MEDICAL RADIOLOGY

Diagnostic Imaging

A. L. Baert
M. Knauth

Imaging of Bone Tumors and Tumor-Like Lesions

Techniques and Applications

A. M. Davies
M. Sundaram
S. L. J. James
Editors

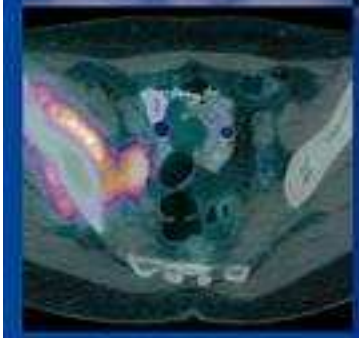

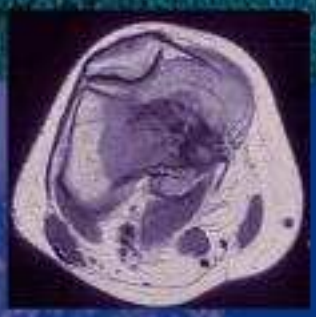

Springer

MEDICAL RADIOLOGY

Diagnostic Imaging

Editors:
A. L. Baert, Leuven
M. Knauth, Göttingen

A. M. Davies · M. Sundaram · S. L. J. James
(Eds.)

Imaging of Bone Tumors and Tumor-Like Lesions

Techniques and Applications

With Contributions by

S. Anderson-Sembach · L. W. Bancroft · J. L. Bloem · M. A. Bredella · P. Brys
R. S. D. Campbell · V. N. Cassar-Pullicino · P. Choong · A. Davies · A. M. Davies
A. M. de Schepper · R. Erlemann · A. Gogna · R. A. R. Green · D. Hobin · A. J. Huang
S. Hwang · H. Ilaslan · S. L. J. James · Karl J. Johnson · G. Jundt · A. W. Kao
S. V. Kattapuram · L. G. Kindblom · M. Koplas · N. A. Kotnis · M. J. Kransdorf
R. K. Lalam · K. Ludwig · N. M. Major · D. Malfair · D. C. Mangham · S. Mannava
P. L. Munk · M. D. Murphey · P. G. O'Donnell · D. M. Panicek · K. M. Patel · B. Peersman
W. C. G. Peh · Etienne Pluot · V. N. Cassar-Pullicino · D. Ritchie · A. Saifuddin
D. Sanghvi · C. Simpfendorfer · J. A. Skinner · A. S. Suhardja · M. Sundaram · B. J. Tins
P. N. M. Tyrrell · F. M. Vanhoenacker · F. van Kerkhove · S. Verbeke · K. Verstraete
R. W. Whitehouse · M. H. Willis

Foreword by
A. L. Baert

Springer

A. Mark Davies, MBCHB, FRCR
Consultant Radiologist
MRI Department
Royal Orthopaedic Hospital NHS Foundation Trust
Bristol Road South
Northfield
Birmingham B31 2AP
UK

Steven J. James, MD
Consultant Radiologist
Imaging Department
Royal Orthopaedic Hospital NHS Foundation Trust
Bristol Road South
Northfield
Birmingham B31 2AP
UK

Murali Sundaram, MD
Section of Musculoskeletal Radiology, Imaging Institute, Cleveland Clinic
Professor of Radiology, Cleveland Clinic Lerner School of Medicine
of Case Western Reserve University
Diagnostic Radiology/A21
The Cleveland Clinic Foundation
9500 Euclid Avenue
Cleveland, OH 44195
USA

Medical Radiology · Diagnostic Imaging and Radiation Oncology
Series Editors:
A.L. Baert · L.W. Brady · H.-P. Heilmann · M. Knauth · M. Molls · C. Nieder

Continuation of Handbuch der medizinischen Radiologie
Encyclopedia of Medical Radiology

ISBN 978-3-540-77982-7 e-ISBN 978-3-540-77984-1

DOI 10.1007/978-3-540-77984-1

Library of Congress Control Number: 2008 9307 83

Cover design: Verlagsservice Teichmann, Mauer, Germany
Production, reproduction and typesetting: le-tex publishing services GmbH, Leipzig, Germany

Printed on acid-free paper

9 8 7 6 5 4 3 2 1

springer.com

Foreword

Detection and characterization of bone tumors with imaging remains a big challenge for every radiologist notwithstanding the impressive progress achieved by the introduction of several new imaging modalities. Moreover, new concepts in surgical and oncological treatment of these lesions require from the radiologist appropriate and focused answers to the specific questions asked by the referring physicians in order to choose the best therapeutic approach for the individual patient.

This comprehensive textbook describes in detail the possibilities and limits of all modalities, including MRI, CT, nuclear medicine and interventional radiological procedures, employed for the modern imaging of tumoral and tumor-like lesions of bone. Their role in the diagnosis, surgical staging, biopsy and assessment of response to therapy is discussed in detail, covering all tumor subtypes as well as their specific anatomical location.Well selected and technically impeccable illustrations strongly enhance the didactic value of this work.

I am very much indebted and grateful to the three editors: A. Mark Davies, Murali Sundaram and Steven L. J. James, world authorities in musculoskeletal radiology, for their superb scientific achievement in preparing and editing this wonderful volume as well as for their individual chapters. I would also like to thank the large international group of collaborating authors, who are also widely acknowledged for their specific expertise in the area of bone tumors, for their outstanding contributions.

I am convinced that this unique book will be of great help to certified radiologists and radiologists in training to assist them in their daily clinical duties. However, orthopedic surgeons and oncologists also will find it extremely helpful to guide them in the therapeutic management of their patients.

I have no doubt that it will meet great success with the readership of this book series.

Leuven

Albert L. Baert
Series Editor

Preface

As our understanding of the complex subject of bone tumours improves, there is a need for the continuous updating of radiologists, orthopaedic surgeons, oncologists and other professionals working in this area. This book takes a multifaceted approach to the subject.

After an initial introductory chapter covering classification and epidemiology the first section acquaints the reader with the range of techniques available for imaging bone tumours. These five chapters cover magnetic resonance imaging, computed tomography, ultrasound, interventional techniques and nuclear medicine. The expanding role of PET scanning is included in this last chapter. The next six chapters apply these techniques to the general diagnosis and management of bone tumours including image-guided biopsy techniques, surgical staging and assessment of tumour response to different treatments. The third and largest section comprises 18 chapters detailing the salient clinical and imaging features of all the important tumour subtypes (cartilaginous, osteogenic etc.). The fourth section reviews the types of tumours that may be found at particular anatomical sites such as the ribs, scapula, spine and so on. Finally there is a chapter covering the important topic of compartmental anatomy and a further chapter giving potted biographies of those whose names over the past 150 years have become synonymous with bone tumours.

The editors are grateful to the international panel of authors for their contributions to this book, which aims to provide a comprehensive overview of current imaging of tumours and tumour-like lesions of bone.

Birmingham, UK — A. Mark Davies
Cleveland, US — Murali Sundaram
Birmingham, UK — Steven L. J. James

Contents

Bone Tumors: Epidemiology, Classification, Pathology

1

Lars Gunnar Kindblom

CONTENTS

KEY POINTS

- Primary bone tumors are rare; non-neoplastic conditions, metastatic disease, and lymphohematologic malignancies, which may simulate primary bone tumors, by far outnumber genuine bone tumors.
- Excluding myeloma and lymphoma, malignant primary bone tumors constitute only 0.2% of all malignancies in adults and approximately 5% of childhood malignancies.
- Bone tumor classification is based on morphologic findings: cell type, architecture, and matrix production. The morphologic features of benign and malignant as well as non-neoplastic conditions and true tumors may overlap.
- Many bone tumor entities show a striking consistency in clinical setting and age and anatomic site distribution.
- The final diagnosis of bone tumors should be based on a synthesis of histopathologic findings, clinical presentation, and imaging characteristics, preferably in the setting of a multidisciplinary team conference.
- Adjunctive immunohistochemical and genetic/molecular genetic techniques are important for the definite classification of certain bone tumors.
- A number of congenital, hereditary, and non-hereditary syndromes are associated with increased risk of bone tumors.

L.-G. Kindblom, MD, PhD
Professor of Pathology, Department of Musculoskeletal Pathology at the Royal Orthopaedic Hospital NHS Foundation Trust, Robert Aitken Institute for Clinical Research, The Medical School, University of Birmingham, Birmingham B15 2TT, UK

1.1 Introduction

Primary bone tumors are fairly rare. Conditions that may simulate primary bone tumors, such as metastasis and non-neoplastic conditions such as inflammatory processes, bone cysts, fibrous dysplasia, non-ossifying fibroma, Paget's disease of bone, etc., by far outnumber the cases of true bone tumors. Compared to other malignancies, primary malignant bone tumors are very rare. The three most common genuine primary bone malignancies (osteosarcoma, chondrosarcoma, and Ewing's sarcoma) account for only 0.2% of all malignancies in the UK and USA; however, in children (< 15 years) malignant bone tumors account for approximately 5% of all malignancies (Dorfman and Czerniak 1995, 1998; Unni et al. 2005). This chapter reviews the epidemiology and pathologic classification of bone tumors. In addition, it gives an overview of the pathologist's role in diagnosis and management.

1.2 Epidemiology

The vast majority of primary bone tumors are benign and since many are non-symptomatic they remain undetected or are detected only incidentally at radiographic examinations for other reasons. The true incidence of benign bone tumors has therefore been difficult to determine. The incidence of primary bone malignancies is, in contrast, fairly well documented in various national cancer registries. Excluding the most common lymphohematopoietic malignancies (particularly plasma cell tumor/myeloma and malignant lymphoma, more rarely leukemia) that are of bone marrow origin rather than true bone tumors, the yearly incidence in the USA has been estimated to be $8/10^6$. This corresponds well with the approximately 500 cases diagnosed yearly in the UK and some 2,500 cases in the USA. More than 75% of malignant bone tumors are osteosarcoma, chondrosarcoma, and Ewing's sarcoma (Table 1.1). The incidence of malignant bone tumors shows a striking age-specific distribution: in the age group 0–40 years, there is an incidence peak between 10 and 20 years (primarily osteosarcoma and Ewing's sarcoma) and for the age group above 40 years there is a steady increase in incidence up to 80 years (primarily chondrosarcoma and to a lesser degree Paget's related osteosarcoma) (Dorfman and Czerniak 1995, 1998; Unni et al. 2005).

Benign bone tumors and many bone simulating, non-neoplastic conditions also show a striking age distribution. This together with a likewise striking site distribution for both benign and malignant bone tumors is most helpful in the diagnosis of bone lesions. The combined information of age, site, and imaging findings can in reality in many instances indicate a definite diagnosis, sometimes to the point that morphologic confirmation is considered unnecessary (such as in cases of bone cysts, fibrous dysplasia, non-ossifying fibroma, Paget's disease of bone). For the pathologist, awareness of these age and site distributions is essential; when a suggested morphologic diagnosis occurs at a highly unusual site or in "the wrong" age group, the definite diagnosis should be carefully reevaluated. The age and anatomic site distributions of some of the most common bone tumors are summarized in Tables 1.2 and 1.3.

Table 1.1. Relative frequency of most common primary bone malignancies (excluding myeloma/malignant lymphoma) (Dorfman and Czerniak 1995)

Primary bone malignancy	Frequency (%)
Osteosarcoma	35.1
Chondrosarcoma	25.8
Ewing's sarcoma	16.0
Chordoma	8.4
Malignant fibrous histiocytoma	5.7
Angiosarcoma	1.4
Unspecified	1.2
Other	6.4

Table 1.2. Classification of primary benign bone tumors, peak age, and most common sites distribution

Histologic type	Peak age (years)	Most common sites	Comments
Cartilage tumors			
Osteochondroma	10–30	Distal femur, proximal tibia, proximal humerus, rarely from flat bones	> 2 cm cartilage cap may indicate malignant transformation
Enchondroma	10–40	Hands, feet, long tubular bones	
Periosteal chondroma	10–40	Proximal humerus, distal femur, hip region, and pelvis	Sharply demarcated from cortex
Chondroblastoma	10–30	Distal femur, proximal tibia and humerus, calcaneus	Typically epiphyseal
Chondromyxoid fibroma	10–30	Proximal tibia, distal femur, pelvis, feet (metatarsal)	
Osteogenic tumors			
Osteoid osteoma	5–25	Proximal femur, any long bones	Distinguished from osteoblastoma by size and imaging
Osteoblastoma	10–40	Spine, long tubular bones, jaws	
Fibrogenic tumors			
Desmoplastic fibroma	10–30	Mandible, femur, pelvis	Very rare; distinction from FD, low-grade osteosarcoma, and fibrosarcoma may be difficult
Fibrohistiocytic tumors			
Benign fibrous histiocytoma	20–60	Pelvis, femur	Diaphyseal or metaphyseal; rarely used concept, distinguished from non-ossifying fibroma only by clinical setting
Giant cell tumor	20–45	Distal femur, proximal tibia, distal radius, sacrum	Epiphyseal; pulmonary metastases occur in 2%; very rarely transformation to high-grade sarcoma
Vascular tumors			
Hemangioma (cavernous, capillary, epithelioid, etc.)	Classic hemangiomas, usually adults	Craniofacial bones, vertebrae	Hemangiomas are often multicentric
Angiomatosis, lymphangioma(tosis)	Often children	Highly variable	
Glomus tumor	Usually adults	Hands, distal phalanx	
Hemangiopericytoma	Usually adults	Pelvis	
Epithelioid hemangioendothelioma	Adults	Long tubular bones, spine	
Soft tissue type tumors			
Lipoma	Adults	Femur, calcaneus	All very rare
Schwannoma		Sacrum, mandible	
Leiomyoma		Mandible, tibia	

FD fibrous dysplasia

Table 1.3. Classification of primary malignant bone tumors, peak age, and most common sites distribution

Histologic type	Peak age (years)	Most common sites	Comments
Chondrosarcoma			
Primary	50–80	Pelvis, proximal/distal femur, proximal humerus, ribs	Usually large, intraosseous; very rarely periosteal
Secondary	20–60	Ex osteochondroma(tosis): pelvis, hip and shoulder	In Ollier's/Maffucci's at any site affected
Dedifferentiated chondrosarcoma	50–70	Pelvis, femur, humerus	Usually small component of low-grade chondrosarcoma juxtaposed with high-grade osteo-, spindle cell-, MFH-, or other sarcoma
Clear cell chondrosarcoma	25–60	Proximal femur, humerus	Typically epiphyseal location
Mesenchymal chondrosarcoma	10–40	Jaws, ribs, pelvis, spine	20–30% occur in soft tissues
Osteosarcoma			
Conventional	10–30	Distal femur, proximal tibia, hip and shoulder	Typically metaphyseal
Telangiectatic osteosarcoma	10–30	Femur, tibia, humerus	Typically metaphyseal; ABC-like, purely lytic
Low-grade central osteosarcoma	20–40	Distal femur, proximal tibia	May dedifferentiate to high grade
Parosteal osteosarcoma	20–50	Posterior distal femur, proximal humerus	May invade the bone, may dedifferentiate to high grade
Periosteal osteosarcoma	10–30	Femur, tibia	Diaphyseal, surface lesion, predominantly chondroblastic, intermediate grade
High-grade surface	10–40	Distal femur, shoulder	Diaphyseal or metaphyseal
Secondary osteosarcoma			
Paget's associated	50–90	Pelvis, hip and shoulder, craniofacial	High-grade osteosarcoma
Post-radiation	50–80	Pelvis, craniofacial, hip and shoulder, chest wall	High-grade osteosarcoma
Other conditions	40–70	Bones affected by FD, bone infracts, chronic osteomyelitis, etc.	
Ewing´s sarcoma, PNET	5–30	Pelvis, longbones of lower and upper extremities	
Fibrosarcoma, MFH, spindle cell sarcoma	40–70	Knee, hip and shoulder regions, pelvis	
Malignant giant cell tumor	20–60	Knee region, pelvis, shoulder region	High-grade sarcoma arising in GCT; classic GCT may rarely metastasize
Chordoma	30–80	Sacrococcygeal, skull base, vertebrae	May rarely dedifferentiate

ABC aneurysmal bone cyst, *FD* fibrous dysplasia, *GCT* giant cell tumor, *MFH* malignant fibrous histiocytoma, *PNET* primitive neuroectodermal tumor

Table 1.3. *(continued)* Classification of primary malignant bone tumors, peak age, and most common sites distribution

Histologic type	Peak age (years)	Most common sites	Comments
Angiosarcoma	20–70	Spine, pelvis, hip and shoulder regions	May be multicentric
Other soft tissue type sarcomas	20–70	Long bones, around major joints	Rare examples of leiomyosarcoma, liposarcoma, extraskeletal myxoid chondrosarcoma, synovial sarcoma, rhabdomyosarcoma, etc.
Adamantinoma	10–40	Tibia, rarely ulna, radius and fibula	Typically diaphyseal

ABC aneurysmal bone cyst, *FD* fibrous dysplasia, *GCT* giant cell tumor, *MFH* malignant fibrous histiocytoma, *PNET* primitive neuroectodermal tumor

1.3 Morphologic Diagnosis of Bone Tumors

The pathologic diagnosis of primary bone tumors poses particular problems:

1. Their rarity prevents most pathologists from gaining sufficient diagnostic experience.
2. There is an unusual need for the pathologist to be familiar with and to integrate clinical, laboratory, and imaging findings in the final diagnosis.
3. Despite their rarity, there is a wide spectrum of bone lesions with overlapping morphologic features.
4. The distinction between neoplastic, reactive/inflammatory, and metabolic bone lesions as well as some developmental disorders is sometimes difficult.
5. The diagnosis of malignant bone tumors, which frequently involve children or young adults, often has dramatic consequences in terms of surgical and adjuvant treatment. Moreover, there are a number of rare hereditary and non-hereditary conditions associated with increased risk of developing bone tumors that the pathologist needs to be aware of.

Even if clinical presentation and imaging studies are very often highly suggestive of a particular diagnosis, it is the morphologic findings that form the basis for the definite diagnosis of bone tumors. It is expected that the pathologists reporting primary bone malignancies participate in multidisciplinary team conferences and appropriately integrate clinical, laboratory, and imaging findings in the final diagnosis. Within these teams the pathologists have the important role to establish the correct diagnosis, to arrange for and interpret required adjunctive diagnostic tests (immunohistochemistry, cytogenetic/molecular analyses), to provide prognostic information, to identify patients that should be considered for adjuvant treatment protocols or trials, and to assess treatment response.

The possibility for the pathologist to correctly diagnose a bone tumor depends to a large extent on the completeness of the clinical and imaging information provided. The request forms for bone tumors should therefore contain information regarding pertinent clinical history, family history, laterality and exact anatomic site of tumor, whether the patient has solitary or multicentric disease or clinical evidence of metastatic disease, information on type and timing of any preoperative treatment, type of surgical procedure (fine-needle aspiration, core needle biopsy, open surgical biopsy, curettage, resection, amputation, etc.), and nature of specimen and, if indicated, orientation markers on specimen.

Whenever practically possible, it is advantageous if malignant bone tumor specimens are delivered fresh and unfixed to the pathology laboratory with the shortest possible delay. This will enable the pathologist to obtain material for studies that require fresh, unfixed tissue, to decide on the most appropriate way to obtain material from surgical margins, to decide on techniques for decalcification procedures, and to decide when dealing with large specimens if sectioning of skin, soft tissues, and bone is required to facilitate fixation.

1.4 Types of Bone Tumor Specimens

1.4.1 Intraoperative Procedures/ Frozen Sections

There are inherent problems with intraoperative diagnosis of bone tumors: hard, bony specimens cannot be processed since decalcification is needed, the pathologist needs to be familiar with the artifacts introduced by freezing specimens, and the overlapping morphologic features of different entities may be difficult to correctly interpret in frozen sections. However, where this technique is widely used, specialized bone tumor pathologists can acquire a very high degree of expertise. Frozen sections may be particularly helpful in determining if the biopsy is representative of the lesion and can help to immediately distinguish primary genuine bone tumors from inflammatory processes, other non-neoplastic conditions, metastases, and lymphohematologic malignancies.

1.4.2 Fine-needle Aspiration Biopsy

With the exception of Scandinavia, there are few bone tumor centers that have adopted this technique as a routine in the diagnosis of bone tumors. The reluctance to apply fine-needle aspiration biopsy (FNAB) is explained by the lack of experienced cytopathologists in this field, the limitations of the technique to obtain material from bony, calcified components, the loss of architecture and matrix characteristics, and the limited volume of tissue obtained (prohibiting extensive immunohistochemical and cytogenetic/molecular workup). In the hands of experienced cytopathologists, FNAB has, however, proven practically useful. For example, it is a very quick method to identify a lesion as a cartilage-producing neoplasm or hematologic malignancy (lymphoma/myeloma) and helps to distinguish osteosarcoma from Ewing's sarcoma and metastatic disease from primary bone tumors (Willen 1997). There are also reports of the diagnostic FNAB characteristics of many individual bone tumor entities such as osteosarcoma, chondrosarcoma, Ewing's sarcoma, and chordoma (Dahl et al. 1986; Walaas and Kindblom 1990, 1991; Walaas et al. 1990; Willen 1997).

1.4.3 Biopsy

Today "closed" transcutaneous, core needle biopsy techniques are widely used, often assisted by radiographic imaging techniques. Material can be obtained from both soft tissue components (preferable when possible) and intraosseous components, and the material obtained is usually sufficient for adjunctive studies such as immunohistochemistry and cytogenetic/molecular genetic analyses. If RNA-based molecular analyses are to be carried out it is important that decalcification processes if required are adjusted to allow such techniques (formic acid can be used, not nitric acid!) (Mangham et al. 2006). When for various reasons "closed" biopsy techniques cannot provide material sufficient for a definite diagnosis an open surgical biopsy has to be performed. It is important that decalcification techniques are not routinely applied on all bone lesion specimens since many specimens need no decalcification at all or at least parts of the biopsy can be processed without such procedures. The decalcification procedure has also to be adjusted for each specimen in order not to overdecalcify the tissue, which can severely hamper the possibilities to reach a correct diagnosis.

1.4.4 Curettage

A bone lesion can be curetted as a one-step diagnostic and treatment procedure or as definite treatment after previous biopsy. Generous sampling for microscopic examination is essential and the same principles for decalcification procedures should be applied as for biopsies.

1.4.5 Resections and Amputations

Resections and amputations are performed as part of curative definite treatment of bone tumors. For a correct approach to dissection of such specimens it is important that the pathologist can review pertinent radiographic images and that that the surgeon has indicated orientation if necessary. In addition to a correct histopathologic diagnosis, the examination of such specimens should include assessment of tumor size (three dimensions), margins (tissue type and dimensions), involvement of the marrow, cortex, periosteum, joints, surrounding soft tissues, etc., and possible vascular invasion. If preoperative treatment has been given, the response should be assessed based on a detailed mapping of the tumor.

1.5 Adjunctive Diagnostic Techniques

1.5.1 Histochemistry, Immunohistochemistry, and Electron Microscopy

These techniques have helped to better define many bone tumors but are, with some important exceptions, not required in routine diagnosis. For the vast majority of bone tumors the diagnosis is based on the histologic appearance in routine-stained sections with appropriate consideration of clinical setting and imaging findings. Immunohistochemical characterization, however, is of special importance for classification of metastatic bone disease (identification of primary sites if unknown) and for the subclassification of lymphohematologic malignancies and small round cell malignancies, in particular Ewing's sarcoma. Other examples where immunohistochemical findings may be helpful include the diagnosis of chordoma in biopsies, the recognition of endothelial differentiation in poorly differentiated angiosarcomas, and for the distinction between osteofibrous dysplasia (OFD) and OFD-like adamantinoma.

1.5.2 Cytogenetic/Molecular Genetic Techniques

Genetic characterization of various bone tumors has helped to better understand their nature and the pathogenetic mechanisms involved and has also given additional support for the morphology-based classifications. Examples of this include the identification of the role of the EXT 1 and 2 genes in the development of osteochondroma, osteochondromatosis, and secondary chondrosarcomas (Bovée et al. 1999). Another example is the identification of the CDH11-USP6 fusion gene caused by a 16; 17 translocation in aneurysmal bone cysts, suggesting that these lesions are probably of neoplastic nature (Oliveira et al. 2004). Other genetic findings have also made the distinction between what in the past were considered non-neoplastic, developmental disorders, such as fibrous dysplasia and Paget's disease, and true neoplasia less clear. There are even some genetic observations suggesting that synovial chondromatosis and pigmented villonodular synovitis may represent neoplastic conditions (Fletcher et al. 2002).

In a few instances karyotyping and molecular genetic techniques (such as FISH and RT-PCR techniques) have provided highly valuable diagnostic tools. The most striking example is the identification of the Ewing's sarcoma-specific translocation between the long arms of chromosomes 11 and 22 involving a fusion of the EWS gene (or rarely the FUS gene) with various other genes of the ETS transcription factor family; mostly these translocations involve the FLI1 gene, less frequently the ERG, ETV1, E1A-F, FEV or ZSG genes. FISH- and/or RT-PCR-based techniques, designed to identify these gene translocations, are today widely applied in the routine diagnosis of Ewing's sarcoma and its distinction from other small round cell malignancies (Fletcher et al. 2002; Mangham et al. 2006; Unni et al. 2005).

1.6 Classification of Bone Tumors

The histologic classification of bone tumors is based on cytologic findings (in particular cell type such as osteocyte/osteoblast, chondrocyte/chondroblast, osteoclast, etc.), architecture, and type of matrix produced by the tumor. Despite the rarity of bone tumors there is a very wide spectrum of entities with sometimes overlapping features; the current WHO classification (2002) includes a total of 45 main bone tumor types. For some malignant bone tumors, such as osteosarcoma and chondrosarcoma, malignancy grading is important, while for others such as Ewing's sarcoma and chordoma the degree of malignancy is implicated in the diagnosis. In addition to correct classification and in some cases grading, the pathologist has to report on margins, relation of tumor to cortex, periosteum, surrounding soft tissues, joints, etc., and the presence of vascular invasion as well as give information of importance for staging (Dorfman and Czerniak 1998).

The current classifications of benign and malignant bone tumors are summarized in Tables 1.2 and 1.3 and the most common non-neoplastic bone tumor-simulating conditions in Table 1.4.

1.7 Comments on the Morphologic Classification of Bone Tumors

1.7.1 Cartilage Tumors

The morphologic diagnosis of cartilage tumors poses particular problems. The distinction between benign cartilage lesions and chondrosarcoma is tradition-

Table 1.4. Classification of most common conditions simulating primary bone tumors, peak age, and common sites

Histologic type	Peak age (years)	Most common sites	Comments
Aneurysmal bone cyst	5–20	Femur, tibia, humerus, vertebrae	Metaphyseal in long bones
Simple bone cyst	Infancy to 20	In childhood: proximal femur, humerus and tibia In adults: calcaneus, ilium	
Fibrous dysplasia	5–30	Long bones, jaws, skull, ribs	One third polyostotic Rarely combined with endocrine disorders
Non-ossifying fibroma	5–20	Distal femur, proximal and distal tibia	Synonym: metaphyseal fibrous (cortical) defect
Osteofibrous dysplasia	Infancy to 20	Tibia	Diaphyseal Rarely in fibula, ulna, radius
Langerhans cell histiocytosis	Infancy to 30	Skull, femur, pelvis, mandible	May be polyostotic Very rarely disseminated disease, visceral involvement
Pigmented villonodular synovitis	10–40	Localized: fingers Diffuse: knee, hip, ankle	Synonym for localized: GCT of tendon sheath Diffuse: may destroy bone
Synovial chondromatosis	20–40	Knee, hip	May erode bone Chondrosarcoma may involve synovium and simulate synovial chondromatosis
Paget's disease	50–90	Pelvis, craniofacial bones, spine, femur, tibia	Sporadic cases may develop secondary high-grade sarcoma (1%) Familial cases may present at young age

GCT giant cell tumor

ally stated to be based on cellularity, degree of atypia, myxoid stromal change, and growth characteristics in relation to native bone. However, the vast majority of chondrosarcomas are low grade and very highly differentiated with minimal atypia and the identification of permeating, infiltrative growth in native bone may not be possible to find in biopsies. Moreover, several types of benign cartilage lesions may show overlapping morphology with chondrosarcoma by being fairly cellular and showing myxoid change and variation in cell size and shape. Periosteal chondroma, enchondroma of phalanxes, soft tissue chondroma, and synovial chondromatosis as well as enchondromas in the setting of Ollier's disease and Maffucci's syndrome are such examples. The interobserver variability in distinguishing benign cartilage lesions from chondrosarcomas and grade 1 chondrosarcomas from grade 2 tumors has been found to be remarkably poor even among specialized bone tumor pathologists (Eefting et al. 2008). This fact underscores the importance of integrating clinical setting and imaging findings in all diagnoses of cartilage lesions. Even when all clinical, imaging, and morphologic information is considered, a significant number of cartilage lesions remains of uncertain malignant potential (so-called CLUMPs). CLUMP has therefore become a useful concept when dealing with intraosseous well-differentiated cartilage tumors without obvious malignant features histologically but of significant size (> 5 cm).

1.7.2 Bone-forming Tumors

The distinction between osteoid osteoma and osteoblastoma is primarily based on clinical setting and imaging findings since they have very similar or identical histologic characteristics. A subset of osteoblastomas is characterized by unusually large epithelioid osteoblasts, larger tumor size, and occurrence in an older age group. The term aggressive osteoblastoma has been suggested for these since they have been reported to recur and cause clinical problems more frequently than the classic ones (Dorfman and Weiss 1984). This finding remains controversial, however.

The most important and sometimes problematic distinction is of course between osteoblastoma and osteosarcoma. The diagnosis of osteosarcoma is usually fairly uncomplicated, the vast majority being high grade of either osteoblastic, chondroblastic, or fibroblastic types. Diagnostic problems typically occur when osteosarcomas occur at unusual sites and in unusual age groups or have unusual morphologic features. Moreover, osteoblastoma-, chondroblastoma-, and chondromyxoid fibroma-like variants of osteosarcoma do occur. A telangiectatic osteosarcoma may in a biopsy show areas that with difficulty can be distinguished from an aneurysmal bone cysts and giant cell-rich osteosarcomas may focally closely mimic giant cell tumors. The very rare small cell variant of osteosarcoma may show features overlapping with Ewing's sarcoma.

The very low grade osteosarcomas may also pose difficulties for the pathologist. Parosteal osteosarcoma may show features overlapping with heterotopic ossification and when presenting a "cartilage cap" with osteochondroma. The low-grade central osteosarcomas may be difficult to distinguish from fibrous dysplasia and desmoplastic fibroma (Dorfman and Czerniak 1998; Unni et al. 2005).

1.7.3 Ewing's Sarcoma and Other Small Round Cell Malignancies

The vast majority of primary small round cell malignancies occurring in bone are within the family of Ewing's sarcomas. Primitive neuroectodermal tumor (PNET) is a term sometimes used for the subset with distinctive neuroectodermal features as seen light microscopically, ultrastructurally, or immunohistochemically. In biopsy material, the distinction from malignant lymphoma is the most important. Immunohistochemical findings (positive for CD99 but negative for lymphocytic markers) and genetic/molecular genetic characteristics (11;22 translocation and identification of typical fusion transcripts) help to recognize the Ewing's sarcomas (Dorfman and Czerniak 1998; Mangham et al. 2006; Unni et al. 2005).

Rarely other small round cell malignancies enter the differential diagnoses, such as metastatic neuroblastoma, primary rhabdomyosarcoma of bone, and the rare small cell variant of osteosarcoma (Dorfman and Czerniak 1998; Unni et al. 2005).

1.7.4 Giant Cell Tumors

The morphologic characteristics of giant cell tumor of bone, combined with the striking consistency in age and site distribution make the diagnosis fairly straightforward in most instances. Sometimes, however, giant cell tumors present unusual features that may cause problems, such as extensive spindle cell areas, prominent new bone formation, rarely cartilage formation, secondary aneurysmal bone cyst development, and nuclear enlargement and hyperchromasia. Moreover, a number of other bone lesions are also characterized by numerous osteoclast-type giant cells, such as chondroblastoma (also an epiphyseal lesion), solid variants of aneurysmal bone cysts, non-ossifying fibroma, and, not least, brown tumor associated with hyperparathyroidism. Metaphyseal location and obvious anaplasia help to recognize the giant cell-rich osteosarcomas.

A very small percentage (probably less than 3%) of histologically benign giant cell tumors metastasizes, particularly to lungs. Such metastases may follow a protracted indolent course or may be progressive and lead to the patient's death. A high-grade sarcoma component may occur de novo in giant cell tumors (primary malignant giant cell tumor or dedifferentiated giant cell tumor) or in recurrent giant cell tumors or at sites previously affected by giant cell tumors (secondary malignant giant cell tumor) (Meis 1991; Meis et al. 1989). Many of the reported secondary malignant giant cell tumors have received radiotherapy as part of their original treatment.

1.7.5 Fibrogenic/ Fibrohistiocytic Tumors

Desmoplastic fibroma, defined as a benign but locally aggressive lesion with histologic resemblance to des-

moid-type fibromatosis of soft tissues, is a rarely used concept. Its distinction from low-grade central osteosarcoma and low-grade fibrosarcoma may be problematic (Unni et al. 2005).

Fibrosarcoma is a term used for malignant spindle cell tumors with a distinct fascicular pattern and lacking osteoid or mineralized bone production (Bertoni et al. 1984). Low-grade fibrosarcomas may be difficult to distinguish from desmoplastic fibromas and high-grade fibrosarcomas from fibroblastic osteosarcomas which in biopsies may lack obvious bone matrix production. Also the distinction from malignant fibrous histiocytoma is often arbitrary and may depend on sampling.

Benign fibrous histiocytoma of bone is a term sometimes used for lesions histologically indistinguishable from non-ossifying fibroma but with a different clinical setting (usually older patients and non-metaphyseal locations).

Malignant fibrous histiocytoma remains a somewhat controversial term used for high-grade spindle cell and pleomorphic bone sarcomas lacking bone matrix production (Dahlin et al. 1977). The distinction from osteosarcomas with minimal osteoid/bone matrix production may be difficult. Malignant fibrous histiocytoma tend to occur in an older age group than osteosarcomas, peak after 40 years, and about one third of reported cases have occurred after radiotherapy or are associated with Paget's disease (Dorfman and Czerniak 1998; Unni et al. 2005).

1.7.6 Chordoma

The characteristic histologic and immunohistochemical features and site distribution of chordoma usually make the diagnosis fairly uncomplicated. In cases in which the microscopy and immunoprofile overlap with metastatic carcinoma, detection of the newly reported chordoma marker brachyury, a regulator of notochordal development, may be helpful (Vujovic et al. 2006). So-called chondroid chordoma is a rare variant occurring in the skull base, presenting classic chordoma features as well as chondroid components (Rosenberg et al. 1994). Rarely chordomas may undergo dedifferentiation to high-grade sarcomas (Bergh et al. 2000; Meis 1991). Very rare examples of chordoma have been reported in bone or soft tissues outside the midline, so-called chordoma peripheric um (Tirabosco et al. 2008).

1.7.7 Vascular Tumors

Classic hemangiomas of capillary or cavernous types are common in the spine (Dorfman et al. 1971). Many of these are multicentric and often incidental findings. Other rare benign vascular lesions include epithelioid hemangioma (O'Connell et al. 1993), various types of angiomatosis, lymphangioma(tosis), and glomus tumors (Dorfman and Czerniak 1998; Unni et al. 2005).

Epithelioid hemangioendothelioma of bone is a skeletal counterpart to the same entity in soft tissues and visceral organs. They are viewed as borderline or low-grade lesions that frequently affect multiple sites (Tsuneyoshi et al. 1986). In overtly malignant cases the distinction from epithelioid angiosarcomas becomes arbitrary.

Angiosarcomas of bone show a range of differentiation and atypia from low-grade lesions with obvious vascular differentiation to predominantly solid, poorly differentiated sarcomas for which immunotechniques to demonstrate endothelial markers may be required to support the diagnosis. Practically any bone can be affected but most cases are seen in the axial skeleton and pelvic bones. When angiosarcomas affect multiple sites they are often confined to one anatomic area, such as an extremity (Dorfman et al. 1971; Unni et al. 2005).

1.7.8 Soft Tissue Tumor Types Occurring as Primary Bone Tumors

Rarely both benign and malignant tumors, typically occurring in soft tissues, present as primary bone tumors. Among such benign tumors are intraosseous lipomas (Milgram 1988), schwannomas, and leiomyomas (Fletcher et al. 2002; Unni et al. 2005). Among the malignant ones leiomyosarcoma is the most common (Berlin et al. 1987). Very rarely liposarcoma, synovial sarcoma, malignant peripheral nerve sheath tumor, clear cell sarcoma of tendons and aponeurosis, rhabdomyosarcoma, and alveolar soft part sarcoma may be primary in bone (Dorfman and Czerniak 1998; Unni et al. 2005).

1.7.9 Conditions Simulating Primary Bone Tumors

In the elderly, metastatic disease is by far the most common condition simulating primary bone tumors. Practically, the distinction becomes particularly problematic

when presenting as a solitary lesion without previous history of malignancy. Almost any type of cancer can metastasize to the skeleton but, in particular, cancer of breast, prostate, thyroid, lung, and kidney tend to metastasize to bone (Unni et al. 2005). Renal cell carcinoma is by far the most common cancer associated with solitary bone metastases.

In addition to the bone tumor-simulating conditions summarized in Table 1.4, there are a number of other lesions that may cause diagnostic problems. These include cysts, such as intraosseous ganglion cysts and epidermal inclusion cysts, and bone and cartilage-forming lesions, such as heterotopic ossification, subungual exostosis, bizarre parosteal osteochondromatous proliferation, and fracture callus. Giant cell-rich lesions that may simulate giant cell tumor of bone include so-called giant cell reparative granuloma of jaws and small bones of the hands and feet as well as "brown tumors" associated with hyperparathyroidism (Dorfman and Czerniak 1998; Unni et al. 2005).

Characteristic morphologic aspects of bone tumor diagnosis are illustrated in Figs. 1.1–1.3.

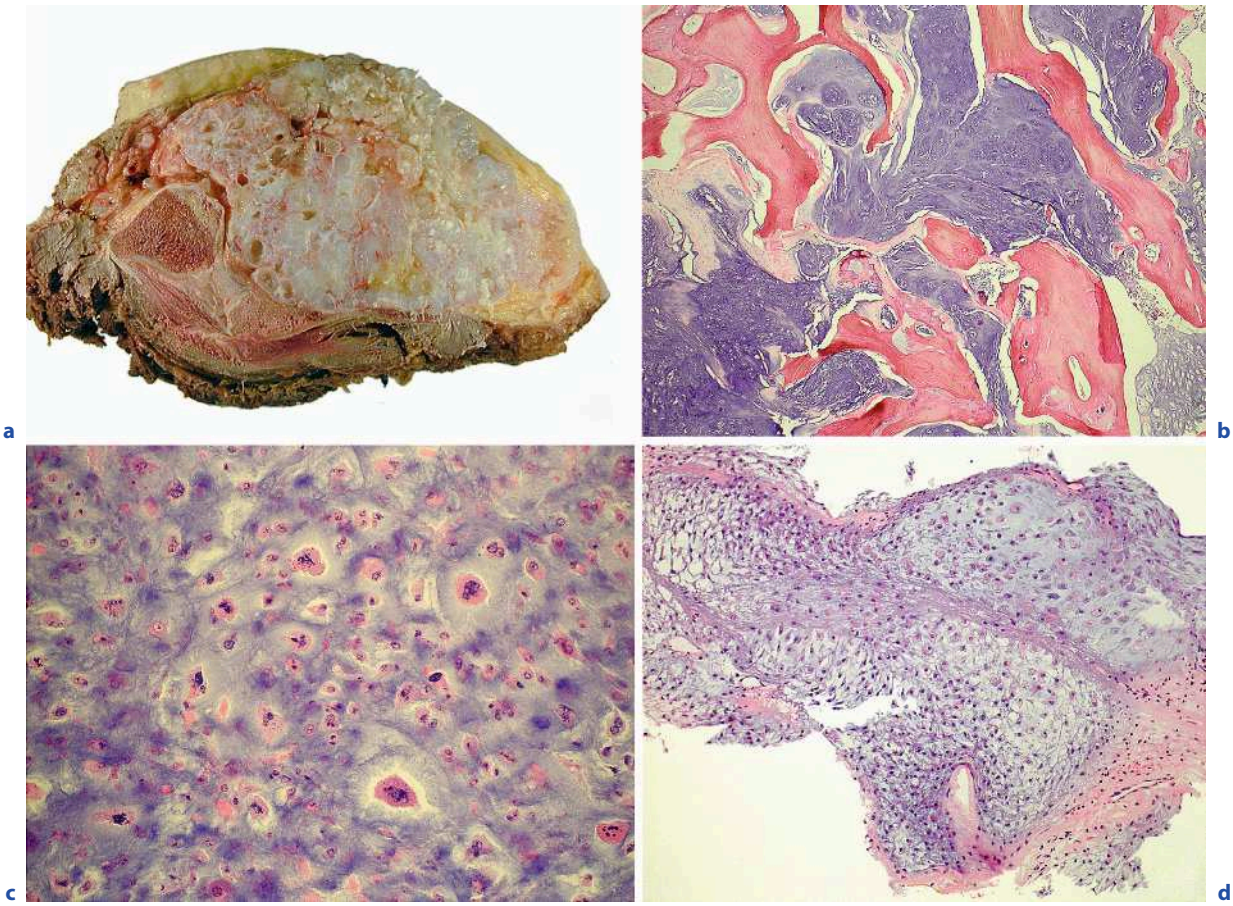

Fig. 1.1. a Pelvic resection for a large chondrosarcoma. **b** Well-differentiated chondrosarcoma with diffuse permeating growth between the bony lamellae. **c** High-grade chondrosarcoma showing prominent cytologic atypia and atypical mitotic figures. **d** Biopsy from enchondroma of a distal phalanx. Increased cellularity and myxoid change can make the distinction from chondrosarcoma difficult if clinical setting and imaging findings are not considered in the final diagnosis

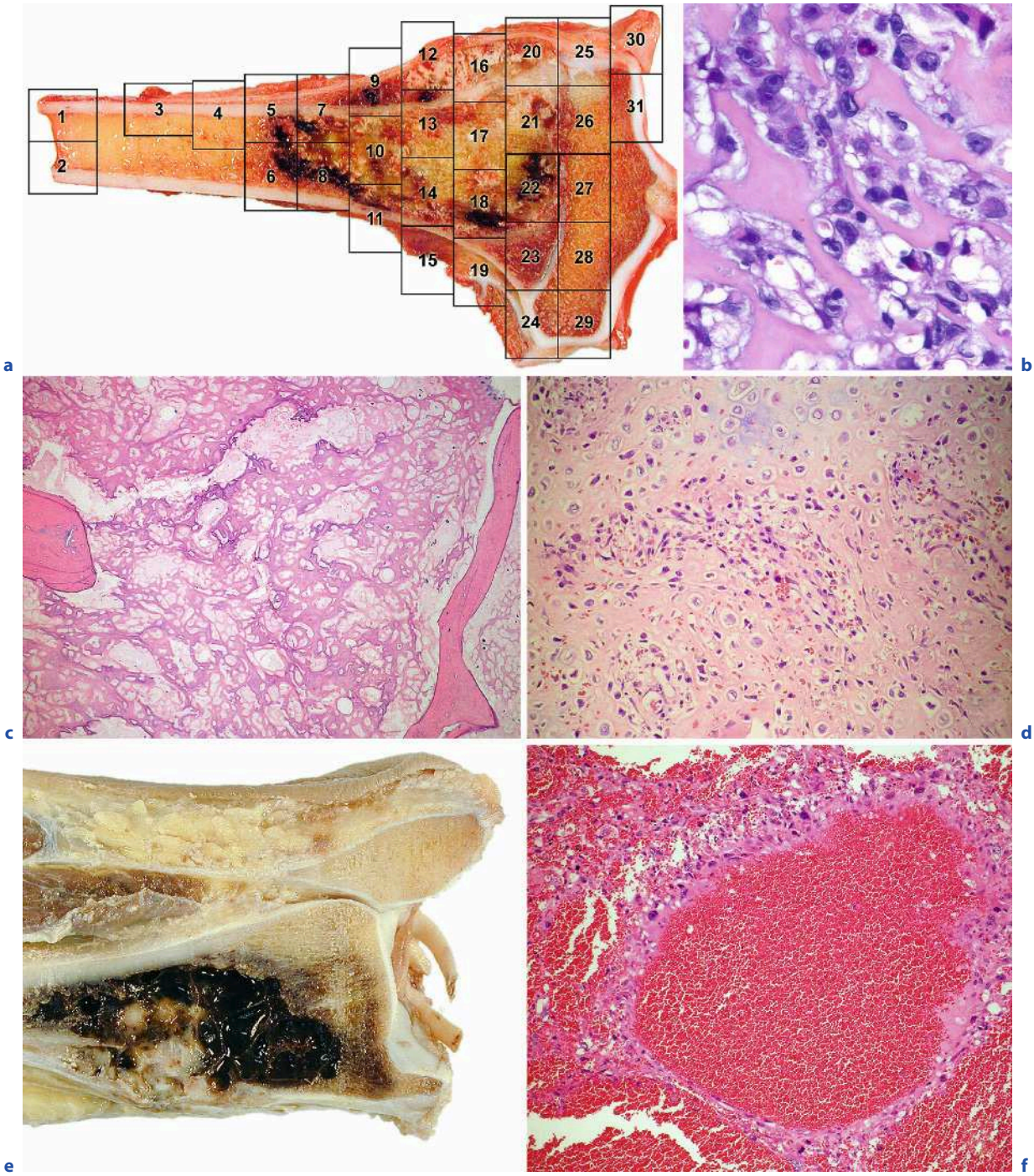

Fig. 1.2. **a** Resection of proximal tibia with typical features of osteosarcoma. Mapping of the specimen is done in order to evaluate the response to given preoperative chemotherapy. **b** Pretreatment biopsy of high-grade osteoblastic osteosarcoma. **c** After treatment the tumor is replaced by a network of acellular mineralized bone indicating good response. **d** Active fracture callus may show features resembling osteosarcoma but lack true anaplasia. **e** Resection of lower leg showing a telangiectatic osteosarcoma in the distal tibia. **f** Telangiectatic osteosarcoma resembles an aneurysmal bone cyst but shows severe cytologic atypia

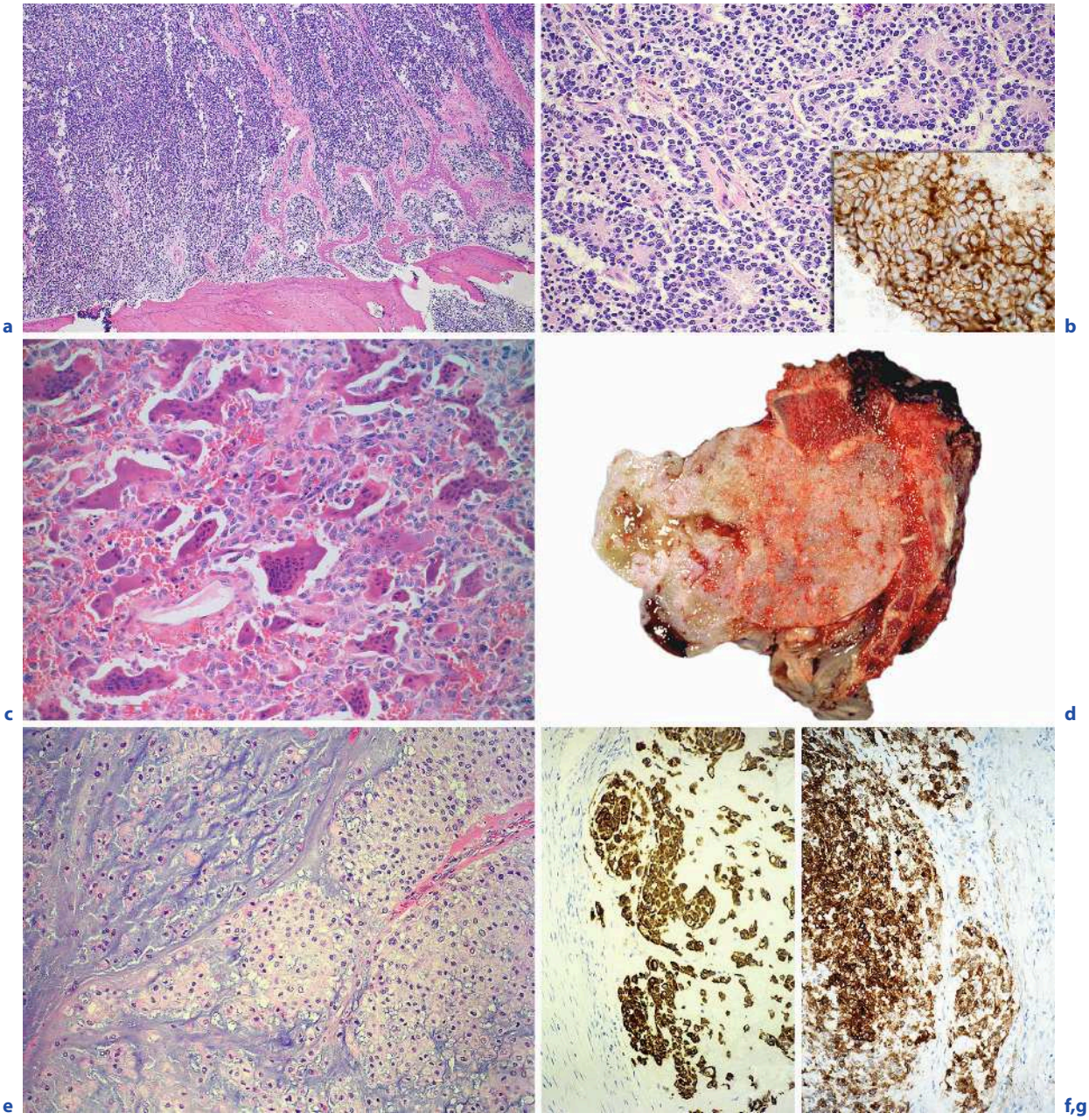

Fig. 1.3. a,b Ewing's sarcoma showing a diffuse proliferation of small primitive cells, focally with rosette-like formations (**b**). *Inset* in **b** is immunohistochemical demonstration of CD99. **c** Giant cell tumor of bone showing very large osteoclasts in a mononuclear cell background. **d** Total resection of sacrum with a large chordoma. **e** Chordomas resemble notochordal tissue and are characterized by epithelioid tumor cells in sheaths and strands, enclosed by an abundant myxoid matrix. **f,g** Chordomas show epithelial features immunohistochemically, thus positivity for cytokeratin (**f**) and epithelial membrane antigen (**g**)

Table 1.5. Syndromes associated with bone tumors

Syndrome	Manifestations
Bloom syndrome	AR; growth deficiency, immunodeficiency, early development of cancer including osteosarcoma
Familial expansile osteolysis	AD; osteosarcoma
Langer-Giedion syndrome	Sporadic; combination of tricho-rhino-phalangeal syndrome II and multiple osteochondromas; chondrosarcomas
Li-Fraumeni syndrome	AD; early onset of various malignancies including osteosarcomas and soft tissue sarcomas
Maffucci's syndrome	Sporadic; multiple enchondromas, chondrosarcoma, hemangioma, spindle cell hemangioma, angiosarcoma
Ollier's disease	Sporadic; multiple enchondromas
Multiple osteochondromas (osteochondromatosis)	AD; multiple osteochondromas, secondary chondrosarcoma, very rarely osteosarcoma
Mazabraud syndrome	Sporadic; polyostotic fibrous dysplasia, osteosarcoma, intramuscular myxoma
McCune-Albright syndrome	Sporadic; polyostotic fibrous dysplasia, osteosarcoma, endocrine disorders, skin pigmentation
Familial Paget's disease	AD; early onset Paget's, osteosarcoma
Retinoblastoma	AD; osteosarcoma, soft tissue sarcomas
Rothmund-Thomson syndrome	AR; poikiloderma, sparse hair, small stature, skeletal abnormalities, increased risk of cancer including osteosarcoma
Werner's syndrome	AR; premature aging, increased risk of various bone and soft tissue sarcomas

AD autosomal dominant, *AR* autosomal recessive

1.8 Congenital, Hereditary, and Non-hereditary Syndromes Associated with Bone Tumors

There are a large number of hereditary and non-hereditary conditions and syndromes associated with an increased risk of developing bone tumors. For many of these the genetic background has recently been clarified giving important knowledge of the pathogenetic mechanisms involved. Table 1.5 summarizes the most important of these conditions (Fletcher et al. 2002).

References

Bergh P, Kindblom LG, Gunterberg B, et al. (2000) Prognostic factors in chordoma of the sacrum and mobile spine: a study of 39 patients. Cancer 88:2122–2134

Berlin O, Angervall L, Kindblom LG, et al. (1987) Primary leiomyosarcoma of bone. A clinical, radiographic, pathologic-anatomic and prognostic study of 16 cases. Skeletal Radiol 16:364–376

Bertoni F, Capanna R, Calderoni P, et al. (1984) Primary central (medullary) fibrosarcoma of bone. Semin Diagn Pathol 1:185–198

Bovée JV, Cleton-Jansen AM, Wuyts W, et al. (1999) EXT-mutation analysis and loss of heterozygosity in sporadic and hereditary osteochondromas and secondary chondrosarcomas. Am J Hum Genet 65:689–698

Dahl I, Akerman M, Angervall L (1986) Ewing's sarcoma of bone. A correlative cytological and histological study of 14 cases. Acta Pathol Microbiol Immunol Scand (A) 94:363–369

Dahlin DC, Unni KK, Matsuno T (1977) Malignant (fibrous) histiocytoma of bone: fact or fancy? Cancer 39:1508–1516

Dorfman HD, Czerniak B (1995) Bone cancers. Cancer 75:203–210

Dorfman HD, Czerniak B (1998) Bone tumors. Mosby, St Louis

Dorfman HD, Weiss SW (1984) Borderline osteoblastic tumors: problems in the differential diagnosis of aggressive osteoblastoma and low grade osteosarcoma. Semin Diagn Pathol 1:215–234

Dorfman HD, Steiner GC, Jaffe HL (1971) Vascular tumors of bone. Hum Pathol 2:349–376

Eefting D, et al. (2008) Assessment of interobserver variability and histological parameters to improve reliability in classification and grading of central cartilaginous tumors. Am J Surg Pathol (in press)

Fletcher CDM, Unni KK, Mertens F (eds) (2002) Pathology and genetics of tumours of soft tissue and bone. WHO classification of tumours. IARC Press, Lyon

Mangham DC, Williams A, McMullan DJ, et al. (2006) Ewing's sarcoma of bone: detection of specific transcripts in a large consecutive series of formalin-fixed decalcified paraffin-embedded tissue samples using the reverse transcriptase-polymerase chain reaction. Histopathology 48:363–376

Meis JM (1991) "Dedifferentiation" in bone and soft-tissue tumors. A histological indicator of tumor progression Pathol Annu 26:37–62

Meis JM, Dorfman HD, Nathanson SD, et al. (1989) Primary malignant giant cell tumor of bone: "dedifferentiated" giant cell tumor. Mod Pathol 2:541–546

Milgram JW (1988) Intraosseous lipomas. A clinicopathologic study of 66 cases. Clin Orthop 231:277–302

O'Connell JX, Kattapuram SV, Mankin HJ, et al. (1993) Epithelioid hemangioma of bone. A tumor often mistaken for low-grade angiosarcoma or malignant hemangioendothelioma. Am J Surg Pathol 17:610–617

Oliveira AM, His BL, Weremowicz S, et al. (2004) USP6 (Tre2) fusion oncogenes in aneurysmal bone cyst. Cancer Res 64:1920–1923

Rosenberg AE, Brown GA, Bhan AK, et al. (1994) Chondroid chordoma: a variant of chordoma. A morphologic and immunohistochemical study. Am J Clin Pathol 101:36–41

Tirabosco R, Mangham DC, Rosenberg AE, et al. (2008) Brachyury in extra-axial skeletal and soft tissue chordomas: a marker that distinguishes chordoma from mixed tumor/myoepithelioma/parachordoma in soft tissue. Am J Surg Pathol 32:572–580

Tsuneyoshi M, Dorfman HD, Bauer TW (1986) Epithelioid hemangioendothelioma of bone. A clinico-pathologic, ultrastructural and immunohistochemical study. Am J Surg Pathol 10:754–764

Unni KK, et al. (2005) Tumors of the bones and joints. AFIP atlas of tumor pathology, series 4. American Registry of Pathology, Washington DC

Vujovic S, Henderson S, Presneau N, et al. (2006) Brachyury, a crucial regulator of notochordal development, is a novel biomarker for chordomas. J Pathol 209:157–165

Walaas L, Kindblom LG (1990) Light and electron microscopic examination of fine-needle aspirates in the preoperative diagnosis of osteogenic tumors: a study of 21 osteosarcomas and two osteoblastomas. Diagn Cytopathol 6:27–38

Walaas L, Kindblom LG (1991) Fine-needle aspiration biopsy in the preoperative diagnosis of chordoma: a study of 17 cases with application of electron microscopy, histochemical and immunocytochemical examination. Hum Pathol 22:22–28

Walaas L, Kindblom LG, Gunterberg B, et al. (1990) Light and electron microscopic examination of fine-needle aspirates in the preoperative diagnosis of cartilaginous tumors. Diagn Cytopathol 6:396–408

Willen H (1997) Fine needle aspiration in the diagnosis of bone tumors. Acta Orthop Scand Suppl 273:47–53

Computed Tomography of Bone Tumours

2

Richard W. Whitehouse

CONTENTS

KEY POINTS

- Computed tomography (CT) is a high-radiation-dose examination, which should therefore be both justified and tailored to the clinical need.
- CT of solitary bone lesions may provide information on tumour mineralization difficult to identify on plain film or MR.
- Non-contrast-enhanced CT of the thorax is appropriate for staging of metastatic bone sarcoma.
- Whole-body CT in older patients should be considered where the "index" bone lesion may be a metastasis.
- CT with CT fluoroscopy is ideal for guiding bone biopsy and interventional procedures. Steps to minimize radiation dose are important for both the patient and operator.
- Ingenuity in patient positioning can produce high-quality scans of limb lesions (by removing unnecessary parts of the patient from the scan plane).

2.1 Introduction

Although magnetic resonance (MR) imaging has become the primary imaging modality for local staging of bone tumours, computed tomography (CT) has complementary roles in the diagnosis and local staging of bone tumours, as well as operation planning, custom prosthesis production, biopsy and percutaneous treatment guidance. Scanning the chest for detection of pulmonary metastases is also a primary role for CT. Computed tomography remains essential for the assessment of patients in whom MR is contraindicated (e. g.

R. W. Whitehouse, MD
Department of Clinical Radiology, Manchester Royal Infirmary, Oxford Road, Manchester, M13 9WL, UK

due to intracranial aneurysm clips or cardiac pacemakers). By comparison with histological measurement of metastatic tumour size in resected spinal lesions, CT underestimates size, whereas MR overestimates it (Fujita et al. 2000), an observation probably also true for other tumours and in other locations.

2.2 Developments in Computed Tomography

A CT image is a map of normalized X-ray attenuation coefficients, generated by computer, from filtered back projection of X-ray transmission measurements in multiple directions through the object in question. Each pixel in the image represents the averaged attenuation of the material that occupies the corresponding voxel in the subject. Recent developments in CT include helical scanning, multislice acquisition, single rotation volume scanning, simultaneous dual-energy scanning and real-time CT "fluoroscopy" (Dawson and Lees 2001). The number of slices acquired in a single rotation of the gantry continues to increase with newer scanners able to perform a scan with over 300 sub-millimetre slices using a single gantry rotation in under 1 s.

2.2.1 CT Technology

The CT gantry carries the X-ray tube(s), X-ray detectors and associated electronics. Developments in power transfer to the X-ray tubes and data transfer from the detectors over the past three decades have increased scan data acquisition speeds from approximately one slice every 5 s in the early 1980s to several hundred slices in under a second in 2008. The speed of digital processing of the data to produce images has also improved exponentially, giving almost instant image display. The continuous supply of detector output data allows both helical scanning and CT fluoroscopy.

Shorter slice acquisition times result in a requirement for X-ray tubes to have both a higher heat capacity and a higher maximum tube current, as the mAs required for a single slice remains much the same but the time in which the slice is acquired is reduced. In addition, for helical scanning continuous X-ray output for up to 60 s may be required. High mA scans, with extended anatomical coverage, can be obtained with ease from multislice helical scanners, with consequent high radiation doses to patients.

Helical scanning is performed by moving the table continuously during the gantry rotation and X-ray exposure, from the first slice location to the last; thus, a helix of X-ray transmission data through the scan volume is acquired. To generate a CT image the data from adjacent turns of the helix are interpolated to produce transmission data which are effectively from a single slice location (Kalender et al. 1990). This process can be performed at any location within the helix (except the first and last 180° – where there is no adjacent helix of data for interpolation). In this way overlapping slices can be produced without overlapping irradiation to the patient. The relationship between the X-ray fan-beam collimation and the table movement per rotation of the gantry is called the pitch ratio. Extended or stretched pitch scans are performed with pitch ratios greater than 1. Such extended pitches can be used to trade off between greater scan volumes, shorter scan acquisition times and lower scan radiation doses. Stretching the pitch ratio to 1.25 has little effect on the image appearances, but pitch ratios greater than 1.5 produce images with effective slice thickness, significantly greater than the nominal fan-beam collimation thickness. Multislice scanners in particular may use pitch ratios of less than 1. This increases patient radiation dose and scan acquisition time but reduces image noise and some spiral scanner artefacts. By increasing the number of detector arrays ("multislice scanner") several interlaced helices can be acquired simultaneously with the table increment per gantry rotation increased proportionately (McCollough and Zink 1999). Initial developments in multislice scanners were aimed at reducing individual slice thicknesses, but once z-axis resolution is equivalent to in-plane resolution, further reduction in slice thickness is of limited value. Adding further rows of detectors will then increase the total width of the detector bank. While offering the potential for faster scan acquisition, the increasing divergence of the X-ray beam to the outer rows of detectors creates a "cone-beam" geometry for the X-ray-beam paths, requiring complex data corrections to reduce artefacts in the resultant images. Currently, scanners offering up to 320 detector rows with up to 16 cm total detector width are available. Flat-panel detectors, based on the Direct Digital Radiography technology, for CT data acquisition are under development. These detectors will allow higher resolution, increased total detector width and variable effective slice thickness (Obenauer et al. 2007). The result of these developments will be a scanner that can acquire the full examination data from a single gantry rotation without table movement. Although this offers significant reduction in acquisition time and total X-ray tube loading, radiation dose reduction techniques

that modulate the X-ray tube current according to slice location will no longer be applicable.

Currently available individual detector widths of between 0.5 and 0.75 mm can achieve y-axis resolution equivalent to in-plane resolution, giving true isometric voxels and consequent equivalent quality reformats in any plane. Even with the thinnest detector widths, the best y-axis resolution is achieved from overlapping sections reconstructed at the thinnest available slice width and reconstructed at half-slice-width spacing (or less).

The combination of multislice and helical scanning results in volume scan acquisition times which are many times faster than a single-slice helical scanner with the same gantry rotation speed, and one or even two orders of magnitude faster than a non-spiral scanner. Multislice scanning reduces X-ray tube loading requirements as the scanner acquires several slices simultaneously with the same tube loading as a single slice would require. The patient radiation dose, however, is not directly reduced and may be increased if greater volumes are scanned.

2.2.2 Dual-Energy Scanning

Although dual-energy CT scanning has been performed by repeating scans after changing the tube voltage, the time delay between these two acquisitions results in misregistration of data from the two acquisitions due to patient movement. A helical scanner with two X-ray tubes set at different kVp levels in the same gantry allows almost simultaneous acquisition of dual-energy X-ray attenuation data. From these data separate CT images of soft tissue (bone) mineral and contrast media can be generated. The use of this scanner in assessment of bone tumours has not been evaluated; it may offer higher sensitivity and specificity to the presence of mineralization in tumours and may also increase sensitivity to contrast enhancement.

2.2.3 Single Gantry Rotation Volume Scanning

With increasing detector row numbers and coverage, true volume scanning becomes possible without requiring the table movement that is used to give a helical acquisition. A single, sub-second gantry rotation then produces hundreds of sub-millimetre-thick sections simultaneously, with a coverage of over 15 cm. The value of such scanners in the assessment of bone tumours has not yet been evaluated. Apart from increased throughput and reduced movement artefact, the potential to perform tumour perfusion studies warrants consideration.

2.2.4 CT "Fluoroscopy"

Continuous CT gantry rotation and data acquisition without table movement provides continuously updated X-ray transmission data from which revised images can be generated. With extremely rapid processors and appropriate reconstruction algorithms, further delay for image reconstruction can be minimized and a continuously updated CT image displayed in "near real time" (Hsieh 1997). Such "CT fluoroscopy" imaging can be used for CT-guided interventional procedures (De Mey et al. 2000). As with all fluoroscopic procedures care should be taken to reduce fluoroscopy time to the minimum necessary and to avoid operator irradiation – instruments designed to keep the operators hands out of the CT section (Daly et al. 1998) and use of the lowest selectable tube current are advocated (50 mA is claimed to be sufficient; Froelich et al. 1999). The present author routinely uses 10-mA tube current for CT fluoroscopy of limbs. To assist in maintaining short CT fluoroscopy exposure times, routine recording and auditing of fluoroscopy exposure times is advocated. An audible alarm after a preset exposure time may also assist in keeping exposures as short as possible. The use of a lead drape adjacent to the irradiated volume has been demonstrated to reduce operator exposure (Nawfel et al. 2000). High skin doses to patients and operators will occur if care is not taken.

2.2.5 Data Manipulation

The vast masses of imaging data acquired from a multislice spiral scanner produces problems of data storage and interpretation. With isometric voxels, reformatted images in any other image plane will have the same image quality as the acquisition images. Fast workstations, allowing rapid reformatting and display of examinations in the most appropriate plane for the pathology being demonstrated, are therefore necessary. Post-processing image reconstructions (curved planes, surface-rendered 3D images, minimum or maximum intensity projections, "transparent bone") can also be applied to assist in diagnosis or treatment (Figs. 2.1, 2.2).

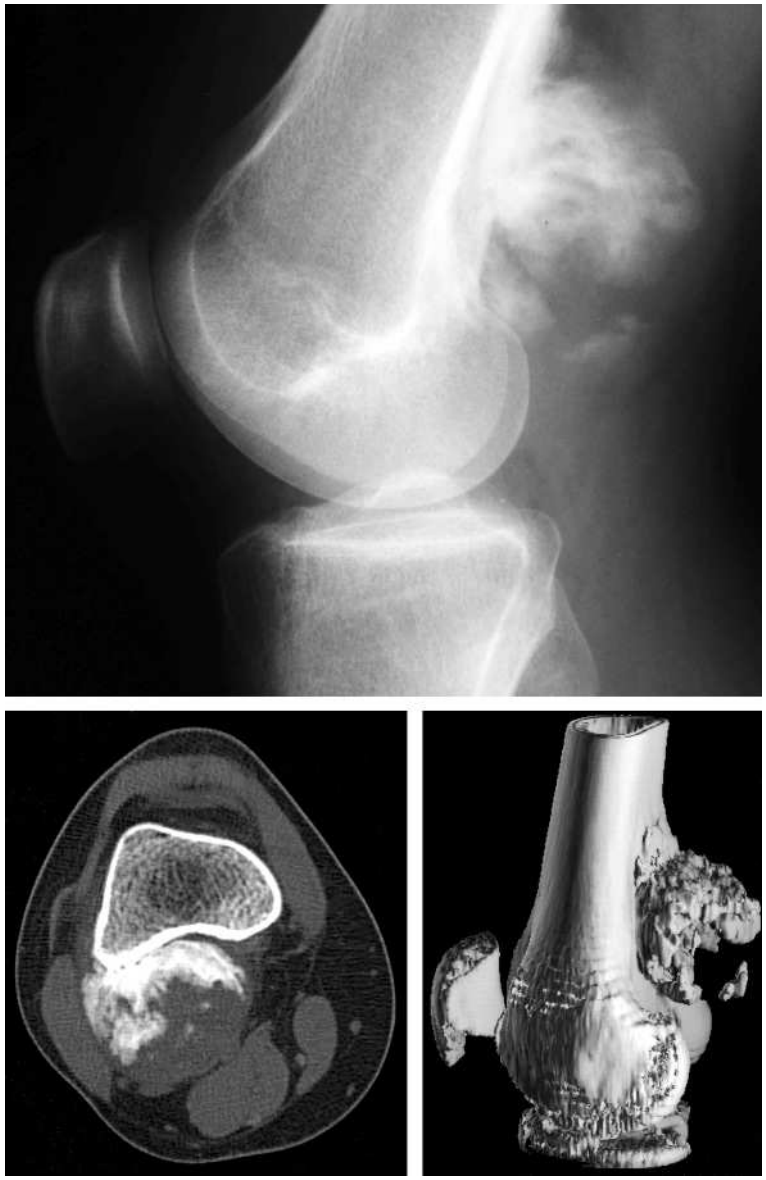

Fig. 2.1. Plain film (**a**), axial CT (**b**) and (**c**) surface reconstruction of a parosteal osteosarcoma of the distal femur. (Courtesy of A.M. Davies)

2.3 Scan Image Quality

The amount of noise, beam-hardening and streak artefacts in a CT image are dependent upon the following factors:

1. Collimation slice thickness
2. Partial or full rotation data set
3. Mass and distribution of tissue in the scan plane
4. Scan acquisition time/patient movement
5. High-density extraneous material (e.g. contrast medium spills, surgical metalwork)
6. KVp and mAs
7. Field of view
8. Matrix size
9. Reconstruction algorithm
10. Post-processing image sharpening or softening filters
11. Viewing window width and level settings

Most of these factors are amenable to selection or modification by the scanner operator and can markedly affect the quality of the final image. The relationships between image noise, mAs and patient size are non-linear, with a halving of patient size (cross-sectional area) resulting in

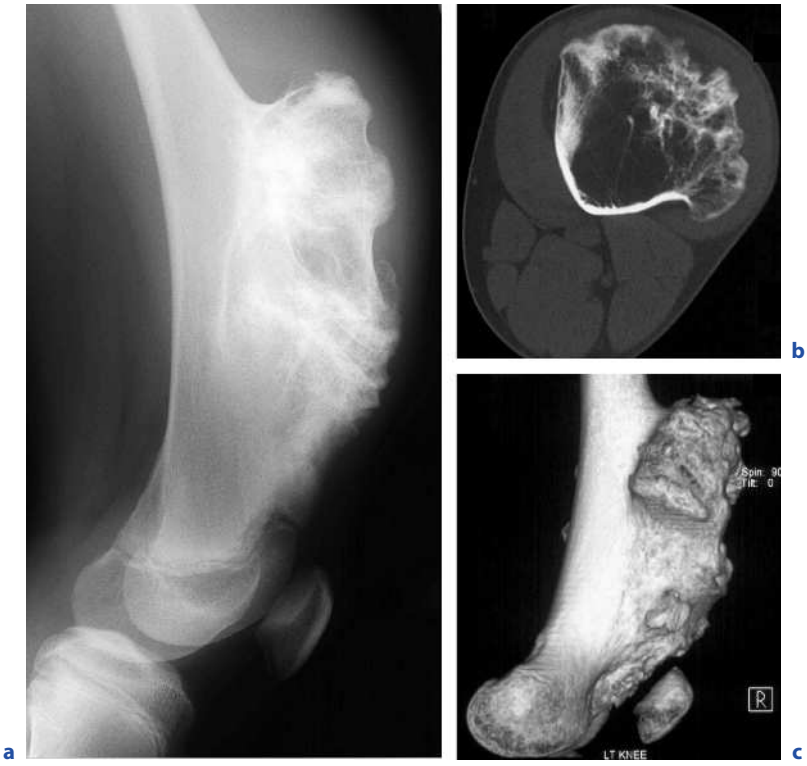

Fig. 2.2a–c. Plain film (**a**), axial CT (**b**) and (**c**) surface reconstruction of an osteochondroma of the distal femur. (Courtesy of A.M. Davies)

a quartering of image noise, whereas a fourfold increase in mAs is needed to halve the image noise. For small patients, image noise is effectively low at all mAs settings and the absolute reduction in image noise achieved by quadrupling the mAs is small.

In addition, when imaging osseous lesions, the width of the usual viewing window for bone renders noise less perceptible. As children are more radiation sensitive than adults as well as smaller, particular attention should be paid to reducing the mAs in this group of patients. Reducing the kVp also reduces patient radiation dose while also increasing the CT number difference between mineral and soft tissue. For small patients (paediatric patients in particular) this should also be considered.

Streak artefacts can be generated by high-density material within the scan plane but outside the field of view of the scanner. Tabletops, which contain edge grooves, tracks for the fixing of attachments or detachable mattresses can act as traps for spilt contrast media. Contrast droplets on the gantry window will also cause imaging artefacts. Scrupulous care to keep the tabletop and gantry clean is needed to remove these sources of artefact. Lightweight casts and plaster of paris casts do not significantly impair CT scan images of the contained limb, unless metallic components have been incorporated.

2.3.1 Internal Metalwork from Fixation Devices

The streak artefact generated from in-situ intramedullary rods is rarely excessive and does not prevent adequate assessment of the bone cortex, making CT valuable in assessing cortical bone near prostheses in selected cases. More intrusive streak artefact is seen when the CT image plane is through locking screws in intramedullary rods, bone surface plates, hip-joint replacements or fixation screws. Care in patient positioning (including decubitus positions where necessary) combined with gantry angulation in order to align the scan plane with the long axis of any screws present will reduce the number of sections degraded by streak artefact from the screws to a minimum.

In scanners with operator-selectable kVp, the use of the highest kVp setting and the use of higher mAs settings are claimed to reduce streak artefact from metalwork, although this has not been confirmed in some studies (Haramati et al. 1994; Lee et al. 2007; Link et al. 2000). The combination of increased kVp and mAs results in considerably greater tube loading and patient irradiation; consequently, the value of significantly increasing these parameters in the presence of metalwork should be considered with care. Streak artefact may appear visually less intrusive on volume-rendered (3D) images (Pretorius and Fishman 1999). The streak artefact from titanium prostheses is less than that from cobalt–chrome (Haramati et al. 1994). The use of an extended CT number scale (with a maximum window width of 40,000) may also improve the demonstration of metalwork (Link et al. 2000).

2.3.2 CT Number, Hounsfield Units, Window Width and Levels

The scale of numbers used to define the grey scale in CT images is artificially limited by data-storage constraints. The CT number scale runs from –1,000 for air, through 0 for water. The top end of the scale is usually constrained to fit into a 12-bit binary number (allowing number values from –1024 to +3072 to be stored), although extended-scale imaging with a maximum window width approximately ten times greater than this may be of value for imaging in the presence of metalwork. The Hounsfield unit (HU) is the true value which the CT number should represent. Scanner drift, calibration error, artefact or other limitation may render this inaccurate, which is why measurements made from scan images are best called CT numbers.

The Hounsfield unit value for any material is defined by Eq. 2.1:

$$HU_s = 1{,}000\ (m_s\text{-}m_w/m_w), \qquad 2.1$$

where HUs = the Hounsfield unit value for substance s, m_s = linear attenuation coefficient for substance s and m_w = linear attenuation coefficient for water.

This formula relates the HU value to the linear attenuation coefficients of the material being measured and water. As the linear attenuation coefficients of all materials change with X-ray-beam energy, there are consequently only two fixed points on the Hounsfield scale. These points are –1,000, which is the HU value for no X-ray attenuation (i.e. a vacuum), and zero, which corresponds to the HU value for water (at the calibration pressure and temperature for the scanner). The HU scale is open ended, with high-atomic-number, high-density materials having values much in excess of the upper end of the usual scale (even on "extended-scale" scanners).

The theoretical Hounsfield value for dense cortical bone calculated at an effective beam energy of 65 keV (equivalent to a scanner operating at around 120 kVp) is in the region of 1,600 (Fig. 2.3). At lower energies (e.g. 55 KeV – the approximate effective energy of a scanner operating at 80 kVp), the HU value for dense cortical bone is over 2,000. Other high-atomic-number materials (contrast media, aluminium and metal fixation devices) also show marked variation in HU value with beam energy. By contrast, the HU values of soft tissues, collagen and fat vary very little with effective beam energy as the linear attenuation coefficients because these materials closely follow those of water. Consequently, in scanners which allow the operating voltage to be changed, the CT number for bone can be increased by using a low kVp (around 80 kVp). This increases the dependence of the CT number on the presence of bone or calcification.

For lower-atomic-number materials, such as are present in soft tissues, the X-ray attenuation and consequent CT number is predominantly influenced by the electron density of the material, which is, in turn, closely related to the physical density of the material. Even the CT number of water is influenced by differences in temperature and differences in density exist between water at room and body temperature (Whitehouse et al. 1993). The presence of protein or high concentrations of salts will increase the CT number of body fluids. Measurement of the CT number of a region of interest in an image must therefore be considered only a guide to its composition.

The visual impression of the density of a region of interest is influenced by the window and level settings of the image, the calibration of the display and the densities in the surrounding part of the image. Particularly within bone, the surrounding high density of bone can give a lytic lesion the visual impression of a lower density than actually exists. Consequently, measurement rather than estimation of any region of interest is essential.

The window width and level are calibrated contrast and brightness settings for image display. The most appropriate window level for cortical bone will be influenced by the bone density and the effective scan energy, whereas the window width may need to be quite narrow to demonstrate subtle intracortical density changes.

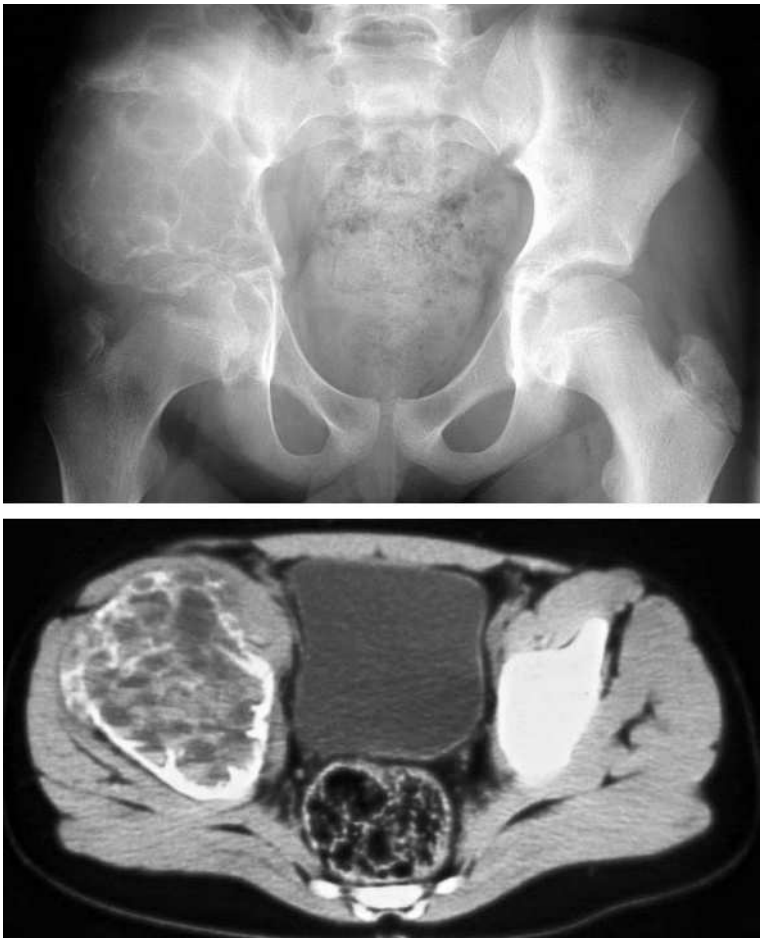

Fig. 2.3a,b. Aneurysmal bone cyst of the pelvis demonstrates fluid/fluid levels on CT. (Courtesy of A.M. Davies)

2.3.3 Radiation Dose Reduction

As regulatory authorities require medical exposure to ionizing radiation to be both justified and minimized if performed, the relatively high radiation burden that CT delivers requires particular consideration. The increased ease with which CT scans can be obtained due to the speed and availability of multislice scanners is also generating debate about safety and dose-reduction strategies (Kalra et al. 2004). For scans that are justified, use of the scout view to accurately identify the required limits of the scan should be mandatory, with rapid review of the top and bottom section to confirm adequate coverage. The mAs setting should be chosen to suit the size of the patient (Jangland et al. 2004), with particular care to select the lowest acceptable setting for children (Frush et al. 2003) and also the required image noise – images for high-contrast structures, such as bone or CT-guided biopsy needles, are adequate at a much lower mAs than images for soft tissue lesions. Modern scanners offer tube-current modulation, which varies the mAs during a scan, with the most sophisticated systems altering the mAs continuously to suit the attenuation of the patient in each projection. In the chest and pelvis the markedly higher attenuation in the lateral projection compared with the anteroposterior projection results in a sinusoidal variation in mAs during scanning which can reduce the effective radiation dose by around 30% while not affecting, or even improving, image noise and streak artefacts (Kalender et al. 1999). Where available such dose modulation should be the default scanner setting. Specific female gonad shielding is not possible on CT, but encasement of the testicles by a "testis capsule" has been shown to reduce testicular radiation dose by 95% for abdominal CT scans (Hidajat et al. 1996). The CT fluoroscopy systems may offer the option of turning off the tube current over an arc where the tube is above the patient. Although this is primarily intended to reduce operator exposure during interventional procedures, it will also reduce male patient testicular dose in pelvic scans.

2.4 CT of Bone Tumours

Particularly in regions of complex anatomy, such as the head and face (Cavalcanti et al. 2000) spine, pelvis or hind foot, CT demonstrates small regions of osteolysis not seen on conventional radiography. Cortical destruction, tumour matrix mineralization and soft tissue extension of tumour is also demonstrated (Fig. 2.4; Priolo and Cerase 1998), although CT underestimates bone marrow invasion compared with MR (Gerber et al. 2008). Lesions arising in the thorax will commonly be demonstrated on CT as part of the thoracic staging (Fig. 2.5).

Computed tomography is particularly useful in assessing tumours with cartilaginous content (Masciocchi et al. 1998). The presence of fat or fluid/fluid levels within a lesion (Fig. 2.3) can also be demonstrated on CT. Other indications include CT-guided biopsy (Dupuy et al. 1998) or ablation procedures.

2.4.1 Anatomy

Detailed knowledge of the anatomy and its appearances in all imaging planes is a prerequisite for adequate scan interpretation. Knowledge of anatomical structures not easily or consistently demonstrated on CT is still needed to assess the likelihood of their involvement by any pathology that is demonstrated. The anatomy of the region is best reviewed in appropriate detailed texts.

2.4.2 Patient Positioning

As described above, volume acquisitions obtained in any plane can be reformatted into other planes without marked loss of image quality. For scanners not capable of such fine collimation, CT scanning in the most appropriate plane for the expected pathology is still preferable. For scanning of a limb, positioning of the patient such that the single affected limb region is the only body part in the scanner aperture will result in scans with higher signal-to-noise at lower mA and lower patient radiation exposure. Gantry angulation may facilitate this aim, but not all scanners can perform multislice acquisitions with an angled gantry.

2.5 Indications

Intraosseous tumours are well demonstrated, for example, the nidus of an osteoid osteoma, which can be overlooked on MR imaging, is characteristic and clearly demonstrated on CT. In addition, osteoid osteomas may be mistaken for more aggressive lesions on MR (Hosalkar et al. 2005).

The presence of tumour matrix ossification or calcification is also clear on CT (Fig. 2.6).

Benign spinal tumours may be better characterized by CT than MR (Shaikh et al. 1999). Soft tissue pathology is less well demonstrated than with MR and intravenous contrast medium injection provides less satisfactory contrast enhancement than the equivalent

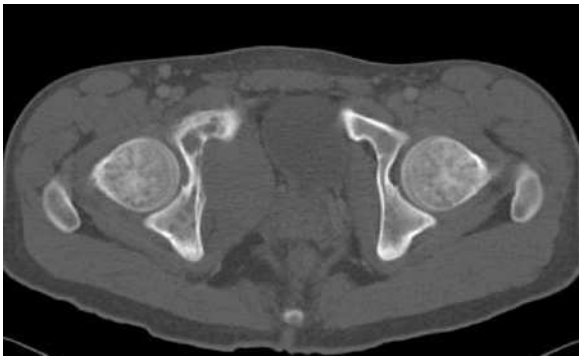

Fig. 2.4. Axial CT through the pelvis demonstrates bone destruction with periosteal reaction and a surrounding soft tissue mass in a patient with Ewing's sarcoma

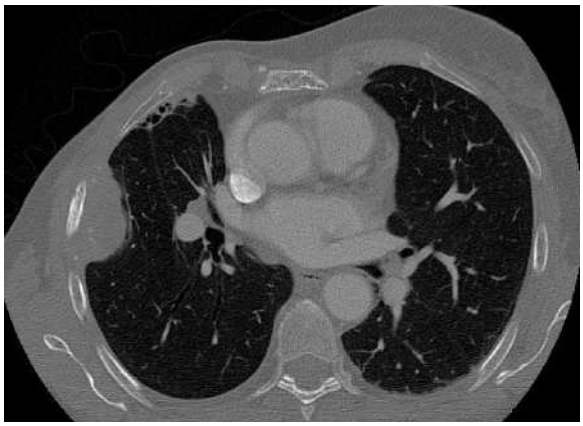

Fig. 2.5. CT of an osteosarcoma arising from a rib 20 years after mastectomy and radiotherapy for carcinoma of the breast. Tumour matrix mineralization is demonstrated

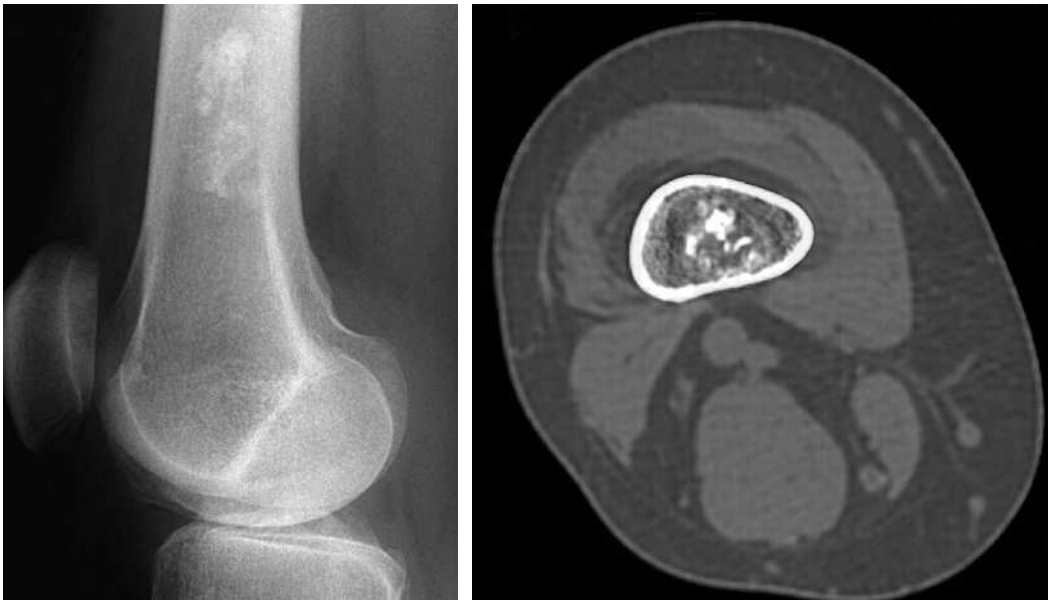

Fig. 2.6a,b. Enchondroma on plain film (**a**) and CT (**b**). The CT demonstrates the distribution of calcification within the lesion and also confirms its intramedullary location, with no endosteal scalloping. (Courtesy of A.M. Davies)

MR examination, but valuable information on soft tissue lesions is still obtainable from CT (e.g. size, extent, tumour calcification, enhancement, articular involvement). Computed tomography can be used to guide biopsy and aspiration procedures.

The accurate three-dimensional localization of the bone anatomy with CT can be used to calculate the mechanical axes of long bones and the relationships of the joints. This can then be used in the pre-operative planning of prostheses. The CT scanogram, usually used to identify the start and finish points for a CT investigation, can also be used for limb-length measurements.

The limitations of CT are usually described in relationship to MR, and consequently the poorer soft tissue contrast of CT is top of the list. Where MR is available and not itself contraindicated, it is the most appropriate modality for imaging soft tissue lesions. The other limitations of CT in relation to MR are the direct multiplanar capability of MR and the use of ionizing radiation with CT.

2.5.1 Thoracic Staging

In primary malignant tumours of bone, metastatic spread is most commonly to the lungs. Routine staging therefore includes chest radiograph. If this is normal, a CT scan of the thorax is indicated for the detection of sub-centimetre pulmonary nodules, as these are often not identified on chest radiography. As peripheral pulmonary metastasis is the usual earliest site of spread for bone sarcoma, non-contrast-enhanced CT of the thorax is usually sufficient for staging. If metastatic lung disease is identified on chest radiography, a CT scan may still be indicated if surgical resection of the pulmonary metastases is being contemplated. The significance of small pulmonary nodules can be uncertain. For example, in regions where histoplasmosis or TB is endemic, then pulmonary granulomata may account for nodules seen on CT. Repeated scanning to assess change in size or number of pulmonary nodules may then be of value. Pulmonary metastases are usually seen as rounded soft tissue density lesions in the lungs (Fig. 2.7); consequently, they can be demonstrated on scans performed at low mA. Because of the marked variation in tissue distribution and density in the thorax (shoulder girdle, breasts and liver, for example), scan protocols that utilise mA modulation are particularly effective in optimizing image quality at lower radiation doses. Computer-aided detection of pulmonary nodules on CT scans is possible. Pulmonary nodules lying immediately inferior to the hilum are otherwise particularly prone to be overlooked. The routine use of reformatted images in the sagittal and coronal planes is advocated to reduce the risk of overlooking pulmonary nodules. The significance of pulmonary nodules in patients with sarcoma requires consideration. In one study of 51 patients with

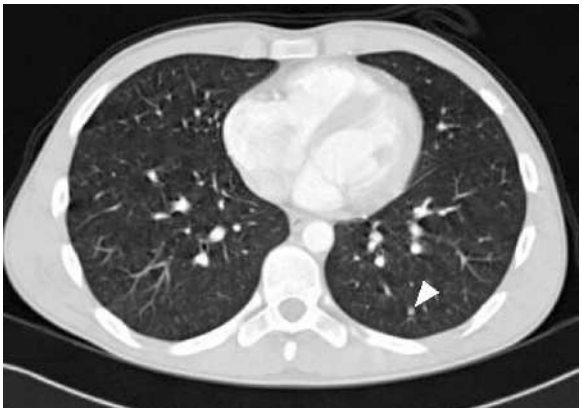

Fig. 2.7. Thoracic CT demonstrates a small pulmonary nodule (*arrowhead*) in a patient with Ewing's sarcoma of the pelvis

osteosarcoma and lung nodules, of 13 patients with one nodule, only 4 were metastatic, whereas all patients with more than 7 nodules had pulmonary metastases, although a quarter of all nodules removed from patients with metastases were benign (Picci et al. 2001). On serial CT scanning, increase in number of nodules was the only feature significantly associated with confirmed metastases.

2.5.2 Whole-Body CT Scanning

An apparently solitary malignant bone lesion may be primary or secondary, with the latter becoming more probable in older patients. As biopsy of a primary malignant bone tumour is best performed at a specialist centre, further investigation of an indeterminate lesion in non-specialist centres can become problematic. It has recently been shown that whole-body multislice CT could replace skeletal scintigraphy for detection of bone lesions (Groves et al. 2006). In a patient with an apparently solitary bone tumour, this examination could confirm or refute the presence of multiple skeletal lesions and may also demonstrate a previously occult primary tumour. This approach could replace skeletal scintigraphy, chest radiography and other investigations aimed at identifying an occult malignancy in appropriate patients (Destombe et al. 2007). Oral and intravenous contrast-enhanced CT of the thorax, abdomen and pelvis should therefore be considered in the assessment of older patients presenting with an apparently solitary malignant-appearing bone lesion.

2.6 CT-Guided Interventions

Computed tomography is being increasingly used to guide interventional procedures, recently encouraged by the development of CT fluoroscopy which enables more rapid and accurate placement of needles and interventional devices (De mey et al. 2000). As described above (see Sect. 2.2.5) care needs to be taken to minimize operator and patient X-ray exposure during CT-guided biopsy. The CT fluoroscopy times of around 10 s should suffice for most biopsy procedures (Goldberg et al. 2000). Limiting the fluoroscopy to identification of the needle tip rather than the entire needle will also reduce operator and patient radiation dose (Silverman et al. 1999). The use of needle holders may also reduce the operator hand radiation exposure (Kato et al. 1996).

The CT section thickness should be appropriate to the size of the lesion; otherwise, partial-volume averaging may include both the needle tip and the lesion in the same section, erroneously suggesting an accurate needle location. Computed tomography can be used to guide biopsy of sclerotic and lytic bone lesions (Leffler and Chew 1999). Where primary malignancy is present the course of the biopsy track and the compartment(s) through which it passes may need excision with the tumour at the time of definitive surgery. Biopsy of such lesions must therefore only be performed after consultation and agreement of the approach with the surgeon who will carry out the definitive treatment. Accuracy of CT-guided biopsy is increased if specimens are obtained for both cytology and pathology, and overall accuracy of around 80% should be achieved (Hodge et al. 1999).

Percutaneous treatment of osteoid osteoma can also be performed with CT guidance. A preliminary diagnostic scan is usually performed (Fig. 2.8). For the procedure a planned approach avoiding vascular structures is required, and a preliminary contrast-enhanced scan to identify the relevant vessels can be performed if necessary. It is possible to treat osteoid osteomas by complete removal via CT-guided biopsy (Voto et al. 1990; Katz et al. 2000), although this may be difficult to achieve with biopsy needles unless a large-bore needle is used and several passes are made through the lesion. More recently techniques aimed at destroying the tumour with heat, either from a radiofrequency ablation probe or a laser-heated probe, both of which are available with fine probes for passage down a biopsy needle have been used. In either case, to avoid

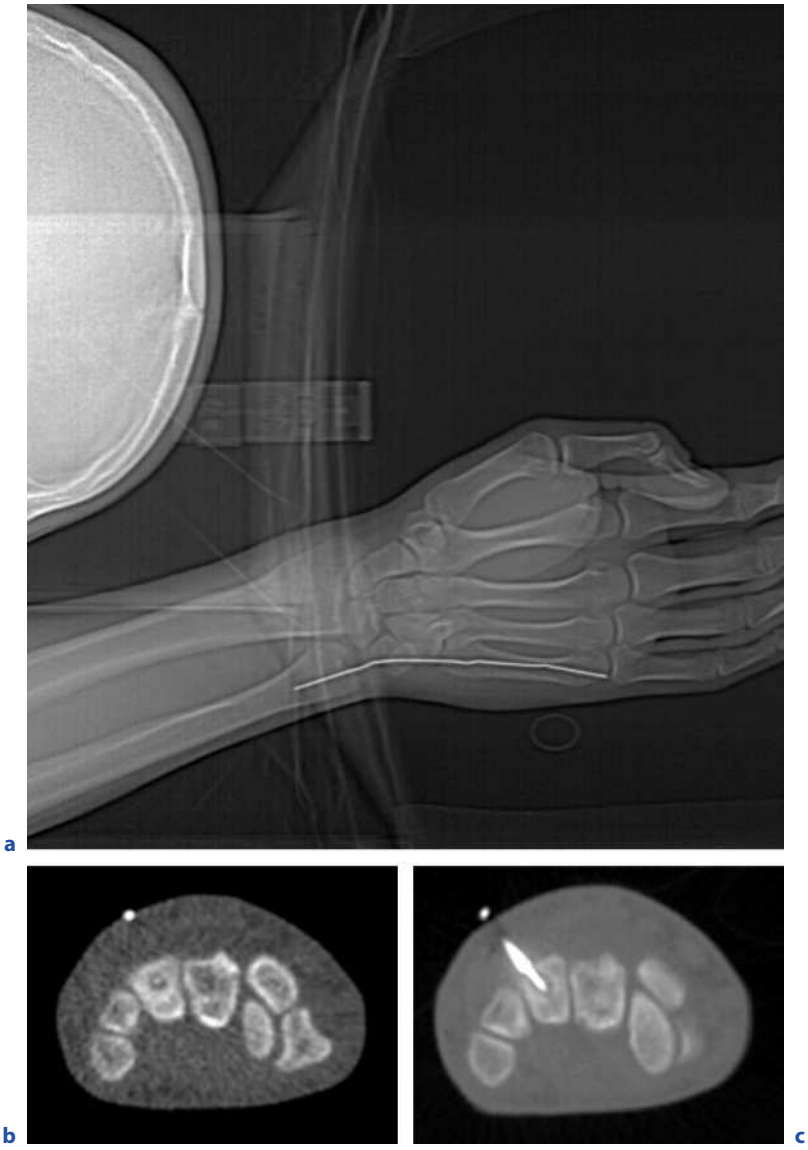

Fig. 2.8. **a** Scout view demonstrates the patient positioning used to allow CT through the wrist to guide percutaneous ablation of an osteoid osteoma of the hamate. A radio-opaque marker has been placed on the wrist along the long axis of the scanner table. This is a reference point for guiding the skin entry point. **b** Axial CT through the wrist. Due to the very small volume of tissue in the scan plane, reducing both the mA to 10 and the kVp to 80 was possible, minimizing radiation exposure while still adequately localizing the lesion. **c** Axial CT demonstrates the ablation probe lying centrally within the nidus. Despite the low kVp and mA, no significant artefact from the probe or cannula is evident

complications the lesion to be treated should be more than a centimetre from neurovascular or other critical structures. The use of radiofrequency ablation under CT guidance has been the subject of over 50 publications from around the world in the past few years, all reporting high success rates with minimal risk of complication. There is a risk of sparks from RF equipment; thus, alcohol-based skin preparations are therefore best avoided. As part of the procedure, a preliminary biopsy for histological confirmation of the diagnosis is necessary, as in one series 16% of lesions were not osteoid osteomas (Sans et al. 1999). Osteoid osteomas can cause severe pain when biopsied; thus, although some series report the use of local anaesthesia, epidural or general anaesthesia is recommended. Although the bulk of CT-guided interventional procedures are performed by radiologists in the Radiology Department, the development of mobile CT scanners has allowed the use of CT guidance for procedures performed in theatre, allowing the orthopaedic surgeon to make greater use of CT guidance for minimally invasive procedures. The CT guidance has also been described for guidance of intralesional alcohol injection in spinal haemangioma (Doppman et al. 2000).

2.7 Conclusion

With appropriate attention to technique, CT continues to play a role in the diagnosis, staging and management of many bone tumours. Scanning of the primary tumour is most appropriate where MR is contraindicated, or where plain films do not adequately demonstrate the tumour mineralization, such as in the spine, pelvis or ribs. Thoracic staging remains the province of CT. Whole-body assessment may be of value where the bone lesion is suspected to be a metastasis.

References

Cavalcanti MG, Ruprecht A, Bonomie JM, Vannier MW (2000) Accuracy and precision of spiral CT in the assessment of neoplastic lesions associated with the mandible. Acad Radiol 7:94–99

Daly B, Templeton PA, Krebs TL, Carroll K, Wong You Cheong JJ (1998) Evaluation of biopsy needles and prototypic needle guide devices for percutaneous biopsy with CT fluoroscopic guidance in simulated organ tissue. Radiology 209:850–855

Dawson P, Lees WR (2001) Multi-slice technology in computed tomography. Clin Rad 56:302–309

De Mey J, Op de Beeck B, Meysman M, Noppen M, De Maeseneer M, Vanhoey M, Vincken W, Osteaux M (2000) Real time CT-fluoroscopy: diagnostic and therapeutic applications. Eur J Radiol 34:32–40

Destombe C, Botton E, Le Gal G, Roudaut A, Jousse-Joulin S, Devauchelle-Pensec V, Saraux A (2007) Investigations for bone metastasis from an unknown primary. Joint Bone Spine 74:85–89

Doppman JL, Oldfield EH, Heiss JD (2000) Symptomatic vertebral hemangiomas: treatment by means of direct intralesional injection of ethanol. Radiology 214:341–348

Dupuy DE, Rosenberg AE, Punyaratabandhu T, Tan MH, Mankin HJ (1998) Accuracy of CT-guided needle biopsy of musculoskeletal neoplasms. Am J Roentgenol 171:759–762

Froelich JJ, Ishaque N, Saar B, Regn J, Walthers EM, Mauermann F, Klose KJ (1999) Control of percutaneous biopsy with CT fluoroscopy. Rofo Fortschr Geb Rontgenstr Neuen Bildgeb Verfahr 170:191–197 [in German]

Frush DP, Donnelly LF, Rosen NS (2003) Computed tomography and radiation risks: what pediatric health care providers should know. Pediatrics 112:951–957

Fujita T, Ueda Y, Kawahara N, Tomita K (2000) Preoperative estimation of metastatic vertebral tumors. Int Orthop 24:71–74

Gerber S, Ollivier L, Leclère J, Vanel D, Missenard G, Brisse H, de Pinieux G, Neuenschwander S (2008) Imaging of sacral tumours. Skeletal Radiol 37:277–289

Goldberg SN, Keogan MT, Raptopoulos V (2000) Percutaneous CT-guided biopsy: improved confirmation of sampling site and needle positioning using a multistep technique at CT fluoroscopy. J Comput Assist Tomogr 24: 264–266

Groves AM, Beadsmoore CJ, Cheow HK, Balan KK, Courtney HM, Kaptoge S, Win T, Harish S, Bearcroft PW, Dixon AK (2006) Can 16-detector multislice CT exclude skeletal lesions during tumour staging? Implications for the cancer patient. Eur Radiol 16:1066–1073

Haramati N, Staron RB, Mazel-Sperling K, Freeman K, Nickoloff EL, Barax C, Feldman F (1994) CT scans through metal: scanning technique versus hardware composition. Comput Med Imaging Graph 18:429–434

Hidajat N, Schröder RJ, Vogl T, Schedel H, Felix R (1996) The efficacy of lead shielding in patient dosage reduction in computed tomography. Rofo Fortschr Geb Rontgenstr Neuen Bildgeb Verfahr:165:462–465 [in German]

Hodge JC (1999) Percutaneous biopsy of the musculoskeletal system: a review of 77 cases. Can Assoc Radiol J 50:121–125

Hosalkar HS, Garg S, Moroz L, Pollack A, Dormans JP (2005) The diagnostic accuracy of MRI versus CT imaging for osteoid osteoma in children. Clin Orthop Relat Res 433:171–177

Hsieh J (1997) Analysis of the temporal response of computed tomography fluoroscopy. Med Phys 24:665–675

Jangland L, Sanner E, Persliden J (2004) Dose reduction in computed tomography by individualized scan protocols. Acta Radiol 45:301–307

Kalender WA, Seissler W, Klotz E, Vock P (1990) Spiral volumetric CT with single-breathhold technique, continuous transport and continuous scanner rotation. Radiology 176:181–183

Kalender WA, Wolf H, Suess C (1999) Dose reduction in CT by anatomically adapted tube current modulation. II. Phantom measurements. Med Phys 26:2248–2253

Kalra MK, Maher MM, Saini S (2004) Radiation exposure and projected risks with multidetector-row computed tomography scanning: clinical strategies and technologic developments for dose reduction. J Comput Assist Tomogr 28 (Suppl 1):S46–S49

Kato R, Katada K, Anno H, Suzuki S, Ida Y, Koga S (1996) Radiation dosimetry at CT fluoroscopy: physician's hand dose and development of needle holders. Radiology 201:576–578

Katz K, Kornreich L, David R, Horev G, Soudry M (2000) Osteoid osteoma: resection with CT guidance. Isr Med Assoc J 2:151–153

Lee IS, Kim HJ, Choi BK, Jeong YJ, Lee TH, Moon TY, Won Kang D (2007) A pragmatic protocol for reduction in the metal artifact and radiation dose in multislice computed tomography of the spine: cadaveric evaluation after cervical pedicle screw placement. J Comput Assist Tomogr 31:635–641

Leffler SG, Chew FS (1999) CT-guided percutaneous biopsy of sclerotic bone lesions: diagnostic yield and accuracy. Am J Roentgenol 172:1389–1392

Link TM, Berning W, Scherf S, Joosten U, Joist A, Engelke K, Daldrup-Link HE (2000) CT of metal implants: reduction of artifacts using an extended CT scale technique. J Comput Assist Tomogr 24:165–172

Masciocchi C, Sparvoli L, Barile A (1998) Diagnostic imaging of malignant cartilage tumors. Eur J Radiol 27 (Suppl 1):S86–S90

McCollough CH, Zink FE (1999) Performance evaluation of a multi-slice CT system. Med Phys 26:2223–2230

Nawfel RD, Judy PF, Silverman SG, Hooton S, Tuncali K, Adams DF (2000) Patient and personnel exposure during CT fluoroscopy-guided interventional procedures Radiology 216:180–184 (and comments: 9–10)

Obenauer S, Dullin C, Alves F, Missbach-Guentner J, Grabbe E, Heuser M (2007) Flat-panel-detector-based volumetric CT: performance evaluation of imaging for skeletal structures of small animals in comparison to multislice CT. Clin Imaging 31:18–22

Picci P, Vanel D, Briccoli A, Talle K, Haakenaasen U, Malaguti C et al. (2001) Computed tomography of pulmonary metastases from osteosarcoma: the less poor technique. A study of 51 patients with histological correlation. Ann Oncol 12:1601–1604

Priolo F, Cerase A (1998) The current role of radiography in the assessment of skeletal tumors and tumor-like lesions. Eur J Radiol 27 (Suppl 1):S77–S85

Pretorius ES, Fishman EK (1999) Volume-rendered three-dimensional spiral CT: musculoskeletal applications. Radiographics 19:1143–1160

Sans N, Morera-Maupome H, Galy-Fourcade D, Jarlaud T, Chiavassa H, Bonnevialle P, Giron J, Railhac JJ (1999) Percutaneous resection under computed tomography guidance of osteoid osteoma. Mid-term follow-up of 38 cases. J Radiol 80:457–465 [in French]

Shaikh MI, Saifuddin A, Pringle J, Natali C, Sherazi Z (1999) Spinal osteoblastoma: CT and MR imaging with pathological correlation. Skeletal Radiol 28:33–40

Silverman SG, Tuncali K, Adams DF, Nawfel RD, Zou KH, Judy PF (1999) CT fluoroscopy-guided abdominal interventions: techniques, results, and radiation exposure. Radiology 212:673–681

Voto SJ, Cook AJ, Weiner DS, Ewing JW, Arrington LE (1990) Treatment of osteoid osteoma by computed tomography guided excision in the pediatric patient. J Pediatr Orthop 10:510–513

Whitehouse RW, Economou G, Adams JE (1993) The influence of temperature on quantitative computed tomography: implications for mineral densitometry. J Comput Assist Tomogr 17:945–951

Imaging Techniques: Magnetic Resonance Imaging

3

Sinchun Hwang and David M. Panicek

CONTENTS

KEY POINTS

- MR imaging is a powerful tool in the detection, diagnosis, staging, and follow-up of bone tumors.
- Images should be obtained with the smallest practical field of view in order to maximize image detail, while performing the entire study in a clinically practical time period.
- T1-weighted spin-echo images are particularly important in the evaluation of bone marrow, whereas intermediate-weighted images should be avoided.
- Fat suppression must be applied when obtaining T2-weighted fast spin-echo images to demarcate tumor from surrounding bone marrow and edema.
- Administration of a gadolinium-chelate contrast material can provide useful information in characterization of bone lesions, as well as in assessment of response to therapy and detection of recurrent tumor.
- Various MR imaging artifacts need to be recognized and appropriate steps taken to minimize their occurrence during image acquisition.
- The signal characteristics of a bone lesion, combined with its demonstrated morphology, location, and anatomic relationships, provide essential information that facilitates state-of-the-art patient care.

S. Hwang, MD
Weill Medical College of Cornell University,
Department of Radiology, Memorial Sloan-Kettering Cancer Center, 1275 York Avenue, New York, NY 10065, USA

D. M. Panicek, MD
Weill Medical College of Cornell University,
Department of Radiology, Memorial Sloan-Kettering Cancer Center, 1275 York Avenue, New York, NY 10065, USA

3.1 Introduction

After its introduction into clinical practice in the 1980s, MR imaging rapidly became established as the preferred imaging modality in the detection, characterization, staging, and post-therapy assessment and surveillance of bone tumors. (Radiographs, of course, still make an invaluable contribution to the characterization of a bone lesion but are often omitted in the rush to obtain an MR imaging examination.) When a tumor is suspected clinically or radiographically, MR imaging can confirm the presence of a tumor or demonstrate an alternative, nonneoplastic diagnosis. The excellent tissue contrast provided at MR imaging can occasionally yield sufficient information to allow a specific histologic diagnosis to be made (e.g., intraosseous lipoma, enchondroma, or aneurysmal bone cyst). The detailed depiction of anatomic relationships at MR imaging enables accurate local staging of a tumor, including delineation of neurovascular and joint involvement and intraosseous skip lesions, key features in planning for limb-salvage surgery. MR imaging also is essential in assessing the response to therapy and detecting local tumor recurrence.

To achieve these goals, it is important to have a thorough understanding of several basic technical issues in MR imaging in order to optimize the imaging protocols and the interpretation of the MR images produced. This chapter focuses on such practical issues as they pertain specifically to the evaluation of bone tumors. Detailed descriptions of MR imaging physics and general scanning techniques are beyond the scope of this chapter.

3.2 Technical Considerations

The first step in MR imaging of a bone tumor is to plan an appropriate MR imaging protocol, focused on the region of interest. Given the wide range of sizes of bone tumors, it is often a challenge to produce detailed images of the entire tumor within a reasonable time period. To successfully optimize MR imaging protocols, it is important to understand some major factors involved in image formation and their impacts on image quality.

3.2.1 Coils

In order to generate an image of a body part, more than one coil is used to send and receive the MR signals. Most of the coils (e.g., gradient and shim) are built directly into the scanner. Another local radiofrequency (RF) coil usually needs to be placed directly on the relevant body part to transmit and/or receive the signals from a bone tumor, as the MR signal is stronger when the tissues of interest are located closer to the coil. Appropriate local coil selection and correct coil positioning are critical to maximize the amount of MR signal acquired, which is essential in obtaining high-resolution images. A wide range of coils is available for different MR scanners. The particular RF coil selected depends on the size and shape of the body part of interest; for example, a cylindrical-shaped body part, such as the knee or wrist, is better scanned with a volume coil, which surrounds the entire region of interest. In contrast, a flatter, noncylindrical body part, such as a shoulder, is better imaged with a surface coil, which overlies but does not completely surround the region scanned. Phased-array coils consist of multiple small coils that receive signal simultaneously from a single excitation. These coils enable larger anatomic regions to be scanned in shorter time periods, with higher spatial resolution and improved signal-to-noise ratios (SNR), facilitating the imaging of large tumors.

The body coil or a long-bone coil is used to image the entire bone in a longitudinal plane to ensure that the full length of tumor will be included on subsequent image series, and to detect any other lesions present in that bone. Then, a smaller, dedicated local coil should be employed to obtain detailed, small field-of-view (FOV) images of the tumor.

3.2.2 MR Imaging Pulse Sequences

Various MR imaging pulse sequences provide different tissue contrast (Bitar et al. 2006) to allow characterization of tumors and definition of their anatomic extent. The most useful pulse sequences in the evaluation of a bone tumor are T1-weighted spin-echo (SE), T2-weighted fast SE with fat suppression, and gadolinium-chelate-enhanced T1-weighted SE with fat suppression (Hwang and Panicek 2007a,b). Gradient-echo (GE) sequences can provide specific information in certain circumstances. The short-tau inversion recovery (STIR) sequence should be avoided in initial evaluation of a bone tumor, as it is extremely sensitive to the presence

of water; many tissues as well as surrounding edema have very high signal on STIR images, diminishing the ability to distinguish various tissue types and often resulting in overstaging of malignant lesions. However, STIR can be quite useful for providing uniform fat suppression in the presence of orthopedic hardware, and it thus represents an important option for obtaining fluid-sensitive images in post-surgical follow-up examinations. Also, it is important to be aware that intermediate-weighted imaging is a poor choice for evaluation of bone tumors, as both marrow fat, any surrounding marrow edema, and the tumor itself often have similar, moderately high signal intensity, markedly limiting the visibility of the tumor.

3.2.2.1 T1-weighted SE

The T1-weighted SE sequence is often thought of as making an "anatomic" image, as it produces excellent contrast between cortical bone, bone marrow, and surrounding soft tissues, as well as relatively high spatial resolution. Most bone tumors are readily evident as well-defined regions of low signal against a background of surrounding fatty marrow. Although T1-weighted images also can be obtained with fast SE or GE pulse sequences, virtually all the articles that have described the signal characteristics of various bone tumors have reported on T1-weighted SE images. Until equivalence of SE and fast SE implementations of T1-weighted sequences has been proven, the SE sequence is preferred.

The repetition time (TR) and echo time (TE) should be kept as low as possible to increase the T1 contribution and decrease the T2 contribution to the images. Fluid or fluid-rich tissues, such as hyaline cartilage, have long T1 times and thus show low signal intensity on T1-weighted SE images. Fat and fatty bone marrow, on the other hand, have short T1 times and show very bright signal intensity.

T1-weighted SE images are some of the most useful for detection and evaluation of a primary bone tumor or bone metastasis. Tumor replaces the normal marrow and typically produces low signal similar to that of muscle (Fig. 3.1a; Vanel et al. 1998; Hwang and Panicek 2007a,b). The signal intensity of surrounding marrow

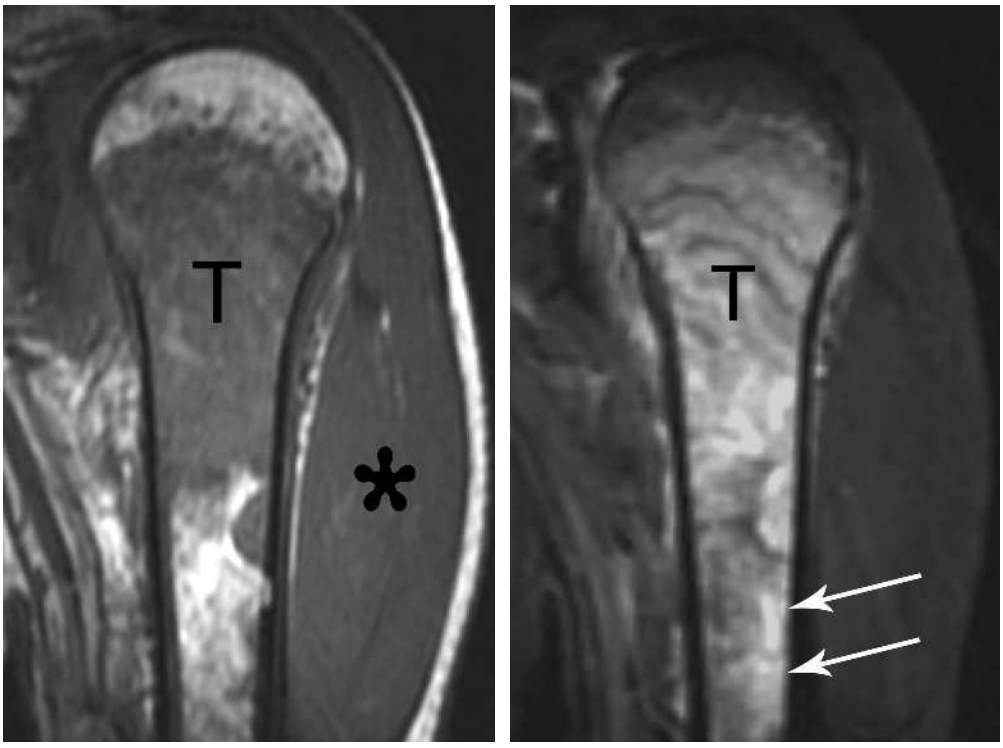

a b

Fig. 3.1a,b. Primary lymphoma of humerus. **a** Coronal T1-weighted SE image shows that signal intensity of tumor (*T*) in medullary cavity is low, similar to that of muscle (*asterisk*). **b** Coronal short-tau inversion recovery (STIR) image demonstrates diffusely high signal intensity both within the tumor (*T*) and throughout extensive surrounding edema (*arrows*). Note that margins of tumor cannot be visualized in **b**

edema is often slightly higher than that of tumor on T1-weighted SE images, whereas the high signal intensity of edema on T2-weighted fast SE and STIR sequences is frequently difficult to distinguish from that of the tumor itself (Fig. 3.1b). This difference in contrast exists because T1-weighted SE images detect the replaced lipid content of the marrow (where marrow is replaced by tumor), whereas T2-weighted fast SE and STIR images demonstrate the increased water content within tumor and surrounding edema. It is noteworthy that the presence of normal marrow fat within a bone lesion is highly predictive of a benign etiology (Simpfendorfer et al. 2008) and is best demonstrated on T1-weighted SE images.

3.2.2.2 T2-weighted Fast SE

The T2-weighted SE sequence can be considered to produce a "pathology scan," which shows high signal within most tumors due to their increased water content. The "fast" modification of the standard SE pulse sequence is preferred because it offers shorter imaging times without significant changes in image quality; however, frequency-selective fat suppression becomes essential when using these fast SE sequences, as they often show both fat and tumor with similar, relatively high signal intensity (Fig. 3.2). Fat suppression also enhances the overall tissue contrast by decreasing the dynamic range of the image, thus improving delineation of different tissues. Frequency-selective fat suppression is available in scanners with 1.0 T or stronger magnets.

One drawback of using fat suppression is that it reduces SNR and worsens some motion-related artifacts (Mirowitz et al. 1994). In addition, homogeneous fat suppression is often difficult to achieve due to local magnetic field inhomogeneities (either inherent to the particular magnet or due to susceptibility artifacts caused by the presence of air or metallic materials in or on the patient). These field inhomogeneities often cause nonuniform fat suppression – or even inadvertent suppression of water – that can potentially obscure underlying lesions (Fig. 3.3). A typical example is the inhomogeneous fat suppression caused by the ferromagnetic effects of orthopedic hardware, yielding nondiagnostic regions within the images.

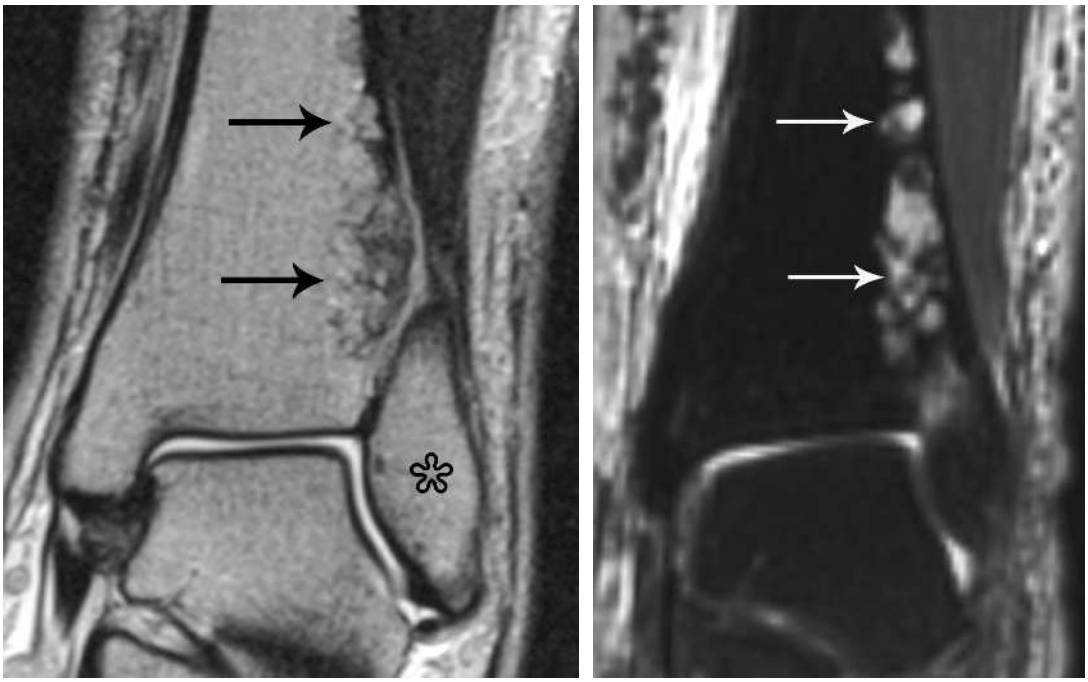

a b

Fig. 3.2a,b. Importance of fat suppression for lesion evaluation at T2-weighted fast SE imaging. **a** In coronal T2-weighted fast SE without fat suppression, the lesion (*arrows*) in distal tibia has high signal intensity similar to that of normal marrow (*asterisk*), and its border is poorly defined. **b** T2-weighted fast SE image with fat suppression clearly demonstrates margins of the lesion (*arrows*), and also clearly demonstrates very high signal within multiple lobules, consistent with a chondroid lesion

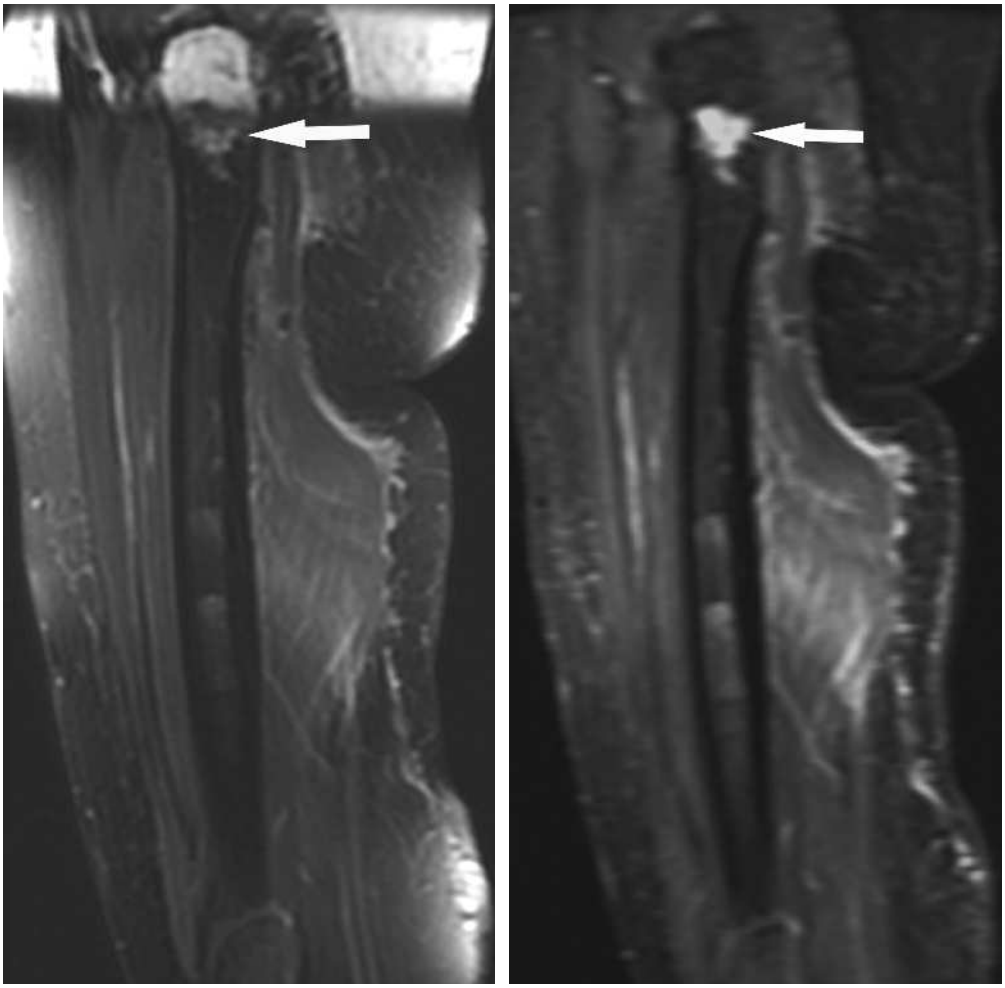

Fig. 3.3a,b. Fat suppression on T2-weighted fast SE and STIR images. **a** Sagittal T2-weighted fast SE image shows heterogeneous high signal intensity near the edge of the coil due to inhomogeneous fat suppression as a result of the large field of view (FOV). The marrow lesion (*arrow*) in proximal femur is partially obscured by inhomogeneous fat suppression. **b** Sagittal STIR image shows the entirety of the lesion (*arrow*). Note the markedly improved uniformity of fat suppression

3.2.2.3 Gadolinium-enhanced SE

Contrast-enhanced MR images are important in characterization of bone tumors, as well as in assessment of response to therapy and detection of recurrent tumor. A gadolinium-chelate contrast material, in the doses given clinically, predominantly decreases the T1 relaxation time in tissues where it accumulates. The decreased T1 relaxation time manifests as increased signal intensity in T1-weighted SE images. Because fat also has high signal on T1-weighted SE images, it is essential to apply frequency-selective fat suppression with both pre- and post-gadolinium-enhanced images; otherwise, the difference between tumor and surrounding fat can be masked by the large dynamic range of the image (Fig. 3.4). In some cases, it can be helpful to subtract the pre-contrast images from the post-contrast images to emphasize the regions that enhanced (De Baere et al. 1992).

The increased signal intensity from contrast enhancement can improve the conspicuity of small tumor nodules and better delineate the borders of tumor surrounded by less-enhancing edema. Contrast enhancement also aids in characterizing the internal composition of a tumor (e.g., solid, cystic, or necrotic components). That information, for example, may help in selecting the most appropriate region of a bone tumor

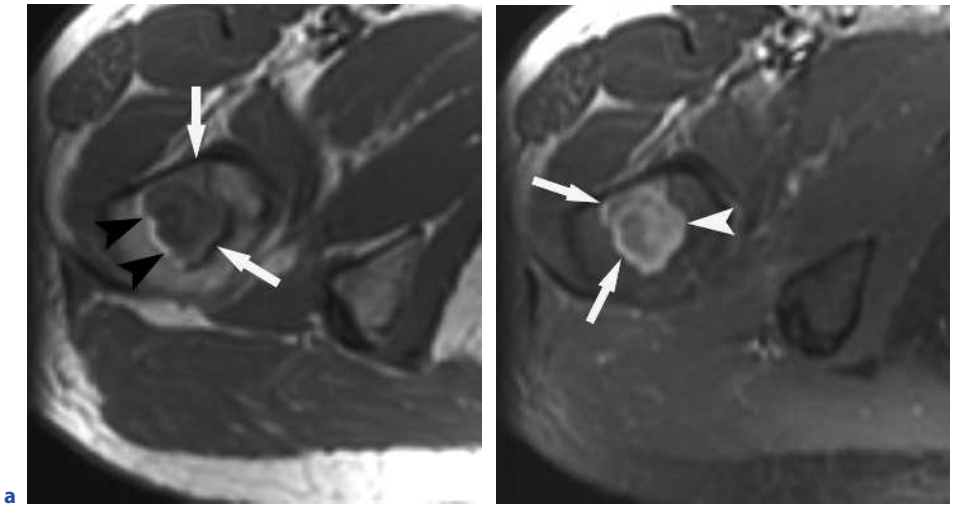

Fig. 3.4a,b. Lesion conspicuity in gadolinium-enhanced images with and without fat suppression. **a** Gadolinium-enhanced transverse T1-weighted SE image obtained without fat suppression shows subtle mild peripheral contrast enhancement (*arrows*) of the lesion in proximal femur. Peripheral high signal (*arrowheads*) due to chemical shift artifact partly obscures the border of the lesion. **b** Subsequent image obtained with same parameters and fat suppression reveals more peripheral (*arrows*) and nodular (*arrowhead*) regions of enhancement. The previous chemical shift artifact is no longer present. Biopsy revealed liposclerosing myxofibrous tumor

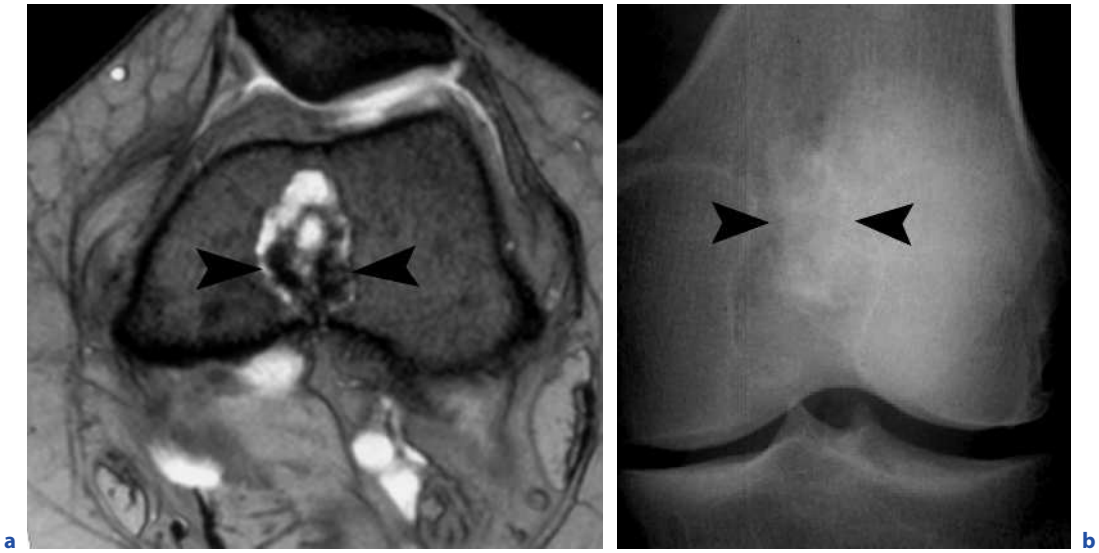

Fig. 3.5a,b. Calcification demonstrated on T2*-weighted GE image. **a** Transverse T2*-weighted GE image (TE=24 ms) shows several small signal voids (*arrowheads*) within a low-grade chondrosarcoma in distal femur. **b** Anteroposterior radiograph of the knee demonstrates faint foci of calcification (*arrowheads*) in distal femur, corresponding to the signal voids seen in GE image

to biopsy, or in showing small solid elements within a background of (secondary) aneurysmal bone cyst. Gadolinium-enhanced SE images with fat suppression may also help delineate a focus of recurrent tumor amidst a background of post-surgical or post-radiation changes.

3.2.2.4 Gradient Echo

Gradient echo (GE) sequences are less useful in the routine evaluation of bone tumors, but can provide additional information in some specific situations. Susceptibility-weighted (also known as T2*-weighted) GE images, obtained by using a TE of 12 ms or longer, can demonstrate foci of calcium (Fig. 3.5) or other metals, as well as hemosiderin from prior hemorrhage. Those foci will appear as signal voids larger than their actual size (due to "blooming" of signal).

In-phase and opposed-phase GE images (also called chemical shift imaging) differ in their TEs: at 1.5 T, in-phase images are obtained with a TE of 4.2 ms, and opposed-phase images with a TE of 2.1 ms. The lipid and water protons present in normal marrow (whether hematopoietic or fatty) have opposite phases on opposed-phase images; this results in signal cancellation and a decrease in signal intensity relative to their signal on in-phase images (in which their signals are additive). Because bone tumors replace normal marrow, tumor will not show signal loss on opposed-phase images. The GE chemical shift images are thus useful in assessing the bone marrow in equivocal cases.

Flow-sensitive GE sequences, such as gradient-recalled echo in the steady state obtained with a flip angle of ~30°, demonstrate blood flowing perpendicular to the image plane as high signal ("bright blood"); stationary tissues are of lower signal intensity. A gadolinium-chelate contrast material can be administered intravenously in conjunction with these sequences to improve image quality. These MR angiography sequences can be used to demonstrate flow in vessels near or within a bone tumor, information useful in characterizing and staging a tumor. Narrowing of a major artery by the extraosseous soft tissue component of a bone tumor, for example, suggests arterial invasion by the tumor (Feydy et al. 2006).

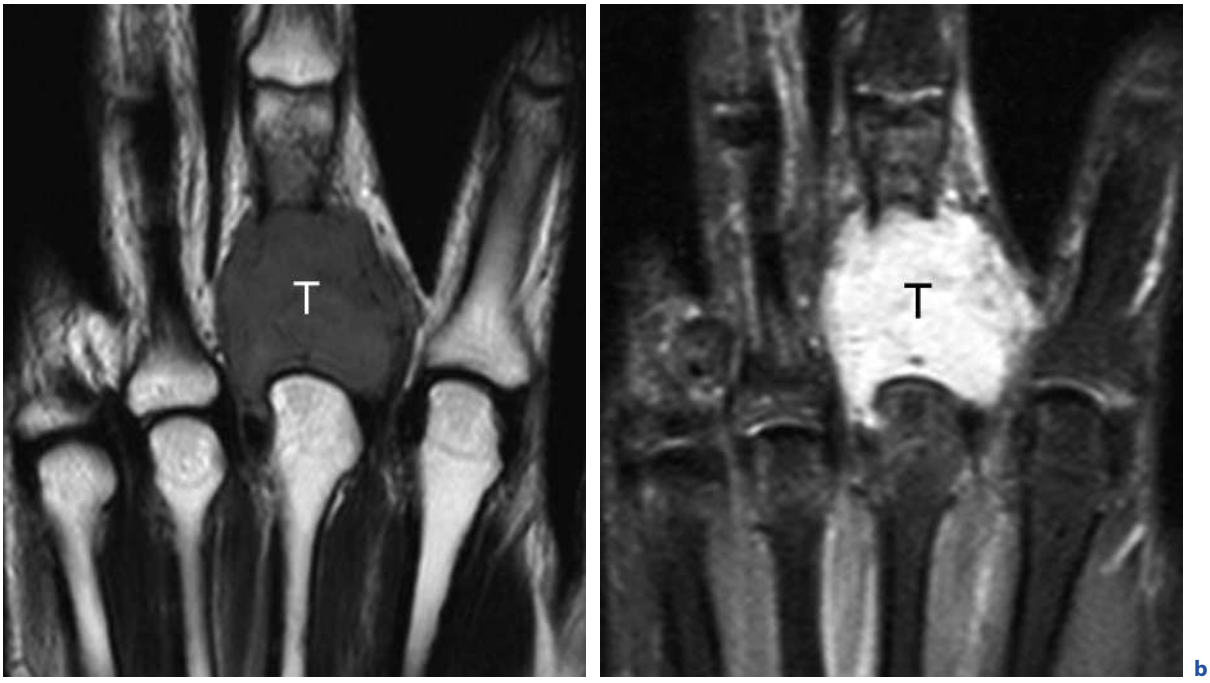

a b

Fig. 3.6a,b. Nonspecific signal intensity of tumor on STIR sequence. On **a** coronal T2-weighted SE image without fat suppression, diffusely low signal intensity throughout the giant cell tumor (*T*) suggests chronic internal hemorrhage. On **b** coronal STIR image, tumor (*T*) is diffusely very high in signal intensity, which improves conspicuity of the tumor but diminishes the ability to characterize it

3.2.2.5 STIR

Short-tau inversion recovery (STIR) frequently is used as an alternative fat-suppression sequence to achieve homogeneous fat suppression and T2-weighting, particularly in situations where fat suppression with T2-weighted fast SE would be unsatisfactory (Fig 3.3). Those circumstances include scanning through a large anatomic region or in the presence of extensive metallic hardware. Unlike the frequency-selective fat-suppression option that depends on a homogeneous magnetic field throughout the entire region of the scan, the STIR sequence depends only on selection of the appropriate inversion time (TI) in order to null the signal from fat. This specific TI is proportional to the magnetic field strength: at 1.5 T, the appropriate TI is 140–160 ms. The STIR sequence is now typically implemented as fast STIR.

At STIR imaging, the T1 and T2 effects of a tissue or other material are additive (unlike at SE imaging, where the T1 and T2 effects are competitive; Fig. 3.6). STIR is a sensitive sequence in detecting pathology, but because high signal intensity at STIR can be seen in any tissue having a T1 time similar to that of water, its ability to characterize lesions is diminished, and tumor extent is often overestimated (Fig. 3.1b; Shuman et al. 1991; Delfaut et al. 1999). STIR is limited in its depiction of anatomic details due to its lower spatial resolution.

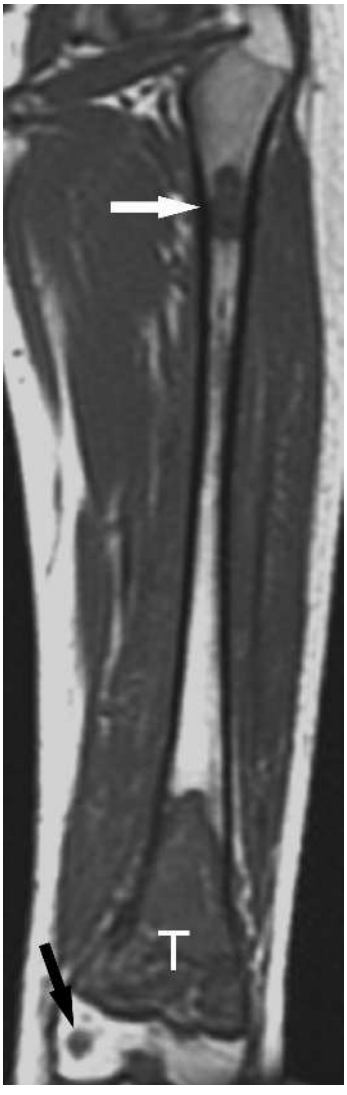

Fig. 3.7. Skip lesions of osteogenic sarcoma in left femur. Coronal T1-weighted SE image reveals skip (metastatic) lesions in the proximal diaphysis and distal epiphysis of femur (*arrows*), in addition to the primary tumor (*T*) in distal metaphysis

3.2.3 Anatomic Coverage and Image Orientation

Before the MR images are acquired, it is important to place markers (e.g., vitamin E capsules) on the ends of any surgical scars or palpable masses. In the absence of physical findings, the body coil or a long-bone coil often is used to obtain localizer images of the entire bone of interest along its long axis to determine the location and gross overall extent of the lesion or its postoperative bed. (For lesions in small bones, such as in the hand or foot, a surface or volume coil would be used for this purpose.) Also, the entire bone should be scanned in its coronal or sagittal plane to detect any skip metastases or other lesions present within the bone (Fig. 3.7).

Then, a surface or volume coil should be employed to obtain small-FOV transverse and longitudinal images through the tumor. If an associated extraosseous soft tissue component of the bone tumor is present, the optimal longitudinal plane can be determined from the line connecting the center of the extraosseous mass and the center of the subjacent bone. Scanning in this plane ensures that both the extraosseous and intraosseous components will be included on the same image.

3.2.4 Signal-to-Noise Ratio, Spatial Resolution, and Scan Time: Trade-offs in MR Image Optimization

Whereas a given pulse sequence determines tissue contrast, other parameters, such as SNR, spatial resolution,

and scan time, are some of the major determinants of overall image quality. Like many MR imaging parameters, these three are interrelated, with the positive effects achieved from changing one parameter typically offset by adverse effects in others. Understanding the interplay between SNR, spatial resolution, and scan time is essential in MR image optimization.

As for other body parts, there is no one correct MR imaging protocol for bone tumors. The routine MR imaging protocol used at our institution for bone tumors is described in Table 3.1, but other modifications that incorporate the principles described throughout this chapter can be equally valid if they accurately and reliably provide the information needed by the referring physicians.

3.2.4.1 Signal-to-Noise Ratio

The SNR is one of the most important parameters in MR imaging, as it reflects the basic "currency" of the technique: Insufficient signal equals inadequate images. The SNR is proportional to many factors, including TR, flip angle, voxel volume, number of excitations, magnetic field strength, and scan time. Increasing the FOV or the slice thickness, or decreasing the number of frequency-encoding and/or phase-encoding steps with a constant FOV, increases SNR. On the other hand, an increase in TE decreases the SNR. Because TR and TE determine tissue contrast, the ability to adjust either in an attempt to improve SNR is limited.

Table 3.1. MR imaging protocol for bone tumor of extremity at 1.5 T

	Coronal T1-weighted (long bone)	Transverse T1-weighted	Transverse T2-weighted	Longitudinal T1-weighted[c]	Longitudinal T2-weighted[c]	Transverse T1-weighted, pre-gadolinium	Transverse T1-weighted, post-gadolinium
Sequence	2D SE	2D SE	2D Fast SE	2D SE	2D Fast SE	2D SE	2D SE
Coil[a]	Long bone/ torso	Extremity	Extremity	Extremity	Extremity	Extremity	Extremity
TR (ms)	400–600	400–600	2,500	400–600	2,500	400–600	400–600
TE (ms)	Min–Full	Min–Full	60	Min–Full	60	Min–Full	Min–Full
Field of view (cm)[b]	14–48	16–24	16–24	16–24	16–24	16–24	16–24
Slice thickness (mm)3	10	4	4	4	4	4–6	4–6
Intersection gap (mm)[b]	2	0.5	1	1	1	1–1.5	1–1.5
Phase encoding Steps	128	256	256	256	256	192	192
Frequency steps	256	256	256	256	256	256	256
Excitations	2–3	2–3	2–3	2–3	2–3	2–3	2–3

[a]After entire long bone is imaged, change to smallest dedicated local coil that best covers anatomic region of entire tumor

[b]FOV, slice thickness, and intersection gap should be as small as possible; need to be increased for large tumors

[c]The optimal longitudinal plane is determined from line connecting center of extraosseous component and center of subjacent bone

Practical methods to optimize SNR include one or more of the following: selecting and properly positioning an optimal local coil; increasing the slice thickness, FOV, or number of excitations; and decreasing the bandwidth. Reducing the bandwidth by half increases SNR by a factor of 1.4 (the square root of 2), but increases the amount of chemical shift artifact. It is important to remember that although increasing the number of excitations will increase SNR, that change will also increase the scan time. On the other hand, doubling the slice thickness doubles the SNR without increasing scan time.

3.2.4.2 Spatial Resolution

Spatial resolution refers to the ability to resolve two points as separate in an image, and is inversely proportional to pixel size. Pixel size itself is proportional to the FOV and inversely proportional to matrix size; therefore, spatial resolution can be increased by increasing the matrix size or decreasing the FOV. Spatial resolution is also inversely proportional to voxel size, because partial volume averaging of the various materials present within the voxel increases with larger slice thickness.

In bone tumor imaging, the FOV and matrix size need to be tailored to the anatomic extent of each tumor, unlike in routine orthopedic imaging protocols that involve standard anatomic landmarks (e.g., MR imaging of the knee to evaluate for internal derangement). In general, for a small bone tumor, a small FOV and large matrix would be desirable to obtain maximal detail; similarly, thinner slices (e.g., 3–4 mm) would be useful in a small tumor, whereas in a large tumor, 7-mm slice thickness might be required to image the entire tumor in a clinically practical time period.

3.2.4.3 Scan Time

As the amount of time a patient remains in the MR scanner increases, the patient's tolerance of the scanning process decreases, and motion artifacts typically then increase. Balancing the scan time with the number and quality of MR images obtained is thus a constant challenge in the clinical setting. Scan time is proportional to TR, the number of phase-encoding steps, and the number of excitations; in fast imaging, time is also inversely proportional to the echo train length (i.e., the number of phase-encoding steps acquired during each TR). Because the TR determines signal intensity and tissue contrast, usually only minor changes are made in TR, in order to slightly modify the number of slices obtained in an imaging sequence. Increasing the number of phase-encoding steps increases spatial resolution, but scan times are also increased. It is important to consider the effect on overall scan time when changing the spatial resolution or SNR, and to achieve an acceptable balance between these competing issues.

3.2.5 Benefits and Technical Challenges of Higher Magnetic Field Strengths

Although MR imaging systems operating at field strengths between 0.2 and 1.5 T have been considered effective for clinical practice, potential benefits of higher field strengths have stimulated increasing clinical use of 3.0-T magnets (and research using even stronger magnets). The benefits include improved SNR, more homogeneous fat suppression, and increased separation of various spectral peaks at MR spectroscopy (Fayad et al. 2007). Also, parallel imaging can be more effectively used at 3.0 T, allowing shorter scan times and reduced energy deposition (Ladd 2007).

As with other parameters in MR imaging, higher magnetic field strengths incur other technical challenges, including increases in T1 and T2 relaxation times (and, therefore, changes in tissue contrast), increases in amount of chemical shift and magnetic susceptibility effects, and larger amounts of energy deposited in the patient (Gold et al. 2004). To date, it has not been determined whether use of higher field strengths produces any substantial benefits in routine clinical imaging of bone tumors.

3.2.6 Advanced MR Techniques

Several MR imaging techniques that have applications in bone tumors are not yet in routine clinical use at most facilities but deserve mention because their potential seems promising.

3.2.6.1 Quantitative Dynamic MR Imaging

Physicians treating a patient with a malignant bone tumor would like to know whether the therapy is working

before the patient has completed the therapy, to allow a modification of that therapy sooner if it is not effective. For example, it has been shown that in osteosarcoma treated with neoadjuvant chemotherapy, those patients with at least 90% necrosis in the remaining tumor at histopathologic examination have a better event-free survival than do those with less than 90% necrosis (Meyers et al. 1998). Because the histopathologic examination can be performed only once, after the bone tumor has been resected, there is a role for a noninvasive, repeatable imaging examination that could assess necrosis occurring during therapy.

Quantitative dynamic MR imaging estimates the amount of necrosis in bone tumors based on the principle that viable tumor enhances faster than nonviable tumor and post-treatment changes (Dyke et al. 2003). At our institution, fast multiplanar spoiled GE imaging is performed through all sections of the entire tumor every 8–9 s, yielding data for each voxel at 20–40 time points in less than 5 min. The necessary post-processing software, which currently is proprietary at each institution that performs this examination, calculates the percentage of voxels within the tumor that enhance relatively slowly. This technique has been shown to correlate reasonably well with results obtained at histopathologic analysis in osteogenic sarcoma and Ewing sarcoma (Dyke et al. 2003). Exact correlation is not expected, because the histopathologic findings are obtained from examination of 5-μm-thick sections obtained through the center of the tumor, whereas the MR-based estimates of necrosis are determined from virtually the entire tumor. The results of quantitative dynamic MR imaging continue to be compared to those obtained at histopathologic examination, as well as with the most clinically relevant parameter, patient outcomes. If confirmed to be of clinically predictive value, the post-processing software for this technique likely would become more widely available.

3.2.6.2 Diffusion-weighted Imaging

Diffusion-weighted imaging (DWI) of tumors is based on the principle that the diffusion of water is more restricted in a tumor than in normal tissue, manifesting as less loss of signal on DWI (Fig. 3.8). DWI has shown potential in some cases for distinguishing benign from malignant bone tumors (Baur and Reiser 2000). Infection also has restricted diffusion and may be indistinguishable from malignant tumor at DWI alone.

Another promising application of DWI is in assessing the response of bone tumors to therapy (Hayashida et al. 2006). As viable tumor is effectively treated, cell membranes break down, resulting in increased diffusion of water; this manifests as a decrease in signal intensity in the tumor on DWI compared with the higher signal present prior to therapy.

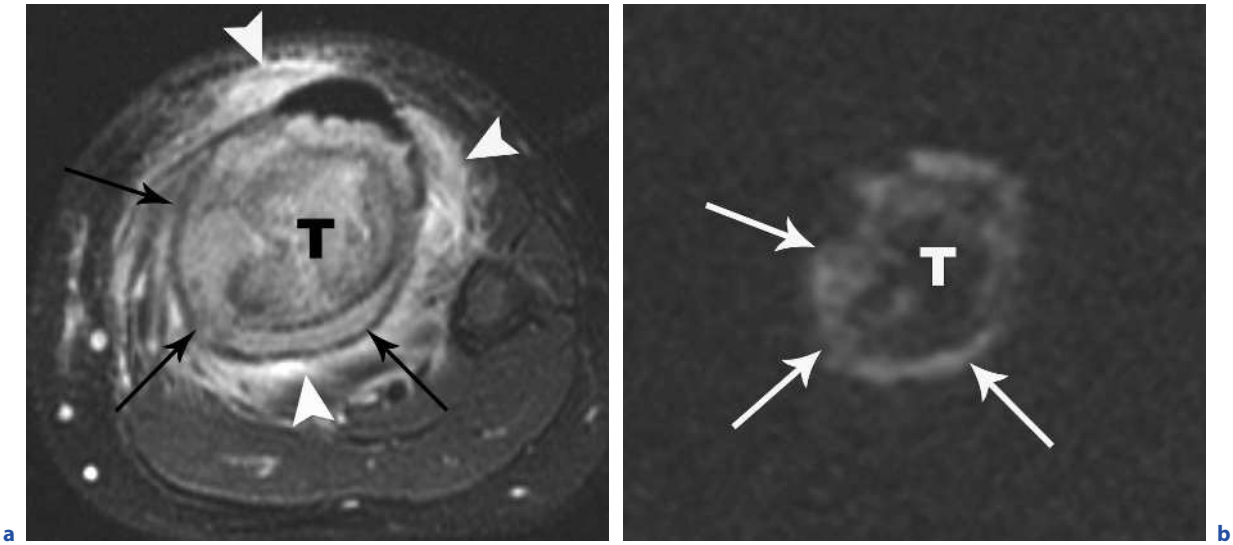

a b

Fig. 3.8a,b. Diffusion-weighted imaging (DWI) in Ewing sarcoma of tibia. **a** Transverse T2-weighted SE image with fat suppression shows extensive high signal in the tumor (*T*) and its subperiosteal component (*arrows*), as well as in surrounding soft tissue edema (*arrowheads*). **b** Transverse DWI (b=1000) allows differentiation of tumor (*T*) from surrounding edema by demonstrating increased signal in the tumor (*arrows*) but not in surrounding edema

3.2.6.3 MR Spectroscopy

Preliminary studies using single-voxel (Wang et al. 2004; Fayad et al. 2007) and multivoxel (Fayad et al. 2006, 2007) MR spectroscopy have shown that choline levels are elevated in many malignant musculoskeletal tumors; however, similar findings may be seen with some benign tumors, including giant cell tumor of bone (Sah et al. 2008). Changes in levels of choline and possibly other metabolites may be useful indicators of tumor response to therapy as well as of recurrent tumor, but further work is needed before MR spectroscopy can be used in routine clinical practice.

3.3 Common MR Imaging Artifacts

Artifacts often occur at MR imaging during the relatively long imaging sequences, degrading both spatial resolution and tissue contrast and potentially obscuring important anatomic and pathologic findings (Zhuo and Gullapalli 2006). It is important to recognize certain artifacts in order to prevent or reduce them as much as possible. Artifacts that commonly are problematic in bone tumor imaging include susceptibility artifacts, inhomogeneous fat suppression, motion artifacts, chemical shift artifact, phase wrapping, and truncation artifacts.

3.3.1 Susceptibility Artifacts

Susceptibility artifacts occur when a ferromagnetic material alters its local magnetic field, causing changes in the resonant frequency of protons. This leads to mismapping of MR signals along the frequency-encoding direction, with local signal loss and geometric distortion. The severity of the artifact depends on the size, anatomic orientation, and specific composition of the offending material, as well as the magnetic field strength, pulse sequence, voxel size, receiver bandwidth, and TE (Suh et al. 1998; Petersilge et al. 1996).

Susceptibility artifact is particularly problematic in bone tumor imaging because the surgical hardware used for reconstruction after tumor resection is generally made of metal. Susceptibility artifact due to metal typically causes a rim of high signal intensity at the periphery of a signal void (Fig. 3.9). Other common sources of susceptibility artifact include hemorrhage, air (Fig. 3.10), and radiation-portal tattoos. Susceptibility artifacts can occur with all pulse sequences but are more pronounced with GE sequences (due to lack of any refocusing pulses).

In some circumstances, the pronounced artifact in a GE sequence is diagnostically useful, such as in detecting hemosiderin or calcification within a tumor. But in general, efforts should be undertaken to minimize susceptibility artifacts (Eustace et al. 1997). Use of a fast SE sequence decreases T2* effects by applying multiple 180° refocusing pulses during each TR. Selection of the minimum TE in SE, fast SE, or GE pulse sequences reduces the time for T2* dephasing to occur. Use of wider receiver bandwidths and smaller voxel size (by choosing a smaller FOV and thinner slices) is also helpful in decreasing the artifact. To minimize the amount of tissue that is obscured by artifact, the frequency-encoding direction should be made parallel to the long axis of a metal prosthesis, when possible.

3.3.2 Inhomogeneous Fat Suppression

Fat suppression that is not equally effective in different areas of the image is one of the most frequently encountered artifacts in clinical MR imaging (Fig. 3.11). Inhomogeneous fat suppression occurs because local field

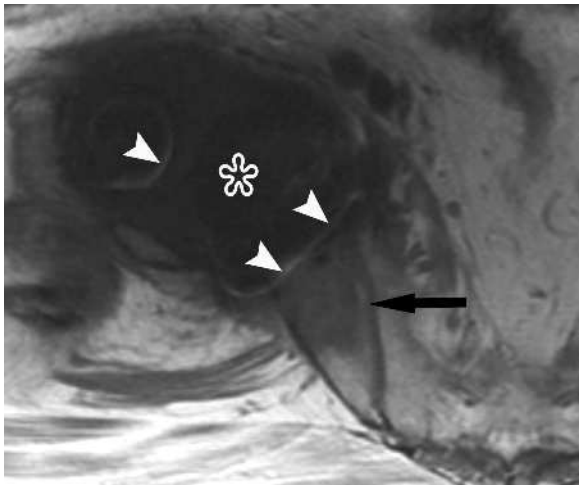

Fig. 3.9. Susceptibility artifacts from metallic hardware. Transverse T1-weighted SE image demonstrates a large area of signal void (*asterisk*) caused by metal hardware in the right hip (placed after resection of chondrosarcoma). The artifact partially obscures recurrent tumor (*arrow*) in remaining ilium. Rims of high signal intensity (*arrowheads*) caused by mismapped signal are present around the right femoral and acetabular components

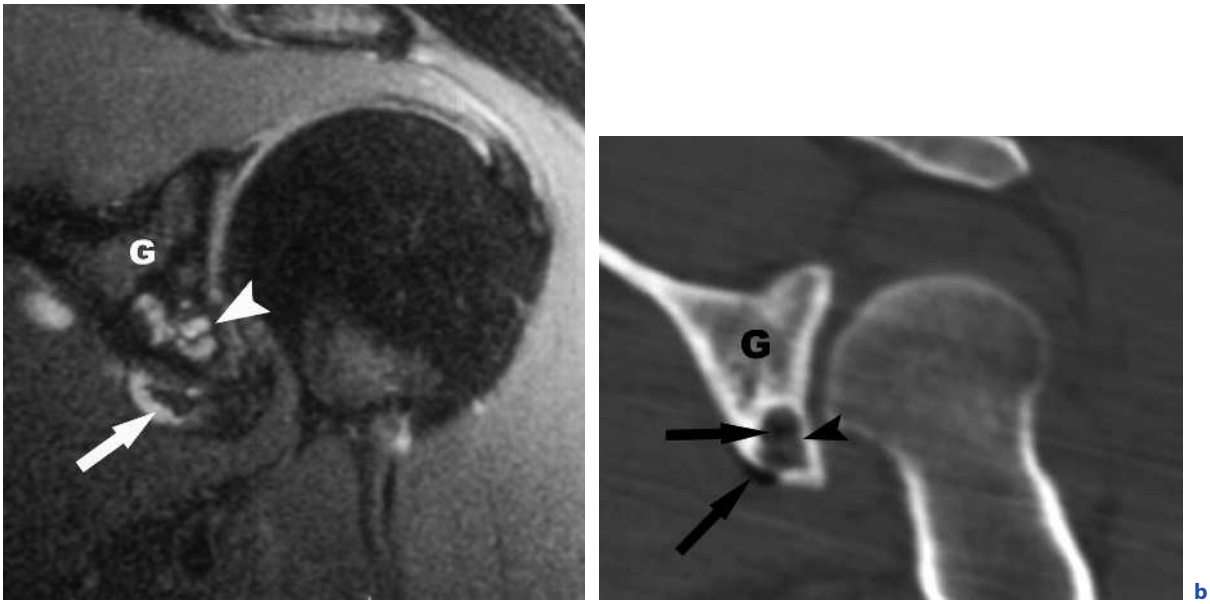

a b

Fig. 3.10a,b. Susceptibility artifacts from air. **a** Coronal intermediate-weighted SE image with fat suppression shows a focus of signal loss (*arrow*) caudal to a lesion (*arrowhead*) in the glenoid (*G*). Findings are suspicious for a bone lesion, possibly of chondroid nature. **b** Coronal CT image shows foci of air (*arrows*) within and outside the glenoid, consistent with intraosseous pneumatocyst (*arrowhead*), accounting for the complex signal changes at MR imaging

inhomogeneities, both within the patient and inherent to the particular magnet, cause the lipid protons in different regions to precess at slightly different frequencies. Consequently, the RF pulse applied for fat suppression does not match the different precessional frequencies of lipid protons at various locations throughout the image slice. Given that the differences in frequencies of protons in lipid and water are quite small (3.5 parts per million), small variations in the homogeneity of the magnetic field can severely interfere with homogeneous fat suppression.

To obtain homogeneous fat suppression, proper positioning of both the local coil and the patient is an important initial step. An excessive amount of air between a body part being imaged and the overlying coil, or a body part contacting the scanner gantry, can produce perturbations in the local magnetic field. These situations need to be minimized by the use of padding or better positioning. Use of a smaller FOV is helpful to improve field homogeneity, but this may not be practical when imaging large bone tumors. In the presence of metallic hardware, STIR is preferred over fat-suppressed T2-weighted fast SE, because the fat suppression in STIR is independent of local field homogeneity.

3.3.3 Physiologic Motion Artifacts

Gross patient motion, as may occur if the patient is in pain during the MR scan, will cause degradation of the images. Scanning the patient in a position that they find comfortable, and after the patient has received adequate pain medication, can usually minimize that degradation.

Physiologic motion artifacts at MR imaging, on the other hand, are usually inevitable – even in the most cooperative patients – and have readily recognizable features. Such artifacts are mostly related to vascular and cardiac pulsations, respiratory motion, and bowel peristalsis, and create blurring or ghosting on the images. Their cause(s) and magnitude in a given patient will vary depending on the location of the bone tumor being scanned. Physiologic motion artifacts occur along the phase-encoding direction because physiologic motion typically occurs on a slower time scale than the frequency-encoding process, but faster than the phase-encoding process. The motion thus generates ghost signals that no long represent the true position of the proton signal along the phase-encoding direction. Because the

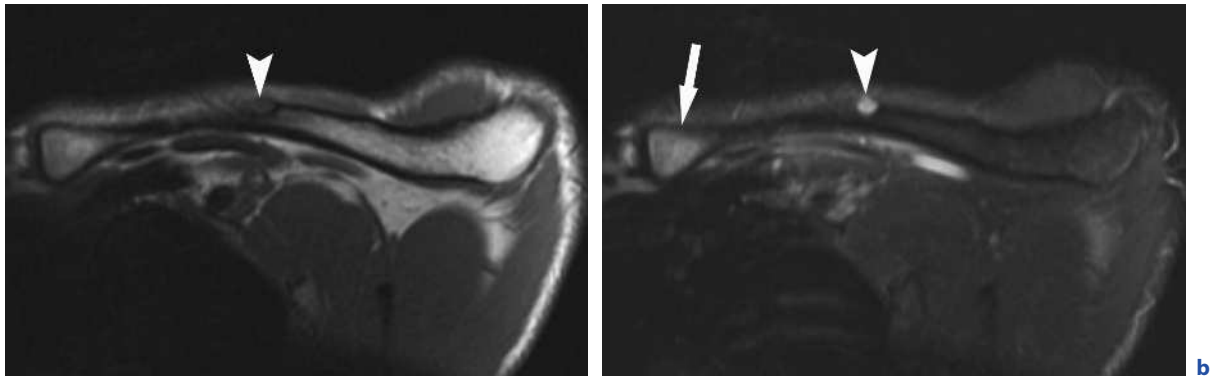

a b

Fig. 3.11a,b. Inhomogeneous fat suppression in clavicle, mimicking bone marrow edema pattern. **a** Transverse T1-weighted SE image shows a small lesion (*arrowhead*) in the mid clavicle. **b** Transverse T2-weighted fast SE image with fat suppression clearly reveals the intracortical location of the lesion (*arrowhead*), shown at biopsy to represent schwannoma. High signal intensity in the clavicular head (*arrow*) caused by inhomogeneous fat suppression could be mistaken for marrow edema. This pitfall is avoidable by careful correlation with T1-weighted images, which demonstrated no corresponding abnormality

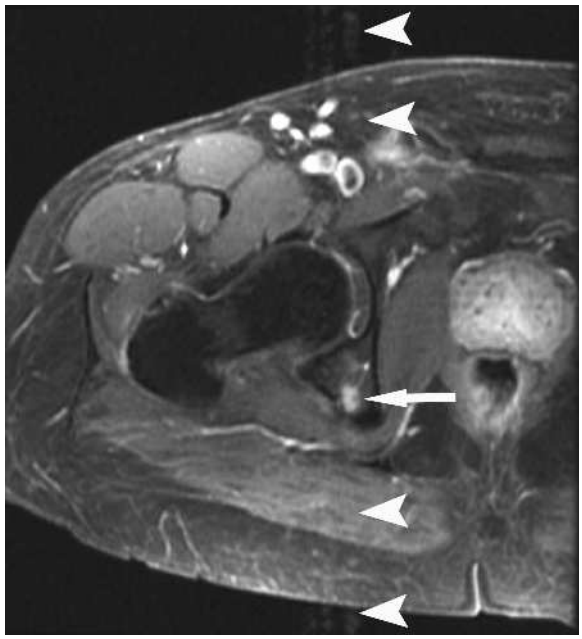

Fig. 3.12. Pulsation artifacts mimicking a bone lesion. Transverse post-gadolinium T1-weighted SE image with fat suppression demonstrates multiple ghosted signals (*arrowheads*) arising from the femoral vessels, projected in the anteroposterior (phase-encoding) direction. One such mismapped signal (*arrow*) mimics an enhancing lesion in the posterior acetabulum. Axial T1-weighted image (not shown) showed no corresponding abnormality, confirming that finding was an artifact

motion is often periodic, many phase-encoding errors are easily recognizable by the repetitive misregistration of signals at regular intervals along the phase-encoding direction ("ghost artifacts"; Fig. 3.12). The distance between the ghosts in an image is proportional to TR and number of excitations.

Physiologic motion-induced artifacts can be reduced in several ways. Use of cardiac gating if the bone tumor is located in the chest, and a respiratory compensation technique if located in the chest, abdomen or pelvis, can help to reduce the signal misregistration. Increasing the number of excitations will increase the SNR but may inadvertently lead to an increase in artifacts because of the increased scan time (and resultant patient motion). Increasing the receiver bandwidth decreases the minimum TE attainable, thus reducing the time during which motion can adversely affect the signal. Swapping the frequency-encoding and phase-encoding directions is another practical way to minimize motion artifact if it obscures the region of interest.

3.3.4 Chemical Shift Artifacts

Chemical shift artifacts are a consequence of differences in the resonant frequencies of the protons in lipid and those in water. These difference occur because lipid protons are shielded by adjacent electrons within the large lipid molecules, thus slightly reducing the effect of the external magnetic field on the lipid protons. Chemical shift artifact can occur in all pulse sequences and is proportional to magnetic field strength. Two manifes-

tations of this resonant frequency difference occur in clinical MR imaging.

The first manifestation, variously referred to as chemical shift artifact, chemical misregistration artifact, and chemical shift artifact of the first kind, is a spatial misregistration of the lipid proton signals with respect to the water proton signals along the frequency-encoding direction. This artifact appears as a bright (high-signal) band on the lower frequency side and a dark band (signal void) on the higher-frequency side of a structure. One of the first reports of this artifact in MR imaging of bone described apparent asymmetrical cortical thickening in long bones, due to shifting of the bright marrow signal relative to the water image. On axial images of both femurs, for example, the right side of each femoral cortex appeared thicker than the left side (Fig. 3.13; Dick et al. 1988). This artifact is commonly seen where fat- and water-containing structures are apposed, such as bone–vertebral disc interfaces. Although it can mimic pathology, such as cortical thickening or endplate infraction, this artifact can be easily recognized by correlating the findings on images obtained in different planes. Increasing the receiver bandwidth and decreasing the FOV can help to reduce this chemical shift artifact, although those changes also decrease SNR. Swapping the frequency- and phase-encoding directions and using a fat-suppression technique are two additional useful options.

The second manifestation, known as phase cancellation artifact, black line artifact, and chemical shift artifact of the second kind, is seen at GE imaging when voxels containing both lipid and water show a reduction in signal on opposed-phase images. This artifact appears as a black line (signal void) at the boundaries between fat-containing and nonfatty tissues, such as at the margins of muscles. (Note that this artifact can also be seen at the boundary of an intramedullary tumor where it contacts fatty marrow.) This type of chemical shift artifact can be minimized at GE imaging by selecting a TE at which lipid and water protons are in phase, or can be avoided altogether by using a SE sequence instead.

3.3.5 Phase Wrapping

Phase wrapping, also known as aliasing, wraparound, and foldover artifact, occurs when the imaged body part is larger than the selected FOV. Structures outside the FOV are spatially mismapped, becoming directly superimposed on the contralateral side of the image (Fig. 3.14). Phase wrapping occurs along the phase-encoding direction in two-dimensional acquisitions, but can also occur along the frequency-encoding direction in three-dimensional acquisitions. Depending on its size and location, phase-wrapping artifact may obscure anatomy or even abnormalities in the region of interest.

Phase-wrapping artifact is reduced by selecting a FOV that includes all the structures within the coil, as well as by using the shortest axis of the imaged body part as the phase-encoding direction. The penalty, though, for choosing a larger FOV is a decrease in spatial resolution. Another option is to use a phase-oversampling option (e.g., "no phase-wrap"), which allows acquisition of signal data along the phase-encoding direction outside

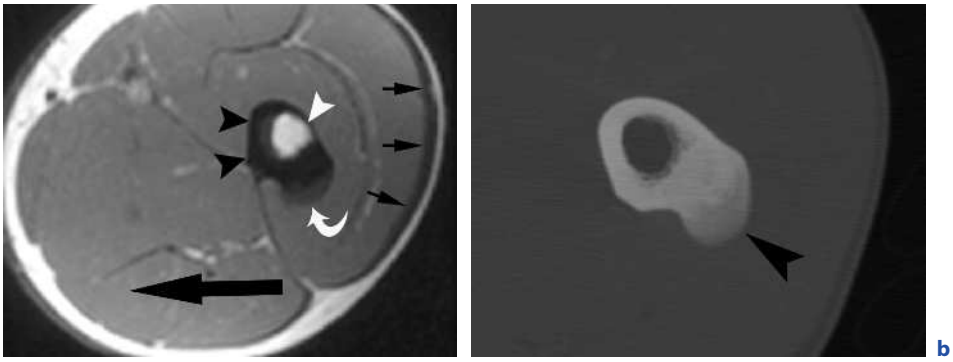

Fig. 3.13a,b. Chemical shift artifact mimicking cortical abnormality. **a** Transverse T1-weighted SE image shows a parosteal osteosarcoma (*curved arrow*) associated with apparent cortical thinning (*white arrowhead*) on one side and thickening (*black arrowheads*) on the other. The apparent variation in cortical thickness is due to signal shift of a few pixels along the frequency-encoding direction (*large arrow*). This artifact is also seen as a dark band of signal at muscle–fat interfaces (*small arrows*). **b** Transverse CT image through tumor (*arrowhead*) confirms that cortical changes at MR imaging were artifactual

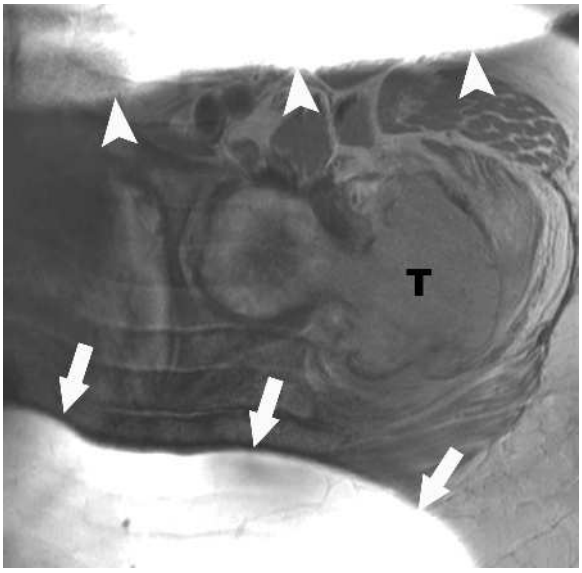

Fig. 3.14. Phase wrapping. Transverse intermediate-weighted SE image of the left hip (FOV 20 cm) demonstrates overlap of signal from the soft tissues of the anterior (*arrows*) and posterior (*arrowheads*) pelvis located outside of the FOV. The overlap occurs in the opposite portion of the image, rather than in the correct anatomic position. *T* shows tumor position

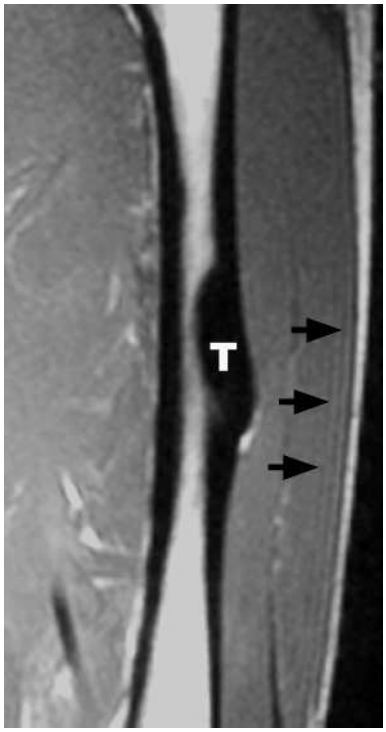

Fig. 3.15. Truncation artifact. Coronal T1-weighted SE image of the thigh demonstrates multiple alternating bands of bright and dark signal (*arrows*) that fade with increasing distance from the muscle–fat interface. Tumor (*T*) is partially visualized

the selected FOV. Unwanted signals from structures located outside the FOV are subsequently discarded during data processing. This phase-oversampling option does not otherwise affect overall image quality, but it does increase scan time. Use of a spatial saturation band can also reduce phase wrapping. The additional 90° RF pulses applied before the main imaging RF pulses saturate structures located outside the selected FOV, and a dephasing gradient is later used to cancel the signal from those structures.

3.3.6 Truncation Artifacts

Truncation artifacts, also called ring-down or Gibbs artifact, occur when the matrix size is smaller than needed to accurately represent an abrupt, high-contrast boundary between two structures at Fourier transform. Truncation artifacts appear as alternating bright and dark bands adjacent and parallel to a high-contrast tissue interface, such as the borders between cortical bone or muscle and surrounding fat (Fig. 3.15). These artifacts become less visible with increasing distance from the boundary that produced them. Truncation artifacts typically occur in the phase-encoding direction, because the imaging matrix is usually smaller in the phase-encoding than in the frequency-encoding direction (to shorten scan time). Increasing the number of phase-encoding steps or using a smaller FOV can minimize truncation artifacts.

3.4 Overview of MR Imaging in Bone Tumors

The specific features of various bone tumors are described in detail in subsequent chapters, as well as information about tumor staging, post-treatment assessment, and routine surveillance imaging. In the remainder of this chapter, some general strengths and limitations of MR imaging in the evaluation of bone tumors are presented.

3.4.1 Advantages of MR Imaging in Bone Tumors

One of the most important attributes of MR imaging is its unparalleled depiction of soft tissue contrast. For bone tumors, this translates into an opportunity to examine the composition and distribution of bone marrow in great detail, as well as the integrity of various related anatomic structures that previously could be evaluated only at surgery or pathologic examination. Differential diagnosis can often be refined beyond that obtained with radiographs alone, and, coupled with the multiplanar capabilities of MR imaging, the borders and location of a bone tumor and any associated muscular, joint, or neurovascular involvement can be delineated. Pretherapy planning is thus facilitated in ways that generally allow limb-salvage surgery to be performed in lieu of amputation, with at least comparable oncologic control. MR imaging also shows the effects of therapy and any complications that occur during or after therapy.

The lack of ionizing radiation at MR imaging is beneficial for all, but especially for pediatric and pregnant patients. The use of iodinated intravenous CT contrast material and its attendant risks are obviated.

Some specific tissue characteristics and findings at MR imaging of bone tumors are presented as examples of the contributions of MR imaging to the care of these patients.

3.4.1.1 Fluid

Fluid content is readily demonstrated at MR imaging and is a prime attribute in the detection and characterization of bone tumors. For example, enchondroma and intraosseous ganglion both have a very high water content, shown as low signal intensity on T1-weighted SE images and very high signal intensity (similar to that of water) on T2-weighted SE images. The presence of such fluid-like signal intensity within multiple small lobules comprising an intramedullary lesion is consistent with enchondroma (Fig. 3.16), whereas a more homogeneous lesion with similar signal intensity, but in a periarticular location within a weight-bearing bone, would be in keeping with an intraosseous ganglion. Lymphoma, in contrast, is much more cellular and has a lower water content, seen as low or mildly increased signal intensity on T2-weighted SE images.

Fluid collections are commonly present after surgical intervention and are readily distinguished from recurrent or residual tumor by the presence of only thin, peripheral enhancement and no internal enhancement on gadolinium-chelate-enhanced MR images.

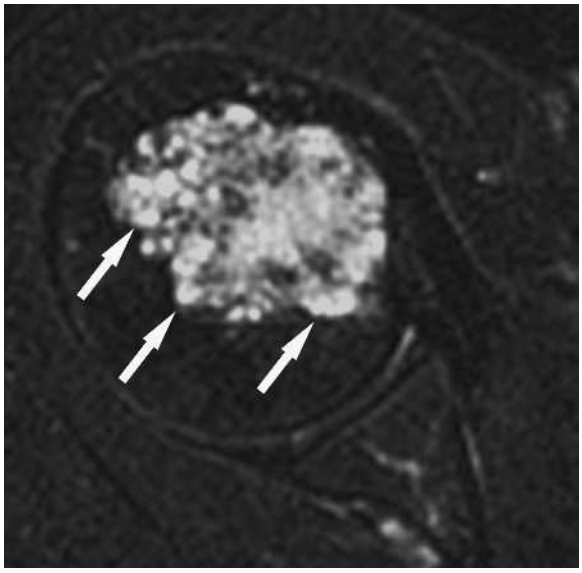

Fig. 3.16. Fluid-like intensity within enchondroma. Transverse T2-weighted SE image with fat suppression demonstrates a medullary lesion in humeral head consisting of multiple small chondroid lobules with very high signal intensity (*arrows*)

3.4.1.2 Fluid-fluid levels

Fluid-fluid levels demonstrated within a bone tumor at MR imaging usually represent blood-fluid levels, and are relatively nonspecific as a diagnostic finding (Van Dyck et al. 2006). Although most commonly seen in aneurysmal bone cyst, they also occur in (the much less common) telangiectatic osteosarcoma, as well as in various other lesions ranging from simple bone cyst to fibrous dysplasia and chondroblastoma (Fig. 3.17; Mahnken et al. 2003; Van Dyck et al. 2006); therefore, unless a bone lesion consists solely of blood-fluid levels (and is thus an aneurysmal bone cyst), the presence of some other, solid bone tumor must be assumed until proven otherwise.

3.4.1.3 Edema

The presence of extensive edema in the marrow around a bone lesion can be an important diagnostic aid, as some tumors (e.g., osteoid osteoma, osteoblastoma,

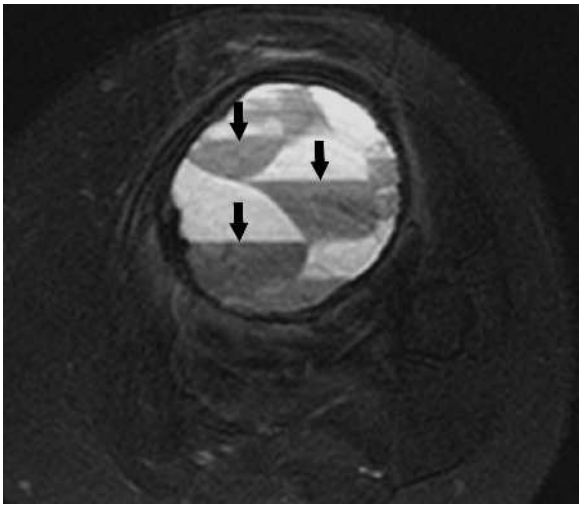

Fig. 3.17. Fluid-fluid levels in aneurysmal bone cyst. Transverse T2-weighted SE image with fat suppression demonstrates an expansile lesion consisting solely of multiple fluid-fluid levels (*arrows*) in proximal tibia. The rather low signal intensity of the dependent portions of the levels is compatible with old blood products

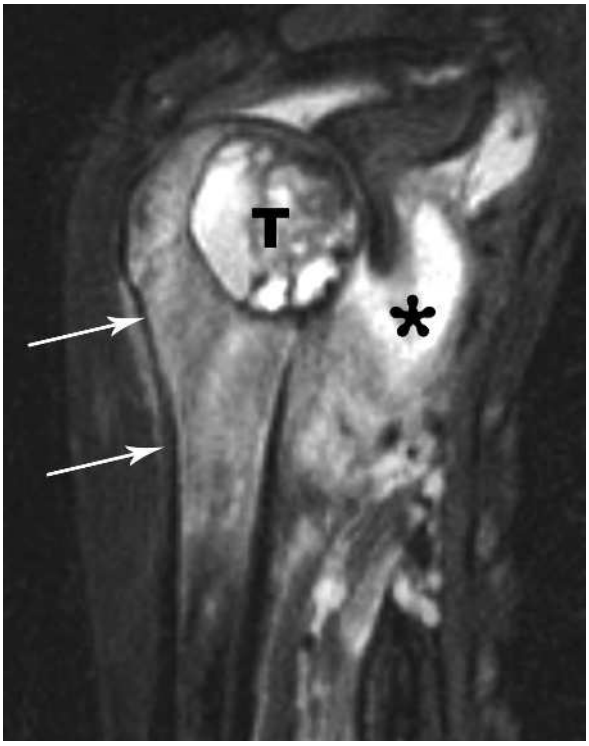

a

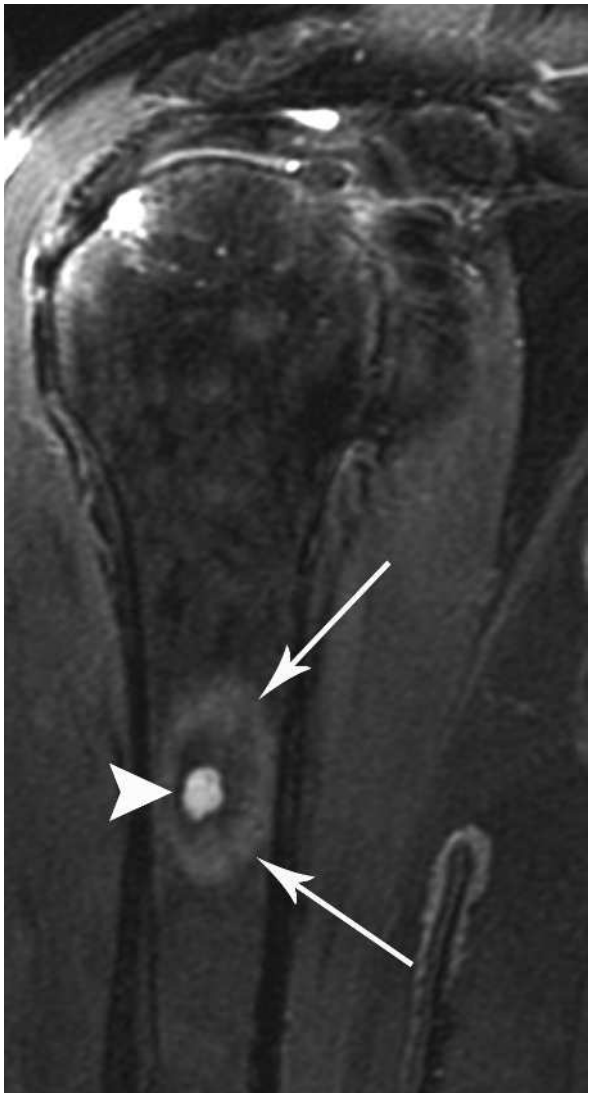

b

Fig. 3.18a,b. Edema around bone tumors. **a** Coronal T2-weighted SE image with fat suppression demonstrates a lesion (*T*) with high signal intensity in the humeral head. Bone marrow edema (*arrows*) throughout the proximal humerus is substantially larger in extent than the lesion (chondroblastoma) itself. Moderate joint effusion (*asterisk*) is present. **b** Coronal T2-weighted fast SE image with fat suppression demonstrates a small metastasis from thyroid cancer (*arrowhead*), surrounded by a halo of marrow edema (*arrows*)

chondroblastoma, and Langerhans cell histiocytosis) tend to have extensive surrounding marrow edema (Fig. 3.18a; James et al. 2008). Also, it has been reported that the greater the extent of marrow edema around a bone lesion, the more likely it is to be benign (James et al. 2006). Edema around a malignant bone tumor, however, constitutes the so-called reactive zone, which may contain viable tumor cells (Fig. 3.18b).

When present, marrow edema can lead to overestimation of the size of bone tumors on T2-weighted SE or STIR images (Fig. 3.1). In order to accurately assess the local extent of a tumor, assessment of T1-weighted SE and gadolinium-chelate-enhanced T1-weighted SE images with fat suppression can be helpful.

3.4.1.4 Hemorrhage

The MR imaging appearance of hemorrhage depends on the temporal evolution of blood products (Table 3.2; Bush 2000) and may be more complex than that of intracranial hemorrhage, depending on the size of the hemorrhage. In the acute stage of hemorrhage (<1 week), oxyhemoglobin is converted to deoxyhemoglobin, which causes T2 shortening due to local magnetic inhomogeneity. The signal on T2-weighted SE images is decreased, and susceptibility artifacts are evident at T2*-weighted GE imaging, without much change in T1-weighted signal. In the early subacute stage, deoxyhemoglobin is transformed into methemoglobin. Because its molecular structure is similar to that of gadolinium-chelate agents, methemoglobin shortens the T1 relaxation time, causing an increase in signal that is readily identifiable as a ring around the periphery of a hematoma on T1-weighted images (Fig. 3.19). Intracellular methemoglobin shortens the T2 relaxation time by causing local magnetic field inhomogeneity; the resultant signal on T2-weighted images is low. In the late subacute stage, methemoglobin becomes extracellular, where it no longer has much T2* effect; its signal on T2-weighted images is therefore increased. Finally, in the

Table 3.2. MR signal intensity of hemorrhage in different stages

	Acute (deoxyhemoglobin)	Subacute		Chronic (hemosiderin)
		Early (intracellular methemoglobin)	Late (extracellular methemoglobin)	
T1 signal intensity[a]	Isointense ●	Hyperintense ○	Hyperintense ○	Hypointense ●
T2 signal intensity[a]	Hypointense ●	Hypointense ●	Hyperintense ○	Hypointense ●

[a]Signal intensity relative to muscle

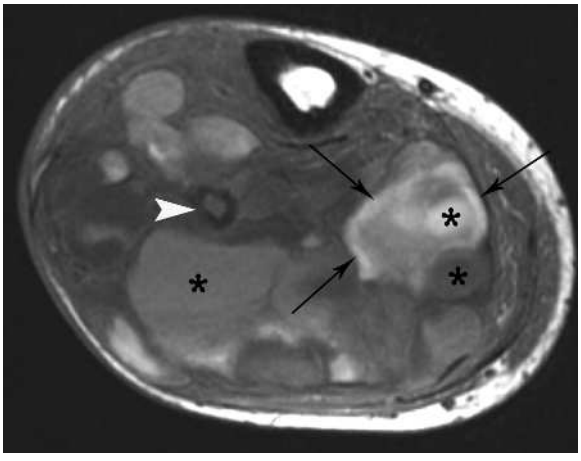

Fig. 3.19. Hemorrhage in different stages within fibular metastasis from cardiac atrial osteosarcoma. Transverse T1-weighted SE image of the calf demonstrates rims of high signal intensity (*arrows*) within portions of the extraosseous component of the fibular metastasis (*arrowhead*). Regions of intermediate to high signal intensities (*asterisk*) in extraosseous mass are due to different stages of hemorrhage

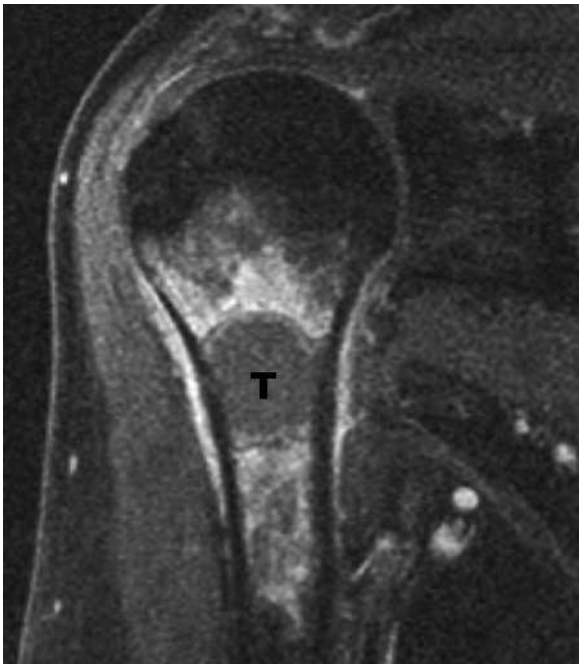

Fig. 3.20. Necrosis in poorly differentiated carcinoma in humerus. Coronal post-gadolinium-enhanced T1-weighted SE image with fat suppression demonstrates relatively little enhancement in tumor (*T*), and poorly defined enhancement in surrounding edematous region. Gross pathologic examination revealed extensive necrosis and hemorrhage

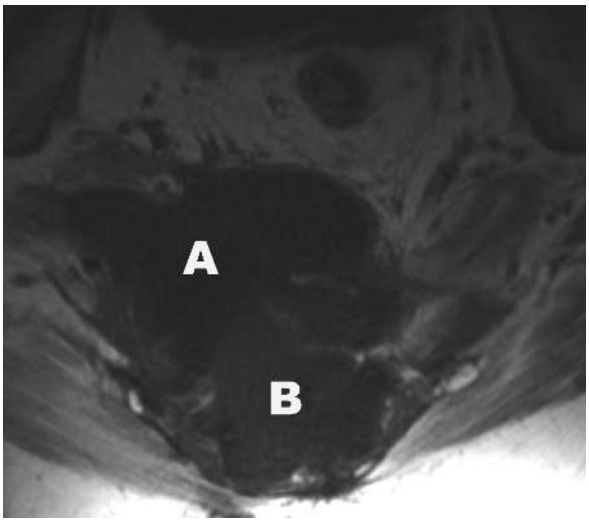

a

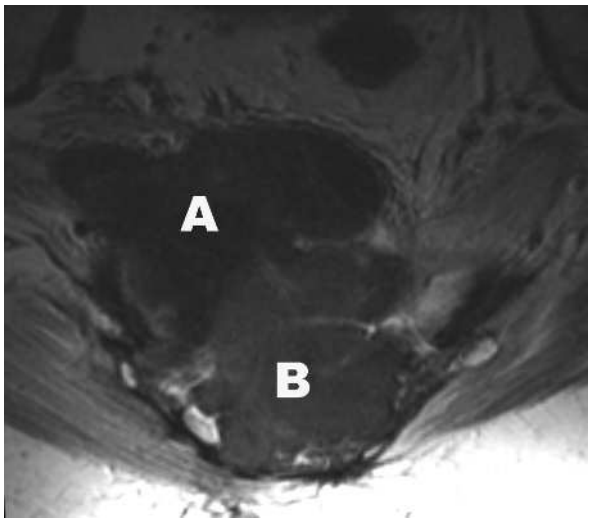

b

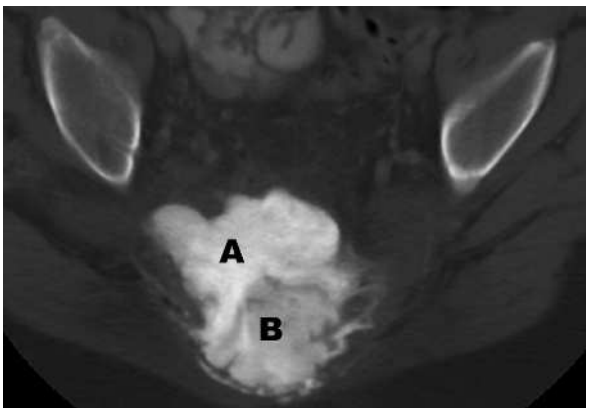

c

Fig. 3.21a–c. Limitations of MR imaging in demonstrating calcification. Transverse **a** T1-weighted and **b** T2-weighted SE images demonstrate lower signal intensity within the anterior portion (*A*) than within the posterior portion (*B*) of the sacral tumor. The cause of the low signal is not evident. **c** Transverse CT image readily reveals extensive ossification throughout the osteoblastoma, more pronounced in portion A than in B

chronic stage, methemoglobin is converted into hemosiderin, leading to low signal on both T1-weighted and T2-weighted sequences.

These findings can be useful, for example, when multiple small foci of subacute or chronic hemorrhage are demonstrated within a bone tumor; if in an appropriate (epiphyseal) location, the findings would lead to the diagnosis of giant cell tumor.

3.4.1.5 Necrosis

Recognizing the presence and location of necrotic regions within a bone tumor is important in order to prevent biopsy of those regions, thereby avoiding nondiagnostic specimens and a delay in diagnosis. Necrosis can also occur after therapy, and when extensive, can be a useful sign of response. An increase in the amount of gross necrosis is helpful in the qualitative clinical assessment of therapeutic response, even without the quantitative information provided with dynamic MR imaging (described in section 3.2.6.1). The most reliable indicator of necrosis at MR imaging is a lack of enhancement after intravenous administration of a gadolinium-chelate contrast material (Fig. 3.20). On noncontrast images, the MR imaging appearance of necrosis is usually heterogeneous, reflecting complex post-treatment changes. Liquefactive ("wet") necrosis can mimic a fluid collection on T2-weighted images, whereas coagulative ("dry") necrosis may appear as nonenhancing solid tissue. Occasionally, myxoid matrix within a bone tumor may resemble necrosis due to the high fluid content of both.

3.4.2 Limitations of MR Imaging in Bone Tumors

Despite its strengths, MR imaging of bone tumors has several limitations that need to be recognized, in addition to the well known, generic contraindications (relative or absolute) to MR imaging (e.g., cardiac pacemakers, intracranial aneurysm clips, and metallic foreign bodies in the globe). Also, severe renal failure or dialysis now must be added to that list of contraindications, as they are the critical risk factors for the recently described, rare but serious syndrome known as nephrogenic systemic fibrosis (Collidge et al. 2007; Shabana et al. 2008).

MR imaging is rather insensitive to the presence of calcifications or even gross ossification (Fig. 3.21), because calcium and bone cortex lack mobile hydrogen protons to contribute to the MR signal. Radiography and CT are important complementary techniques to evaluate suspected mineralized tumor matrix, cortical erosion or destruction, or bone formation.

MR imaging has limited ability to show tissues in the vicinity of metal, which can be a substantial issue after orthopedic surgery. Nevertheless, newer prostheses are composed of metal alloys that produce fewer susceptibility artifacts at MR imaging, and some new sequences are being developed that minimize metal-related artifacts (Chang et al. 2001). Important diagnostic information usually can be obtained except in the immediate vicinity of the prosthesis and other surgical hardware (Fig. 3.9), so MR imaging should not be summarily denied solely in anticipation of metal artifacts.

Despite improved software, coils, and pulse sequences, MR imaging scan time remains relatively long. This is especially problematic in pediatric patients and in those who cannot comply with the requirements of MR imaging, such as patients with claustrophobia or who are in pain. Patients with bone tumors are not infrequently uncooperative children or even infants, and a patient of any age with a bone tumor may find it uncomfortable to remain still within the magnet for long periods of time, despite the technologist's best efforts to make them as comfortable as possible. Enlisting the assistance of an anesthesiologist who is familiar with all the specific requirements of the MR imaging environment can be invaluable for enabling the successful scanning of these patients.

References

Baere T de, Vanel D, Shapeero LG, Charpentier A, Terrier P, Paola M di (1992) Osteosarcoma after chemotherapy: evaluation with contrast material-enhanced subtraction MR imaging. Radiology 185:587–592

Baur A, Reiser MF (2000) Diffusion-weighted imaging of the musculoskeletal system in humans. Skeletal Radiol 29:555–562

Bitar R, Leung G, Perng R, Tadros S, Moody AR, Sarrazin J, McGregor C, Christakis M, Symons S, Nelson A, Roberts TP (2006) MR pulse sequences: what every radiologist wants to know but is afraid to ask. RadioGraphics 26:513–537

Bush CH (2000) The magnetic resonance imaging of musculoskeletal hemorrhage. Skeletal Radiol 29:1–9

Chang SD, Lee MJ, Munk PL, Janzen DL, MacKay A, Xiang QS (2001) MRI of spinal hardware: comparison of conventional T1-weighted sequence with a new metal artifact reduction sequence. Skeletal Radiol 30:213–218

Collidge TA, Thomson PC, Mark PB, Traynor JP, Jardine AG, Morris ST, Simpson K, Roditi GH (2007) Gadolinium-enhanced MR imaging and nephrogenic systemic fibrosis: retrospective study of a renal replacement therapy cohort. Radiology 245:168–175

Delfaut EM, Beltran J, Johnson G, Rousseau J, Marchandise X, Cotten A (1999) Fat suppression in MR imaging: techniques and pitfalls. RadioGraphics 19:373–382

Dick BW, Mitchell DG, Burk DL, Levy DW, Vinitski S, Rifkin M (1988) The effect of chemical shift misrepresentation on cortical bone thickness on MR imaging. Am J Roentgenol 151:537–538

Dyke JP, Panicek DM, Healey JH, Meyers PA, Huvos AG, Schwartz LH, Thaler HT, Tofts PS, Gorlick R, Koutcher JA, Ballon D (2003) Osteogenic and Ewing sarcomas: estimation of necrotic fraction during induction chemotherapy with dynamic contrast-enhanced MR imaging. Radiology 228:271–278

Eustace S, Goldberg R, Williamson D, Melhem ER, Oladipo O, Yucel EK, Jara H (1997) MR imaging of soft tissues adjacent to orthopaedic hardware: techniques to minimize susceptibility artefact. Clin Radiol 52:589–594

Fayad LM, Bluemke DA, McCarthy EF, Weber KL, Barker PB, Jacobs MA (2006) Musculoskeletal tumors: use of proton MR spectroscopic imaging for characterization. J Magn Reson Imaging 23:23–28

Fayad LM, Barker PB, Jacobs MA, Eng J, Weber KL, Kulesza P, Bluemke DA (2007) Characterization of musculoskeletal lesions on 3-T proton MR spectroscopy. Am J Roentgenol 188:1513–1520

Feydy A, Anract P, Tomeno B, Chevrot A, Drapé J-L (2006) Assessment of vascular invasion by musculoskeletal tumors of the limbs: use of contrast-enhanced MR angiography. Radiology 238:611–621

Gold GE, Han E, Stainsby J, Wright G, Brittain J, Beaulieu C (2004) Musculoskeletal MRI at 3.0 T: relaxation times and image contrast. Am J Roentgenol 183:343–351

Hayashida Y, Yakushiji T, Awai K, Katahira K, Nakayama Y, Shimomura O, Kitajima M, Hirai T, Yamashita Y, Mizuta H (2006) Monitoring therapeutic responses of primary bone tumors by diffusion-weighted image: initial results. Eur Radiol 16:2637–2643

Hwang S, Panicek DM (2007a) Magnetic resonance imaging of bone marrow in oncology, part 1. Skeletal Radiol 36:913–920

Hwang S, Panicek DM (2007b) Magnetic resonance imaging of bone marrow in oncology, part 2. Skeletal Radiol 36:1017–1027

James SL, Hughes RJ, Ali KE, Saifuddin A (2006) MRI of bone marrow oedema associated with focal bone lesions. Clin Radiol 61:1003–1009

James SL, Panicek DM, Davies AM (2008) Bone marrow oedema associated with benign and malignant bone tumours. Eur J Radiol 67:11–21

Ladd ME (2007) High-field-strength magnetic resonance: potential and limits. Top Magn Reson Imaging 18:139–152

Mahnken AH, Nolte-Ernsting CC, Wildberger JE, Heussen N, Adam G, Wirtz DC, Piroth W, Bücker A, Biesterfeld S, Haage P, Günther RW (2003) Aneurysmal bone cyst: value of MR imaging and conventional radiography. Eur Radiol 13:1118–1124

Meyers PA, Gorlick R, Heller G, Casper E, Lane J, Huvos AG, Healey JH (1998) Intensification of preoperative chemotherapy for osteogenic sarcoma: results of the Memorial Sloan-Kettering (T12) protocol. J Clin Oncol 16:2452–2458

Mirowitz SA, Apicella P, Reinus WR, Hammerman AM (1994) MR imaging of bone marrow lesions: relative conspicuousness on T1-weighted, fat-suppressed T2-weighted, and STIR images. Am J Roentgenol 162:215–221

Petersilge CA, Lewin JS, Duerk JL, Yoo JU, Ghaneyem AJ (1996) Optimizing imaging parameters for MR evaluation of the spine with titanium pedicle screws. Am J Roentgenol 166:1213–1218

Sah PL, Sharma R, Kandpal H, Seith A, Rastogi S, Bandhu S, Jagannathan NR (2008) In vivo proton spectroscopy of giant cell tumor of the bone. Am J Roentgenol 190:W133–W139

Shabana WM, Cohan RH, Ellis JH, Hussain HK, Francis IR, Su LD, Mukherji SK, Swartz RD (2008) Nephrogenic systemic fibrosis: a report of 29 cases. Am J Roentgenol 190:736–741

Shuman WP, Patten RM, Baron RL, Liddell RM, Conrad EU, Richardson ML (1991) Comparison of STIR and spin-echo MR imaging at 1.5 T in 45 suspected extremity tumors: lesion conspicuity and extent. Radiology 179:247–252

Simpfendorfer CS, Ilaslan H, Davies AM, James SL, Obuchowski NA, Sundaram M (2008) Does the presence of focal normal marrow fat signal within a tumor on MRI exclude malignancy? An analysis of 184 histologically proven tumors of the pelvic and appendicular skeleton. Skeletal Radiol 37:797–804, 10.1007/s00256-008-0523-7

Suh JS, Jeong EK, Shin KH, Cho JH, JB Na, Kim DK, Han CD (1998) Minimizing artifacts caused by metallic implants at MR imaging: experimental and clinical studies. Am J Roentgenol 171:1207–1213

Van Dyck P, Vanhoenacker FM, Vogel J, Venstermans C, Kroon HM, Gielen J, Parizel PM, Bloem JL, De Schepper AM (2006) Prevalence, extension and characteristics of fluid-fluid levels in bone and soft tissue tumors. Eur Radiol 16:2644–2651

Vanel D, Bittoun J, Tardivon A (1998) MRI of bone metastases. Eur Radiol 8:1345–1351

Wang CK, Li CW, Hsieh TJ, Chien SH, Liu GC, Tsai KB (2004) Characterization of bone and soft-tissue tumors with in vivo 1H MR spectroscopy: initial results. Radiology 232:599–605

Zhuo J, Gullapalli RP (2006) MR artifacts, safety, and quality control. RadioGraphics 26:275–297

Nuclear Medicine

4

Ruth A. R. Green

CONTENTS

KEY POINTS

^{99m}Technechium labelled methylene diphosphonate (^{99m}Tc-MDP) bone scan:

- Detects bone metabolism
- Is a non-specific imaging modality
- Remains one of the primary investigations in the evaluation of bone malignancy
- May show patterns of disease or disease distribution which may help to confirm a diagnosis
- Should always be viewed in conjunction with other imaging modalities

Positron emission tomography (PET) in combination with CT (PET/CT):

- Has an undefined role in the management of bone sarcoma
- The primary lesion must be avid for ^{18}Florine labelled floro-2-deoxy-d-glucose (FDG) or other radiopharmaceutical for the application of this modality
- Knowledge of the limitations and normal variants is necessary in order to avoid false positive results
- Sufficient time delay is necessary between imaging and previous surgery or radiotherapy to differentiate between recurrence and inflammatory reaction
- May have a future role in demonstrating response to therapy and as a prognostic indicator in the management of bone sarcoma

R. A. R. Green, MBBS, MRCP, FRCR
Consultant Radiologist, Royal National Orthopaedic Hospital, Radiology Department, Brockley Hill, Stanmore, Middlesex, HA7 4LP, UK

4.1 Introduction

Nuclear medicine scanning for imaging bone pathology is sensitive to detecting changes in bone metabolism; although non-specific in diagnosing pathology. There are several radiopharmaceuticals that have been used to image bone and bone malignancy, e.g. ^{67}Ga-citrate, ^{201}Tl-choloride and ^{99m}Tc-MIBI (2-methyoxy-isobutyl-isonitrile). This chapter, however, will focus on the use of the more commonly used radiopharmaceutical in relation to bone scintigraphy: Technetium labelled methylene diphosphonate (^{99m}Tc-MDP).

The evidence base for the application of positron emission tomography (PET) in combination with CT (PET/CT) using ^{18}F-labelled floro-2-deoxy-D-glucose (FDG) in the management of primary bone tumour will be discussed; together with the use of the more bone specific radiopharmaceutical, ^{18}F-labelled fluoride (^{18}F-fluoride). ^{18}F-3-fluoro-3-deoxy-L-thymidine (FLT) application and limitations will also be discussed.

4.2 ^{99}Tc MDP Bone Scan

4.2.1 Principles and Technique of ^{99m}Tc-MDP Bone Scan

Methylene diphosphonate is a phosphate analogue which is labelled with technetium to form ^{99m}Tc-MDP and has a half life of 6 h. The uptake by bone depends on the metabolism of phosphates which are absorbed by bone and incorporated into the crystalline lattice and collagen matrix (Subramanian et al. 1972; Subramanian and McAfee 1971). The uptake of this radiopharmaceutical is related to a number of factors including: blood supply, rate of bone turnover or osteoblastic activity, quantity of mineralised bone, capillary permeability, fluid pressure in bone and local acid/base balance (Rosenthall and Kaye 1975; Kaye et al. 1975; Charkes 1980).

Intravenous injection of 350–750 MBq of ^{99m}Tc-MDP depending on body weight is an effective dose equivalent of 3.2 mSv. Of the dose, 50%–60% will be taken up by bone and soft tissue, the rest excreted by the kidneys. By 3–4 h post-injection in a well hydrated patient, a high enough bone to background ratio will be achieved to enable satisfactory static delayed phase imaging using a gamma camera (Robinson 1992; Smith 1998). Early dynamic vascular phase and/or blood pool phase imaging may be carried out in certain circumstances to evaluate the vascularity of a lesion, e.g. osteoid osteoma (Fig. 4.1).

Single photon emission computed tomography (SPECT), may also be carried out on delayed imaging to obtain spatial information (Fig. 4.2) and hence improve the sensitivity of the bone scan. This may be particularly helpful where there is significant bone overlap, e.g. in the spine, where if uptake is found in the pedicle, there is a high probability that this represents malignancy, compared to uptake seen in the vertebral body or spinous process where no such differentiation can be made (Reinartz et al. 2000).

4.2.2 Application and Interpretation of the Bone Scan

In evaluating a bone lesion, one of the first steps is to determine if it is a solitary lesion or if there are multiple bone lesions. From this and the radiographic appearance, a decision as to whether the lesion represents a primary bone tumour or metastatic disease can often be made.

If multiple lesions exist, the bone scan may demonstrate a characteristic distribution of the abnormality that could indicate a skeletal dysplasia or metabolic bone disorder (Hain and Fogelman 2002) rather than metastatic disease, e.g. fibrous dysplasia, Paget's disease, osteomalacia, osteoporosis or chronic recurrent multifocal osteomyelitis (CRMO) (Fig. 4.3).

Characteristic features of metastatic bone disease are multiple areas of asymmetric increased uptake, in particular the sternum, scapula and ribs (Ryan and Fogelman 1995). The ribs are difficult to evaluate on most imaging modalities, but on the bone scan are well demonstrated; the uptake is often elongated along the rib in metastatic disease rather then focal as in a rib fracture (Fig. 4.3a,c). Bone scintigraphy in detecting metastases, for example in breast cancer, has been shown to have a sensitivity and specificity of 98% and 95%, respectively; positive and negative predictive values were 73% and 100% respectively with an accuracy of 96% (Crippa et al. 1993) (Fig. 4.4). However, the sensitivity and specificity depends on the type of metastasis, bone scanning being less sensitive in detecting lytic lesions, although there is often adjacent reactive change which will show uptake of isotope (Fig. 4.2a,d).

The pattern and distribution of uptake of isotope in bone lesions may be characteristic of certain bone pathology. This is particularly evident in Paget's disease

a

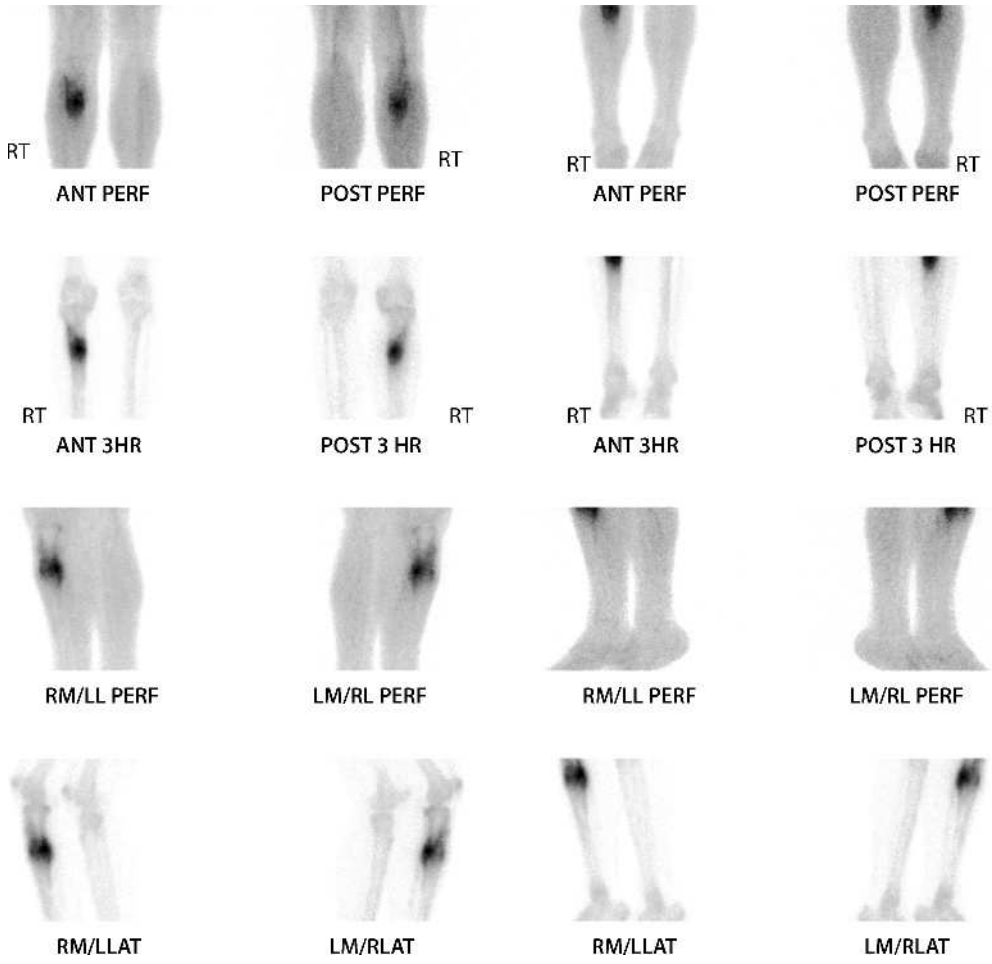

b

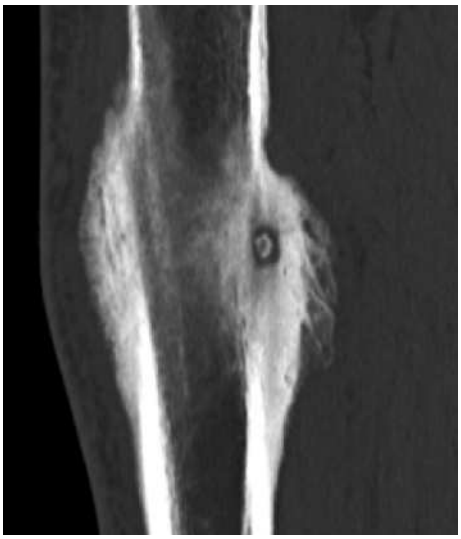

Fig. 4.1a,b. Osteoid osteoma. **a** Two phase scintigram demonstrates the intense uptake of the vascular nidus and the "double density" sign on the delayed images. **b** CT sagittal MPR demonstrates the calcified nidus and surrounding reactive sclerosis and periosteal reaction

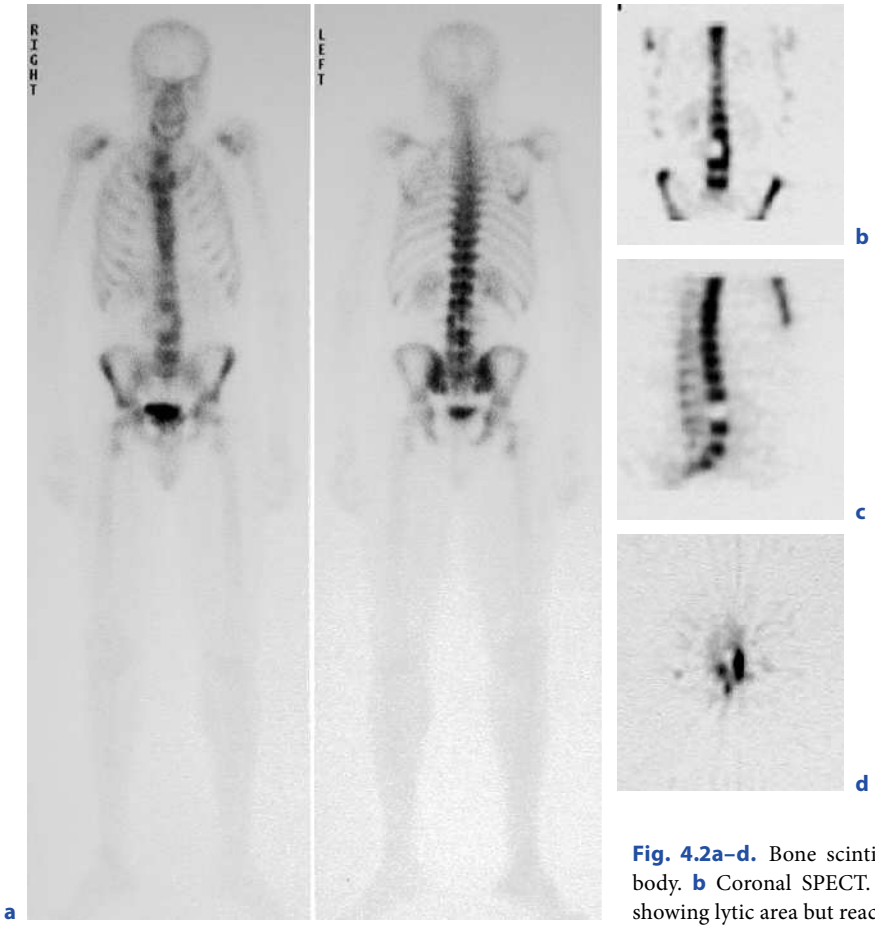

Fig. 4.2a–d. Bone scintigram of lytic metastasis. **a** Whole body. **b** Coronal SPECT. **c** Sagittal SPECT. **d** Axial SPECT showing lytic area but reactive high uptake in the pedicle

(Serafini 1976), where the uptake may eventually involve the whole bone, in a long bone starting from the articular surface and extending into the shaft with well defined flame shaped leading edge. The abnormality being very vascular will be demonstrated in early phase imaging, with intense uptake on delayed imaging. Skull involvement of osteoporosis circumscripta distribution and intense leading edge activity will also be demonstrated. Correlation with other imaging would be necessary to confirm the diagnosis, particularly when uptake has been altered by treatment, becoming less intense and non-uniform and where there may be clinical suspicion of malignant change (Fig. 4.5).

In CRMO, a typical presentation may be at the medial end of the clavicle. Further lesions may be demonstrated by the bone scan, where distal femur and proximal tibiae are frequently involved (Mandell et al. 1998). The metaphyseal area is a common site for CRMO or any infection. In a growing skeleton the metaphysis and physis can be difficult areas to evaluate due to the high metabolic turnover; therefore, evaluation for asymmetry with reference to an atlas of normal uptake for the age of the patient should be made (Gordon et al. 1993) to try to avoid misinterpretation of the bone scan (Fig. 4.6).

4.2.3 ^{99}Tc MDP Bone Scan and Benign Bone Tumour and Tumour-like Lesions

Benign bone tumours and tumour-like lesions describe a number of lesions of different cell type, the majority of which show some degree of uptake of isotope on bone scintigraphy. Although these lesions demonstrate metabolic activity, the investigation is often non-specific in making a diagnosis. SPECT may be used where structures are overlapping, e.g. the skull, pelvis and spine (Reinartz et al. 2000).

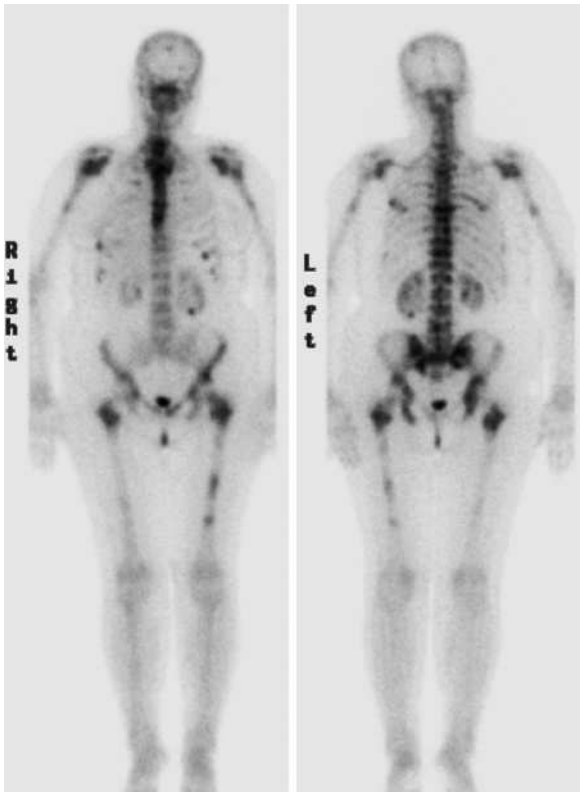

a

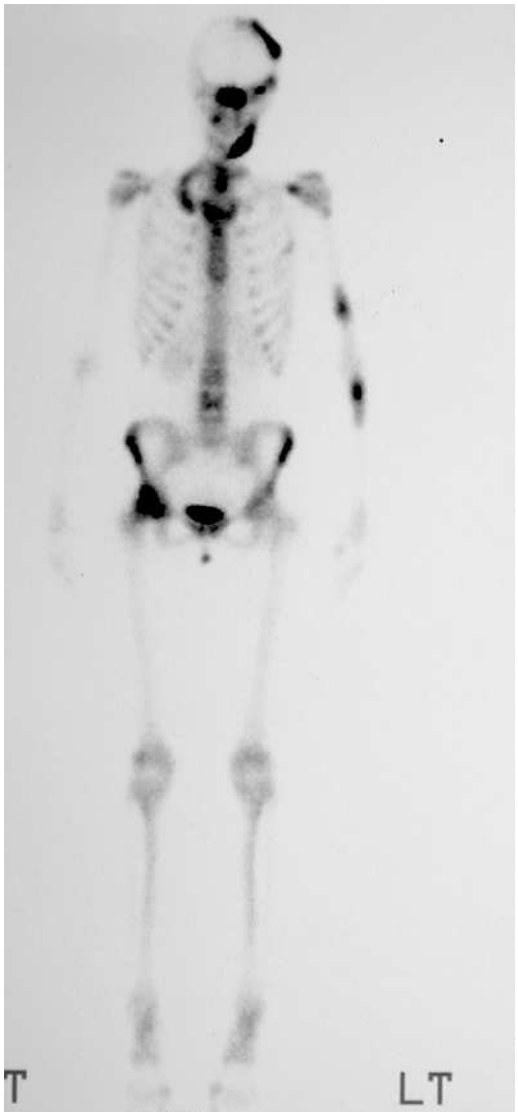

b

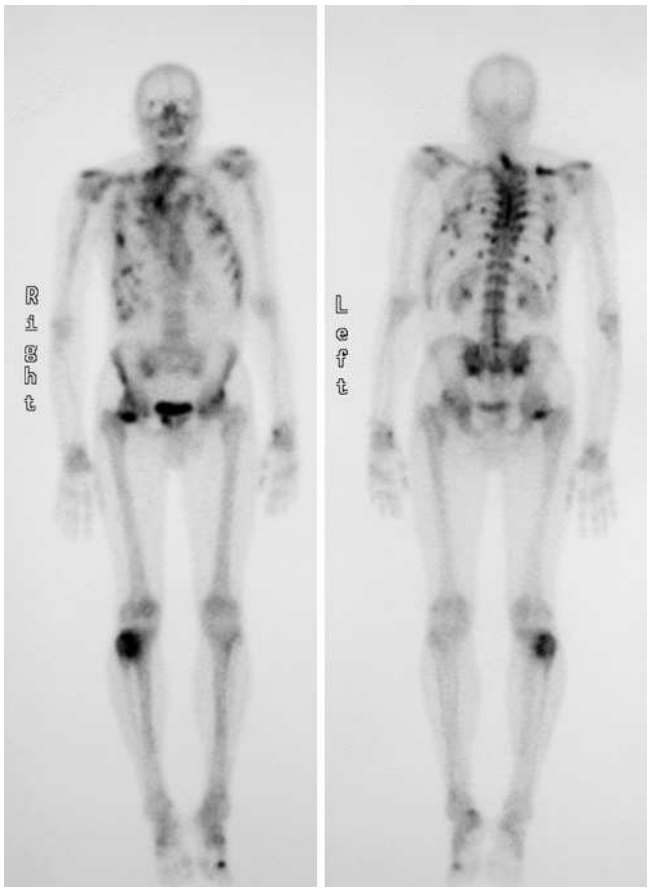

c

Fig. 4.3a–c. Bone scintigram. **a** Metastases. **b** Polyostotic fibrous dysplasia. **c** Hypophosphataemic tumour induced osteomalacia with high uptake of isotope in right fibula at the site of sarcoma, Looser's zone in the right neck of femur and right scapula with multiple rib fractures

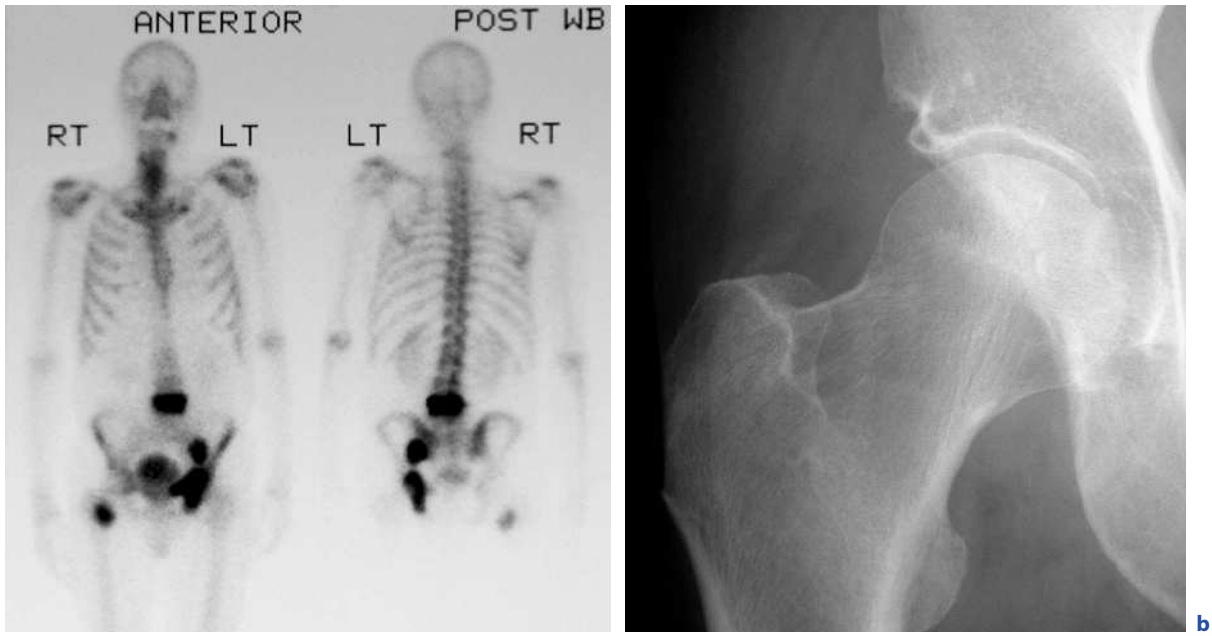

a b

Fig. 4.4. **a** Prostatic metastases shown on scintigram, most were sclerotic on radiographs however the right hip metastasis was more easily on scintigram than on the radiograph. **b** Radiograph of right hip

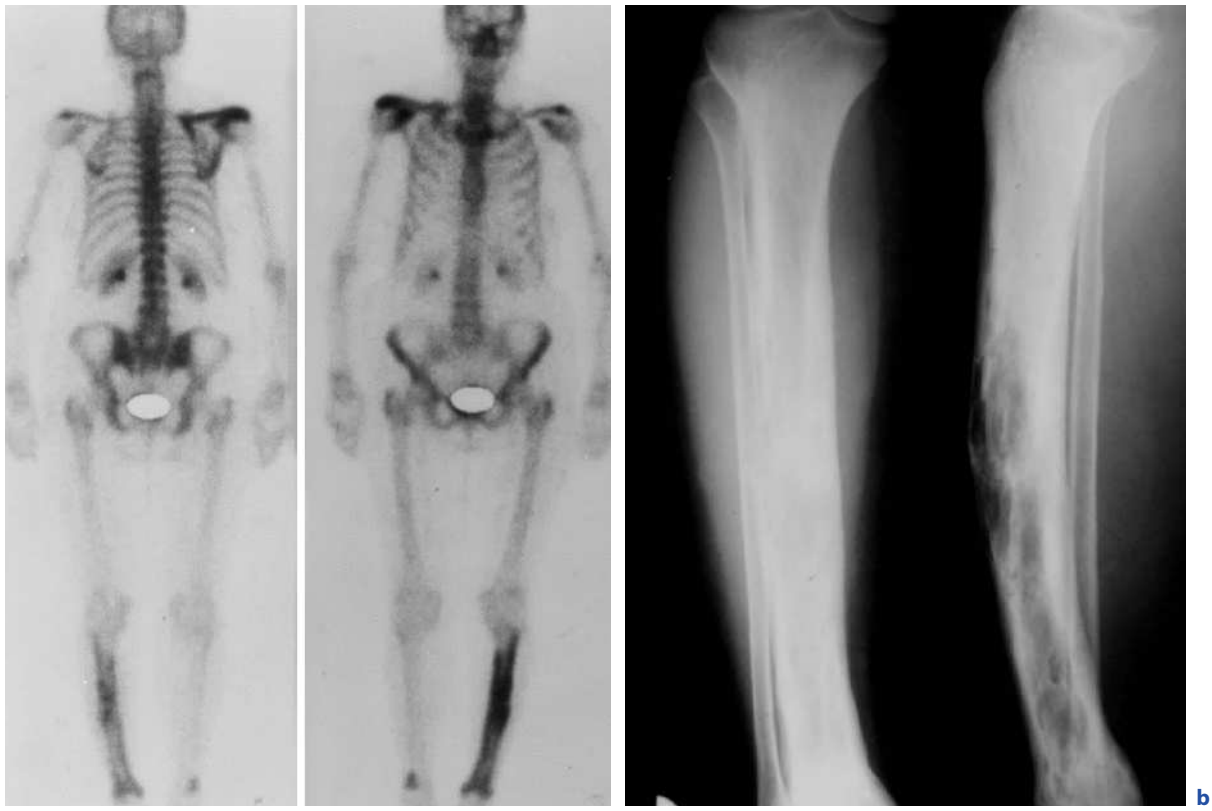

a b

Fig. 4.5. **a** Bone scintigram of Paget's disease shows intense uptake in relation to right scapula, right distal tibia, left tibia shows typical uptake extending from the tibial plafond involving almost the whole bone, non-uniform uptake in the mid shaft could be secondary to bisphosphonate treatment or sarcoma. **b** Radiograph of right tibia. (**c**) *see next page*

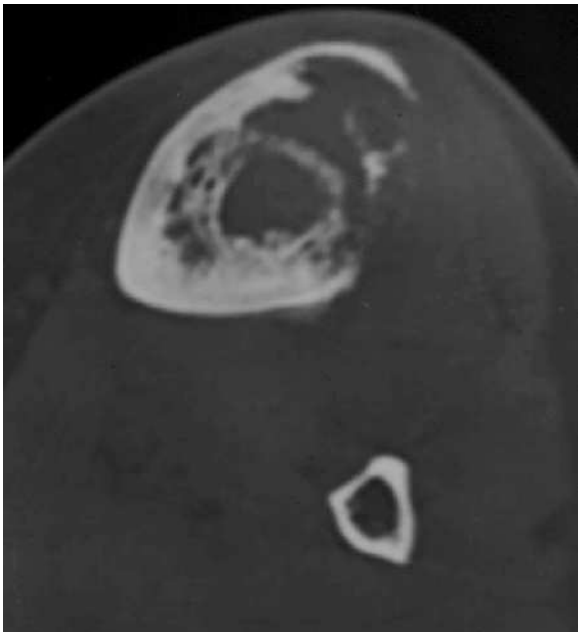

c

Fig. 4.5. (*continued*) **c** CT scan shows destruction of tibia and associated soft tissue mass of sarcoma

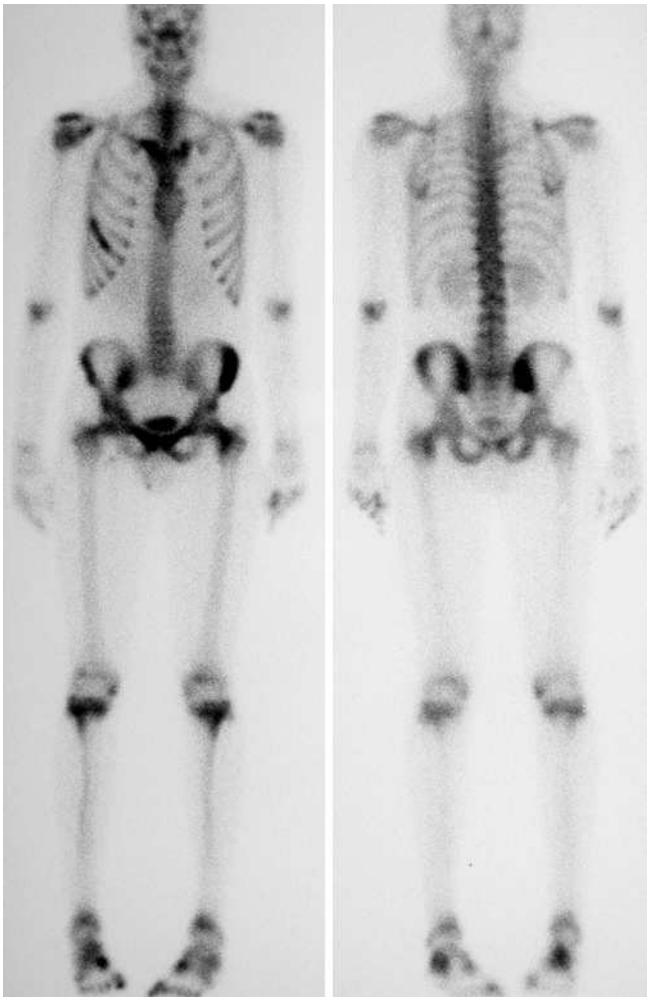

a

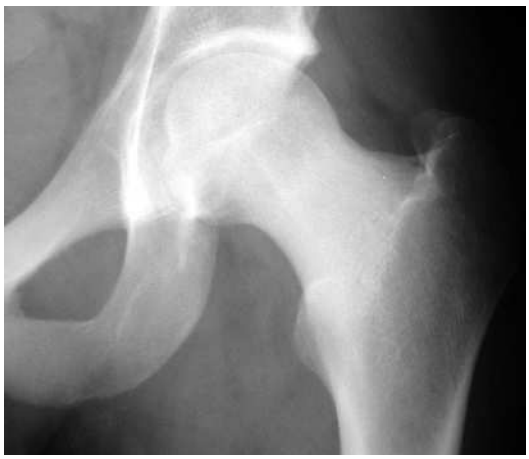

b

Fig. 4.6. **a** Bone scintigram of CRMO with high uptake in the medial end of right clavicle, right rib, left ilium and right sacroiliac joint, left femoral neck, right metatarsal. **b** Radiograph of sclerotic left neck of femur

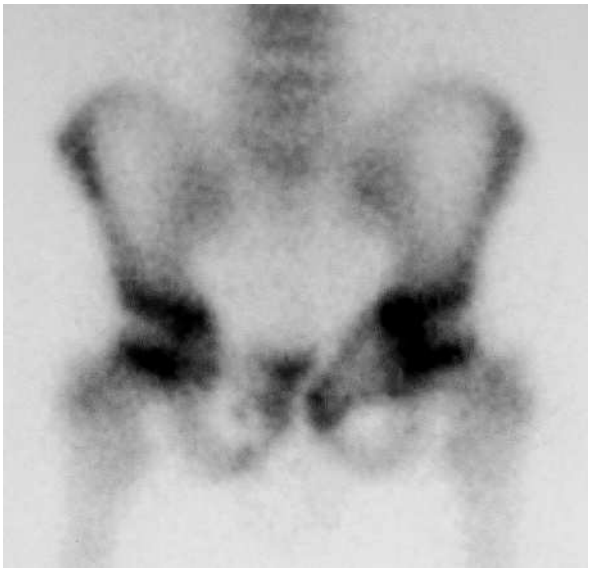

a

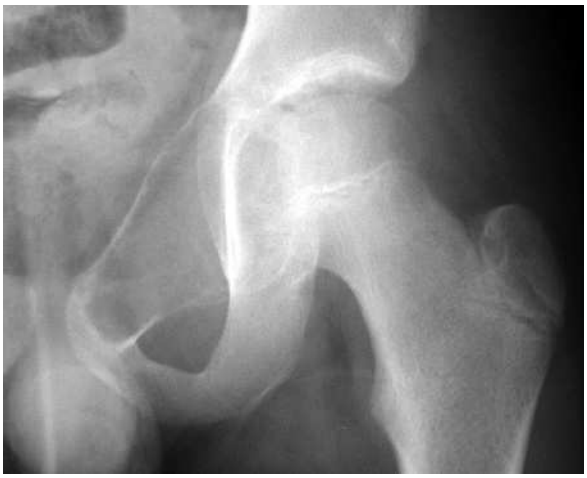

b

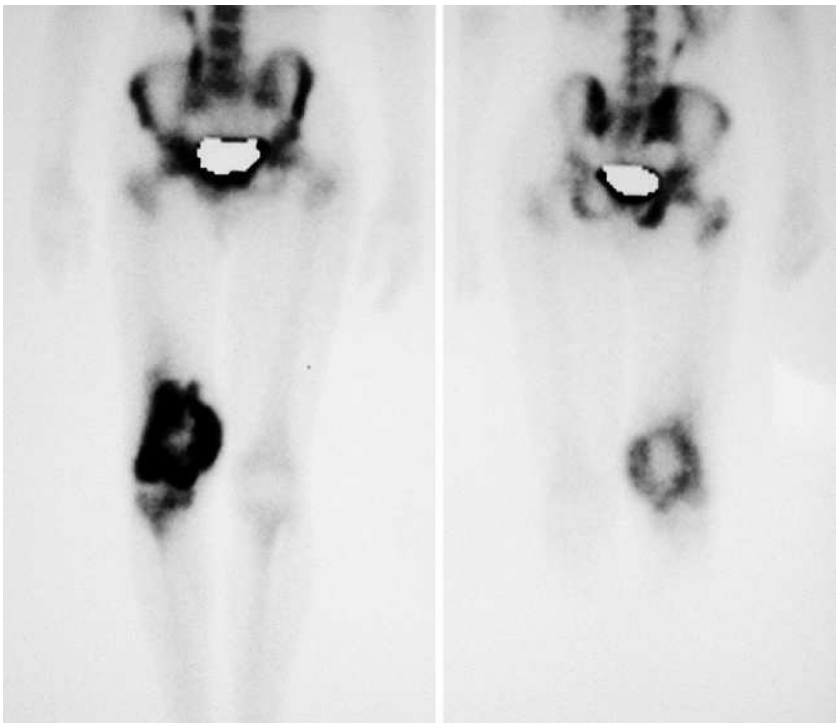

c

Fig. 4.7. **a** Aneurysmal bone cyst scintigram. **b** Aneurysmal bone cyst radiograph. **c** Telangiectatic osteosarcoma scintigram. (**d,e,f**) *see next page*

Where a lesion is cystic there may be a rim of activity with central photopenia; this is termed a "doughnut sign" (Fig. 4.7) and maybe seen in a number of lesions, e.g.: aneurismal bone cyst (ABC), giant cell tumour (GCT) which may have ABC change within, or simple bone cyst (SBC). However, the doughnut sign is nonspecific and can also be present in chondrosarcoma or telangiectatic osteosarcoma which can resemble an ABC on a radiograph. Any lesion that shows ABC change within, such as fibrous dysplasia, can also have this sign. An SBC will have less activity in the rim as compared to an ABC and will not show as much uptake in early phase imaging unless there has been fracture. The clinical presentation and radiographs of these lesions are often more helpful in making the diagnosis than the bone scan (Wang et al. 2005).

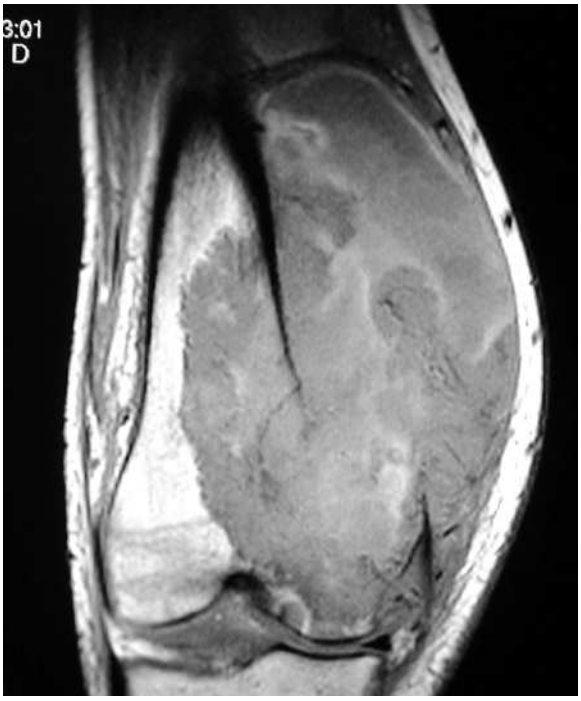

d

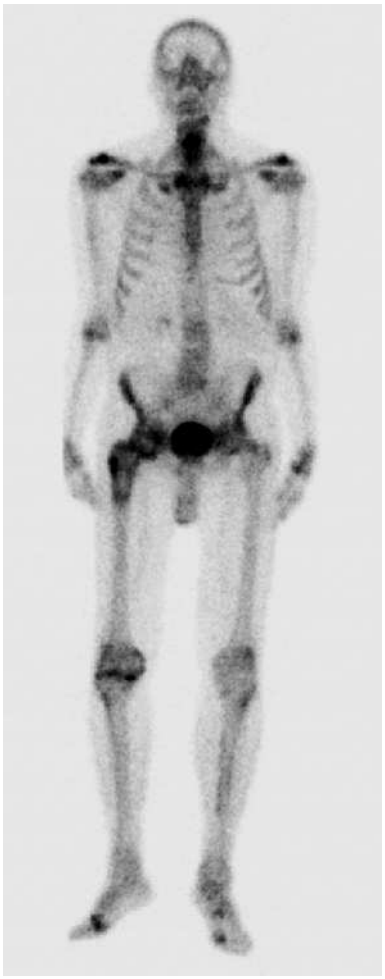

e

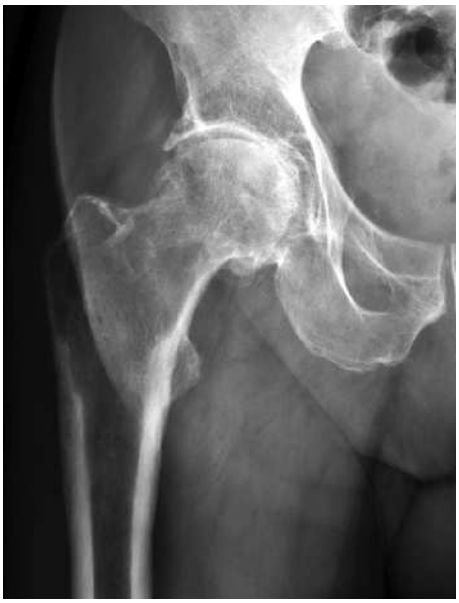

f

Fig. 4.7. (*continued*) **d** Telangiectatic osteosarcoma MRI, coronal T1. **e** Chondrosarcoma scintigram. **f** Chondrosarcoma radiograph. All these lesions show a rim of varying degrees of increased uptake of isotope, the "doughnut" sign, indicating the non-specific nature of the sign

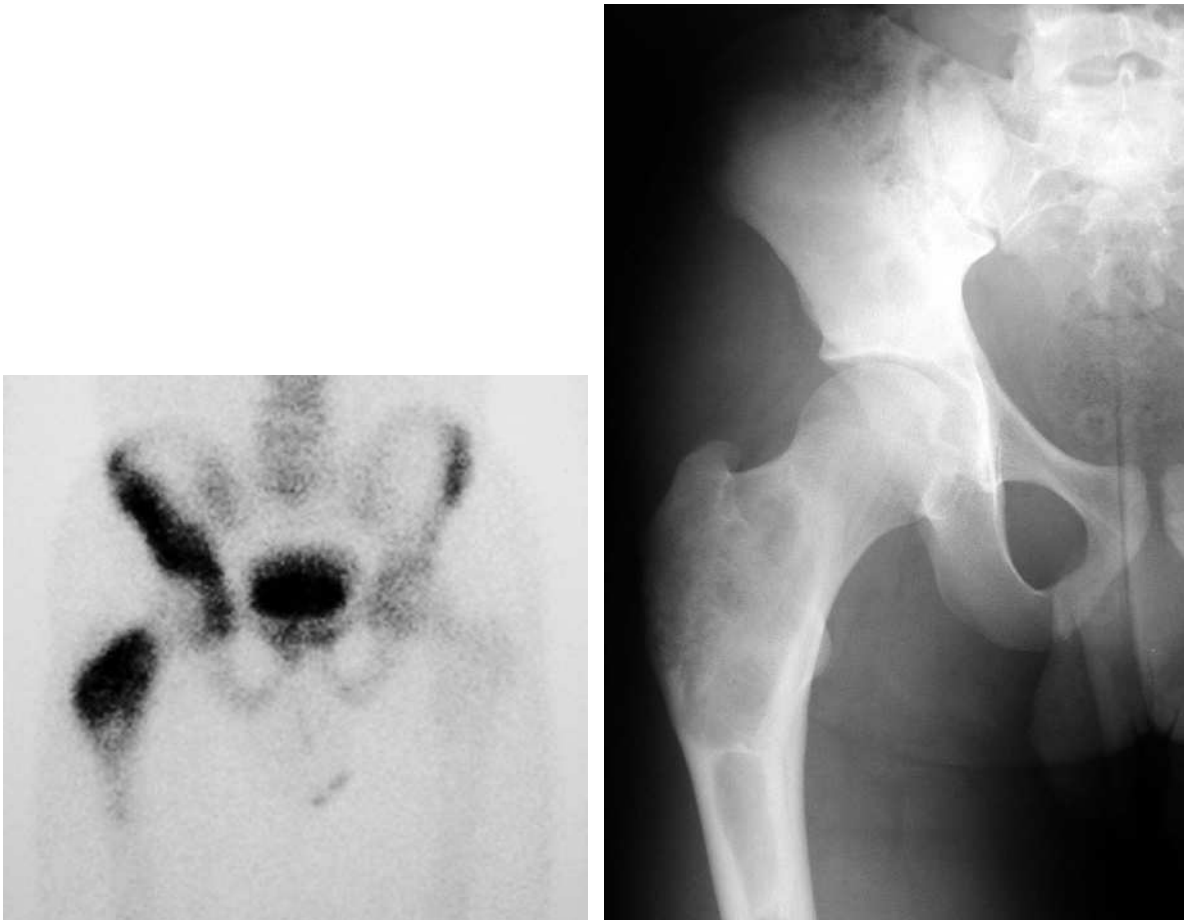

a b

Fig. 4.8a–d. Fibrous dysplasia. **a** Scintigram of polyostotic disease with high uptake in the ilium, but mixed uptake with "doughnut" sign in right femur. **b** Radiograph correlation with area of sclerosis in ilium and characteristic ground glass bone matrix of lytic lesion in the femur. (**c**,**d**) *see next page*

Fibrous dysplasia may be mono- or polyostotic. Lesions will generally show uptake in all three phases of the bone scan, which is often intense on delayed images. The bone scan helps to demonstrate the polyostotic nature of the condition with distribution of lesions in skull, ribs, limbs and spine (Fig. 4.3b) (Zhibin et al. 2004). Some lesions may show aneurismal change with a "doughnut sign". However, as the skeleton matures or the lesion is shown to have ground glass density on a radiograph or CT, or where there has been bone infarction, there may be less or very little uptake on the bone scan (Machida et al. 1986; Han et al. 2000) (Fig. 4.8).

Nonossifying fibroma or fibrocortical defect which has a characteristic appearance on a radiograph of a cortically based lytic lesion, with thin sclerotic margin, can show mild uptake on bone scan with more intense uptake during the healing sclerotic phase due to osteoblastic activity (Fig. 4.9).

Giant cell tumour, which is a lytic expansile lesion with non-sclerotic margin, found adjacent to the joint line or apophyses in mature skeleton will show uptake on all three phases of a bone scan, and may show a "doughnut sign". It is rarely multicentric, which would justify evaluation with bone scanning (Fig. 4.10).

Eosinophilic granuloma may be solitary or multiple. It is the benign form of the spectrum of disease that is Langerhan's cell histiocytosis. These lesions can have variable appearance on radiographs at presentation and hence show variable uptake on bone scan. Depending on the associated adjacent reactive change, the bone scan may show uptake but is sometimes photopaenic at the site of the lesion (Siddiqui et al. 1981; Wang et al.

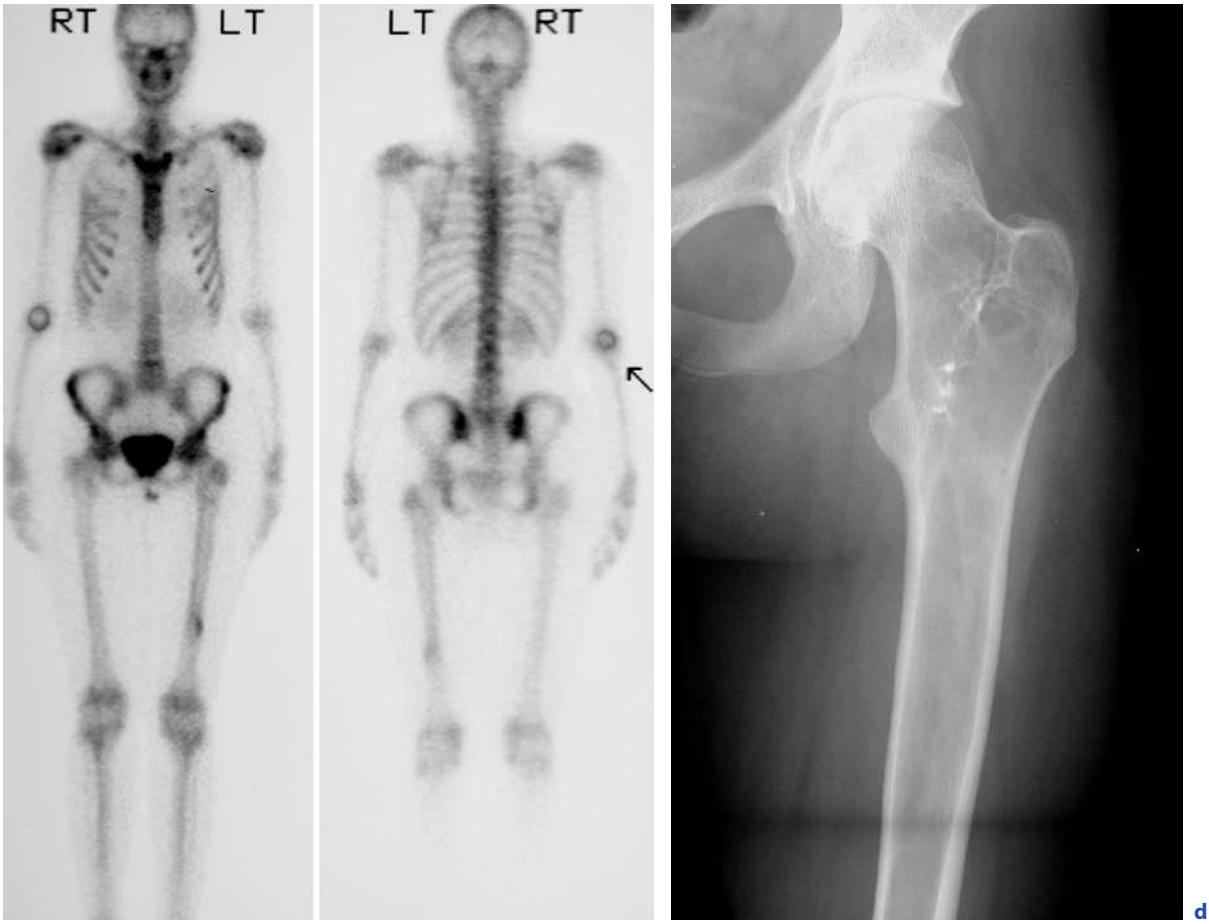

c d

Fig. 4.8a–d. (*continued*) **c** Scintigram of whole body but minimal uptake in left femur at the site fibrous dysplasia shown on the radiograph (**d**)

2005). The bone scan may be less sensitive than the radiograph but where radiographs are equivocal can be complementary in detecting lesions (Fig. 4.11).

Enchondroma – whether solitary or multiple as in the dysplasias of Ollier's disease or Maffucci syndrome – will show little if any uptake on early phase bone scans but, depending on the amount of matrix mineralisation, will show some uptake on delayed imaging. The presence of multiple lesions and their distribution can be demonstrated by the bone scan. A change in the metabolic activity of a lesion and correlation with clinical presentation and other imaging modalities may indicate malignant change (Gruning and Franke 1999; Trikha et al. 2003) (Fig. 4.12).

Exostoses, whether solitary or associated with diaphyseal aclasis or hereditary multiple exostoses, may show uptake on early phases of the bone scan due to adjacent inflammatory soft tissue uptake or the presence of bursa, as well as in an immature skeleton, in relation to the lesion itself. Delayed imaging of exostoses in an immature skeleton will show uptake; however this will be reduced with maturation of the skeleton and fusion of epiphyses. Uptake of isotope however has been observed in exostoses in mature skeleton whether actively growing or with malignant change (Epstein and Levin 1978) (Fig. 4.13).

Osteoid osteoma and osteoblastoma are benign osteoblastic rich tumours. They have a vascular nidus which can become calcified and hence appear dense on imaging. In osteoid osteoma, if the nidus is in cortical bone, reactive sclerosis occurs; however, if the nidus is in cancellous bone or within a joint where periosteum

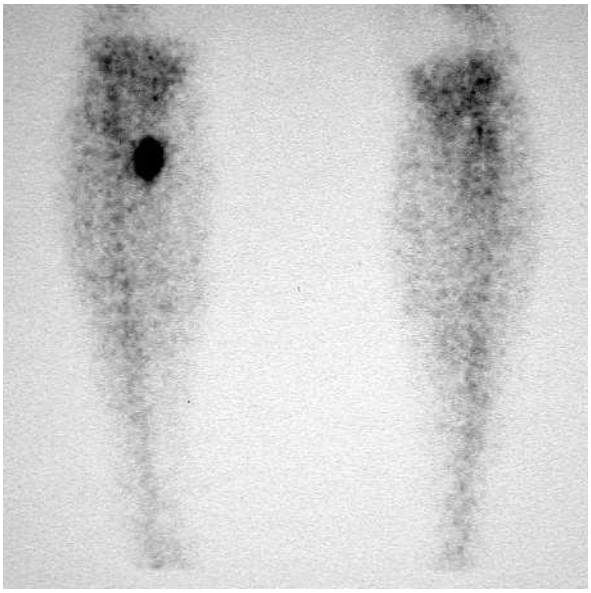

a

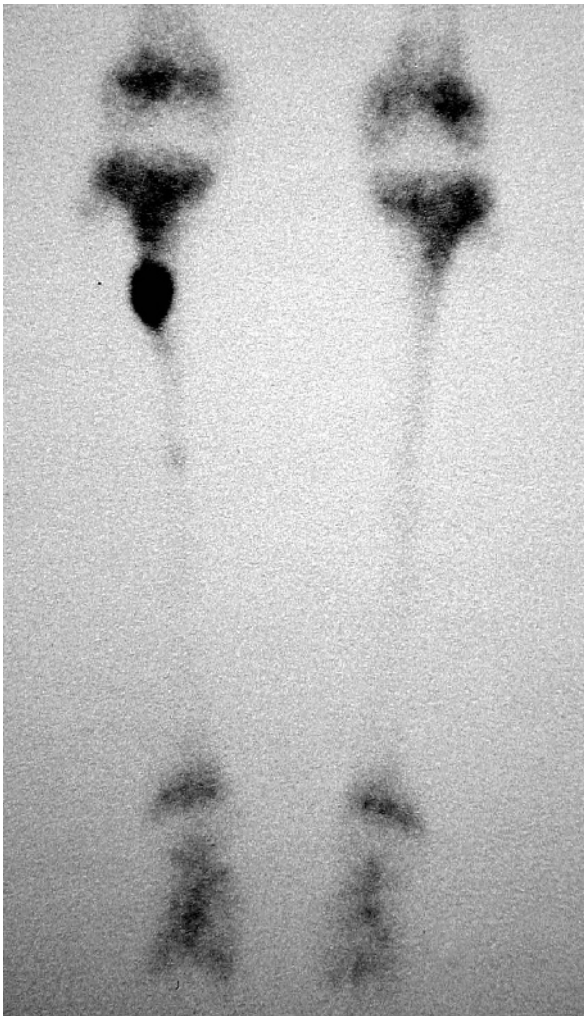

b

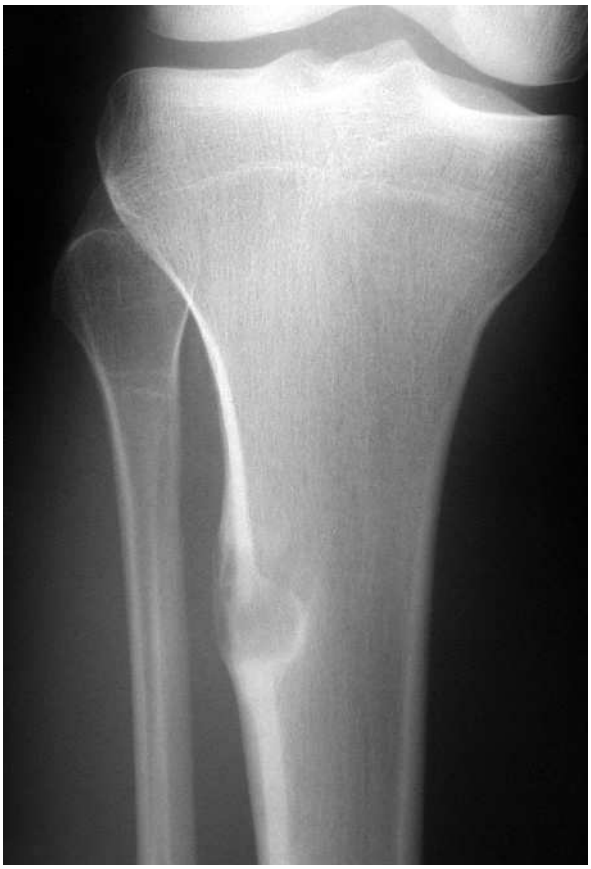

c

Fig. 4.9a–c. Non-ossifying fibroma scintigram high uptake in healing or osteoblastic phase. **a** Blood pool. **b** Delayed. **c** Radiograph

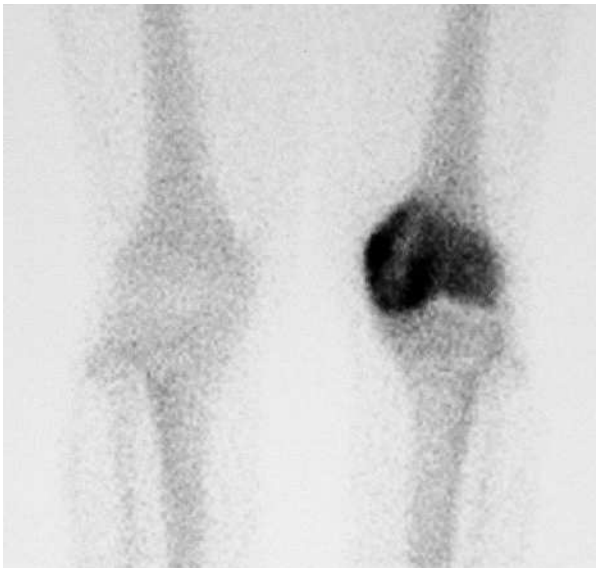

a

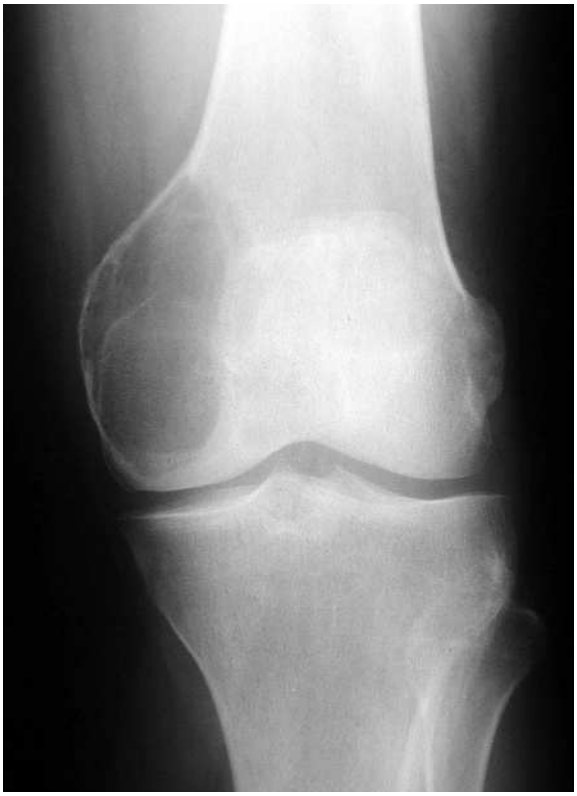

b

Fig. 4.10a,b. Giant cell tumour. **a** Scintigram with rim high uptake consistent with "doughnut sign". **b** Radiograph of the lytic lesion adjacent to joint line in mature skeleton

is not present within the capsule, sclerosis may be minimal or distant (Allen and Saifuddin 2003). Because of the vascular nature of the nidus, the early phases of the bone scan show intense uptake, with equally intense uptake on delayed imaging. On delayed imaging a "double density" sign may be seen (Helms et al. 1984; Helms 1987), which is thought to be secondary to the intense uptake of the nidus and less intense uptake of surrounding reactive osteoblastic activity (Fig. 4.1).

The spine is the site for osteoid osteoma in 10% of cases and for 36% of osteoblastoma (Jackson et al. 1977), arising mainly in the posterior elements. SPECT imaging can be useful to localize the lesion (Ryan and Fogelman 1994; Reinartz et al. 2000). Once localised, other imaging such as CT and MRI may be used to demonstrate the morphology and position of the lesion and hence plan management (Fig. 4.14).

In summary, the bone scan in benign tumour and tumour-like lesions is helpful in demonstrating focal or multifocal nature of a condition, position and distribution of lesions and the metabolic activity or change in metabolic activity of a lesion. In this way, confirming the diagnosis in conjunction with other imaging and helping in the planning of management and follow-up of the lesions.

4.2.4 ^{99}Tc MDP Bone Scan and Malignant Bone Tumours

The most common application of the ^{99}Tc MDP bone scan is in staging for tumour metastases although other modalities such as whole body MRI and PET/CT are proving to be as sensitive and specific (Daldrup-Link et al. 2001). The bone scan is less sensitive in detecting lytic lesions. In myeloma, more lesions may be detected with a radiological skeletal survey, although the bone scan will detect lesions where there has been fracture, new bone formation or reactive change, particularly in the spine (Tamir et al. 1983) (Fig. 4.2). Patterns of uptake in relation to metastatic disease can also be demonstrated on a bone scan, e.g. a flare response and a superscan.

A "flare response" on a bone scan occurs where there is an increase in uptake of isotope in bone metas-

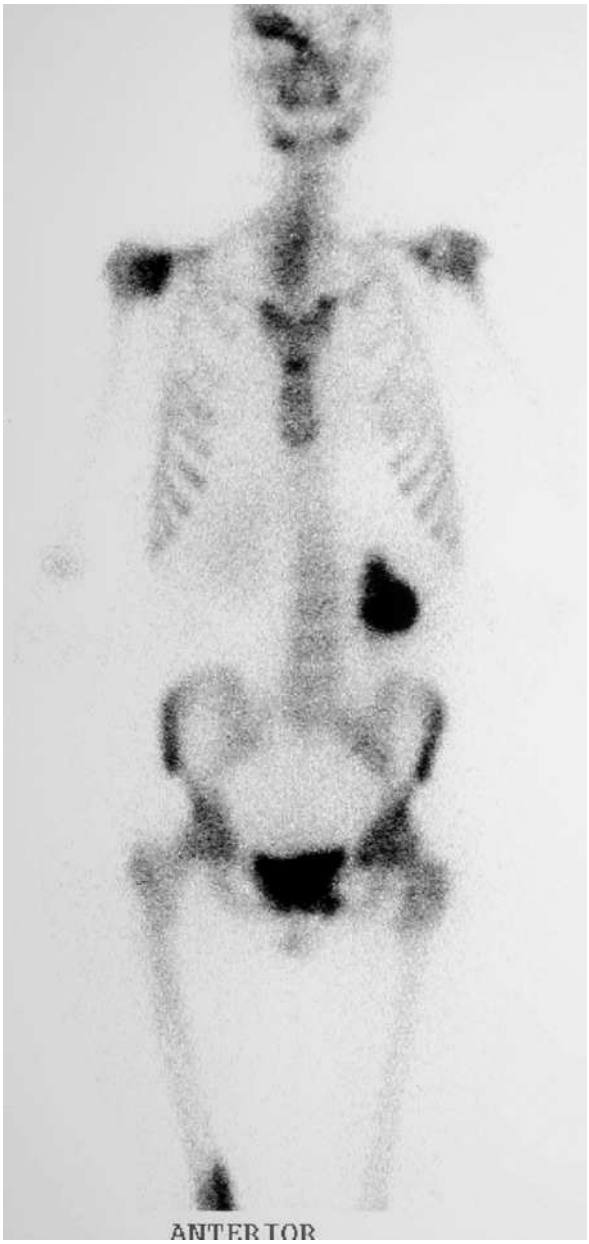

a

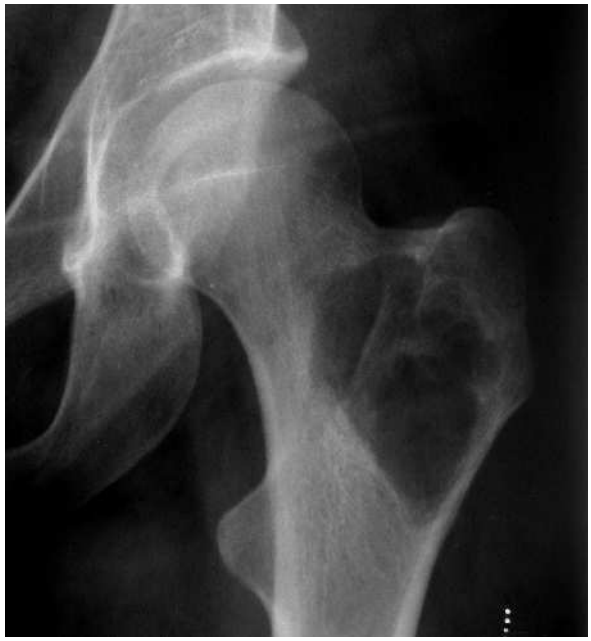

b

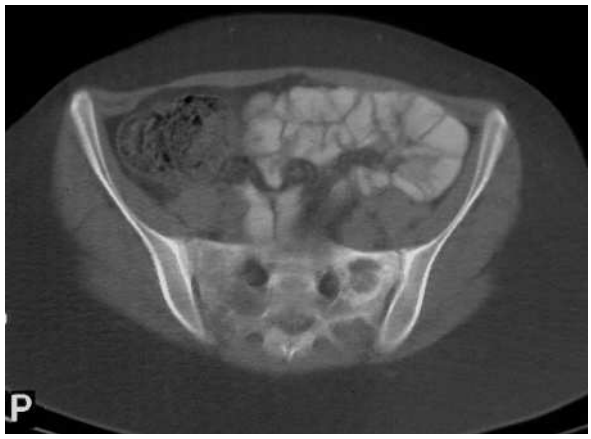

c

Fig. 4.11a–c. Langerhans cell histiocytosis. **a** Scintigram showing areas of high uptake in skull, right humeral head, right femur with intermediate uptake in relation to left sacrum and left femur (left hydronephrosis noted). **b** Radiograph of left femoral lytic lesion with narrow zone of transition non-sclerotic margin. **c** CT of sacrum showing lytic lesion with sclerotic margin. This case demonstrates the variable presentation of lesions

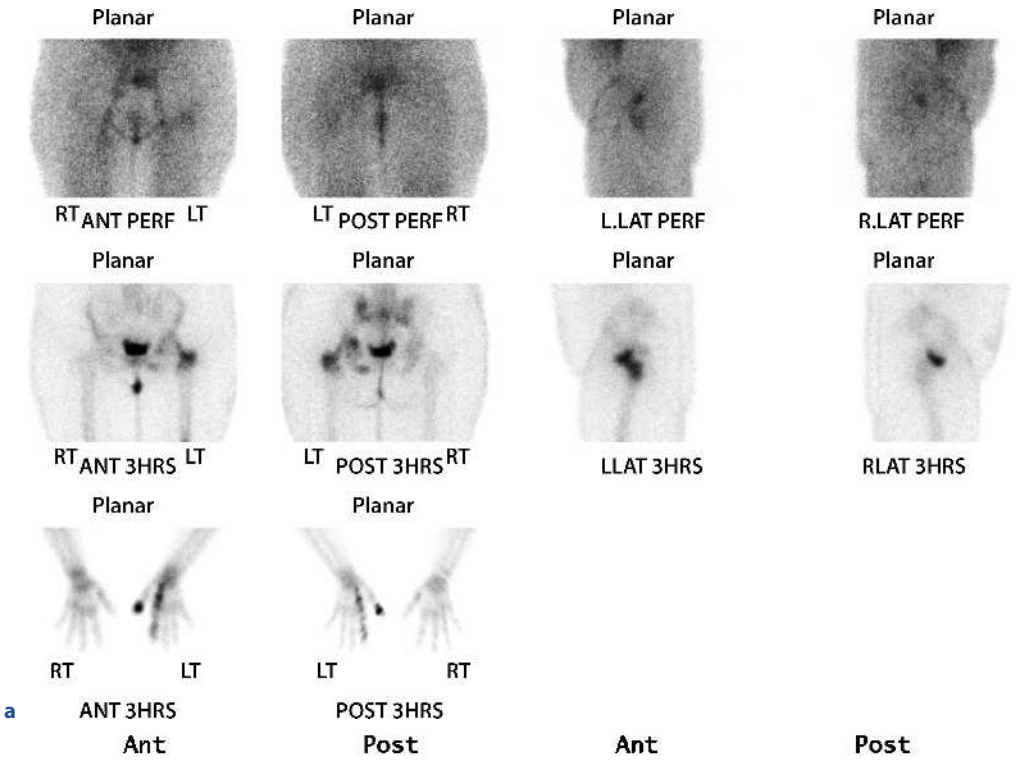

a

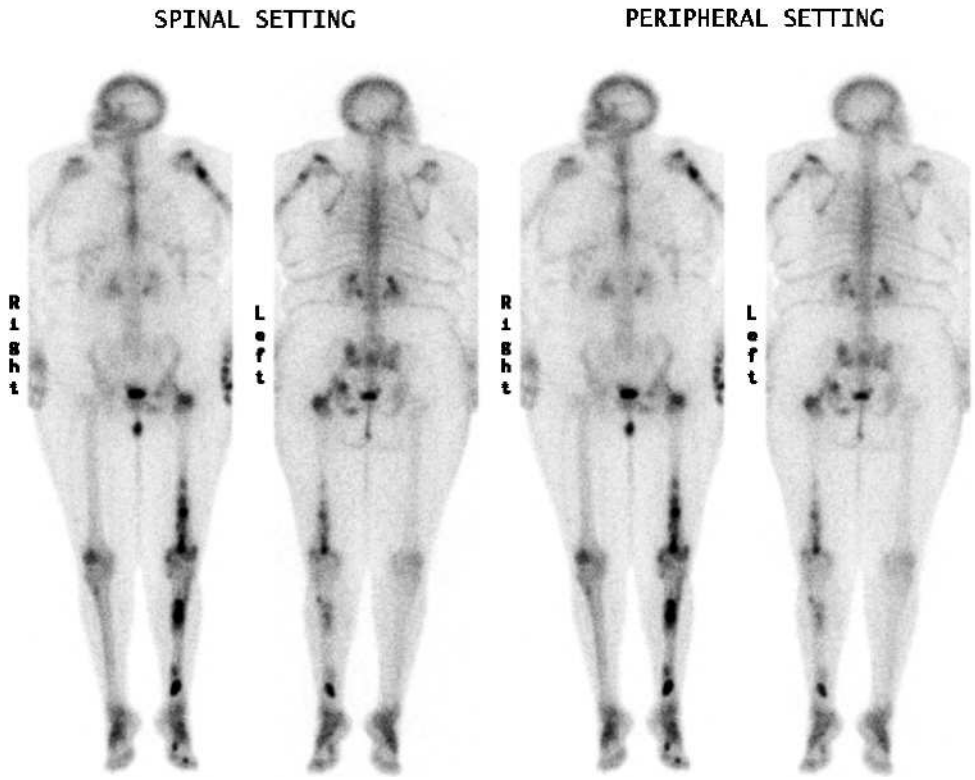

b

Fig. 4.12a–d. Ollier's disease. **a** Blood pool images show mild uptake in the left femoral enchondroma but no uptake in other enchondroma in the pelvis. Spot hand images show variable uptake in the left hand enchondroma. **b** Delayed whole body imaging shows variable uptake in the multiple enchondroma. (**c,d**) *see next page*

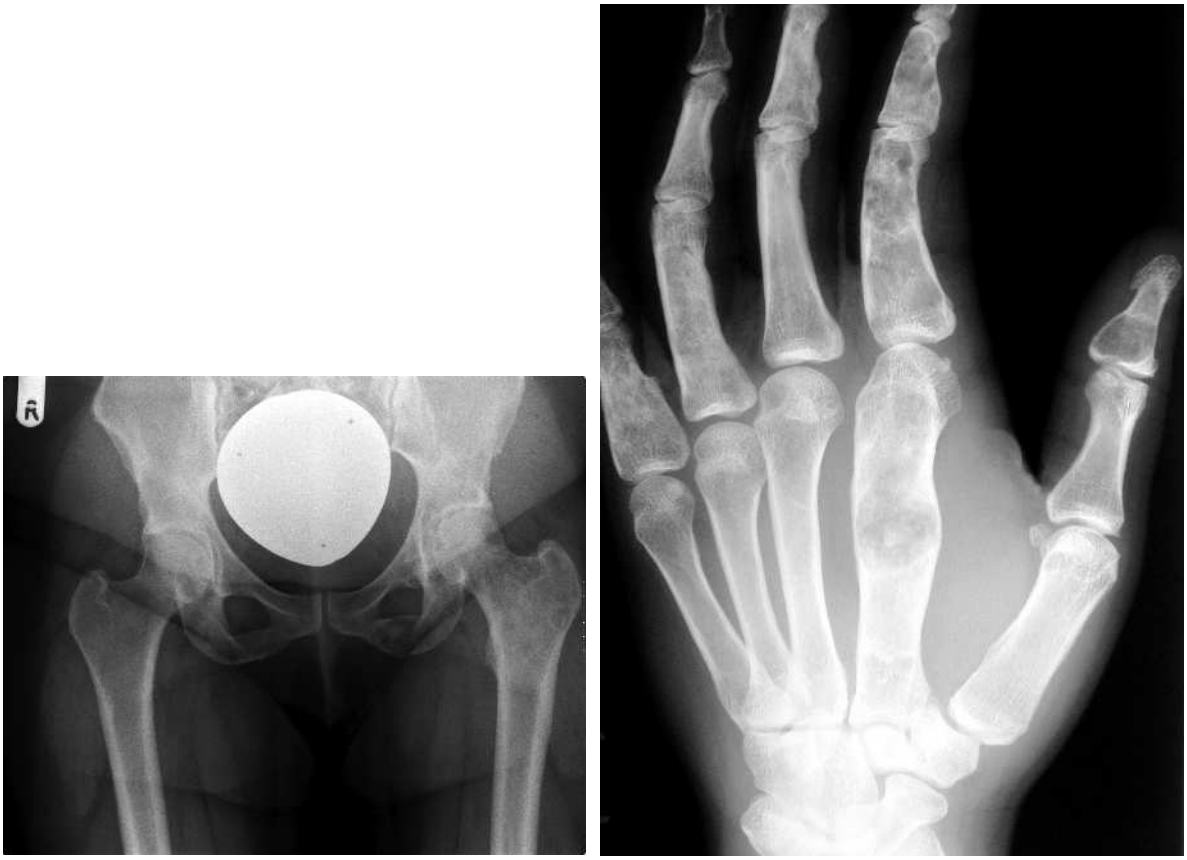

c d

Fig. 4.12a–d. (*continued*) **c** Radiograph of the pelvis shows not only left femoral lesion but also lesions in left hemipelvis. **d** Radiograph of multiple enchondroma in the bones of the left hand, some showing matrix calcification

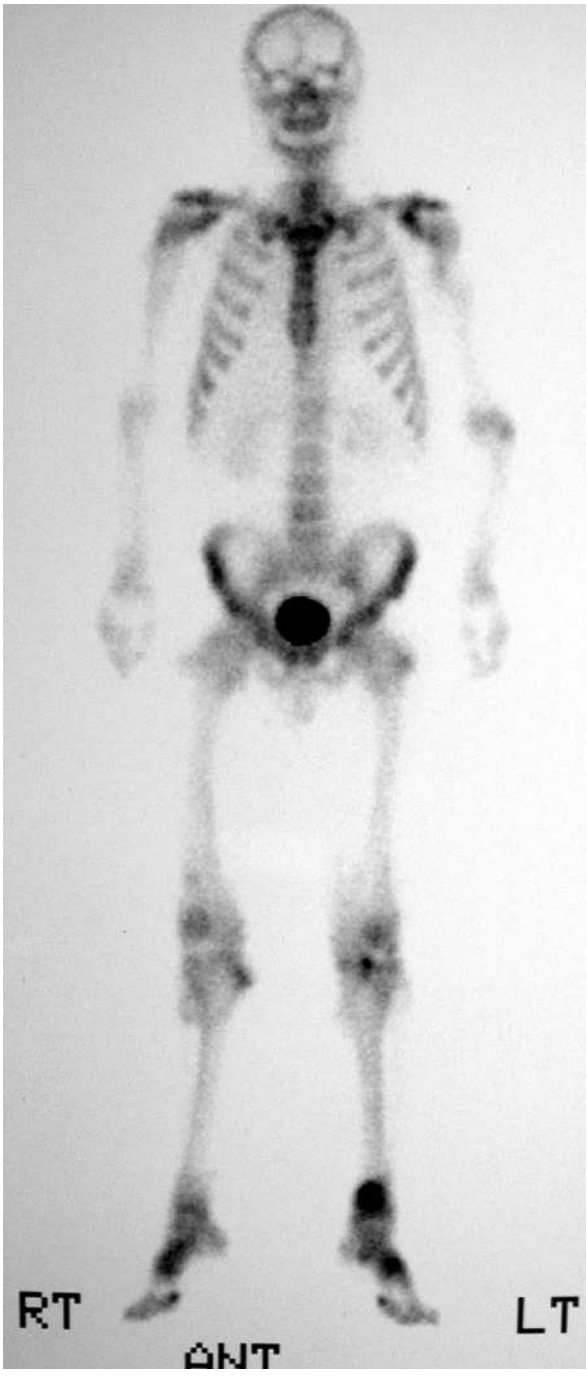

a

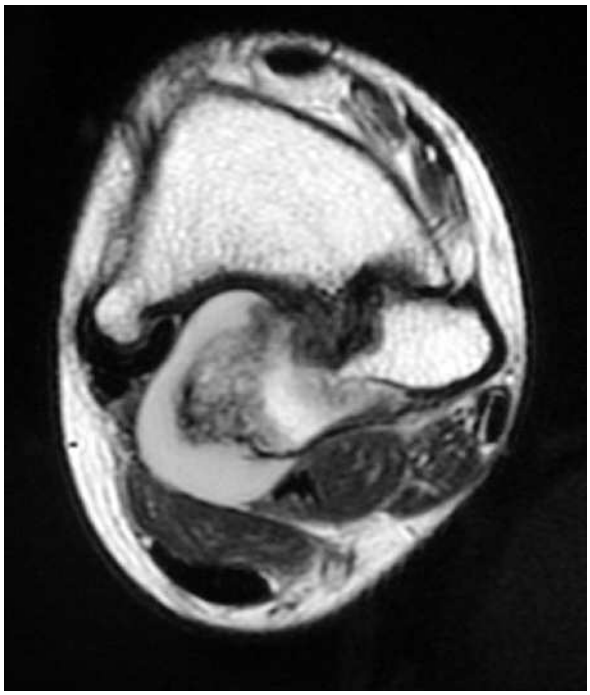

b

Fig. 4.13a,b. Diaphyseal aclasis. **a** Whole body scintigram demonstrates the abnormal modelling in the proximal humeri, neck of femora, distal femora, proximal and distal tibia, particularly high uptake is seen in distal left tibia. **b** MRI axial T2 shows the high signal cartilage cap of a large exostosis with smaller exostoses in the distal tibia, all of which will be contributing to impingement between the bones, and a reactive response, which also contributes to the high uptake on the bone scan

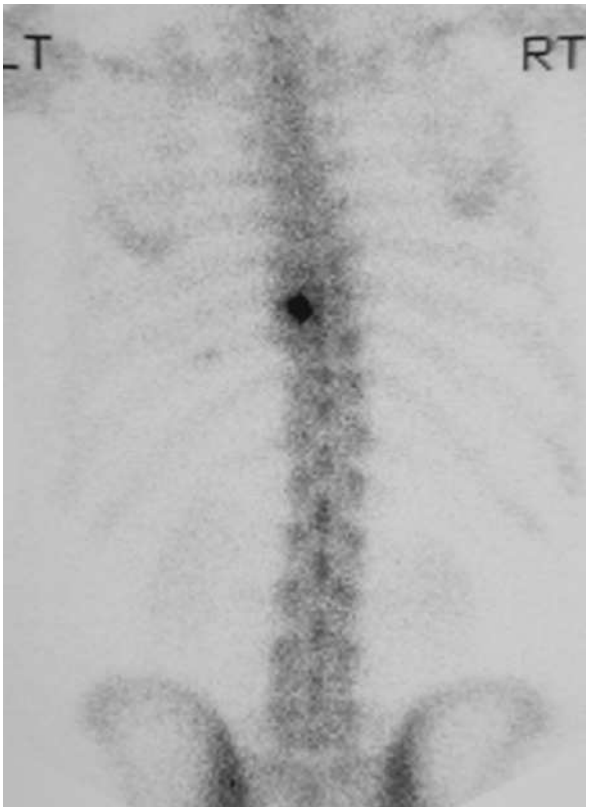

a

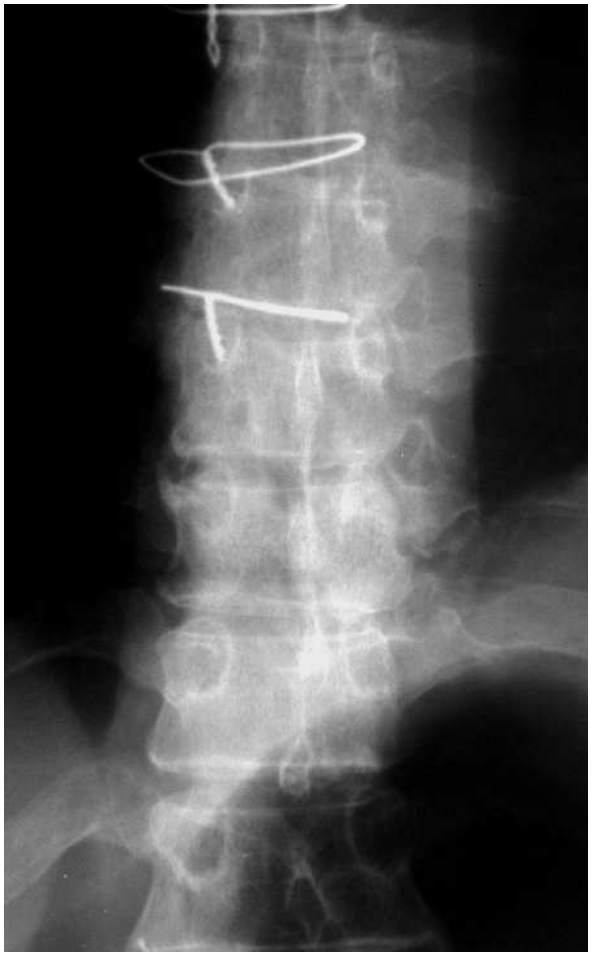

b

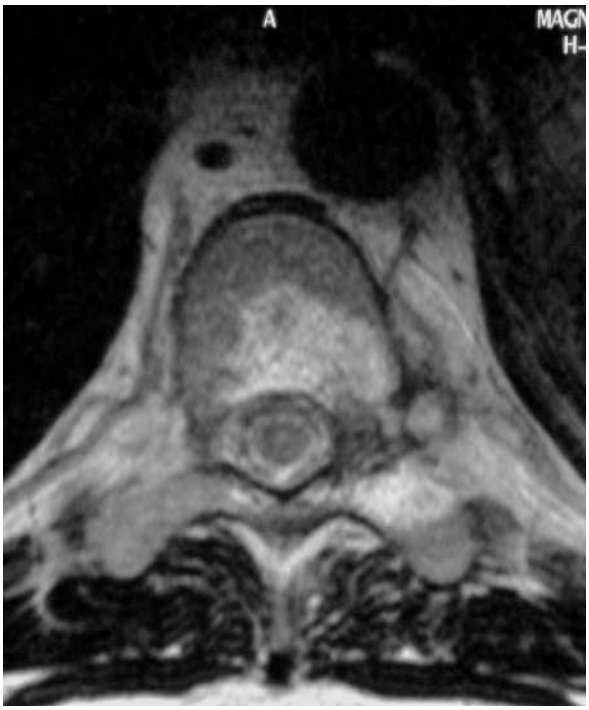

c

Fig. 4.14a–c. Osteoid osteoma at T9 vertebra. **a** Scintigram demonstrating high uptake in region of the left pedicle with associated scoliosis. **b** Radiograph demonstrates missing left pedicle of T9. **c** MRI axial T2 shows high signal bone oedema and low signal of the sclerotic nidus

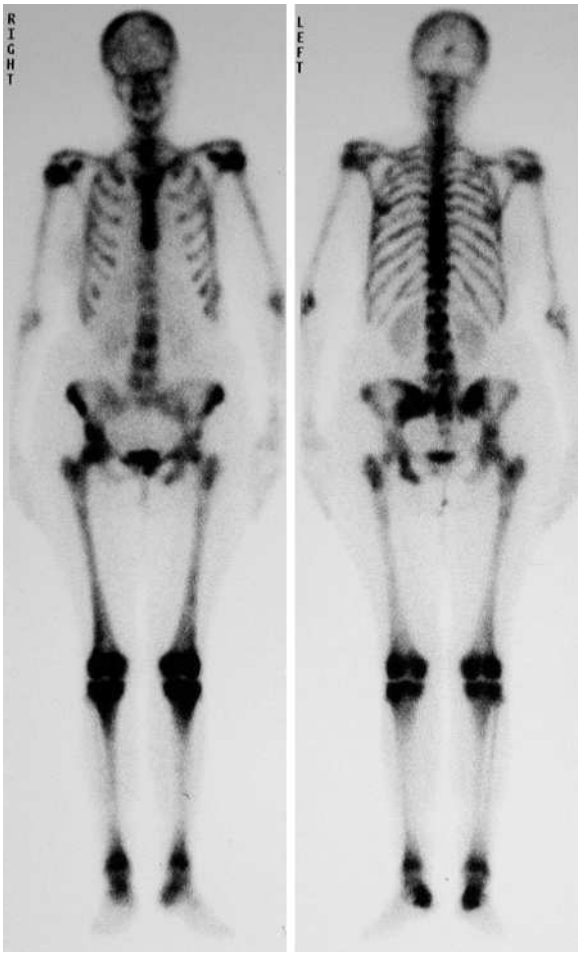

Fig. 4.15. "Superscan" due to multiple breast metastases

tases post-chemotherapy if the bone scan has been carried out at 3 months or less than 6 months post-chemotherapy. This phenomenon may demonstrate previously undetected metastases but can also indicate a likely response to treatment (Coleman et al. 1988).

The "superscan" occurs where there is a high ratio of bone to soft tissue activity and an apparent uniform high uptake, with absence of focal lesions in the axial skeleton, with apparently little or no uptake seen in the renal areas. This occurs when there are widespread bone metastases, e.g. prostatic or breast carcinoma (Fig. 4.15) (Constable and Cranage 1981), although a more uniform high uptake may also be seen in hyperparathyroidism.

In chondrosarcoma, when developing in a dysplasia of multiple enchondromatosis or exostoses, the bone scan, as already discussed, can be helpful in demonstrating change in metabolic activity of a lesion with sarcomatous change. A chondral lesion with high uptake and heterogenous uptake in a mature skeleton raises suspicion of malignancy, the difference between benign lesions being significant ($P<0.0005$) (Murphey et al. 1998). In the staging of a biopsy proven chondrosarcoma, bone scan is important in detecting the presence of metastatic disease when planning surgery (Fig. 4.7c).

In osteosarcoma, whether primary or secondary, due to the oseoblastic nature of the cell type, early and intense uptake will be shown in the lesion. The radiographic appearance of the lesion however may be lytic or poorly differentiated, although will still show uptake. On the bone scan an "extended pattern of uptake" has been described in the limb in which the sarcoma arises. This pattern of uptake describes a less intense, more diffuse uptake of isotope in the rest of the limb involved including the joints, where no occult tumour exists (Chew and Hudson 1982). In the areas of increased uptake marrow hyperaemia, reactive medullary bone formation and periosteal reaction have been described (Chew and Hudson 1982) (Fig. 4.16).

Although the bone scan will detect soft tissue extension, bone metastases and skip lesions (lesions within the same bone as the primary tumour with normal bone between), there are reported cases (Chew and Hudson 1982; Bhagia et al. 1997) where the bone scan has not detected uptake in skip lesions. The detection of skip metastases is particularly important when considering limb salvage surgery in order to have margins free of tumour; hence the need to use other imaging modalities, in particular MRI of the whole bone, to detect these lesions (Fig. 4.17).

In Ewing's sarcoma and other primary bone tumours, e.g. malignant fibrous histiocytoma, which may be permeative and destructive on a radiograph with periosteal reaction associated, lesions will be detected on the bone scan due to increase in blood flow and osteoblastic reactive changes. The bone scan is used in the initial staging and evaluation for metastatic disease. The bone scan can also be used to demonstrate response to treatment, particularly the early phase of uptake, where there is a correlation with a mean change in tumour blood flow ratio following treatment. This can be detected in responders to therapy which correlates with tumour necrosis demonstrated by histology (Ozcan et al. 1999).

In the presence of a massive prosthesis, the bone scan can be helpful in demonstrating complications, such as loosening or infection, as well as soft tissue recurrence (Fig. 4.18).

In summary, in malignant bone disease, the bone scan is mainly used in the staging, restaging and follow-up, in planning management of the disease.

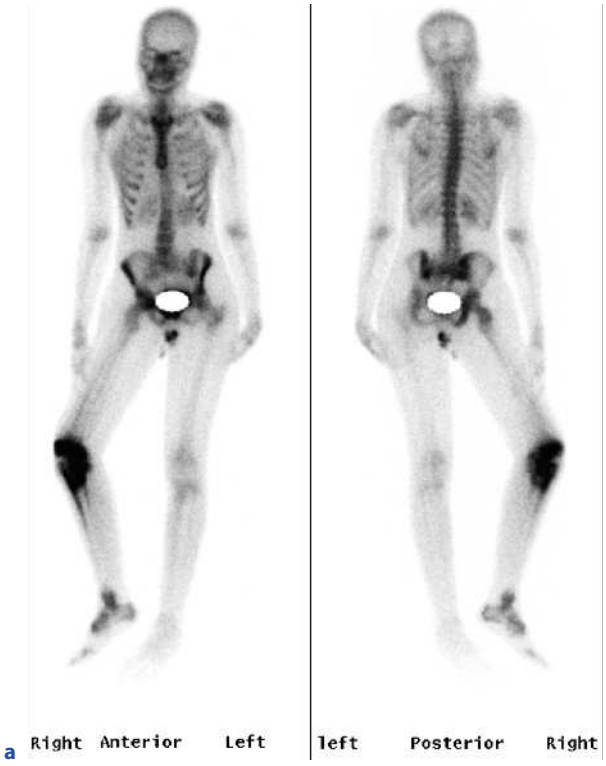

a

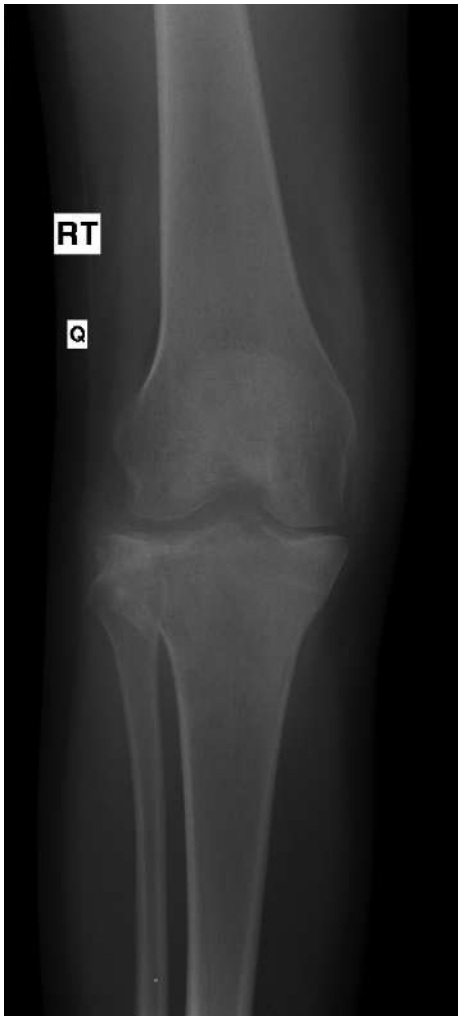

b

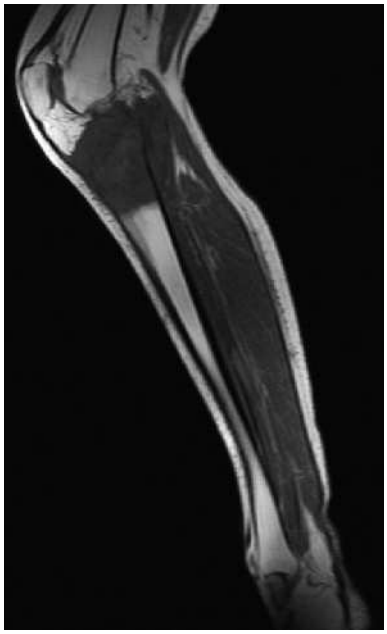

c

Fig. 4.16a–c. Osteosarcoma. **a** Scintigram shows very high uptake in the tibia and distal femur (possibly relating to joint involvement seen on MRI), although high uptake in the right lower limb in particular hip joint and bones of the ankle. **b** Radiograph shows osteopenia distal femur and relative sclerosis in the proximal tibia. **c** MRI sagittal T1 whole tibia shows no lesions in the ankle hence uptake on scintigram relates to an "extended pattern of uptake", most likely secondary to hyperaemia

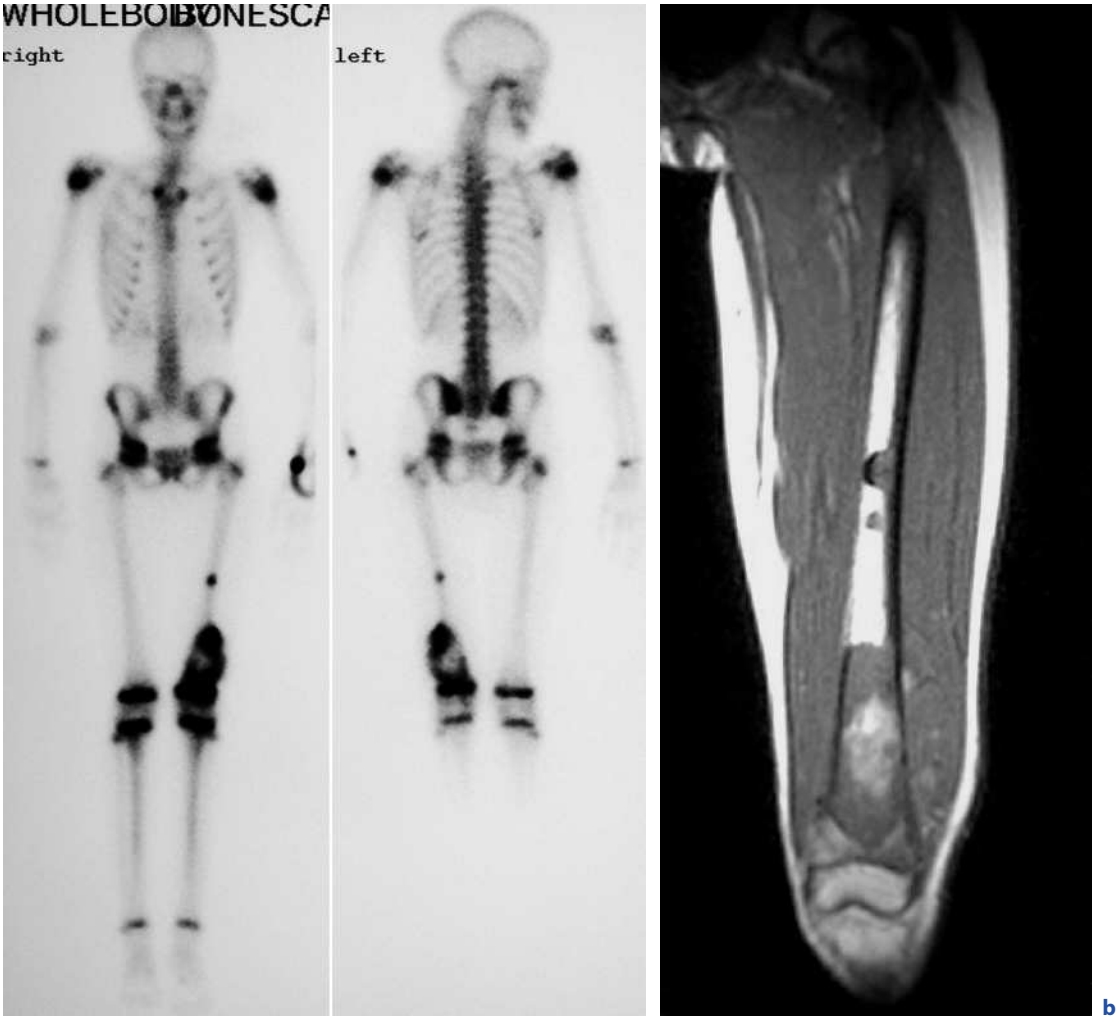

a b

Fig. 4.17a,b. Osteosarcoma. **a** Scintigram with high uptake in primary tumour in the distal left femur with small focus of high uptake in proximal femoral shaft consistent with skip lesion. **b** MRI coronal T1 demonstrates the skip lesion in the left femoral shaft

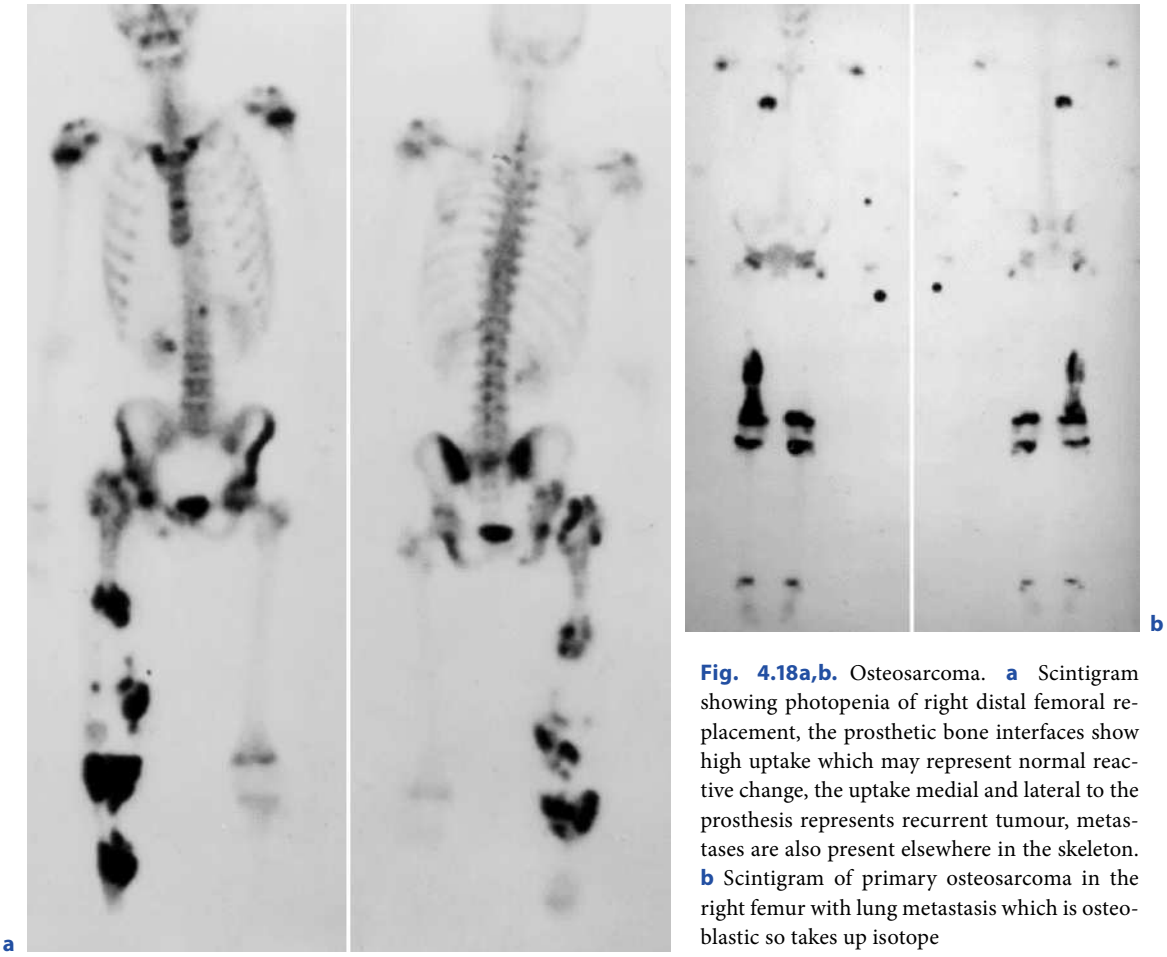

Fig. 4.18a,b. Osteosarcoma. **a** Scintigram showing photopenia of right distal femoral replacement, the prosthetic bone interfaces show high uptake which may represent normal reactive change, the uptake medial and lateral to the prosthesis represents recurrent tumour, metastases are also present elsewhere in the skeleton. **b** Scintigram of primary osteosarcoma in the right femur with lung metastasis which is osteoblastic so takes up isotope

4.3 PET and PET/CT

4.3.1 Principles and Technique of PET and PET/CT

Positron emission tomography (PET) imaging relies on positrons (positively charged electrons emitted from nuclei with an excess of protons), which, on encountering negatively charged electrons, lose energy, briefly combining with electrons to form positronium before annihilating. The total mass of the positronium is converted to a photon of energy in the form of 511-keV gamma rays, which are emitted at approximately 180° to each other. These gamma rays are then detected by a ring of detectors around the patient. In this way it is possible to localise the source of emission by detecting the simultaneous or coincident arrival of the photons. The source of these photons is localised along a line of response. Using iterative expectation-maximization algorithms for reconstruction (which are independent of the acquisition geometry), so reducing the image noise, an image is produced. The attenuation correction of the images was originally achieved by a transmission scan using a Germanium-68 source in pure PET scanners. However, with the integration of a CT scanner in combination with the PET scanner, an attenuation map is achieved more efficiently. The attenuation corrected images achieved by CT are susceptible to movement artefacts, misregistration and streak artefact produced by metallic implants; therefore uncorrected images are also produced and viewed in conjunction with the corrected images.

The combination of anatomical detail from the CT in the co-registered images in PET/CT adds signifi-

cantly to the sensitivity and specificity of the investigation (Valk et al. 2002). The attenuated corrected data also improves and allows quantitative analysis of uptake of radiopharmaceutical.

The radioisotopes used in PET scanning have short half lives, e.g. fluorine-18, 110 min, carbon-11, 20.3 min, oxygen-15, 124 s, nitrogen-13, 9.97 min. These radioisotopes, produced in a cyclotron, combine with other molecules to produce radiopharmaceuticals that are metabolised, so a measure of metabolism and the site of metabolism can be made by the PET scanner. The most commonly used isotope fluorine-18, has a longer half life and is more easily transported, if there is no cyclotron on site. Fluorine-18 decays producing 97% positrons. It forms a strong covalent bond with carbon compounds and can be incorporated into a wide variety or organic molecules. For use in PET, it substitutes a hydroxyl group in deoxyglucose to produce [^{18}F]-2-floro-2-deoxy-D-glucose (FDG). FDG acts as a glucose analogue but as such is not tumour specific. The FDG is taken up into the cell and phosphorylated but, unlike glucose-6-phosphate, is not metabolised any further and therefore will accumulate in cells with high glucose metabolism. Some tumour cells have high expression of the GLUT1, a glucose transporter molecule on the cell membrane; they also have increased hexokinase and glucose-6-phosphatase reactions and hence higher accumulation of phosphorylated FDG. However, any cell or organ that has a high glucose metabolism, e.g. brain, myocardium and particularly inflammatory cells, will also accumulate FDG.

The patient preparation prior to FDG PET scanning is integral to achieving satisfactory image quality. The patient must have been fasting for at least 6 h prior to injection with a blood glucose between 4–6 mmol/L. This ensures that serum insulin levels are low, so reducing uptake in liver and muscle, and also reducing cardiac uptake by switching to fatty acid metabolism in the heart. The patient should have an empty bladder and be kept warm and quiet, as this helps reduce adrenalin levels and hence uptake of FDG in brown fat. The patient should move as little as possible prior to and after injection of radiopharmaceutical, to reduce muscle uptake. An intravenous injection of 300–400 MBq of FDG (a dose of 5–6 mSv) is given after which imaging may then be carried out at 1 h to 90 min. The CT part of the examination is carried out with quiet breathing taking seconds (the CT is usually without contrast agents and is of lower than normal mA). The total radiation dose of PET/CT is approximately 17 mSv, depending on the method of CT acquisition. The emission scan is carried out from skull base to groin and may include the legs depending on the site of pathology, taking at least 20–25 min, with CT having been acquired over the same volume. Motion artefact is the predominant concern due to the long acquisition time of the PET element of the scan, with risk of misregistration.

It has been demonstrated that peak uptake of FDG in benign lesions occurs within 30 min whereas peak uptake in malignant lesions occurs at approximately 4 h (Lodge et al. 1999). A compromise is made for technical, patient comfort and economic reasons, in imaging at 60–90 min.

Various uptake measurements of FDG can be made using a region of interest, including tumour to non-tumour ratios. More commonly a measurement of standard uptake value (SUV) is made:

$$\text{SUV} = \frac{\text{decay-corrected activity (kBq)/tissue volume (mL)}}{\text{injected activity (kBq)/body weight (g)}}$$

There are however potential sources for error in the calculation of SUV or indeed SUV maximum (SUVmax) for a lesion, namely:

- The patient size, as there is generally a reduced uptake of FDG in fat, so a higher uptake in normal tissue will occur, hence an over estimation of SUV (lean body mass or surface area may be used in the calculation).
- Time of acquisition post-injection depending on uptake peak may alter the SUV in inter study measurement.
- Plasma glucose level can be variable between studies.
- Partial volume averaging; if a lesion is 5–10 mm it can have an artificially low SUV.
- Dose of FDG, particularly if there has been extravasation at the site of injection (but has less effect on tumour to normal tissue ratio measurement).
- Image processing; differs between different manufactures of equipment, variable number of iterations in image production may occur, this will effect SUV max but not average SUV.
- Attenuation correction has more effect on SUV; hence motion or the presence of a prosthesis will result in higher SUV readings. One cannot compare SUV calculations from a PET scanner, with a PET/CT scanner.

PET/CT can be extremely helpful in locating sites of disease where the anatomy is complex or altered by surgery. It may locate disease in unexpected sites or where other cross sectional imaging has demonstrated normal size nodes. PET/CT however does have limitations in spatial resolution. In certain tumour types, e.g.

lymphoma, PECT/CT is valuable in staging and restaging. Some tumour types show poor uptake, hence a false negative result could occur, if a baseline study has not been carried out to demonstrate this.

Difficulties in interpretation may also occur as a result of physiological uptake, normal variants and artefacts. False positive results can occur due to non-specific uptake relating to surgery, radiotherapy, chemotherapy and inflammation or infection. Necrosis in lymph nodes or tumour and sclerotic metastases may show reduced uptake. The other concern of the PET/CT scan that should be taken into account, particularly when imaging young patients, is the radiation dose and time for the acquisition of the data (Valk et al. 2002).

4.3.2 Application and Interpretation of PET and PET/CT

There is some controversy as to where PET and PET/CT should be applied to bone sarcoma management. In this section the evidence base will be explored in relation to primary bone tumours. A range of methodology has been applied in the literature including tumour to non-tumour ratios as well as the use of SUV. Because primary bone sarcoma makes up approximately 0.2% of the total human tumour burden, the sample sizes are often small with grouping of different cell types.

Kole et al. (1998) compared the uptake in bone lesions with contra lateral normal muscle tissue in 26 patients, who had 7 benign and 19 malignant bone lesions. All the lesions other than a small bone infarct showed an increase uptake compared to normal muscle tissue. However, they were unable to demonstrate a clear correlation between the glucose metabolism and aggressive nature of the lesion or to differentiate benign from malignant lesions.

4.3.2.1 The Diagnosis and Grading of Bone Tumours

Some studies have looked at the value of PET in grading bone tumours. In one study of Schulte et al. (2000), 202 cases were evaluated – 40 benign lesions, 47 tumour-like and 115 malignant bone tumours which included 70 high grade sarcoma, 21 low grade sarcoma, 6 osseous lymphomas, 6 plasmacytomas and 12 metastases of unknown primary. In this study, tumour to background ratio was used to evaluate metabolic activity. Using a cut off of 3 to differentiate benign from malignant lesions, a sensitivity of 93% and specificity of 66.7% with accuracy of 81.7% was shown. An overlap of uptake was demonstrated between metabolically active benign lesions such as giant cell tumours and some sarcomas.

SUV measurement has also been applied to differentiating between benign and malignant bone tumours. In one study (Aoki et al. 2001), with 52 cases of which 33 were benign and 19 were malignant lesions, a significant difference (P=0.002) between benign (SUV 2.18 ± 1.52 SD) and malignant (SUV 4.34 ± 3.19 SD) lesions was demonstrated. Again, an overlap in uptake of FDG in benign lesions, e.g. chondroblastomas, sarcoid and Langerhans cell histiocytosis and malignant lesions, e.g. osteosarcoma was shown. Using SUV (Dimitrakopoulou-Strauss et al. 2002) evaluating 83 cases, 46 benign, 37 malignant, a sensitivity of 54% and specificity of 91.3% with accuracy of 77% was demonstrated; however an improvement in the sensitivity, specificity and accuracy was achieved when more kinetic data was applied. However, with more complex kinetic measurements, some benign lesions showed as high metabolic activity as malignant lesions.

The question then arises, whether by evaluating a more specific cell type, the differentiation between benign and malignant lesions could be achieved using PET. In a small sample of 11 cases (Aoki et al. 1999), SUVmax showed that there was a range of uptake in benign, low grade malignant and high grade malignant cartilage tumours, with an overlap between the grades.

A larger study of 35 cartilaginous tumours (Lee et al. 2004) involved 13 benign cartilage tumours, 12 grade I, and 10 grade II or III chondrosarcoma. Using a cut off SUVmax of 2.3 for grade II and III chondrosarcoma, there was a sensitivity of 0.90 and specificity of 0.92 in differentiating between grade 0–I and grade II–III chondrosarcoma with positive predictive value of 0.82 and negative predictive value of 0.96, although wide 95% confidence intervals were seen for sensitivity and positive predictive values. This paper however emphasised the inability of PET to differentiate between the benign cartilage tumour and grade I chondrosarcoma.

A further study (Feldman et al. 2005) used a cut off SUVmax of 2 to differentiate benign and malignant cartilage lesions. A total of 29 lesions, of which 18 were benign and 11 malignant, showed a sensitivity of 90.9%, specificity of 100% and accuracy 96.6% in differentiating.

All of the aforementioned papers re-emphasise the need for biopsy in diagnosing and grading cartilage tumours (Fig. 4.19).

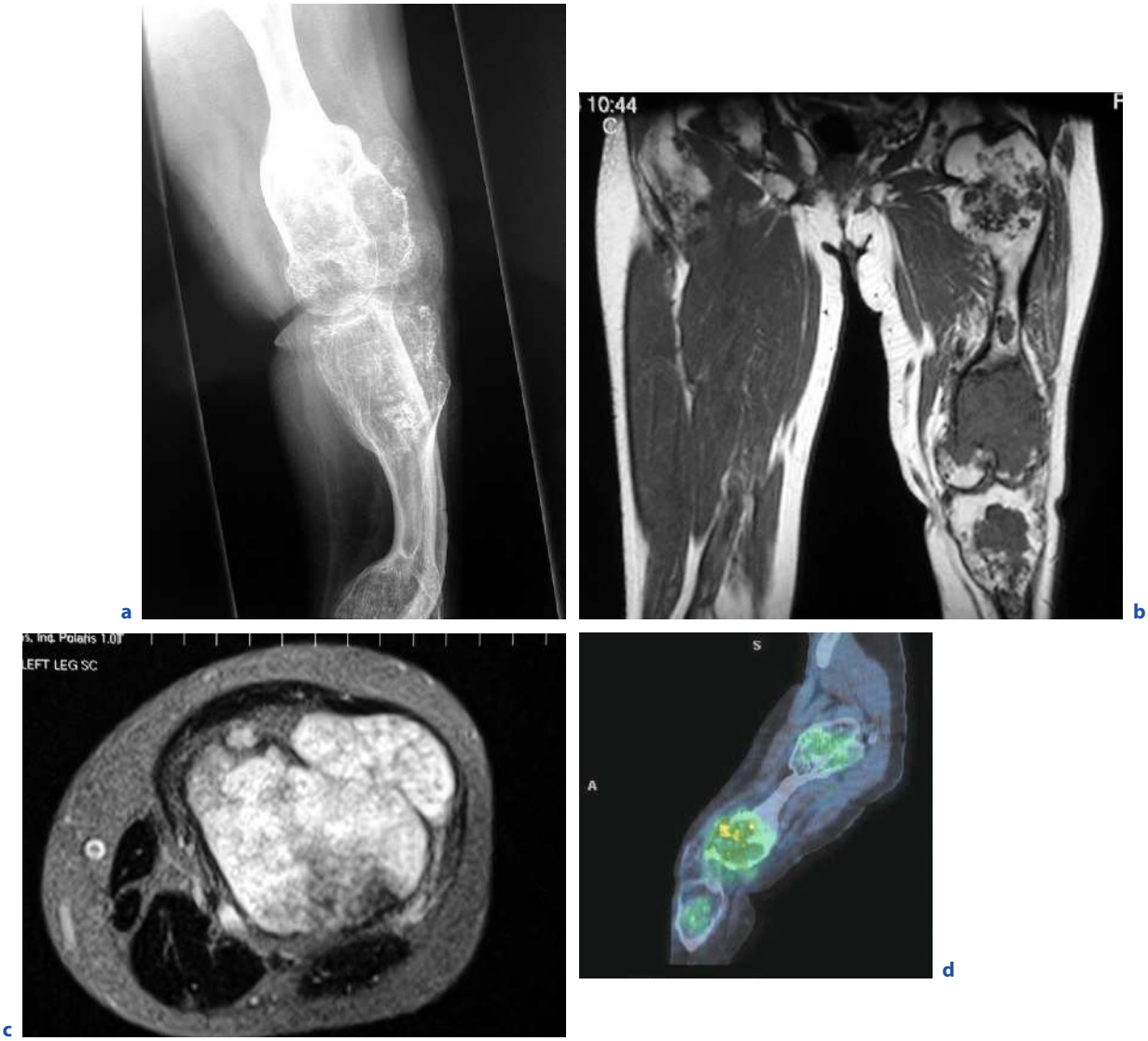

Fig. 4.19a–d. Ollier's disease. **a** Radiograph shows multiple enchondroma in the tibia and fibula with extension beyond the cortex of the distal femoral enchondroma. **b** MRI coronal T1 demonstrates a small skip lesion in the distal femur as well as the extent of the intermediate signal of then enchondroma within the femur as well as the tibia. **c** The MRI axial T2 fat saturated image demonstrates the presence of high signal chondrosarcoma breaking through the cortex of the distal femoral lesion. A PET/CT was carried out to help in the management decisions. **d** Shows a sagittal PET/CT with areas of higher FDG uptake in the distal femoral enchondroma with SUVmax = 3; however other lesions showed SUV of less than 2. Biopsy of the distal femur showed grade 2 chondrosarcoma. A management decision based on biomechanical outcome to carry out disarticulation and placement of prosthetic amputation stump was made. Microscopic foci of grade 2 chondrosarcoma were present in the proximal femoral enchondroma which were too small to be detected by the PET/CT

4.3.2.2 Staging of Sarcomas

PET and PET/CT are well established in the staging of some tumours, e.g. bronchogenic carcinoma; however, its place in the staging of primary bone tumour is still being evaluated. Primary bone sarcomas, particularly Ewing's and osteosarcoma, occur in a young age group and therefore the use of a high radiation dose investigation poses significant ethical concern when applying the modality for research purposes. There are however some studies that have compared PET and PET/

CT with conventional imaging in sarcoma patients. A combination of ultrasound (US), CT, MRI and bone scan were prospectively evaluated in relation to PET (Volker et al. 2007). A lesion and patient based analysis of a combination of 23 Ewing sarcoma, 11 osteosarcoma and 12 rhabdomyosarcoma were staged by different modalities. Conventional imaging and PET were 100% accurate in detecting the primary tumour. PET was found to be superior to conventional imaging in detecting lymph node involvement (sensitivity 95% and 25% respectively) and bone manifestations (sensitivity 89% and 57% respectively). CT, however, was more sensitive in detecting lung metastases than PET (sensitivity 100% and 25% respectively) probably secondary to the poor resolution of PET compared to CT. On the patient based analysis, the best results were achieved by a side by side analysis with 91% correct therapy decisions, significantly superior to conventional imaging alone 59% $P<0.001$.

A retrospective study of 117 bone and soft tissue sarcoma patients (Tateishi et al. 2007) of which 32 were bone sarcomas were reviewed where a combination of MRI, chest radiography, contrast enhanced whole body CT and bone scan were reviewed in relation to PET and PET/CT. PET/CT performed better than PET alone (accuracy of 96% and 80% respectively). Overall tumour, node and metastasis detection was superior in PET/CT as compared to conventional imaging. PET/CT achieved correct staging in 83% of patients, although overstaged in 12%. However, where PET/CT was combined with conventional imaging it achieved correct staging in 87% of patients, with reduced overstaging to 4% and helped change management to resectable in 2% of cases.

Both of these studies suggest improved staging of sarcoma with a combination of conventional imaging and PET/CT. Whether the new generation of multislice (64 slice) CT scanners or using a more diagnostic CT with contrast, in combination with PET will improve the diagnostic accuracy of PET/CT, has yet to be determined.

4.3.2.3 Prognostic Indicator and Response to Therapy

In 31 patients with chondrosarcoma (Brenner et al. 2004), the SUVmax demonstrated again an overlap in each grade of tumour, with particularly high SUVmax noted in three grade I extraskeletal myxoid chondrosarcoma compared to grade I skeletal chondrosarcoma. With a mean follow-up of 4 years, significant differences in SUVmax of patients with and without disease progression were found. Using a cut off SUVmax of 4, sensitivity, specificity, positive and negative predictive values were 90%, 76%, 64% and 94% respectively. Combining histological tumour grade and SUV, sensitivity, specificity, positive and negative predictive values were improved to 90%, 95%, 90% and 95% respectively. This study demonstrated that pretreatment SUV in combination with histology tumour grade can improve prediction of outcome, identifying patients at high risk of local relapse or metastatic disease. The paper highlighted a difference in the cases of extraskeletal myxoid chondrosarcoma, which although of histological grade I, have a tendency to recur locally, with a poor prognosis compared to skeletal grade I chondrosarcoma. It is not known whether extraskeletal myxoid chondrosarcoma have a generally higher SUVmax and should be considered as a unique tumour entity having a t(9;22) translocation not seen in conventional skeletal chondrosarcoma.

Osteosarcoma cells have the specific capability to produce primitive osseous matrix; a measure of this production can be made by ^{99}Tc MDP scanning, although this will also measure osteoblastic activity of adjacent normal bone reacting to the presence of tumour and healing. FDG uptake as a measure of metabolic activity of osteosarcoma cells and ^{99}Tc MDP uptake were evaluated prospectively as prognostic indicators of the tumour (Franzius et al. 2002a) in 29 patients. All the lesions were high grade although of different cell subtype, received the same neoadjuvant chemotherapy, were resected, and their histology response to therapy was evaluated. Tumour to non-tumour (T/NT) uptake ratios of FDG and ^{99}Tc MDP were measured with a positive correlation between the T/NT maximum FDG uptake and T/NT average ^{99}Tc MDP uptake. The T/NT maximum FDG uptake could be used to discriminate between high probability of overall event free survival and poor prognosis.

Response of osteosarcoma patients to neoadjuvant chemotherapy when considering limb salvage treatment is an important prognostic indicator (Picci et al. 1994). In a study of 27 cases of osteosarcoma (Schulte et al. 1999) using FDG uptake tumour to background ratio and a cut off of 0.6 for post-therapeutic to pre-therapeutic measurements, detection of response to therapy with a sensitivity 100%, specificity 80%, and accuracy 92.6%, with a positive predictive value 89.5% and negative predictive value 100% was demonstrated. A difference in responders and non-responders ($P<0.01$) was evident, with a correlation of FDG response ratio with tumour necrosis also demonstrated ($P<0.001$). This correlation most likely relates to the fact that FDG is a more accurate measure of tumour cell viability than, for example,

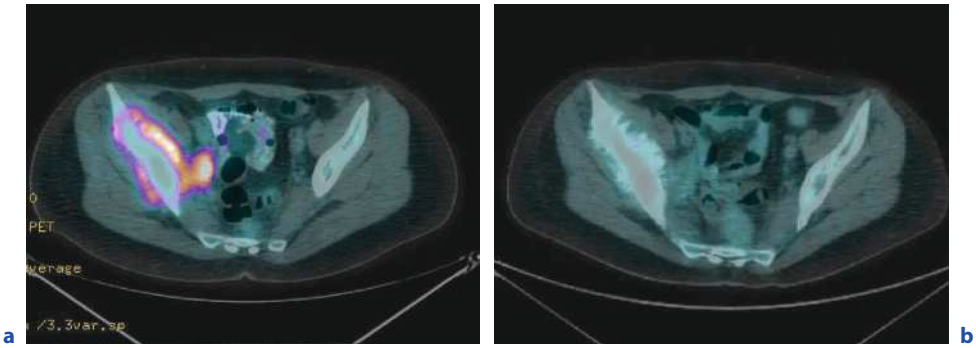

a b

Fig. 4.20a,b. Osteosarcoma. **a** Axial PET/CT demonstrating high uptake of FDG in the right ilium in area of spiculated new bone formation of the osteosarcoma SUVmax=8; similar high uptake was and right iliac vein also noted in the inferior vena cava (IVC) consistent with tumour thrombus. **b** Axial PET/CT image after two cycles of chemotherapy demonstrating significant response with reduced uptake of FDG (SUVmax=3 in some areas of previous uptake). This response to therapy prompted the oncologist to continue chemotherapy with a view to surgical intervention

contrast enhanced MRI as a measure of perfusion or ^{99}Tc MDP a measure of osteogenesis.

A study (Hawkins et al. 2002) combining osteosarcoma and Ewing sarcoma family of tumours used SUVmax to evaluate tumour cell metabolism before and after treatment in 33 patients – 18 osteosarcoma and 15 Ewing sarcoma family of tumours. Applying a cut off post-treatment SUVmax of <2, a positive predictive value for a favourable response (>90% necrosis) was 93%, whereas a negative predictive value for a unfavourable response (<90% necrosis) was 75% (P=0.01). Using SUVmax post-treatment to SUVmax pretreatment ratio <0.5 led to positive predictive value of favourable response of 78%; with ratio of >0.5 having a negative predictive value of unfavourable response of 63% (P=0.01). It should be noted that the SUVmax is a measure of maximum metabolic activity in a specific area of the tumour, whereas the histology measure of percentage necrosis takes into account the whole tumour.

A more recent study (Hawkins et al. 2005) evaluated a 36 Ewing sarcoma family of tumours and found concordance with a histologically good response to treatment defined by a post-treatment SUVmax <2.5 in 68% of patients and SUVmax post treatment to SUVmax pretreatment ratio <0.5 in 69% of patients. At 4 year follow-up, the ratio of post- to pretreatment SUVmax was found to be non-predictive of progression free survival. In all patients, progression free survival was seen in 72% with SUVmax <2.5, although only in 27% with SUVmax >2.5 (P=0.01). In patients with localised disease, progression free survival was seen in 80% with SUVmax <2.5, although only in 33% with SUVmax >2.5 (P=0.036).

Neither histology response nor SUVmax are completely concordant or predictive of disease free survival, although they may be helpful in planning management changes (Fig. 4.20). Larger prospective studies are needed in conjunction with meticulous methodology, in relation to timing of scan post chemotherapy, in deciding the correct application of PET/CT, in modifying treatment for patients with higher risk of disease recurrence.

4.3.2.4 Recurrence and Metastatic Disease

FDG PET has been demonstrated to have a small advantage for detecting osseous and soft tissue recurrence in primary bone tumours (Franzius et al. 2002b), with higher specificity and overall accuracy. This study however reviewed only 27 patients – 6 osteosarcoma, and 21 Ewing sarcoma – and compared FDG PET with CT thorax, bone scan and MRI. Another small study that reviewed 28 soft tissue and bone sarcoma patients (Johnson et al. 2003) compared FDG PET with body CT and regional MRI. In this small sample FDG PET proved 100% effective in detecting recurrence, particularly where there had been previous extensive surgery or radiotherapy (Fig. 4.21). Both the aforementioned papers however are PET studies and do not include coregistration with CT.

Pulmonary metastases are one area where CT performs better in detecting metastases than FDG PET (Franzius et al. 2001) with sensitivity of 0.75 and 0.50 respectively. With the addition of CT coregistration

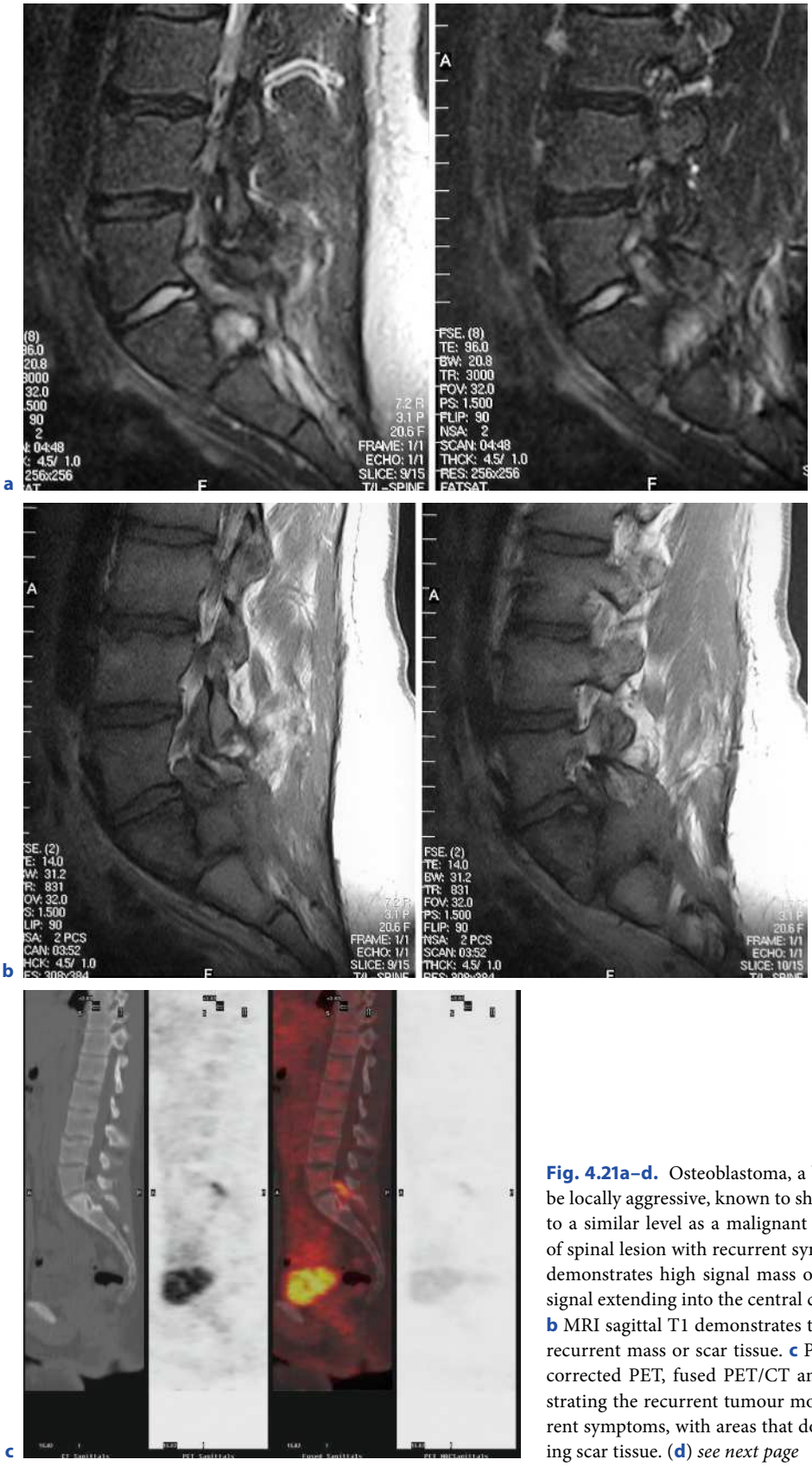

Fig. 4.21a–d. Osteoblastoma, a benign bone tumour but can be locally aggressive, known to show high uptake on FDG PET to a similar level as a malignant bone tumour. Post resection of spinal lesion with recurrent symptoms. **a** MRI sagittal STIR demonstrates high signal mass or scar tissue which has high signal extending into the central canal and exit foramina at L5. **b** MRI sagittal T1 demonstrates the intermediate signal of the recurrent mass or scar tissue. **c** PET/CT with CT, attenuation corrected PET, fused PET/CT and uncorrected PET demonstrating the recurrent tumour most likely the source of recurrent symptoms, with areas that do not show uptake representing scar tissue. (**d**) *see next page*

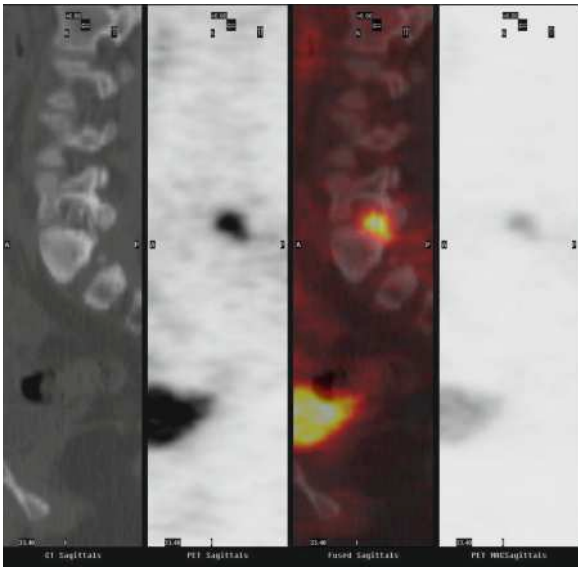

d

Fig. 4.21a–d. (*continued*) **d** PET/CT with CT, attenuation corrected PET, fused PET/CT and uncorrected PET demonstrating the recurrent tumour most likely the source of recurrent symptoms, with areas that do not show uptake representing scar tissue

(Iagaru et al. 2006) there was still a reduced sensitivity in detecting lung metastasis in PET and PET/CT as compared to CT with sensitivities of 68.3% and 95.1% respectively. Metastases of greater than 10 mm diameter may be negative on PET which may be secondary to reduced spatial resolution of the PET scan and breathing artifact causing blur.

In detecting bone metastases in general FDG PET performs well compared to other modalities such as whole body MRI and bone scan (Daldrup-Link et al. 2001) with sensitivities (P=0.05) for FDG PET, whole body MRI, and bone scan 90%, 82% and 71% respectively. Most false positives occurred in the FDG PET studies. All modalities had some false negatives depending on lesion location, MRI being less sensitive in the ribs, small and flat bones, bone scan in the spine and PET in the skull. A study in cases of primary bone sarcoma (Franzius et al. 2000) – 5 osteosarcoma and 49 Ewing's sarcoma – metastatic lesions compared bone scan to FDG PET in detecting metastases. The bone scan sensitivity, specificity and accuracy were 0.71, 0.92 and 0.88 respectively compared to FDG PET sensitivity, specificity and accuracy of 0.90, 0.96 and 0.95 respectively. FDG PET, however, did not detect the five osteosarcoma metastases. Although the osteosarcoma sample size in this study is very small, there could have been various reasons for this finding: a different pattern of glucose metabolism or expression of glucose transporter from the primary tumour site compared to the metastasis or a difference between cell subtype of osteosarcoma which may have different FDG uptake.

4.3.2.5 ^{18}F-Fluoride PET and PET/CT

The uptake of ^{18}F-fluoride in bone is rapid and once absorbed onto hydroxyapatite is then exchanged for a hydroxyl group of the hydroxyapatite in the bone and forms ^{18}F-fluoroapatite, which then deposits at the bone surface where turnover is greatest (Blau et al. 1972). ^{18}F-Fluoride PET has been shown to be more accurate than ^{99}Tc MDP scanning for detection of lytic and sclerotic bone lesions (Schirrmeister et al. 1999). The use of this more specific radiopharmaceutical for detection metabolically active bone lesions in PET has been evaluated for detection of metastatic disease in oncology patients (Evan-Sapir et al. 2004). ^{18}F-Fluoride PET/CT in comparison to ^{18}F-fluoride PET demonstrated higher sensitivity as one would expect 100% and 88% respectively for detection of bone metastases in oncology patients.

The use of more specific radiopharmaceutical for bone metabolism shows improved detection of bone lesions compared to FDG (Langsteger et al. 2006); this as yet, has not been applied to primary bone sarcoma specifically.

4.3.2.6 ^{18}F-3-Fluoro-3-deoxy-L-thymidine PET and PET/CT

^{18}F-3-Fluoro-3-Deoxy-L-Thymidine (FLT) is an analogue of thymidine, which is a nucleoside precursor in DNA synthesis, so it can be used as a measure of cell division. When FLT is phosphorylated by the enzyme thymidine kinase 1, intracellular trapping occurs. During DNA synthesis, thymidine kinase 1 concentration increases almost ten times and can therefore accurately reflect cellular proliferation (Valk et al. 2002). FLT is more specific in detecting high cell turnover than FDG, although resulting in high uptake in normal bone marrow, particularly at sites of growth in an immature skeleton. Normal high uptake is also seen in the heart, liver, kidneys and bladder. The half-life is 1.2 h and patients can be imaged at 60 min. A recent study (Buck et al. 2008) prospectively applied FLT PET and FDG PET/CT to 22 patients with bone or soft tissue tumours – 5 benign tumours of which 3 were bone tumours and 2 soft tissue tumours; this left 17 malignant sarcoma of which

7 were primary bone sarcomas and 10 soft tissue sarcomas. All the sarcomas showed uptake of FLT; an overlap between uptake of the benign lesions and low grade sarcomas was demonstrated but a significant difference between low grade and grade 2 and 3 sarcomas was demonstrated, particularly when using a cut off SUV of 2. FLT correlated significantly with tumour grade as compared to FDG in this small study. The study suggests that FLT could be used for noninvasive grading of sarcomas.

As with previous studies discussed, this is not a cell specific study, with a small sample size. However, it does indicate an additional potential for the application of PET in bone sarcoma evaluation, although it may be of limited value in the detection of bone metastases or local extension in view of the uptake at sites of normal cell division in the bone marrow.

4.3.3 The Future Application of PET/CT

As has been demonstrated, there is a need for larger and more cell specific prospective studies to demonstrate the value of PET/CT as applied to bone sarcoma. This would require carefully standardized multi-centre studies. The advance of cell specific radiopharmaceuticals has yet to be achieved.

At present it would appear that the value of PET/CT in the management of primary bone sarcoma lies in knowing that the primary tumour is FDG avid, before applying the modality to answer a specific management question. Measurement of response to therapy and survival or outcome measures may be where the value of PET/CT lies in the management of bone sarcoma.

References

Allen SD, Saifuddin A (2003) Imaging of intra-articular osteoid osteoma. Clin Rad 58:845–852

Aoki J, Watanabe H, Shinozaki T et al. (1999) FDG-PET in differential diagnosis and grading of chondrosarcoma. JCAT 23:603–608

Aoki J, Watanabe H, Shinozaki T et al. (2001) FDG PET of primary benign and malignant bone tumors: standardized uptake value in 52 lesions. Radiology 219:774–777

Bhagia SM, Grimer RJ, Davies AM et al. (1997) Scintigramically negative skip metastasis in osteosarcoma. Eur Radiol 7:1446–1448

Blau M, Ganatra R, Bender MA (1972) ^{18}F-Fluoride for bone imaging. Semin Nucl Med 2:31–37

Brenner W, Conrad EU, Eary JF (2004) FDG PET imaging for grading and prediction of outcome in chondrosarcoma patients. J Nucl Med Mol Imaging 31:189–195

Buck AK, Herrmann K, Büschenfelde CM et al. (2008) Imaging bone and soft tissue tumors with the proliferation marker [18F]fluorodeoxythymidine. Clin Cancer Res 14:2970–2977

Charkes ND (1980) Skeletal blood flow: implications for bone-scan interpretation. J Nucl Med 21:91–98

Chew FS, Hudson TM (1982) Radionuclide bone scanning of osteosarcoma: falsely extended uptake patterns. Am J Roentgenol 139:49–54

Coleman RE, Mashiter G, Whitaker KB et al. (1988) Bone scan flare predicts successful systemic therapy for bone metastases. J Nucl Med 29:1354–1359

Constable AR, Cranage RW (1981) Recognition of the superscan in prostatic bone scintigraphy. Br J Radiol 54:122–125

Crippa F, Seregni E, Agresti R et al. (1993) Bone scintigraphy in breast cancer: a ten-year follow-up study. J Nucl Biol Med 37:57–61

Daldrup-Link HE, Franzius C, Link TM et al. (2001) Whole-body MR imaging for detection of bone metastases in children and young adults: comparison with skeletal scintigraphy and FDG PET. AJR Am J Roentgenol 177:229–236

Dimitrakopoulou-Strauss A, Strauss LG, Heichel T et al. (2002) The role of quantitative ^{18}F-FDG PET in the differentiation of malignant and benign bone lesions. J Nucl Med 43:510–518

Epstein DA, Levin EJ (1978) Bone scintigraphy in hereditary multiple exostoses Am J Roentgenol 130:331–333

Even-Sapir E, Metser U, Flusser G et al. (2004) Assessment of malignant skeletal disease: initial experience with 18F-fluoride PET/CT and comparison of 18F-fluoride PET and 18F-fluoride PET/CT. J Nucl Med 45:272–278

Feldman F, Van Heertum R, Saxena C et al. (2005) ^{18}FDG-PET applications for cartilage neoplasms. Skeletal Radiol 34:367–374

Franzius C, Sciuk J, Daldrup-Link HE et al. (2000) FDG PET for detection of osseous metastases from malignant primary bone tumours: comparison with bone scintigraphy. Eur J Nucl Med 27:1305–1311

Franzius C, Daldrup-Link HE, Sciuk J et al. (2001) FDG- PET for detection of pulmonary metastases from malignant primary bone tumors: comparison with spiral CT. Ann Oncol 12:479–486

Franzius C, Bielack S, Flege S et al. (2002a) Prognostic significance of ^{18}F-FDG and ^{99m}MDP uptake in primary osteosarcoma. J Nucl Med 43:1012–1017

Franzius C, Daldrup-Link HE, Wagner-Bohn A et al. (2002b) FDG-PET for detection of recurrences from malignant primary bone tumors: comparison with conventional imaging. Ann Oncol 13:157–160

Gordon I, Hahn K, Fischer S (1993) Atlas of bone scintigraphy in the developing paediatric skeleton. Springer, Berlin Heidelberg New York

Grüning T, Franke WG (1999) Bone scan appearances in a case of Ollier's disease. Clin Nucl Med 24:886–887

Hain SF, Fogelman I (2002) Nuclear medicine studies in metabolic bone disease. Semin Musculoskelet Radiol 6:323–329

Han J, Ryu JS, Shin MJ et al. (2000) Fibrous dysplasia with barely increased uptake on bone scan: a case report. Clin Nucl Med 25:785–788

Hawkins DS, Rajendran JG, Conrad EU III et al. (2002) Evaluation of chemotherapy response in pediatric bone sarcomas by [F-18]-fluorodeoxy-D-glucose positron emission tomography. Cancer 94:3277–3284

Hawkins DS, Schuetze SM, Butrynski JE et al. (2005) [F-18]-Fluorodeoxy-D-glucose positron emission tomography predicts outcome for Ewing sarcoma family of tumors. J Clin Oncol 23:8828–8833

Helms CA (1987) Osteoid osteoma. The double density sign. Clin Orthop Relat Res 222:167–173

Helms CA, Hattner RS, Vogler JB III (1984) Osteoid osteoma: radionuclide diagnosis. Radiology 151:779–784

Iagaru A, Chawla S, Menendez L et al. (2006) 18F-FDG PET and PET/CT for detection of pulmonary metastases from musculoskeletal sarcomas. Nucl Med Commun 27:795–802

Jackson RP, Reckling FW, Mants FA (1977) Osteoid osteoma and osteoblastoma. Similar histologic lesions with different natural histories. Clin Orthop Relat Res 128:303–313

Johnson GR, Zhuang H, Khan J et al. (2003) Role of positron emission tomography with fluorine-18-deoxyglucose in the detection of local recurrent and distant metastatic sarcoma. Clin Nucl Med 28:815–820

Kaye M, Silverton S, Rosenthall L (1975) Technetium-99m-pyrophosphate: studies in vivo and in vitro J Nucl Med 16:40–45

Kole AC, Nieweg OE, Hoekstra HJ et al. (1998) Fluorine-18-fluorodeoxyglucose assessment of glucose metabolism in bone tumors. J Nucl Med 39:810–815

Langsteger W, Heinisch M, Fogelman I (2006) The role of fluorodeoxyglucose, 18F-dihydroxyphenylalanine, 18F-choline, and 18F-fluoride in bone imaging with emphasis on prostate and breast. Semin Nucl Med 36:73–92

Lee FY, Yu J, Chang SS et al. (2004) Diagnostic value and limitations of fluorine-18 florodeoxyglucose positron emission tomography for cartilaginious tumors of bone. J Bone Joint Surg Am 86:2677–2685

Lodge MA, Lucas JD, Marsden PK et al. (1999) A PET study of ^{18}FDG uptake in soft tissue masses. Eur J Nucl Med 26:22–30

Machida K, Makita K, Nishikawa J et al. (1986) Scintigramic manifestation of fibrous dysplasia. Clin Nucl Med 11:426–429

Mandell GA, Contreras SJ, Conard K et al. (1998) Bone scintigraphy in the detection of chronic recurrent multifocal osteomyelitis. J Nucl Med 39:1778–1783

Murphey MD, Flemming DJ, Boyea SR et al. (1998) Enchondroma versus chondrosarcoma in the appendicular skeleton: differentiating features. Radiographics 18:1213–1237

Ozcan Z, Burak Z, Kumanlioğlu K et al. (1999) Assessment of chemotherapy-induced changes in bone sarcomas: clinical experience with ^{99}Tc^{m}-MDP three phase dynamic bone scintigraphy. Nucl Med Commun 20:41–48

Picci P, Sangiorgi L, Rougraff BT et al. (1994) Relationship of chemotherapy-induced necrosis and surgical margins to local recurrence in osteosarcoma. J Clin Oncol 12:2699–2705

Reinartz P, Schaffeldt J, Sabri O et al. (2000) Benign versus malignant osseous lesions in the lumbar vertebrae: differentiation by means of bone SPECT. Eur J Nucl Med 27:721–726

Robinson PJ (1992) Bone scanning. Br J Hosp Med 48:99–103

Rosenthall L, Kaye M (1975) Technetium-99m-pyrophosphate kinetics and imaging in metabolic bone disease. J Nucl Med 16:33–39

Ryan PJ, Fogelman I (1994) Bone SPECT in osteoid osteoma of the vertebral lamina. Clin Nucl Med 19:144–145

Ryan PJ, Fogelman I (1995) The bone scan: where are we now? Semin Nucl Med 25:76–91

Schirrmeister H, Guhlmann A, Elsner K et al. (1999) Sensitivity in detecting osseous lesions depends on anatomic localization: planar bone scintigraphy versus ^{18}F PET. J Nucl Med 40:1623–1629

Schulte M, Brecht-Krauss D, Werner M et al. (1999) Evaluation of neoadjuvant therapy response of osteogenic sarcoma using FDG PET. J Nucl Med 40:1637–1643

Schulte M, Brecht-Krauss D, Heymer B et al. (2000) Grading of tumors and tumor-like lesions of bone: evaluation by FDG PET. J Nucl Med 41:1695–1701

Serafini AN (1976) Paget's disease of bone. Semin Nucl Med 6:47–58

Siddiqui AR, Tashjian JH, Lazarus K et al. (1981) Nuclear medicine studies in evaluation of skeletal lesions in children with histiocytosis X. Radiology 140:787–789

Smith FW (1998) The skeletal system. In: Sharp PE, Gemmell HG, Smith FW (eds) Practical nuclear medicine, 2nd edn. Oxford University Press, Oxford, pp 235–252

Subramanian G, McAfee JG (1971) A new complex of 99mTc for skeletal imaging. Radiology 99:192–196

Subramanian G, McAfee JG, Bell EG et al. (1972) 99m Tc-labeled polyphosphate as a skeletal imaging agent. Radiology 102:701–704

Tamir R, Glanz I, Lubin E et al. (1983) Comparison of the sensitivity of 99mTc-methyl diphosphonate bone scan with the skeletal X-ray survey in multiple myeloma. Acta Haematol 69:236–242

Tateishi U, Yamaguchi U, Seki K et al. (2007) Bone and soft-tissue sarcoma: preoperative staging with 18FDG PET/CT and conventional imaging. Radiology 245:839–847

Trikha V, Gupta V, Kumar R (2003) Ollier's disease: characteristic Tc-99m MDP scan features. Clin Nucl Med 28:56–57

Valk PE, Bailey DL, Townsend DW et al. (2002) Positron emission tomography: basic science and clinical practice. Springer, Berlin Heidelberg New York

Volker T, Denecke T, Steffen I et al. (2007) Positron emission tomography for staging of pediatric sarcoma patients: results of a prospective multicenter trial. J Clin Oncol 34:5435–5441

Wang K, Allen L, Fung E (2005) Bone scintigraphy in common tumors with osteolytic components. Clin Nucl Med 30:655–671

Zhibin Y, Quanyong L, Libo C et al. (2004) The role of radionuclide bone scintigraphy in fibrous dysplasia of bone. Clin Nucl Med 29:177–180

Ultrasonography

5

Alun Davies and Asif Saifuddin

CONTENTS

A. Davies, MD
Department of Radiology, Royal National Orthopaedic Hospital Trust, Brockley Hill, Stanmore, Middlesex, London HA7 4LP, UK

A. Saifuddin, MD
Department of Radiology, Royal National Orthopaedic Hospital Trust, Brockley Hill, Stanmore, Middlesex, London HA7 4LP, UK

KEY POINTS

- Ultrasound can be used to assess subperiosteal or extraosseous bone tumour extension.
- Ultrasound can accurately assess the cartilage cap of an osteochondroma.
- Bone tumours are frequently amenable to sonographically guided core needle biopsy with excellent results.
- Ultrasound can prove useful in the detection of local tumour recurrence, especially in the presence of an endoprosthetic replacement.
- Ultrasound may have a future role in the assessment of tumour response to neoadjuvant chemotherapy.

5.1 Introduction

The inherent inability of ultrasound (US) to penetrate adult cortical bone limits its role in the assessment of intramedullary bone tumours; however, once the bony cortex is breached with production of a subperiosteal or extraosseous mass, such lesions can be assessed by US. Similarly, tumours arising from the bone surface can also be evaluated.

Imaging plays a vital role in the identification, diagnosis, as well as local and distant staging of bone tumours. Plain radiographs, magnetic resonance imaging (MRI), bone scintigraphy and computed tomography (CT) adequately perform these roles; however, US has a role to play in the initial work-up of bone tumours and also in subsequent management, and this is discussed in the current chapter.

5.2 Imaging Features of Bone Tumours on Ultrasound

The normal cortex of a long bone is seen as a thin hyperechoic line which produces posterior acoustic shadowing (Fig. 5.1a,b; Lund et al. 1996). Ultrasound should be used to assess the integrity of the cortex, with the bone being scanned in the longitudinal and transverse planes. For appendicular bones and bones with little overlying soft tissue, for example, the pubic symphysis, a high-frequency (5–12 Mhz) linear-array probe enables optimal resolution of the bony cortex and any associated soft tissue mass. A lower-frequency (3.5 MHz) curvilinear probe may be necessary in bones with greater soft tissue coverage, for example, the posterior iliac crest or the femoral shaft. Colour Doppler should also be routinely used to assess areas of tumour neovascularity and to identify tumour relationship to any adjacent neurovascular structures (Fig. 5.1c).

5.3 Morphological Features of Bone Tumours on Ultrasound

5.3.1 Cortex

Ultrasound can demonstrate an intact underlying cortex where a lesion is arising in a juxtacortical location and is not involving the bone itself (Fig. 5.2). Pathological fractures are seen as a discontinuity and step of the normal hyperechoic linear cortical line, which can also be associated with an extraosseous extension of the tumour mass.

If the cortex is sufficiently thinned, then it may be possible to visualise the underlying medullary bone. In such circumstances, the posterior wall of a bone cyst can be seen.

Cortical destruction from primary intramedullary tumours, particularly osteosarcoma and Ewing sarcoma,

a

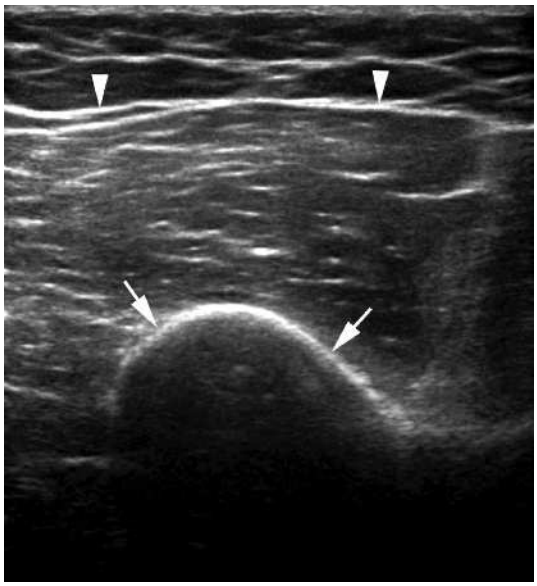

b

c

Fig. 5.1a–c. Normal bone. **a** Longitudinal and **b** transverse images of the mid-humerus show the hyperechoic thin line of the bone cortex (*arrows*) and the deep fascia (*arrowheads*), between which lies the muscle compartment. **c** Transverse Doppler US through the forearm in a patient with Ewing sarcoma of the proxiaml radius demonstrates the eroded radial cortex (*short arrow*), the extraosseous tumour mass (*arrowheads*) and the adjacent brachial vessels (*double-headed arrow)*

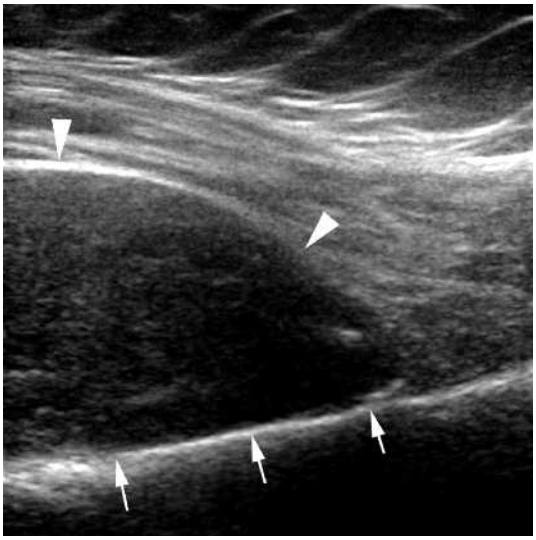

Fig. 5.2. Longitudinal US of the humerus in a woman with a periosteal chondroma shows the tumour mass (*arrowheads*) and the intact underlying cortex (*arrows*)

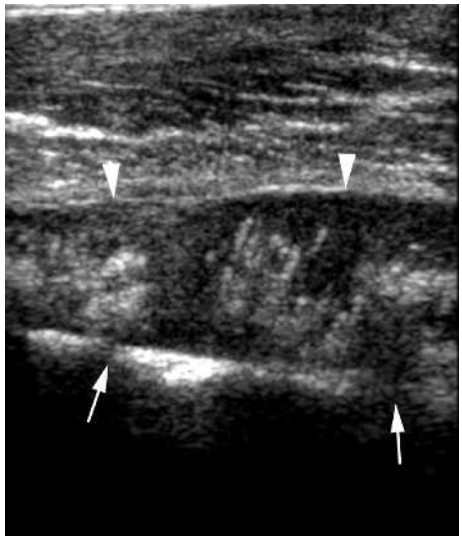

Fig. 5.3. Longitudinal US of the femur in a child with osteosarcoma shows irregular discontinuity of the femoral cortex (*arrows*) with an associated extraosseous mass (*arrowheads*)

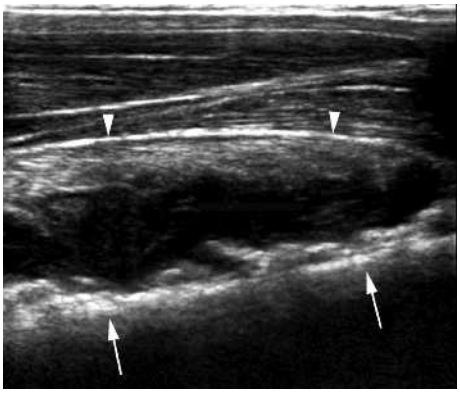

a

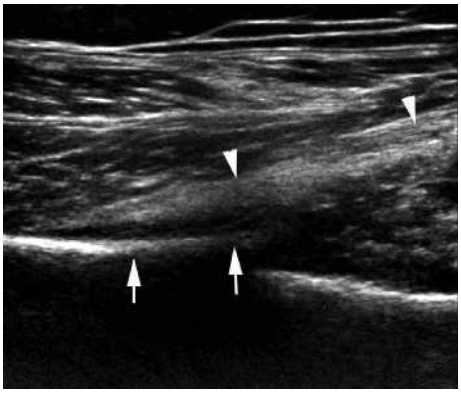

b

Fig. 5.4a,b. Periosteal response. **a** Longitudinal US through the upper forearm in a child with a proximal radial Ewing sarcoma shows the tumour mass extending through the permeated cortex (*arrows*) and covered by the intact periosteum (*arrowheads*). **b** Longitudinal US in a child with a distal femoral osteosarcoma shows a Codman's triangle (*arrows*) at the site of extraosseous tumour extension (*arrowheads*)

appears as a discontinuity or marked irregularity of the smooth hyperechoic line of the normal cortex, with the associated extraosseous tumour mass (Fig. 5.3).

5.3.2 Periosteum

Ultrasound can demonstrate the unmineralised periosteum as a thin, hyperechoic line overlying the extraosseous tumour mass (Fig. 5.4a). A multilaminated periosteal reaction may be seen as multiple thin hyperechoic lines. A Codman's triangle seen on plain radiographs manifests as a smooth angulation of the cortex at the tumour margin (Fig. 5.4b).

5.3.3 Neurovascular Bundle

Ultrasound can demonstrate displacement or encasement of the neurovascular bundle (Fig. 5.5), which is

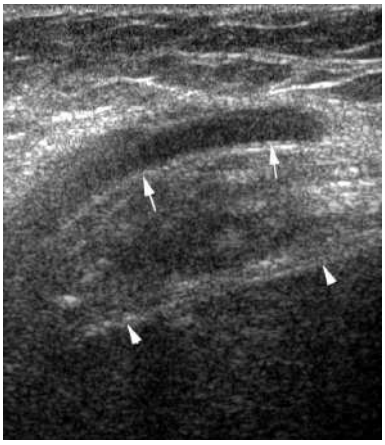

Fig. 5.5. Longitudinal US through the arm in a patient with lymphoma of the humerus shows a large soft tissue mass extending from the bone surface (*arrows*) and displacing and partially encasing the brachial artery (*arrowheads*)

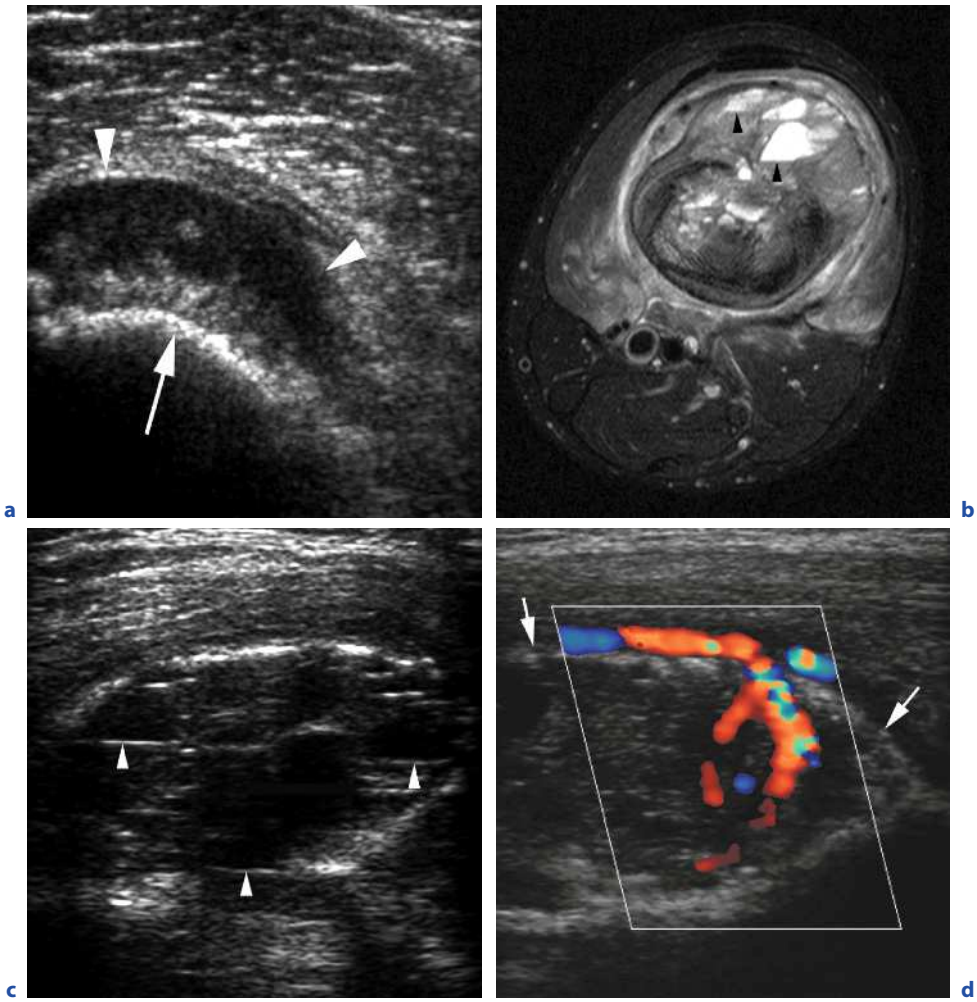

Fig. 5.6a–d. Osteosarcoma. **a** Transverse US through the femur (*arrow*) shows an extraosseous mass (*arrowheads*) containing heterogeneous hyerechoic areas due to matrix ossification. **b** Axial fat-suppressed, proton-density-weighted, fast spin-echo (PDW FSE) MR image and **c** transverse US show multiple fluid levels (*arrowheads*). **d** Longitudinal colour Doppler US shows marked neovascularity within th extraosseous mass (*arrows*)

most frequently seen in tumours with large extraosseous components; however, US is no more sensitive than MRI in demonstrating the tumour relationship with the neurovascular bundle, but is useful in assessing flow within the vessels and ensuring that biopsy approaches are remote from the neurovascular bundle, which can sometimes be difficult to appreciate with CT-guided biopsy.

5.4 Tumour Characterisation

Ultrasound adds little to the plain radiographic findings in differentiating tumour types due to the non-specific appearances of tumours on US.

5.4.1 Osteosarcoma

The US appearances reflect the plain radiographic findings with irregular hyperechoic areas representing matrix ossification with variable degrees of posterior acoustic shadowing depending on the extent of matrix mineralization (Fig. 5.6a). Lytic tumours are heterogenous in echotexture with necrotic areas appearing hypo- or anechoic with occasional fluid levels (Fig. 5.6b,c); however, the majority of osteosarcomas are hypervascular on colour flow imaging (Fig. 5.6d; Saifuddin et al. 1998).

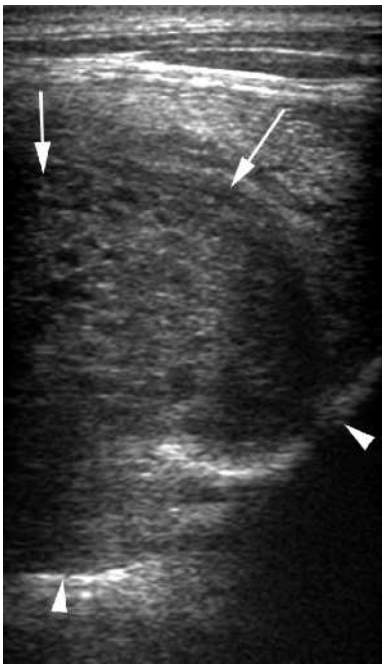

Fig. 5.7. Ewing sarcoma. Transverse US through the lower abdomen shows a large, relatively homogeneous mass (*arrows*) arising from the iliac blade (*arrowheads*)

5.4.2 Malignant Round Cell

The US appearances of malignant round cell tumour [Ewing sarcoma, peripheral neuroectodermal tumour (PNET), primary bone lymphoma (PBL)] can be variable (Fig. 5.7). Tumours with a small extraosseous component appear homogenously hypoechoic, but as the extraosseous component enlarges the tumour matrix becomes more heterogeneous due to necrosis. These tumours tend to be relatively hypovascular (Saifuddin et al. 1998).

5.4.3 Giant Cell Tumour

Heterogeneous echotexture with areas of necrosis and fluid-fluid levels may be seen in giant cell tumours. The majority of these tumours are hypervascular.

5.4.4 Aneurysmal Bone Cyst

Fluid-fluid levels and septae may be identified in aneurysmal bone cysts if the tumour is located in a subperiosteal location (Habear et al. 1993).

5.4.5 Osteochondroma

Ultrasound can accurately assess the cartilage cap of an osteochondroma (OC), (Malghem et al. 1992). The cartilage cap appears as a hypoechoic layer covering the hyperechoic surface of the deeper calcified part (Fig. 5.8a). Increased thickness of the cartilage cap is considered an extremely important criterion for the diagnosis of peripheral chondrosarcoma, since malignant transformation occurs in the cartilage cap (Garrison et al. 1982; Malghem et al. 1992). Although a thickness value specific for malignancy cannot be determined, a cap thinner than 1 cm usually indicates a benign exostosis, a cap between 1 and 2 cm thick may be considered suspicious, while a cap thicker than 2 cm generally

corresponds to malignant transformation (Fig. 5.8b,c). In addition, US allows the recognition of other complications such as bursa formation; however, US is limited in evaluating cartilage caps that are inwardly orientated or deeply located in soft tissue, both situations being relatively uncommon.

5.4.6 Chondrosarcoma

Ultrasound can assess the extraosseous component of high-grade central CS or peripheral CS complicating an osteochondroma (see above). The morphology of the lesion is typically hypoechoic and multilobular with internal hyperechoic septation (Fig. 5.9). The matrix mineralization pattern can be seen as either punctate, hyperechoic areas or more extensive curvilinear hyperechoic areas with posterior acoustic shadowing. These tumours are relatively hypovascular on colour Doppler (Saifuddin et al. 1998).

5.5 US-Guided Biopsy

The diagnostic accuracy of image-guided percutaneous needle biopsy of bone tumours with either fine-needle or larger-gauge core biopsy needles is well established in the literature. Traditionally percutaneous needle biopsy of primary or metastatic bone neoplasms is either fluoroscopically or CT guided (Ayala and Zornosa 1983; Dupuy et al. 1998; Harish et al. 2006; White et al. 1996).

Although US has the disadvantage in its inability to show purely intraosseous lesions, a large proportion of tumours that require biopsy have some degree of subperiosteal or extraosseous extension at presentation, which can be identified on US (Carrasco et al. 1991; Civardi et al. 1994; Saifuddin et al. 1998). Due to the presence of this soft tissue mass, bone tumours are frequently amenable to sonographically guided core biopsy with excellent results. A diagnostic accuracy of up

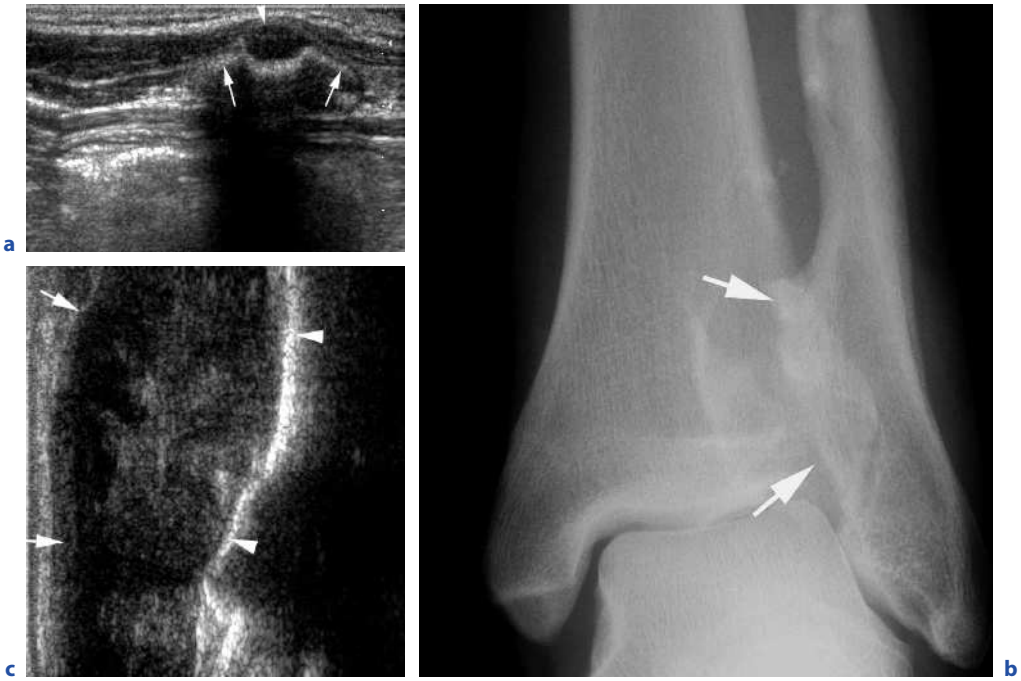

Fig. 5.8a–c. Osteochondroma. **a** Longitudinal US of the rib shows a sessile osteochondroma (*arrows*) with a small overlying hypoechoic cap (*arrowhead*). Peripheral chondrosarcoma. **b** Anteroposterior radiograph of the ankle shows a sessile osteochondroma (*arrows*) of the fibula. **c** Longitudinal US shows a very thick, heterogeneous mass (*arrows*) arising from the surface of the osteochondroma (*arrowheads*)

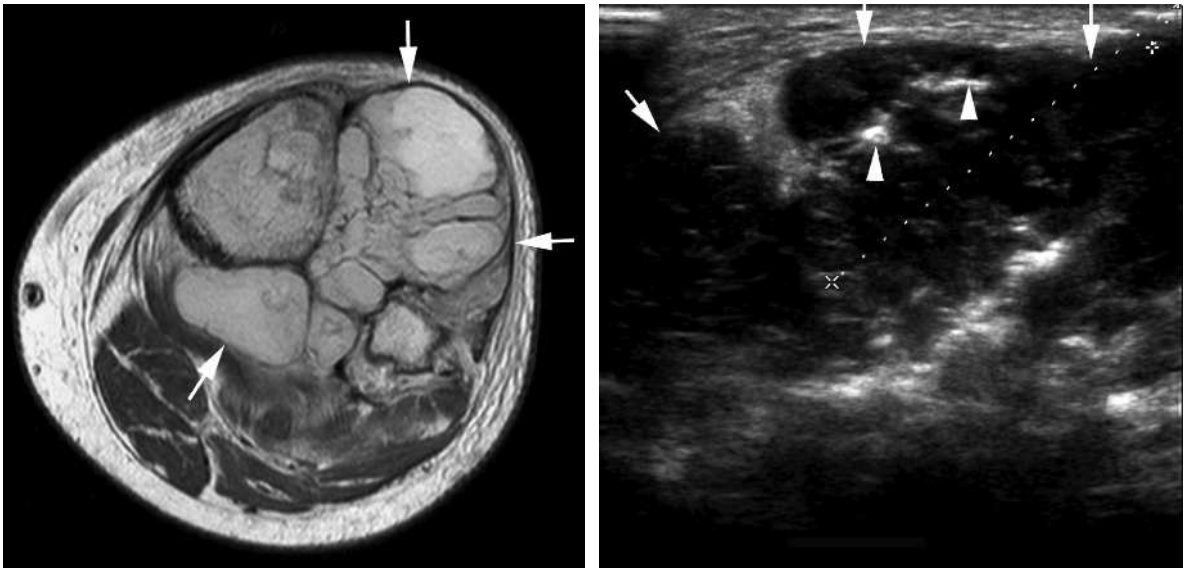

a b

Fig. 5.9a,b. High-grade central chondrosarcoma. **a** Axial PDW FSE MR image through the proximal tibia shows a tumour with a large extraosseous component (*arrows*). **b** Longitudinal US shows the hypoechoic, lobular morphology of the lesion (*arrows*) with internal punctate and linear echogenic calcifications (*arrowheads*)

to 98% for surface bone lesions and aggressive tumours with extension through the cortex has been reported (Civardi et al. 1994; Saifuddin et al. 2000; Torriani et al. 2002; Yeow et al. 2000).

Ultrasound has several advantages over CT and fluoroscopy. The adjacent neurovascular bundle can be easily identified and marked such that the biopsy can be made away from major vessels. The tumour should be scanned in longitudinal and transverse planes to identify a solid area to biopsy. Demonstration of neovascularity within the tumour with colour Doppler increases the chances of the biopsy being obtained from an area of viable tumour, rather than a solid-appearing area of necrosis. For hypovascular tumours, such as Ewing sarcoma and peripheral chondrosarcoma, a biopsy from the edge of the lesion increases the chances of sampling viable tumour (Saifuddin et al. 2000). Ultrasound has further advantages in being relatively inexpensive and readily available, and also lacking the risk from ionising radiation to both patients and staff. Ultrasound-guided biopsy can be performed more quickly and cheaply compared with CT, especially when it is necessary to sample several areas of a neoplasm.

5.6 Monitoring of Tumour Response

For patients with osteosarcoma or Ewing sarcoma, the clinical outcome can be predicted by the histological response to neoadjuvant chemotherapy, as determined by pathological assessment of the resection specimen. Those patients who respond poorly may benefit from a change of chemotherapy regimen, or early surgery to reduce the risk of metastasis.

Van Der Woude et al. (1995) used colour Doppler US to assess intratumoral blood flow in the extraosseous component of patients with either osteosarcoma or Ewing sarcoma, before, during and after chemotherapy. They found that resistive indices in arteries that fed tumours were significantly lower in the contralateral normal arteries. After chemotherapy, persistent intratumoral flow corresponded to poor histological response. In practical terms, if after chemotherapy there is less vascularity in a lesion, and the resistive index of the feeding vessel decreases, tumour necrosis can be assumed. For findings to be reliable, probe repositioning for follow-up studies must be exact, a problem which may partly be overcome by employing a single operator and using fixed anatomical landmarks.

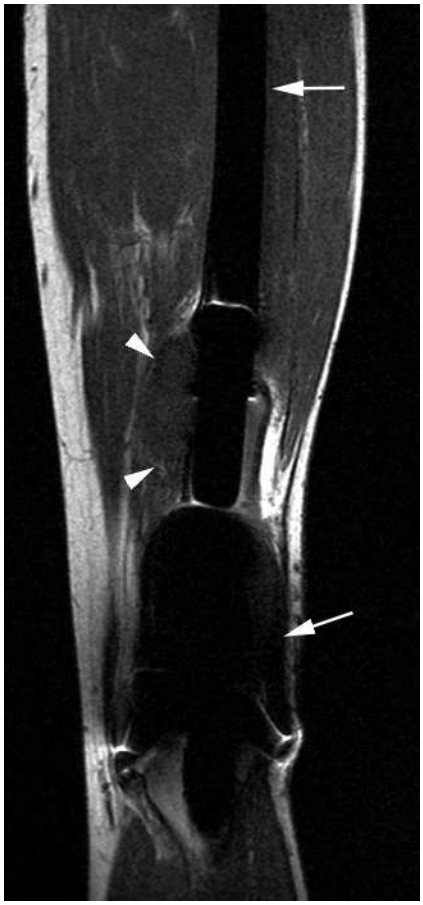

a

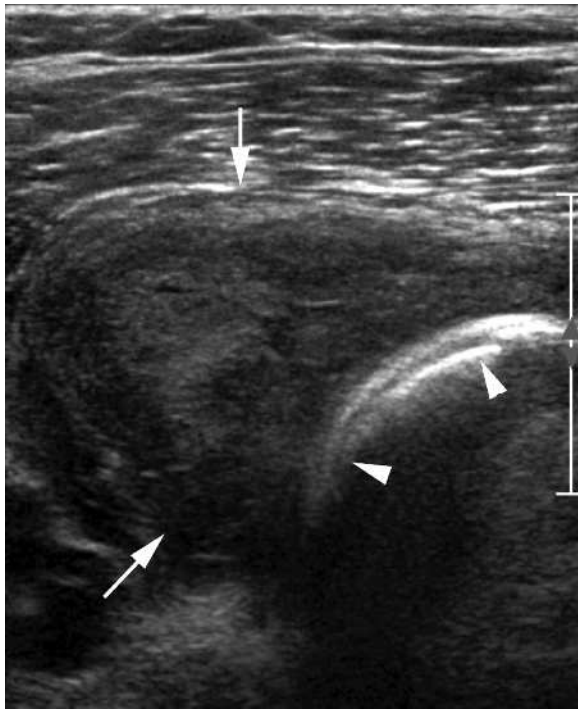

b

Fig. 5.10a,b. Assessment of endoprosthetic replacement. **a** Coronal T1W SE MR image shows a soft tissue mass (*arrowheads*) adjacent to a distal femoral massive replacement (*arrows*). **b** Axial US shows the lesion (*arrows*) with no associated artefact from the prosthesis (*arrowheads*)

5.7 Assessment of Local Recurrence

Ultrasound has the advantage over MRI and CT in the assessment of clinically suspected local recurrence at the site of previous surgery, as images are not degraded by artefact from endoprosthetic replacement (Fig. 5.10). Solid lesions can be distinguished from post-operative fluid collections, which appear anechoic on US, are compressible and may demonstrate posterior acoustic enhancement. Ultrasound can be used to guide needle aspiration of peri-prosthetic fluid collections when infection is a clinical concern. Differentiation between chronic infection and scar tissue may be difficult, as both can appear as poorly defined, hypervascular soft tissue masses. Tumour recurrence tends to be more spherical or lobular and well defined (Fig. 5.11) compared with scar formation and chronic infection. If there is any suspicion of recurrence, then a biopsy can be performed under US guidance.

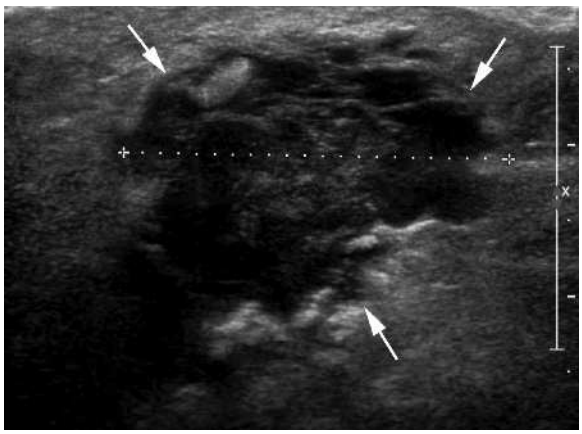

Fig. 5.11. Longitudinal US of the thigh shows a lobular, hypoechoic mass (*arrows*) due to local recurrence of dedifferentiated chondrosarcoma of the femur

5.8 Conclusion

Although US adds little to the initial diagnosis and staging of primary bone tumours, it plays a potentially important role in guiding needle biopsy of surface tumours or tumours with extraosseous extension. Ultrasound can also be useful in the detection of local recurrence, especially in the presence of endoprosthetic replacement, and may have a future role in assessing tumour response to chemotherapy.

References

Ayala AG, Zornosa J (1983) Primary bone tumors: percutaneous needle biopsy: radiologic–pathological study of 222 biopsies. Radiology 149:675–679

Carrasco CH, Wallace S, Richli WR (1991) Percutaneous skeletal biopsy. Cardiovasc Intervent Radiol 14:69–72

Civardi G, Livraghi T, Colombo P, Fornari F, Cavanna L, Buscarini L (1994) Lytic bone lesions suspected for metastasis: ultrasonically guided fine-needle aspiration biopsy. J Clin Ultrasound 22:307–311

Dupuy DE, Rosenberg AE, Punyaratabandhu T, Tan MH, Mankin HJ (1998) Accuracy of CT-guided needle biopsy of musculoskeletal neoplasm. Am J Roentgenol 171:759–762

Garrison RC, Unni KK, McLeod RA, Pritchard DJ, Dahlin DC (1982) Chondrosarcoma arising in osteochondroma. Cancer 49:1890

Habear HP, Drews K, Scheel-Walter H, Klinbiel T (1993) Aneurysmal bone cysts in early childhood: ultrasound findings. Pediatr Radiol 23:405–406

Harish S, Hughes RJ, Saifuddin A, Flanagan AM (2006) Image-guided percutaneous biopsy of intramedullary lytic bone lesions: utility of aspirated blood clots. Eur Radiol 16:2120–2125

Lund PJ, Nisbet JK, Valencia FG, Ruth JT (1996) Pictorial essay: current sonographic applications in orthopaedics. Am J Roentgenol 166:889–895

Malghem J, Vande Berg B, Noël H, Maldague B (1992) Benign osteochondromas and exostotic chondrosarcomas: evaluation of cartilage cap thickness by ultrasound. Skeletal Radiol 21:33–37

Saifuddin A, Burnett SJD, Mitchell R (1998) Pictorial review: ultrasonography of primary bone tumours. Clin Radiol 53:239–246

Saifuddin A, Mitchell R, Burnett SJ, Sandison A, Pringle JA (2000) Ultrasound-guided needle biopsy of primary bone tumours. J Bone Joint Surg Br 82:50–54

Torriani M, Etchebehere M, Amstalden EMI (2002) Sonographically guided core needle biopsy of bone and soft tissue tumours. J Ultrasound Med 21:275–281

Van der Woude HJ, Bloem JL, van Oostayen JA, Nooy MA, Taminiau AH, Hermans J et al. (1995) Treatment of high-grade bone sarcomas with neoadjuvant chemotherapy: the utility of sequential color Doppler sonography in predicting histopathological response. Am J Roentgenol 165(1):125–133

White LM, Schweitzer ME, Deely DM (1996) Coaxial percutaneous needle biopsy of osteolytic lesions with intact cortical bone. Am J Roentgenol 166:143–144

Yeow K-M, Tan C-F, Chen J-S, Hsueh C (2000) Diagnostic sensitivity of ultrasound-guided needle biopsy in soft tissue masses about superficial bone lesions. J Ultrasound Med 19:849–855

Interventional Techniques

6

Steven L. J. James

CONTENTS

KEY POINTS

- Multiple percutaneous therapies are available for the treatment of both benign and malignant bone neoplasms.
- Thermal ablation is the procedure of choice for the treatment of osteoid osteoma and is increasingly being used for chondroblastoma.
- Palliative thermal ablation of metastatic disease can be performed for pain relief.
- Spinal cementoplasty incorporates both vertebroplasty and balloon kyphoplasty. The aim of treatment is to provide pain relief and prevent further collapse.
- Cementoplasty can be performed in the pelvis for pain relief in metastatic disease.
- Vascular embolization can be undertaken either pre-operatively to reduce the risk of intraoperative haemorrhage or for symptomatic control in patients with metastatic disease.

6.1 Introduction

Image-guided percutaneous techniques are increasingly being utilized in the treatment and palliation of both benign and malignant primary and secondary bone tumours. The indication for these therapies continues to expand and they form an integral part of the multidisciplinary management of bone neoplasms. In some instances, for example in the treatment of osteoid osteoma, percutaneous radiofrequency ablation has largely replaced surgical excision as the primary treatment of choice for this benign tumour (Rosenthal et al. 2003).

This chapter considers the role of these interventional techniques in the management of bone tumours.

S. L. J. James, MB, ChB, FRCR
Consultant Radiologist, Department of Radiology, The Royal Orthopaedic Hospital, NHS Foundation Trust, Bristol Road South, Northfield, Birmingham B31 2AP, UK

The different methods of thermal ablation, including radiofrequency ablation, microwave therapy, laser coagulation and cryotherapy, are considered. Percutaneous cementoplasty in both spinal and extraspinal sites is discussed as is the role of bone substitutes. Finally, preoperative embolization is briefly addressed. The theory behind these techniques is described and the indications, procedure technique and clinical outcomes following treatment are reviewed. All percutaneous interventions require a good knowledge and understanding of compartmental anatomy to allow a safe access route to be planned. A number of articles have been published on this subject and are useful reference sources for those undertaking these procedures (Liu et al. 2007; Logan et al. 1996; Bancroft et al. 2007). Biopsy techniques are covered in Chap. 8.

6.2 Thermal Ablation

Over recent years, thermal ablation in its different guises has become increasingly used in the treatment of a number of benign and malignant bone tumours. Its role is continuing to expand as experience with these techniques increases and new indications continue to be described. The thermal ablation techniques, including radiofrequency ablation, cryotherapy, laser coagulation and microwave therapy, are discussed. The procedural technique is discussed in detail for radiofrequency ablation, but as there is significant overlap in terms of bone access methods between the thermal ablation techniques, this is not repeated in order to avoid repetition.

6.2.1 Radiofrequency Ablation

High-frequency alternating current (460–480 kHz) is applied through an exposed needle tip creating a local heating phenomenon. As the alternating current is applied, ions in the targeted tissue attempt to follow the directional changes leading to frictional heating. This causes denaturation of proteins, tissue dessication and coagulative necrosis (Nahum Goldberg and Dupuy 2001). As tissue is ablated, the resistance to electrical current (impedance) increases. A number of manufacturers allow active monitoring of impedance during the radiofrequency ablation cycle thereby enabling an estimation of complete ablation of a given tissue volume. The size of the treatment area is determined by the size of the exposed needle tip and this can be chosen according to case requirements. Technical advances in needle design now allow lesions up to 5 cm in diameter to be treated with a single multi-tined array probe and some manufacturers allow multiple needle placements to be performed and ablated simultaneously.

The most common bone tumour to be treated with radiofrequency ablation is osteoid osteoma. This is a benign osteogenic tumour that typically occurs in the metaphysis/diaphysis of long bones in children and young adults. Traditional treatments include surgical resection and curettage; however, the small size makes intra-operative localization of the tumour difficult, and often quite large surgical exposures can be required to identify and treat these lesions. Some authors have advocated the use of intra-procedural radionuclide localization to aid in lesion detection during surgery (Szypryt et al. 1986; Hay et al. 2007).

CT-guided radiofrequency ablation is now firmly established as the therapeutic method of choice in the treatment of osteoid osteoma (Rosenthal et al. 2003; Woertler et al. 2001). The procedure is most frequently performed under general anaesthesia, although some authors advocate the use of sedation. An initial CT is performed to localize the nidus and allow planning of an access route for biopsy and radiofrequency ablation. A long-acting local anaesthetic should be infiltrated along the needle tract and in the periosteum at the site of bone penetration. A bone biopsy needle is then used to access the lesion and allow placement of

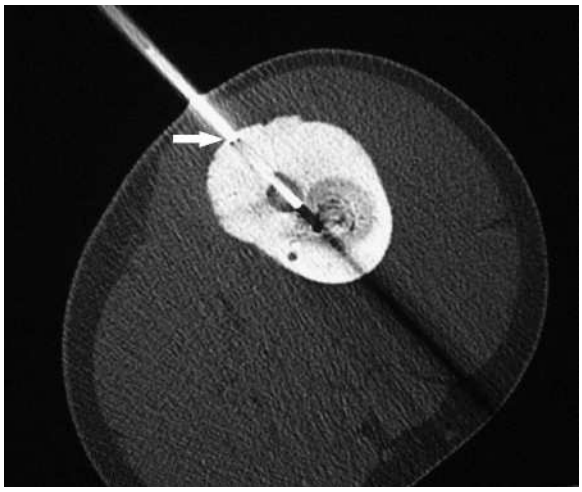

Fig. 6.1. Axial CT through the mid thigh illustrates the Bonopty needle in situ passing through the soft tissues to the cortical bone surface (*arrow*). The inner needle is demonstrated in the centre of the osteoid osteoma nidus

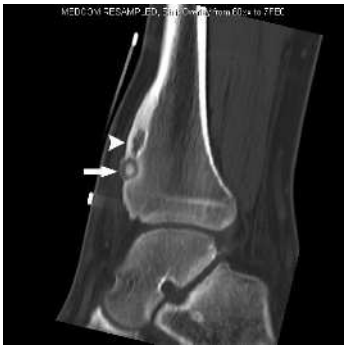

Fig. 6.2. Sagittal CT reconstruction of the distal tibia. Biopsy confirmed the inferior area (*arrow*) to be the osteoid osteoma nidus with the more cranially located abnormality (*arrowhead*) representing reactive tissue only. Regardless, separate access for biopsy and ablation was required to treat both sites adequately

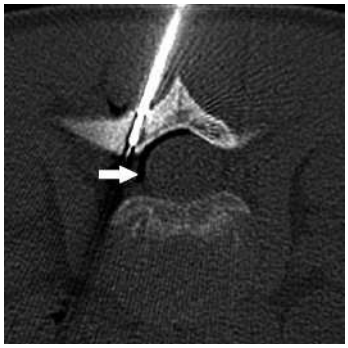

Fig. 6.3. Axial CT through the L2 level shows the ablation needle in situ in the right lamina. Air had been instilled into the epidural space under CT guidance prior to ablation to act as a "thermoprotective agent"

the ablation needle. Tissue is routinely sent for histology and microbiology. The present author's preference is for the Bonopty coaxial bone biopsy system (Radi Medical Systems, Uppsala, Sweden) which incorporates a drill, although other manufacturers' systems are available for this purpose. In view of the size of the lesion it is particularly important that a good technique be used to access the nidus. The needle should be inserted parallel to the CT beam and placed as centrally within the nidus as possible. Following bone access an insulated probe is inserted through the biopsy needle (Fig. 6.1). Most frequently a 5-mm exposed needle tip is required, but in cases where a larger nidus is identified a 10- or 15-mm exposed tip may be required. In some cases where an elongated nidus is identified in cranio-caudal direction or in rare cases of a "double" nidus, more than one access point and ablation site is required (Fig. 6.2). It is the present author's preference to perform two cycles of 3 min at 90°C with cleaning of the exposed tip between cycles, although many operators would perform a single 6-min cycle. At the start of the ablation it is not infrequent that the patient develops a transient tachycardia due to the stimulation of the painful nidus. When the ablation is complete, the needles are then withdrawn and a skin dressing is applied. Patients can usually be discharged the same day but should be advised that some post-procedural pain of different character is normal in the days following treatment.

The typical pre-procedure pain usually responds within 2–5 days (Donkal et al. 2008). Overall, therapeutic success is between 73 and 91% according to different series with a single treatment (Vanderschueren et al. 2007; Donkol et al. 2008). Outpatient follow-up at approximately 6 weeks allows the clinical response to be assessed, but routine imaging is not required. Recurrent or residual symptoms following a single treatment should prompt a further attempt at radiofrequency ablation; however, the success rates are somewhat lower for second treatment (approximately 60%; Rosenthal et al. 2003). The imaging findings in these cases are, however, somewhat variable with no reliable imaging sign which accurately predicts residual or recurrent tumour (Vanderschueren et al. 2007). Tumour location in a non-diaphyseal region is more likely to be associated with tumour recurrence (Cribb et al. 2005). Long-term follow-up at 2–5 years again shows success rates in the region of 90% (Sung et al. 2007).

Complications from the procedure are minimal. Occasionally, thermal burns have been reported particularly in the treatment of very superficial lesions (Finstein et al. 2006). This occurs due to contact between the exposed needle tip and the coaxial needle with heat passage along the access needle to the skin. Local anaesthetic can be usefully injected as this swells the subcutaneous tissues before bone needle access in subcutaneous lesions, potentially reducing this risk. If a spinal lesion is being treated, air can be injected into the epidural space to allow a degree of increased thermal protection for the spinal cord (Fig. 6.3).

Recently, a number of authors have described the use of radiofrequency ablation in the treatment of chondroblastoma (Tins et al. 2006; Petsas et al. 2007; Christie-Large et al. 2008). The typical epiphyseal location of this tumour often makes surgical treatment challenging both in terms of potential injury to the growth plate and articular cartilage when the lesion

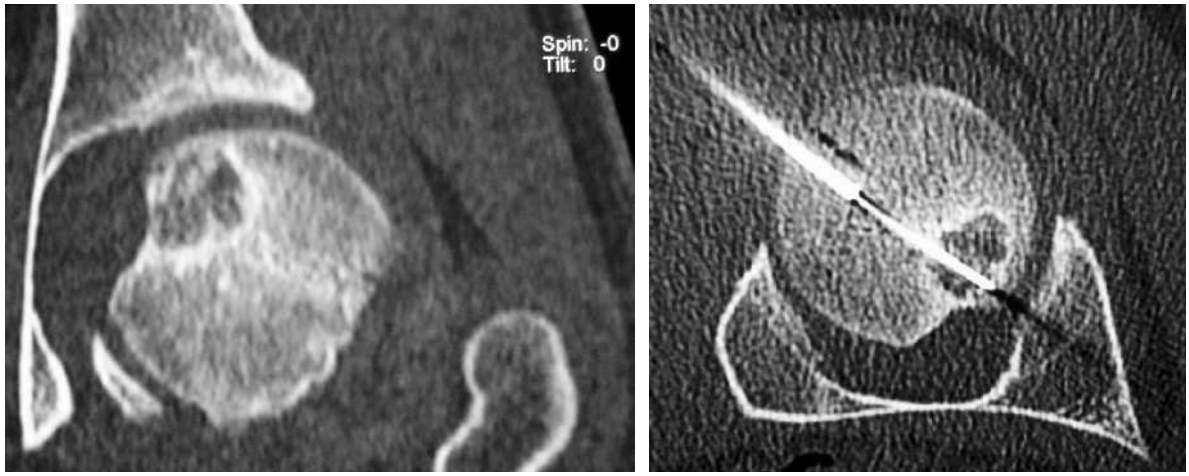

a b

Fig. 6.4. **a** Coronal CT reconstruction of the proximal femur shows the typical epiphyseal subchondral location of chondroblastoma. **b** Axial CT shows the ablation needle positioned in the posterior medial aspect of the lesion. In this case multiple needle placements were required to ablate the chondroblastoma (not shown)

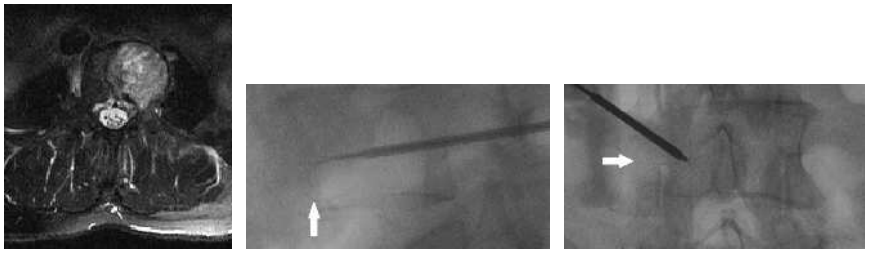

a,b c

Fig. 6.5. **a** Axial fat-suppressed T2-weighted MR image shows a renal metastasis in the left side of the body of L3. Lateral (**b**) and anteroposterior (**c**) views during the ablation procedure (patient in prone position) show the multi-tined umbrella probe in situ (*arrow*). This procedure was combined with vertebroplasty (not illustrated)

lies adjacent to a joint surface. This has led to increased interest in minimally invasive methods of treating this benign bone tumour. Each of the published series differs in the technique used. Tins and co-workers (2006) used a multi-tined electrode to provide a sufficiently large ablation zone to treat the lesion. In their series of four patients there were two complications, namely end-plate infraction and articular cartilage injury. A recent series published by the present author's institution described multiple single-needle placements into the lesion rather than the use of a single multi-tined probe (Fig. 6.4). This potentially allows better control of the ablation zone and no complications were encountered in the four patients treated with this technique. Mean follow-up of just over 12 months showed resolution of the typical oedema pattern encountered with chondroblastoma and fatty ingrowth in the periphery of the lesion on T1-weighted images (Christie-Large et al. 2008). It seems likely that this technique will continue to gain favour in the treatment of this tumour. Additional long-term data will be required, however, to establish the potential for local recurrence.

In terms of primary malignant bone tumours, radiofrequency ablation currently has no defined role. Treatment of these conditions consists of surgical resection with the aim of clear margins followed by adjuvant therapy if indicated. In the management of metastatic disease, treatment is palliative, so clear margins are of less concern; thus, percutaneous therapies can be utilized more often. Pain from bone metastases can be extremely debilitating, often requiring large amounts of opiate analgesia. This can significantly affect patient quality of life during the palliative phase of management (Nielsen et al. 1991). Traditionally, local radiotherapy,

chemotherapy or hormone treatment is used for pain control in symptomatic bone metastases. There is, however, a group of up to 30% of patients who are refractory to these therapies who are still troubled with ongoing pain (Callstrom et al. 2006b). It is in this group that radiofrequency ablation has found a role (Fig. 6.5). Initial results show promise with a number of studies demonstrating reduction in mean pain scores albeit in small patient groups (Callstrom et al. 2002; Callstrom et al. 2006a; Goetz et al. 2004; Gronemeyer et al. 2002; Thanos et al. 2008). As one would expect, smaller metastases respond better to radiofrequency ablation with large pelvic tumours often not gaining significant pain relief.

6.2.2 Laser Therapy

Laser ablation effectively provides an alternative to radiofrequency ablation and the same indications apply for this technique. Interstitial laser ablation involves the use of an optic fiber which delivers a fixed energy, thus acting as a heat source. The size of the ablation zone relates to the duration of energy application, power used, fiber diameter and tip size. Gangi and co-workers (2007) reported 114 cases of osteoid osteoma treated with laser ablation with mean follow-up of 58.5 months. The treatment was effective in 112 patients and they reported six recurrences in the study period. These results are comparable with previous reported series treated with radiofrequency ablation. Laser ablation has also been reported in conjunction with percutaneous vertebroplasty for the treatment of metastatic spinal lesions to reduce the potential risk of cement migration (Ahn et al. 2007).

6.2.3 Cryotherapy

Cryotherapy refers to the use of freezing to obtain tissue destruction and a number of different mechanisms of action have been suggested including tissue ischaemia, protein denaturation, membrane destabilization and cellular rupture (Simon and Dupuy 2006). Cryosurgery has been evaluated and found to be effective in the local control of metastases, benign aggressive bone lesions and low-grade chondrosarcoma (Bickels et al. 1999; Ahlmann et al. 2006). Advances in needle design have allowed this technique to be performed percutaneously. Argon gas is delivered through an insulated probe which undergoes rapid expansion resulting in cooling to −100°C within seconds. Recently, Tuncali and co-workers (2007) described the use of MR-guided cryotherapy in the treatment of bone metastases. This allows active monitoring of the ablation zone using standard pulse sequences during the procedure. The frozen tissue creates an "ice ball" which causes a signal void on MR imaging. The ability to monitor the ablation intraoperatively provides a potential advantage over radiofrequency ablation. During radiofrequency ablation, MR imaging is used to monitor between cycles and image distortion occurs when the generator is activated (Zhang et al. 1998). Initial results for cryoablation demonstrate improvements in pain control following treatment in the majority of patients with the potential advantage of increased procedure safety and a reduction in damage to adjacent vital structures (Tuncali et al. 2007). Other workers have also reported significant reduction in patients' pain scores following percutaneous cryotherapy for metastases (Callstrom et al. 2006a).

6.2.4 Microwave Therapy

Microwave ablation refers to the use of electromagnetic waves with a frequency ≥900 MHz (Shibata et al. 2002; Simon et al. 2005). A number of workers have described the potential benefits of microwave therapy over conventional radiofrequency ablation. These benefits include faster ablation times, larger ablation volume, improved convection profile and no need for the placement of a grounding pad (Simon et al. 2005). Microwave radiation causes movement in water molecules due to interaction with its electric charge. This vigorous movement causes local heating which induces cellular death by coagulative necrosis. As with radiofrequency ablation, the procedure is performed under CT guidance using either general anaesthesia or conscious sedation. There are scant reports of the utility of the technique in the treatment of bone metastases (Simon and Dupuy 2006).

6.3 Cementoplasty

6.3.1 Spinal

Spinal cementoplasty incorporates vertebroplasty and kyphoplasty. Both techniques represent a minimally invasive procedure compared with surgical intervention

in which bone cement (typically polymethylmethacrylate, PMMA) is injected into the vertebra. The most frequent indication for vertebroplasty is benign vertebral compression fractures secondary to osteoporosis (Kobayashi et al. 2005); however, the use of this technique in malignant spinal disease is widespread (Alvarez et al. 2003). The common indications include metastases (Fig. 6.6) and myeloma (Fig. 6.7); however, benign tumours, such as haemangioma, may also be treated. As has been previously mentioned, up to 30% of patients treated with metastatic disease with adjuvant therapies continue to have ongoing pain and radiotherapy does not provide immediate vertebral stabilization (Callstrom et al. 2006b). The primary aim is therefore to provide pain relief in this refractory group but also to obtain some structural support and prevent further vertebral collapse (Jakobs et al. 2007). This should enable analgesic requirements to be reduced in the postoperative period. It is vital that appropriate patient selection for the procedure be undertaken and this is best facilitated by a multidisciplinary team incorporating a spinal surgeon, radiologist and oncologist. In particular, the likely prognosis can be advised by the oncologist so that the appropriate choice can be made between surgical stabilization and percutaneous therapy. Frequently, when life expectancy is limited, it is the latter option which is more appropriate. Furthermore, this multidisciplinary discussion allows follow-up and adjuvant therapy to be planned as part of the patients' ongoing care.

When considering patients for vertebroplasty or kyphoplasty, pre-procedure imaging should include MR imaging of the whole spine. This allows the potential treatment levels to be identified and assessed for suitability, but it is also important to ensure that there is no further evidence of more critical spinal canal compromise elsewhere. If MR imaging is contraindicated, then bone scintigraphy will aid in localization in the majority of cases and is often available as part of the staging investigations. Computed tomography can be useful in

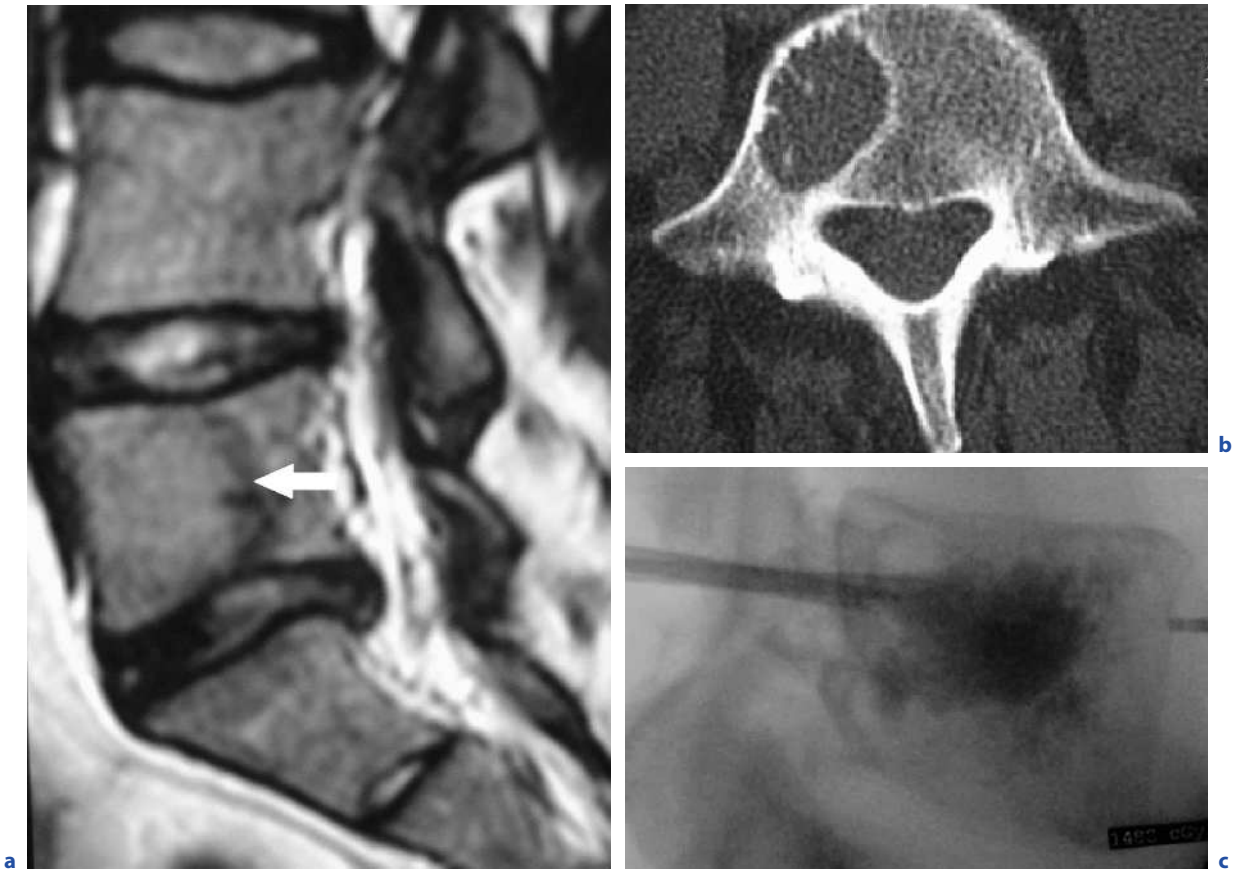

Fig. 6.6. **a** Sagittal T2-weighted MR image shows a renal metastasis in the anterior part of the L5 vertebral body (*arrow*). **b** Axial CT demonstrates a lytic lesion in the right side of the vertebral body. **c** Lateral fluoroscopy image shows a bipedicular approach with needles in situ at the end of the procedure

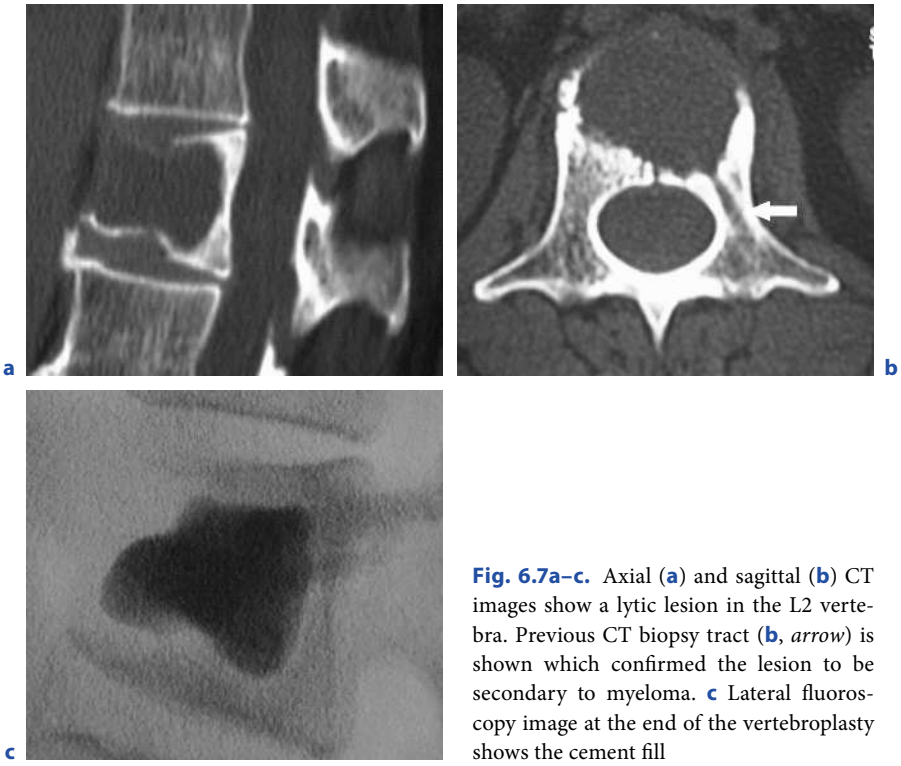

Fig. 6.7a–c. Axial (**a**) and sagittal (**b**) CT images show a lytic lesion in the L2 vertebra. Previous CT biopsy tract (**b**, *arrow*) is shown which confirmed the lesion to be secondary to myeloma. **c** Lateral fluoroscopy image at the end of the vertebroplasty shows the cement fill

evaluating the degree of bone osteolysis which can be underestimated on MR imaging.

Prior to the procedure, the patient receives intravenous antibiotics and is positioned prone on the examination table. Vertebroplasty can be performed under both fluoroscopic, CT guidance or using CT fluoroscopy (Jakobs et al. 2007). In general, intravenous sedation is utilized, although some patients may elect for the procedure to be performed under general anaesthesia. The route of access into the vertebral body will depend on the level of the lesion and anatomical factors such as pedicle size. In the thoracic region either a costotransverse or transpedicular approach may be adopted. In the lumbar spine most frequently a transpedicular route is employed, although a number of operators would advocate the use of a posterolateral approach particularly when the lesion involves the pedicles. The needles are sited in the anterior portion of the vertebral body or in the predominant area of osteolysis. The author prefers a bi-pedicular approach when treating tumour cases. This seems to allow more control of the cement injection particularly if venous leaking is encountered. When this is identified under screening, the injection is terminated and the cement left to act as a "cement plug" in the vessel. The opposite side can then be injected before returning to continue injection down the other needle once it has been repositioned. The volume of injection is to some extent dependent on the degree of bone destruction. Often 2–3 cc is all that is required and the volume of cement injected does not seem to bear a relationship with the degree of pain relief (Cotten et al. 1996). If there is extensive osteolysis and the aim is to provide some structural support, then larger volumes of cement may be required. Once satisfactory fill has been obtained, the central stylet is inserted down the needle which should be monitored with fluoroscopy. The needles can then be withdrawn and a skin dressing applied. If there is involvement in the pedicles, it is possible to perform a "pediculoplasty" to reinforce this region (Fig. 6.8).

The precise mechanism of pain relief in vertebroplasty is poorly understood. It has been postulated that mechanisms of action include stabilization of the destroyed bone and the analgesic effect from the thermal properties of PMMA (Deramond et al. 1999). The success of newer cement products which have a lower temperature profile in providing symptomatic relief in vertebral fractures may suggest that stabilization is the most important factor in pain relief. Furthermore, long-term pain control may be the result of a combination of factors such as stabilization of painful periosteum, reduction in tumour volume and the antitumoral effect from PMMA itself (Uemura et al. 2005; Hierholzer et al. 2003).

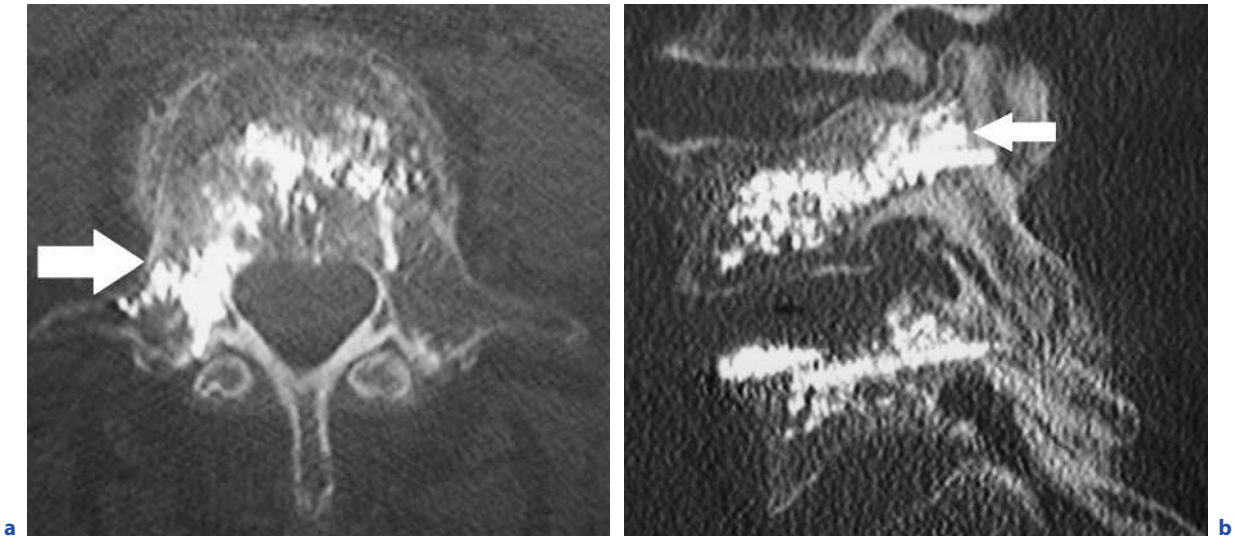

Fig. 6.8a,b. Axial (**a**) and sagittal (**b**) CT images demonstrate the cement in the pedicle (*arrow*) following pediculoplasty in a patient with breast metastases

Improvement in pain is identified in the majority of patients in the hours and days following the procedure. Jakobs et al. (2007) have reviewed seven studies incorporating 185 patients and reported a mean good to excellent response regarding pain in 77.4% of patients. Pain relief is usually persistent at follow-up, and if recurrent pain is a feature then this is usually due to further lesions developing in adjacent vertebra rather than failure of the previously treated levels (Weill et al. 1996; Hodler et al. 2003). Alvarez and co-workers (2003) have also reported that 69% of patients bed-bound before the procedure subsequently became ambulatory due to significant pain relief.

Kyphoplasty represents a variation in the technique of cement augmentation in the spine, although indications remain the same (Peh et al. 2008; Hadjipavlou et al. 2005). Needle access is again performed via either a transpedicular or parapedicular approach. It requires somewhat larger needles so that a balloon can be inserted into the vertebral body. This can be done as either a single step or by inserting a smaller needle and the use of an exchange wire before the definitive needle is inserted. The aim of balloon inflation is to create a cavity for the cement to fill. The advantages that are advocated include a low-pressure injection, potential for vertebral height restoration and reduced risk of cement leakage and subsequent complications (Pflugmacher et al. 2007). In fact, the degree of cement leakage is multifactorial and the tumour vascularity, cement viscosity and operator technique all play a role.

Minor complications of both vertebroplasty and kyphoplasty include infection, local bleeding, rib or pedicle fracture and are reported to have an incidence of less than 1%. The major concern is the risk of cement leakage, and this is thought to be higher for osteolytic vertebral lesions than compression fractures (Jakobs et al. 2007). This may occur either into the central canal or exit foramen (Fig. 6.9). Radiculopathy may therefore be encountered due to foraminal leakage; however, this is usually well tolerated and can be managed with a combination of medication and nerve blocks.

The use of cement augmentation within the sacrum, frequently termed sacroplasty, is increasingly being performed as a treatment for sacral insufficiency fractures including those secondary to previous radiotherapy (Heron et al. 2007; Frey 2008). This procedure has naturally expanded as a treatment of painful tumour infiltration of the sacrum typically from metastases or myeloma (Wee et al. 2008). There are limited reports describing successful treatments of pulmonary, hepatocellular, bronchial and renal metastases (Fig. 6.10) as well as sacral involvement from myeloma (Fig. 6.11; Wee et al. 2008). A number of techniques have been described including fluoroscopic guidance using spinal needles inserted into the anterior sacral exit foramina prior to cement injection (Garant 2002). Other workers suggest needle placement under CT guidance with transfer of the patient to the fluoroscopy suite for cement injection (Butler et al. 2005). Brook and coworkers (2005) have described a simplified technique

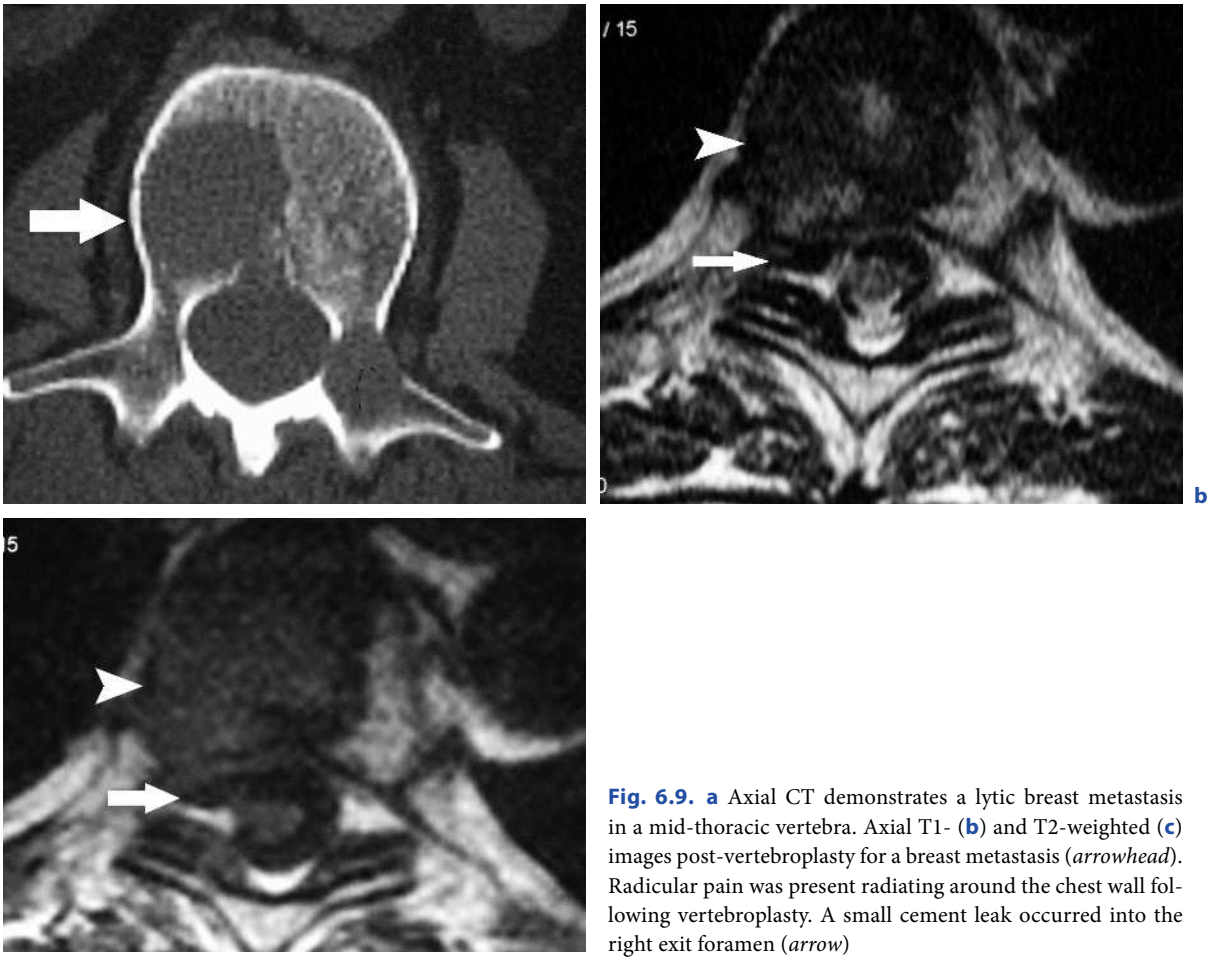

Fig. 6.9. **a** Axial CT demonstrates a lytic breast metastasis in a mid-thoracic vertebra. Axial T1- (**b**) and T2-weighted (**c**) images post-vertebroplasty for a breast metastasis (*arrowhead*). Radicular pain was present radiating around the chest wall following vertebroplasty. A small cement leak occurred into the right exit foramen (*arrow*)

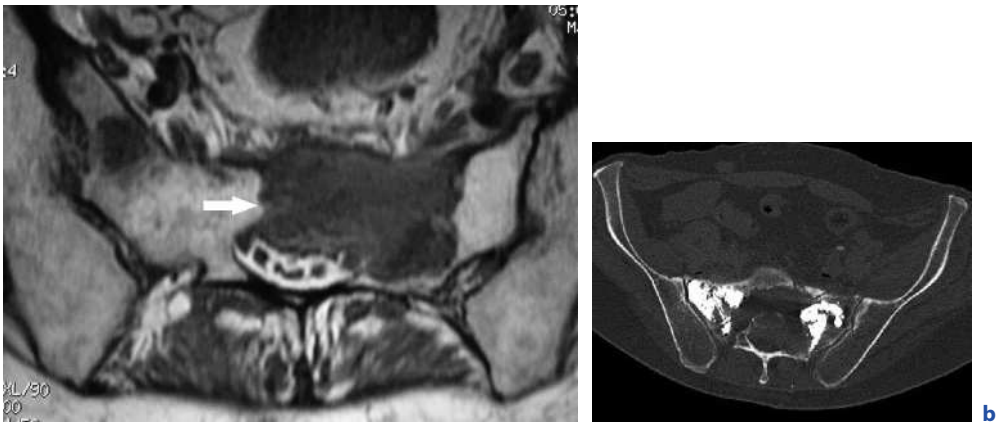

Fig. 6.10. **a** Axial T1-weighted image shows a focal renal metastasis in the left sacral ala extending across the midline (*arrow*). **b** Axial CT image following CT-guided sacroplasty shows the cement fill in both sacral ala. Despite little cement distribution in the midline, the patient experienced excellent pain relief

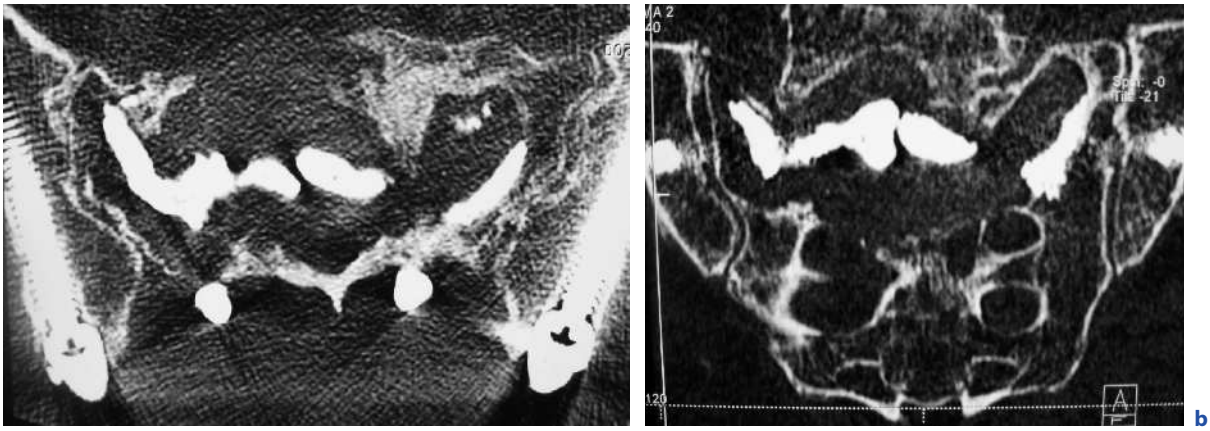

Fig. 6.11a,b. Axial (**a**) and coronal (**b**) CT images in a patient with advanced sacral destruction from multiple myeloma. A limited volume of cement was injected in this case as the tumour encased a number of sacral nerve roots. Again good symptomatic relief was obtained from the procedure

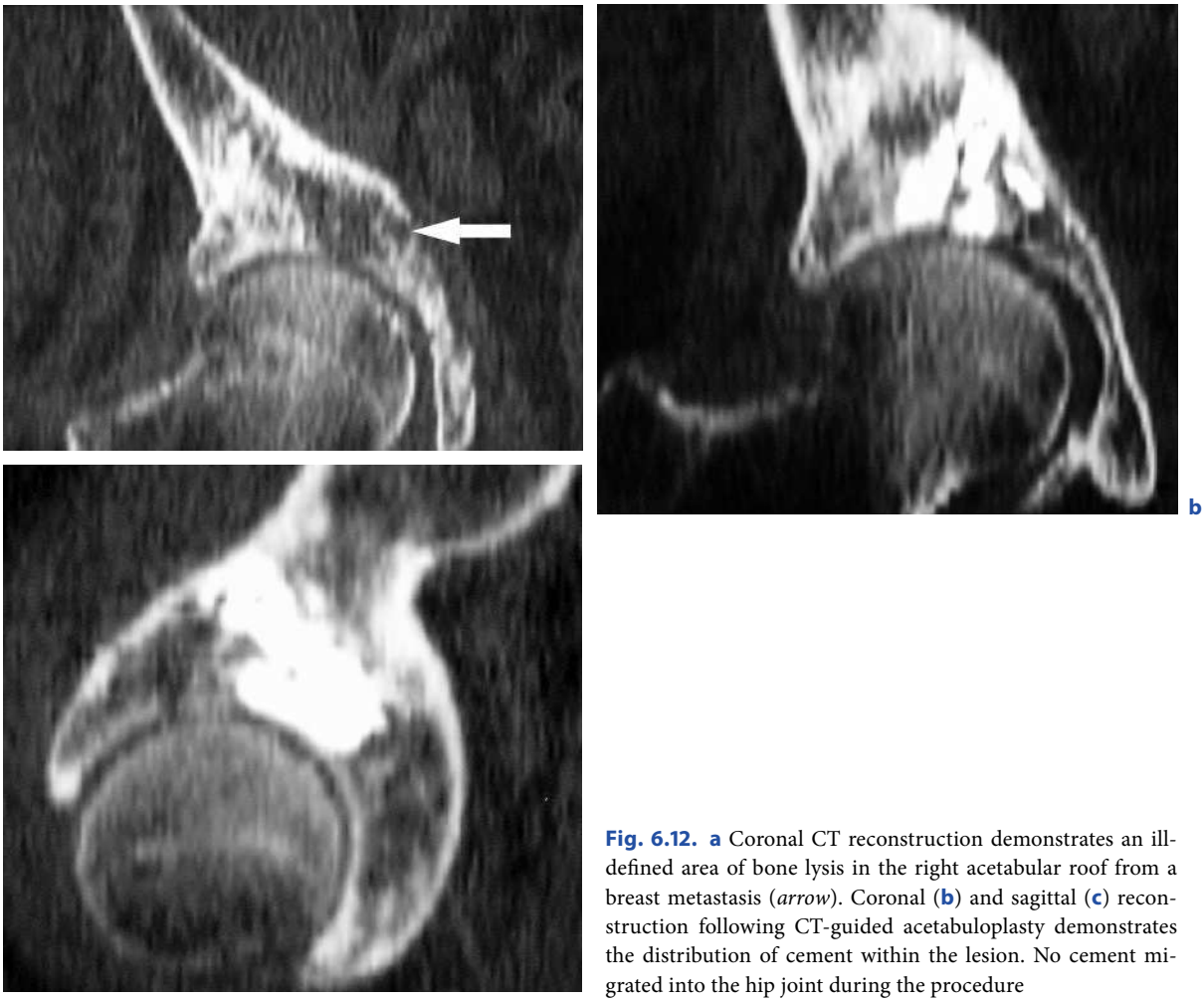

Fig. 6.12. a Coronal CT reconstruction demonstrates an ill-defined area of bone lysis in the right acetabular roof from a breast metastasis (*arrow*). Coronal (**b**) and sagittal (**c**) reconstruction following CT-guided acetabuloplasty demonstrates the distribution of cement within the lesion. No cement migrated into the hip joint during the procedure

with both needle placement and cement injection under CT guidance, without fluoroscopy. Two recent articles published from the present author's institution describe our preferred technique for CT-guided sacroplasty (Heron et al. 2007; Wee et al. 2008). When treating sacral tumour infiltration, the lesion is typically lytic making identification of sacral landmarks extremely problematic on fluoroscopy. We have found that needle placement under CT guidance is quick and easy. Cement may be injected in 0.2-ml aliquots reducing the risk of cement leakage. If the cement is cooled during the procedure, the working time of the cement can be dramatically increased thus reducing time pressure during injection (James and Connell 2006). Frequently larger volumes of cement are required to be injected than in insufficiency fractures to fill or partially fill the bony defect. Pain relief is often immediate and dramatic. The complications are similar to those of vertebroplasty, but when there is significant bony destruction there is increased risk of cement leakage into the sacral exit foramina and towards the lumbar plexus.

6.3.2 Extraspinal

The predominant indication for the use of cementoplasty in an extraspinal site is in the palliative treatment of osteolytic lesions of the pelvis (Figs. 6.12, 6.13). There are multiple case reports and series describing excellent pain responses for lesions in the pubic rami, ischium and acetabulum (Kelekis et al. 2005; Harris et al. 2007). A number of workers have described its use to include the appendicular skeleton including the femur, humerus, scapula and sternum (Basile et al. 2008; Anselmetti et al. 2008; Masala et al. 2007). In a series by Anselmetti and co-workers (2008), two patients with lesions in the femoral diaphysis reported pathological fractures within a month of treatment. It seems likely that lesions in the lower limb, particularly in the femur and tibia, remain best treated by surgical intervention to prevent this complication rather than via a percutaneous technique. Indeed, one could postulate that the needle access for such procedures could increase the potential for pathological fracture as is occasionally seen following percutaneous biopsy.

The basic technique for cement augmentation is the same for spinal and extraspinal sites. Fluoroscopic or CT guidance can be used depending on local availability and operator preference. As with sacroplasty, it is the present author's preference to use CT guidance. The volume of cement injected will depend to some extent on the size of the defect and little guidance is available on suitable cement volumes. It is therefore a matter of experience and observation during the procedure to decide on an end point to cement injection.

A number of workers have combined the use of cementoplasty with radiofrequency ablation both in spinal and extraspinal sites. There is currently little convincing evidence that the addition of radiofrequency ablation significantly improves symptom control. Anselmetti and co-workers (2008) found no statistical difference in pain relief rates between patients treated with cementoplasty alone and those where radiofrequency ablation was combined with cementoplasty. Some studies have, however, shown improvement in vertebral stability and reduced cement leakage rates when radiofrequency ablation is performed prior to vertebroplasty (Masala et al. 2004; Schaefer et al. 2003; Buy et al. 2006).

6.4 Bone Substitutes

The use of a "bone substitute" has long been in the realm of orthopaedic surgeons who have utilized bone-grafting techniques for decades for a wide variety of indications. The clear aim is to restore bone strength and integrity and this can be applied in different areas

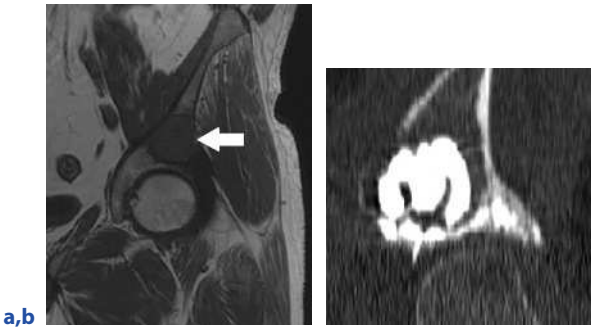

a,b

Fig. 6.13. **a** Coronal T1-weighted sequence demonstrates a focal lesion in the left acetabulum in a patient with multiple renal metastases to the skeleton. **b** Coronal CT reconstruction demonstrates good fill of the lesion and the patient experienced complete symptomatic relief following the procedure

of both the axial and appendicular skeleton. Increasing application of percutaneous techniques has reinstituted interest in bone augmentation delivery via this rather than the open surgical route. Unfortunately, although many materials are available, such as autograft, allograft and xenograft, these are not suitable for percutaneous injection. Any compound needs to be "fluid" enough for injection via a needle and visible under image guidance. Some compounds, such as PRO-DENSE (Wright Medical Technology, Arlington, Tenn.), represent an injectable regenerative graft. Following injection, an initial phase of resorption reveals a porous scaffold which is conductive to vascular infiltration. Growth factors stimulate proliferation and differentiation of mesenchymal stem cells. Differentiated osteoblasts than lay down osteoid which later mineralizes to bone. This type of injectable form of bone reconstitution is likely to see continued development with the potential that this will provide alternatives to some traditional surgical treatment options.

6.5 Embolization

Embolization can be utilized both in the axial and appendicular skeleton in both benign and malignant bone tumours. Treatment in malignant disease primarily consists of pre-operative embolization before a definitive surgical procedure is undertaken (Wirbel et al. 2005; Hallscheidt et al. 2006). The primary aim in these cases is to reduce the vascular supply to these tumours reducing the potential of haemorrhage during surgical resection (Olerud et al. 1993). Some authors have also recommended its use as a palliative treatment for pain relief (Chiras et al. 2004; Hallscheidt et al. 2006; Forauer et al. 2007). In the present author's institution, the most common indication for pre-operative embolization is bone metastases from renal carcinoma. There are, however, multiple reports in the literature describing the use of this technique for thyroid and he-

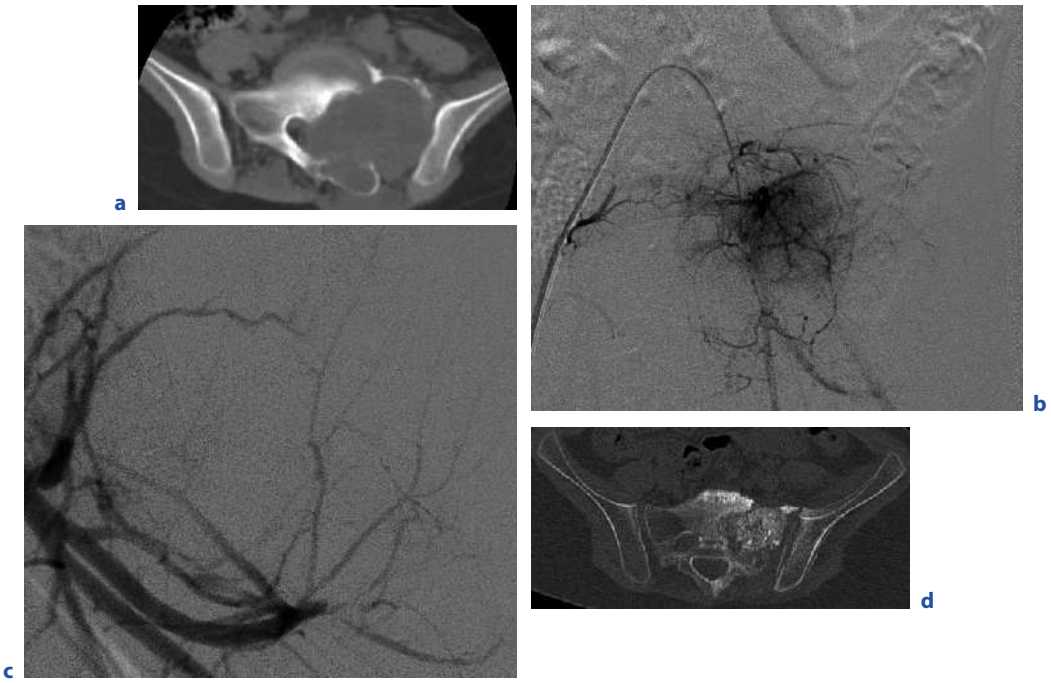

Fig. 6.14. **a** Axial CT demonstrates a lytic lesion in the left sacral ala demonstrated on biopsy to be an aneurysmal bone cyst. **b** Fluoroscopic spot image following selective catheterization shows the vascular configuration of the lesion. **c** Post-embolization angiogram demonstrates lack of contrast within the lesion on this and delayed runs (not shown) confirming satisfactory embolization. **d** Axial CT at follow-up shows consolidation of the left sacral ala following embolization

patocellular metastases to bone (Uemura et al. 2001; Eustatia-Rutten et al. 2003).

Embolization has been used in the treatment of a number of benign primary tumours of bone. Probably the best recognized of these indications is in the treatment of giant cell tumours particularly in a pelvic location (Lin et al. 2002; Hosalkar et al. 2007; Lackman et al. 2002). Surgical treatment for large lesions involving the sacrum can have considerable morbidity. Hosalkar and co-workers (2007) have demonstrated that selective arterial embolization can provide symptomatic pain relief and prevention of disease progression in the majority of the cases in their series. There are a small number of case reports describing embolization of aneurysmal bone cysts (Fig. 6.14; Wathiong et al. 2003; Yildirim 2007). Both embolization and sclerotherapy are increasingly being utilized in the treatment of benign soft tissue vascular anomalies. These anomalies include venous, lymphatic and mixed venous–lymphatic malformations with sclerotherapy and arteriovenous malformations, haemangiomas and arteriovenous fistulas with embolization (Konez 2006). These lesions are briefly mentioned here as they can occasionally involve adjacent bones and joints.

The aim of embolization is to close off the abnormal vascular channels which feed or drain the lesion. Angiographic catheters are used to access the lesion and intravenous contrast is injected to demonstrate the vascular configuration. Various agents and devices can be utilized including absolute ethanol, n-BCA, detachable coils and particle agents. The technical aspects of this procedure are beyond the scope of this chapter.

Alcoholization has been used in the treatment of bone malignancy predominantly for pain relief in osteolytic bone metastases. Ethanol causes tissue dehydration with subsequent coagulation necrosis. As with radiofrequency ablation, this technique can be combined with cementoplasty if some structural support is required. In general, a rapid reduction in pain is seen within 24–48 h. This treatment provides successful symptomatic relief in 74% of cases (Gangi et al. 1994).

References

Ahlmann ER, Menendez LR, Fedenko AN, Learch T (2006) Influence of cryosurgery on treatment outcome of low-grade chondrosarcoma. Clin Orthop Relat Res 451:201–207

Ahn H, Mousavi P, Chin L et al. (2007) The effect of pre-vertebroplasty tumor ablation using laser-induced thermotherapy on biomechanical stability and cement fill in the metastatic spine. Eur Spine J 16(8):1171–1178

Alvarez L, Pérez-Higueras A, Quiñones D et al. (2003) Vertebroplasty in the treatment of vertebral tumors: post-procedural outcome and quality of life. Eur Spine J 12(4):356–360

Anselmetti GC, Manca A, Ortega C et al. (2008) Treatment of extraspinal painful bone metastases with percutaneous cementoplasty: a prospective study of 50 patients. Cardiovasc Intervent Radiol [Epub ahead of print]

Bancroft LW, Peterson JJ, Kransdorf MJ et al. (2007) Compartmental anatomy relevant to biopsy planning. Semin Musculoskelet Radiol 11(1):16–27

Basile A, Giuliano G, Scuderi V et al. (2008) Cementoplasty in the management of painful extraspinal bone metastases: our experience. Radiol Med (Torino) [Epub ahead of print]

Bickels J, Meller I, Shmookler BM, Malawer MM (1999) The role and biology of cryosurgery in the treatment of bone tumors. A review. Acta Orthop Scand 70(3):308–315

Brook A, Mirsky D, Bello J (2005) Computerized tomography guided sacroplasty: a practical treatment for sacral insufficiency fracture. Spine 30:E450–E454

Butler C, Given C, Michel S, Tibbs P (2005) Percutaneous sacroplasty for the treatment of sacral insufficiency fractures. AJR 184:1956–1959

Buy X, Basile A, Bierry G et al. (2006) Saline-infused bipolar radiofrequency ablation of high-risk spinal and paraspinal neoplasms. AJR 186(5 Suppl):S322–S326

Callstrom MR, Charboneau JW, Goetz MP et al. (2002) Painful metastases involving bone: feasibility of percutaneous CT- and US-guided radio-frequency ablation. Radiology 224(1):87–97

Callstrom MR, Atwell TD, Charboneau JW et al. (2006a) Painful metastases involving bone: percutaneous image guided cryoablation – prospective trial interim analysis. Radiology 241(2):572–580

Callstrom MR, Charboneau JW, Goetz MP et al. (2006b) Image-guided ablation of painful metastatic bone tumors: a new and effective approach to a difficult problem. Skeletal Radiol 35(1):1–15

Chiras J, Adem C, Vallée JN et al. (2004) Selective intra-arterial chemoembolization of pelvic and spine bone metastases. Eur Radiol 14(10):1774–1780

Christie-Large M, Evans N, Davies AM, James SL (2008) Radiofrequency ablation of chondroblastoma: procedure technique, clinical and MR imaging follow up of four cases. Skeletal Radiol 37(11):1011–1017

Cotten A, Dewatre F, Cortet B et al. (1996) Percutaneous vertebroplasty for osteolytic metastases and myeloma: effects of the percentage of lesion filling and the leakage of methyl methacrylate at clinical follow-up. Radiology 200(2):525–530

Cribb GL, Goude WH, Cool P et al. (2005) Percutaneous radiofrequency thermocoagulation of osteoid osteomas: factors affecting therapeutic outcome. Skeletal Radiol 34(11):702–706

Deramond H, Wright NT, Belkoff SM (1999) Temperature elevation caused by bone cement polymerization during vertebroplasty. Bone 25(2 Suppl):17S–21S

Donkol RH, Al-Nammi A, Moghazi K (2008) Efficacy of percutaneous radiofrequency ablation of osteoid osteoma in children. Pediatr Radiol 38(2):180–185

Eustatia-Rutten CF, Romijn JA, Guijt MJ et al. (2003) Outcome of palliative embolization of bone metastases in differentiated thyroid carcinoma. J Clin Endocrinol Metab 88(7):3184–3189

Finstein JL, Hosalkar HS, Ogilvie CM, Lackman RD (2006) Case reports: an unusual complication of radiofrequency ablation treatment of osteoid osteoma. Clin Orthop Relat Res 448:248–251

Forauer AR, Kent E, Cwikiel W et al. (2007) Selective palliative transcatheter embolization of bony metastases from renal cell carcinoma. Acta Oncol 46(7):1012–1018

Frey ME, Depalma MJ, Cifu DX et al. (2008) Percutaneous sacroplasty for osteoporotic sacral insufficiency fractures: a prospective, multicenter, observational pilot study. Spine J 8(2):367–373

Gangi A, Kastler B, Klinkert A et al. (1994) Injection of alcohol into bone metastases under CT guidance. J Comput Tomogr 18:932–995

Gangi A, Alizadeh H, Wong L et al. (2007) Osteoid osteoma: percutaneous laser ablation and follow-up in 114 patients. Radiology 242(1):293–301

Garant M (2002) Sacroplasty: a new treatment for sacral insufficiency fracture. J Vasc Interv Radiol 13:1265–1267

Goetz MP, Callstrom MR, Charboneau JW et al. (2004) Percutaneous image-guided radiofrequency ablation of painful metastases involving bone: a multicenter study. J Clin Oncol 15; 22(2):300–306

Gronemeyer DH, Schirp S, Gevargez A (2002) Image guided radiofrequency ablation of spinal tumors: preliminary experience with an expandable array electrode. Cancer 8:33–39

Hadjipavlou AG, Tzermiadianos MN, Katonis PG, Szpalski M (2005) Percutaneous vertebroplasty and balloon kyphoplasty for the treatment of osteoporotic vertebral compression fractures and osteolytic tumours. J Bone Joint Surg Br 87(12):1595–1604

Hallscheidt P, Besharati S, Noeldge G, Haferkamp A, Lopez R, Kauffmann GW (2006) Preoperative and palliative embolization of renal cell carcinomas: follow-up of 49 patients. Rofo 178(4):391–399

Harris K, Pugash R, David E et al. (2007) Percutaneous cementoplasty of lytic metastasis in left acetabulum. Curr Oncol 14(1):4–8

Hay PD, Griffiths KM, Smith RM et al. (2007) Radionuclide localization of skeletal tumours within the spine. RAD Magazine 33:388;17–18

Heron J, Connell DA, James SL (2007) CT-guided sacroplasty for the treatment of sacral insufficiency fractures. Clin Radiol 62(11):1094–1100

Hierholzer J, Anselmetti G, Fuchs H et al. (2003) Percutaneous osteoplasty as a treatment for painful malignant bone lesions of the pelvis and femur. J Vasc Interv Radiol 14:773–777

Hodler J, Peck D, Gilula LA (2003) Midterm outcome after vertebroplasty: predictive value of technical and patient-related factors. Radiology 227(3):662–668

Hosalkar HS, Jones KJ, King JJ, Lackman RD (2007) Serial arterial embolization for large sacral giant-cell tumors: mid- to long-term results. Spine 32(10):1107–1115

Jakobs TF, Trumm C, Reiser M, Hoffmann RT (2007) Percutaneous vertebroplasty in tumoral osteolysis. Eur Radiol 17:2166–2175

James SLJ, Connell DA (2006) The effect of temperature reduction on cement working time in percutaneous vertebroplasty. Clin Radiol 61:797–799

Kelekis A, Lovblad KO, Mehdizade A et al. (2005) Pelvic osteoplasty in osteolytic metastases: technical approach under fluoroscopic guidance and early clinical results. J Vasc Interv Radiol 16(1):81–88

Kobayashi K, Shimoyama K, Nakamura K, Murata K (2005) Percutaneous vertebroplasty immediately relieves pain of osteoporotic vertebral compression fractures and prevents prolonged immobilization of patients. Eur Radiol 15(2):360–367

Konez O (2006) Treatment of musculoskeletal vascular anomalies. Semin Musculoskelet Radiol 10(2):145–158

Lackman RD, Khoury LD, Esmail A, Donthineni-Rao R (2002) The treatment of sacral giant-cell tumours by serial arterial embolisation. J Bone Joint Surg Br 84(6):873–877

Lin PP, Guzel VB, Moura MF et al. (2002) Long-term follow-up of patients with giant cell tumor of the sacrum treated with selective arterial embolization. Cancer 95(6):1317–1325

Liu PT, Valadez SD, Chivers FS et al. (2007) Anatomically based guidelines for core needle biopsy of bone tumors: implications for limb-sparing surgery. Radiographics 27(1):189–205

Logan PM, Connell DG, O'Connell JX, Munk PL, Janzen DL (1996) Image-guided percutaneous biopsy of musculoskeletal tumors: an algorithm for selection of specific biopsy techniques. AJR 166(1):137–141

Masala S, Roselli M, Massari F et al. (2004) Radiofrequency heat ablation and vertebroplasty in the treatment of neoplastic vertebral body fractures Anticancer Res 24(5B):3129–3133

Masala S, Manenti G, Roselli M et al. (2007) Percutaneous combined therapy for painful sternal metastases: a radiofrequency thermal ablation (RFTA) and cementoplasty protocol. Anticancer Res 27(6C):4259–4262

Nahum Goldberg S, Dupuy DE (2001) Image-guided radiofrequency tumor ablation: challenges and opportunities – part 1. J Vasc Interv Radiol 12:1021–1032

Nielsen OS, Munro AJ, Tannock IF (1991) Bone metastases: pathophysiology and management. J Clin Oncol 9:509–524

Olerud C, Jónsson H Jr, Löfberg AM et al. (1993) Embolization of spinal metastases reduces peroperative blood loss. Twenty-one patients operated on for renal cell carcinoma. Acta Orthop Scand 64(1):9–12

Peh WC, Munk PL, Rashid F, Gilula LA (2008) Percutaneous vertebral augmentation: vertebroplasty, kyphoplasty and skyphoplasty. Radiol Clin North Am 46(3):611–635

Petsas T, Megas P, Papathanassiou Z (2007) Radiofrequency ablation of two femoral head chondroblastomas. Eur J Radiol 63(1):63–67

Pflugmacher R, Schulz A, Schroeder RJ et al. (2007) A prospective two-year follow-up of thoracic and lumbar osteolytic vertebral fractures caused by multiple myeloma treated with balloon kyphoplasty. Z Orthop Ihre Grenzgeb 145(1):39–47

Rosenthal DI, Hornicek FJ, Torriani M et al. (2003) Osteoid osteoma: percutaneous treatment with radiofrequency energy. Radiology 229:171–175

Schaefer O, Lohrmann C, Markmiller M et al. (2003) Technical innovation. Combined treatment of a spinal metastasis with radiofrequency heat ablation and vertebroplasty. AJR 180(4):1075–1077

Shibata T, Iimuro Y, Yamamoto Y et al. (2002) Small hepatocellular carcinoma: comparison of radiofrequency ablation and percutaneous microwave coagulation therapy. Radiology 223:331–337

Simon CJ, Dupuy DE (2006) Percutaneous minimally invasive therapies in the treatment of bone tumors: thermal ablation. Semin Musculoskelet Radiol 10(2):137–144

Simon CJ, Dupuy DE, Mayo-Smith WW (2005) Microwave ablation: principles and applications. Radiographics 25:S69–S83

Sung KS, Seo JG, Shim JS, Lee YS (2007) Computed-tomography-guided percutaneous radiofrequency thermoablation for the treatment of osteoid osteoma: 2 to 5 years follow-up. Int Orthop [Epub ahead of print]

Szypryt EP, Hardy JG, Colton CL (1986) An improved technique of intra-operative bone scanning. J Bone Joint Surg Br 68(4):643–646

Thanos L, Mylona S, Galani P et al. (2008) Radiofrequency ablation of osseous metastases for the palliation of pain. Skeletal Radiol 37(3):189–194

Tins B, Cassar-Pullicino V, McCall I et al. (2006) Radiofrequency ablation of chondroblastoma using a multi-tined expandable electrode system: initial results. Eur Radiol 16(4):804–810

Tuncali K, Morrison PR, Winalski CS et al. (2007) MRI-guided percutaneous cryotherapy for soft-tissue and bone metastases: initial experience. AJR 189(1):232–239

Uemura A, Fujimoto H, Yasuda S et al. (2001) Transcatheter arterial embolization for bone metastases from hepatocellular carcinoma. Eur Radiol 11(8):1457–1462

Uemura A, Matsusako M, Numaguchi Y et al. (2005) Percutaneous sacroplasty for haemorrhagic metastases for hepatocellular carcinoma. Am J Neuroradiol 26:493–495

Vanderschueren GM, Taminiau AH, Obermann WR et al. (2007) The healing pattern of osteoid osteomas on computed tomography and magnetic resonance imaging after thermocoagulation. Skeletal Radiol 36(9):813–821

Wathiong J, Brys P, Samson I, Maleux G (2003) Selective arterial embolization in the treatment of an aneurysmal bone cyst of the pelvis. JBR–BTR 86(6):325–328

Wee B, Shimal A, Stirling AJ, James SL (2008) CT-guided sacroplasty in advanced sacral destruction secondary to tumour infiltration. Clin Radiol 63(8):906–912

Weill A, Chiras J, Simon JM et al. (1996) Spinal metastases: indications for and results of percutaneous injection of acrylic surgical cement. Radiology 199(1):241–247

Wirbel RJ, Roth R, Schulte M et al. (2005) Preoperative embolization in spinal and pelvic metastases. J Orthop Sci 10(3):253–257

Woertler K, Verstring T, Boettner F et al. (2001) Osteoid osteoma: CT-guided percutaneous radiofrequency ablation and follow-up in 47 patients. J Vasc Interv Radiol 12:717–722

Yildirim E, Ersözlü S, Kirbaş I et al. (2007) Treatment of pelvic aneurysmal bone cysts in two children: selective arterial embolization as an adjunct to curettage and bone grafting. Diagn Interv Radiol 13(1):49–52

Zhang Q, Chung YC, Lewin JS, Duerk JL (1998) A method of simultaneous RF ablation and MRI. J Magn Reson Imaging 8:110–114

Principles of Detection and Diagnosis

7

A. Mark Davies and Victor N. Cassar-Pullicino

CONTENTS

KEY POINTS

- The majority of bone tumours are detected using conventional radiographs.
- Occasionally occult lesions may be detected using more sensitive techniques such as bone scintigraphy and MR imaging.
- Careful analysis of the pattern of bone destruction, periosteal reaction and matrix mineralisation on radiographs allow for characterisation of many bone tumours.
- Additional factors that should be included in determining the likely diagnosis include the age of the patient, location of the tumour in bone and any history of a pre-existing bone abnormality, e. g. Paget's disease.
- A multidisciplinary approach to diagnosis, which includes review of the imaging and any histological findings, is emphasised.

7.1 Introduction

There is a very large variety of tumours and tumour-like lesions that can involve the skeleton (see Chaps. 1 and 30). To the unwary observer they present a bewildering spectrum of radiographic appearances that all too often can lead to misinterpretation and suboptimal management. Although primary malignancies are relatively rare, they often pose an intriguing diagnostic problem for the radiologist, particularly as the pathology is frequently equally challenging (Sliced Study Group 2007). Conventional teaching identifies that the ultimate responsibility for definitive diagnosis resides with the pathologist (Moser and Madewell 1987); however, the input of the radiologist in the process should be neither overlooked nor ignored. The radiologist has the benefit of

A. M. Davies, MBChB, FRCR
Consultant Radiologist, Department of Radiology, Royal Orthopaedic Hospital, Birmingham B31 2AP, UK

V. N. Cassar-Pullicino, MD
Department of Radiology, Robert Jones and Agnes Hunt Orthopaedic Hospital, Oswestry, Shropshire SY10 7AG, UK

seeing the "bigger picture" able to view the entire bone lesion in two or more planes and with different imaging techniques thereby appreciating the "gross pathology", whereas the pathologist views the biopsy material from a selected portion of the lesion that may or may not be representative of the lesion as a whole (Kricun 1983; Moser and Madewell 1987).

The purpose of this chapter is to review the role of imaging in the detection and subsequent diagnosis of bone tumours stressing the pre-eminent role of the radiograph. Individual tumour types are not discussed in detail and the reader can further his/her knowledge of specific tumours by referring to Chaps. 13–30.

7.2 Detection

Part of the problem in detecting a bone tumour is that the level of awareness among clinicians and radiologists of the disease is low due to its rarity. To put it into context, an individual is five times more likely to be killed on the roads in the United Kingdom each year than develop a primary sarcoma of bone and only ten times less likely to be hit by a lightning strike (Watanabe et al. 2007). The patient with a bone tumour, irrespective of its nature, will typically present with either pain or swelling. Frequently, tumours, particularly around the knee, are initially misdiagnosed as an athletic injury (Muscolo et al. 2003). The pain may be mild and intermittent initially but later becomes more severe and unremitting, particularly if it is a malignancy. Alternatively, a pathological fracture may be the precipitous presenting feature. Occasionally, a bone tumour, typically a benign lesion, can be an incidental radiographic finding. Despite newer imaging techniques, the radiograph is the preliminary and single most important imaging investigation. It remains cheap, easily obtainable and universally available. Frequently, the diagnosis may be obvious to the trained eye and further imaging is then directed towards staging the lesion. Alternatively, if an abnormality is present on the film and the exact nature is not immediately apparent, certain findings will indicate a differential diagnosis and other forms of imaging can then be employed to assist in making a more definitive radiological diagnosis. If the initial radiograph is normal, however, with persisting and increasing symptoms a repeat radiograph may be indicated in due course. The concept of a latent period between onset of symptoms and the appearance of the first radiographic abnormalities of a bone tumour should be appreciated (Brailsford 1946, 1949).

Early signs of a bone tumour and/or infection include areas of ill-defined lysis or sclerosis, cortical destruction, periosteal new bone formation and soft tissue swelling (DeSantos and Edeiken 1985; Rosenberg et al. 1995). Bone lesions are frequently missed or overlooked on the initial radiograph (Fig. 7.1). In an audit performed at one of the author's (A.M.D.) institutions over 20 years ago in approximately 20% of cases neither the clinician nor the radiologist at the referring centre detected the bone tumour on the initial radiographs, although evidence was present on retrospective review of the films (Grimer and Sneath 1990). Another study, reviewing delays in diagnosis of primary sarcomas of the pelvis, showed that in 26% cases the initial radiographs were misinterpreted as showing normal findings or degenerative arthritis (Wurtz et al. 1999). A more recent study has shown fewer misses but problems can still occur (Müller et al. 2005). A number of features may improve the rate of detection. Attention to good radiographic technique is essential. The fundamental prerequisite for skeletal radiology, that at least two views of a structure are obtained, preferably at right angles to one another, must be strictly followed. Often subtle signs of a lesion may be discernible on one view but not visualised on another (Fig. 7.2). It is ironic that the more complex the bony anatomy, the fewer the routine projections obtained. The prime example is the pelvis, where early lesions may be missed due to the curvature of the bones and can be obscured by the overlying soft tissues, bowel gas and in the elderly vascular calcifications. Problems may be exacerbated by the overzealous use of gonad shielding (Fig. 7.3). Careful scrutiny of the entire image, including the periphery, is necessary, and if an abnormality is seen at the edge of the image, further, more extensive views will be required. In the past inadequate exposure of films might make detection more difficult. In the current era of digital radiography it may be necessary to alter the windowing of the image on the PACS workstation to highlight subtle changes. In the presence of a normal radiograph, referred pain needs to be considered, in which case further radiographs would be indicated. Hip joint pathology presenting with referred pain to the knee is a well-recognised entity in the child.

The pathological process may be well established even in the presence of a normal radiographic image. At least 40–50% of trabecular bone must be destroyed before a discrete area of lucency can be seen on the radiographs (Ardran 1951; Edelstyn et al. 1967). Erosion or destruction of the cortex is more readily apparent. A typical example is the vertebral metastasis. Classically, the first radiographic abnormality detected is destruction of the pedicle, by virtue of its small size and easily visible cortex. Cross-sectional imaging has shown

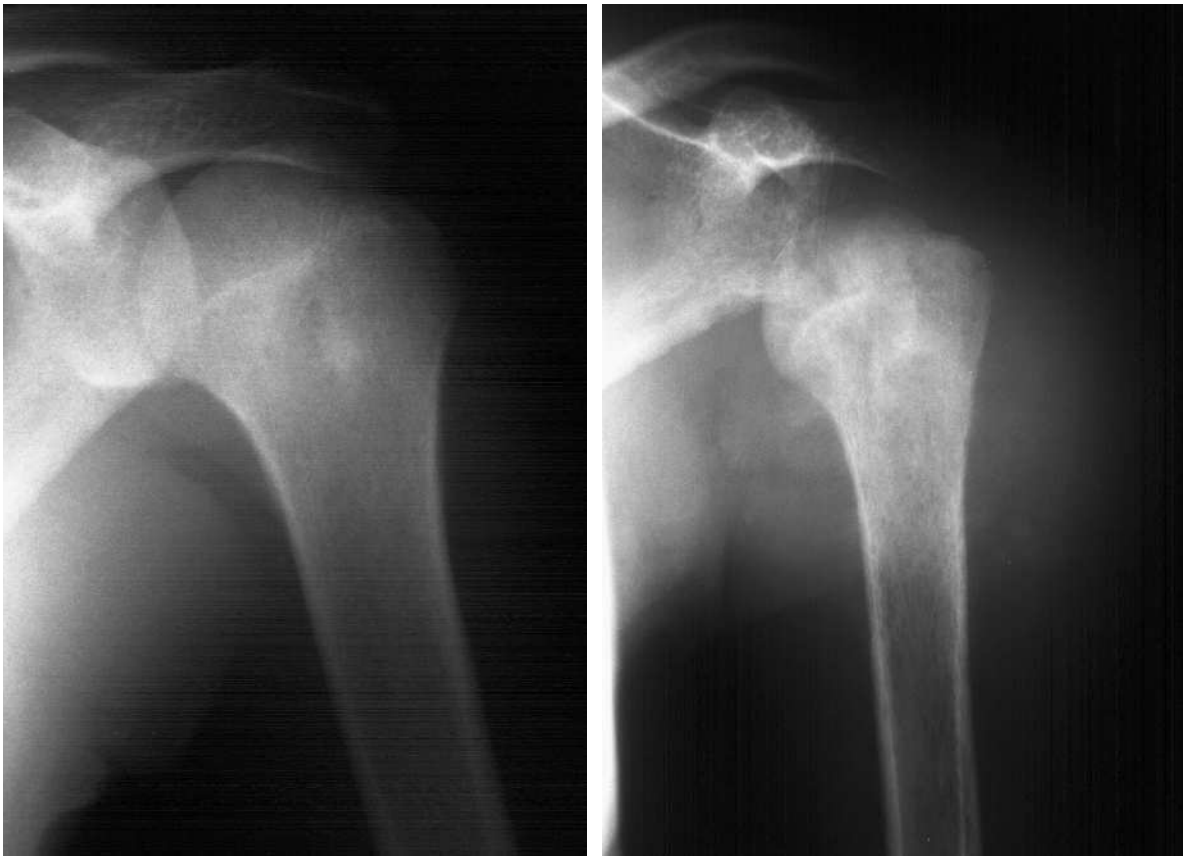

a b

Fig. 7.1a,b. Osteosarcoma humerus. **a** AP radiograph. The subtle signs in the proximal humeral metaphysis were initially overlooked. **b** AP radiograph 5 months later when the diagnosis was first made. There is mixed lysis and sclerosis with a large soft tissue mass containing some amorphous mineralisation. The tumour mass is causing the humeral head to sublux inferiorly

that the vast majority of these metastases arise within the vertebral body and that the pedicle is only involved secondarily (Fig. 7.4; Algra et al. 1991); however, the destruction of the trabecular bone within the vertebral body is frequently poorly seen on the initial radiographs. It is clear that the smaller the bone involved, with a greater proportion of cortical to medullary bone, the earlier it will be possible to detect an abnormality on the radiographs.

On occasion, radiographically occult lesions can be detected by imaging techniques more sensitive to marrow pathology notably bone scintigraphy and/or magnetic resonance (MR) imaging (Fig. 7.2c). A typical example in this regard is the painful adolescent scoliosis due to an osteoid osteoma, the nature of which may not be immediately obvious on the radiograph. An intense focus of increased activity/uptake on bone scintigraphy will suggest the diagnosis (Fig. 7.5). Often, however, the high sensitivity of bone scintigraphy will highlight pathology, but its lack of specificity means that other imaging, frequently a retrospective review of the radiographs, will be required to establish the diagnosis. Localisation of a lesion can be improved by using single photon emission tomography (SPECT). The high sensitivity of MR imaging for marrow abnormalities means it has to be interpreted with caution or else incidental findings might be considered unduly significant. Asymptomatic enchondromas are not an infrequent finding in the proximal humerus and distal femur on routine MR imaging in the investigation of shoulder and knee pain (Fig. 7.6a; Levy et al. 2005). A recent study has shown that incidental enchondromas can be identified in 2.9% of routine MR knee examinations (Walden et al. 2008). Frequently MR imaging is performed for musculoskeletal complaints without prior radiography. Indeed, in certain clinical situations it is suggested that radiographs are no longer a prerequisite (ter Braak et al. 2007). The prudent radiologist will, however, insist on radiographic correlation of any bony abnormality revealed by MR imaging (Fig. 7.6b).

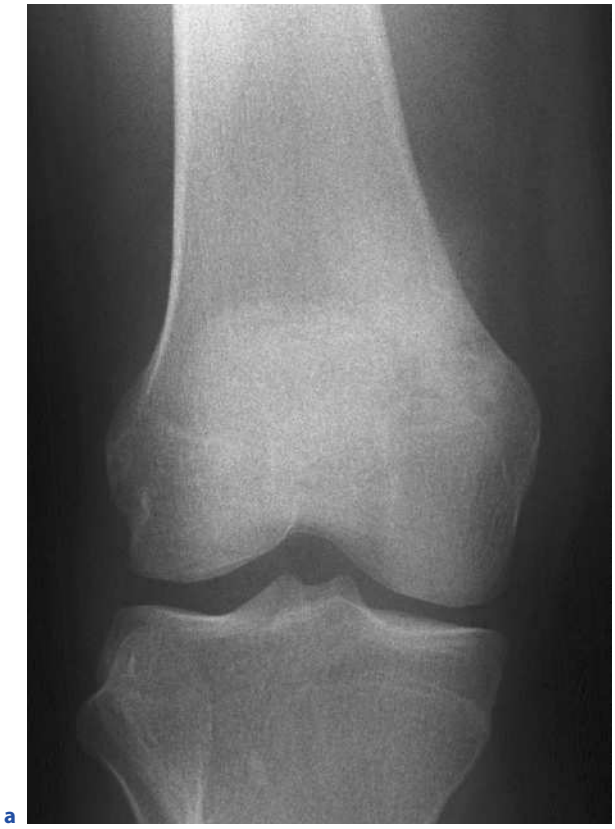

a

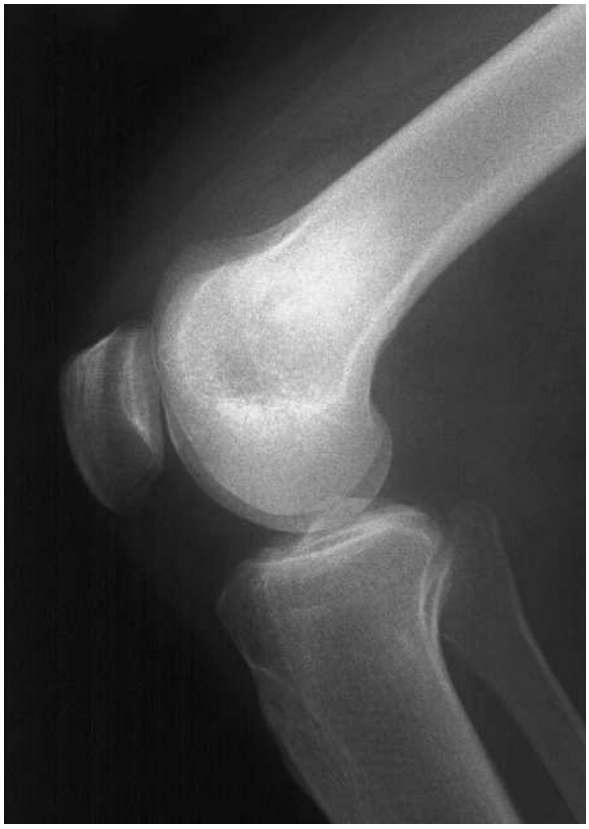

b

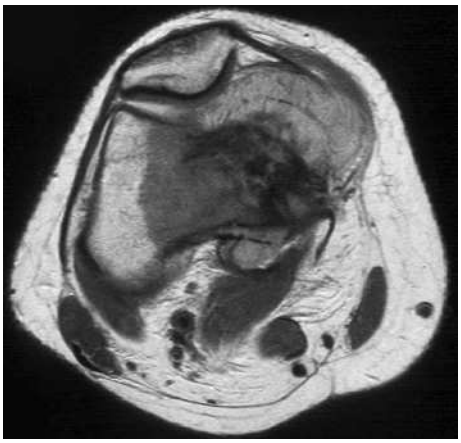

c

Fig. 7.2a–c. Osteosarcoma femur not detected on the initial radiographs. **a** AP radiograph which is virtually normal even in retrospect. **b** Lateral radiograph shows some ill-defined sclerosis in the distal femoral metaphysis due to malignant osteoid. **c** Axial intermediate-weighted image obtained 10 days later as part of a study to confirm or exclude a meniscal tear. There is tumour infiltration with marked soft tissue extension anteriorly into the knee joint. The malignant osteoid is indicated by the low signal intensity area in the intraosseous component of the tumour

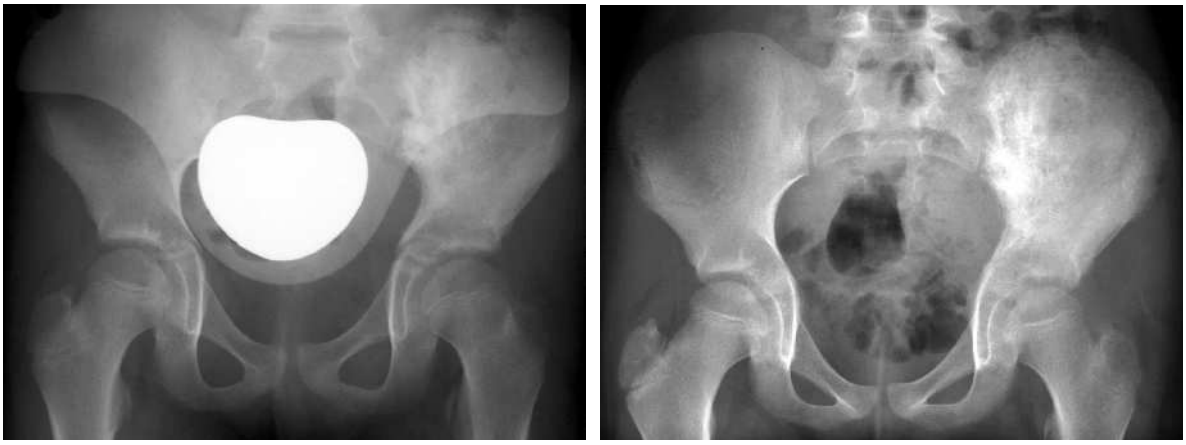

Fig. 7.3a,b. Ewing's sarcoma in the pelvis. **a** AP radiograph at presentation. The reporting radiologist overlooked the sarcoma in the left ilium partially obscured by the gonad shield. **b** AP radiograph 1 month later without a gonad shield. It is now much easier to identify the sarcoma

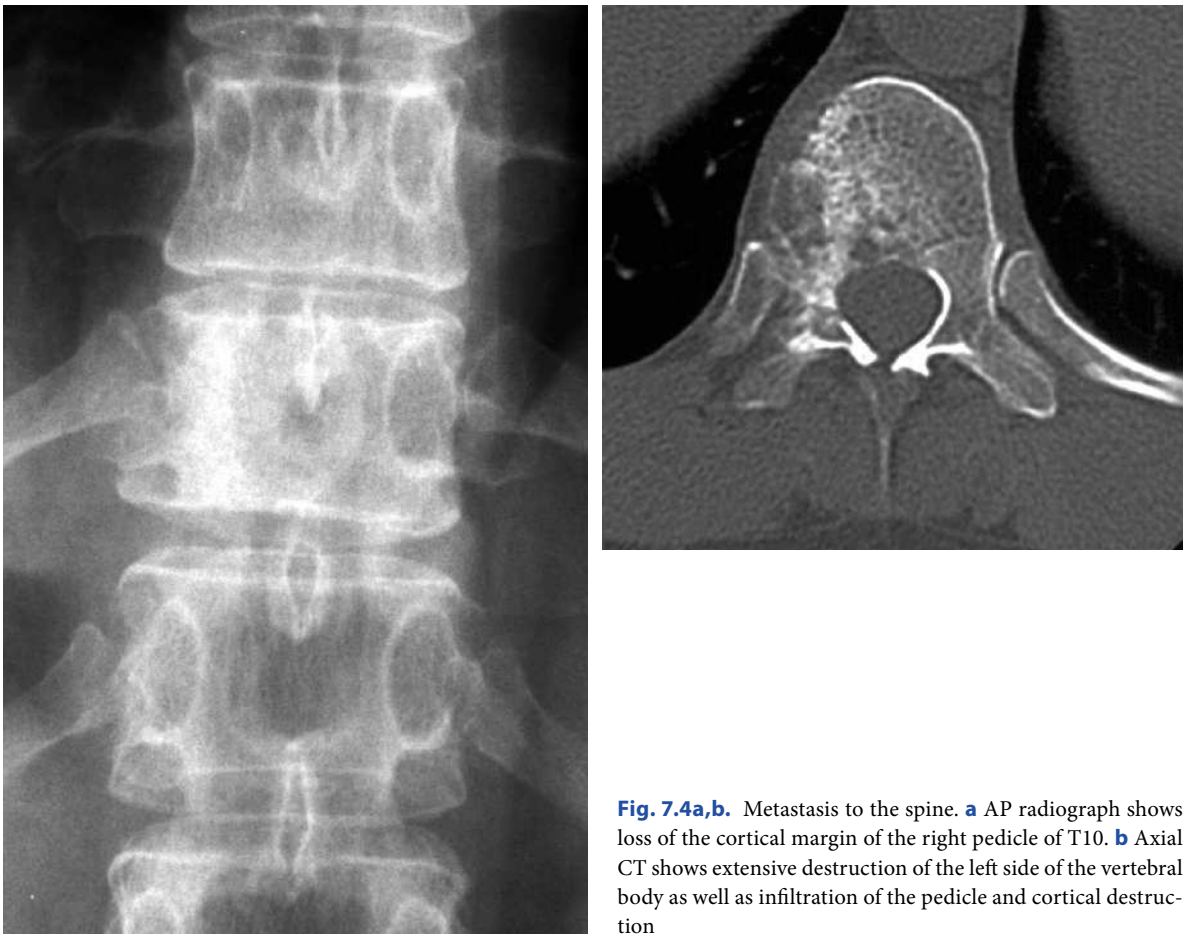

Fig. 7.4a,b. Metastasis to the spine. **a** AP radiograph shows loss of the cortical margin of the right pedicle of T10. **b** Axial CT shows extensive destruction of the left side of the vertebral body as well as infiltration of the pedicle and cortical destruction

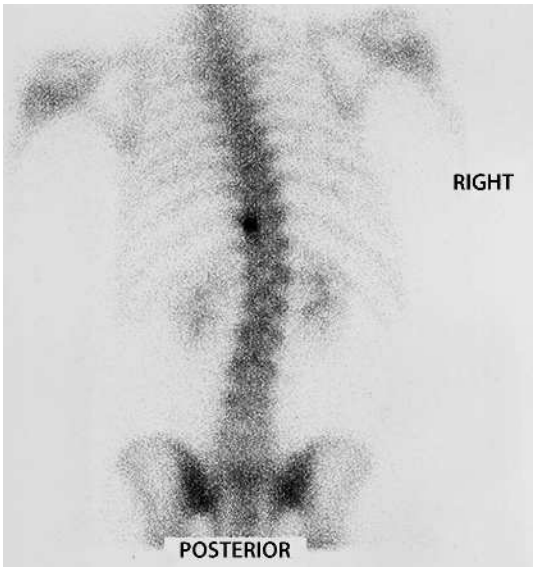

Fig. 7.5. Osteoid osteoma in the thoracic spine. Three-hour-delayed posterior image from a bone scan in an adolescent presenting with a painful scoliosis. The spinal deformity is obvious as is the small focus of intense increased activity at the site of the osteoid osteoma. Further imaging with CT and/or MR imaging would be required to localise and characterise the lesion further

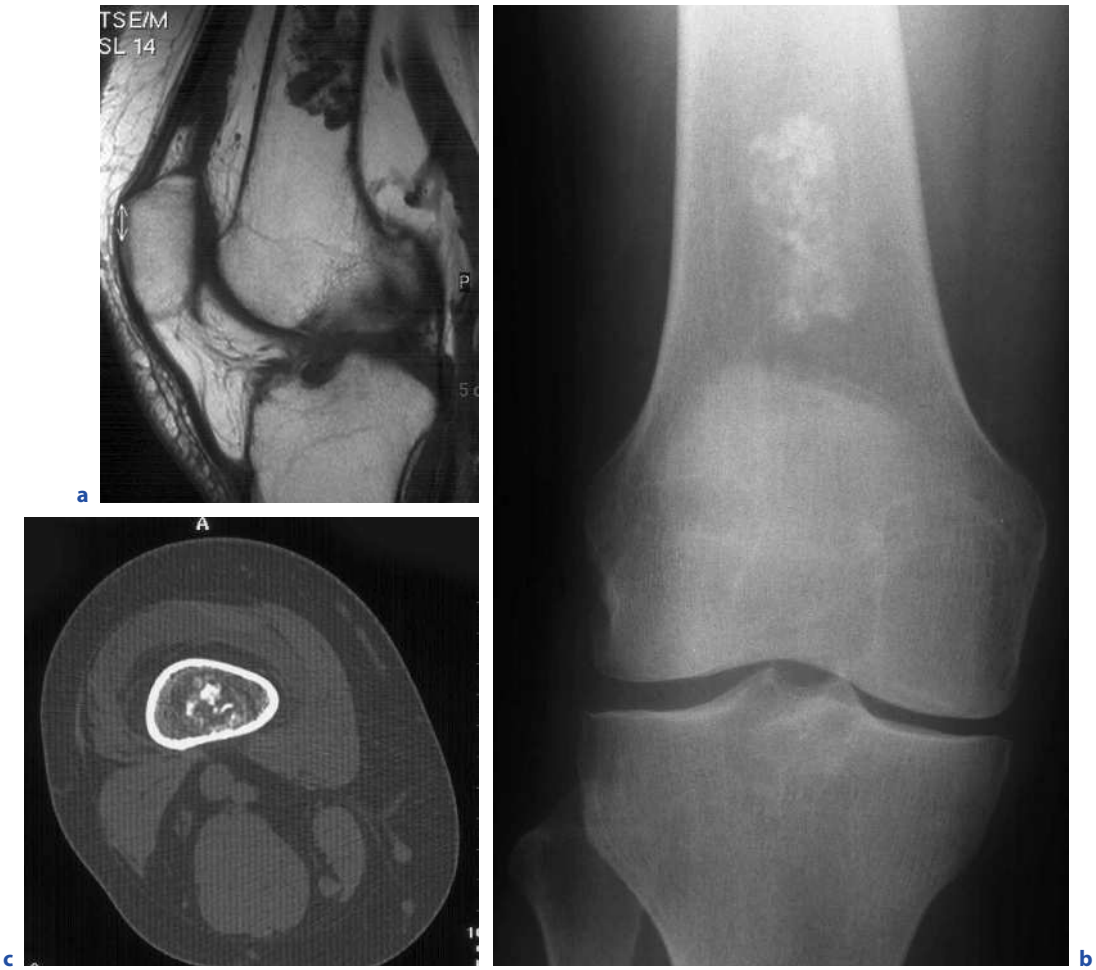

Fig. 7.6a–c. Enchondroma femur. **a** Sagittal T1-weighted MR image obtained for a suspected meniscal injury reveals an incidental lesion in the distal femoral diaphysis. **b** AP radiograph and **c** axial CT show punctate calcification typical of a cartilage tumour

7.3 Diagnosis

The author, Conan Doyle, the inventor of the archetypal British detective and fictional contemporary of Roentgen, Sherlock Holmes, identified three qualities for the ideal detective: "observation, deduction and knowledge" (Doyle 1890). Analogies can be readily drawn between the optimum profiles of detectives and clinicians (Rapezzi et al. 2005) that can be aptly applied to the radiologist faced with an undiagnosed bone lesion. Once a skeletal abnormality has been detected, the next objective of imaging is to attempt to characterize the lesion and, in doing so, indicate an appropriate differential diagnosis to the referring clinician. At this stage important maxims that should be appreciated include not over-treating a benign lesion, not under-treating a malignant lesion and not misdirecting the approach to biopsy that might prejudice subsequent surgical management (Moser and Madewell 1987).

In drawing up a differential diagnosis for a particular case the radiologist must first have knowledge of the different pathologies that may arise in the musculoskeletal system. While an understanding of the microscopic features is not required, it is clear that an entity will not appear in the differential diagnosis if the radiologist involved is unaware of its existence. Musculoskeletal tumours can best be categorised according to their tissue of origin and then into benign and malignant subtypes (see Chap. 1).

Before assessing the imaging the prudent radiologist should establish some basic facts regarding the patient. In recognizing the relevance of certain clinical details the differential diagnosis may then be significantly reduced even before the imaging is taken into account. Important factors to be noted that can help narrow down the differential diagnosis to a greater or lesser extent include the following:

1. Age. The age of the patient is arguably the single most useful piece of information as it frequently influences the differential diagnosis. Many musculoskeletal neoplasms exhibit a peak incidence at different ages (Table 7.1). The late eminent skeletal radiologist, Jack Edeiken, reasonably claimed that approximately 80% of bone tumours could be correctly diagnosed on the basis of age alone (Edeiken 1981). He observed that tumours could be grouped according to age so that neuroblastoma metastases were commonest in the first 2 years of life, osteosarcoma and Ewing's sarcoma in the first and second decades, spindle cell sarcoma (i.e. malignant fibrous histiocytoma), parosteal osteosarcoma, giant cell tumour and lymphoma during the third and fourth decades and finally metastases, myeloma and chondrosarcoma above 40 years of age. The radiologist can also apply the opposite principle. At what ages are certain diagnoses more or less unlikely? For example, it is unusual to see cystic lesions of bone, such as a simple bone cyst or an aneurysmal bone cyst (ABC), after skeletal fusion, i.e. in the adult. Osteosarcoma is unlikely to be included in the differential diagnosis of a bone-forming lesion in a middle-aged or elderly patient except in the presence of a pre-existing bone lesion such as Paget's disease. Similarly, a bone tumour arising in adolescence or early adult life is unlikely to be a metastasis.
2. Gender. When looking at large series of patients with different types of bone tumour it can be seen that many occur slightly more commonly in boys. In the individual case this fact does not play a significant role in formulating the differential diagnosis.
3. Ethnic and geographic origin. Among the bone neoplasms, Ewing's sarcoma is unusual in that it is prevalent in Caucasians but is rarely seen in the Afro-Caribbean races. A number of non-neoplastic bone conditions that may on occasion simulate neoplasia also show a racial predisposition, e.g. sickle cell, Gaucher's and Paget's diseases. It is only in isolated cases that the ethnic origin of the patient provides a useful pointer to the diagnosis. Osseous TB can mimic a bone tumour and in developed countries is more commonly seen in immigrants from the Indian subcontinent and South Asia.
4. Family history. There is little evidence of a familial predisposition to the formation of musculoskeletal neoplasms in most instances. The exceptions are certain hereditary bone conditions that may be found in association with malignant change, e.g. diaphyseal aclasis (hereditary multiple exostoses), Ollier's disease and Maffucci's syndrome. Several congenital conditions may be associated with a higher risk of developing osteosarcoma including congenital retinoblastoma and Rothmund–Thomson syndrome.
5. Past medical history. Information that should be noted in all patients, whenever present, is a history of a prior malignancy or a pre-existing bone condition. If such relevant details are forthcoming, it is important to establish if previous imaging records exist and, if so, obtain them for correlation with the present imaging results.
6. Multiplicity. It is critical early in the investigation of a patient to establish whether a bone lesion is solitary or multiple as it will influence the differential diagnosis. Frequently, this question will not be de-

Table 7.1. Peak age incidence of benign and malignant tumours and tumour-like lesions of bone

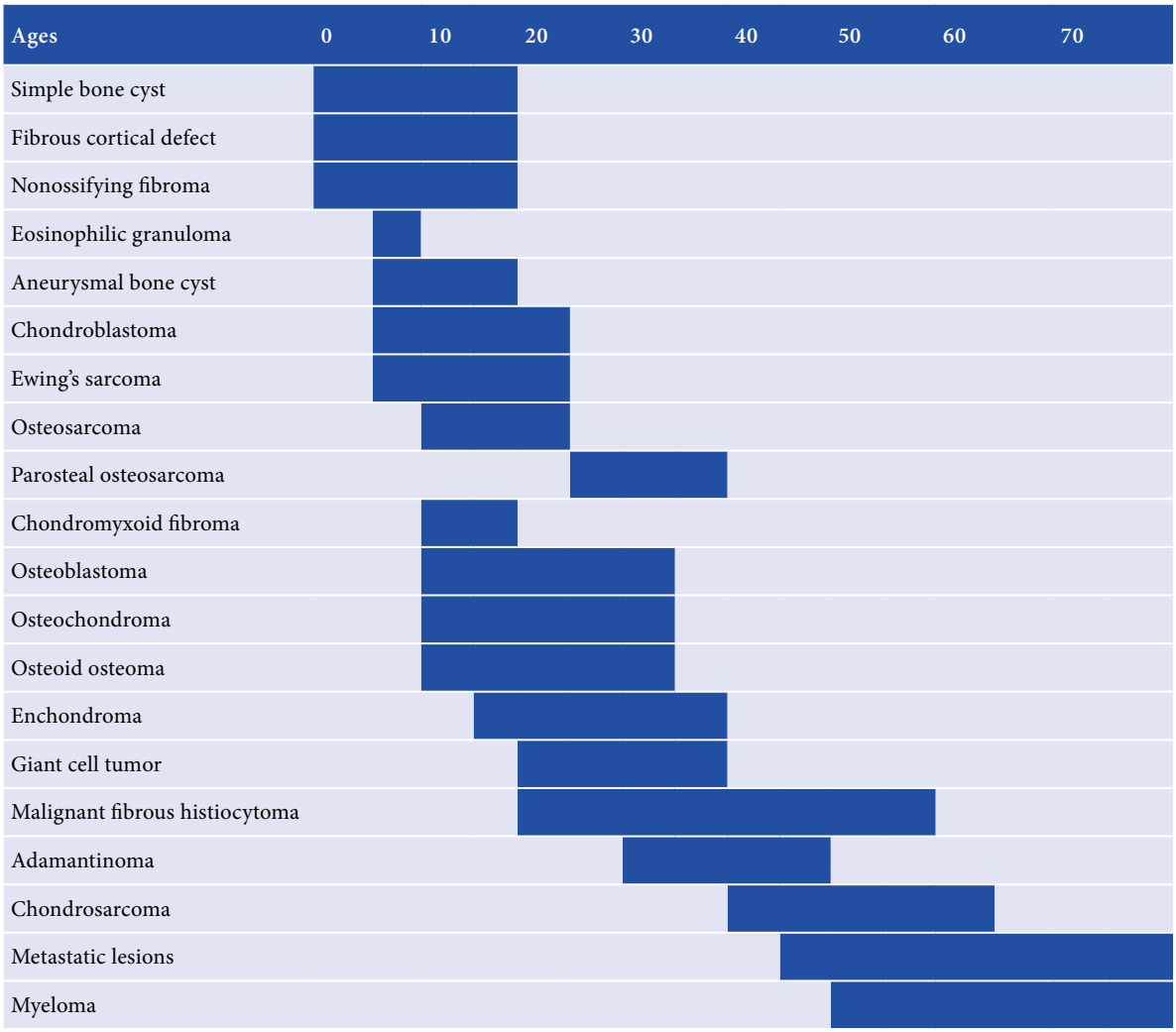

finitively answered until the staging imaging, such as bone scintigraphy, has been performed.

7. Serology. Abnormal serological tests, such as raised erythrocyte sedimentation rate (ESR) and white cell count, together with the examination findings of a hot swollen limb, are highly suggestive of a bone or soft tissue infection. Ewing's sarcoma, however, is notorious for presenting with similar clinical and serological findings. The brown tumour of hyperparathyroidism may mimic a true bone tumour on both imaging and histology. Raised serum calcium and alkaline phosphatase levels should alert the clinician to the possibility of this diagnosis. Similarly, a raised prostatic serum antigen level in an elderly male patient presenting with a bone-forming tumour is highly suggestive of a prostate metastasis.

In establishing a perspective of the patient as a whole the factors detailed above should be taken in conjunction with one another, for example, age and multiplicity. Multiple bone lesions in the young child will suggest a bone dysplasia, Langerhans cell histiocytosis, leukaemia or metastatic neuroblastoma, whereas in the adult, metastatic disease and myeloma are the most likely lesions. It is at this stage that attention should turn to the imaging of the lesion itself.

7.3.1 Radiographic Diagnosis

The radiograph remains the most accurate of all the imaging techniques currently available in determining the differential diagnosis of a bone lesion (Kricun 1983; Priolo and Cerase 1998; Miller 2008). The radiologist may attempt a diagnosis from the radiograph in one of two ways. Firstly, the not-so-sophisticated but oft-used method of radiographic interpretation commonly referred to as the "Aunt Minnie approach". This epithet was attributed by the late Ben Felson to Ed Neuhauser, Chief of Radiology at the Boston Children's Hospital over half a century ago (Teele and Griscom 1998). It consists of a question and answer. "How do you know that woman is your Aunt Minnie?" "Because I've seen her before and it looks like her" (Kricun 1983). This approach relies on familiarity with the typical overall appearances of a particular lesion. This is all very satisfactory if the abnormality under investigation is classic in appearance, but problems arise if the lesion has atypical features, arises at an unusual site or is mimicked by a differing pathology. The second, preferred approach, which might best be termed pattern analysis, relies on meticulous recognition of various radiographic signs (Lodwick 1965, 1966). The analysis can be best illustrated by answering a series of five questions: Which bone is affected? Where in that bone is the lesion located? What is the tumour doing to the bone (pattern of destruction)? What form of periosteal reaction, if any, is present? What type of matrix mineralisation, if any, is present?

7.3.1.1 Site in Skeleton

Most bone tumours and infections occur around the knee and in the proximal humerus, and as such, little diagnostic information can be deduced from noting the affected bone in many cases. There are notable exceptions. Cartilage tumours of the hands and feet, while common, are almost invariably benign or, if shown to be malignant histologically, have remarkably little potential for metastatic spread. Both osteofibrous dysplasia and adamantinoma classically involve the diaphysis of the tibia and are extremely rare at any other site (Fig. 7.7). The majority of lesions arising in the medial third of the clavicle in children and adolescents are osteomyelitis or part of the spectrum of chronic recurrent multifocal osteomyelitis and are, therefore, not neoplastic (see Chap. 31). Conversely, most lesions arising in the sternum are malignant. Chordoma characteristically

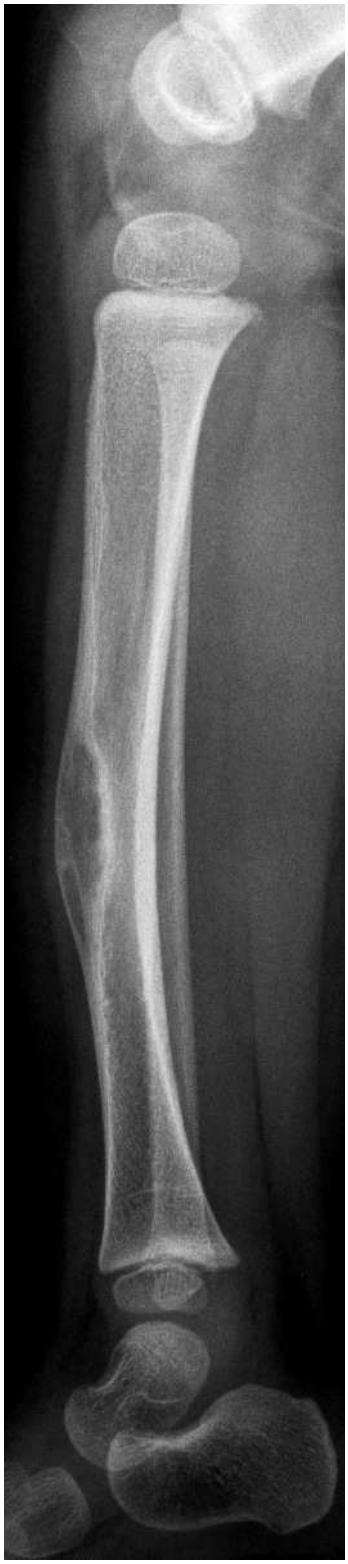

Fig. 7.7. Osteofibrous dysplasia (OFD) tibia. Lateral radiograph shows a typical mildly expansile lytic lesion arising in the anterior cortex of the diaphysis. This is the typical site for OFD and adamantinoma; both are rare at other skeletal sites

arises from the clivus or sacrum. Although many different tumours may arise in the bony spine, malignant lesions are found predominantly in the anterior part of the vertebra (body), while benign lesions, with a few exceptions, are characteristically found in the posterior elements (neural arch; see Chap. 33). Most spinal infections develop first in the vertebral endplate and rapidly extend to involve the disc space, which is uncommon in neoplasia.

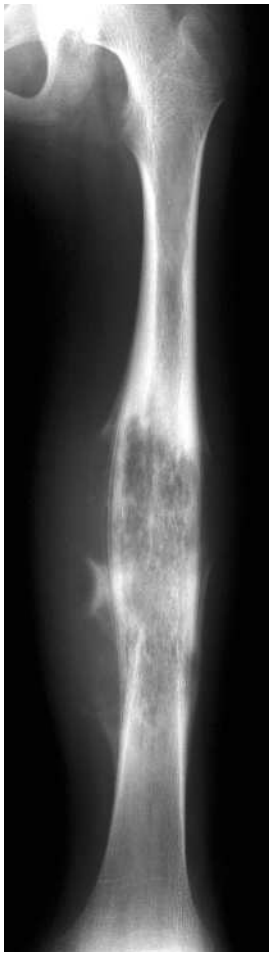

Fig. 7.8. Ewing's sarcoma in the femur. AP radiograph shows the classical diaphyseal location, permeative bone destruction, lamellated periosteal reaction, multiple Codman angles and soft tissue extension

7.3.1.2 Location in Bone

The site of the original bone tumour is an important parameter of diagnosis (Madewell et al. 1981). It reflects the site of greatest cellular activity. During the adolescent growth spurt the most active areas are the metaphyses around the knee and the proximal humerus. Tumour originating from marrow cells may occur anywhere along the bone. Conventional osteosarcoma will tend, therefore, to originate in the metaphysis or metadiaphysis (see Fig. 7.2), whereas Ewing's sarcoma will arise in the metaphysis or, more distinctively, in the diaphysis (Fig. 7.8). In the child the differential diagnosis of a lesion arising within an epiphysis can be realistically limited to chondroblastoma (Fig. 7.9), epiphyseal abscess (pyogenic or tuberculous) and rarely, Langerhans cell histiocytosis. Following skeletal fusion subarticular lesions, analogous in the adult to the epiphyseal lesions in children, include giant cell tumour, clear cell chondrosarcoma (rare) and intraosseous ganglion. With the exception of epiphyseal abscess most osteomyelitis will arise within the metaphysis of a long bone, typically the tibia and femur.

It is also helpful to identify the origin or epicentre of the tumour with respect to the transverse plane of the bone. Is the tumour central, eccentric or cortically based? For example, a simple bone cyst, fibrous dysplasia and Ewing's sarcoma will tend to be centrally located (Figs. 7.8, 7.10). Giant cell tumour, chondromyxoid fibroma and non-ossifying fibroma are typically eccentric in location (Figs. 7.11, 7.12). Lesions that usually arise in an eccentric position may appear central if the tumour is particularly large or the involved bone is of a small calibre. There are numerous surface lesions of bone that are related to the outer surface of the bony cortex (Kenan et al. 1993; Seeger et al.1998). A benign example is the periosteal or juxtacortical chondroma. Most of the malignant surface lesions of bone are the rarer forms of osteosarcoma, e.g. periosteal, high-grade surface and parosteal osteosarcoma (Fig. 7.13). Of parosteal osteosarcomas, 50% arise on the posterior surface of the distal femoral metaphysis.

Analysis of the location of a tumour in bone should, therefore, recognize the position in both the longitudinal and transverse planes. Combining these factors can then help to narrow down the differential diagnosis. For example, a giant cell tumour will be subarticular and eccentric, whereas both non-ossifying fibroma and chondromyxoid fibroma will tend to be metaphyseal and eccentric in location (Figs. 7.11, 7.12). In the sacrum, chordoma classically arises in the midline, whereas giant cell tumour, a not uncommon tumour in the sacrum at a similar age, will be eccentric bordering on one of the sacroiliac joints, i.e. subarticular in origin. Figure 7.14 illustrates the typical sites of origin of bone tumours.

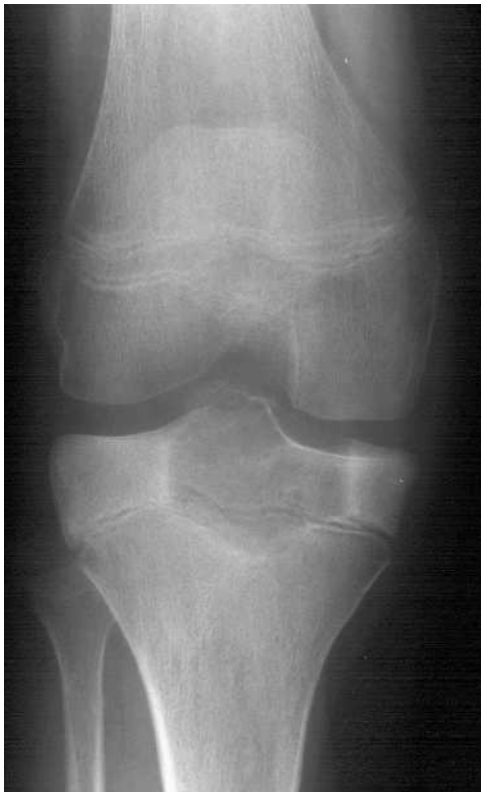

a

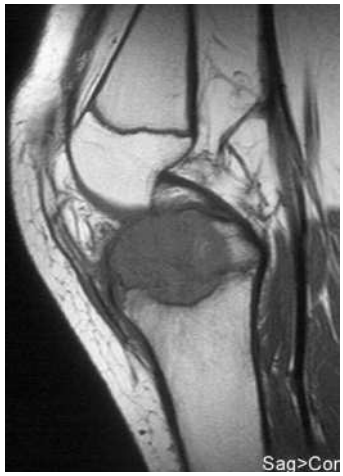

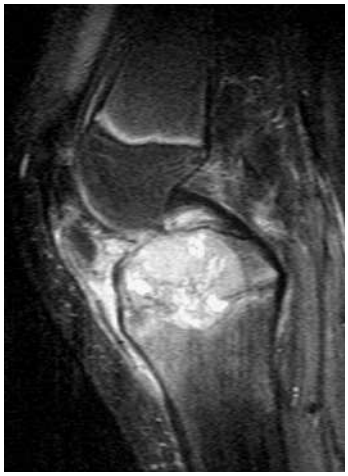

b, c

Fig. 7.9a–c. Chondroblastoma tibia. **a** AP radiograph shows a lytic lesion arising in the proximal tibial epiphysis. **b** Sagittal T1-weighted and **c** Sagittal STIR images confirm the epiphyseal lesion and shows early breaching of the growth plate and moderate surrounding marrow oedema

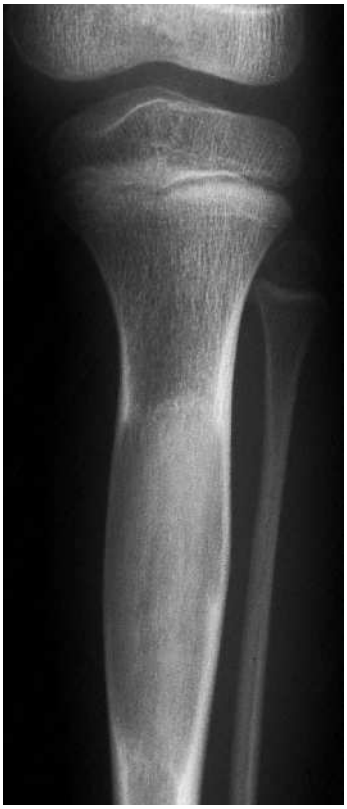

Fig. 7.10. Fibrous dysplasia tibia. AP radiograph shows typical features being well defined and central, mildly expansile with a ground-glass density matrix

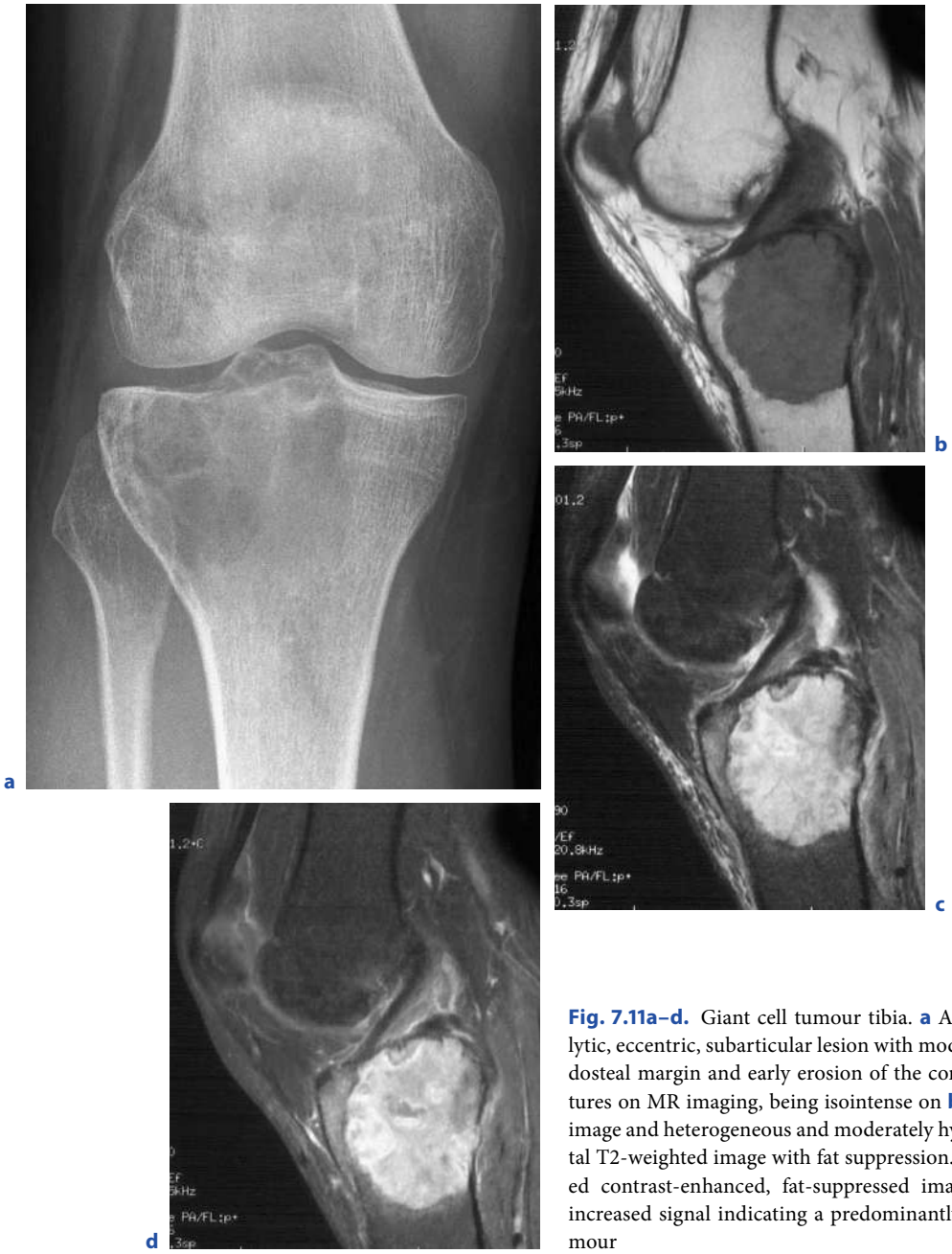

Fig. 7.11a–d. Giant cell tumour tibia. **a** AP radiograph shows a lytic, eccentric, subarticular lesion with moderately ill-defined endosteal margin and early erosion of the cortex. Non-specific features on MR imaging, being isointense on **b** sagittal T1-weighted image and heterogeneous and moderately hyperintense on **c** sagittal T2-weighted image with fat suppression. **d** Sagittal T1-weighted contrast-enhanced, fat-suppressed image shows extensively increased signal indicating a predominantly solid, not cystic, tumour

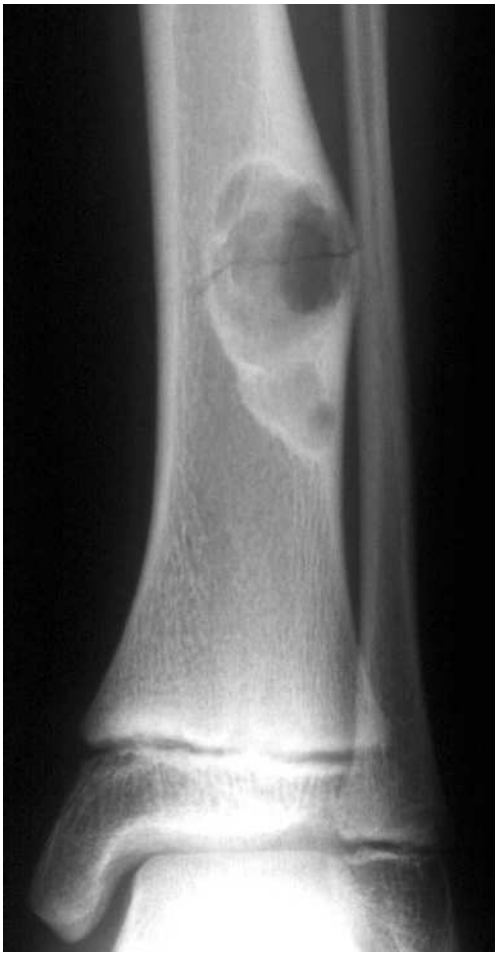

Fig. 7.12. Non-ossifying fibroma tibia. AP radiograph shows a typical example with a well-defined sclerotic margin arising in an eccentric location complicated by a pathological fracture

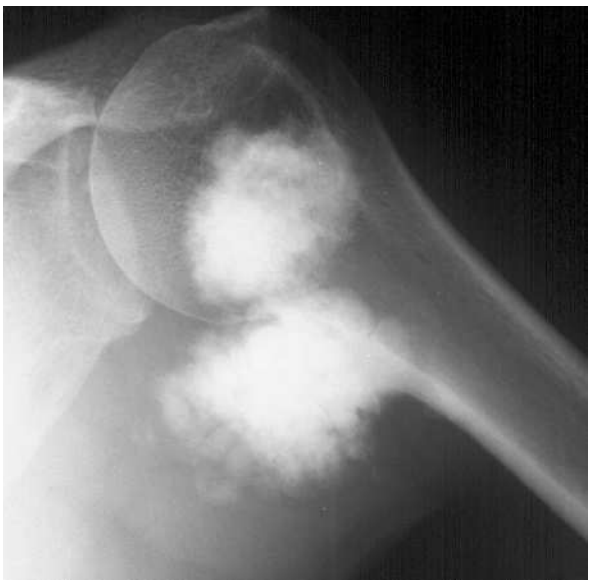

a

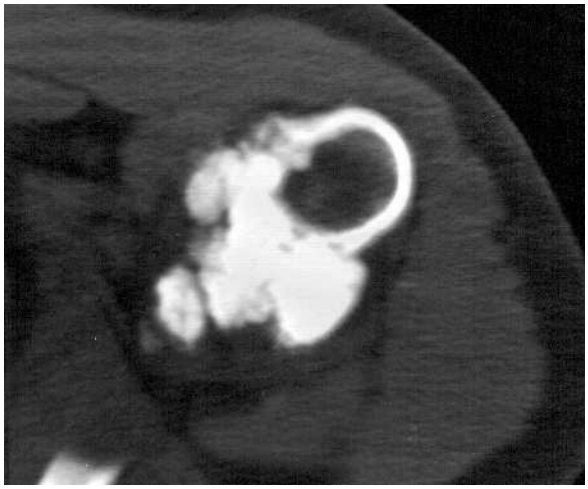

b

Fig. 7.13a,b. Parosteal osteosarcoma humerus. **a** AP radiograph shows dense malignant osteoid overlying the proximal humeral metaphysis and adjacent soft tissues. **b** Axial CT shows the lesion to be arising on the surface of the bone, hence a parosteal osteosarcoma

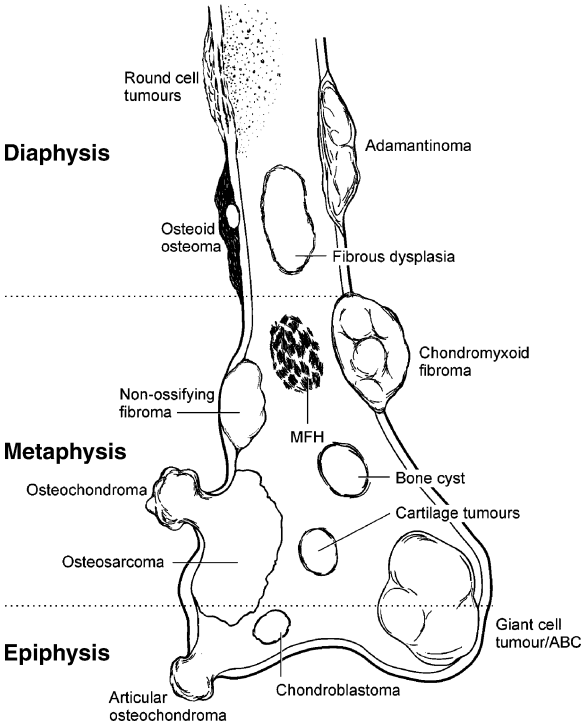

Fig. 7.14. The typical sites of bone tumours. *MFH* malignant fibrous histiocytoma, *ABC* aneurysmal bone cyst

7.3.1.3 Pattern of Bone Destruction

Bone destruction is usually the first radiographic sign of disease and may be the only evidence of pathology. Trabecular bone is more easily destroyed than cortical bone. As individual trabeculae contribute less to the overall radiographic image, relatively large amounts of spongy bone must be destroyed before it is visible (Edeiken 1981). Analysis of the interface between tumour and host bone is a good indicator of the rate of growth in the lesion. A sharply marginated lesion usually denotes slower growth than a non-marginated lesion. The faster the growth, the more "aggressive" the pattern of destruction and the wider the zone of transition between tumour and the normal bone. Aggressivity, per se, does not conclusively indicate malignancy, but the malignant tumours tend to be faster growing than their benign counterparts. The American skeletal radiologist, Gwilym Lodwick, can be credited with introducing a semi-quantitative classification of patterns of bone destruction that is regularly reproduced in almost every text dealing with this subject (Lodwick 1965a, 1965b, 1966; Lodwick et al. 1980a,b). Each pattern reflects a particular growth rate and thereby suggests a differential diagnosis (Madewell et al. 1981; Kricun 1983). It must be noted that any classification is artificial and that a category of bone tumour can exhibit a spectrum of bone destruction from well- to ill-defined. Lodwick described three patterns of bone destruction associated with tumours and tumour-like lesions of bone: type 1, known as geographic bone destruction (Fig. 7.15a); type 2, known as moth-eaten bone destruction; and type 3, known as permeative bone destruction (Fig. 7.15b). A description and discussion of the significance of these three patterns follows.

7.3.1.3.1 Type 1: Geographic

In this pattern the growth rate is sufficiently indolent that the lesion will appear well marginated with a thin zone of transition. The geographic pattern may be further subdivided into types 1A, 1B and 1C depending on the appearance of the margin and the effect on the cortex (Fig. 7.15a). Type 1A, the slowest growing of all the lesions and thereby the least aggressive, is typified by a sclerotic margin. The thicker the sclerotic rim, the longer the host bone has had time to respond to the lesions indicating a slow rate of growth. The vast majority of these lesions will prove to be benign (see Fig. 7.10). In type 1B the lesion is well defined without the sclerotic margin. While still relatively slow growing, the rate is slightly greater than that of type 1A. Again, the majority of type-1B lesions are benign, although some malignancies may on occasion demonstrate this pattern. In type 1C the margin is less well defined, indicating a more aggressive pattern. The cortex is also destroyed. Few benign tumours exhibit a type-1C pattern. The differential diagnosis in this situation includes giant cell tumour, malignant fibrous histiocytoma and lymphoma of bone (Fig. 7.11).

7.3.1.3.2 Type 2: Moth-eaten; Type 3: Permeative

Moth-eaten and permeative patterns of bone destruction reflect the increasingly aggressive nature of these tumours compared with geographic lesions (Fig. 7.15b). Again, this is a spectrum of change varying from multiple foci of bone destruction which may coalesce (moth-eaten; see Fig. 7.8) to multiple tiny defects, best seen

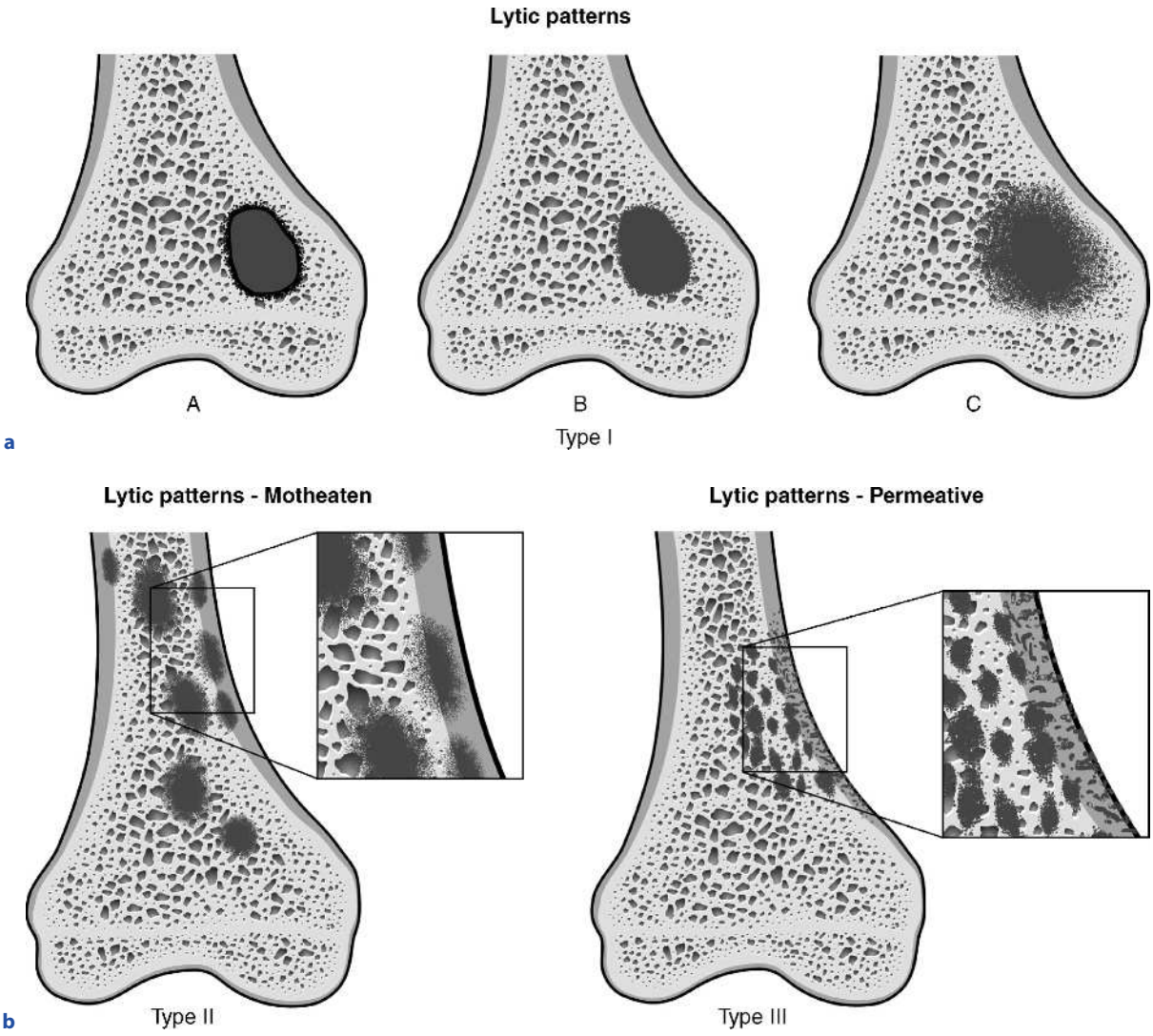

Fig. 7.15a,b. The patterns of bone destruction. **a** Geographic (types 1A–1C). **b** Type 2 (moth-eaten) and type 3 (permeative)

a

b

Fig. 7.16a,b. Ewing's sarcoma in the humerus. **a** AP radiograph and **b** magnified detail show a highly aggressive permeative pattern of bone destruction

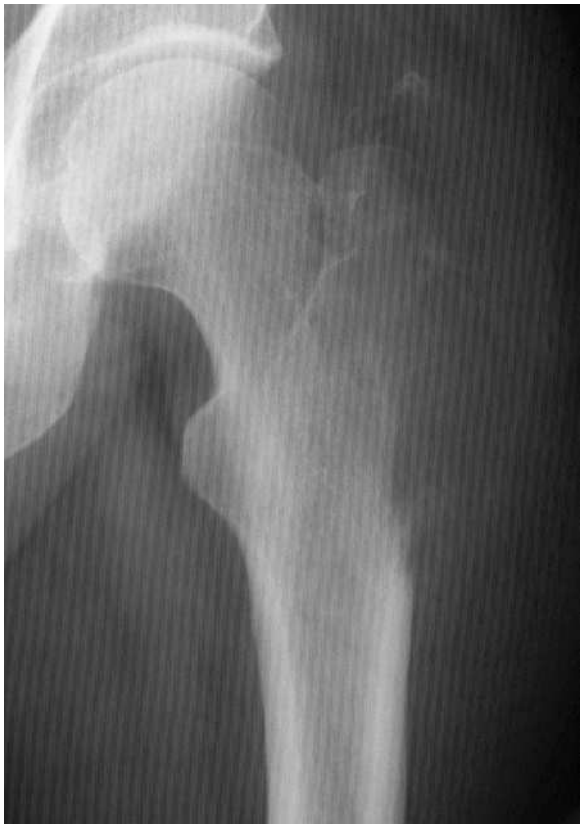

Fig. 7.17. Bronchial metastasis in the femur. There is destruction of the greater trochanter with extraosseous tumour extension and an ill-defined inner margin

in the cortical bone, which gradually diminish in size and frequency from the centre to periphery of the lesion (permeative) resulting in an ill-defined wide zone of transition (Fig. 7.16). The highly aggressive nature of these lesions does not allow the host bone sufficient time to react and produce a response (Kricun 1993). Typically, malignancies, including metastasis, Ewing's sarcoma and osteosarcoma, exhibit a moth-eaten or permeative appearance (Figs. 7.8, 7.16, 7.17). Benign tumours in general do not show this pattern of bone destruction. Acute osteomyelitis may also give a moth-eaten pattern of bone destruction.

7.3.1.4 Periosteal Reaction

The periosteum is the thin layer of soft tissue with osteoblastic properties that lines the outer cortex of bone. It is normally radiolucent but will mineralise when the osteoid-producing cells of the inner cambium layer are stimulated by an adjacent bony or para-osseous process. The rate of mineralisation is partly dependent on the age of the patient. The younger the patient, the more rapid the appearance of the radiographic change, and vice versa. Periosteal reaction, otherwise known as pe-

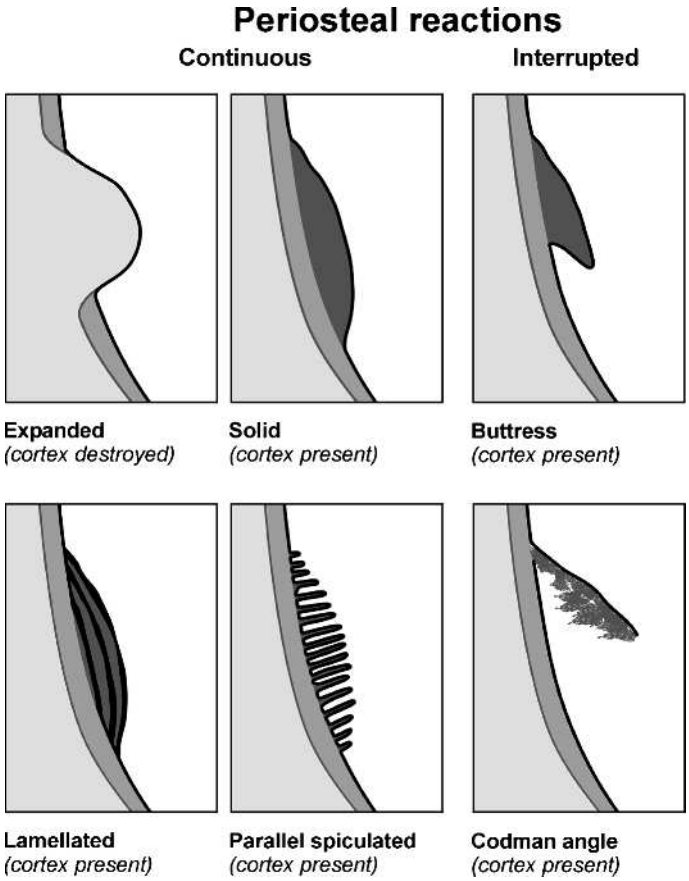

Fig. 7.18. Periosteal reactions

riosteal new bone formation, may occur in any condition that elevates the periosteum, whether it be blood, pus or tumour. The term "periostitis", favoured in older texts, is best avoided as it implies an inflammatory aetiology. The appearance and nature of a periosteal reaction is frequently valuable in narrowing down the differential diagnosis of a bone tumour. A good, albeit complex, classification identified three broad categories: continuous; discontinuous; or interrupted and complex (Fig. 7.18; Ragsdale et al. 1981; Moser and Madewell 1987).

7.3.1.4.1 Continuous Periosteal Reaction

A continuous periosteal reaction may be observed with either an intact or a destroyed underlying cortex; in the latter the bone can be described as "expanded", but this is a misnomer as bone cannot be inflated like a balloon (Ragsdale et al. 1981). Nevertheless, the term "cortical expansion" is well entrenched in common usage (Fig. 7.19a,b). It represents a relatively slow process by which endosteal bone resorption is balanced by periosteal new bone formation. In faster-growing lesions the endosteal resorption will exceed periosteal apposition and a thin outer "shell" will be produced. The thickness of this shell is another indicator of the rate of growth of the lesion, but it is not a good discriminator of benign from malignant. Shells are typically found in benign lesions such as simple bone cyst, aneurysmal bone cyst (ABC), chondromyxoid fibroma, fibrous dysplasia and giant cell tumour. They are also well recognised in "expansile" metastases of renal (Fig. 7.20) and thyroid origin and plasmacytoma (Fig. 7.21). Additions to, rather than substitutes for, the original cortex occur with a continuous periosteal reaction with an intact cortex. The periosteal reaction may be solid, a single lamella, lamellated ("onion skin") or spiculated ("hair-on-end"; Fig. 7.18). The solid type implies the slow apposition of layers of new bone to the cortex, sometimes termed "cortical thickening" or "cortical hyperostosis".

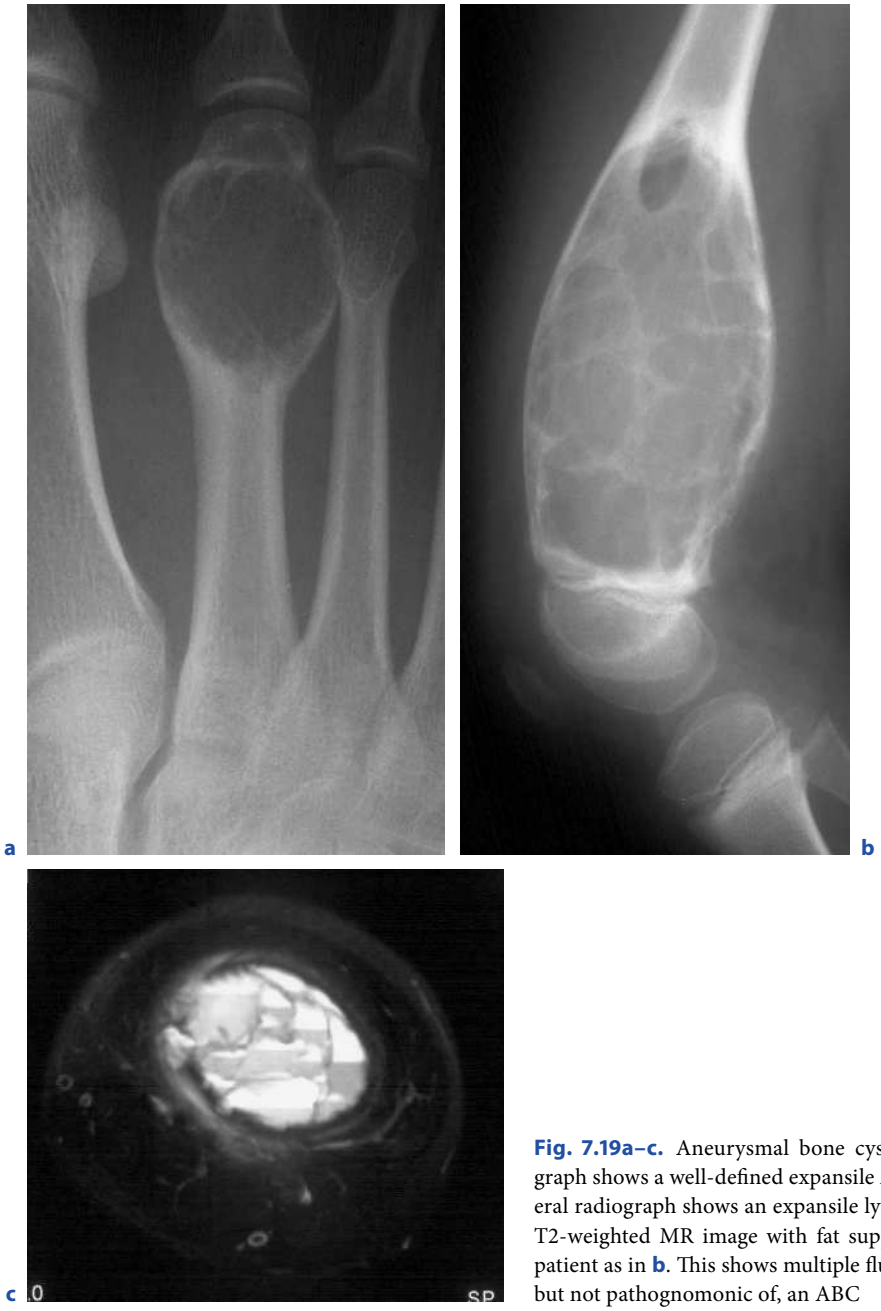

Fig. 7.19a–c. Aneurysmal bone cysts (ABC). **a** Dorso-plantar radiograph shows a well-defined expansile ABC in the distal metatarsal. **b** Lateral radiograph shows an expansile lytic ABC in the distal femur. **c** Axial T2-weighted MR image with fat suppression of the femur in the same patient as in **b**. This shows multiple fluid-fluid levels highly suggestive of, but not pathognomonic of, an ABC

It is seen in chondroma, central chondrosarcoma, and eccentrically in osteoid osteoma. If the solid periosteal reaction is extensive with an undulating quality the differential diagnosis includes chronic osteomyelitis, hypertrophic osteoarthropathy (Fig. 7.22), chronic lymphoedema and varicosities.

A single lamellar periosteal reaction is formed by a thin radiodense line separated from the cortex by a narrow radiolucent zone. It usually denotes a benign disorder and is frequently seen with traumatic and inflammatory conditions. It should be appreciated that a periosteal reaction is a dynamic process and a single lamella may fill in to produce a solid appearance or go on to the addition of further lamellae ("onion skin"). The lamellated periosteal reaction is seen in Ewing's sarcoma (see Fig. 7.8), osteosarcoma, Langerhans cell histiocytosis (eosinophilic granuloma) of the long bones in children and acute osteomyelitis. A spicu-

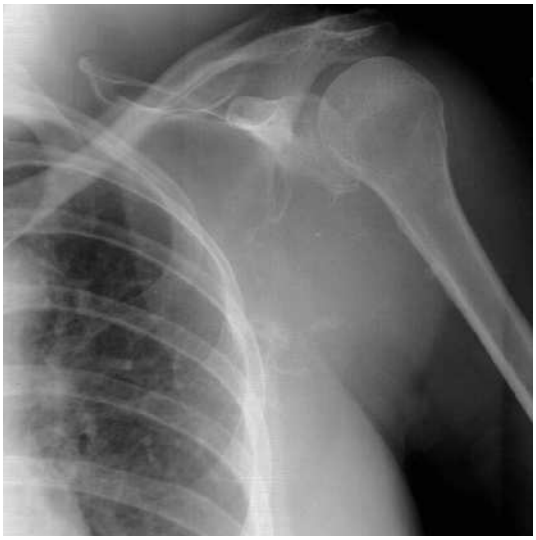

a

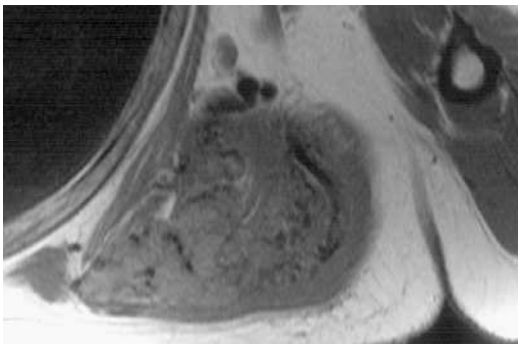

b

Fig. 7.20a,b. Renal metastasis scapula. **a** AP radiograph shows a lytic expansile lesion destroying the lateral border of the scapula. **b** Axial T1-weighted MR image shows the tumour to be of intermediate signal intensity with multiple small flow voids due to prominent vessels

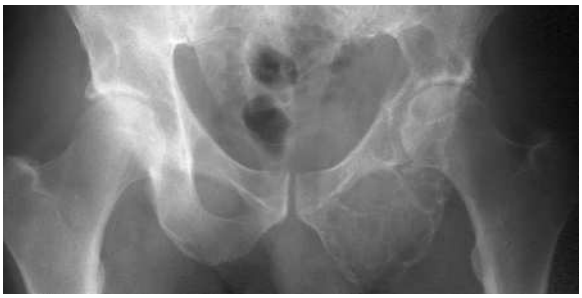

Fig. 7.21. Plasmacytoma in the pelvis. AP radiograph shows a large expansile lytic lesion involving the left acetabulum and ischium

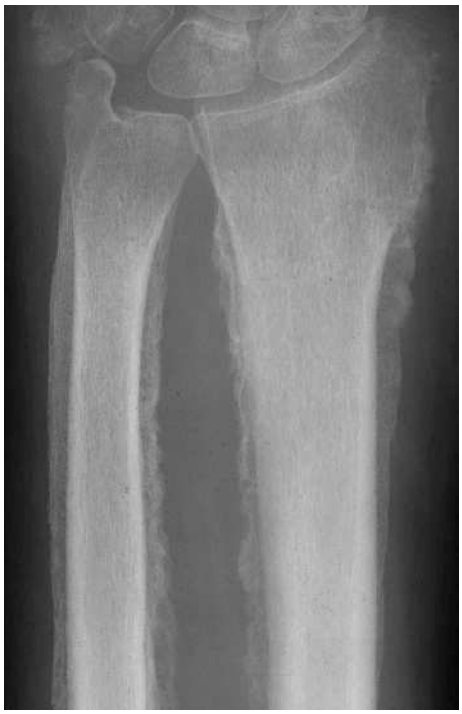

Fig. 7.22. Hypertrophic osteoarthropathy. PA radiograph shows florid continuous periosteal reaction along the radius and ulna. The patient had a history of bronchial carcinoma

lated ("hair-on-end") periosteal reaction occurs when the mineralisation is oriented perpendicular to the cortex and denotes a more rapidly evolving process. It is typical of malignant tumours such as osteosarcoma (Fig. 7.23) and Ewing's sarcoma but may be seen in benign tumours including meningioma, haemangioma of bone and non-neoplastic conditions such as thalassemia and thyroid acropachy. The location of a spiculated periosteal reaction significantly influences the differential diagnosis.

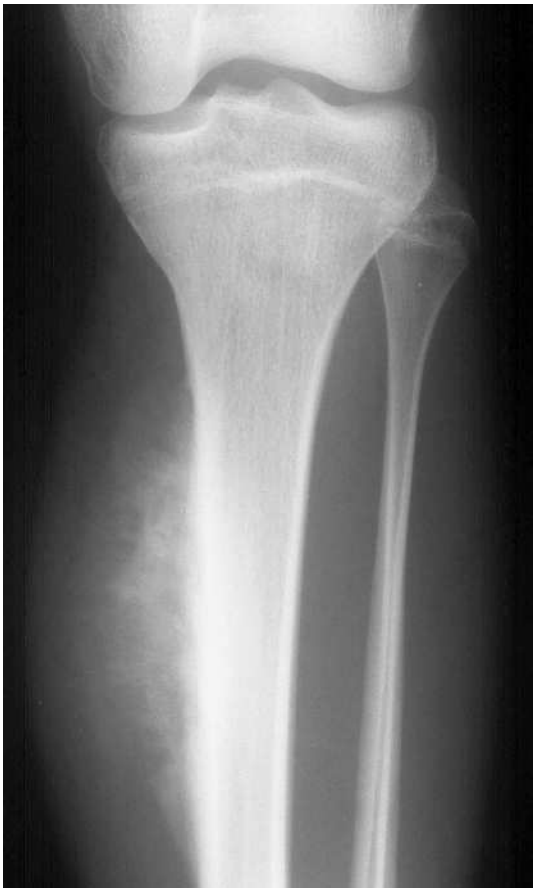

Fig. 7.23. Periosteal osteosarcoma in the tibia. The AP radiograph shows a spiculated periosteal reaction arising from the medial aspect of the proximal diaphysis. The obliquity of the spicules at the periphery of the lesion means that the pattern could also be described as "sun-ray" or "sun-burst"

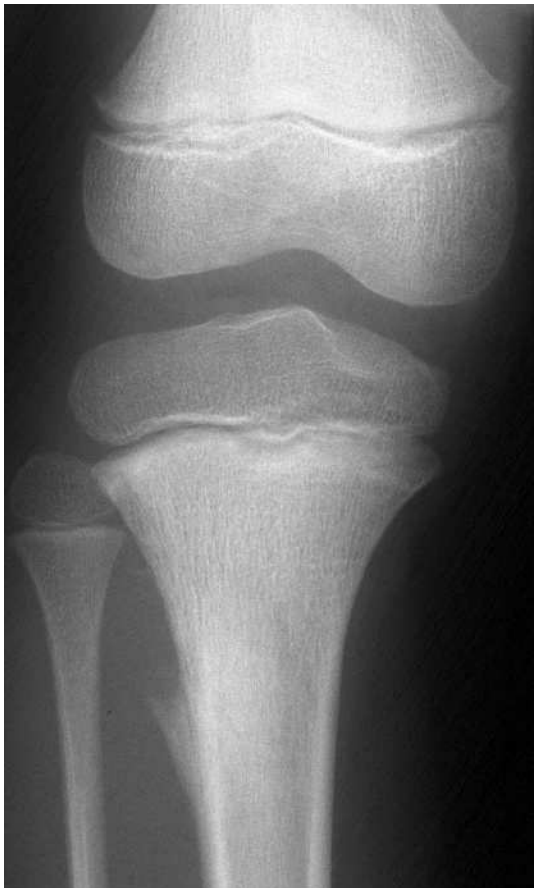

Fig. 7.24. Osteosarcoma tibia. AP radiograph shows a typical Codman angle arising on the lateral aspect of the proximal metaphysis. This is virtually the only sign of the underlying sarcoma in this image

7.3.1.4.2 Discontinuous Periosteal Reaction

A discontinuous or interrupted periosteal reaction indicates that the mineralisation has been breached in one of two ways: either the process, usually a tumour, simply occupies the available space, or the rate of apposition of new bone is exceeded by the rate of resorption. Close attention should be paid to the margins of the periosteal reaction. Rapidly growing benign tumours may exhibit a peripheral wedge or buttress with a thin or even non-existent shell. The buttress should be distinguished from the so-called Codman triangle (see Fig. 7.18; Codman 1926). This refers to an elevation of interrupted periosteum with one or more layers of new bone located at the periphery of the lesion (Figs. 7.8, 7.24). It might be more appropriately termed Codman angle as only two sides (the host cortex and the interrupted periosteal reaction) are typically mineralised. This pattern is suggestive, if not diagnostic, of malignancy as it may also be seen in osteomyelitis as well as being a classic feature of both osteosarcoma and Ewing's sarcoma. In malignant bone tumours the site of interruption of a periosteal reaction is usually the area of maximum extra-osseous tumour growth.

7.3.1.4.3 Combined Periosteal Reaction

More than one pattern of periosteal reaction may be manifest in the same case and is called a combined or

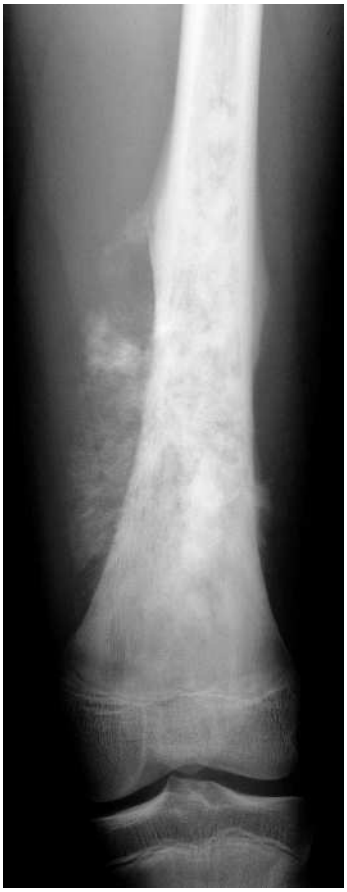

Fig. 7.25. Osteosarcoma femur. AP radiograph shows all the typical features of the tumours including permeative bone destruction, malignant osteoid mineralisation and a complex periosteal reaction

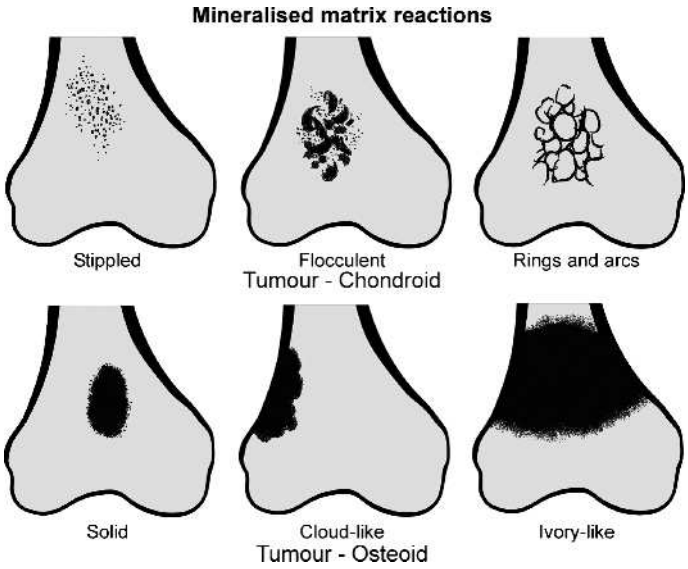

Fig. 7.26. Mineralised matrix patterns

complex pattern (see Fig. 7.8). This reflects the varying rate of growth at different sites in the same lesion. The divergent spiculated periosteal reaction, otherwise known as "sun-burst" or "sun-ray", is a typical example of a complex pattern and is suggestive of osteosarcoma (Figs. 7.23, 7.25).

7.3.1.5 Tumour Mineralisation

New bone formation is a frequent finding in numerous diseases of bone and can originate from the normal bone-forming elements (trabeculae and periosteum) as well as from particular types of tumour cells. Reactive new bone formation arising within the host bone may be seen with many tumours but also with other pathologies including trauma and infection. It can be difficult to distinguish reactive new bone from tumour new bone; the former usually produces thickening and increased density of the pre-existing trabeculae (Edeiken 1981). Other pitfalls in the diagnosis of tumour new bone include apparent increased radiodensity of a lesion due to the contribution of an overlying soft tissue mass to the attenuation of the X-ray beam and the presence of a mineralised periosteal reaction seen en face (Fig. 7.3b). Tumour new bone is the matrix of intercellular substance produced by certain tumour cells that can calcify or ossify. Radiodense tumour matrix is of either osteoid (osteogenic tumours) or chondroid (chondrogenic tumours) origin. The exception is fibrous dysplasia, where the collagenous matrix may be sufficiently dense to give a ground-glass appearance (Fig. 7.10). Tumour osteoid is typified by solid (sharp-edged) or cloud to ivory-like

(ill-defined edge) patterns (Figs. 7.13, 7.25, 7.26; Sweet et al. 1981). Tumour cartilage is variously described as stippled, flocculent, ring and arc and popcorn in appearance (Figs. 7.6b, 7.26; Sweet et al. 1981). Identifying the pattern of matrix calcification will significantly reduce the differential diagnosis, but matrix per se has no influence as to whether the lesion is benign or malignant, just whether the tumour is of osteogenic or chondrogenic origin. The distribution can also be helpful. For example, both enchondroma and medullary infarction may show calcification of a similar nature. The distribution is typically central in enchondroma and peripheral in medullary infarction.

7.3.2 CT Diagnosis

Computed tomography (CT) may be useful in establishing a differential diagnosis of a bone lesion in selected cases only. The CT features that should be assessed are similar to those previously described when evaluating the radiographs. This reflects the fact that both are radiographic techniques relying on the attenuation of an X-ray source. Cortical destruction, soft tissue extension and faint mineralisation are all more readily appreciated on CT scans than on radiographs, as is the epicentre of a bone lesion (medullary, cortical, periosteal or parosteal; Fig. 7.13b; Bloem and Kroon 1993; Magid 1993; Woertler et al. 2003). The presence of cortical breaching and a soft tissue mass are highly suggestive of malignancy or osteomyelitis (Brown et al. 1986). Computed tomography is of particular value in assessing complex anatomical areas such as the pelvis, spine and scapula (Woertler 2003). Computed tomography is also helpful in revealing the nidus of a suspected osteoid osteoma and is the technique of choice for subsequent image-guided radiofrequency ablation. In the long bones CT can be used to predict fracture risk associated with focal bone lesions (van der Linden et al. 2004). Direct measurement of the thickness of the cap of a peripheral cartilage tumour with CT can help differentiate an osteochondroma from a peripheral chondrosarcoma (Kenney et al. 1981). A cap thickness of <2 cm when measured perpendicular to the osteochondroma is likely to be benign. A cap thickness >2 cm is associated with an increased likelihood of malignancy. Both ultrasound and MR imaging can also be used in a similar manner to measure cartilage-cap thickness (Woertler et al. 2000).

7.3.3 Scintigraphic Diagnosis

Whole-body bone scintigraphy, utilizing 99mtechnetium methylene diphosphonate (^{99m}TcMDP), is routinely used in the investigation of a bone lesion to determine whether it is solitary or multiple. Identification of multifocal involvement clearly has implications for the surgical staging of a known disease but can also be helpful in suggesting a differential diagnosis in a patient with a previously undiagnosed abnormality detected on radiographs. The role of bone scintigraphy in surgical staging may be challenged in the future by whole-body MR imaging.

In the patient over 40 years of age, multiple bone lesions are much more likely to indicate metastases or myeloma than a primary bone tumour. The caveat is that in the same age group multiple foci of increased activity can be seen with Paget's disease, intermediate-grade vascular tumours and insufficiency-type stress fractures. Distinctive features that suggest Paget's disease include subarticular location, bone expansion, deformity and a higher uptake in the advancing edge of the disease (Wellman et al. 1977). Intermediate-grade vascular tumours, such as multifocal haemangioendothelioma, are frequently confined to a single limb, typically the lower limb. This monomelic distribution would be most unusual for either metastases or myeloma. Insufficiency-type stress fractures commonly occur in the pelvic bones in high-risk patients, namely postmenopausal women, long-term steroid therapy or any other cause of osteoporosis, and following radiotherapy for gynaecological malignancies (Mumber et al. 1997; Moreno et al. 1999). There is a classic association between parasymphyseal and sacral insufficiency fractures; the latter are frequently difficult to see on radiographs, but bone scintigraphy reveals the typical Honda or H-shaped pattern of vertical fractures arising in the sacral ala with a horizontal fracture extending across the body of the sacrum (Ries 1983).

In the past attempts have been made to characterize solitary bone lesions by assessing the shape, size, pattern and intensity of ^{99m}TcMDP uptake (Goodgold et al. 1983), but it is rarely used for this purpose today. For example, giant cell tumour frequently shows a "doughnut" appearance with a rim of high uptake surrounding a central area of lower uptake (Levine et al. 1984). A similar appearance can be seen in other tumours, however. Bone scintigraphy cannot be reliably used to distinguish enchondroma with persistent enchondral ossification from a low-grade central chondrosarcoma. Where the bone scan can be helpful in a patient with an indeterminate solitary bone lesion is in giving a crude

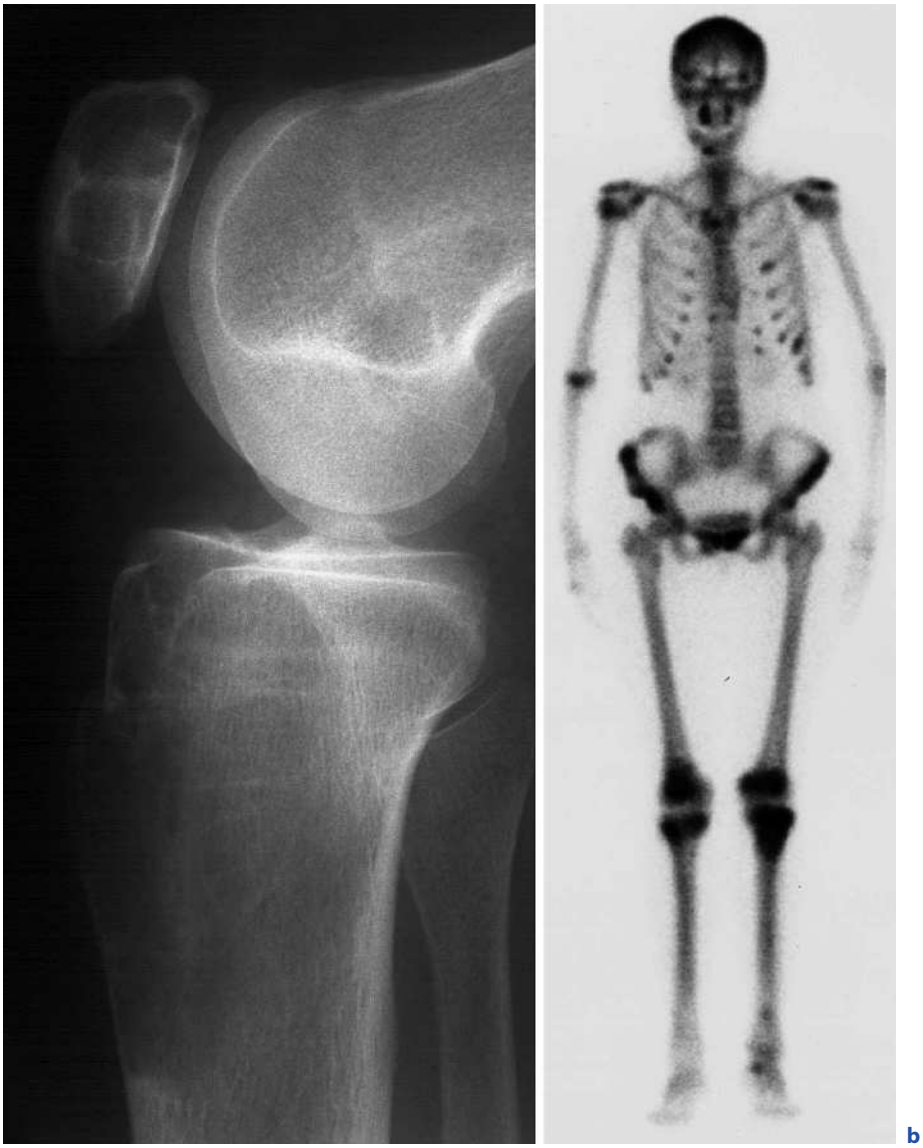

a b

Fig. 7.27a,b. Brown tumours of hyperparathyroidism. **a** Lateral radiograph and **b** whole-body bone scan. The multiple lytic lesions detected on the radiographs were first mistakenly thought to be metastases or myeloma. The bone scan performed to identify the full extent of the disease shows a "superscan". Note the marked activity in the calvarium and the paucity of renal activity

measure of the physiological activity of the lesion. Activity similar to the background skeletal activity suggests an indolent lesion and can be useful in distinguishing an isolated bone island from a sclerotic metastasis (Go et al. 1980), although increased activity has also been described in large bone islands (Hall et al. 1980).

A generalised high bone uptake of ^{99m}TcMDP with a high bone-to-soft tissue ratio and corresponding faint renal uptake is known as a superscan (Ryan and Fogelman 1997). This can be seen in the presence of diffuse marrow infiltration such as breast and prostate metastases but also in metabolic bone diseases such as osteomalacia, hyperparathyroidism and renal osteodystrophy. The authors have seen several patients, investigated for a suspected bone tumour, where the superscan was the first pointer to the correct diagnosis of a brown tumour due to underlying hyperparathyroidism (Fig. 7.27).

The role of positron emission tomography (PET) and PET/CT in bone tumours is evolving (see Chap. 4). Fluorine-18 FDG uptake has been shown to correlate with histopathological grading in sarcomas (Folpe et al. 2000). There is, however, an overlap of uptake between benign and malignant tumours with some benign conditions showing marked FDG uptake including Brodie's abscess, fibrous dysplasia and chondroblastoma (Strobel et al. 2006, 2007).

7.3.4 MR Imaging Diagnosis

In most cases MR imaging contributes little additional information in the characterisation of a bone tumour when compared with the radiographs (Leung and Dalinka 2000; Rechl et al. 2001). The majority exhibit a non-specific pattern with a low to intermediate signal intensity on T1-weighted and intermediate to high signal intensity on T2-weighted sequences (Alyas et al. 2007). In selected cases attention to signal characteristics and morphological features can be helpful (see Fig. 7.11b–d). At the most basic level, the identification, in an indeterminate lesion, of cortical destruction and solid soft tissue extension should alert the radiologist to the presence of an aggressive lesion likely to be malignant (see Fig. 7.2c). Many of the most useful signs are covered in the chapters on the various tumour subtypes (see Chaps. 13–30). Some general comments on the diagnostic value of MR imaging are discussed below. It is stressed that any MR features should always be correlated with the radiographic findings to minimise errors in interpretation. For example, signal voids (i.e. low signal intensity on all sequences) within a bone lesion may be due to mineralisation, such as might be seen with malignant osteoid production in an osteosarcoma. Similar appearances may be seen due to flow voids from fast-flowing blood which is typical of renal metastases (see Fig. 7.20b; Choi et al. 2003) and other hypervascular bone lesions. A quick reference to the radiographs enables the correct distinction to be made.

Oedema may be found around bone tumours both in the adjacent marrow and also the soft tissues. Marrow oedema is characterised by signal intensity on T1-weighted images between that of fat and skeletal muscle and hyperintensity on fluid-sensitive sequences with fat suppression. As a rule of thumb the more marked the marrow oedema as compared with the size of the main lesion, the less likely it is to be malignant. Prominent marrow oedema is common in a number of benign tumours; notably osteoid osteoma, osteoblastoma, chondroblastoma (Fig. 7.9b,c) and Langerhans cell histiocytosis (Davies et al. 1994; Beltran et al. 1993; Assoun et al. 1994; Kroon et al. 1994; Oxtoby and Davies 1996; James et al. 2006; James et al. 2008). Prominent marrow oedema is also a feature of non-neoplastic, and therefore also benign, conditions such as osteomyelitis, stress fractures, bone bruises, osteonecrosis and transient osteoporosis (Alyas et al. 2007). Clearly, the oedema may be extensive if a malignant bone tumour presents with a pathological fracture.

Fluid-fluid levels may occur due to the separation of blood products or occasionally tumour necrosis with sedimentation of cells within cystic lesions (Alyas et al. 2007). The sign, first described in ABCs (see Fig. 7.19c; Hudson et al. 1985), is now recognised to occur in many bony lesions as diverse as telangiectatic osteosarcoma, brown tumour of hyperparathyroidism, intraosseous ganglion and adamantinoma (Davies et al. 2001). While fluid-fluid levels are considered non-specific (Tsai et al. 1995; Van Dyck et al. 2006), the commonest cause in a child is an ABC (Davies and Cassar-Pullicino 1992) and lesions comprising greater than two-thirds fluid-fluid levels are more likely to be a primary or secondary ABC than a malignancy (O'Donnell and Saifuddin 2004).

Most bone lesions containing hyperintense fat signal on T1-weighted MR images are benign and include intraosseous lipoma (Campbell et al. 2003), haemangioma and non-tumorous conditions such as medullary infarction (Beltran et al. 1988) and uncomplicated Paget's disease (Sundaram et al. 2001). A recent study has shown that identification of fat signal within an untreated bone tumour is rare in bone malignancy with the possible exception of lymphoma (Simpfendorfer et al. 2008).

Well-differentiated cartilaginous tumours typically show a lobulated configuration, low signal intensity on T1-weighted images and high signal on T2-weighted STIR sequences (Woertler et al. 2003). As with other cross-sectional imaging techniques, MR imaging can be used to measure the thickness of the cartilage cap of peripheral lesions. Irrespective of the imaging technique employed, a cap thickness of <2 cm when measured perpendicular to the osteochondroma is likely to be benign. A cap thickness >2 cm is associated with an increased likelihood of malignancy (Woertler et al. 2000). The distinction of an enchondroma from a low-grade central chondrosarcoma remains more controversial. Static contrast-enhanced MR imaging is of little value as it will show peripheral and septal enhancement in both. One study has shown more rapid enhancement in chondrosarcoma than enchondroma using dynamic contrast-enhanced MR imaging (Geirnaerdt et al. 2000). This is, however, one of those diagnoses that the

pathologists find equally challenging (Sliced Study Group 2007), which begs the question as to what is the gold standard when evaluating the accuracy of this particular imaging technique?

7.4 Conclusion

In their heart of hearts most busy radiologists will admit to having failed to detect a subtle (or not always so subtle) bone metastasis at some point in their career. Although such an occurrence is unfortunate, it is unlikely to have fundamentally altered the long-term prognosis for that particular patient. The same cannot be said for primary sarcomas of bone that can present with equally deceptive appearances on radiographs. In the modern era, with chemotherapy and limb-salvage surgery, the 5-year survival rate for most patients presenting with a primary high-grade sarcoma of bone in the absence of metastases ranges from 55 to 75%. Delays in diagnosis either due to failure to detect or correctly diagnose the sarcoma may lead to more mutilating surgery being required to achieve a cure (i.e. amputation of a limb rather than limb salvage surgery) or, with the development of metastases, a 5-year survival rate of 10% or less. The impact of delayed detection and diagnosis on the patient is clear, and it can have major medico-legal implications for the radiologist at fault. The radiograph remains preeminent in the detection and initial diagnosis of bone tumours. The importance of the multidisciplinary approach to the diagnosis and subsequent management of bone sarcomas cannot be overemphasised.

References

Algra PR, Heimans JJ, Valk J, Nauta JJ, Lachniet M, Kooten van B (1991) Do metastases in vertebra begin in the body or the pedicles? Am J Roentgenol 158:1275–1279

Alyas F, James SL, Davies AM, Saifuddin A (2007) The role of MR imaging in the diagnostic characterization of appendicular bone tumours and tumour-like conditions. Eur Radiol 17:2675–2686

Ardran GM (1951) Bone destruction not demonstrable by radiography. Br J Radiol 24:107–109

Assoun J, Richardi G, Railhac JJ (1994) Osteoid osteoma: MR imaging versus CT. Radiology 191:217–223

Beltran J, Herman LJ, Burk JM et al. (1988) Femoral head avascular necrosis: MR imaging with clinical–pathologic and radionuclide correlation. Radiology 166:215–220

Beltran J, Aarisi F, Bonmati LM, Rosenberg ZS et al. (1993) Eosinophilic granuloma: MRI manifestations. Skeletal Radiol 22:157–161

Bloem JL, Kroon HM (1993) Imaging of bone and soft tissue tumors: osseous lesions. Radiol Clin N Am 31:261–278

Braak BPM ter, Vincken PWJ, van Erkel et al. (2007) Are radiographs needed when MR imaging is performed for non-acute knee symptoms in patients younger than 45 years of age? Skeletal Radiol 36:1129–1139

Brailsford JF (1946) Evaluation of the negative radiological report. The Practioner 157:200–205

Brailsford JF (1949) The diagnosis of bone tumours. Lancet 26:973–981

Brown KT, Kattapuram SV, Rosenthal DI (1986) Computed tomography analysis of bone tumors: patterns of cortical destruction and soft tissue extension. Skeletal Radiol 15:448–451

Campbell RSD, Grainger AJ, Mangham DC, Beggs I, Teh J, Davies AM (2003) Intraosseous lipoma: a report of 35 new cases and a review of the literature. Skeletal Radiol 32:209–222

Choi JA, Lee KH, Jun WS et al. (2003) Osseous metastasis from renal carcinoma: "flow-void" sign at MR imaging. Radiology 228:629–634

Codman EA (1926) Registry of bone sarcoma. Surg Gynecol Obstet 42:381–393

Davies AM, Cassar-Pullicino VN (1992) The incidence and significance of fluid-fluid levels on computed tomography of osseous lesions. Br J Radiol 65:193–198

Davies AM, Pikoulas C, Griffiths J (1994) MRI of eosinophilic granuloma. Eur J Radiol 18:205–209

Davies AM, Evans N, Mangham DC, Grimer RJ (2001) MR imaging of brown tumors with fluid-fluid levels: a report of three cases. Eur Radiol 11:1445–1449

DeSantos LA, Edeiken BS (1985) Subtle early osteosarcoma. Skeletal Radiol 13:44–48

Doyle C (1890) The sign of four. Lippincott's Magazine, February, London

Edeiken J (1981) Roentgen diagnosis of diseases of bone. Williams and Wilkins, Baltimore, pp 8–32

Edelstyn GA, Gillespie PJ, Grebbel FS (1967) The radiological demonstration of osseous metastases: experimental observations. Clin Radiol 18:158–162

Folpe AL, Lyes RH, Sprouse JT et al. (2000) F-18 fluorodeoxyglucose positron emission tomography as a predictor of pathologic grade and other prognostic variables in bone and soft tissue sarcoma. Clin Cancer Res 6:1279–1287

Geirnaerdt MJA, Hogendoorn PCW, Bloem JL et al. (2000) Cartilaginous tumors: fast contrast-enhanced MR imaging. Radiology 214:539–546

Go RT, El Khoury GY, Wehbe MA (1980) Radionuclide bone image in growing and stable bone islands. Skeletal Radiol 5:15–18

Grimer RJ, Sneath RS (1990) Diagnosing malignant bone tumors: editorial. J Bone Joint Surg Br 72:754–756

Hall FM, Goldberg RP, Davies JA et al. (1980) Scintigraphic assessment of bone islands. Radiology 135:737–742

Hudson TM, Hamlin DJ, Fitzsimmons JR (1985) Magnetic resonance imaging of fluid levels in an aneurysmal bone cyst and in anticoagulated human blood. Skeletal Radiol 3:267–270

James SLJ, Hughes RJ, Ali KE, Saifuddin A (2006) MRI of bone marrow oedema associated with focal bone lesions. Clin Radiol 61:1003–1009

James SLJ, Panicek DM, Davies AM (2008) Bone marrow oedema associated with benign and malignant bone tumours. Eur J Radiol 67:11–21

Kenan S, Abdelwahab IF, Klein MJ, Herman G, Lewis MM (1993) Lesions of juxtacortical origin (surface lesions of bone). Skeletal Radiol 22:337–357

Kenney PJ, Gilula LA, Murphy WA (1981) The use of computed tomography to distinguish osteochondroma and chondrosarcoma. Radiology 139:129–137

Kricun ME (1983) Radiographic evaluation of solitary bone lesions. Orthop Clin North Am 14:39–64

Kricun ME (1993) Imaging of bone tumors. Saunders, Philadelphia, pp 2–45

Kroon HM, Bloem JL, Holscher HC et al. (1994) MR imaging of edema accompanying benign and malignant bone tumors. Skeletal Radiol 23:261–269

Leung JC, Dalinka MK (2000) Magnetic resonance imaging in primary bone tumors. Semin Roentgenol 35:297–305

Levine E, De Smet AA, Neff JR et al. (1984) Scintigraphic evaluation of giant cell tumor of bone. AJR 143:343–348

Levy JC, Temple HT, Mollabashy A, Sanders J, Kransdorf M (2005) The causes of pain in benign solitary enchondromas of the proximal humerus. Clin Orthop Relat Res 431:181–186

Lodwick GS (1965a) A probabilistic approach to the diagnosis of bone tumors. Radiol Clin North Am 3:487–497

Lodwick GS (1965b) A systematic approach to the Roentgen diagnosis of bone tumors. In: Tumors of bone and soft tissue: a collection of papers presented at the 8th Annual Clinical Conference on Cancer 1963. Year-Book Medical Publishers, Chicago, pp 49–68

Lodwick GS (1966) Solitary malignant tumors of bone: the application of predictor variables in diagnosis. Semin Roentgenol 1:293–313

Lodwick GS, Wilson AJ, Farrell C, Virtama P, Dittrich F (1980a) Determining growth rates of focal lesions of bone from radiographs. Radiology 134:577–583

Lodwick GS, Wilson AJ, Farrell C, Virtama P, Dittrich F (1980b) Estimating rate of growth in bone lesions: observer performance and error. Radiology 134:585–590

Madewell JE, Ragsdale BD, Sweet DE (1981) Radiologic and pathologic analysis of solitary bone lesions. Part I: Internal margins. Radiol Clin North Am 19:715–748

Magid D (1993) Two-dimensional and three-dimensional computed tomographic imaging in musculoskeletal tumors. Radiol Clin N Am 31:425–447

Miller TT (2008) Bone tumors and tumor-like conditions: analysis with conventional radiography. Radiology 246:662–674

Moreno A, Clemente J, Crespo C (1999) Pelvic insufficiency fractures in patients with pelvic irradiation. In J Radiat Oncol Biol Phys 44:61–66

Moser RP, Madewell JE (1987) An approach to primary bone tumors. Radiol Clin North Am 25:1049–1093

Müller C, Huber W, Imhof H, Kainberger F (2005) Detektion von primär malignen intermediären Knochentumoren:Wertigkeit der Projektionsradiographie. Fortschr Röntgenstr 177:210–216

Mumber MP, Greven KM, Haygood TM (1997) Pelvic insufficiency fractures associated with radiation atrophy: clinical recognition and diagnostic evaluation. Skeletal Radiol 26:94–99

Muscolo DL, Ayerza MA, Mokino A, Costa-Paz M, Aponte-Tinao LA (2003) Tumors about the knee misdiagnosed as athletic injuries. J Bone Joint Surg (Am) 85:1209–1214

O'Donnell P, Saifuddin A (2004) The prevalence and diagnostic significance of fluid-fluid levels in focal lesions of bone. Skeletal Radiol 33:330–336

Oxtoby JW, Davies AM (1996) MRI characteristics of chondroblastoma. Clin Radiol 5:22–26

Priolo F, Cerase A (1998) the current role of radiography in the assessment of skeletal tumors and tumor-like lesions. Eur J Radiol 27(Suppl 1):S77–S85

Ragsdale BD, Madewell JE, Sweet DE (1981) Radiologic and pathologic analysis of solitary bone lesions. Part II. Periosteal reaction. Radiol Clin North Am 19:749–783

Rapezzi C, Ferrar R, Branzi A (2005) White coats fingerprints: diagnostic reasoning in medicine and investigative methods of fictional detectives. Br Med J 331:1491–1494

Rechl H, Hof N, Gerdesmeier L (2001) Differential diagnosis of bone and soft tissue tumors by MRI. Orthopade 30:528–539

Ries T (1983) Detection of osteoporotic sacral fractures with radionuclides. Radiology 146:783–785

Rosenberg ZS, Lev S, Schmahmann S, Steiner GC, Beltran J, Present D (1995) Osteosarcoma: subtle, rare, and misleading plain film features. AJR 165:1209–1214

Ryan PJ, Fogelman I (1997) Bone scintigraphy in metabolic bone disease. Semin Nucl Med 17:291–305

Seeger LL, Yao L, Eckardt JJ (1998) Surface lesions of bone. Radiology 206:17–33

Simpfendorfer CS, Ilaslan H, Davies AM, James SL, Obuchowski N, Sundaram M (2008) Does the presence of focal normal marrow fat signal within a tumor on MRI exclude malignancy? An analysis of 184 histologically proven tumors of the pelvis and appendicular skeleton. Skeletal Radiol 37:797–804

Skeletal Lesions Interobserver Correlation Amongst Expert Diagnosticians (SLICED) Study Group (2007) Reliability of histopathologic and radiologic grading of cartilaginous neoplasms in long bones. J Bone Joint Surg (Am) 89:2113–2123

Strobel K, Hany TF, Exner GU (2006) PET/CT of a Brodie abscess. Clin Nucl Med 31:210

Strobel K, Bode B, Lardinois D, Exner U (2007) PET positive fibrous dysplasia: a potentially misleading incidental finding in a patient with intimal sarcoma of the pulmonary artery. Skeletal Radiol 36(Suppl):S24–S28

Sundaram M, Khanna G, El-Khoury GY (2001) T1-weighted MR imaging for distinguishing large osteolysis of Paget's disease from sarcomatous degeneration. Skeletal Radiol 30:378–383

Sweet DE, Madewell JE, Ragsdale BD (1981) Radiologic and pathologic analysis of solitary bone lesions. Part III. Matrix patterns. Radiol Clin North Am 19:785–814

Teele RL, Griscom NT (1998) Letter: Aunt Minnie. Radiology 208:829–830

Tsai JC, Dalinka MK, Fallon MD et al. (1995) Fluid-fluid level: a non-specific finding in tumors of bone and soft tissue. Radiology 175:779–782

Van der Linden YM, Dijkstra PDS, Kroon HM, Lok JJ, Noordijk EM, Leer JWH, Marijnen CAM (2004) Comparative analysis of risk factors for pathological fracture with femoral metastases. J Bone Joint Surg (Br) 86B:566–573

Van Dyck P, Vanhoenacker FM, Vogel J et al. (2006) Prevalence, extension and characteristics of fluid-fluid levels in bone and soft tissue tumors. Eur Radiol 16:2644–2651

Walden MJ, Murphey MD, Vidal JA (2008) Incidental enchondromas of the knee. AJR 190:1611–1615

Watanabe N, Inaoka T, Shuke N et al. (2007) Acute rhabdomyolysis of the soleus muscle induced by a lightning strike: magnetic resonance and scintigraphic findings. Skeletal Radiol 36:671–675

Wellman HN, Schauwecker D, Robb JA et al. (1977) Skeletal scintimaging and radiography in the diagnosis and management of Paget's disease. Clin Orthop Relat Res 127:55–62

Woertler K (2003) Benign bone tumors and tumor-like lesions: value of cross-sectional imaging. Eur Radiol 13:1820–1835

Woertler K, Lindner N, Gosher G, Brinkschmidt C, Heindel W (2000) Osteochondroma: MR imaging of tumor-related complications. Eur Radiol 10:832–884

Wurtz LD, Peabody TD, Simon MA (1999) Delay in the diagnosis and treatment of primary sarcoma of the pelvis. J Bone Joint Surg (Am) 81A:317–325

Biopsy

8

Apoorva Gogna, Wilfred C. G. Peh and Peter L. Munk

CONTENTS

KEY POINTS

- Biopsy of bone lesions should be performed as a final diagnostic step, after completion of appropriate imaging and non-imaging workup.
- Do not rush into a poorly planned biopsy. Prior imaging should guide the technique and approach.
- Certain "do-not-touch" lesions should not be biopsied in order to avoid an unnecessary invasive procedure, or worse, over-diagnosis resulting in harmful over-treatment.
- For primary tumors, biopsy at the same center as the definitive treatment is advisable. Close collaboration between the radiologist, orthopedic oncologist, and pathologist is vital to reducing diagnostic errors and complications. The biopsy approach should be carefully planned according to oncological principles to prevent local recurrence.
- Biopsy methods can be broadly divided into open surgical biopsy and percutaneous methods which include fine-needle aspiration cytology (FNAC) and core-needle biopsy (CNB). When a CNB of bone is obtained, the term "trephine" is applied.
- Percutaneous biopsy is often guided by imaging, which allows access to deeper lesions, avoidance of vital structures, and selective targeting in order to sample those areas of the lesions most likely to yield a true diagnosis.

A. Gogna, MBBS, FRCR
Department of Diagnostic Radiology, Singapore General Hospital, Outran Road, Singapore 169608, Republic of Singapore

W.C.G. Peh, MBBS, MHSM, MD, FRCPE, FRCPG, FRCR
Department of Diagnostic Radiology, Alexandra Hospital, 378 Alexandra Road, Singapore 159964, Republic of Singapore; Clinical Professor, National University Hospital, 5 Lower Kent Ridge Road, Singapore 119074, Republic of Singapore

P. L. Munk, MD, CM, FRCPC
Musculoskeletal Division, Department of Radiology, Vancouver General Hospital and Health Sciences Centre, University of British Columbia, 855 West 12th Avenue, Vancouver BC V5Z 1M9, Canada

8.1 Introduction

Half a century ago, Henry L. Jaffe stated that a biopsy should be regarded as a final diagnostic procedure, not a shortcut to diagnosis (Jaffe 1958). The advice is still relevant today, and with the current advances in imaging technology there is increasing confidence that a diagnosis can often be made on imaging findings. Biopsy continues to play a central role in the management of lesions of the musculoskeletal system, especially bone tumors, for which histological type and grade influence management protocols. It is important that logical steps be followed to ensure appropriate selection of patients in order to optimize the risk–benefit ratio of this invasive procedure. While sampling of bone and marrow for analysis has been recognized for millennia (Parapia 2007), and has been performed as an open procedure for centuries, percutaneous biopsy is a relatively recent development (Coley et al. 1931; Martin and Ellis 1930), led by innovations in imaging guidance and interventional hardware (Lalli 1970).

This chapter reviews the issues related to image-guided percutaneous bone biopsy and is targeted at radiologists in practice and in training. Table 8.1 shows a checklist for performing a successful biopsy.

8.2 Planning of Biopsy

The interventionist must ensure that a biopsy is definitely indicated, after an adequate non-invasive investigative approach. The presence of a lesion in bone does not immediately imply the need for histology. Clinical information, laboratory findings, and imaging features may be sufficient to provide high diagnostic confidence for certain lesions, allowing for a therapeutic trial (Parsons et al. 2007). In addition, certain clearly benign lesions ("do not touch lesions") should not require biopsy purely for academic satisfaction. Worse, these lesions can appear histologically worrying (Choi et al. 2004), raising the potential for over-aggressive management. A wide range of benign bone lesions have been described in the literature and familiarity with these may help obviate an unnecessary biopsy (Chew et al. 2003; Greenspan 1993, 1995; Lambiase et al. 1998; Unni and Dahlin 1996). Conversely, bone tumors often present with

Table 8.1. Checklist for biopsy

Why do I need to perform this biopsy? Review indications and contraindications
Has all necessary imaging been performed? Complete all imaging prior to biopsy, especially for suspected sarcomas
Is this a primary sarcoma and is limb-sparing surgery indicated?
Which biopsy is most appropriate, percutaneous or open?
Which is the most appropriate imaging guidance modality?
Schedule a pre-procedure visit
Obtain informed consent
Perform sedation assessment
Review/obtain coagulation profile, i.e., INR, PTT, hemoglobin and platelet count
Patient preparation: instructions on fasting, medication adjustment, admission to ward
Select appropriate biopsy equipment
Request appropriate pathology support, e.g., onsite cytotechnician
Choose appropriate biopsy route
Note appropriate handling of specimen
Post-procedure instructions and follow-up; ensure patient is escorted home
Management of complications and inadequate biopsy

Table 8.2. "Red flags" for aggressive bone tumors

New lesions, not seen on previous imaging
Enlarging lesions; however, benign lesions do enlarge slowly but the radiologist should be satisfied that any change in size is appropriate for the given time period
Rapid growth should be viewed with suspicion
Symptomatic lesions; note that benign lesions can also be symptomatic, e.g., pathological fracture of a simple bone cyst
Known primary tumor elsewhere – could this be a metastasis?
Invasion of adjacent tissue compartment
Permeative or moth-eaten pattern of involvement
Bone lesions with soft tissue components
Aggressive periosteal reactions

non-specific imaging characteristics, and a high index of suspicion should be maintained for "red flags" (Table 8.2).

When a biopsy is indicated, the first step is to decide whether the lesion could be a primary sarcoma, and whether curative limb-sparing surgical resection is an option. This is because biopsy of primary bone sarcomas entails additional precautions to prevent track seeding. For metastatic lesions, the biopsy can be planned according to the safest and easiest route. Orthopedic oncology surgery principles require en-bloc resection of the biopsy track during definitive surgery (Liu et al. 2007; Mankin et al. 1982, 1996). A multi-disciplinary approach to patient management has been advocated by numerous authors for primary bone tumors, where limb conservation is an option. This ideally includes an orthopedic oncology surgeon, musculoskeletal radiologist, bone pathologist, oncologist, and radiotherapist.

Mankin et al. (1982) studied results of open biopsy in 329 patients with primary malignant musculoskeletal sarcomas and reported an overall 18.2% major diagnostic error rate and a 10.3% inadequate biopsy rate. Moreover, unnecessary amputation occurred in 4.5% and prognosis considered adversely affected in 8.5% of cases. The results were unchanged when the study was repeated more than a decade later (Mankin et al. 1996). The adverse results were 2–12 times greater for biopsies performed in referral centers, compared with definitive treatment centers, highlighting the hazards of an improperly conducted open biopsy and the need for management of primary musculoskeletal tumors by appropriately trained staff.

8.2.1 Indications and Contraindications

Table 8.3 outlines the indications and contraindications for bone biopsies. The most common indications are suspected tumors, infections, and investigation of unknown lesions (Gogna et al. 2008; Peh 1999). Histological identification of primary tumors is required to facilitate subsequent surgical planning, chemotherapy, and radiotherapy regimes. While not always necessary, pretreatment biopsy is considered mandatory when the lesion appears to involve a critical structure or when neoadjuvant chemotherapy is considered (Hueman et al. 2008), in order to justify the risk of treatment. Often, biopsy may be the only method of exclusion of sinister solitary bone lesions in the absence of classic benign features, especially when the history is suggestive (Fig. 8.1; Greenspan 1993). Suspected metastatic bone lesions may be biopsied in an attempt to identify the primary tumor, particularly as tumor markers are generally unhelpful in identifying an unknown primary lesion, with the exception of prostate-specific antigen (Altuntas et al. 2005; Dupuy et al. 1998; Hau et al. 2002).

Early stages of spondylodiscitis may be difficult to differentiate from degenerative Modic 1 endplate changes, inflammatory lesions, e.g., seronegative spondyloarthropathy, amyloidosis, or crystal deposition disease (Altuntas et al. 2005; Hau et al. 2002) on magnetic resonance (MR) imaging, and scintigraphy (Turpin and Lambert 2001). While biopsy was often necessary to distinguish pathological and osteoporotic vertebral compression fractures in the past, the distinction can often now be made with imaging, reducing the

Table 8.3. Indications and contraindications for percutaneous bone biopsy

Indications	Contraindications (relative)
Determine the nature of a bone lesion with non-specific imaging findings	Uncorrected bleeding diathesis, e.g., decreased platelet count, increased prothrombin time
Suspected metastasis in the presence of a primary tumor, usually when the imaging features of the lesions are not typical of metastasis	No safe available access path, e.g., infected soft tissues surrounding a non-infective lesion, intervening structures, e.g., large bowel
Suspected bone metastases of an unknown primary; biopsy of a bone lesion may identify the primary tumor	Inaccessible sites, e.g., C1 vertebral body, odontoid process
Determine the etiology of a suspected pathological fracture	Suspected vascular lesion, e.g., hemangioma in a site where hematoma formation may be hazardous, e.g., cervical/thoracic spine where cord compression could occur
Evaluate recurrence at a tumor resection margin	Uncooperative patients: the risk/benefit ratio of an open vs percutaneous biopsy should be re-evaluated, as general anesthesia may be required anyway
Differentiate infection, metabolic bone disease, and other bone lesions from tumor	Pregnancy: precludes use of ionizing radiation for image guidance

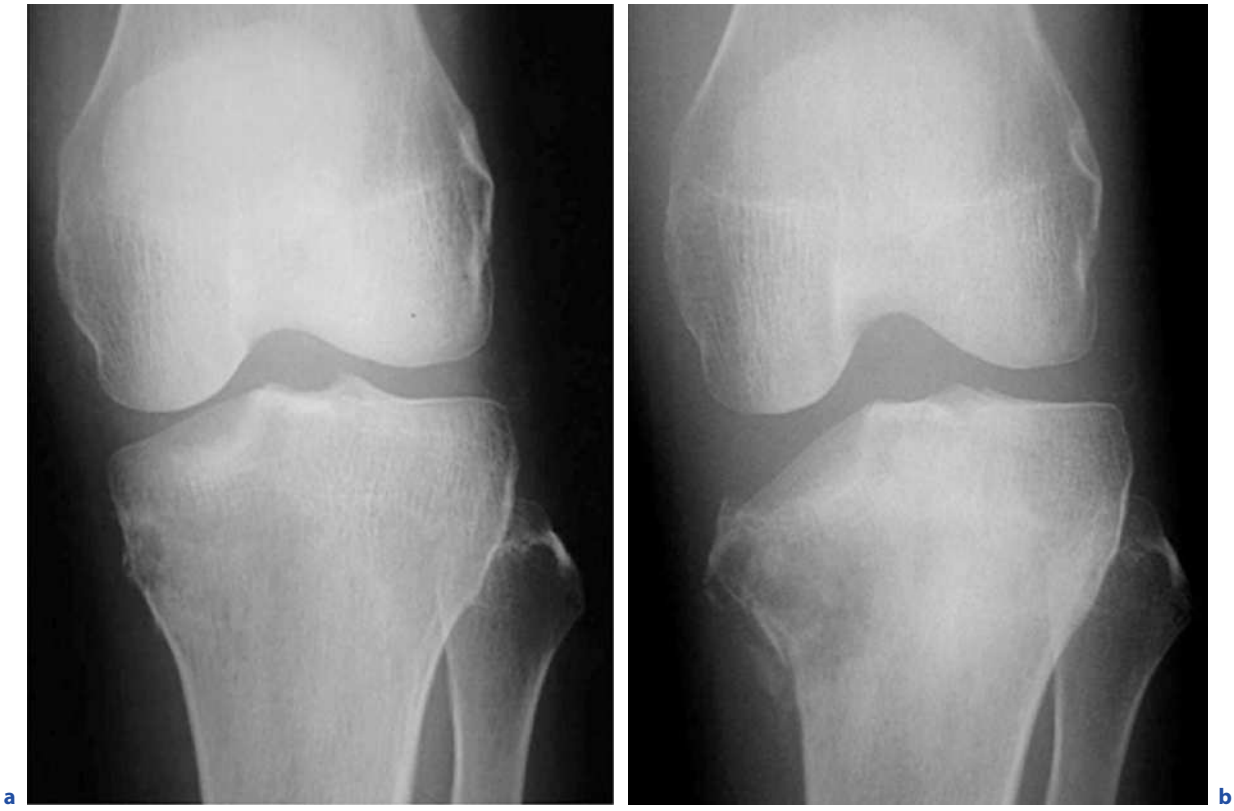

a b

Fig. 8.1a–c. Patient with renal osteodystrophy who presented with a pathological fracture of the proximal tibia. **a** Initial frontal radiograph shows a small osteolytic lesion in the medial proximal shaft, with a small cortical break. **b** Follow-up radiograph shows enlargement of an aggressive-appearing osteolytic lesion, with pathological fracture fragments and progressive collapse. **c** *see next page*

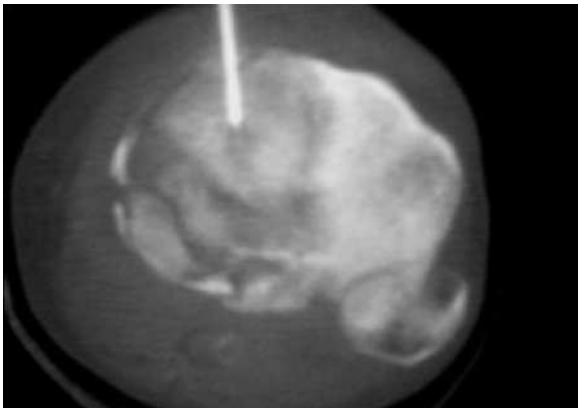

c

Fig. 8.1a–c. (*continued*) **c** CT-guided biopsy was performed to exclude malignancy. Final diagnosis was insufficiency fracture secondary to renal osteodystrophy

proportion of cases referred for this indication (Vieillard et al. 2005).

Several precautions are essential to prevent harm. For example, C1 and odontoid biopsy often requires the trans-oral route and general anesthesia. Alternative biopsy sites should probably be chosen if available, and if not, referral to an ENT surgeon for trans-oral biopsy should be considered. Severe coagulopathy or thrombocytopenia should be corrected prior to the procedure. For certain cases, a hematological consult may be required to deal with coagulopathies that the interventionist may not have experience in correcting.

Biopsy may sometimes be required to distinguish a tumor from an infective focus; however, it should be noted that the culture positivity rate of biopsy for osteomyelitis may be low, ranging from 34 to 60% in several studies (Altuntas et al. 2005; Ayala et al. 1995; Bennert and Abdul-Karim 1994; Dupuy et al. 1998; Hau et al. 2002; Schweitzer et al. 1995; Wu et al. 2007), although higher rates of up to 90% have been reported for spinal infections (Chew and Kline 2001). Biopsy of suspected bone tumors adjacent to a known infective focus is contraindicated, as it may result in iatrogenic infection of the target lesion, e.g., bone biopsy through infected skin or subcutaneous tissue.

8.2.2 Lesion Selection and Biopsy Method

8.2.2.1 Lesion Selection

For multiple lesions, the largest and most superficial lesion is often the most ideal one for biopsy; however, the integrity of the underlying bone should be considered. The biopsy should preferably be done in a non-weight-bearing portion of bone to prevent iatrogenic fracture. Also, the location of the adjacent structures must be considered. An iliac biopsy may thus be safer than thoracic vertebral biopsy for multiple bone metastases from an unknown primary. If possible, choose lesions that are more likely to have viable tissue, i.e., which are solid rather than cystic, show contrast enhancement, or have areas of color flow on Doppler ultrasonography (US). These imaging techniques also show adjacent vascular structures, which should obviously be avoided during biopsy. Clearly necrotic and cystic areas of the lesion have a far lower diagnostic yield (Jelinek et al. 2002), compared with solid lesions.

8.2.2.2 Biopsy Method

While open surgical biopsy has long been the mainstay of diagnosis, percutaneous biopsy has all but replaced primary open biopsy in recent years (Lopez et al. 2005; Mitsuyoshi et al. 2006; Yamamoto et al. 2003) for patients of all ages (Shin et al. 2007). Open biopsy remains a "fall-back" option for cases which are non-diagnostic on initial percutaneous attempts.

Table 8.4 summarizes the strengths of percutaneous and open methods of biopsy. The major limitation of percutaneous biopsy has always been the relatively lower accuracy compared with open biopsy, which is considered the gold standard. Errors in diagnosis including non-diagnostic sample, misclassification of malignant tumors as benign (false negative), benign tumors as positive (false positive), and inaccurate staging and grading of tumors have all been highlighted (Bommer et al. 1997; El-Khoury et al. 1983; Fraser-Hill and Renfrew 1992; Logan et al. 1996; Wu et al. 2007).

Many studies report high accuracy in classifying lesions as benign or malignant but lower accuracy in specifying exact pathology and grade. For example, in

Table 8.4. Percutaneous vs open biopsy methods

Percutaneous biopsy	Open biopsy
Less trauma to surrounding structures	Larger tissue size allowing ancillary studies, e.g., immunohistochemistry, cytogenetics, molecular genetics, flow cytometry, and electron microscopy
Faster wound healing, allowing faster initiation of neoadjuvant chemotherapy and radiotherapy which can begin the next day, compared with a delay of 10–21 days for open biopsy	Single-stage procedure, when combined with frozen-section histology, leading to definitive surgery
Lower risk of contamination of adjacent structures and of tumor dissemination; easier excision of biopsy track	Allows surgeon to view the tumor directly
Less disruption of structural integrity of cortical bone leading to lower likelihood of iatrogenic pathological fracture	Greater familiarity among orthopedic surgeons
Preoperative diagnosis allowing pre-treatment multidisciplinary discussion and patient counseling	"Gold standard diagnostic procedure": cases which are equivocal on percutaneous biopsy may be diagnosed on open biopsy; reported accuracy rate is up to 98%
Significantly lower cost (two to six times lower cost has been reported)	Avoidance of radiation exposure to staff and patient compared with fluoroscopic or CT-guided biopsy
Lower morbidity including faster post-procedural mobility, less pain at wound site, and faster healing of biopsy site	
Repeatability in case of negative biopsy	
Biopsy of areas most likely to yield diagnostic information (e.g., different quadrants, non-sclerotic areas, viable areas); areas of lesion showing enhancement or even higher grade may be identified	
Potentially able to biopsy surgically inaccessible sites or multiple lesions	
Potential for unrepresentative biopsy: higher-grade foci within a heterogeneous lesion may be missed, leading to diagnosis of a low-grade tumor or benign lesion	
Cystic tumors can be particularly difficult to diagnose accurately	

a study of 155 sarcoma patients, Welker et al. (2000) reported that needle biopsy was 92.4% accurate in differentiating benign from malignant, 88.6% accurate in providing exact grade, and 72.7% accurate in determining exact pathology.

The negative biopsy raises problems about further management. A repeat percutaneous biopsy attempt is reasonable if additional material will change patient management. Viellard et al. (2005) reported a 7% rebiopsy rate; however, they reported that when two biopsies fail to provide the diagnosis, additional attempts are likely to be unsuccessful. Low inherent diagnostic yield of bone lesions caused by hematological malignancies and highest diagnostic yield for metastatic lesions has been reported (Vieillard et al. 2005).

The choice of fine-needle aspiration cytology (FNAC) versus core biopsy for lesion type is still controversial. Koscick et al. (1998) advocated a combined approach of both FNAC and core biopsy in order to improve accuracy. In some specialized centers with adequate cytopathological support (Akerman 1997; Kilpatrick et al. 2001; Ward et al. 2001), FNAC of primary bone tumors may be performed with high diagnostic accuracy. The FNA has a lower risk of hemorrhage (e.g., in suspected hemangiomas or vascular metastases such as renal cell carcinoma), can traverse small

bowel safely when deemed necessary, and theoretically, has a lower risk of biopsy track seeding. With improved cytological techniques, ancillary tests can now be performed on FNAC specimens and collaboration with one's pathology department is important to establish appropriate biopsy protocols for the individual institution. The FNAC specimens can be applied to rapid staining and preliminary assessment techniques. For certain cases, FNA may even yield a micro cell-block, allowing assessment of tissue architecture; however, this is rarely obtained in tumors with a collagenous matrix (Domanski et al. 2005).

Generally, for metastatic tumors and infections, FNAC is often sufficient (Kattapuram and Rosenthal 1991) for diagnosis; however, core biopsy is still usually required for determining cell type and tumor grade (Espinosa et al. 2008). Crushing and insufficient sample sizes are major limitations of FNA, where one may be able to diagnose a malignancy, but the tumor morphology may not be definable (Yaffe et al. 2003). Also, the thin needles tend to bend during biopsy of deep lesions, are difficult to redirect without reinsertion, are unable to penetrate intact bone, and provide small specimens which may be under-representative of the whole lesion.

Core-needle biopsy (CNB) is more likely to provide micro-tissue blocks, which can be used for analysis of tissue architecture, and inter-cellular relationships, which are important for primary malignant tumors.

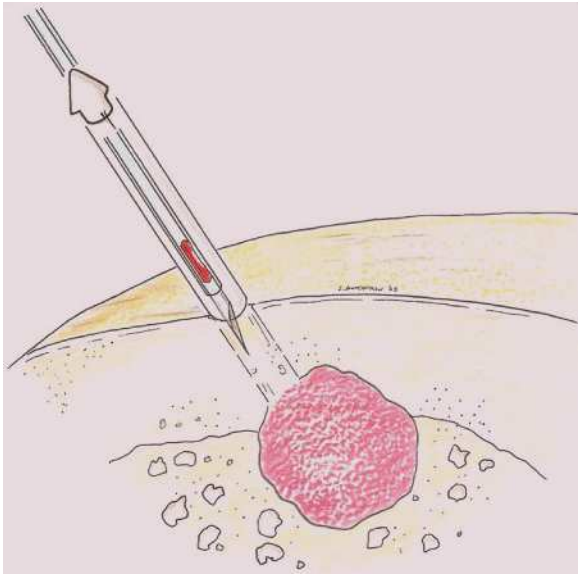

Fig. 8.2. Coaxial passage of a cutting needle through a trephine needle

CNB needles can be drilled into bone, allowing coaxial insertion of smaller core and fine needles. The coaxial technique also allows multiple passes through a single skin puncture (Fig. 8.2). The advantage of core specimens is greater tissue volume in general, allowing ancillary tests to be performed, e.g., staining for cytokeratin, epithelial membrane, CD, light chain and factor-VIII antibody markers (Domanski et al. 2005). The spindle cell tumors are reportedly difficult to diagnose by percutaneous biopsy due to sampling error in these mixed mesenchymal tumors, (Welker et al. 2000) and CNB is preferred over FNA alone. Lesions which are difficult to diagnose on CNB are usually also challenging on open biopsy.

Lesions which have been reportedly misdiagnosed on percutaneous biopsy include osteofibrous dysplasia, as it can be very difficult to distinguish from its main differentials of adamantinoma and monostotic fibrous dysplasia on a small biopsy specimen (Khuu et al. 1999), de-differentiated chondrosarcoma (Altuntas et al. 2005; Wu et al. 2007), hemangioendothelioma (Ward and Kilpatrick 2000), chondroblastoma of bone (Kilpatrick et al. 1997) and telangiectatic osteosarcoma, which may resemble giant cell tumor on percutaneous and intra-operative frozen-section biopsy (Jelinek et al. 2002).

The sampling methods are not mutually exclusive, and some authors have shown addition benefit from combination sampling protocols (Gibbon 1996; Schweitzer et al. 1996). Using a coaxial system allows multiple passes through a single skin/soft tissue track, and allows both CNB and FNA techniques to be used. In general, percutaneous biopsy is highly accurate and can be used for most cases; however, correlation with imaging findings is necessary, with performance of repeat biopsy or open surgical biopsy if the results of percutaneous biopsy do not match the clinical and imaging findings. The final choice of biopsy method is determined by available expertise and experience.

8.2.3 Imaging Guidance Method

The lesion should ideally be well visualized on the imaging modality to be used, and ideally, a formal assessment should have already been done with that same modality; however, information from several modalities may have to be combined in order to achieve optimum targeting, e.g., a metabolically active, non-necrotic and non-sclerotic portion of a large mixed tumor. The imaging modality should be safe and provides adequate visualization of relevant anatomy, in order to allow a safe

approach to the lesion. The radiation exposure, if any, should be justified, e.g., the higher radiation dose of computed tomography (CT) may be justified for complex bony anatomy but not for simple cases, especially in pediatric patients.

8.2.3.1 Fluoroscopy

Fluoroscopy is a time-honored, inexpensive, fast, and widely available technique that delivers a lower radiation dose compared with CT for the same imaging duration. Patient movement does not degrade image quality as severely as for CT or MR imaging (Ahrar et al. 2004). Unlike CT, there is no "streaking" caused by metallic implants which may impair visualization on other modalities. The X-ray beam can often be angulated and collimated to allow needle advancement under continuous fluoroscopy with much less radiation dose delivered to the operator and the patient, compared with CT; however, visualization of small intra-medullary lesions and the soft tissue component of bone tumors is suboptimal. Soft tissue structures in the biopsy path are poorly seen and depth perception is absent in the plane of imaging. For lesions close to vital structures and anatomical boundaries, cross-sectional image guidance is preferred. Complex-shaped bones, e.g., pelvis and vertebrae, may be difficult or hazardous to access on fluoroscopic guidance; hence, for selected lesions which are adequately visualized, relatively large and with no closely related or overlying important structures, fluoroscopy may be used to guide biopsy. This technique is most often used for large tumors located in long bones (Fig. 8.3).

8.2.3.2 Ultrasonography

Ultrasonography (US) offers high soft tissue resolution, allows real-time continuous imaging guidance, multiplanar visualization, flexible patient positioning and identification of blood flow, all with no exposure to ionizing radiation. Color Doppler US can be used to identify tumor neovascularity and the relationship of the tumor to the neurovascular bundle. Ultrasonography can be used for lesions on or near a bone surface, especially if there is an associated soft tissue component (Konermann et al. 2000; Saifuddin et al. 2000). Non-sclerotic portions of mixed sclerotic–lytic lesions can be

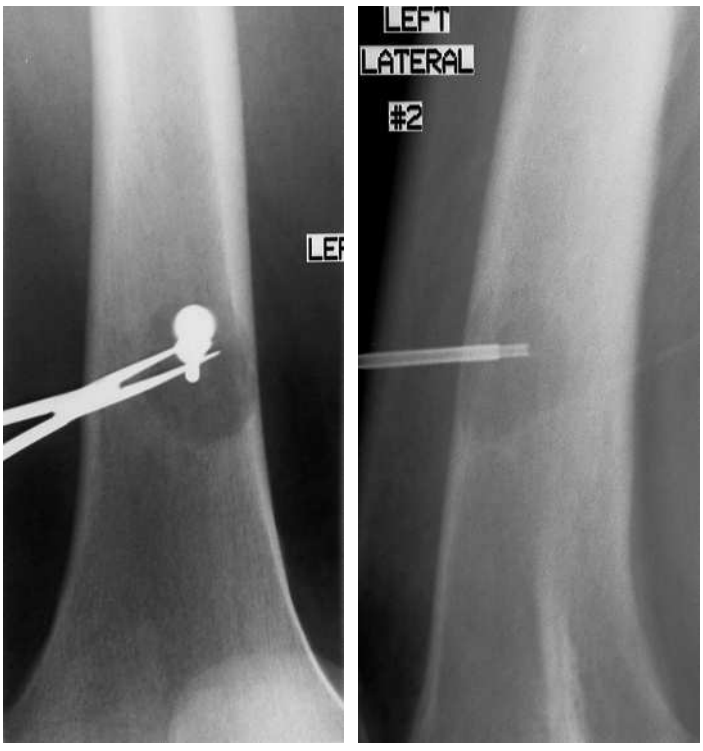

a,b

Fig. 8.3a,b. Fluoroscopic-guided biopsy of a long bone lesion. **a** Frontal and **b** lateral fluoroscopic images show direction of a trephine needle into the distal femoral osteolytic lesion

sampled, thus potentially providing higher yield. The CT- or fluoroscopy-directed procedures tend to oversample the sclerotic areas, which are more clearly seen on these modalities. Clearly cystic or necrotic areas and areas showing significant blood flow on Doppler imaging can be avoided, and solid areas are sampled instead. Nearby vascular structures can be identified on color Doppler imaging and thus be avoided (Gibbon 1996); however, US cannot be used for lesions that are completely encased by bone. Ultrasound-guided spinal biopsy has been described (Gupta et al. 1999); however, for thoracolumbar spinal biopsies, its use is limited to the posterior elements.

8.2.3.3 MR Imaging

Magnetic resonance imaging guidance is attractive for its lack of radiation and superior delineation of pathology that is often not visible using other modalities; however, equipment compatibility issues, patient positioning, cost and availability of MR imaging scan room time are all factors to consider. While several authors have reported excellent results with MR imaging-guided biopsy, its routine role in biopsy remains limited at present.

8.2.3.4 CT Fluoroscopy

Technical advances in high-speed array processors, partial reconstruction algorithms, slip-ring technology, and higher heat capacitance of X-ray tubes have allowed near real-time visualization of structures on CT (Ahlstrom and Astrom 1993), with images reconstructed up to 6 frames per second. The modality allows excellent visualization of lesions within bone, and of overlying soft tissues. A wide field of view demonstrates anatomical relations of adjacent and overlying structures. Accurate needle localization is possible due to high tissue resolution and depth perception, and with CT fluoroscopy and gantry tilt available on many newer machines, real-time needle-track visualization is also often available (Fig. 8.4).

Radiation dose is an important consideration. In contrast to fluoroscopy, where radiation doses are several centigrays per minute, in CT fluoroscopy the dose delivered is of the order of several centigrays per second. The CT fluoroscopy doses are small compared with conventional CT, however, and this can be further minimized by using short bursts of imaging. Paulson et al. (2001) assessed CT fluoroscopy doses to radiologists in various procedures using low milliampere (10 mA) settings and predominantly intermittent imaging. The majority of procedures used the "quick-check" method, where only a few consecutive slices are imaged at a time, and the needle is advanced after studying these images. For spine biopsy, radiation doses to whole body, ocular lens, and skin (measured outside the lead gown) were in the range of 0.66–2.8, 1.0–2.8, and 1.5–2.8 mrem, respectively, when the quick-check method was used (NB: occupational whole body limit = 5000 mrem, i.e., 50 mSv per year). The average fluoroscopy time was also considerably shorter, about one-fourth to one-seventh that reported by other authors, and average patient doses were 3.2 cGy per procedure.

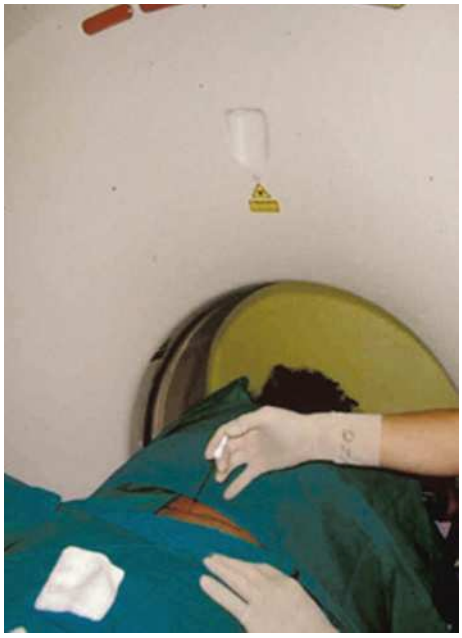

Fig. 8.4. A CT fluoroscopic unit taken during a thoracic spine biopsy using an Ostycut needle. The needle passage and direction into the spinal lesion can be done under near real-time imaging guidance

8.2.4 Biopsy Route Selection

As a general principle, the shortest path between skin and lesion that avoids structures such as the neurovascular bundles, pleura, solid organs, bowel, and joints is selected. The biopsy route is also influenced by the nature of the suspected lesion and imaging modality.

8.2.4.1 Axial Skeleton

For thoracolumbar spine biopsies, most lesions can be accessed posteriorly, with the patient in prone position. Approaches include transpedicular (most common), posterolateral (transcostovertebral), and transforaminodiscal. The transpedicular approach can be used if the posterior half of the vertebral body or if the pedicle is involved. Access through the pedicle limits risk of damage to the adjacent lung, soft tissue, and exiting nerve roots. Access for difficult-to-reach lesions can be improved by using curved needles. The size of the pedicle limits the size of the needle used (Fig. 8.5).

Zindrick et al. (1987) studied pedicle sizes from T1 to L5 levels in 2905 pedicles and found the widest pedicle (axial plane) to be at L5 level and the narrowest at T5 level (average 4.6 mm). The cranio-caudal width of the pedicle was reported to be the smallest at T1 level (9.9 mm); hence, while sufficient space is available above and below the needle, large-bore needles should be used with caution as they may traverse the medial border of the pedicle. We usually use the 14.5-G (2.1-mm outer diameter) Ostycut (Angiomed/Bard, Karlsruhe, Germany) trephine needle which gives a sufficient safety margin and also allows some room for needle angulation (Fig. 8.4).

The posterolateral approach can be used for lesions predominantly involving the disc space and for lesions in the lower aspect of the vertebral body (Fig. 8.6; Pierot and Boulin 1999; Yaffe et al. 2003). However, this approach can lead to pulmonary complications, e.g., pneumothorax and pneumonia, when used in the thoracic spine; hence, great caution is required and CT is preferable for guidance. Saline injection into the posterolateral soft tissues may be used to displace the pleura away from the needle path, but the injection may be painful. The transforaminodiscal approach has been described as an alternative to the posterolateral approach (Daly et al. 1999).

A lateral approach has also been described, to allow access to the vertebral body and the disc. The advantage of this approach is that the needle tip remains away from the nerve roots. For the lateral approach, the patient lies in a decubitus position, displacing the abdominal viscera anteriorly. This approach provides access to the vertebral body and disc, and avoids the nerve roots; however, it should not be used when there is insufficient

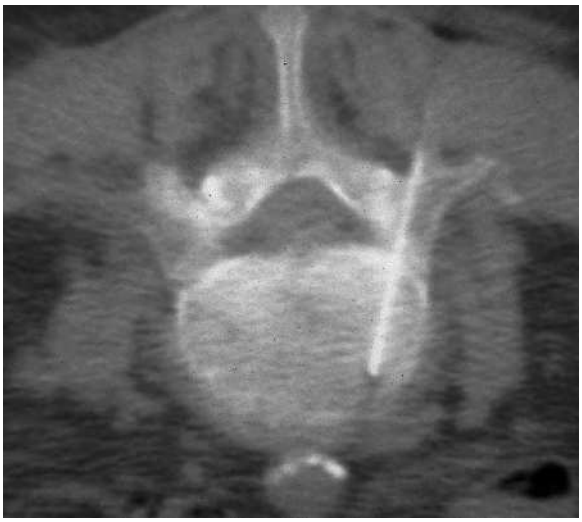

Fig. 8.5. A CT-guided biopsy of L4 vertebral body performed with the patient lying prone and using the transpedicular approach

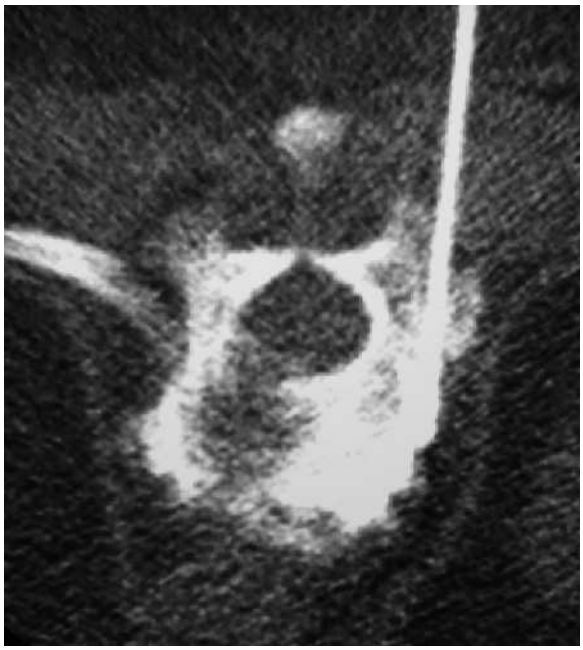

Fig. 8.6. A CT-guided biopsy of T12 vertebral body performed with the patient lying prone and using the transcostovertebral approach

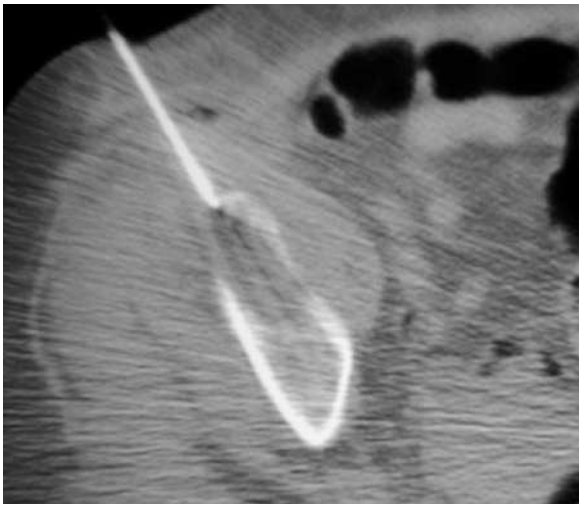

Fig. 8.7. A CT-guided biopsy of an osteolytic lesion in the anterior ilium performed with the patient lying supine

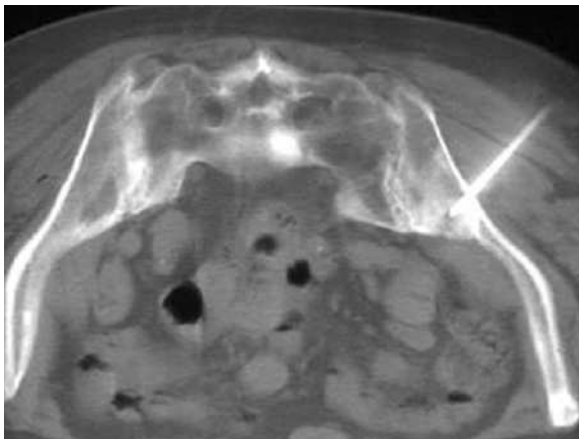

Fig. 8.8. A CT-guided biopsy of a sclerotic lesion in the posterior ilium performed with the patient lying prone

anterior displacement of the abdominal viscera. In the cervical spine, an anterolateral approach can be used for lesions in the vertebral body, while lesions in pedicles or posterior elements may be approached posteriorly (Daly et al. 1999). Iliac lesions can be accessed via an anterior or posterior approach (Figs. 8.7, 8.8; Espinosa et al. 2008). For primary bone lesions, the gluteal muscles and rectus femoris muscles should not be traversed, as far as possible.

8.2.4.2 Appendicular Skeleton

Special precautions apply for possible primary limb sarcomas due to the risk of needle track seeding. The en-bloc resection of the biopsy tract is required at time of definitive limb-conservation surgery (Hueman et al. 2008). Bone sarcoma recurrence along biopsy tracks of 16-G needles or larger has been reported (Davies et al. 1993; Schwartz and Spengler 1997), and the patient survival rate drops significantly after local recurrence (Weeden et al. 2001). Although the risk of tumor seeding with fine-needle biopsy using 22- to 25-G needles has been reported to be insignificant (Kilpatrick et al. 2001), for reasons discussed previously, primary sarcomas generally undergo core biopsy.

Limb-sparing surgery techniques aim to replace tumor-containing bone while preserving major neurovascular and myotendinous structures needed to maintain limb function. Uninvolved anatomical compartments of extremities, uninvolved muscles, and neurovascular bundles which may be used for reconstruction should therefore not be compromised.

For skeletally immature patients, the uninvolved physis should not be crossed, so as to allow the option of a physis-sparing resection (Espinosa et al. 2008); hence, careful planning of biopsy route in consultation with the operating team is recommended, and preferably, the biopsy should be performed in the same center as the planned definitive surgery. The puncture site should be marked, e.g., with an indelible marker or tattoo, to facilitate recognition intra-operatively.

Lesions in the proximal humerus should be approached through the anterior deltoid, rather than posteriorly, because the deltoid fibers are innervated from posterior to anterior; hence, resection of a posteriorly placed biopsy track may denervate the anterior muscle fibers, which then cannot be used for reconstruction. The deltopectoral groove should be avoided to prevent contamination of the pectoral muscle and the neurovascular bundle at this location.

As far as possible, thigh masses should not be accessed anteriorly through the rectus femoris. For lesions closely related to the femoral vessels, a medial approach may allow intra-operative exploration of the bundle; otherwise, a lateral approach is advised, as this avoids the neurovascular bundle and is more ergonomic

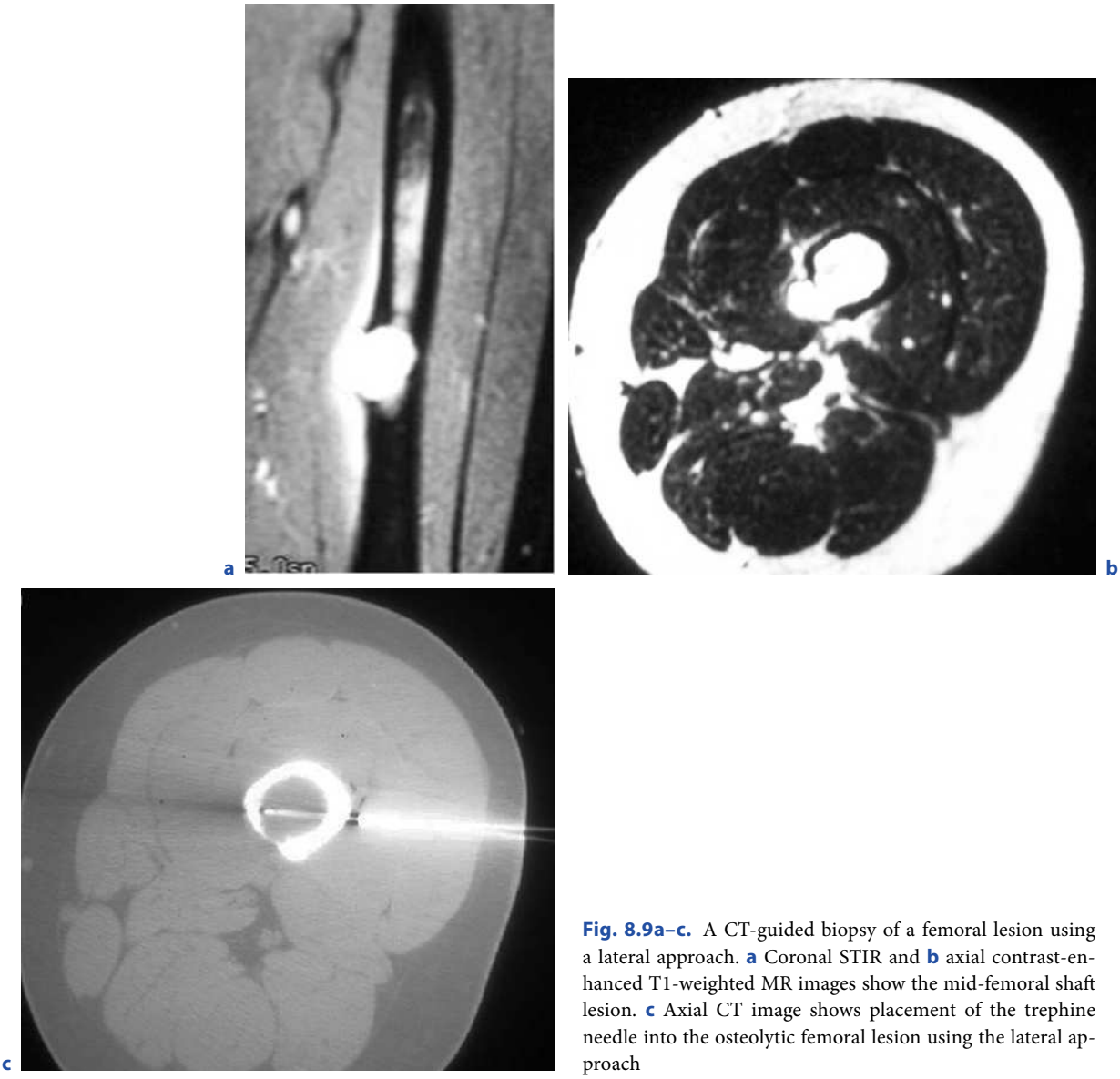

Fig. 8.9a–c. A CT-guided biopsy of a femoral lesion using a lateral approach. **a** Coronal STIR and **b** axial contrast-enhanced T1-weighted MR images show the mid-femoral shaft lesion. **c** Axial CT image shows placement of the trephine needle into the osteolytic femoral lesion using the lateral approach

(Fig. 8.9). Also, care should be taken not to accidentally traverse the supra-patellar recess of the knee joint and the greater trochanteric bursa, both of which are difficult to remove entirely during surgery (Espinosa et al. 2008).

Forearm and calf biopsies should not traverse the interosseous membrane, as this structure divides the flexor and extensor compartments. Ulnar lesions can be approached via the subcutaneous border of the ulna. If this is not possible, the extensor carpi ulnaris or flexor carpi ulnaris muscles can usually be traversed with the least morbidity. The anteromedial border of the tibia is subcutaneous and is hence the preferred route as this avoids both anterior and posterior compartments (Fig. 8.10).

Liu et al. (2007) described approaches based on lesion location in extremities, which may serve as a useful reference for the reader. Hand and foot biopsies are often complex, requiring very careful planning. The palm of the hand and sole of the foot should be avoided as these are highly pain sensitive. Rib lesions should be approached tangentially to prevent inadvertent pleural puncture.

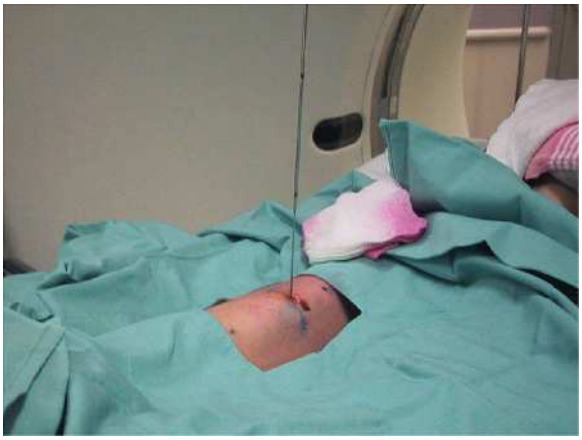

Fig. 8.10. Needle position for biopsy of an anterior tibial lesion using the anteromedial approach

8.2.5 Needle Characteristics and Types

The optimal needle type depends on the type of lesion to be biopsied, its location, and the operator preference. The chosen needle should be long enough to reach the lesion and provide an adequate core of tissue. Table 8.5 summarizes some available needles. The full range offered by manufacturers is far wider, and the ones included are some with which we have had experience.

Percutaneous biopsy can be divided into fine-needle aspiration (FNA), which uses needles of 20 G or smaller, generally providing samples for ultrastructural (cytological) analysis; and core-needle biopsy (CNB) – 18 G or larger, which generally allows sufficient tissue for histological analysis. The CNB can be further divided into soft tissue core biopsy, which is performed with cutting needles (e.g., Tru-Cut, Quick-core, Temmo), and trephine (e.g., Ostycut, Craig, Ackerman), which uses special cutting needles or drill-bit-type needles to traverse intact overlying cortical bone (Fig. 8.11). Air-powered drills or hammers may be needed in conjunction with trephine needles to aid controlled penetration of cortical bone (Fig. 8.12).

A coaxial system allows multiple passes though a single percutaneous puncture, minimizing collateral soft tissue damage, reducing the need for repeated needle localization and reducing procedure time (Fig. 8.13). The traditional sizing system for needles is based on the Stubs Iron wire gauge system, with gauge being inversely proportionate to the diameter. Each gauge increment roughly correlates to a 0.1-in. decrease, although not strictly linear. Inner and outer diameters are determined by the needle thickness, and vary slightly. This influences coaxial assembly when products of different manufacturers are combined, e.g., core- and fine-needle biopsy. The product literature should be reviewed prior to embarking on a coaxial biopsy using the available needles in one's own department. As a guide, corresponding inner- and outer-needle diameters are presented in Table 8.6.

An eccentric drill tip allows a channel to be drilled just wider than the external diameter of the cannula of the coaxial system, so that the cannula can be advanced into the bone window. When sampling sclerotic or calcified ("hard") lesions, a large-bore bone cutting needle of at least 15 G should be used. Larger-bore needles tend to show better targeting precision, cause less crushing artifact in hard bone, and can collect more tissue. Osteolytic lesions in bone may be sampled using a bone trephine needle or a soft tissue cutting needle; the latter is particularly useful if the bone lesion is perceived to be very "soft" from MR images and has overlying cortical destruction, and also for sampling of an associated extraosseous soft tissue component (Fig. 8.14). Needle sizes of 16–18 G are advised (Jelinek et al. 2002).

Yaffe et al. (2003) described a technique of cutting the hub of a 24-cm, 18-G spinal needle after delivering periosteal anesthetic, thus converting the needle into a guidewire. A 5.2-mm (6-G) sheath is then advanced over the "guidewire" and coaxial biopsies are obtained using 8-G Jamshidi needles. Generally three to five good cores should be obtained if the lesion is of sufficient size. Adequacy of sample is best guided by an on-site cytopathologist.

Table 8.5. Selected needle types. *FNA* fine-needle aspiration, *Soft* soft tissue core biopsy; *Bone* trephine needles to penetrate intact bone or hard lesions

Type	Name	Manufacturer	Size (G)	Comments
FNA	Chiba	Cook Medical (Bloomington, Ind.)	18–22	Inexpensive, high rigidity, high ultrasound visibility
FNA	Westcott type side-cutting	Becton-Dickenson (Franklin Lakes, N.J.)	20–22	Similar in design to Tru-Cut but smaller gauge
FNA	Tru-Guide	Bard (Covington, Ga.)	17	
Soft	Temno	Bauer Medical International (Santo Domingo, Dominican Republic)	8–11	Bevelled-point stylet advanced into lesion, before firing cutting outer cannula
Soft	Monopty	Medi-Tech (Boston Scientific Group, Nalick, Mass.)	16	Adjustable throw length, lightweight
Soft	BioPince	Ascendia AB (Sollentuna, Sweden)	18	Adjustable throw length, lightweight
Soft	Tru-Cut	Baxter Health Care Corp. (Deerfield, Ill.)	14	Side-cutting, outer-cutting cannula which slides over an inner-slotted needle, holding sample within the needle slot (prevents specimen loss)
Soft	Quick-core	Cook Medical (Bloomington, Ind.)	14–20	Lightweight; needle comes with a handle and spring-loaded trigger for one-handed operation. Bevelled stylet point; rapid-firing cutting cannula which closes over the slotted stylet to capture a core
Bone	Jamshidi needle	Kormed Co. (Minneapolis, Minn.)	8–11	
Bone	Ostycut needle	Angiomed/Bard (Karlsruhe, Germany)	14–17	Comprises a threaded cannula, inner-pointed stylet, and probe for dislodging specimen
Bone	Bonopty needle	RADI Medical Systems (Uppsala, Sweden)	14	Diamond tip provides better purchase on curved surface of long bones; eccentric drill tip 15-G needle accompanies the 14-G outer needle
Bone	SD-Allen	Special Devices Inc. (Grass Valley, Calif.)	11	A k-wire is placed toward the lesion through a tissue protector to guide the biopsy needle; "bit-design" of the needle captures a core during drilling and retains it during withdrawal
Bone	Ackerman	Cook Medical (Bloomington, Ind.)	14	12-G skin perforator, 12-G needle guide, 14-G trephine needles of long and short lengths, which protrude by 2 cm and 1 cm beyond the needle guide

Fig. 8.11. A trephine bone biopsy needle (11 G, Cook, Bloomington, Ind.)

Fig. 8.12. An air-powered drill that can be attached to a biopsy needle

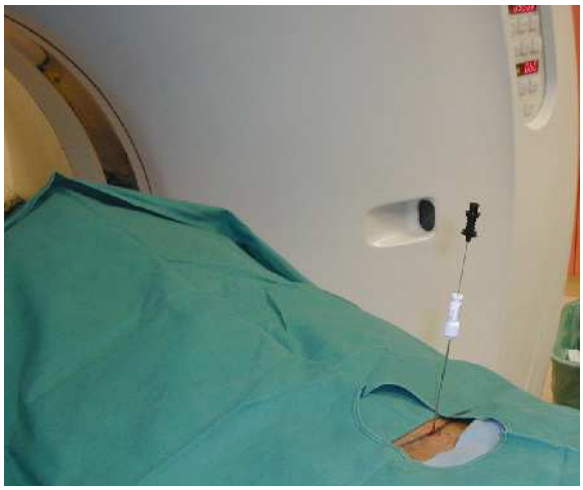

Fig. 8.13. The coaxial technique with placement of a Chiba needle within an Ostycut needle

Table 8.6. Needle gauge conversion chart

Needle size (G)	Outer diameter		Inner diameter	
	(mm)	(in.)	(mm)	(in.)
6	5.2	0.203	4.4	0.173
8	4.2	0.165	3.5	0.135
10	3.4	0.134	2.7	0.106
12	2.8	0.109	2.2	0.085
14	2.1	0.083	1.6	0.063
16	1.7	0.065	1.2	0.047
18	1.3	0.050	0.8	0.033
20	0.9	0.035	0.6	0.023
22	0.7	0.028	0.4	0.015
25	0.5	0.020	0.2	0.010

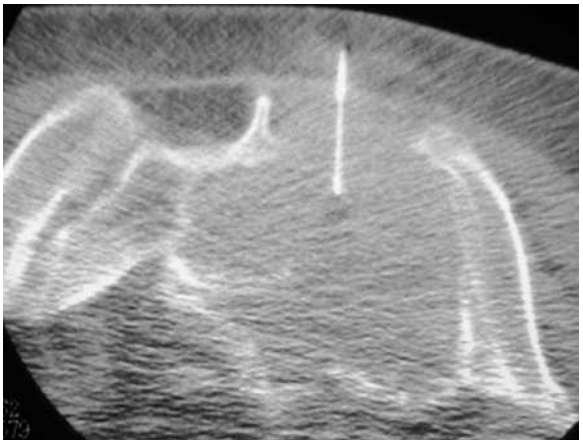

Fig. 8.14. A CT-guided biopsy of a large osteolytic lesion in the sacrum performed with the patient lying prone. As there is a large cortical window, biopsy of this "soft" lesion was performed using a cutting needle (11 G, Temno, Bauer Medical International, Santo Domingo, Dominican Republic)

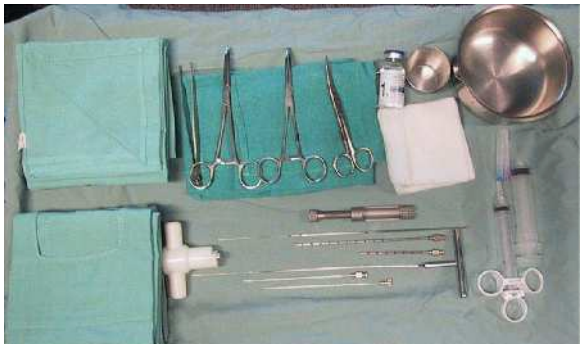

Fig. 8.15. The trolley settings for a bone biopsy. This includes sterile drapes, various forceps, containers for cleansing solutions, syringes for administration of local anesthetic, and various needles including biopsy needles

8.3 Procedure

8.3.1 Preliminary Preparation

It is desirable to schedule a pre-procedural consultation with the patient, if possible. This provides a valuable opportunity to establish rapport, allay the patient's fears, engage in a risk/benefit discussion, discuss alternatives, and provide relevant details of the procedure. Obtain a relevant history, including allergies, medications, and co-morbidities, and perform a targeted physical examination; the latter may be valuable in evaluating the post-procedure status of the patient.

It is important to order necessary laboratory investigations, including platelet count, hemoglobin, international normalized ratio (INR), and activated partial thromboplastin time (APTT), prior to the procedure. Platelet levels above 100,000/mm^3 are adequate for most procedures, while levels below 50,000/mm^3 require prophylactic transfusion just prior to the procedure (due to short half life of transfused platelets). An INR of below 1.5 is ideal, and fresh frozen plasma transfusion should be considered for values over 1.5 if core biopsy is to be obtained or if the lesion is deep. If intravenous (IV) contrast is to be used, measurements of serum creatinine, urea, and glomerular filtration rate calculation are appropriate.

The patient should be assessed for suitability of sedation, if that procedure is required. This includes assessment of ASA (American Society of Anesthesiologists) grading and assessment of risk of airway compromise (e.g., obesity, tonsillar hypertrophy, micrognathia, known obstructive sleep apnea). Patients deemed to be of higher risk for sedation (ASA score of 4 or greater) or at significant risk of upper airway compromise are best scheduled for anesthesiologist-supervised sedation. Informed consent should be obtained during this visit, and pre-/post-procedure instructions conveyed, ideally supplemented with printed information sheets.

The procedure should be scheduled allowing some extra time for unexpected delays and ensuring the availability of appropriate support staff. Anticoagulants should be withheld prior to the biopsy. Stop warfarin for 3 days prior to a biopsy. For selected cases where anti-coagulation is critical, e.g., prosthetic heart valves, heparin may be used up to 4 h prior to the procedure, usually in consultation with the patient's cardiologist. Aspirin should be stopped for at least a week, as it causes permanent inhibition of platelet activity, thus requiring between 4 and 10 days for return to normal platelet function. Uremia in renal failure causes platelet dysfunction, which can be reversed by scheduling hemodialysis prior to the procedure.

It is advisable to stop antimicrobials for a minimum of 24 h prior to the biopsy to facilitate microbiological assessment (Peh 2003). Although no studies have conclusively demonstrated significantly higher yields when antibiotics are stopped before biopsy, there is suggestion of benefit. Wu et al. (2007) obtained 24% culture positivity rates in patients who were given antibiotics within 24 h of biopsy vs 42% in patients who were not,

although the result was not statistically significant. Fasting for 6–8 h is advised, with oral medications allowed with sips of water up to the morning of the procedure. Insulin-dependent diabetic patients are instructed to take only half their normal dose of insulin and a 5% dextrose-containing infusion is started before the procedure, along with capillary glucose monitoring.

Post-procedure monitoring in the hospital may be required for checking of vital signs, pain control, or treatment of complications (if any). Planning for possible admission should be done early and the patient forewarned appropriately. For day-case procedures, we instruct the patient to arrange for a responsible adult to accompany them home. This should be someone who is able to recognize and report any post-procedure problems.

8.3.2 Pre-procedure Patient Preparation

Pre-procedure patient preparation consists of choosing an appropriate position based on the previously selected biopsy route, with attention to the patient's (and operator's) comfort, and the imaging modality. One must ensure adequate padding over bony prominences, especially for prolonged procedures and in debilitated patients where the risk of pressure sores is higher. Optimum positioning may not always be possible, e.g., a patient with recent abdominal surgery may not be able to lie prone for biopsy. The patient's vital signs are continually monitored and recorded every 15 min by a trained person who is not involved in performing or assisting with the procedure, preferably an interventional radiology nurse. All patients should have an IV cannula in situ, preferably running a slow IV saline infusion. This is particularly useful for sedated patients and management of the occasional vasovagal reaction.

Medications are given, if necessary. For sedatives and anti-anxiety drugs, we usually titrate intravenous doses of midazolam (0.5–5.0 mg) and fentanyl (25–200 mcg) with monitoring of vital signs and pulse oximetry. Platelet, fresh frozen plasma, or cryoprecipitate cover is also initiated, if required. Prophylactic antibiotics are not routinely indicated. The operator should wear sterile gloves, gown, and eye-protective gear after performing a surgical hand scrub. A generous area around the puncture site is cleansed with povidone iodine and alcohol or chlorhexidine and sterile drapes are placed (Fig. 8.15). Local anesthetic is delivered at the planned site of entry, and if needed, right up to the lesion. Subcutaneous injection is given with a 25-G needle, and then the track is anesthetized with an 18-G, 24-cm long needle up to the periosteum. The adjacent muscles and the periosteum of bone should also be infiltrated to minimize pain. Lignocaine 1% is used to infiltrate the skin, subcutaneous tissue, and muscles. The periosteum may be infiltrated with bupivacaine 0.5%, which provides a longer duration of action, with a slightly longer onset time compared with lignocaine. Bupivacaine should be used with caution in skeletal muscle, as it is more toxic to muscle, compared with lignocaine.

8.3.3 Specific Biopsy Techniques

8.3.3.1 US-Guided Biopsy

The lesion to be targeted is visualized in two planes and a solid area of tumor, preferably with evidence of neovascularity seen on color Doppler US, is selected. If the lesion is hypovascular, then sampling of the tumor margin is recommended (Saifuddin et al. 2000; Sartori et al. 2002). Using the biopsy function of the ultrasound machine, the distance and angle to lesion are calculated in a suitable plane that avoids important intervening structures. The probe is placed in a sterile probe cover and a sterile transparent drape is applied to the ultrasound console to facilitate adjustment. A sterilized biopsy transducer guide may be applied to the probe, if required. The "longitudinal" position of the transducer allows visualization of the entire needle tract, and is recommended during needle advancement. Once the needle tip is in the target site, the "transverse" position is used to confirm its location. The echogenic needle tip should be visualized during approach to the lesion and documented within the lesion on two planes before taking the biopsy. Color Doppler US can be applied to guide the needle to perfused areas. A screw stylet can be used to increase visualization of the needle tip. "Enhanced" needle tips are also available, e.g., Biosponder needle (Advanced Technology Laboratories, Bothel, Wash.). Another method is to trap a tiny bubble of air in the needle tip by withdrawing and reinserting the stylet before inserting the needle.

8.3.3.2 CT-Guided Biopsy

We routinely set up the monitor to show three consecutive slices reconstructed in a 256×256 matrix and displayed on a 768×768 matrix. The slice number is noted and the operator and staff stand behind a lead

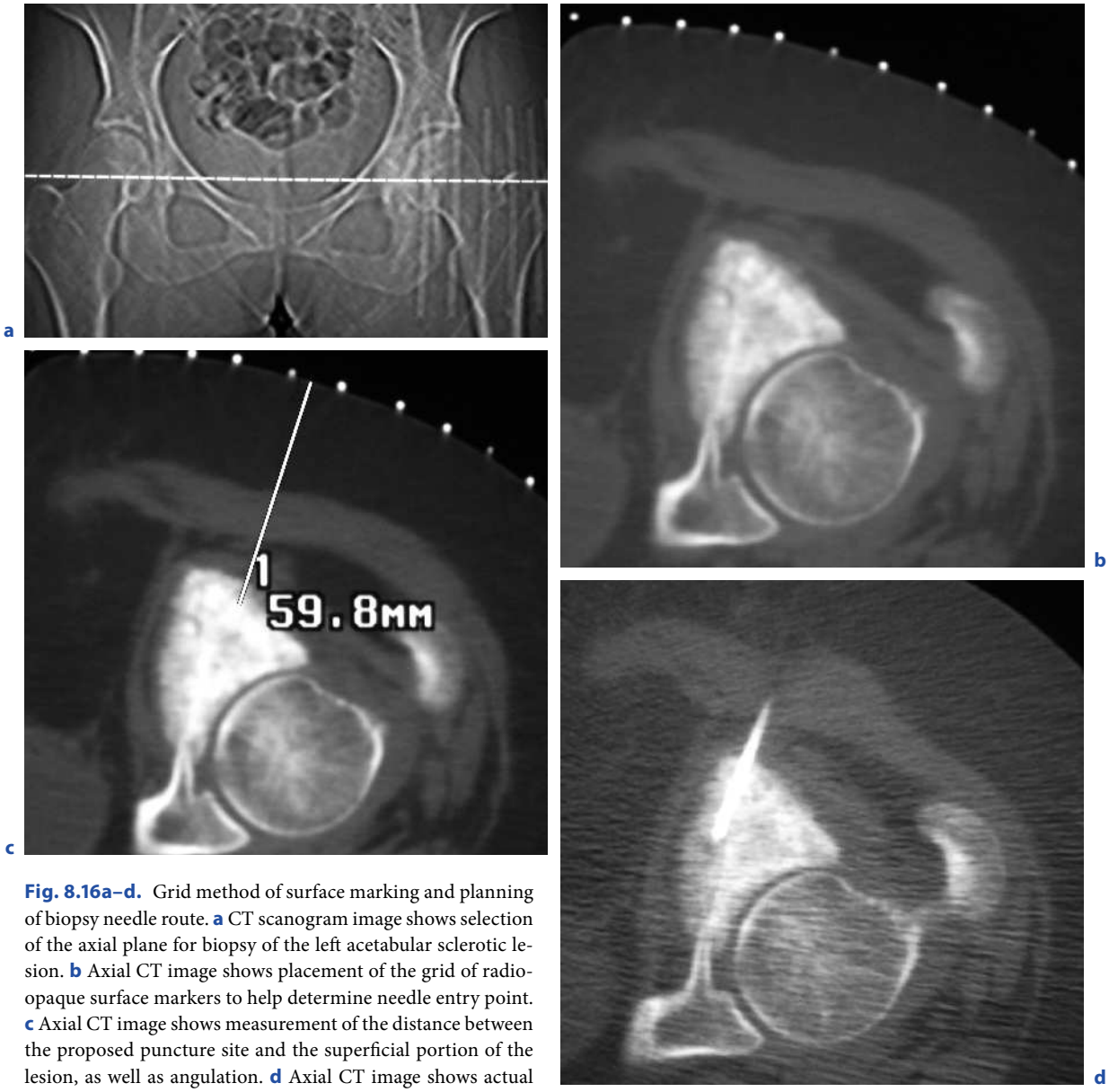

Fig. 8.16a–d. Grid method of surface marking and planning of biopsy needle route. **a** CT scanogram image shows selection of the axial plane for biopsy of the left acetabular sclerotic lesion. **b** Axial CT image shows placement of the grid of radiopaque surface markers to help determine needle entry point. **c** Axial CT image shows measurement of the distance between the proposed puncture site and the superficial portion of the lesion, as well as angulation. **d** Axial CT image shows actual needle placement into the acetabular lesion

glass screen during imaging to reduce radiation exposure. The couch top can be moved via the console or manually. For console operation, we use a transparent sterile cover to drape the console to allow the operator to adjust the table independently. The lesion to skin distance and trajectory angle are estimated by assessing the preliminary images. The representative slice number is marked. A grid can be placed on the patient's skin, or alternatively, a skin surface marker is placed to determine the puncture site (Fig. 8.16). A localizer laser beam from the scanner gantry assists in surface marking of the skin.

The needle tip can be located by the low-attenuation beam-hardening artifact (Fig. 8.17). Perpendicular insertion of the needle is simplest; however, for angulated approaches, the CT gantry should be tilted to the plane of insertion so as to try to achieve a perpendicular needle direction. For selected cases, the needle can be held with sponge forceps and inserted under continuous fluoroscopy; however, the radiation dose to the patient

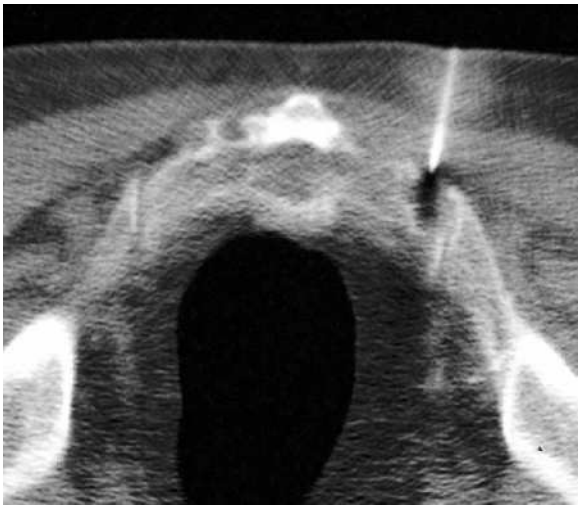

Fig. 8.17. A CT-guided biopsy of the posterior sacrum performed with the patient lying prone. The biopsy needle tip is identified by the presence of the beam-hardening artifact

and operator are increased. Several guidance devices and techniques have been described in the literature, aimed to reduce exposure (Roberts et al. 2007; Yaffe et al. 2003). We prefer the intermittent-exposure approach. The operator stands behind a lead screen while screening, and then makes frequent small adjustments to a localizer needle without continuous fluoroscopy.

8.3.3.3 Spinal Biopsy

For anterior biopsy of cervical lesions (C3–C7), an anterolateral approach is adopted. The operator's hand is used to displace the carotid bundle laterally and guard the structures from the biopsy needle. The positions of the esophagus and trachea are noted on the image. The needle is directed toward the vertebral body, preferably from the patient's right side, while avoiding the carotid–jugular bundle, trachea, and esophagus. For posterior biopsies, the transpedicular and posterolateral routes are the most commonly used, yielding similar accuracy (Pierot and Boulin 1999). The patient is positioned prone and the pedicle profiled en-face, using a slight 5–10° ipsilateral and cranio-caudal tilt. The needle is advanced toward the center of the pedicle, with repeated confirmation of positioning using orthogonal fluoroscopic views or CT. Care is taken not to traverse the medial pedicle margin, to prevent inadvertent entry into the spinal canal. For the transpedicular route, the needle should remain within the pedicle at all times.

The CT guidance is preferred for thoracic spine biopsies to better visualize the closely related viscera. On fluoroscopy, due to the curved outline of the vertebral body, the needle tip may protrude beyond the anterolateral margin of the vertebral body, despite appearing to be within the vertebra on frontal and lateral projections (Gibbon 1996). This possibility is eliminated with CT and is of importance when critical adjacent structures

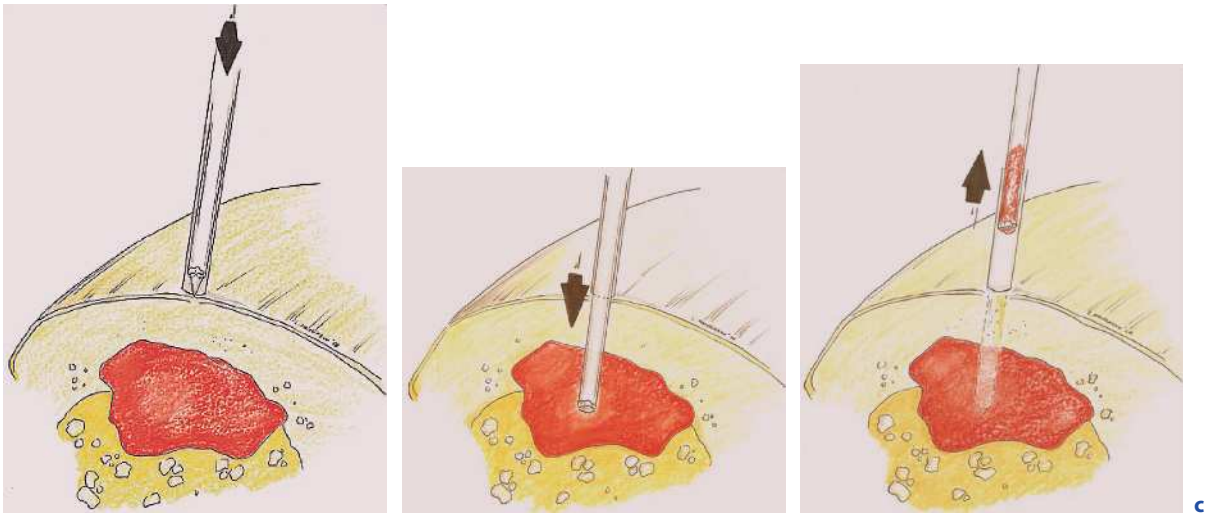

a,b c

Fig. 8.18a–c. Technique for trephine biopsy of a bone lesion

Table 8.7. Additional tips for a successful biopsy

While coring through healthy bone, keep the obturator in place to prevent the hard normal bone from clogging the lumen. The obturator is withdrawn when the lesion is reached
Target the lytic or soft tissue component of the tumor. Sampling only the sclerotic areas may result in a poor yield, comprising crushed bony fragments. In a study of 222 patients with 38 inadequate biopsies, the most common cause for failure was the sclerotic nature of the lesion, especially osteosarcoma (Ayala and Zornosa 1983)
Avoid clearly cystic or necrotic areas. Ultrasound may be useful to show solid, more likely viable tumor tissue. Jelinek et al. (2002) found insufficient tumor cells in aspirates from the center of cystic lesions, and supplemented biopsy of cystic lesions with "microcuretting." The lesion is first accessed with a 7- to 9-G outer needle and a 16- to 18-G Ostycut needle passed through it to scrape the wall of the lesion
Obtain adequate samples. Most authors recommend at least three good cores of specimen, if feasible. False-positive histological results can have serious therapeutic implications, accounting for a generally conservative pathological approach. If the obtained specimen is insufficient for a confident diagnosis, an inconclusive result is likely
Blood clots obtained during the biopsy should not be discarded but can instead be sent for histology and microbiology in a sterile container (Hewes et al. 1983). Harish et al. (2006) found that 73% of aspirated blood clots from lytic medullary lesions provided an accurate diagnosis when compared with surgical histology
Try to have a cytopathologist or technician on stand-by to ensure adequacy of sample. The presence of spindle cells from a tumor biopsy shows that a sarcoma has indeed been correctly targeted. Although this does not completely guarantee a diagnostic result, the adequacy of biopsy is more likely
For suspected infections, specimens should be sent routinely for histopathological and microbiological assessment, because 40–60% of histologically proven infections turn out to be culture negative (White et al. 1995). Send samples for histology, cytopathology, and microbiology. Cytopathology improves sensitivity for fungal infections
Lesions more than 10 cm deep should be targeted with thicker needles, e.g., 20-G rather than 22-G needles, when fine-needle aspiration is attempted, as they are more resistant to bending. For deep lesions, a coaxial method is advised to allow multiple passes via a single tract
Excessive local bleeding after biopsy can be controlled by instilling gel foam or absorbable collagen hemostatic sponge through the outer needle (Espinosa et al. 2008). During coaxial bone biopsy, bleeding may also be tamponaded by fitting the obturator back into the outer sheath for several minutes
Consider giving a mixture of lignocaine and bupivacaine for local anesthesia, as the bupivacaine has a longer duration of action and overlaps with the oral analgesics

are present. For fine-needle biopsy, multiple small to-and-fro passes are done through the most optimal portion of the lesion to maximize cellular yield. The needle is attached via an extension tubing to a 20-ml syringe. Five milliliters of air is included in the syringe and the plunger is withdrawn to the 20-ml mark to create a vacuum effect. The vacuum must be released before withdrawing the needle. For core biopsy, a corkscrew rotating movement is used to advance the serrated needle into the lesion (Fig. 8.18). Alternatively, a spring-loaded biopsy gun can be employed for solid non-sclerotic tumors. Some additional tips for obtaining a successful biopsy are listed in Table 8.7.

8.3.4 Handling of Specimens

The FNAC specimens can be injected onto glass slides and smeared using a second glass slide (Fig. 8.19). Some slides are air dried and stained with Diff-Quick (Fisher Scientific Biomedical Sciences Incorporated, Swedesboro, N.J.) for immediate cytological assessment (to check adequacy). Other slides are fixed immediately with 95% ethanol for later staining using the Papanicolaou method. Core-biopsy specimens can be placed on wet gauze and sent to the pathology department immediately (Fig. 8.20). Alternatively, they may be placed in 10% formalin. If infection is suspected, additional ma-

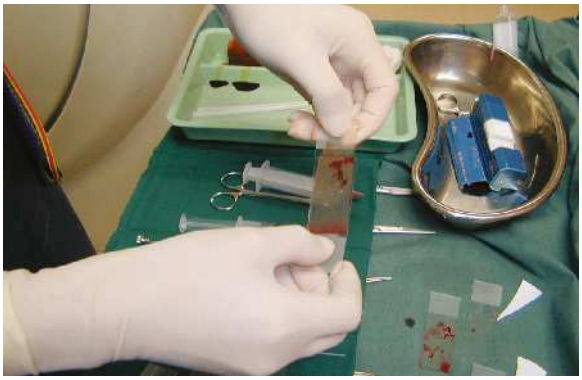

Fig. 8.19. Smearing of FNAC specimens using glass slides

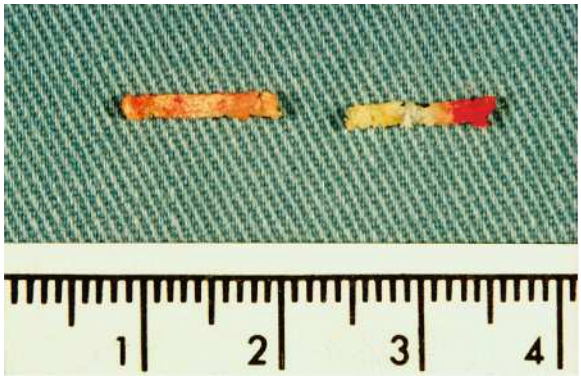

Fig. 8.20. Two bone-core specimens obtained by needle biopsy

Table 8.8. Complications of bone biopsy

Bleeding requiring transfusion
Needle breakage
Infection
Neurological injury including paralysis, cord compression (e.g., from vertebral hemangioma or metastatic renal cell carcinoma
Pneumothorax. For thoracic spine biopsy, rates are 4–11%. This is much lower if biopsy is performed under CT guidance

terial should be sent in a sterile container and/or placed directly into culture material.

For suspected lymphoma it is advisable to flush some aspirate into Hank's solution for flow cytometric immunophenotyping (Domanski et al. 2005). Imprints of the core specimen may be obtained by touching the tissue core onto a glass slide before dislodging it into the specimen container. The imprint cytology allows a quick review for adequacy and may even provide a provisional diagnosis (Chang et al. 2008; Domanski et al. 2005) – effectively functioning as a "frozen section" for the biopsy procedure.

8.3.5 Post-procedure Routine

Hemostasis is secured immediately after completion of biopsy. For superficial lesions direct compression is usually effective. For deeper lesions embolization of the biopsy track may sometimes be required to stop persistent bleeding. The puncture site is covered with a sterile dressing. The patient should be monitored in a recovery area for 2–4 h for any deterioration in vital signs and puncture-site hematoma. Vital signs are charted every 15 min for the first hour, 30 min for the next 2 h, and hourly thereafter. Obtaining a chest radiograph following rib and thoracic spine biopsy to exclude pneumothorax is an added precaution, but this is usually not necessary if biopsy has been carefully performed under CT guidance.

At discharge, the patient is given a printed information sheet listing potential late complications and containing instructions on how to proceed and who to contact if any do occur. Adequate, preferable long-acting pain medications should be prescribed for at least 2 days post-procedure. Check that a follow-up appointment had been scheduled with the referring clinician to discuss the biopsy findings and management plan. We generally discourage patients from driving on the day of biopsy, especially if IV sedatives have been administered.

8.3.6 Complications

Reported complication rates range between 0 and 10% (Welker et al. 2000), with serious complications occurring in less than 1% of cases. Murphy et al. (1981) reported a 0.2% complication rate in more than 9500 procedures. This compares favorably against the up to 16% reported complication rate of open biopsy (Mankin et al. 1996). The most frequently reported complications are listed in Table 8.8.

8.4 Conclusion

Biopsy plays a central role in the diagnosis and management of bone tumors and is increasingly being performed percutaneously under imaging guidance. Factors to consider include careful pre-procedure planning, consideration of indications and contraindications, lesion site selection, biopsy method, imaging guidance method, biopsy route, needle types and biopsy techniques, and possible complications. Awareness of these factors and application of the correct technique will help ensure a successful outcome.

Acknowledgement

We thank L. Marchinkow for providing the line diagrams.

References

Ahlstrom KH, Astrom KG (1993) CT-guided bone biopsy performed by means of a coaxial biopsy system with an eccentric drill. Radiology 188(2):549–552

Ahrar K, Himmerich JU, Herzog CE, Raymond AK, Wallace MJ, Gupta S, Madoff DC, Morello FA Jr, Murthy R, McRae SE, Hicks ME (2004) Percutaneous ultrasound-guided biopsy in the definitive diagnosis of osteosarcoma. J Vasc Interv Radiol 15(11):1329–1333

Akerman M (1997) The cytology of soft tissue tumours. Acta Orthop Scand Suppl 273:54–59

Altuntas AO, Slavin J, Smith PJ, Schlict SM, Powell GJ, Ngan S, Toner G, Choong PF (2005) Accuracy of computed tomography guided core needle biopsy of musculoskeletal tumours. Aust N Z J Surg 75(4):187–191

Ayala AG, Zornosa J (1983) Primary bone tumors: percutaneous needle biopsy. Radiologic–pathologic study of 222 biopsies. Radiology 149(3):675–679

Ayala AG, Ro JY, Fanning CV, Flores JP, Yasko AW (1995) Core needle biopsy and fine-needle aspiration in the diagnosis of bone and soft-tissue lesions. Hematol Oncol Clin North Am 9(3):633–651

Bennert KW, Abdul-Karim FW (1994) Fine needle aspiration cytology vs needle core biopsy of soft tissue tumors. A comparison. Acta Cytol 38(3):381–384

Bommer KK, Ramzy I, Mody D (1997) Fine-needle aspiration biopsy in the diagnosis and management of bone lesions: a study of 450 cases. Cancer 81(3):148–156

Chang YC, Yu CJ, Lee WJ, Kuo SH, Hsiao CH, Jan IS, Hu FC, Liu HM, Chan WK, Yang PC (2008) Imprint cytology improves accuracy of computed tomography-guided percutaneous transthoracic needle biopsy. Eur Respir J 31(1):54–61

Chew FS, Kline MJ (2001) Diagnostic yield of CT-guided percutaneous aspiration procedures in suspected spontaneous infectious diskitis. Radiology 218(1):211–214

Chew FS, Bui-Mansfield LT, Kline MJ (2003) Musculoskeletal imaging. Lippincott Williams and Wilkins, Philadelphia

Choi JJ, Davis KW, Blankenbaker DG (2004) Percutaneous musculoskeletal biopsy. Semin Roentgenol 39(1):114–128

Coley BL, Sharp GS, Ellis EB (1931) Diagnosis of bone tumors by aspiration. Am J Surg 13:215–224

Daly B, Krebs TL, Wong-You-Cheong JJ, Wang SS (1999) Percutaneous abdominal and pelvic interventional procedures using CT fluoroscopy guidance. Am J Roentgenol 173(3):637–644

Davies NM, Livesley PJ, Cannon SR (1993) Recurrence of an osteosarcoma in a needle biopsy track. J Bone Joint Surg Br 75(6):977–978

Domanski HA, Akerman M, Carlen B, Engellau J, Gustafson P, Jonsson K, Mertens F, Rydholm A (2005) Core-needle biopsy performed by the cytopathologist: a technique to complement fine-needle aspiration of soft tissue and bone lesions. Cancer 105(4):229–239

Dupuy DE, Rosenberg AE, Punyaratabandhu T, Tan MH, Mankin HJ (1998) Accuracy of CT-guided needle biopsy of musculoskeletal neoplasms. Am J Roentgenol 171(3):759–762

El-Khoury GY, Terepka RH, Mickelson MR, Rainville KL, Zaleski MS (1983) Fine-needle aspiration biopsy of bone. J Bone Joint Surg Am 65(4):522–525

Espinosa LA, Jamadar DA, Jacobson JA, DeMaeseneer MO, Ebrahim FS, Sabb BJ, Kretschmer MT, Biermann JS, Kim SM (2008) CT-guided biopsy of bone: a radiologist's perspective. Am J Roentgenol 190(5):W283–W289

Fraser-Hill MA, Renfrew DL (1992) Percutaneous needle biopsy of musculoskeletal lesions. 1. Effective accuracy and diagnostic utility. Am J Roentgenol 158(4):809–812

Gibbon WW (1996) Interventional radiology techniques in musculoskeletal disease. Baillieres Clin Rheumatol 10(4):711–727

Gogna A, Peh WCG, Munk PL (2008) Image-guided musculoskeletal biopsy. Radiol Clin North Am 46(3):455–473

Greenspan A (1993) Benign bone-forming lesions: osteoma, osteoid osteoma, and osteoblastoma. Clinical, imaging, pathologic, and differential considerations. Skeletal Radiol 22(7):485–500

Greenspan A (1995) Bone island (enostosis): current concept–a review. Skeletal Radiol 24(2):111–115

Gupta S, Takhtani D, Gulati M, Khandelwal N, Gupta D, Rajwanshi A, Suri S (1999) Sonographically guided fine-needle aspiration biopsy of lytic lesions of the spine: technique and indications. J Clin Ultrasound 27(3):123–129

Harish S, Hughes RJ, Saifuddin A, Flanagan AM (2006) Image-guided percutaneous biopsy of intramedullary lytic bone lesions: utility of aspirated blood clots. Eur Radiol 16(9):2120–2125

Hau A, Kim I, Kattapuram S, Hornicek FJ, Rosenberg AE, Gebhardt MC, Mankin HJ (2002) Accuracy of CT-guided biopsies in 359 patients with musculoskeletal lesions. Skeletal Radiol 31(6):349–353

Hewes RC, Vigorita VJ, Freiberger RH (1983) Percutaneous bone biopsy: the importance of aspirated osseous blood. Radiology 148(1):69–72

Hueman MT, Thornton K, Herman JM, Ahuja N (2008) Management of extremity soft tissue sarcomas. Surg Clin North Am 88(3):539–557, vi

Jaffe HL (1958) Tumors and tumorous conditions of the bones and joints. Lea and Febiger, Philadelphia

Jelinek JS, Murphey MD, Welker JA, Henshaw RM, Kransdorf MJ, Shmookler BM, Malawer MM (2002) Diagnosis of primary bone tumors with image-guided percutaneous biopsy: experience with 110 tumors. Radiology 223(3):731–737

Kattapuram SV, Rosenthal DI (1991) Percutaneous biopsy of skeletal lesions. Am J Roentgenol 157(5):935–942

Khuu H, Moore D, Young S, Jaffe KA, Siegal GP (1999) Examination of tumor and tumor-like conditions of bone. Ann Diagn Pathol 3(6):364–369

Kilpatrick SE, Pike EJ, Geisinger KR, Ward WG (1997) Chondroblastoma of bone: use of fine-needle aspiration biopsy and potential diagnostic pitfalls. Diagn Cytopathol 16(1):65–71

Kilpatrick SE, Cappellari JO, Bos GD, Gold SH, Ward WG (2001) Is fine-needle aspiration biopsy a practical alternative to open biopsy for the primary diagnosis of sarcoma? Experience with 140 patients. Am J Clin Pathol 115(1):59–68

Konermann W, Wuisman P, Ellermann A, Gruber G (2000) Ultrasonographically guided needle biopsy of benign and malignant soft tissue and bone tumors. J Ultrasound Med 19(7):465–471

Koscick RL, Petersilge CA, Makley JT, Abdul-Karim FW (1998) CT-guided fine needle aspiration and needle core biopsy of skeletal lesions. Complementary diagnostic techniques. Acta Cytol 42(3):697–702

Lalli AF (1970) Roentgen-guided aspiration biopsies of skeletal lesions. J Can Assoc Radiol 21(2):71–73

Lambiase RE, Levine SM, Terek RM, Wyman JJ (1998) Long bone surface osteomas: imaging features that may help avoid unnecessary biopsies. Am J Roentgenol 171(3):77–58

Liu PT, Valadez SD, Chivers FS, Roberts CC, Beauchamp CP (2007) Anatomically based guidelines for core needle biopsy of bone tumors: implications for limb-sparing surgery. Radiographics 27(1):189–206

Logan PM, Connell DG, O'Connell JX, Munk PL, Janzen DL (1996) Image-guided percutaneous biopsy of musculoskeletal tumors: an algorithm for selection of specific biopsy techniques. Am J Roentgenol 166(1):137–141

Lopez JI, Del Cura JL, Zabala R, Bilbao FJ (2005) Usefulness and limitations of ultrasound-guided core biopsy in the diagnosis of musculoskeletal tumours. APMIS 113(5):353–360

Mankin HJ, Mankin CJ, Simon MA (1996) The hazards of the biopsy, revisited. Members of the Musculoskeletal Tumor Society. J Bone Joint Surg Am 78(5):656–663

Mankin HJ, Lange TA, Spanier SS (1982) The hazards of biopsy in patients with malignant primary bone and soft tissue tumors. J Bone Joint Surg 64:1121–1127

Martin HE, Ellis EB (1930) Biopsy by needle puncture and aspiration. Ann Surg 92(2):169–181

Mitsuyoshi G, Naito N, Kawai A, Kunisada T, Yoshida A, Yanai H, Dendo S, Yoshino T, Kanazawa S, Ozaki T (2006) Accurate diagnosis of musculoskeletal lesions by core needle biopsy. J Surg Oncol 94(1):21–27

Murphy WA, Destouet JM, Gilula LA (1981) Percutaneous skeletal biopsy 1981: a procedure for radiologists–results, review, and recommendations. Radiology 139(3):545–549

Parapia LA (2007) Trepanning or trephines: a history of bone marrow biopsy. Br J Haematol 139(1):14–19

Parsons TW III, Frink SJ, Campbell SE (2007) Musculoskeletal neoplasia: helping the orthopaedic surgeon establish the diagnosis. Semin Musculoskelet Radiol 11(1):3–15

Paulson EK, Sheafor DH, Enterline DS, McAdams HP, Yoshizumi TT (2001) CT fluoroscopy-guided interventional procedures: techniques and radiation dose to radiologists. Radiology 220(1):161–167

Peh WCG (1999) The role of imaging in the staging of bone tumors. Crit Rev Oncol Hematol 31(2):147–167

Peh WCG (2003) Imaging-guided bone biopsy. Ann Acad Med Singapore 32(4):557–561

Pierot L, Boulin A (1999) Percutaneous biopsy of the thoracic and lumbar spine: transpedicular approach under fluoroscopic guidance. Am J Neuroradiol 20(1):23–25

Roberts CC, Morrison WB, Deely DM, Zoga AC, Koulouris G, Winalski CS (2007) Use of a novel percutaneous biopsy localization device: initial musculoskeletal experience. Skeletal Radiol 36(1):53–57

Saifuddin A, Mitchell R, Burnett SJ, Sandison A, Pringle JA (2000) Ultrasound-guided needle biopsy of primary bone tumours. J Bone Joint Surg Br 82(1):50–54

Sartori S, Nielsen I, Trevisani L, Ceccotti P, Abbasciano V, Tassinari D (2002) Sonographically guided biopsy of bone and soft tissue tumors. J Ultrasound Med 21(9):1056

Schwartz HS, Spengler DM (1997) Needle tract recurrences after closed biopsy for sarcoma: three cases and review of the literature. Ann Surg Oncol 4(3):228–236

Schweitzer ME, Deely DM, Beavis K, Gannon F (1995) Does the use of lidocaine affect the culture of percutaneous bone biopsy specimens obtained to diagnose osteomyelitis? An in vitro and in vivo study. Am J Roentgenol 164(5):1201–1203

Schweitzer ME, Gannon FH, Deely DM, O'Hara BJ, Juneja V (1996) Percutaneous skeletal aspiration and core biopsy: complementary techniques. Am J Roentgenol 166(2):415–418

Shin HJ, Amaral JG, Armstrong D, Chait PG, Temple MJ, John P, Smith CR, Taylor G, Connolly BL (2007) Image-guided percutaneous biopsy of musculoskeletal lesions in children. Pediatr Radiol 37(4):362–369

Turpin S, Lambert R (2001) Role of scintigraphy in musculoskeletal and spinal infections. Radiol Clin North Am 39(2):169–189

Unni KK, Dahlin DC (1996) Dahlin's bone tumors: general aspects and data on 11,087 cases. Lippincott-Raven, Philadelphia

Vieillard MH, Boutry N, Chastanet P, Duquesnoy B, Cotten A, Cortet B (2005) Contribution of percutaneous biopsy to the definite diagnosis in patients with suspected bone tumor. Joint Bone Spine 72(1):53–60

Ward WG Sr, Kilpatrick S (2000) Fine needle aspiration biopsy of primary bone tumors. Clin Orthop Relat Res (373):80–87

Ward WG, Savage P, Boles CA, Kilpatrick SE (2001) Fine-needle aspiration biopsy of sarcomas and related tumors. Cancer Control 8(3):232–238

Weeden S, Grimer RJ, Cannon SR, Taminiau AH, Uscinska BM (2001) The effect of local recurrence on survival in resected osteosarcoma. Eur J Cancer 37(1):39–46

Welker JA, Henshaw RM, Jelinek J, Shmookler BM, Malawer MM (2000) The percutaneous needle biopsy is safe and recommended in the diagnosis of musculoskeletal masses. Cancer 89(12):2677–2686

White LM, Schweitzer ME, Deely DM, Gannon F (1995) Study of osteomyelitis: utility of combined histologic and microbiologic evaluation of percutaneous biopsy samples. Radiology 197(3):840–842

Wu JS, Gorbachova T, Morrison WB, Haims AH (2007) Imaging-guided bone biopsy for osteomyelitis: Are there factors associated with positive or negative cultures? Am J Roentgenol 188(6):1529–1534

Yaffe D, Greenberg G, Leitner J, Gipstein R, Shapiro M, Bachar GN (2003) CT-guided percutaneous biopsy of thoracic and lumbar spine: a new coaxial technique. Am J Neuroradiol 24(10):2111–2113

Yamamoto T, Nagira K, Akisue T, Marui T, Hitora T, Kawamoto T, Yoshiya S, Kurosaka M, Tsukamoto R (2003) Fine-needle aspiration biopsy of solid aneurysmal bone cyst in the humerus. Diagn Cytopathol 28(3):159–162

Zindrick MR, Wiltse LL, Doornik A, Widell EH, Knight GW, Patwardhan AG, Thomas JC, Rothman SL, Fields BT (1987) Analysis of the morphometric characteristics of the thoracic and lumbar pedicles. Spine 12(2):160–166

Surgical Staging 1: Primary Tumour

9

Alun Davies, John Skinner and Asif Saifuddin

CONTENTS

KEY POINTS

- The objectives of local staging of primary bone tumours are to detect: (a) the extent of bone marrow involvement, including epiphyseal involvement and the presence of skip lesions; and (b) the presence and extent of extraosseous soft tissue mass including involvement of the adjacent joint, neurovascular bundle and muscle compartments, thus establishing the feasibility of limb salvage, as opposed to amputation.
- MRI of the whole bone containing the primary tumour, including joints at both ends of long bones, should be obtained to show the full extent of bone marrow involvement and skip lesions.
- Longitudinal non-contrast T1-weighted SE sequences are the most accurate for determining intraosseous tumour extent.
- Assessment of neurovascular involvement is optimally demonstrated in the axial plane using fat-suppressed T2-weighted or PDW FSE sequences.
- Dynamic enhanced MRI can aid in the differentiation of extraosseous tumour from adjacent oedema due to the delayed enhancement of the latter, although its clinical utility has not been proven.

A. Davies, MD
Department of Radiology, Royal National Orthopaedic Hospital Trust, Brockley Hill, Stanmore, Middlesex, London HA7 4LP, UK

J. A. Skinner, MD
Department of Bone and Soft Tissue Sarcoma Surgery, Royal National Orthopaedic Hospital Trust, Brockley Hill, Stanmore, Middlesex, London, HA7 4LP, UK

A. Saifuddin, MD
Department of Radiology, Royal National Orthopaedic Hospital Trust, Brockley Hill, Stanmore, Middlesex, London HA7 4LP, UK

9.1 Introduction

Staging of a primary bone tumour refers to the clinical or radiological evaluation of both the local and distant spread. In this chapter we review the imaging aspects of staging local disease, predominantly relating to malignant lesions of the appendicular skeleton. Local staging plays an important role in deciding the oncological and surgical management of a patient. Also, disease prognosis can be determined by accurate staging of the tumour. Finally, staging systems allow communication between the medical profession allowing meaningful comparison of data from different groups of patients, facilitating both an understanding of the natural history of the disease and the development of clinical trials.

The local staging of a primary bone tumour can be divided into determining its intramedullary and extramedullary extent, as summarised in Table 9.1 (Saifuddin 2002).

9.2 Bone Tumour Staging Systems

The surgical staging system of bone tumours was initially proposed by Enneking et al. (1980). The purpose of a surgical staging system for musculoskeletal neoplasms is to incorporate the significant prognostic factors into a model that describes the progressive degrees of risk for local recurrence and distant metastases to which a patient is subject, stratify the stages so they have specific implications for surgical management and provide guidelines for adjunctive therapies (Enneking et al. 1980).

The Enneking staging system is based on three criteria: The first criterion is that of tumour extent: The tumour is designated T1 if it remains confined to a single anatomical compartment (intracompartmental; Fig. 9.1) and is designated T2 if it spreads into any additional compartment or compartments (extracompartmental; Fig. 9.2). The second criterion is that of metastases: The tumour is designated M0 if there are no metastases and M1 if there are either regional or distant metastases. The third criterion is that of tumour grade, which is a histological assessment of cellular atypia and is related to the tumour's tendency to metastasise. This staging system is summarised in Table 9.2 and was adopted by the Musculoskeletal Tumour Society (MSTS).

According to the original MSTS staging system, low-grade tumours were classified as stage I, high-grade tumours were classified as stage II and tumours that had metastasised were classified as stage III (regardless of grade). These stages were sub-classified based on the local extent of growth of the tumour. Bone tumours that had not grown beyond the compartment of origin had an A sub-classification, whereas tumours that extended into the adjacent soft tissue compartment had a B sub-classification.

In 1983, the American Joint Committee on Cancer (AJCC) recommended a staging system for malignant tumours of bone (Peabody et al. 1998; AJCC 1997). The original AJCC staging system was almost identical to the MSTS, with the exception of metastatic disease being classified as stage IV while stage III was left undefined. Also stage IV was subdivided on the presence of lymph node metastasis only (stage IV-A) or the presence of distant metastases (stage IV-B).

The AJCC system was updated in 2002 when three major revisions were made (AJCC 2002). Rather than using the intraosseous or extraosseous extent of the tumour for subdividing stages I and II, tumour size was suggested as a better prognostic indicator. Specifically, a tumour size of less than 8 cm in any dimension was recommended as a favourable prognostic indicator. Secondly, tumours associated with skip metastases defined as discontinuous disease in the same bone were classified separately as stage III. Finally, stage-IV tumours (those associated with distant metastases) were subdivided by the presence of pulmonary metastases only (stage IV-A) or metastases to other locations including bone (stage IV-B; Table 9.3).

Table 9.1. Local staging objectives

Intramedullary	Extramedullary
Extent of bone marrow involvement	Joint involvement
Epiphyseal involvement	Muscle compartmental involvement
Skip metastases	Neurovascular bundle involvement

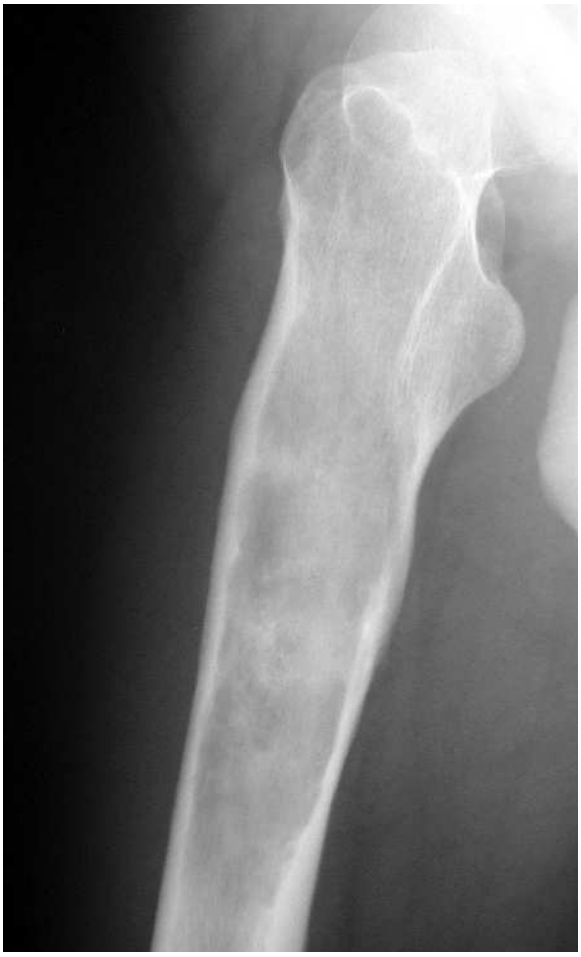

Fig. 9.1. Stage T1 (intracompartmental) tumour. Lateral radiograph shows a proximal femoral low-grade chondrosarcoma, which is limited to the intramedullary compartment

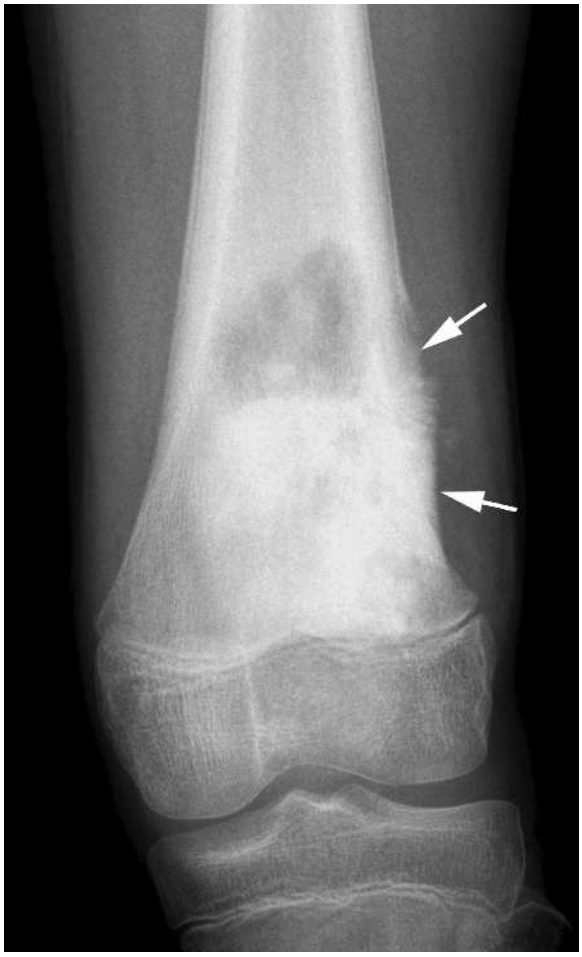

Fig. 9.2. Stage T2 (extracompartmental) tumour. Anteroposterior radiograph shows a distal femoral osteosarcoma, which has extended through the lateral cortex (*arrows*)

Table 9.2. Staging system for primary malignant tumours of bone according to Enneking et al. (1980) *T1* tumour is intracompartmental, *T2* tumour is extracompartmental, *M0* no regional or distant metastases, *M1* regional or distant metastases, *G1* low grade, *G2* high grade. (Modified from Stacey et al. 2006)

Stage	Tumour	Metastases	Grade
IA	T1	M0	G1
IB	T2	M0	G1
IIA	T1	M0	G2
IIB	T2	M0	G2
III	T1 or T2	M1	G1 or G2

Table 9.3. American Joint Committee on Cancer Staging System for primary malignant tumours of bone for those tumours diagnosed on or after 1 January 2003. *T0* no evidence of primary tumour, *T1* tumour 8 cm or less in greatest dimension, *T2* tumour >8 cm in greatest dimension, *T3* skip metastases, *N0* no regional lymph node metastases, *N1* regional lymph node metastases, *M0* no distant metastases, *M1a* lung, *M1b* other distant sites, *G1* well differentiated (low grade), *G2* moderately differentiated (low grade), *G3* poorly differentiated (high grade), *G4* undifferentiated (high grade). (Modified from Stacey et al. 2006)

Stage	Tumour	Lymph node	Metastases	Grade
IA	T1	N0	M0	G1 or G2
IB	T2	N0	M0	G1 or G2
IIA	T1	N0	M0	G3 or G4
IIB	T2	N0	M0	G3 or G4
III	T3	N0	M0	Any G
IVA	Any T	N0	M1a	Any G
IVB	Any T	N1	Any M	Any G
IVB	Any T	Any N	M1b	Any G

9.3 Staging of Long Bone Tumours

9.3.1 Intramedullary Extent

The degree of intramedullary tumour extension is unreliably assessed on plain radiographs (Fig. 9.3). Lytic lesions are often not detectable on standard radiographs until the tumour has resulted in 30–50% loss of trabecular bone (Ardran 1951).

Prior to the advent of computed tomography (CT) and magnetic resonance imaging (MRI), intramedullary tumour extent was assessed by bone scintigraphy; however, it has been shown that scintigraphy can commonly overestimate the extent of intraosseous tumour due to falsely extended uptake patterns (Figs. 9.4, 9.5; Chew and Hudson 1982; Hudson et al. 1983; Sundaram et al. 1986). Scintigraphy can also produce apparent extension across the adjacent joint (Chew and Hudson 1982). Bloem et al. (1988) demonstrated that scintigraphy has a relatively poor correlation for the assessment of intraosseous tumour when compared with pathological specimens, both underestimating and overestimating the intraosseous extent.

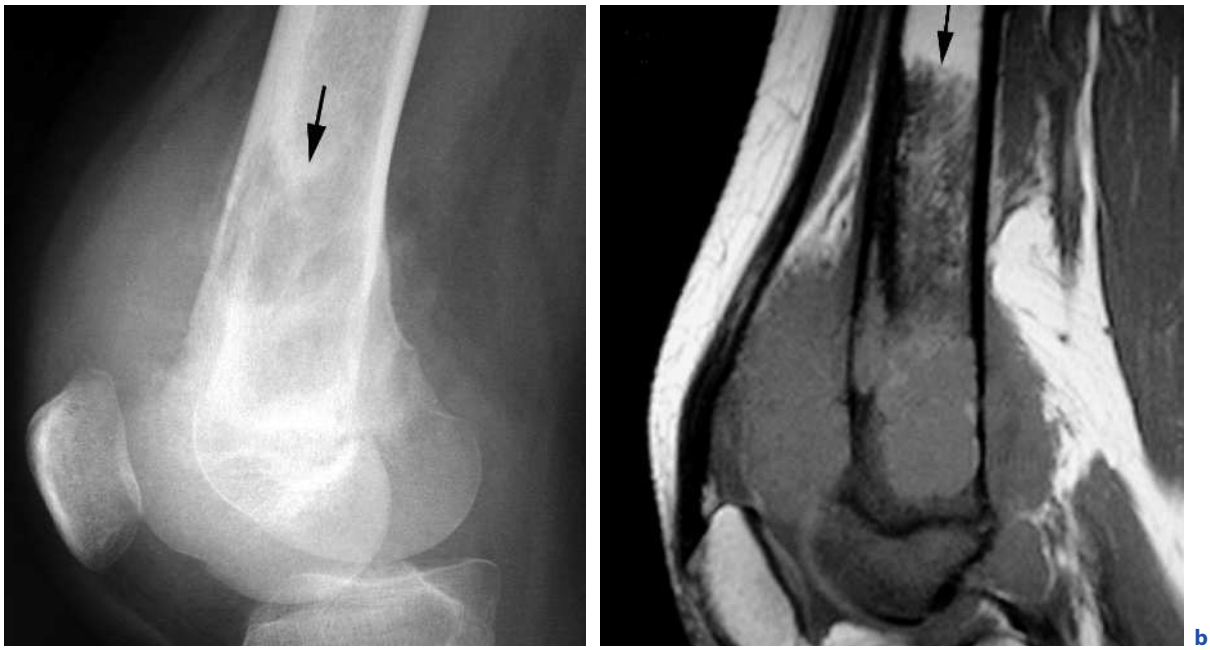

a b

Fig. 9.3a,b. Osteosarcoma of the distal femur. **a** Lateral radiograph demonstrates a mixed sclerotic/lytic lesion with the proximal margin (*arrow*) in the metaphysis. **b** Sagittal T1W SE MRI shows a significantly more proximal extension of intramedullary tumour into the distal metadiaphysis (*arrow*)

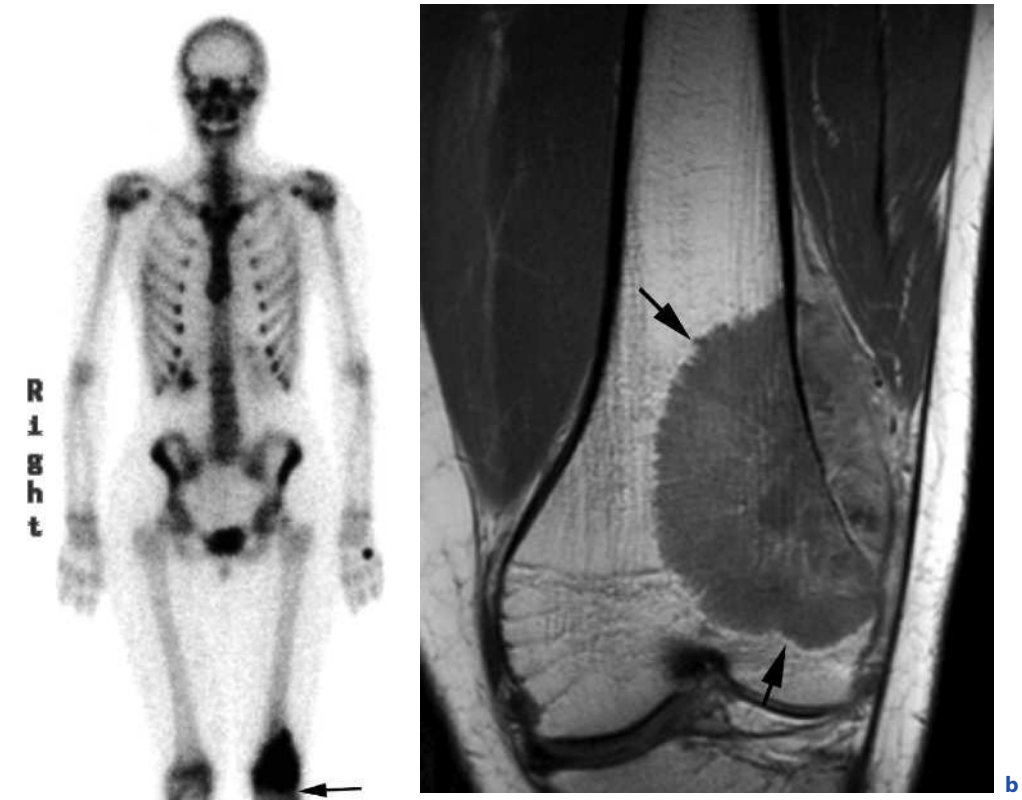

a b

Fig. 9.4a,b. Osteosarcoma of the distal femur. **a** Whole-body bone scan shows a single focus of intense increased activity in the distal left femur, extending to the joint margin (*arrow*). **b** Coronal post-contrast T1W SE MR image shows the intramedullary tumour extent, which does not reach the distal femoral articular surface (*arrows*)

Magnetic resonance imaging has become the technique of choice for the intraosseous staging of bone tumours. Studies comparing CT and MRI with pathological specimens have shown that MRI is superior to CT at evaluating the extent of intraosseous involvement (Bohndorf et al. 1986; Bloem et al. 1988; O'Flanagan et al. 1991; Gillespy et al. 1988).

The most accurate MRI sequence for the measurement of intraosseous spread is debatable. For osteosarcoma, Onikul et al. (1996) compared short-tau inversion recovery (STIR) and T1-weighted spin-echo (W SE) sequences with pathological specimens in 20 children and found that STIR significantly overestimated the degree of macroscopic intraosseous tumour in 73% of cases due to its sensitivity to marrow hyperplasia and oedema; however, Golfieri et al. (1990, 1991) found that the STIR sequence was slightly more accurate than the T1W SE sequences in approximately 20% of bone tumours of various histological types. If the suspicion is of osteosarcoma, then imaging should include a non-contrast-enhanced coronal or sagittal T1W SE sequence (Fig. 9.6).

As a general rule, intravenous gadolinium administration is of limited value in the evaluation of primary bone tumours because the inherent contrast between the tumour, which has intermediate-low T1W signal intensity (SI) and normal high SI marrow fat, is optimal without it (Sundaram 1997; May et al. 1997; Verstraete and Lang 2000); however, gadolinium will occasionally allow one to better identify areas of solid

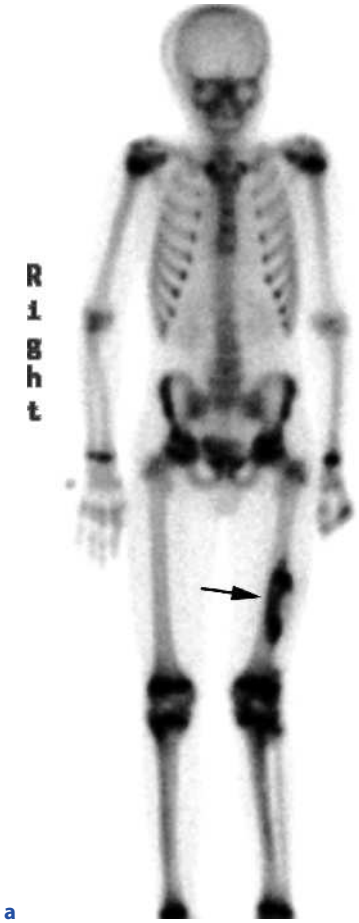

a

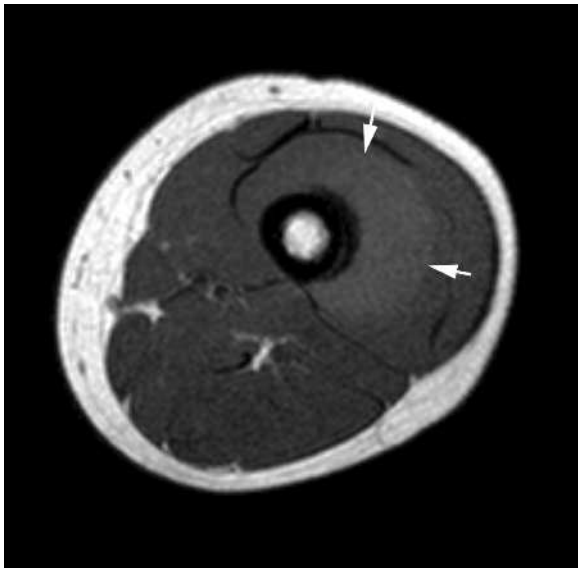

b

Fig. 9.5a,b. High-grade surface osteosarcoma of the femur. **a** Whole-body bone scan shows intense increased activity in the left femoral diaphysis, extending to almost the whole width of the bone (*arrow*), implying intramedullary extension. **b** Axial T1W SE MR image shows the surface tumour (*arrows*) without intramedullary extension, the marrow showing normal-fat SI

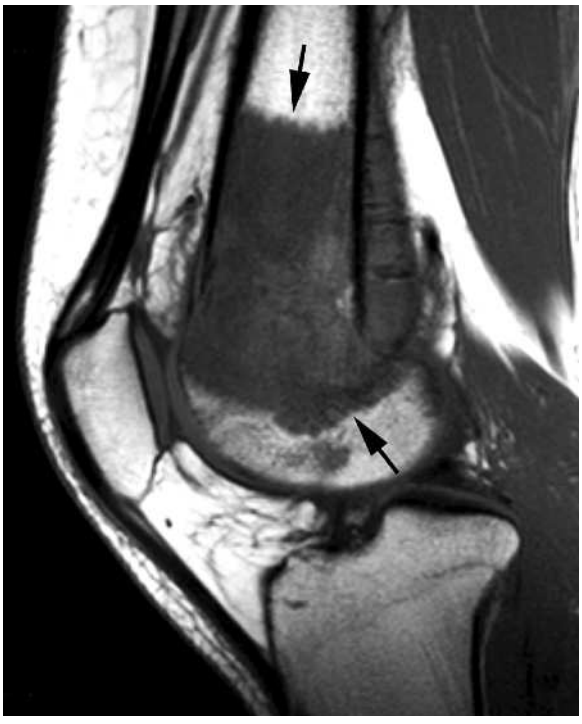

Fig. 9.6. Osteosarcoma of the distal femur. Sagittal T1W SE MR image shows the local intramedullary extent of tumour (*arrows*)

tumour from haemorrhage and necrosis, which is important for biopsy planning. Our experience would indicate that this differentiation is just as easy on T2W FSE images, where solid tumour shows intermediate SI and necrosis appears of fluid SI. Although some investigators have shown encouraging results using dynamic enhanced MRI (DEMRI) to distinguish tumour from reactive oedema after chemotherapy and residual tumour from non-tumour tissue post-operatively (Brisse et al. 2004; Reddick et al. 2001; Egmont-Peterson et al. 2000; Ongolo-Zogo et al. 1999; El Khadrawy et al. 1999), this technique currently has no proven role in the initial staging of tumours.

9.3.2 Epiphyseal Involvement

The growth plate had long been considered a barrier to the spread of tumour into the epiphysis (Aegerter and Kirkpatrick 1975; Mahoubi 1989). These data were supported by experimental work identifying protein substances within the physis that inhibit angiogenesis (Langer et al. 1976; Kuettner et al. 1978); however, pathological studies have reported that transphyseal spread of tumour occurs in 50–88% of cases of osteosarcoma and Ewing sarcoma (ES; Enneking and Kagan 1978; Simon and Bos 1980; Norton et al. 1991; Panuel et al. 1993).

It is important to determine the involvement of the physis and epiphysis in skeletally immature children in order to determine whether joint-sparing surgery can be performed, thus allowing continued growth of the limb.

The MRI criteria for determining epiphyseal involvement include the extension of intermediate SI tumour on T1W SE sequences across the growth plate with associated evidence of physeal destruction (Fig. 9.7; Onikul et al. 1996; Norton et al. 1991; Panuel et al. 1993). This gives a high sensitivity, but false-positive cases arise from the presence of focal or diffuse areas of red marrow resulting in reduced SI in the physis, with subsequent low specificity (Onikul et al. 1996).

Hoffer et al. (2000) compared standard T1W SE sequences, STIR and DEMRI in patients with appendicular osteosarcoma to determine the most reliable MRI

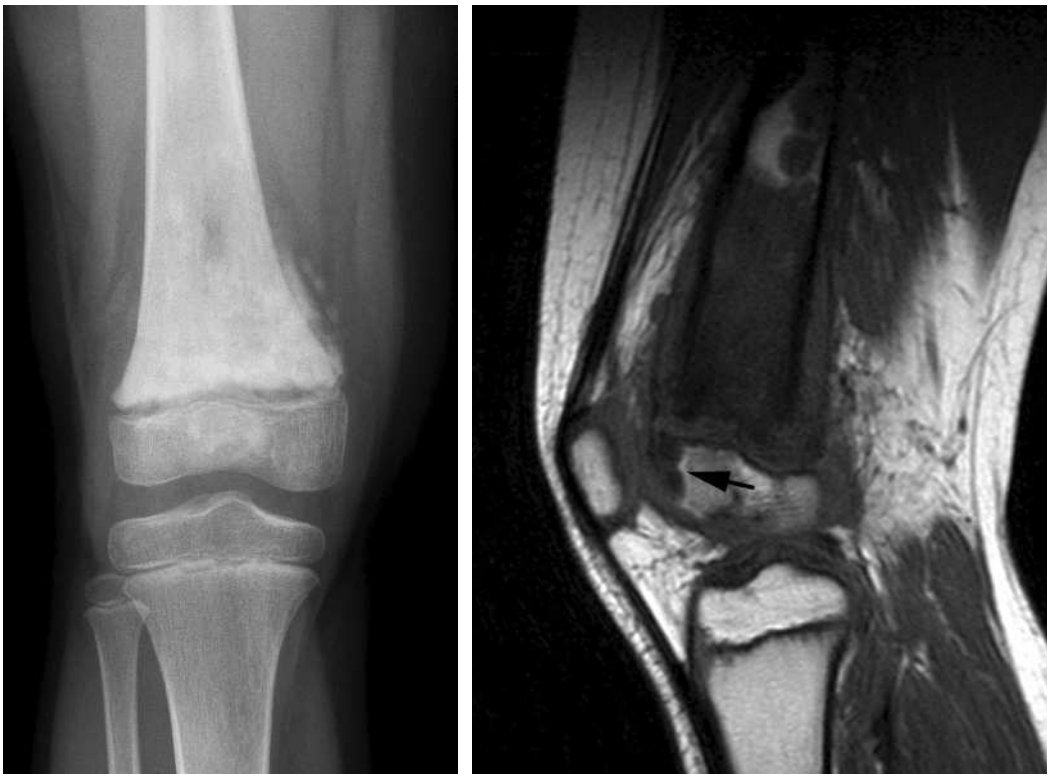

Fig. 9.7a,b. Distal femoral osteosarcoma with epiphyseal involvement. **a** Anteroposterior radiograph shows an osteoblastic tumour extending to the open growth plate. **b** Sagittal T1W SE MR image shows epiphyseal extension of tumour across the growth plate anteriorly (*arrow*)

signs of epiphyseal involvement. When any epiphyseal SI abnormality was considered to represent epiphyseal involvement, both T1W SE and STIR sequences had a sensitivity of 100% but a specificity of 60 and 40%, respectively; however, if the epiphyseal abnormality was only considered to represent tumour when it had the same SI as the metaphyseal lesion, then T1W SE sequences had a sensitivity and specificity of 90% while STIR sequences had a sensitivity of 95% but a specificity of 70%. The diagnostic accuracy of DEMRI was slightly less than the conventional sequences.

In conclusion, the T1W SE sequence is more specific and the STIR sequence slightly more sensitive for determining epiphyseal involvement.

9.3.3 Skip Metastases

A skip lesion, or skip metastasis, is defined as a second smaller focus of histologically proven tumour occurring within the same bone but separated from the larger primary tumour by an area of normal medullary bone. Less commonly, it may be a second focus of tumour on the opposing side of the joint, when it is referred to as a trans-articular skip (Enneking and Kagan 1975; Wuisman and Enneking 1990).

Skip metastases are a well-recognised feature of osteosarcoma and are associated with a poorer prognosis (Wuisman and Enneking 1990; Malawer and Dunham 1983). The incidence of skip metastases has been reported to be as high as 25% in one early series of osteosarcomas (Enneking and Kagan 1975). More recent studies quote much lower incidences (from 1.5 to 9%; Kager et al. 2006; Sajadi et al. 2004; Wuisman and Enneking 1990). There is limited literature on the incidence of skip metastases in Ewing sarcoma (ES) (Sundaram et al. 1989). In a series of 69 cases of ES the incidence of skip metastases was only 4.5% (Davies et al. 1997).

It is well established that diagnostic imaging procedures, including plain radiographs, CT and bone scintigraphy, are not reliable enough to detect skip metastases, particularly in ES (Fig. 9.8a–c; Wuisman and Enneking 1990; Davies et al. 1997; Bhagia et al. 1997). Whole-bone MRI has been shown to be the most accurate modality for detecting skip metastases (Kaeger et al. 2006; Saifuddin 2002; Wetzel et al. 1990; Bhagia et al. 1997); however, there is no study which has defined the sensitivity and specificity of whole-bone MRI for the detection of skip lesions. Trans-articular skip lesions appear as focal areas of marrow signal abnormality, which is the same as that of the primary lesion (Fig. 9.8d) and must be differentiated from other incidental lesions such as chondroma.

Patients with skip lesions were shown by Wuisman and Enneking (1990) to have a poorer prognosis than those without, with a higher incidence of distant metastases, local recurrence and reduced disease-free survival, suggesting that these patients should be classified as having stage-III disease according to the Enneking staging system.

Recently Kager et al. (2006) showed that a subset of osteosarcoma patients who present with skip metastases, but who are treated aggressively with chemotherapy and surgery, have improved disease-free survival; however, patients with trans-articular lesions and/or whose tumours respond poorly to neoadjuvant chemotherapy have a significantly lower survival probability than other patients with skip metastases. These results support the AJCC staging system where skip lesions are defined as "discontinuous tumours in the primary site bone" and are classified as stage III, whereas patients with trans-articular lesions are classified as having synchronous distant bone metastases (stage-IV disease).

9.3.4 Joint Involvement

The presence or absence of intra-articular extension of a malignant bone tumour is the major criterion that determines whether a patient is a candidate for an intra- or extra-articular resection, when limb-preserving surgery is to be performed. In cases of tumour extension into the joint space or into the cruciate ligaments of the knee, an extra-articular resection is required, which means that the joint must be resected en bloc resulting in poorer post-operative function (Tsuboyama et al. 1993).

Peritumoral inflammatory changes and oedema can be difficult to distinguish from the tumour itself. Furthermore, when tumours are located adjacent to synovial joint surfaces, it is difficult to determine the extent of involvement of local tissues such as capsular, musculo-tendinous, ligamentous and other soft tissue attachments within and around the joints, and consequently it is often difficult to confirm or exclude synovial joint involvement on pre-operative imaging. Pathological fracture into the joint is, however, considered unequivocal evidence of joint involvement. These uncertainties may lead to overstaging and false-positive diagnoses of joint involvement by tumour and, in turn, excessive radical surgery.

Extension of metaphyseal intraosseous sarcomas across the osseous–tendinous junction has been dem-

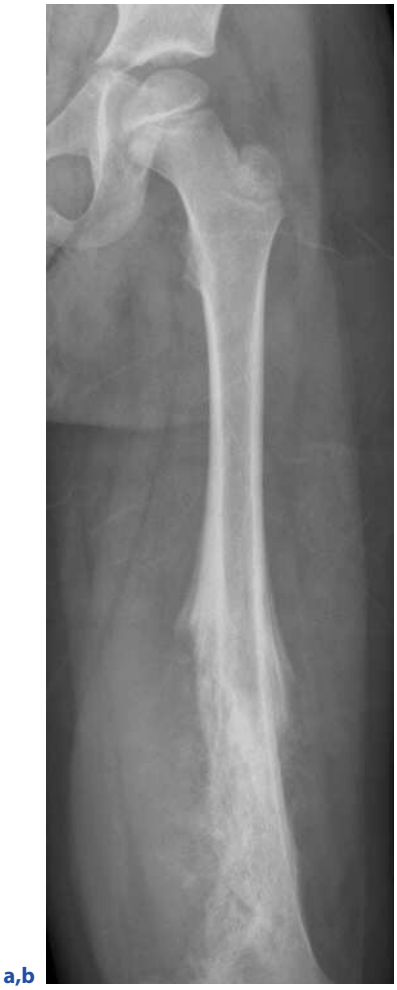

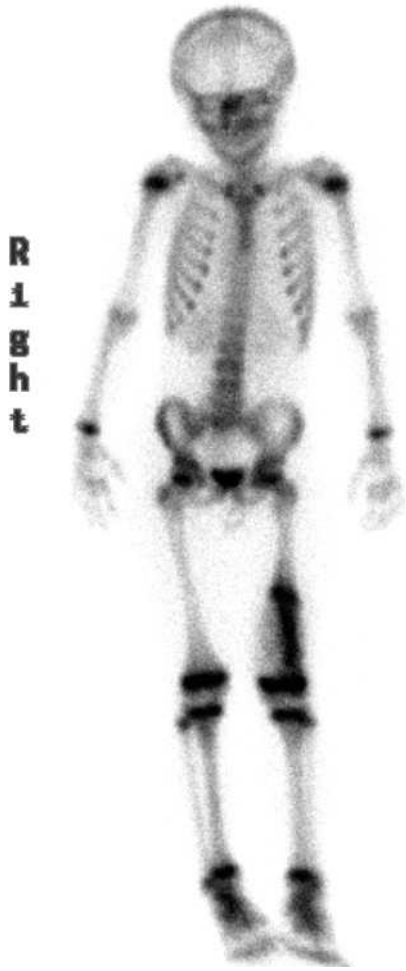

a,b

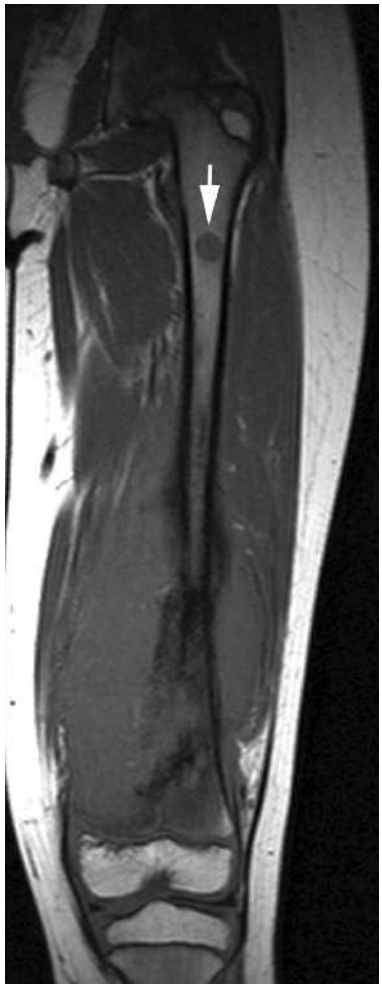

c

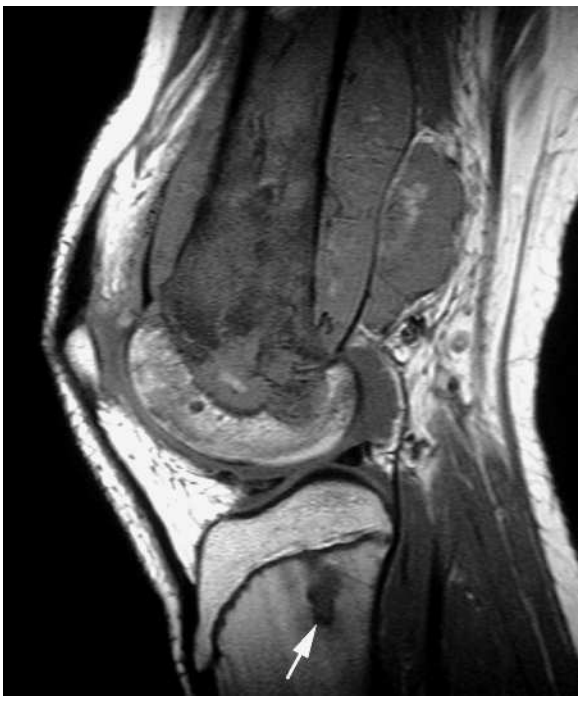

d

Fig. 9.8a–d. Ewing sarcoma of the distal femur with a skip metastasis. **a** Anteroposterior radiograph shows a lytic destructive lesion with a normal appearance of the proximal femur. **b** Whole-body bone scan shows intense increased activity in the left femoral metaphysis and diaphysis, but no increased activity in the proximal femur. **c** Coronal T1W SE MR image shows the extensive distal femoral lesion and also a small proximal femoral skip metastasis (*arrow*). **d** Sagittal T1W SE MR image shows a trans-articular skip metastasis (*arrow*) of the proximal tibia in a patient with distal femoral osteosarcoma

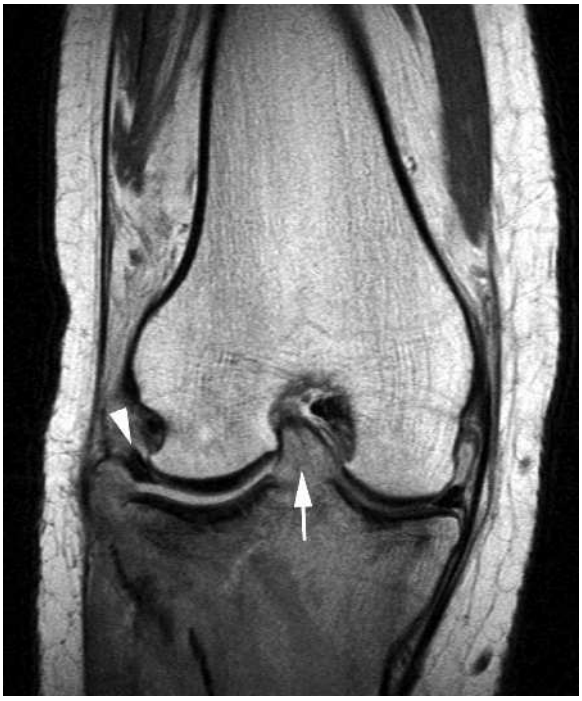

Fig. 9.9. Proximal tibial osteosarcoma with joint involvement. Coronal PDW FSE MR image shows tumour in the proximal tibia extending into the ACL (*arrow*) and also surrounding the lateral meniscus (*arrowhead*)

onstrated (Simon and Hecht 1982), with tumour extension along the cruciate ligaments of the knee and also the knee joint capsule (Fig. 9.9). Similarly, tumour extension has been shown to cross the hip joint along the ligamentum teres into the femoral head, or from the femoral head into the acetabulum (Alkalay et al. 1998).

A major difficulty is the difference in the criteria used in various studies to define joint involvement. Schima et al. (1994) defined joint involvement as being present if an enhancing tumour mass could be seen extending into the joint, either through the joint capsule or through the destroyed sub-articular cortex. Although their sensitivity for correctly identifying joint invasion was 100%, their specificity of 69% was low with 10 patients incorrectly diagnosed as having joint invasion. Cases of false-positive MRI diagnosis of joint-space invasion were thought to be due to displacement of the joint capsule by tumour, without penetration. This is commonly seen with tumours extending through the anterior distal femoral cortex, deep to the suprapatellar pouch.

Van Trommel et al. (1997) used wider definitions of joint involvement; these included the presence of tumour reaching the sub-articular surface such that a clear surgical plane could be achieved, involvement of the collateral or cruciate ligaments or the suprapatellar pouch. All cases of joint involvement (19 of 29 cases) were identified on MRI with only one false positive.

The most recent study is by Quan et al. (2005). In a total of 27 patients they defined joint involvement as present only if tumour penetrated the entire thickness of articular cartilage, and using this criterion, none of the patients had joint involvement. They concluded that if MRI was negative for joint involvement, it is likely to be safe to proceed with intra-articular resection; however, as their patient cohort did not include any with defined joint involvement, an assessment of false-negative rate cannot reliably be made.

The use of intravenous gadolinium has not been shown to improve the assessment of joint invasion. Schima et al. (1994) suggested that the differentiation between intra-articular tumour and joint effusion was improved with intravenous contrast. This is not supported by the study by Seeger et al. (1991) who suggested that tumour could be differentiated from effusion by identifying invasion of the high SI synovial fat on T1-weighted images without contrast.

Schima et al. (1994) noted that the presence of joint effusion in itself did not predict the presence of tumour extension into the joint; however, they found that the absence of a joint effusion had a high negative predictive value for joint involvement by tumour.

9.3.5 Neurovascular Involvement

The accurate assessment of extraosseous tumour relationship to any major adjacent neurovascular bundle is a vital aspect of local staging, as encasement of the neurovascular bundle is the major reason for the inability to perform limb-salvage surgery.

Neurovascular structures can be defined as being either completely free of tumour, abutted by tumour or partially/completely encased by tumour (Fig. 9.10; Bloem et al. 1988; Seeger et al. 1991).

A study by Bloem et al. (1988) demonstrated that MRI was superior to CT or conventional angiography in detecting involvement of the neurovascular bundle, having a sensitivity of 100% and specificity of 98%.

Seeger et al. (1991) evaluated the role of intravenous gadolinium in determining neurovascular involvement. When comparing non-contrast T1W SE images, where tumour is seen as intermediate SI tissue invading the high SI fat around the neurovascular bundle, the addition of gadolinium reduced the contrast between tumour and fat; however, Gronemeyer et al. (1997) showed that fat-saturated contrast-enhanced T1W SE

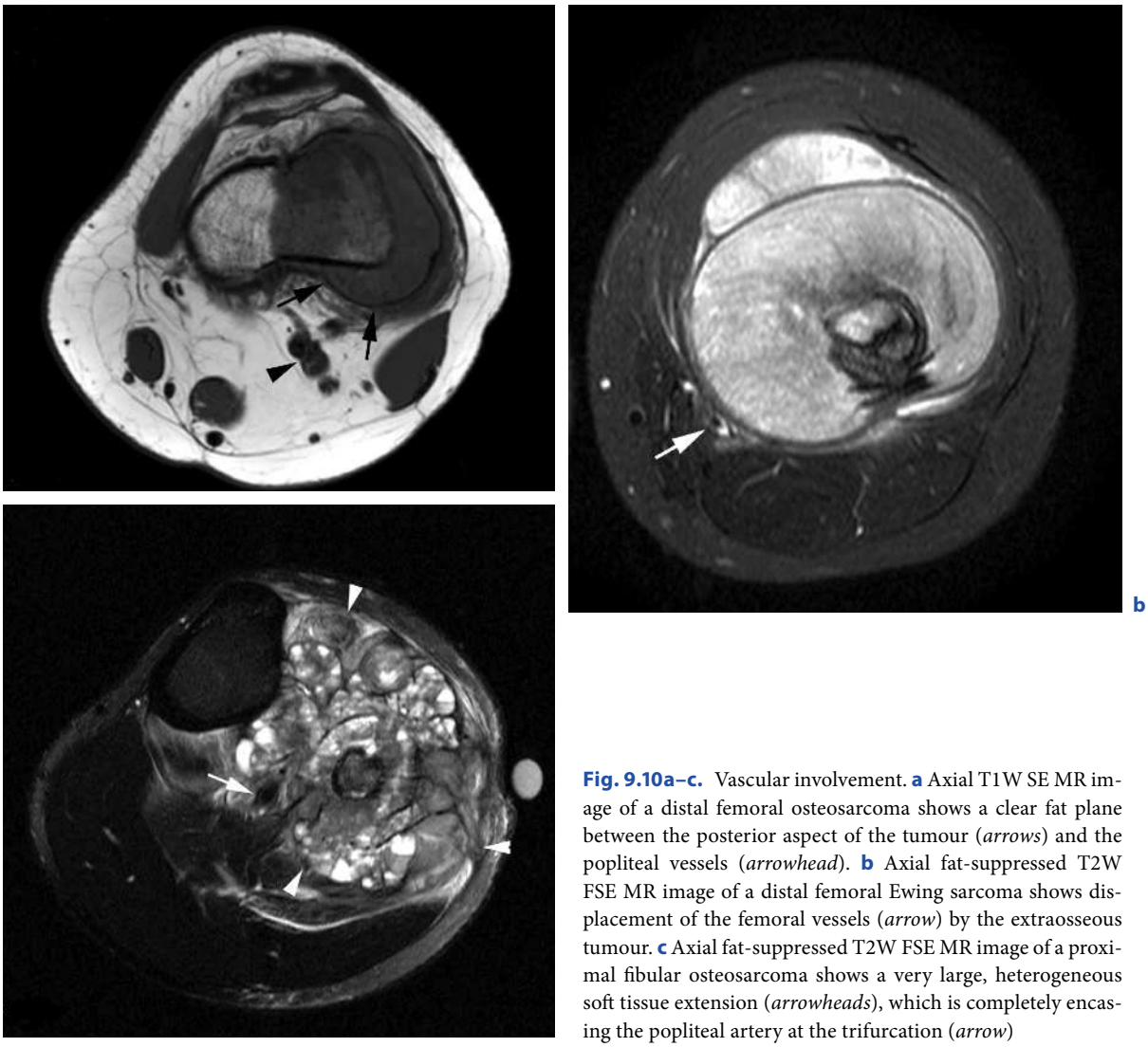

Fig. 9.10a–c. Vascular involvement. **a** Axial T1W SE MR image of a distal femoral osteosarcoma shows a clear fat plane between the posterior aspect of the tumour (*arrows*) and the popliteal vessels (*arrowhead*). **b** Axial fat-suppressed T2W FSE MR image of a distal femoral Ewing sarcoma shows displacement of the femoral vessels (*arrow*) by the extraosseous tumour. **c** Axial fat-suppressed T2W FSE MR image of a proximal fibular osteosarcoma shows a very large, heterogeneous soft tissue extension (*arrowheads*), which is completely encasing the popliteal artery at the trifurcation (*arrow*)

sequences were superior to conventional T2W images. The routine use of intravenous contrast requires cannulation, which can be traumatic, is time-consuming, especially in children, and is not without risk of adverse reaction.

In a more recent study by Feydy et al. (2006), the accuracies of contrast-enhanced MR angiography (MRA) and conventional MRI were compared for evaluating vascular invasion. On MRA, the presence of a stenosis was 82% sensitive, 85% specific and had an accuracy of 84% for vascular invasion. This was compared with a 64% sensitivity, 95% specificity and an accuracy of 84% on conventional MR imaging. By combining the two studies they showed that this increased the specificity to 100% and accuracy to 90%, although sensitivity remained low at 79%. If they had included the loss of fat around the vessels as a sign of vascular invasion, this would have improved sensitivity but at the expense of specificity. The number of patients in their study was small (31 patients with 11 cases of vascular invasion), and further evidence is required to confirm if the added study time and use of contrast is of enough benefit to justify performing MRA in selected cases where vascular invasion is suspected.

As tumour tends to be relatively hyperintense on T2-weighted FSE sequences, and this gives the maximal contrast between tumour and muscle, but the neurovascular bundle can be difficult to appreciate. Our experience suggests that axial PDW FSE images give optimal definition of the bone cortex, periosteum, extraosseous tumour, muscle compartment and neurovascular bundle (Fig. 9.11a), whereas the addition of fat suppression reduces the signal from perivascular fat, thus increasing the contrast between tumour and vessels (Fig. 9.11b). Assessment of neurovascular and muscle involvement is optimally demonstrated in the axial plane (Saifuddin et al. 2000b).

A significant proportion of high-grade primary malignant bone tumours will have an extraosseous component at the time of presentation (Boyko et al. 1987; Saifuddin et al. 2000a). As well as the neurovascular structures, it is important to document which muscle compartments are involved (see Chap. 38). Table 9.4 lists the important anatomical structures that need to be identified for various sites in the appendicular skeleton.

Extraosseous tumour-related oedema has a "feathery" appearance, does not demonstrate any mass effect (Fig. 9.12a) and has poorly defined margins with a SI on fat-suppressed T2W FSE and STIR sequences that is lower than the tumour itself (Alyas et al. 2007; Golfieri et al. 1990; Hanna et al. 1991). On conventional post-contrast T1W SE imaging, peritumoral oedema may demonstrate isointense or hyperintense enhancement compared with the tumour, which does not allow differentiation between oedematous uninvolved muscle and tumour infiltrated muscle (Fig. 9.12b; Seeger et al. 1991); however, DEMRI can aid in the differentiation of tumour from adjacent oedema due to its delayed enhancement, oedema having an enhancement curve with a slope at least 20% less than the tumour itself (Lang

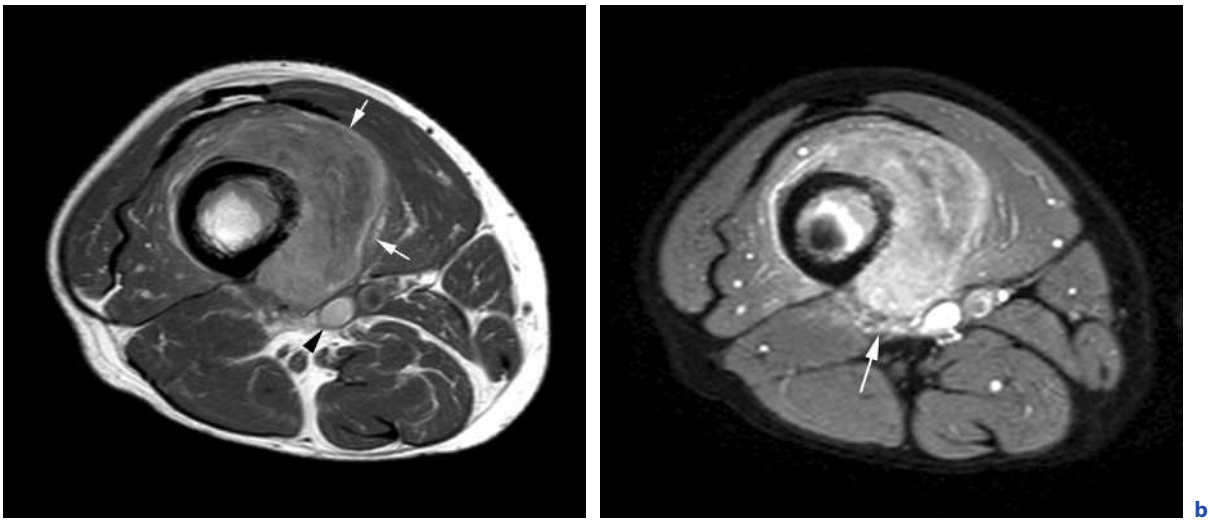

Fig. 9.11a,b. Use of PDW sequences for extraosseous tumour assessment in a patient with a malignant tumour of the femoral diaphysis. **a** Axial PDW FSE MR image clearly shows the differentiation between extraosseous tumour (*arrows*), muscle, bone cortex and the femoral vessels (*arrowhead*). **b** Fat-suppressed PDW FSE MR image shows a small amount of peritumoral oedema (*arrow*)

Table 9.4. Anatomical structures for various sites in the appendicular skeleton

Site	Structures
Proximal humerus	Distal brachial plexus; axillary artery and vein quadrilateral space; tumour relationship to the deltoid insertion[a]; glenohumeral joint
Humeral shaft/distal humerus	Brachial vessels; median, radial and ulnar nerves; elbow joint
Proximal forearm	Brachial vessels; median, radial, ulnar and posterior interosseous nerves; elbow joint
Distal forearm	Radial nerve and artery; ulnar nerve and artery; wrist joint
Proximal femur[c]	Femoral vessels/nerve and sciatic nerve; hip joint; greater trochanter[b]
Femoral shaft[c]	Femoral vessels/nerve and sciatic nerve
Distal femur[c]	Popliteal vessels; tibial and common peroneal nerves; knee joint
Proximal tibia/fibula	Popliteal trifurcation and anterior tibial artery through interosseous membrane; tibial and common peroneal nerves
Tibial/fibular shaft Distal tibia/fibular	Anterior/posterior tibial and peroneal vessels; tibial and peroneal nerves; ankle joint
Fibular shaft Distal fibula	Posterior tibial neurovascular bundle

[a] This is important since the ability to preserve the deltoid muscle will significantly improve shoulder function

[b] If the greater trochanter is free of tumour, the abductor insertions can be preserved, improving hip function and stability

[c] For femoral tumours, relationship to the extensor mechanism is important since if all the anterior compartment muscles and the femoral nerve are involved, and have to be sacrificed, the knee cannot be locked in extension and arthrodesis or amputation need to be considered

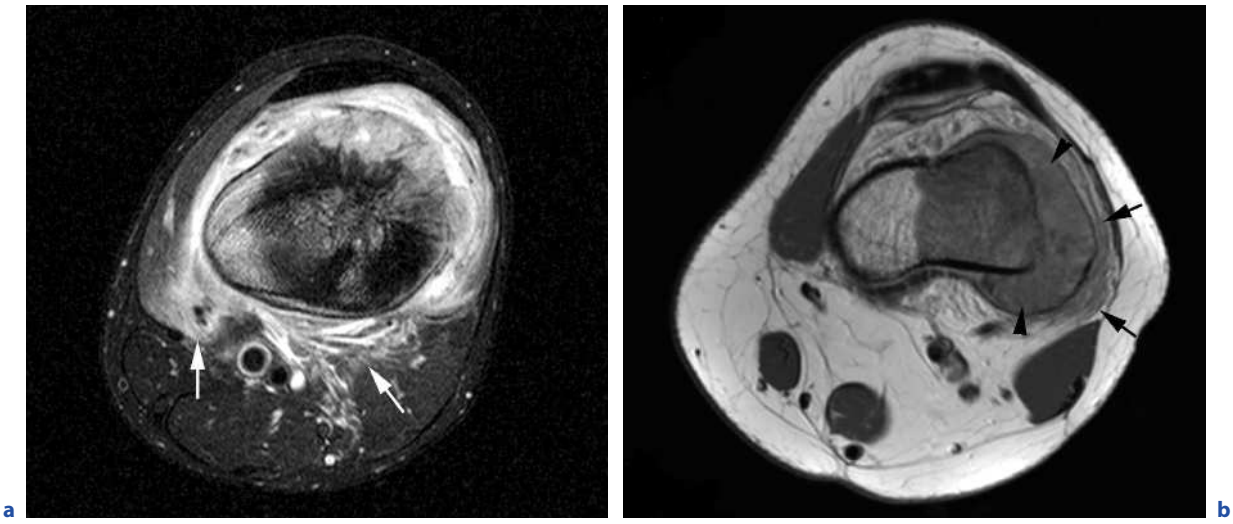

a **b**

Fig. 9.12a,b. MRI appearance of tumour-related oedema. **a** Axial fat-suppressed T2W FSE MR image of a distal femoral osteosarcoma shows feathery increased SI of oedema (*arrows*) in the popliteal fossa. **b** Axial post-contrast T1W SE MR image of a distal femoral osteosarcoma (same case as Fig. 9.10a) shows enhancement of tumour-related oedema (*arrows*) to the same degree as extraosseous tumour (*arrowheads*)

et al. 1995). There are no studies correlating the presence of oedema and local recurrence.

Massive oedema represents oedema that is seen to involve the whole of a muscle in continuity with its attachment to bone, which has been disrupted by tumour, and is most commonly seen with osteosarcoma. Patients with this pattern of oedema are more likely to have large tumours and distant metastases at presentation (Hanna et al. 1991).

9.4 Staging of Tumours of the Shoulder Girdle

Tumours arising from the scapula may be managed with partial scapulectomy, or may require forequarter amputation. The major criterion which will determine the type of resection is involvement of the glenoid, the axillary vessels and the brachial plexus. If the glenoid is

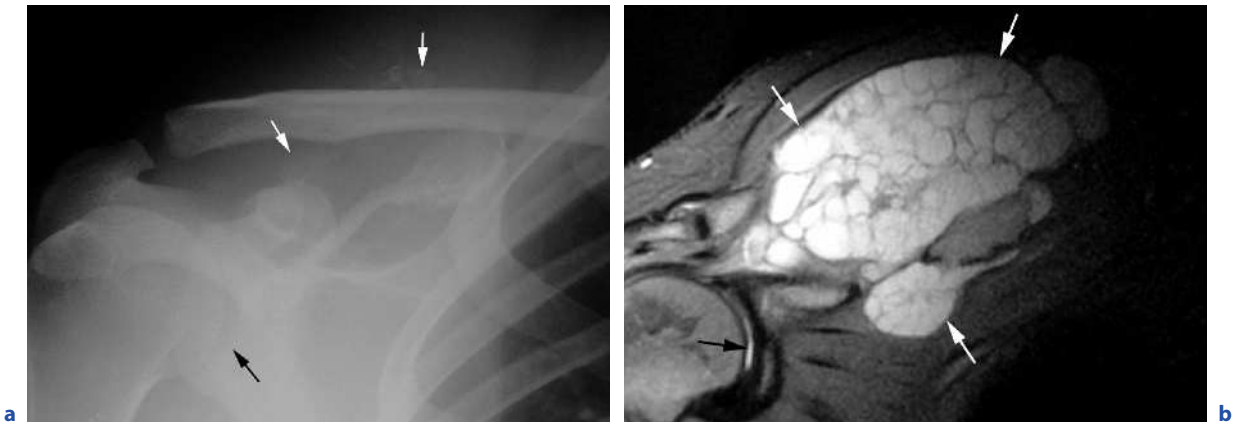

Fig. 9.13a,b. Low-grade chondrosarcoma of the scapular spine. **a** Anteroposterior radiograph shows a mineralised mass (*white arrows*) arising from the scapular spine, with no involvement of the glenohumeral joint (*black arrow*). **b** Coronal fat-suppressed T2W FSE MR image shows the typical hyperintense, lobular appearance of a chondral tumour (*white arrows*) with an intact glenoid (*black arrow*)

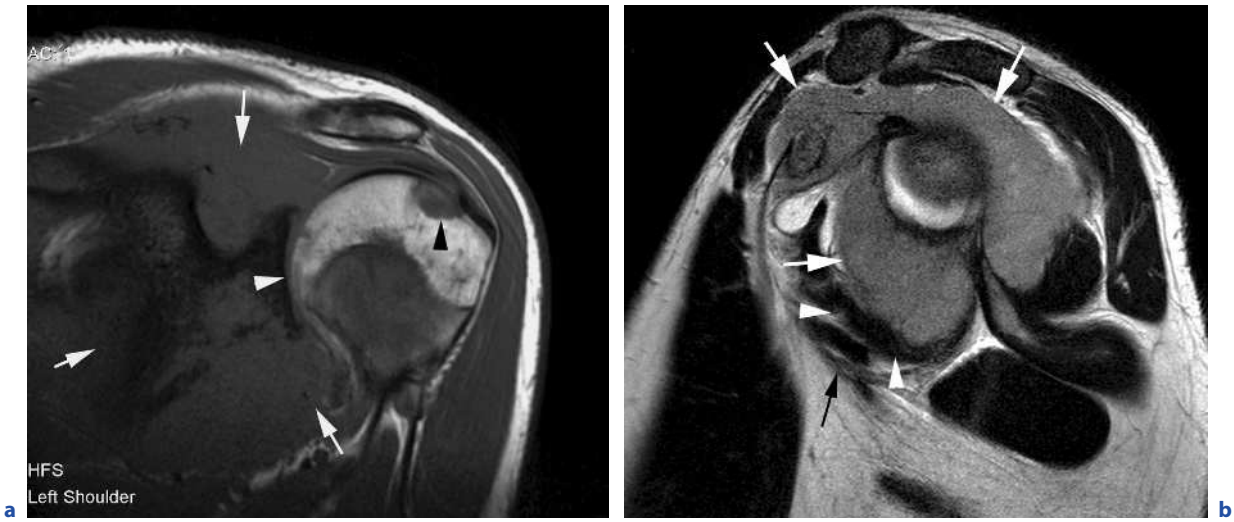

Fig. 9.14a,b. Ewing sarcoma of the left scapula. **a** Coronal T1W SE MR image shows a large tumour mass (*arrows*) extending to involve the glenoid (*white arrowhead*). A transarticular skip lesion is present in the humeral head (*black arrowhead*). **b** Sagittal T2W FSE image shows the intermediate SI mass (*white arrows*) which is separated from the axillary vessels and brachial plexus (*black arrow*) by the subscapularis muscle (*arrowheads*)

not involved and the vessels/plexus are clear (Fig. 9.13), the shoulder girdle and upper limb can be spared by performing a partial scapulectomy; however, involvement of the glenoid (Fig. 9.14a) together with the vessels/plexus will require forequarter amputation. Large scapular tumours can involve the brachial plexus and axillary vessels, but these are usually separated from tumour by an intact subscapularis muscle (Fig. 9.14b). If the glenohumeral joint is involved by tumour, but the vessels and plexus are clear, the patient can be treated by total scapulectomy and resection of the lateral clavicle and glenohumeral joint leaving a poorly functioning "hanging" upper limb (modified Tikoff-Lindberg procedure), or with a limited shoulder girdle reconstruction.

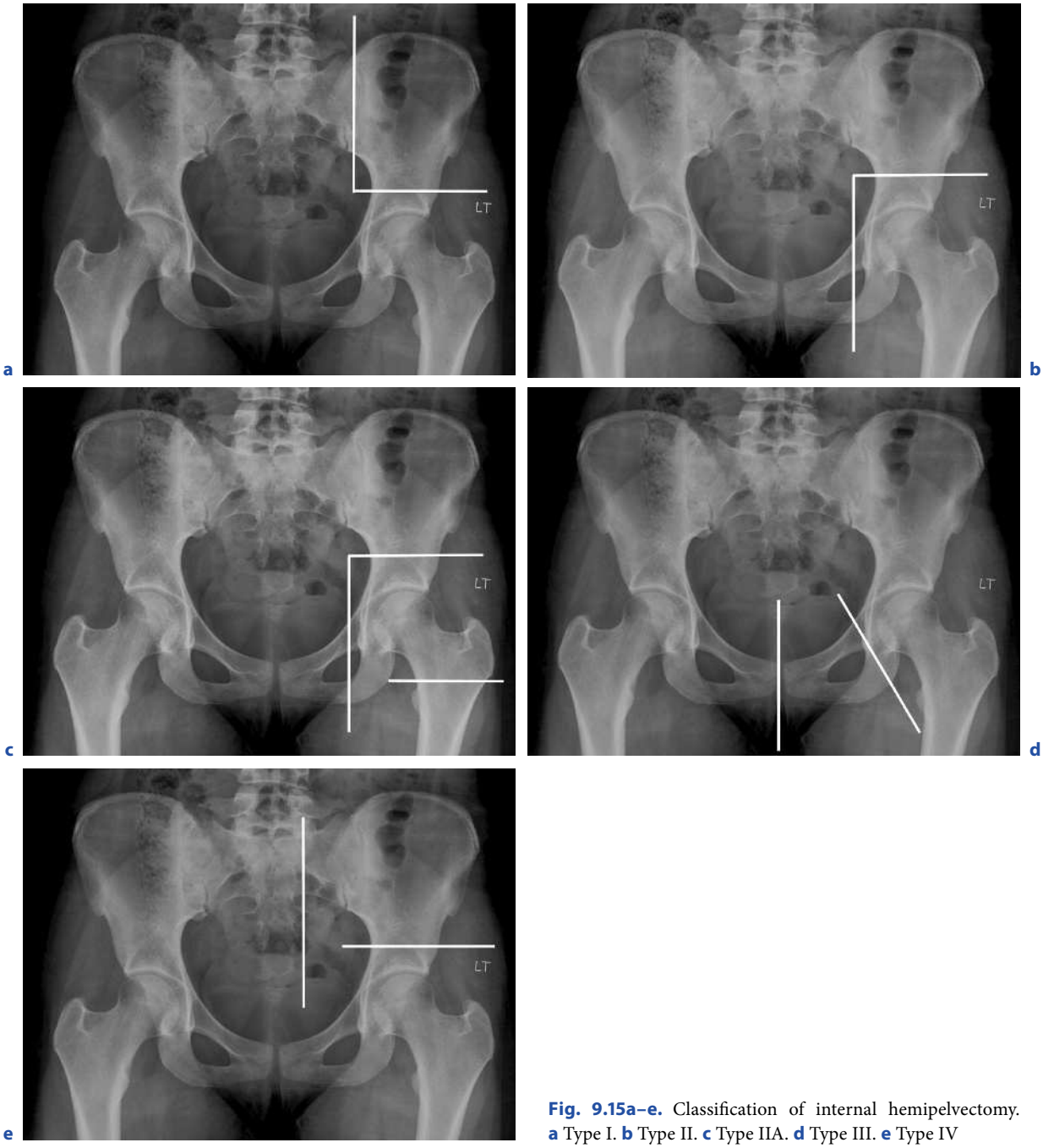

Fig. 9.15a–e. Classification of internal hemipelvectomy. **a** Type I. **b** Type II. **c** Type IIA. **d** Type III. **e** Type IV

9.5 Staging of Tumours of the Bony Pelvis

Hindquarter amputation (classical hemipelvectomy) was for decades the standard treatment for large tumours involving the proximal thigh, groin or the periacetabular region. An extended hemipelvectomy includes resection of the sacrum through the neural foramina. If resection includes a viscus in addition to any part of the bony pelvis, it is termed compound hemipelvectomy.

In recent years, internal hemipelvectomy with limb salvage has become more popular than classical hemipelvectomy (Fig. 9.15; Huth et al. 1988). Internal hemipelvectomy involves resection of part or all of the innominate bone with limb preservation. The surgical classification for internal hemipelvectomy was initially proposed by Enneking and Dunham (1978) and is presented in Table 9.5.

This classification system is somewhat impractical, however, as tumours do not confine themselves to bony pelvic segments, and the advent of MRI has resulted in a more accurate staging of bone and soft tissue extent of tumour (Fig. 9.16). A more recent classification system proposed by Mayilvahanan and Bose (2005) is based on the anatomical segments resected, including the bony as well as soft tissue resections.

The ability to avoid hindquarter amputation is largely dependent upon involvement of the sacroiliac joint (SIJ), acetabulum and iliac vessels. Involvement of both the SIJ and acetabulum renders limb salvage impossible (Fig. 9.16). The SIJ is the commonest joint invaded by tumour (Abdelwahab et al. 1991). Assessment of trans-articular tumour invasion across the SIJ is of critical importance as it necessitates an extended or external hemipelvectomy, which is a much more demanding procedure due to the complex regional anatomy and close relationship to the lumbosacral plexus. Similarly, a sacrectomy may be extended to include resection of the SIJ. Chhaya et al. (2005) defined SIJ involvement as direct, contiguous tumour extension across the joint as demonstrated on axial and oblique coronal T1W SE and fat-suppressed T2W FSE images. In their study, 12 of 24 patients demonstrated imaging and histopathological evidence of SIJ invasion. There were no cases of false-positive or false-negative SIJ involvement. Tumour was demonstrated to preferentially cross the joint at its interosseous ligamentous portion, and therefore, it is important to pay particular attention to this area when staging pelvic tumours adjacent to the SIJ. Invasion of the hip joint by periacetabular tumours should also be carefully assessed (Fig. 9.17).

Table 9.5. Pelvic surgical resection classification. (Modified from Enneking and Dunham 1978). *SIJ* sacroiliac joint

Type	Surgical resection
Type I	Wide excision of part or the whole of the iliac blade from the SIJ to the neck of the ilium (see Fig. 9.15a)
Type IA	Type I plus wide excision or radical resection of the gluteal muscles and sciatic nerve
Type II	Periacetabular excision/wide excision of the whole acetabulum, adjacent neck of ilium, ischium and lateral portion of the pubic rami (see Fig. 9.15b)
Type IIA	Type II plus excision of the proximal femur for tumours invading the hip joint (see Fig. 9.15c)
Type III	Pubic excision/wide excision of a portion or the whole of the pubis from the symphysis to the lateral margin of the obturator foramen, preserving the hip joint (see Fig. 9.15d)
Type IIIA	Radical resection of the pubic rami, femoral neurovascular bundle and enveloping muscles with preservation of the hip joint
Type IV	En-bloc resection of the ilium and sacral ala (extended type-I resection; see Fig. 9.15e)

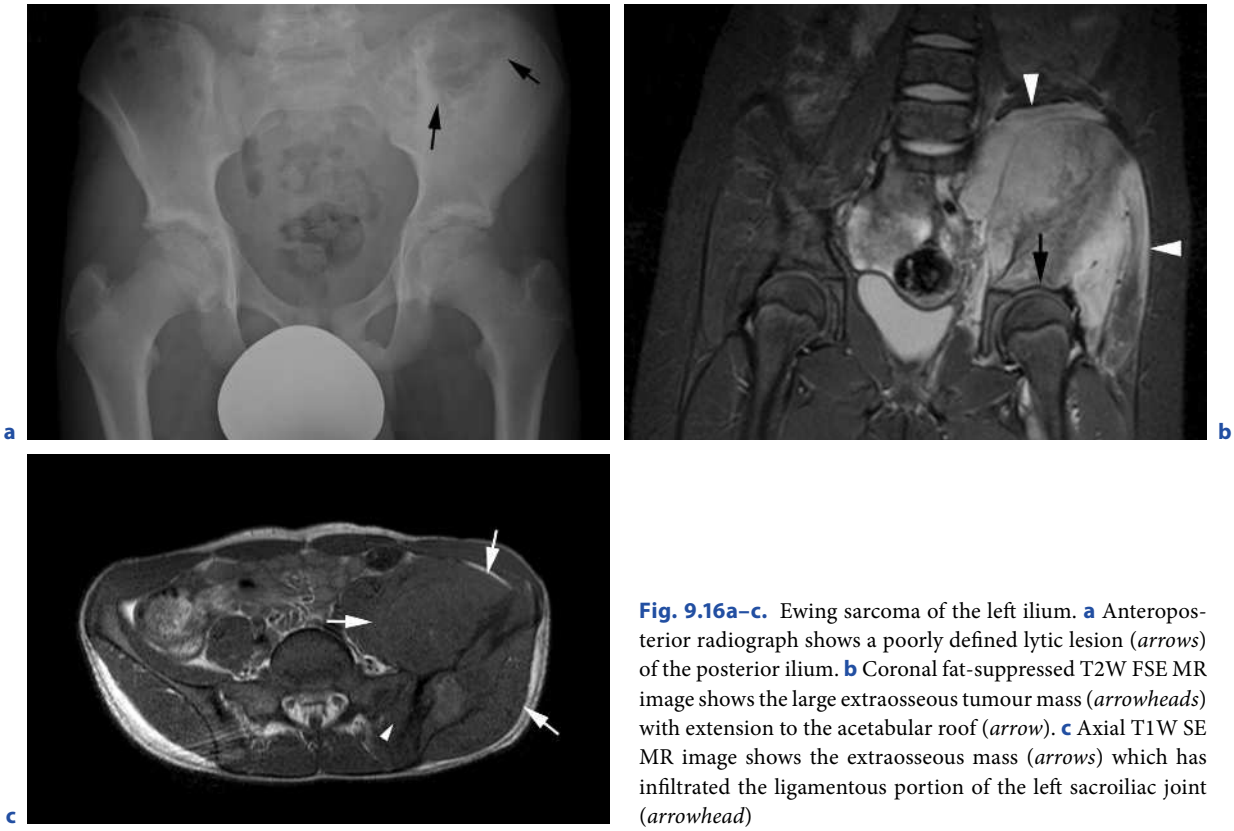

Fig. 9.16a–c. Ewing sarcoma of the left ilium. **a** Anteroposterior radiograph shows a poorly defined lytic lesion (*arrows*) of the posterior ilium. **b** Coronal fat-suppressed T2W FSE MR image shows the large extraosseous tumour mass (*arrowheads*) with extension to the acetabular roof (*arrow*). **c** Axial T1W SE MR image shows the extraosseous mass (*arrows*) which has infiltrated the ligamentous portion of the left sacroiliac joint (*arrowhead*)

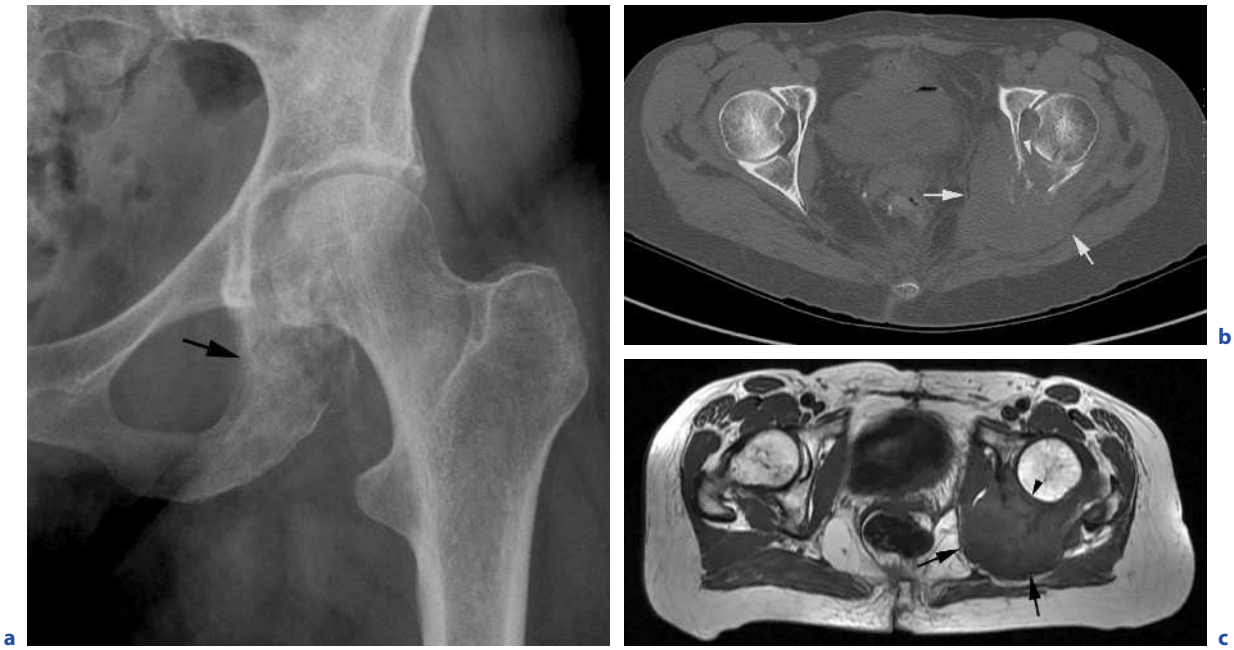

Fig. 9.17a–c. Post-radiation sarcoma of the ischium. **a** Anteroposterior radiograph of the left hip shows a destructive lesion of the ischium (*arrow*). **b** CT shows the extraosseous tumour mass (*arrows*) and destruction of the posterior acetabular wall (*arrowhead*). **c** Axial T1W SE MR images shows the extraosseous tumour mass (*arrows*) and extension of intra-articular tumour to the femoral head (*arrowhead*)

9.6 Conclusion

Proper selection of appropriate imaging techniques for the evaluation of a patient with a suspected bone tumour is crucial for accurate local staging. Recent changes in the AJCC system emphasises the importance of tumour size over trans-cortical extension and also address skip metastases. Magnetic resonance imaging is the imaging technique of choice for local staging, although consensus is lacking on the definition of neurovascular involvement and joint extension. There is little evidence for the role of static post-contrast MR imaging, although DEMRI may be more useful in improving the accuracy of local staging.

References

Abdelwahab IF, Miller TT, Hermann G et al. (1991) Transarticular invasion of joints by bone tumours: hypothesis. Skeletal Radiol 20:279–283

Aegerter E, Kirkpatrick JA (1975) Orthopedic diseases: physiology, pathology, radiology, 4th edn. Saunders, Philadelphia, pp 519–520

Alkalay D, Kollender Y, Mozes M et al. (1998) Transarticular tumor invasion via ligamentum teres: a clinical pathologic study of 12 patients. Acta Orthop Scand (Suppl) 445:25–35

Alyas F, James SL, Davies AM et al. (2007) The role of MR imaging in the diagnostic characterisation of appendicular bone tumours and tumour-like conditions. Eur Radiol 17:2675–2686

American Joint Committee on Cancer (1997) Bone. In: Fleming ID, Cooper JS, Henson DE et al. (eds) AJCC cancer staging manual. Lippincott-Raven, Philadelphia, pp 143–147

American Joint Committee on Cancer (2002) Bone. In: Greene FL, Page DL, Fleming ID et al. (eds) AJCC cancer staging manual. Springer, Berlin Heidelberg New York, pp 213–219

Ardran GM (1951) Bone destruction not demonstrable by radiography. Br J Radiol 24:107–109

Bhagia SM, Grimer RJ, Davies AM et al. (1997) Scintigraphically negative skip metastasis in osteosarcoma. Eur Radiol 7:1446–1448

Bloem JL, Taminiau AH, Eulderink F et al. (1988) Radiologic staging of primary bone sarcoma: MR imaging, scintigraphy, angiography, and CT correlated with pathologic examination. Radiology 169:805–810

Bohndorf K, Reiser M, Lochner B et al. (1986) Magnetic resonance imaging of primary tumours and tumour-like lesions of bone. Skeletal Radiol 15(7):511–517

Boyko OB, Cory DA, Cohen MD et al. (1987) MR imaging of osteogenic and Ewing's sarcoma. Am J Roentgenol 148:317–322

Brisse H, Ollivier L, Edeline V et al. (2004) Imaging of malignant tumours of the long bones in children: monitoring response to neoadjuvant chemotherapy and preoperative assessment. Pediatr Radiol 34:595–605

Chew FS, Hudson TM (1982) Radionuclide bone scanning of osteosarcoma: falsely extended uptake patterns. Am J Roentgenol 139:49–54

Chhaya S, White LM, Kandel R et al. (2005) Transarticular invasion of bone tumours across the sacroiliac joint. Skeletal Radiol 34:771–777

Davies AM, Makwana NK, Grimer RJ et al. (1997) Skip metastases in Ewing's sarcoma: a report of three cases. Skeletal Radiol 26:379–384

Egmont-Petersen M, Hogendoorn PCW, van der Geest RJ et al. (2000) Detection of areas with viable remnant tumor in postchemotherapy patients with Ewing's sarcoma by dynamic contrast-enhanced MRI using pharmacokinetic modeling. Magn Reson Imaging 18:525–535

El Khadrawy AM, Hoffer FA, Reddick WA (1999) Ewing sarcoma recurrence vs radiation necrosis in dynamic contrast-enhanced MR imaging: a case report. Pediatr Radiol 29:272–274

Enneking WF, Dunham WK (1978) Resection and reconstruction for primary neoplasms involving the innominate bone. J Bone Joint Surg Am 60:731–746

Enneking WF, Kagan A (1975) Skip metastases in osteosarcoma. Cancer 36:2192–2205

Enneking WF, Kagan A (1978) Transepiphyseal extension of osteosarcoma: incidence, mechanism, and implications. Cancer 41:1526–1537

Enneking WF, Spanier SS, Goodman MA (1980) A system for the surgical staging of musculoskeletal sarcoma. Clin Orthop 153:106–120

Feydy A, Anract P, Tomeno B et al. (2006) Assessment of vascular invasion by musculoskeletal tumors of the limbs: use of contrast enhanced MR angiography. Radiology 238:611–621

Gillespy T III, Manfrini M, Ruggieri P et al. (1988) Staging of intraosseous extent of osteosarcoma: correlation of preoperative CT and MR imaging with pathologic macroslides. Radiology 167:765–767

Golfieri R, Baddeley H, Pringle JS et al. (1990) The role of the STIR sequence in magnetic resonance imaging examination of bone tumours. Br J Radiol 1990 63:251–256

Golfieri R, Baddeley H, Pringle JS et al. (1991) MRI in primary bone tumors: therapeutic implications. Eur J Radiol 12:201–207

Gronemeyer SA, Kauffman WM, Rocha MS et al. (1997) Fat-saturated contrast-enhanced T1-weighted MRI in the evaluation of osteosarcoma and Ewing sarcoma. J Magn Reson Imaging 7:585–589

Hanna SL, Fletcher BD, Parham DM et al. (1991) Muscle edema in musculoskeletal tumours: MR imaging characteristics and clinical significance. J Magn Reson Imaging 1:441–449

Hoffer FA, Nikanorov AY, Reddick WE et al. (2000) Accuracy of MR imaging for detecting epiphyseal extension of osteosarcoma. Pediatr Radiol 30:289–298

Hudson TM, Schiebler M, Springfield DS et al. (1983) Radiologic imaging of osteosarcoma: role in planning surgical treatment. Skeletal radiol 10:137–146

Huth JF, Eckardt JJ, Pignatti G et al. (1988) Resection of malignant bone tumors of the pelvic girdle without extremity amputation. Arch Surg 123:1121–1124

Kager l, Zoubek A, Kastner U et al. (2006) Skip metastases in osteosarcoma: experience of the cooperative osteosarcoma study group. J Clin Oncol 24(10):1535–1541

Kuettner KE, Pauli BU, Soble L (1978) Morphological studies on the resistance of cartilage to invasion by osteosarcoma cells in vitro and in vivo. Cancer Res 38:277

Lang P, Honda G, Roberts TW et al. (1995) Musculoskeletal neoplasms: perineoplastic edema versus tumor on dynamic postcontrast images with spatial mapping of instantaneous enhancement rates. Radiology 197:831–839

Langer R, Brem H, Falterman K et al. (1976) Isolation of a cartilage factor that inhibits tumour neovascularization. Science 193:70

Mahboubi S (1989) Radiologic approach to primary bone lesions. In: Mahboubi S (ed) Pediatric bone imaging: a practical approach. Little, Brown, Boston, pp 175

Malawer MM, Dunham WK (1983) Skip metastases in osteosarcoma: recent experience. J Surg Oncol 22:236–245

May DA, Good RB, Smith DK et al. (1997) MR imaging of musculoskeletal tumors and tumor mimickers with intravenous gadolinium: experience with 242 patients. Skeletal Radiol 26:2–15

Mayilvahanan N, Bose JC (2005) Reconstructive options in pelvic tumours. Indian J Orthop 39:151–157

Norton KI, Hermann G, Abdelwahab IF et al. (1991) Epiphyseal involvement in osteosarcoma. Radiology 180:813–816

O'Flanagan SJ, Stack JP, McGee HM et al. (1991) Imaging of intramedullary tumour spread in osteosarcoma: a comparison of techniques. J Bone Joint Surg Br 73:998–1001

Ongolo-Zogo P, Thiesse P, Sau J et al. (1999) Assessment of osteosarcoma response to neoadjuvant chemotherapy: comparative usefulness of dynamic gadolinium-enhanced spin-echo magnetic resonance imaging and technetium-99m skeletal angioscintigraphy. Eur Radiol 9:907–914

Onikul E, Fletcher BD, Parham DM et al. (1996) Accuracy of MR imaging for estimating intraosseous extent of osteosarcoma. Am J Roentgenol 167:1211–1215

Panuel M, Gentet JC, Scheiner C et al. (1993) Physeal and epiphyseal extent of primary malignant bone tumours in childhood. Pediatr Radiol 23:421–424

Peabody TD, Gibbs CP Jr, Simon MA (1998) Evaluation and staging of musculoskeletal neoplasms. J Bone Joint Surg Am 80:1204–1218

Quan GMY, Slavin JL, Schlicht SM et al. (2005) Osteosarcoma near joints: assessment and implications. J Surg Oncol 91:159–166

Reddick WE, Wang S, Xiong X et al. (2001) Dynamic magnetic resonance imaging of regional contrast access as an additional prognostic factor in pediatric osteosarcoma. Cancer 91:2230–2237

Saifuddin A (2002) The accuracy of imaging in the local staging of appendicular osteosarcoma. Skeletal Radiol 31:191–201

Saifuddin A, Mitchell, Burnett SJD et al. (2000a) Ultrasound-guided needle biopsy of primary bone tumours. J Bone Joint Surg Br 82-B:50–54

Saifuddin A, Twinn P, Emanuel R et al. (2000b) An audit of MRI for bone and soft-tissue tumours performed at referral centres. Clin Radiol 55:537–541

Sajadi KR, Heck RK, Neel MD et al. (2004) The incidence and prognosis of osteosarcoma skip metastases. Clin Orthop Relat Res 426:92–96

Schima W, Amann G, Stiglbauer R et al. (1994) Preoperative staging of osteosarcoma: efficacy of MR imaging in detecting joint involvement. Am J Roentgenol 163:1171–1175

Seeger LL, Widoff BE, Bassett LW et al. (1991) Preoperative evaluation of osteosarcoma: value of gadopentetate dimeglumine-enhanced MR imaging. Am J Roentgenol 157:347–351

Simon MA, Bos GD (1980) Epiphyseal extension of metaphyseal osteosarcoma in skeletally immature individuals. J Bone Joint Surg Am 62:195–204

Simon MA, Hecht JD (1982) Invasion of joints by primary bone sarcomas in adults. Cancer 50:1649–1655

Stacy GS, Mahal RS, Peabody TD (2006) Staging of bone tumours: a review with illustrative examples. Am J Roentgenol 186:967–976

Sundaram M (1997) The use of gadolinium in the MR imaging of bone tumors. Semin Ultrasound CT MR 18:307–311

Sundaram M, McGuire MH, Herbold DR et al. (1986) Magnetic resonance imaging in planning limb-salvage surgery for primary malignant tumours of bone. J Bone Joint Surg Am 68:809–819

Sundaram M, Merenda G, McGuire MM (1989) A skip lesion in association with Ewing's sarcoma: report of a case. J Bone Joint Surg Am 71:764–768

Tsuboyama T, Windhager R, Dock W et al. (1993) Knee function after operation for malignancy of the distal femur. Quadriceps muscle mass and knee extension strength in 21 patients with hinged endoprostheses. Acta Orthop Scand 64(6):673–677

Van Trommel MF, Kroon HM, Bloem JL et al. (1997) MR imaging based strategies in limb salvage surgery for osteosarcoma of the distal femur. Skeletal Radiol 26:636–641

Verstraete KL, Lang P (2000) Bone and soft tissue tumors: the role of contrast agents for MR imaging. Eur J Radiol 34:229–246

Wetzel LH, Schweiger GD, Levine E (1990) MR imaging of transarticular skip metastases from distal osteosarcoma. J Comput Assist Tomogr 14:315–317

Wuisman P, Enneking WF (1990) Prognosis for patients who have osteosarcoma with skip metastasis. J Bone Joint Surg Am 72:60–68

Surgical Staging 2: Metastatic Disease

10

Ambrose J. huang, Marc H. Willis, Susan V. Kattapuram
and Miriam A. Bredella

CONTENTS

KEY POINTS

- Advances in the treatment of bone sarcomas have increased patient survival.
- Accurate staging of primary bone tumors influences treatment planning, determines patient prognosis, and improves patient outcomes.
- Bone sarcomas metastasize primarily to the lungs and other bones.
- Chest CT is the most sensitive modality for detecting pulmonary metastases.
- MRI of the entire bone containing the primary tumor is the most accurate modality for the detection of skip lesions.
- Tc-99m MDP skeletal scintigraphy is traditionally the modality employed for the detection of distant osseous metastases.
- Newer imaging techniques include FDG-PET and whole body MRI, which show promise for efficient and earlier detection of distant osseous and soft tissue metastases.
- Since FDG-PET and whole body MRI have different strengths and weaknesses, their roles in tumor staging may be complementary.
- Additional studies evaluating their performance on metastases from primary bone tumors, their effect on patient outcome, and their cost-effectiveness are needed.

A. J. Huang, MD
Massachusetts General Hospital, Department of Radiology, Musculoskeletal Division, 55 Fruit Street, Yawkey 6E, Boston, MA 02114, USA

M. H. Willis, DO
Massachusetts General Hospital, Department of Radiology, Musculoskeletal Division, 55 Fruit Street, Yawkey 6E, Boston, MA 02114, USA

S. V. Kattapuram, MD
Massachusetts General Hospital, Department of Radiology, Musculoskeletal Division, 55 Fruit Street, Yawkey 6E, Boston, MA 02114, USA

M. Bredella, MD
Massachusetts General Hospital, Department of Radiology, Musculoskeletal Division, 55 Fruit Street, Yawkey 6E, Boston, MA 02114, USA

10.1 Introduction

Bone sarcomas are uncommon high-grade tumors derived from mesenchyma. Fewer than 2,500 cases are diagnosed per year in the United States, and the death rate from these tumors is decreasing (Jemal et al. 2007). Bone sarcomas encompass a heterogeneous group of malignancies, the most common of which include osteosarcoma, chondrosarcoma, Ewing sarcoma, and undifferentiated high-grade pleomorphic sarcoma (also known as malignant fibrous histiocytoma of bone) (Murphey et al. 2003; Reid 2007; Skubitz and D'Adamo 2007).

Each entity within this heterogeneous group of malignancies requires a different treatment approach (Skubitz and D'Adamo 2007), and the approaches are changing. Limb amputation was the mainstay of treatment of bone sarcomas before the 1970s, and the overwhelming majority of patients died from metastatic disease, mostly involving the lungs. Because of strides and developments in inductive and adjuvant chemotherapy, limb sparing surgery has become the standard of care (McDonald 1994). For example, more than 90% of osteosarcoma patients are currently treated with limb-sparing surgery, and 60–80% of osteosarcoma patients are long-term survivors (Link et al. 1986; Fuchs et al. 1998; Bacci et al. 2001).

Evolving treatments are delaying the appearance of metastatic disease or altering their appearance or location. This chapter reviews the most common patterns of spread of metastatic bone tumors and the imaging approach to their evaluation.

10.2 Sites of Metastatic Spread

As with other malignancies, staging of primary bone tumors is crucial because it influences treatment planning and determines patient prognosis, and patient outcomes improve with accurate staging (Enneking et al. 1980; Mentzel et al. 2004; Heck et al. 2006). Distant metastases are the most predictive factor of poor prognosis (Bacci et al. 2001; Heck et al. 2006).

10.2.1 Pulmonary Metastases

Most primary bone tumors metastasize primarily to the lungs, reflecting hematogenous spread (van der Woude et al. 1998; Bearcroft and Davies 1999; Reid 2007; Skubitz and D'Adamo 2007). Ewing sarcoma, in addition to metastasizing to the lungs, also has a particular propensity for metastasizing to marrow and other bones (Reid 2007; Skubitz and D'Adamo 2007).

The proliferation and continued improvement of multidetector CT has increased the ability to resolve pulmonary nodules of ever-decreasing size. Although the sensitivity of CT for the detection of pulmonary metastases has increased, specificity can be decreased,

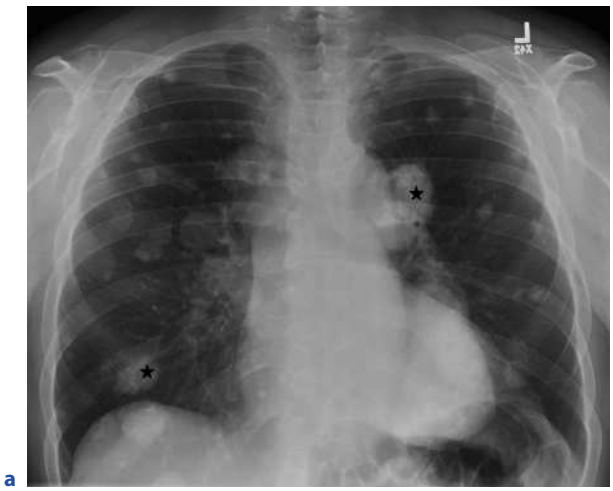

a

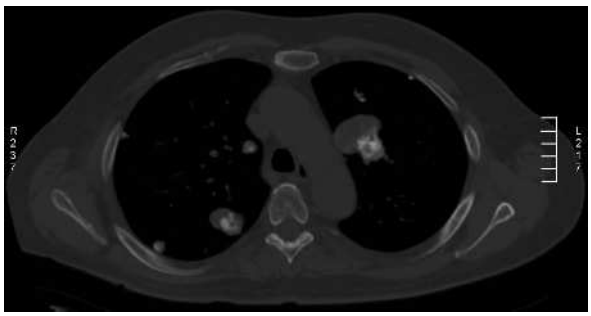

b

Fig. 10.1a–c. A 70-year-old male with osteosarcoma, primary to the left proximal femur, with calcified metastases to the lungs. **a** PA chest radiograph shows innumerable pulmonary metastases, many of which are calcified (*black stars*). **b** Chest CT demonstrates internal calcifications in several of the upper lobe lesions. (**c**) *see next page*

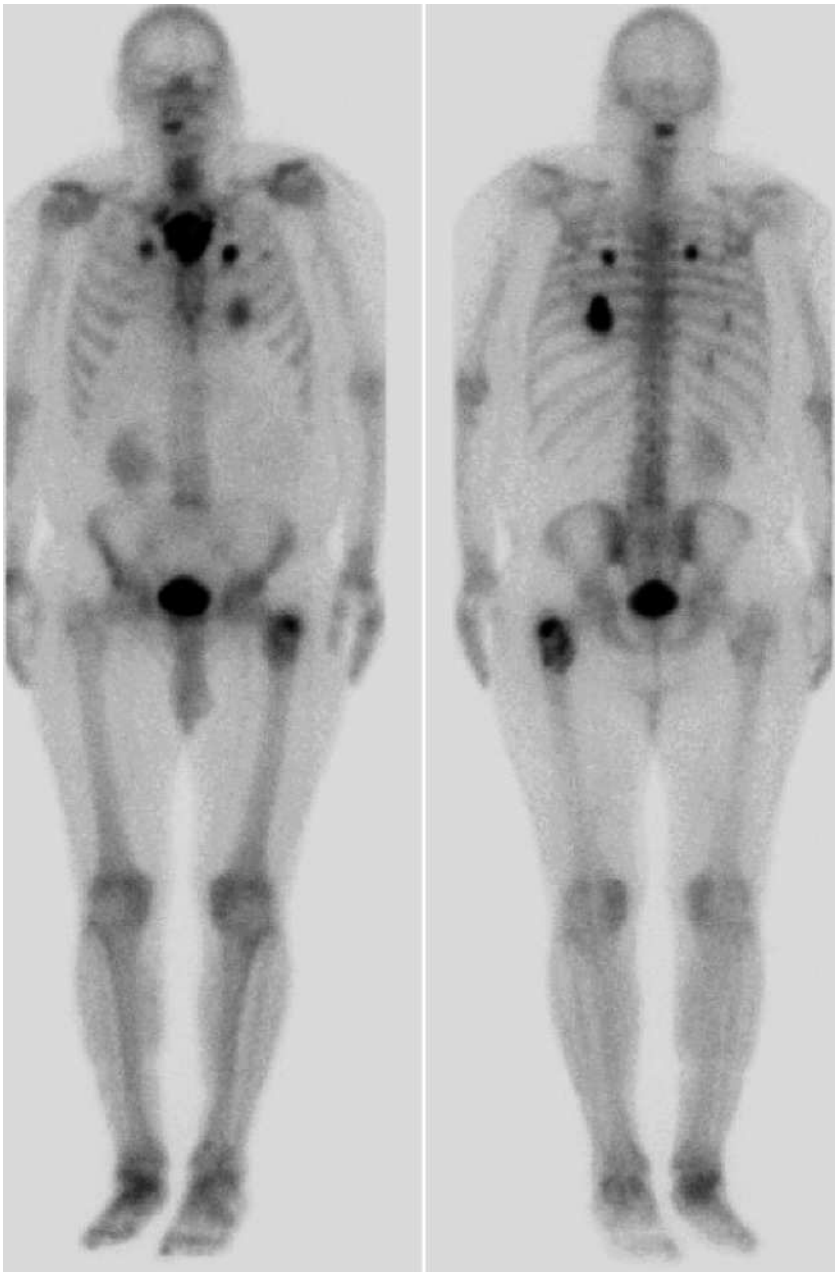

c

Fig. 10.1a–c. *(continued)* **c** Anterior and posterior images from the Tc-99m MDP skeletal scintigram show intense radiopharmaceutical uptake in numerous of the calcified pulmonary metastases as well as in the primary tumor located in the proximal left femur

especially where there is a high prevalence of non-metastatic pulmonary nodules, such as prior granulomatous infection (e.g. tuberculosis, histoplasmosis) (van der Woude et al. 1998; Bearcroft and Davies 1999; Franzius et al. 2001).

By permitting the evaluation of whether or not a pulmonary nodule exhibits increased metabolic activity, FDG-PET/CT shows promise in recovering some of that lost specificity. Franzius et al. (2001), however, showed that though specificity of FDG-PET for detection of pulmonary metastases from primary bone tumors is improved over conventional CT, sensitivity is lacking. Thus, although FDG-PET cannot be used to exclude a pulmonary metastasis, a positive result can

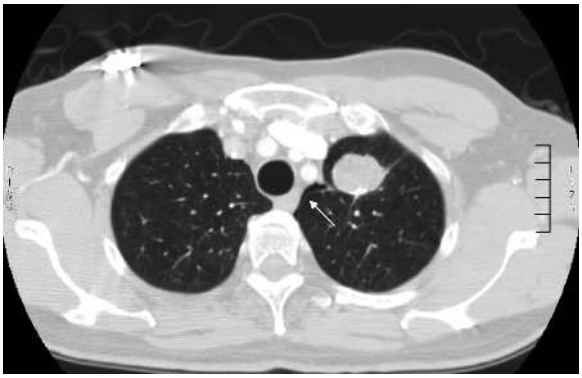

Fig. 10.2. A 65-year-old male with a left upper lobe pulmonary metastasis from osteosarcoma and a small adjacent pneumothorax (*arrow*)

be used to confirm an abnormality detected by conventional CT. Brenner et al., however, concluded that many of the studies evaluating FDG-PET used only small series, thus preventing definite conclusions from being drawn (Brenner et al. 2003).

Detection of pulmonary metastases even after the treatment of the primary tumor is important. Osteosarcoma patients with pulmonary metastases experience substantially improved 3–5-year survival rates following their surgical resection (metastasectomy), especially for solitary lesions, and cure can be achieved in up to 33% of select cases (Giritsky et al. 1978; Han et al. 1981; Putnam et al. 1983; Goorin et al. 1984; al-Jilaihawi et al. 1988; Pastorino et al. 1988; Belli et al. 1989; Carter et al. 1991b; Briccoli et al. 2005). Since most pulmonary metastases occur within two years after completion of therapy, recommended screening regimens include chest CT every 3–6 months for the first 2 years after primary surgery (Bearcroft and Davies 1999; Wittig et al. 2002).

Pulmonary metastases from primary bone tumors have similar appearances to pulmonary metastases from non-bone primary tumors. They appear as round nodules or masses. Since they are hematogenously spread, they tend to be predominantly located in the peripheral and lower lungs, where there is increased blood flow compared to the upper lungs. Osteosarcoma and chondrosarcoma metastases can occasionally appear calcified (Fig. 10.1) (Brown et al. 1994). Rarely, pulmonary metastases from primary bone sarcomas result in a spontaneous pneumothorax, postulated to be the result of necrosis and subsequent bronchopleural fistula formation (Fig. 10.2) (Seo et al. 2001).

10.2.2 Osseous Metastases

Osseous metastases of primary bone tumors appear similar to metastases from non-bone primary malignancies and can be either lytic or blastic on radiographs and CT (Fig. 10.3). On MRI, osseous metastases typically are hypointense to skeletal muscle on T1-weighted images, hyperintense on T2-weighted images, and enhance (Fig. 10.4).

Metastases to other bones can occur locally—within the same bone or across an adjacent joint—or distantly. The former are termed "skip lesions," and these are best identified by MRI (Fig. 10.5) (Wittig et al. 2002; Teo and Peh 2004; Heck et al. 2006; Stacy et al. 2006). The detection of skip lesions at the time of initial workup renders the patient's prognosis as though he or she had metastases to lymph nodes or more distant sites (Bearcroft and Davies 1999; Stacy et al. 2006).

Without a predisposing factor, such as Paget disease or previous radiation therapy, distant osseous metastases of primary bone tumors at initial presentation are rare, and in these cases pulmonary metastases are almost always present (Bearcroft and Davies 1999; Stacy et al. 2006). More often, osseous metastases occur after treatment of the primary tumor and thus perhaps are more accurately classified as recurrence. Occasionally, multifocal osseous osteosarcomas are identified at presentation, and pulmonary metastases are either absent or appear late in the course. These cases suggest a multicentric rather than a metastatic etiology and can be further classified as multiple metachronous or synchronous osteosarcomas. Metachronous osteosarcomas can manifest as multiple lesions that occur asymmetrically within long and flat bones or as new lesions that occur following successful treatment of the primary tumor, as though multiple primary osteosarcomas are present, and imply a favorable prognosis with successful treatment of each individual lesion (Fitzgerald et al. 1973; Simodynes et al. 1981). On the other hand, multiple synchronous osteosarcomas, usually bilaterally symmetric without an apparent dominant lesion, portend a poor prognosis (Jones et al. 1993; Skubitz and D'Adamo 2007).

Tc-99m MDP skeletal scintigraphy is most commonly employed to evaluate for multifocal skeletal involvement of primary bone tumors and shows increased radiopharmaceutical activity in areas of metastatic involvement (van der Woude et al. 1998; Franzius et al. 2000; Teo and Peh 2004; Heck et al. 2006; Stacy et al. 2006). Since most benign osseous lesions also demonstrate increased radiopharmaceutical activity on

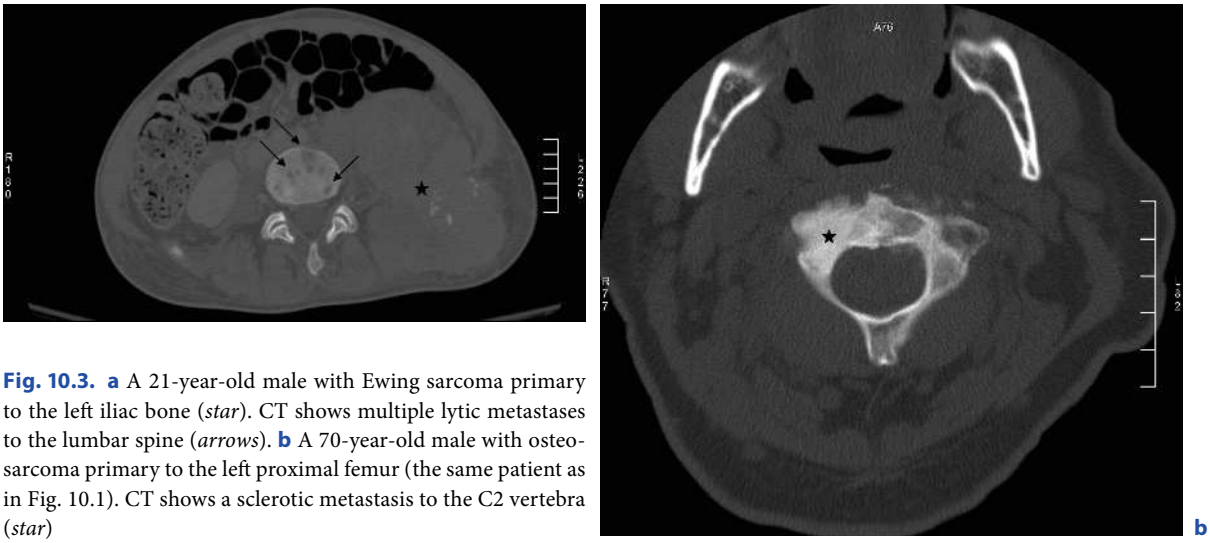

Fig. 10.3. **a** A 21-year-old male with Ewing sarcoma primary to the left iliac bone (*star*). CT shows multiple lytic metastases to the lumbar spine (*arrows*). **b** A 70-year-old male with osteosarcoma primary to the left proximal femur (the same patient as in Fig. 10.1). CT shows a sclerotic metastasis to the C2 vertebra (*star*)

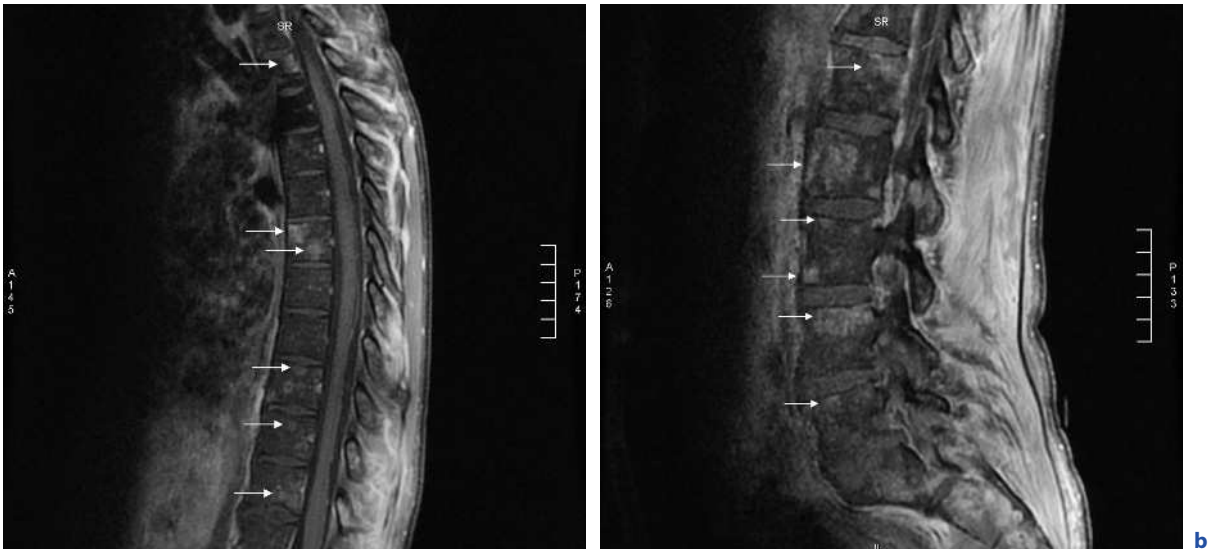

Fig. 10.4a,b. A 21-year-old male with Ewing sarcoma primary to the left iliac bone (the same patient as in Fig. 10.3a). Sagittal T1-weighted gadolinium-enhanced fat-suppressed images reveal innumerable enhancing metastases throughout the thoracic (**a**) and lumbar (**b**) spines (*arrows*)

Tc-99m MDP skeletal scintigraphy, confirmatory tests are usually required for complete evaluation of such lesions, either by imaging (e.g. radiography, CT, MRI) or tissue sampling (Teo and Peh 2004).

Although distant skeletal metastases of primary bone tumors at presentation are uncommon, their presence will affect the treatment plan (Stacy et al. 2006). Therefore, skeletal scintigraphy is recommended during initial staging. Thereafter, skeletal scintigraphy is required only when the patient reports symptomatic bone pain. Routine screening skeletal scintigraphy is not recommended, since earlier scintigraphic detection of metastases that are already present does not improve patient survival or otherwise alter patient outcome (Bearcroft and Davies 1999).

In skeletal scintigraphy, visualization of metastases is due to accumulation of radiopharmaceutical in osteoblastic new bone formation in response to the metastatic lesion (Rosenthal 1997). Tracer accumulation is dependent on blood flow to the lesion, so metasta-

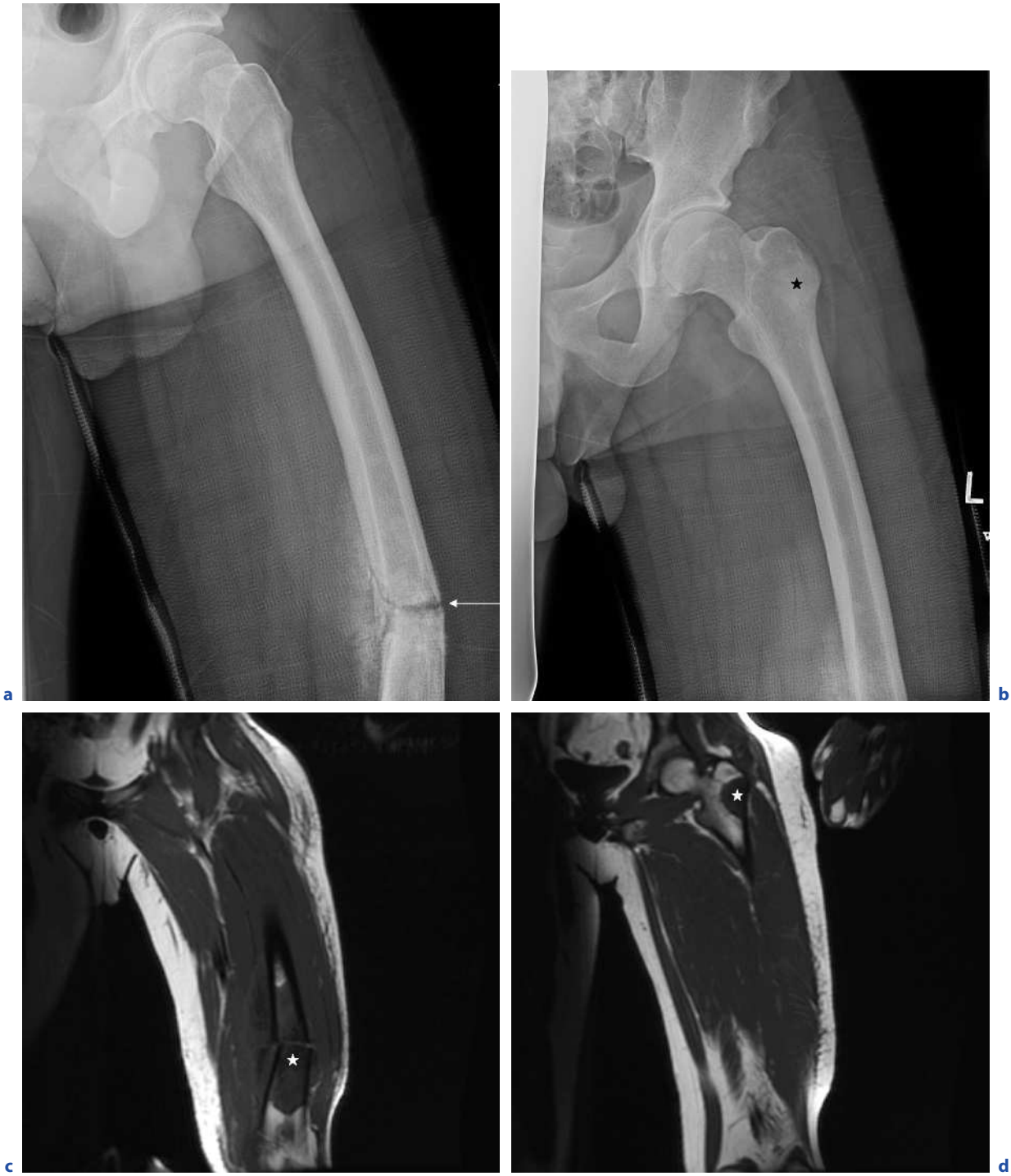

Fig. 10.5a–f. A 19-year-old with osteosarcoma of the distal femur. **a** Radiographs of the casted left femur show an intramedullary lesion in the distal diaphysis with osteoid matrix, a soft tissue component, and a pathologic fracture (*arrow*). **b** Closer inspection of the greater trochanter reveals a second sclerotic lesion (*black star*). **c** In addition to the primary lesion in the distal femur (*white star*), coronal T1-weighted MR images of the left femur reveal an intramedullary low signal intensity lesion (**d**) in the greater trochanter (*white star*), corresponding to the sclerotic lesion identified on the radiographs, and representing a skip lesion. (**e,f**) *see next page*

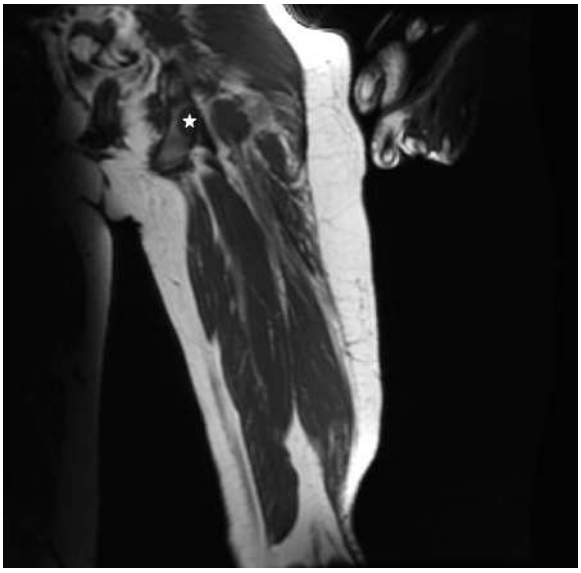

e

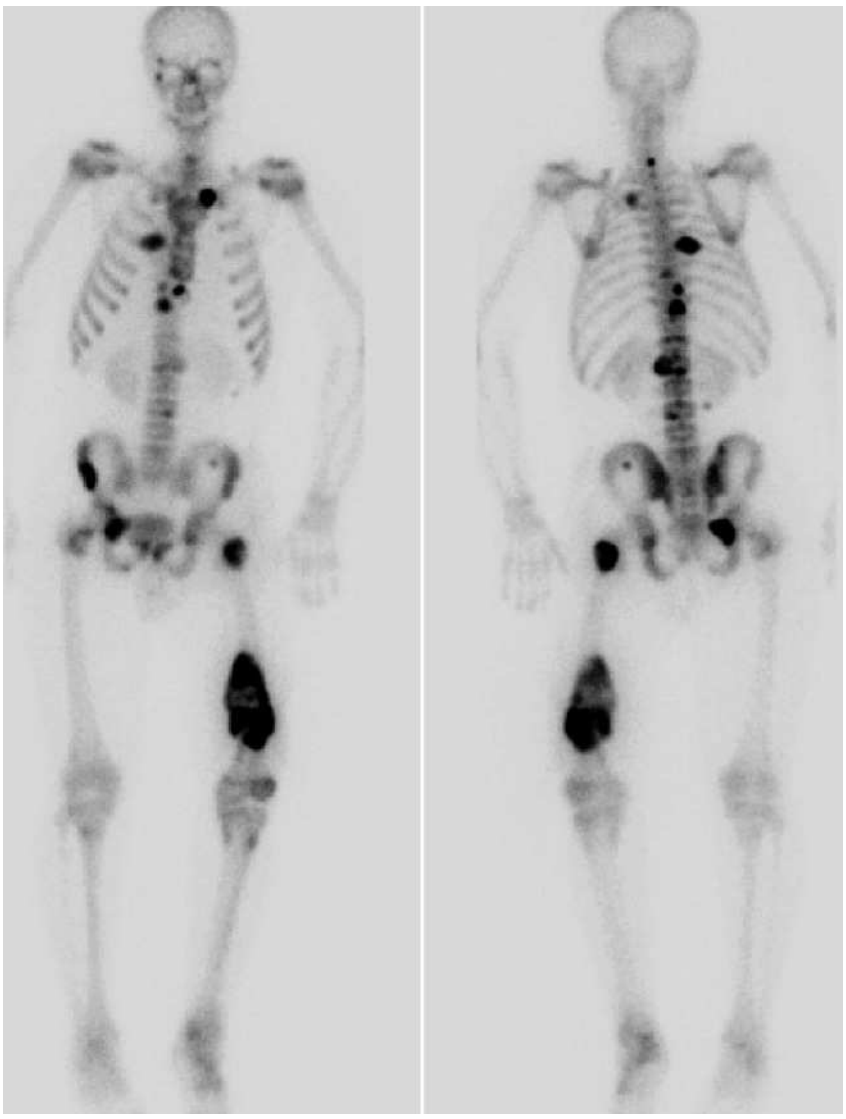

f

Fig. 10.5a–f. *(continued)* **e** An additional skip lesion is seen in the ischium (*white star*). **f** Anterior and posterior images from a Tc-99m MDP skeletal scintigram show increased radiopharmaceutical activity in the primary lesion within the distal left femur, the skip lesion in the proximal left femur and left ischium, as well as several other lesions in the spine, contralateral bony pelvis, a right rib, and the left sternoclavicular joint

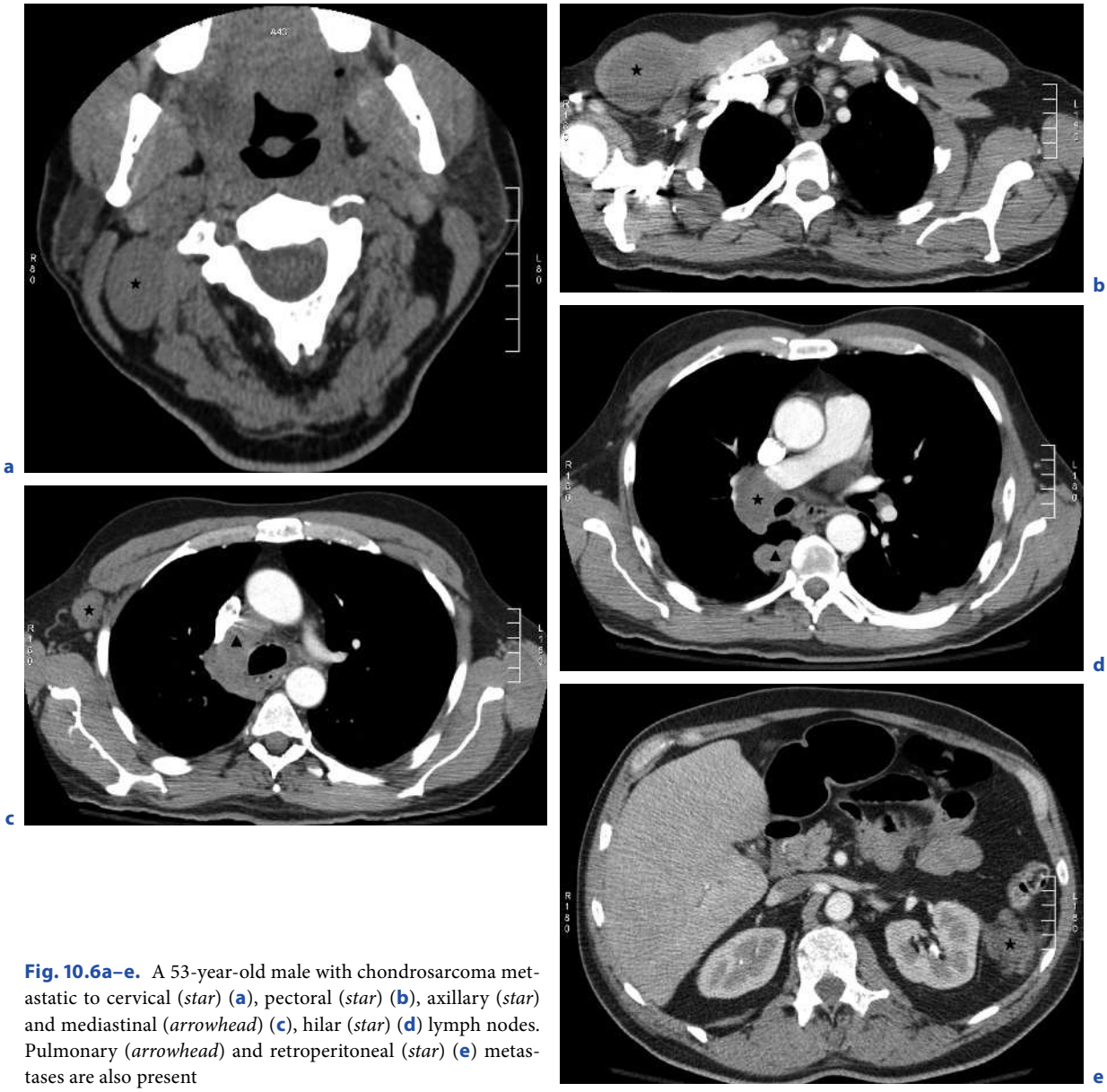

Fig. 10.6a–e. A 53-year-old male with chondrosarcoma metastatic to cervical (*star*) (**a**), pectoral (*star*) (**b**), axillary (*star*) and mediastinal (*arrowhead*) (**c**), hilar (*star*) (**d**) lymph nodes. Pulmonary (*arrowhead*) and retroperitoneal (*star*) (**e**) metastases are also present

ses with poor blood flow or aggressive lesions whose growth outstrips the body's ability to mount an osteoblastic response can be missed.

FDG-PET and whole body MRI are newer modalities that can detect skeletal metastases at an earlier stage than can skeletal scintigraphy. FDG-PET images glucose metabolism, which is increased with skeletal metastases before reactive bone formation occurs. The initial site of seeding of skeletal metastases is the bone marrow, and increased contrast between metastases and surrounding normal bone marrow allows their earlier identification with MRI.

10.2.3 Other Sites

Extrapulmonary, extraosseous sites of metastatic disease include the brain, retroperitoneum, abdominal or pelvic organs, and the mediastinum (Dalinka et al. 1971; Dunnick et al. 1981; Pakter and Fishman 1983; von Hochstetter et al. 1987; Kauffman et al. 1995; George and Zamber 1996; Salvati et al. 1998; Ryan et al. 2000; Banfic et al. 2001; van Rijswijk et al. 2001; Kpodonu et al. 2005; Secil et al. 2005; Izzo et al. 2007; Oh et al. 2007; Takeuchi et al. 2007).

These are uncommon manifestations and rarely occur outside of recurrent or metastatic disease involving the lungs or other bones. FDG-PET has shown to be sensitive in detecting these soft tissue metastases (Franzius et al. 2000; Tateishi et al. 2007). Occasionally, skeletal scintigraphy is able to detect extraosseous metastases (Bearcroft and Davies 1999).

It is rare for primary bone tumors to metastasize to lymph nodes (Fig. 10.6). Evaluation by conventional morphologic/anatomic imaging lacks specificity, and accuracy is statistically significantly improved when morphologic imaging techniques are combined with metabolic imaging techniques, e.g. FDG-PET (Tateishi et al. 2007).

Occasionally, metastases can occur at the site of the bone graft donor site or along a tract used for percutaneous biopsy of the primary lesion. These iatrogenic metastases emphasize the importance of a multidisciplinary approach to the workup and care of the patient with a primary bone tumor (Wittig et al. 2002).

10.3 Imaging Evaluation

10.3.1 CT

Chest CT has largely supplanted chest radiography for the evaluation and detection of pulmonary metastases from primary bone tumors, since chest CT allows the detection of smaller pulmonary nodules (van der Woude et al. 1998; Bearcroft and Davies 1999; Wittig et al. 2002; Heck et al. 2006; Reid 2007). Chest CT lacks specificity, however, especially in populations where there is a high prevalence of granulomatous diseases (most commonly from histoplasmosis or tuberculosis), which produce multiple small pulmonary nodules which are often calcified (van der Woude et al. 1998; Bearcroft and Davies 1999). Nevertheless, early detection of pulmonary metastases substantially affects prognosis, since long-term survival is possible if patients undergo pulmonary metastasectomy, especially if the metastases are solitary (Goorin et al. 1984; Belli et al. 1989; Carter et al. 1991a; Mialou et al. 2005). Although the optimal imaging interval has not been determined, most groups recommend chest CT every 3–6 months for the first 2 years after primary surgery, when pulmonary metastases are most likely to occur (Bearcroft and Davies 1999; Wittig et al. 2002).

10.3.2 MRI

MRI of the bone containing the primary tumor site is the most accurate modality for the detection of skip lesions, either within the same bone or across the adjacent joint (McDonald 1994; Wittig et al. 2002; Stacy et al. 2006). This is due to the increased contrast resolution between the lesion and surrounding normal marrow. These lesions often can be missed on other modalities, including radiography, CT, and skeletal scintigraphy (Bloem et al. 1988; Bhagia et al. 1997; Bearcroft and Davies 1999; Heck et al. 2006). Skip lesions often have the same imaging features as the primary lesion.

10.3.3 Tc-99m MDP Skeletal Scintigraphy

The ability for whole body imaging renders Tc-99m MDP skeletal scintigraphy advantageous for the detection of distant osseous metastases. Metastatic foci will most often appear as foci of increased radiopharmaceutical activity at the involved location, since the lesions generate an osteoblastic response. Increased radiopharmaceutical activity is not specific for skeletal metastases, since many benign bone lesions appear similar, including trauma, infection, and degenerative joint disease. When such foci are detected, anatomic imaging studies, such as radiography, CT, or MRI of the involved area can occasionally be helpful to confirm or deny the presence of a metastatic lesion (Teo and Peh 2004; Heck et al. 2006). Occasionally, Tc-99m MDP skeletal scintigraphy identifies non-osseous osteosarcoma metastases (Fig. 10.1) (Brown et al. 1994; Kauffman et al. 1995).

The presence of osseous metastatic disease indicates widespread dissemination of tumor, and scintigraphic detection of these lesions after the initial staging period does not change patient outcome or improve survival (Bearcroft and Davies 1999). Thus, routine screening Tc-99m MDP skeletal scintigraphy is not generally recommended.

Before osseous metastases have had time to produce an osteoblastic response, they may appear as foci of decreased radiopharmaceutical activity, since they occupy the intramedullary space of the involved bone and decrease the ability of the radiopharmaceutical to accumulate in that area. These lesions are more subtle and difficult to detect compared to lesions that generate an osteoblastic response and therefore can be missed (Basu et al. 2008). Newer imaging techniques for earlier detection of osseous metastatic disease focus on bone

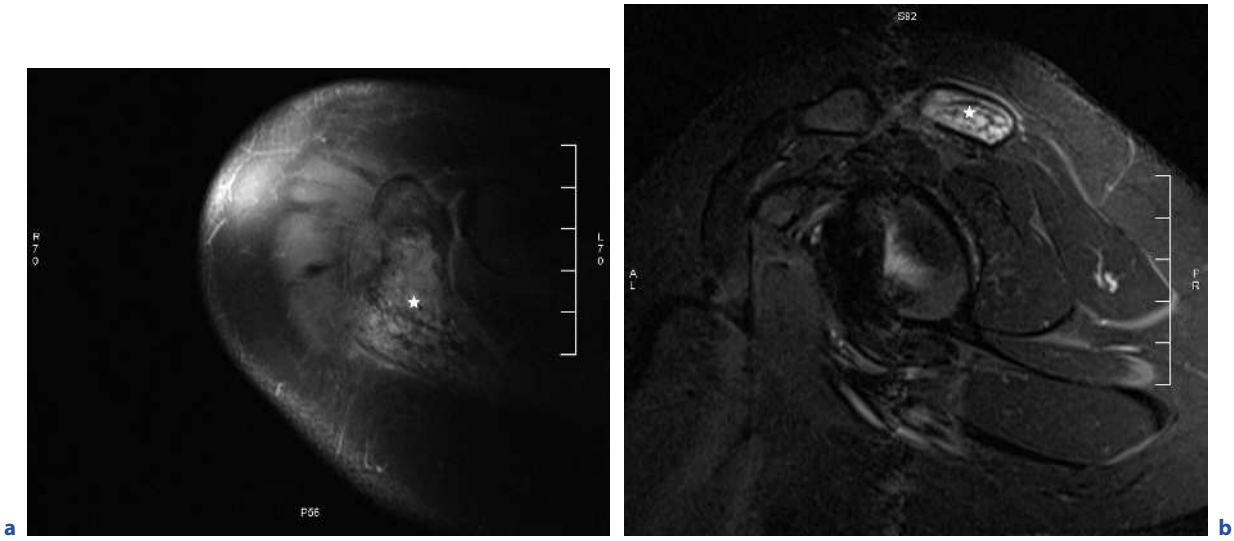

a b

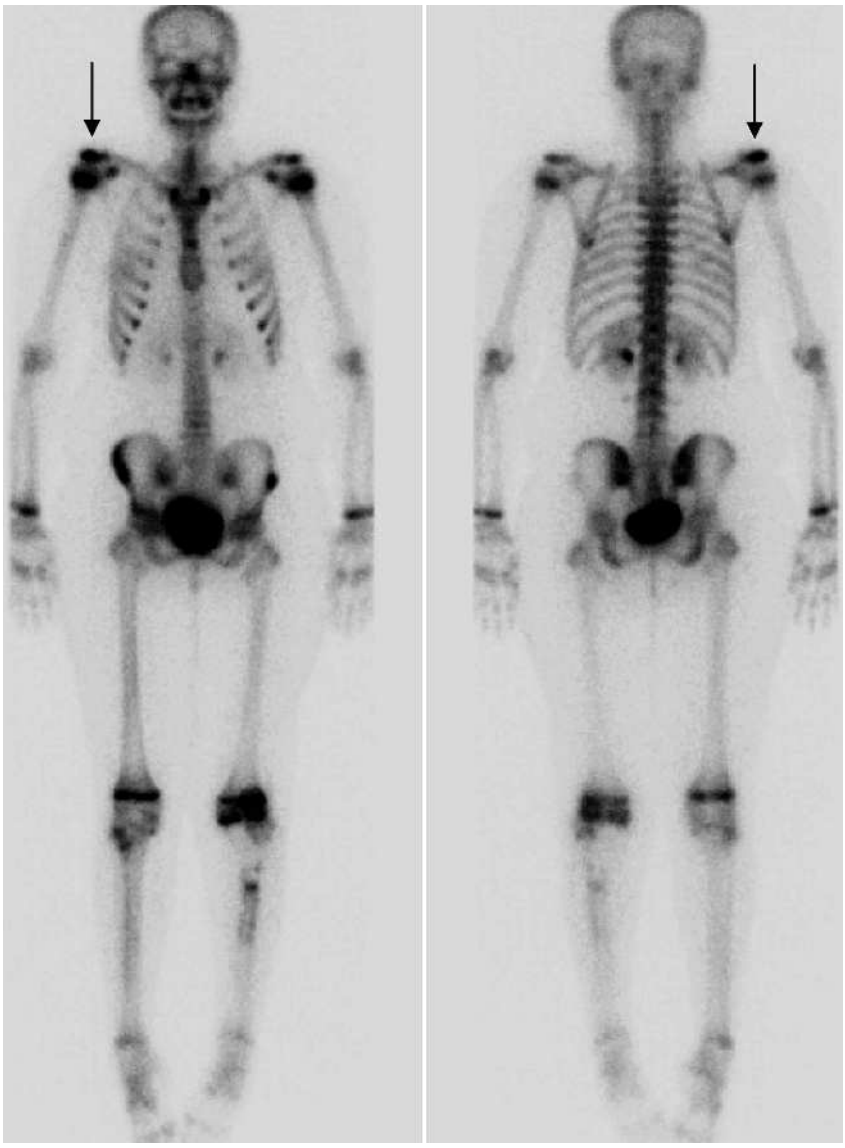

c

Fig. 10.7a–e. A 16-year-old female with osteosarcoma primary to the left tibia, which metastasized to the right acromion. Axial (**a**) and sagittal (**b**) T1-weighted, gadolinium-enhanced, fat-suppressed images reveal the enhancing metastasis in the right acromion (*stars*). **c** Anterior and posterior images from a Tc-99m MDP skeletal scintigram reveal increased radiopharmaceutical activity in the right acromion metastasis (*black arrows*). Increased radiopharmaceutical activity in the proximal left tibia is related to postsurgical change. (**d,e**) *see next page*

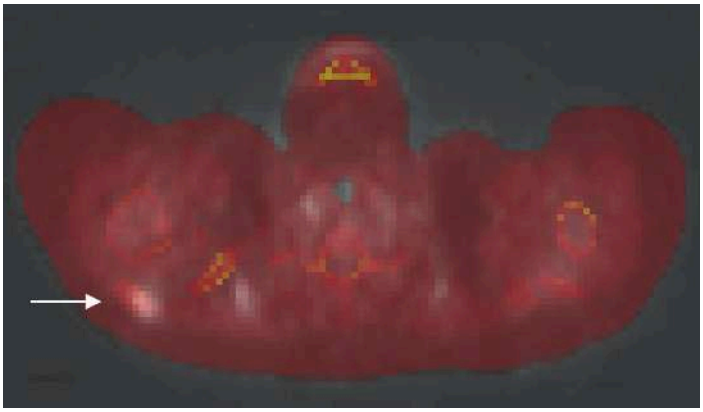

d

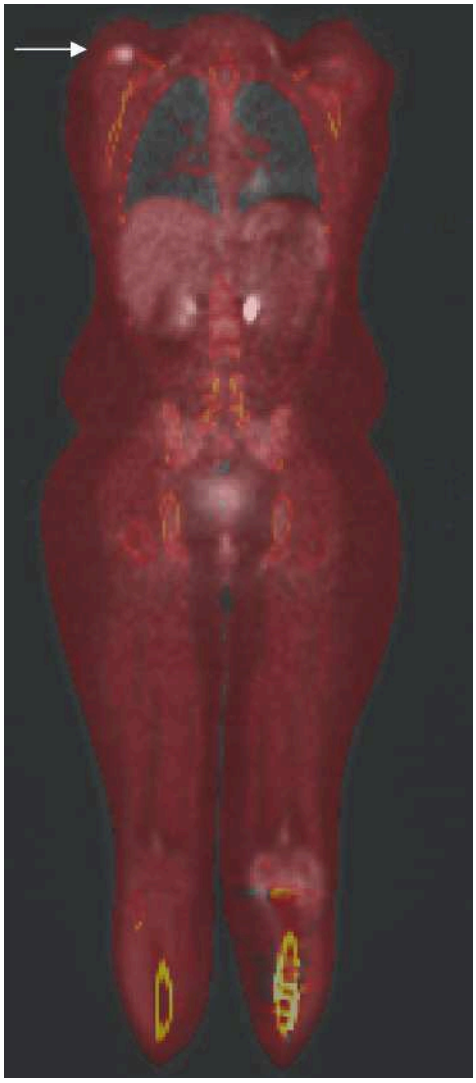

e

Fig. 10.7a–e. *(continued)* **d,e** Fused FDG-PET/CT images show increased FDG avidity within the right acromion metastasis (white arrows)

marrow imaging. These modalities include FDG-PET and whole body MRI.

The presence of osseous metastatic disease indicates widespread dissemination of tumor, and scintigraphic detection of these lesions after the initial staging period does not change patient outcome or improve survival (Bearcroft and Davies 1999). Thus, routine screening Tc-99m MDP skeletal scintigraphy is not generally recommended.

10.3.4 FDG-PET

FDG-PET traces foci of increased glucose metabolism, which is demonstrated by primary bone metastatic lesions and will be seen on imaging as areas of increased radiopharmaceutical activity. Multiple studies comparing FDG-PET to Tc-99m MDP skeletal scintigraphy regarding the ability of each modality to detect osseous metastases from primary bone tumors concluded that FDG-PET is superior to Tc-99m MDP skeletal scintigraphy in detecting osseous metastases from Ewing sarcoma but is less sensitive than Tc-99m MDP skeletal scintigraphy for detecting osseous metastases from osteosarcoma (Franzius et al. 2000; Volker et al. 2007). However, Franzius et al. (2002) have also reported that FDG-PET is superior to Tc-99m MDP skeletal scintigraphy for detection of skeletal metastases, including metastases from osteosarcoma (Fig. 10.7).

Studies comparing FDG-PET and chest CT for the detection of pulmonary metastases from primary bone tumors have demonstrated a lower sensitivity of FDG-PET, especially for nodules smaller than 7–10 mm

(Franzius et al. 2001; Volker et al. 2007). Tateishi et al. (2007) concluded in their study that preoperative staging of primary bone sarcomas was most accurate when FDG-PET was combined with conventional imaging methods (including radiography, CT, MRI, and Tc-99m MDP skeletal scintigraphy) than when either FDG-PET or conventional imaging modalities were utilized in isolation.

Since FDG-PET is a whole body imaging technique, one of its principle advantages lies in its potential ability to identify extrapulmonary, extraosseous sites of soft tissue spread (Franzius et al. 2002). An additional potential application of FDG-PET is the detection of skip metastases in children, since increased hematopoietic marrow in these patients may render bone marrow imaging, either by MRI or by Tc-99m MDP skeletal scintigraphy, insensitive (Fletcher 1997; Basu et al. 2008). This hypothesis remains unproven, however (Brenner et al. 2003).

To date, the role of FDG-PET is not to replace other imaging modalities. It seems to be best suited for confirming suspicious but equivocal findings identified on other imaging modalities or to screen those areas of the body not included in the field of view of the other imaging modalities during initial workup (Schuetze 2006). In fact, most FDG-PET systems today are combined with CT as dual FDG-PET/CT systems, underscoring the benefits of pairing metabolic with anatomic imaging (Schmidt et al. 2006).

10.3.5 Whole Body MRI

Whole body MRI is another emerging modality whose utility for assessment of various malignancies is being actively studied (Daldrup-Link et al. 2001; Antoch et al. 2003; Mentzel et al. 2004; Schlemmer et al. 2005; Frat et al. 2006; Schmidt et al. 2006; Nakanishi et al. 2007). Potential advantages of whole body MRI over FDG-PET/CT include detailed anatomic information without ionizing radiation. Although whole body MRI is not a new technique, relatively recent advances, including the rolling platform, parallel imaging, and phased-array coils have made the technique more viable for clinical use by decreasing imaging times to one hour or less (Schmidt et al. 2005, 2006). Several studies working with different whole body imaging protocols have shown the ability of a streamlined whole body protocol to detect intraosseous and extraosseous metastases (Mentzel et al. 2004; Schlemmer et al. 2005; Frat et al. 2006; Nakanishi et al. 2007).

Preliminary work has shown whole body MRI to be superior in assessing some types of metastatic disease, whereas FDG-PET/CT is advantageous in others. Whole body MRI is deficient in the evaluation of the lung parenchyma and lymph nodes (Schmidt et al. 2006). For lymph nodes, increased metabolic activity demonstrated by FDG-PET/CT is more specific than morphologic (i.e. size) abnormalities detected by whole body MRI (Antoch et al. 2003; Schmidt et al. 2006). Regarding lung metastases, FDG-PET/CT benefits from superior contrast between pulmonary nodules and background parenchyma as well as decreased motion artifact.

Whole body MRI outperforms FDG-PET/CT with respect to brain and liver metastases (Antoch et al. 2003; Schmidt et al. 2006, 2007a). High background cerebral FDG activity decreases the conspicuity of metastases. In the liver, the small size of metastatic lesions, low contrast between suspicious foci and background liver parenchyma on CT, and heterogeneous background liver FDG activity make metastatic lesions more difficult to detect. At our institution, an unenhanced CT for attenuation correction is followed by a contrast-enhanced CT, which increases the conspicuity of suspicious liver lesions. Regarding metastases to bone, some groups report the superiority of whole body MRI (Antoch et al. 2003; Schmidt et al. 2007b), while others report the superiority of FDG-PET (Daldrup-Link et al. 2001).

Compared to Tc-99m MDP skeletal scintigraphy, most studies report increased sensitivity of whole body MRI for the detection of skeletal metastases (Daldrup-Link et al. 2001; Mentzel et al. 2004). The identification of osseous metastases by Tc-99m MDP skeletal scintigraphy requires an osteoblastic reaction, a relatively advanced phenomenon (Daldrup-Link et al. 2001; Mentzel et al. 2004), since the bone marrow is the first site of hematogenous seeding of malignancy to bone (Nakanishi et al. 2007). Since MRI evaluates intramedullary pathology, metastatic foci to the skeleton, which reside in the intramedullary space, can be detected sooner than by Tc-99m MDP skeletal scintigraphy (Frank et al. 1990). The potential exception is in the pediatric population, where increased cellularity of the bone marrow may decrease the sensitivity of MRI for detection of osseous lesions (Fletcher 1997; Daldrup-Link et al. 2001; Basu et al. 2008).

Currently, there are few studies that have evaluated whole body MRI for the detection of metastases specifically from primary bone tumors. Mentzel et al. (2004) had a comparatively higher proportion of patients with primary musculoskeletal malignancies in their study group and found that whole body MRI identified more malignant lesions than did Tc-99m MDP skeletal scin-

tigraphy. Daldrup-Link et al. (2001) also studied a relatively higher proportion of patients with primary musculoskeletal malignancies, and they reported that whole body MRI and FDG-PET demonstrated higher sensitivity for identifying skeletal metastases compared to Tc-99m MDP skeletal scintigraphy. However, the lesions these modalities failed to depict differed from one another, supporting the notion that they may have complementary roles in tumor staging that play to their individual strengths.

10.3.6 Other Imaging Modalities

Optical imaging has experienced recent advances and is being used to study the biological behavior of malignancy, including metastatic disease, in small animals. Some of these techniques are already being applied to humans, such as near-fluorescence imaging for breast cancer detection and fluorescent probes used intraoperatively for analysis of tumor margins and detection of metastases (Kaijzel et al. 2007). As research continues and new advances are made, one can expect that these techniques will find their way into the primary bone tumor arena.

10.4 Conclusion

Advances in the treatment options for primary bone sarcomas have resulted in dramatic improvements in patient survival and patient morbidity. As a result, patterns of metastatic disease have changed, although sites of metastases still remain predominantly to the lungs and to bones distant from the primary tumor site. No one imaging modality is perfect for the detection of primary bone tumor metastases. Current staging protocols require MRI of the affected and adjacent limbs, chest CT, and Tc-99m MDP skeletal scintigraphy for the complete evaluation of metastases.

Emerging modalities for the detection of metastases of primary bone tumors include whole body MRI and FDG-PET/CT. These newer modalities show promise for efficient and earlier detection of distant metastases. By evaluating intramedullary abnormalities, these tools may further improve patient survival by detecting osseous lesions while they are still treatable. Additional investigations to assess their performance on metastases from primary bone tumors as well as their overall effect on patient outcome and their cost-effectiveness are required and promise to be exciting. Continuing advances in optical imaging can also be expected to impact the care of the patient with metastases from a primary bone tumor.

References

al-Jilaihawi AN, Bullimore J, Mott M et al. (1988) Combined chemotherapy and surgery for pulmonary metastases from osteogenic sarcoma. Results of 10 years experience. Eur J Cardiothorac Surg 2(1):37–42

Antoch G, Vogt FM, Freudenberg LS et al. (2003) Whole-body dual-modality PET/CT and whole-body MRI for tumor staging in oncology. JAMA 290(24):3199–3206

Bacci G, Briccoli A, Ferrari S et al. (2001) Neoadjuvant chemotherapy for osteosarcoma of the extremity: long-term results of the Rizzoli's 4th protocol. Eur J Cancer 37(16):2030–2039

Banfic L, Jelic I, Jelasic D et al. (2001) Heart metastasis of extraskeletal myxoid chondrosarcoma. Croat Med J 42(2):199–202

Basu S, Torigian D, Alavi A et al. (2008) Evolving concept of imaging bone marrow metastasis in the twenty-first century: critical role of FDG-PET. Eur J Nucl Med Mol Imaging 35(3):465–471

Bearcroft PW, Davies AM (1999) Follow-up of musculoskeletal tumours. 2. Metastatic disease. Eur Radiol 9(2):192–200

Belli L, Scholl S, Livartowski A et al. (1989) Resection of pulmonary metastases in osteosarcoma. A retrospective analysis of 44 patients. Cancer 63(12):2546–2550

Bhagia SM, Grimer RJ, Davies AM et al. (1997) Scintigraphically negative skip metastasis in osteosarcoma. Eur Radiol 7(9):1446–1448

Bloem JL, Taminiau AH, Eulderink F et al. (1988) Radiologic staging of primary bone sarcoma: MR imaging, scintigraphy, angiography, and CT correlated with pathologic examination. Radiology 169(3):805–810

Brenner W, BohuslavizkiKH, Eary JF (2003) PET imaging of osteosarcoma. J Nucl Med 44(6):930–942

Briccoli A, Rocca M, Salone M et al. (2005) Resection of recurrent pulmonary metastases in patients with osteosarcoma. Cancer 104(8):1721–1725

Brown K, Mund DF, Aberle DR et al. (1994) Intrathoracic calcifications: radiographic features and differential diagnoses. Radiographics 14(6):1247–1261

Carter SR, Grimer RJ, Sneath RS (1991a) A review of 13-years experience of osteosarcoma. Clin Orthop Relat Res 270:45–51

Carter SR, Grimer RJ, Sneath RS et al. (1991b) Results of thoracotomy in osteogenic sarcoma with pulmonary metastases. Thorax 46(10):727–731

Daldrup-Link HE, Franzius C, Link TM et al. (2001) Whole-body MR imaging for detection of bone metastases in children and young adults: comparison with skeletal scintigraphy and FDG PET. AJR Am J Roentgenol 177(1):229–236

Dalinka MK, Fiveash AE, Aston JK (1971) Metastatic extraosseous osteosarcoma to the liver: a case demonstrated by 85 Sr and 99m Tc-colloid scanning. J Nucl Med 12(11):754–755

Dunnick NR, Seibert K, Cramer HR Jr (1981) Cardiac metastasis from osteosarcoma. J Comput Assist Tomogr 5(2):253–255

Enneking WF, Spanier S, Goodman MA (1980) Current concepts review. The surgical staging of musculoskeletal sarcoma. J Bone Joint Surg Am 62(6):1027–1030

Fitzgerald RH Jr, Dahlin DC, Sim FH (1973) Multiple metachronous osteogenic sarcoma. Report of twelve cases with two long-term survivors. J Bone Joint Surg Am 55(3):595–605

Fletcher BD (1997) Imaging pediatric bone sarcomas. Diagnosis and treatment-related issues. Radiol Clin North Am 35(6):1477–1494

Frank JA, Ling A, Patronas NJ et al. (1990) Detection of malignant bone tumors: MR imaging vs scintigraphy. AJR Am J Roentgenol 155(5):1043–1048

Franzius C, Sciuk J,Daldrup-Link HE et al. (2000) FDG-PET for detection of osseous metastases from malignant primary bone tumours: comparison with bone scintigraphy. Eur J Nucl Med 27(9):1305–1311

Franzius C, Daldrup-Link HE, Sciuk J et al. (2001) FDG-PET for detection of pulmonary metastases from malignant primary bone tumors: comparison with spiral CT. Ann Oncol 12(4):479–486

Franzius C, Daldrup-Link HE, Wagner-Bohn A et al. (2002) FDG-PET for detection of recurrences from malignant primary bone tumors: comparison with conventional imaging. Ann Oncol 13(1):157–160

Frat A, Agildere M, Gencoglu A et al. (2006) Value of whole-body turbo short tau inversion recovery magnetic resonance imaging with panoramic table for detecting bone metastases: comparison with 99MTc-methylene diphosphonate scintigraphy. J Comput Assist Tomogr 30(1):151–156

Fuchs N, Bielack SS, Epler D et al. (1998) Long-term results of the co-operative German-Austrian-Swiss osteosarcoma study group's protocol COSS-86 of intensive multidrug chemotherapy and surgery for osteosarcoma of the limbs. Ann Oncol 9(8):893–899

George DP, Zamber RW (1996) Chondrosarcoma metastatic to the eye. Arch Ophthalmol 114(3):349–351

Giritsky AS, Etcubanas E, Mark JB (1978) Pulmonary resection in children with metastatic osteogenic sarcoma: improved survival with surgery, chemotherapy, and irradiation. J Thorac Cardiovasc Surg 75(3):354–362

Goorin AM, Delorey MJ, Lack EE et al. (1984) Prognostic significance of complete surgical resection of pulmonary metastases in patients with osteogenic sarcoma: analysis of 32 patients. J Clin Oncol 2(5):425–431

Han MT, Telander RL, Pairolero PC et al. (1981) Aggressive thoracotomy for pulmonary metastatic osteogenic sarcoma in children and young adolescents. J Pediatr Surg 16(6):928–933

Heck RK Jr, Peabody TD, Simon MA (2006) Staging of primary malignancies of bone. CA Cancer J Clin 56(6):366–375

Izzo P, Ricci N, Capolupo R et al. (2007) A rare case of primary chondrosarcoma of the heart. J Cardiovasc Med (Hagerstown) 8(3):210–213

Jemal A, Siegel R, Ward E et al. (2007) Cancer statistics, 2007. CA Cancer J Clin 57(1):43–66

Jones RD, ReidR, Balakrishnan G et al. (1993) Multifocal synchronous osteosarcoma: the Scottish Bone Tumour Registry experience. Med Pediatr Oncol 21(2):111–116

Kaijzel EL, van der Pluijm G, Lowik CW. (2007) Whole-body optical imaging in animal models to assess cancer development and progression. Clin Cancer Res 13(12):3490–3497

Kauffman WM, Winer-Muram H, Sandlund JT (1995) Detection of adrenal metastasis from osteosarcoma by Tc-99m MDP scintigraphy. Clin Nucl Med 20(8):741

Kpodonu J, Warso MA, Massad MG (2005) Osteosarcoma invading adrenal gland: rare cause of adrenal mass. Urology 65(6):1226

Link MP, Goorin AM, Miser AW et al. (1986) The effect of adjuvant chemotherapy on relapse-free survival in patients with osteosarcoma of the extremity. N Engl J Med 314(25):1600–1606

McDonald DJ (1994) Limb-salvage surgery for treatment of sarcomas of the extremities. AJR Am J Roentgenol 163(3):509–513; discussion 514–516

Mentzel HJ, Kentouche K, Sauner D et al. (2004) Comparison of whole-body STIR-MRI and 99mTc-methylene-diphosphonate scintigraphy in children with suspected multifocal bone lesions. Eur Radiol 14(12):2297–2302

Mialou V, Philip T, Kalifa C et al. (2005) Metastatic osteosarcoma at diagnosis: prognostic factors and long-term outcome – the French pediatric experience. Cancer 104(5):1100–1109

Murphey MD, Walker EA, Wilson AJ et al. (2003) From the archives of the AFIP: imaging of primary chondrosarcoma: radiologic-pathologic correlation. Radiographics 23(5):1245–1278

Nakanishi K, Kobayashi M, Nakaguchi K et al. (2007) Whole-body MRI for detecting metastatic bone tumor: diagnostic value of diffusion-weighted images. Magn Reson Med Sci 6(3):147–155

Oh BG, Han YH, Lee BH et al. (2007) Primary extraskeletal mesenchymal chondrosarcoma arising from the pancreas. Korean J Radiol 8(6):541–544

Pakter RL, Fishman EK (1983) Metastatic osteosarcoma to the heart and mediastinum presenting as esophageal obstruction. J Comput Assist Tomogr 7(6):1114–1115

Pastorino U, Valente M, Gasparini M et al. (1988) Lung resection as salvage treatment for metastatic osteosarcoma. Tumori 74(2):201–206

Putnam JB Jr, Roth JA, Wesley MN et al. (1983) Survival following aggressive resection of pulmonary metastases from osteogenic sarcoma: analysis of prognostic factors. Ann Thorac Surg 36(5):516–523

Reid R (2007) Update on sarcomas of bone and soft tissue. Scott Med J 52(2):31–35

Rosenthal DI (1997) Radiologic diagnosis of bone metastases. Cancer 80(Suppl 8):1595–1607

Ryan JM, Dupuy DE, Pitman M et al. (2000) Metastases to the liver from extraskeletal myxoid chondrosarcoma and successful treatment with percutaneous ethanol injection. Clin Radiol 55(4):314–317

Salvati M, Cervoni L, Caruso R et al. (1998) Sarcoma metastatic to the brain: a series of 15 cases. Surg Neurol 49(4):441–444

Schlemmer HP, Schafer J, Pfannenberg C et al. (2005) Fast whole-body assessment of metastatic disease using a novel magnetic resonance imaging system: initial experiences. Invest Radiol 40(2):64–71

Schmidt GP, Baur-Melnyk A, Herzog P et al. (2005) High-resolution whole-body magnetic resonance image tumor staging with the use of parallel imaging versus dual-modality positron emission tomography-computed tomography: experience on a 32-channel system. Invest Radiol 40(12):743–753

Schmidt GP, Haug AR, Schoenberg SO et al. (2006) Whole-body MRI and PET-CT in the management of cancer patients. Eur Radiol 16(6):1216–1225

Schmidt GP, Kramer H, Reiser MF et al. (2007a) Whole-body magnetic resonance imaging and positron emission tomography-computed tomography in oncology. Top Magn Reson Imaging 18(3):193–202

Schmidt GP, Schoenberg SO, Schmid R et al. (2007b) Screening for bone metastases: whole-body MRI using a 32-channel system versus dual-modality PET-CT. Eur Radiol 17(4):939–949

Schuetze SM (2006) Utility of positron emission tomography in sarcomas. Curr Opin Oncol 18(4):369–373

Secil M, Mungan U, Yorukoglu K et al. (2005) Case 89: Retroperitoneal extraskeletal osteosarcoma. Radiology 237(3):880–883

Seo JB, Im JG, Goo JM et al. (2001) Atypical pulmonary metastases: spectrum of radiologic findings. Radiographics 21(2):403–417

Simodynes EE, Jardon OM, Connolly JF (1981) Multiple metachronous osteosarcoma with eleven-year survival. A case report. J Bone Joint Surg Am 63(2):317–322

Skubitz KM, D'Adamo DR (2007) Sarcoma. Mayo Clin Proc 82(11):1409–1432

Stacy GS, Mahal RS, Peabody TD (2006) Staging of bone tumors: a review with illustrative examples. AJR Am J Roentgenol 186(4):967–976

Takeuchi I, Kawaguchi T, Kimura Y et al. (2007) Primary cardiac osteosarcoma in a young man with severe congestive heart failure. Intern Med 46(10):649–651

Tateishi U, Yamaguchi U, Seki K et al. (2007) Bone and soft-tissue sarcoma: preoperative staging with fluorine 18 fluorodeoxyglucose PET/CT and conventional imaging. Radiology 245(3):839–847

Teo HE, Peh WC (2004) The role of imaging in the staging and treatment planning of primary malignant bone tumors in children. Eur Radiol 14(3):465–475

van der Woude HJ, Bloem JL, Hogendoorn PC (1998) Preoperative evaluation and monitoring chemotherapy in patients with high-grade osteogenic and Ewing's sarcoma: review of current imaging modalities. Skeletal Radiol 27(2):57–71

van Rijswijk CS, Lieng JG, Kroon HM et al. (2001) Retroperitoneal extraskeletal osteosarcoma. J Clin Pathol 54(1):77–78

Volker T, Denecke T, Steffen I et al. (2007) Positron emission tomography for staging of pediatric sarcoma patients: results of a prospective multicenter trial. J Clin Oncol 25(34):5435–5441

von Hochstetter AR, Hattenschwiler J, Vogt M (1987) Primary osteosarcoma of the liver. Cancer 60(9):2312–2317

Wittig JC, Bickels J, Priebat D et al. (2002) Osteosarcoma: a multidisciplinary approach to diagnosis and treatment. Am Fam Physician 65(6):1123–1132

Assessment of Response to Chemotherapy and Radiotherapy

11

Koenraad Verstraete

CONTENTS

KEY POINTS

- The most valuable, readily available and easy-to-use techniques to assess response to radiation therapy and chemotherapy in malignant bone tumours are DCE-MR imaging, diffusion MR imaging and colour-Doppler ultrasound.
- Dynamic contrast-enhanced MR imaging allows to study the physiological effects of therapy graphically in TICs or in parametric images, that display tumour microvascularisation, perfusion, capillary permeability and volume of the interstitial space.
- There is not enough evidence to use F-18 FDG-PET routinely for monitoring therapy in bone sarcomas.

Findings indicating good response to therapy in bone sarcomas are:

- Disappearance of high systolic Doppler frequency shifts and an increased resistive index on colour-Doppler ultrasound
- Appearance of high signal intensity in bone marrow on T2-weighted images (after radiation therapy)
- Change to slow and moderate to absent enhancement on DCE-MR imaging
- Increased diffusion of water molecules with high ADC values on diffusion MR imaging

Findings indicating poor response to therapy in bone sarcomas are:

- Persistence of high systolic Doppler frequency shifts and decreased resistive index on colour-Doppler ultrasound
- Increased extent of bone marrow invasion

K. Verstraete, MD, PhD
Full Professor of Radiology, Ghent University, Chief Department of Radiology, Ghent University Hospital – UZG/MR/1K12, De Pintelaan 185, 9000 Ghent, Belgium

- Increased tumour volume or identification of a new soft tissue mass
- No decrease in the amount of peritumoral oedema
- Persistence of fast and intense enhancement on DCE-MR imaging
- Persistence of decreased diffusion of water molecules with low ADC values on diffusion MR imaging

11.1 Introduction

After detection, local staging, biopsy and initial treatment of a bone tumour, the radiologist's task is to assess response to radiation therapy or chemotherapy. The aim of monitoring therapy is to predict the percentage of tumour necrosis in order to differentiate responders from non-responders, as response to initial chemotherapy is an important predictor of outcome and may influence further treatment.

11.2 Assessment of Response to Radiotherapy

Radiotherapy is not frequently used for treatment of bone tumours. In Ewing's sarcoma it is used when local resection is not possible. Because dynamic contrast-enhanced magnetic resonance (DCE-MR) imaging may be misleading in the early weeks after radiotherapy, due to radiation-induced neovascularisation that resembles viable tumour tissue, one must mainly rely on volume reduction and changes in signal intensity on T2-weighted images. The tumoral tissue in Ewing's sarcoma will change into myxoid tissue with typical high signal intensity on T2-weighted images, comparable to that of water (Lemmi et al. 1990). After a few months the radiation-induced neovascularisation will disappear and (dynamic) contrast-enhanced studies will show little enhancement in this myxoid tissue. Later on, DCE-MR imaging is a reliable method to confirm tumour response and demonstrate tumour necrosis and the absence of tumour recurrence (El Khadrawy et al. 1999; Verstraete et al. 1996).

11.3 Assessment of Response to Chemotherapy

Patients with malignant bone tumours such as osteosarcoma and Ewing's sarcoma are treated with neoadjuvant chemotherapy for about 3 months before local surgery is performed, and will receive postoperative chemotherapy for about one more year. Treatment response is considered successful if, histologically, more than 90% of tumour cells show necrosis. Histological response to chemotherapy is an important prognostic factor in bone sarcoma, influencing therapeutic considerations. It is advantageous to be able to assess chemotherapy response, and predict survival, prior to tumour resection. The radiologist has the task to assess response to preoperative chemotherapy because, in case of non-response, another chemotherapy agent will have to be used postoperatively. Moreover, after local resection histopathological assessment of response may take several days to weeks before results are available.

Assessment of local response to chemotherapy can be done using conventional MR imaging and DCE-MR imaging. Other, less frequently used methods are colour-Doppler ultrasound, diffusion imaging and fluorine-18 2-fluoro-2-deoxyglucose positron emission tomography (F-18 FDG-PET).

11.3.1 Colour-Doppler Ultrasound

Colour-Doppler ultrasound is non-invasive, non-demanding for the patient and easy to plan. This makes the method especially suitable for children, who comprise the majority of patients. It can be used for planning treatment immediately prior to definitive surgery by predicting chemotherapy response with high sensitivity and specificity, especially for negative response (predictive value > 90%) (Bramer et al. 2004).

After two cycles of chemotherapy a decreased or unaltered resistive index in the arteries that feed tumours in addition to persistent intratumoral flow and high-frequency Doppler shifts suggest poor histological response to chemotherapy in osteosarcoma and Ewing's sarcoma. Disappearance of high systolic Doppler frequency shifts and an increased resistive index after two cycles of chemotherapy are indicative of good response (van der Woude et al. 1994a, 1995a).

Ultrasonography can also be used in addition to MR imaging when susceptibility artefacts secondary to orthopaedic hardware (including prostheses) prevent evaluation of specific areas (van der Woude et al. 1999).

11.3.2 Fluorine-18 2-Fluoro-2-Deoxyglucose Positron Emission Tomography (F-18 FDG-PET) and PET-CT

The most common application of FDG-PET in the musculoskeletal system is the detection of osseous metastatic disease in patients with primary carcinoma. Another potential, but not yet evidence-based and still controversial role for FDG-PET imaging is staging and restaging of primary bone sarcoma and assessing response to chemotherapy and radiation therapy. Although a meta-analysis performed in 2004 revealed that there was no indication to use FDG-PET in the standard treatment of sarcomas (Bastiaannet et al. 2004), more recent studies indicated that this technique might be sensitive, specific and accurate in the detection of recurrence of tumour especially at the primary site and for assessing treatment response (Arush et al. 2007; McCarville et al. 2005; Peterson 2007). However, a study by Iagaru et al. revealed that the pathologically determined degree of necrosis post-neoadjuvant chemotherapy was concordant with PET-assessed classification of response only in 57.1% of patients (Iagaru et al. 2008). A significant number of patients had discrepancies, which could in part be explained by chemotherapy-induced inflammation that also results in higher glycolysis.

Prospective studies with large patient groups are still required to further evaluate the real benefit of FDG-PET in these indications.

11.3.3 Diffusion MR Imaging

Diffusion-weighted MR imaging depicts differences in random motion of water molecules and, ultimately, in membrane integrity between viable and necrotic tumour and may therefore be used to monitor tumour viability by demonstration of the appearance of tumour necrosis during treatment. Only a few studies have been published (Hayashida et al. 2006; Lang et al. 1998; Uhl et al. 2006a, b). The technique has been used successfully to assess, non-invasively, tumour necrosis in rats and patients with osteosarcoma and Ewing's sarcoma. On diffusion-weighted images, necrotic sarcoma has high apparent diffusion coefficients (ADC) (mean ADC value 2.3×10^{-3} mm^2s^{-1}) visible as areas with low signal intensity, indicating rapid diffusion of water molecules as a result of loss of membrane integrity, while viable tumour has lower ADC (mean ADC value 0.8×10^{-3} mm^2s^{-1}) and is visible as areas with higher signal intensity (Uhl et al. 2006a, b). Diffusion MR imaging seems to be more efficient than contrast-enhanced MR imaging to demonstrate tumour necrosis because on gadolinium-enhanced images signal intensity overlap between viable and necrotic tumour may be caused by the small molecular size of the contrast medium, which permeates the interstitial space freely, thereby also enhancing necrosis (Lang et al. 1998). This statement is only true for *static* contrast-enhanced MR imaging, but not for *dynamic* contrast-enhanced MR imaging, which can easily differentiate tumour from peritumoral oedema and necrosis.

11.3.4 Conventional MR Imaging

To assess response to preoperative chemotherapy on conventional MR imaging, changes in intra- and extramedullary signal intensities, in tumour demarcation, in tumour volume and in the appearance of residual extramedullary tumour can be evaluated.

In osteosarcoma, poor responders can be identified if an increase in tumour volume or no decrease in the amount of oedema is seen (Holscher et al. 1992). In Ewing's sarcoma, increased extent of abnormal marrow invasion and increase in tumour volume or identification of a new soft tissue mass indicate non-response (Kauffman et al. 1994). Except for these signs of non-response, conventional MR imaging alone has low predictive value: minimal residual disease (< 10% of the entire tumour volume), observed histologically, cannot be identified. Therefore, conventional MR imaging should be combined with DCE-MR imaging and eventually other physiological or molecular imaging methods to allow prediction of response with higher accuracy. Nevertheless, both in osteosarcoma and Ewing's sarcoma, determination of tumour volume by conventional, unenhanced MR imaging at the time of diagnosis is a simple and reliable method of predicting the clinical outcome (progression-free survival and disease-free survival) (Kaste et al. 2004; Miller et al. 2001).

11.3.4.1 Changes in Extramedullary Tumour

In Ewing's sarcoma, tumour volume, necrosis and residual extramedullary tumour, rather than changes of signal intensity, are major features for evaluating the response to chemotherapy. A limited decrease of tumour volume (< 25%) and/or residual soft tissue mass following chemotherapy correlates with a poor response. Development of necrosis and reduction of tumour volume

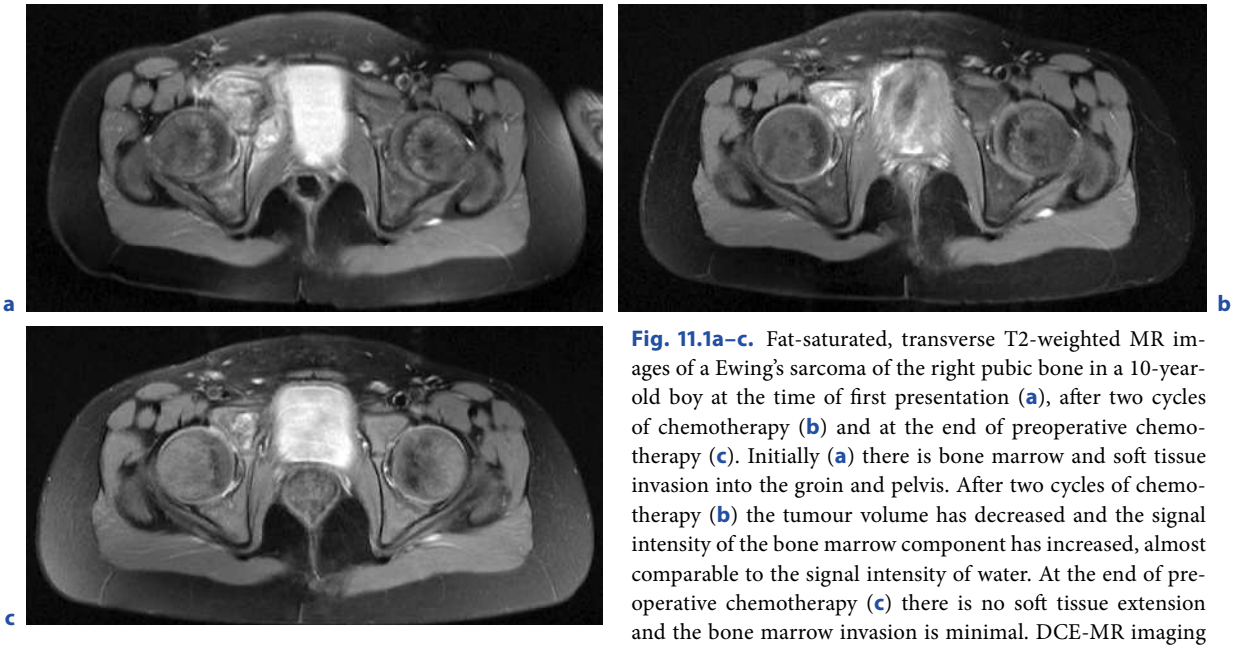

Fig. 11.1a–c. Fat-saturated, transverse T2-weighted MR images of a Ewing's sarcoma of the right pubic bone in a 10-year-old boy at the time of first presentation (**a**), after two cycles of chemotherapy (**b**) and at the end of preoperative chemotherapy (**c**). Initially (**a**) there is bone marrow and soft tissue invasion into the groin and pelvis. After two cycles of chemotherapy (**b**) the tumour volume has decreased and the signal intensity of the bone marrow component has increased, almost comparable to the signal intensity of water. At the end of preoperative chemotherapy (**c**) there is no soft tissue extension and the bone marrow invasion is minimal. DCE-MR imaging and histopathological examination of the resected specimen confirmed a good response

is significantly higher in good responders. An inhomogeneous, well-defined cuff of abnormal tissue encircling the bone and/or radiological disappearance of the soft tissue tumour component following chemotherapy correlates with good response (Abudu et al. 1999; van der Woude et al. 1994b) (Fig. 11.1).

In osteosarcoma, only an increase in tumour volume and persistence of high signal intensity of the tumour and peritumoral oedema on T2-weighted images are reliable indicators of poor response, even after one cycle of chemotherapy (Holscher et al. 1995). A decreased or stable tumour volume is less reliable in predicting good histopathological response, as poor responders also may show these signs (Shin et al. 2000).

11.3.4.2 Change in the Bone Marrow Component

In poor responders, an increase in the extent of tumoral bone marrow invasion may be observed.

In patients with a chemotherapy-sensitive Ewing's sarcoma, the bone marrow component may show a change in signal intensity that becomes comparable to that of water (Fig. 11.1). The increase in marrow signal intensity on T2-weighted images is associated with replacement of marrow elements by a loose, hypocellular myxoid matrix containing modest amounts of collagen, consistent with response to chemotherapy and eradication of disease. Therefore, an increase in the T2-weighted signal intensity of the bone marrow component of Ewing's sarcoma of bone after at least two cycles of chemotherapy reflects a favourable response to chemotherapy (Lemmi et al. 1990). This sign is, however, not reliable within 10 days after one cycle of chemotherapy because clusters of viable tumour cells may show similar signal characteristics (MacVicar et al. 1992). In patients treated with chemotherapy for Ewing's sarcoma, MR signal changes are not predictive of resolution of malignant disease within adjacent soft tissue.

11.3.5 Dynamic Contrast-enhanced MR Imaging

Dynamic contrast-enhanced MR imaging is a method of physiological imaging, based on ultrafast imaging, with the possibility to follow the early enhancement kinetics of a water-soluble gadolinium-chelate within the first 3 min after intravenous bolus injection. This technique provides clinically useful information by depicting tissue vascularisation and perfusion, capillary permeability and composition of the interstitial space (Verstraete et al. 1994b, 1996). The aim of DCE-MR imaging

is to detect and depict differences in early intravascular and interstitial distribution of the gadolinium-chelate, as this process is influenced by pathological changes in tissues. The most important applications of this technique are its abilities to monitor response to preoperative chemotherapy, to identify areas of viable tumour before biopsy and to provide physiological information for improved tissue characterisation and detection of residual or recurrent tumour tissue after therapy.

Dynamic contrast-enhanced MR imaging should be part of every MR tumour imaging protocol, because it assists in the detection of the most viable parts of the tumour and serves as an initial standard for follow-up of the metabolic activity of the tumour during and after chemotherapy, both in small intraosseous tumours and in tumours with an associated soft tissue mass. In combination with selected morphological features, dynamic imaging parameters are therefore advocated for monitoring the effect of neoadjuvant chemotherapy in patients with bone sarcoma (Reddick et al. 1995, 1999; van der Woude et al. 1998; Verstraete et al. 1994a, b, 1996).

11.3.5.1 Practical Guidelines

Dynamic contrast-enhanced MR imaging is a physiological imaging method with low spatial resolution but very high temporal resolution that allows to study the contrast-enhancement dynamics during and immediately after the first-pass of a gadolinium-chelate in the tissues. According to the Nyquist theorem limit, the physiological process of interest must be sampled at twice the frequency of the dynamic event being measured. As the first-pass of the contrast medium in tumours usually takes less than 6–10 s, an imaging frequency of at least one image per 2 s is mandatory to obtain at least three images during this phase of enhancement. Ultrafast T1-weighted 'snapshot' sequences like Turbo-FLASH (turbo fast low angle shot), Turbo Fast Field Echo (TFFE) and Fast Spoiled Gradient Echo (FSPGR) with a temporal resolution of 1 s per image and an imaging matrix of 128 × 128 or 256 × 256 are very suitable to study this physiological phenomenon during the first 2–3 min after bolus injection. The result is a set of 100–200 images displaying second by second the arrival of the bolus in the capillary network and its initial distribution into the interstitial space of the tumoral tissue. Image thickness usually varies between 3 and 10 mm with a field-of-view of at least twice the largest diameter of the tumour, usually 200 × 200 mm.

Dynamic contrast-enhanced MR imaging is frequently performed in one imaging plane (i.e. the 'single slice' method), whereby the most representative imaging plane through the tumour is chosen. It is presumed that this section represents the contrast-enhancement behaviour of the entire lesion. To minimise a sampling error, the different components of the lesion should be thoroughly evaluated on the precontrast T1- and T2-weighted images, in order to find an imaging plane which includes most components of the lesion (Figs. 11.2, 11.3). This preselection may provide a representative longitudinal or transverse imaging plane. Inclusion of an artery in the imaging plane is useful to evaluate differences in time of onset of enhancement in various parts of the lesion, compared with the time of arrival of the bolus. In follow-up studies during chemotherapy, the same imaging plane should be used for comparison and assessment of response (Figs. 11.2, 11.3). Multislice DCE-MR imaging allows to cover the whole tumour volume, but this may be at the cost of temporal resolution, which has to remain very high in the order of 1 s per image.

In practice, one test snapshot image is obtained after preselection of a representative imaging plane. If the lesion, the regional artery and a normal neighbouring muscle are displayed well on this image, the dynamic snapshot sequence can be started simultaneously with the bolus injection. During all acquisitions of the dynamic study, the transmitter and receiver gains are held constant. Overall, the dynamic imaging study lasts for 2–3 min after bolus injection. If the infusion line is placed before the patient has entered the MR unit, the whole procedure lengthens the MR examination for about 5 min. In order to obtain high concentrations of contrast medium during the first-pass, the bolus injection is performed at an injection rate of 3 ml/s in the right antecubital vein, which is easily accessible and nearer to the heart than the left one: this causes less dilution of the bolus. To empty the contrast medium completely from the infusion line, the bolus is followed immediately by a saline flush of about 20 ml at the same injection rate. At this rapid injection rate, no serious side effects exist.

11.3.5.2 Physiological Background

Dynamic contrast-enhanced MR imaging after bolus injection of a gadolinium-chelate allows to study tissue vascularisation (number of capillaries), tissue perfusion, capillary permeability, volume of the interstitial

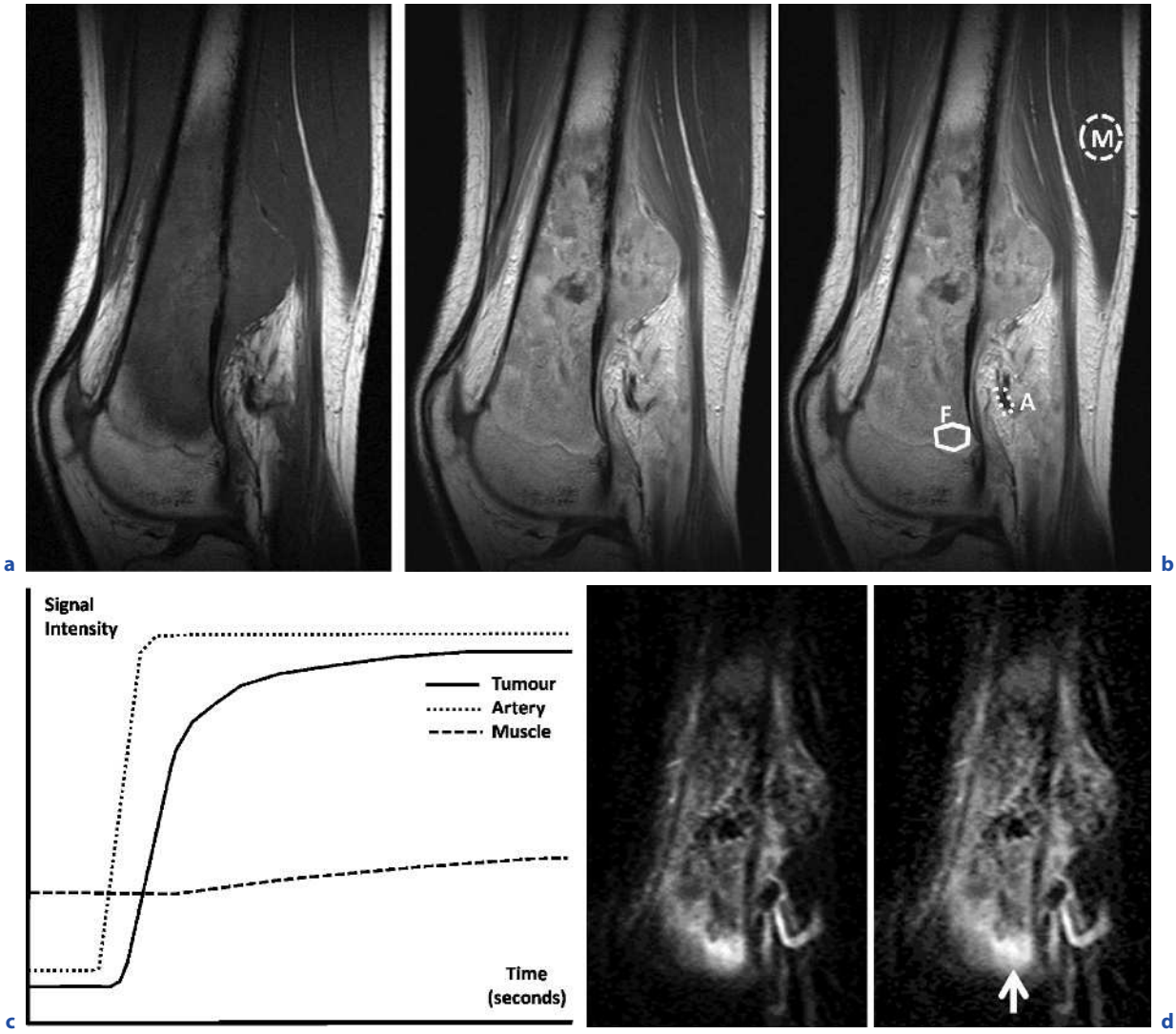

Fig. 11.2a–d. Sagittal T1-weighted MR image of an osteosarcoma of the femur in a 16-year-old girl at the time of first presentation, before (**a**) and after (**b**) intravenous contrast medium administration, shows extensive bone marrow and soft tissue infiltration, posteriorly. This imaging plane was selected as representative for the whole tumour. Three ROIs were selected (**b**) (*A* artery, *F* fastest enhancing area in tumour, *M* unaffected muscle). The corresponding TIC (**c**) shows similar enhancement in the artery and fastest enhancing tumoral area, with a steep slope during the first-pass of the contrast medium, followed by an early plateau phase. The muscle shows slow enhancement without a plateau phase within the first 120 s after bolus injection. The first-pass image or slope image (**d**) shows many bright areas indicating a high number of leaky capillaries with high perfusion in highly malignant tumoral tissue. The fastest enhancing area is easily recognised near the physis (*arrow*) and can be chosen as preferential site for biopsy

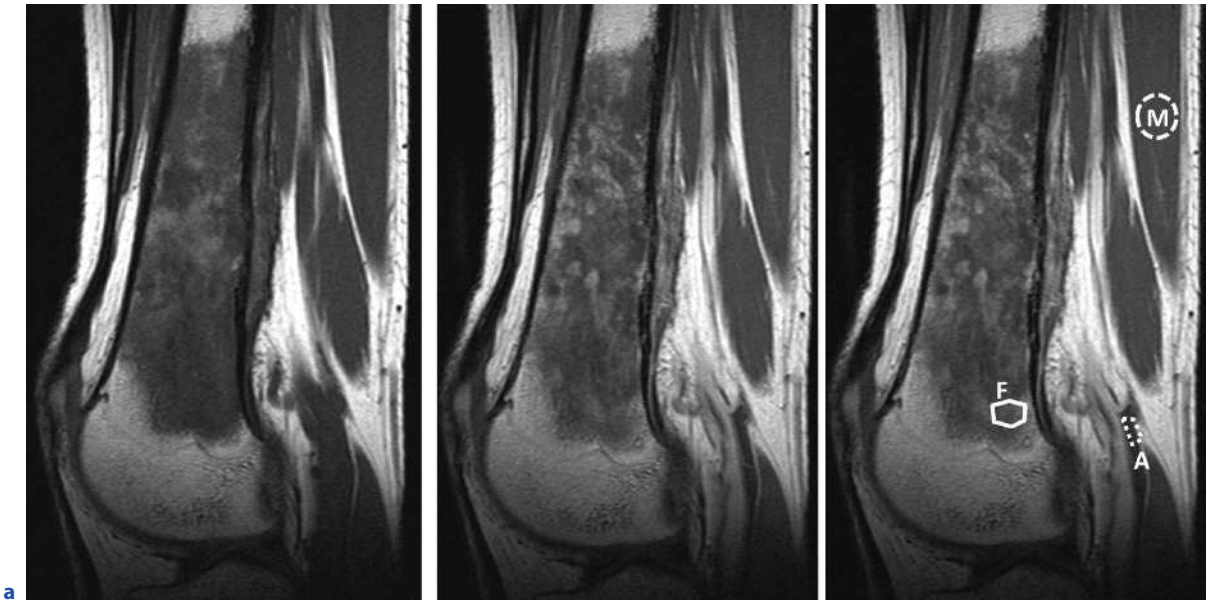

a b

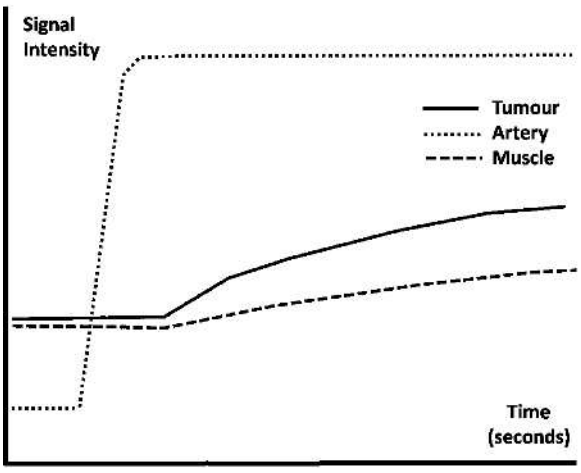

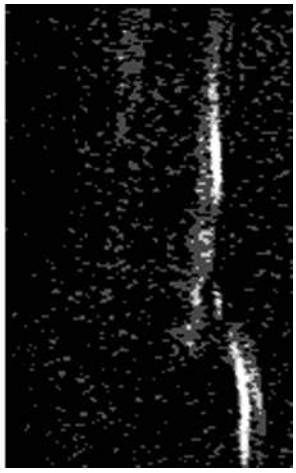

c d

Fig. 11.3a–d. Sagittal T1-weighted MR image of an osteosarcoma of the femur in a 16-year-old girl after 3 months of preoperative chemotherapy, before (**a**) and after (**b**) intravenous contrast medium administration. For assessment of response, the imaging plane is the same as before the start of chemotherapy. The bone marrow infiltration is unchanged and the soft tissue extension has decreased, posteriorly. The signal intensities in the static contrast-enhanced image (**b**) do not allow to assess response to chemotherapy. Three ROIs were selected (**b**) (*A* artery, *F* fastest enhancing area in tumour, *M* unaffected muscle). The corresponding TIC (**c**) shows slowly progressive enhancement in the tumoral area, not more than twice the enhancement of muscle, indicating good response to chemotherapy. The first-pass image or slope image (**d**) shows no bright areas (except for the popliteal artery) indicating good response to chemotherapy

space and thus indirectly tissue cellularity (= number of cells).

During the *first-pass* of the contrast medium in the tissue there is no gadolinium-chelate in the interstitial space yet and the concentration gradient between the blood plasma and interstitial space is maximal, resulting in a net unidirectional fast diffusion of the gadolinium-chelate into the tissue. Whereas in normal tissues during the first-pass approximately 50% of the circulating contrast medium will diffuse from the blood into the extravascular compartment, in tumours with a high number of capillaries with increased permeability, leakage during the first-pass is much higher and may even reach 100% in some tumours or tumour parts.

The enhancement rate of the tissue during the first-pass is mainly determined by tissue vascularisation (i.e. the number of capillaries), tissue perfusion and capillary permeability. This phase of the dynamic contrast-enhanced study can be evaluated graphically using the *region-of-interest (ROI) method* (Figs. 11.2b, c, 11.3b, c). In this method, signal intensities in one or more circular or freely determined ROIs are measured and plotted against time in a time–intensity curve (TIC). This graph displays the change in signal intensity versus time in one or more ROIs. Most often, ROIs encircling a feeding artery, the whole tumour, the fastest enhancing area within the tumour and, for comparison, a neighbouring unaffected muscle are drawn (Figs. 11.2b, 11.3b). To find the fastest enhancing area within a tumour, review of the native or subtraction images is necessary.

Before treatment there is usually a very fast enhancement rate in a malignant bone tumour during the first-pass of the contrast medium because these tumours have a very high number of vessels with increased flow and very high capillary permeability. In the TIC this is visible as a steep slope of the curve, which has an early time of onset of enhancement and high maximal enhancement (Fig. 11.2c).

Quantitative data that can be obtained from the TIC are the time of onset of enhancement, slope (= enhancement rate during the first-pass), maximum enhancement and, eventually, negative slope (i.e. wash-out rate). The time of onset of enhancement in a lesion can be measured relative to arterial enhancement.

In the *second phase*, i.e. immediately after the first-pass of the contrast bolus, the diffusion of the gadolinium-chelate and the enhancement rate of the tissue drop significantly because the plasma concentration of the contrast medium in the blood has become much lower after passage of the bolus due to abundant leakage into the interstitial space, recirculation with further dilution in the remaining blood volume and start of renal excretion. The length of the time interval between the end of the first pass and the *equilibrium phase*, with equal concentrations of contrast medium in plasma and interstitial space, is now mainly determined by the volume of the interstitial space. This time interval may vary from less than 5 s in lesions with a very small interstitial space to more than 3–5 min in tissues with a larger interstitial space (Verstraete et al. 1996) (Figs. 11.2c, 11.3c).

The equilibrium phase is followed by the *wash-out phase*, in which the contrast medium is progressively washed out from the interstitial space as the arterial concentration decreases. Only in highly vascular lesions with a small interstitial space does early wash-out occur within the first minutes after bolus injection.

In tissues with increased capillary permeability, a very high cellularity and small volume of the interstitial space, the equilibrium in concentration between blood and interstitial space will be reached within the first minute after arrival of the bolus because the gadolinium-chelate will fill in the total volume of the small interstitial space very fast. This is visible in a TIC as an early plateau phase, which can be followed by early wash-out within the first 2–3 min after bolus injection, when the gadolinium-chelate diffuses back from the interstitial space, with the high initial concentration, to the vascular space with already diluted and much lower concentration of contrast medium. This type of TIC with a very high first-pass, early plateau phase, immediately followed by early wash-out is frequently seen in many (but not all) patients with Ewing's sarcoma, osteosarcoma, giant cell tumour of bone and multiple myeloma. Chemotherapy or radiation therapy resistant areas of these bone tumours and recurrences of giant cell tumour of bone can be identified by this type of dynamic contrast-enhancement (Fig. 11.4).

On the contrary, in tissues with a lower cellularity and larger interstitial space, the equilibrium in concentration between blood and interstitial space will be reached later and often not within the first 2–3 min after bolus injection because the volume of the interstitial space is too large and more time is required to fill in this space with the gadolinium-chelate. This is visible on a TIC as a continuously, rather slow enhancement after the initial first-pass phase, without reaching a plateau phase within the first 2–3 min after bolus injection. This type of TIC with gradual increase of signal intensity after the first-pass is not specific for any tumour type, but mainly indicative of lower cellularity and a larger interstitial space. Although this type of TIC is observed in many benign and malignant bone tumours, it can be used for monitoring therapy.

In follow-up MR examinations during therapy, a change of type of TIC, e.g. from a TIC with an early and fast wash-in, early plateau phase (and sometimes

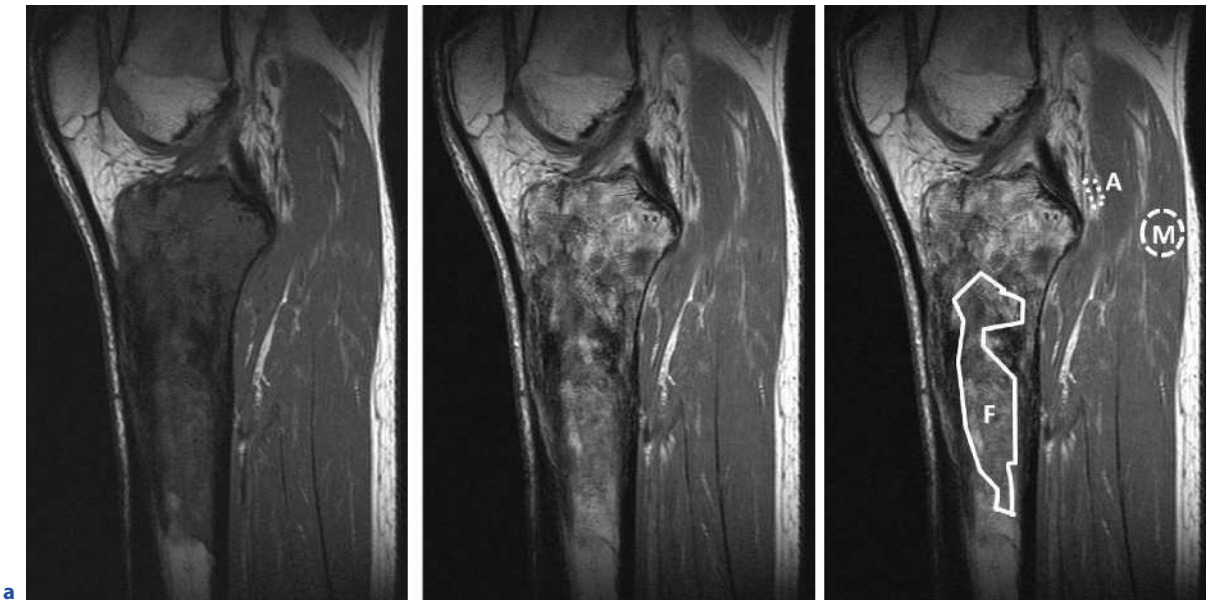

a b

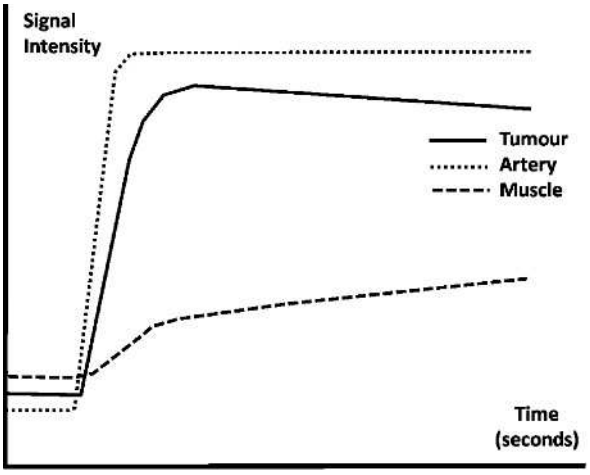

c

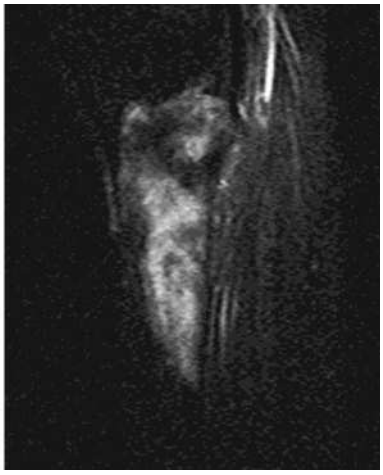

d

Fig. 11.4a–d. Sagittal T1-weighted MR image of an osteosarcoma of the tibia in a 17-year-old boy after 3 months of preoperative chemotherapy, before (**a**) and after (**b**) intravenous contrast medium administration, shows extensive bone marrow infiltration. The signal intensities in the static contrast-enhanced image (**b**) do not allow to assess response to chemotherapy. Three ROIs were selected (**b**) (*A* artery, *F* fastest enhancing area in tumour, *M* unaffected muscle). The corresponding TIC (**c**) shows similar enhancement in the artery and fastest enhancing tumoral area, with a steep slope during first-pass of contrast medium, followed by an early plateau phase and immediate wash-out, histopathologically corresponding to non-responsive, highly vascular tumoral tissue, with numerous cells and small interstitial space. The muscle shows slow enhancement without a plateau phase within the first 120 s after bolus injection. The first-pass image or slope image (**d**) shows many bright areas indicating a high number of leaky capillaries with high perfusion in the non-responsive tumour

also an immediate wash-out) to a TIC with a slower first-pass followed by moderate further enhancement within the first 3 min, without wash-out, is observed in responders to chemotherapy and can be used to assess response to chemotherapy (Figs. 11.2c, 11.3c). For good response the TIC has to drop towards values at most twice the perfusion of muscle tissue. However, small nests of residual tumour tissue may be missed using the ROI method. To detect these small viable tumour nests, smaller areas of interest have to be investigated with subtraction or, alternatively, more sophisticated pixel-by-pixel post-processing methods, which display physiological parameters in one or only a few, usually coloured, parametric images.

11.3.5.3 Post-processing Methods

Other methods than the graphical ROI method to evaluate a DCE-MR imaging study are the native review method, the subtraction method and computerised pixel-by-pixel post-processing methods that calculate dynamic parameters such as the fastest-enhancement rate (= 'wash-in rate' or 'slope'), the maximal enhancement, the time to start of tumoral enhancement after the start of arterial enhancement, the time to peak enhancement and other more complex parameters, according to two- or three-compartment pharmacokinetic models (Dyke et al. 2003; Egmont-Petersen et al. 2000). Pixel-by-pixel post-processing tools are available in the MR manufacturer's software or they can be obtained as freeware on the internet or in commercially available software packets (Duke University School of Medicine website; National Institute of Health ImageJ website).

In the *native review method*, the more than one hundred dynamic images are reviewed one by one to visually assess the enhancement in different parts of the tumour. This can be done by fast 'scrolling' through all dynamic contrast-enhanced images or by using the cine-display method. Because visual assessment of enhancement can be difficult in small areas, in areas with discrete enhancement and in areas with already high signal intensity before arrival of the gadolinium-chelate (such as fatty and haemorrhagic areas), it is preferable that the physiological information behind the dynamic MR images is extracted by post-processing.

In the *subtraction* method, subtraction of a precontrast image from all subsequent images allows to review the images of the dynamic study one by one without any difficulty to see the arrival of the bolus in the artery, the immediate enhancement of highly vascular tumour areas and later enhancement of tumoral oedema and reactive tissue that has replaced tumoral tissue after chemotherapy.

The *first-pass* method is a computerised pixel-by-pixel post-processing method that calculates the fastest-enhancement rate during the first-pass of the contrast medium for each individual pixel, resulting in one parametric 'first-pass' image or 'slope' image, displaying pixels with a signal intensity equal to their individual highest enhancement rate. In this way areas with fast-enhancing tissue, such as viable tumour tissue, are displayed as white areas, whereas areas with slower enhancement, such as oedema, reactive tissue and tumour necrosis, will be displayed as dark grey to black areas (Lang et al. 1995; Reddick et al. 1995, 1999; Verstraete et al. 1994a, b, 1996) (Figs. 11.2d, 11.3d, 11.4d). Using this technique, good response to chemotherapy (> 90% necrosis) is predictable in bone tumours in which, at the end of chemotherapy, the first-pass image shows no bright areas with high first-pass enhancement rates (Fig. 11.3d). Whenever areas with a bright appearance are detected, poor response, with more than 10% of tumour tissue remaining vital should be suspected (Fig. 11.4d). In such cases, the first-pass image can be useful to guide a new biopsy or to focus the attention of the pathologist on those areas in the resected specimen in which tumour cells may have survived chemotherapy.

11.3.5.4 Assessment of Response

Assessment of response to neoadjuvant chemotherapy is one of the most important applications of DCE-MR imaging. After the completion of the preoperative chemotherapy, this technique allows the prediction of histological response with very high accuracy (> 90%) (Ongolo-Zogo et al. 1999). To evaluate the effect of chemotherapy, the dynamic contrast-enhanced images acquired before chemotherapy have to be compared to those obtained during and after neoadjuvant chemotherapy. For optimal comparison, it is useful to examine the patient in the same imaging planes and with the same acquisition parameters (Figs. 11.2, 11.3). Histopathologically, good response means that 90% or more of the viable tumour tissue has disappeared. At midpoint of the chemotherapy, DCE-MR imaging fails in predicting final histological response, mainly because early reactive granulation tissue in good responders may mimic persistent viable tumour areas. Therefore, after the first cycle of preoperative chemotherapy (i.e. after about 4 weeks), interpretation of the dynamic contrast-enhanced study should be done carefully and with a certain amount of reserve. Definitive classification of a patient as responder or non-responder should be postponed until the last preoperative dynamic MR examination, about 3 months after the first chemotherapy. At this time, the perfusion in the granulation tissue will have decreased, whereas residual tumour tissue will still be highly vascularised and perfused.

Another pitfall exists in the interpretation of DCE-MR imaging and the parametric post-processing techniques: low vascular tumour tissue, like chemotherapy-resistant chondroblastic areas in osteosarcoma, may mimic tumour necrosis (van der Woude et al. 1998; Verstraete et al. 1996).

Assessment of response can be done practically and quickly using the ROI method in combination with the native review method, subtraction method or a pixel-

by-pixel evaluation method like the first-pass images (De Baere et al. 1992; Reddick et al. 1999; van der Woude et al. 1995b; Verstraete et al. 1994a, b, 1996) (Figs. 11.2–11.4).

Scrolling through the series of more than hundred native or subtracted images allows to identify the early and very fast enhancing non-responsive active tumoral areas and differentiate them from later and slower-enhancing oedema or reactive tissue that has replaced the tumour after chemotherapy. Several ROIs can then be evaluated individually and displayed in a TIC to study the contrast-enhancement dynamics graphically.

On dynamic subtraction images the interval between the arrival of the bolus of contrast medium in an artery and the start of tissue enhancement can be used to detect residual viable tumour. A short time interval of less than 3 s between arterial enhancement and tissue enhancement with high wash-in rate followed by further progressive and intense enhancement within the first 2 min after bolus injection corresponds to feeding arteries, physeal vessels or residual viable tumour, often located subperiosteally and at the margins of the tumour. Viable tumour areas with scarce formation of matrix on microscopy, such as small cell osteosarcoma areas or Ewing's sarcoma, show early enhancement with rapid wash-out of contrast medium on the dynamic MR images. Late and gradually enhancing or non-enhancing areas correspond histopathologically to regions of chemotherapy-induced necrosis, mucomyxoid degeneration or fibrosis. Late or non-enhancing areas are associated with reactive changes such as oedema, haemorrhage or osteomyelitis or with tumour-related extracellular matrices such as abundant osteoid or chondroid.

References

Abudu A, Davies AM, Pynsent PB, Mangham DC, Tillman RM, Carter SR, Grimer RJ (1999) Tumour volume as a predictor of necrosis after chemotherapy in Ewing's sarcoma. J Bone Joint Surg Br 81:317–322

Arush MW, Israel O, Postovsky S, Militianu D, Meller I, Zaidman I, Sapir AE, Bar-Shalom R (2007) Positron emission tomography/computed tomography with 18fluoro-deoxyglucose in the detection of local recurrence and distant metastases of pediatric sarcoma. Pediatr Blood Cancer 49:901–905

Bastiaannet E, Groen H, Jager PL, Cobben DC, van der Graaf WT, Vaalburg W, Hoekstra HJ (2004) The value of FDG-PET in the detection, grading and response to therapy of soft tissue and bone sarcomas: a systematic review and meta-analysis. Cancer Treat Rev 30:83–101

Bramer JA, Gubler FM, Maas M, Bras H, de Kraker J, van der Eijken JW, Schaap GR (2004) Colour Doppler ultrasound predicts chemotherapy response, but not survival in paediatric osteosarcoma. Pediatr Radiol 34:614–619

De Baere T, Vanel D, Shapeero LG, Charpentier A, Terrier P, di Paola M (1992) Osteosarcoma after chemotherapy: evaluation with contrast material-enhanced subtraction MR imaging. Radiology 185:587–592

Duke University School of Medicine website: http://dblab.duhs.duke.edu/modules/PhysiologicalModels

Dyke JP, Panicek DM, Healey JH, Meyers PA, Huvos AG, Schwartz LH, Thaler HT, Tofts PS, Gorlick R, Koutcher JA, Ballon D (2003) Osteogenic and Ewing sarcomas: estimation of necrotic fraction during induction chemotherapy with dynamic contrast-enhanced MR imaging. Radiology 228:271–278

Egmont-Petersen M, Hogendoorn PC, van der Geest RJ, Vrooman HA, van der Woude H, Janssen JP, Bloem JL, Reiber JH (2000) Detection of areas with viable remnant tumour in postchemotherapy patients with Ewing's sarcoma by dynamic contrast-enhanced MRI using pharmacokinetic modeling. Magn Reson Imaging 18:525–535

El Khadrawy AM, Hoffer FA, Reddick WE (1999) Ewing's sarcoma recurrence versus radiation necrosis in dynamic contrast-enhanced MR imaging: a case report. Pediatr Radiol 29:272–274

Hayashida Y, Yakushiji T, Awai K, Katahira K, Nakayama Y, Shimomura O, Kitajima M, Hirai T, Yamashita Y, Mizuta H (2006) Monitoring therapeutic responses of primary bone tumours by diffusion-weighted image: initial results. Eur Radiol 16:2637–2643

Holscher HC, Bloem JL, Vanel D, Hermans J, Nooy MA, Taminiau AH, Henry-Amar M (1992) Osteosarcoma: chemotherapy-induced changes at MR imaging. Radiology 182:839–844

Holscher HC, Bloem JL, van der Woude HJ, Hermans J, Nooy MA, Taminiau AH, Hogendoorn PC (1995) Can MRI predict the histopathological response in patients with osteosarcoma after the first cycle of chemotherapy? Clin Radiol 50:384–390

Iagaru A, Masamed R, Chawla SP, Menendez LR, Fedenko A, Conti PS (2008) F-18 FDG PET and PET/CT evaluation of response to chemotherapy in bone and soft tissue sarcomas. Clin Nucl Med 33:8–13

Kaste SC, Liu T, Billups CA, Daw NC, Pratt CB, Meyer WH (2004) Tumour size as a predictor of outcome in pediatric non-metastatic osteosarcoma of the extremity. Pediatr Blood Cancer 43:723–728

Kauffman WM, Fletcher BD, Hanna SL, Meyer WH (1994) MR imaging findings in recurrent primary osseous Ewing sarcoma. Magn Reson Imaging 12:1147–1153

Lang P, Honda G, Roberts T, Vahlensieck M, Johnston JO, Rosenau W, Mathur A, Peterfy C, Gooding CA, Genant HK (1995) Musculoskeletal neoplasm: perineoplastic edema versus tumour on dynamic postcontrast MR images with spatial mapping of instantaneous enhancement rates. Radiology 197:831–839

Lang P, Wendland MF, Saeed M, Gindele A, Rosenau W, Mathur A, Gooding CA, Genant HK (1998) Osteogenic sarcoma: noninvasive in vivo assessment of tumor necrosis with diffusion-weighted MR imaging. Radiology 206:227–235

Lemmi MA, Fletcher BD, Marina NM, Slade W, Parham DM, Jenkins JJ, Meyer WH (1990) Use of MR imaging to assess results of chemotherapy for Ewing sarcoma. AJR Am J Roentgenol 155:343–346

MacVicar AD, Olliff JF, Pringle J, Pinkerton CR, Husband JE (1992) Ewing sarcoma: MR imaging of chemotherapy-induced changes with histologic correlation. Radiology 184:859–864

McCarville MB, Christie R, Daw NC, Spunt SL, Kaste SC (2005) PET/CT in the evaluation of childhood sarcomas. AJR Am J Roentgenol 184:1293–1304

Miller SL, Hoffer FA, Reddick WE, Wu S, Glass JO, Gronemeyer SA, Haliloglu M, Nikanorov AY, Xiong X, Pappo AS (2001) Tumour volume or dynamic contrast-enhanced MRI for prediction of clinical outcome of Ewing sarcoma family of tumours. Pediatr Radiol 31:518–523

National Institute of Health ImageJ website: http://rsbweb.nih.gov/ij/index.html

Ongolo-Zogo P, Thiesse P, Sau J, Desuzinges C, Blay JY, Bonmartin A, Bochu M, Philip T (1999) Assessment of osteosarcoma response to neoadjuvant chemotherapy: comparative usefulness of dynamic gadolinium-enhanced spin-echo magnetic resonance imaging and technetium-99m skeletal angioscintigraphy. Eur Radiol 9:907–914

Peterson JJ (2007) F-18 FDG-PET for detection of osseous metastatic disease and staging, restaging, and monitoring response to therapy of musculoskeletal tumours. Semin Musculoskelet Radiol 11:246–260

Reddick WE, Bhargava R, Taylor JS, Meyer WH, Fletcher BD (1995) Dynamic contrast-enhanced MR imaging evaluation of osteosarcoma response to neoadjuvant chemotherapy. J Magn Reson Imaging 5:689–694

Reddick WE, Taylor JS, Fletcher BD (1999) Dynamic MR imaging (DEMRI) of microcirculation in bone sarcoma. J Magn Reson Imaging 10:277–285

Shin KH, Moon SH, Suh JS, Yang WI (2000) Tumour volume change as a predictor of chemotherapeutic response in osteosarcoma. Clin Orthop Relat Res 376:200–208

Uhl M, Saueressig U, van Buiren M, Kontny U, Niemeyer C, Köhler G, Ilyasov K, Langer M (2006a) Osteosarcoma: preliminary results of in vivo assessment of tumour necrosis after chemotherapy with diffusion- and perfusion-weighted magnetic resonance imaging. Invest Radiol 41:618–623

Uhl M, Saueressig U, Koehler G, Kontny U, Niemeyer C, Reichardt W, Ilyasof K, Bley T, Langer M (2006b) Evaluation of tumour necrosis during chemotherapy with diffusion-weighted MR imaging: preliminary results in osteosarcomas. Pediatr Radiol 36:1306–1311

van der Woude HJ, Bloem JL, Schipper J, Hermans J, van Eck-Smit BL, van Oostayen J, Nooy MA, Taminiau AH, Holscher HC, Hogendoorn PC (1994a) Changes in tumour perfusion induced by chemotherapy in bone sarcomas: color Doppler flow imaging compared with contrast-enhanced MR imaging and three-phase bone scintigraphy. Radiology 191:421–431

van der Woude HJ, Bloem JL, Holscher HC, Nooy MA, Taminiau AH, Hermans J, Falke TH, Hogendoorn PC (1994b) Monitoring the effect of chemotherapy in Ewing's sarcoma of bone with MR imaging. Skeletal Radiol 23:493–500

van der Woude HJ, Bloem JL, van Oostayen JA, Nooy MA, Taminiau AH, Hermans J, Reynierse M, Hogendoorn PC (1995a) Treatment of high-grade bone sarcomas with neoadjuvant chemotherapy: the utility of sequential color Doppler sonography in predicting histopathologic response. AJR Am J Roentgenol 165:125–133

van der Woude HJ, Bloem JL, Verstraete KL, Taminiau AH, Nooy MA, Hogendoorn PC (1995b) Osteosarcoma and Ewing's sarcoma after neoadjuvant chemotherapy: value of dynamic MR imaging in detecting viable tumour before surgery. AJR Am J Roentgenol 165:593–598

van der Woude HJ, Bloem JL, Hogendoorn PC (1998) Preoperative evaluation and monitoring chemotherapy in patients with high-grade osteogenic and Ewing's sarcoma: review of current imaging modalities. Skeletal Radiol 27:57–71

van der Woude HJ, Vanderschueren G (1999) Ultrasound in musculoskeletal tumours with emphasis on its role in tumour follow-up. Radiol Clin North Am 37:753–766

Verstraete KL, Dierick A, De Deene Y, Uyttendaele D, Vandamme F, Roels H, Kunnen M (1994a) First-pass images of musculoskeletal lesions: a new and useful diagnostic application of dynamic contrast-enhanced MRI. Magn Reson Imaging 12:687–702

Verstraete KL, De Deene Y, Roels H, Dierick A, Uyttendaele D, Kunnen M (1994b) Benign and malignant musculoskeletal lesions: dynamic contrast-enhanced MR imaging–parametric "first-pass" images depict tissue vascularisation and perfusion. Radiology 192:835–843

Verstraete KL, Van der Woude HJ, Hogendoorn PC, De-Deene Y, Kunnen M, Bloem JL (1996) Dynamic contrast-enhanced MR imaging of musculoskeletal tumours: basic principles and clinical applications. J Magn Reson Imaging 6:311–321

Assessment of Locally Recurrent Disease

12

Marc H. Willis, Ambrose J. Huang, Miriam A. Bredella and Susan V. Kattapuram

CONTENTS

M. H. Willis, DO
Massachusetts General Hospital, Department of Radiology, Musculoskeletal Division, 55 Fruit Street, Yawkey 6E, Boston, MA 02114, USA

A. J. Huang, MD
Massachusetts General Hospital, Department of Radiology, Musculoskeletal Division, 55 Fruit Street, Yawkey 6E, Boston, MA 02114, USA

M. A. Bredella, MD
Massachusetts General Hospital, Department of Radiology, Musculoskeletal Division, 55 Fruit Street, Yawkey 6E, Boston, MA 02114, USA

S. V. Kattapuram, MD
Massachusetts General Hospital
Department of Radiology, Musculoskeletal Division
55 Fruit Street, Yawkey 6E, Boston, MA 02114, USA

KEY POINTS

- Imaging is a key component of routine screening to evaluate local control of disease and for the evaluation of suspected local recurrence.
- Proper utilization of the available imaging modalities is important to optimize the early detection of local recurrence. In order to obtain this goal, one must also have knowledge of the imaging characteristics of these tumors when they recur locally.

12.1 Introduction

In recent years, there has been significant improvement in the diagnosis and treatment of bone tumors. Local control remains a challenge in both benign and malignant bone tumors. Imaging plays a significant role in management of these neoplasms. An understanding of the proper utilization of the various imaging tools is extremely important. One should also have a grasp of the imaging features of these recurrences. Knowledge of the original tumor's typical appearance at recurrence, predilection to recur at a specific site, and imaging findings that affect management are essential.

12.2 Imaging Modalities

Radiographs are valuable to evaluate osteolysis, new bone formation, and the presence of mineralization. Gross soft tissue abnormalities may be detected on radiographs; however, radiographs alone do not provide a reliable imaging option for soft tissue recurrence (Costelloe et al. 2007).

Bone scintigraphy is highly sensitive for detecting bone formation. The principal role of bone scintigraphy in evaluating osseous lesions is to determine whether the process is monostotic or polyostotic. Neoplasms have an enhanced glucose metabolism when compared with normal tissue, and FDG-PET has been shown to be sensitive and specific in detecting abnormal metabolic activity suggestive of tumor recurrence (see Fig. 12.3d; Johnson et al. 2003). The metabolic and anatomic information provided by FDG-PET/CT can be very valuable in the assessment for possible recurrence, even in patients with extensive changes secondary to surgery and radiation therapy (Johnson et al. 2003).

CT demonstrates subtle bone changes and the presence of mineralization. The availability of 3D reconstructions is invaluable, especially in the axial skeleton. Intravenous contrast improves the sensitivity and specificity of soft tissue abnormalities and is valuable in patients with contraindications to MRI (Costelloe et al. 2007); however, one should consider the patient's prior cumulative radiation dose and site of the tumor before selecting CT as the modality for serial follow-up. This is especially true with the current improvements in treatment regimens and the significant increase in the number of disease-free years, particularly in younger patients with tumors of the head, chest wall, spine, and pelvis.

The bone marrow and soft tissues are best evaluated with MRI. With the appropriate protocols, MRI provides detailed evaluation of the surgical bed, even in the presence of hardware. With intravenous gadolinium, MRI can distinguish viable tumor from adjacent necrotic, fibrous, or normal tissue. This may prove indispensable when planning biopsy of a suspected local recurrence (Costelloe et al. 2007).

12.3 Imaging Findings

An understanding of the expected imaging findings with tumor recurrence is necessary for the evaluation of local control. Bone changes include lytic or destructive processes, marrow replacement, or new bone formation. Any new or expanding destructive focus at the resection margin is suspicious for tumor recurrence (Murphey et al. 2001). Mineralized matrix may be osteoid, which appears "cloud-like," or chondroid, described as "rings-and-arcs." Osteolysis and tumor matrix are best evaluated with radiographs and/or CT. On MRI, the intramedullary and soft tissue extent of disease, particularly the relationship between the tumor mass and major neurovascular structures, is well demonstrated. Marrow replacement is seen as foci of signal intensity that are hypointense to normal muscle on T1-weighted images and hyperintense on T2-weighted images. Mineralized osteoid matrix is seen on MRI as low signal intensity areas within the marrow or soft tissues. Chondroid matrix is hypointense on T1-weighted images and hyperintense on T2-weighted images. In the presence of enchondral ossification, heterogenous low signal intensity foci are seen on both T1- and T2-weighted images. Cortical abnormalities may present as periostitis, cortical thinning, scalloping, remodeling, or cortical disruption.

The changes from prior surgery and/or radiation present one of the major challenges in imaging of local recurrence. The importance and availability of baseline studies at the time of follow-up interpretation cannot be overemphasized. Treatment-related changes often significantly distort the anatomy and signal characteristics. Without proper comparison, the sensitivity and specificity for detection of early local recurrence is significantly diminished. If polymethyl methacrylate is present, the marked difference in density between it and the adjacent bone on radiography or CT helps in the detection of early destructive foci. On MRI, polymethyl methacrylate results in a signal void on all pulse sequences (Costelloe et al. 2007).

12.4 Benign Tumors

The benign bone tumors that have a propensity for local recurrence include giant cell tumor, aneurysmal bone cyst, and chondroblastoma.

12.4.1 Giant Cell Tumor

Giant cell tumors result in a geographic region of bone lysis, have a narrow zone of transition, and most commonly lack surrounding sclerosis. The tumor is eccentrically located in the juxta-cortical or metaepiphyseal region, extends to the subchondral bone, and results in expansile remodeling and cortical thinning. Giant cell tumor is histologically benign but can be aggressive and may recur locally. Wide resection of the tumor has a low local recurrence rate; however, wide resection can result in impaired joint function. With simple curettage, the local recurrence rate can be as high as 60%. With bone grafting, the local bone recurrence rate is 40–60%. Newer surgical techniques include the use of adjuvants such

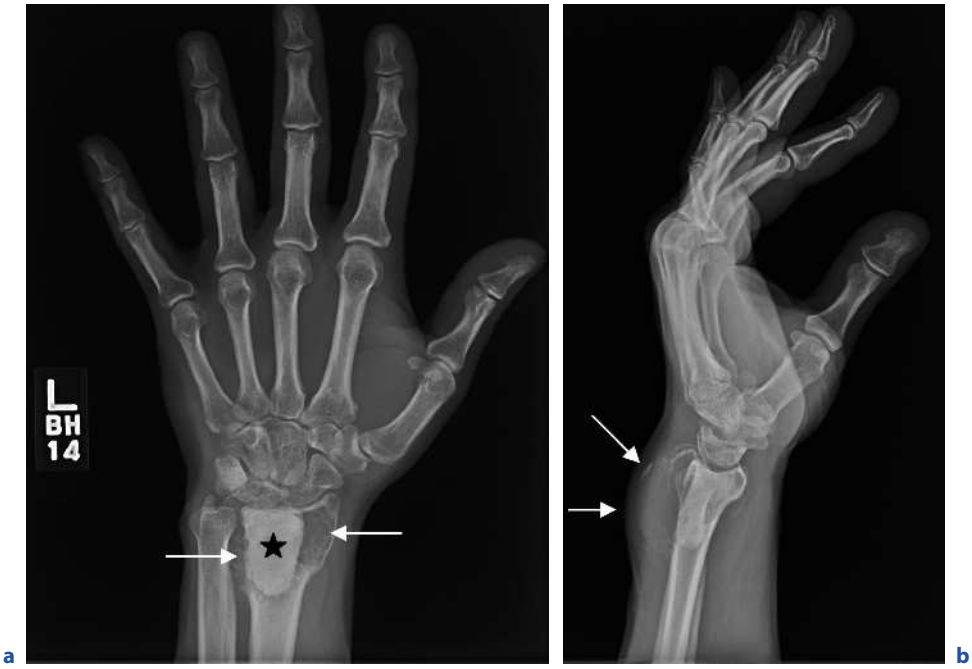

a b

Fig. 12.1a,b. A 50-year-old man presents with an enlarging mass on the dorsum of the distal left forearm 12 years after curettage and polymethyl methacrylate packing of a giant cell tumor involving the distal radius. **a** Frontal radiograph demonstrates radiodense polymethyl methacrylate centrally within the distal radius (*star*) with osteolysis and expansile osseous remodeling (*arrows*) at the margin of the prior curettage, that involves the adjacent bone. **b** Lateral radiograph shows expansile remodeling of the distal radius with a thin osseous rim resulting in the dorsal mass (*white arrows*) for which the patient sought evaluation

as polymethyl methacrylate, liquid nitrogen, phenol, or thermal cautery. Polymethyl methacrylate provides added mechanical stability and allows early weight-bearing. The use of these adjuvants has decreased the local recurrence rate to less than 25% (McGough et al. 2005; Murphey et al. 2001; O'Donnell et al. 1994; Turcotte 2006; Vidyadhara and Rao 2007).

The site of the original tumor also plays a significant role in local recurrence. Locations such as the axial skeleton and distal radius have increased rates of recurrence. The proximity of the axial lesions to the adjacent neurologic structures greatly limits wide surgical resections (Caudell et al. 2003; O'Donnell et al. 1994; Refai et al., in press).

Of giant cell tumor recurrences, 80–90% occur during the first 3 years after treatment, and the peak incidence of recurrence is between 12 and 18 months. Recurrence after 3 years is rare but has been reported up to decades after the initial treatment. Imaging at 3- to 6-month intervals for the first 5–6 years after treatment and then yearly has been recommended (Murphey et al. 2001). Recurrence typically presents with pain. If there is resorption of intralesional bone graft or areas of bone destruction at the resection margins, local recurrence should be suspected. In the presence of polymethyl methacrylate, a lucent rim, up to 2 mm, at the cement-bone interface, is normal because of the thermal cytotoxic effect of the cement, and typically does not progress after 6–8 months. Surrounding this lucent rim, it is normal for a sclerotic margin to form around the cement. Progressive lysis or failed development of the sclerotic rim between the cement and cancellous bone suggests recurrence (Fig. 12.1). Since the cement creates signal void on all MRI sequences, any subtle nodular foci of bone marrow replacement are indicative of recurrence. Additionally, high signal intensity within the surgical bed that exhibits a rounded mass effect and eccentric growth is highly suggestive of tumor. Differentiation of recurrent tumor from cement-related giant cell reaction can be difficult. Giant cell granulomas usually develop after several years, whereas the majority of tumor recurrences occur within 18 months after the initial surgery. In addition, tumor recurrence grows more rapidly than giant cell granuloma; however, when there is overlap of the imaging features, a biopsy for histologic evaluation may be needed (McGough et al.

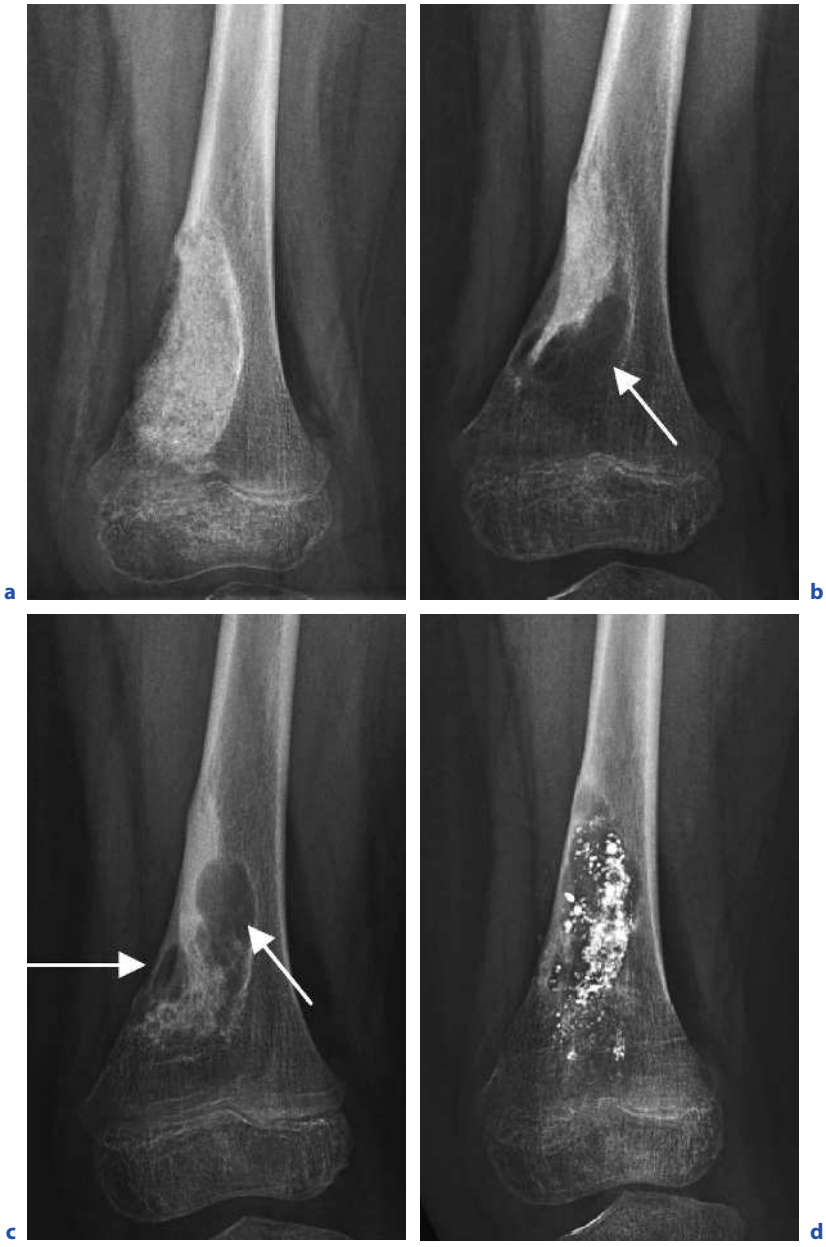

Fig. 12.2a–d. An 8-year-old boy with multiple recurrences of an aneurysmal bone cyst involving his distal femur. Multiple frontal radiographs of the distal femur. **a** Six weeks after curettage and allograft packing of the aneurysmal bone cyst. **b** Five months after the initial surgery, there is lysis of the allograft and the adjacent bone by the recurrent tumor (*arrow*). **c** Five months after the second curettage and allograft packing, there is again lysis of the allograft and adjacent bone by the second recurrence of the tumor (*arrows*). **d** After a third recurrence, the patient underwent sclerotherapy and embolization

2005; Mendenhall et al. 2006b; Murphey et al. 2001; O'Donnell et al. 1994; Turcotte 2006; Vidyadhara and Rao 2007).

There is a 1% risk of local soft tissue recurrence due to contamination during treatment. Soft tissue recurrence typically appears as a mass with a peripheral rim of calcification. Differentiating the rim of calcification associated with recurrence from myositis ossificans can be difficult. When faced with this challenge, several key concepts can aid this distinction. The factors suggesting local recurrence include continued slow growth of the abnormality, occurrence more than 2 months after surgical treatment, and failure of ossific maturation (Costelloe et al. 2007; Murphey et al. 2001; Turcotte 2006).

Despite their classification as benign tumors, giant cell tumors have generally enhanced FDG uptake, mainly attributable to an enhanced vascular fraction and increased FDG transport (Kern et al. 1988).

Of giant cell tumors, 14% have cystic components (secondary aneurysmal bone cyst). Giant cell tumors are the most common tumors associated with second-

ary aneurysmal bone cysts, and recurrent lesions may also present with cystic areas. This is important, since biopsies must be directed at the solid portion of the tumor to yield diagnostic tissue. On CT, the solid components will demonstrate attenuation similar to that of adjacent normal muscle. CT or MRI with intravenous contrast is the best modality to detect the solid components of the tumor (Murphey et al. 2001).

12.4.2 Aneurysmal Bone Cyst

Aneurysmal bone cyst (ABC) is a benign neoplasm, typically eccentric in location within the metaphyseal areas of long bones. The flat bones (pelvis and scapula) and posterior elements of the spine are also well-known locations. It presents as a lytic lesion with cortical thinning and expansile remodeling (Lin et al. 2008; Mankin et al. 2005; Mendenhall et al. 2006a; Papagelopoulos et al. 2001; Rastogi et al. 2006). The origin remains controversial, but most feel it is a benign vascular tumor (Rastogi et al. 2006). The tumor may be primary or arise secondarily within the bone, associated with an underlying lesion such as giant cell tumor, unicameral bone cyst, non-ossifying fibroma, fibrous dysplasia, chondroblastoma, or osteoblastoma (Mankin et al. 2005; Mendenhall et al. 2006a).

Aneurysmal bone cysts are commonly treated with curettage and bone graft or cement placement. Local control rates range between 60–95% (Mankin et al. 2005; Mendenhall et al. 2006a). Sclerotherapy has been successfully used as an alternative treatment with low rates of local recurrence (Rastogi et al. 2006). The site of the lesion plays a significant role in the rate of local recurrence. Lesions of the clavicle and distal femur have the highest rates of recurrence. Lesions involving the pelvis and spine can be extremely difficult to treat due to their proximity to neurovascular structures (Mankin et al. 2005; Mendenhall et al. 2006a; Papagelopoulos et al. 2001).

Most local recurrences occur within the first 2 years after treatment (Mendenhall et al. 2006a; Papagelopoulos et al. 2001). A new focus of lysis or mass at the treatment site is worrisome for recurrence (Fig. 12.2). A diagnosis of ABC from a percutaneous needle biopsy can be difficult, especially if the biopsy sample contains only blood products (Mankin et al. 2005).

12.4.3 Chondroblastoma

Chondroblastoma classically is an eccentric lesion that involves the epiphysis or apophysis of long bones (de Silva and Reid 2003; Ramappa et al. 2000; van der Geest et al. 2007). The lesion may be purely lytic

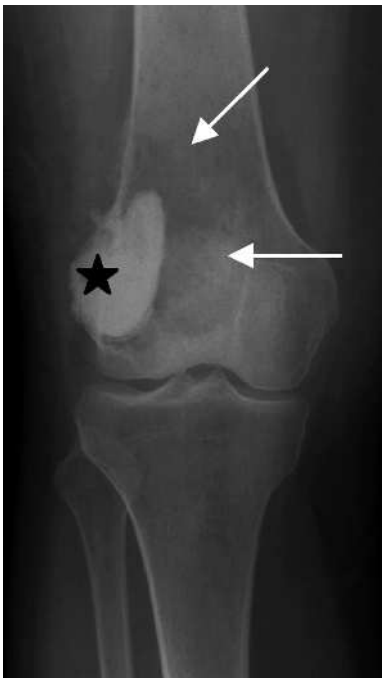

a

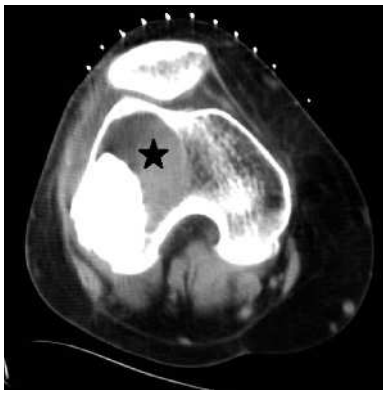

b

Fig. 12.3a–d. A 52-year-old woman with a long-standing history of locally recurrent chondroblastoma with pulmonary metastases. **a** Frontal radiograph of the distal femur reveals radiodense polymethyl methacrylate eccentrically within the distal femur from curettage and packing of the tumor 12 years prior (*star*). Adjacent to the polymethyl methacrylate, there is subtle lysis of the adjacent bone from tumor recurrence (*arrows*). **b** Subsequent CT performed for a CT-guided biopsy. The target for the biopsy was the area of osteolysis adjacent to the polymethyl methacrylate (*star*). (**c,d**) *see next page*

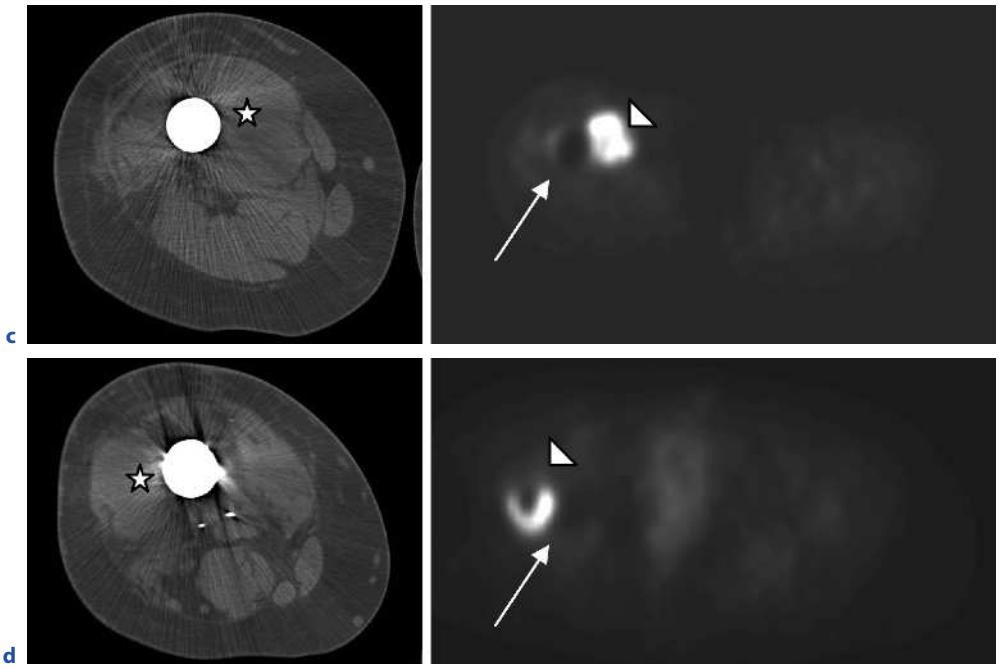

Fig. 12.3a–d. (*continued*) **c,d** CT and FDG-PET images performed 4 years after resection and endoprosthetic reconstruction of a second local recurrence, which resulted in a pathologic fracture. CT images demonstrate soft tissue masses (*stars*) that are partially obscured by the beam-hardening artifact from the endoprosthetic device. On FDG-PET images, the soft tissue masses demonstrate avid FDG uptake (*arrowheads*). The voids of FDG uptake are from the endoprosthetic device (*arrows*)

or may contain punctuate calcifications (Ramappa et al. 2000; van der Geest et al. 2007). The treatment of chondroblastoma is focused on local control while preserving function; however, this can be problematic. Recurrence rates are around 10% for most long bones. The location of the tumor can be associated with a higher risk of recurrence, and lesions around the hip joint are associated with higher recurrence rates (Ramappa et al. 2000). The presence of secondary ABC adds to the recurrence risk (de Silva and Reid 2003; Ramappa et al. 2000). As with many other tumors, a new focus of lysis or mass at the treatment site is worrisome for recurrence (Fig. 12.3).

12.5 Malignant Tumors

The malignant bone tumors that have a propensity for local recurrence include osteosarcoma, chondrosarcoma, undifferentiated high-grade pleomorphic sarcoma (also known as malignant fibrous histiocytoma), Ewing sarcoma family of tumors, chordoma, and adamantinoma.

12.5.1 Osteosarcoma

Osteosarcoma is the most common primary malignant bone tumor. Primary tumors typically occur at sites of rapid bone turnover and are classically characterized by osteoid production by the tumor cells which appears "cloud-like" on radiographs and CT (Skubitz and D'Adamo 2007). The majority of patients are treated with neoadjuvant chemotherapy and surgery (DeLaney et al. 2005). More than 80% of patients with osteosarcoma of the extremities are now offered limb-sparing surgery (Bacci et al. 2006).

Local recurrence rates range from 4–10% and the prognosis after local recurrence remains poor (Nathan et al. 2006; Rodriguez-Galindo et al. 2004). Lesions that recur two or more years after treatment, in a location where surgical resection is possible, portend a better prognosis (Rodriguez-Galindo et al. 2004).

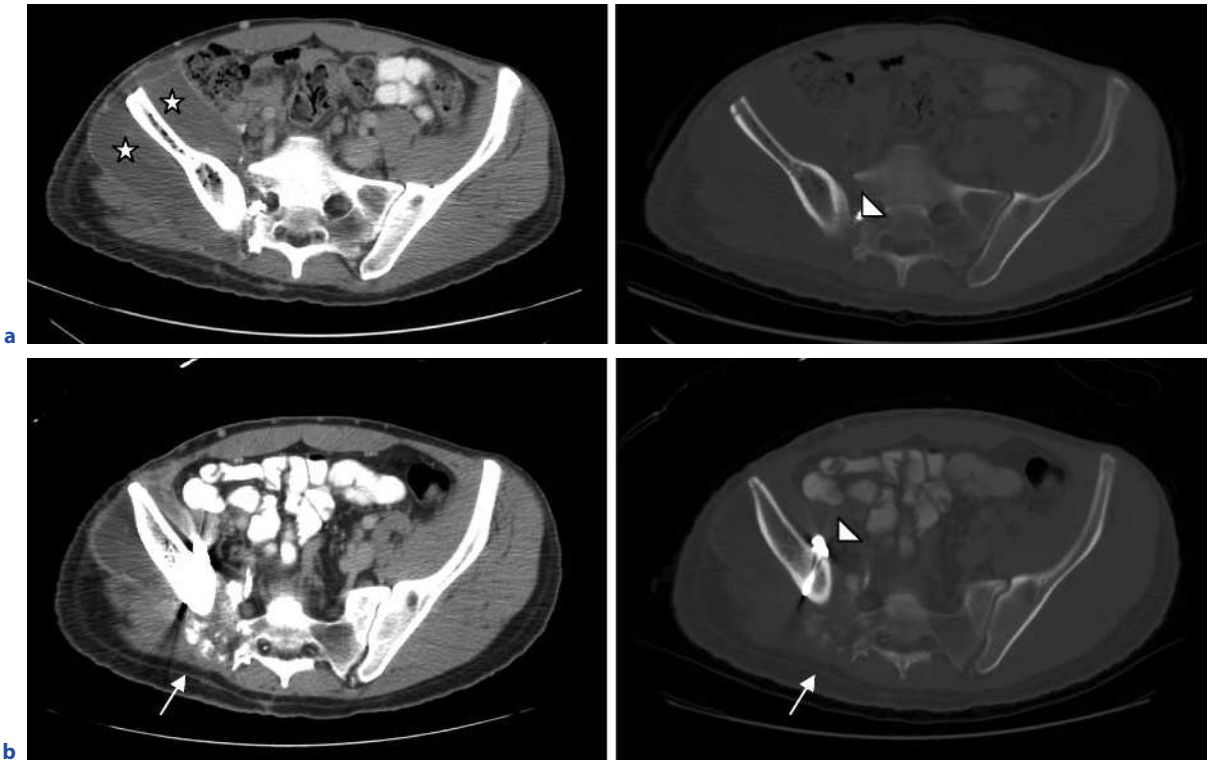

Fig. 12.4a,b. A 21-year-old man treated with chemotherapy and right internal hemipelvectomy and reconstruction with a hemipelvic allograft for a large right pelvic osteosarcoma. **a** CT of the pelvis windowed for soft tissues and bone 1 month after surgery demonstrates a fluid collection surrounding the iliac bone, likely secondary to the allograft (*stars*). Partially visualized is a portion of a fixation screw (*arrowhead*). **b** CT of the pelvis windowed for soft tissue and bone 5 months after surgery. Now there is mineralization posterior and lateral to the sacroiliac joint, which proved to be recurrence of the osteosarcoma (*arrows*). Partially visualized is a portion of the fixation hardware with adjacent beam-hardening artifact (*arrowhead*)

Recurrence rates have dramatically decreased with the use of neoadjuvant chemotherapy (Nathan et al. 2006; Skubitz and D'Adamo 2007). The strongest predictor of local recurrence is the adequacy of the surgical margin (Bacci et al. 2007). Lesions in the pelvis, spine, head, or neck present a surgical challenge (Skubitz and D'Adamo 2007). Proton-beam therapy shows promise as an adjuvant in these locations (DeLaney et al. 2005).

The significance and management of patients with a pathologic fracture in osteosarcoma remains controversial. Limb-sparing surgery is an option in some of these patients. The tumor response and fracture healing during chemotherapy indicate whether limb salvage can be performed without increased risk of recurrence (Bramer et al. 2007; Scully et al. 2002).

The imaging features of local recurrence include soft tissue calcifications, ossifications (35%), and bone and soft tissue involvement on CT or MRI (53%; Fig. 12.4). Treatment of osteosarcoma often involves the placement of hardware; therefore, MRI with metal-suppression techniques may be beneficial in detecting soft tissue recurrence in these patients (Rodriguez-Galindo et al. 2004). The FDG-PET may help detect the most appropriate regions for biopsy, aiding differentiation of viable tumor from treatment-related scar, which can be extremely difficult by other modalities (Johnson et al. 2003).

12.5.2 Chondrosarcoma

Primary chondrosarcoma is the third most common primary malignant bone tumor after osteosarcoma and multiple myeloma. Chondrosarcomas classically show a chondroid matrix described as "rings-and-arcs," endosteal scalloping, and possible soft tissue involvement (Murphey et al. 2003). Local recurrence is common, but the impact on survival remains somewhat contro-

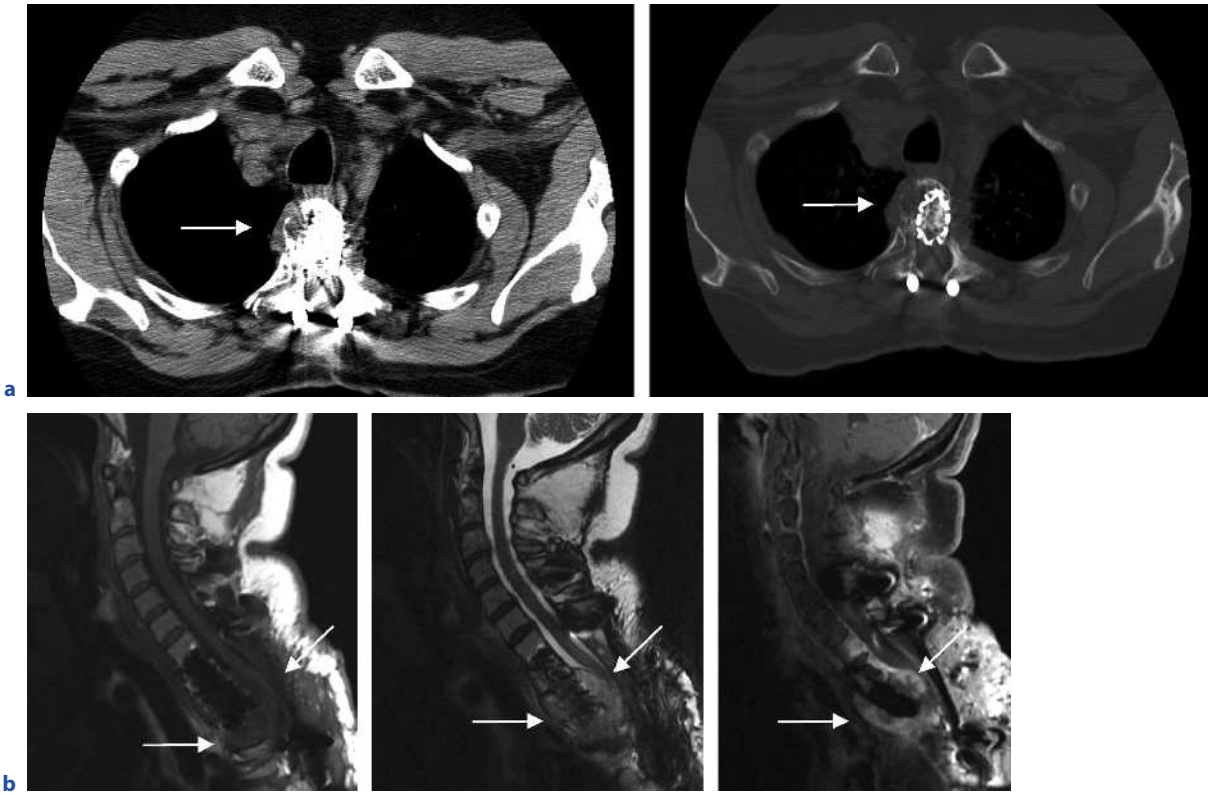

Fig. 12.5a,b. A 51-year-old woman with a history of multiple recurrences of a thoracic chondrosarcoma presented approximately 3 years after T1–T3 corpectomies, interbody cage placement, posterior decompression, and posterior fusion from C7–T5 with a complaint of increasing numbness in her lower extremities. **a** CT of the thoracic spine windowed for soft tissue and bone shows a soft tissue mass involving the right side of the T2 and T3 vertebral bodies with right paraspinal extension (*arrows*). Assessment for involvement within the central canal is difficult because of the beam-hardening artifact from the spinal fusion hardware. **b** Sagittal T1-weighted, T2-weighted, and T1-weighted gadolinium-enhanced fat-suppressed MRI of the cervicothoracic junction reveal a large heterogeneous mass extending into the ventral epidural space and compressing the adjacent spinal cord (*arrows*)

versial (Donati et al. 2005). Patients that have pulmonary metastases at the time of local recurrence have the poorest prognosis (Fiorenza et al. 2002). FDG-PET analysis of chondrosarcomas utilizing maximum (SUV), combined with histopathology, can be useful for tumor grading and outcome prediction for local recurrence and metastases (Feldman et al. 2005).

Local recurrence rates for chondrosarcoma range from 28–45% (Pring et al. 2001). The standard surgical treatment is wide excision. Successful complete resection of the tumor, including the biopsy tract, without contamination of the adjacent tissues provides the best chance of local control. The recurrence rates are highest for tumors involving the pelvis, spine, craniofacial bones, scapula, and ribs (Fig. 12.5; Fiorenza et al. 2002; Leerapun et al. 2007; Murphey et al. 2003; Schneiderbauer et al. 2004). Chondrosarcoma of the pelvis may cross the sacroiliac joint, and these patients have a higher incidence of local failure (Donati et al. 2005).

There is a risk for locally recurrent chondrosarcoma to recur at a higher grade than the original tumor (up to 13%); therefore, when planning a biopsy, targeted areas for tissue sampling should include the solid component of the tumor without calcification, any soft tissue components, and areas of aggressive endosteal scalloping, diffuse enhancement, or maximum FDG-PET avidity. Following the biopsy, communication with the orthopedic surgeon is extremely important to assure that the biopsy path is included in the future surgical bed (Bovée et al. 2005; Murphey et al. 2003).

12.5.3 Undifferentiated High-grade Pleomorphic Sarcoma/Malignant Fibrous Histiocytoma

Undifferentiated high-grade pleomorphic sarcoma/malignant fibrous histiocytoma (MFH) is a malignant neoplasm of uncertain origin (Murphey 2007). This tumor is more common in soft tissues than bone. This malignancy typically arises as a primary bone lesion in younger patients. Up to 25% of MFH arise secondary to an underlying benign bone lesion. These lesions include Paget disease, irradiated bone, bone infarcts, enchondroma, and fibrous dysplasia. The secondary lesions typically affect older patients.

The tumor tends to infiltrate the medullary compartment of bone without significant tissue reaction; therefore, MRI is helpful in evaluating the extent of disease. Recurrence rates range from 6–19% with radical and wide surgical margins, but recurrence is as high as 64% if margins are inadequate. A combined treatment approach of neoadjuvant chemotherapy and wide surgical resection is recommended (Natarajan et al. 2007). Any new site of bone destruction, soft tissue mass, or marrow replacement on CT or MRI should be considered highly suspicious for recurrence.

12.5.4 Ewing Sarcoma Family of Tumors

Ewing sarcoma family of tumors (ESFT) is a group of small round-cell neoplasms that comprise the second most common malignant bone tumor in childhood and adolescents. Most ESFTs develop in the extremities, but

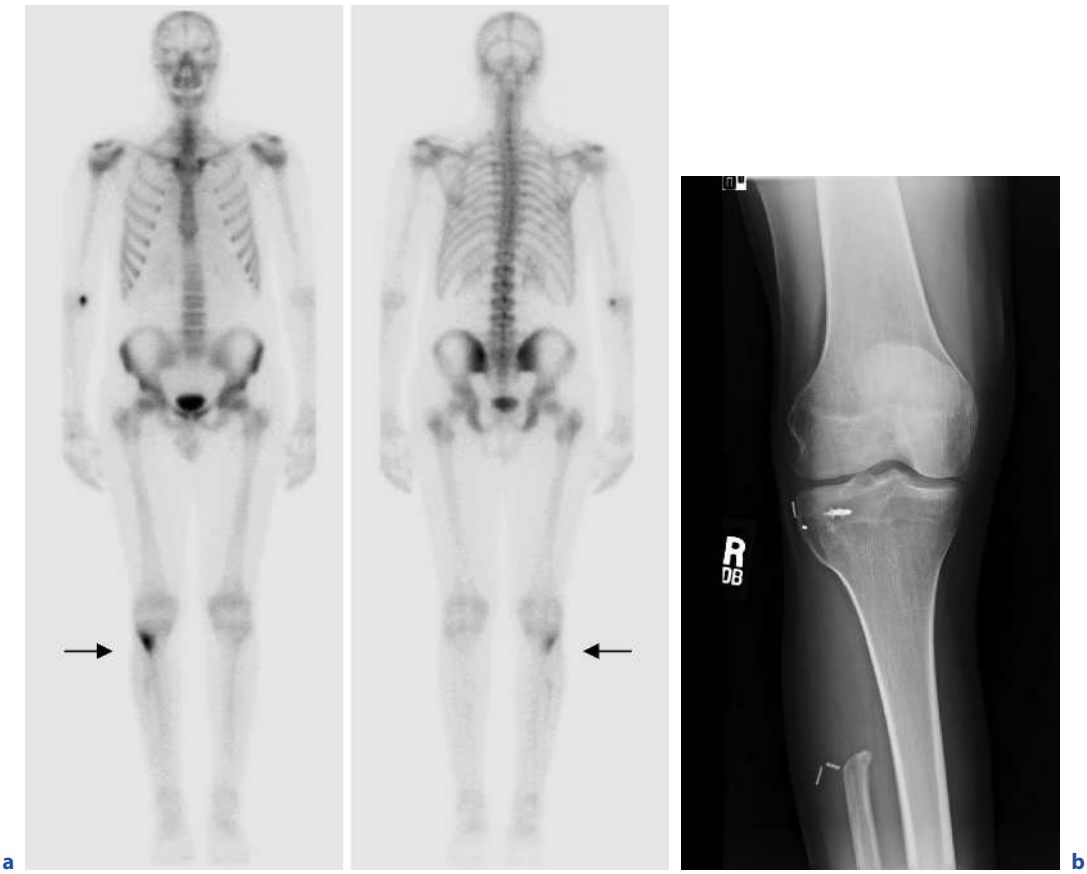

a b

Fig. 12.6a–c. A 24-year-old man with metastatic disease to his chest from Ewing sarcoma family of tumors involving his right fibula. **a** Bone scintigram performed 4 years after the original resection to evaluate the extent of metastatic disease revealed no evidence of metastases, but increased Tc-99m MDP activity at the site of his prior resection warranted additional evaluation (*arrows*) **b** Frontal radiograph of the knee shows the changes of prior treatment, but no definite abnormality to explain the abnormality on bone scintigraphy. (**c**) *see next page*

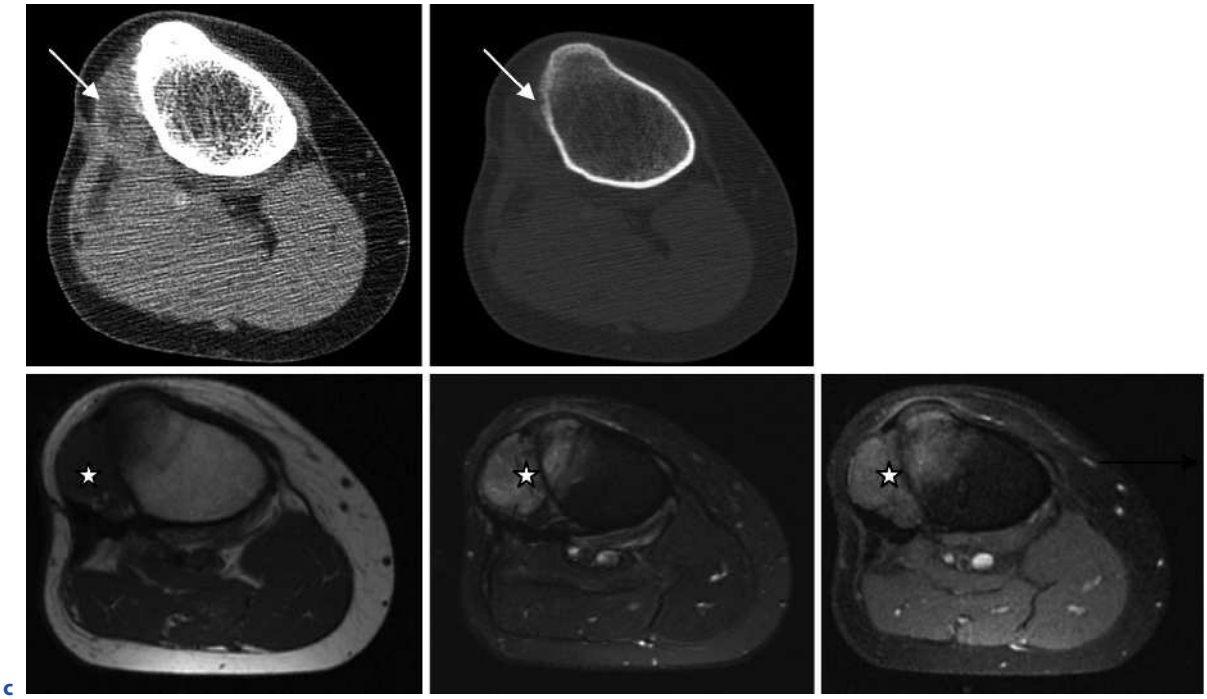

Fig. 12.6a–c. *(continued)* **c** CT of the knee, windowed for soft tissues and bone, demonstrates subtle periosteal reaction of the lateral tibia and an adjacent soft tissue mass (*arrows*). T1-weighted, T2-weighted, and T1-weighted gadolinium-enhanced fat-suppressed MRI show a T1 hypointense, T2 hyperintense, enhancing mass involving the lateral tibia and adjacent soft tissues at the site of the prior resection

any bone can be involved. The most common radiographic finding is an aggressive permeative lesion that often elicits multilayered periostitis and an "onion-skin" appearance. CT and MRI help to define the extent of the tumor, especially the involvement of the bone marrow and wheter an associated soft tissue component is present.

During the past three decades, there has been marked improvement in the outcomes of these patients. Utilizing a multimodal approach, disease-free survival and overall survival are approaching 70% and > 80%, respectively. Combined treatment with surgery, radiation, and systemic chemotherapy results in the best rate local control. The prognosis of patients with an ESFT that does relapse is very poor, and only 13% achieve a second remission; therefore, judicious use of intensive chemotherapy and aggressive local treatment are advocated (Bacci et al. 2003; Rodriguez-Galindo et al. 2008). Any new area of bone destruction or soft tissue mass in the surgical bed is suspicious for local recurrence (Fig. 12.6).

12.5.5 Chordoma

Chordomas arise when notochord rests within the axial skeleton undergo malignant degeneration (Chugh et al. 2007; Park et al. 2006; Rutz et al. 2007). Despite the relatively slow growth, chordomas are locally aggressive, and local control of the disease is extremely difficult (Chugh et al. 2007). The surgical margin is the most important factor in predicting local recurrence. Obtaining negative surgical margins is often a challenge because of the close proximity to important neurologic structures (Park et al. 2006). Preservation of the sacral nerves is crucial in order to retain rectal and urinary control (Park et al. 2006).

Local recurrence is approximately 20% with adequate surgical margins and reaches 70% with positive margins. The role of radiation is debated due to the relative resistance of the tumor and high doses needed. Protons, other forms of radiation, and radiosensitization are being investigated (Chugh et al. 2007; Park et al. 2006). On the follow-up images, areas of bone destruction along the resected margin and/or soft tis-

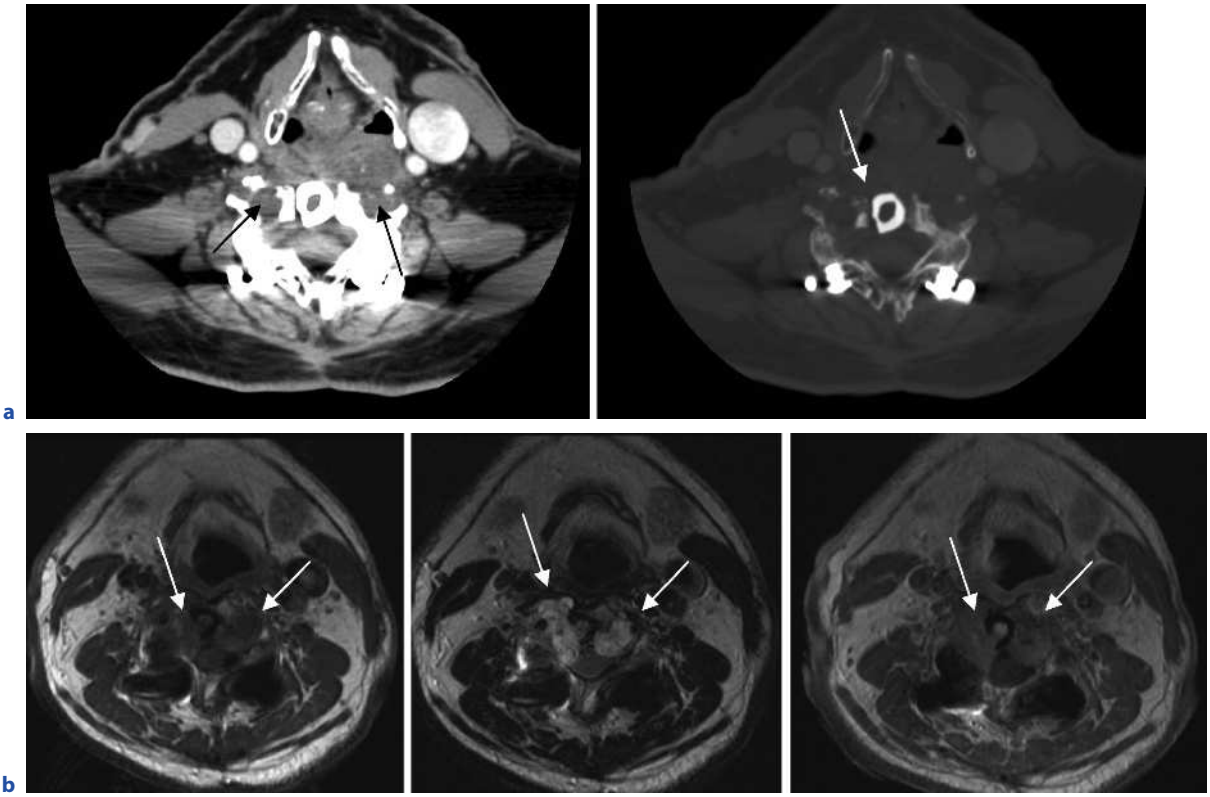

Fig. 12.7a,b. A 72-year-old man with a chordoma involving C4 and C5, status post-interbody allograft placement and posterior fusion from C3–C7. **a** CT of the cervical spine approximately 2 years after the surgery windowed for soft tissues and bone shows a large soft tissue mass involving the vertebral body and extending into the anterior soft tissues. The tumor invades the transverse foramina and encases the vertebral arteries (*black arrows*) There is lysis of the right side of the allograft by the mass (*white arrow*) **b** The extent of the soft tissue component is better demonstrated on MRI performed near the same time. The mass is hypointense on T1-weighted images, hyperintense on T2-weighted images, enhances following gadolinium administration (*arrows*), invades the transverse foramina, encases the vertebral arteries, and causes stenosis of the central canal

sue masses in the surgical bed or track is suggestive of recurrence (Fig. 12.7).

12.5.6 Adamantinoma

Adamantinoma is a rare malignant bone tumor that classically involves the anterior cortex of the tibial diaphysis, causes bone lysis and expansile remodeling, and may result in bowing deformities (Jain et al. 2008; Levine et al. 2003a). Adamantinoma is a slow-growing tumor that can be locally aggressive. Treatment is primarily surgical with en-bloc resection and limb-salvaging procedures. The goal of treatment is to obtain a wide surgical margin while preserving function (Jain et al. 2008). The rate of local recurrence after surgical resection is 8.6% at 5 years and 18.6% at 10 years. If a wide margin cannot be obtained, the recurrence rate increases to 32% (Qureshi et al. 2000; Van der Woude et al. 2004). Any new site of bone destruction or marrow replacement is worrisome for recurrence.

12.6 Conclusion

In conclusion, it is important to understand the significant role imaging plays in the evaluation and management of local recurrence of many benign and malignant bone neoplasms. Proper utilization of the available modalities and knowledge of the imaging features of these tumors when they recur locally is also important.

References

Bacci G, Ferrari S, Longhi A, Donati D, Paolis M de, Forni C et al. (2003) Therapy and survival after recurrence of Ewing's tumors: the rizzoli experience in 195 patients treated with adjuvant and neoadjuvant chemotherapy from 1979 to 1997. Ann Oncol 14(11):1654(1659

Bacci G, Longhi A, Cesari M, Versari M, Bertoni F (2006) Influence of local recurrence on survival in patients with extremity osteosarcoma treated with neoadjuvant chemotherapy: the experience of a single institution with 44 patients. Cancer 106(12):2701-2706

Bacci G, Forni C, Longhi A, Ferrari S, Mercuri M, Bertoni F et al. (2007) Local recurrence and local control of nonmetastatic osteosarcoma of the extremities: a 27-year experience in a single institution. J Surg Oncol 96(2):118-123

Bovée JV, Cleton-Jansen A, Taminiau AH, Hogendoorn PC (2005) Emerging pathways in the development of chondrosarcoma of bone and implications for targeted treatment. Lancet Oncol 6(8):599-607

Bramer JAM, Abudu AA, Grimer RJ, Carter SR, Tillman RM (2007) Do pathological fractures influence survival and local recurrence rate in bony sarcomas? Eur J Cancer 43(13):1944-1951

Caudell JJ, Ballo MT, Zagars GK, Lewis VO, Weber KL, Lin PP et al. (2003) Radiotherapy in the management of giant cell tumor of bone. Int J Radiat Oncol Biol Phys 57(1):158-165

Chugh R, Tawbi H, Lucas DR, Biermann JS, Schuetze SM, Baker LH (2007) Chordoma: the nonsarcoma primary bone tumor. Oncologist 12(11):1344-1350

Costelloe CM, Kumar R, Yasko AW, Murphy WA Jr, Stafford RJ, Lewis VO et al. (2007) Imaging characteristics of locally recurrent tumors of bone. Am J Roentgenol 188(3):855-863

DeLaney TF, Park L, Goldberg SI, Hug EB, Liebsch NJ, Munzenrider JE et al. (2005) Radiotherapy for local control of osteosarcoma. Int J Radiat Oncol Biol Phys 61(2):492-498

Donati D, El Ghoneimy A, Bertoni F, Bella C di, Mercuri M (2005) Surgical treatment and outcome of conventional pelvic chondrosarcoma. J Bone Joint Surg Br 87(11):1527-1530

Feldman F, Van Heertum R, Saxena C, Parisien M (2005) 18FDG-PET applications for cartilage neoplasms. Skeletal Radiol 34(7):367-374

Fiorenza F, Abudu A, Grimer RJ, Carter SR, Tillman RM, Ayoub K et al. (2002) Risk factors for survival and local control in chondrosarcoma of bone. J Bone Joint Surg Br 84(1):93-99

Jain D, Jain VK, Vasishta RK, Ranjan P, Kumar Y (2008) Adamantinoma: a clinicopathological review and update. Diagn Pathol 3(1):8

Johnson GR, Zhuang H, Khan J, Chiang SB, Alavi A (2003) Roles of positron emission tomography with fluorine-18-deoxyglucose in the detection of local recurrent and distant metastatic sarcoma. Clin Nucl Med 28(10):815-820

Kern KA, Brunetti A, Norton JA, Chang AE, Malawer M, Lack E et al. (1988) Metabolic imaging of human extremity musculoskeletal tumors by PET. J Nucl Med 29(2):181-186

Leerapun T, Hugate RR, Inwards CY, Scully SP, Sim FH (2007) Surgical management of conventional grade I chondrosarcoma of long bones. Clin Orthop Relat Res 463:166-172

Levine SM, Lambiase RE, Petchprapa CN (2003a) Cortical lesions of the tibia: characteristic appearances at conventional radiography. Radiographics 23(1):157-177

Levine SM, Lambiase RE, Petchprapa CN (2003b) Cortical lesions of the tibia: characteristic appearances at conventional radiography. Radiographics 23(1):157-177

Lin PP, Brown C, Raymond AK, Deavers MT, Yasko AW (2008) Aneurysmal bone cysts recur at juxtaphyseal locations in skeletally immature patients. Clin Orthop Relat Res 466:722-728

Mankin HJ, Hornicek FJ, Ortiz-Cruz E, Villafuerte J, Gebhardt MC (2005) Aneurysmal bone cyst: a review of 150 patients. J Clin Oncol 23(27):6756-6762

McGough RL, Rutledge J, Lewis VO, Lin PP, Yasko AW (2005) Impact severity of local recurrence in giant cell tumor of bone. Clin Orthop Relat Res 438:116-122

Mendenhall WM, Zlotecki RA, Gibbs CP, Reith JD, Scarborough MT, Mendenhall NP (2006a) Aneurysmal bone cyst. Am J Clin Oncol 29(3):311-315

Mendenhall WM, Zlotecki RA, Scarborough MT, Gibbs CP, Mendenhall NP (2006b) Giant cell tumor of bone. Am J Clin Oncol 29(1):96-99

Murphey MD (2007) World health organization classification of bone and soft tissue tumors: modifications and implications for radiologists. Semin Musculoskelet Radiol 11(3):201-214

Murphey MD, Nomikos GC, Flemming DJ, Gannon FH, Temple HT, Kransdorf MJ (2001) From the archives of AFIP: imaging of giant cell tumor and giant cell reparative granuloma of bone: radiologic-pathologic correlation. Radiographics 21(5):1283-1309

Murphey MD, Walker EA, Wilson AJ, Kransdorf MJ, Temple HT, Gannon FH (2003) From the archives of the AFIP: imaging of primary chondrosarcoma: radiologic-pathologic correlation. Radiographics 23(5):1245-1278

Natarajan MV, Mohanlal P, Bose JC (2007) Limb salvage surgery complimented by customised mega prostheses for malignant fibrous histiocytomas of bone. J Orthop Surg (Hong Kong) 15(3):352-356

Nathan SS, Gorlick R, Bukata S, Chou A, Morris CD, Boland PJ et al. (2006) Treatment algorithm for locally recurrent osteosarcoma based on local disease-free interval and the presence of lung metastasis. Cancer 107(7):1607-1616

O'Donnell RJ, Springfield DS, Motwani HK, Ready JE, Gebhardt MC, Mankin HJ (1994) Recurrence of giant-cell tumors of the long bones after curettage and packing with cement. J Bone Joint Surg Am 76(12):1827-1833

Papagelopoulos PJ, Choudhury SN, Frassica FJ, Bond JR, Unni KK, Sim FH (2001) Treatment of aneurysmal bone cysts of the pelvis and sacrum. J Bone Joint Surg Am 83-A(11):1674-1681

Park L, Delaney TF, Liebsch NJ, Hornicek FJ, Goldberg S, Mankin H et al. (2006) Sacral chordomas: impact of high-dose proton/photon-beam radiation therapy combined with or without surgery for primary versus recurrent tumor. Int J Radiat Oncol Biol Phys 65(5):1514-1521

Pring ME, Weber KL, Unni KK, Sim FH (2001) Chondrosarcoma of the pelvis. A review of sixty-four cases. J Bone Joint Surg Am 83-A(11):1630-1642

Qureshi AA, Shott S, Mallin BA, Gitelis S (2000) Current trends in the management of adamantinoma of long bones. an international study. J Bone Joint Surg Am 82-A(8):1122-1131

Ramappa AJ, Lee FY, Tang P, Carlson JR, Gebhardt MC, Mankin HJ (2000) Chondroblastoma of bone. J Bone Joint Surg Am 82-A(8):1140-1145

Rastogi S, Varshney MK, Trikha V, Khan SA, Choudhury B, Safaya R (2006) Treatment of aneurysmal bone cysts with percutaneous sclerotherapy using polidocanol. A review of 72 cases with long-term follow-up. J Bone Joint Surg Br 88(9):1212-1216

Refai D, Dunn GP, Santiago P (in press) Giant cell tumor of the thoracic spine: case report and review of the literature. Surg Neurol

Rodriguez-Galindo C, Shah N, McCarville MB, Billups CA, Neel MN, Rao BN et al. (2004) Outcome after local recurrence of osteosarcoma: the St. Jude Children's Research Hospital experience (1970-2000) Cancer 100(9):1928-1935

Rodriguez-Galindo C, Navid F, Liu T, Billups CA, Rao BN, Krasin MJ (2008) Prognostic factors for local and distant control in Ewing sarcoma family of tumors. Ann Oncol 19(4):814-820

Rutz HP, Weber DC, Sugahara S, Timmermann B, Lomax AJ, Bolsi A et al. (2007) Extracranial chordoma: outcome in patients treated with function-preserving surgery followed by spot-scanning proton beam irradiation. Int J Radiat Oncol Biol Phys 67(2):512-520

Schneiderbauer MM, Blanchard C, Gullerud R, Harmsen WS, Rock MG, Shives TC et al. (2004) Scapular chondrosarcomas have high rates of local recurrence and metastasis. Clin Orthop Relat Res (426):232-238

Scully SP, Ghert MA, Zurakowski D, Thompson RC, Gebhardt MC (2002) Pathologic fracture in osteosarcoma: prognostic importance and treatment implications. J Bone Joint Surg Am 84-A(1):49-57

Silva MVC de, Reid R (2003) Chondroblastoma: varied histologic appearance, potential diagnostic pitfalls, and clinicopathologic features associated with local recurrence. Ann Diagn Pathol 7(4):205-213

Skubitz KM, D'Adamo DR (2007) Sarcoma. Mayo Clinic Proc 82(11):1409-1432

Turcotte RE (2006) Giant cell tumor of bone. Orthop Clin North Am 37(1):35-51

Van der Geest IC, van Noort MP, Schreuder HW, Pruszczynski M, de Rooy JW, Veth RP (2007) The cryosurgical treatment of chondroblastoma of bone: long-term oncologic and functional results. J Surg Oncol 96(3):230-234

Van der Woude HJ, Hazelbag HM, Bloem JL, Taminiau AH, Hogendoorn PC (2004) MRI of adamantinoma of long bones in correlation with histopathology. Am J Roentgenol 183(6):1737-1744

Vidyadhara S, Rao SK (2007) Techniques in the management of juxta-articular aggressive and recurrent giant cell tumors around the knee. Eur J Surg Oncol 33(2):243-251

Cartilage Tumours

13

Karl Ludwig

CONTENTS

K. Ludwig, MD
Associate Professor of Radiology, Department of Diagnostic Radiology, Orthopedic University Hospital, University of Heidelberg, Schlierbacher Landstraße 200a, 69118 Heidelberg, Germany

KEY POINTS

- Cartilage tumours include a range of benign and malignant entities characterised by more or less differentiated cartilage tissue.
- Imaging findings reflect this range with specific findings of well-differentiated cartilage on one side and findings of high aggressiveness without specific criteria on the other.
- The findings of well-differentiated cartilage are chondrogenic calcifications, lobulated structure with high water content and a rings-and-arcs type enhancement of the fibrovascular interlobular septae.
- There is a gradual transition between benign and low-grade malignant cartilage tumours that makes thorough workup of lesions using a combination of clinical information, radiology and pathology especially important.

13.1 Introduction

Cartilage tumours represent a wide spectrum of entities ranging from lesions that are more like hamartomas than neoplasms to highly aggressive sarcomatous tumours. There is a gradual transition between benign and low-grade malignant chondrogenic tumours, making differential diagnosis and treatment decisions difficult and leading to an especially important role of radiology. Like other primary bone tumours, most chondrogenic tumours have a certain predilection for the age and site of manifestation.

Within the benign chondrogenic lesions, especially those of hamartomatous origin, enchondromas and osteochondromas are extremely frequent, while chondro-

blastomas and chondromyxoid fibromas are infrequent. Within the malignant chondrogenic lesions, conventional chondrosarcoma represents one of the most frequent malignant primary bone tumours. Within the malignant part of the spectrum there are exceptionally rare histological variants of chondrosarcomas, the clear cell chondrosarcoma and the mesenchymal chondrosarcoma. Juxtacortical chondrosarcomas, even rarer, are characterised by their localisation on the bone surface and are difficult to distinguish from juxtacortical chondromas. Dedifferentiated chondrosarcomas and secondary chondrosarcomas eventually are bimorphic lesions and include a benign or low-grade malignant chondrogenic tumour as a component.

13.2 Chondroblastoma

Chondroblastoma is a benign chondrogenic tumour with a strong predilection for the epiphysis of long tubular bones and for the adolescent age group. It accounts for less than 1% of all bone tumours and thus is the fourth most frequent chondrogenic tumour (Dahlin and Unni 1986). Approximately 70% of chondroblastomas present during the second decade of life, but manifestation ages from 3 to 73 years have been reported (Brower et al. 1990). There is a slight predominance of the male gender. About 75% of chondroblastomas are located in the epiphyses or apophyses of long tubular bones, most frequently in the proximal tibia, the proximal humerus, the distal femur and the apophysis of the greater trochanter (Dahlin and Unni 1986). Interestingly, the proximal epiphysis of the femur is not a very frequent localisation. Manifestation in equivalent sites of the flat bones occur as well, predominantly in the ileum. Extension in the metaphysis is reported in up to 50% of chondroblastomas (Bloem and Mulder 1985). Within other localisations described—chondroblastoma can generally manifest in any skeletal region—the temporal bone, the talus and the calcaneus are more frequent (Davila et al. 2004). Patients with chondroblastomas in these atypical regions tend to be of a greater age at the time of diagnosis and the development of secondary aneurysmal bone cysts is described more frequently (Kyriakos et al. 1985). It should be mentioned that in chondroblastoma, though generally a benign tumour, a few cases of malignant behaviour and with distant metastases have been reported (Brien et al. 1997).

The typical radiograph of a chondroblastoma is that of a round or oval lytic lesion with a geographic pattern of destruction located eccentrically in the epiphysis of a long tubular bone (Fig. 13.1). It is sharply demarcated with a thin complete or incomplete sclerotic rim. Matrix mineralisation is found in approximately 50% of chondroblastomas (Bloem and Mulder 1985). It tends to be more of an amorphous pattern instead of a punctuate or rings-and-arcs pattern. Lack of a sclerotic rim, however, does not exclude the diagnosis of a chondroblastoma. Mostly lesion size does not exceed the size of the parent bone. If it does, which is rarely the case in the long bones but frequent in flat bones, it is surrounded by a thin neocortex. Penetration of the cortex is rare but has been described. Thus, most chondroblastomas are Lodwick grade Ia or Ib lesions, seldom Lodwick Ic lesions. Aggressive periosteal reactions or ill-defined margins usually do not occur in chondroblastomas. Some degree of periosteal reaction may be present in chondroblastomas. Interestingly and not fully explained up to date, pronounced periosteal reaction in the metaphysis has been reported in chondroblastomas confined to the epiphysis (Brower et al. 1990) (Fig. 13.2).

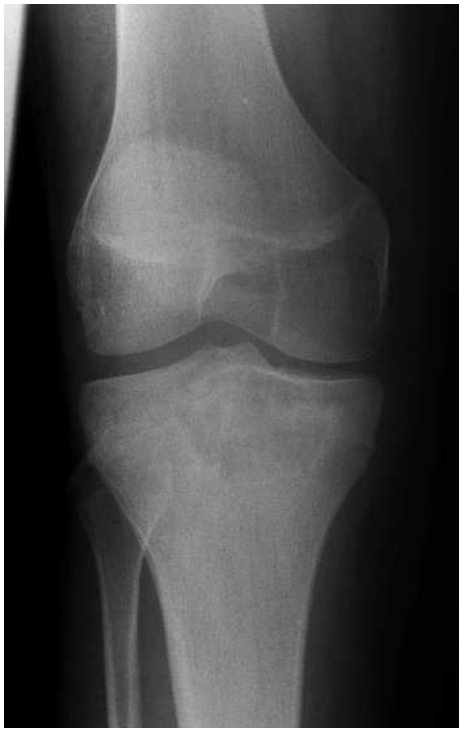

Fig. 13.1. Chondroblastoma: Anteroposterior radiograph shows a well-demarcated lytic lesion in the proximal epimetaphyseal tibia. It is surrounded by an incomplete thin rim of sclerosis and shows slight amorphous matrix calcifications. The subchondral bone lamella is intact

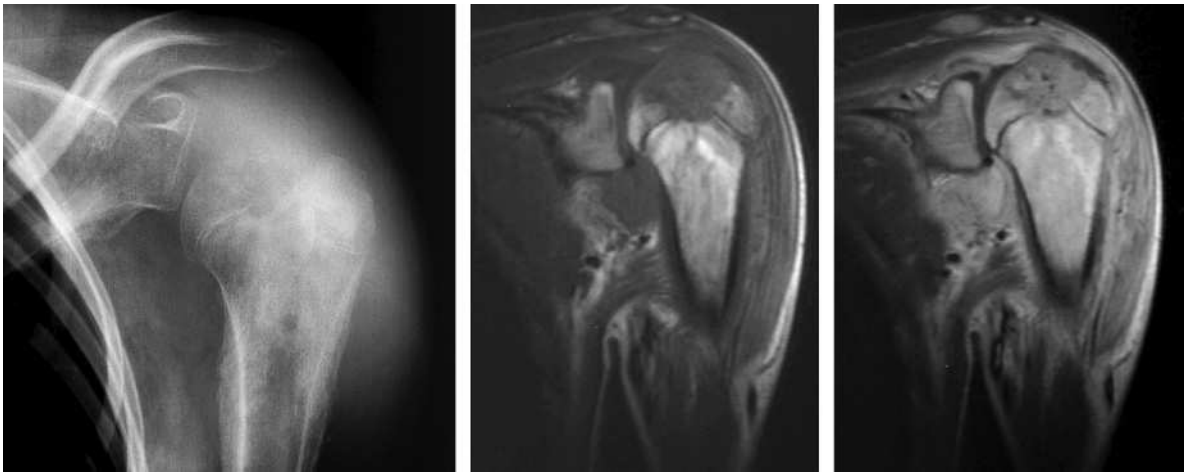

a b,c

Fig. 13.2a–c. Chondroblastoma: Anteroposterior radiograph (**a**) shows a lytic lesion in the proximal epiphyseal humerus with slight extension into the metaphysis. The pattern of destruction is geographic. The subchondral bone lamella is destroyed. There is considerable metaphyseal sclerosis and periosteal reaction. T1-weighted MR images without (**b**) and with (**c**) contrast enhancement show the demarcation of the lesion and the slight extension into the metaphysis

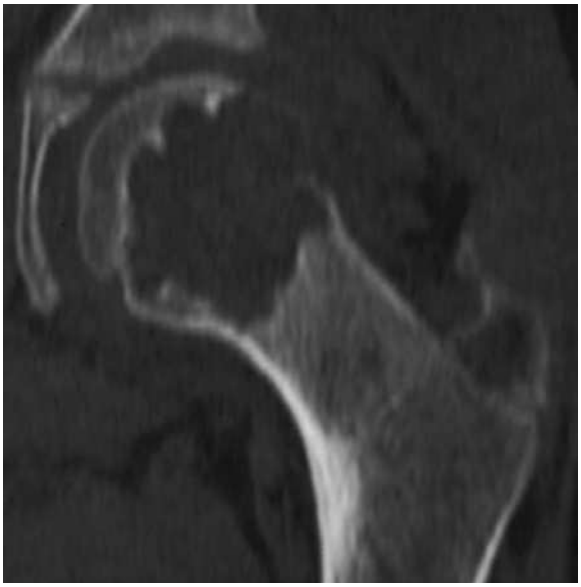

Fig. 13.3. Chondroblastoma: Computed tomography in a coronal reconstruction shows a well-demarcated lytic lesion in the proximal epimetaphyseal femur, one of the less frequent locations of chondroblastoma. There is an incomplete thin rim of sclerosis and the cortex is partially destroyed. No matrix calcifications can be seen

In typical cases of chondroblastomas—epiphyseal location, young patient, typical morphology of bone destruction and matrix mineralisation—the diagnosis can be made on a plain radiograph. Computed tomography can help in the detection of matrix mineralisation and in the assessment of the sclerotic rim (Fig. 13.3). MR imaging can be useful in the exclusion of a soft tissue component or intra-articular extension. Due to their high cellularity chondroblastomas frequently show a low to intermediate signal in T1-weighted images and a heterogeneous intermediate signal in T2-weighted images. Chondroblastomas usually present with an intense perifocal oedema and sometimes cystic regions within the chondroblastoma can be seen (Weatherall et al. 1994; Kaim et al. 2002). MR imaging can help in the differentiation from bone abscess in which it shows a ring enhancement around a liquid centre in contrast to the solid tissue of a chondroblastoma.

Localisation is a key point in the differential diagnosis of chondroblastoma as only a few other lesions share this predilection site. Giant cell tumours are located metaepiphyseally, are more aggressive in terms of cortex penetration and prefer a slightly older age group. Bone abscesses have a wider sclerotic rim, but can occur in a metaepiphyseal location and produce a profound perifocal oedema as well. Metastases predominantly occur in a much older age group. Ganglia, frequently located in the epiphyseal area of long bones, do not show matrix mineralisation, are more frequent in higher age groups and can mostly be distinguished by the fluid signal they show on MR imaging. An important but difficult differential diagnosis is clear cell carcinoma, a rare low-grade malignant lesion that can be morphologically indistinguishable from chondroblastoma. Its peak manifestation age is slightly higher than that of chon-

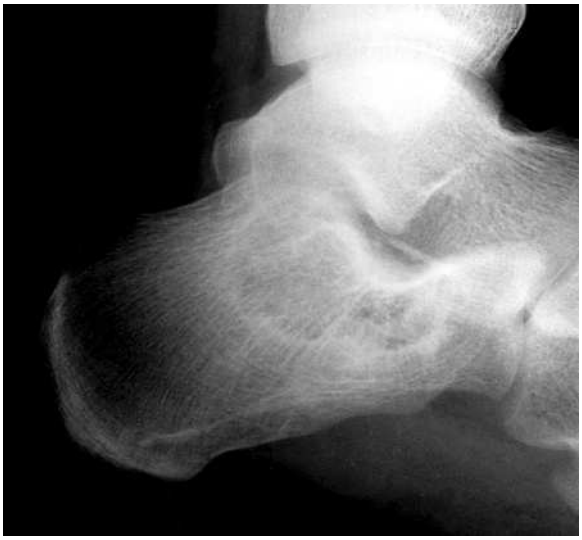

Fig. 13.4. Chondroblastoma: Lateral radiograph of the heel of the foot shows a well-demarcated lytic lesion with a thin rim of sclerosis in the calcaneus adjacent to the subtalar joint. Within the calcaneus, chondroblastoma, chondromyxoid fibroma and chondrosarcoma are the cartilaginous tumours to take into the differential diagnosis. Enchondromas hardly occur in the calcaneus

droblastoma, but age distribution overlaps widely. Its most frequent localisation is the proximal epiphysis of the femur, a site that is infrequent in chondroblastoma. Chondromyxoid fibromas usually arise in the metaphysis. If they extend into the epiphysis differentiation from a chondroblastoma with extension into the metaphysis can be difficult.

Chondroblastomas frequently develop secondary aneurysmal bone cysts, which should be taken into account in the radiologic–pathologic correlation after biopsy of a chondroblastoma.

Outside the epiphyseal location and especially in the flat bones of the pelvis, differential diagnosis can be difficult (Fig. 13.4). The presence of matrix calcifications is helpful, leading to the diagnosis of a chondrogenic tumour. Young patient age then leads to the correct diagnosis, as primary chondrosarcomas are rare in this age group and other chondrogenic tumours only rarely occur in the flat bones. A fibrous dysplasia can be diagnosed by its ground-glass density, if not radiographically then on computed tomography. In contrast to chondroblastoma it usually shows little perifocal reaction on MR imaging.

13.3 Chondroma

13.3.1 Enchondroma

Enchondroma is one of the most frequent benign entities in the spectrum of tumorous and tumour-like bone lesions. It is believed to be more like a hamartomatous lesion than a neoplasm, developing from embryonic rests of the physis which are displaced into the metaphysis during growth (Brien et al. 1997).

The vast majority of enchondromas are asymptomatic and are detected only as incidental findings. Otherwise pathologic fracture is the most common situation in which enchondromas are detected. The precise incidence of enchondroma is unknown and the frequency of enchondroma reported in large bone tumour series, e.g. 11% of benign and 3% of all lesions in a series of 8,542 bone tumours, can only be interpreted as an underestimation of its real frequency (Dahlin and Unni 1986). Because of the lack of symptoms, most enchondromas probably exist for a long time before they are diagnosed. Age distribution reported for the diagnosis of enchondroma, however, includes a wide range from 14 months to 90 years (Moser et al. 1990a).

Enchondromas have a predilection for the short tubular bones followed by the long tubular bones. Localisation outside the tubular bones is much less frequent but generally possible in any chondrogenic preformed bone. Large series report a frequency of approximately 4% in the axial skeleton (Dahlin and Unni 1986). This is especially important because one of the major differential diagnoses, chondrosarcoma, shows an almost complementary distribution with a high frequency in the axial skeleton and a low frequency peripherally (see Sect. 13.7).

Within its most frequent localisation in the short tubular bones, enchondroma is generally located metaphyseally or metadiaphyseally or involves all parts of the bone (Dahlin and Unni 1986). Within the long tubular bones it is mostly located centrally in the metaphyseal region, but can extend into the diaphysis and even into the opposed metaphysis. Eccentric location is not infrequent, especially in the distal femur. Epiphyseal or metaepiphyseal manifestation is rare (Potter et al. 2005).

The typical radiographic appearance of enchondroma depends on its location. In the short tubular bones lytic lesions with a thin sclerotic rim and a varying degree of chondrogenic calcification are typical. The sclerotic rim can be hard to see at the diaphyseal margin

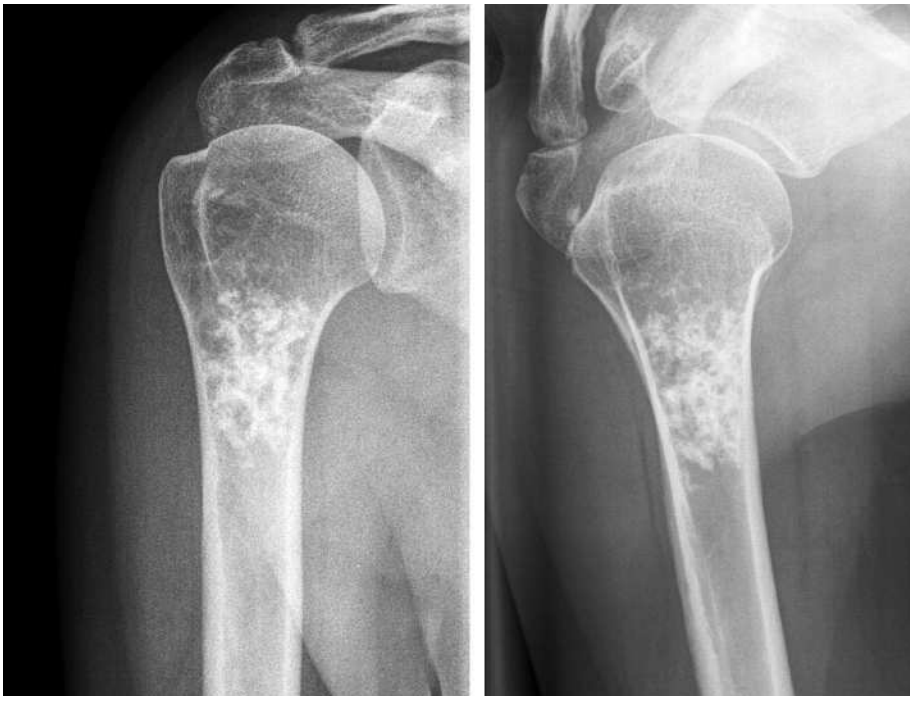

a b

Fig. 13.5a,b. Enchondroma: Radiographs show dense chondrogenic calcifications in the form of rings and arcs in the proximal metadiaphyseal humerus. The underlying osteolysis is completely obscured by the calcifications. There is no sclerotic rim and the cortex is intact. The patient is asymptomatic in this region

of the lesion due to the only minimal amount of trabeculae within the diaphyseal marrow cavity. Radiographic appearance can be suggestive of an aggressive or malignant lesion with destruction of the cortex and without neocortex formation. The biologic behaviour of such lesions, important for the treatment regime, however, is benign (Moser et al. 1990a).

Enchondromas of the long tubular bones may have two different radiographic patterns. First, they can show as dense chondrogenic calcifications completely obscuring the underlying destruction and typically showing no sclerotic rim (Fig. 13.5). The lack of a sclerotic rim has been interpreted as the ability of the enchondromas to connect closely to the surrounding trabeculae (Brien et al. 1997) (Fig. 13.6). This type of radiographic manifestation is typically located centrally in the medullary canal of the metaphysis. With larger size it may have contact to the cortex and show slight scalloping or even extend into the diaphysis. Deep scalloping (see Sect. 13.7), extension over a considerable length within the medullary canal (see Sect. 13.7) or expansile growth are not features of enchondroma but suggestive of chondrosarcoma (Murphey et al. 1998). Second, they can present as sharply demarcated lytic lesions with a thin rim of sclerosis and a varying degree of chondrogenic or amorphous calcification. Within the long bones they may occur in an eccentric location and have a slightly expansile pattern of bone destruction with formation of a thin neocortex (Moser et al. 1990a). A rare intracortical localisation has been described, as well as an extension from the bone surface called enchondroma protruberans. All radiographic manifestations have in common that they do not grow after skeletal maturity is reached and that they per se do not cause pain. However, pain can be present secondary to a pathologic fracture or an insufficiency fracture.

In the vast majority of cases enchondroma is a simple and unambiguous diagnosis based on the clinical and radiographic presentation. Neither computed tomography nor MR imaging is required. Computed tomography and MR imaging can be helpful in atypical cases and in atypical localisations in the axial skeleton. Computed tomography allows assessment of cortical integrity as well as matrix calcifications more accurately than radiography. MR imaging can show a typical pattern with a lobular lesion morphology, high signal in T2-weighted sequences, low to intermediate signal in T1-weighted sequences and a so-called rings-and-arcs

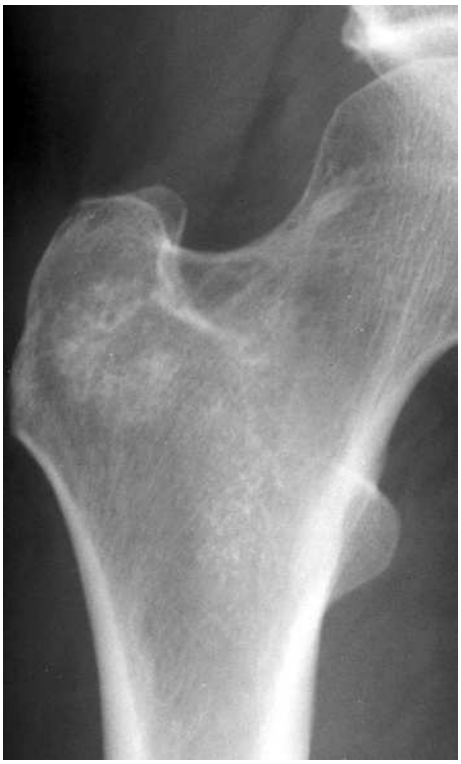

Fig. 13.6. Enchondroma: Radiograph shows chondrogenic calcifications in the form of rings and arcs in the proximal meta-apophyseal femur. The underlying osteolysis is completely obscured by the calcifications. There is no sclerotic rim and the cortex is intact. The patient is asymptomatic in this region

pattern of enhancement showing the fibrovascular septae between the cartilage lobules. This pattern, however, can also be found in highly differentiated chondrosarcomas (Aoki et al. 1991). If the amount of calcification is severe, the MR images can show low signal in T1- and T2-weighted images and the rings-and-arcs pattern of enhancement may be absent.

Within the differential diagnosis of enchondroma low-grade chondrosarcoma is of special importance and is discussed separately in Sect. 13.7. Besides low-grade chondrosarcoma, differential diagnoses of densely calcified enchondromas may be sclerotic lesions of any kind. These can normally be separated very well as they lack the typical chondrogenic pattern of calcification. Metaphyseal bone infarcts, however, can resemble densely calcified enchondromas radiographically. The differential diagnosis of lytic forms of enchondroma comprises fibrous dysplasia and non-ossifying fibroma. Within the chondrogenic tumours, chondromyxoid fibroma and chondroblastoma rarely can be differential diagnoses for atypical cases of enchondroma (Potter et al. 2005).

13.3.2 Periosteal Chondroma

Chondromas in a periosteal or juxtacortical localisation are rare entities believed to originate from the periosteum. Indicating the very low incidence of this lesion, in a series of 3,067 bone tumours only 16 periosteal chondromas were found (Brien et al. 1997). The leading localisations in these lesions are the metaphyseal regions of the short tubular bones, the femur and the humerus. Patient age at diagnosis in the series mentioned above commonly was under 30 years.

Radiographically, periosteal chondromas present as lesions scalloping the cortex from the periosteal side and eventually forming a sclerotic rim separating them from the medullary cavity of the parent bone (Moser et al. 1990a). Periosteal reaction at their margins causes the typical saucer-shaped profile of a periosteal lesion (Fig. 13.7). These reactions must not be mistaken for Codman's triangles and do not indicate aggressive growth. Periosteal chondromas show matrix calcifications in approximately 50% of cases and do present with a round to ovoid form on MR images (Robinson et al. 2001).

The main differential diagnosis is periosteal chondrosarcoma, an especially rare entity with a frequency about five times lower than periosteal chondroma. Differences between periosteal chondroma and periosteal chondrosarcoma are believed to be that periosteal chondrosarcomas are generally larger, may contain hazy windblown densities and do not show an endosteal border of sclerosis (Moser et al. 1990a). Published series on both lesions are small, so that the validity of these criteria is not well examined (Robinson et al. 2001).

13.3.3 Enchondromatosis

Enchondromatosis (Ollier's disease) is a rare condition in which multiple enchondromas are present, frequently with a preference for a certain limb or for one side of the body. In a series of 3,067 bone tumours 25 patients with an enchondromatosis are reported (Brien et al. 1997). In contrast to osteochondromatosis enchondromatosis does not have an inheritance pattern with a significant familial accumulation.

The radiographic morphology of single lesions of enchondromatosis is identical to that of solitary enchondromas (Fig. 13.8). The frequency of lesions, however, can lead to significant deformity. Diagnosis is commonly established within the first two decades of life. Patients with enchondromatosis are much more prone

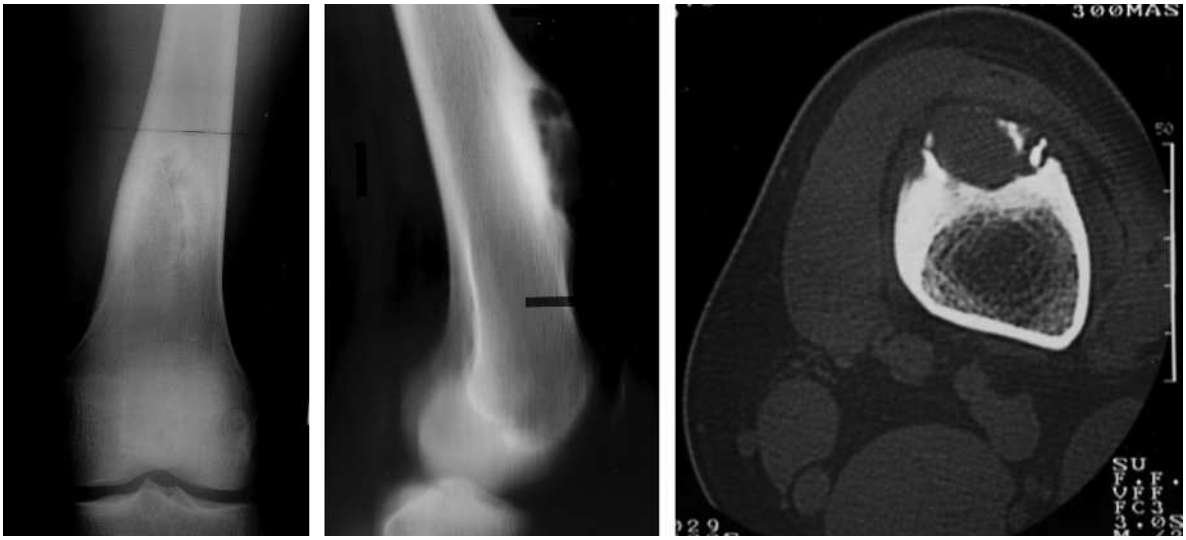

a b,c

Fig. 13.7a–c. Juxtacortical chondroma: Radiographs (**a,b**) and computed tomography (**c**) show a saucer-like juxtacortical lesion separated by a thick sclerotic rim from the medullary cavity

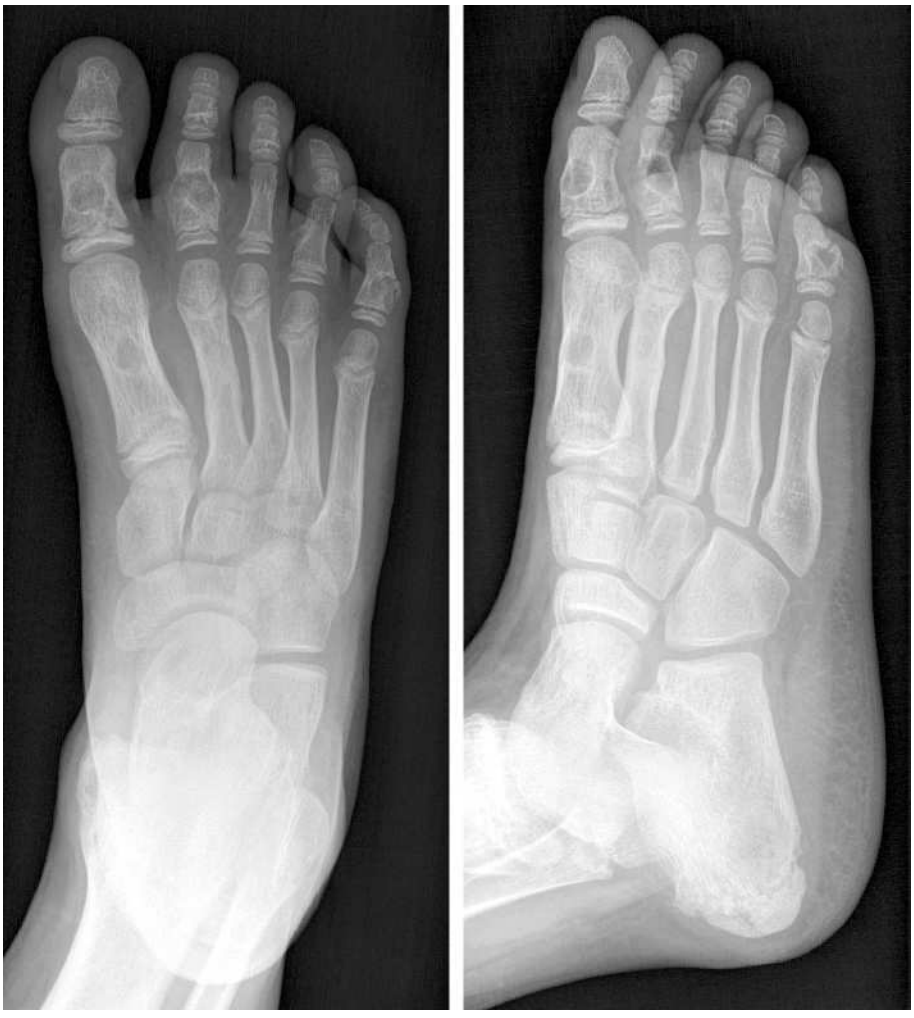

a,b

Fig. 13.8a,b. Enchondromatosis: Radiographs (**a,b**) show multiple osteolytic lesions in the meta- and diaphyseal areas of the short tubular bones. Some of the lesions do not show a completely intact cortex. This is in accordance with the diagnosis of enchondromatosis, which can be radiographically more aggressive in the short tubular bones than in other localisations. However, the lesions are biologically benign

to the development of secondary chondrosarcoma than patients with a solitary enchondroma: rates between 10% and 25% are reported in the literature (Lucas and Bridge 2002).

The role of radiology in the detection of an early malignant transformation is even more challenging than the differential diagnosis of solitary enchondroma and chondrosarcoma, as histology in enchondromatosis shows features that may aggravate the difficulties in differentiating between a benign and a malignant condition, similar to the solitary enchondromas of the short tubular bones.

There is a very rare condition that combines the features of enchondromatosis and osteochondromatosis, termed metachondromatosis. In the series mentioned above two cases are reported in 3,067 bone tumours (Brien et al. 1997).

13.3.3.1 Maffucci's Disease

Maffucci's disease is a disease with multiple enchondromas and multiple soft tissue haemangiomas. Patients usually have deformities of long bones. Secondary development of chondrosarcomas is reported to be even more frequent than in Ollier's disease (Lucas and Bridge 2002).

13.4 Osteochondroma

Osteochondroma (exostosis, cartilaginous exostosis) is one of the most frequent entities within the spectrum of tumorous and tumour-like bone lesions. It is considered to be more like a hamartoma than a neoplasm. It is believed to develop from embryonic rests of the physis which are displaced not into the metaphysis, as in enchondroma, but to the bone surface during growth (Brien et al. 1999). Morphologically, it consists of two components: a bony protrusion that is a continuous extension of both the cortex and the medullary cavity of the parent bone and a cartilage cap adjacent to it. The form of the bony protrusion can be pedunculated or broad-based (Fig. 13.9). Similar to enchondroma osteochondroma is frequently asymptomatic, so that its incidence can only be estimated. Within large series of bone tumours, frequencies of up to 35% of benign and 8% of all lesions have been reported (Dahlin and Unni 1986). Most cases are diagnosed within the first three decades of life. There is no sex predilection.

The most common sites involved are the metaphyseal regions of long tubular bones, especially the regions around the knee joint that grow fast during adolescence. Flat bones can be involved as well, most frequently the scapula or ileum. Pedunculated osteochondromas of the long bones frequently follow the direction away from the epiphysis and towards the diaphysis following the tendon pull. According to their aetiology osteochondromas may increase in size as long as the parent bone grows. An increase in size after skeletal maturity is reached is not consistent with the diagnosis of an osteochondroma.

Complications of osteochondromas include nerve and vascular compression, and rarely succeeding formation of arterial pseudoaneurysms, neobursa formation and bursitis, fracture of the stalk (Fig. 13.10), growth disturbances caused by compression of other bony structures (Fig. 13.11) and malignant transformation (Woertler et al. 2000).

Diagnosis is almost always possible on the basis of plain radiographs, which show a bony protrusion as an extension of the cortical and medullary component of the parent bone. The cartilage cap can be seen in radiographs only if matrix mineralisation is present. The degree of matrix mineralisation, however, is highly variable. In anatomically complex regions as well as in anatomically complex osteochondromas computed tomography can be helpful in showing the extension of the medullary cavity and of the host bone cortex into the osseous component of the osteochondroma, which is the key feature for the differential diagnosis (Murphey et al. 2000). MR imaging can show this extension as well and additionally depict the thickness of the cartilage cap, which is important in the detection of malignant transformation. It should be mentioned that in adults sometimes a cartilage cap may be completely replaced due to enchondral ossification. MR imaging can also detect a neobursa or bursitis as a lesion with fluid signal surrounded by a rim of contrast enhancement (Woertler et al. 2000).

The risk of malignant transformation of solitary osteochondromas is very low and almost always seen in skeletally mature patients. Atypical location in the skeleton, large size and broad-based morphology are risk factors. In particular, secondary chondrosarcomas of the pelvis, scapula and thigh can get very large. Features suggestive of malignant transformation are the disturbance of a formerly well-ordered and homogeneous cartilage cap, a nodular mass arising from the cartilage cap with a signal and/or calcification pattern different

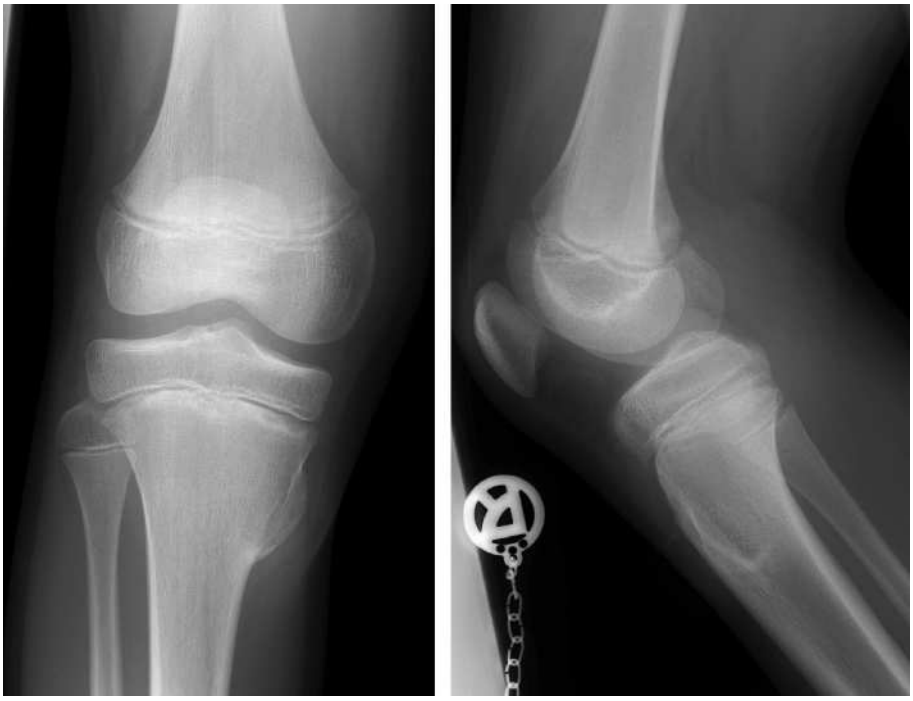

a b

Fig. 13.9a,b. Osteochondroma: Radiographs (**a,b**) show a broad-based osteochondroma in the proximal metaphyseal tibia. Cortex and medullary cavity of the parent bone extend harmonically into the osseous component of the osteochondroma. Only the osseous component can be perceived, as there are no matrix calcifications of the cartilaginous component. This constellation is frequent

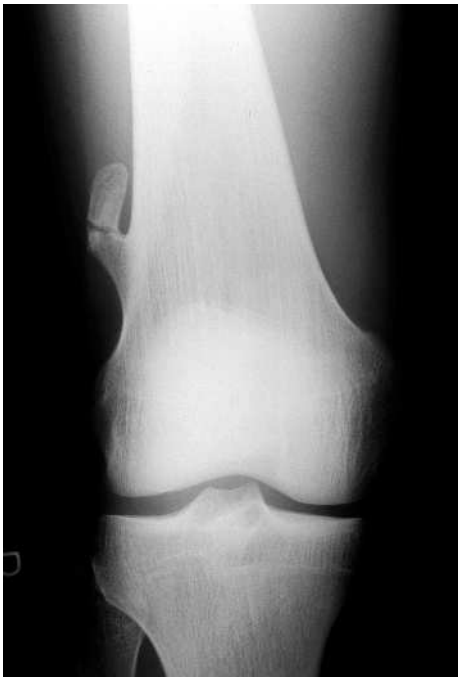

Fig. 13.10. Osteochondroma: Anteroposterior radiograph shows a pedunculated osteochondroma in the distal metaphyseal femur. Cortex and medullary cavity of the parent bone extend harmonically into the osseous component of the osteochondroma. The osteochondroma points towards the diaphysis. This is typical and is believed to be a result of tendon pull on these lesions. The osteochondroma is fractured, which is one of its possible complications. The cartilaginous cap cannot be seen as there are no matrix calcifications

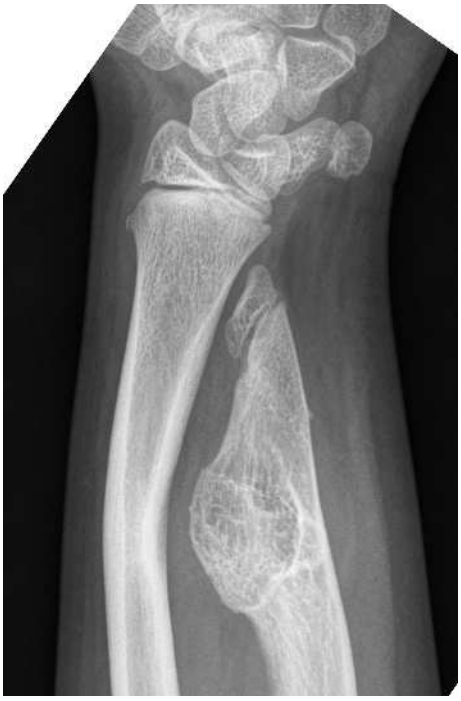

Fig. 13.11. Osteochondroma: Radiograph shows a bizarre deformity of the forearm caused by a broad-based osteochondroma of the distal metadiaphyseal ulna

from the rest, and blurring or destruction of the osseous component. Also, a cartilage cap thickness of more than 1.5–2.0 cm in skeletally mature patients and the development of pain should raise suspicion of a malignant transformation. A cartilage cap must not be confused with a neobursa formation. Any recurrence of a previously removed osteochondroma is also suspicious for a malignant transformation.

The great majority of malignant tumours deriving from osteochondroma are low-grade malignant chondrosarcomas (Brien et al. 1999). If unrecognised, about 10% of these low-grade osteosarcomas dedifferentiate into high-grade sarcomas (Brien et al. 1999).

The differential diagnosis of osteochondroma includes parosteal osteosarcoma, periosteal chondroma and chondrosarcoma. In this differential diagnosis, computed tomography or MR imaging can be of special value in the evaluation of the lesion in relation to the cortex of the parent bone: only osteochondroma shows a continuous extension of both medullary cavity and cortex of the parent bone. Parosteal osteosarcoma, periosteal chondroma and periosteal chondrosarcoma originate at the surface of bone, though parosteal osteosarcoma and periosteal chondrosarcoma can secondarily infiltrate the marrow cavity (Hatano et al. 1997).

13.4.1 Osteochondromatosis

Osteochondromatosis (hereditary multiple exostosis, HME) is an autosomal dominant inherited trait with an incidence of at least one in 50,000 (Porter et al. 2004). Multiple osteochondromas in all parts of the skeleton develop during childhood and adolescence. It is believed that in the pathogenesis the separation of physeal cartilage may occur as a result of defects of the periosteal cuff that surrounds the physis (Keith 1920).

Osteochondromas may already be present at birth. The severity of the disease varies significantly. About 75% of affected individuals have a clinically apparent deformity and about 40% have a short stature (Schmale et al. 1994). Lesion size and number of lesions are the most relevant factors for the risk of malignant transformation (Brien et al. 1999). The rate of malignant transformation is reported to be in the range of 5–25% of patients (Woertler et al. 2000). The imaging appearance of osteochondromas in osteochondromatosis does not differ from that in solitary osteochondromas (see Sect. 13.4) (Fig. 13.12).

13.5 Chondromyxoid Fibroma

Chondromyxoid fibroma is a rare benign chondrogenic tumour, accounting for less than 1% of the 8,542 bone tumours in Dahlin and Unni's series (Dahlin and Unni 1986). The typical age at presentation is in the second or third decade of life, though a wide age distribution from 4 to 79 years has been reported. A slight male predominance is also described.

Predilection sites for chondromyxoid fibroma are the metadiaphyses of long tubular bones, especially around the knee joint where about two thirds of all chondromyxoid fibromas occur (Rahimi et al. 1972). An eccentric location within the medullary canal is typical. The tarsal bones as well as the short bones of the feet follow in frequency (Brien et al. 1997). However, almost any other location in chondrogenic preformed bone has been reported.

Chondromyxoid fibroma is a slowly growing tumour. At diagnosis it is frequently larger than 3 cm.

Radiographically, the typical chondromyxoid fibroma is a round or oval, well-defined, sharply marginated lytic lesion, sometimes lobulated and surrounded by a thin sclerotic rim (Moser et al. 1990b). Growth is usually expansile with formation of a thin neocortex, but manifestations without a neocortex can be found as

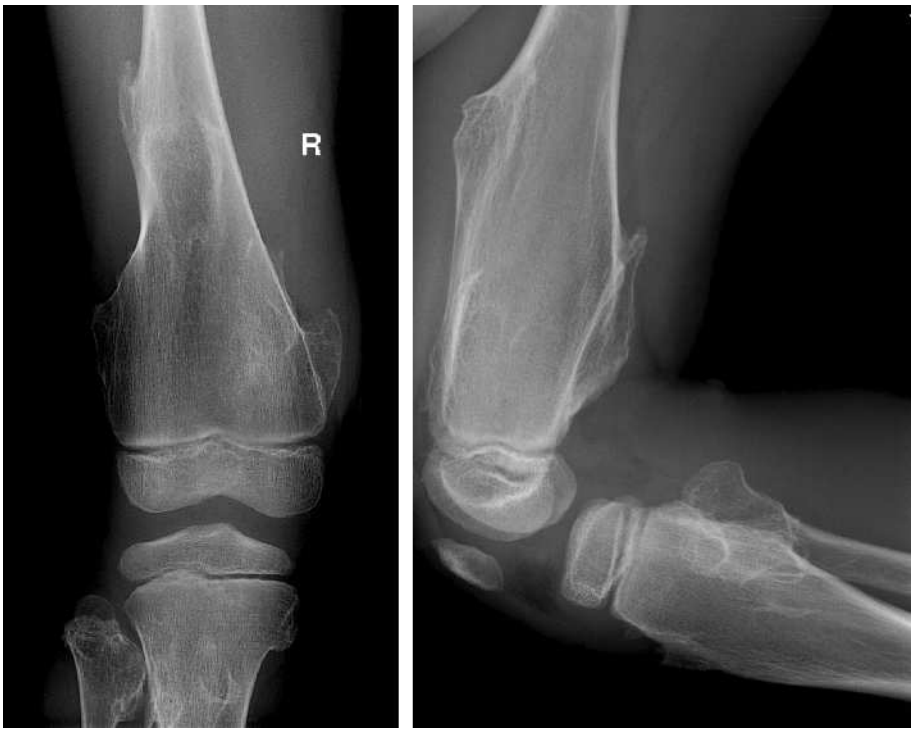

a b

Fig. 13.12a,b. Osteochondromatosis: Radiographs (**a,b**) show multiple osteochondromas in the metaphyses and metadiaphyses around the knee joint in a child with osteochondromatosis

well (Fig. 13.13). Chondromyxoid fibromas show only little periosteal reaction. Occasionally, matrix calcifications can be seen in a punctuate, flocculent or rings-and-arcs pattern (Yamaguchi and Dorfman 1998). Bony ridges that seem to transverse the lesion are frequent.

Most often the diagnosis of a chondromyxoid fibroma can be achieved radiographically. Computed tomography can add some information on matrix calcification, sclerotic rim and neocortex formation but is not routinely required. The signal in MR imaging is unspecific. It may show small areas of haemorrhage or cyst formation.

The differential diagnosis of chondromyxoid fibroma includes a number of predominantly benign lesions (Moser et al. 1990b). Juvenile and aneurysmal bone cysts, which can be found in the metaphysis or diaphysis of long bones and show morphologic signs of slow growth as well, can resemble chondromyxoid fibroma. Matrix calcifications detected radiographically or by computed tomography exclude these entities. MR imaging is able to differentiate a solid lesion like a chondromyxoid fibroma from these cystic lesions, even if they might have small solid portions. Giant cell tumour is more likely than chondromyxoid fibroma to reach the subchondral bone in the epiphysis and more frequently penetrates the cortex without neocortex formation. Though it may have some local dystrophic calcification the presence of uniform mineralisation throughout large parts of the lesion is inconsistent with giant cell tumour. Enchondroma of the long bones is typically located centrally and mostly does not affect the cortex. Enchondroma in the short bones is much more frequent than chondromyxoid fibroma but can show a similar radiographic pattern.

Non-ossifying fibroma is usually asymptomatic, as long as no complicating pathologic fracture occurs. In particular, larger non-ossifying fibromas can be radiographically indistinguishable from chondromyxoid fibroma. Fibrous dysplasia can show a typical ground-glass pattern which is pathognomonic. In contrast to chondromyxoid fibroma, it is usually an asymptomatic lesion. Polyostotic involvement as found in fibrous dysplasia is not described in chondromyxoid fibroma. Eosinophilic granuloma can present with a wide variety of radiographic patterns, but is usually more aggressive than chondromyxoid fibroma, shows some periosteal reaction and frequently lacks a thin and uniform scle-

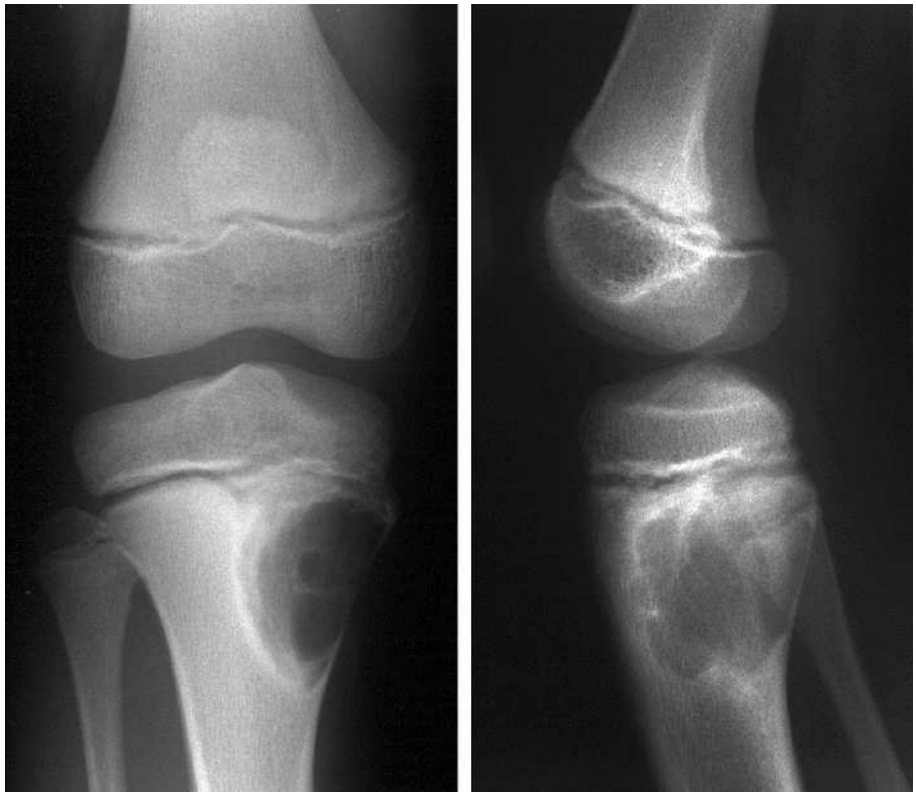

a b

Fig. 13.13a,b. Chondromyxoid fibroma: Radiographs (**a,b**) show a well-demarcated lytic lesion in the proximal metaphyseal tibia. The lesion is located eccentrically within the medullary cavity. It has partially destroyed the cortex and is separated from the medullary cavity by a 1- to 2-mm-wide sclerotic rim. Some bony ridges can be seen within the lesion, but no matrix calcifications are present. These findings are typical for a chondromyxoid fibroma

rotic rim. Furthermore, it shows significant perifocal reaction in MR imaging. Rarely, chondrosarcoma can be a differential diagnosis (Fig. 13.14).

13.6 Chondrosarcoma

Chondrosarcoma is the most common malignant cartilage tumour and the third most common malignant bone tumour after myeloma and osteosarcoma (Dorfman and Czerniak 1995). Pathogenically there is primary chondrosarcoma, a chondrosarcoma without evidence of a precursor lesion, and secondary chondrosarcoma, which develops out of an enchondroma or osteochondroma. The most frequent histologic type, accounting for more than 90% of chondrosarcomas, is conventional chondrosarcoma (medullary chondrosarcoma, central chondrosarcoma) (Bertoni et al. 2002). Rare histologic varieties are clear cell carcinoma and mesenchymal chondrosarcoma. An exceptionally rare subtype of chondrosarcoma defined by its localisation is juxtacortical chondrosarcoma. The term dedifferentiated chondrosarcoma eventually describes a chondrosarcoma in which both areas of low-grade chondrosarcoma and, developed out of these, areas of a high-grade malignant tumour exist. Clear cell chondrosarcoma, mesenchymal chondrosarcoma and juxtacortical chondrosarcoma are only reported as being primary chondrosarcomas. Dedifferentiation is reported both in primary and secondary chondrosarcomas.

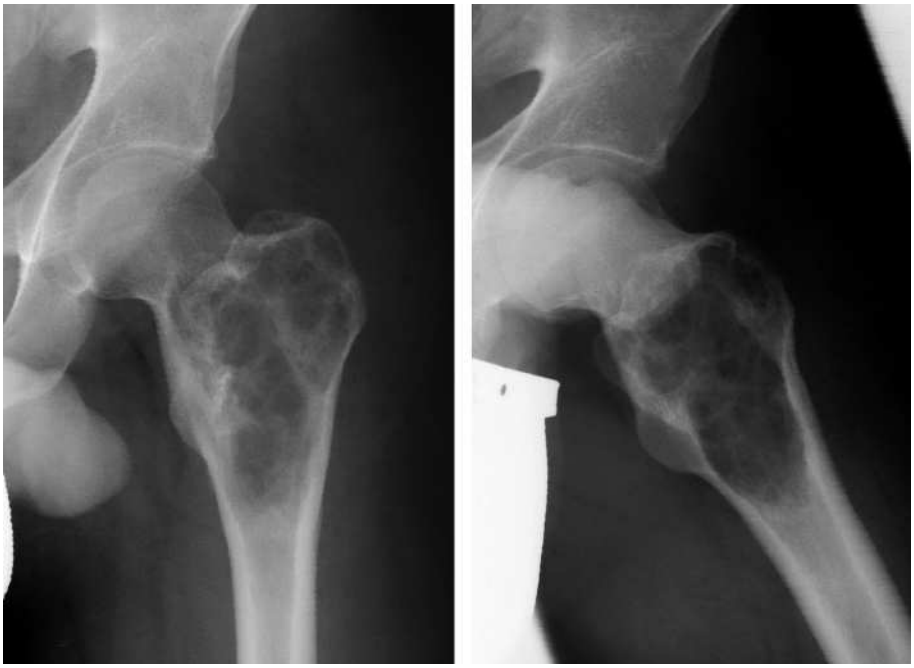

Fig. 13.14a,b. Chondromyxoid fibroma: Radiographs (**a,b**) show a lytic lesion in the proximal metaphyseal femur extending into the apophyses of the lesser and greater trochanter. Cortex is thinned out but not penetrated and there is an incomplete rim of sclerosis with a thickness of 1–2 mm surrounding the lesions. No matrix calcifications can be seen. There is slight cortical remodelling in the distal part of the lesion. Radiographically, a chondrosarcoma has also to be considered in the differential diagnosis

13.6.1 Primary Chondrosarcoma

13.6.1.1 Conventional Chondrosarcoma

Primary conventional chondrosarcoma accounts for approximately 20% of malignant bone tumours in large series (Dahlin and Unni 1986). It has a strong localisation predilection for the pelvis, the proximal femur, proximal humerus, distal femur and ribs, all together central localisations in or close to the trunk. Within long tubular bones, conventional chondrosarcoma is usually located in the metaphysis or metadiaphysis. It is rare in the skeletal periphery, especially in the short tubular bones of the hand and feet and in the spine. The age distribution of primary conventional chondrosarcoma shows an age peak in the sixth decade and the vast majority of cases are diagnosed in patients above the age of 50 years.

Histologically, chondrosarcomas are graded on a scale of I–III based primarily on nuclear size, staining and cellularity. Grade I and II chondrosarcomas are much more frequent than grade III chondrosarcomas (Bertoni et al. 2002).

Radiographic appearance differs significantly with histologic grade, reflecting the different aggressiveness. The spectrum of findings starts with osteolytic lesions difficult to differentiate from enchondromas (see Sect. 13.7) and ends with the radiographic pattern of high-grade malignant tumours: moth-eaten destruction and aggressive periosteal reaction. Many chondrosarcomas, especially those with a higher grade of differentiation, show chondrogenic calcifications, which is helpful in the diagnosis.

A frequent radiographic finding for a conventional chondrosarcoma is a lytic lesion with a geographic pattern of destruction, some cortical destruction in the form of scalloping, penetration and/or expansile growth (Brien et al. 1997). Thickening of the cortex or formation of a complete or incomplete periosteal shell may be present, but otherwise only little periosteal reaction is found. Frequently, there is some chondrogenic or amorphous calcification and frequently, conven-

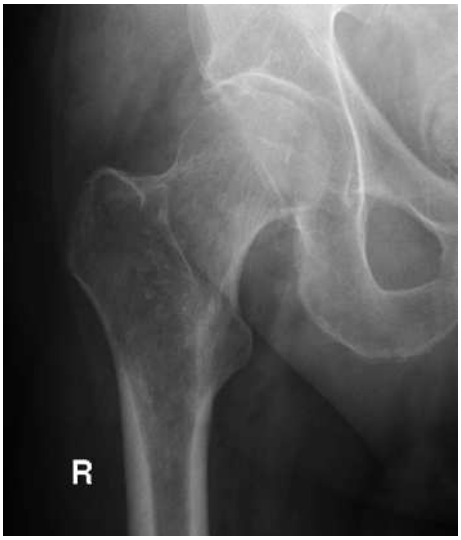

Fig. 13.15. Chondrosarcoma: Radiograph shows an ill-defined lytic lesion in the proximal metaphyseal femur with extension into the lesser and greater trochanter. There is some cortical destruction especially in the cortex distal to the greater trochanter. A sclerotic rim cannot be seen. There is slight chondrogenic calcification as a key feature for the correct diagnosis

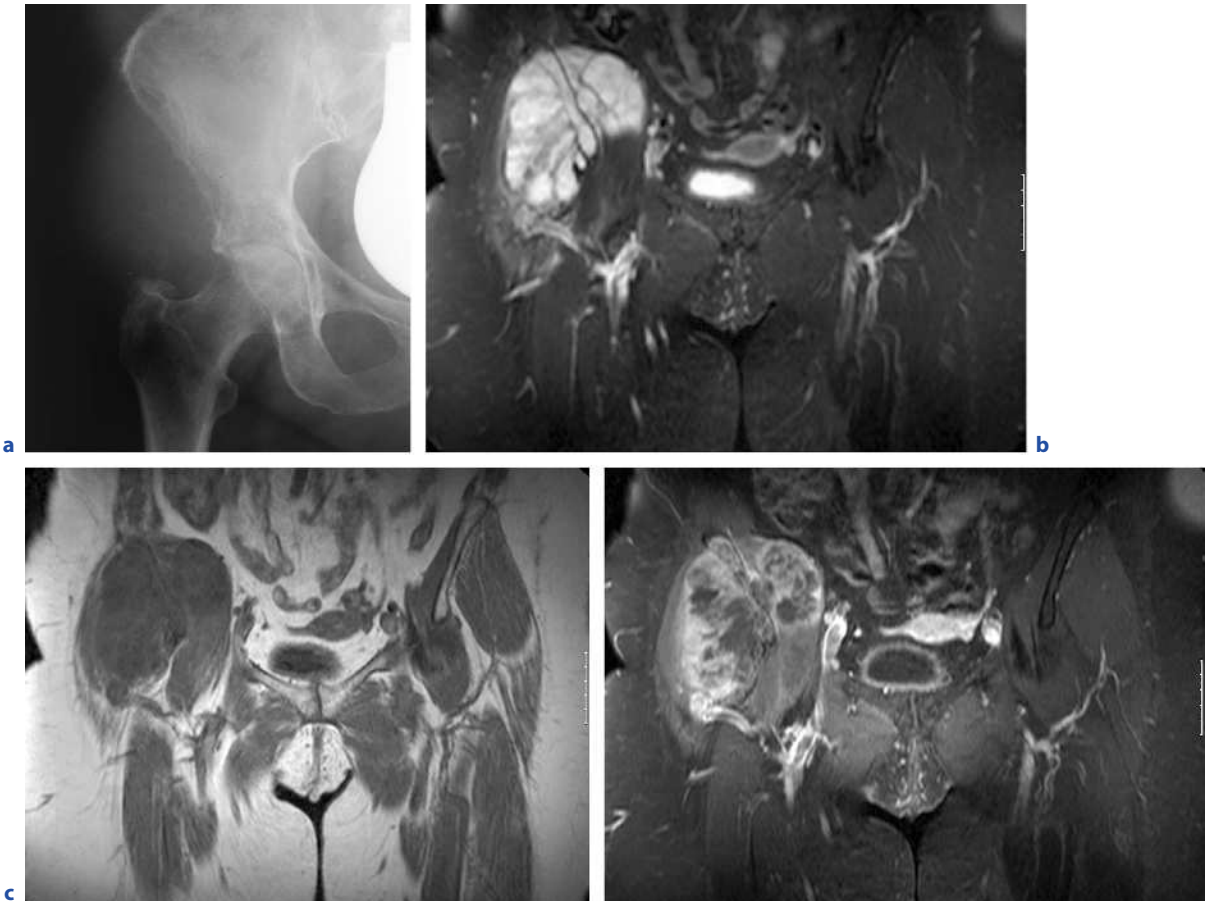

Fig. 13.16a–d. Chondrosarcoma: Radiograph (**a**) shows an ill-defined lytic lesion in the ileum with considerable cortical irregularity and slight chondrogenic matrix calcification. MR imaging shows a large intra- and extraosseous mass with a high signal in fat-saturated T2-weighted sequences (**b**), a low signal in T1-weighted sequences (**c**) and some enhancement in fat-saturated contrast-enhanced T1-weighted sequences (**d**). Though MR images show some degree of lobulation and of the rings-and-arcs type enhancement, the pattern is not regular enough for a purely low-grade chondrosarcoma, especially in the laterocaudal parts of the mass. Histology showed significant areas of grade III chondrosarcoma

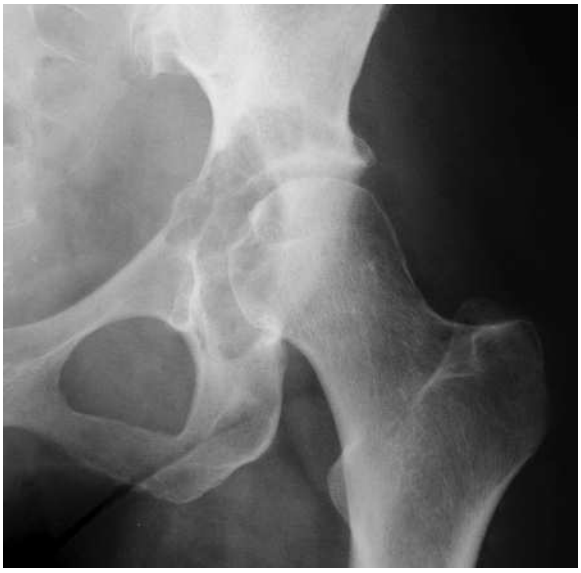

Fig. 13.17. Chondrosarcoma: Radiograph shows a well-demarcated, lobulated lytic lesion in the acetabulum. Slight matrix calcifications can be visualised especially medially. There is at least some expansile growth, if not cortical penetration

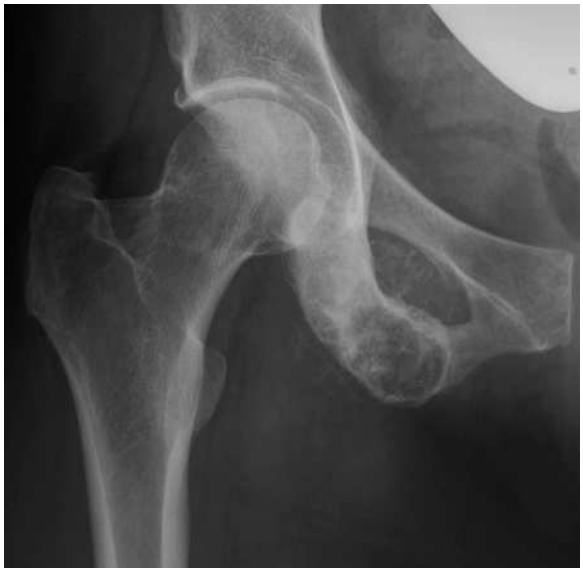

Fig. 13.18. Chondrosarcoma: Radiograph shows a well-demarcated lytic lesion in the ischium. There is some cortical remodelling and a 1- to 2-mm-wide incomplete sclerotic rim. Matrix calcifications within the soft tissues indicate a large soft tissue component

tional chondrosarcomas are of large size (Fig. 13.15). Pathologic fractures are not infrequent (Hudson et al. 1990).

In well-differentiated chondrosarcomas MR imaging frequently shows a lobular pattern with high signal in T2-weighted sequences, reflecting the high water content of these cartilage tumours, and a rings-and-arcs type of contrast enhancement, corresponding to the interlobular fibrovascular septae (Aoki et al. 1991). This pattern can be found in benign chondrogenic lesions as well. Large conventional chondrosarcomas with this pattern frequently show areas of grade II chondrosarcoma histologically (Fig. 13.16). Computed tomography can be especially helpful in the assessment of cortical destruction and detection of matrix calcification.

Differential diagnosis depends on the detection of chondrogenic calcifications. If these can be identified ensuring that the lesion is a chondrogenic tumour, the main differential diagnosis is that of an enchondroma (see Sect. 13.7). If no chondrogenic calcifications are seen, a larger group of tumours of the higher age group has to be included in the differential diagnosis, e.g. metastasis, malignant fibrous histiocytoma, fibrosarcoma or lytic secondary osteosarcoma (Figs. 13.17, 13.18).

13.6.1.2 Clear Cell Chondrosarcoma

Clear cell chondrosarcoma is a low-grade variant of chondrosarcoma. It accounts for 1–2% of all chondrosarcomas and is three times more common in men than in women (McCarthy et al. 2002). It is most frequent in the third and fourth decades of life, but cases have been reported within the range from 12 to 84 years. Its most frequent location is the epiphyseal region of long bones, especially of the femur and the humerus. This location accounts for approximately two thirds of all cases. It has been described in various other regions as well, including the ribs, skull, spine, hands and feet (Collins et al. 2003). Clear cell chondrosarcoma is a slowly growing tumour, frequently with a clinical history of pain for several months or even years.

The radiographic appearance of clear cell carcinoma is that of a well-defined osteolytic lesion that can have a thin sclerotic rim and, in larger lesions, the growth can be slightly expansile. Except for a thin neocortex in expansile lesions, no periosteal reaction is found. Thus, clear cell carcinomas usually are in the range of Lodwick grade Ia–Ic. Chondrogenic calcifications occur in approximately one third of cases.

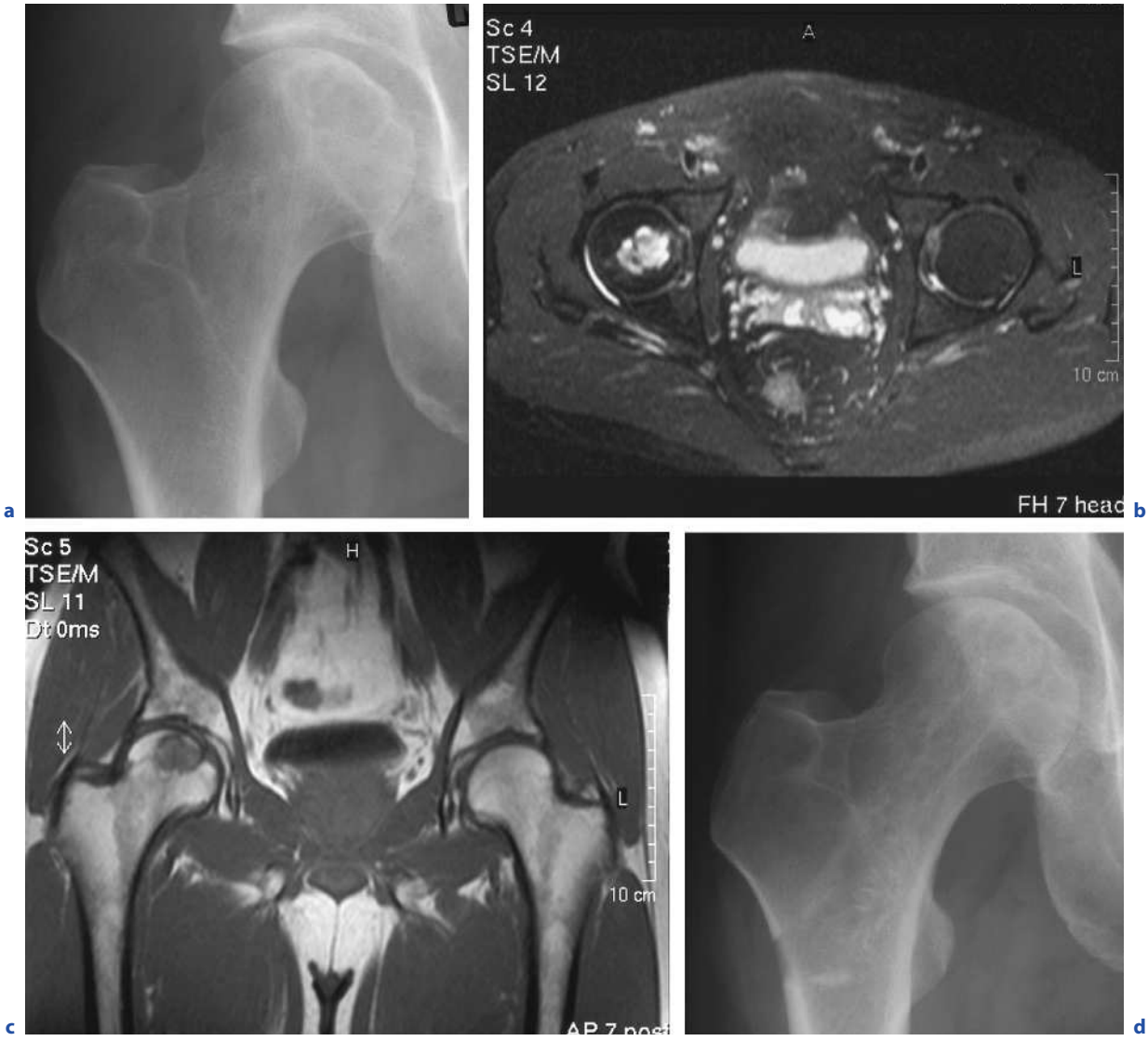

a b c d

Fig. 13.19a–d. Clear cell chondrosarcoma: Radiograph (**a**) shows a well-demarcated lytic lesion, slightly lobulated, in the proximal epiphysis of the femur. The lesion is surrounded by a thin sclerotic rim. No matrix calcification is present. T1-weighted (**b**) and fat-saturated T2-weighted (**c**) images show a lobulated lesion with high water content and without surrounding oedema. The lesion, which is typical of a clear cell carcinoma, was misdiagnosed as an avascular necrosis and treated by core decompression (**d**) and later referred to our institution for correct oncologic treatment. A possible differential diagnosis would be chondroblastoma

In its classical location in the epiphyses of long bones the radiographic pattern is mostly indistinguishable from chondroblastomas, which are an important differential diagnosis (Kaim et al. 2002). Patient age is considered as an important discriminator between both entities. It must be taken into account that the age distribution of both tumours overlaps widely. Some cases will require histology to clarify diagnosis (Cannon et al. 2002).

Clear cell chondrosarcoma in a typical epiphyseal location must be furthermore considered as a rare differential diagnosis for ganglion cysts and, in the femoral head, for avascular necrosis (Hudson et al. 1990). The presence of chondrogenic matrix mineralisation and the presence of a thin sclerotic rim are the most important radiographic criteria for the differentiation between a clear cell carcinoma and a ganglion cyst. In both criteria, computed tomography can be helpful. MR imaging can

be helpful if it shows a uniform fluid signal proving the presence of a ganglion cyst. The differentiation of a clear cell chondrosarcoma from an avascular necrosis is easy in typical cases of the latter. The special importance of clear cell carcinoma lies in the fact that, due to its rarity, it is sometimes not considered as a differential diagnoses for this frequent, non-tumorous condition (Fig. 13.19). Furthermore, metastases can occur in an epiphyseal localisation. In contrast to clear cell chondrosarcoma, they mostly show a more aggressive pattern of destruction and also lack any chondrogenic calcification.

13.6.1.3 Mesenchymal Chondrosarcoma

Mesenchymal chondrosarcoma is a rare form of chondrosarcoma characterised by a bimorphic histologic pattern with highly undifferentiated small round cells and islands of well-differentiated cartilage (Hudson et al. 1990). With age peaks in the second and third decades its age distribution is quite different from conventional chondrosarcoma, but it has been reported in older age groups as well. Mesenchymal chondrosarcoma can originate in bone (approximately two thirds of cases) and in soft tissue (approximately one third of cases). In those cases originating in bone distribution is widespread, with a preference for the craniofacial bones, ribs, ileum and vertebrae (Hudson et al. 1990). Soft tissue lesions involve the somatic soft tissue as well as the meninges.

Radiographically, skeletal manifestations of mesenchymal chondrosarcoma have been described as being similar to conventional chondrosarcomas. Specific criteria of differentiation are not known. About 75% of mesenchymal chondrosarcomas originating from bone contain chondrogenic calcifications. In soft tissue mesenchymal chondrosarcomas granules of chondrogenic calcifications are frequent and can lead to the specific diagnosis. In soft tissue mesenchymal chondrosarcomas MR imaging typically shows a well-demarcated mass composed of calcified and non-calcified areas (Hashimoto et al. 2005).

13.6.1.4 Juxtacortical Chondrosarcoma

Juxtacortical chondrosarcomas (periosteal chondrosarcomas) originate at the surface of bone. They are rare with a frequency of 3 cases in 667 chondromas in a series of 2,267 bone tumours (Brien et al. 1999). Their most common localisation is the metaphysis of long tubular bones, especially the distal femur.

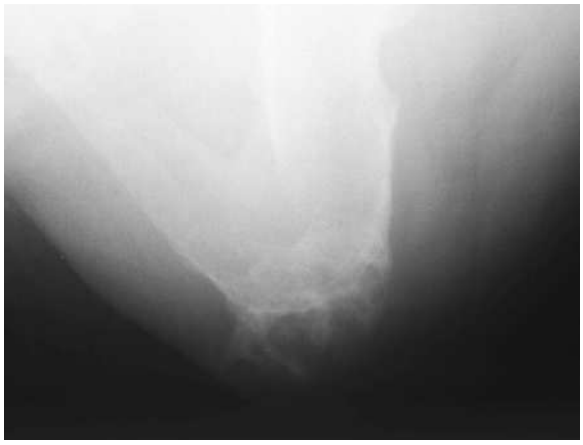

Fig. 13.20. Juxtacortical chondrosarcoma: Tangential view of the ischial tuberosity shows ridge-like calcifications perpendicular to the cortex. Cortical destruction cannot be visualised. No sclerotic rim is seen separating this juxtacortical lesion from the medullary cavity

Radiographically, juxtacortical chondrosarcomas resemble juxtacortical chondromas. Criteria mentioned in the literature for the presence of a juxtacortical chondrosarcoma instead of a juxtacortical chondroma include large size and presence of striated calcifications (Robinson et al. 2001) (Fig. 13.20). Large, controlled studies, however, do not exist due to the very low incidence of both entities. Besides the juxtacortical chondroma, juxtacortical osteosarcoma may be a differential diagnosis. Juxtacortical osteosarcoma is usually more aggressive, frequently with a pattern resembling a sunburst-type periosteal reaction and may have an osteogenic matrix seen radiographically. In a series of 24 periosteal chondrosarcomas a strong preference for the posterior distal metaphysis of the femur was found with 8 cases in this localisation (Vanel et al. 2001). Age distribution ranged from 17 to 65 years. There was a male predominance with 20 men and 4 women. Lesion size varied from 4 to 11 cm. The underlying cortex was altered in all cases, but never fully destroyed. Marrow involvement was found in 2 of 16 cases evaluated with computed tomography/MR imaging. Thick, radial periosteal bone formation was found in 9 cases (Vanel et al. 2001).

13.6.2 Dedifferentiated Chondrosarcoma

Dedifferentiated chondrosarcoma is an entity that consists of two different components: a well-differentiated

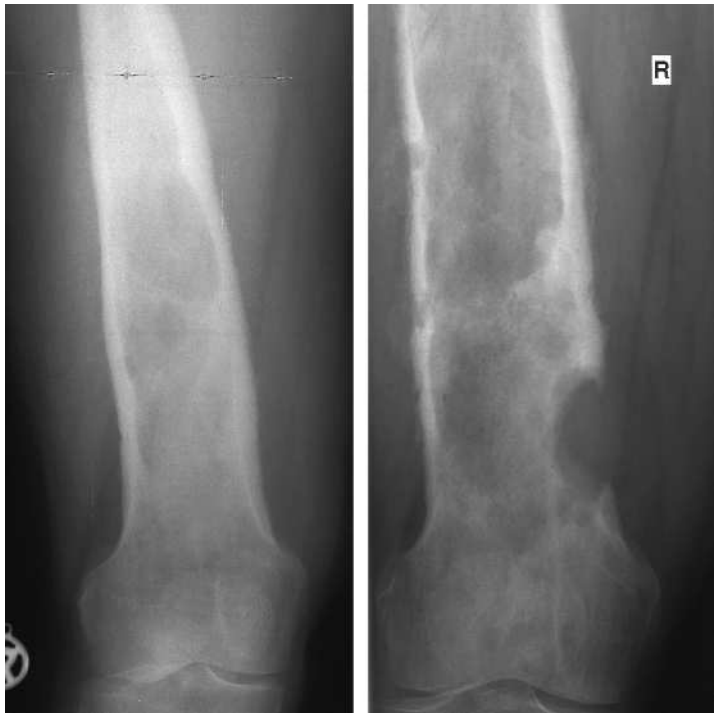

a b

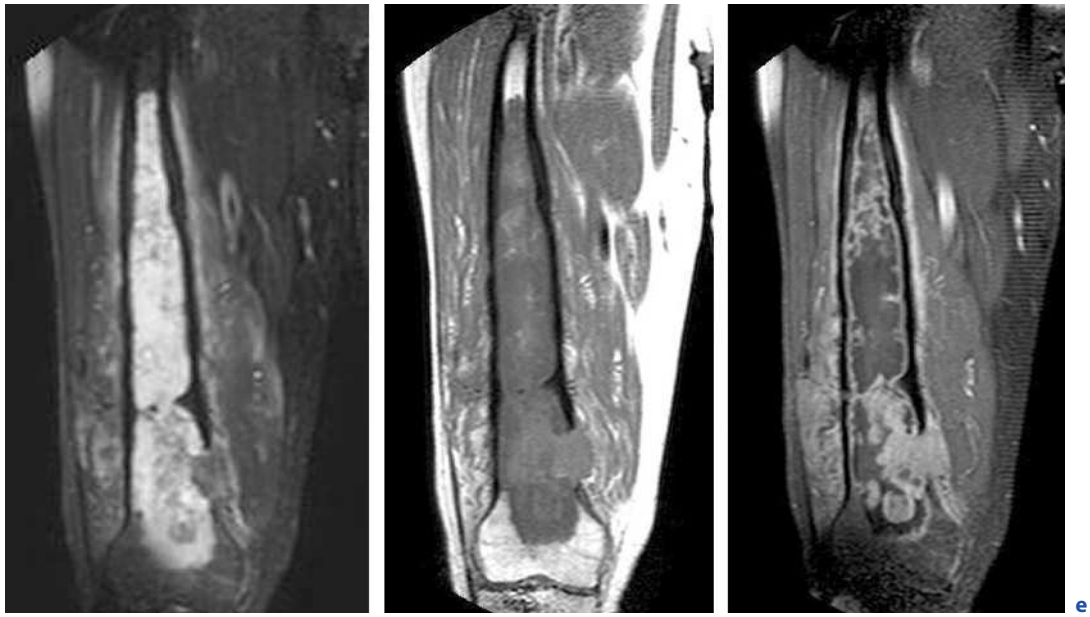

c,d e

Fig. 13.21a–e. Dedifferentiated chondrosarcoma: Anteroposterior radiograph (**a**) shows a large lytic lesion of the distal diametaphyseal femur. Considerable cortical remodelling is present. Biopsy showed well-differentiated cartilage tissue, so that in conjunction with histology and radiology the diagnosis of a chondrosarcoma was made and operative treatment recommended. Despite repeated information the patient denied treatment. Ten months later he came back with the findings presented in radiographic (**b**) and MR imaging (**c–e**) showing a lytic destruction with complete penetration of the cortex in the medial aspect of the metaphysis. MR imaging in this location shows a mass with low signal in fat-saturated T2-weighted images (**c**), intermediate signal in T1-weighted images (**d**) and homogeneous enhancement in fat-saturated contrast-enhanced T1-weighted sequences (**e**). This mass was shown histologically to be a high-grade sarcoma. MR imaging clearly depicts the bimorphism of the lesion

chondrogenic component, enchondroma, low-grade chondrosarcoma or osteochondroma, and a high-grade, non-cartilaginous component, frequently malignant fibrous histiocytoma, fibrosarcoma or osteosarcoma. Dedifferentiated chondrosarcomas account for approximately 10% of chondrosarcomas. They are most frequent in the fifth to ninth decades of life, with cases reported from 15 to 93 years in large series. Most commonly they are located in the pelvis, femur and humerus (Littrell et al. 2004).

The typical imaging appearance reflects the presence of the two different components, with one component showing the characteristics of a well-differentiated chondrogenic tumour, including chondrogenic calcifications in about 50% of cases, and a second, highly aggressive component with penetration of the cortex,

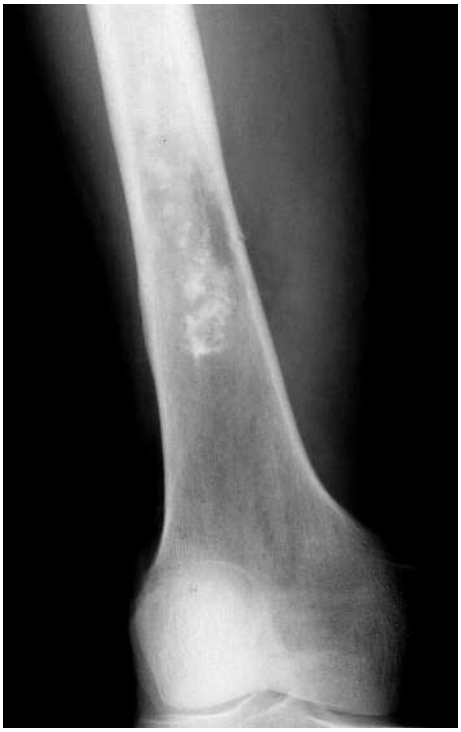

Fig. 13.22. Dedifferentiated chondrosarcoma: Radiograph shows a bimorphic lesion with a dense chondrogenic calcification centrally in the medullary cavity of the distal diaphyseal femur and an adjacent, ill-defined lytic lesion with a pathologic fracture in the cortex

a,b

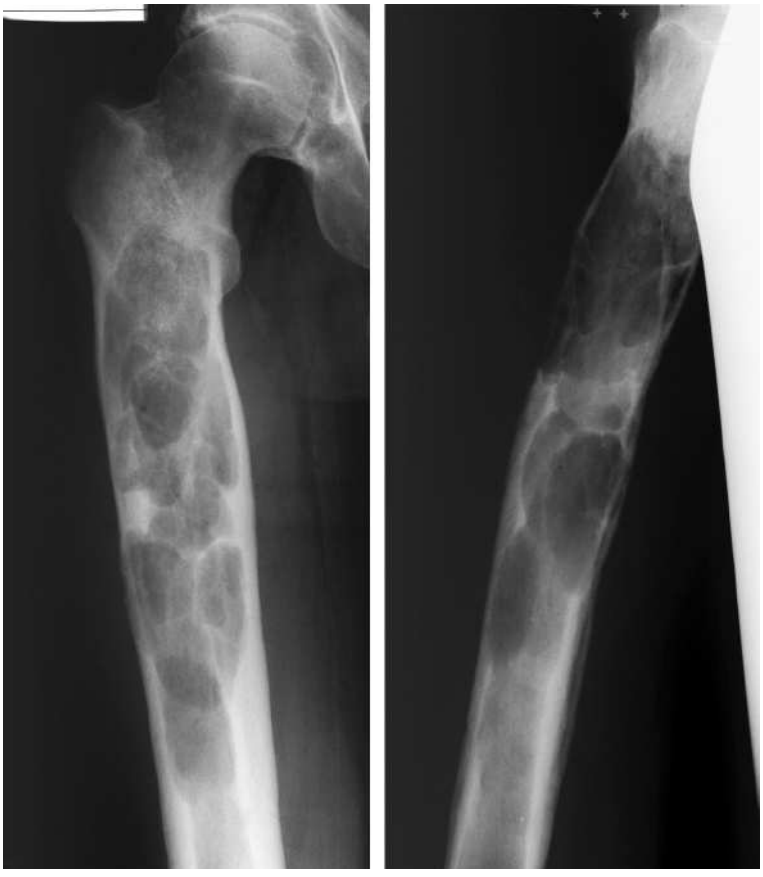

Fig. 13.23a,b. Dedifferentiated chondrosarcoma: Radiographs (**a,b**) show a large lytic lesion with deep scalloping and significant remodelling of the cortex in the proximal diametaphyseal femur. There is an incomplete rim of sclerosis separating the lesion from the medullary cavity. In the proximal part of the lesion slight matrix calcifications can be seen that are lacking in the distal part, showing bimorphism of the lesion. This finding, however, is very discrete

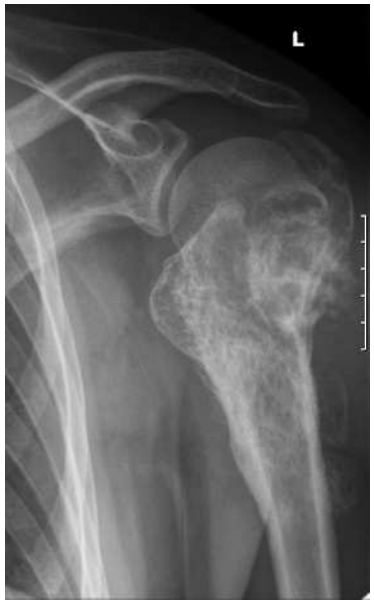

a

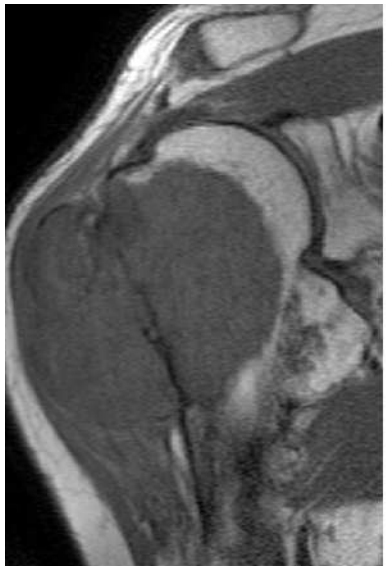

b,c

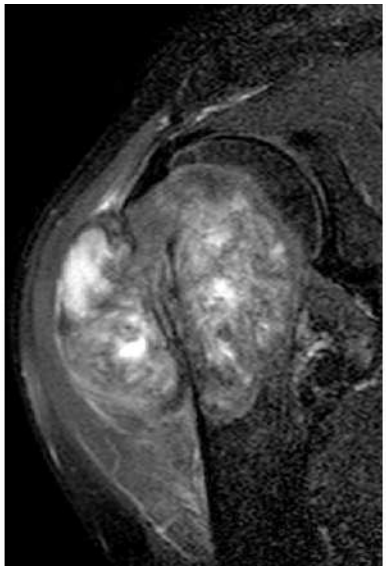

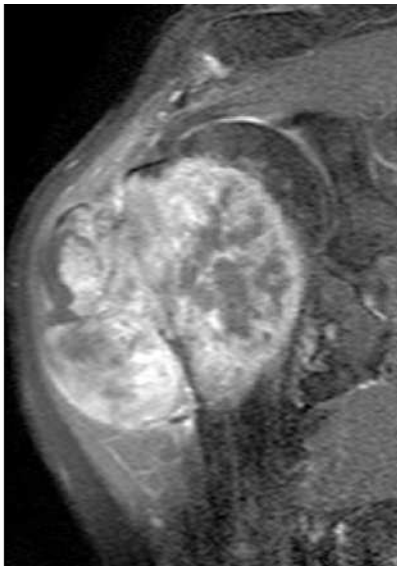

d

Fig. 13.24a–d. Secondary chondrosarcoma: Radiograph (**a**) shows a large osteochondroma of the proximal metaphyseal humerus. The lateral cortex is partially destroyed suggestive of malignant transformation. MR images show a huge intra- and extraosseous mass, with heterogeneous high signal in fat-saturated T2-weighted images (**b**), low signal in T1-weighted images (**c**) and considerable enhancement in fat-saturated contrast-enhanced T1-weighted sequences (**d**)

ill-defined margin and a large soft tissue component (Littrell et al. 2004) (Figs. 13.21, 13.22). Most dedifferentiated chondrosarcomas arise from the medullary cavity. Juxtacortical origin is described, but rare (Staals et al. 2007).

Radiographs and MR imaging show bimorphic features in one third of cases, while computed tomography shows these features in half of cases. Diagnosis of this bimorphic pattern is of special importance, as biopsy must be directed to the high-grade malignant component to ensure correct interpretation (MacSweeney et al. 2003). Cases of dedifferentiated chondrosarcoma with the imaging features of conventional chondrosarcomas are described as well, so that differentiation is not always possible and there should be careful evaluation for bimorphism (Mercuri et al. 1995) (Fig. 13.23). In lesions located in the pelvis, computed tomography and MR imaging should be performed additionally to radiography. Pathologic fracture is not infrequent.

13.6.3 Secondary Chondrosarcoma

Secondary chondrosarcomas are chondrosarcomas developing out of underlying benign chondrogenic le-

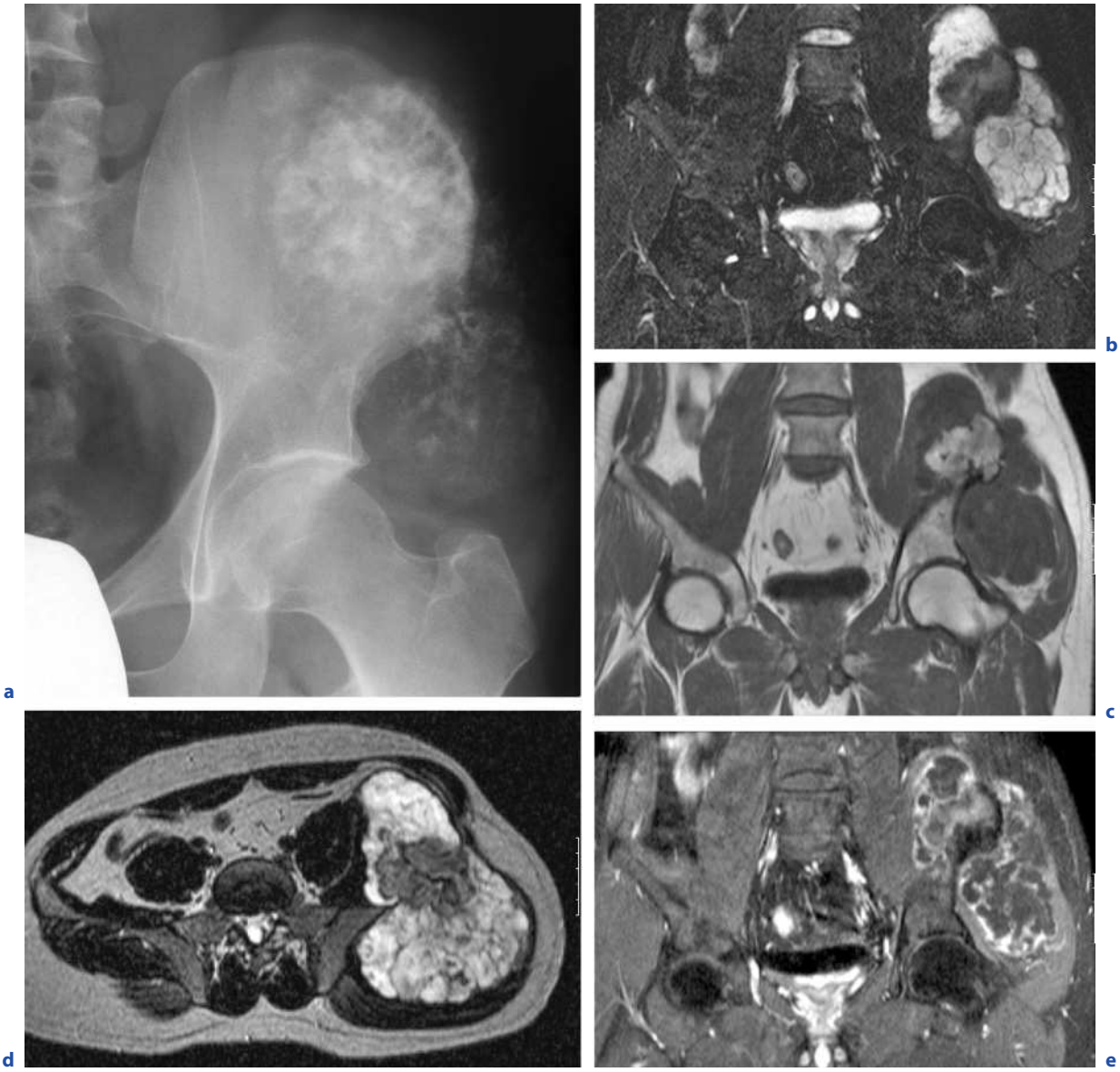

Fig. 13.25a–e. Secondary chondrosarcoma: Radiograph (**a**) shows a large intra- and extraosseous lesion of the left ileum characterised by chondrogenic calcifications. There is some bimorphism in that the craniomedial calcifications are much denser and much more regular than the caudolateral calcifications. MR imaging reveals the presence of an underlying osseous component of an osteochondroma that can be seen with the signal of normal bone marrow in fat-saturated T2-weighted images (**b**), T1-weighted images (**c**), T2-weighted sequences (**d**) and fat-saturated contrast-enhanced T1-weighted sequences (**e**). MR imaging also reveals the lobular pattern and rings-and-arcs type enhancement of a highly differentiated chondrogenic lesion. Additionally to the bimorphism suspected in radiography, the size of the cartilaginous mass is suggestive of secondary chondrosarcoma

sions such as enchondromas or osteochondromas. Patients with enchondromatosis are much more prone to the development of secondary chondrosarcoma than patients with a solitary enchondroma: rates between 10% and 25% are reported in the literature (Lucas and Bridge 2002). In osteochondromatosis the rate of malignant transformation is reported to be in the range of 5–25% of patients (Woertler et al. 2000) (Figs. 13.24, 13.25).

13.7 Differential Diagnosis: Enchondroma Versus Low-grade Chondrosarcoma

The differentiation between enchondroma and low-grade chondrosarcoma is a major challenge for several reasons. Histologically, the borderline between enchondroma and low-grade chondrosarcoma is not clearly defined (Welkerling et al. 1996). Cytologic presentation can be identical and differences in the growth pattern are crucial for the differentiation (WELKERLING et al. 1996). Mirra and co-workers have postulated different growth patterns, which they call 'benign islands of cartilage pattern' and 'chondrosarcoma permeation pattern' for benign and low-grade malignant cartilage lesions (Brien et al. 1997). No controlled study exists to validate these criteria. Reliability of histopathologic criteria in the differentiation of both entities has been shown to be low (Sliced Study Group 2007). To what extent sampling error may play a role in lesions containing benign and malignant areas remains unclear. Thus, histology alone is unable to offer a clear gold standard in the distinction between benign and malignant in these borderline cases.

It is generally agreed that radiology can play an important role in the assessment of the growth pattern and biologic behaviour of these entities. Criteria have been described for the differentiation of enchondroma from chondrosarcoma, including deep endosteal scalloping (greater than two thirds of cortical thickness), cortical destruction, soft tissue mass, periosteal reaction, marked uptake of radionuclide (greater than the anterior iliac crest) and pain related to the lesion in a large retrospective series, allowing a radiologic assessment that correlated with histology in more than 90%

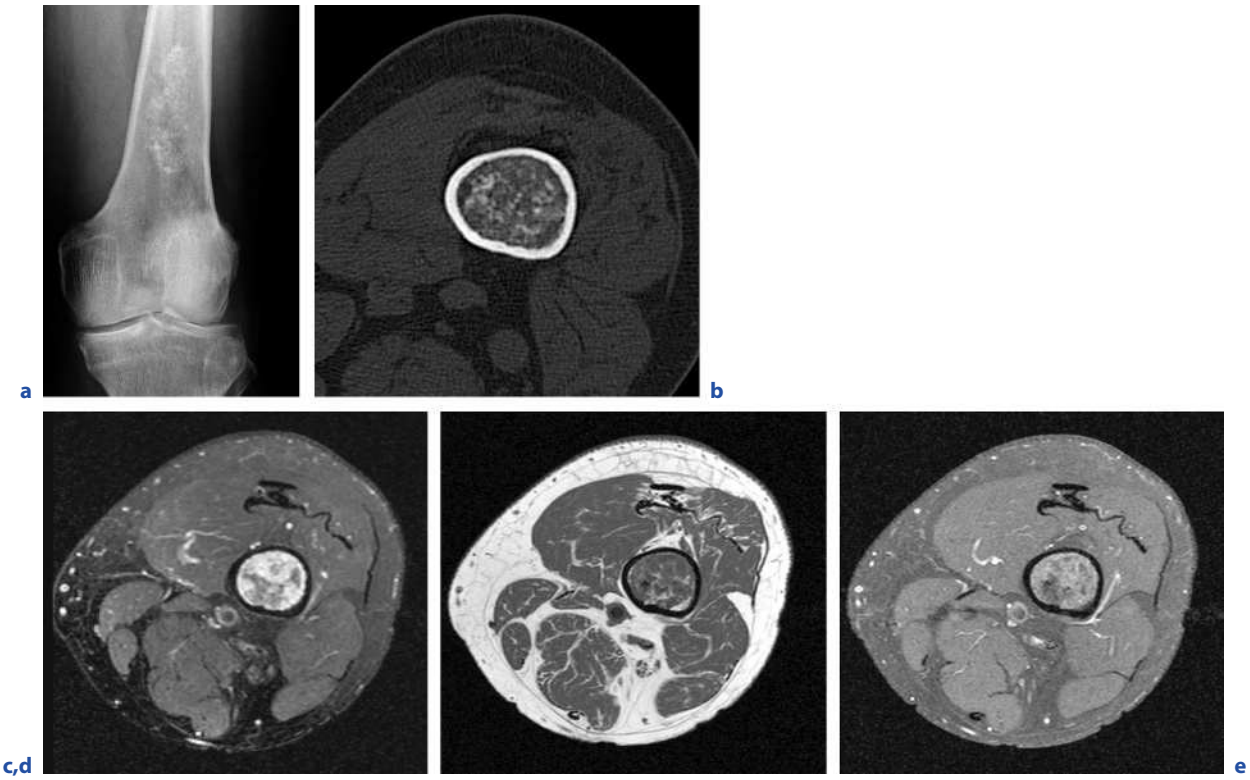

Fig. 13.26a–e. Borderline lesion: Radiograph (**a**) shows chondrogenic calcifications in the distal metadiaphyseal femur. Slight scalloping of the lateral cortex adjacent to the lesion gave the indication for further workup with computed tomography (**b**) and MR imaging (**c–e**). Computed tomography shows that scalloping is only minimal, deep scalloping could be excluded. Neither computed tomography nor MR imaging shows bimorphism within the lesion. MR imaging excluded the presence of a soft tissue mass. The patient was asymptomatic. The lesion was classified as an enchondroma, but further observation was recommended and surgical treatment seriously taken into account. MR imaging consisted of fat-saturated T2-weighted images (**c**), T1-weighted images (**d**) and fat-saturated contrast-enhanced T1-weighted sequences (**e**)

of lesions (Murphey et al. 1998; Kendell at al. 2004). Importantly, in their series of 92 enchondromas and 95 chondrosarcomas all grades of chondrosarcomas were present, so that study results do not refer to the differentiation of enchondroma from low-grade chondrosarcoma, but from all chondrosarcomas. Thus, the authors give helpful criteria to look for in the differential diagnosis, but are not able to quantify the accuracy of the special differential diagnosis described here. Also, by implication, they state that in almost 10% of cases differential diagnosis based on their criteria was not possible.

In an examination of radiography in differentiating enchondroma from grade I chondrosarcoma, another group found no morphologic criteria improving the differentiation between these entities in a series of 35 enchondromas and 43 grade I chondrosarcomas (Geirnaerdt et al. 1997). Limitations of their study were that localisations such as the short tubular bones, known to underlie different histologic and radiologic criteria (see below), were not excluded, and that computed tomography and MR imaging were not routinely included in the radiologic decision process.

Finally, a sophisticated study on the reliability of histologic and radiologic grading of cartilaginous neoplasms showed a low reliability for both in a series of 64 cartilaginous neoplasms (Sliced Study Group 2007). Critically, in their study pathology specimens and imaging were collected in a series over 15 years, and quality of the imaging material, e.g. MR imaging or computed tomography, can be assumed to be heterogeneous.

The use of newer imaging techniques such as positron emission tomography and dynamic MR imaging has been evaluated in initial studies (Geirnaerdt et al. 2000; Feldman et al. 2005). Study results, however, are difficult to interpret because the patient groups in these

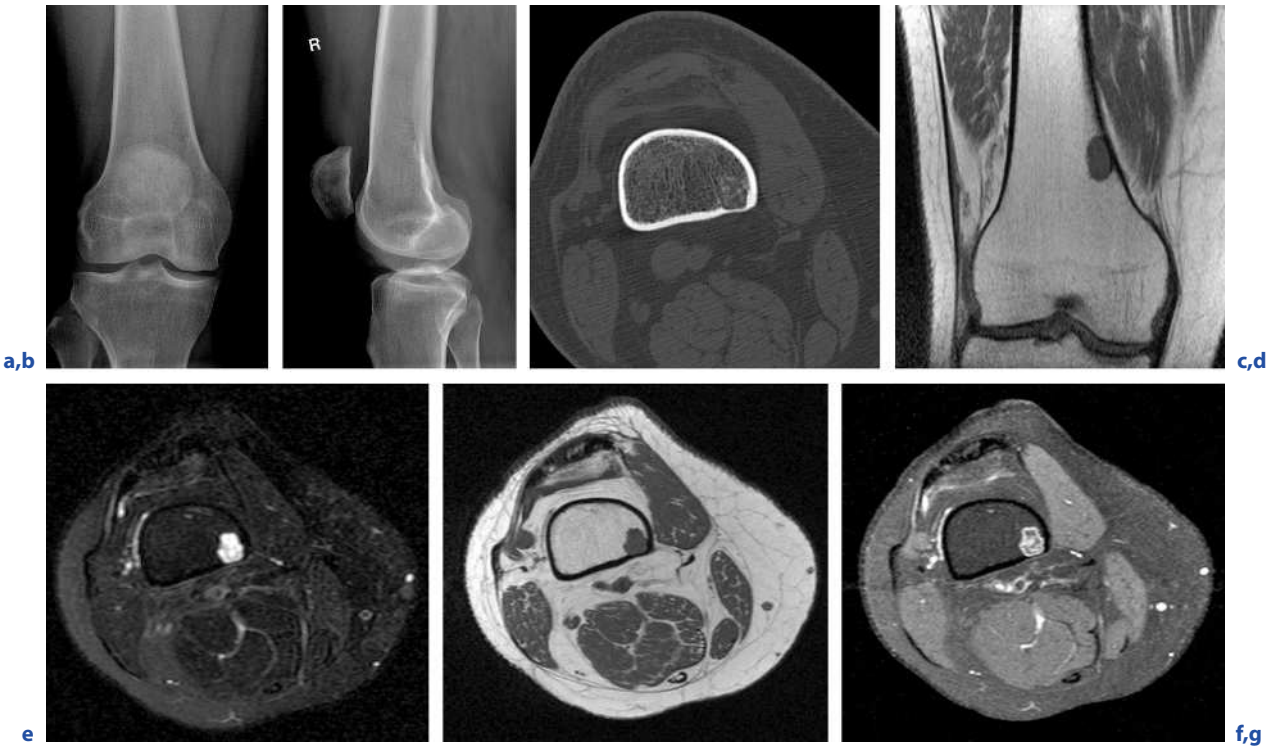

Fig. 13.27a–g. Borderline lesion: Radiographs (**a,b**) show a lytic lesion in the lateral aspect of the distal metaphyseal femur. Interestingly the lesion had been imaged in another institution one year before and at that time been classified as a non-ossifying fibroma (images not shown). Comparison of images showed a slight progression in size, not consistent with either non-ossifying fibroma or with enchondroma in the mature skeleton. Further workup showed deep cortical scalloping and chondrogenic calcifications in computed tomography (**c**) and a lobular mass with high water content and rings-and-arcs type enhancement in MR imaging (**d–g**). MR imaging consisted of T1-weighted images (**d,f**), fat-saturated T2-weighted images (**e**) and fat-saturated contrast-enhanced T1-weighted sequences (**g**). The patient was asymptomatic. Histology was that of a well-differentiated chondrogenic tumour. Because of the progression in size the lesion was classified as a low-grade chondrosarcoma

studies contain either higher grade lesions as well, or the number of borderline lesions is low, and a gold standard is difficult to define.

As examples, these data reflect the difficulties in the scientific workup of this diagnostic challenge which is explained by the lack of a uniform histologic gold standard, by the low numbers of lesions in which a borderline situation is given and by the difficulty in collecting those cases under constant personal and technical circumstances over a longer period of time.

The situation is even more complicated as localisation plays a role in the assessment of biologic behaviour as well: enchondromas in their most frequent localisation, the small tubular bones, are known to have histologic and radiologic features of more aggressive lesions but still show a benign biological behaviour. Localisation in general should be considered in the differential diagnosis: chondrosarcomas and enchondromas show an almost complimentary skeletal distribution. Enchondromas are rare in the axial skeleton, chondrosarcomas in the short tubular bones. It should be kept in mind that though they are rare in these localisations, respectively, they do occur (Ogose et al. 1997; Cawte et al. 1998). It should be noted that enchondroma is exceptionally rare in the talus and the calcaneus and a well-differentiated, purely chondrogenic neoplasm in these bones should be rather classified as a chondrosarcoma.

Despite all the problems indicated above, the following principles should be followed as a general concept as derived from the literature. Lesions with the typical radiographic appearance of an enchondroma (see Sect. 13.3), in a typical localisation and without symptoms can be diagnosed by plain radiography and do not need further workup. Certain criteria, however, do not belong to the typical presentation of an enchondroma and should initiate further workup. These are:

- Lesion-related pain, especially when not explained by the mechanical situation of the parent bone, i.e. if the lesion is not likely to cause a stress phenomenon. Clinical differentiation, e.g. involving the application of local anaesthetics to nearby joints to exclude joint-related pain, may be helpful.
- Atypical localisation.
- Large lesion size, e.g. larger than 5 cm.
- Any radiographic change in the mature skeleton.
- Penetration of the cortex.
- Deep cortical scalloping, more than two thirds of the cortical thickness.
- Periosteal reaction or cortical remodelling, except for a thin neocortex.
- Different calcification patterns within a lesion.
- Different signal patterns within a lesion in MR imaging.
- Soft tissue extension.
- Marked uptake of radionuclide (greater than the anterior iliac crest).

It is generally agreed, that the ideal situation for the workup of these entities is an experienced team of a clinician, radiologist and pathologist working together closely (Sliced Study Group 2007). As the crucial imaging findings may be very subtle, it is furthermore important to have a dedicated imaging workup that in critical cases includes optimised radiographs, computed tomography and MR imaging (Figs. 13.26, 13.27). Imaging should be performed before any biopsy to avoid problems in the differentiation of postoperative tissue changes from tumour spread.

References

Aoki J, Sone S, Fujioka F, Terayama K, Ishii K, Karakida O, Imai S, Sakai F, Imai Y (1991) MR of enchondroma and chondrosarcoma: rings and arcs of Gd-DTPA enhancement. J Comput Assist Tomogr 15:1011–1016

Bertoni F, Baccini P, Hogendoorn PCW (2002) Chondrosarcoma. In: Fletcher DM, Unni KK, Mertens F (eds) Pathology and genetics. Tumours of soft tissue and bone. WHO classification of tumours, Geneva, pp 247–251

Bloem JL, Mulder JD (1985) Chondroblastoma: a clinical and radiological study of 104 cases. Skeletal Radiol 14:1–9

Brien EW, Mirra JM, Kerr R (1997) Benign and malignant cartilage tumors of bone and joint: their anatomic and theoretical basis with an emphasis on radiology, pathology and clinical biology. I. The intramedullary cartilage tumors. Skeletal Radiol 26:325–353

Brien EW, Mirra JM, Luck JV Jr (1999) Benign and malignant cartilage tumors of bone and joint: their anatomic and theoretical basis with an emphasis on radiology, pathology and clinical biology. II. Juxtacortical cartilage tumors. Skeletal Radiol 28:1–20

Brower AC, Moser RP, Gilkey FW, Kransdorf MJ (1990) Chondroblastoma. In: Moser RP (eds) Cartilaginous tumors of the skeleton. Mosby-Year Book, St. Louis, pp 74–113

Cannon CP, Nelson SD, Seeger LL, Eckardt JJ (2002) Clear cell chondrosarcoma mimicking chondroblastoma in a skeletally immature patient. Skeletal Radiol 31:369–372

Cawte TG, Steiner GC, Beltran J, Dorfman HD (1998) Chondrosarcoma of the short tubular bones of the hands and feet. Skeletal Radiol 27:625–632

Collins MS, Koyama T, Swee RG, Inwards CY (2003) Clear cell chondrosarcoma: radiographic, computed tomographic, and magnetic resonance findings in 34 patients with pathologic correlation. Skeletal Radiol 32:687–694

Dahlin, DC, Unni KK (1986) Benign chondroblastoma. In: Dahlin CC, Unni KK (eds) Bone tumors, general aspects and data of 8,542 cases. Thomas, Springfield, p 52

Davila JA, Amrami KK, Sundaram M, Adkins MC, Unni KK (2004) Chondroblastoma of the hands and feet. Skeletal Radiol 33:582–587

Dorfman HD, Czerniak B (1995) Bone cancers. Cancer 75:203–210

Feldman F, Van Heertum R, Saxena C, Parisien M (2005) 18FDG-PET applications for cartilage neoplasms. Skeletal Radiol 34:367–374

Geirnaerdt MJ, Hermans J, Bloem JL, Kroon HM, Pope TL, Taminiau AH, Hogendoorn PC (1997) Usefulness of radiography in differentiating enchondroma from central grade 1 chondrosarcoma. AJR Am J Roentgenol 169:1097–1104

Geirnaerdt MJ, Hogendoorn PC, Bloem JL, Taminiau AH, van der Woude HJ (2000) Cartilaginous tumors: fast contrast-enhanced MR imaging. Radiology 214:539–546

Hashimoto N, Ueda T, Joyama S, Araki N, Beppu Y, Tatezaki S, Matsumoto S, Nakanishi K, Tomita Y, Yoshikawa H (2005) Extraskeletal mesenchymal chondrosarcoma: an imaging review of ten new patients. Skeletal Radiol 34:785–792

Hatano H, Ogose A, Hotta T, Otsuka H, Takahashi HE (1997) Periosteal chondrosarcoma invading the medullary cavity. Skeletal Radiol 26:375–378

Hudson TM, Moser RP, Gilkey FW, Aoki J (1990) Chondrosarcoma. In: Moser RP (eds) Cartilaginous tumors of the skeleton. Mosby-Year Book, St. Louis, pp 155–204

Kaim AH, Hügli R, Bonél HM, Jundt G (2002) Chondroblastoma and clear cell chondrosarcoma: radiological and MRI characteristics with histopathological correlation. Skeletal Radiol 31:88–95

Keith A (1920) Studies on the anatomic changes which accompany certain growth disorders of the human body. J Anat 54:101

Kendell SD, Collins MS, Adkins MC, Sundaram M, Unni KK (2004) Radiographic differentiation of enchondroma from low-grade chondrosarcoma in the fibula. Skeletal Radiol 33:458–466

Kyriakos M, Land VJ, Penning LH, et al. (1985) Metastatic chondroblastoma: report of a fatal case with a review of the literature on atypical, aggressive and malignant chondroblastoma. Cancer 55:1770

Littrell LA, Wenger DE, Wold LE, Bertoni F, Unni KK, White LM, Kandel R, Sundaram M (2004) Radiographic, CT, and MR imaging features of dedifferentiated chondrosarcomas: a retrospective review of 174 de novo cases. Radiographics 24:1397–1409

Lucas DR, Bridge JA (2002) Chondromas: enchondroma, periosteal chondroma, and enchondromatosis. In: Fletcher DM, Unni KK, Mertens F (eds) Pathology and genetics. Tumours of soft tissue and bone. WHO classification of tumours, Geneva, pp 237–240

MacSweeney F, Darby A, Saifuddin A (2003) Dedifferentiated chondrosarcoma of the appendicular skeleton: MRI–pathological correlation. Skeletal Radiol 32:671–678

McCarthy EF, Freemont A, Hogendoorf PCW (2002) Clear cell chondrosarcoma. In: Fletcher DM, Unni KK, Mertens F (eds) Pathology and genetics. Tumours of soft tissue and bone. WHO classification of tumours, Geneva, pp 257–258

Mercuri M, Picci P, Campanacci L, Rulli E (1995) Dedifferentiated chondrosarcoma. Skeletal Radiol 24:409–416

Moser RP, Gilkey FW, Madewell JE (1990a) Enchondroma. In: Moser RP (ed) Cartilaginous tumors of the skeleton. Mosby-Year Book, St. Louis, pp 8–34

Moser RP, Kransdorf MJ, Gilkey FW, Aoki J (1990b) Chondromyxoid fibroma. In: Moser RP (ed) Cartilaginous tumors of the skeleton. Mosby-Year Book, St. Louis, pp 114–154

Murphey MD, Flemming DJ, Boyea SR, Bojescul JA, Sweet DE, Temple HT (1998) Enchondroma versus chondrosarcoma in the appendicular skeleton: differentiating features. Radiographics 18:1213–1237

Murphey MD, Choi JJ, Kransdorf MJ, Flemming DJ, Gannon FH (2000) Imaging of osteochondroma: variants and complications with radiologic–pathologic correlation. Radiographics 20:1407–1434

Ogose A, Unni KK, Swee RG, May GK, Rowland CM, Sim FH (1997) Chondrosarcoma of small bones of the hands und feet. Am Cancer Soc 80:50–59

Porter DE, Lonie L, Fraser M, Dobson-Stone C, Porter JR, Monaco AP, Simpson AH (2004) Severity of disease and risk of malignant change in hereditary multiple exostoses. A genotype–phenotype study. J Bone Joint Surg Br 86:1041–1046

Potter BK, Freedman BA, Lehman RA Jr, Shawen SB, Kuklo TR, Murphey MD (2005) Solitary epiphyseal enchondromas. J Bone Joint Surg Am 87:1551–1560

Rahimi A, Beabout JW, Ivins JC, Dahlin DC (1972) Chondromyxoid fibroma: a clinicopathologic study of 76 cases. Cancer 30:726–736

Robinson P, White LM, Sundaram M, Kandel R, Wunder J, McDonald DJ, Janney C, Bell RS (2001) Periosteal chondroid tumors: radiologic evaluation with pathologic correlation. AJR Am J Roentgenol 177:1183–1188

Schmale GA, Conrad EU 3rd, Raskind WH (1994) The natural history of hereditary multiple exostoses. J Bone Joint Surg Am 76:986–992

Skeletal Lesions Interobserver Correlation among Expert Diagnosticians (SLICED) Study Group (2007) Reliability of histopathologic and radiologic grading of cartilaginous neoplasms in long bones. J Bone Joint Surg Am 89:2113–2123

Staals EL, Bacchini P, Mercuri M, Bertoni F (2007) Dedifferentiated chondrosarcomas arising in preexisting osteochondromas. J Bone Joint Surg Am 89:987–993

Vanel D, De Paolis M, Monti C, Mercuri M, Picci P (2001) Radiological features of 24 periosteal chondrosarcomas. Skeletal Radiol 30:208–212

Weatherall PT, Maale GE, Mendelsohn DB, Sherry CS, Erdman WE, Pascoe HR (1994) Chondroblastoma: classic and confusing appearance at MR imaging. Radiology 190:467–474

Welkerling H, Werner M, Delling G (1996) Histologic grading of chondrosarcoma. A qualitative and quantitative analysis of 74 cases of the Hamburg bone tumor register. Pathologe 17:18–25

Woertler K, Lindner N, Gosheger G, Brinkschmidt C, Heindel W (2000) Osteochondroma: MR imaging of tumor-related complications. Eur Radiol 10:832–840

Yamaguchi T, Dorfman HD (1998) Radiographic and histologic patterns of calcification in chondromyxoid fibroma. Skeletal Radiol 27:559–564

Osseous Tumors

14

Mark J. Kransdorf and Mark D. Murphey

CONTENTS

M. J. Kransdorf, MD
Department of Radiology, Mayo Clinic, Jacksonville, FL 32224-3899, USA
Department of Radiologic Pathology, Armed Forces Institute of Pathology, Washington, DC 20306-6000, USA

M. D. Murphey, MD
Department of Radiologic Pathology, Armed Forces Institute of Pathology, Washington, DC 20306-6000, USA
Department of Radiology and Nuclear Medicine, Uniformed Services University of the Health Sciences, Bethesda, MD 20814-4799, USA

KEY POINTS

- Enostosis is overwhelmingly the most frequently encountered osseous lesion; one that possesses an imaging appearance which is almost always characteristic.
- Osteoma, while much rarer, also has diagnostic imaging features, and shares the same nonneoplastic classification.
- Osteoid osteoma and osteoblastoma are similar but distinct lesions with different clinical presentations and natural histories.
- The pain in osteoid osteoma is worse at night and relieved promptly by salicylates.
- Osteoblastoma occurs most commonly in the appendicular skeleton, with about one-third of cases arising in the spine, typically in the posterior elements, or in the posterior elements growing into the vertebral body.
- Osteosarcoma is the most common primary osseous malignancy (excluding multiple myeloma) and the most common nonhematologic malignancy.
- There are numerous subtypes of osteosarcoma with a wide spectrum of clinical and radiographic features.
- Conventional osteosarcoma is the most common subtype, and is typically in the metaphysis of long bones, with the knee being the most common skeletal site.
- Radiographs are frequently characteristic.
- MR imaging is essential for local staging and surgical and biopsy planning.
- CT scanning is a useful adjunct and especially helpful to demonstrate small areas of mineralized matrix.
- CT is also useful to assess lesions in areas with complex anatomy, such as the pelvis, spine, wrist, etc., and remains the modality of choice for evaluation of pulmonary metastases.
- Telangiectatic osteosarcoma is the subtype most likely to be confused with aneurysmal bone cyst and can be distinguished by identification of solid, viable tumor on contrast enhanced MR imaging.

Abstract

Osseous tumors are common. Although not considered a neoplasm, enostosis is overwhelmingly the most frequently encountered osseous lesion; one that possesses an imaging appearance which is almost always characteristic. Osteoma, while much rarer, also has diagnostic imaging features, and shares the same nonneoplastic classification. Osteoid osteoma and osteoblastoma are benign osseous neoplasms that represent 17% of all benign primary lesions of bone. While osteoid osteoma and osteoblastoma can have similar histological features, they are considered to be separate and distinct lesions with different clinical presentations and natural histories. Of these, osteoid osteoma is four times more common than osteoblastoma.

Osteosarcoma is the most common primary malignant bone tumor in children, and second only to myeloma in overall incidence. The radiologic appearance of osteosarcoma varies over a wide spectrum. Recognized subtypes of osteosarcoma can be grouped into three general categories: intramedullary (conventional, telangiectatic, small cell, low grade and gnathic), juxtacortical (intracortical, parosteal, periosteal, and high grade surface), and secondary. The radiographic appearance of these lesions is often characteristic and suggestive of the specific diagnosis. Additional imaging modalities, including bone scintigraphy, CT, and MR imaging, provide vital information for preoperative staging and planning surgical management. Radiologic examination also allows evaluation of tumor response to chemotherapy, identification of metastatic disease, and postoperative evaluation of recurrent neoplasm, all of which have important prognostic implications.

14.1 Introduction

Osseous tumors are defined by the World Health Organization (WHO) as neoplasms that produce an osseous matrix (Fletcher et al. 2002). These lesions are divided into benign and malignant on the basis of their biological behavior (Fletcher et al. 2002). Although bone island (enostosis) and osteoma are not considered neoplasms and not included the WHO classification of osseous tumors, they will be included in this review because they are not uncommonly encountered in clinical practice.

14.2 Benign Osseous Tumors

Osseous lesions produce osteoid, as well as woven and lamellar bone (Mirra 1989a). The benign osseous lesions can be divided into tumor-like lesions (enostosis and osteoma) and tumors (osteoid osteoma and osteoblastoma). While these benign lesions may share some clinical and imaging characteristics, they are considered to be separate and distinct lesions.

14.2.1 Enostosis (Bone Island)

An enostosis (bone island) represents a focus of mature compact (cortical) bone within the cancellous bone (Greenspan 1995). Initially described in 1905 by Stieda (1905) as "compact bone nuclei" (Greenspan 1995), they are best considered to be a benign, tumor-like lesion, and may be thought of as an intramedullary, cortical hamartoma (Mirra 1989a). The origin of this lesion is unknown, but Greenspan (1995) suggests that it is probably congenital or developmental, reflecting a failure of resorption during enchondral ossification.

14.2.1.1 Pathology

Enostosis is a lesion composed of compact lamellar bone and Haversian systems which blend with the surrounding spongiosa (Mirra 1989a). The surrounding cancellous bone forms thorn-like, trabeculae radiating from the lesion and merging with the surrounding cancellous bone (Fig. 14.1) (Greenspan 1995). Active enostoses may contain foci of woven, nonlamellar bone, but foci of osteoblastic and/or osteoclastic activity are rare (Greenspan et al. 1991; Greenspan 1995).

14.2.1.2 Clinical Presentation

Patients with enostoses typically have no symptoms and lesions are discovered as incidental findings on radiologic exams obtained for other purposes (Mirra 1989a; Greenspan 1995; Cerase and Priolo 1998). Lesions are small, ranging in size from 1 mm to 2 cm, and are found more frequently in adults than in children; males and females are affected equally (Mirra 1989a; Murphey et al. 1996; Cerase and Priolo 1998). Lesions are most commonly encountered in the pelvis, femur, and other long bone (Greenspan 1995), although they may be found anywhere within the skeleton.

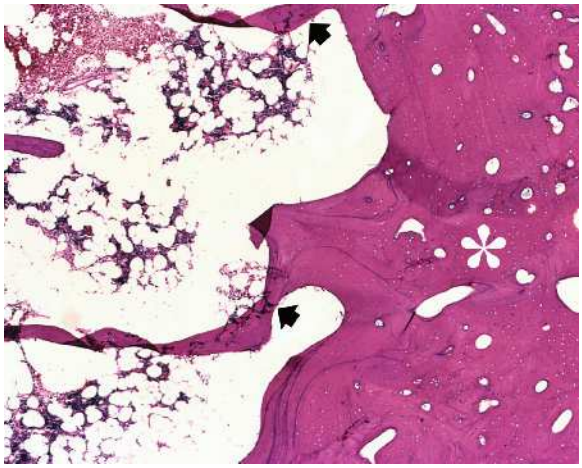

Fig. 14.1. Enostosis histology. Scanning power photomicrograph (hematoxylin-eosin stain) shows enostosis (*asterisk*) composed of compact lamellar bone which blends with the surrounding cancellous bone (*black arrows*)

As enostoses are common and are almost always incidental findings, it is difficult to get accurate data on their prevalence. The generally accepted incidence of 1% stems from a 1964 review of 5000 consecutive patients, in which 42 (0.8%) lesions were identified (Kim SK and Barry 1964). Resnick et al. (1983) reviewed the thoracic and lumbar radiographs of 100 consecutive cadavers, identifying 14 enostoses in 13 patients. Only 4 (29%) of these lesions were identified prospectively, likely as a result of their small size, emphasizing the difficulty of recognizing small lesions. It has been our experience that these lesions are exceedingly common on CT and MR imaging studies.

14.2.1.3 Imaging

The radiographic features of enostosis are quite characteristic and mirror the pathologic features. Lesions are round to oval, with the long axis of oval lesions paralleling the long axis of the affected bone (Greenspan 1995). The surrounding cancellous bone which blends imperceptibly with the surface of the lesion provides a "brush-like" margin (Fig. 14.2). As the enostosis is composed entirely of lamellar bone, there is no associated mass or periosteal reaction (Resnick et al. 1983;

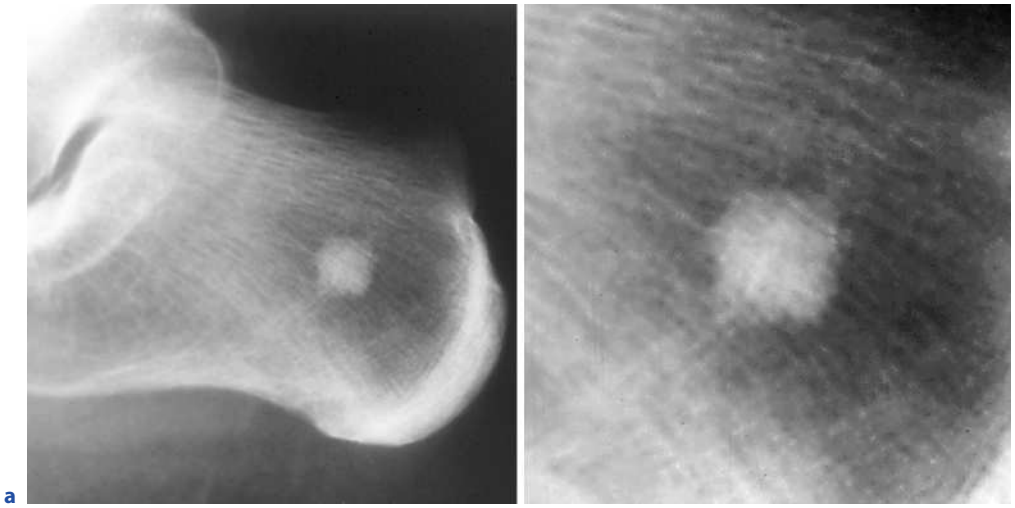

Fig. 14.2a,b. Enostosis of the calcaneous. **a** Lateral radiograph of the calcaneous shows a rounded dense (sclerotic) lesion with radiating osseous spicules that merge with the adjacent trabeculae giving a brush-like border. **b** Magnified image shows these features to better advantage

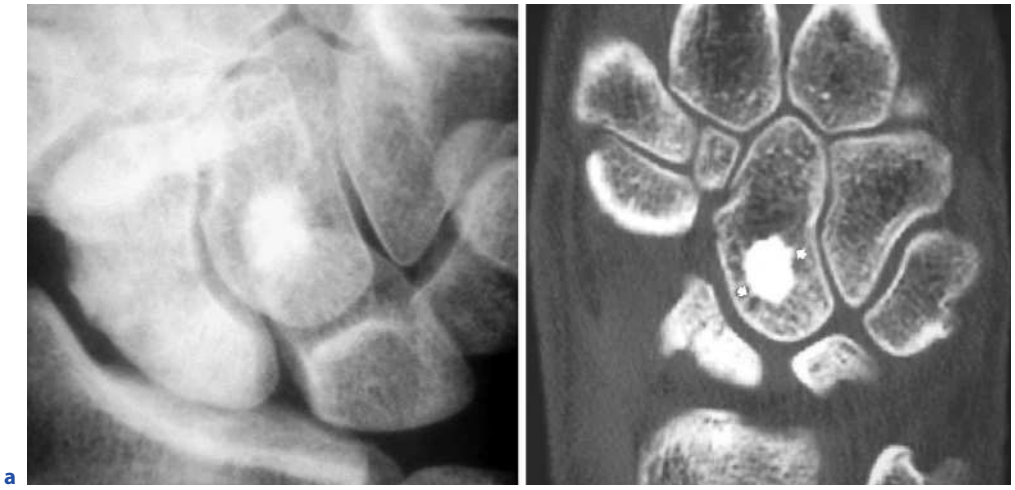

Fig. 14.3a,b. Enostosis of the capitate. **a** Anteroposterior radiograph of the wrist shows a rounded (sclerotic) lesion with radiating osseous spicules. **b** Corresponding direct coronal CT shows the attenuation of the lesion to be similar to that of the adjacent cortex. Note brush-like border with radiating osseous spicules (*arrows*).

Mirra 1989a; Greenspan 1995; Greenspan and Stadalnik 1995). Spinal lesions are often located just below the cortex, and in our experience, often extend to the endosteal surface. Similar features may be seen in appendicular enostoses.

Scintigraphy is typically normal (Greenspan and Stadalnik 1995), although in a study of 12 patients with lesions at least 12 mm in size, 4 (33%) had positive studies (Hall et al. 1980). While the increased tracer accumulation is usually mild, this has not be quantified or compared to an internal standard such as the anterior superior iliac crest. The increased uptake likely is due to a combination of factors such as the lesion size, location and growth rate (Hall et al. 1980; Greenspan and Stadalnik 1995). Because scintigraphy is characteristically normal with enostoses, this modality has been used to distinguish enostoses from blastic metastases (Greenspan and Stadalnik 1995).

MR and CT imaging will reflect those features seen on radiographs (Figs. 14.3 and 14.4). The lesion appear-

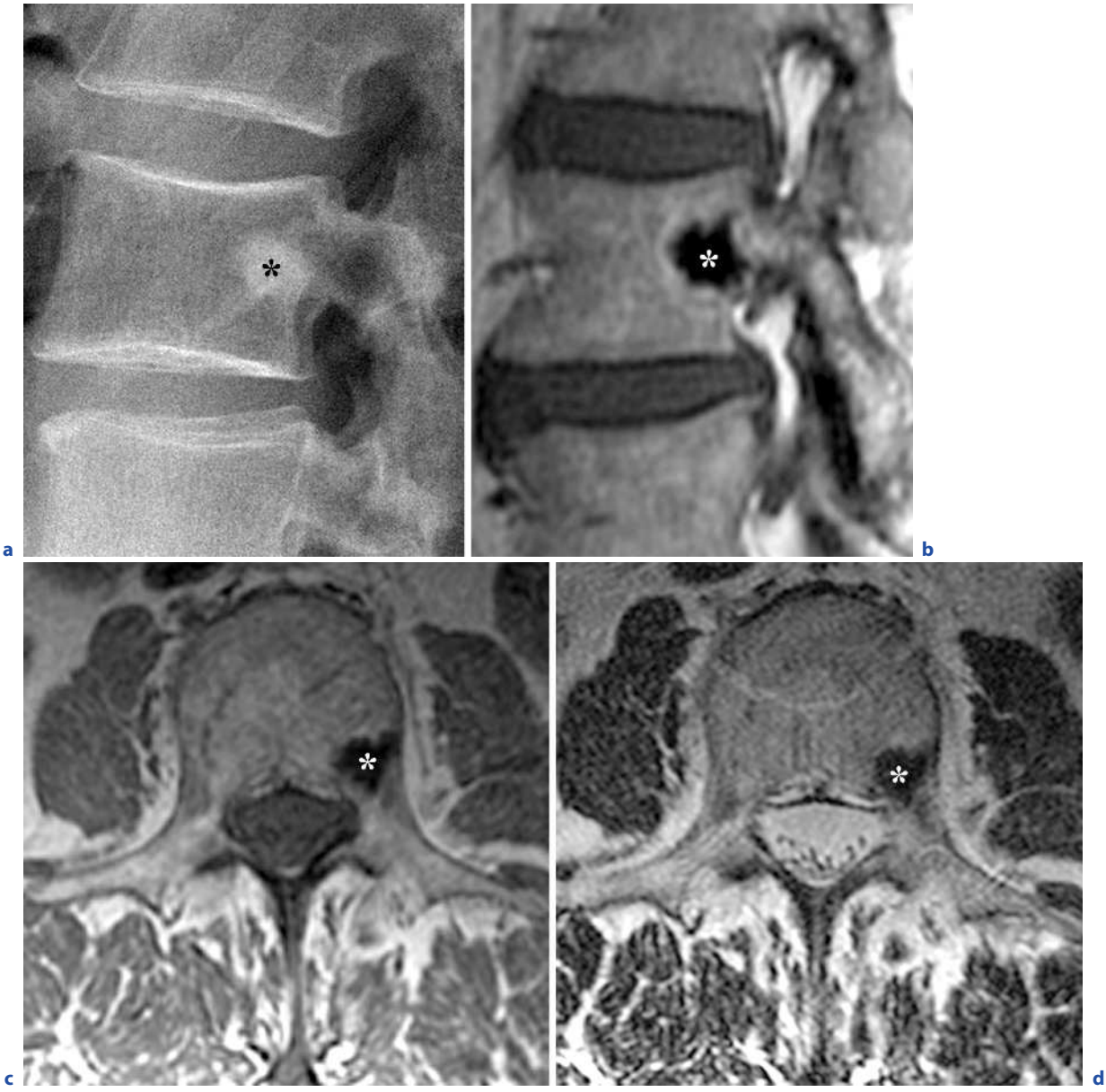

Fig. 14.4a–d. Enostosis of the L3 vertebral body. **a** Lateral radiograph of the spine shows a rounded sclerotic lesion having the typical radiographic features of an enostosis (*asterisk*) with a radiating, spiculated border. Sagittal (**b**) and axial (**c**) T1-weighted spin-echo MR images of the lesion (*asterisk*) show a signal intensity similar to that of cortical bone with radiating speculated margin. Note peripheral location of the lesion. **d** Corresponding axial fast spin-echo T2-weighted image shows similar features (*asterisk*)

ance will duplicate that of cortical bone with no associated soft tissue or mass. The spiculated margin seen on microscopic analysis is usually well demonstrated on CT and MR imaging (Cerase and Priolo 1998; Rodallec et al. 2008). Strict adherence to the required diagnostic imaging appearance for enostosis will ensure that the lesion is not confused with a blastic metastasis.

14.2.1.4 Giant Bone Island

While most enostoses are small, these lesions may become quite large and the term *giant bone island* is given to those lesions larger than 2 cm (Gold et al. 1989). In a literature review in 2005, Park HS et al. (2005) noted

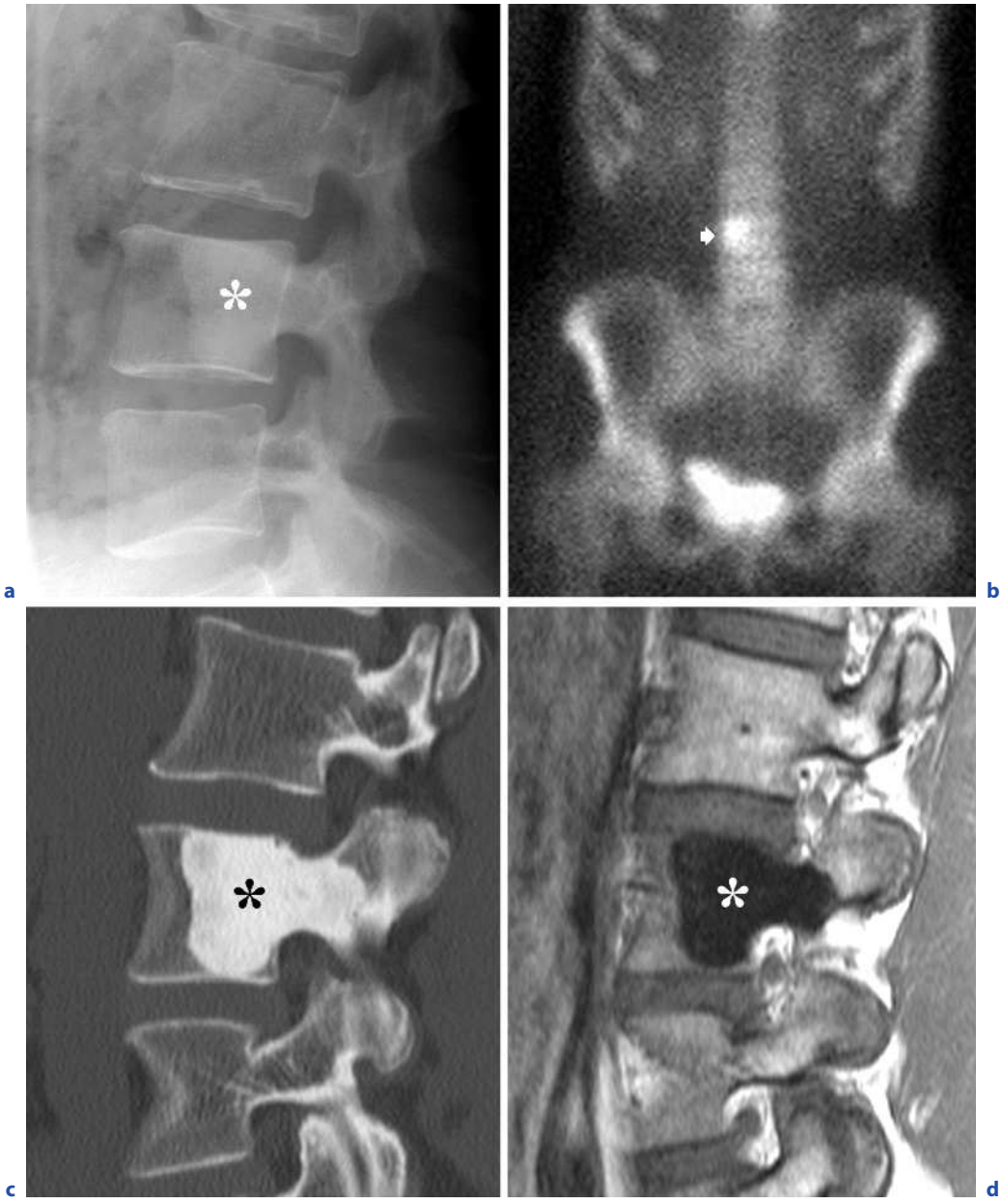

Fig. 14.5a–d. Giant bone island of the spine. **a** Lateral radiograph of the spine shows a large sclerotic lesion (*asterisk*) extending into the pedicle. **b** Delayed static image from bone scintigram shows the lesion (*arrow*) to demonstrate increased tracer accumulation, consistent with the mass of cortical bone present. Corresponding sagittal reformatted CT (**c**) and T1-weighted spin-echo MR (**d**) images show a giant bone island (*asterisks*) involving the body and right pedicle of L3

some degree of pain in eight of ten patients with giant lesions. While it has been our experience that these lesions will demonstrate imaging features similar to those seen in conventional enostoses, some differences may be identified. On scintigraphy, large lesions may show increased radiotracer accumulation as noted above (Fig. 14.5). On CT and MR imaging, the appearance of the lesion, usually centrally, may vary from that of cortical bone (Fig. 14.5). The basis for these changes is not documented; however, Avery et al. (1995) noted it to be due to central resorption in reporting a symptomatic lesion of the proximal femur.

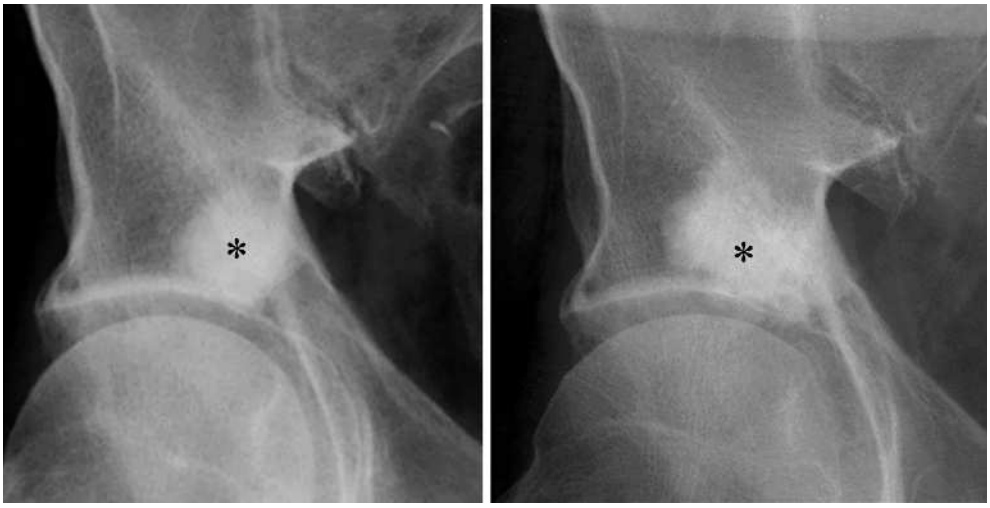

Fig. 14.6a,b. Interval growth of an enostosis over 7 years. Initial (**a**) and 7 year follow-up (**b**) anteroposterior radiographs of the pelvis show interval growth of the acetabular enostosis (*asterisk*)

14.2.1.5 Natural History

While most enostoses are small and remain stable, changes in size are not rare. Previous reports have shown that as many as one-third of enostoses will demonstrate changes in size, typically increasing slowly (Fig. 14.6), although lesions may decrease in size as well (Onitsuka 1977; Petrikowski and Peters 1997). The change in size can be marked with Trombetti and Noël (2002) reporting a change in maximal size of a pelvic lesion from 1 to 5.5 cm over an observation period of 31 years. Although there are no absolutes, Mirra (1989a) recommends that radiographic follow-up at 1, 3, 6, and 12 months should show should no more than 25% change in size at 1, 3 or 6 months, or no more than 50% at 1 year.

14.2.2 Osteoma

An osteoma is a relatively rare lesion composed entirely of osteoid tissue, representing a focal exaggeration of intramembranous bone formation, and accordingly, is identified in areas associated with periosteum (Resnick et al. 2002a). It is typically found within the paranasal sinuses and the skull, but may rarely be identified in a long bone. Osteomas are found in both children and adults and may be associated with Gardner syndrome. Osteoma of soft tissue has been described, but is quite rare (Schweitzer et al. 1992).

14.2.2.1 Pathology

Osteomas are nodular osteoid forming masses on the surface of bone (Resnick et al. 2002a). Microscopically, an osteoma is composed of lamellar bone, often with a mixture of woven bone, which may or may not contain Haversian systems (Fig. 14.7) (Mirra 1989a). This variability in the type of bone present and its mineralization influences the lesion's radiologic appearance. Densely mineralized lesions are sometimes termed *ivory osteomas* to emphasize this pattern. In striking contrast to

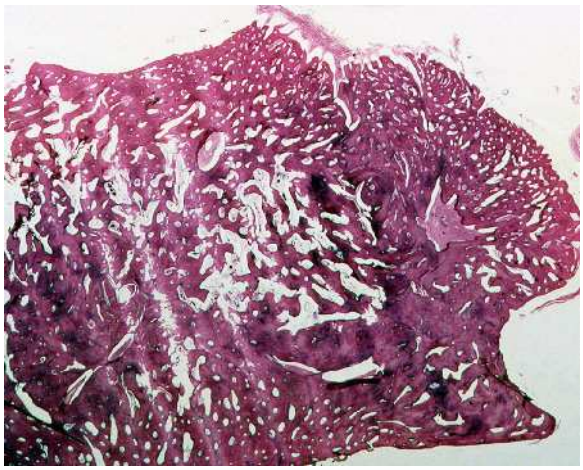

Fig. 14.7. Osteoma histology. Scanning power photomicrograph (hematoxylin-eosin stain) shows osteoma composed of a mixture of lamellar bone and woven bone

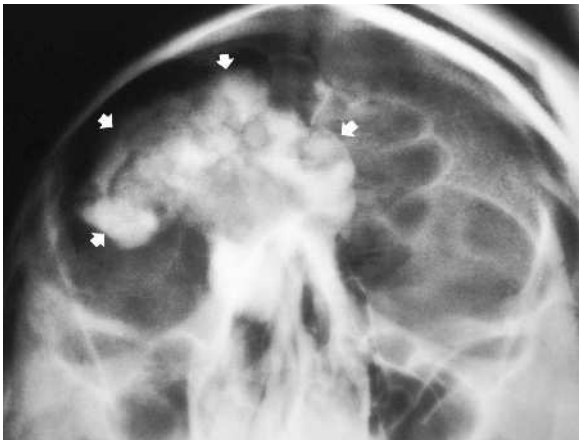

Fig. 14.8. Osteoma of the frontal-ethmoid sinuses. Waters view radiograph of the sinuses shows a large, lobulated, dense osteoma (*arrows*) involving the frontal and ethmoid sinuses. The lesion is heterogeneous, with the dense areas representing lamellar bone and the more radiolucent areas representing less well mineralized fibro-osseous tissue

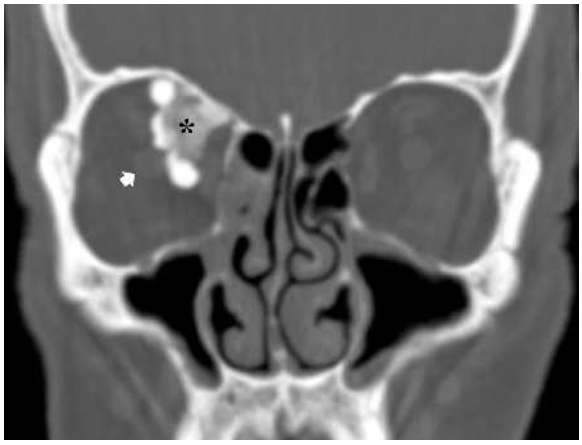

Fig. 14.9. Osteoma of the orbit in a 72-year-old man presenting with double vision. Reformatted noncontrast coronal CT scan of the orbits shows an osteoma displacing the optic nerve (*arrow*). The more radiolucent area (*asterisk*) represents less well mineralized fibro-osseous tissue

enostoses, they are associated with the cortical margin of bone and do not involve the intramedullary space (Mirra 1989a).

14.2.2.2 Clinical Presentation

Osteomas are usually small and patients frequently have no symptoms. Lesions are often discovered as incidental findings on radiologic exams obtained for other purposes. The much quoted frequency on sinus radiographs of 0.42% stems from a 1959 retrospective study of 16,000 patients (Eckel and Palm 1959).

Lesions are reported most frequently in the third and fourth decades and are twice as common in men as in women (Sadry et al. 1988). They are found in children and are thought to have their peak growth at the time of maximal skeletal development (Greenspan 1993). Lesions are most commonly found in the frontal and ethmoid sinuses, with these areas accounting for 75% of osteomas (Sadry et al. 1988).

Lesions are usually small; however, large or giant lesions may be seen. Larger lesions are more likely to cause symptoms based on their size and location, typically affecting the sinuses and orbits. Most frequently, this is the result of blockage of the fronto-nasal ducts causing sinusitis, headache and mucocele (Leiberman and Tovi 1984; Sadry et al. 1988). Orbital involvement may cause unilateral, non-pulsatile exophthalmos, proptosis and visual disturbances (Sadry et al. 1988). Rarely, lesions may invade the anterior cranial fossa with serious intracranial complications (Sadry et al. 1988; Greenspan 1993).

In addition to the sinuses, osteomas may also be found in the long bones. We generally refer to this lesion as appendicular osteoma; although it is also termed *parosteal osteoma* or *surface osteoma* (Sundaram et al. 1996). Appendicular osteoma is distinctly unusual. In a review of 40,000 recorded bone lesions in the Mayo Clinic tumor files, only 14 (0.035%) long bone osteomas were identified (Unni 1996b). Parosteal osteomas have been reported in patients between 10 and 75 years of age (Sundaram et al. 1996), often with a long history of a mass that may extend to 40 years (Stern et al. 1985). Lesions are most common in the ilium, clavicle, and femur, but have been reported in various other locations to include the tibia, humerus, fibula, and metacarpal (Stern et al. 1985; Houghton et al. 1995; Sundaram et al. 1996).

14.2.2.3 Imaging

On radiography, lesions are typically small, round, smoothly marginated, well-defined, homogeneous, osteoid forming masses (Sadry et al. 1988), becoming more lobulated with increasing size (Figs. 14.8 and 14.9). Radiographs reflect the histologic composition of the dense lamellar bone within the lesions, although variable radiolucency may be seen (Shibata et al.

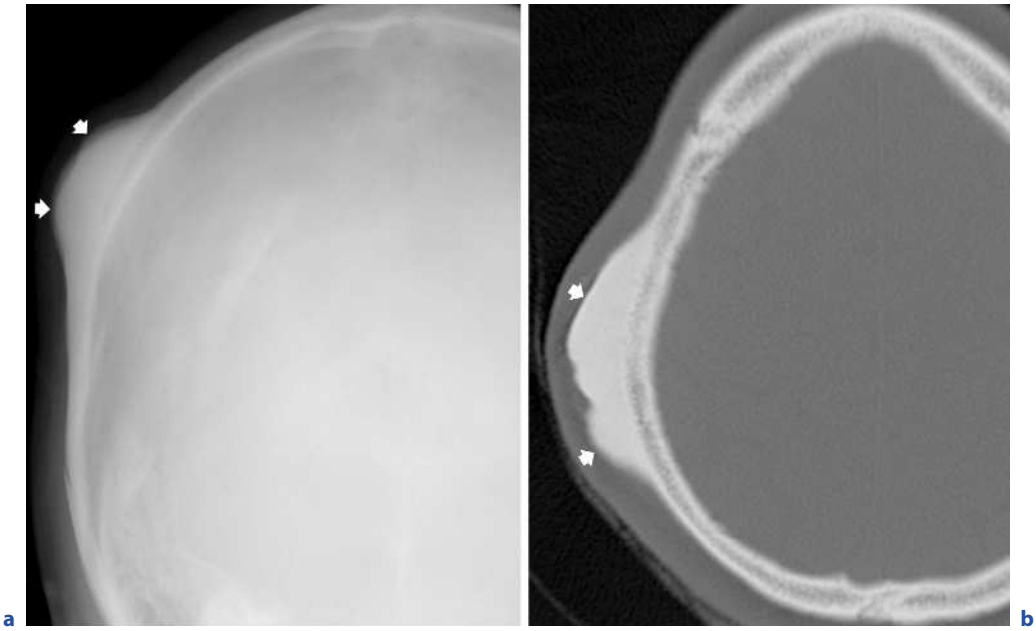

Fig. 14.10a,b. Osteoma of the skull in a 40-year-old woman with 12 year history of a "hard" mass. **a** Townes view of the skull shows the osteoma (*arrows*) as a dense osseous mass arising from the outer table of the skull. **b** Axial noncontrast CT displayed on bone window shows the lobulated mass (*arrows*) arising from the outer table. The mass images similar to the adjacent cortical bone

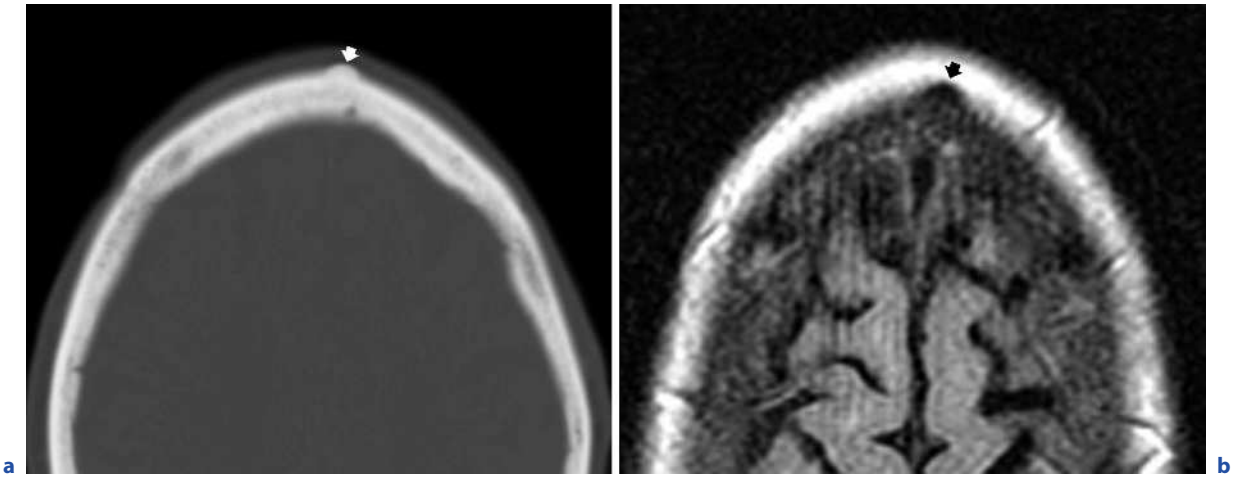

Fig. 14.11a,b. Osteoma of the skull. Corresponding axial noncontrast CT (**a**) and FSE proton density MR (**b**) images show a typical small osteoma (*arrows*) arising from the outer table of the skull

1991), reflecting zones of fibro-osseous dysplasia (Unni 1996b). Osteomas arise from the surface of bone and do not demonstrate the cortical medullary continuity seen in an osteochondroma.

The CT and MR imaging appearance of osteoma parallel that of cortical bone, and although there may be some variability, the dominant feature mirrors cortex (Figs. 14.10 and 14.11). Scintigraphy generally shows no increased tracer accumulation on flow or blood pool imaging, with delayed imaging demonstrating slightly increased radionuclide uptake relative to cortical bone (Lambiase et al. 1998). In general, scintigraphy shows variable tracer accumulation reflecting the biological activity of the lesion (Noyek et al. 1989) as well as its size, but will not show the marked uptake anticipated for osteosarcoma (Lambiase et al. 1998).

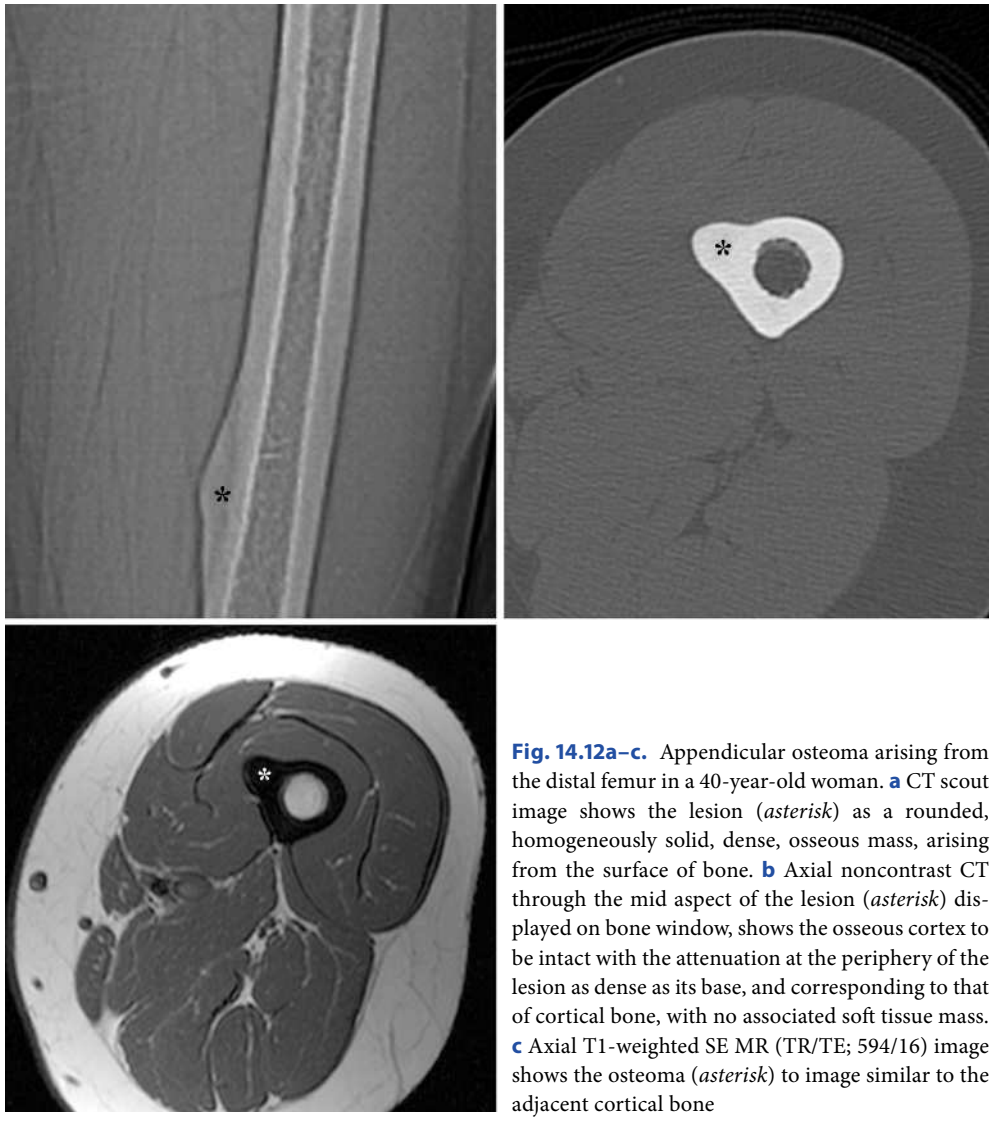

Fig. 14.12a–c. Appendicular osteoma arising from the distal femur in a 40-year-old woman. **a** CT scout image shows the lesion (*asterisk*) as a rounded, homogeneously solid, dense, osseous mass, arising from the surface of bone. **b** Axial noncontrast CT through the mid aspect of the lesion (*asterisk*) displayed on bone window, shows the osseous cortex to be intact with the attenuation at the periphery of the lesion as dense as its base, and corresponding to that of cortical bone, with no associated soft tissue mass. **c** Axial T1-weighted SE MR (TR/TE; 594/16) image shows the osteoma (*asterisk*) to image similar to the adjacent cortical bone

The imaging of long bone lesions is more problematic as a result of their rarity and their similarity to parosteal osteosarcoma. Sundaram et al. (1996) succinctly summarized the diagnostic imaging criteria noting that: (1) radiographs reveal a rounded homogeneously solid, dense, osseous mass extending parallel to the cortex, with virtually no lucency arising from the surface of bone, (2) CT scanning shows the osseous cortex to be intact with the attenuation of the periphery of the lesion to have an attenuation as dense as its base, and corresponding to that of cortical bone, with no associated soft tissue mass, and (3) MR imaging also shows decreased signal intensity, consistent with that of cortical bone without intramedullary extension (Fig. 14.12). Variations to these criteria have been described to include periosteal reaction (Sundaram et al. 1996), intramedullary extension (Houghton et al. 1995), and intramedullary sclerosis (Soler Rich et al. 1998); however, strict adherence to the above criteria will allow successful distinction from parosteal osteosarcoma, the lesion with which an appendicular osteoma is most likely to be confused.

14.2.2.4 Gardner Syndrome

Multiple osteomas are commonly associated with Gardner syndrome; a familial autosomal-dominant disorder characterized by multiple osteomas, intestinal polyposis, dentigerous cysts, epidermoid cysts, desmoid tumors and skin fibromas (Gardner and Richards 1953).

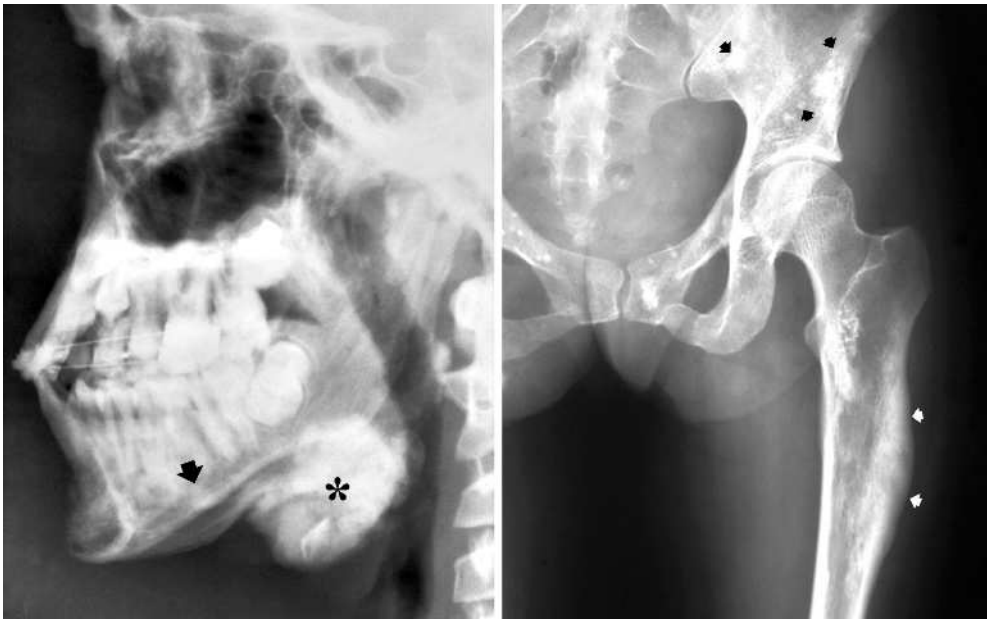

Fig. 14.13a,b. Multiple craniofacial and appendicular osteomas in a patient with Gardner syndrome presenting with a mass at the angle of the jaw. **a** Lateral radiograph of the mandible shows the presenting osteoma (*asterisk*). Note additional mandibular osteoma viewed en-face (*arrow*). **b** Anteroposterior radiograph of the left hip shows multiple osteomas, with large appendicular osteoma (*white arrows*) of the femur and multiple smaller, round lesions within the pelvis (*black arrows*)

Approximately half of patients with Gardner syndrome will have osteomas, which may be the presenting manifestation of the disease (Weary et al. 1964), most commonly in the skull, sinuses and mandible. Lesions are also common in long bones, and in this location they are not necessarily well-defined, but may instead appear as a thickening of the cortex (Resnick et al. 2002a), the thickened cortex representing periosteal intramembranous new bone formation (Fig. 14.13).

14.2.3 Osteoid Osteoma

Osteoid osteoma is defined by the WHO as "…a benign bone-forming tumor characterized by small size, limited growth potential and disproportionate pain" (Klein et al. 2002). The term *osteoid osteoma* was introduced into the medical literature in 1935 by Jaffe, who described five benign osteoblastic tumors composed of osteoid and atypical bone. In all of these cases, surgery was performed on the "assumption that the condition was inflammatory-osteomyelitis or an abscess of the bone-but pus was not found in any instances" (Jaffe 1935). Although similar cases were published previously, Jaffe was the first to recognize the lesion as a distinct clinical and pathologic entity (Jaffe 1935). After his initial report, Jaffe reported an additional 28 cases in 1940 (Jaffe and Lichtenstein 1940) and 29 cases in 1945 (Jaffe 1945), for a cumulative total of 62 cases. Osteoid osteoma is now recognized to be a relatively common skeletal lesion which accounts for approximately 12% of benign skeletal neoplasms (Unni 1996a).

14.2.3.1 Pathology

Osteoid osteoma is a lesion composed of osteoid and woven bone, both of which can be seen as interconnected trabeculae, sheets, or isolated islands (Kransdorf et al. 1991). The trabeculae can be thin or broad, well-formed, or haphazard. Plump osteoblasts are often obvious at the edge of the osteoid (osteoblastic "rimming"). The tissue between the osteoid elements is composed of loose, fibrovascular tissue, and osteoclasts are usually only present in small numbers. There may or may not be a zone of loose tissue without osteoid between the lesion and surrounding bone, but lesional tissue does not insinuate itself into surrounding bone more than in minute foci. Host bone surrounding the lesion is typically robust and is composed of varying mixtures

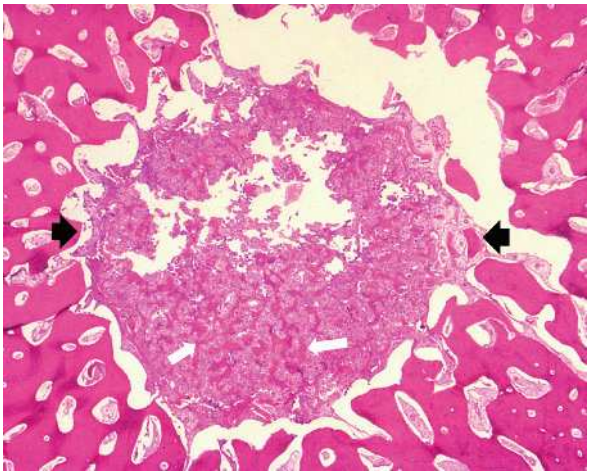

Fig. 14.14. Osteoid osteoma histology. Scanning power photomicrograph (hematoxylin-eosin stain) shows osteoid osteoma (*black arrows*) surrounded by dense cortical and periosteal bone. Note woven bone trabeculae (*long white arrows*) on a background of intervening loose connective tissue

of woven and lamellar bone (Fig. 14.14) (Kransdorf et al. 1991; Klein et al. 2002).

14.2.3.2 Classification

In 1966, Edeiken et al. (1966) categorized three types of osteoid osteoma, each with differing amounts of associated osteosclerosis, based on radiographic localization of the nidus: cortical, cancellous, and subperiosteal.

Cortical osteoid osteoma, the most common type, accounts for approximately 75% of lesions and typically demonstrates fusiform, sclerotic, cortical thickening in the shaft of a long bone, most frequently affecting the tibia and femur. A characteristic radiolucent area, representing the lesion itself, is usually located within the center of the osteosclerosis. The latter is reactive and can regress after surgical removal of the osteoid osteoma (Unni 1996a).

Cancellous (also referred to as medullary) osteoid osteoma, is intermediate in frequency and classically accounts for about 25% of lesions. It has a predilection for the femoral neck, small bones of the hand and foot, and the vertebral posterior elements. When present, osteosclerosis is usually mild to moderate and may be distant from the lesion. Unlike its classic cortical counterpart, a cancellous osteoid osteoma is not necessarily situated in the center of the accompanying sclerosis. This feature has surgical ramifications, since removal of the nidus is necessary for cure.

Subperiosteal osteoid osteoma is traditionally considered to be the rarest type and arises as a soft-tissue mass immediately adjacent to the affected bone. Subperiosteal osteoid osteoma is typically located along the medial aspect of the femoral neck as well as in the hands and feet (Edeiken et al. 1966). It is also common in the neck of the talus (Capanna et al. 1986). The subjacent bone may have pressure atrophy or irregular bone resorption (Edeiken et al. 1966). Subperiosteal osteoid osteomas produce almost no reactive sclerosis (Swee et al. 1979). While subperiosteal osteoid osteoma has traditionally been considered to be rare, Kayser et al. (1998) have suggested that almost half of all cortical lesions may arise in this location. Analysis of many lesions that may have previously been considered cortical, shows that the lesion was likely to have originated in a subperiosteal location, being incorporated into the cortex by extensive periosteal new bone production. In our experience, most orthopedic surgeons still use the Edeiken system. Accordingly, we generally refer to all lesions surrounded by cortex (either original or the result of extensive periosteal new bone formation) as intracortical osteoid osteomas.

Cancellous and classic subperiosteal osteoid osteomas typically arise in an intraarticular or juxtaarticular location. As broadly defined by Kattapuram et al. (1983), osteoid osteomas occurring at the ends of long bone, in or around the joint, or in the bone surrounded by or very close to the capsule and synovium (although not within the synovial cavity itself such as a loose body), are considered to be intraarticular osteoid osteomas.

14.2.3.3 Clinical Presentation

Patients with osteoid osteoma are usually young, with about half presenting between the ages of 10 and 20 years. and is uncommon in patients less than 5 or greater than 40 years of age (Mirra 1989a). In a series of 225 patients seen at the AFIP, the average age at presentation was 19 years (range, 19 months to 56 years) (Kransdorf et al. 1991). There is an unmistakable male prevalence, with most larger series reporting a ratio of male to female patients of approximately 1.6:1 to 4:1 (Jaffe 1945; Freiberger et al. 1959; Kendrick and Evarts 1967; Mirra 1989a; Kransdorf et al. 1991; Unni 1996a).

Osteoid osteoma is uncommon in the non-white population (Kendrick and Evarts 1967). In the vast

majority of patients the presenting complaint is pain varying in duration from weeks to years. The pain is usually described as mild and intermittent at first, later becoming more constant and severe (Jaffe and Lichtenstein 1940; Swee et al. 1979). Intense pain may be present even before the lesion is apparent radiologically (Schulman and Dorfman 1970; Kattapuram et al. 1983). Pain is typically worse at night (Sherman 1947a; Swee et al. 1979; Pettine and Klassen 1986) and may awaken the patient from sleep (Sherman 1947b). Pain is often referred to a nearby joint (Freiberger et al. 1959; Unni 1996a) or may be so distant from the lesion that radiographic examinations are misdirected (Freiberger et al. 1959; Unni 1996a). Pain, typically relieved by aspirin, was noted by Jaffe (Jaffe and Lichtenstein 1940) and has been regarded as a significant diagnostic feature (Freiberger et al. 1959). Response to aspirin is clearly not universal (Mitnick et al. 1979; Kattapuram et al. 1983; Healey and Ghelman 1986); however, approximately 75% of patients report relief of symptoms after treatment with salicylates (Healey and Ghelman 1986; Unni 1996a).

Rarely, osteoid osteoma may be painless; Jackson et al. (1977) identified 14 (1.6%) such lesions in a review of 860 cases. These patients may present with swelling, a mass, deformity, or painless limp (Freiberger et al. 1959; Healey and Ghelman 1986; Pettine and Klassen 1986). In the AFIP series, 5% of patients presented with a mass or painless swelling, although 17% of this small group noted associated tenderness. Interestingly, half of the painless lesions in the AFIP series occurred in lesions involving the fingers (Kransdorf et al. 1991). Swelling may be associated with superficial lesions (i.e., those arising in the fingers, toes, or superficially located long bones, such as the radius or anterior aspect of the tibia) (Sim et al. 1975; Kayser et al. 1998). Systemic symptoms are almost invariably absent and results of laboratory studies are normal (Jaffe 1945; Sherman 1947a,b; Healey and Ghelman 1986). Osteoid osteoma in the lower extremities is often associated with limp and muscle atrophy, possibly due to disuse (Sherman 1947b; Freiberger et al. 1959; Unni 1996a).

Patients with osteoid osteoma of the spine commonly have scoliosis (Azouz et al. 1986; Pettine and Klassen 1986); moreover, osteoid osteoma is the most common cause of painful scoliosis in adolescents (Pettine and Klassen 1986). Spinal deformity in these patients is due to spasm and is not a true scoliosis (Mirra 1989a). Atrophy and fatty replacement of the paraspinal muscles may occur as well (McConnell and Daneman 1984). Typically, there are no signs of motor or sensory loss or neurologic dysfunction associated with spinal lesions (Corbett et al. 1974). Diagnosis of spinal lesions is often delayed and Pettine and Kiassen (1986) noted that when diagnosis of spinal osteoid osteoma was made by means of scintigraphy, the average duration of symptoms decreased by approximately two-thirds, from 35 to 12 months.

Intraarticular osteoid osteoma is typically associated with nonspecific symptoms. Physical examination may reveal a joint effusion and synovitis, the latter being histologically characterized by some authors as lymphofollicular (Sherman 1947b; Goldberg and Jacobs 1975; Swee et al. 1979; Kattapuram et al. 1983; Mirra 1989a; Resnick et al. 2002c). Limitation of joint motion, stiffness, weakness, flexion deformity, atrophy, contracture, and advanced epiphyseal development (maturation) have also been reported (Jaffe and Lichtenstein 1940; Swee et al. 1979; Kumar SJ et al. 1984).

Norman et al. (1986) reported osteoarthritis as a "not infrequent" complication of intraarticular osteoid osteoma of the hip, noting it in 50% of 30 patients with intraarticular lesions. In these patients, the osteoarthritis was moderate and developed 1.5–22 years after the clinical onset of symptoms (Norman et al. 1986).

14.2.3.4 Skeletal Distribution

Osteoid osteoma may occur in virtually any bone, although there is a strong predilection for the lower extremity, with 50% or more of lesions occurring in the femur and tibia (Jackson et al. 1977; Unni 1996a; Resnick et al. 2002c). The majority of lesions arise in the cortex of long bones, where the lesion is usually diaphyseal or metadiaphyseal (Mirra 1989a; Raymond et al. 2002). Of the remaining lesions, approximately 30% are equally distributed among the spine, hand, and foot (Jackson et al. 1977; Resnick et al. 2002c). When osteoid osteoma occurs in the spine, the most commonly affected area is the lumbar spine, typically in the neural arch (Swee et al. 1979; Pettine and Klassen 1986). Lesions limited to the vertebral body are unusual (Pettine and Klassen 1986). Other atypical locations include the skull, ribs, ischium, mandible, and patella (Jackson et al. 1977). Intraarticular lesions are most commonly encountered in the hip (Swee et al. 1979; Kattapuram et al. 1983). Epiphyseal lesions have been reported but are rare (Dunlap and Martin 1985; Destian et al. 1988); in a review of the literature through 1988, Destian et al. (1988) noted only seven such cases.

14.2.3.5 Imaging

The radiologic appearance of classic cortical osteoid osteoma arising in the shaft of a long bone is characteristic. The osteoid osteoma, which may be radiolucent or contain a variable amount of mineralization, is often referred to as the "nidus," because it is the focus of the underlying pathologic process and is usually centrally positioned within an area of dense, fusiform, reactive osteosclerosis (Figs. 14.15 and 14.16). This sclerosis is reversible and may regress after treatment (Unni 1996a).

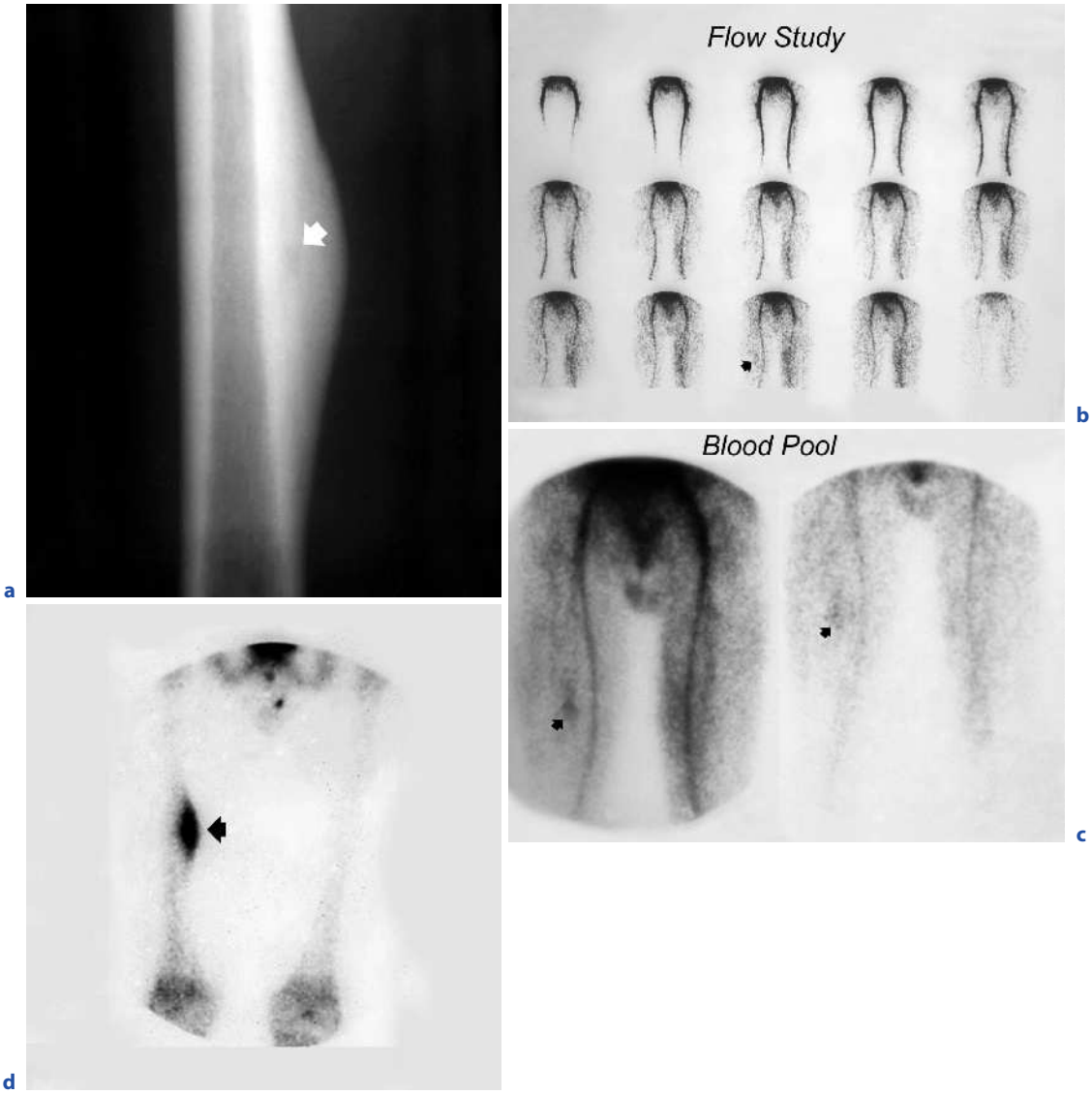

Fig. 14.15a–i. Cortical osteoid osteoma of the femur in a 19-year-old man with thigh pain. This is the type of lesion that likely originated subperiostally, and was incorporated into the cortex by extensive periosteal new bone. **a** Anteroposterior radiograph of the distal femoral shaft shows marked cortical thickening and fusiform periosteal new bone formation with a faint central radiolucent lesion (*arrow*) representing the osteoid osteoma. **b** Flow study from three-phase bone scintigram reveals minimally increased flow to the right thigh in the region of the lesion (*arrow*) and moderately increased flow to the left thigh musculature, presumably related to increased weight-bearing because the patient favored the right leg. **c** Blood pool images demonstrate a focus of increased uptake in the middle of the right femoral diaphysis (*arrow*), corresponding to the region of the lesion. **d** Delayed scintigram shows focal radionuclide activity corresponding to the cortical osteoid osteoma and reactive new bone formation (*arrow*) identified on the radiograph

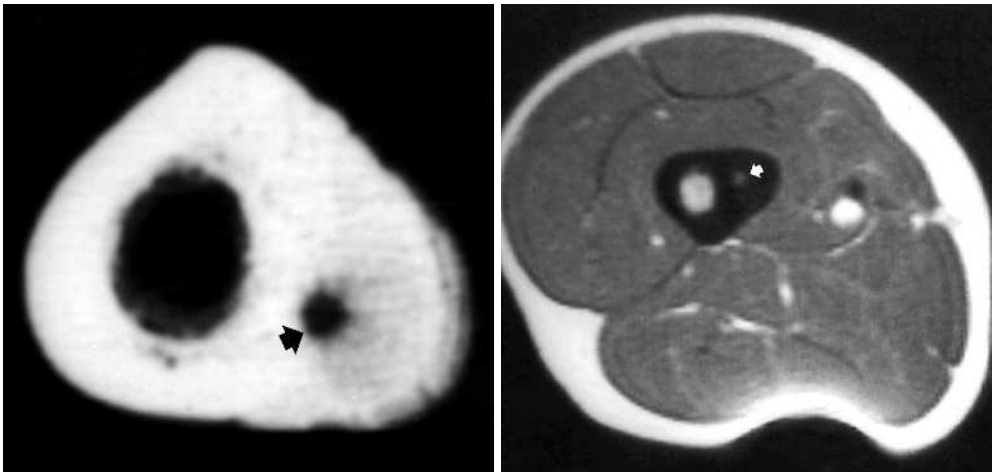

e f

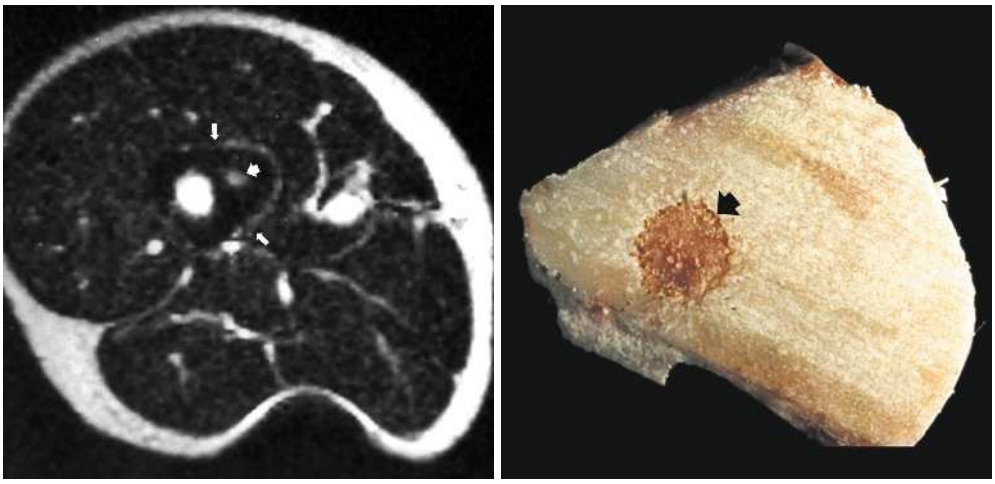

g h

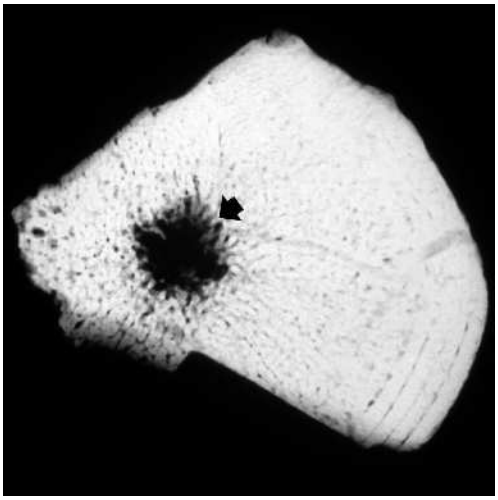

i

Fig. 14.15a–i. (*continued*) Cortical osteoid osteoma of the femur in a 19-year-old man with thigh pain. This is the type of lesion that likely originated subperiostally, and was incorporated into the cortex by extensive periosteal new bone. **e** Axial CT image through the center of the osteoid osteoma demonstrates the central location of the lesion (*arrow*) within the surrounding periosteal new bone. Corresponding axial T1-weighted (TR/TE; 700/20) (**f**) and T2-weighted (TR/TE; 2000/80) (**g**) spin-echo MR images show the lesion (*short arrows*) to have an intermediate signal intensity. Signal intensity of the marrow within the right femur adjacent to the lesion is abnormal, being slightly decreased on T1-weighted and increased on T2-weighted images, compatible with minimal associated marrow edema. Note mild associated edema-like change in the adjacent soft tissue (*long arrows*). **h** Photograph of resected wedge specimen after fixation. Note brown color of nidus (*arrow*) as well as small trabeculae within it. **i** Corresponding radiograph of the specimen **h** shows the irregular periphery of the nidus (*arrow*), which appears smooth on CT scan. Also note subtle internal trabeculae matching those seen in the gross photograph

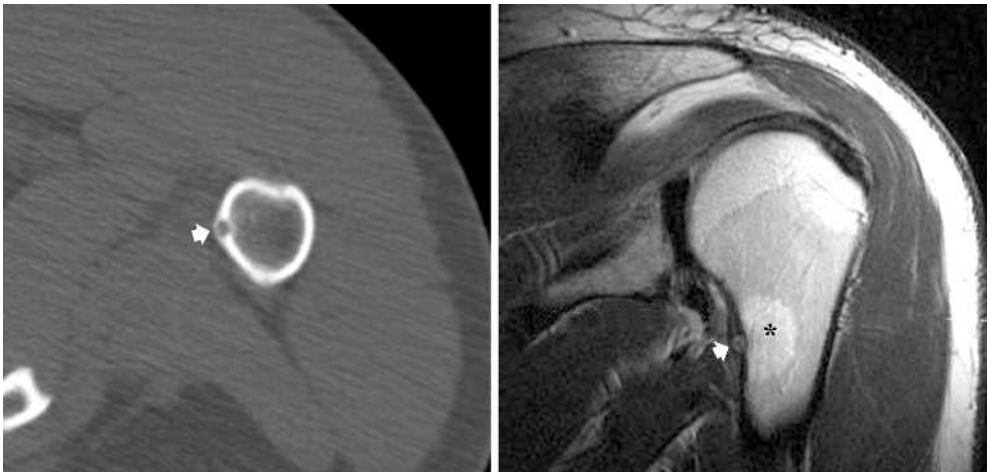

Fig. 14.16a,b. Intracortical osteoid osteoma of the humerus in a 28-year-old man. **a** Axial noncontrast CT of the proximal humerus shows the lesion (*arrow*) centered within the cortex. **b** Coronal T2-weighted SE MR image shows the lesion (*arrow*) within the cortex with associated marrow edema (*asterisk*)

Interestingly, Jaffe and Lichtenstein first used the term *nidus* to describe lesions that were radioopaque, referring to a "dense circular nidus . . . which may . . . stand out from the neighboring opaque bone [reactive sclerosis] by a narrow zone which is more permeable to the rays" (Jaffe and Lichtenstein 1940).

The tumor has a limited growth potential and is rarely larger than 1.5 cm in diameter (Klein et al. 2002). The reactive periosteal bone is usually solid but may be laminated (Edeiken et al. 1966). The circumference of the bone may be greatly increased and the bone so sclerotic that the nidus may not be demonstrated on radiographs (Jaffe 1945; Sherman 1947b; Kendrick and Evarts 1967). Osteoporosis of the surrounding bones may be present, likely from disuse (Swee et al. 1979). Intraarticular osteoid osteomas are generally the cancellous and subperiosteal types (Figs. 14.17 and 14.18) and present a far more formidable diagnostic challenge to the radiologist. Most intraarticular osteoid osteomas occur in the hip, where osteosclerosis is minimal or even absent (in sharp contrast to cortical lesions). Initial radiographs may be normal or positive findings are seen only retrospectively (Kumar SJ et al. 1984). The joint may be widened secondary to synovitis and joint effusion (Snarr et al. 1973; Corbett et al. 1974; Goldberg and Jacobs 1975; Cronemeyer et al. 1981; Schlesinger and Hernandez 1990). Regional osteoporosis may also be present, particularly about the hip (Spence and Lloyd-Roberts 1961; Wiener and Kirschenbaum 1980; Kumar SJ et al. 1984). Such changes are more likely to be identified when both hips are radiographed (Spence and Lloyd-Roberts 1961). Structural alterations of the hip, including widening and foreshortening of the femoral neck and reduction in the height of the capital femoral epiphysis (as measured from the apex of the femoral head to the superior margin of the growth plate), have been observed in patients having symptoms for at least 3 months (Kumar SJ et al. 1984). Advanced epiphyseal development may also be seen. Not all intraarticular osteoid osteomas demonstrate synovitis, as illustrated in a report by Destian et al. (1988) of a lesion of the distal femoral epiphysis with no associated joint effusion, soft-tissue mass, or osteoporosis.

The lack of extensive reactive sclerosis associated with intraarticular osteoid osteoma is due to functional differences between the intra- and extracapsular periosteum (Freiberger et al. 1959), with the former being incapable of a proliferative sclerotic response (analogous to the lack of callus formation after intraarticular fracture). The results reported by Kattapuram et al. (1983) in review of 25 intraarticular osteoid osteomas support this concept. Osteoid osteomas with the nidus located within 1 cm of the articular surface demonstrated little or no periosteal new bone formation, while lesions with the nidus more than 4 cm from the articular surface of the joint demonstrated thick periosteal new bone formation (Kattapuram et al. 1983).

Although intraarticular lesions usually do not stimulate significant periosteal new bone, in our experience they are commonly associated with reactive changes in the adjacent cancellous bone. The intensity of this re-

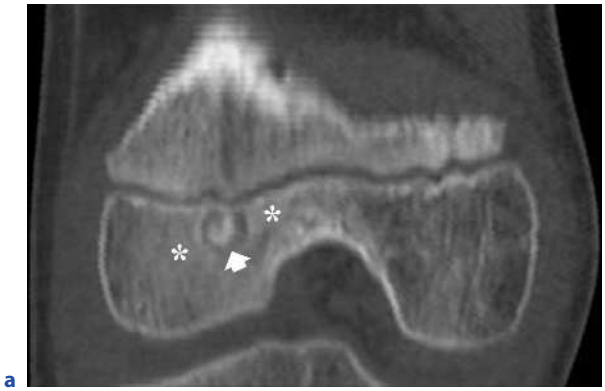

a

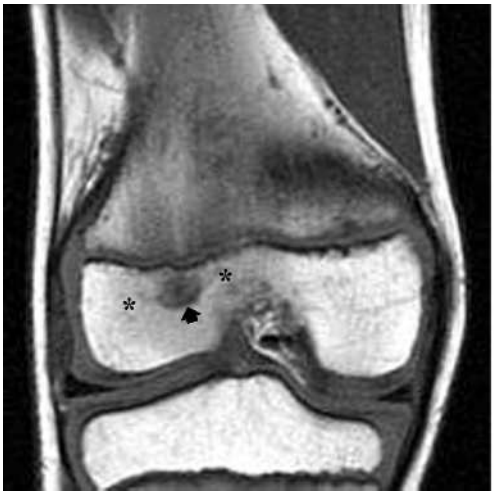

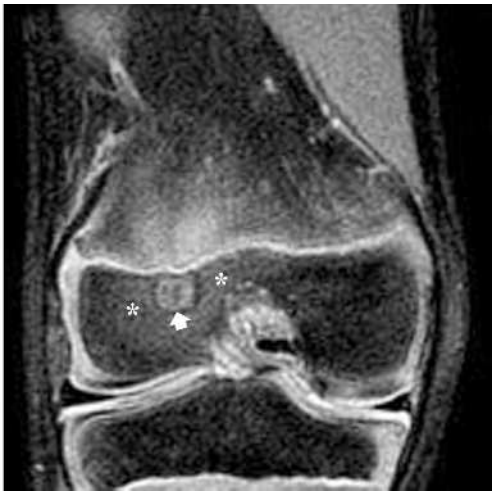

b c

Fig. 14.17a–c. Cancellous osteoid osteoma of the distal femoral epiphysis in an 8-year-old girl. **a** Reformatted coronal noncontrast CT of the distal femur shows the mineralized osteoid osteoma in the epiphysis (*arrow*) with mild associated sclerosis (*asterisks*). Corresponding coronal T1-weighted (TR/TE; 450/11) (**b**) and fat-suppressed proton density (TR/TE; 1850/30) (**c**) spin-echo MR images show the lesion (*arrows*) to have an intermediate signal intensity. There are subtle areas of decreased signal within the lesion representing the mineralized matrix. Note mild associated edema (*asterisks*). Reactive sclerosis is not appreciated on MR imaging

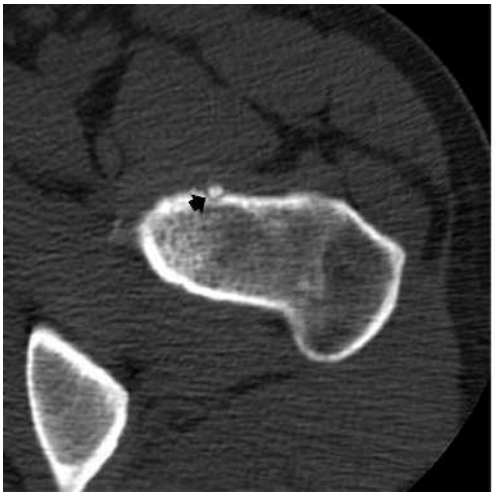

a

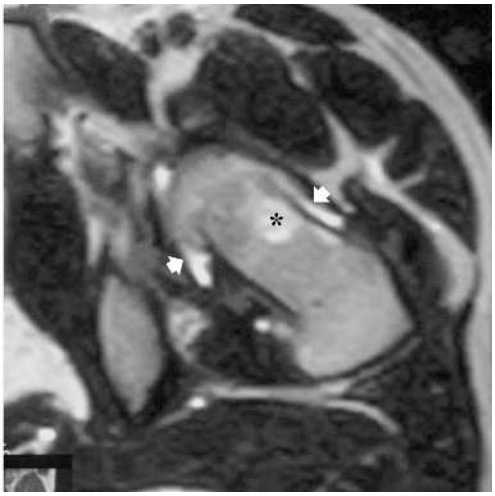

b

Fig. 14.18a,b. Subperiosteal osteoid osteoma of the femoral neck in a 35-year-old man. **a** Axial nontrast CT of the femoral neck shows a small subperiosteal lesion (*arrow*) causing extrinsic scalloping of the anterior femoral cortex. **b** Corresponding turbo-spin-echo MR image shows the associated marrow edema (*asterisks*), as well as a small joint effusion (*arrows*) related to the coincident synovitis

active change varies and tends to be mild in the hip, although it may be extensive in other joints. With intraarticular osteoid osteoma, periosteal reaction may occur outside the limits of the joint capsule and may be seen on both sides of the joint (Morton and Bartlett 1966; Schlesinger and Hernandez 1990).

The classic subperiosteal osteoid osteoma typically appears as a juxtacortical mass, extrinsically eroding cortex. Associated sclerosis is usually absent (Swee et al. 1979; Capanna et al. 1986). Osteoid osteoma may also be difficult to diagnose when it occurs in the spine. Radiographs are often normal or may demonstrate osteosclerosis, which can be subtle. Lesions typically occur in the posterior elements (facet, pedicle, or lamina), although a small number arise in the vertebral body.

Bone scintigraphy of osteoid osteoma usually reveals focal radiotracer activity on both the immediate and delayed images (Winter et al. 1977; Swee et al. 1979; Smith and Gilday 1980; Helms et al. 1984; Kumar SJ et al. 1984). Scintigraphy is particularly valuable in assessing osteoid osteoma in patients whose initial radiographs are negative or symptoms are atypical (Swee et al. 1979; Smith and Gilday 1980; Azouz et al. 1986). Subsequent CT scans obtained on the basis of the localization afforded by the scintigram will detect the lesion (Gamba et al. 1984; Azouz et al. 1986) On scintigrams, intraarticular osteoid osteoma may demonstrate diffuse distribution about the joint with a specific increase in tracer accumulation at the site of the nidus (Mitnick et al. 1979; Cronemeyer et al. 1981; Kumar SJ et al. 1984). This diffuse activity is likely secondary to associated synovitis and reactive hyperemia (Mitnick et al. 1979). A scintigraphic double density sign has been described in which there is a small area of focal radionuclide activity, corresponding to the nidus, superimposed on a second, larger area of increased tracer accumulation (Helms et al. 1984; Helms 1987). Although nonspecific, this sign may be used to suggest the diagnosis of osteoid osteoma and to locate the nidus (Helms et al. 1984).

CT is especially useful in evaluating those areas with complex anatomy (Gamba et al. 1984), such as the spine, hips, and joints. Rarely, CT results can be falsely negative (Kattapuram et al. 1983). On CT scans, the nidus of a cortical or cancellous osteoid osteoma is a well-defined round or oval lesion of decreased attenuation, with a variable amount of surrounding sclerosis, ranging from mild to extensive periosteal new bone. The periphery of the nidus is smooth at CT examination; however, on gross examination the periphery is irregular due to the coarse host lamellar bone which circumscribes and sharply demarcates the lesion (Kransdorf et al. 1991). The smooth contour seen on CT scans likely reflects volume averaging. CT may show variable amounts of mineralization within the nidus, ranging from punctate, amorphous, or ringlike to dense central mineralization. When dense central mineralization is present, it is often, although not invariably, smooth. Mineralization within the nidus is seen in approximately half of CT scans (Kransdorf et al. 1991). As a generalization, an osteoid osteoma is better seen on CT than MR imaging in almost two-thirds of cases (Assoun et al. 1994).

On conventional, nonenhanced MR imaging, osteoid osteoma demonstrates an intermediate signal intensity on T1-weighted images and intermediate to high signal on fluid-sensitive sequences (Kransdorf et al. 1991; Assoun et al. 1994; Liu et al. 2003). Osteoid within the lesion may be sufficiently mineralized to demonstrate decreased signal, while associate marrow and soft tissue edema-like signal will show an abnormal fluid-like signal (Glass et al. 1986; Yeager et al. 1987; Houang et al. 1990; Kransdorf et al. 1991; Assoun et al. 1994; Nogues et al. 1998; Ehara et al. 1999; Spouge and Thain 2000; Liu et al. 2003). Additionally, osteoid osteoma has been noted to be less conspicuous on MR than CT imaging, probably being obscured due to a combination of insufficient spatial resolution and obscuration by surrounding marrow and soft tissue edema-like signal (Liu et al. 2003). More recently, high-resolution and dynamic contrast-enhanced MR imaging have been found to correct this issue (Spouge and Thain 2000; Liu et al. 2003). Liu et al. (2003), in a study of 11 patients, showed that on dynamic MR imaging 82% of lesions showed a peak enhancement in the arterial phase with early partial washout, compared with slower, progressive enhancement of the adjacent marrow. We have found this technique useful in equivocal cases.

While sonography has not been used in the evaluation of osteoid osteoma, its utilization in the assessment of joint pain and articular disease has increased significantly in the last decade. In many cases, it may be the initial imaging study for patients presenting with an unexplained arthropathy. Ebrahim et al. (2001), in a report of three patients with intraarticular lesions, noted that osteoid osteoma should be considered when sonography reveals intraarticular cortical irregularity and adjacent focal synovitis.

14.2.3.6 Natural History

In reality, the "true" natural history of osteoid osteoma is impossible to obtain. Although the diagnosis may be

strongly suggested by radiologic findings, an absolute diagnosis may be made only after histologic examination of the lesion. Even biopsy or incomplete removal of a lesion assuredly alters its natural course. The fact that osteoid osteomas are overwhelmingly encountered in young patients suggests that the lesion may heal spontaneously (Freiberger et al. 1959). Only 12 years after Jaffe's original article, Sherman (1947b) reported what may be the earliest cases with findings suggestive of the natural course of the disease. She described two patients, one of whom presented in 1916 at the age of 18 with a history of 18 months of pain, tenderness, and swelling in the distal tibia. Radiographic findings in the patient were compatible with an osteoid osteoma and demonstrated a central nidus. The patient refused surgery, and the pain and tenderness decreased until he became asymptomatic 7 years after original presentation. At a follow-up examination in 1940, 24 years after initial presentation, persistent sclerosis and cortical thickening were seen, but the nidus was no longer discernible. Subsequently, numerous examples of spontaneous regression of osteoid osteoma have been noted (Freiberger et al. 1959; Vickers et al. 1959; Goldberg and Jacobs 1975; Sim et al. 1975; Jackson et al. 1977). However, in these cases, the diagnosis was established on the basis of clinical and radiologic findings only. Sim et al. (1975) described 54 patients for whom the diagnosis of osteoid osteoma was made on the basis of clinical and radiographic findings, but the surgical specimen failed to show a nidus. Initial surgery resulted in symptomatic relief in 31 patients, two of whom subsequently proved to have Brodie abscesses. It is tempting to speculate whether these clinically and radiographically diagnosed "osteoid osteomas" would have healed spontaneously in the absence of surgical intervention.

14.2.3.7 Treatment

Radiofrequency ablation has become the standard of care for treatment of osteoid osteoma (Rosenthal et al. 1998, 2003), with an initial treatment success rate of more than 90%, and a repeat success rate (following unsuccessful surgery or ablation) of 60% (Rosenthal et al. 2003). While a discussion of this technique is beyond the scope of this text, the success rate for this procedure is similar to that of surgery. As previously stated, the reactive bone regresses after removal of the nidus (Unni 1996a).

Complete ablation or excision of the osteoid osteoma nidus is curative and brings immediate and dramatic relief of symptoms (Freiberger et al. 1959; Kendrick and Evarts 1967; Kransdorf et al. 1991). Conversely, symptoms persist if the nidus is incompletely treated (Sim et al. 1975; Norman 1978; Swee et al. 1979; Sadry et al. 1988) and "recurrence" is typically the result of incomplete excision or ablation (Norman 1978). Patients may experience a symptom-free interval after unsuccessful treatment. Recurrence of symptoms following successful treatment may indicate the presence of a second osteoid osteoma. Although such cases are rare, lesions with as many as three distinct nidi have been reported (Glynn and Lichtenstein 1973; Greenspan et al. 1974). Multifocal lesions may occur adjacent to one another within the same bone, at distinct separate locations within the same bone, or at separate sites (Keret et al. 1989).

14.2.4 Osteoblastoma

Osteoblastoma is defined by the WHO as "… a benign bone-forming neoplasm which produces woven bone spicules, which are bordered by prominent osteoblasts" (Malcolm et al. 2002).

The lesion now recognized as osteoblastoma was first introduced into the literature by Jaffe and Mayer (1932) in a report of "an osteoblastic osteoid-tissue-forming tumor of the metacarpal bone." Established as a distinct entity in 1956 by Jaffe and Lichtenstein in separate articles (Jaffe 1956; Lichtenstein 1956), Jaffe chose the term *benign osteoblastoma* to emphasize its benign nature and histologically conspicuous proliferating osteoblasts (Jaffe 1956).

14.2.4.1 Pathology

Osteoblastoma is a relatively rare lesion that is typically larger than 1.5–2.0 cm in diameter. Macroscopically, the lesion has an extremely rich vascular supply and is usually red to red-brown in color, with a gritty cut surface due to the woven bone produced (Malcolm et al. 2002). It is the rich vascularity which is likely to be responsible for the aneurysmal bone cyst component identified in 10–15% of cases (Schajowicz and Lemos 1970).

Histologic examination reveals a lesion composed of pure osteoid and woven bone (Mirra 1989a). These features are very similar to those of osteoid osteoma (interconnecting trabecular bone and fibrovascular stroma), but overall, the microscopic pattern is not as well organized as that seen in osteoid osteoma (Schajowicz and Lemos 1970). The osseous spicules

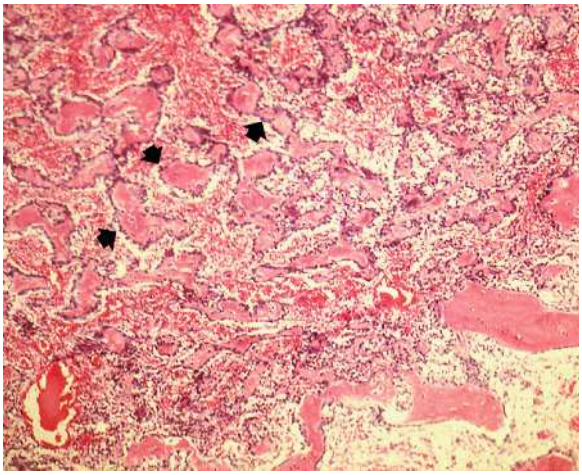

Fig. 14.19. Osteoblastoma histology. Scanning power photomicrograph (hematoxylin-eosin stain) shows numerous thick, irregularly shaped woven bone trabeculae, many with prominent osteoblastic rimming (*arrows*)

are haphazardly arranged and are lined by a single layer of osteoblasts, a phenomenon termed "osteoblastic rimming" (Fig. 14.19) (Malcolm et al. 2002). Despite differences, the histopathology of osteoblastoma may overlap that of osteoid osteoma (McLeod et al. 1976). Mayer described a subgroup of osteoblastomas, which appeared to be similar to osteosarcoma and contained prominent epithelioid osteoblasts, and referred to these lesions as aggressive osteoblastomas (see below discussion) (Mayer 1967).

14.2.4.2 Classification

The WHO does not subclassify osteoblastoma; although, they do recognize the term *epithelioid osteoblastoma* for those lesions in which there are large, plump osteoblasts with prominent nucleus and nucleoli (Malcolm et al. 2002). The terms *aggressive osteoblastoma* (Dorfman and Weiss 1984) or *malignant osteoblastoma* (Schajowicz and Lemos 1970) have also been applied to these lesions with epithelioid osteoblasts, in order to emphasize the diagnostic difficulties in distinguishing these lesions from osteosarcoma. The term *conventional osteoblastoma* is sometimes used to distinguish osteoblastoma from the more aggressive epithelioid variant.

The term *toxic osteoblastoma* comes from a 1979 report by Mirra et al. (Mirra et al. 1979) and is used to describe a rare subset of patients in which osteoblastoma is associated with severe systemic symptoms. The systemic symptoms are thought to be due to an exaggerated immunological response to the tumor and include fever, anorexia, weight loss and cachexia (Dale et al. 2001; Theologis et al. 2007).

14.2.4.3 Clinical Presentation

Patients with osteoblastoma are usually adolescents or young adults, with 70–80% of cases diagnosed in the first three decades of life; however, cases have been reported in patients aged less than 1 year to 72 years (Mirra 1989a; Kroon and Schurmans 1990; Lucas et al. 1994; Berry et al. 2008). There is a male predominance of 2:1 (Murphey et al. 1996; Berry et al. 2008).

Pain is the most common presenting symptom, being present in 80–90% of patients (McLeod et al. 1976; Murphey et al. 1996; Berry et al. 2008). The pain of osteoblastoma is less likely to respond to NSAIDS (approximately 7%) (McLeod et al. 1976) and, in contradistinction to osteoid osteoma, is usually not more severe at night (Berry et al. 2008).

Clinical symptoms often differ from those of osteoid osteoma, with osteoblastoma producing dull localized pain, as opposed to the intense night pain caused by osteoid osteoma. Unlike osteoid osteoma, osteoblastoma is commonly manifested by neurologic symptoms, including paresthesias, paraparesis, and paraplegia. Kroon and Schurmans (1990) reported neurogenic defects in 12 (38%) of 38 spinal lesions, Scoliosis occurs in less than half of patients and is seen less frequently with osteoblastoma than with osteoid osteoma (Kroon and Schurmans 1990; Murphey et al. 1996). Scoliosis may also be seen with osteoblastoma of the rib (Kroon and Schurmans 1990).

14.2.4.4 Skeletal Distribution

Osteoblastoma of the spine accounts for about one-third (range 32–46%) of all osteoblastomas (Kroon and Schurmans 1990; Lucas et al. 1994; Murphey et al. 1996; Berry et al. 2008). Lesions have been reported to be equally distributed in the cervical, thoracic, and lumbar segments, although Berry et al. noted a predilection for the lumbar region (Kroon and Schurmans 1990; Berry et al. 2008). Lesions most frequently involve the posterior vertebral elements, although extension into the vertebral body is also common (McLeod et al. 1976; Kroon and Schurmans 1990). Osteoblastoma confined to only the vertebral body is relatively rare

(3–6%) (Kroon and Schurmans 1990; Lucas et al. 1994; Murphey et al. 1996).

Osteoblastoma of long bones accounts for about 26–56% of cases, typically involving the femur, humerus or tibia (Kroon and Schurmans 1990; Unni 1996a; Berry et al. 2008). When in the long bones, lesions are typically proximal (about 75%), and usually in the diaphysis (36–76%) or metaphysis (24–42%) (McLeod et al. 1976; Kroon and Schurmans 1990; Lucas et al. 1994; Berry et al. 2008). Long bone lesions are usually medullary or cortical; juxtacortical lesions are relatively infrequent. The hands and feet account for approximately 8–26% of cases; about 15% of cases arise in the skull, maxilla and mandible (Unni 1996a).

14.2.4.5 Imaging

Three radiographic patterns have been described with osteoblastoma (McLeod et al. 1976; Kroon and Schurmans 1990; Greenspan 1993; Lucas et al. 1994; Murphey et al. 1996). The first consists of a central radiolucent area (with or without calcification) and surrounding osseous sclerosis and is similar to the radiographic appearance of osteoid osteoma, but the lesion is larger than 1.5 cm in diameter. The second, an expansile lesion with multiple small calcifications and a peripheral sclerotic rim, is the most common appearance of spinal osteoblastoma (Kumar R et al. 1988). The third pattern has a more aggressive appearance, consisting of osseous expansion, bone destruction, infiltration of surrounding soft tissue, and intermixed matrix calcification. Mineralization within an osteoblastoma may have the radiologic appearance simulating chondroid matrix (rings and arcs), and suggesting a cartilage tumor (Murphey et al. 1996). An aneurysmal bone cyst component may be seen in 10–15% of cases (Schajowicz and Lemos 1970).

In the spine, osteoblastoma is usually a geographic lytic lesion within the posterior elements or within the posterior elements extending into the vertebral body. A well-defined margin with surrounding sclerosis of variable thickness is usually identified (59–91%), as is variable expansile remodeling (64–94%) and mineralized matrix (55–72%) (Figs. 14.20 and 14.21) (McLeod et al. 1976; Kroon and Schurmans 1990; Lucas et al. 1994; Murphey et al. 1996).

The appearance of long bone lesions is more variable. The majority of lesions are spherical or oval in shape with a well-defined margin (McLeod et al. 1976; Kroon and Schurmans 1990). Surrounding sclerosis

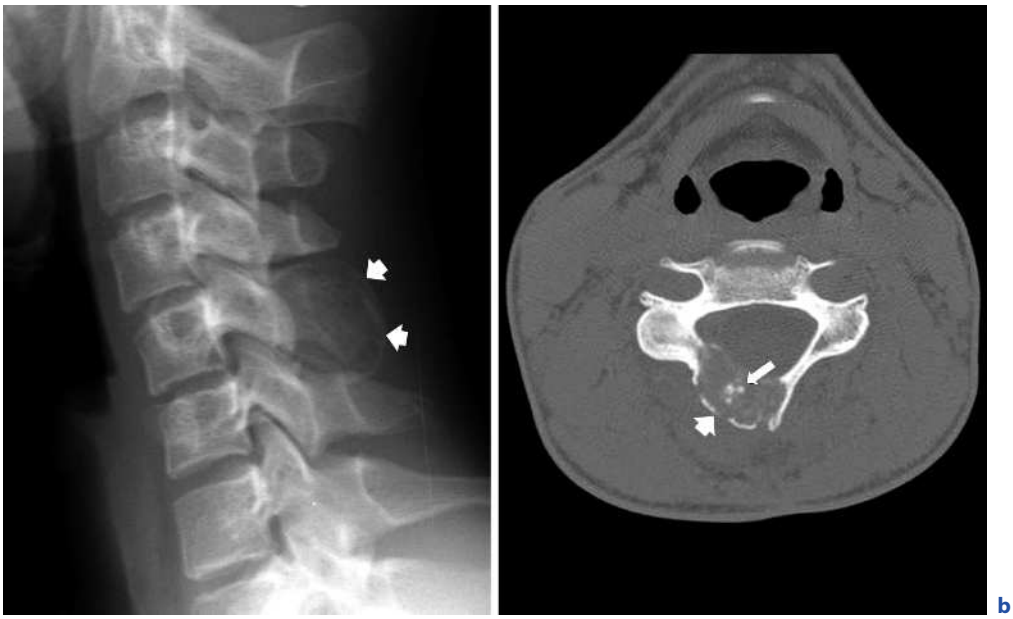

a b

Fig. 14.20a–f. Osteoblastoma of the cervical spine in a 13-year-old boy. **a** Lateral radiograph of the cervical spine shows a lytic lesion in the posterior elements of the C5 vertebra (*arrows*) with moderate expansile remodeling. Axial (**b**) and reformatted sagittal (**c**) noncontrast CT images of the cervical spine show the degree of expansile remodeling (*short arrows*) to better advantage, as well as the internal mineralized matrix (*long arrows*). **c–f** *see next page*

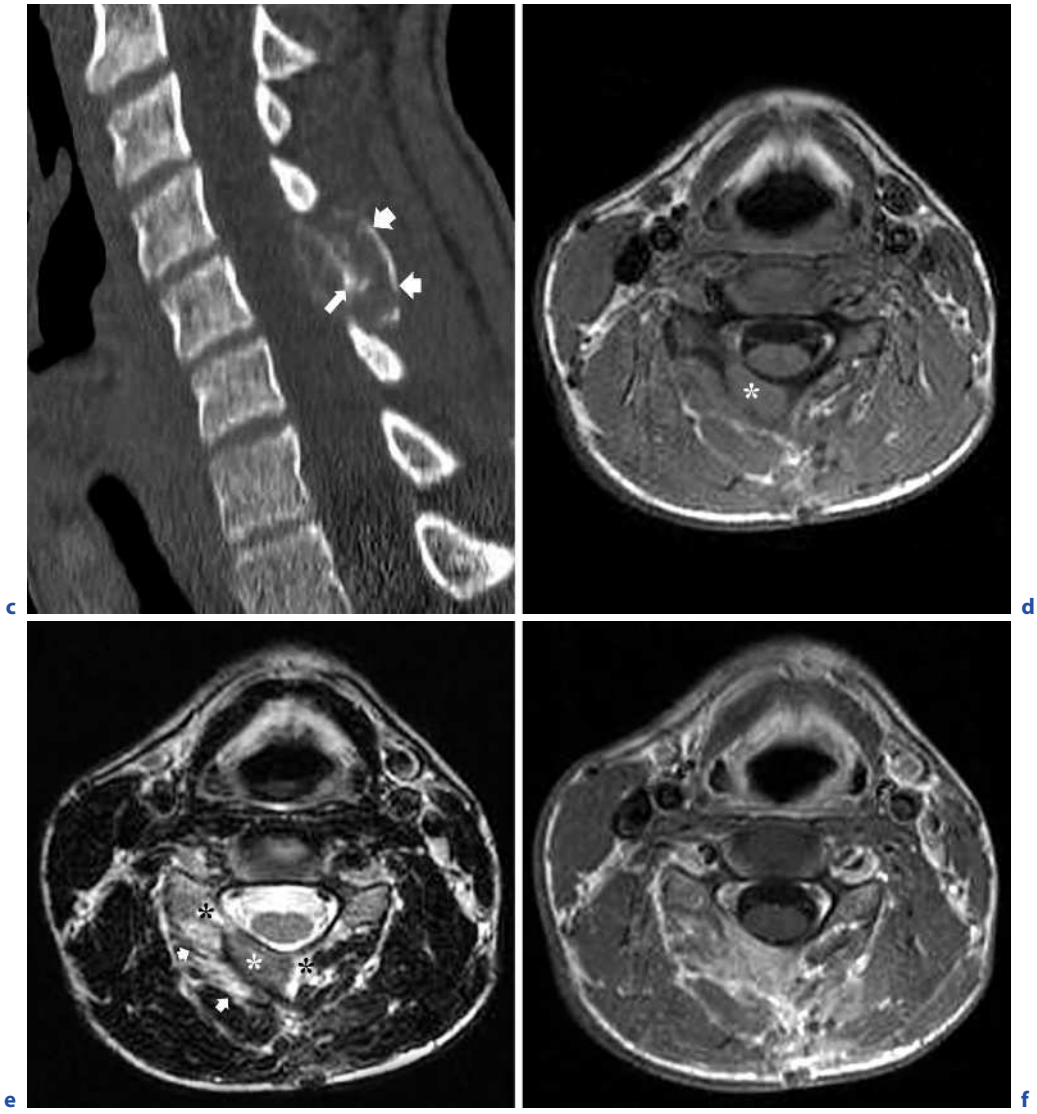

Fig. 14.20a–f. (*continued*) Osteoblastoma of the cervical spine in a 13-year-old boy. Axial T1-weighted (TR/TE; 416/9) (**d**) and turbo-T2-weighted (TR/TE; 4950/112) (**e**) spin-echo MR images show the lesion (*white asterisks*) with an intermediate signal intensity, but do not identify the internal matrix. Note associated inflammatory changes in the adjacent bone (*black asterisks*) and soft tissue (*arrows*). **f** Corresponding enhanced axial T1-weighted (TR/TE; 416/9) spin-echo MR image shows prominent enhancement of the lesion and adjacent inflammation

is common and is seen in about half of cases (McLeod et al. 1976; Lucas et al. 1994). The lesion is frequently lucent (35–64%), with varying degrees of mineralization seen in the remaining cases (McLeod et al. 1976; Kroon and Schurmans 1990; Lucas et al. 1994). Limited cases with serial imaging suggests mineralization is time dependent (McLeod et al. 1976; Lucas et al. 1994). Expansile remodeling of bone is also common and seen in the majority of cases. An associated periosteal reaction is often present (36–58%); typically demonstrating a solid, continuous new bone formation (Figs. 14.22 and 14.23) (McLeod et al. 1976; Lucas et al. 1994). Occasionally, a more aggressive lamellated or spiculated periosteal reaction may be seen suggesting a malignancy (McLeod et al. 1976). Unfortunately, the diagnosis of osteoblastoma in the appendicular skeleton is difficult. In a review by McLeod et al. (McLeod et al. 1976), the correct diagnosis of osteoblastoma was suggested in two-thirds of patients presenting with spinal lesions, while it was suggested in only 29% of those pre-

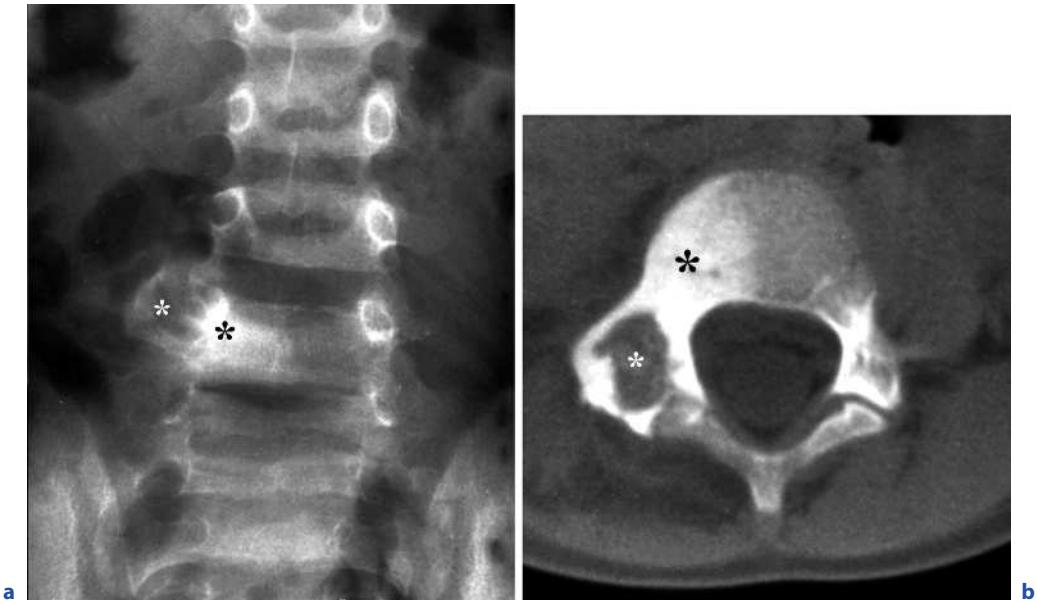

Fig. 14.21a,b. Osteoblastoma of the lumbar spine. **a** Anteroposterior radiograph of the lumbar spine shows a lesion in the posterior elements of L4 (*white asterisk*) with prominent sclerosis (*black asterisk*). **b** Axial noncontrast CT scan shows the lesion (*white asterisk*) with subtle mineralized matrix, moderate expansile remodeling and prominent sclerosis (*black asterisk*)

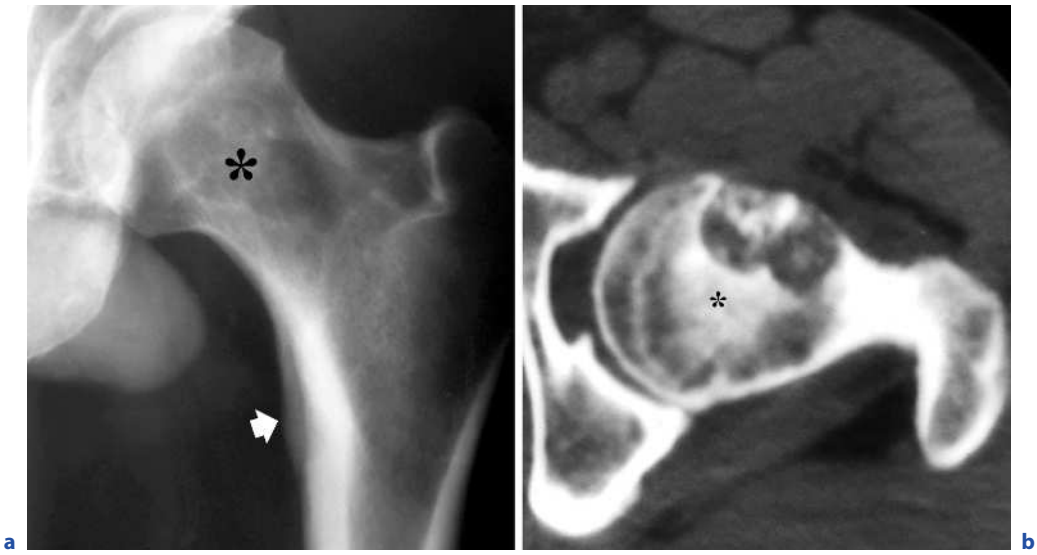

Fig. 14.22a,b. Osteoblastoma of the femur. **a** Anteroposterior radiograph of the proximal femur shows a geographic lytic lesion (*asterisk*) with solid continuous periosteal new bone (*arrow*) distant from the lesion. **b** Axial noncontrast CT scan shows the lesion with prominent mineralized matrix and associated sclerosis (*black asterisk*)

senting with appendicular lesions. Findings similar to those in long bones may be seen in the hands, feet and ilium (Resnick et al. 2002c).

At bone scintigraphy, osteoblastoma typically demonstrates marked radionuclide uptake, presumably secondary to hypervascularity and new bone formation (Martin et al. 1976; Kroon and Schurmans 1990). At CT, the lesion shows areas of mineralization, expansile bone remodeling, and sclerosis or a thin osseous shell about its margins. Shaikh et al. (1999) suggested

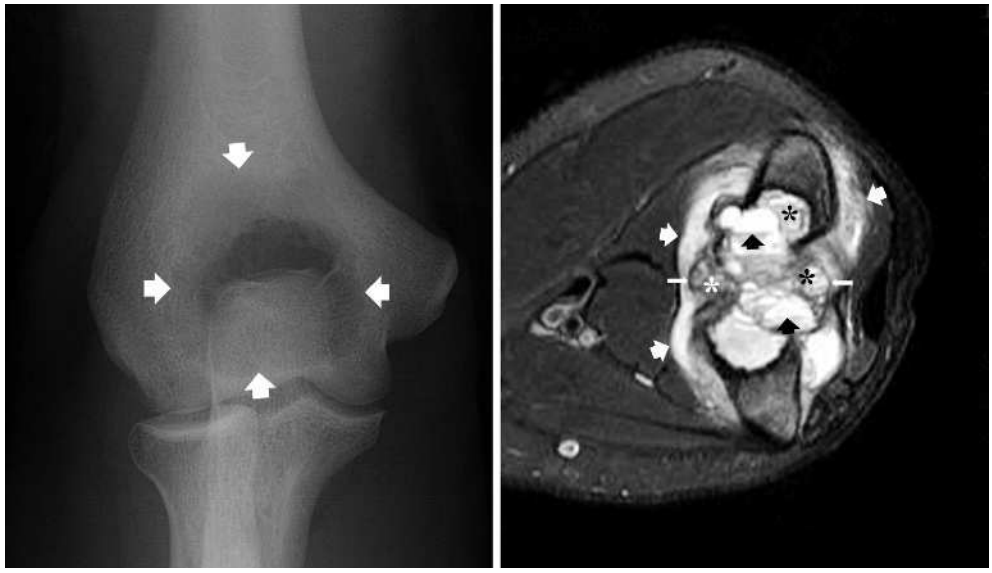

a b

Fig. 14.23a,b. Osteoblastoma of the humerus. **a** Anteroposterior radiograph of the elbow shows a geographic lytic lesion in the distal humerus (*arrows*) with ill-defined margins. **b** Axial fat-suppressed proton (TR/TE; 4000/48) FSE MR image of the distal humerus shows a lesion with intermediate signal intensity (*asterisks*), with expansile remodeling (*long white arrows*), secondary aneurismal bone cyst change (*black arrows*) and associate edema-like (*short white arrows*)

that CT is the modality of choice for the evaluation of suspected spinal osteoblastomas, with MR imaging showing no characteristic features and overestimating the extent of the lesion due to the associated reactive changes.

The MR imaging appearance of osteoblastoma is generally nonspecific, with low to intermediate signal intensity seen on T1-weighted images and variable (low to high) signal intensity seen on T2-weighted images (Murphey et al. 1996; Shaikh et al. 1999). MR imaging optimally depicts the effects of the tumor on adjacent structures and surrounding soft tissues and we have found the extensive peritumoral edema-like signal (Crim et al. 1990) can be helpful in suggesting the diagnosis in equivocal cases.

Imaging studies of aggressive osteoblastoma, in our experience, reveal large, infiltrative, soft tissue components that reflect its pathologic appearance and clinical behavior. Clinical, imaging, and pathologic characteristics usually allow differentiation of osteoblastoma from osteoid osteoma in the spine. The radiologic features favoring osteoblastoma include lesion diameters larger than 1.5–2.0 cm, osseous expansile remodeling, soft-tissue component, and multifocal (as opposed to central) matrix mineralization. The clinical course of osteoblastoma is slow growth, compared with the stable lesion size usually encountered in cases of osteoid osteoma.

14.2.4.6 Treatment

Treatment of spinal osteoblastoma is surgical resection, and the recurrence rate for conventional lesions is 10–24% (McLeod et al. 1976; Kroon and Schurmans 1990; Lucas et al. 1994; Berry et al. 2008). Typically, this entails curettage with allograft or autograft augmentation; tumors that are locally aggressive, exceptionally large, invasive or involve expendable bones are likely best treated with en block resection (Malcolm et al. 2002; Berry et al. 2008). The diagnosis of aggressive osteoblastomas is important because they have a far greater recurrence rate (approaching 50%), which is probably related to their larger size and the resultant inability to perform complete resection (Lucas et al. 1994).

14.3 Osteosarcoma

Prior to the establishment of the Registry of Bone Sarcoma by The American College of Surgeons in 1925, there was no standardized nomenclature or organized systematic method for the classification of bone tumors (McCarthy 1995). Using material submitted to the

Sarcoma Registry, Earnest A. Codman, a Boston Surgeon and the organization's Registrar, divided primary bone tumors into six groups. One of these groups was malignant osteogenic tumors (McCarthy 1995); defining members of this group as sarcomas derived from tissue presumably intended to form bone, irrespective of whether or not it eventually does so (Jaffe 1958). The following year, in an attempt to establish an acceptable standard nomenclature and criteria for malignancy, Codman published 25 historical, clinical, radiographic and microscopic criteria for the diagnosis of osteosarcoma (Codman 1926). Codman's initial description predates the recognition of chondrosarcoma and fibrosarcoma as distinct diagnoses in 1939 (Codman 1926), and may explain the current broad definition of this lesion. Today, the WHO defines the conventional osteosarcoma as a high grade malignant tumor in which the cells produce osteoid, even if only in small amounts (Raymond et al. 2002).

Osteosarcoma is the most common primary osseous malignancy (excluding multiple myeloma) and the most common nonhematologic malignancy of bone in children and adults, accounting for approximately 35% of cases, followed by chondrosarcoma (26%) and Ewing sarcoma (16%) (Dorfman and Czerniak 1995; Tang et al. 2008). While most osteosarcomas are high grade tumors with a tendency for pulmonary metastases, there is a spectrum of clinical and radiographic features in the numerous subtypes that have been described (Unni et al. 2005), often with distinctive radiologic appearances. In this section we describe the imaging spectrum of this malignant tumor, emphasizing the specific subtypes and their diagnostic imaging appearances.

14.3.1 Classification

In 2002, the WHO Committee for the Classification of Bone Tumors divided malignant osteogenic tumors into eight distinct diagnoses: (1) conventional osteosarcoma; (2) telangiectatic osteosarcoma; (3) small cell osteosarcoma; (4) low grade central osteosarcoma; (5) secondary osteosarcoma; (6) parosteal osteosarcoma; (7) periosteal osteosarcoma; and (8) high grade surface osteosarcoma (Ayala et al. 2002; Dorfman et al. 2002; Forest et al. 2002; Inwards and Knuutila 2002; Kalil and Bridge 2002; Matsuno et al. 2002; Raymond et al. 2002; Unni and Knuutila 2002; Wold et al. 2002).

Although the new WHO Classification system provides an excellent basis for diagnosis, we find greater clinical utility for radiologic diagnosis in a modification of this classification, in which malignant osseous lesions are grouped into three major categories which are subsequently further divided. This categorization includes:

1. *Intramedullary osteosarcoma:* Lesions in this group arise within the medullary cavity and represent the typical high grade intramedullary osteosarcoma. They are usually pleomorphic and produce varying amounts of cartilage and/or fibrous tissue, and rarely, other histological components. While these lesions can be, and sometimes are, further subdivided by their predominant matrix (see below), the WHO uses the umbrella term *conventional osteosarcoma* for these various forms, since they have a similar biological behavior (Raymond et al. 2002). Additional members of this group are telangiectatic, small cell, gnathic and low grade central osteosarcoma.
2. *Juxtacortical osteosarcoma:* Lesions in this group are located on or in the cortex and include parosteal, periosteal and high grade surface osteosarcoma, as well as intracortical osteosarcoma.
3. *Secondary osteosarcoma:* Included in this group are lesions derived from benign precursors, such as osteosarcoma associated with Paget disease, radiation therapy and other benign lesions. Metastatic osteosarcoma is also included in this group, as is osteosarcomatosis, which is now generally accepted to represent the multicentric metastases (Parham et al. 1985; Hopper et al. 1990).

The above organization recognizes the radiological and/or clinical similarities among the members of each group, and helps in the formulation of a differential diagnosis. These major groups are discussed in greater detail below, emphasizing the typical features of lesions as encountered in the musculoskeletal system.

14.3.2 Pathology

Osteosarcoma is pathologically classified as a malignant mesenchymal neoplasm in which the tumor cells directly produce osteoid, or immature bone (Fig. 14.24). Lesions are typically pleomorphic and often contain other elements, particularly fibrous or chondroid components; however, by convention, even if only a minority of the intraosseous tumor is producing osteoid, it is designated as an osteosarcoma (Mirra 1989a). Macroscopically, osteosarcoma is usually a large (5–10 cm) intraosseous tumor with frequent soft-tissue extension.

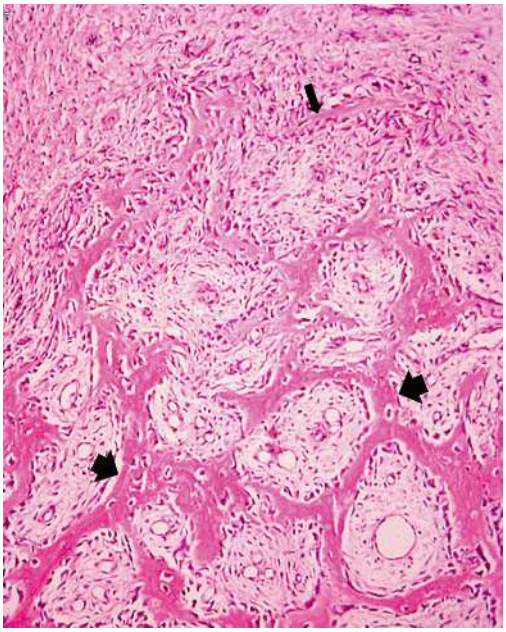

Fig. 14.24. Osteosarcoma histology. High power photomicrograph (hematoxylin-eosin stain) shows osteoid production by malignant tumors cells. Note woven bone trabeculae (*short arrows*) as well as more immature osteoid (*long arrow*)

Mineralized regions of osteoid and cartilage, as well as hemorrhagic foci, are frequent (Fig. 14.25).

Histologically, osteosarcoma has classically been divided into osteoblastic, chondroblastic, and fibroblastic varieties, depending on the dominant cell type present. Although most lesions have a mixed (pleomorphic) histologic appearance, subtyping is generally used when there is a dominant histologic pattern of differentiation. For example, the term chondroblastic osteosarcoma is used for those lesions in which more than 90% of the tumor is cartilaginous (Mirra 1989a), while the designation of telangiectatic osteosarcoma is reserved for those high grade osteosarcomas with more than 90% of the lesion characterized by large, blood-filled spaces (Matsuno et al. 2002; Murphey et al. 2003). In general, the dominant pattern is osteoblastic in 50–80% of osteosarcomas, fibroblastic-fibrohistocytic in 7–25%, chondroblastic in 5–25%, telangiectatic in 2.5–12%, and small cell in 1% (Dahlin and Coventry 1967; Mirra 1989a; Resnick et al. 2002c; Unni et al. 2005). As with other malignant neoplasms, osteosarcoma is graded from I to IV according to the degree of anaplasia, although the prognostic significance of this parameter is controversial.

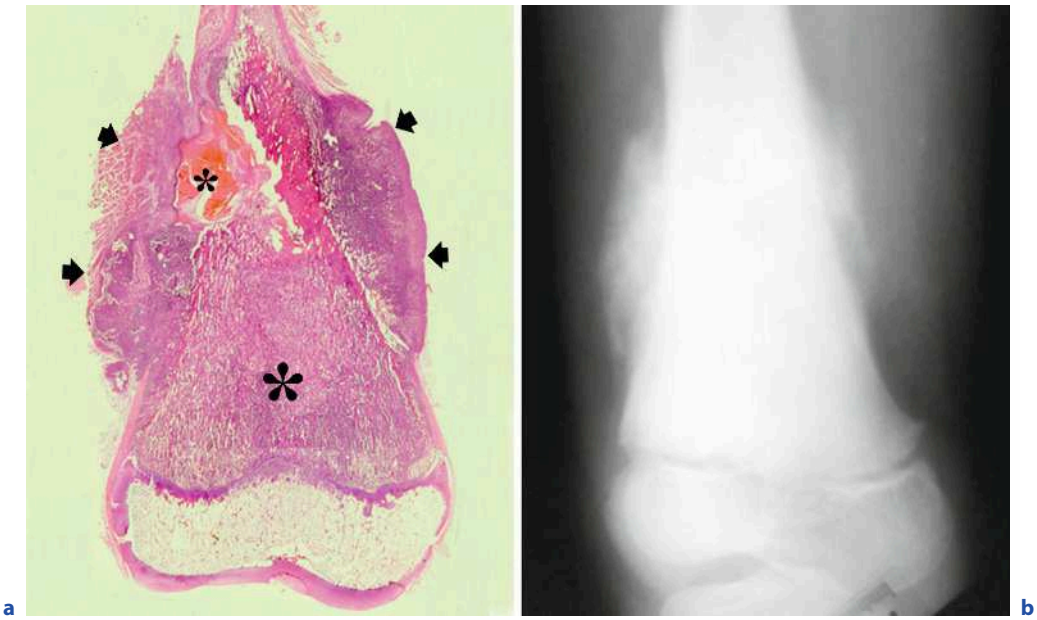

a **b**

Fig. 14.25a,b. Macroscopic appearance osteosarcoma distal femur. **a** Macro section shows a large intamudullary tumor with prominent osteoid production (*large asterisk*), soft tissue extension (*arrows*) and hemorrhagic focus (*small asterisk*). **b** Corresponding radiograph shows a large tumor in the distal femur with extensive matrix production, extending into the soft tissues

14.4 Intramedullary Osteosarcoma

As noted above, lesions in this group arise within the medullary cavity and represent the typical high grade intramedullary osteosarcoma, termed *conventional osteosarcoma* by the WHO, and are most frequently either osteoblastic or pleomorphic, with most cases demonstrating features of both (Unni et al. 2005). Other unusual histological subtypes of conventional osteosarcoma include MFH-like osteosarcoma, osteoblastoma-like osteosarcoma, and giant cell rich osteosarcoma (Raymond et al. 2002). Additional lesions in this group, which are described separately below, include telangiectatic, small cell, gnathic, and low grade central osteosarcoma. These latter forms of osteosarcoma are distinguished from conventional osteosarcoma by the WHO because of different, or unusual, biological, imaging, and histological features (Unni et al. 2005).

14.4.1 Conventional Osteosarcoma

The conventional osteosarcoma is a high grade intramedullary form of osteosarcoma that originates centrally and often involves the entire width of the bone. These lesions account for approximately 75% of all osteosarcomas and, as noted above, have been categorized into numerous subtypes on the basis of their histologic appearance. They are most common in patients in the second and third decades of life, with 75% of cases encountered in patients 15–25 years of age (Dahlin and Coventry 1967; Mirra 1989a; Resnick et al. 2002c). Primary osteosarcoma occurring in patients younger than 6 years of age or older than 60 years of age is unusual. Osteosarcoma typically affects whites and males, with a male-to-female ratio of 1.5–2:1 (Dahlin and Coventry 1967; Mirra 1989a; Resnick et al. 2002c). In fact, the incidence of osteosarcoma in black females is nearly five times less than that for white males (Murphey et al. 1997). There have been isolated reports of a familial form of osteosarcoma, but the vast majority of cases occur as sporadic tumors (Miller and McLaughlin 1977). As with all types of osteosarcoma, the clinical manifestations are usually nonspecific, with pain and swelling being the most frequent symptoms. Patients commonly have a history of trauma, which brings the lesion to clinical attention. Pathologic fracture is seen in approximately 15–20% of cases, either at presentation or occurring during therapy (Dahlin and Coventry 1967; Mirra 1989a; Resnick et al. 2002c).

Conventional osteosarcoma most frequently affects long bones (70–80% of cases), particularly about the knee (50–55%) (Fig. 14.25) (Dahlin and Coventry 1967; Mirra 1989a; Resnick et al. 2002c). Specifically, the femur is involved in 40–45% of cases, the tibia in 16–20%, and the humerus in 10–15% (Dahlin and Coventry 1967; Mirra 1989a; Murphey et al. 1997; Resnick et al. 2002c). Involvement of the pelvis, fibula, facial bones, and spine is unusual. The skull, clavicle, ribs, scapula, forearm, and small bones of the feet and hands are rarely affected. The majority (90–95%) of conventional osteosarcomas arise in the metaphysis (Dahlin and Coventry 1967; Mirra 1989a; Murphey et al. 1997; Resnick et al. 2002c). Primary involvement of the diaphysis is seen in 2–11% of cases, and these patients may have a longer duration of symptoms prior to diagnosis (Swaney 1973; Sim et al. 1995). Although osteosarcoma with metaphyseal involvement often extends into the epiphysis (75–88% of cases with open physis), initial manifestation within the epiphysis is very rare (< 1%) (Norton et al. 1991; Panuel et al. 1993).

Metastases most commonly affect the lungs, bones, and regional and distant lymph nodes. Ossification of pulmonary and lymph node metastases may be apparent on radiographs, CT scans, MR images, and bone scans. Pulmonary metastases may be associated with spontaneous pneumothorax and, when few in number, are often treated aggressively with local resection. Skip metastases, defined as "discontinuous tumors in the primary bone site," represent foci of tumor occurring in the same bone anatomically as the primary lesion, but which show no continuity with the primary lesion, being separated by normal marrow (Greene et al. 2002). These "skip" lesions have been reported to occur in 1–25% of high-grade intramedullary osteosarcomas (Enneking and Kagan 1975; Kager et al. 2006); although a recent study of 1765 patients by the Cooperative Osteosarcoma Study Group identified only 24 (1.4%) such patients (Kager et al. 2006). This frequency is in keeping with our experience. The identification of skip metastases is important not only for defining the extent of disease, but also for directing treatment. Patients with skip metastases have traditionally been thought to have an extremely poor prognosis (Malawer and Dunham 1983); however, a recent report has identified prolonged survival in this group following aggressive multimodality therapy (Kager et al. 2006). Skip metastases are best identified with MR imaging, and a study of the entire length of an affected bone should be performed at the time of primary evaluation.

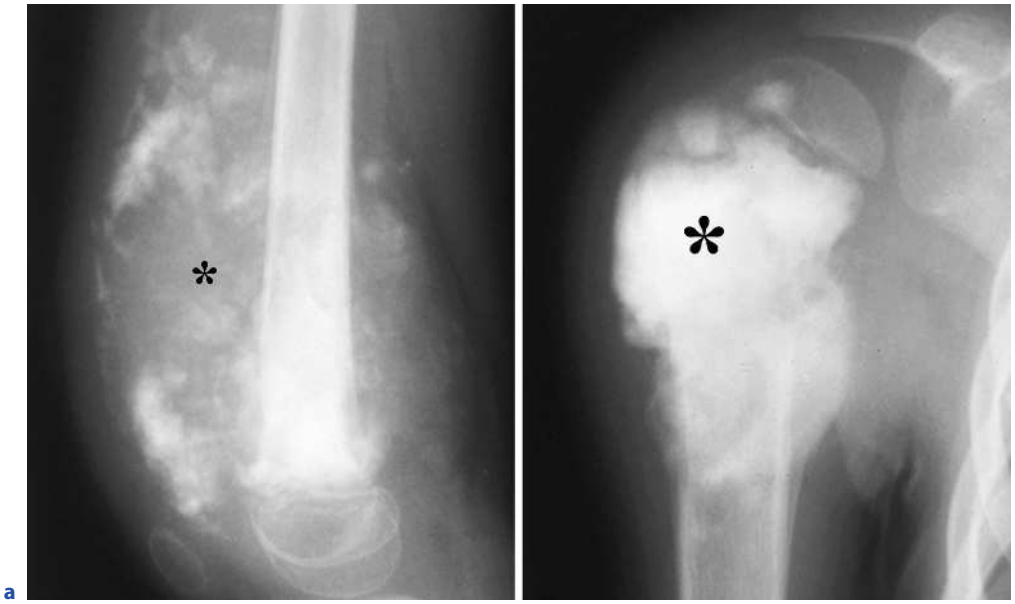

Fig. 14.26a,b. Radiographic appearance of osteoid matrix in osteosarcoma. **a** Lateral radiograph of the distal femur shows predominantly fluffy osteoid matrix (*asterisk*) in bone and within the large soft tissue component. **b** Anterioposterior radiograph shows a predominantly cloudlike (cumulous) opacity (*asterisk*) in the proximal humerus and adjacent soft tissue

14.4.1.1 Radiography

As in all cases of a bone lesion, the primary evaluation of an osteosarcoma begins with radiographic assessment. Conventional osteosarcomas are aggressive lesions with rapid doubling times (20–30 days) and therefore are often large (typically >6 cm) at the time of diagnosis (Fig. 14.26). At radiographic examination, the vast majority (approximately 90%) of osteosarcomas demonstrate a variable amount of fluffy, cloudlike (cumulous) opacities within the lesion, characteristic of osteoid matrix production (Fig. 14.26) (Dahlin and Coventry 1967; Mirra 1989a; Murphey et al. 1997; Resnick et al. 2002c). Occasionally, the lesion may be completely blastic (osteoblastic subtype) or lytic (fibroblastic subtype), but a mixed pattern of sclerosis and lucent areas is most frequent. Conventional osteosarcoma tends to violate the cortex without expanding the osseous contours, a characteristic that reflects its aggressive pathologic behavior. This growth pattern is associated with an aggressive periosteal reaction (Codman triangle, laminated, hair-on-end, or sunburst patterns) and soft-tissue mass in 80–90% of cases (Fig. 14.27) (Dahlin and Coventry 1967; Mirra 1989a; Murphey et al. 1997; Resnick et al. 2002c).

Most osteosarcomas have a radiographic appearance that poses little diagnostic dilemma. Additional imaging techniques such as CT, MR imaging, and bone scintigraphy are typically not needed to diagnose an osteosarcoma. However, an unusual radiographic appearance can lead to delay in diagnosis and confusion with benign disease (Rosenberg et al. 1995). This situation is particularly likely when the osteosarcoma involves anatomically complex areas such as the pelvis and in the case of small lesions (often < 5 cm and adjacent to the endosteum). In these cases, cross-sectional imaging may not only help confirm the presence of the lesion, but also help identify mineralized matrix that is not appreciable at radiography. More important, these imaging modalities are vital in the preoperative assessment and staging of osteosarcoma (Redmond et al. 1989; Seeger et al. 1989; O'Flanagan et al. 1991; Schima et al. 1994).

14.4.1.2 Scintigraphy

At bone scintigraphy, marked uptake of radiotracer is seen on blood flow, blood pool, and delayed images. Extended uptake patterns, presumably due to hyperemia,

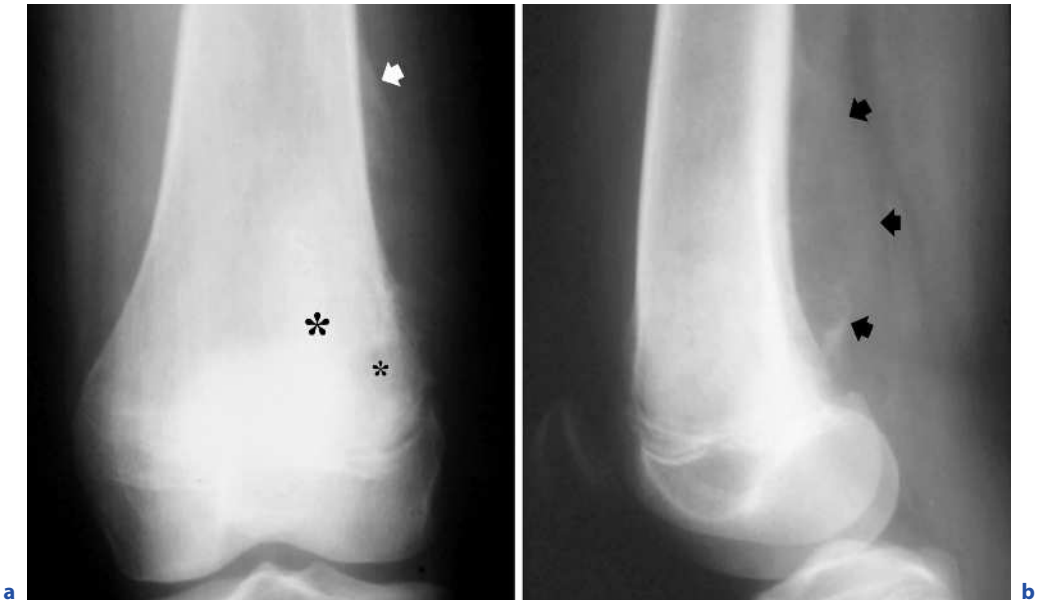

Fig. 14.27a,b. Osteosarcoma of the distal femur with periosteal reaction and soft tissue mass. **a** Anteroposterior radiograph of the distal femur shows a small triangle of interrupted periosteal reaction (*arrow*) at the superior margin or the tumor (Codman triangle). Note that the lesion shows areas of sclerosis (*large asterisk*) and lysis (*small asterisk*). **b** Lateral radiograph shows the associated soft tissue mass (*arrows*) to better advantage

have been reported (Chew and Hudson 1982; Murphey et al. 1997). Presently, however, the chief role of scintigraphy is to evaluate for distant metastases. Both osseous and extraosseous metastatic disease may be detected (Fig. 14.28).

14.4.1.3 CT Scanning

The primary advantage of CT scanning is its ability to demonstrate small areas of mineralized matrix that might not be detected with radiographs, particularly in areas in which the osseous anatomy is complex, such as in the pelvis or spine (Fig. 14.29). CT scanning is also excellent in identifying mineralized matrix that may not be apparent on MR imaging in predominantly lytic lesions. The aggressive characteristics of conventional osteosarcoma, both intraosseous and soft-tissue components, are also well seen at CT (Destouet et al. 1979; Schreiman et al. 1986; Seeger et al. 1989; Rosenberg et al. 1995). Nonmineralized portions of tumor usually demonstrate a soft-tissue attenuation and replace the normal low attenuation of fatty marrow. Chondroblastic components may be of low attenuation on CT scans, reflecting a higher water content. Areas of central hemorrhage or necrosis, which also have low attenuation, are frequent. Osteoid matrix production is easily appreciated in both intraosseous and soft-tissue tumor components as areas of very high attenuation.

14.4.1.4 MR Imaging

MR imaging has become the cross-sectional imaging modality of choice for preoperative evaluation and staging of osteosarcoma because of its superior contrast resolution and multiplanar capabilities. Tumor is seen primarily as areas of intermediate signal intensity on Tl-weighted images and as areas of high signal intensity, replacing the normal marrow, on T2-weighted images. Areas of low signal intensity on both T1- and T2-weighted MR images are frequent and represent mineralized matrix (Figs. 14.29 and 14.30). Foci of central hemorrhage (which have high signal intensity with all MR pulse sequences) and necrosis (which has low signal intensity on T1-weighted images and high signal intensity on T2-weighted MR images) are common in both the intraosseous and soft-tissue tumor components.

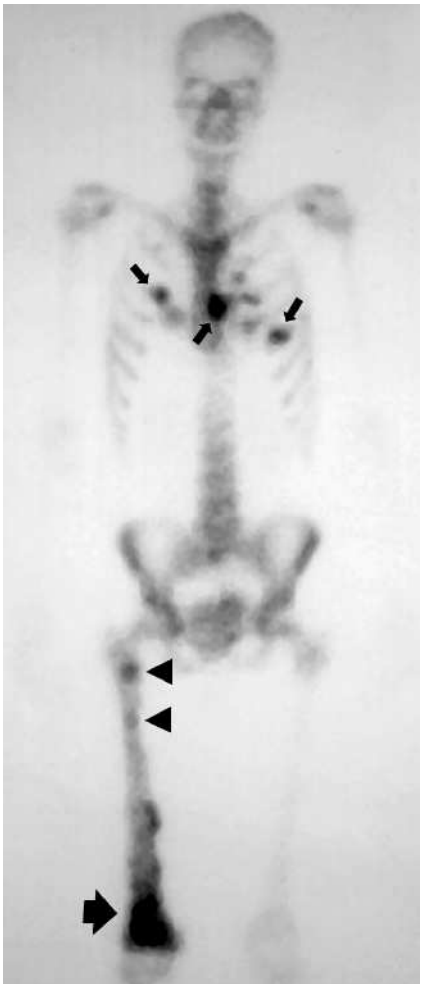

a

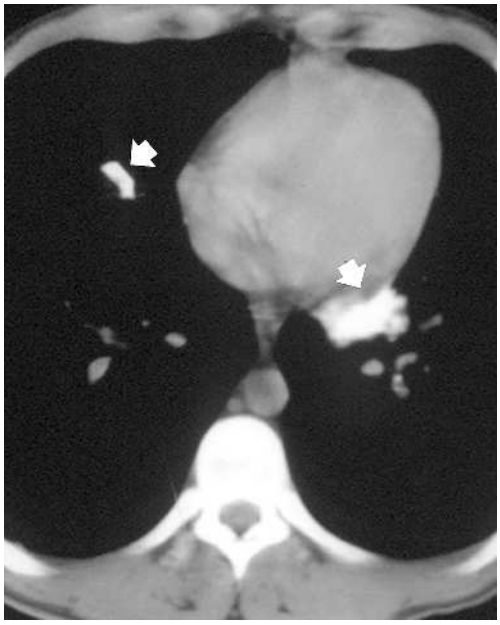

b

Fig. 14.28a,b. Osteosarcoma with multiple metastases. **a** Delayed static anterior image from MDP scintigraphy shows the primary tumor in the distal femur (*short arrow*), multiple femoral skip lesions (*arrowheads*), and multiple pulmonary metastases (*long arrows*). **b** Corresponding axial chest CT image shows multiple ossified pulmonary metastases (*arrows*)

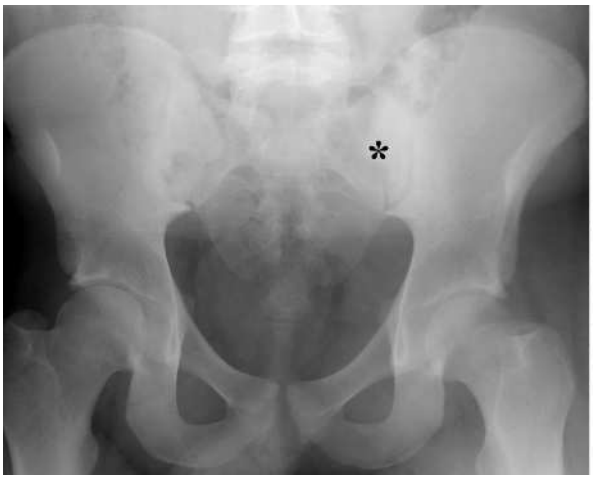

a

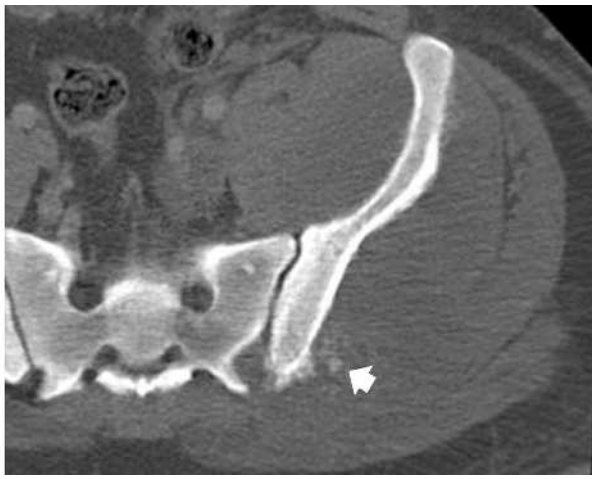

b

Fig. 14.29a–e. Osteosarcoma of the pelvis in a 20-year-old, presenting with an acute DVT in the left lower extremity. **a** Anteroposterior radiograph of the pelvis does not readily identify the subtle osseous matrix and lysis in the left ilium (*asterisk*). **b** Axial enhanced CT scan displayed at bone window shows subtle osseous matrix and tumor soft tissue extension (*arrow*) in the posterior left ilium. **c–e** *see next page*

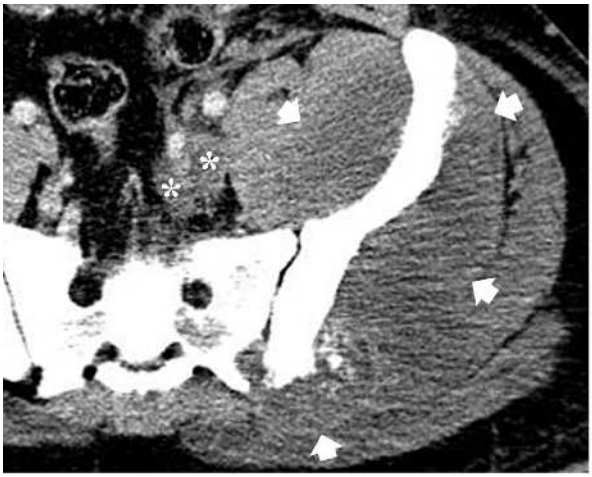

c

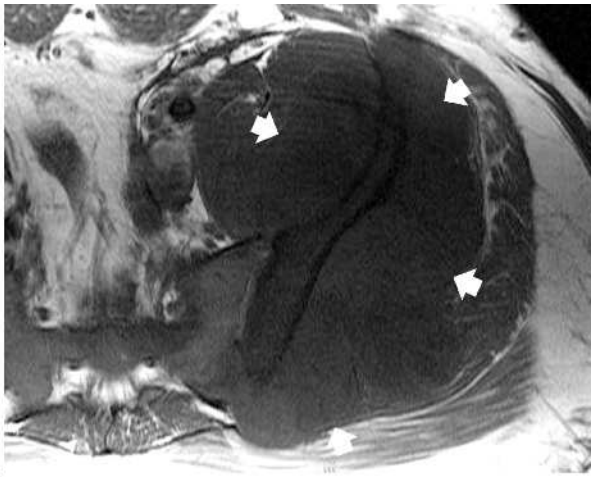

d

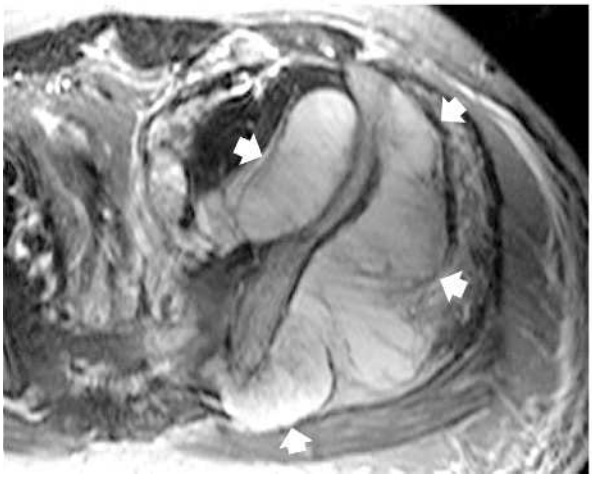

e

Fig. 14.29a–e. (*continued*) Osteosarcoma of the pelvis in a 20-year-old, presenting with an acute DVT in the left lower extremity. **c** Corresponding axial enhanced CT scans displayed at soft tissue window shows the DVT in the iliac veins (*asterisks*). Note large associated soft tissue mass (*arrows*). Corresponding axial T1 (TR/TE; 450/16) (**d**) and T2-weighted (TR/TE; 2250/80) (**e**) spin-echo MR images show the soft tissue mass to better advantage (*arrows*)

As with other musculoskeletal neoplasms, accurate assessment of the intra- and extraosseous extent of osteosarcoma is critical in directing limb-salvage procedures. Multiplanar imaging allows assessment of the following vital information: (1) anatomic landmarks for the extent of marrow and soft-tissue involvement and their relationship to surrounding structures, (2) invasion of the epiphysis, (3) involvement of the joint or neurovascular structures, (4) identification of skip metastases, and (5) identification of areas of viable tumor and mineralized matrix which improve biopsy accuracy (Figs. 14.30 and 14.31) (Schreiman et al. 1986; Redmond et al. 1989; O'Flanagan et al. 1991; Seeger et al. 1991; Panuel et al. 1993; Schima et al. 1994). The true margins of a lesion, whether intra- or extraosseous, may be obscured by perilesional edema on MR images obtained with water-sensitive pulse sequences (inversion recovery and T2-weighting with fat suppression).

The physis has long been considered by radiologists to be a barrier to tumor growth. However, pathologic evaluation has shown that approximately 75–88% of metaphyseal osteosarcomas extend through the open physis into the epiphysis (Simon and Bos 1980; Ghandur-Mnaymneh et al. 1983). Epiphyseal extension may be identified at radiography in as few as 17% of osteosarcomas, although this pattern of spread is easily recognized on coronal or sagittal MR images in 80% of metaphyseal osteosarcomas (Fig. 14.30) (Ghandur-Mnaymneh et al. 1983; Schreiman et al. 1986; Norton et al. 1991; Panuel et al. 1993). Joint involvement (most frequently in the knee) can be seen in 19–24% of osteosarcomas, although the synovium is rarely involved (Schima et al. 1994).

A diagnosis of joint involvement by tumor on MR images is difficult, but is suggested when the hyaline cartilage is penetrated or more commonly, when tumor extends through the capsule, such as into the suprapatellar bursa anteriorly or posteriorly, to encompass the cruciate ligaments (Schima et al. 1994). Fat-suppressed T1-weighted gadolinium-enhanced images are helpful for delineating extension of tumor into the joint, but enhancing synovium may mimic tumor spread. Al-

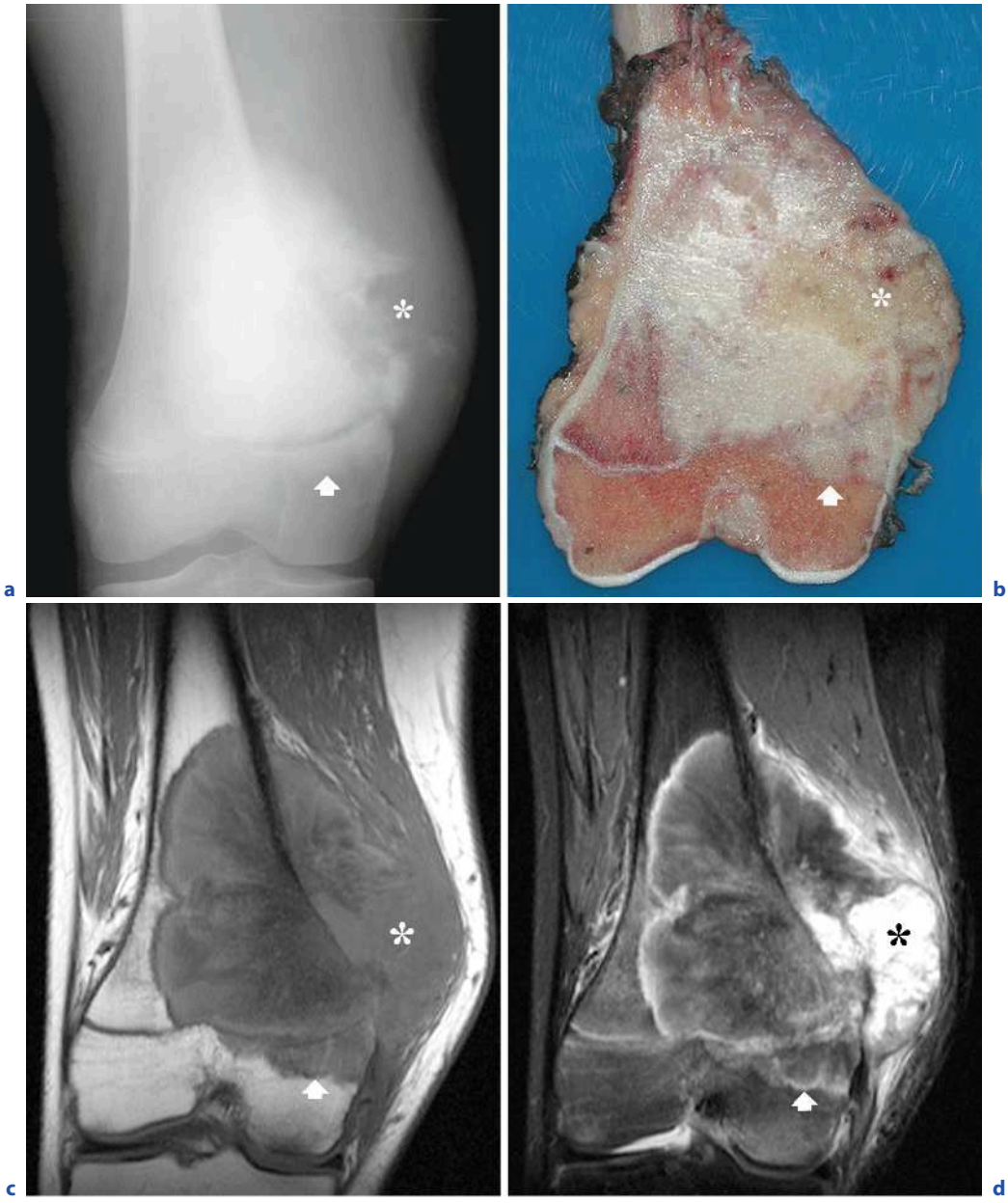

Fig. 14.30a–e. Osteosarcoma of the distal femur in a 13-year-old, presenting with knee pain and swelling. **a** Anteroposterior radiograph shows a large, osteoblastic mass with a large associated soft tissue mass, a portion of which is not mineralized (*asterisk*). Note epiphysesal extension (*arrow*). **b** Corresponding coronal gross photograph shows the different gross appearance between the sclerotic (osteoblastic) and lucent (chondroblastic) (*asterisk*) portions of the tumor. Epiphyseal extension is well demonstrated (*arrow*). Corresponding coronal T1-weighted (TR/TE; 516/14) (**c**) spin-echo and STIR (TR/TE/TI; 6886/30/140) MR images show variable signal intensity with the osteoblastic areas of the tumor demonstrating low-intermediate signal intensity and the chondroblastic portion showing intermediate signal intensity on T1-weighted image (**d**). On fluid sensitive image, the osteoblastic portion of the mass shows low signal, while the chondroblastic portion shows high signal (*asterisk*). The epiphyseal extension is also well demonstrated on MR imaging (*arrow*). **e** *see next page*

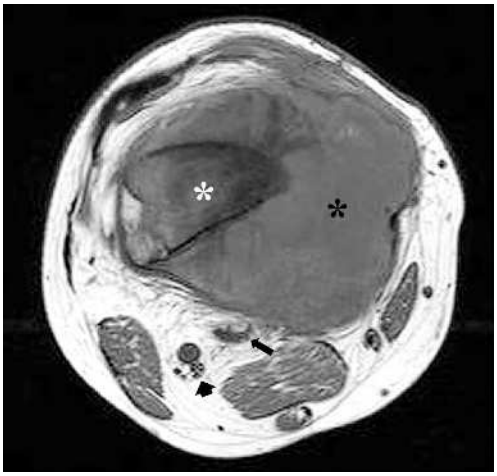

e

Fig. 14.30a–e. (*continued*) Osteosarcoma of the distal femur in a 13-year-old, presenting with knee pain and swelling. **e** Axial MR image at the level of the mid metaphysis shows a low to intermediate signal from the tumor (*asterisks*), as well as the relationship of the lesion to the superficial femoral artery and vein (*small long arrow*) and tibial and common peroneal nerves (*arrow*)

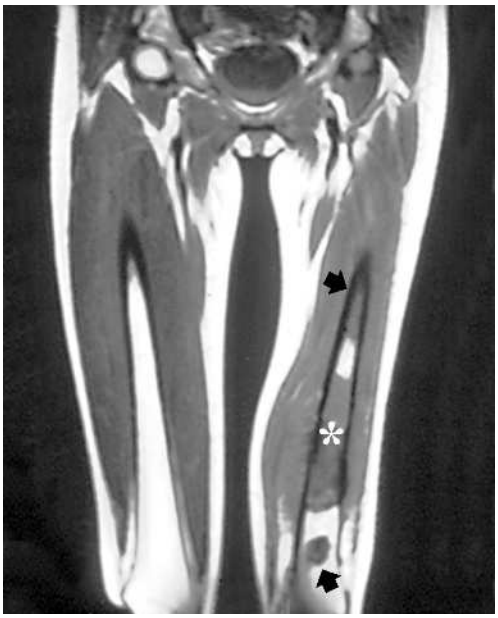

Fig. 14.31. Osteosarcoma with skip metastases. Large field-of-view coronal imaging of the lower extremity done following local staging of the left distal diaphyseal osteosarcoma (*asterisk*) shows multiple skip metastases (*arrows*)

though invasion of the joint is unlikely in the absence of an effusion, the presence of an effusion does not allow an accurate prediction of intraarticular invasion.

14.4.1.5 Treatment

Treatment of high-grade intramedullary osteosarcoma consists of chemotherapy, followed by wide surgical resection and limb salvage (amputation if salvage is not possible). Clinical outcome of osteosarcoma has dramatically improved over the past 25 years. Currently, the 5-year survival rate is 60–80% (Goorin et al. 1985; Glasser et al. 1992). Tumor size (>10 cm) and advanced stage at presentation are important factors that significantly worsen patient outcome. Evidence of pathologic fracture increases the likelihood of local recurrence. Perhaps the most important determinant of long-term survival of patients with osteosarcoma is tumor response to chemotherapy. Patients with greater than 90% tumor necrosis after therapy have a statistically significantly higher likelihood of long-term survival. Ongoing research is being conducted to quantitate the degree of tumor necrosis radiologically, by using various modalities, including Doppler sonography, PET. bone scintigraphy, and MR imaging (dynamic subtraction studies) before therapy (Goorin et al. 1985; Glasser et al. 1992; van der Woude et al. 1994, 1995; Reddick et al. 1995; Ohtomo et al. 1996).

14.4.2 Uncommon Intramedullary Osteosarcoma

While the majority of intramedullary osteosarcomas are classified as conventional osteosarcoma, additional uncommon forms of osteosarcoma include telangiectatic, small cell, gnathic, and low grade central osteosarcoma. These lesions are distinguished by a specific clinical setting and/or a characteristic histological appearance, as well as a different biological behavior.

14.4.2.1 Telangiectatic Osteosarcoma

Telangiectatic osteosarcoma was described by Paget in 1854 (Murphey et al. 2003) and was subsequently referred to by Gaylord as a "malignant bone aneurysm" in 1903 (Gaylord 1903). Ewing (1922) was the first to classify telangiectatic osteosarcoma as a distinct histologic variant, characterized by a malignant, osteoid-forming sarcoma of bone with large blood-filled vascular channels. This subtype of osteosarcoma is now well recognized, although unusual, representing 2.5–12.0% of all lesions (Farr et al. 1974; Matsuno et al. 1976;

Huvos et al. 1982; Mervak et al. 1991). Characteristically, telangiectatic osteosarcoma is primarily (>90%) composed of multiple aneurysmally dilated cavities that contain blood, with viable high-grade sarcomatous cells in the peripheral rim and septations around these spaces. It is therefore not surprising that telangiectatic osteosarcomas may be confused with aneurysmal bone cysts, both radiologically (with all imaging modalities) and pathologically (Ruiter et al. 1977; Kaufman and Towbin 1981). Patient demographics, clinical symptoms, and lesion locations are similar to those in conventional osteosarcoma (Murphey et al. 1997, 2003).

In the first large series of telangiectatic osteosarcomas described by Matsuno et al. (1976), lack of sclerosis on radiographs was one of the diagnostic criteria. In a follow-up series (Mervak et al. 1991) from the same institution, however, this criterion was modified to "lack of significant sclerosis." The WHO, in its definition of telangiectatic osteosarcoma, now notes the radiograph "… typically shows a purely lytic destructive process without matrix mineralization" and that the finding of "… significant sclerosis within the lesion militates against the diagnosis of telangiectatic osteosarcoma" (Matsuno et al. 2002).

Radiographs typically show a metaphyseal location with a geographic pattern of bone destruction and ill-defined margins; however, more aggressive patterns of osteolysis may be seen (Rosen et al. 1986; Vanel et al. 1987; Pignatti et al. 1991; Bacci et al. 1994; Murphey et al. 2003). A pattern of parallel striations was described by Vanel et al. (1987) in 28% of their 14 cases of telangiectatic osteosarcoma, and they suggested the cause to be hypertrophy of normal veins, a feature that may also be seen with other hyperemic bone lesions or the result of aggressive bone loss (Murphey et al. 2003). Expansile remodeling of bone is also common, although only infrequently marked and aneurysmal. Periosteal reaction, which is usually aggressive in character, cortical destruction, and associated soft-tissue mass are also frequent findings (Murphey et al. 2003).

The hemorrhagic nature of telangiectatic osteosarcoma is reflected in its imaging appearance. Bone scintigraphy typically shows heterogeneous marked uptake of radionuclide with photopenia centrally (donut sign) in 65% of cases. On CT scanning, the central portion of the lesion often demonstrates an attenuation lower than that of muscle (80% of cases) (Murphey et al. 2003). This central region also shows very high signal intensity on fluid sensitive MR images. At MR imaging, hemorrhage is frequently observed, with multiple fluid-fluid levels. While fluid levels may also be seen at CT, they are best demonstrated at MR imaging, being identified in approximately 90% of cases (Fig. 14.32) (Murphey et al. 2003).

The lesion most often confused with telangiectatic osteosarcoma is aneurysmal bone cyst. The most important features for distinguishing telangiectatic osteosarcoma from aneurismal bone cyst, in our opinion, are the identification of solid, viable tumor, osteoid matrix and an aggressive pattern of growth (Murphey et al. 2003).

The first imaging feature that favors the diagnosis of telangiectatic osteosarcoma as opposed to aneurysmal bone cyst is the detection of thick, solid or nodular tissue surrounding or associated with the cystic/hemorrhagic spaces. This appearance is best depicted after intravenous contrast material administration, with the thick, enhancing tissue corresponding to viable sarcoma associated with hemorrhagic and necrotic spaces. The thick peripheral and septal nodular tissue can also be seen before contrast material administration, although not as well (Murphey et al. 2003). It is vital to direct biopsy to this viable tissue to ensure an accurate diagnosis.

The second imaging feature is the detection of matrix mineralization in the lesion, which reflects an underlying osteoid-producing tumor. As would be expected, this mineralization can only occur in the previously described viable neoplastic tissue around the periphery and septations of the necrotic and/or hemorrhagic spaces. This is often subtle on radiographs and of limited extent because the viable tumor cells comprise only a small amount of the lesion (<10%) compared with the volume of cystic spaces (>90%). In our experience, subtle osteoid matrix can be identified on radiographs in 58% of cases and with CT scanning in 85% of cases (Murphey et al. 2003).

The final imaging feature that that is useful in distinguishing telangiectatic osteosarcoma from aneurysmal bone cyst reflects the more aggressive growth of the former lesion. Cortical destruction with associated soft-tissue mass is a frequent finding in telangiectatic osteosarcoma. The growth pattern of aneurismal bone cyst is much different, typically showing expansile remodeling of a large portion of the cortical circumference (>33%), not focal protrusion, and an intact outer periosteum (Murphey et al. 2003).

Treatment of telangiectatic osteosarcoma is similar to that of conventional osteosarcoma and consists of chemotherapy followed by wide surgical resection and limb salvage or amputation. Results of biopsy of these lesions can be misleading if specimens of only hemorrhagic tissue are obtained. Imaging can be helpful in directing the biopsy sampling to the peripheral regions of

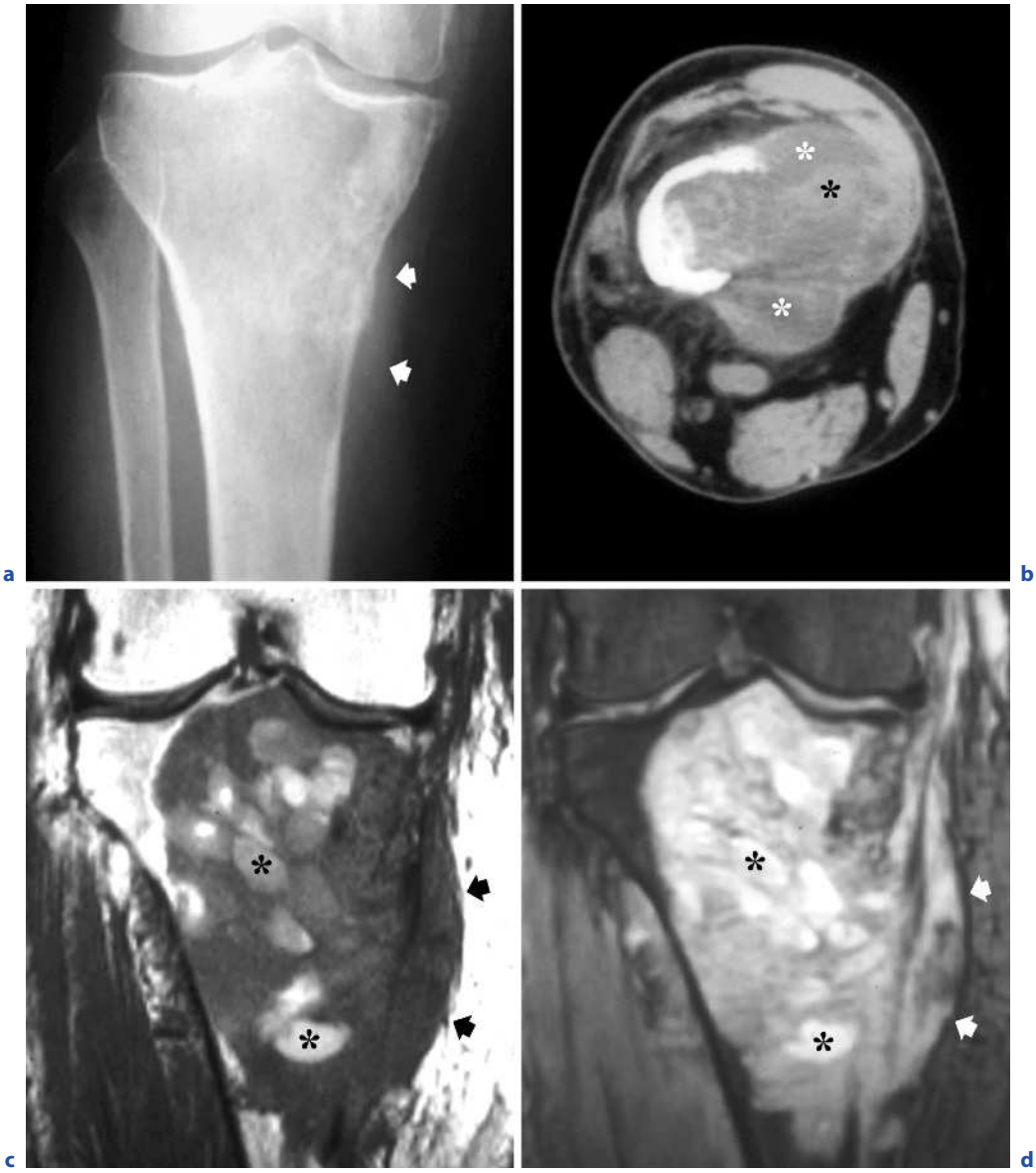

Fig. 14.32a–h. Telangiectatic osteosarcoma of the proximal tibia. **a** Anteroposterior radiograph shows a large lytic lesion in the proximal tibia with soft tissue extension (*arrows*) and no definitive osteoid formation. **b** Axial noncontrast CT scan reveals areas of low attenuation (*white asterisks*), as well as others with soft tissue attenuation (*black asterisk*). Corresponding coronal T1-weighted (**c**) spin-echo and STIR (**d**) MR images show a predominantly hemorrhagic mass with areas of subacute hemorrhage (*asterisks*) and soft tissue extension (*arrows*). **e–h** *see next page*

viable tumor. Prognosis of telangiectatic osteosarcoma was previously thought to be much worse than that of conventional osteosarcoma (Matsuno et al. 1976); however, newer studies suggest that the 5-year survival rate of telangiectatic osteosarcoma (68%) is similar to that of conventional osteosarcoma (Huvos et al. 1982; Rosen et al. 1986; Pignatti et al. 1991).

14.4.2.2 Small Cell Osteosarcoma

Small cell osteosarcoma is a distinct subtype of conventional osteosarcoma, composed of small, round, blue cells. It was first described by Sim et al. (1979) and histologically it may be difficult to distinguish from other

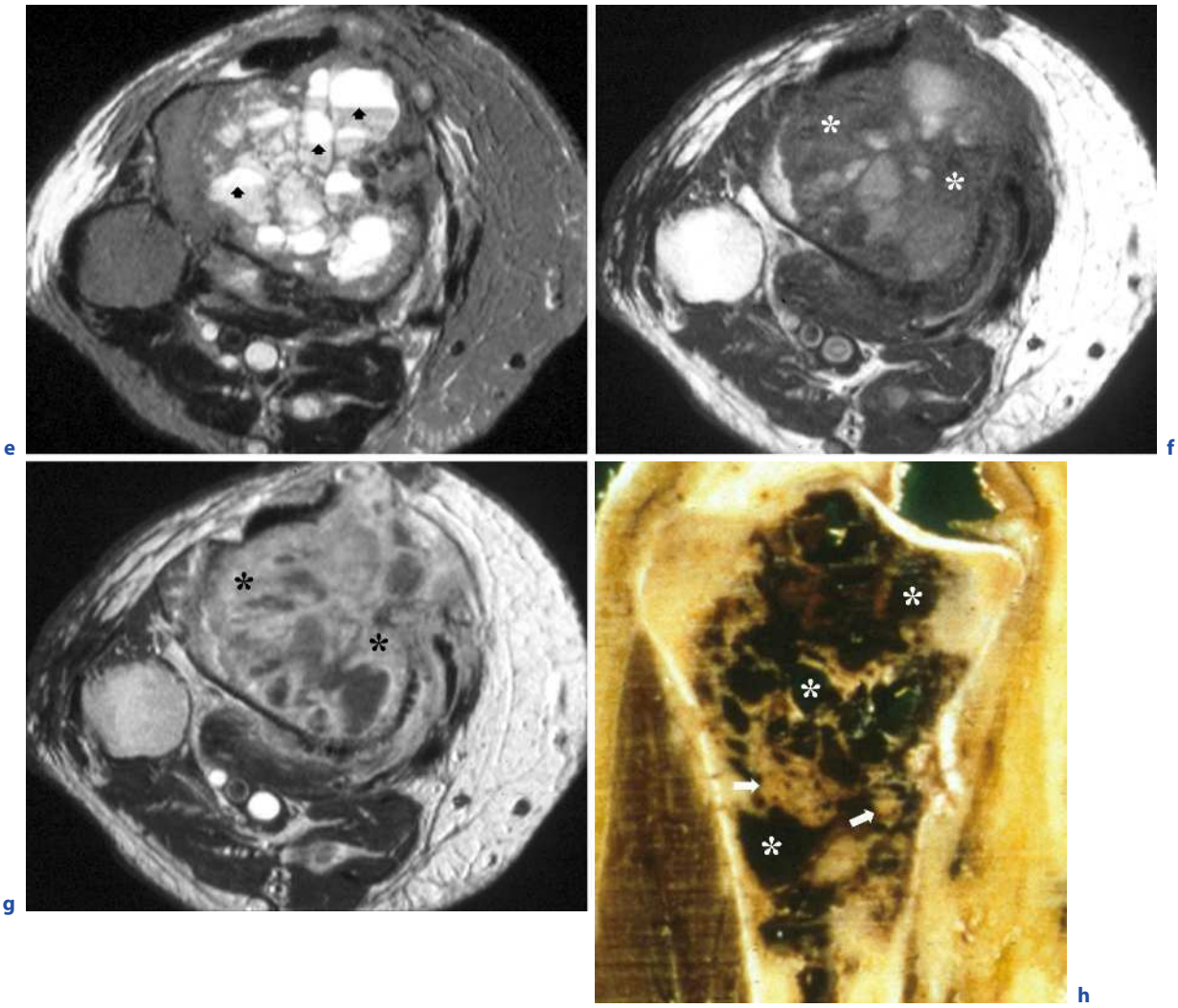

Fig. 14.32a–h. (*continued*) Telangiectatic osteosarcoma of the proximal tibia. **e** Axial T2-weighted spin-echo MR image shows the hemorrhagic component to better advantage with multiple fluid levels (*arrows*). Corresponding axial T1-weighted images preceding (**f**) and following (**g**) contrast administration show extensive enhancement of the viable tumor (*asterisks*) within the hemorrhagic mass. **h** Photograph of coronally sectioned gross specimen shows multiple hemorrhagic spaces (*asterisks*) with surrounding rinds of viable tumor (*arrows*), correlating well with coronal MR image in **c**

small round cell malignancies, particularly Ewing sarcoma, lymphoma, and mesenchymal chondrosarcoma (Nakajima et al. 1997). Small cell osteosarcoma is estimated to represent between 1% and 4% of osteosarcomas (Edeiken et al. 1987; Ayala et al. 1989; Bertoni et al. 1989; Park YK et al. 1995; Nakajima et al. 1997; Hameed 2007). Males and females are affected equally, and the patient age distribution and tumor location is similar to that for conventional osteosarcoma, with the distal femur being the most common site. Patients typically present with pain and swelling, also similar to those with conventional osteosarcoma (Nakajima et al. 1997).

The lesions are typically metaphyseal with frequent extension into the epiphysis, but 15% of cases solely involve the diaphysis (Sim et al. 1979; Edeiken et al. 1987; Ayala et al. 1989; Bertoni et al. 1989). The pathologic characteristics of this tumor are similar to those of Ewing sarcoma: both lesions are composed of small, round, blue cells. However, small cell osteosarcoma lacks the cellular uniformity seen in Ewing sarcoma and consistently produces osteoid (fine and reticular) (Sim et al. 1979; Ayala et al. 1989). Ewing sarcoma does not produce osteoid, even though at times reactive bone formation may be encountered and histologic differentiation can be difficult. In this setting, molecular and immuno-

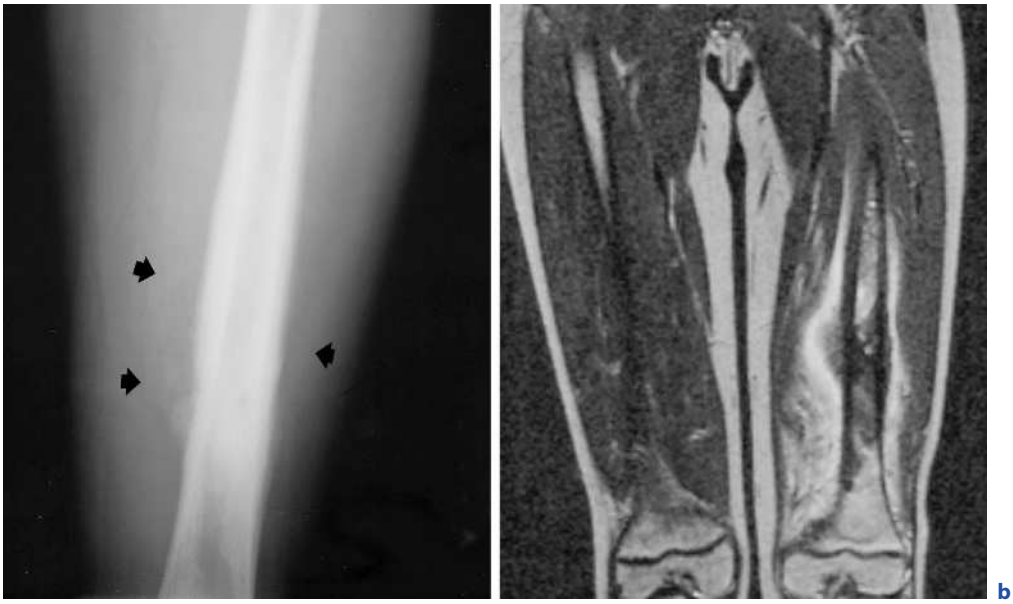

Fig. 14.33a,b. Small cell osteosarcoma. **a** Anteroposterior radiograph of the distal femur shows a destructive, predominantly lytic lesion, with associated soft tissue extension (*arrows*). **b** Coronal T2-weighted spin-echo MR image shows the mass and the associated periosteal reaction

histochemical markers are very helpful for distinguishing between the two tumors.

At radiologic examination, small cell osteosarcoma typically manifests as a predominantly permeative, lytic, medullary lesion with cortical breakthrough, aggressive periosteal reaction, and an associated soft-tissue mass (Sim et al. 1979; Ayala et al. 1989; Bertoni et al. 1989). Osteoid matrix is usually apparent in the medullary and/or soft-tissue component and is best detected with CT scanning (Fig. 14.33) (Edeiken et al. 1987; Ayala et al. 1989). Lesions may be entirely lytic with no radiologic evidence of osteoid matrix to suggest the diagnosis of osteosarcoma, and such lytic lesions have been reported in up to 40% of patients (Nakajima et al. 1997).

The prognosis for patients with small cell osteosarcoma is extremely poor, regardless of treatment, and is generally slightly worse than that for patients with conventional osteosarcoma (Kalil and Bridge 2002).

14.4.2.3 Gnathic Osteosarcoma

Lesions of the mandible and maxilla constitute 6% of all osteosarcomas (Garrington et al. 1967; Finkelstein 1970; Clark et al. 1983). Gnathic osteosarcoma is often considered to be a distinct category because of its predilection to affect older patients (average age, 34–36 years) (Garrington et al. 1967; Finkelstein 1970; Russ and Jesse 1980; Clark et al. 1983). Lesions most commonly affect the alveolar ridge, maxillary antrum, and body of the mandible. Patients most frequently present with pain or swelling. Less common symptoms include paresthesias, tooth loosening, toothache, bleeding and nasal obstruction (Garrington et al. 1967).

At histologic analysis, the lesions are often predominantly chondroblastic (Clark et al. 1983). The radiologic appearance of gnathic osteosarcoma is similar to that of conventional osteosarcoma, with evidence of osteoid matrix (60–80% of cases), aggressive periosteal reaction in mandibular lesions, and soft-tissue extension (Fig. 14.34) (Finkelstein 1970; Lee et al. 1988). Opacification of the maxillary sinuses is also a frequent finding of maxillary lesions. CT is the optimal modality for detecting areas of mineralized osteoid in this complex anatomic location. MR imaging demonstrates the intramedullary and extraosseous components to best advantage. Treatment of gnathic osteosarcoma is difficult and includes radical and local surgical resection, radiation therapy, and chemotherapy. Unfortunately, local recurrence is common (50–80% of cases), particularly in cases of maxillary lesions, and is often uncontrollable, typically leading to patient death (Russ and Jesse 1980; Clark et al. 1983). Distant metastases are less frequent than in other osteosarcomas, and the

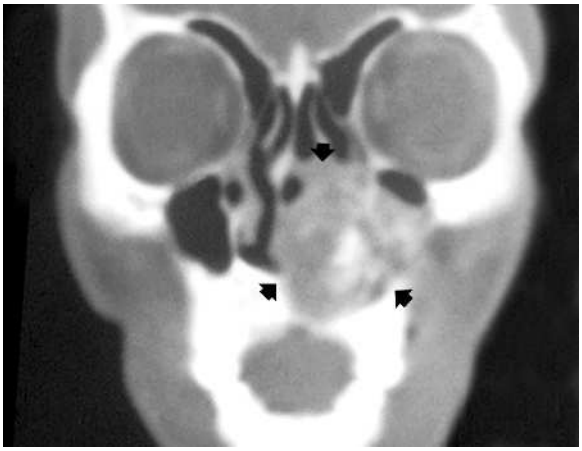

Fig. 14.34. Gnathic osteosarcoma. Reformatted coronal CT displayed at bone window shows a well defined lytic maxillary mass (*arrows*) with osteoid production

5-year survival rate is approximately 40% (Russ and Jesse 1980; Clark et al. 1983).

14.4.2.4 Low Grade Intraosseous Osteosarcoma

Low grade intraosseous osteosarcoma is an unusual variant of conventional osteosarcoma and represents 1–2% of all osteosarcomas (Inwards and Knuutila 2002); it has also been referred to as well-differentiated or sclerosing osteosarcoma (Unni et al. 1977; Ellis et al. 1988; Mirra 1989a; Kurt et al. 1990). It occurs most frequently in patients in the third decade of life (a decade older than that for conventional osteosarcoma), but patients have a wide age range, and unlike high-grade intramedullary osteosarcoma, men and women are affected equally (Unni et al. 1977; Ellis et al. 1988; Kurt et al. 1990). Patients usually present after a protracted clinical course with nonspecific symptoms, but they may be asymptomatic, with the lesion being discovered incidentally. The sites of low grade intraosseous osteosarcoma are similar to those of conventional osteosarcoma: the femur and tibia (about the knee) are most frequently affected, and the lesion most commonly involves the metaphysis, often with extension into the epiphysis (Kurt et al. 1990). Unlike conventional osteosarcoma, low grade intraosseous osteosarcomas frequently have radiologic and pathologic characteristics that simulate a benign process, including fibrous dysplasia, nonossifying fibroma, chondroblastoma, and chondromyxoid fibroma (Kurt et al. 1990). At radiographic examination, the lesion may show well-defined margins, a sclerotic rim, prominent internal trabeculation, and diffuse sclerosis, and it may cause expansile remodeling of bone (Fig. 14.35) (Ellis et al. 1988). However, radiographic evidence of a more aggressive process, such as associated bone lysis, focally indistinct margins, cortical destruction, soft-tissue mass and, uncommonly, periosteal reaction, is apparent even if subtle (Ellis et al. 1988).

Low grade intraosseous osteosarcoma usually behaves as a locally aggressive tumor, with multiple recurrences developing after intralesional resection. Time to recurrence is variable and can be delayed up to 20 years after surgery (Unni et al. 1977; Kurt et al. 1990). In general, for those patients whose lesions are initially treated by wide excision with limb salvage, the long-term prognosis is excellent. In 15% of incompletely resected lesions, Kurt et al. (1990) found transformation of the initial lesion into a higher-grade osteosarcoma, resulting in an increased prevalence of metastatic disease and a poor prognosis. Rarely, low grade intraosseous osteosarcoma may manifest as a more aggressive tumor with significant metastatic potential.

14.5 Juxtacortical Osteosarcoma

Juxtacortical osteosarcomas account for 4–10% of all osteosarcomas (Levine et al. 1985; Mirra 1989a; Raymond 1991). While it is convenient to separate juxtacortical osteosarcomas into four distinct entities – parosteal, periosteal, high grade surface, and intracortical osteosarcoma, it is important to remember that these lesions may have overlapping clinical and imaging features. Accordingly, some authors prefer to group all these osteosarcomas into a "juxtacortical" category; however, with this caveat in mind, we prefer to distinguish these lesions because of differences in radiologic and pathologic appearances, as well as in treatment and prognosis.

14.5.1 Parosteal Osteosarcoma

Parosteal osteosarcomas account for 65% of all juxtacortical osteosarcomas and are thought to originate from the outer layer of periosteum (Campanacci et al. 1984; Wold et al. 1984b; Levine et al. 1985; Mirra 1989b; Raymond 1991; Okada et al. 1994; Jelinek et al. 1996). These lesions usually affect patients in the third and fourth decades of life and show a slight female

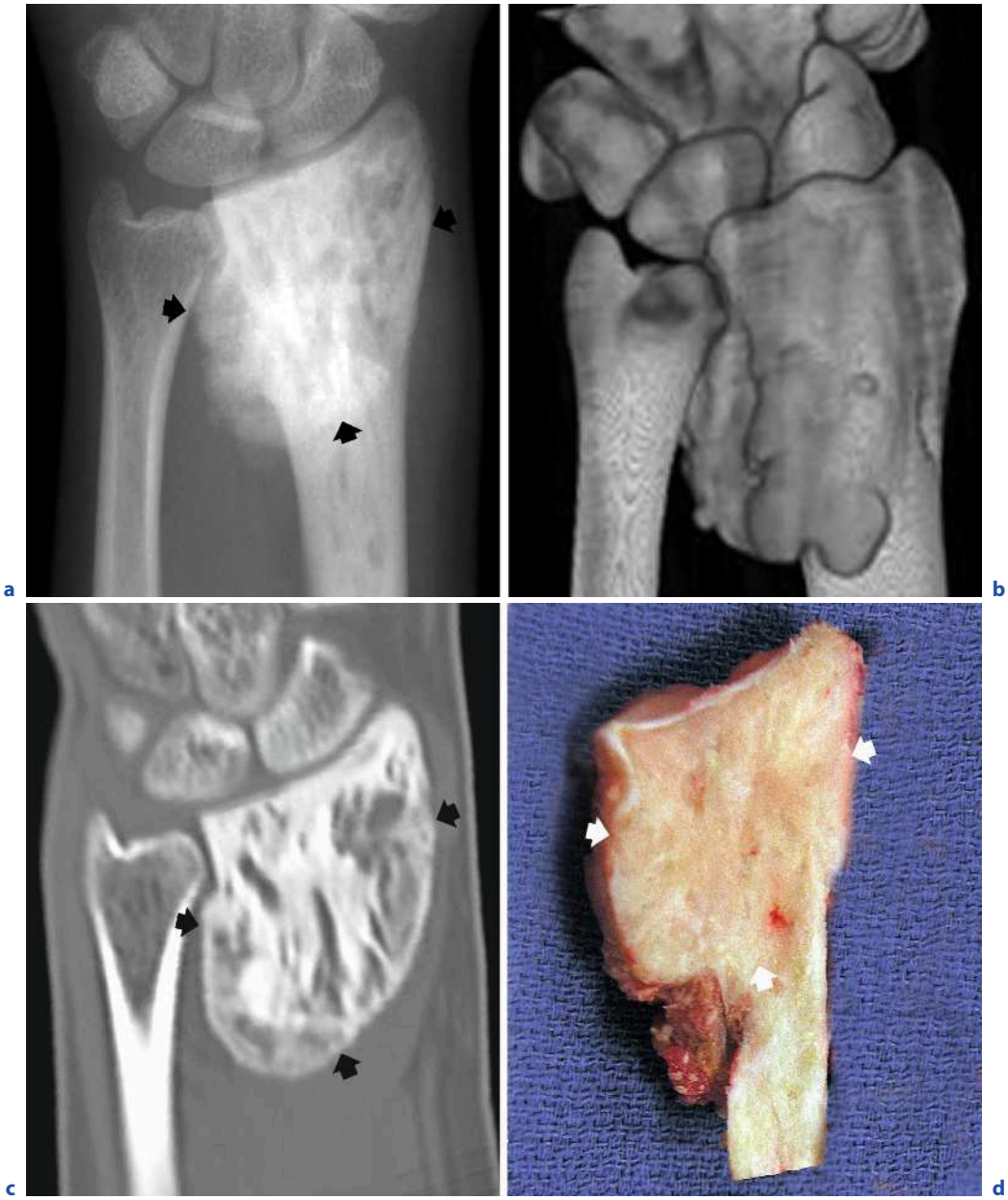

Fig. 14.35a–d. Low grade intramedullary osteosarcoma of the radius. **a** Anteroposterior radiograph of the wrist shows a densely sclerotic mass with prominent expansile remodeling (*arrows*). **b** Surface rendered 3-D CT scan shows the expansile remodeling of the mass to better advantage. Reformatted coronal CT displayed at bone window (**c**) and corresponding gross photograph (**d**) shows the well defined osseous character of the mass (*arrows*)

predilection. Clinical symptoms frequently include a palpable mass. Parosteal osteosarcomas affect the metaphyseal region of long bones (80–90% of cases), most frequently the posterior distal femur (50–65%) (Unni et al. 1976; Campanacci et al. 1984). Other commonly involved regions are the proximal humerus, tibia, and fibula.

Parosteal osteosarcomas are frequently low grade lesions, as suggested in the original description by Geschickter and Copeland (1951), who used the term *parosteal osteoma*. However, these large, lobulated, parosteal lesions contain higher grade regions in 22–64% of cases and may demonstrate invasion (back growth) into the medullary canal (8–59%) (Cam-

PANACCI et al. 1984; RAYMOND 1991; OKADA et al. 1994; UNNI and KNUUTILA 2002). Fibrous stroma and extensive osteoid are the predominant histologic characteristics, although smaller foci of cartilage are also frequent.

The radiologic appearance of parosteal osteosarcoma is often characterized by a large, lobulated (cauliflower-like), ossific (denser centrally), juxtacortical mass. Initially, only a narrow zone (stalk) of attachment to the cortex may be apparent, creating a partial radiolucent cleavage plane between the lobulated ossific mass and the remaining cortical bone (LEVINE et al. 1985; JELINEK et al. 1996). However, continued tumor growth often obliterates the cleavage plane. Cortical thickening without aggressive periosteal reaction may be seen. CT and MR imaging can demonstrate both the soft-tissue extent and evidence of medullary involvement. The ossified regions show high attenuation on CT scans and low signal intensity on all MR images, regardless of pulse sequence. In addition, JELINEK et al. (1996) have recently shown that nonmineralized soft-tissue components larger than 1 cm^3 identified at CT or MR imaging correspond to high-grade foci. Parosteal osteosarcomas may be confused both pathologically and radiologically with myositis ossificans (VAN ONGEVAL et al. 1993). However, in contradistinction to parosteal osteosarcoma, myositis ossificans is denser peripherally and is usually not attached to the cortex (Fig. 14.36).

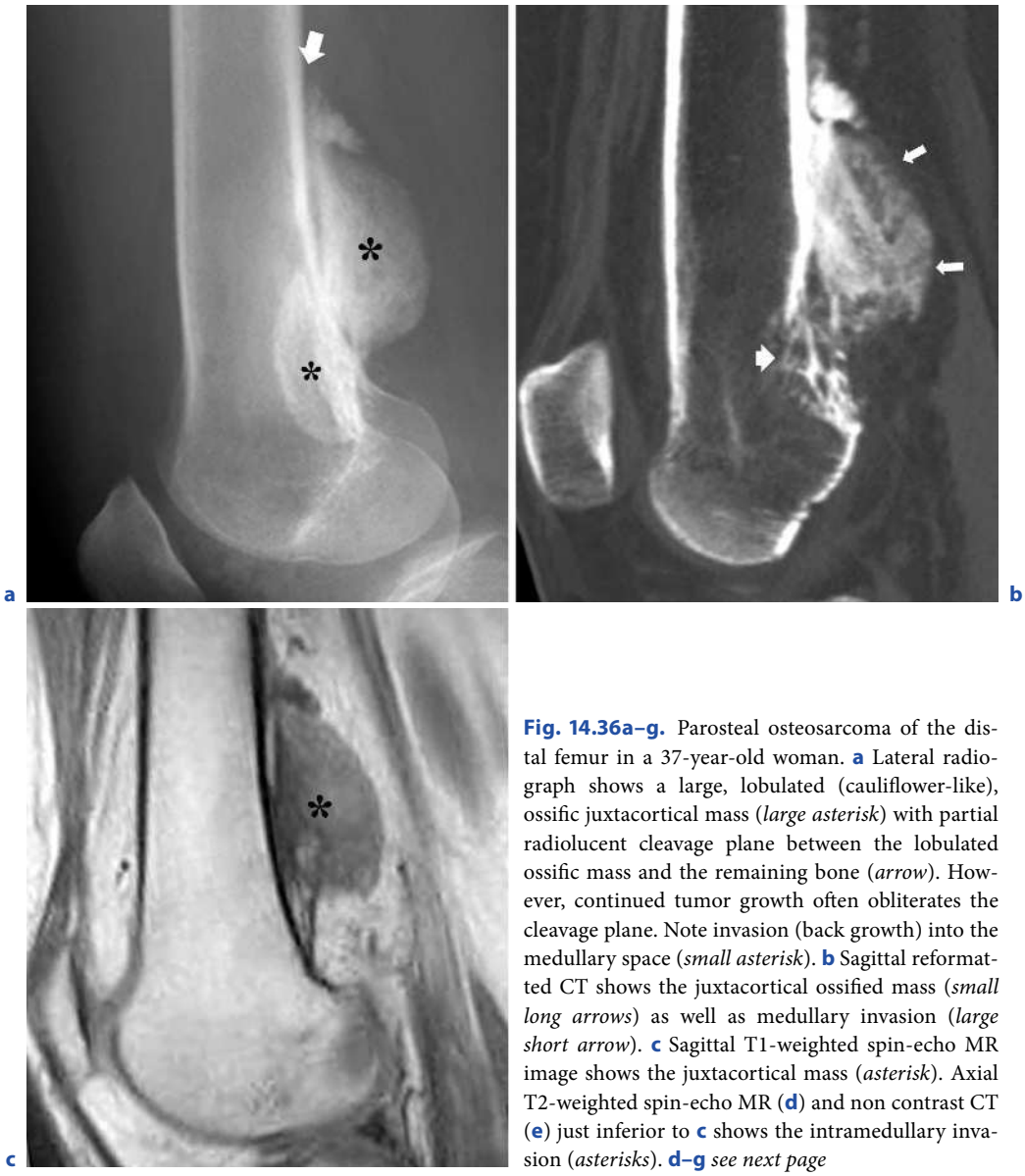

Fig. 14.36a–g. Parosteal osteosarcoma of the distal femur in a 37-year-old woman. **a** Lateral radiograph shows a large, lobulated (cauliflower-like), ossific juxtacortical mass (*large asterisk*) with partial radiolucent cleavage plane between the lobulated ossific mass and the remaining bone (*arrow*). However, continued tumor growth often obliterates the cleavage plane. Note invasion (back growth) into the medullary space (*small asterisk*). **b** Sagittal reformatted CT shows the juxtacortical ossified mass (*small long arrows*) as well as medullary invasion (*large short arrow*). **c** Sagittal T1-weighted spin-echo MR image shows the juxtacortical mass (*asterisk*). Axial T2-weighted spin-echo MR (**d**) and non contrast CT (**e**) just inferior to **c** shows the intramedullary invasion (*asterisks*). **d–g** *see next page*

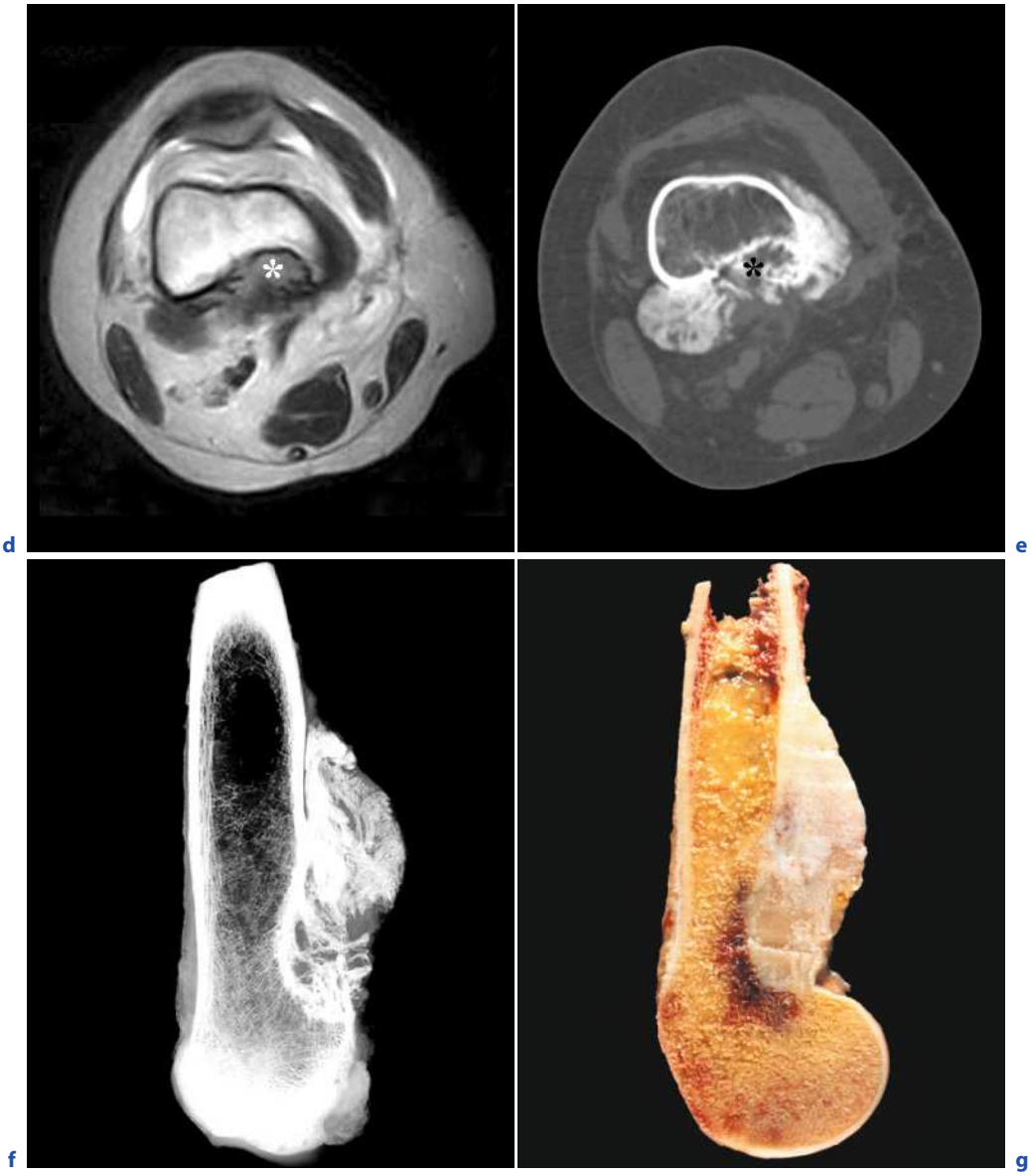

Fig. 14.36a–g. (*continued*) Parosteal osteosarcoma of the distal femur in a 37-year-old woman. Axial T2-weighted spin-echo MR (**d**) and non contrast CT (**e**) through the femoral metaphysis shows the just inferior to **c** shows the intramedullary invasion (*asterisks*). Corresponding specimen radiograph (**f**) and gross photograph (**g**) show the juxtacortical mass with medullary invasion to better advantage

Prognosis for patients with parosteal osteosarcoma is excellent, with 5- and 10-year survival rates of 80–90% (Campanacci et al. 1984; Unni and Knuutila 2002). Detection of higher-grade foci may alter therapy, and presurgical biopsy should be directed toward these sites. Higher-grade parosteal osteosarcomas may warrant neoadjuvant chemotherapy.

Lesions of higher grade have been called *dedifferentiated parosteal osteosarcoma*, although the term *dedifferentiated* is generally reserved for those lesions that contain a second tumor cell line (often fibrosarcoma or malignant fibrous histiocytoma) (Wold et al. 1984b). The presence of intramedullary back growth has previously been reported to imply a worse prognosis. More recent studies suggest that this finding does not change the overall excellent prognosis of patients with parosteal osteosarcoma (Wold et al. 1984b; Okada et al. 1994; Jelinek et al. 1996). However, it remains important to

identify medullary extension in order to ensure adequate surgical resection during limb-salvage operations.

14.5.2 Periosteal Osteosarcoma

Periosteal osteosarcoma accounts for 25% of all juxtacortical osteosarcomas and was originally described in 1976 by Unni and coworkers (Unni et al. 1976; Mirra 1989b). The age group affected is similar to that for conventional osteosarcoma (patients in the second and third decades of life). However, unlike conventional osteosarcoma, these lesions show a strong propensity to arise in the diaphysis or metadiaphysis of bone. The most commonly affected sites are the tibia and femur (85–95% of cases), followed by the ulna and humerus (5–l0%) (Unni et al. 1976; deSantos et al. 1978). Periosteal osteosarcomas are intermediate grade lesions that arise from the deep layer of periosteum and cause cortical scalloping, classically without intramedullary invasion (Unni et al. 1976). Pathologic assessment demonstrates a highly chondroblastic lesion with smaller areas of osteoid formation.

The radiologic appearance of periosteal osteosarcomas is usually characteristic and distinctive from that of parosteal lesions. The surface of the thickened diaphyseal cortex is scalloped, with perpendicular periosteal reaction extending into a broad-based soft-tissue mass (deSantos et al. 1978). Lesions are often chondroblastic and matrix mineralization may be subtle. Solid (cortical thickening) or aggressive (Codman triangle) periosteal reaction may also be apparent at the upper and lower margins of the lesion. CT and MR imaging show similar findings, with the highly chondroblastic areas corresponding to relatively low-attenuation regions on CT scans, low-signal-intensity areas on T1-weighted images, and very high-signal-intensity areas on T2-weighted MR images (deSantos et al. 1978). In a recent study, we demonstrated that these lesions usually involve approximately 50% of the osseous circumference and that the perpendicular periosteal reaction is seen as rays of low signal intensity with all MR pulse sequences (Figs. 14.37 and 14.38) (Murphey et al. 2004). Marrow invasion is rare and, when seen, is directly continuous with the surface mass (Fig. 14.38). Marrow invasion should be distinguished from reactive marrow changes, which appear as foci of marrow replacement (low signal intensity on T1-weighted MR images and high signal intensity on T2-weighted or inversion recovery images) adjacent to, but noncontiguous with, the surface mass, and has been described in more than 50% of cases (Murphey et al. 2004). Prognosis for patients with periosteal osteosarcoma is improved compared

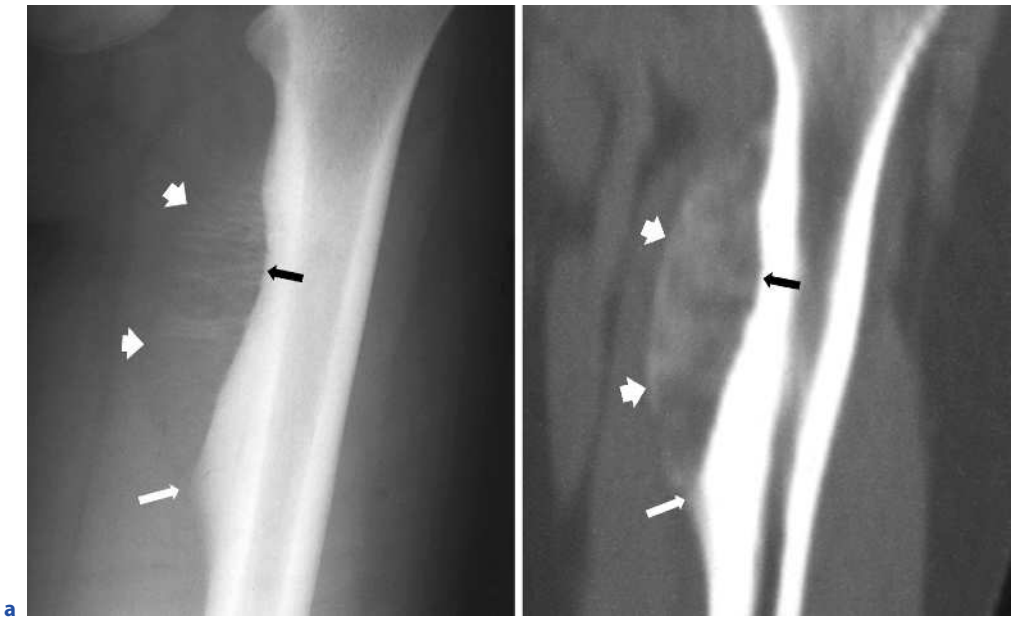

Fig. 14.37a,b. Periosteal osteosarcoma of the mid femur. Lateral radiograph (**a**) and reformatted CT (**b**) show a thickened (*long white arrows*), scalloped (*long black arrows*) diaphyseal cortex with perpendicular periosteal reaction extending into a broad-based soft-tissue mass (*short arrows*)

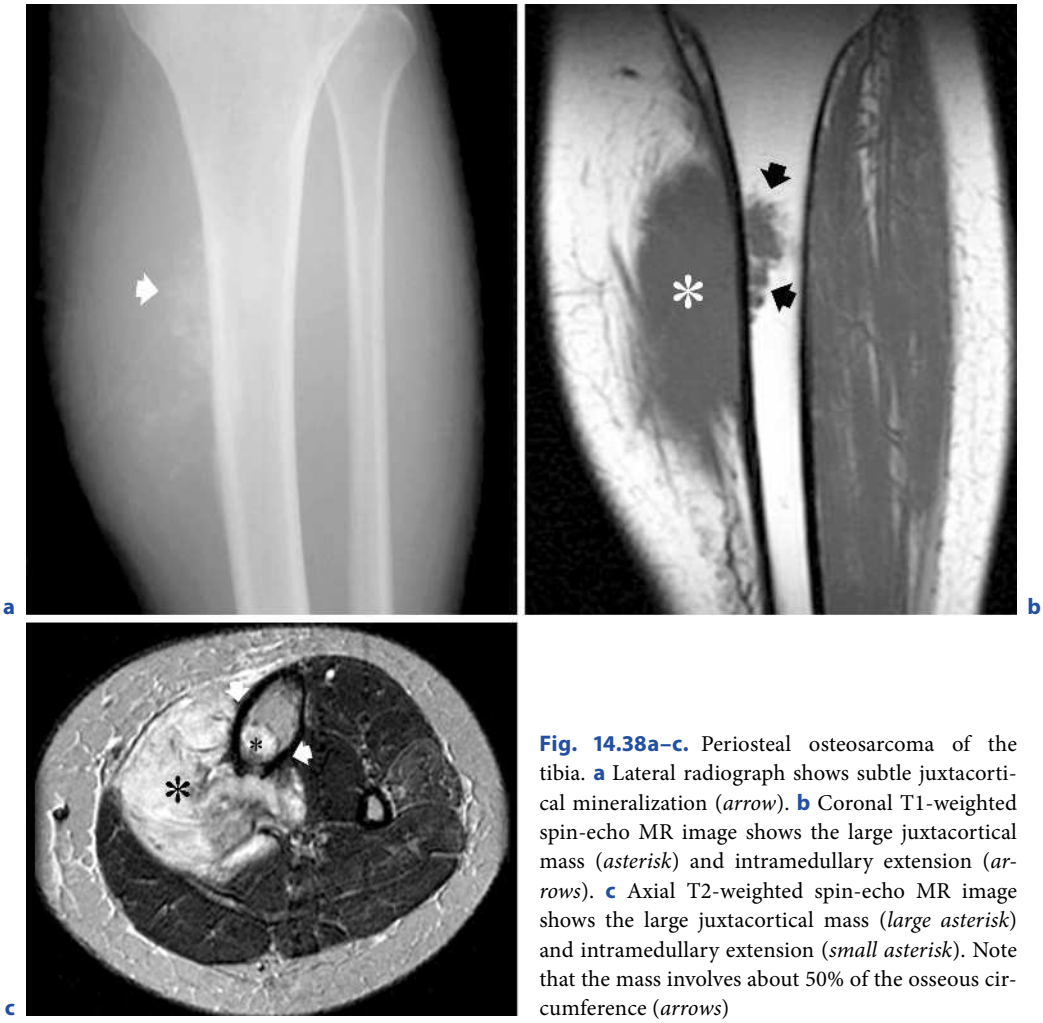

Fig. 14.38a–c. Periosteal osteosarcoma of the tibia. **a** Lateral radiograph shows subtle juxtacortical mineralization (*arrow*). **b** Coronal T1-weighted spin-echo MR image shows the large juxtacortical mass (*asterisk*) and intramedullary extension (*arrows*). **c** Axial T2-weighted spin-echo MR image shows the large juxtacortical mass (*large asterisk*) and intramedullary extension (*small asterisk*). Note that the mass involves about 50% of the osseous circumference (*arrows*)

with that for patients with conventional osteosarcoma, but it is not as good as that for patients with parosteal lesions. Metastatic disease leads to patient death in 8–16% of cases (Unni et al. 1976; Ritts et al. 1987). Surgical treatment is usually wide local excision with an associated limb-salvage procedure.

14.5.3 High Grade Surface Osteosarcoma

High grade surface osteosarcoma is rare and accounts for 10% of all juxtacortical osteosarcomas (Wold et al. 1984a; Mirra 1989b). These lesions have a high predilection to involve the diaphysis of bone and most commonly affect the femur, humerus, and fibula. Pathologically and prognostically, high-grade surface osteosarcomas are identical to conventional intramedullary lesions (Mirra 1989b). Radiologically, these lesions are similar in appearance to periosteal osteosarcoma (Wold et al. 1984a; Mirra 1989b). However, in our experience, high grade surface osteosarcomas often involve the entire circumference of bone and frequently invade the medullary canal (Fig. 14.39).

14.5.4 Intracortical Osteosarcoma

Intracortical osteosarcoma is the rarest form of osteosarcoma; the term applies to those cases in which the lesion arises within the cortex. It was originally described by Jaffe (1960) in 1960 in a report of two cases, and through 2002 only 16 cases were published (Jaffe 1960; Kyriakos 1980; Vigorita et al. 1984; Mirra et al. 1991; Griffith et al. 1998; Hasegawa et al. 1999; Hermann et al. 2002). The lesion is histologically characterized as a sclerosing variant of osteosarcoma, which

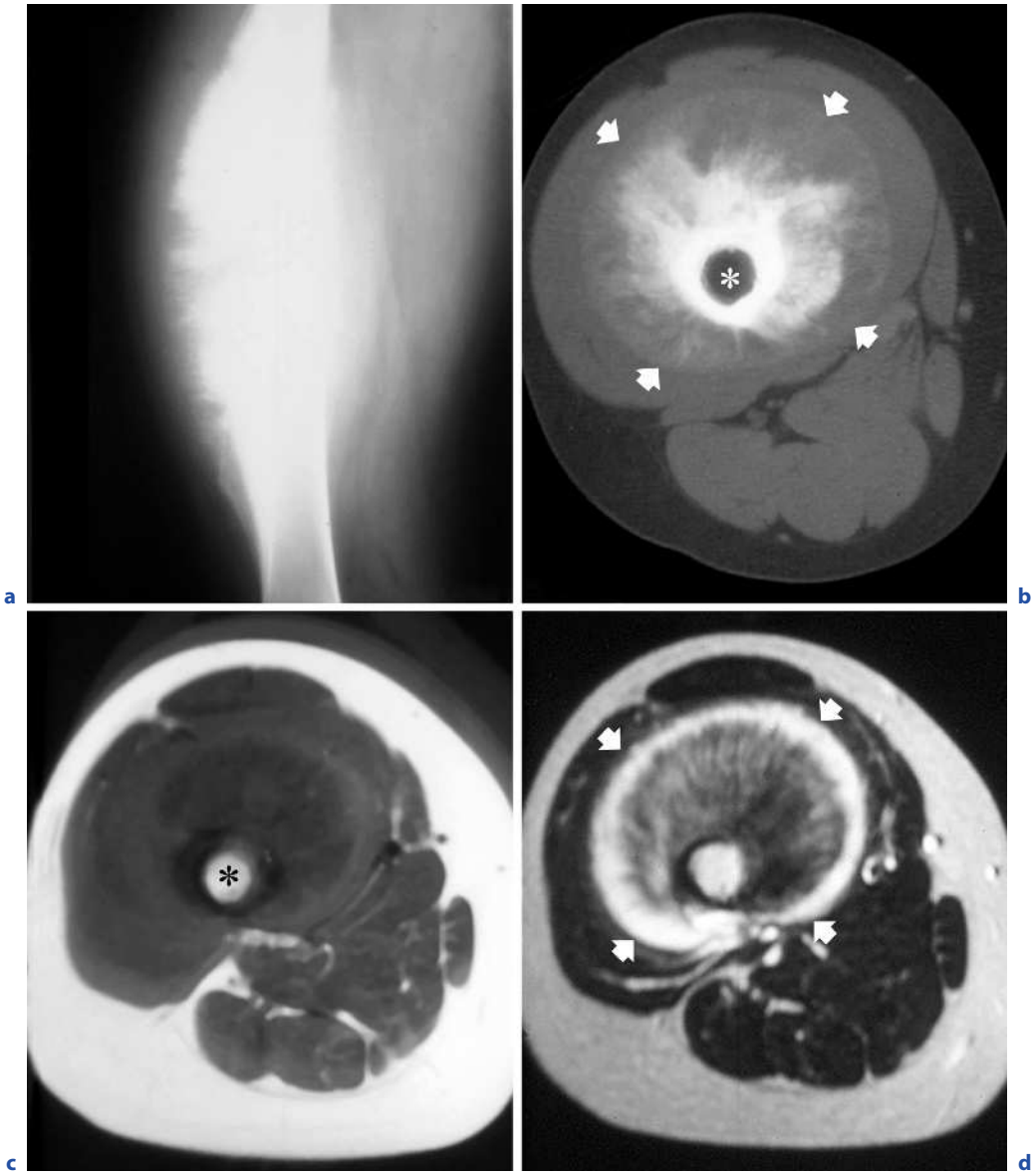

Fig. 14.39a–d. High grade surface osteosarcoma of the femur. **a** Lateral radiograph shows extensive juxtacortical mineralization (*arrow*). **b** Axial CT displayed at bone window shows a large juxtacortical mass (*arrows*) with sparing of the marrow (*asterisk*). Corresponding axial T1-weighted (**c**) and T2-weighted (**d**) spin-echo MR images confirm the juxtacortical origin with marrow sparing (*asterisk*) and reactive marrow change seen in **d**. Note the lesion involves the entire circumference of bone (*arrows*)

may contain small foci of chondrosarcoma or fibrosarcoma (Kyriakos 1980; Vigorita et al. 1984; Mirra et al. 1991; Hermann et al. 2002).

Reported patients have ranged between 9 and 43 years of age, with half being in the second decade of life. Males are affected more commonly than females (2:25:1) (Griffith et al. 1998; Hermann et al. 2002). All previously reported cases have occurred in the diaphysis of the tibia or femur, and while it is difficult to make generalizations on the basis of such a small number of cases, the typical lesion shows geographic bone lysis with variable amounts of mineralized osteoid, which may be small. The lesion is intracortical and typically measures less than 4 cm in diameter (Picci et al. 1983; Mirra et al. 1991; Hermann et al. 2002). The tumor margin may be remarkably well defined, with thickening of the surrounding cortex, while medullary invasion is only rarely reported (Fig. 14.40) (Picci et al.

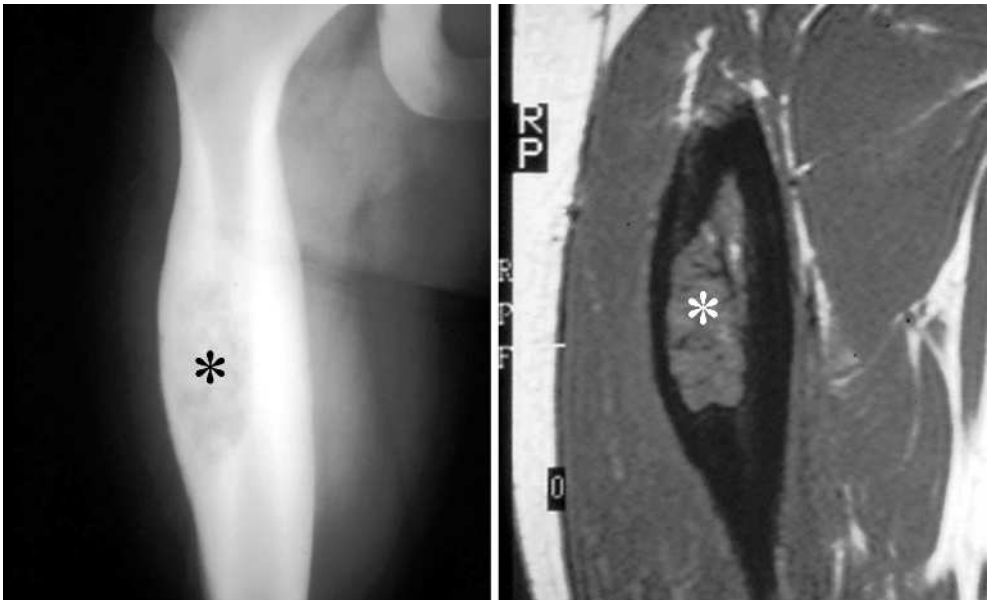

a b

Fig. 14.40a,b. Intracortical osteosarcoma of the mid femur. **a** Anteroposterior radiograph shows a focal osteoid producing intracortical mass (*asterisk*). **b** Coronal T1-weighted spin-echo MR image confirms the lesion (*asterisk*) is confined to the osseous cortex

1983; Mirra et al. 1991). Small lesions may resemble osteoid osteoma (Hermann et al. 2002). Perilesional and intramedullary high (edema-like) signal were reported in two previous cases (Hermann et al. 2002) and tumor-induced rickets (osteomalacia) in one case (Hasegawa et al. 1999).

Patients typically present with moderate pain and tenderness; less than half of patients develop a palpable "lump" (Hermann et al. 2002). Duration of symptoms is quite variable and ranges from 1 month to 2 years (Hermann et al. 2002). Although long-term data are lacking, metastases in patients with intracortical osteosarcoma have been well documented. Griffith et al. (1998), in a review of 14 cases in the literature, noted metastases in three patients (21%) and local recurrence in two (14%).

14.6 Secondary Osteosarcoma

Most osteosarcomas occur as primary neoplasms; however, approximately 5–7% of all osteosarcomas are the result of malignant transformation of a preexisting benign lesion (Mirra 1989a). The vast majority of these secondary osteosarcomas are associated with Paget disease (67–90% of cases) (Fig 14.41) or previous irradiation (6–22%) (Mirra 1989a; Resnick et al. 2002c). We include metastatic osteosarcoma within this group, as well as osteosarcomatosis, which is now generally accepted to represent multifocal metastases (Parham et al. 1985; Hopper et al. 1990).

14.6.1 Paget Osteosarcoma

Sir James Paget described osteosarcoma as a complication of osteitis deformans, the disease which would eventually bear his name, in his initial description of the disorder in 1876 (Resnick et al. 2002b). He would eventually describe five such cases, with this complication occurring in 22% of the 23 patients he described (Resnick et al. 2002b). The frequency of malignant transformation to osteosarcoma in Paget disease is generally accepted to be approximately 1%. This figure is derived from a 1981 Mayo Clinic study by Wick et al. (1981), in which 38 (0.95%) osseous sarcomas were identified in the 3964 patients with a diagnosis of Paget disease during a 50 year period (1927–1977). Of the 38 sarcomas, 32 (84%) were osteosarcoma, and while this is the most frequently encountered sarcoma identified with Paget disease of bone (73–84%), fibrosarcoma (9–16%), chondrosarcoma (14%), and malignant fibrous histiocytoma (5%) have also been noted (Wick et al. 1981; Moore et al. 1991).

While the figure of 1% is a reasonable estimate of the prevalence of malignant transformation, one must

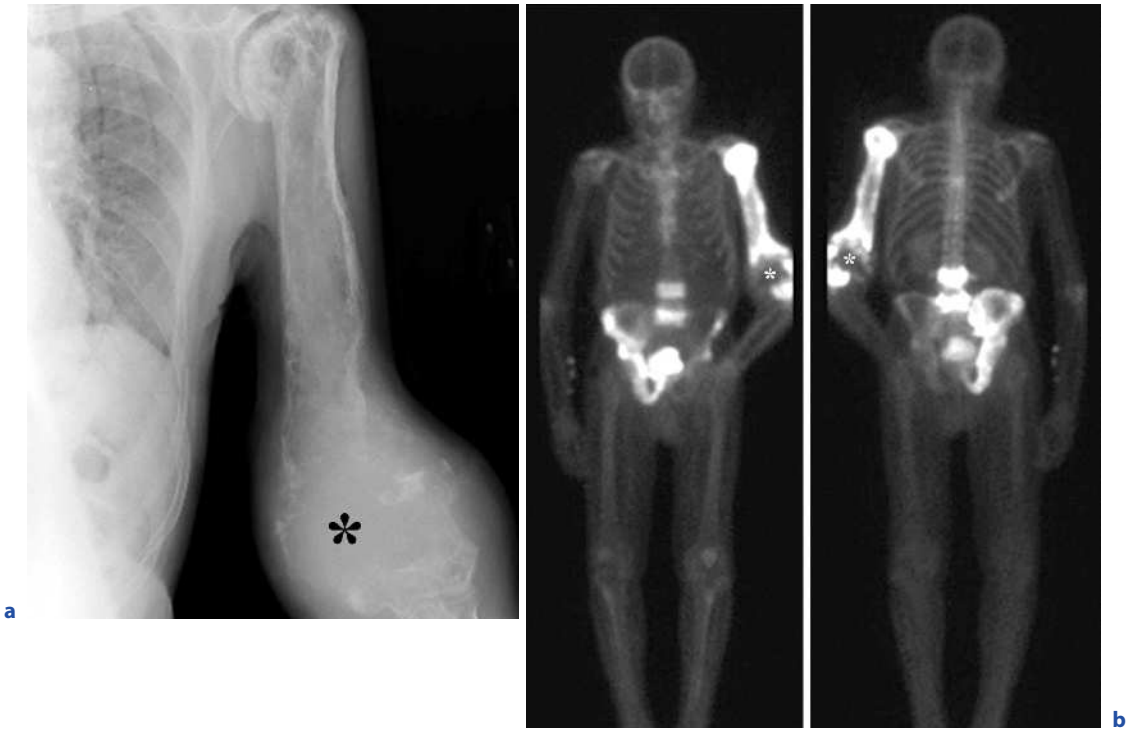

Fig. 14.41a,b. Secondary osteosarcoma associated with Paget disease. **a** Anteroposterior radiograph shows a focal destructive lytic process (*asterisk*) in the distal humerus with an associated soft tissue mass. Note absence of osteoid matrix and periosteal reaction. **b** Anterior and posterior delayed static images from bone scintigraphy show Pegetoid changes in the pelvis, spine and left humerus. Note focus of decreased traced accumulation (*asterisk*) at the tumor site

remember that Paget disease of bone shows geographic and ethnic trends; it is rare in Scandinavia, India, and the Far East, while it is common in Great Britain and Western Europe (Hansen et al. 2006). In addition, the frequency of transformation varies with the degree of skeletal involvement; reports range from 0.2% in patients having limited involvement, to as much as 7.5% in those patients having extensive skeletal manifestations (Porretta et al. 1957).

Patients with malignant transformation in association with Paget disease most frequently present with pain (90%) and a palpable associated mass; pathologic fracture is reported in 14–32% of patients (Greditzer et al. 1983; Smith et al. 1984; Moore et al. 1991; Hansen et al. 2006). Radiographs reveal a destructive process which is most often lytic (50–65%), or less commonly, mixed or blastic, and an associated soft tissue mass. In contradistinction to primary osteosarcoma, this is usually without associated periosteal reaction (Fig. 14.41) (Smith et al. 1984; Hansen et al. 2006).

The overall prognosis for Paget sarcoma is quite poor, with patients having a 5-year survival rate of only 5–8%; the Mayo Clinic series reported 29% of patients having metastatic disease at the time of presentation (Moore et al. 1991; Hansen et al. 2006). It is important to remember that not all soft-tissue masses associated with Paget disease represent malignant transformation. A rarely reported entity termed *pseudosarcoma* has also been noted in Paget disease, representing florid Paget disease with exuberant, associated, benign periosteal bone formation and soft-tissue mass (Tins et al. 2001). Differentiation of benign, pagetic pseudosarcomatous proliferation from sarcomatous degeneration may require biopsy.

14.6.2 Radiation Induced Osteosarcoma

Radiation induced sarcoma is the most dreaded complication following radiotherapy, occurring much more frequently in soft tissue than in bone (2.3:1) (Lagrange et al. 2000). When it occurs in bone, osteosarcoma is the most frequently encountered radiation induced malignancy, representing 3–5% of all osteosarcomas and 50–60% of all radiation induced sarcomas

(Forest et al. 2002). Malignant fibrous histiocytoma is a distant second at about 20% (Arlen et al. 1971; Kim JH et al. 1978; Lorigan et al. 1989; Lagrange et al. 2000). Overall, radiation induced osteosarcoma is a relatively rare lesion having an estimated prevalence of 0.02–4%, developing following an exposure of usually greater than 1,000 cGy (Garner et al. 2009). There is great variability in the reported latent period for radiation induced sarcoma, although it generally ranges between 4 to 30 years, with a mean of 8 to 12 years. In general, osseous lesions have a longer latency period than soft tissue lesions. The reported radiation dose is also quite variable, but in general the mean reported dose is about 50 Gy, in keeping with current therapeutic practices (Garner et al. 2009).

14.6.3 Osteosarcoma Associated with Other Benign Lesions

Osteosarcoma may also complicate other benign processes, with or without previous radiation, including fibrous dysplasia, bone infarct, osteogenesis imperfecta, multiple hereditary exostoses, chronic osteomyelitis, and osteoblastoma (Fig. 14.42) (Mirra 1989a).

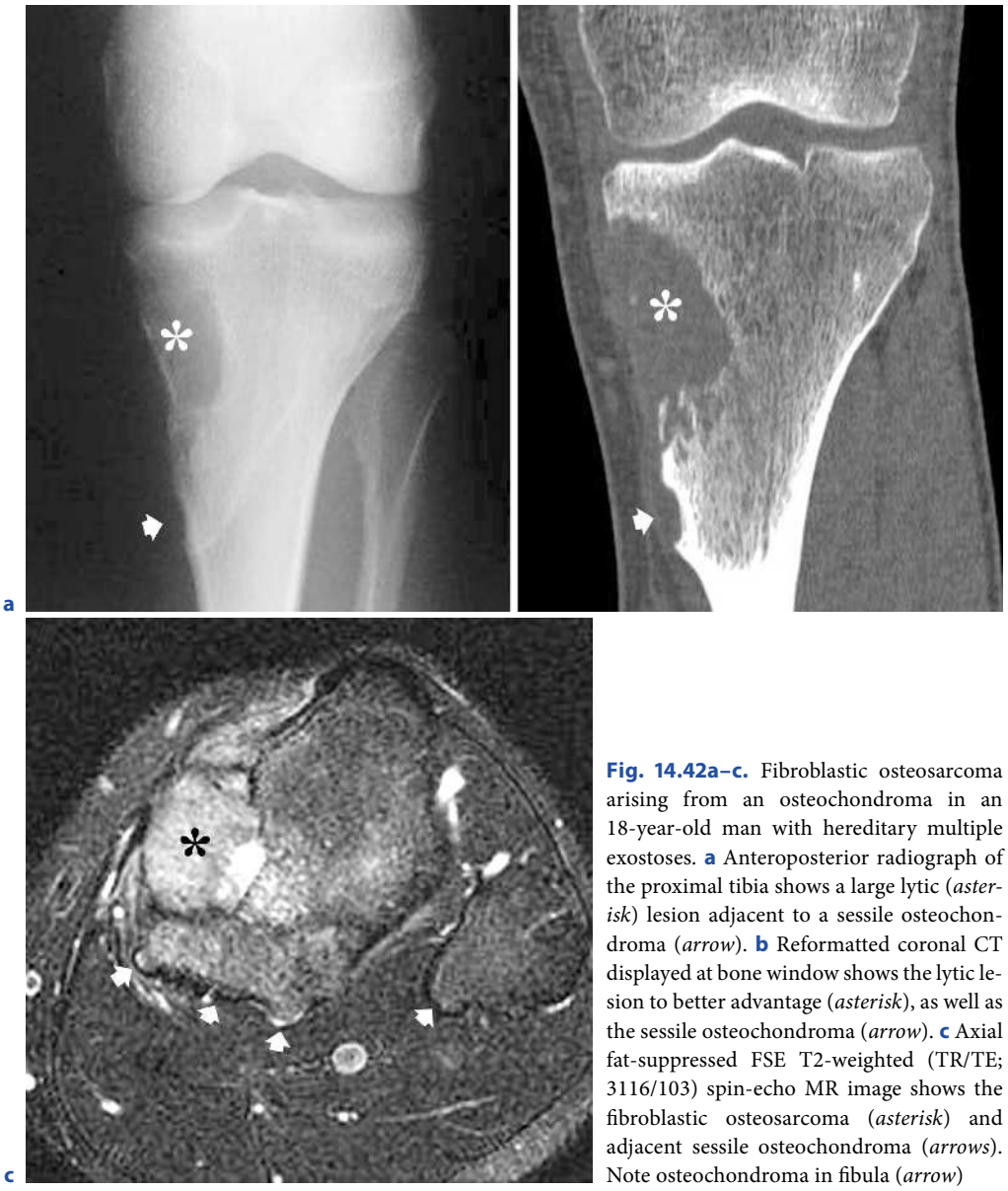

Fig. 14.42a–c. Fibroblastic osteosarcoma arising from an osteochondroma in an 18-year-old man with hereditary multiple exostoses. **a** Anteroposterior radiograph of the proximal tibia shows a large lytic (*asterisk*) lesion adjacent to a sessile osteochondroma (*arrow*). **b** Reformatted coronal CT displayed at bone window shows the lytic lesion to better advantage (*asterisk*), as well as the sessile osteochondroma (*arrow*). **c** Axial fat-suppressed FSE T2-weighted (TR/TE; 3116/103) spin-echo MR image shows the fibroblastic osteosarcoma (*asterisk*) and adjacent sessile osteochondroma (*arrows*). Note osteochondroma in fibula (*arrow*)

14.6.4 Osteosarcomatosis

Osteosarcomatosis (also known as *multifocal osteosarcoma* or *multiple sclerotic osteosarcoma*) describes a condition in which there are multiple intraosseous foci of osteosarcoma at the time of presentation. Previous investigators have considered osteosarcomatosis to represent multicentric primary neoplasia (Amstutz 1969). More recently, it has been suggested that all cases of osteosarcomatosis represent rapidly progressive metastatic disease (Jeffree et al. 1975; Hopper et al. 1990). Although the latter concept is still somewhat controversial, we strongly endorse it, based on the identification of a radiographically dominant (large) lesion in virtually all patients having otherwise symmetric disease. In addition, the presence of pulmonary metastases is evident on chest CT scans in the majority of these patients.

Osteosarcomatosis is uncommon, accounting for approximately 3–4% of osteosarcoma cases (Amstutz 1969; Jeffree et al. 1975; Mahoney et al. 1979; Mirra 1989a; Hopper et al. 1990; Olson et al. 1991; Resnick et al. 2002c). However, multifocal skeletal involvement by osteosarcoma has been found at autopsy in as many as 48% of patients (Jeffree et al. 1975; Hopper et al. 1990). Although osteosarcomatosis has been believed to be more common in skeletally immature patients, Hopper et al. (1990) reported a series of 29 cases in which there were relatively equal numbers of skeletally immature and mature patients. Younger, skeletally immature patients tend to have rapidly appearing, usually symmetric, sclerotic lesions, whereas older patients typically have fewer, asymmetric sclerotic lesions. In 97% of those cases reported by Hopper et al. (1990), a radiologically dominant skeletal tumor was seen. The radiologic features of the dominant lesion include ill-defined margins, aggressive periosteal reaction, cortical disruption, and adjacent soft-tissue extension (Amstutz 1969; Parham et al. 1985; Hopper et al. 1990; Olson et al. 1991). Although lesions usually contain cloudlike osteoid (Fig. 14.43), purely lytic dominant lesions may be seen. In contrast to the dominant lesions, the secondary foci are often smaller, more sclerotic, better defined and lack periosteal reaction or cortical destruction. The existence of multifocal skeletal osteo-

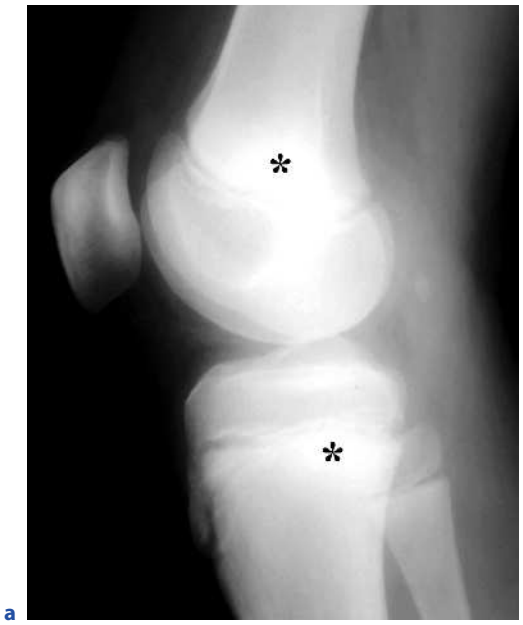

a

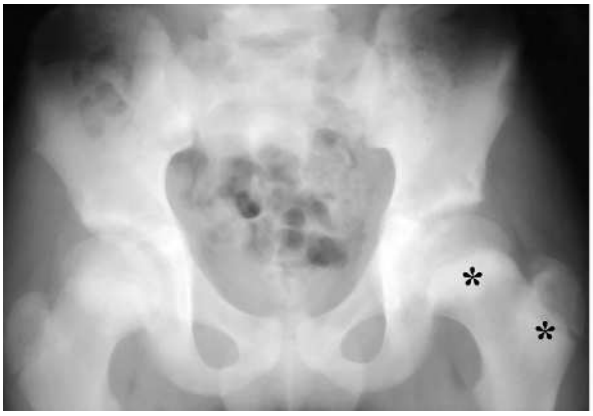

b

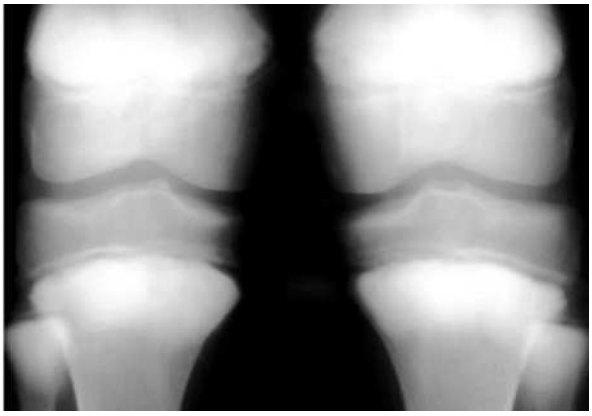

c

Fig. 14.43a–f. Osteochondromatosis in a 12-year-old boy presenting with knee pain. **a** Lateral radiograph of the knee shows subtle metaphyseal sclerosis (*asterisks*). **b** Anteroposterior radiograph of the pelvis obtained 4-weeks following initial presentation shows prominent sclerosis at multiple metaphyses (*asterisks*). **c** Anteroposterior radiograph of both knees, done at the same time as **b**, shows the rapid progression of the metaphyseal sclerosis. **d–f** *see next page*

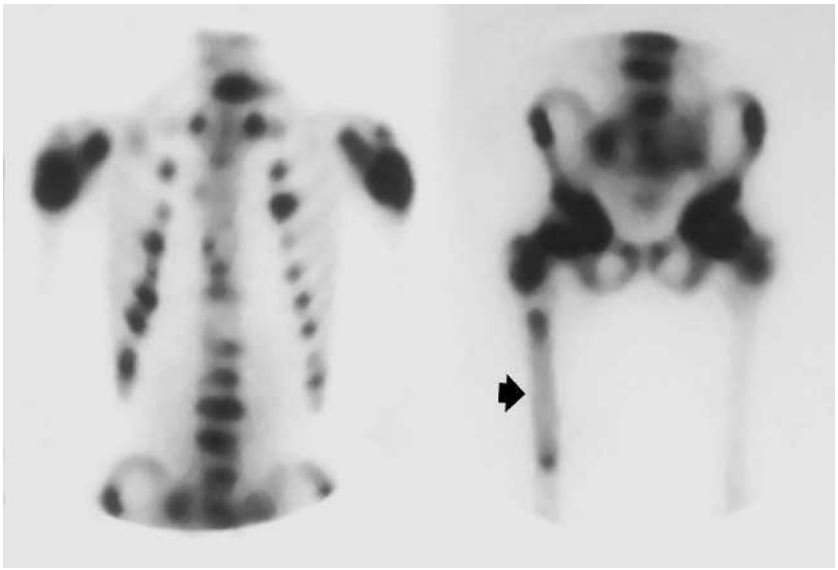

d

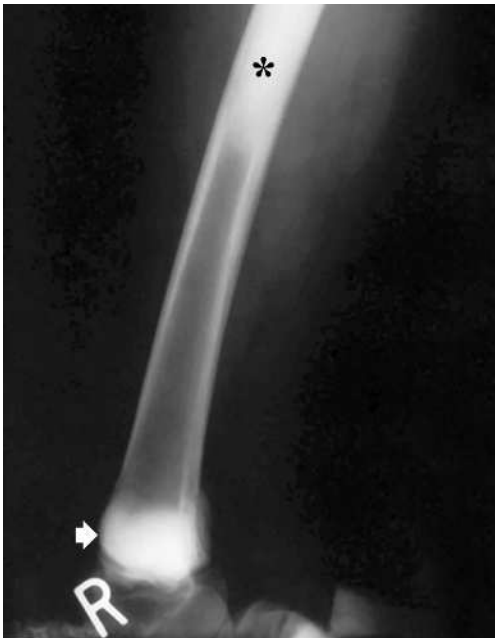

e

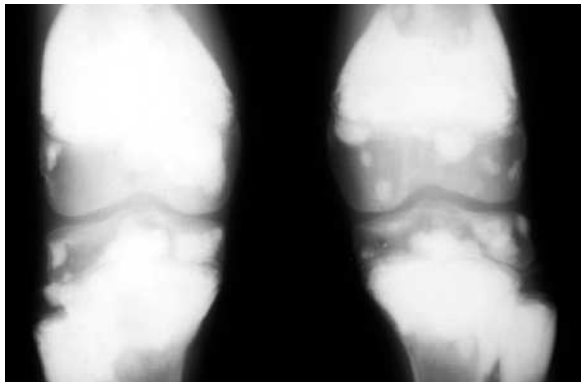

f

Fig. 14.43a–f. (*continued*) Osteochondromatosis in a 12-year-old boy presenting with knee pain. **d** Bone scintigraphy shows the marked extend of the metastatic disease, with a dominant lesion in the right femur (*arrow*). **e** Corresponding lateral radiograph of the right femur shows the dominant femoral lesion (*asterisk*) with metaphyseal metastasis (*white arrow*). **f** Radiograph of the knees at autopsy shows extensive metastatic involvement

sarcoma substantially alters both treatment and anticipated prognosis. In a report of nine patients, Parham et al. (1985) noted that, despite intensive chemotherapy, all patients died, with a mean survival of 12 months (range, 6–37 months).

14.7 Summary

Osseous tumors are common. Osteosarcoma is the most common primary malignant bone tumor in children. Its radiologic appearances vary over a wide spectrum. We have reviewed the radiologic and pathologic features of the various types of primary osteosarcoma, including intramedullary (high grade, telangiectatic, low grade, small cell, osteosarcomatosis, and gnathic), surface (intracortical, parosteal, periosteal, and high grade surface), and secondary lesions. The radiographic appearances of these lesions are often characteristic and suggestive of the specific diagnosis. Perhaps more important, additional imaging modalities, including bone scintigraphy, CT, and MR imaging, provide vital information for preoperative staging in planning surgical management. Radiologic examination also allows evaluation of tumor

response to chemotherapy, identification of metastatic disease, and postoperative evaluation of recurrent neoplasm, all of which have important prognostic implications. Recognition of these imaging features is an important guide to our clinical colleagues throughout the often difficult and complex treatment of patients with osteosarcoma and results in improved clinical outcome.

Benign osseous tumors are also common, representing 17% of all benign primary lesions of bone. While osteoid osteoma and osteoblastoma can have similar histological features, they are considered to be separate and distinct lesions with different clinical presentations and natural histories. Of these benign osseous lesions, osteoid osteoma is four times more common than osteoblastoma.

While not considered a neoplasm, enostosis is overwhelmingly the most frequently encountered osseous lesion; one that possesses an imaging appearance which is almost always characteristic. Osteoma, while much rarer, also has diagnostic imaging features, and shares the same nonneoplastic classification.

References

Amstutz HC (1969) Multiple osteogenic sarcomata–metastatic or multicentric? Report of two cases and review of literature. Cancer 24:923–931

Arlen M, Higinbotham NL, Huvos AG, Marcove RC, Miller T, Shah IC (1971) Radiation-induced sarcoma of bone. Cancer 28:1087–1099

Assoun J, Richardi G, Railhac JJ, Baunin C, Fajadet P, Giron J, Maquin P, Haddad J, Bonnevialle P (1994) Osteoid osteoma: MR imaging versus CT. Radiology 191:217–223

Avery GR, Wilsdon JB, Malcolm AJ (1995) Giant bone island with some central resorption. Skeletal Radiol 24:59–60

Ayala AG, Ro JY, Raymond AK, Jaffe N, Chawla S, Carrasco H, Link M, Jimenez J, Edeiken J, Wallace S, et al. (1989) Small cell osteosarcoma. A clinicopathologic study of 27 cases. Cancer 64:2162–2173

Ayala AG, Raymond AK, Czerniak B, Knuutila S (2002) Periosteal osteosarcoma. In: Fletcher DM, Unni KK, Mertens F (eds) WHO classification of tumors. Pathology and genetics: tumors of soft tissue and bone. IARC Press, Lyon, France, pp 282–283

Azouz EM, Kozlowski K, Marton D, Sprague P, Zerhouni A, Asselah F (1986) Osteoid osteoma and osteoblastoma of the spine in children. Report of 22 cases with brief literature review. Pediatr Radiol 16:25–31

Bacci G, Picci P, Ferrari S, Sangiorgi L, Zanone A, Brach del Prever A (1994) Primary chemotherapy and delayed surgery for non-metastatic telangiectatic osteosarcoma of the extremities. Results in 28 patients. Eur J Cancer 30A:620–626

Berry M, Mankin H, Gebhardt M, Rosenberg A, Hornicek F (2008) Osteoblastoma: a 30-year study of 99 cases. J Surg Oncol 98:179–183

Bertoni F, Present D, Bacchini P, Pignatti G, Picci P, Campanacci M (1989) The Istituto Rizzoli experience with small cell osteosarcoma. Cancer 64:2591–2599

Campanacci M, Picci P, Gherlinzoni F, Guerra A, Bertoni F, Neff JR (1984) Parosteal osteosarcoma. J Bone Joint Surg Br 66:313–321

Capanna R, Van Horn JR, Ayala A, Picci P, Bettelli G (1986) Osteoid osteoma and osteoblastoma of the talus. A report of 40 cases. Skeletal Radiol 15:360–364

Cerase A, Priolo F (1998) Skeletal benign bone-forming lesions. Eur J Radiol 27 Suppl 1:S91–97

Chew FS, Hudson TM (1982) Radionuclide bone scanning of osteosarcoma: falsely extended uptake patterns. AJR Am J Roentgenol 139:49–54

Clark JL, Unni KK, Dahlin DC, Devine KD (1983) Osteosarcoma of the jaw. Cancer 51:2311–2316

Codman EA (1926) Registry of bone sarcoma. Part I – Twenty-five criteria for establishing the diagnosis of osteogenic sarcoma. Part II – Thirteen registered cases of "five year cures" analyzed according to these criteria. Surg Gynecol Obstet 42:381–393

Corbett JM, Wilde AH, McCormack LJ, Evarts CM (1974) Intra-articular osteoid osteoma; a diagnostic problem. Clin Orthop Relat Res 225–230

Crim JR, Mirra JM, Eckardt JJ, Seeger LL (1990) Widespread inflammatory response to osteoblastoma: the flare phenomenon. Radiology 177:835–836

Cronemeyer RL, Kirchmer NA, De Smet AA, Neff JR (1981) Intra-articular osteoid-osteoma of the humerus simulating synovitis of the elbow. A case report. J Bone Joint Surg Am 63:1172–1174

Dahlin DC, Coventry MB (1967) Osteogenic sarcoma. A study of six hundred cases. J Bone Joint Surg Am 49:101–110

Dale S, Breidahl WH, Baker D, Robbins PD, Sundaram M (2001) Severe toxic osteoblastoma of the humerus associated with diffuse periostitis of multiple bones. Skeletal Radiol 30:464–468

deSantos LA, Murray JA, Finklestein JB, Spjut HJ, Ayala AG (1978) The radiographic spectrum of periosteal osteosarcoma. Radiology 127:123–129

Destian S, Hernanz-Schulman M, Raskin K, Genieser N, Becker M, Crider R, Greco MA (1988) Case report 468. Epiphyseal osteoid osteoma distal end of femur. Skeletal Radiol 17:141–143

Destouet JM, Gilula LA, Murphy WA (1979) Computed tomography of long-bone osteosarcoma. Radiology 131:439–445

Dorfman HD, Czerniak B (1995) Bone cancers. Cancer 75:203–210

Dorfman HD, Weiss SW (1984) Borderline osteoblastic tumors: problems in the differential diagnosis of aggressive osteoblastoma and low-grade osteosarcoma. Semin Diagn Pathol 1:215–234

Dorfman HD, Czerniak R, Kootz R (2002) WHO classification of tumors of bone: introduction. In: Fletcher DM, Unni KK, Mertens F (eds) WHO classification of tumors. Pathology and genetics: tumors of soft tissue and bone. IARC Press, Lyon, France, pp 227–232

Dunlap H, Martin DJ (1985) Osteoid osteoma of the femoral head. Pediatr Radiol 15:262–263

Ebrahim FS, Jacobson JA, Lin J, Housner JA, Hayes CW, Resnick D (2001) Intraarticular osteoid osteoma: sonographic findings in three patients with radiographic, CT, and MR imaging correlation. AJR Am J Roentgenol 177:1391–1395

Eckel W, Palm D (1959) [Statistical and roentgenological studies on some problems of osteoma of the paranasal sinuses.]. Arch Ohren Nasen Kehlkopfheilkd 174:440–457

Edeiken J, DePalma AF, Hodes PJ (1966) Osteoid osteoma. (Roentgenographic emphasis). Clin Orthop Relat Res 49:201–206

Edeiken J, Raymond AK, Ayala AG, Benjamin RS, Murray JA, Carrasco HC (1987) Small-cell osteosarcoma. Skeletal Radiol 16:621–628

Ehara S, Rosenthal DI, Aoki J, Fukuda K, Sugimoto H, Mizutani H, Okada K, Hatori M, Abe M (1999) Peritumoral edema in osteoid osteoma on magnetic resonance imaging. Skeletal Radiol 28:265–270

Ellis JH, Siegel CL, Martel W, Weatherbee L, Dorfman H (1988) Radiologic features of well-differentiated osteosarcoma. AJR Am J Roentgenol 151:739–742

Enneking WF, Kagan A (1975) "Skip" metastases in osteosarcoma. Cancer 36:2192–2205

Ewing J (1922) A review and classification of bone sarcomas. Ann Surg 4:483–533

Farr GH, Huvos AG, Marcove RC, Higinbotham NL, Foote FW Jr (1974) Telangiectatic osteogenic sarcoma. A review of twenty-eight cases. Cancer 34:1150–1158

Finkelstein JB (1970) Osteosarcoma of the jaw bones. Radiol Clin North Am 8:425–443

Fletcher DM, Unni KK, Mertens F (2002) Osteogenic tumors. In: Fletcher DM, Unni KK, Mertens F (eds) WHO classification of tumors. Pathology and genetics: tumors of soft tissue and bone. IARC Press, Lyon, France, p 258

Forest M, De Pinieux G, Knuutila S (2002) Secondary osteosarcoma. In: Fletcher DM, Unni KK, Mertens F (eds) WHO classification of tumors. Pathology and genetics: tumors of soft tissue and bone. IARC Press, Lyon, France, pp 277–278

Freiberger RH, Loitman BS, Helpern M, Thompson TC (1959) Osteoid osteoma; a report on 80 cases. Am J Roentgenol Radium Ther Nucl Med 82:194–205

Gamba JL, Martinez S, Apple J, Harrelson JM, Nunley JA (1984) Computed tomography of axial skeletal osteoid osteomas. AJR Am J Roentgenol 142:769–772

Gardner EJ, Richards RC (1953) Multiple cutaneous and subcutaneous lesions occurring simultaneously with hereditary polyposis and osteomatosis. Am J Hum Genet 5:139–147

Garner HW, Kransdorf MJ, Bancroft LW, Peterson JJ, Berquist TH, Murphey MD (2009) Benign and malignant soft-tissue tumors: posttreatment MR imaging. Radiographics 29:119–134

Garrington GE, Scofield HH, Cornyn J, Hooker SP (1967) Osteosarcoma of the jaws. Analysis of 56 cases. Cancer 20:377–391

Gaylord HR (1903) On the pathology of so-called bone aneurisms. Ann Surg 37:834–847

Geschickter CF, Copeland MM (1951) Parosteal osteoma of bone: a new entity. Ann Surg 133:790–807

Ghandur-Mnaymneh L, Mnaymneh WA, Puls S (1983) The incidence and mechanism of transphyseal spread of osteosarcoma of long bones. Clin Orthop Relat Res 210–215

Glass RB, Poznanski AK, Fisher MR, Shkolnik A, Dias L (1986) MR imaging of osteoid osteoma. J Comput Assist Tomogr 10:1065–1067

Glasser DB, Lane JM, Huvos AG, Marcove RC, Rosen G (1992) Survival, prognosis, and therapeutic response in osteogenic sarcoma. The Memorial Hospital experience. Cancer 69:698–708

Glynn JJ, Lichtenstein L (1973) Osteoid-osteoma with multicentric nidus. A report of two cases. J Bone Joint Surg Am 55:855–858

Gold RH, Mirra JM, Remotti F, Pignatti G (1989) Case report 527: Giant bone island of tibia. Skeletal Radiol 18:129–132

Goldberg VM, Jacobs B (1975) Osteoid osteoma of the hip in children. Clin Orthop Relat Res 41–47

Goorin AM, Abelson HT, Frei E III (1985) Osteosarcoma: fifteen years later. N Engl J Med 313:1637–1643

Greditzer HG III, McLeod RA, Unni KK, Beabout JW (1983) Bone sarcomas in Paget disease. Radiology 146:327–333

Greene FL, Page DL, Fleming ID, Fritz AG, Balch CM, Haller OG, Morrow M (2002) AJCC cancer staging manual. Springer, Berlin Heidelberg New York

Greenspan A (1993) Benign bone-forming lesions: osteoma, osteoid osteoma, and osteoblastoma. Clinical, imaging, pathologic, and differential considerations. Skeletal Radiol 22:485–500

Greenspan A (1995) Bone island (enostosis): current concept – a review. Skeletal Radiol 24:111–115

Greenspan A, Stadalnik RC (1995) Bone island: scintigraphic findings and their clinical application. Can Assoc Radiol J 46:368–379

Greenspan A, Steiner G, Knutzon R (1991) Bone island (enostosis): clinical significance and radiologic and pathologic correlations. Skeletal Radiol 20:85–90

Greenspan A, Elguezabel A, Bryk D (1974) Multifocal osteoid osteoma. A case report and review of the literature. Am J Roentgenol Radium Ther Nucl Med 121:103–106

Griffith JF, Kumta SM, Chow LT, Leung PC, Metreweli C (1998) Intracortical osteosarcoma. Skeletal Radiol 27:228–232

Hall FM, Goldberg RP, Davies JA, Fainsinger MH (1980) Scintigraphic assessment of bone islands. Radiology 135:737–742

Hameed M (2007) Small round cell tumors of bone. Arch Pathol Lab Med 131:192–204
Hansen MF, Seton M, Merchant A (2006) Osteosarcoma in Paget's disease of bone. J Bone Miner Res 21 Suppl 2:P58–63
Hasegawa T, Shimoda T, Yokoyama R, Beppu Y, Hirohashi S, Maeda S (1999) Intracortical osteoblastic osteosarcoma with oncogenic rickets. Skeletal Radiol 28:41–45
Healey JH, Ghelman B (1986) Osteoid osteoma and osteoblastoma. Current concepts and recent advances. Clin Orthop Relat Res 76–85
Helms CA (1987) Osteoid osteoma. The double density sign. Clin Orthop Relat Res 167–173
Helms CA, Hattner RS, Vogler JB III (1984) Osteoid osteoma: radionuclide diagnosis. Radiology 151:779–784
Hermann G, Klein MJ, Springfield D, Abdelwahab IF, Dan SJ (2002) Intracortical osteosarcoma; two-year delay in diagnosis. Skeletal Radiol 31:592–596
Hopper KD, Moser RP Jr., Haseman DB, Sweet DE, Madewell JE, Kransdorf MJ (1990) Osteosarcomatosis. Radiology 175:233–239
Houang B, Grenier N, Greselle JF, Vital JM, Douws C, Broussin J, Caille JM (1990) Osteoid osteoma of the cervical spine. Misleading MR features about a case involving the uncinate process. Neuroradiology 31:549–551
Houghton MJ, Heiner JP, De Smet AA (1995) Osteoma of the innominate bone with intraosseous and parosteal involvement. Skeletal Radiol 24:455–457
Huvos AG, Rosen G, Bretsky SS, Butler A (1982) Telangiectatic osteogenic sarcoma: a clinicopathologic study of 124 patients. Cancer 49:1679–1689
Inwards CY, Knuutila S (2002) Low grade central osteosarcoma. In: Fletcher DM, Unni KK, Mertens F (eds) WHO classification of tumors. Pathology and genetics: tumors of soft tissue and bone. IARC Press, Lyon, France, pp 275–276
Jackson RP, Reckling FW, Mants FA (1977) Osteoid osteoma and osteoblastoma. Similar histologic lesions with different natural histories. Clin Orthop Relat Res 303–313
Jaffe HL (1935) Osteoid osteoma: a benign osteoblastic tumor composed of osteoid and atypical bone. Arch Surg 31:709–728
Jaffe HL (1945) Osteoid osteoma of bone. Radiology 45:319–334
Jaffe HL (1956) Benign osteoblastoma. Bull Hosp Joint Dis 17:141–151
Jaffe HL (1958) Tumors and toumorous conditions of the bones and joints. Lea & Febiger, Philadelphia
Jaffe HL (1960) Intracortical osteogenic sarcoma. Bull Hosp Joint Dis 21:189–197
Jaffe HL, Lichtenstein L (1940) Osteoid osteoma: further experience with this benign tumor of bone. J Bone Joint Surg 22:645–682
Jaffe HL, Mayer L (1932) An osteoblastic-osteoid tissue forming tumor of a metacarpal bone. Arch Surg 24:550–564
Jeffree GM, Price CH, Sissons HA (1975) The metastatic patterns of osteosarcoma. Br J Cancer 32:87–107
Jelinek JS, Murphey MD, Kransdorf MJ, Shmookler BM, Malawer MM, Hur RC (1996) Parosteal osteosarcoma: value of MR imaging and CT in the prediction of histologic grade. Radiology 201:837–842
Kager L, Zoubek A, Kastner U, Kempf-Bielack B, Potratz J, Kotz R, Exner GU, Franzius C, Lang S, Maas R, Jurgens H, Gadner H, Bielack S (2006) Skip metastases in osteosarcoma: experience of the Cooperative Osteosarcoma Study Group. J Clin Oncol 24:1535–1541
Kalil R, Bridge JA (2002) Small cell osteosarcoma. In: Fletcher DM, Unni KK, Mertens F (eds) WHO classification of tumors. Pathology and genetics: tumors of soft tissue and bone. IARC Press, Lyon, France, pp 273–274
Kattapuram SV, Kushner DC, Phillips WC, Rosenthal DI (1983) Osteoid osteoma: an unusual cause of articular pain. Radiology 147:383–387
Kaufman RA, Towbin RB (1981) Telangiectatic osteosarcoma simulating the appearance of an aneurysmal bone cyst. Pediatr Radiol 11:102–104
Kayser F, Resnick D, Haghighi P, Pereira Edo R, Greenway G, Schweitzer M, Kindynis P (1998) Evidence of the subperiosteal origin of osteoid osteomas in tubular bones: analysis by CT and MR imaging. AJR Am J Roentgenol 170:609–614
Kendrick JI, Evarts CM (1967) Osteoid-osteoma: a critical analysis of 40 tumors. Clin Orthop Relat Res 54:51–59
Keret D, Harcke HT, MacEwen GD, Bowen JR (1989) Multiple osteoid osteomas of the fifth lumbar vertebra. A case report. Clin Orthop Relat Res 163–168
Kim JH, Chu FC, Woodard HQ, Melamed MR, Huvos A, Cantin J (1978) Radiation-induced soft-tissue and bone sarcoma. Radiology 129:501–508
Kim SK, Barry WF Jr (1964) Bone Island. Am J Roentgenol Radium Ther Nucl Med 92:1301–1306
Klein MJ, Parisien MV, Schneider-Stock R (2002) Osteoid osteoma. In: Fletcher DM, Unni KK, Mertens F (eds) WHO classification of tumors. Pathology and genetics: tumors of soft tissue and bone. IARC Press, Lyon, France, pp 260–261
Kransdorf MJ, Stull MA, Gilkey FW, Moser RP Jr (1991) Osteoid osteoma. Radiographics 11:671–696
Kroon HM, Schurmans J (1990) Osteoblastoma: clinical and radiologic findings in 98 new cases. Radiology 175:783–790
Kumar R, Guinto FC Jr, Madewell JE, David R, Shirkhoda A (1988) Expansile bone lesions of the vertebra. Radiographics 8:749–769
Kumar SJ, Harcke HT, MacEwen GD, Ger E (1984) Osteoid osteoma of the proximal femur: new techniques in diagnosis and treatment. J Pediatr Orthop 4:669–672
Kurt AM, Unni KK, McLeod RA, Pritchard DJ (1990) Low-grade intraosseous osteosarcoma. Cancer 65:1418–1428
Kyriakos M (1980) Intracortical osteosarcoma. Cancer 46:2525–2533

Lagrange JL, Ramaioli A, Chateau MC, Marchal C, Resbeut M, Richaud P, Lagarde P, Rambert P, Tortechaux J, Seng SH, de la Fontan B, Reme-Saumon M, Bof J, Ghnassia JP, Coindre JM (2000) Sarcoma after radiation therapy: retrospective multiinstitutional study of 80 histologically confirmed cases. Radiation Therapist and Pathologist Groups of the Federation Nationale des Centres de Lutte Contre le Cancer. Radiology 216:197–205

Lambiase RE, Levine SM, Terek RM, Wyman JJ (1998) Long bone surface osteomas: imaging features that may help avoid unnecessary biopsies. AJR Am J Roentgenol 171:775–778

Lee YY, Van Tassel P, Nauert C, Raymond AK, Edeiken J (1988) Craniofacial osteosarcomas: plain film, CT, and MR findings in 46 cases. AJR Am J Roentgenol 150:1397–1402

Leiberman A, Tovi F (1984) A small osteoma of the frontal sinus causing headaches. J Laryngol Otol 98:1147–1149

Levine E, De Smet AA, Huntrakoon M (1985) Juxtacortical osteosarcoma: a radiologic and histologic spectrum. Skeletal Radiol 14:38–46

Lichtenstein L (1956) Benign osteoblastoma: a category of osteoid-and-bone forming tumors other than classical osteoid osteoma, which may be mistaken for giant-cell tumor or osteogenic sarcoma. Cancer 9:1044–1052

Liu PT, Chivers FS, Roberts CC, Schultz CJ, Beauchamp CP (2003) Imaging of osteoid osteoma with dynamic gadolinium-enhanced MR imaging. Radiology 227:691–700

Lorigan JG, Libshitz HI, Peuchot M (1989) Radiation-induced sarcoma of bone: CT findings in 19 cases. AJR Am J Roentgenol 153:791–794

Lucas DR, Unni KK, McLeod RA, O'Connor MI, Sim FH (1994) Osteoblastoma: clinicopathologic study of 306 cases. Hum Pathol 25:117–134

Mahoney JP, Spanier SS, Morris JL (1979) Multifocal osteosarcoma: a case report with review of the literature. Cancer 44:1897–1907

Malawer MM, Dunham WK (1983) Skip metastases in osteosarcoma: recent experience. J Surg Oncol 22:236–245

Malcolm AJ, Schiller AL, Schneider-Sock R (2002) Osteoblastoma. In: Fletcher DM, Unni KK, Mertens F (eds) WHO classification of tumors. Pathology and genetics: tumors of soft tissue and bone. IARC Press, Lyon, France, pp 262–263

Martin NL, Preston DF, Robinson RG (1976) Osteoblastomas of the axial skeleton shown by skeletal scanning: case report. J Nucl Med 17:187–189

Matsuno T, Unni KK, McLeod RA, Dahlin DC (1976) Telangiectatic osteogenic sarcoma. Cancer 38:2538–2547

Matsuno T, Okada K, Knuutila S (2002) Telangiectatic osteosarcoma. In: Fletcher DM, Unni KK, Mertens F (eds) WHO classification of tumors. Pathology and genetics: tumors of soft tissue and bone. IARC Press, Lyon, France, pp 271–272

Mayer L (1967) Malignant degeneration of so-called benign osteoblastoma. Bull Hosp Joint Dis 28:4–13

McCarthy EF (1995) The registry of bone sarcoma. A history. Iowa Orthop J 15:74–78

McConnell JR, Daneman A (1984) Fatty replacement of muscles adjacent to spinal osteoid osteoma. J Comput Assist Tomogr 8:147–148

McLeod RA, Dahlin DC, Beabout JW (1976) The spectrum of osteoblastoma. AJR Am J Roentgenol 126:321–325

Mervak TR, Unni KK, Pritchard DJ, McLeod RA (1991) Telangiectatic osteosarcoma. Clin Orthop Relat Res 135–139

Miller CW, McLaughlin RE (1977) Osteosarcoma in siblings. Report of two cases. J Bone Joint Surg Am 59:261–262

Mirra JM (1989a) Osseous tumors of intramedullary origin. In: Mirra JM (ed) Bone tumors: clinical, radiologic, and pathologic correlations. Lea & Febiger, Philadelphia, pp 248–438

Mirra JM (1989b) Parosteal tumors. In: Mirra JM (ed) Bone tumors: clinical, radiologic, and pathologic correlations. Lea & Febiger, Philadelphia, pp 1587–1753

Mirra JM, Cove K, Theros E, Paladugu R, Smasson J (1979) A case of osteoblastoma associated with severe systemic toxicity. Am J Surg Pathol 3:463–471

Mirra JM, Dodd L, Johnston W, Frost DB, Barton D (1991) Case report 700: Primary intracortical osteosarcoma of femur, sclerosing variant, grade 1 to 2 anaplasia. Skeletal Radiol 20:613–616

Mitnick JS, Braunstein P, Genieser NB (1979) Osteoid osteoma of the hip: unusual isotopic appearance. AJR Am J Roentgenol 133:322–323

Moore TE, King AR, Kathol MH, el-Khoury GY, Palmer R, Downey PR (1991) Sarcoma in Paget disease of bone: clinical, radiologic, and pathologic features in 22 cases. AJR Am J Roentgenol 156:1199–1203

Morton KS, Bartlett LH (1966) Benign osteoblastic change resembling osteoid osteoma. Three cases with unusual radiological features. J Bone Joint Surg Br 48:478–484

Murphey MD, Andrews CL, Flemming DJ, Temple HT, Smith WS, Smirniotopoulos JG (1996) From the archives of the AFIP. Primary tumors of the spine: radiologic pathologic correlation. Radiographics 16:1131–1158

Murphey MD, Robbin MR, McRae GA, Flemming DJ, Temple HT, Kransdorf MJ (1997) The many faces of osteosarcoma. Radiographics 17:1205–1231

Murphey MD, wan Jaovisidha S, Temple HT, Gannon FH, Jelinek JS, Malawer MM (2003) Telangiectatic osteosarcoma: radiologic-pathologic comparison. Radiology 229:545–553

Murphey MD, Jelinek JS, Temple HT, Flemming DJ, Gannon FH (2004) Imaging of periosteal osteosarcoma: radiologic-pathologic comparison. Radiology 233:129–138

Nakajima H, Sim FH, Bond JR, Unni KK (1997) Small cell osteosarcoma of bone. Review of 72 cases. Cancer 79:2095–2106

Nogues P, Marti-Bonmati L, Aparisi F, Saborido MC, Garci J, Dosda R (1998) MR imaging assessment of juxta cortical edema in osteoid osteoma in 28 patients. Eur Radiol 8:236–238

Norman A (1978) Persistence or recurrence of pain: a sign of surgical failure is osteoid-osteoma. Clin Orthop Relat Res 263–266

Norman A, Abdelwahab IF, Buyon J, Matzkin E (1986) Osteoid osteoma of the hip stimulating an early onset of osteoarthritis. Radiology 158:417–420

Norton KI, Hermann G, Abdelwahab IF, Klein MJ, Granowetter LF, Rabinowitz JG (1991) Epiphyseal involvement in osteosarcoma. Radiology 180:813–816

Noyek AM, Chapnik JS, Kirsh JC (1989) Radionuclide bone scan in frontal sinus osteoma. Aust N Z J Surg 59:127–132

O'Flanagan SJ, Stack JP, McGee HM, Dervan P, Hurson B (1991) Imaging of intramedullary tumour spread in osteosarcoma. A comparison of techniques. J Bone Joint Surg Br 73:998–1001

Ohtomo K, Terui S, Yokoyama R, Abe H, Terauchi T, Maeda G, Beppu Y, Fukuma H (1996) Thallium-201 scintigraphy to assess effect of chemotherapy in osteosarcoma. J Nucl Med 37:1444–1448

Okada K, Frassica FJ, Sim FH, Beabout JW, Bond JR, Unni KK (1994) Parosteal osteosarcoma. A clinicopathological study. J Bone Joint Surg Am 76:366–378

Olson PN, Prewitt L, Griffiths HJ, Cherkna B (1991) Case report 703: multifocal osteosarcoma. Skeletal Radiol 20:624–627

Onitsuka H (1977) Roentgenologic aspects of bone islands. Radiology 123:607–612

Panuel M, Gentet JC, Scheiner C, Jouve JL, Bollini G, Petit P, Bourliere-Najean B, Devred P (1993) Physeal and epiphyseal extent of primary malignant bone tumors in childhood. Correlation of preoperative MRI and the pathologic examination. Pediatr Radiol 23:421–424

Parham DM, Pratt CB, Parvey LS, Webber BL, Champion J (1985) Childhood multifocal osteosarcoma. Clinicopathologic and radiologic correlates. Cancer 55:2653–2658

Park HS, Kim JR, Lee SY, Jang KY (2005) Symptomatic giant (10-cm) bone island of the tibia. Skeletal Radiol 34:347–350

Park YK, Ryu KN, Ahn JH, Yang MH (1995) A small cell osteosarcoma on the calcaneus–a case report. J Korean Med Sci 10:147–151

Petrikowski CG, Peters E (1997) Longitudinal radiographic assessment of dense bone islands of the jaws. Oral Surg Oral Med Oral Pathol Oral Radiol Endod 83:627–634

Pettine KA, Klassen RA (1986) Osteoid-osteoma and osteoblastoma of the spine. J Bone Joint Surg Am 68:354–361

Picci P, Gherlinzoni F, Guerra A (1983) Intracortical osteosarcoma: rare entity or early manifestation of classical osteosarcoma? Skeletal Radiol 9:255–258

Pignatti G, Bacci G, Picci P, Dallari D, Bertoni F, Bacchini P, Capanna R (1991) Telangiectatic osteogenic sarcoma of the extremities. Results in 17 patients treated with neoadjuvant chemotherapy. Clin Orthop Relat Res 99–106

Porretta CA, Dahlin DC, Janes JM (1957) Sarcoma in Paget's disease of bone. J Bone Joint Surg Am 39-A:1314–1329

Raymond AK (1991) Surface osteosarcoma. Clin Orthop Relat Res 140–148

Raymond AK, Ayala AG, Knuutila S (2002) Conventional osteosarcoma. In: Fletcher DM, Unni KK, Mertens F (eds) WHO classification of tumors. Pathology and genetics: tumors of soft tissue and bone. IARC Press, Lyon, France, pp 264–272

Reddick WE, Bhargava R, Taylor JS, Meyer WH, Fletcher BD (1995) Dynamic contrast-enhanced MR imaging evaluation of osteosarcoma response to neoadjuvant chemotherapy. J Magn Reson Imaging 5:689–694

Redmond OM, Stack JP, Dervan PA, Hurson BJ, Carney DN, Ennis JT (1989) Osteosarcoma: use of MR imaging and MR spectroscopy in clinical decision making. Radiology 172:811–815

Resnick D, Nemcek AA Jr, Haghighi P (1983) Spinal enostoses (bone islands). Radiology 147:373–376

Resnick D, Kyriakos M, Greenway GD (2002a) Enostosis, hyperostosis, and periostitis. In: Resnick D (ed) Diagnosis of bone and joint disorders, 4th edn. W. B. Saunders Company, Philadelphia, pp 4844–4919

Resnick D, Kyriakos M, Greenway GD (2002b) Paget's disease. In: Resnick D (ed) Diagnosis of bone and joint disorders, 4th edn. W. B. Saunders Company, Philadelphia, pp 1947–2000

Resnick D, Kyriakos M, Greenway GD (2002c) Tumors and tumor-like lesions of bone: imaging and pathology of specific lesions. In: Resnick D (ed) Diagnosis of bone and joint disorders, 4th edn. W. B. Saunders Company, Philadelphia, pp 3763–4128

Ritts GD, Pritchard DJ, Unni KK, Beabout JW, Eckardt JJ (1987) Periosteal osteosarcoma. Clin Orthop Relat Res 299–307

Rodallec MH, Feydy A, Larousserie F, Anract P, Campagna R, Babinet A, Zins M, Drape JL (2008) Diagnostic imaging of solitary tumors of the spine: what to do and say. Radiographics 28:1019–1041

Rosen G, Huvos AG, Marcove R, Nirenberg A (1986) Telangiectatic osteogenic sarcoma. Improved survival with combination chemotherapy. Clin Orthop Relat Res 164–173

Rosenberg ZS, Lev S, Schmahmann S, Steiner GC, Beltran J, Present D (1995) Osteosarcoma: subtle, rare, and misleading plain film features. AJR Am J Roentgenol 165:1209–1214

Rosenthal DI, Hornicek FJ, Wolfe MW, Jennings LC, Gebhardt MC, Mankin HJ (1998) Percutaneous radiofrequency coagulation of osteoid osteoma compared with operative treatment. J Bone Joint Surg Am 80 815–821

Rosenthal DI, Hornicek FJ, Torriani M, Gebhardt MC, Mankin HJ (2003) Osteoid osteoma: percutaneous treatment with radiofrequency energy. Radiology 229:171–175

Ruiter DJ, Cornelisse CJ, van Rijssel TG, van der Velde EA (1977) Aneurysmal bone cyst and telangiectatic osteosarcoma. A histopathological and morphometric study. Virchows Arch A Pathol Anat Histol 373:311–325

Russ JE, Jesse RH (1980) Management of osteosarcoma of the maxilla and mandible. Am J Surg 140:572–576

Sadry F, Hessler C, Garcia J (1988) The potential aggressiveness of sinus osteomas. A report of two cases. Skeletal Radiol 17:427–430

Schajowicz F, Lemos C (1970) Osteoid osteoma and osteoblastoma. Closely related entities of osteoblastic derivation. Acta Orthop Scand 41:272–291

Schima W, Amann G, Stiglbauer R, Windhager R, Kramer J, Nicolakis M, Farres MT, Imhof H (1994) Preoperative staging of osteosarcoma: efficacy of MR imaging in detecting joint involvement. AJR Am J Roentgenol 163:1171–1175

Schlesinger AE, Hernandez RJ (1990) Intracapsular osteoid osteoma of the proximal femur: findings on plain film and CT. AJR Am J Roentgenol 154:1241–1244

Schreiman JS, Crass JR, Wick MR, Maile CW, Thompson RC Jr (1986) Osteosarcoma: role of CT in limb-sparing treatment. Radiology 161:485–488

Schulman L, Dorfman HD (1970) Nerve fibers in osteoid osteoma. J Bone Joint Surg Am 52:1351–1356

Schweitzer ME, Greenway G, Resnick D, Haghighi P, Snoots WE (1992) Osteoma of soft parts. Skeletal Radiol 21:177–180

Seeger LL, Eckardt JJ, Bassett LW (1989) Cross-sectional imaging in the evaluation of osteogenic sarcoma: MRI and CT. Semin Roentgenol 24:174–184

Seeger LL, Gold RH, Chandnani VP (1991) Diagnostic imaging of osteosarcoma. Clin Orthop Relat Res 254–263

Shaikh MI, Saifuddin A, Pringle J, Natali C, Sherazi Z (1999) Spinal osteoblastoma: CT and MR imaging with pathological correlation. Skeletal Radiol 28:33–40

Sherman MS (1947a) Osteoid osteoma associated with changes in adjacent joints. J Bone Joint Surg 29:483–490

Sherman MS (1947b) Osteoid osteoma:review of the literature and report of thirty cases. J Bone Joint Surg 29:918–930

Shibata Y, Yoshii Y, Tsukada A, Nose T (1991) Radiolucent osteoma of the skull: case report. Neurosurgery 29:776–778

Sim FH, Dahlin CD, Beabout JW (1975) Osteoid-osteoma: diagnostic problems. J Bone Joint Surg Am 57:154–159

Sim FH, Unni KK, Beabout JW, Dahlin DC (1979) Osteosarcoma with small cells simulating Ewing's tumor. J Bone Joint Surg Am 61:207–215

Sim FH, Frassica FJ, Unni KK (1995) Osteosarcoma of the diaphysis of long bones: clinicopathologic features and treatment of 51 cases. Orthopedics 18:19–23

Simon MA, Bos GD (1980) Epiphyseal extension of metaphyseal osteosarcoma in skeletally immature individuals. J Bone Joint Surg Am 62:195–204

Smith FW, Gilday DL (1980) Scintigraphic appearances of osteoid osteoma. Radiology 137:191–195

Smith J, Botet JF, Yeh SD (1984) Bone sarcomas in Paget disease: a study of 85 patients. Radiology 152:583–590

Snarr JW, Abell MR, Martel W (1973) Lymphofollicular synovitis with osteoid osteoma. Radiology 106:557–560

Soler Rich R, Martinez S, de Marcos JA, Salas A, Lluc P, Granados J (1998) Parosteal osteoma of the iliac bone. Skeletal Radiol 27:161–163

Spence AJ, Lloyd-Roberts GC (1961) Regional osteoporosis in osteoid osteoma. J Bone Joint Surg Br 43-B:501–507

Spouge AR, Thain LM (2000) Osteoid osteoma: MR imaging revisited. Clin Imaging 24:19–27

Stern PJ, Lim EV, Krieg JK (1985) Giant metacarpal osteoma. A case report. J Bone Joint Surg Am 67:487–489

Stieda A (1905) Über umschriebene Knochenverdichtungen im Bereich der Substantia spongiosa im Röntgenbilde. Bruns Beitr Klin Chir Tuebing 45:700–703

Sundaram M, Falbo S, McDonald D, Janney C (1996) Surface osteomas of the appendicular skeleton. AJR Am J Roentgenol 167:1529–1533

Swaney JJ (1973) Familial osteogenic sarcoma. Clin Orthop Relat Res 64–68

Swee RG, McLeod RA, Beabout JW (1979) Osteoid osteoma. Detection, diagnosis, and localization. Radiology 130:117–123

Tang N, Song WX, Luo J, Haydon RC, He TC (2008) Osteosarcoma development and stem cell differentiation. Clin Orthop Relat Res 466:2114–2130

Theologis T, Ostlere S, Gibbons CL, Athanasou NA (2007) Toxic osteoblastoma of the scapula. Skeletal Radiol 36:253–257

Tins BJ, Davies AM, Mangham DC (2001) MR imaging of pseudosarcoma in Paget's disease of bone: a report of two cases. Skeletal Radiol 30:161–165

Trombetti A, Noel E (2002) Giant bone islands: a case with 31 years of follow-up. Joint Bone Spine 69:81–84

Unni KK (1996a) Osteoid osteoma. In: Unni KK (ed) Dahlin's bone tumors. General aspects and data on 11,087 cases, 5th edn. Lippincott-Raven, Philadelphia, pp 121–130

Unni KK (1996b) Osteoma. In: Unni KK (ed) Dahlin's bone tumors. General aspects and data on 11,087 cases, 5th edn. Lippincott-Raven, Philadelphia, pp 117–120

Unni KK, Knuutila S (2002) Parosteal osteosarcoma. In: Fletcher DM, Unni KK, Mertens F (eds) WHO classification of tumors. Pathology and genetics: tumors of soft tissue and bone. IARC Press, Lyon, France, pp 279–281

Unni KK, Dahlin DC, Beabout JW (1976) Periosteal osteogenic sarcoma. Cancer 37:2476–2485

Unni KK, Dahlin DC, McLeod RA, Pritchard DJ (1977) Intraosseous well-differentiated osteosarcoma. Cancer 40:1337–1347

Unni KK, Inwards CY, Bridge JA, Kindblom LG (2005) Tumors of bones and joints. The American Registry of Pathology, Washington, D.C.

van der Woude HJ, Bloem JL, Schipper J, Hermans J, van Eck-Smit BL, van Oostayen J, Nooy MA, Taminiau AH, Holscher HC, Hogendoorn PC (1994) Changes in tumor perfusion induced by chemotherapy in bone sarcomas: color Doppler flow imaging compared with contrast-enhanced MR imaging and three-phase bone scintigraphy. Radiology 191:421–431

van der Woude HJ, Bloem JL, Verstraete KL, Taminiau AH, Nooy MA, Hogendoorn PC (1995) Osteosarcoma and Ewing's sarcoma after neoadjuvant chemotherapy: value of dynamic MR imaging in detecting viable tumor before surgery. AJR Am J Roentgenol 165:593–598

Van Ongeval C, Lateur L, Baert AL (1993) Parosteal osteosarcoma. J Belge Radiol 76:173–175

Vanel D, Tcheng S, Contesso G, Zafrani B, Kalifa C, Dubousset J, Kron P (1987) The radiological appearances of telangiectatic osteosarcoma. A study of 14 cases. Skeletal Radiol 16:196–200

Vickers CW, Pugh DC, Ivins JC (1959) Osteoid osteoma; a fifteen-year follow-up of an untreated patient. J Bone Joint Surg Am 41-A:357–358

Vigorita VJ, Jones JK, Ghelman B, Marcove RC (1984) Intracortical osteosarcoma. Am J Surg Pathol 8:65–71

Weary PE, Linthicum A, Cawley EP, Coleman CC Jr, Graham GF (1964) Gardner's syndrome. a family group study and review. Arch Dermatol 90:20–30

Wick MR, Siegal GP, Unni KK, McLeod RA, Greditzer HG III (1981) Sarcomas of bone complicating osteitis deformans (Paget's disease): fifty years' experience. Am J Surg Pathol 5:47–59

Wiener SN, Kirschenbaum D (1980) Osteoid osteoma presenting as regional osteoporosis. Clin Nucl Med 5:68–69

Winter PF, Johnson PM, Hilal SK, Feldman F (1977) Scintigraphic detection of osteoid osteoma. Radiology 122:177–178

Wold LE, Unni KK, Beabout JW, Pritchard DJ (1984a) High-grade surface osteosarcomas. Am J Surg Pathol 8:181–186

Wold LE, Unni KK, Beabout JW, Sim FH, Dahlin DC (1984b) Dedifferentiated parosteal osteosarcoma. J Bone Joint Surg Am 66:53–59

Wold L, McCarthy E, Knuutila S (2002) High grade surface osteosarcoma. In: Fletcher DM, Unni KK, Mertens F (eds) WHO classification of tumors. Pathology and genetics: tumors of soft tissue and bone. IARC Press, Lyon, France, pp 284–285

Yeager BA, Schiebler ML, Wertheim SB, Schmidt RG, Torg JS, Perosio PM, Dalinka MK (1987) MR imaging of osteoid osteoma of the talus. J Comput Assist Tomogr 11:916–917

Fibrogenic and Fibrohistiocytic Tumors

15

Monica Koplas and Murali Sundaram

CONTENTS

M. Koplas, MD
Diagnostic Radiology/Hb6, The Cleveland Clinic Foundation, 9500 Euclid Avenue, Cleveland OH 44195, USA

M. Sundaram, MD, FRCR
Section of Musculoskeletal Radiology, Imaging Institute, Cleveland Clinic, Professor of Radiology, Diagnostic Radiology/A21, The Cleveland Clinic Foundation, 9500 Euclid Avenue, Cleveland OH 44195, USA

KEY POINTS

- Lesions of fibrous origin include those tumors of fibrogenic and fibrohistiocytic origin.
- Tumors of fibrogenic origin are those that produce collagen and demonstrate absence of bone and cartilage formation
- Desmoplastic fibroma and fibrosarcoma make up the fibrogenic tumor category.
- Desmoplastic fibroma is a rare benign tumor often associated with recurrence.
- Desmoplastic fibroma is also one of those rare lytic bone tumors that demonstrate predominantly low signal intensity on T2-weighted MR images, reflecting its collagenous nature.
- Microscopically, differentiation may be difficult between desmoplastic fibroma and a low-grade fibrosarcoma, with the absence of herringbone pattern and pleomorphism being the distinguishing factor.
- Tumors of fibrohistiocytic origin encompass both benign and malignant fibrous histiocytoma.
- Fibrohistiocytic tumors are surrounded in controversy, which is further underscored by the fact that the rare entity of benign fibrous histiocytoma is histologically identical to nonossifying fibroma (NOF), with clinical and radiographic features and location being the distinguishing factors between the two.
- Fibrosarcoma and malignant fibrous histiocytoma (MFH) are rare primary bone tumors with overlapping histologic and radiographic appearance.
- Only a close histological examination may differentiate fibrosarcoma and malignant fibrous histiocytoma.

15.1 Introduction

Lesions of fibrous origin have been subdivided according to the World Health Organization (WHO) classification to include those tumors of fibrogenic and fibrohistiocytic origin. Tumors of fibrogenic origin are those that produce collagen and demonstrate absence of bone and cartilage formation; desmoplastic fibroma and fibrosarcoma are the two tumors included in this category. Tumors of fibrohistiocytic origin encompass both benign and malignant fibrous histiocytoma. These tumors are surrounded in controversy, which is further underscored by the fact that the rare entity of benign fibrous histiocytoma is histologically identical to nonossifying fibroma (NOF), with clinical and radiographic features and location being the distinguishing factors between the two. Thus, the inclusion of NOF in this chapter is warranted and is a significantly more commonly encountered lesion than benign fibrous histiocytoma.

15.2 Desmoplastic Fibroma

15.2.1 Incidence, Age and Site Distribution, and Clinical Features

Desmoplastic fibroma (DF) is a rare benign fibrogenic tumor of bone first described by Jaffe in 1958 (Jaffe 1958). It is also known as a desmoid tumor of the bone, and the intraosseous counterpart of soft tissue fibromatosis. Desmoplastic fibroma is reported to constitute 0.3% of benign bone tumors and 0.06% of all bone tumors (Dahlin 1978; Mirra et al. 1989). There is no sex predilection, and mean age is 23 years of age, with approximately 75% of these tumors arising during the first three decades of life (Dahlin 1978; Yoon et al. 2006; Wolfe et al. 2005). The age range varies from 15 months (Bullens et al. 1975) to 75 years of age (Penneau et al. 1978). While more than 200 DF have now been described in the literature, most reports consist of single cases, with only a few large case series reported in the literature to date (Taconis et al. 1994; Frick et al. 2005).

The most common location of desmoplastic fibroma is within the mandible, the long bones, and the ilium, with the femur, tibia, humerus, and radius being involved most often in the long bones. However, DF has been reported in almost all bones, with more unusual sites being the skull, vertebrae, ribs, scapula, and calcaneus (Gephardt et al. 1985; Taconis et al. 1994). Within the long bones, most lesions arise in the (meta) diaphyseal area, with rare reports of pure diaphyseal location or epiphyseal extension.

Presenting symptoms are often nonspecific, with pain and swelling being the most common symptoms reported. Other symptoms include a limp, with some lesions being found incidentally. Some patients may have long-standing complaints of up to 2- to 4-years' duration. Lesions may also become manifest after pathologic fracture, which occurs in up to 11% of patients (Taconis et al. 1994).

DF is considered a benign but locally aggressive lesion, which does not metastasize. Local recurrence rates of up to 48% are present. Curettage is most often associated with recurrence, with best treatment results reported after wide resection of the tumor (Bohm et al. 1996). Only rare reports of malignant degeneration into osteosarcoma exist (Abdelwahab et al. 2002; Takazawa et al. 2003), arising 11 to 16 years after initial treatment of DF.

15.2.2 Pathology and Genetics

Grossly, DF may be gray or white, with a tough and rubbery consistency. Occasionally, the tumor may invade the adjacent soft tissues. Microscopically, the tumor is characterized by an abundant collagenous stoma with interlacing bundles of spindle shaped fibroblasts and myofibroblasts. The absence of pleomorphism and herringbone pattern allows from differentiation from a malignant lesion, such as low-grade fibrosarcoma. A few normal mitoses may be present, and there is a varying degree of cellularity. It is histologically similar to the soft tissue desmoids tumor (Lagace et al. 1979). When the tumor is located in the jaw, the distinction between desmoplastic fibroma and intra-osseous odontogenic fibroma may not be easy, especially if there is absence of odontogenic epithelium, which is needed for diagnosis of the odontogenic tumor (Ikeshima and Utsunomiya 2005).

Fluorescence in situ hybridization (FISH) analysis has identified trisomies 8 and 20 to be present in a subset of desmoplastic fibromas, a finding previously demonstrated in desmoids tumors of the soft tissues. This demonstrates that the trisomies are nonrandom aberrations in DF, and further links this lesion to the soft tissue counterpart (Bridge et al. 1999).

15.2.3 Imaging Features

The imaging characteristics of desmoplastic fibromas are of a benign, slow-growing lesion, which may occasionally demonstrate focal aggressive features of cortical disruption, best seen on CT and MR imaging. Larger lesions that do demonstrate features of local invasion should prompt further workup to exclude a more aggressive, malignant lesion, such as a low-grade osteosarcoma.

Radiographically, desmoplastic fibromas are lytic, well-defined lesions (Fig. 15.1) which may have a sclerotic border (Taconis et al. 1994, Bertoni et al. 1984a). The lesion is usually located within the (meta)diaphysis. Most cases demonstrate internal trabeculation or ridges, which may result in a soap-bubble appearance. Larger lesions may infiltrate the adjacent soft tissues, with resultant cortical thinning and destruction. Periosteal reaction is only rarely seen. The soft tissue component may be underestimated on the radiographs.

CT usually demonstrates an osteolytic lesion most often, with a mixed sclerotic component seen in up to 35% of cases (Frick et al. 2005). Up to 88% of lesions will have cortical destruction, with good visualization of an associated soft tissue component. Skull lesions may show enlargement of the diploic space, with occasional intracranial extension.

MR imaging will often show the lesion to be iso- or hypointense to adjacent muscle. T2-weighted images show that in up to 89% of the lesions, there is iso- or hypointense signal relative to the adjacent muscle (Fig. 15.2) (Frick et al. 2005). This short T2 signal is felt to relate to the abundant collagen formation seen in this tumor, and is analogous to the signal seen in the soft tissue counterpart, the desmoid tumor. A factor that may confound MR characteristics includes the presence of a pathologic fracture, which is commonly associated with high T2-weighted signal. Thus, it is one of those rare osteolytic lesions of bone with a short T2 on MR imaging.

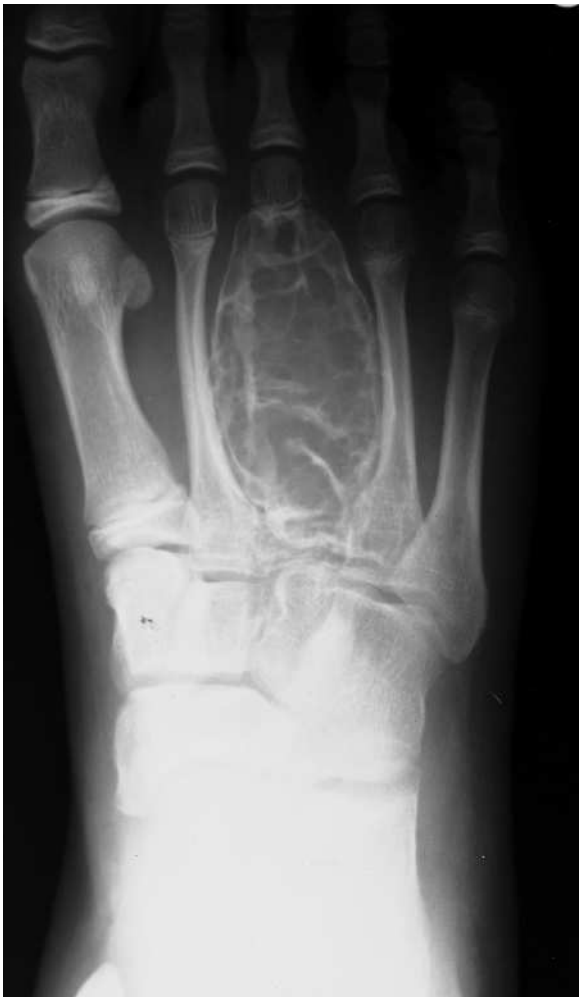

Fig. 15.1. Anteroposterior radiograph of the foot of a young male shows an expansive, septated osteolytic lesion that occupies the entire shaft of the third metatarsal bone. This is a large fibro-osseous lesion, which based on location, would include giant cell reparative granuloma (solid ABC) and secondary ABC in the differential diagnosis. Histological analysis demonstrated this lesion to be a desmoplastic fibroma

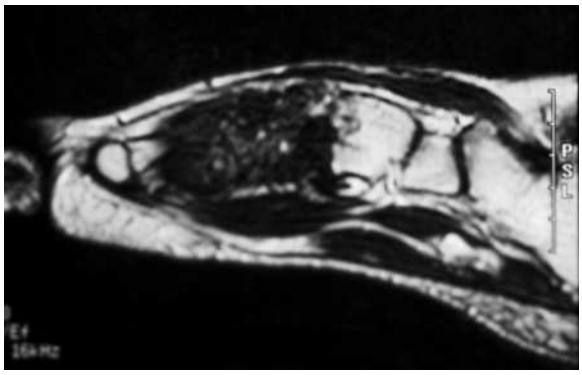

Fig. 15.2. Sagittal non–fat-suppressed T2 spin echo MR image (TR/TE, 3,500/105) of the desmoplastic fibroma within the third metatarsal bone shows the entire lesion to be isointense with muscle (short T2)

15.3 Fibrosarcoma

15.3.1 Incidence, Age and Site Distribution, and Clinical Features

Fibrosarcoma is a relatively rare bone tumor, accounting for less than 5% of bone sarcomas. Older case series of fibrosarcomas included examples of malignant fibrous histiocytoma, making true incidence of the tumor difficult to ascertain (Papagelopoulos et al. 2002). Primary medullary fibrosarcoma makes up approximately 75–85% of the tumors. Most arise as a solitary lesion; however, multiple diffuse fibrosarcoma of the bone has rarely been reported and is associated with poor outcome (Ninomiya et al. 1998). Primary periosteal fibrosarcoma is rare and more controversial, as some authors believe that this represents a fibrosarcoma of the soft tissue, which secondarily abuts the bone and/or the periosteum. Distinction from primary medullary fibrosarcoma is necessary, as a better prognosis exists for the periosteal subtype (Huvos and Higinbotham 1975). Secondary fibrosarcoma may arise from preexisting benign bone lesions, such as Paget's disease, bone infarct, fibrous dysplasia, or chronic osteomyelitis, from prior radiation, or may dedifferentiate from other bone neoplasms, such as giant cell tumor and chondrosarcoma (Bertoni et al. 2003; Sharma et al. 2006; Papagelopoulos et al. 2000a; Ruggieri et al. 1994; McGrory et al. 1999).

While fibrosarcoma occurs most frequently between the third and sixth decade of life, a wide range distribution has been reported, with the tumor occurring in both the pediatric age group as well as the elderly (Papagelopoulos et al. 2000a). The occurrence of fibrosarcoma in the elderly frequently relates to a preexisting bone lesion. No sex predilection exists.

Long tubular bones are involved most often, in 70% of cases, with the femur (40%), tibia (16%), humerus (10%), fibula (3%), and ulna (1%) being involved in decreasing order of frequency (Papagelopoulos et al. 2002). The tumor frequently occurs about the knee. Flat bones may also be involved, with the pelvis affected in 9%, the mandible in 5%, and the maxilla in 2% of cases. Unusual locations of involvement, such as the spine or skull, usually relate to underlying lesions such as Paget's disease or prior radiation (Lustig et al. 1997; Sharma et al. 2006). When the long bones are affected, the metaphysis or metadiaphysis is most commonly involved, with secondary extension into the epiphysis occasionally occurring.

The most common presenting symptom is pain, occurring in most patients, with swelling or a lump occurring less frequently. A pathologic fracture may be present in up to 18.5% of patients. Less common symptoms include a limp, restricted range of motion about a joint, and scoliosis.

Prognosis for patients depends upon histologic grade, with poorly differentiated tumors corresponding to higher grade and poorer prognosis. Five-year survival is low, and ranges from 28 to 34% (Papagelopoulos et al. 2000a; Taconis and van Rijssel 1985). Common sites of metastases include the lung (79%) and bones (7%), with a local recurrence rate of 15% reported.

15.3.2 Pathology and Genetics

Fibrosarcoma is a destructive and locally aggressive tumor. Macroscopically, they appear as low-grade lesions that are well differentiated, with abundant collagen formation, appear well circumscribed with a white color and firm consistency. Higher-grade lesions tend to have infiltrating margins, are soft or friable, with areas of hemorrhage, necrosis, or cystic areas, especially in larger tumors. There is a variable appearance in color.

Histologically, fibrosarcoma is characterized by spindle-shaped cells that are arranged in a herringbone pattern. The degree of collagen production is variable, with a decreased amount of collagen present in higher-grade (moderately or poorly differentiated) fibrosarcoma, as well as a concomitant increase in cellularity and greater nuclear atypia in these lesions (Kahn and Vigorita 2002). There is an absence of cartilage or bone production.

A lesion that may pose difficulty histologically in terms of differentiation from a low-grade fibrosarcoma is desmoplastic fibroma (Saito et al. 2003). However, DF demonstrates an absence of mitoses and atypical cells, and collagen production is not as prominent in fibrosarcoma as in DF. Conversely, in cases of severe cytological atypia, it may be difficult to distinguish fibrosarcoma from malignant fibrous histiocytoma. However, the presence of fibroblasts in a cartwheel or storiform pattern is a clue to the diagnosis of malignant fibrous histiocytoma (Smith and Kransdorf 2000).

While the pathogenesis of fibrosarcoma has not yet been fully elucidated, recent genetic and immunohistochemical analysis demonstrates that a gain of chromosome region 22q, corresponding to an over-representation of the platelet-derived growth factor-beta (*PDGF-B*) gene, may represent an important pathway

in the pathogenesis of fibrosarcoma arising in the bone (Hattinger et al. 2004).

15.3.3 Imaging Features

The radiographic appearance of fibrosarcoma is that of an aggressive and malignant osteolytic lesion with a moth-eaten, geographic, or permeative pattern of bone destruction. Cortical destruction with extension into the soft tissues is common, but periosteal reaction and sclerotic margins are rare (Papagelopoulos et al. 2000a). The lesions tend to be large, and when occurring in long tubular bones, the tumor may be central or eccentric in location. Metaphyseal location is most frequent, and there often is extension to the epiphysis or diaphysis. Residual bony trabeculae may be found. The low-grade fibrosarcoma tend to have more defined borders and sclerosis (Bertoni et al. 1984b).

Unlike chondrosarcoma or osteosarcoma, neither calcification nor ossification is found in the matrix of the lesion. However, based upon radiographic features, a desmoplastic fibroma, chondromyxoid fibroma or giant cell tumor are reasonable differential diagnoses for a low-grade fibrosarcoma; lymphoma, malignant fibrous histiocytoma, plasma cell myeloma and skeletal metastasis, especially from carcinoma, would provide differential diagnoses for a high-grade fibrosarcoma.

MR imaging would be the optimal imaging modality to delineate the intramedullary extent of the lesion, and define the soft tissue extent of the lesion. However, findings are nonspecific for the diagnosis of fibrosarcoma.

15.4 Benign Fibrous Histiocytoma

15.4.1 Incidence, Age and Site Distribution, and Clinical Features

Benign fibrous histiocytoma (BFH), also known as fibroxanthoma, fibrous xanthoma, xanthofibroma, and xanthogranuloma, is a rare tumor of the bone, with most reports in the literature existing as single-case reports. Indeed, less than 100 cases have been reported thus far (Kyriakos 2002), with some larger series reporting that BFH represents approximately 1% of their operated benign bone tumors (Grohs et al. 2002). It is histologically indistinguishable from NOF, with clinical and radiographic features and location being the distinguishing factors between the two (Matsuno 1990; Clarke et al. 1985).

Symptoms related to BFH are usually seen patients older than 20 years of age (Grohs et al. 2002; Hamada et al. 1996), although a few rare cases have been reported in the pediatric population, with age as young as 6 years (the lesion arose in the posterior arch of C1, an unusual location for NOF) (van Giffen et al. 2003). Most often,

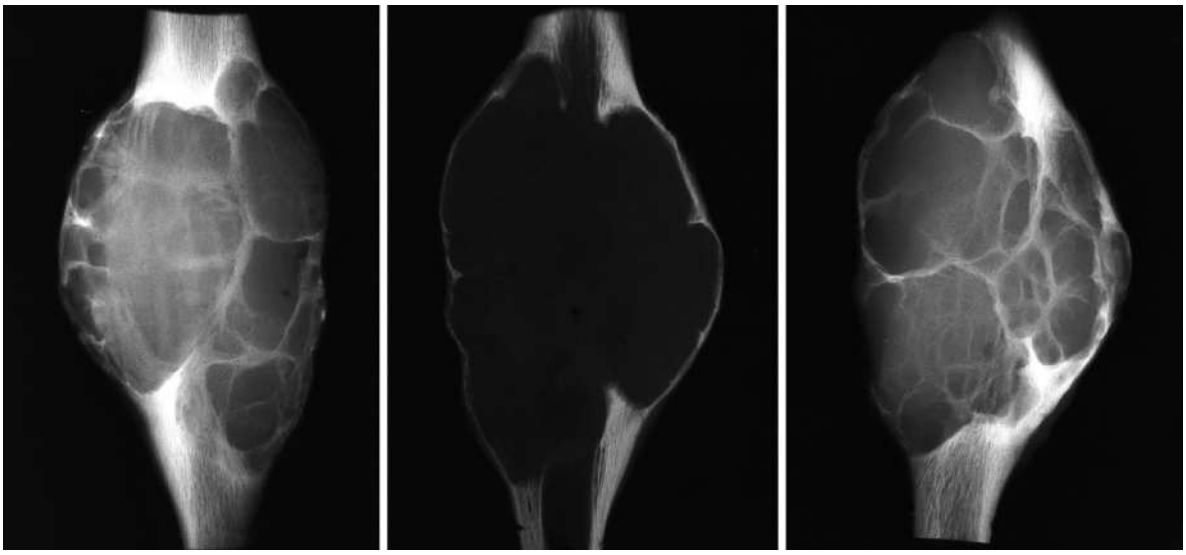

Fig. 15.3. Resected fibula from a 10 year old shows a massively expansive lesion in the diaphysis. The histological features were those of NOF. Because of the location (mid-diaphysis), the lesion was characterized as benign fibrous histiocytoma. (Photo courtesy of Michael Kyriakos, M.D., Department of Pathology, Washington University School of Medicine, St. Louis, Mo.)

BFH comes to clinical attention due to symptoms of local pain, with pathologic fracture being present in up to 60% of patients in some series (Grohs et al. 2002). Pain may precede presentation by weeks to a few years, and almost always precedes the fracture as well. Because most pathologists would not render a diagnosis of BFH in a patient whose age is in the NOF range and whose lesion is in the most commonly encountered sites for NOF, this rare diagnosis is reserved for older patients or lesions in sites not associated with NOF (Fig. 15.3).

There is no sex predilection. Forty percent of BFH occurs in the long bones, with the femur and tibia being the most commonly involved long bones. Twenty-five percent may occur in the pelvis, usually the ilium. Other less common locations for BFH include the rib, acromion, vertebrae, and mandible, and almost any bone may be involved. When the lesion occurs in the long tubular bones, the lesion is centered in the epiphysis or diaphysis. However, rare reports of metaphyseal location of BFH (Bertoni et al. 1986; Clarke et al. 1985) may make distinction between BFH and NOF more difficult. Therefore, BFH differs from NOF in that NOF occurs in patients younger than 20 years, is painless, usually being an incidental finding, and centered in the metaphyseal region of long bones. BFH is usually successfully treated by curettage and bone graft, or resection in the case of non–weight-bearing bone such as a rib. A few rare reports of local recurrences have resulted in eventual amputation (Clarke et al. 1985). BFH does not metastasize.

15.4.2 Pathology and Genetics

Macroscopically, the tumor is gray–white, and from soft to firm in terms of consistency. The mass may be partially cystic, with occasional yellow or hemorrhagic fluid present. On histological examination (Clarke et al. 1985), benign fibrous histiocytoma presents with spindle-shaped fibroblasts, which are interlaced in a whorled or characteristic storiform pattern. The spindle-shaped fibroblast may be associated with a variable degree of collagen, and areas of the tumor may appear fibrous. The nuclei of the spindle cells should demonstrate bland cytologic features, and nuclear atypia should be absent. Foam cells and multinucleated giant cells resembling histiocytes may be intermixed within this lesion to a variable degree. Some cases may demonstrate haemosiderin deposits.

The lesion is histologically identical to nonossifying fibroma (Clarke et al. 1985; Kyriakos 2002), necessitating correlation to clinical and radiographic features. Histologic differentiation from a malignant fibrous histiocytoma may be based on absence of pleomorphism and atypical mitoses. As some BFH lesions may have a predominance of giant cells, simulating a giant cell tumor, differentiation may be made based on a storiform pattern of spindle cells present with collagen formation, which is not seen in giant cell tumor. Finally, the predominant fibrous nature of some BFH may make differentiation from a low-grade fibrosarcoma challenging. However, a careful search for storiform pattern of fibroblasts, coupled with presence of giant cells and absence of nuclear atypia, allows for differentiation of the two. The genetics of this rare tumor have yet to be elucidated.

15.4.3 Imaging Features

On radiographic imaging, benign fibrous histiocytoma presents as a lytic, well-defined, and benign-appearing lesion, which may have a sclerotic rim and internal trabeculations or a soap-bubble appearance (Bertoni et al. 1986; Grohs et al. 2002; Hamada et al. 1996). Within long bones, location is most often diaphyseal or epiphyseal, with either an eccentric or a central location when present at the end of the bone. When present at the end of long bones, differentiation from a giant cell tumor or regressing giant cell tumor may be difficult and ultimately relies on histological findings (Hamada et al. 1996; Matsuno 1990). Expansion and thinning of the cortex is not unusual, although there is an absence of periosteal reaction. The presence of soft tissue extension has only been described in a few rare cases (Grohs et al. 2002). A few authors emphasize that the BFH has a more aggressive-appearing pattern of bone destruction than does NOF (Grohs et al. 2002; Matsuno 1990), although this has not been seen in all case series (Hamada et al. 1996).

When present, CT shows BFH to be a lytic and well-defined lesion, which may have marginal sclerosis. There may also be better delineation of the internal bony trabeculation, which may be present in BFH. The few MR imaging descriptions which have been reported are nonspecific, although several authors have described varying degrees of high T2-weighted signal intensity within the lesion (Hamada et al. 1996; van Giffen et al. 2003; Sanatkumar et al. 2005).

15.5 Nonossifying Fibroma/Fibrous Cortical Defect

15.5.1 Incidence, Age and Site Distribution, and Clinical Features

NOF is a common and benign fibrous tumor that was first described by Jaffe and Lichtenstein in 1942, at which time it was termed *non-osteogenic fibroma* (Jaffe and Lichtenstein 1942). The related fibrous cortical defect (FCD) and NOF are both similar lesions histologically, and distinction between the two has been arbitrarily designated as being based on size, with the larger (usually larger than 2 cm in size) and more proliferating lesion involving the medullary cavity being termed NOF. Some authors prefer to refer to the two lesions as a metaphyseal fibrous defect or fibroxanthoma instead.

These two lesions are the most common benign bone lesions, with an estimated incidence of 30–40% in asymptomatic children and teens. These lesions are rarely seen in children younger than 2 years of age, and are not usually seen above 20 years of age. Lesions in older patients are usually termed BFH. Long tubular bones are affected in approximately 90% of cases, with the femur and tibia being most commonly involved, and lesions about the knee making up more than 55% of cases. When arising in long tubular bones, NOF and FCD have a predominantly metaphyseal location. More unusual locations have been described, such as the mandible (Bailey et al. 2001), although when present in such unusual locations, these tumors may instead be referred to as BFH. Lesions in males are seen at a 2:1 ratio as compared with females.

NOFs are most often discovered incidentally following minor trauma, in which the study is performed to exclude fracture. Both NOF and FCD are not associated with pain, especially if noted incidentally. However, if size of the NOF exceeds more than 50% of the transverse plane in both the anterior–posterior and lateral directions, there is an increased risk of pathologic fracture occurring through the lesion, at which time they may become symptomatic (Arata et al. 1981).

The origin of NOF and FCD is felt to relate to local trauma that is often unrecognized, and occurs at the site of muscular attachment onto the periosteum, with focal edema and hemorrhage occurring. This may explain why lesions are rarely seen in children younger than 2 years of age, as they are not yet weight bearing and experiencing muscular pulls at the site of their osseous attachment (Resnick et al. 2002). Ultrastructure studies of NOF and FCD support the theory of cellular proliferations occurring due to developmental defects in long bones (Steiner 1974).

NOF and FCD are frequently solitary, but multiple lesions may be seen, especially when present in the lower extremities (Blau et al. 1988). Neurofibromatosis can also occasionally be associated with multiple NOF (Schwartz and Ramos 1980). When multiple NOFs are associated with café-au-lait spots, without other stigmata of neurofibromatosis, these findings have been given the designation Jaffe-Campanacci syndrome, and other findings, including mental retardation, hypogonadism, cryptorchidism, and cardiovascular and ocular anomalies may be present (Mirra et al. 1982). In this syndrome, the NOF tends to be present in multiple and symmetric distribution, most often about the knee, as well as in other more rare locations, such as the mandible. Other conditions that have been associated with NOF include hypophosphatemic vitamin D–refractory rickets and osteomalacia, with NOF being responsible for approximately 5% of these cases (oncogenic osteomalacia). Symptoms resolve upon excision of the lesion (Nuovo et al. 1989; Pollack et al. 1973).

15.5.2 Pathology

Grossly, NOF and FCD are usually yellow, with small brown areas within the lesion, and a soft or rubbery consistency. Analysis of histological appearance demonstrates spindle shaped fibroblasts arranged in an interlacing whorled or storiform pattern. Intermixed within this fibrous stoma are multinucleated giant cells and groups of foam cells. Focal areas of hemorrhage are frequently noted. Periostitis and a soft tissue mass are absent. Electron microscope studies have revealed the identical nature of NOF and FCD (Steiner 1974). This histological pattern is also identical to that described for BFH, underscoring the need to correlate clinical and radiographic findings to the ultimate diagnosis.

15.5.3 Imaging Features

The radiographic findings of NOF are usually characteristic. The lesion is a lytic, well-defined lesion centered in the metaphysis with geographic bone destruction and marginal sclerosis (Friedland et al. 1995). Once again, size and location are the discriminating features between NOF and FCD. FCD involves the cortex (Fig. 15.4) and

NOF the cancellous bone (Fig. 15.5), and larger lesions may demonstrate a septated or multiloculated appearance. Studies documenting the natural history of these lesions over time demonstrate that the lesions tend to move away from the epiphysis as bone growth continues, and gradually the lesions develop sclerotic margins. If these lesions do not completely involute, then they migrate over time to become situated in the diaphysis. Usually, as these lesions tend to become sclerotic over time, new bone formation tends to gradually fill in the lucent lesion, and usually the lesion disappears altogether (Ponsetti and Friedman 1949). Occasionally, FCD has been observed to enlarge with time, becoming a NOF. If a radiograph of NOF is obtained during these stages of involution, then diagnosis may be more challenging if the interpreter is unaware of these varying evolutionary appearances.

As the radiographic appearance of NOF/FCD is characteristic, further workup with other imaging modalities is not needed. The CT appearance is similar to the radiographic appearance, with soft tissue attenuation demonstrated within the lytic lesion. When seen on MR imaging, variable results have been reported. Araki and colleagues (1994) found FCD to be isointense to muscle on T1-weighted imaging, and high in signal intensity on T2-weighted imaging, with the lesions surrounded by bands of low signal intensity. Jee and colleagues (1998) found NOF to be hypointense compared to muscle on T1-weighted imaging, and 79% of the lesions to be hypointense as well on T2-weighted imaging (1998). They felt that this related to the extensive fibrous tissue and haemosiderin, which was seen on histological examination. Internal septation was noted in 95% of the lesions, and this correlated to trabeculations that were seen on radiographic imaging. T1-weighted images may show fat signal within the lesion indicative of its benign nature (Fig 15.6) (Simpfendorfer et al. 2008).

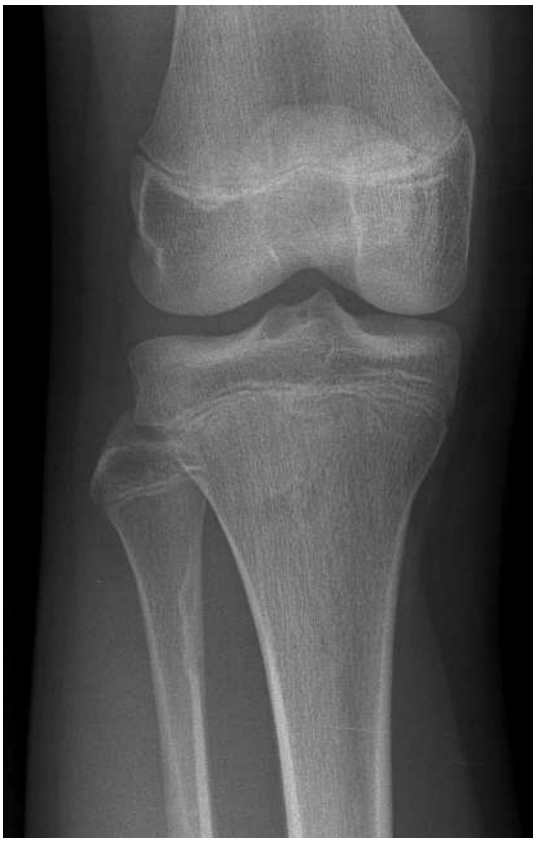

Fig. 15.4. Anteroposterior radiograph of the right knee of a 13-year-old female demonstrates a cortically based lytic and well-defined lesion with sclerotic margins in the proximal metaphysis of the fibula. This characteristic appearing fibrous cortical defect was seen incidentally when images were obtained for left knee pain

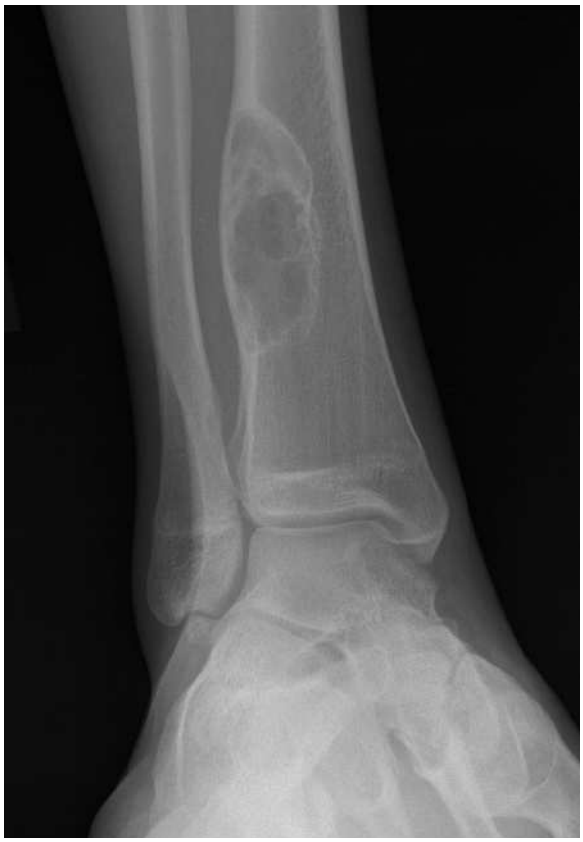

Fig. 15.5. Oblique view of the right ankle of a 15-year-old male who presented with pain after an injury sustained while playing basketball. There is a well-defined and expansive lytic lesion with sclerotic margins in the distal metaphysis of the tibia that extends from the cortex to the center of the bone. The findings are characteristic of nonossifying fibroma

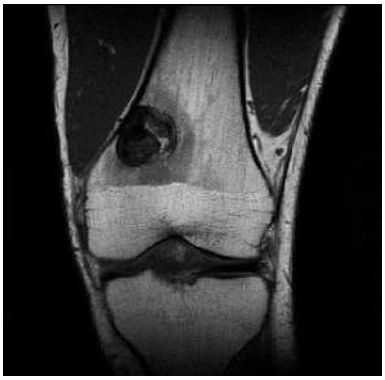

Fig. 15.6. Coronal T1-weighted image of the right knee of a young male obtained unnecessarily (radiographs showed characteristic features of NOF) demonstrates a lession proven to be a nonossifying fibroma with focal area of high T1 signal within it, which shows fat signal, indicating its benign nature

15.6 Malignant Fibrous Histiocytoma

15.6.1 Incidence, Age and Site Distribution, and Clinical Features

Malignant fibrous histiocytoma (MFH) was first described in the bone by Feldman and Norman in 1972 (Feldman and Norman 1972), and remains much less common than its soft tissue counterpart. It is indeed a rare bone tumor, accounting for less than 2% of primary bone malignancies. MFH has been variably termed malignant histiocytoma, xanthosarcoma, malignant fibrous xanthoma, and fibroxanthoma. Controversy exists as to its true origin, whether that of a true histocytic origin, or whether it derives from a single primitive mesenchymal cell, which then differentiates into histiocytes and fibroblasts. It is believed that many older cases of fibrosarcoma reported in the literature in the past instead represented MFH.

MFH can arise de novo, representing primary MFH, or may arise secondarily in preexisting osseous conditions such as Paget's disease, bone infarct, chronic osteomyelitis, giant cell tumor, aneurysmal bone cyst, prior radiation, and total joint replacements (Anract et al. 2002; Bertoni et al. 2003; Desai et al. 1996; Hoshi et al. 2006; Matsuo et al. 2005; Sharma et al. 2006; Visuri et al. 2006; Zlowodzki et al. 2005). Approximately 20% of MFH is secondary and is associated with a worse prognosis (Yokoyama et al. 1993). The rare, autosomal dominant condition diaphyseal medullary stenosis, which is characterized by cortical thickening of trabecular bone and longitudinal linear striations, has been found to be associated with secondary MFH (Douya et al. 2002).

MFH has a small predilection towards the male sex. The range of patients affected is broad, from 6 to 81 years of age, with a mean age of the third and fourth decade of life (Bielack et al. 1999; Nishida et al. 1997; Yokoyama et al. 1993). MFH occurs most often in the long tubular bones, most often about the knee in 29–68% of cases. The femur is most often long bone affected, followed by the tibia, and then the humerus. The metaphysis is most commonly involved when occurring in long bones. The ilium is the most common flat bone affected. However, MFH can arise in any bone, with more uncommon locations reported including the rib, the mandible, and the calcaneus. Pain is reported in nearly all patients, which is then followed by local swelling or mass. Other clinical symptoms may include limp, deformity, or joint stiffness. Pathologic fracture occurs in up to 12% of patients (Bielack et al. 1999).

Prognosis depends on histologic grade of the tumor, with better prognosis reported in lower grade tumors. Five-year disease free survival ranges from 43 to 59% in recent series, with a younger age, use of chemotherapy and limb-salvage surgery associated with better outcome (Bielack et al. 1999; Nishida et al. 1997; Yokoyama et al. 1993). MFH metastases occur most frequently in the lung, up to 37% of the time, and are followed by osseous metastasis in 15% of patients. Only rarely does lymph node involvement occur.

15.6.2 Pathology and Genetics

Grossly, the tumor appears as a poorly marginated mass, with areas of hemorrhage within it. It is centrally located within bone, and cortical destruction and extension into the soft tissues is found in almost all cases. On histologic examination, the tumor is found to be composed of fibroblasts, which may be arranged in a characteristic cartwheel, whorled, or storiform pattern. Admixed within this are histiocytes, multinucleated giant cells, inflammatory cells, and foamy cells. Mitotic figures are commonly seen, with varying degree of pleomorphism and cellularity seen within the tumor (Papagelopoulos et al. 2000b). Five different subtypes of MFH have been described in the bone and soft tissue: storiform-pleomorphic, histocytic, myxoid, inflammatory, and giant cell, classified according to the most common cell type seen. The most common in bone is the storiform–pleomorphic subtype (Steiner et al. 2002). Histologic considerations in the differential diagnosis include osteosarcoma, particularly the MFH-like variant, fibrosarcoma, malignant giant cell tumor, and malignant schwannoma, (Naka et al. 1995; Papagelopoulos et al. 2000b). The presence of osteoid within the tumor will point in the direction of osteosarcoma; however, thin bands of collagen found within MFH may simulate osteoid, making the differentiation more difficult. The differentiation between MFH and fibrosarcoma, both of which may appear similar histologically, is based upon finding spindle shaped fibroblasts in a herringbone pattern that is characteristically seen in fibrosarcoma.

Seventy-one percent of sporadic MFH cases tested have been found to demonstrate loss of heterozygosity at the marker on the chromosome band 9p21-22 (Martignetti et al. 2000). The same researchers have also demonstrated the same loss of heterozygosity to MFH, arising in the rare syndrome of diaphyseal medullary stenosis, suggesting a common underlying etiology to both the sporadic and inherited forms of MFH.

15.6.3 Imaging Features

The typical radiographic presentation of MFH is that of an osteolytic, aggressive tumor demonstrating a permeative or moth-eaten pattern of bone destruction with cortical destruction (Fig. 15.7). Reactive sclerosis may be seen in up to 10% of patients. Periosteal reaction and expansive growth are less commonly seen. Calcification and ossification should not be seen. Typical location is

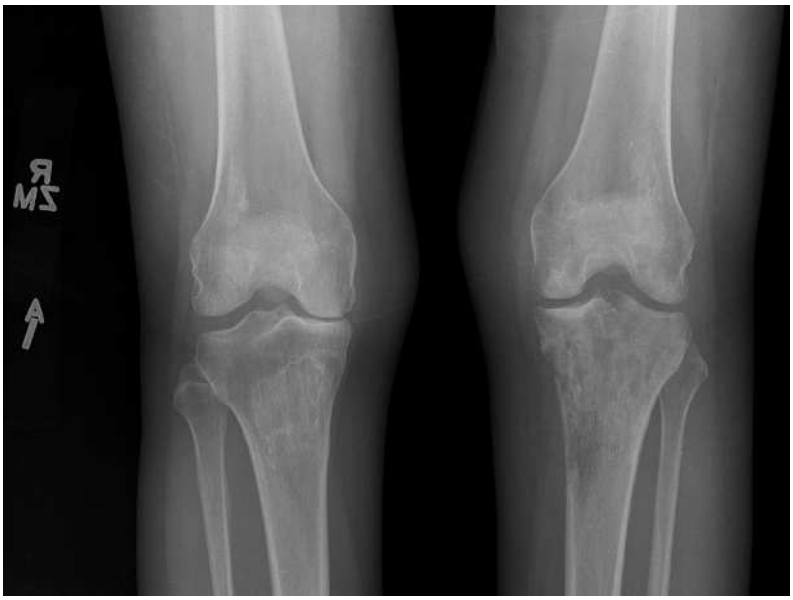

Fig. 15.7. Anteroposterior radiograph of the knees of a 56-year-old female reveals a permeative lesion involving the proximal left tibia with disruption of the cortex medially. Serpentine lucencies and sclerosis noted in the other demonstrated bones are characteristic of medullary infarcts. This lesion was shown histologically to be a malignant fibrous histiocytoma arising in bone infarct

within the metaphysis, but the tumor may extend into the epiphysis or diaphysis as well (Link et al. 1998). The radiographic appearance is not specific for MFH, but may be seen in metastatic carcinoma from the breast or lung, plasmacytoma, lymphoma, and osteosarcoma.

As with other malignant neoplasms, MR imaging optimally defines local extent of disease. MR imaging signal characteristically are nonspecific for MFH, and predominantly demonstrates hypointensity on T1-weighted imaging, high signal intensity on T2-weighted imaging, with contrast enhancement following the administration of gadolinium contrast agent, especially at the periphery of the tumor.

References

Abdelwahab IF, Klein MJ, Hermann G et al. (2002) Osteosarcoma arising in a desmoplastic fibroma of the proximal tibia. AJR Am J Roentgenol 178:613–615

Anract P, de Pinieux G, Jeanrot C et al. (2002) Malignant fibrous histiocytoma at the site of a previously treated aneurysmal bone cyst. A case report. J Bone Joint Surg 84:106–111

Araki Y, Tanaka H, Yamamoto H et al. (1994) MRI of fibrous cortical defect of the femur. Radiat Med 12:93–98

Arata MA, Peterson HA, Dahlin DC (1981) Pathological fractures through non-ossifying fibromas. J Bone Joint Surg 63:980–988

Bailey JS, Nikitakis NG, Lopes M et al. (2001) Nonossifying fibroma of the mandible in a 6-year old girl: A case report and review of the literature. J Oral Maxillofac Surg 59:815–818

Bertoni F, Calderoni P, Bacchini P et al. (1984a) Desmoplastic fibroma of bone. A report of six cases. J Bone Joint Surg Br 66:265–268

Bertoni F, Capanna R, Calderoni P et al. (1984b) Primary central (medullary) fibrosarcoma of bone. Semin Diagn Pathol 1:185–198

Bertoni F, Calderoni P, Bacchini P et al. (1986) Benign fibrous histiocytoma of bone. J Bone Joint Surg 68:1225–1230

Bertoni F, Bacchini P, Staals EL (2003) Malignancy in giant cell tumor of bone. Cancer 97:2520–2529

Bielack SS, Schroeders A, Fuchs N et al. (1999) Malignant fibrous histiocytoma of bone. A retrospective EMSOS study of 125 cases. Acta Orthop Scand 70:353–360

Blau RA, Zwick DL, Westphal RA (1988) Multiple nonossifying fibromas: a case report. J Bone Joint Surg Am 70:299–304

Bohm P, Krober S, Greschniok A et al. (1996) Desmoplastic fibroma of the bone. A report of two patients, review of the literature, and therapeutic implications. Cancer 78:1011–1023

Bridge JA, Swats SJ, Buresh C et al. (1999) Trisomies 8 and 20 characterize a subgroup of benign fibrous lesions arising in both soft tissue and bone. Am J Pathol 154:729–733

Bullens R, Boddaert J, Schautteet H et al. (1975) Osseous desmoplastic fibroma of the mandible. An unusual case in a 15 month old infant. Rev Stomatol Chir Maxillofac 76:45–52

Clarke BE, Xipell JM, Thomas DP (1985) Benign fibrous histiocytoma of bone. Am J Surg Pathol 9:806–815

Dahlin DC (1978) Bone tumors: General aspects and data on 6,221 cases, 3rd edn. C.C. Thomas, Springfield, Ill., pp 325–326

Desai P, Perino G, Present D et al. (1996) Sarcoma in association with bone infarcts. Report of five cases. Arch Pathol Lab Med 120:482–489

Douya H, Yokoyama R, Beppu Y et al. (2002) Malignant fibrous histiocytoma associated with diaphyseal medullary stenosis. Clin Orthop Relat Res (400):211–216

Feldman F, Norman D (1972) Intra- and extraosseous malignant histiocytoma (malignant fibrous xanthoma). Radiology 104:497–508

Frick MS, Sundaram M, Unni KK et al. (2005) Imaging findings in desmoplastic fibroma of bone: distinctive T2 characteristics. AJR Am J Roentgenol 184:1762–1767

Friedland JA, Reinus WR, Fisher AJ et al. (1995) Quantitative analysis of the plain radiographic appearance of nonossifying fibroma. Invest Radiol 30:474–479

Gebhardt, MC, Cambell CJ, Schiller AL et al. (1985) Desmoplastic fibroma of the bone. A report of eight cases and review of the literature. J Bone Joint Surg Am 67:732–747

Giffen NH van, van Rhijn WL, van Ooij A et al. (2003) Benign fibrous histiocytoma of the posterior arch of C1 in a 6-year old boy: a case report. Spine 28:E359–E363

Grohs JG, Nicolakis M, Kainberger F et al. (2002) Benign fibrous histiocytoma of bone: A report of ten cases and review of literature. Wein Klin Wochenschr 114:56–63

Hamada T, Ito H, Araki Y et al. (1996) Benign fibrous histiocytoma of the femur: review of three cases. Skeletal Radiol 25:25–29

Hattinger CM, Tarkkanen M, Benini S et al. (2004) Genetic analysis of fibrosarcoma of bone, a rare tumour entity closely related to osteosarcoma and malignant fibrous histiocytoma of bone. Eur J Cell Biol 83:483–491

Hoshi M, Matsumoto S, Manabe J et al. (2006) Malignant change secondary to fibrous dysplasia. Int J Clin Oncol 11:229–235

Huvos AG, Higinbotham NL (1975) Primary fibrosarcoma of the bone. A clinicopathologic study of 130 patients. Cancer 35:837–847

Ikeshima A, Utsunomiya T (2005) Case report of intra-osseous fibroma: a study on odontogenic and desmoplastic fibromas with a review of the literature. J Oral Sci 47:149–157

Jaffe HL (1958) Tumors and tumorous conditions of the bones and joints. Lea and Febiger, Philadelphia, pp 298–303

Jaffe HL, Lichtenstein L (1942) Nonosteogenic fibroma of bone. Am J Pathol 18:205

Jee WH, Choe BY, Kang HS et al. (1998) Nonossifying fibroma: characteristics at MR imaging with pathologic correlation. Radiol 209:197–202

Kahn LB, Vigorita V (2002) Fibrosarcoma of bone. In: Fletcher CDM, Unni KK, Mertens F (eds) World Health Organization classification of tumours. Pathology and genetics, tumours of soft tissues and bone. IARC Press, Lyon, pp 289–290

Kyriakos M (2002) Benign fibrous histiocytoma of bone. In: Fletcher CDM, Unni KK, Mertens F (eds) World Health Organization classification of tumours. Pathology and genetics, tumours of soft tissues and bone. IARC Press Lyon, pp 292–293

Lagace R, Delage C, Bouchard HL (1979) Desmoplastic fibroma of the bone. An ultrastructure study. Am J Surg Pathol 3:423–430

Link TM, Haeussler MD, Poppek S et al. (1998) Malignant fibrous histiocytoma of bone: conventional x-ray and MR imaging features. Skeletal Radiol 27:552–558

Lustig LR, Jackler RK, Lanser MJ (1997) Radiation-induced tumors of the temporal bone. Am J Otol 18:230–235

Martignetti JA, Belb BD, Pierce H et al. (2000) Malignant fibrous histiocytoma: Inherited and sporadic forms have loss of heterozygosity at chromosome band 9p21-22—Evidence for a common genetic defect. Genes Chromosomes Cancer 27:191–195

Matsuno T (1990) Benign fibrous histiocytoma involving the ends of long bone. Skeletal Radiol 19:561–566

Matsuo T, Sugita T, Shimose S et al. (2005) Postradiation malignant fibrous histiocytoma and osteosarcoma of a patient with high telomerase activities. Anticancer Res 25:2951–2956

McGrory JE, Pritchard DJ, Unni KK et al. (1999) Malignant lesions arising in chronic osteomyelitis. Clin Ortho and Relat Res 362:181–189

Mirra JM, Gold RH, Rand R (1982) Disseminated nonossifying fibromas in association with café-au-lait spots (Jaffe-Campanacci Syndrome). Clin Orthop Relat Res 168:192–205

Mirra JM, Picci P, Gold RM (1989) Clinical, radiologic, and pathologic correlations. Lea and Febiger, Philadelphia, pp 735–746

Naka T, Fukuda T, Shinohara N et al. (1995) Osteosarcoma versus malignant fibrous histiocytoma of bone in patients older than 40 years. Cancer 76:972–984

Ninomiya H, Hato T, Yamada T et al. (1998) Multiple diffuse fibrosarcoma of bone associated with extramedullary hematopoiesis. Intern Med 37:480–483

Nishida J, Sim FH, Wenger DE et al. (1997) Malignant fibrous histiocytoma of bone. A clinicopathologic study of 81 patients. Cancer 79:482–493

Nuovo MA, Dorfman HD, Sun CCJ et al. (1989) Tumor-induced osteomalacia and rickets. Am J Surg Pathol 13:588–599

Papagelopoulos PJ, Galanis E, Frassica FJ et al. (2000a) Primary fibrosarcoma of bone. Outcome after primary surgical treatment. Clin Orthop and Relat Res 373:88–103

Papagelopoulos PJ, Galanis EC, Sim FH et al. (2000b) Clinicopathologic features, diagnosis, and treatment of malignant fibrous histiocytoma of bone. Orthopedics 23:59–65

Papagelopoulos PJ, Galanis EC, Triantafyllidis P et al. (2002) Clinicopathologic features, diagnosis, and treatment of fibrosarcoma of bone. Am J Orthop 31:253–257

Penneau M, Desnos J, Desnos JP (1978) Desmoplastic fibroma of the mandible. Rev Stomatol Chir Maxillofac 79:395–399

Pollack JA, Schillller AL, Crawford JD (1973) Rickets and myopathy cured by removal of a nonossifying fibroma of bone. Pediatrics 52:364–371

Ponsetti IV, Friedman B (1949) Evolution of metaphyseal fibrous defects. J Bone Joint Surg Am 31:582–585

Resnick D, Kyriakos M, Greenway GD (2002) Tumors and tumor-like lesions of bone: imaging and pathology of specific lesions. In Resnick D (ed) Diagnosis of bone and joint disorders, 4th edn. Saunders, Philadelphia, pp 3763–4128

Ruggieri P, Sim FH, Bond JR et al. (1994) Malignancies in fibrous dysplasia. Cancer 73:1411–1424

Saito T, Oda Y, Tanaka K et al. (2003) Low grade fibrosarcoma of the proximal humerus. Pathol Int 53:115–120

Sanatkumar S, Rajagopalan N, Mallikarjunaswamy B et al. (2005) Benign fibrous histiocytoma of the distal radius with congenital dislocation of the radial head: A case report. J Orthop Surg 13:83–87

Schwartz AM, Ramos RM (1980) Neurofibromatosis and multiple nonossifying fibromas. AJR 135:617–619

Sharma H, Mehdi SA, MacDuff E et al. (2006) Paget Sarcoma of the spine: Scottish bone tumor registry experience. Spine 31:1344–1350

Simpfendorfer C, Ilaslan I, Davies AM et al. (2008) Does the presence of focal normal marrow fat signal within a tumor on MRI exclude malignancy? An analysis of 184 histologically proven tumors of the pelvic and appendicular skeleton. Skeletal Radiol 37:797–804, doi:10.1007/s00256-008-0523-7

Smith SE, Kransdorf MJ (2000) Primary musculoskeletal tumors of fibrous origin. Semin Musculoskelet Radiol 4:73–88

Steiner GC (1974) Fibrous cortical defect and nonossifying fibroma of bone. A study of the ultrastructure. Arch Pathol 97:205–210

Steiner GC, Jundt G, Martignetti JA (2002) In: Fletcher CDM, Unni KK, Mertens F (eds) World Health Organization classification of tumours. Pathology and genetics, tumours of soft tissues and bone. IARC Press, Lyon, pp 294–296

Taconis WK, van Rijssel TG (1985) Fibrosarcoma of long bones. A study of the significance of areas of malignant fibrous histiocytoma. J Bone Joint Surg Br 67:111–116

Taconis WK, Schutte HE, van der Heul RO (1994) Desmoplastic fibroma of bone: a report of 18 cases. Skeletal Radiol 23:283–288

Takazawa K, Tsuchiya H, Yamamoto N et al. (2003) Osteosarcoma arising from desmoplastic fibroma treated 16 years earlier: a case report. J Orthop Sci 8:864–868

Visuri T, Pulkkinen P, Paavolainen P (2006) Malignant tumors at the site of total hip prosthesis. Analytic review of 46 cases. J Arthroplasty 21:311–323

Wolfe SQ, Cervantes L, Olavarria G et al. (2005) Desmoplastic fibroma of the pediatric skull. J Neurosurg (Pediatrics 4) 103:362–365

Yokoyama R, Tsuneyoshi M, Enjoji M et al. (1993) Prognostic factors of malignant fibrous histiocytoma of bone. A clinical and histopathologic analysis of 34 cases. Cancer 79:1902–1908

Yoon SH, Kim SH, Shin YS et al. (2006) Desmoplastic fibroma of the skull in an infant. Childs Nerv Syst 22:176–181

Zlowodzki M, Allen B, Schreibman KL et al. (2005) Case reports: Malignant fibrous histiocytoma of bone arising in chronic osteomyelitis. Clin Orthop Relat Res 439:269–273

Giant Cell Tumor

16

Mark J. Kransdorf and Mark D. Murphey

CONTENTS

KEY POINTS

- GCTs are relatively common, representing 18–23% of all benign primary tumors.
- The vast majority of patients are between 20–50 years of age.
- About 2–4% of GCTs occur in children.
- Lesion extends to subarticular bone, starting in the metaphysis.
- Radiographs typically show a geographic, lytic lesion, with well-defined, nonsclerotic margins.
- MR imaging will usually show an intermediate signal intensity on T1- and T2-weighted images.
- MR imaging will reflect intralesional hemorrhage and hemosiderin deposition.
- Secondary ABC change is seen in about 10–15% of adult patients and is more common in children.

16.1 Introduction

Giant cell tumor of bone (GCT) is a relatively common, locally aggressive, osseous neoplasm of variable biological activity (Reid et al. 2002; Unni 1996; Wülling et al. 2001). The lesion is composed of sheets of ovoid mononuclear cells interspersed with uniformly distributed, large, multinucleated osteoclast-like giant cells (Reid et al. 2002). It is this multinucleated, osteoclast-like giant cell that initially suggested an osteoclastic lineage to Jaffe et al. in their classic description of the tumor in 1940, in which they separated this distinct lesion from other giant cell-containing tumors and tumor-like lesions. It is now known that the mononuclear component of GCT consists of two cell types: a rounded cell resembling a monocyte and a spindle-shaped, fibroblast-like

M. J. Kransdorf, MD; Mark D. Murphey, MD
Department of Radiological Pathology, Armed Forces Institute of Pathology, Washington, DC, 20306-6000, USA
M. J. Kransdorf, MD
Professor of Diagnostic Radiology
Department of Radiology, Mayo Clinic, Jacksonville, Florida 32224-3899, USA
M. D. Murphey, MD
Department of Radiology and Nuclear Medicine, Uniformed Services University of the Health Sciences, Bethesda, MD 20814-4799, USA

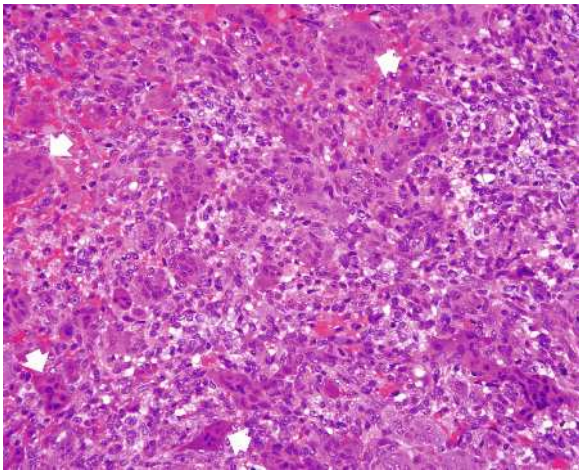

Fig. 16.1. GCT histology. The tumor contains multiple reactive osteoclast-like, multinucleated giant cells (*white arrows*), which are the cells for which the tumor was initially named. The background consists of two types of mononuclear cell: a rounded cell resembling a monocyte and a spindle-shaped, fibroblast-like stromal cell, which is the proliferating component of the tumor

stromal cell, which is the proliferating component of the tumor (Wülling et al. 2001). Recent evidence suggests that this stromal component secretes a variety of cytokines and differentiation factors that are monocyte chemoattractants essential for osteoclast differentiation. This finding suggests that these stromal cells stimulate blood monocyte migration into tumor tissue and enhance their fusion into osteoclast-like, multinucleated giant cells (Wülling et al. 2001). This concept supports the hypothesis that the stromal cells are the neoplastic component of the lesion, while the monocytes and multinucleated giant cells are the reactive components of the lesion (Fig. 16.1) (Wülling et al. 2001).

16.2 Clinical Features

GCT represents approximately 4–9.5% of all primary bone tumors and about 18–23% of benign primary tumors (Larsson et al. 1975; Manaster and Doyle 1993; Murphey et al. 2001; Reid et al. 2002; Resnick et al. 2002; Turcotte 2006; Unni 1996). Patients with GCT of bone present most often in the third decade of life, with approximately 80% of lesions occurring in patients between 20 and 50 years of age (Larsson et al. 1975; Manaster and Doyle 1993; Murphey et al. 2001; Resnick et al. 2002; Unni 1996). Giant cell tumors (GCTs) in children and adolescents are generally considered to be rare, but have been reported with an incidence of 1.7-10.6% of all GCTs (Kransdorf et al. 1992; Picci et al. 1983; Schütte and Taconis 1993; Unni 1996). This great variability reflects the inconsistency in the definition of adolescence, which was defined as those 18 years of age or less in establishing an incidence of 10.6% (Schütte and Taconis 1993). A diagnosis of GCT in patients less than 14 years of age should be viewed with caution; the best estimates of the incidence in this age group are between 2%–4%. In contrast, 9%–13% of affected patients are over 50 years of age (deSantos and Murray 1978; Frassica et al. 1993; Goldenberg et al. 1993; Sung et al. 1993; Unni 1996).

GCT affects all races; however, there is an unusually high prevalence in China and southern India (state of Andhra Pradesh) of 20 and 30%, respectively (Reddy et al. 1974; Sung et al. 1993; Turcotte 2006; Yang 1985). Unlike the majority of osseous neoplasms, benign GCT has been shown to affect women more commonly than men in many series, with ratios ranging from 1.1:1 to 1.5:1, although many researchers believe that there is no gender predilection (Goldenberg et al. 1993; Larsson et al. 1975; Manaster and Doyle 1993; Mirra 1989; Turcotte 2006).

Clinical symptoms are nonspecific and include (in order of decreasing frequency) pain, local swelling, and limited range of motion of the adjacent joint. Pain is usually present for several months and is reduced by rest. Associated pathologic fracture, which may cause the acute onset of pain, is present in about 10%–12% of patients (Resnick et al. 2002; Turcotte 2006). Neurological symptoms may be associated with spine lesions (Murphey et al. 2001).

16.3 Skeletal Distribution

GCTs are most common in long bones (75%–90%), where they are characteristically found at the ends of bones, with approximately 84%–99% of lesions extending to within 1 cm of subarticular bone (Fig. 16.2) (Dahlin et al. 1970; Eckardt and Grogan 1986; Mirra 1989; Resnick et al. 2002; Unni 1996). While these lesions are often considered to be epiphyseal, such a designation is misleading in that in long bones these lesions arise in the metaphysis, adjacent to the physeal plate (Campanacci et al. 1987; Dahlin et al. 1970; Eckardt and Grogan 1986; Mirra 1989; Puri et al. 2007; Resnick et al. 2002; Unni 1996), an observation

that has been confirmed in those infrequent cases in which the lesion is found in skeletally immature patients (Fig. 16.3) (Kransdorf et al. 1992; Turcotte 2006). Moreover, we are unaware of any occurrences of GCT isolated to the epiphysis of a long bone in a skeletally immature patient. It has been our experience that in long bone, the center of an individual lesion is on the metaphyseal side of the physeal plate, reflecting this origin. This feature can be a useful differentiating feature in separating GCT from chondroblastoma having metaphyseal extension, with the latter lesion generally showing its center on the epiphyseal side of the growth plate.

GCTs are most commonly found around the knee, with this location accounting for 50%–65% of cases (Carrasco and Murray 1989; Campanacci et al.

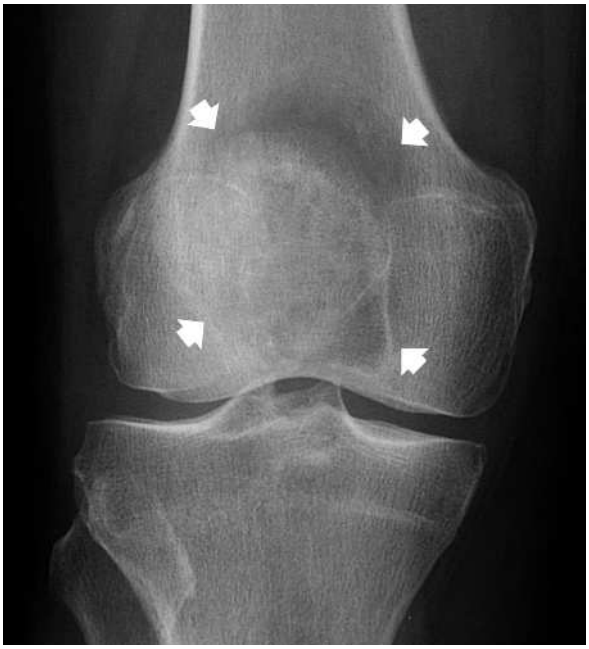

a

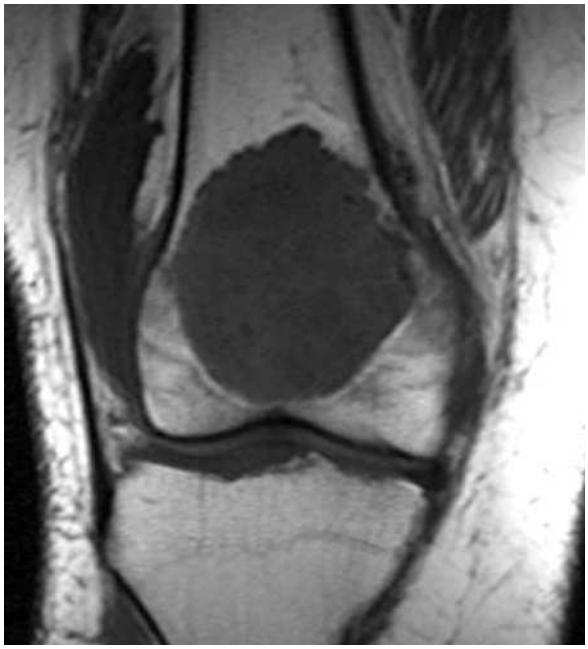

b

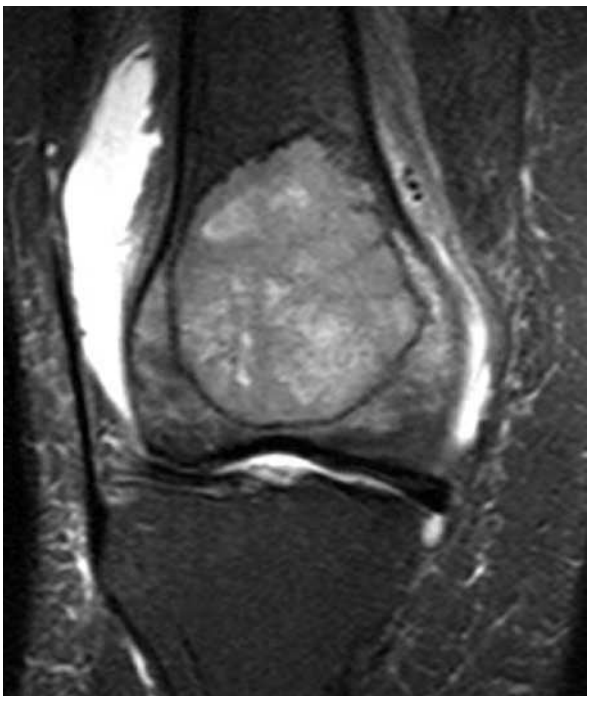

c

Fig.16.2a–c. GCT of the distal femur in a 68-year-old woman. **a** AP radiograph shows the lesion (*arrows*) approaching the end of the bone. **b,c** Corresponding coronal T1-weighted (**b**) and fat-suppressed T2-weighted (**c**) SE MR images of the distal femur show to better advantage the lesion and its relationship to the articular surface. Note that the lesion has intermediate signal intensity with moderate heterogeneity on fluid sensitive sequence **c**

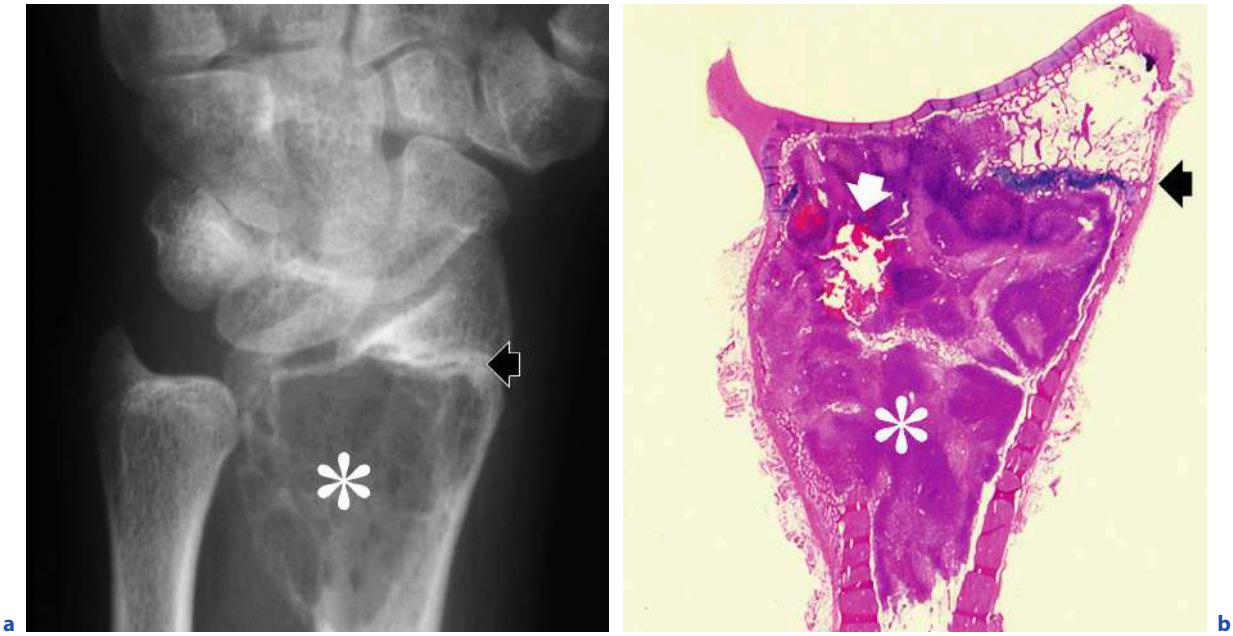

a b

Fig. 16.3a,b. GCT of the distal radius in a 16-year-old girl. **a** Radiograph shows that the giant cell tumor originates in the metaphysis (*asterisk*), and in this patient with a partially open physis, the tumor has crossed the physis (*black arrow*) and extends to the end of the bone. **b** Corresponding macrosection shows the tumor (*asterisk*) and physis (*black arrow*). Note small area of secondary aneurysmal bone cyst formation (*white arrow*)

1975; Dahlin et al. 1970; Eckardt and Grogan 1986; Larsson et al. 1975; Manaster and Doyle 1993; Mirra 1989; Resnick et al. 2002; Turcotte 2006; Unni 1996). The single most common site of occurrence is in the distal femur (23%–30% of cases) (Fig. 16.2), followed by the proximal tibia (20%–25%), distal radius (10%–12%), sacrum (4%–9%), and proximal humerus (4%–8%) (Aoki et al. 1989; Carrasco and Murray 1989; Campanacci et al. 1975; Dahlin et al. 1970; Larsson et al. 1975; Manaster and Doyle 1993; Picci et al. 1983; Turcotte et al. 1975; Unni 1996). Other, less frequent sites of involvement include the proximal femur (4% of cases), innominate bone (3%), vertebral bodies (3%–6%), distal tibia (2%–5%), proximal fibula (3%–4%), hand and wrist (1%–5%), and foot (1%–2%) (Burns et al. 1988; Kumar et al. 1988; Patel et al. 1987; Resnick et al. 2002; Schwimmer et al. 1988; Shankman et al. 1988; Walker et al. 1988; Wold and Swee 1984). GCTs occurring in other anatomic sites are rare (Coumbaras et al. 1999; Lee et al. 1998), but can also occur in sesamoid bones, particularly the patella (the largest sesamoid bone) and apophyses (e.g., the greater trochanter), which are considered to be epiphyseal equivalents in terms of bone neoplasm origin (Kransdorf et al. 1989; Resnick et al. 2002; Wang et al. 1998).

16.4 Classification and Pathologic Features

The World Health Organization's (WHO) Classification of Tumors does not subclassify GCT of bone (Reid et al. 2002). Historically, GCT was categorized into three grades; however, grading has been abandoned because it does not correlate with prognosis and does not predict tumor biological behavior (Reid et al. 2002; Turcotte 2006; Werner 2006).

As previously noted, GCT is composed of mononuclear cells and multinucleated, osteoclast-like giant cells. The spindle-shaped mononuclear cell, representing the neoplastic component of the lesion, is a fibroblast-like cell characterized by longitudinal, often cigar-shaped, nuclei (Wülling et al. 2001). The reactive osteoclast-like giant cells can be very large and may contain 100 or more nuclei (Fig. 16.1) (Reid et al. 2002; Wülling et al. 2001). Mitotic figures are invariably present, although atypical mitoses should suggest the diagnosis of a giant cell-rich sarcoma (Reid et al. 2002; Turcotte 2006). Numerous blood vessels and capillaries are typically present, as are areas of necrosis (Turcotte 2006), and areas of secondary aneurysmal bone cyst (ABC) formation are seen in about 15% of cases, representing

blood-filled cavities devoid of endothelial cells (Murphey et al. 2001; Turcotte 2006). GCTs contain little or no intercellular substrate other than a few collagen fibers (Turcotte 2006).

Cytogenetically, GCT of bone is characterized by the presence of an unusual phenomenon defined as "telomeric associations" (Reid et al. 2002; Unni et al. 2005). Telomeres are located at the linear ends of chromosomes, and telomeric associations lead to fusions of the telomeric ends of different chromosomes, which make them appear "whole" or "intact" (Unni et al. 2005), resulting in a clonal character within the tumor in some cases (Werner 2006). Telomeric associations have been identified in 72% of GCTs (Wülling et al. 2001). While structural and cytogenic abnormalities have been noted in GCT, no uniform aberrations are recognized (Werner 2006).

16.5 Treatment and Prognosis

GCT of bone is a benign lesion, and curettage is generally the preferred treatment (Turcotte 2006). While the tumor is considered to be locally aggressive, occasional distal metastases are identified (Reid et al. 2002). Local recurrence rates vary widely and have been previously reported to be as high as 41% in patients treated with curettage only, to as low as 2% in patients treated with curettage, followed by burring of the tumor walls and liquid nitrogen cryotherapy (Malawer et al. 1999). Local recurrence is usually seen within 2 years; however, local recurrence may be delayed as long as 7 years (Reid et al. 2002; Unni 1996). Pulmonary metastases are seen in about 2–5% of patients, an average of 3–4 years after primary diagnosis (Murphey et al. 2001; Reid et al. 2002). (See discussion on malignant GCT.)

Currently, there are no reliable predictors of recurrence or metastatic disease. A recent array comparative genomic hybridization study of 20 frozen tumors has shown that 20q11.1 is frequently amplified in GCT, and its presence correlates with the occurrence of metastatic disease (Lewis 2007).

16.6 Imaging

The radiographic appearance of GCT is extremely characteristic and usually sufficient to allow a specific diagnosis. Imaging studies are also relatively characteristic.

16.6.1 Radiography

GCT almost invariably presents as a geographic lytic lesion with a well-defined, non-sclerotic margin (80%–85% of cases) (Fig. 16.4). Geographic lysis with an ill-defined margin indicative of a more aggressive growth is seen in approximately 10%–20% of cases (Hudson et al. 1984; Manaster and Doyle 1993; Mirra 1989; Resnick et al. 2002; Unni 1996). A sclerotic margin can be seen, but is rare, and identified in only 1%–2% of lesions (Hudson et al. 1984; McInerney and Middlemiss 1978; Moser et al. 1990). In our experience, while a rim of sclerosis is rare on radiographs, areas of peripheral sclerosis are not infrequent, particularly at CT, where it has been reported in up to 20% of cases (Fig. 16.2) (deSantos and Murray 1978; Levine et al. 1984). Margins will often show a combination of patterns with the geographic, well-defined margin most commonly the dominant pattern (Fig. 16.5a and 16.5b). The majority (42%– 93%) of lesions are eccentrically located (Fig. 16.5); however, large lesions and lesions in small diameter bone, such as the fibula, may appear central (Hudson et al. 1984; Levine et al. 1984; McInerney and Middlemiss 1978).

Expansile remodeling of bone is also frequent, seen in 47% to 60% of cases (Fig. 16.6) (Hudson et al. 1984; Manaster and Doyle 1993), and cortical penetration is seen in 33%–50% of cases, often with an associated soft-tissue mass (deSantos and Murray 1978; Herman et al. 1987; Hudson et al. 1984; Levine et al. 1984; Tehranzadeh et al. 1989). Periosteal reaction is reported at radiography in 10%–30% of cases (Levine et al. 1984; Moser et al. 1990). Pathologic fracture, which may be complete or incomplete, is seen in 11%–37% of patients (Campanacci et al. 1975; Kransdorf et al. 1989; Levine et al. 1984). At radiography, lesions often demonstrate prominent trabeculation (33%–57% of cases), sometimes referred to as a multiloculated or "soap bubble" appearance (Fig. 16.6) (Hudson et al. 1984; Kransdorf et al. 1992; Levine et al. 1984; Moser et al. 1990). We agree with Manaster and Doyle (1993) that this finding has been overemphasized and that this appearance frequently represents pseudotrabeculation from osseous ridges, which are created by endosteal scalloping. This pseudotrabeculation is often well demonstrated by comparing radiographic findings with CT manifestations.

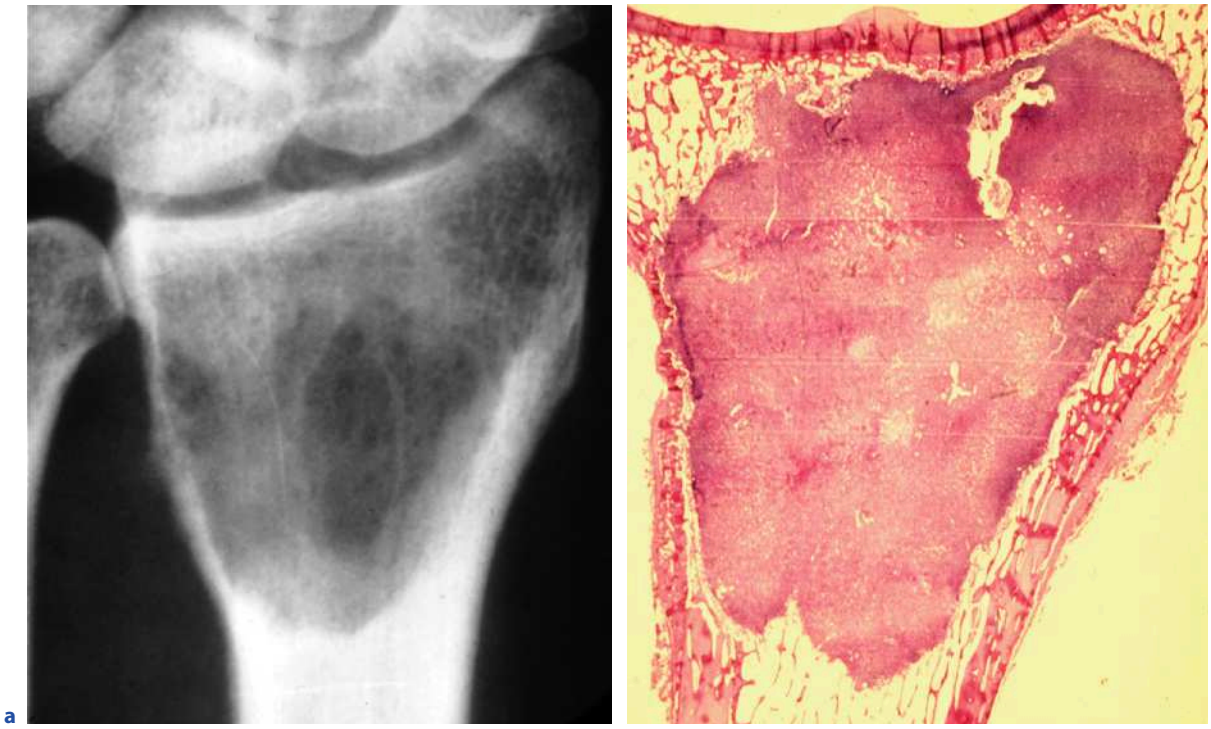

Fig. 16.4a,b. GCT of the distal radius. **a** Radiograph of the distal radius shows a geographic lytic lesion with a well-defined, nonsclerotic margin. **b** Corresponding macrosection shows the well-defined, nonsclerotic margin to better advantage

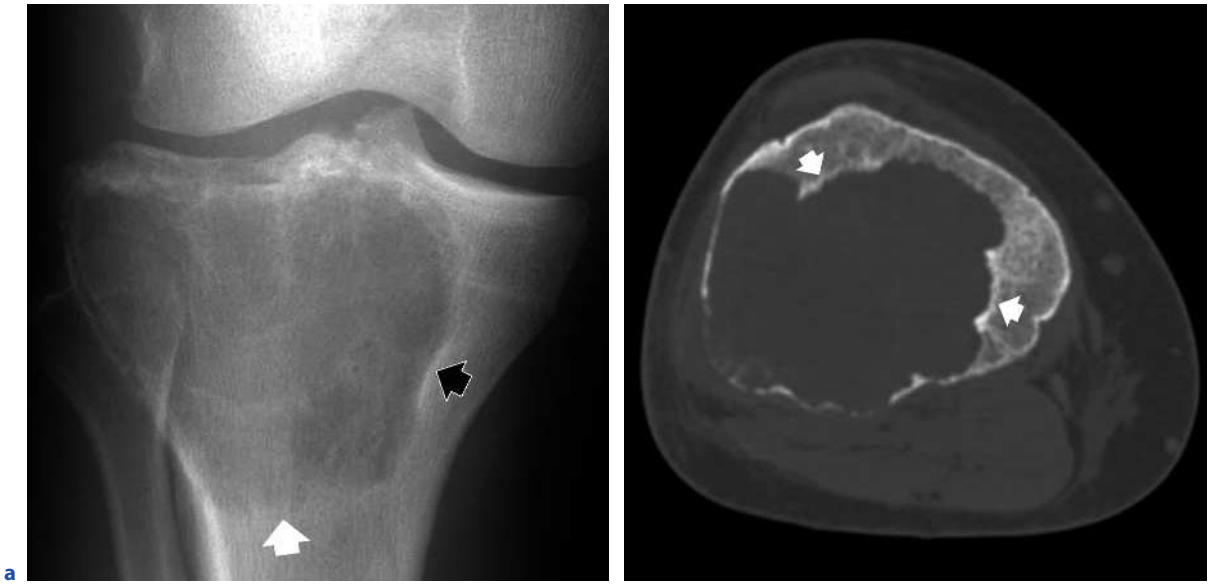

Fig. 16.5a–e. GCT of the proximal tibia in a 23-year-old male. **a** AP radiograph shows a geographic lytic lesion (*arrows*) in the metaphysis, extending to the end of the bone. Portions of the lesion show slight sclerosis (*black arrow*), while other areas are more ill-defined (*white arrow*). **b** Axial noncontrast CT scan displayed at bone window shows areas of sclerosis in the margin (*arrows*). **c-e** *see next page*

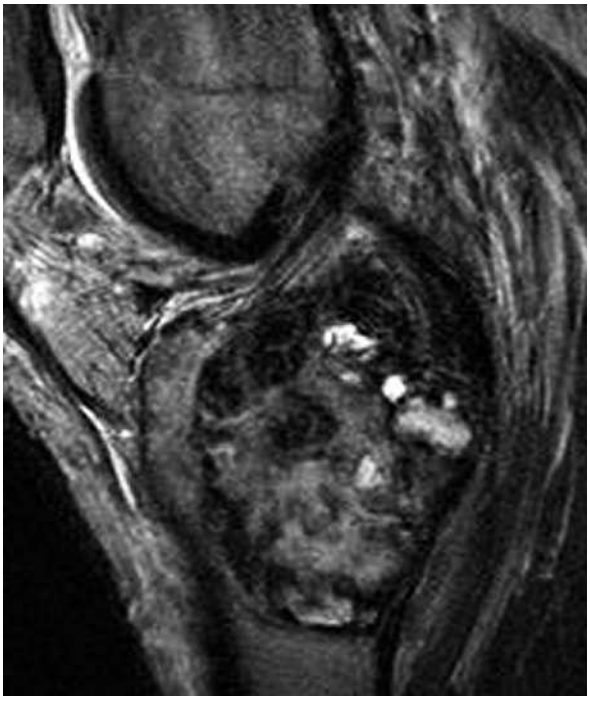

c

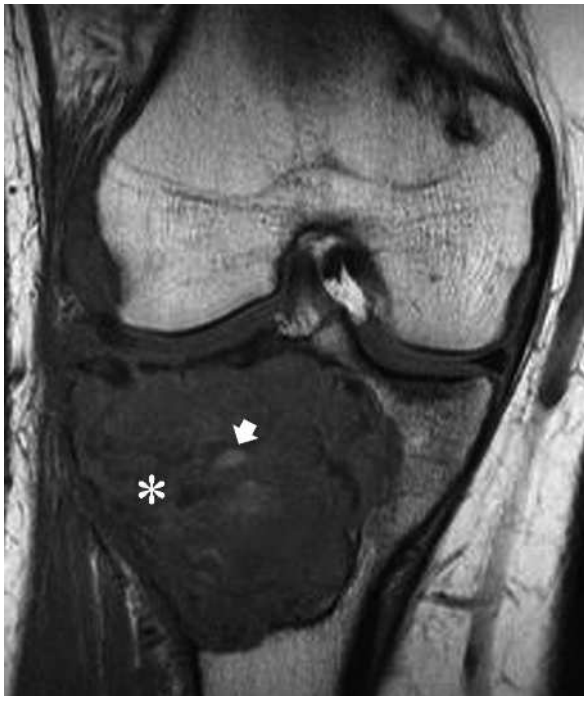

d

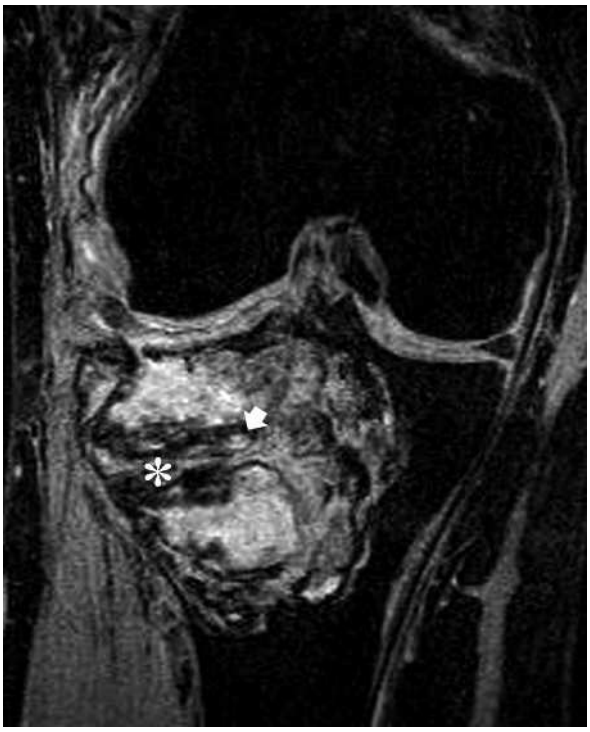

e

Fig. 16.5a–e. (*continued*) **c** Sagittal conventional T2-weighted MR SE image shows the lesion to be heterogeneous, with a predominantly intermediate signal intensity, similar to that of the adjacent marrow fat. The areas of increased and decreased signal are the result of previous intralesional hemorrhage. **d,e** Corresponding coronal T1-weighted SE (**d**) and gradient echo (GRE) (**e**) MR images of the proximal tibia show areas of subacute hemorrhage (*arrows*) and hemosiderin deposition (*asterisks*)

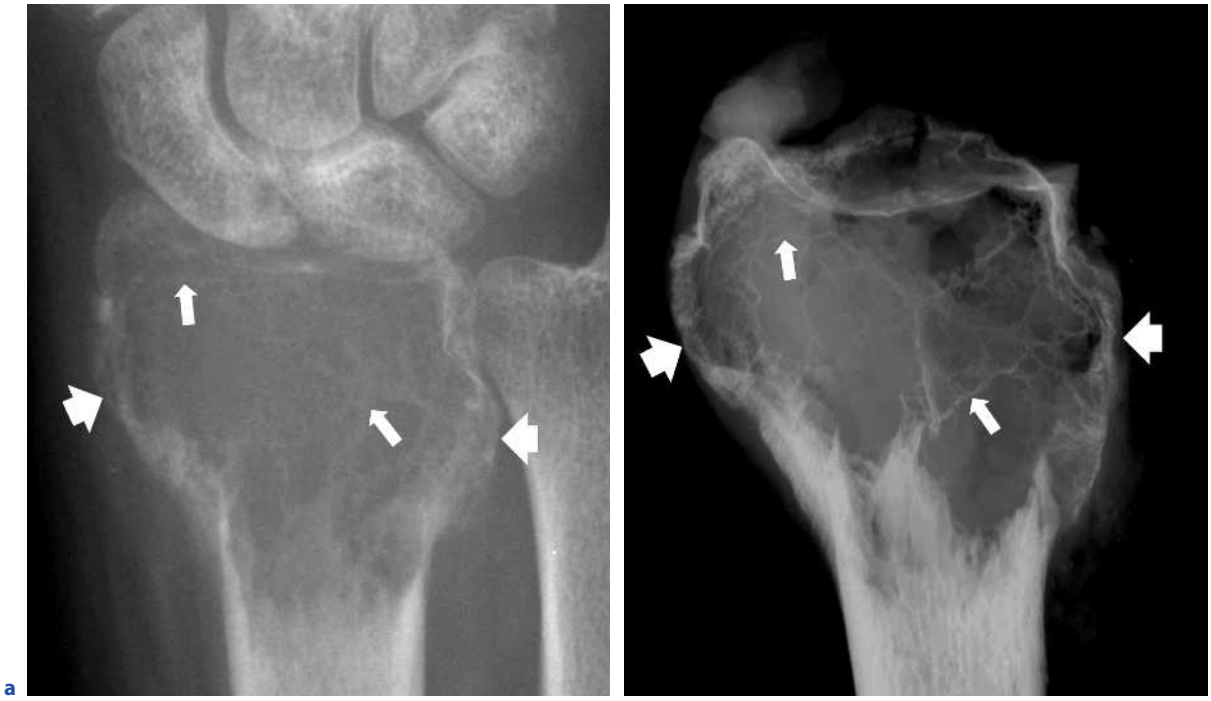

Fig. 16.6a,b. GCT of the distal radius in a 23-year-old woman. **a** AP radiograph of the wrist shows expansile remodeling (*large, short arrows*) of the cortical margins of the distal radius. Trabeculation (*small, long arrows*) can be seen, although it is subtle. **b** Specimen radiograph shows the expansile remodeling (*large, short arrows*), as well as more clearly shows the trabeculated "soap bubble" appearance (*small, long arrows*)

16.6.2 Scintigraphy

Bone scintigraphy demonstrates increased radionuclide uptake in the vast majority of GCTs (Levine et al. 1984a, 1984b; O'Reilly and Chew 1996; Van Nostrand et al. 1986; Wang et al. 2005). Increased radionuclide uptake peripherally with photopenia centrally, termed the "donut sign," was seen in 57% of cases reported by Levine et al. (1984). Blood pool and dynamic flow imaging typically reveals increased radionuclide uptake, although usually to a lesser degree than in delayed static images (Levine et al. 1984a, 1984b). Increased radiotracer uptake in bone across an articulation and in adjacent joints is common (62% of cases) and should not be mistaken for tumor extension (Levine et al. 1984a, 1984b). As with other hyperemic bone neoplasms, this phenomenon, referred to as "contiguous bone activity" or "extended pattern of uptake," is related to increased blood flow and disuse osteoporosis (Fig. 16.7) (Chew and Hudson 1982; Levine et al. 1984a; O'Reilly and Chew 1996; Thrall et al. 1975; Turcotte 2006; Van Nostrand et al. 1986; Wang et al. 2005).

16.6.3 Angiography

Angiography is rarely performed in patients with GCT, and when done, is typically in conjunction with preoperative, therapeutic, transcatheter, arterial embolization used to reduce blood loss during surgical resection (Levine et al. 1984). The majority of lesions are hypervascular (60%–65% of cases) (Fig. 16.7) (deSantos and Prando 1979; Prando et al. 1979; Tehranzadeh et al. 1989), although 26%–30% of cases are hypovascular and about 10% are relatively avascular (deSantos and Prando 1979; Prando et al. 1979; Tehranzadeh et al. 1989). It has been our experience that those lesions with prominent secondary ABC change are less vascular.

16.6.4 Computed Tomography

As with other musculoskeletal neoplasms, CT and MR imaging allow superior delineation and local staging

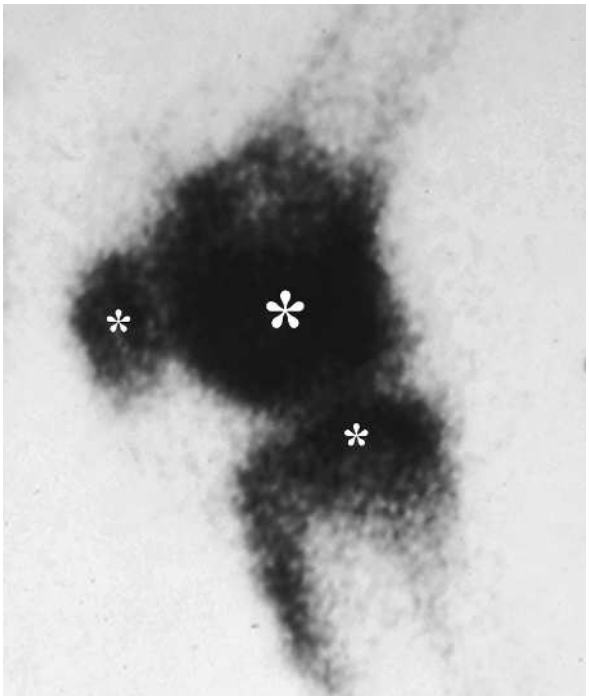

a

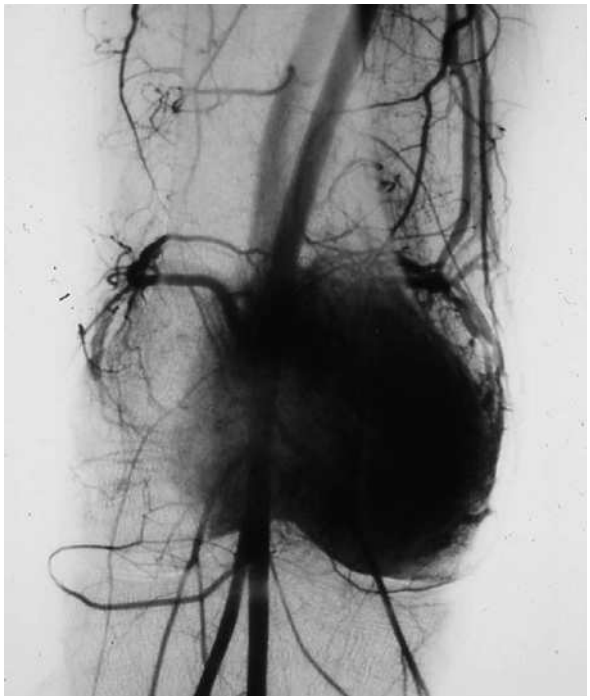

b

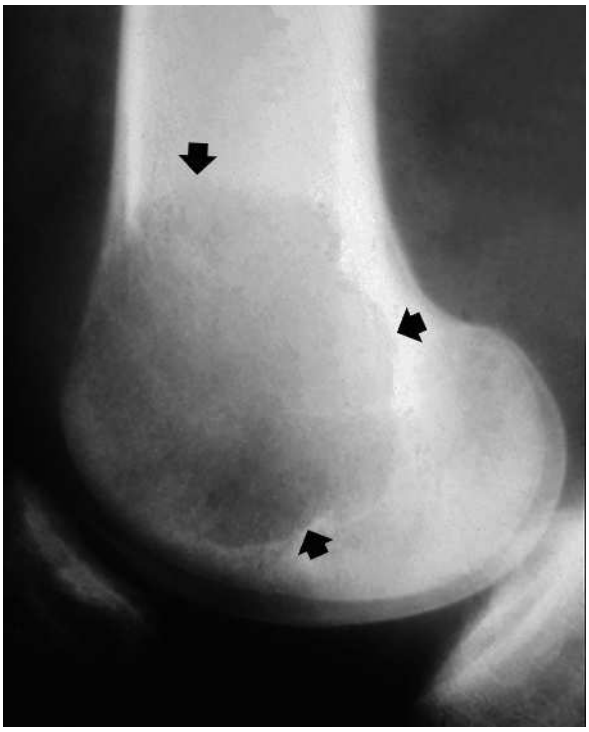

c

Fig. 16.7a–c. GCT of the distal femur in a 24-year-old man. **a** Collimated, lateral, delayed static image from MDP scintigraphy shows marked radiotracer accumulation in the lesion in the distal femur (*large asterisk*). The "extended pattern of uptake" is well demonstrated with increased tracer uptake in the patella and proximal femur (*small asterisks*). **b** Arterial phase film from conventional arteriogram shows the marked hypervascularity of the lesion. **c** Lateral radiograph of the distal femur shows findings of typical giant cell tumor (*arrows*)

of GCTs (Herman et al. 1987; Lee et al. 1998). CT is particularly useful for the identification of cortical thinning, pathologic fracture, periosteal reaction, assessing the degree of osseous expansile remodeling, and confirming the absence of matrix mineralization (Fig 16.5). CT is generally superior to MR imaging in assessing these features (Murphey et al. 2001). Soft-tissue extension is common at CT and MR imaging and has been reported to occur at CT in 33%–44% of cases (Hudson et al. 1984; Levine et al. 1984).

16.6.5 Magnetic Resonance Imaging

As with other musculoskeletal neoplasms, MR imaging is superior to CT in delineating soft-tissue tumor extent because of its improved contrast resolution. In our experience, soft tissue extension typically occurs at the metaphyseal portion of the lesion because the articulate cartilage overlying at the epiphyseal aspect of the tumor is a barrier to tumor extension. This also explains why joint involvement is unusual, despite the subarticular spread of GCT (Murphey et al. 2001). There are exceptions to this general rule, however, exemplified by GCT of the sacrum, which commonly extends across the sacroiliac joint and into the ilium (38% of cases) (Smith et al. 1979). MR imaging frequently reveals a relatively well-defined lesion with a low-signal-intensity margin, representing either osseous sclerosis or a pseudocapsule. In our experience, in the vast majority of cases, the solid components of GCT show a low to intermediate signal intensity at T1- and non-fat-suppressed T2-weighted MR imaging (Figs. 16.2 and 16.5).

16.6.6 Imaging of Secondary ABC Change

Secondary ABC formation in GCT is not uncommon, being seen in about 15% of lesions (Abdelwahab et al. 1994; Hudson et al. 1984; Kaplan et al. 1987; Kransdorf and Sweet 1995; Manaster and Doyle 1993; Martinez and Sissons 1988; Mirra 1989; Resnick et al. 2002; Unni 1996; Vergel De Dios et al. 1992), and GCT is the most common lesion associated with secondary ABC, accounting for 39% of these lesions (Kransdorf and Sweet 1995). While GCTs are uncommon in children, secondary ABC change is much more frequent in the pediatric age group, with 44% of lesions being predominantly cystic, and an additional 36% being partially cystic (Fig. 16.8) (Kransdorf et al. 1992). It is likely that this phenomenon is responsible for GCT in children being misdiagnosed as aneurysmal bone cyst. Cases of GCT with prominent ABC elements may have a more aggressive radiographic appearance, reflecting the expansile cystic component. These cystic/hemorrhagic areas are typically well seen at CT and MR imaging, although the latter modality is superior in this regard because of improved contrast resolution and ability to identify subacute blood and hemosiderin (Fig. 16.5) (Aoki et al. 1996).

GCT with secondary ABC change frequently shows the fluid levels at both CT and MR imaging, with fluid level visualization being influenced by image plane (axial and sagittal planes) and timing of the imaging (10 min may be required for sedimentation to occur) (Fig 16.9) (Hudson 1984). The fluid components show variable attenuation and signal intensity depending on their age and composition, often revealing low attenuation at CT, low or high signal intensity at T1-weighted MR imaging, and markedly increased signal intensity at T2-weighted MR imaging (Abdelwahab et al. 1994; Kaplan et al. 1987; Kransdorf and Sweet 1995; Martinez and Sissons 1988; Vergel De Dios et al. 1992). The areas of ABC change are readily distinguished from the solid component of the GCT. The solid areas are typically lobular and peripheral, showing extensive enhancement following contrast administration, in contradistinction to the thin and delicate peripheral and septal enhancement pattern seen in the cystic areas (Nascimento et al. 1979). Distinction between GCT with secondary ABC change and primary aneurysmal bone cyst is essential for accurate diagnosis and appropriate patient treatment.

16.7 Malignant Giant Cell Tumor

"Malignant GCT" is a term used to describe a heterogeneous group of giant cell-containing lesions that are capable of malignant behavior and of producing pulmonary metastases (Brien et al. 1997; Bullough and Bansal 2002; Horvai and Unni 2006; Maloney et al. 1989; Mauri et al. 2001; Mirra 1989; Murphey et al. 2001; Nascimento et al. 1979; Sanerkin 1980; Tubbs et al. 1992; Turcotte 2006). The prevalence of malignant GCT is controversial, although an incidence of 5%–10% of all GCT appears to be the most frequent consensus (Brien et al. 1997; Murphey et al. 2001; Nascimento et al. 1979; Rock et al. 1984; Tubbs et al. 1992; Turcotte 2006). Nevertheless, this figure must be viewed with caution in view of the lack of a consistent classification or nomenclature, and this percentage seems to be an overestimation in our experience.

We find it useful to use a modification of the classification of malignant GCT described by Mirra (1989). This grouping identifies those lesions that are related to benign conventional GCT and those that represent a giant cell-containing sarcoma, allowing them to be placed in three distinct groups: (1) benign metastasizing GCT, (2) true malignant GCT, and (3) giant cell-containing sarcoma.

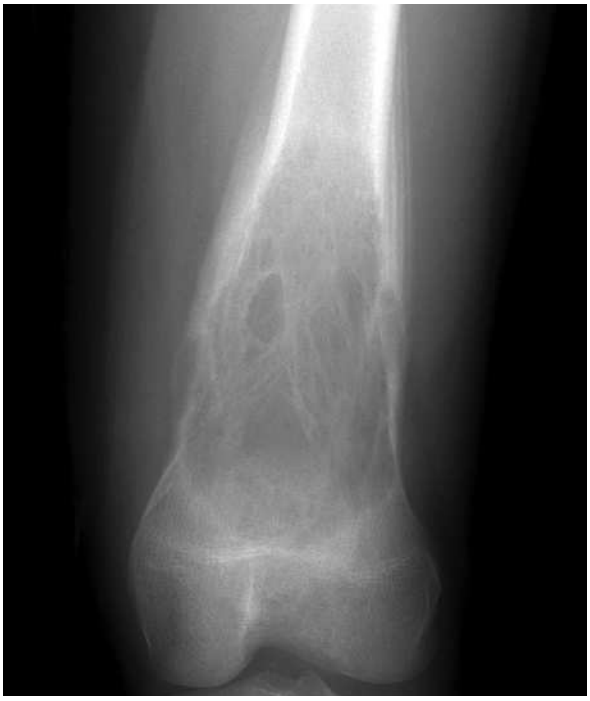

a

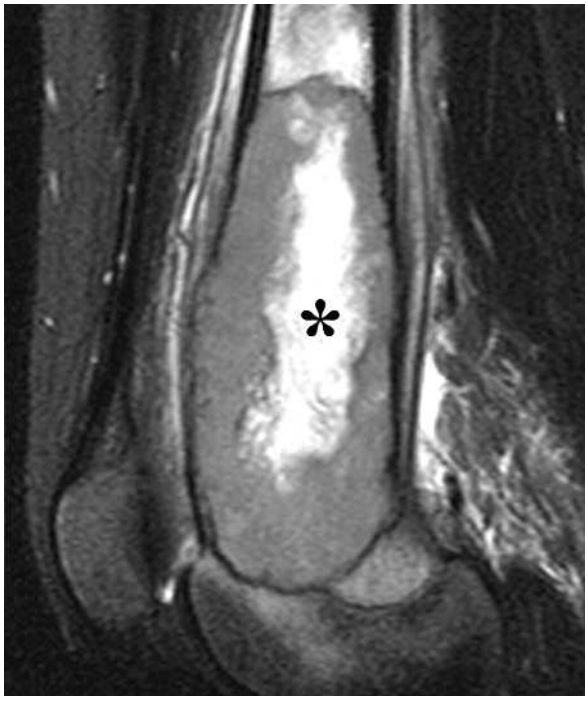

b

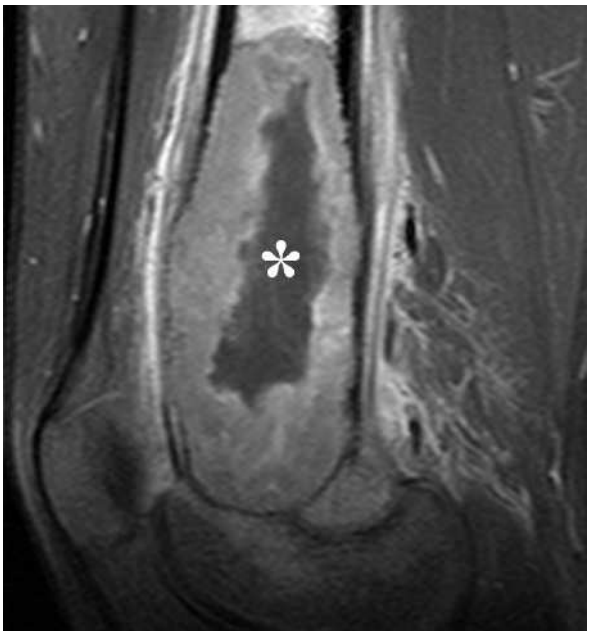

c

Fig. 16.8a–c. GCT of the distal femur with secondary aneurysmal bone cyst. **a** AP radiograph of the distal femur shows a nonmineralized geographic lytic lesion with associated continuous periosteal new bone formation. **b,c** Corresponding sagittal conventional T2-weighted (**b**) and fat-suppressed, post-contrast T1-weighted (**c**) SE MR images show the hemorrhagic area (*asterisks*) within the center of the mass. Note intermediate signal intensity from the solid portion of the tumor on conventional T2-weighted image **b**, as well as intense enhancement in the solid portions of the tumor **c**

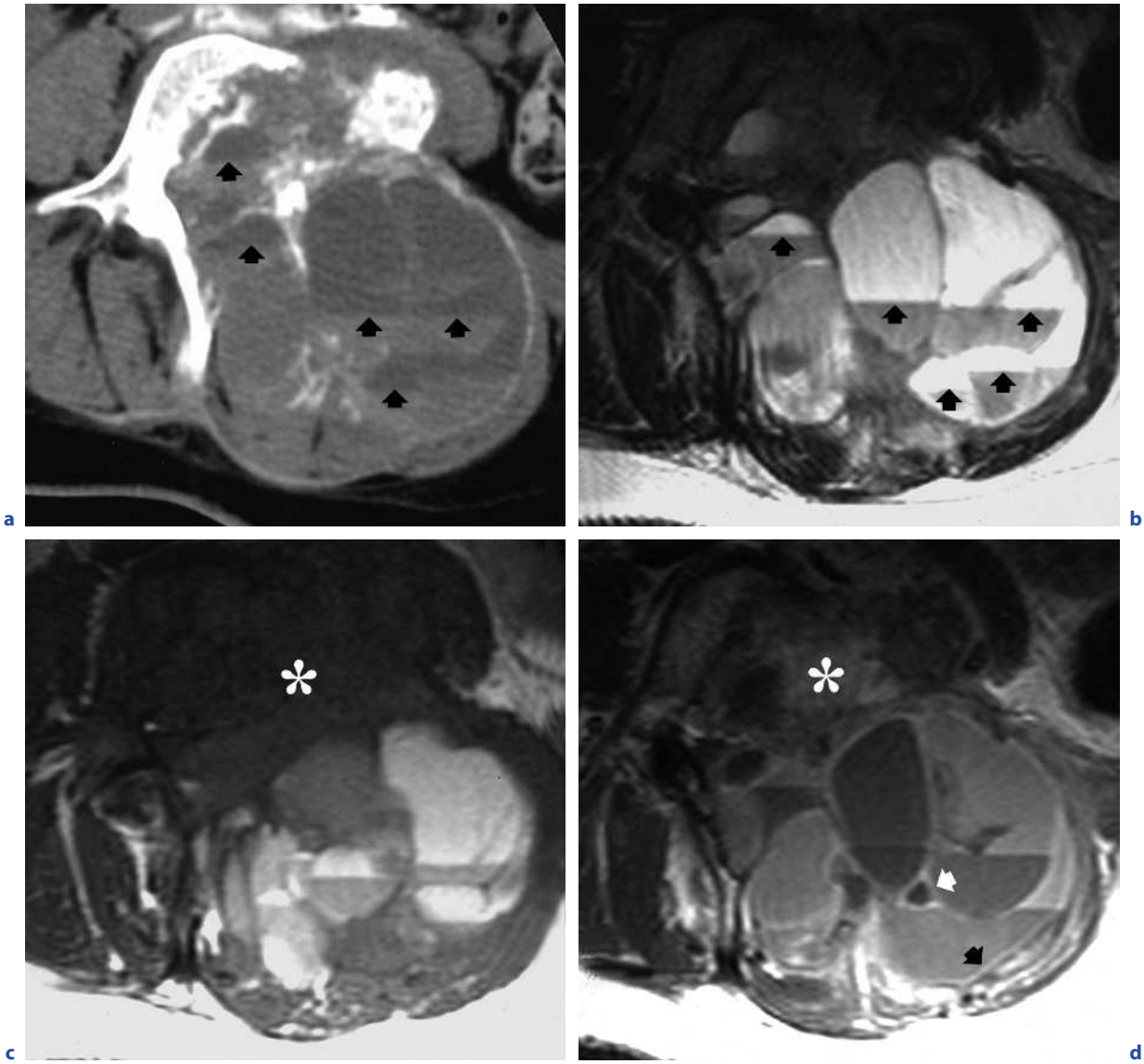

Fig. 16.9a–d. GCT with secondary aneurysmal bone cyst change of the spine. **a,b** Axial noncontrast CT scan (**a**) and conventional T2-weighted SE MR image (**b**) show multiple fluid levels (*arrows*) indicative of previous intralesional hemorrhage. **c,d** Corresponding axial T1-weighted SE MR images preceding (**c**) and following (**d**) intravenous contrast show a nodule of enhancing tumor in the anterior aspect of the mass. Note thin, uniformly enhancing, fibrovascular septations between the many blood-filled spaces (*arrows*; **d**)

16.7.1 Benign Metastasizing Giant Cell Tumor

Benign metastasizing GCT represents a lesion in which the metastases demonstrate a histologically benign appearance identical to that of conventional GCT (Mirra 1989). In a review of the literature in 1994, Nojima et al. (1994) reported 73 cases of pulmonary metastases in benign metastasizing GCT of bone, noting a reported prevalence of 1.8%–5.0%. Detailed information was available in 54 of these patients, and the authors noted that local recurrence preceded pulmonary metastases in 26 patients (48%). Pulmonary metastases were detected within 3 years of initial diagnosis in 74% of patients (Fig. 16.10), while pulmonary metastases were present at the time of initial diagnosis in 6% of patients

(Nojima et al. 1994). In patients with benign metastasizing GCT, pulmonary metastases may regress spontaneously or remain stable. Interestingly, lesions in the distal radius more frequently demonstrate this behavior, with only 12% of GCTs occurring in this location, whereas 38% of patients with pulmonary metastases have lesions at this site (Tubbs et al. 1992). Pulmonary metastases were seen in 3% of 568 patients with benign GCT in the Mayo Clinic series (Unni 1996). In general, the prognosis of patients with pulmonary metastases is good.

16.7.2 Malignant Giant Cell Tumor

The WHO defines malignancy in GCT as a high-grade sarcoma arising in a GCT (primary) or at the site of previously documented GCT (secondary) (Bullough and Bansal 2002). These "true" malignant GCTs represented approximately 6% of the 609 GCTs in the Mayo Clinic files reported by Unni (1996). A primary malignant GCT is more precisely defined as "a malignant tumor of bone that is composed of a sarcomatous growth juxtaposed to zones of typical benign GCT without a history of radiation therapy, repeated curettage, or resection" (Mirra 1989; Murphey et al. 2001; Nascimento et al. 1979; Sanerkin 1980; Unni 1996). A secondary malignant GCT of bone is defined as "a sarcomatous growth that occurs at the site of a previously documented GCT, usually after previous radiation therapy and less commonly after a long latency period or repeated resections (Mirra 1989; Murphey et al. 2001; Unni 1996). Primary malignant GCT represents about 13% of malignant GCTs. It is usually seen in patients older than those with conventional GCT (Horvai and Unni 2006). Secondary malignant GCT is much more common, representing about 87% of such cases. A history of pervious radiation therapy is found in 76% of patients with secondary malignant GCT, usually after a delay of 10 or more years, with the remaining cases occurring following surgical treatment (Horvai and Unni 2006).

16.7.3 Osteoclast-Containing Sarcoma

The final type of malignant GCT is osteoclastic (giant cell) sarcoma. Mirra (1989) defines this lesion as "a highly malignant tumor composed of anaplastic stromal and anaplastic osteoclast-like giant cells in which there is no evidence of tumor osteoid, bone or cartilage," considering it to be the anaplastic counterpart of benign GCT of bone. This rare tumor is most commonly seen in association with other processes, such as severe polyostotic Paget's disease (secondary osteoclastic sarcoma), and must be differentiated from other giant cell–rich sarcoma variants, such as those seen in osteosarcoma, fibrosarcoma, and malignant fibrous histiocytoma (Mirra 1989). Giant cell-containing sarcomas are rare, and there is no uniformly accepted classification scheme.

16.8 Multifocal Giant Cell Tumor

Multifocal GCTs of bone are rare and account for less than 1% of all cases of GCT of bone (Averill 1980; Dahlin 1985; Dhillon and Psasad 2007; Murphey et al. 2001; Tornberg et al. 1975; Sim et al. 1977). In a recent 2007 literature review by Dhillon and Prasad (2007), only 69 of the 101 previously reported cases had sufficient data for comprehensive analysis. Although the age of patients with multifocal GCT varies widely (range, 9–62 years), the mean age is 22.5 years and younger than that for solitary GCT, with about 21% of cases occurring in the skeletally immature (Dhillon and Psasad 2007). As with solitary GCT, most reviews of multifocal GCT report a slight female predilection (Averill 1980; Dahlin 1985; Dhillon and Psasad 2007; Murphey et al. 2001; Tornberg et al. 1975; Sim et al. 1977).

The number of lesions per patient varies. In a review by Sim et al. (1977), 5 of 11 patients had more than two sites of involvement, and up to 12 lesions have been reported (Dhillon and Psasad 2007). Multiple lesions are most often discovered synchronously (diagnosed within 6 month of each other), but may by identified metachronously (diagnosed more than 6 months apart). The latent period between development of the first and second lesion is usually at least 1 to 2 years, but has been reported to be as long as 24 years following initial diagnosis (Dhillon and Psasad 2007).

In general, the radiographic appearance of multifocal GCT is similar to that of solitary GCT. As in solitary lesions, the knee is the most common location for multifocal disease. However, there is an increased prevalence of involvement of the small bones of the hands or feet in patients with multifocal GCT, which are unusual sites for solitary lesions (Dhillon and Prasad 2007).

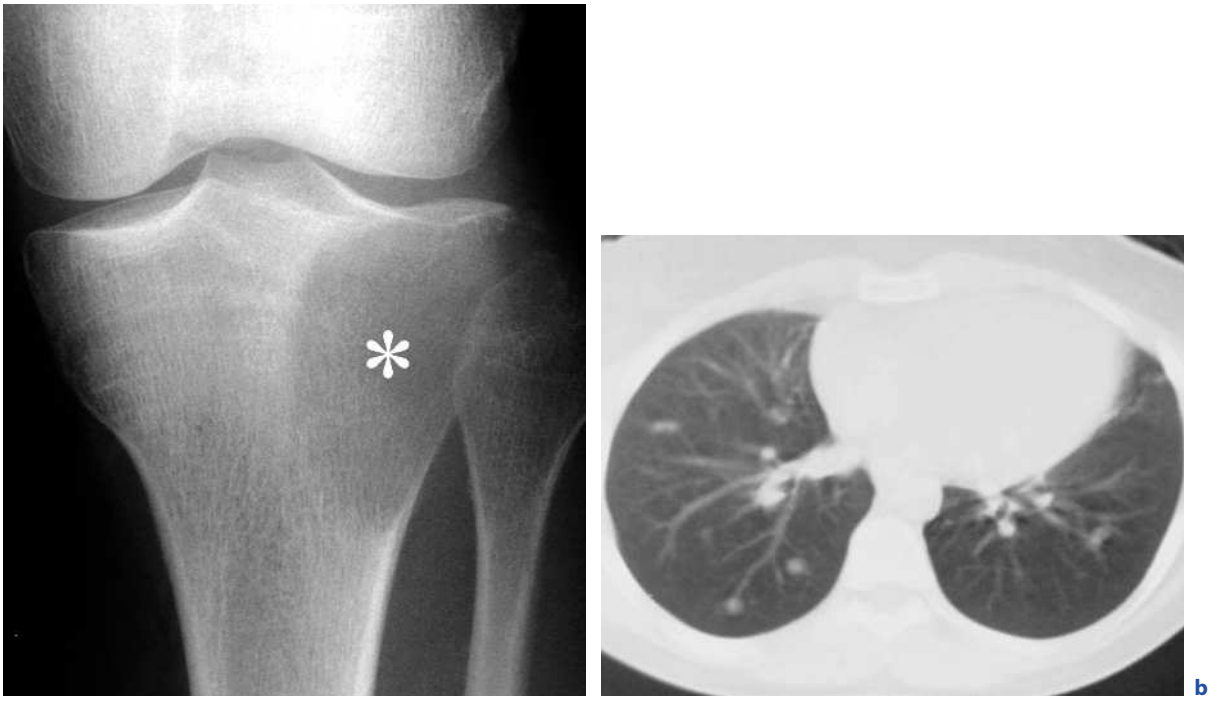

a b

Fig. 16.10a,b. Benign metastasizing GCT of the proximal tibia in a 30-year-old woman. **a** AP radiograph of the original lesion (*asterisk*) shows a nonmineralized geographic lytic lesion with a well-defined, nonsclerotic margin, typical of a GCT. The lesion recurred 6 months following initial resection and was treated with resection of the proximal tibia and allograft reconstruction. **b** Chest CT displayed on lung window approximately 18 months following initial presentation shows multiple pulmonary metastases. Biopsy of lung nodule showed histological features of typical GCT

16.9 Conclusion

The diagnosis of GCT of bone frequently has a characteristic clinical, radiographic, and imaging appearance. The diagnosis is suggested in a young adult by a lytic, nonmineralized, metaepiphyseal lesion involving a long bone. The lesion typically extends to subarticular bone in a skeletally mature patient, although the center of the lesion is usually located in the metaphysis. MR and CT imaging may identify a secondary ABC component, frequently with fluid levels, which are more common in young patients. When both cystic and solid components are present, biopsy must be directed at the solid regions of the tumor to ensure accurate pathologic diagnosis. GCT is typically solitary, with multifocal involvement seen in less than 1% of patients. Malignancy is unusual in GCT, accounting only for 5%–10% of all lesions, and occurs most often following irradiation of a benign GCT. Recognition of the above features will allow an accurate prospective diagnosis.

Comments

The opinions or assertions contained herein are the private views of the authors and are not to be construed as official or as reflecting the views of the Department of the Army or the Department of Defense.

References

Abdelwahab IF, Kenan S, Hermann G, Klein MJ, Lewis MM (1994) Case report 845: fluid-filling giant cell tumor with an aneurysmal bone cyst component. Skeletal Radiol 23:317–319

Aoki J, Moser RP, Vinh TN (1989) Giant cell tumors of the scapula: a review of 13 cases. Skeletal Radiol 18:427–434

Aoki J, Tanikawa H, Ishii K, et al. (1996) MR findings indicative of hemosiderin in giant cell tumor of bone: frequency, cause, and diagnostic significance. AJR Am J Roentgenol 166:145–148

Averill R, Smith R, Campbell C (1980) Giant cell tumors of the bones of the hand. J Hand Surg Am 5:39–50

Brien EW, Mirra JM, Kessler S, Suen M, Ho JKS, Yang WT (1997) Benign GCT of bone with osteosarcomatous transformation ("dedifferentiated" primary malignant GCT): report of two cases. Skeletal Radiol 26:246–255

Bullough PG, Bansal M (2002) Malignancy in giant cell tumour. In: Fletcher DM, Unni KK, Mertens F (eds) WHO classification of tumors. Pathology and genetics: tumors of soft tissue and bone. IARC Press, Lyon, France, pp 313

Burns TP, Weiss M, Snyder M, Hopson CN (1988) Giant cell tumor of the metatarsal. Foot Ankle 8:223–226

Carrasco CH, Murray JA (1989) Giant cell tumors. Orthop Clin North Am 20:395–405

Campanacci M, Baldini N, Boriani S, Sudanese A (1987) Giant cell tumor of bone. J Bone Joint Surg Am 69:106–114

Campanacci M, Giunti A, Olmi R (1975) Giant cell tumors of bone: a study of 209 cases with long-term follow-up in 130. Ital J Orthop Traumatol 1:249–277

Chew FS, Hudson TM (1982) Radionuclide bone scanning of osteosarcoma: falsely extended uptake patterns. AJR Am J Roentgenol 139:1071–1076

Coumbaras M, Pierot L, Felgeres AA, Boulin A, Gaillard S, Derome PJ (1999) Giant cell tumour involving the cranial vault: imaging and treatment. Neuroradiology 41:826–828

Dahlin DC (1985) Caldwell Lecture: Giant cell tumor of bone–highlights of 407 cases. AJR Am J Roentgenol 144:955–960

Dahlin DC, Cupps RE, Johnson EW Jr (1970) Giant cell tumor: a study of 195 cases. Cancer 25:1061–1070

deSantos LA, Murray JA (1978) Evaluation of giant cell tumor by computerized tomography. Skeletal Radiol 2:205–212

deSantos LA, Prando A (1979) Synovial hyperemia in giant cell tumor of bone: angiographic pitfall. AJR Am J Roentgenol 133:281–284

Dhillon MS, Prasad P (2007) Multicentric giant cell tumor of bone. Acta Orthop Belg 73:289–299

Eckardt J, Grogan T (1986) Giant cell tumor of bone. Clin Orthop 204:45–58

Frassica FJ, Sanjay BK, Unni KK, McLeod RA, Sim FH (1993) Benign giant cell tumor. Orthopedics 16:1179–1183

Goldenberg RR, Campbell CJ, Bonfiglio M (1970) Giant cell tumor of bone: an analysis of 218 cases. J Bone Joint Surg Am 52:619–664

Herman SD, Mesgarzadeh M, Bonakdarpour A, Dalinka MK (1987) The role of magnetic resonance imaging in giant cell tumor of bone. Skeletal Radiol 16:635–643

Horvai A, Unni KK (2006) Premalignant conditions of bone. J Orthop Sci 11:412–423

Hudson TM (1984) Fluid levels of aneurysmal bone cysts: a CT feature. AJR Am J Roentgenol 142:1001–1004

Hudson TM, Schiebler M, Springfield DS, Enneking WF, Hawkins IF, Spanier SS (1984) Radiology of giant cell tumors of bone: computed tomography, arthrotomography, and scintigraphy. Skeletal Radiol 11:85–95

Jaffe HL, Lichtenstein L, Portis R (1940) Giant cell tumor of bone. Its pathologic appearance, grading, supposed variants and treatment. Arch Pathol 30:993–1031

Kaplan PA, Murphey MD, Greenway G, Resnik D, Sartoris DJ, Harms S (1987) Fluid–fluid levels in giant cell tumors of bone: report of two cases. J Comput Tomogr 11:151–155

Kransdorf MJ, Moser RP Jr, Vinh TN, Aoki J, Callaghan JJ (1989) Primary tumors of the patella: a review of 42 cases. Skeletal Radiol 18:365–371

Kransdorf MJ, Sweet DE (1995) Aneurysmal bone cyst: concept, controversies, patient presentation, and imaging. AJR Am J Roentgenol 164:573–580

Kransdorf MJ, Sweet DE, Buetow PC, Giudicci MAI, Moser RP (1992) Giant cell tumor in skeletally immature patients. Radiology 184:233–237

Kumar R, Guinto FC, Madewell JE, David R, Shirkhoda A (1988) Expansile bone lesions of the vertebra. RadioGraphics 8:749–769

Larsson SE, Lorentzon R, Boquist L (1975) Giant cell tumor of bone. J Bone Joint Surg Am 57:167–173

Lee JA, Bank WO, Gonzalez–Melendez M, Olan WJ, Tabarra SO (1998) Giant cell tumor of the skull. RadioGraphics 18:1295–1302

Lee MJ, Sallomi DF, Munk PL, et al. (1998) Pictorial review: giant cell tumours of bone. Clin Radiol 53:481–489

Levine E, DeSmet AA, Neff JR (1984a) Role of radiologic imaging in management planning of giant cell tumor of bone. Skeletal Radiol 12:79–89

Levine E, DeSmet AA, Neff JR, Martin NL (1984b) Scintigraphic evaluation of giant cell tumor of bone. AJR Am J Roentgenol 148:343–348

Lewis VO (2007) What's new in musculoskeletal oncology. J Bone Joint Surg Am 98:1399–1407

Malawer MM, Bickels J, Meller I, Buch RG, Henshaw RM, Kollender T (1999) Cryosurgery in the treatment of giant cell tumor. A long-term follow-up study. Clin Orthop 359:176–188

Maloney WJ, Vaughan LM, Jones HH, Ross J, Nagel DA (1989) Benign metastasizing giant cell tumor of bone: report of three cases and review of the literature. Clin Orthop 243:208–214

Marui T, Yamamoto T, Yushihara H, Kurosaka M, Mizonu K, Akamatsu T (2001) De novo malignant transformation of giant cell tumor of bone. Skeletal Radiol 30:104–108

Manaster BJ, Doyle AJ (1993) Giant cell tumors of bone. Radiol Clin North Am 31:299–323

Martinez V, Sissons HA (1988) Aneurysmal bone cyst: a review of 123 cases including primary lesions and those secondary to other bone pathology. Cancer 61:2291–2304

McInerney DP, Middlemiss JH (1978) Giant cell tumor of bone. Skeletal Radiol 2:195–204

Mirra JM (1989) Bone tumors: clinical, radiologic and pathologic correlations, 2nd edn. Lea & Febiger, Philadelphia, pp 941–1020

Moser RP, Kransdorf MJ, Gilkey FW, Manaster BJ (1990) Giant cell tumor of the upper extremity. RadioGraphics 10:83–102

Murphey MD, Nomikos GC, Flemming DJ, Gannon FH, Temple HT, Kransorf MJ (2001) Imaging of giant cell tumor and giant cell reparative granuloma of bone: radiologic-pathologic correlation. RadioGraphics 21:1283–1309

Nascimento NG, Huvos AG, Marcove RC (1979) Primary malignant GCT of bone: a study of eight cases and review of the literature. Cancer 44:1393–1402

Nojima T, Takeda N, Matsuno T, Inoue K, Nagashima K (1994) Case report 896: benign metastasizing GCT of bone. Skeletal Radiol 23:583–585

O'Reilly M, Chew FS (1996) The scintigraphic features of giant cell tumors in relation to other imaging modalities. Clin Nucl Med 21:43–48

Patel MR, Desai SS, Gordon SL, et al. (1987) Management of skeletal giant cell tumors of the phalanges of the hand. J Hand Surg Am 12:70–77

Picci P, Manfrini M, Zucchi V, et al. (1983) Giant cell tumor of bone in skeletally immature patients. J Bone Joint Surg Am 65:486–490

Prando A, DeSantos LA, Wallace S, Murray JA (1979) Angiography in giant cell bone tumors. Radiology 130:323–331

Puri A, Agarwal MG, Shah M, Jambekar NA, Anchan C, Behle S (2007) Giant cell tumor of bone in children and adolescents. J Pediatr Orthop 27:635–639

Reddy CRRM, Rao PS, Rajakumari K (1974) Giant cell tumors of bone in south India. J Bone Joint Surg Am 56:617–619

Reid R, Banerjee SS, Sciot R (2002) Giant cell tumour. In: Fletcher DM, Unni KK, Mertens F (eds) WHO Classification of tumors. Pathology and genetics: tumors of soft tissue and bone. IARC Press, Lyon, France, pp 310–312

Resnick D, Kyriakos M, Greenway GD (2002) Tumors and tumor-like lesions of bone: imaging and pathology of specific lesions. In: Resnick D (ed) Diagnosis of bone and joint disorders, 4th edn. Saunders, Philadelphia, pp 3763–4128

Rock MG, Pritchard DJ, Unni KK (1984) Metastases from histologically benign giant-cell tumor of bone. J Bone Joint Surg Am 66:269–274

Sanerkin NG (1980) Malignancy, aggressiveness, and recurrence in giant cell tumor of bone. Cancer 46:1641–1649

Schütte HE, Taconis WK (1993) Giant cell tumor in children and adolescents. Skeletal Radiol 22:173–176

Schwimmer SR, Bassett LW, Mancuso AA, Mirra JM, Dawson EG (1981) Giant cell tumor of the cervicothoracic spine. AJR Am J Roentgenol 136:63–67

Shankman S, Greenspan A, Klein MJ, Lewis MM (1988) Giant cell tumor of the ischium: a report of two cases and review of the literature. Skeletal Radiol 17:46–51

Sim FH, Dahlin DC, Beabout JW (1977) Multicentric giant cell tumors in the long bones. J Bone Joint Surg Am 59:1052–1060

Smith J, Wixon D, Watson RC (1979) Giant cell tumor of the sacrum: clinical and radiologic features in 13 patients. J Can Assoc Radiol 30:34–38

Sung HW, Kuo WP, Chai YB, Liu CC, Li SM (1982) Giant cell tumor of bone: analysis of 208 cases in Chinese patients. J Bone Joint Surg Am 64:755–761

Tehranzadeh J, Murphy BJ, Mnaymneh W (1989) Giant cell tumor of the proximal tibia: MR and CT appearance. J Comput Assist Tomogr 13:282–286

Thrall JH, Geslien GE, Corcoron RJ, Johnson MC (1975) Abnormal radionuclide deposition patterns adjacent to focal skeletal lesions. Radiology 115:659–663

Tornberg DN, Dick HM, Johnston A (1975) Multicentric giant cell tumors in the long bones. J Bone Joint Surg Am 57:420–422

Tubbs WS, Brown LR, Beabout JW, Rock MG, Unni KK (1992) Benign giant–cell tumor of bone with pulmonary metastases: clinical findings and radiologic appearance of metastases in 13 cases. AJR Am JRoentgenol 158:331–334

Turcotte RE (2006) Giant cell tumor of bone. Orthop Clin N Am 37:35–51

Turcotte RE, Sim FH, Unni KK (1993) Giant cell tumor of the sacrum. Clin Orthop 291:215–221

Unni KK (1996) Dahlin's bone tumors. General aspects and data on 11,987 cases, 5th edn. Lippincott-Raven, Philadelphia, pp 1–10, 263–283

Unni KK, Inwards CY, Bridge JA, Kindblom LG, Wold LE (2005) Tumors of the bones and joints. ARP Press, Silver Spring, pp 281–298

Van Nostrand D, Madewell JE, McNiesh LM, Kyle RW, Sweet DE (1986) Radionuclide bone scanning in giant cell tumor. J Nucl Med 27:329–338

Vergel De Dios AM, Bond JR, Shrives TC, McLeod RA, Unni KK (1992) Aneurysmal bone cyst: a clinicopathologic study of 238 cases. Cancer 69:2921–2931

Walker DR, Rankin RN, Anderson C, Rock MG (1988) Giant cell tumor of the sacrum in a child. Can J Surg 31:47–49

Wang K, Allen L, Fung E, Chan CC, Chan JCS, Griffith JF (2005) Bone scintigraphy in common tumors with osteolytic components. Clin Nucl Med 30:655–671

Wang IC, Shih HN, Hsueh S, Hsu RW (1998) Giant-cell tumor of the patella: report of two cases. Changgeng Yi Xue Za Zhih 21:338–342

Werner M (2006) Giant cell tumour of bone: morphological, biological and histogenetical aspects. Int Orthop 30:484–489

Wold LE, Swee RG (1984) Giant cell tumor of the small bones of the hands and feet. Semin Diagn Pathol 1:173–184

Wülling M, Engels C, Jesse N, Werner M, Delling G, Kaiser E (2001) The nature of giant cell tumor of bone. J Cancer Res Clin Oncol 127:467–474

Yang DZ (1985) Clinicopathologic analysis of giant cell tumor of the bone: report of 35 cases. Zhonghua Zhong Liu Za Zhi 7:200–202

Ewing Sarcoma/PNET Tumors

17

Filip M. Vanhoenacker, Filip van Kerkhove, Benjamin Peersman, Peter Brys and Arthur M. de Schepper

CONTENTS

KEY POINTS

- ES and PNET are part of the same spectrum of neoplastic disorders, irrespective of their localisation or cellular differentiation.
- ES/PNET occurs in young patients.
- On radiographs/CT, 37.5% are located in the axial skeleton and 62.5% in the peripheral skeleton.
- ES/PNET involving the bone is mostly mixed sclerotic-lytic. A spiculated periosteal reaction is most frequent.
- The most characteristic finding on MRI is the presence of a large soft tissue mass.
- At initial presentation, 20%–30% of patients have pulmonary and/or skeletal metastases.
- PET-CT is becoming standard of care for initial staging, in monitoring response to chemotherapy and detection of recurrence or new metastatic disease.

F. M. Vanhoenacker, MD, PhD
Department of Radiology, University Hospital Antwerp, Wilrijkstraat 10, 2650 Edegem, Belgium

B. Peersman, MD
Department of Radiology, University Hospital Antwerp, Wilrijkstraat 10, 2650 Edegem, Belgium

A. M. de Schepper, MD
Department of Radiology, University Hospital Antwerp, Wilrijkstraat 10, 2650 Edegem, Belgium

F. van Kerkhove, MD
Department of Radiology, University Hospital Leuven, Herestraat 49, 3000 Leuven, Belgium

P. Brys, MD
Department of Radiology, University Hospital Leuven, Herestraat 49, 3000 Leuven, Belgium

17.1 Introduction

Ewing Sarcoma (ES) and primitive neuroectodermal tumor (PNET) were originally described as distinct clinicopathologic entities.

ES was named after James Ewing, who described the lesion in 1921 as an undifferentiated tumor involving the diaphysis of the long bones that, in contrast to osteosarcoma, was radiation-sensitive. Although the tumor most frequently involves the bone, ES has also been reported to arise in soft tissue (extraosseous ES) (Angervall and Enzinger 1975).

In 1918, Stout described a tumoral lesion in which small round cells originating from the ulnar nerve formed a rosette. This entity was designated as neuroepithelioma and later as PNET (Jaffe et al. 1984).

Recently, it has become evident that these diseases are actually part of the same spectrum of neoplastic diseases, known as the Ewing sarcoma family of tumors (EFT), which also includes adult neuroblastoma, malignant small-cell tumor of the chest wall or (Askin's tumor) (Askin et al. 1979), paravertebral small-cell tumor, and atypical ES (Delaney et al. 2008).

Although the histogenesis of these tumors has been debated over the years, evidence from immunohistochemical, cytogenetic, and molecular genetic studies supports a common neuroectodermal origin for all EFT. In other words, all tumors from the EFT spectrum should be designated as "Ewing/PNET", irrespective of their localization (intra- or extraosseous; chest wall or other atypical locations), or degree of (neural) differentiation.

Therefore, according to these new insights in the histogenesis, the previously used terminology "Ewing sarcoma" and "PNET" will be discarded and the tumor will be referred to as a unique tumor entity ("Ewing/PNET") in all cases. Table 17.1 summarizes synonyms that have been used in the past, but that should be avoided currently.

This chapter will focus particularly on Ewing/PNET involving the bone.

Table 17.1. Synonyms and old terminology

• Ewing sarcoma
• Primitive neuroectodermal tumors (PNET)
• Peripheral primitive neuroectodermal tumors (pPNET)
• CNS PNET
• Neuroblastoma
• Ewing family of tumors (EFT)
• Ewing sarcoma family of tumors (ESFT)
• Peripheral neuroepithelioma
• Askin tumor
• Neuroectodermal tumor
• Ectomesenchymoma
• Peripheral medulloepithelioma

17.2 Incidence

Ewing/PNET is the second most common primary musculoskeletal neoplasm in children and adolescents after osteosarcoma (Mar et al. 2008), with an annual incidence rate in Caucasians of 3 cases per million children less than 15 years of age (Paulussen et al. 2001). There is a slight male predominance. Most studies report a male/female ratio between 1.5/1 and 2.4/1 (Reinus and Gilula 1984; Peersman et al. 2007).

17.3 Age

Most tumors occur between the age 5 and 25 years of age, with a peak between 10 and 20. Rarely does the tumor develop in adults older than 30 years.

17.4 Location

The preferred sites are the long bones of the lower extremity. The most frequent involved bone is the femur (Fig. 17.1).

In the long bones, involvement of the metadiaphysis (59%) and diaphysis (35%) is most common (Kransdorf and Smith 2000; Peersman et al. 2007). Epiphyseal location is rare.

In the trunk, the pelvis (especially the ilium) is most frequently involved (Figs. 17.2 and 17.6), followed by the spine (Ilaslan et al. 2004) and sacrum (Baker and Dorfman 1996), scapula, ribs (Moser et al. 1990) and

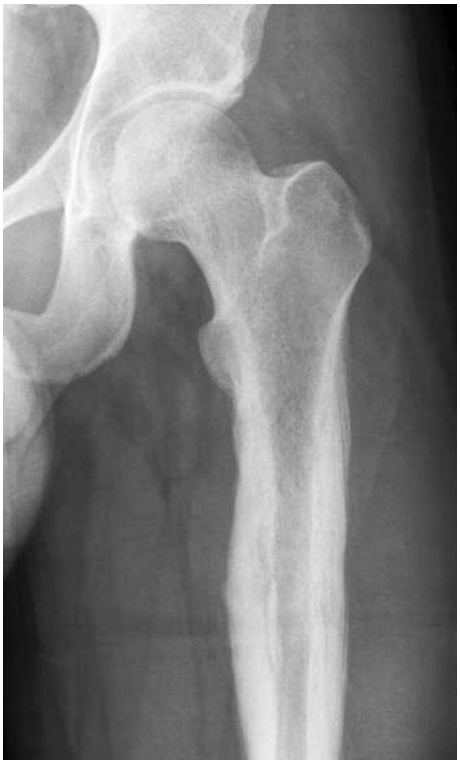

Fig. 17.1. Ewing/PNET of the left femur in a 20-year-old male. Notice the presence of an ill-defined osteolytic lesion, adjacent cortical thickening and lamellar periosteal reaction at the diaphysis of the femur

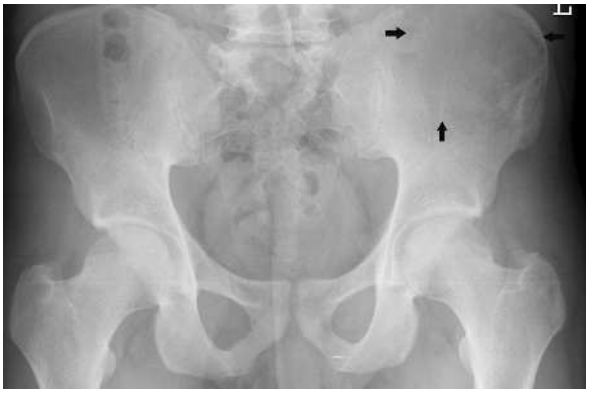

a

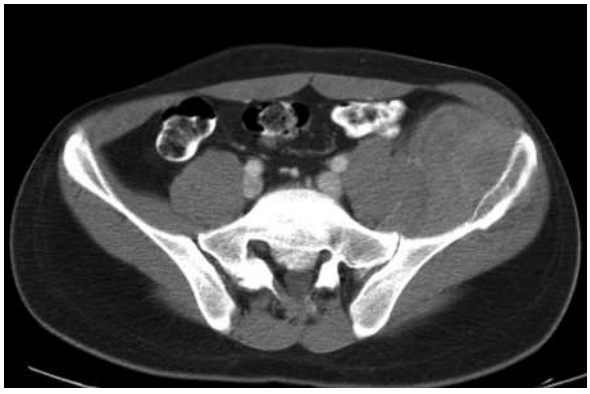

b

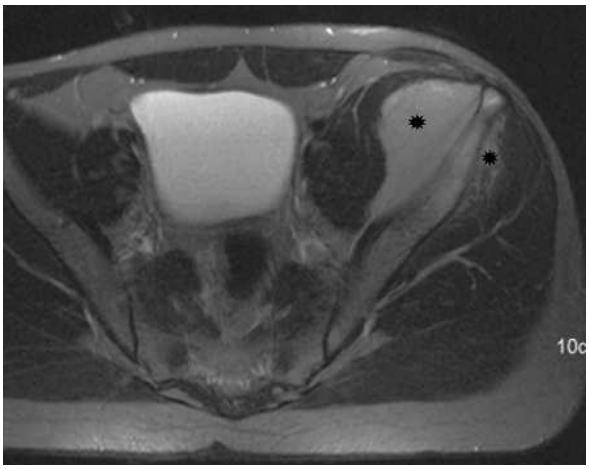

c

Fig. 17.2a–c. Ewing/PNET involving the left iliac bone in a 19-year-old male. **a** Plain radiograph of the pelvis; ill defined osteolytic lesion within the left ilium (*arrows*). **b** CT scan of the pelvis (soft tissue window) shows an extensive soft tissue mass, particularly within the left iliac muscle. **c** Axial fat-suppressed T2-weighted MR image demonstrates better the soft tissue extent due to its better contrast resolution

Fig. 17.3. Ewing/PNET of the left clavicle in a 20-year-old female. The plain radiograph reveals an ill defined permeative lesion at the lateral aspect of the clavicle. Note the subtle interrupted periosteal reaction with a Codman's triangle (*arrow*)

a

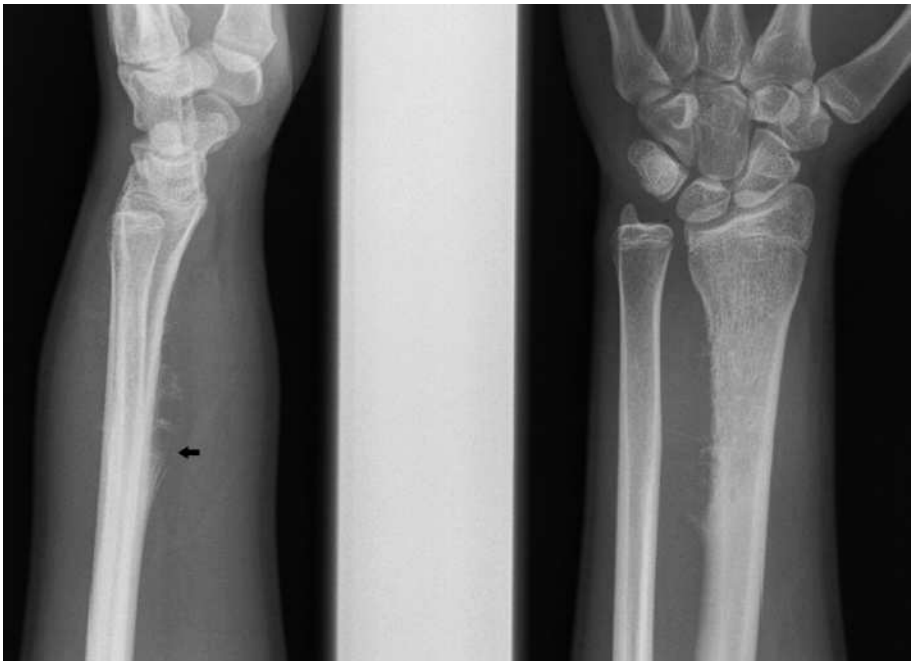

b

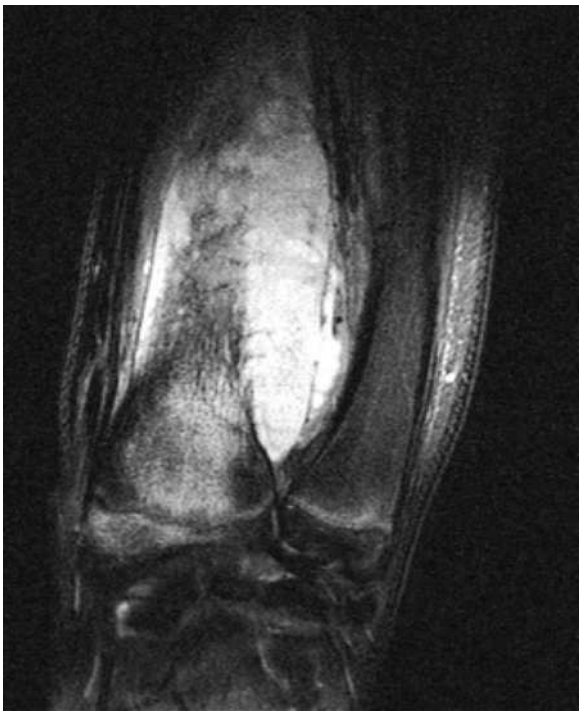

Fig. 17.4a,b. Ewing/PNET involving the distal diaphysis of the right radius in a 14-year-old female. **a** Plain radiograph of the right forearm; there is cortical permeation at the ulnar side of the radius. Notice also the presence of a Codman's triangle, representing an aggressive type of periosteal reaction (*arrow*). **b** Coronal fat-suppressed T2-weighted MR image shows a large associated soft tissue mass

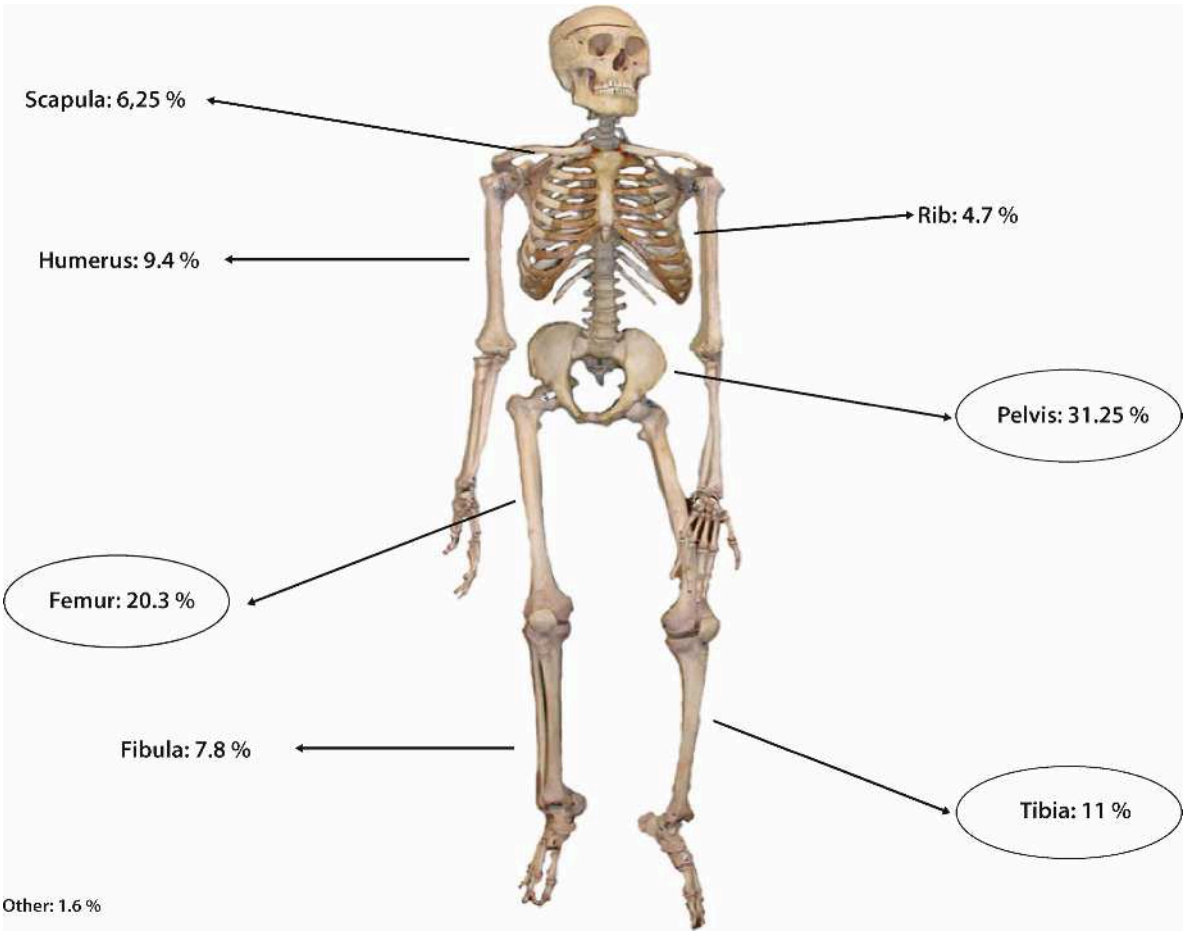

Fig. 17.5. Most frequent locations based on our own series of 64 patients (used with permission from Peersman et al. 2007). On radiographs/CT, 37.5% are located in the axial skeleton and 62.5% in the peripheral skeleton

clavicle (Fig. 17.3). Involvement of the lumbar spine is more frequent than the thoracic and cervical spine.

Less frequent osseous sites are the skull bones (Li et al. 2005), and forearm (Fig. 17.4) and hands and feet (Reinus and Gilula 1984; Baraga et al. 2001).

Ewing/PNET is less frequent in other locations, but can be seen in practically every (musculoskeletal) location (Mar et al. 2008).

Extraosseous EWING/PNET is rare. Virtually every organ system may be affected. The most well described extraskeletal site is the thoracopulmonary region, where it is known as the Askin tumor (Askin et al. 1979). Other sites include the kidney, retroperitoneal/paraspinal regions, head and neck areas and unusual locations in the body, including the uterus, ovary, testis, pancreas, adrenal gland, small bowel mesentery, urinary bladder, parotid gland, skin and subcutaneous tissue (Khong et al. 2002). Further discussion of extraosseous Ewing/PNET is beyond the scope of this chapter.

Figure 17.5 summarizes the most frequent locations based on our own series of 64 patients.

17.5 Clinical and Laboratory Findings

Clinical presentation is usually nonspecific. Pain is the most important and earliest finding (80%). The pain may radiate to the limbs, particularly with tumors in the vertebral or pelvic region.

Trauma, often minor, may be the initiating event that calls attention to the lesion.

Swelling is also a common and early sign, presenting as a firm and tender extraosseous mass. Rarely, a soft tissue mass may be absent.

Constitutional symptoms or signs, such as fever, fatigue, weight loss, or anemia, are present in about 10%–20% of patients at presentation (Rud et al. 1989). Fever is related to cytokines produced by the tumor cells and, along with other systemic symptoms, is associated with advanced disease (Delaney et al. 2008). Pathologic fracture may occur in 7.8% (Peersman et al. 2007).

The tumor is usually solitary and nonfamilial, although multiplicity has been reported in 10% at time of presentation and rare cases of affected siblings have been described in the literature (Kransdorf and Smith 2000). Recently, a Ewing/PNET associated with Nail-Patella syndrome has been described. The significance of these associations is, however, not known (Steens et al. 2007).

Laboratory findings may include an increase of serum lactic dehydrogenase (LDH), increased erythrocyte sedimentation rate, leukocytosis and anemia.

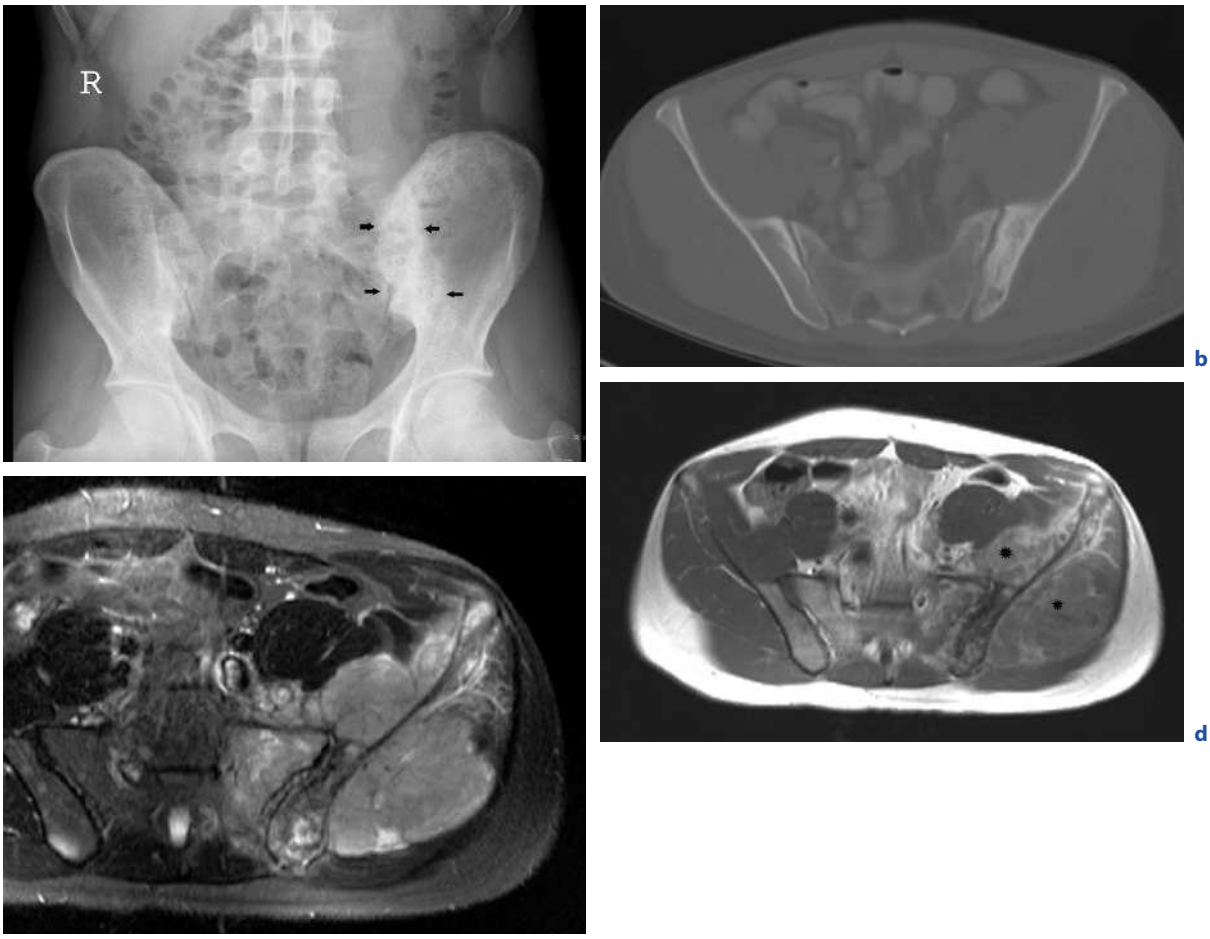

Fig. 17.6a–d. Ewing/PNET involving the left iliac bone in a 24-year-old female. **a** Plain radiograph of the pelvis; ill defined sclerotic lesion within the left iliac bone, adjacent to the sacroiliac joint (*arrows*). Radiographic evaluation does not allow to evaluate involvement of the sacroiliac joint, nor soft tissue involvement. **b** The corresponding CT scan of the pelvis shows extensive sclerosis of the left iliac bone, but fails to demonstrate transarticular tumor extension. **c** Axial fat-suppressed T2-weighted MR image demonstrates far better the bone (involvement of both iliac and sacral bone on the left side) and huge soft tissue extent. **d** Axial T1-weighted MR image after intravenous administration of gadolinium chelates. Heterogeneous contrast uptake of the bone and soft tissue component (*asterisks*) of the lesion

17.6 Imaging Features

17.6.1 Plain Radiography

Reinus and Gilula (1984) reviewed the radiographs of 373 patients and described the radiographic features of ES. Findings were divided into three categories, depending on their frequency of occurrence: common findings (>30%), uncommon findings (>10%, <30%) and rare findings (<10%). Poor margination, soft tissue involvement, bone permeation, laminated periosteal reaction (Fig. 17.1) and sclerotic matrix (Fig. 17.6) were described as common findings. Soft tissue involvement is, however, underestimated on plain radiographs (Figs. 17.1, 17.2, 17.6, and 17.7). Spiculated periosteal reaction, cortical thickening and violation (Fig. 17.4 and 17.8), purely lytic matrix, pathologic fracture, cystic component and bone expansion were described as uncommon findings. Soft tissue calcification, sauceriza-

tion, honeycombing, sharp margins and vertebra plana were described as rare findings.

Poor margination, extensive soft tissue component, sclerotic matrix and permeation were also common findings in a recent multicenter study, including 64 patients (Peersman et al. 2007). On the other hand, laminated periosteal reaction was an uncommon finding in this study (14%).

Although Reinus and Gilula (1984) described spiculated periosteal reaction as an uncommon finding, it is more than common (>50%) in the series of Peersman et al. (2007).

The less aggressive types of periosteal reaction, such as laminated periosteal reaction and onion skin, were described also by Resnick and Kransdorf (2005) to be common manifestations (57%), and the spiculated periosteal reaction as a less frequent manifestation (28%).

Peersman et al. (2007) described cortical permeation and destruction (Fig. 17.4) as common findings (respectively 31% and 42%), whereas cortical thickening (Fig. 17.1) was rather uncommon (20%). A patho-

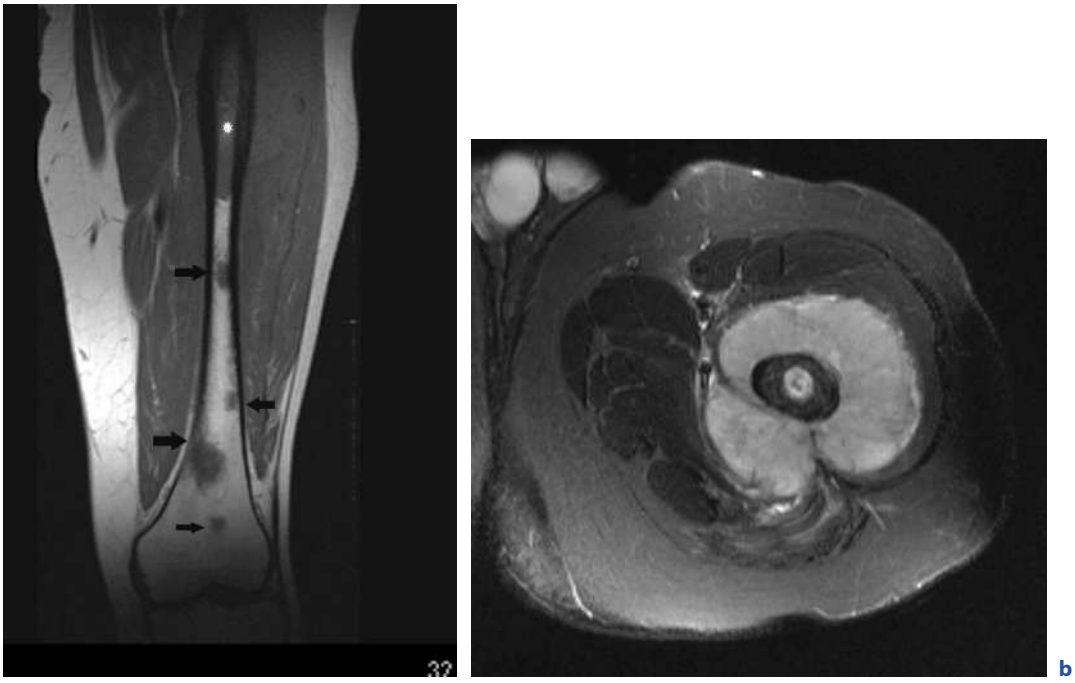

a b

Fig. 17.7a,b. Locoregional tumor spread on MRI. Same patient as in Fig. 17.1. **a** Coronal T1-weighted MR image. The primary tumor – as demonstrated on the plain radiographs – is located within the middiaphysis of the left femur (*asterisk*). Notice the presence of multiple skip metastases within the distal diaphysis (*black arrows*). **b** Axial fat-suppressed T2-weighted MR image shows a huge associated soft tissue mass

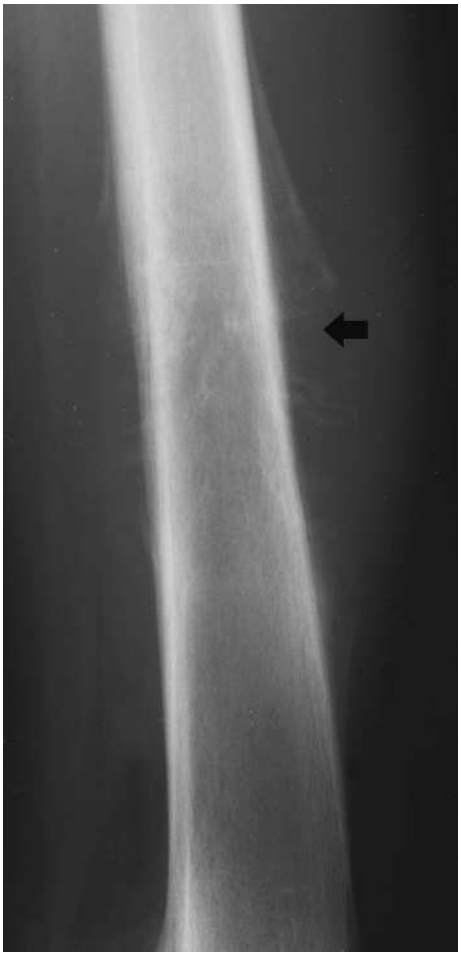

a

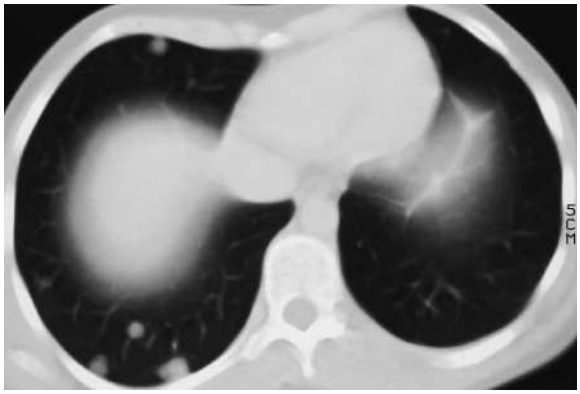

b

Fig. 17.8a,b. Distant pulmonary metastases in Ewing/PNET of the left femur in a 14-year-old male. **a** Plain radiograph showing an ill-defined osseous lesion at the diaphysis with associated Codman's triangle (*black arrow*). **b** Axial CT scan of the chest revealing multiple pulmonary metastases

logic fracture (7.8%), as well as soft tissue calcification and sharp margins were less findings.

Pathologic fracture was seen in 14% in the series of Reinus and Gilula (1984).

Although plain radiography is often the initial method for detection (and imaging characterization) of osseous Ewing/PNET, radiographs are not primarily used for follow-up after treatment.

17.6.2 Computed Tomography (CT)

CT can be helpful to assess bone destruction and lesion's matrix (Fig. 17.6) in anatomically complex areas, such as the spine and pelvis. CT facilitates identification of subtle pathological fracture or cortical breakthrough. However, the preferred method for local staging and follow-up of the Ewing/PNET is MR imaging.

17.6.3 MR Imaging

MRI is the preferred imaging modality for evaluation of local tumor extent.

MRI is particularly accurate in the assessment of the intramedullary tumor extent in patients with bone sarcoma which is documented by the excellent correlation between longitudinal T1-weighted images and identical macrosections of the surgical specimens. Transverse TSE T2-weighted images best display the interface between tumor and adjacent soft tissues (Figs.17.2, 17.6 and 17.7) and the anatomical relationship with the neurovascular structures, allowing differentiation between

intracompartmental and extracompartmental disease (Hanna et al. 1994). Non-homogeneous signal intensity is seen on all pulse sequences.

Contrast between tumor and normal tissue, especially fat-containing tissue, is greatly enhanced by combining TSE with fat-selective presaturation.

T1-weighted images after administration of contrast material can be successfully combined with fat-selective presaturation to enhance contrast resolution.

No specific degree and pattern of enhancement on MRI is seen (Fig. 17.6d). Although Jiya and Wuisman (2005) described the occurrence of skip lesion in ES as rare, skip metastases were found in 14% of cases in Peersman's series (Fig. 17.7b) (Peersman et al. 2007).

Most osseous tumors have a large soft tissue component; 65% presented with a soft tissue component of more than 50% (Figs. 17.2c, 17.4b, 17.6c,d and 17.7b) (Peersman et al. 2007).

MRI is very sensitive, but less specific for the determination of epiphyseal involvement. It is highly sensitive for excluding joint involvement although false-positive results may occur secondary to synovial inflammatory reactions.

In addition to locoregional staging, MRI may also be used for staging of distant metastatic disease. Whole body magnetic resonance has been shown to be more sensitive than bone scintigraphy in detection of osseous metastases and has the advantage of not involving ionizing radiation. According to some authors, however, FDG-PET is more sensitive than whole body MRI for detecting metastatic disease (Daldrup-Link et al. 2001; Mar et al. 2008).

MRI is the best modality to evaluate response to chemotherapy. It can define the decrease in size of the soft tissue mass which is a marker of tumor response (Van der Woude et al. 1994). A decrease in T2 signal of the lesion is thought to represent a favourable response by some authors, whereas an increase in T2 signal is reported to be nonspecific and was found histologically to represent granulation or fibrous tissue, necrosis, solid fields of viable tumor, or clusters of viable tumor within areas of necrosis (Van der Woude et al. 1994).

Dynamic enhanced MRI has been reported to be a sensitive study in evaluation of response to chemotherapy and can aid in differentiating viable from vascularised granulation tissue (Van der Woude et al. 1998). Viable tumor shows enhancement corresponding to the slope on a time-intensity curve greater than that of muscle but less than that of vessel, whereas the necrotic tumor is characterized by a lesser degree of enhancement than that of muscle.

Dynamic enhanced MRI is, however, not widely used in routine clinical practice, as it is relatively time consuming and technically challenging. Moreover, Miller et al. (2001) reported that information obtained from dynamic enhanced MRI did not predict survival rates.

17.6.4 Ultrasound

Ultrasound is not the primary imaging method of choice for imaging of Ewing/PNET. It is, however, frequently used for initial assessment of a patient, presenting with a soft tissue lump and to distinguish between cystic and solid masses. Additionally, it may detect extraosseous Ewing/PNET or soft tissue metastases (Mar et al. 2008).

17.6.5 Bone Scintigraphy

In most institutions, technetium Tc-99m methylene diphosphonate bone scintigraphy is still the routine standard for detection and follow-up of distant osseous metastatic disease. Other tracers, such as thallium-201 (^{201}TI) and gallium-67 (^{67}Ga), were previously used to assess therapeutic response, but these methods are currently replaced by fluorodeoxyglucose positron emission tomography (FDG-PET).

17.6.6 Positron Emission Tomography Scan/ Positron Emission Tomography-Computed Tomography

Fluorodeoxyglucose positron emission tomography (FDG-PET) is more sensitive than conventional bone scintigraphy in the detection of bone metastases, because increased glucose uptake by the tumor precedes any osteoblastic response (Gyorke et al. 2006). Due to its better spatial resolution compared to bone scintigraphy, FDG-PET can also detect nonosseous metastases (Franzius et al. 2000). The initial standardized uptake value of the primary tumor seems to correlate with tumor aggressiveness (Mar et al. 2008). PET-CT has even an increased specificity and sensitivity than FDG-PET alone, because of its capabilities to correlate anatomical information with function. Indeed, FDG-PET alone is insensitive to pulmonary metastases smaller than 1 cm. Adding CT increases sensitivity for smaller lesions. For

lung metastases, Iagaru et al. (2006) reported a 57% sensitivity of FDG-PET and 77% sensitivity of CT and a specificity of 96% for FDG-PET and 88% for CT. Therefore, PET-CT is becoming standard of care for initial staging, in monitoring response to chemotherapy and detection of recurrence or new metastatic disease (McCarville et al. 2005 ; Arush et al. 2007).

17.7 Histology

As noted above, the Ewing sarcoma family tumors represent a spectrum of tumors that range from the undifferentiated ES to atypical poorly differentiated ES and the differentiated PNET.

Histologically, the classic undifferentiated ES is composed of small, round, monotonous cells arranged in a sheet-like configuration. The cells have an increased nuclear-to-cytoplasm ratio, with hyperchromatic nuclei and scant cytoplasm. About 70% of cases demonstrate intracytoplasmic glycogen. Mitotic figures are rare.

Atypical ES contain larger cells, a greater degree of cellular pleiomorphism, and have a higher mitotic rate.

On the other side of the spectrum, PNET is characterized by a neural immunophenotype or there is evidence of neural differentiation on light microscopy (with formation of Flexner-type rosettes or Homer-Wright-type pseudorosettes) or ultrastructural examination.

Immunohistochemically, the neoplasm exhibits a variety of antigenic components ,such as CD99. There is high expression of MIC2p antigen, a membrane protein of unknown function (Ambros et al. 1991).

Cytogenetically, 85% have a balanced t(11;22)(q24;12) chromosome translocation (Szuhai et al. 2006).

17.8 Differential Diagnosis

For Ewing/PNET involving the bone, the differential diagnosis includes both benign and malignant conditions.

The most common benign condition which mimic Ewing/PNET of bone is subacute osteomyelitis. In both conditions, fever and an elevated sedimentation rate may be present, and imaging features may be similar, including an associated soft tissue mass. Aspiration of a necrotic-enflamed Ewing/PNET tumor may yield purulent material. On culture, however, tumor will be sterile (Campanacci 1999). Therefore, both histological examination and culture should be performed in all cases of suspected osteomyelitis or tumor.

Imaging features of eosinophilic granuloma (EG) may be very similar. Destructive EG, however, usually occurs at a younger age. A large soft tissue mass is indicative of Ewing/PNET.

Malignant tumors that should be considered in the differential diagnosis are other solid tumors of childhood, including lytic osteosarcoma, primary lymphoma of bone, spindle cell sarcoma, acute leukemia, and metastasis from a neuroblastoma or embryonal rhabdomyosarcoma. A primarily lytic osteosarcoma may be difficult to distinguish from a bony Ewing/PNET on imaging studies. Osteosarcoma is, however, most often located in the metaphysis and usually has a rim of bone formation, which is uncommon in osseous Ewing/PNET (Delaney et al. 2008). Lymphoma of bone is mostly found in adults, whereas Ewing/PNET is rare after 30 years of age (Campanacci 1999).

Metastatic neuroblastoma is often found before the age of 5 years, whereas Ewing/PNET is rare in this age group. Skeletal lesions are frequently multiple, there is a retroperitoneal or mediastinal mass, and catecholamines metabolites are found in urine (Campanacci 1999).

Embryonal rhabdomyosarcoma may only rarely invade the adjacent bone or metastasize to the bone.

ESS and soft tissue PNETs must be distinguished from a variety of benign and malignant soft tissue tumors, but further discussion of soft tissue lesions is beyond the scope of this chapter.

17.9 Staging Evaluation

For locoregional tumor staging, MRI is the imaging modality of choice (see Sect. 17.6.3).

At initial presentation, 20%–30% of patients have pulmonary (Fig. 17.8b) and/or skeletal metastases.

Classically, work-up for distant metastases includes a CT scan of the chest to evaluate pulmonary metastases and a bone scintigraphy to evaluate the entire skeleton for osseous metastases.

The potential role for PET-CT in the initial staging of Ewing/PNET has been discussed previously (see Sect. 17.6.6). Integrated PET/CT imaging may be particularly useful to detect unusual sites of metastases (McCarville et al. 2005).

No commonly used staging systems (TNM) exist for Ewing/PNET as they do for other solid tumors. A major

drawback of these staging systems is that they do not take the primary tumor site into account, which is one of the most important prognostic factors.

17.10 Prognostic Factors

Important prognostic factors include the age of the patient, primary tumor location and tumor size, the presence of certain chromosomal translocations, the presence or absence of distant metastasis and the response to therapy.

Other parameters such as tumor histology (neural differentiation grade) or extraosseous location do not have a significant adverse influence on disease outcome (Parham et al. 1999; Chow et al. 2000; Lee et al. 1995).

17.10.1 Age

Children younger than 10 seem to have a better prognosis than older ones. The 5-year relapse-free survival was significantly better for younger children (86% vs 55%, respectively) (Craft et al. 1998).

For adults, the relationship between age and prognosis is less clear. Although Baldini et al. (1999) reported a less favourable outcome in older adults as compared to children, a greater tumor bulk in adults may explain this different behavior (Delaney et al. 2008). Others have noted that adults with localized disease fare as well as children, and that adults should be treated in the same way as younger patients (Bacci et al. 2007).

17.10.2 Tumor Site and Size

Patients with a tumor located within the axial skeleton have a worse prognosis than those with extremity lesions (Cotterill et al. 2000).

Patients with small primary tumors (less than 100 mL) have a better outcome than those with large tumors (Cotterill et al. 2000). Fever, anemia and elevated serum LDH are correlated with larger tumor volume and a worse prognosis (Ferrari et al. 2001).

The poorer prognosis of tumors of the axial skeleton and large primary tumors, is at least partly attributable to the difficulty in surgical resection and higher rates of local failure after radiotherapy for larger lesions (Delaney et al. 2008).

17.10.3 Molecular Findings

Ewing/PNET is characterized by distinct non-random chromosomal translocations, which all involve the Ewing's sarcoma (EWS) gene on chromosome 22. These translocations result in the fusion of distinct genes on different chromosomes, and these fused genes encode hybrid proteins, which are thought to be involved in cancer development.

Certain variants in cytogenetic and molecular alterations in Ewing/PNET have been associated with a poor response to chemotherapy and a worse prognosis (Huang et al. 2005; Delaney et al. 2008).

17.10.4 Metastatic Disease

The key prognostic factor in Ewing/PNET is the presence or absence of metastasis. The 5-year relapse-free survival rates for patients with localized and metastatic disease at presentation are 55% and 21%, respectively. Patients with bone and lung metastasis have a significant worse prognosis than those with bone metastases alone, who in turn, fare worse than those with isolated lung metastases. Patients with limited pulmonary metastases may have a reasonable opportunity for cure. Of patients with limited lung metastases, 30% will survive years, as compared to only 10% of those with bone or bone marrow involvement (Cotterill et al. 2000).

17.10.5 Response to Therapy

Response to induction chemotherapy and the completeness of surgical resection are important prognostic factors. Patients with more than 10% residual viable tumor following neoadjuvant chemotherapy have a worse outcome (Cotterill et al. 2000; Oberlin et al. 2001).

The role of the different imaging modalities in the evaluation of response to treatment has been discussed in Sect. 17.6.

Recommended time intervals for follow-up imaging during and after the treatment are 3 to 6 months, depending on the clinical indication.

17.11 Treatment

Patients with apparently localized tumors are presumed to have subclinical metastatic disease. Therefore, current treatment of localized disease consists of initial multiagent neoadjuvant chemotherapy (combination of vincristine, doxorubicin, cyclophosphamide, ifosfamide and etoposide), followed by wide or radical surgery and/or radiotherapy. Preoperative chemotherapy aims to provide a reduction in size of the primary tumor, improve surgical margins, and decreases the possibility of microscopic spread during surgical intervention (Kransdorf and Smith 2000).

After local control, additional systemic therapy is administered for treatment of microscopic residual disease.

Increased survival with this multimodality approach has encouraged development of techniques to preserve or restore limb function, so-called limb salvage procedures. These procedures include reorientation of remaining muscles and/or bones, reconstruction using vascularised fibular autografts or bulk allografts and replacement of resected bone segments, entire bones and/or joints with metal-polymer implants (Mar et al. 2008).

Inoperable tumors receive radiation therapy and/or chemotherapy.

17.12 Conclusion

The current recommended imaging work-up of Ewing/PNET tumors should start with radiography followed by MRI for local tumor staging.

Distant metastatic disease should be evaluated by chest CT for pulmonary metastases and bone scintigraphy and/or PET(-CT) for bone metastases.

Follow-up imaging is performed during and after treatment, using the same imaging modalities as for initial work-up.

References

Ambros IM, Ambros PF, Strehl S et al. (1991) MIC2 is a specific marker for Ewing's sarcoma and peripheral primitive neuroectodermal tumors. Cancer 67:1886–1893

Angervall L, Enzinger FM (1975) Extraskeletal neoplasm resembling Ewing's sarcoma. Cancer 36:240–251

Arush MW, Israel O, Postovsky S et al. (2007) Positron emission tomography/computed tomography with 18fluorodeoxyglucose in the detection of local recurrence and distant metastases of pediatric sarcoma. Pediatr Blood Cancer 49:901–905

Askin FB, Rosai J, Sibley RK et al. (1979) Malignant small cell tumor of the thoracopulmonary region in childhood: a distinctive clinicopathologic entity of uncertain histogenesis. Cancer 43:2438–2451

Bacci G, Balladelli A, Forni C et al. (2007) Adjuvant and neoadjuvant chemotherapy for Ewing sarcoma family tumors in patients aged between 40 and 60: report of 35 cases and comparison of results with 586 younger patients treated with the same protocols in the same years. Cancer 109:780–786

Baker ND, Dorfman DM (1996) Ewing's sacoma of the sacrum. Skeletal Radiol 25:302–304

Baldini EH, Demetri GD, Fletcher CD et al. (1999) Adults with Ewing's sarcoma: primitive neuroectodermal tumor: adverse effect of older age and primary extraosseous disease on outcome. Ann Surg 230:79–86

Baraga JJ, Amrami KK, Swee RG (2001) Radiographic features of Ewing's sarcoma of the bones of the hands and feet. Skeletal Radiol 30:121–126

Campanacci M (1999) Ewings's sarcoma, primitive neuroectodermal tumor (PNET). In: Campanacci M (ed) Bone and soft tissue tumors, 2nd edn. Springer, Berlin Heidelberg New York, pp 653–682

Chow E, Mercant TE, Pappo A et al. (2000) Cutaneous and subcutaneous Ewing's sarcoma: an indolent disease. Int J Radiat Oncol Biol Phys 46:433–438

Cotterill SJ, Ahrens S, Paulussen M et al. (2000) Prognostic factors in Ewing's tumors of bone: analysis of 975 patients from the European Intergroup Cooperative Ewing's Sarcoma Study Group. J Clin Oncol 18:3108–3114

Craft A, Cotterill S, Malcolm A et al. (1998) Ifosfamide-containing chemotherapy in Ewing's sarcoma: The Second United Kingdom Children's Cancer Study Group and the Medical Research Council Ewing's Tumor Study. J Clin Oncol 16:3628–3633

Daldrup-Link HE, Franzius C, Link TM et al. (2001) Whole-body MR imaging for detection of bone metastasis in children and young adults. AJR Am J Roentgenol 177:229–236

Delaney T, Hornicek FJ, Mankin HJ (2008) http://www.uptodate.com

Ferrari S, Bertoni F, Mercuri M et al. (2001) Ewing's sarcoma of bone: relation between clinical characteristics and staging. Oncol Rep 8:553–556

Franzius C, Sciuk J, Daldrup-Link HE et al. (2000) FDG-PET for detection of osseous metastases from malignant primary bone tumours: comparison with bone scintigraphy. Eur J Nucl Med 27:1305–1311

Gyorke T, Zajic T, Lange A et al. (2006) Impact of FDG-PET for staging of Ewing sarcomas and primitive neuroectodermal tumours. Nucl Med Commun 27:17–24

Hanna SL, Fletcher BD, Kaste SC et al. (1994) Increased confidence of diagnosis of Ewing sarcoma using T2-weighted MR images. Magn Reson Imaging 12:559–568

Huang HY, Illei PB, Zhao Z et al. (2005) Ewing Sarcomas with p53 mutation or p16/p14ARF homozygous deletion: a highly lethal subset associated with poor chemoresponse. J Clin Oncol 23:548–558

Iagaru A, Chawla S, Menendez L et al. (2006) 18F-FDG PET and PET/CT for detection of pulmonary metastases from musculoskeletal sarcomas. Nucl Med Commun 27:785–802

Ilaslan H, Sundaram M, Unni KK et al. (2004) Primary Ewing's sarcoma of the vertebral column. Skeletal Radiol 33:506–513

Jaffe R, Santamaria M, Yunis EJ et al. (1984) The neuroectoderal tumor of bone. Am J Surg Pathol 8:885–898

Jiya TU, Wuisman PI (2005) Long-term follow-up of 15 patients with nonmetastatic Ewing's sarcoma and a skip lesion. Acta Orthop 76:899–903

Khong PL, Chan GC, Shek TW et al. (2002) Imaging of peripheral PNET: common and uncommon locations. Clin Radiol 57:272–277

Kransdorf MJ, Smith SE (2000) Lesions of unknown histogenesis: Langerhans cell histiocytosis and Ewing sarcoma. Semin Musculoskelet Radiol 4:113–125

Lee CS, Southey MC, Slater H et al. (1995) Primary cutaneous Ewing's sarcoma/peripheral primitive neuroectodermal tumors in childhood. A molecular, cytogenetic, and immunohistochemical study. Diag Mol Pathol 4:174–181

Li W-Y, Brock P, Saunders DE (2005) Imaging characteristics of primary cranial Ewing sarcoma. Pediatr Radiol 35:612–618

Mar WA, Taljanovic MS, Bagatell R et al. (2008) Update on imaging and treatment of Ewing sarcoma family tumors: what the radiologist needs to know. J Comput Assist Tomogr 32:108–118

McCarville MB, Christie R, Daw NC et al. (2005) PET/CT in the evaluation of childhood sarcomas. AJR Am J Roentgenol 184:1293–1304

Miller SL, Hoffer FA, Reddick WE et al. (2001) Tumor volume or dynamic contrast-enhanced MRI for prediction of clinical outcome of Ewing sarcoma family of tumors. Pediatr Radiol 31:518–523

Moser RP Jr, Davis MJ, Gilkey FW et al. (1990) Primary Ewing sarcoma of rib. Radiographics 10:899–914

Oberlin O, Deley MC, Bui BN et al. (2001) Prognostic factors in localized Ewing's tumours and peripheral neuroectodermal tumours: the third study of the French Society of Paediatric Oncology (EW88 study). Br J Cancer 85:1646–1654

Parham DM, Hijazi Y, Steinberg SM et al. (1999) Neuroectodermal differentiation in Ewing's sarcoma family of tumors does not predict tumor behavior. Human Pathol 30:911–918

Paulussen M, Fröhlich B, Jürgens H (2001) Ewing tumour: incidence, prognosis and treatment options. Paediatr Drugs 3:899–913

Peersman B, Vanhoenacker FM, Heyman S et al. (2007) Ewing's sarcoma: imaging features. JBR-BTR 90:368–376

Reinus WR, Gilula LA (1984) Radiology of Ewing's sarcoma: intergroup study (IESS). Radiographics 4:929–944

Resnick D, Kransdorf MJ (2005) Tumors and tumorlike diseases. In: Resnick D (ed) Bone and joint imaging, 3rd edn. Elsevier, Philadelphia, pp 1192–1198

Rud NP, Reiman HM, Pritchard DJ et al. (1989) Extraosseous Ewing's sarcoma. A study of 42 cases. Cancer 64:1548–1553

Steens SC, Kroon HM, Taminiau AH et al. (2007) Nail-Patella syndrome associated with Ewing sarcoma. JBR-BTR 90:214–215

Szuhai K, Ijszenga M, Tanke HJ et al. (2006) Molecular cytogenetic characterization of four previously established and two newly established Ewing sarcoma cell lines. Cancer Genet Cytogenet 166:173–179

Van der Woude HJ, Bloem JL, Holscher HC et al. (1994) Monitoring the effect of chemotherapy in Ewing sarcoma of bone with MR imaging. Skeletal Radiol 23:493–500

Van der Woude HJ, Bloem JL, Hogendoorn PC et al. (1998) Preoperative evaluation and monitoring chemotherapy in patients with high-grade osteogenic and Ewing's sarcoma: review of current imaging modalities. Skeletal Radiol 27:57–71

Hematopoietic Tumors

18

Laura W. Bancroft

CONTENTS

L. W. Bancroft, MD
Professor of Radiology, Adjunct Faculty, University of Central Florida, Orlando, FL 32816, USA
Radiologist, Florida Hospital, 601 E. Rollins, Orlando, FL 32803, USA
Adjunct Faculty, Mayo Clinic College of Medicine, Rochester, Minnesota 55901, USA

KEY POINTS

- There are overlapping features among hematopoietic tumors, including osteopenia, lytic lesions, and marrow infiltration.
- Myelofibrosis typically demonstrates diffuse osteosclerosis and splenomegaly due to extramedullary hematopoiesis.
- Hematopoietic tumors requiring frequent blood transfusions can lead to hemosiderin deposition and low marrow signal intensity on MRI.
- Myelomatous lesions are usually well-circumscribed lytic lesions, and can demonstrate expansile remodeling of the cortical bone.
- Lymphoma can be radiographically occult and MRI findings are frequently out of proportion to those predicted on radiographs.
- Lymphoma can extensively infiltrate the marrow and extend into the adjacent soft tissues without causing significant cortical destruction.

18.1 Introduction

The World Health Organization classifies hematopoietic tumors into chronic myeloproliferative diseases, myelodysplastic/myeloproliferative diseases, myelodysplastic syndromes, acute myelogenous leukemia, and B-cell neoplasms (Jaffe et al. 2001). In general, the marrow-infiltrating processes of many of these hematopoietic tumors can lead to overlapping features on radiographs, scintigraphy, computed tomography (CT), magnetic resonance imaging (MRI), and positron emission tomography (PET) imaging; however, the following discussion will elucidate several distinguishing imaging features.

18.2 Chronic Myeloproliferative Diseases

Chronic myeloproliferative diseases encompass a variety of disorders with hyperplastic bone marrow, hematopoiesis independent of physiologic stimuli, increased circulating blood cell concentration, tendency to develop marrow fibrosis, and tendency to terminate in acute leukemia (Cloran and Banks 2007); these include chronic myelogenous leukemia, chronic neutrophilic leukemia, chronic eosinophilic leukemia, polycythemia vera, chronic idiopathic myelofibrosis, essential thrombocytopenia, and chronic myeloproliferative disease (unclassifiable) (Jaffe et al. 2001).

18.2.1 Chronic Myelogenous Leukemia

Chronic myelogenous leukemia (CML) is the most common myeloproliferative disease (15–20% of all cases of leukemia), has a median age of diagnosis in the fifth and sixth decades, and a slight male predominance (Vardiman 2001). Patients with CML (as well as any of the leukemias) may demonstrate diffuse osteopenia on radiographs and marrow-infiltration evident on MRI (Kobayashi 2005). Leukemia and multiple other hematopoietic tumors may demonstrate nonspecific marrow infiltration, with hypointense T1 signal and hyperintense T2 signal (Hwang and Panicek 2007). Utilization of in-phase and out-of-phase imaging can be helpful: the literature suggests that a signal intensity loss of more than 20% on out-of-phase imaging is highly worrisome for malignant marrow infiltration (Zajick et al. 2005).

18.2.2 Polycythemia Vera

Polycythemia vera is a myeloproliferative disorder arising in a clonal hematopoietic stem cell, and is characterized by increased red blood cell production independent of autoregulation (Pierre et al. 2001). There is a slight male predominance and the mean age at diagnosis is 60 years (Pierre et al. 2001). Patients will have a disproportionate amount of red marrow relative to yellow, resulting in an infiltrative pattern on MR imaging (Fig. 18.1). Because of the high viscosity of blood in patients with polycythemia vera, slow flow and vessel occlusion can occur. As a result, patients can present with portal venous occlusion and sequelae of portal venous hypertension (Fig. 18.1).

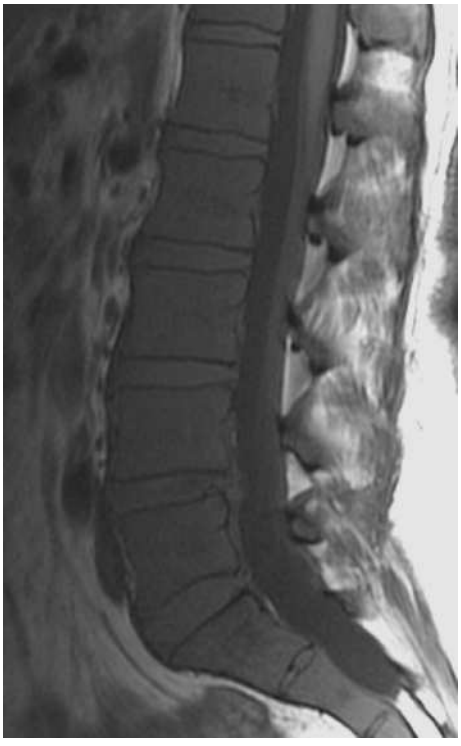

a

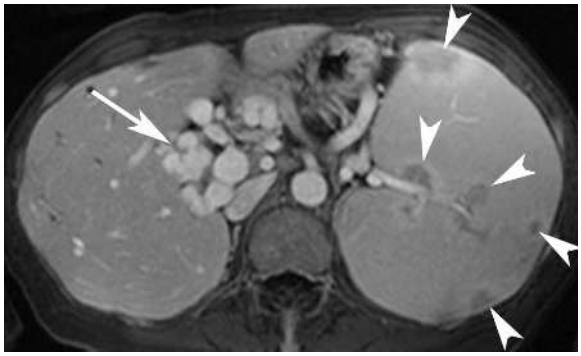

b

Fig. 18.1a,b. Polycythemia vera in a 64-year-old woman. **a** Sagittal T1-weighted image of the lumbar spine demonstrates diffusely abnormal marrow signal that is hypointense to the intervertebral discs. **b** Axial T2-weighted image through the abdomen shows cavernous transformation of the portal vein (*arrow*) and portal vein thrombosis due to polycythemia vera. Splenomegaly is secondary to portal venous hypertension. Multiple small low intensity splenic foci (*arrowheads*) are likely due to infarcts

18.2.3 Chronic Idiopathic Myelofibrosis

Chronic idiopathic myelofibrosis is another chronic myeloproliferative disorder characterized by an abnormal maturation of red blood cells and granulocytes with marrow fibrosis or sclerosis (Cloran and Banks 2007). Myelofibrosis affects 1:100,000 individuals and the median age at diagnosis is 60 years (Cloran and Banks 2007). The etiology of myelofibrosis is incompletely understood, and a clear genetic marker has not been identified. Clinical presentation is variable and 25% of patients are asymptomatic at presentation. Common signs and symptoms include fatigue, weight loss, bruising and bleeding, fever night sweats and splenomegaly. Laboratory findings include anemia and variable neutrophil and platelet counts. Imaging reflects the fibrotic marrow changes and chronic anemia. Radiographs often show sclerosis in the axial skeleton and proximal long bones, with or without associated paravertebral masses from extramedullary hematopoiesis and enlarged splenic silhouette (Resnick and Haghighi 2002). Skeletal scintigraphy may show a "superscan," with little or no appreciable renal activity and increased radioactivity in the skeleton (Fig. 18.2). MRI is useful in confirming the diffuse marrow infiltration, quantifying splenic volume, and detecting additional areas of extramedullary hematopoiesis (Fig. 18.2).

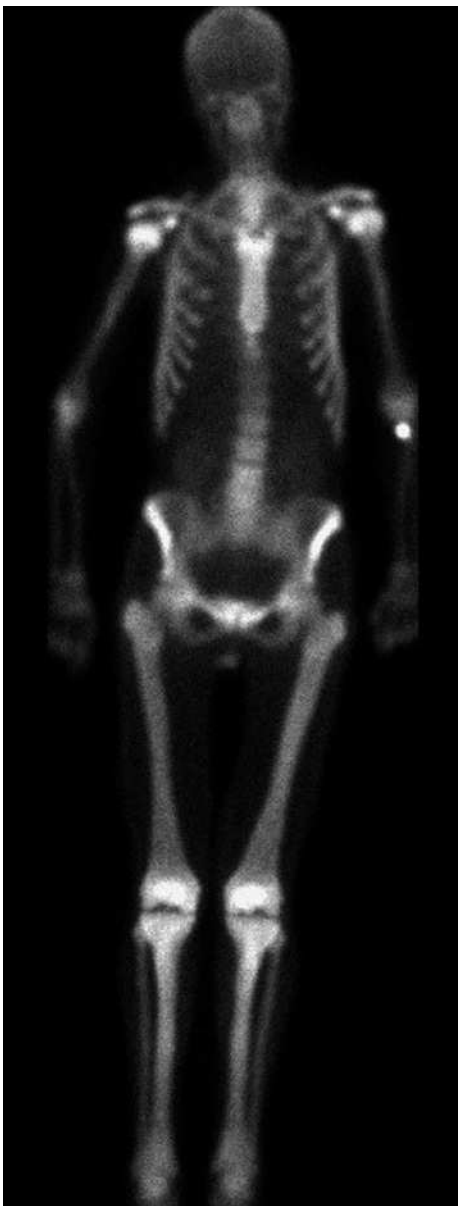

a

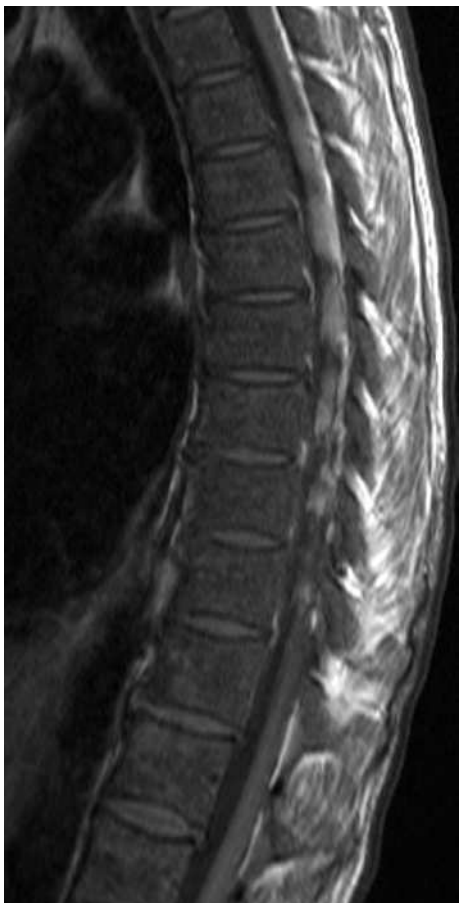

b

Fig. 18.2a–c. Myelofibrosis. **a** Tc-MDP skeletal scintigraphy in a 62-year-old woman with myelofibrosis reveals no appreciable renal activity and increased radioactivity in the skeleton, consistent with a "superscan." **b** Sagittal T1-weighted image through the thoracolumbar spine in the same patient shows diffusely low signal intensity marrow. (**c**) *see next page*

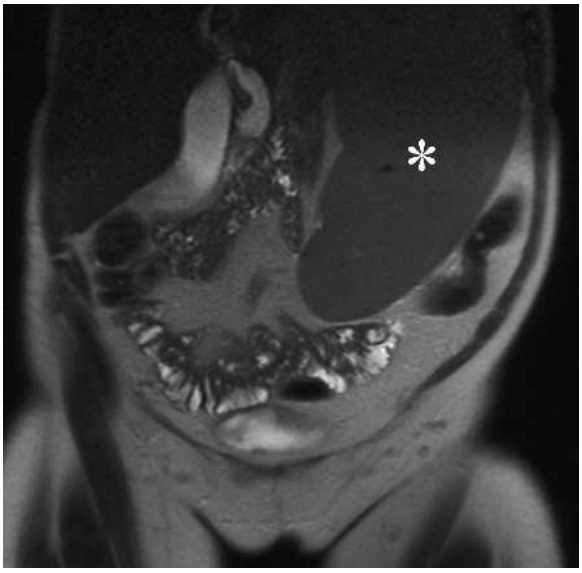

c

Fig. 18.2a–c. (*continued*) **c** Coronal T2-weighted MRI in the same patient shows marked splenomegaly (*asterisk*) caused by extramedullary hematopoiesis

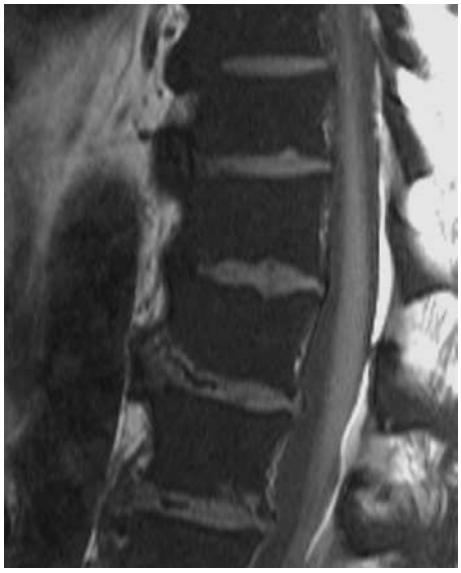

Fig. 18.3. Transfusion-dependent myelodysplastic syndrome in an 80-year-old man. T1-weighted sagittal image through the lower thoracic spine shows diffuse, markedly hypointense marrow signal intensity. Radiographs demonstrated normal bone density. Findings are consistent with hemosiderin deposition in this patient who required biweekly blood transfusions for his anemia caused by myelodysplastic syndrome

18.3 Myelodysplastic Syndromes

Myelodysplastic syndromes include refractory anemia (with or without ringed sideroblasts or excessive blasts), refractory cytopenia with multilineage dysplasia, and myelodysplastic syndrome (unclassifiable or associated with isolated del(5q) chromosome abnormality (Jaffe et al. 2001).

Transfusion-dependent myelodysplastic syndromes can show diffuse, markedly hypointense marrow signal intensity due to hemosiderin deposition and/or hyperplastic marrow due to chronic anemia (Fig. 18.3). Myelodysplastic marrow can also be heterogeneous and nonspecific on MR imaging (Fig. 18.3).

18.4 Acute Myeloid Leukemia

Acute myeloid leukemia (AML) is a clonal expansion of myeloid blasts in the bone marrow, blood or other tissue, accounting for 70% of all cases of acute leukemia (Brunning et al. 2001a). The vast majority of cases occur in adults (median age 60 years) and there is an equal distribution among men and women (Brunning et al. 2001a). Investigators using iron oxide-enhanced imaging have correlated imaging findings and bone marrow angiogenesis in patients with AML (Matuszewski et al. 2006). Change in R2* (gradient echo) relaxation time maps have shown prominent areas of highly vascularized bone marrow in patients with AML, whereas control subjects had only moderately vascularized bone marrow with homogeneous vessel distribution (Matuszewski et al. 2006).

Chloromas (granulocytic sarcomas) are localized extramedullary tumors composed of malignant myeloid-lineage cells that may be the first manifestation of disease in patients with nonlymphocytic leukemia or a secondary lesion in patients with a history of myelodysplastic disorders (Fritz 2006). Chloromas have nonspecific signal intensity on MRI but are typically hyperintense to muscle on fluid-sensitive sequences and avidly enhance (Fig. 18.4).

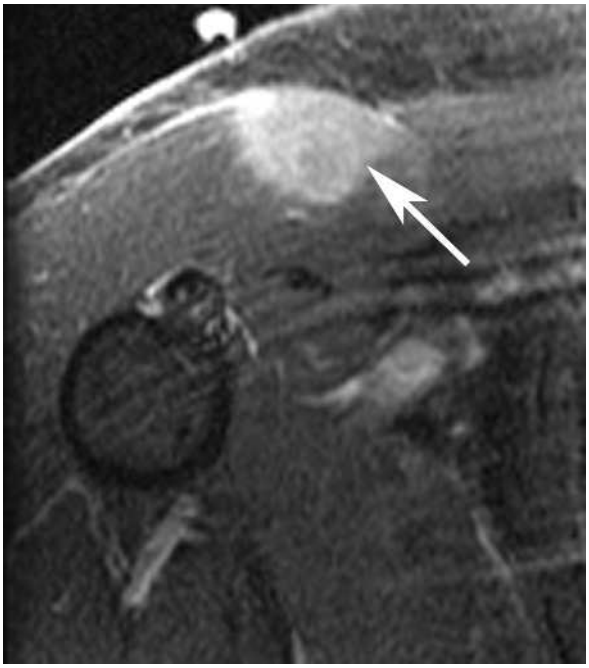

a

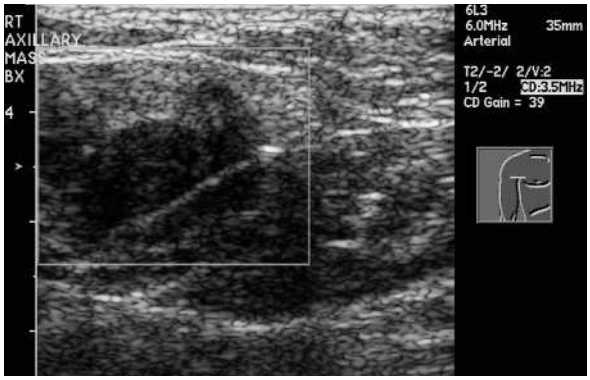

b

Fig. 18.4a,b. Chloroma in 77-year-old man with acute myelogenous leukemia. **a** Axial T1-weighted enhanced image through the right anterior shoulder shows an enhancing mass (*arrow*) within the anterior deltoid. **b** Sonographically guided biopsy of the lobulated, hypoechoic mass proved to be a chloroma (granulocytic sarcoma)

18.5 Precursor B-cell and T-cell Neoplasms

Precursor B and T lymphoblastic leukemia (precursor B-cell/T-cell acute lymphoblastic leukemia) is more commonly known as acute lymphoblastic leukemia (ALL; Brunning et al. 2001b). ALL is a neoplasm of lymphoblasts that involves bone marrow and blood (85% of cases are from precursor B-cell lineage) and is the most common form of childhood malignancy (Brunning et al. 2001b). Nearly 75% of cases occur in patients less than 6 years old (Brunning et al. 2001b). Radiographic findings occur in 50–70% of cases, including diffuse osteopenia, radiolucent and radiodense metaphyseal bands, osteolytic lesions, periostitis and osteosclerosis (Resnick et al. 2002). Complications during or after treatment of leukemia include fractures, osteonecrosis, and osteopenia related to chemotherapy and high-dose steroid treatment (Hughes et al. 2007; Tragiannidis et al. 2006; Hogler et al. 2007; Bertuna 2003). Patients generally have a good prognosis, with a 95% rate of complete remission in children (Brunning et al. 2001b).

18.6 B-Cell Neoplasms

B-cell neoplasms encompass a wide range of disorders, including chronic lymphocytic leukemia (CLL), lymphoplasmacytic lymphoma (Waldenstrom macroglobulinemia), and plasma cell neoplasms (plasma cell myeloma and variants, plasmacytoma, immunoglobulin deposition diseases, osteosclerotic myeloma, and heavy chain diseases).

18.6.1 Chronic Lymphocytic Leukemia

Chronic lymphocytic leukemia (CLL) is a neoplasm of monomorphic B-lymphocytes in the peripheral blood, bone marrow, and lymph nodes (Muller-Hermelink et al. 2001). The median age of patients with CLL is 65 years, and men are afflicted twice as often as women (Muller-Hermelink et al. 2001). As with any of the leukemias, MR imaging appearance of chronic lymphocytic leukemia can reveal homogeneous or heteroge-

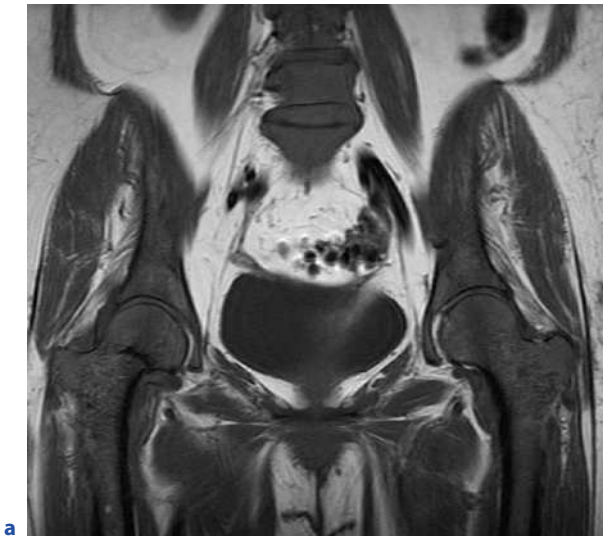

a

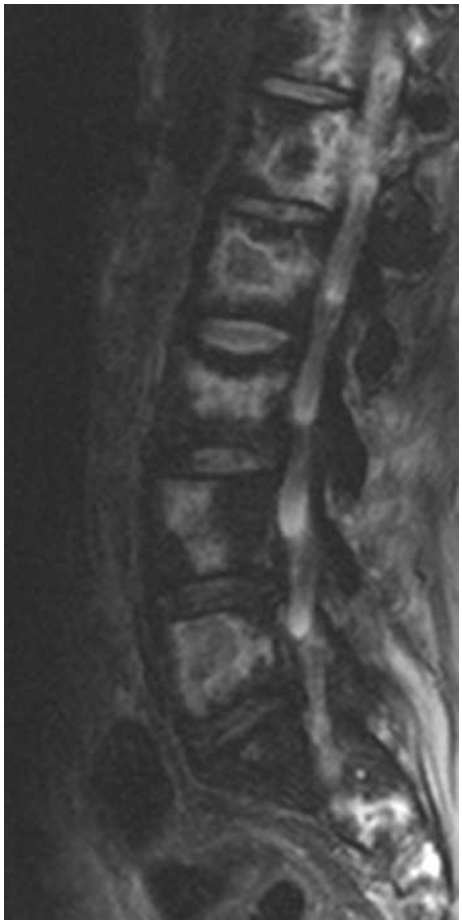

b

Fig. 18.5a,b. Varied MR imaging appearances of chronic lymphocytic leukemia. **a** Coronal T1-weighted image in an 81-year-old woman shows complete marrow replacement with diffusely low signal intensity relative to normal marrow fat and skeletal muscle. **b** Sagittal FSE T2-weighted fat-suppressed image shows diffuse extensive, heterogeneous abnormal signal throughout the lumbar spine in this 30-year-old man with chronic lymphocytic leukemia

neous marrow infiltrative patterns (Fig. 18.5). Extensive lytic lesions simulating multiple myeloma on radiography have been reported in cases of CLL (Greenfield et al. 2006).

18.6.2 Lymphoplasmacytic Lymphoma (Waldenstrom Macroglobulinemia)

Lymphoplasmacytic lymphoma, also known as Waldenstrom macroglobulinemia (WM), is a malignant lymphoplasmo-proliferative disorder with monoclonal IgM production and bone marrow infiltration (Vijay and Gertz 2007). WM accounts for about 1–2% of hematologic malignancies, has a slight male predominance, most often occurs in the seventh decade and predominates in Caucasians (Vijay and Gertz 2007). Although the diagnosis is made by bone marrow biopsy, MRI can demonstrate the extent of marrow infiltration (Fig. 18.6). Specific genetic abnormalities have been identified in cases of WM (deletion of 6q), with implications for disease progression and treatment (Henry and Fonseca 2007). Waldenstrom macroglobulinemia has a median survival of 5 years (Vijay and Gertz 2007).

18.6.3 Plasma Cell Myeloma (Multiple Myeloma)

Plasma cell myeloma (more commonly known as multiple myeloma) is the most common primary bone malignancy. It is a malignant clonal neoplasm of plasma cells of B-lymphocyte origin, resulting in the overproduction of monoclonal immunoglobulins (Angtuaco et al. 2004). Multiple myeloma is characterized by osteolytic lesions (Fig. 18.7), bone pain, hypercalcemia, monoclonal gammopathy, and disorders due to amyloid deposition (Grogan et al. 2001). Plasma cell myeloma most commonly presents in the sixth and seventh decades (less than 10% of individuals are younger than 40 years) and men and women are affected equally

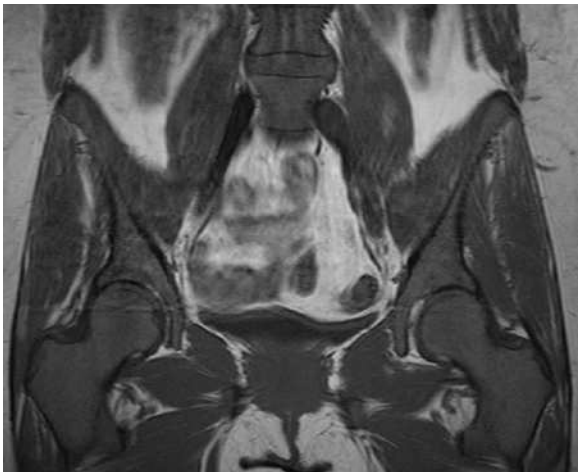

Fig. 18.6. Lymphoplasmacytic lymphoma (Waldenstrom macroglobulinemia) in a 42-year-old woman with recalcitrant hip pain and suspected trochanteric bursitis. Coronal T1-weighted image shows diffuse marrow infiltration, with complete absence of fatty signal intensity. The marrow changes were unsuspected and subsequent biopsy yielded lymphoplasmacytic lymphoma

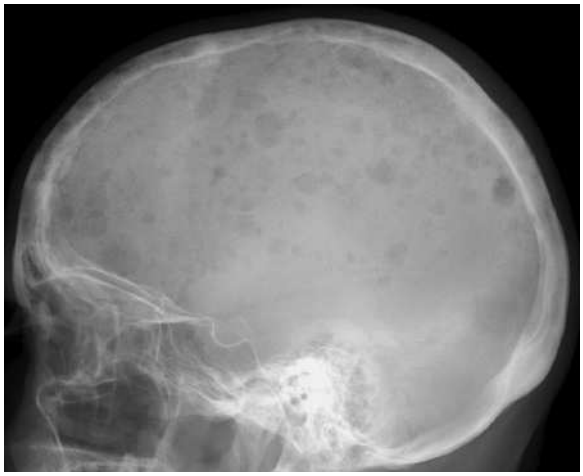

Fig. 18.7. Plasma cell myeloma of the skull in a 46-year-old man. Lateral radiograph shows the typical appearance of plasma cell myeloma, with multiple "punched-out" lytic lesions in the calvarium

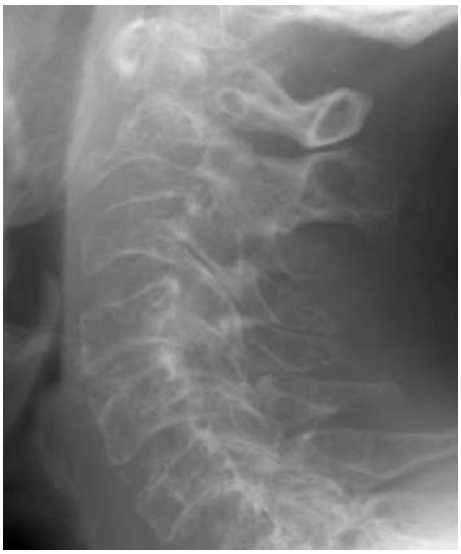

a

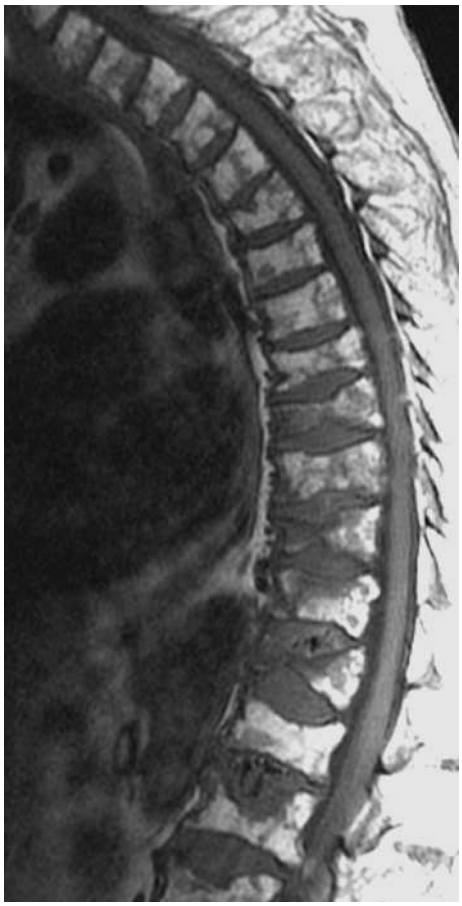

b

Fig. 18.8a,b. Plasma cell myeloma of the spine. **a** Cervical spine radiograph depicts multiple mild compression fractures and osteopenia in a 55-year-old woman with plasma cell myeloma. **b** Sagittal T1-weighted image through the thoracic spine shows innumerable compression fractures and multiple small marrow-replacing lesions in this 64-year-old man with advanced myeloma

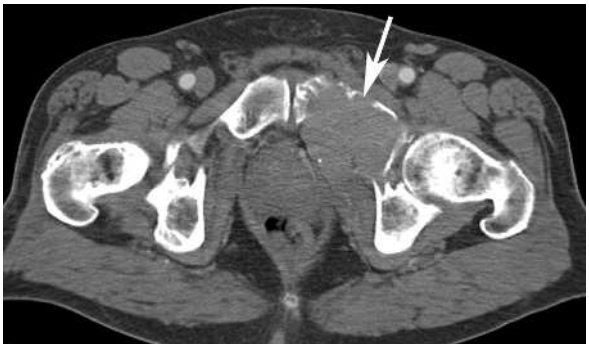

a

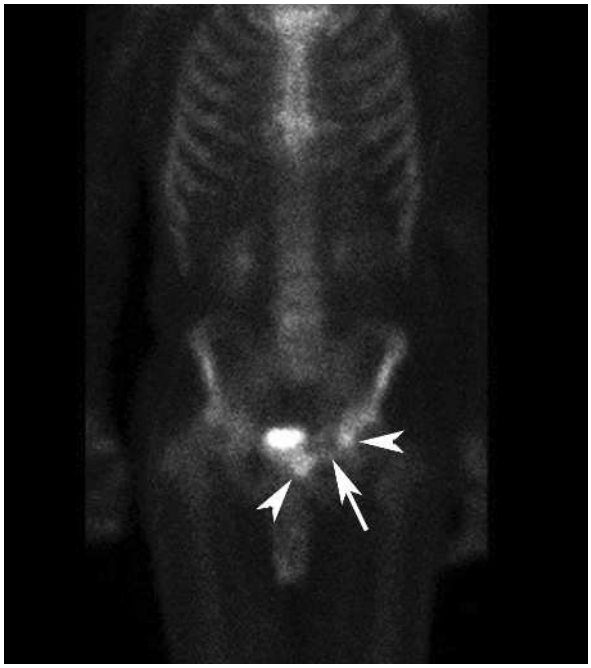

b

Fig. 18.9a,b. Plasma cell myeloma of the left superior pubic ramus. **a** CT depicts the classic expansile, lytic appearance of this biopsy-proven myelomatous lesion (*arrow*). **b** Correlating 99mTc-MDP scintigraphy shows a photopenic defect (*arrow*) with surrounding radiotracer uptake (*arrowheads*). Because of the primarily lytic nature of plasma cell myeloma, skeletal scintigraphy is usually insensitive to lesion detection

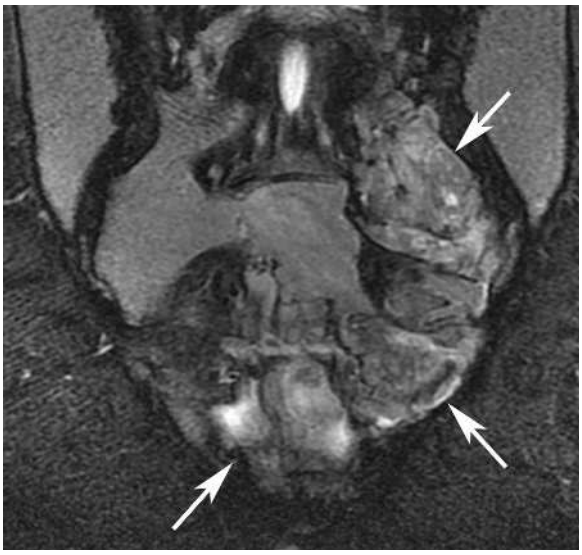

Fig. 18.10. Plasma cell myeloma of the sacrum. Coronal oblique FSE T2-weighted fat-suppressed image shows a heterogeneous, marrow-replacing lesion (*arrows*) occupying the left and inferior mid sacrum with expansile remodeling

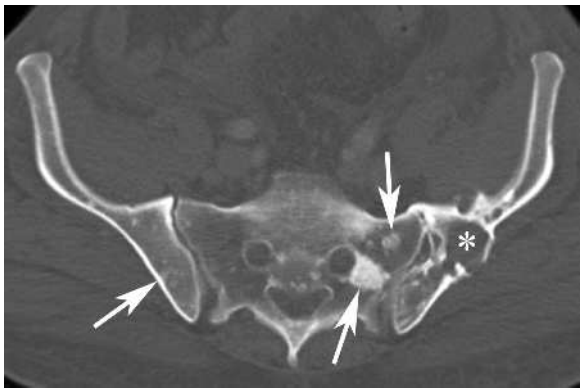

Fig. 18.11. Osteosclerotic myeloma (POEMS syndrome). CT through the pelvis delineates multiple sclerotic lesions (*arrows*) as well as an expansile lytic lesion (*asterisk*) in this patient with POEMS syndrome. The combination of sclerotic and lytic lesions are classic for POEMS syndrome

(Grogan et al. 2001). The diagnosis is made in a clinical setting of symptomatic and progressive disease using a combination of bone marrow biopsy, serum IgG and IgA levels, urine immunoglobulin levels, and lytic bone lesions (Grogan et al. 2001).

Imaging can detect the extent of intramedullary disease, any extramedullary myelomatous foci, complications, and treatment response. Bones containing hematologic (red) marrow are frequently involved – vertebrae (Fig. 18.8), ribs, skull, pelvis (Fig. 18.9), femur, clavicle and scapula. Mandibular involvement can be seen with myeloma, often differentiating it from metastases. Imaging findings of multiple myeloma include osteopenia, lytic lesions, and pathologic fracture. The lytic lesions are typically "punched out" but can exhibit expansile remodeling of the adjacent bone (Figs. 18.9, 18.10). CT can better assess lesions with cortical thinning that are at increased risk for pathologic fracture.

In the sclerotic form of myeloma, there is usually a mixed pattern of lytic and sclerotic lesions (Fig. 18.11); the number of sclerotic foci is usually limited, but can be extensive (Mulligan 2007). Osteosclerotic myeloma can also be associated with POEMS (polyneuropathy, organomegaly, endocrinopathy, monoclonal gammopathy, skin changes) syndrome (Chong et al. 2006).

Skeletal scintigraphy is insensitive to myelomatous lesions (Fig. 18.9). MRI is excellent in evaluating the extent of disease at diagnosis, during and after treatment. CT can be used solely, or more often in combination with PET imaging (Mahnken et al. 2002). FDG-PET is able to detect marrow involvement in patients with multiple myeloma and can be helpful in differentiating residual/recurrent tumor from post-therapeutic changes (Bredella et al. 2005; Jadvar and Conti 2002); however, PET/CT can be insensitive for both small lytic lesions as well as diffuse osseous involvement (Breyer et al. 2006). Less commonly used PET agents in the literature include 18F-FLT (fluorodeoxy-L-thymidine), 11C-methionine, and 11C-choline (Agool et al. 2006; Nanni et al. 2007; Dankerl et al. 2006).

Tumor burden detected on imaging is generally predictive of patient survival. The Durie/Salmon PLUS staging system is currently used to stage patients with multiple myeloma and is based on radiographs, MRI, and PET/CT (Durie 2006; Mulligan 2007). Stage IA is a normal skeletal survey or a single lesion. Stage IB is less than five focal lesions or mild diffuse spine disease. Stage II is 5–20 focal lesions or moderate diffuse spine disease (vertebral body signal intensity greater than disc on T1-weighted imaging). Stage III is more than 20 focal lesions or severe diffuse spine disease (vertebral body signal intensity isointense or hypointense to the adjacent disc on T1-weighted imaging).

18.7 Lymphoma

Lymphoma is characterized pathologically by a proliferation of lymphocytes, histiocytes, and their precursors. Multiple forms of lymphoma (other than Hodgkin's lymphoma) are subcategorized by the WHO classification system under "precursor B- and T-cell neoplasms," "mature B-cell neoplasms," and "mature T-cell and NK-cell neoplasms" (Jaffe et al. 2001). Non-Hodgkin's lymphoma (NHL) accounts for the majority of cases of osseous lymphoma, and diffuse large B-cell is the most common cell type (Ruzek and Wenger 2004).

18.7.1 Non-Hodgkin's Lymphoma

Osseous lymphoma can be categorized as primary lymphoma of bone (PLB), secondary lymphoma, or multifocal osseous lymphoma. PLB is defined as lymphoma presenting within a bone without disease elsewhere for at least 6 months. Secondary lymphoma occurs when systemic disease spreads secondarily to the bone. Multifocal osseous lymphoma occurs in the absence of lymph node or visceral involvement for 6 months after initial diagnosis (Ruzek and Wenger 2004). Primary lymphoma of bone accounts for less than 5% of all malignant bone tumors, can occur at any age, and has a slight male predominance (Mulligan 1999; Ruzek and Wenger 2004; Krishnan et al. 2003). Primary lymphoma has a significantly better 5-year prognosis than secondary lymphoma of bone (Kirsch et al. 2006).

The radiographic appearance can be variable, but lymphoma typically arises in the diaphyses or metadiaphyses of long bones (Fig. 18.12) or flat bones in the axial skeleton. Rare cases of epiphyseal and periosteal locations have been reported (Mounasamy et al. 2006; Abdelwahab et al. 2007). Secondary osseous lymphoma typically involves the axial skeleton such as the skull (Fig. 18.12), spine (Fig. 18.13), pelvis (Figs. 18.12, 18.14), and ribs. Distal extremity lesions are much less common (Fig. 18.15). Lymphomatous lesions are often lytic (with a permeative or moth-eaten pattern) and more than half of cases demonstrate an associated periosteal reaction (Mulligan et al. 1999; Krishnan 2003). Lymphoma can incite a marked osteoblastic response in the spongiosa with diffuse homogeneous sclerotic change, but the "ivory vertebra" sign is not specific for lymphoma (Graham et al. 2005). Lymphoma can also be radiographically occult, with MRI findings frequently out of proportion to those predicted on radiographs.

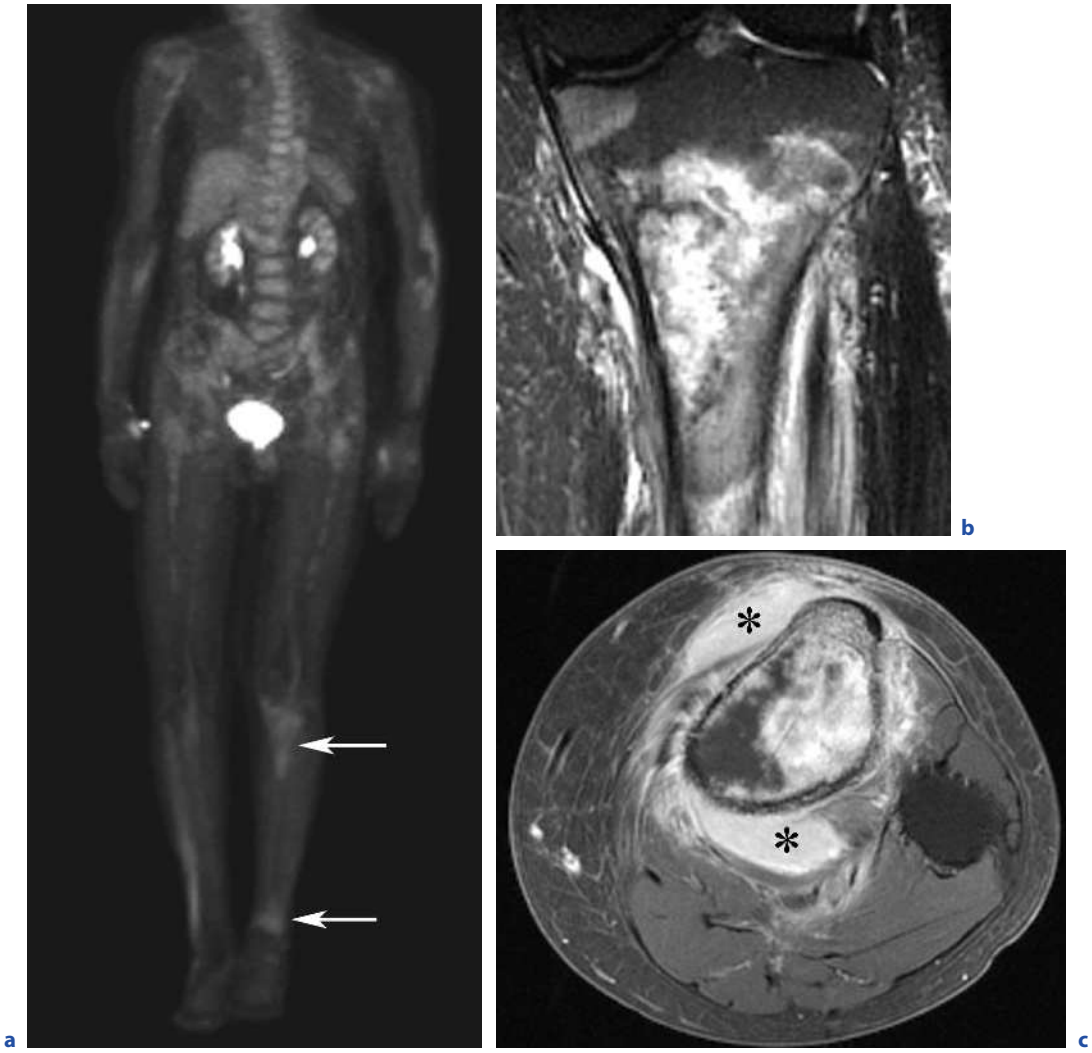

Fig. 18.12a–c. Primary diffuse large B-cell lymphoma of the tibia and ankle in a 70-year-old woman. **a** FDG-PET scan shows hypermetabolic activity within the left proximal tibia and ankle (*arrows*). Corresponding **b** coronal and **c** axial enhanced T1-weighted fat-suppressed images show heterogeneous signal and enhancement throughout the infiltrative lesion. Note the extensive marrow infiltration and extension into the adjacent soft tissues (*asterisks* in **c**) without gross cortical destruction, classic imaging features of osseous lymphoma

The MRI appearance of primary lymphoma of bone is variable; however, lymphoma should be considered in a patient older than 30 years when a soft tissue mass and marrow changes are indentified with little cortical destruction on MRI (Krishnan 2003). Lesions are typically isointense or slightly hypointense to muscle on T1-weighted images, and hyperintense on fluid-sensitive or diffusion-weighted echo-planar imaging with fat suppression (Yasumoto et al. 2002). Lymphoma can appear nonaggressive on MRI because of tumor confined to the bone, linear cortical signal abnormalities, normal or thickened cortical bone, and lack of soft tissue extension (Heyning et al. 2007). Dynamic contrast-enhanced MR images can also be helpful in assessing response to treatment, since decreased contrast enhancement has been shown to correlate with a good response (Rahmouni et al. 2003).

18.7.2 Hodgkin's Lymphoma

Hodgkin's lymphoma is differentiated from other types of lymphoma by the presence of the Reed-Sternberg gi-

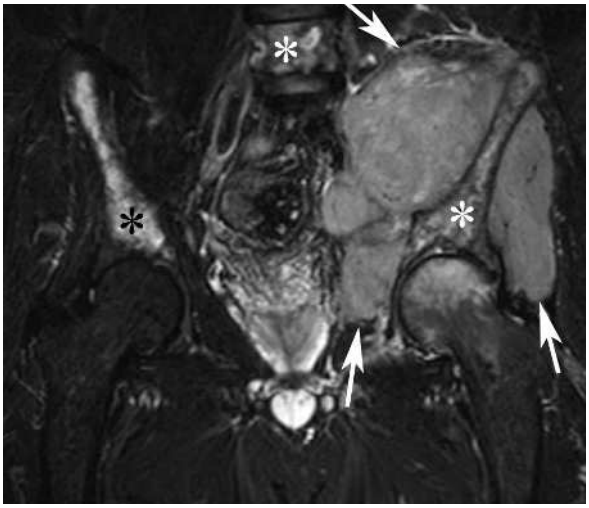

a

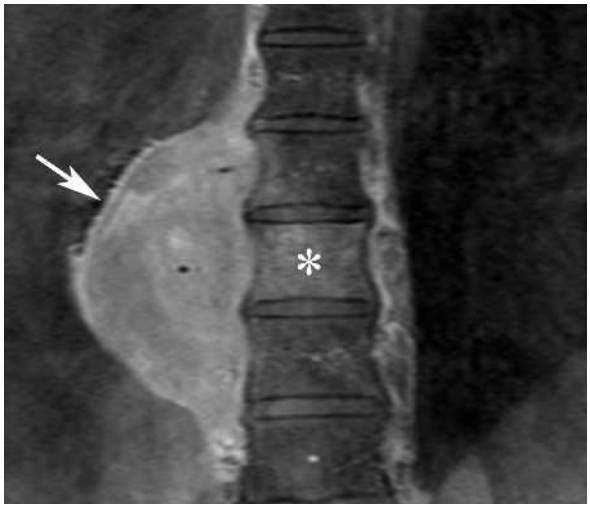

b

Fig. 18.13a,b. Diffuse large B-cell lymphoma. **a** Coronal FSE T2-weighted image through the pelvis in a 55-year-old man shows multiple marrow-replacing, hyperintense lesions (*asterisks*) and a large soft tissue mass (*arrows*) encompassing the left ilium. Grossly intact cortex with extraosseous soft tissue mass is characteristic of lymphoma. **b** Coronal enhanced T1-weighted image through the chest of a 55-year-old man displays a large, homogeneously enhancing right paraspinal mass (*arrow*). Although there is abnormal enhancement in the adjacent vertebrae (*asterisk*), the vertebral cortices are maintained

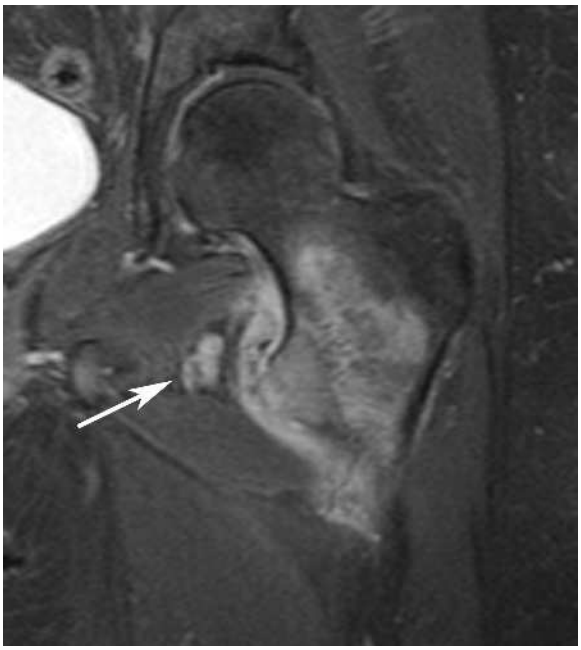

Fig. 18.14. Pathologic fracture of the lesser trochanter of the femur in a 66-year-old woman with splenic marginal zone lymphoma. Coronal FSE T2-weighted image shows the hyperintense avulsed fragment (*arrow*) and extensive, infiltrative lesion involving the proximal femur. The lesion was treated with external beam radiation

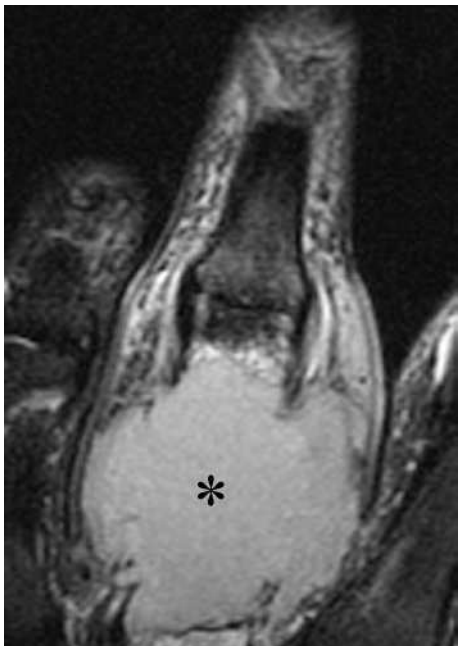

Fig. 18.15. Anaplastic large cell lymphoma of the finger in a 68-year-old man. Coronal MRI shows a destructive, homogeneous soft tissue mass (*asterisk*) that is homogeneously hyperintense on FSE T2-weighted images. This mass of T-cell lineage subsequently responded to radiation therapy

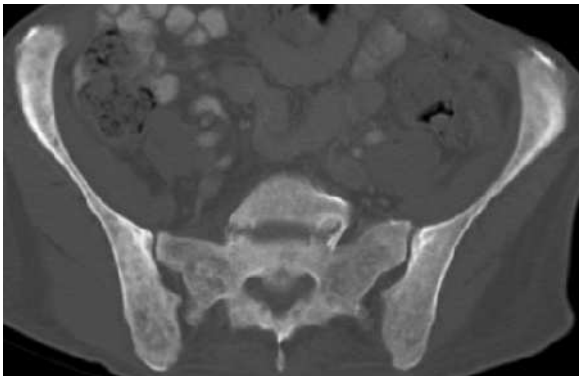

Fig. 18.16. Hodgkin's lymphoma. Axial CT through the pelvis shows diffuse osteosclerosis in this patient with Hodgkin's lymphoma

ant cells. Only about 5–15% of patients with Hodgkin's lymphoma have marrow involvement (Linden et al. 1989). Primary Hodgkin's lymphoma of bone is exceedingly rare (Ruzek and Wenger 2004). In a series of 237 pathologically proven cases of primary lymphoma of bone from the Armed Forces Institute of Pathology, only 6% were Hodgkin's lymphoma (Mulligan et al. 1999). In a Mayo Clinic series of 25 patients with osseous Hodgkin's lymphoma, only 2 patients had primary Hodgkin's lymphoma of bone, whereas secondary osseous involvement occurred in 10–25% of patients (Fig. 18.16; Ostrowski et al. 1999). Patients with diffuse osseous Hodgkin's or non-Hodgkin's lymphoma can have a false-negative CT portion of PET/CT scans, with concordance between the PET and CT findings occurring in less than half of all bone lesions (Taira et al. 2007).

References

Abdelwahab IF, Hoch B, Hermann G, Bianchi S, Klein MJ, Springfield DS (2007) Primary periosteal lymphoma: rare and unusual. Skeletal Radiol 36:335–339

Agool A, Schot B, Jager P, Vellenga E (2006). 18F-FLT PET in hematologic disorders: a novel technique to analyze the bone marrow compartment. J Nucl Med 47:1592–1598

Angtuaco EJ, Fassas ABT, Walker R, Sethi R, Barlogie B (2004) Multiple myeloma: clinical review and diagnostic imaging. Radiology 231:11–23

Bertuna G, Fama P, Lo Nigro L, Russo-Mancuso G, Cataldo A di (2003) Marked osteoporosis and spontaneous vertebral fractures in children: don't forget, it could be leukemia. Med Pediatr Oncol 41:450–451

Bredella MA, Steinbach L, Caputo G, Segall G, Hawkins R (2005) Value of FDG PET in the assessment of patients with multiple myeloma. Am J Roentgenol 185:1199–1204

Breyer RJ III, Mulligan ME, Smith S, Line BR, Badros AZ (2006) Comparison of imaging with FDG PET/CT with other imaging modalities in myeloma. Skeletal Radiol 2006:632–640

Brunning RD, Matutes E, Harris NL et al. (2001a) Acute myeloid leukemia: introduction. In: Jaffe ES, Harris NL, Stein H, Vardiman JW (eds) Pathology and genetics: tumours of haematopoietic and lymphoid tissues. IARC Press, Lyon, pp 77–80

Brunning RD, Borowitz M, Matutes E et al. (2001b) Precursor B lymphoblastic leukemia/lymphoblastic lymphoma (precursor B-cell acute lymphoblastic leukemia). In: Jaffe ES, Harris NL, Stein H, Vardiman JW (eds) Pathology and genetics: tumours of haematopoietic and lymphoid tissues. IARC Press, Lyon, pp 111–114

Chong ST, Beasley HS, Daffner RH (2006) POEMS syndrome: radiographic appearance with MRI correlation. Skeletal Radiol 35:690–695

Cloran F, Banks KP (2007) Diffuse osteosclerosis with hepatosplenomegaly. Am J Roentgenol 188:S18–S20

Dankerl A, Liebiesch P, Glatting G, Friesen C, Blunstein NM, Kocot D et al. (2006) Multiple myeloma: molecular imaging with 11C-methionine PET/CT: initial experience. Radiology 242:498–508

Durie B (2006) The role of anatomic and functional staging in myeloma: description of Durie/Salmon PLUS staging system. Eur J Cancer 42:1539–1543

Fritz J, Vogel W, Claussen CD, Wehrmann M, Pereira PL, Horger MS (2007) Generalized intramuscular granulocytic sarcoma mimicking polymyositis. Skeletal Radiol 36:985–989

Graham TS (2005) The ivory vertebra sign. Radiology 235:614–615

Greenfield HM, Hunt R, Lee LK, Jowitt SN (2006) B-cell chronic lymphocytic leukaemia with extensive lytic lesions. Eur J Haematol 76:356–357

Grogan TM, Van Camp B, Kyle RA, Muller-Hermelink HK, Harris NL (2001) Plasma cell neoplasms. In: Jaffe ES, Harris NL, Stein H, Vardiman JW (eds) Pathology and genetics: tumours of haematopoietic and lymphoid tissues. IARC Press, Lyon, pp 142–156

Henry T, Fonseca R (2007) Genomics and proteomics in multiple myeloma and Waldenström macroglobulinemia. Curr Opin Hematol 14:369–374

Heyning FH, Kroon HMJA, Hogendoorn PCW, Taminiau AHM, van der Woude H-J (2007) MR imaging characteristics in primary lymphoma of bone with emphasis on non-aggressive appearance. Skeletal Radiol 36:937–944

Hogler W, Wehl G, van Staa T, Meister B, Klein-Franke A, Kroshofer G (2007) Incidence of skeletal complications during treatment of childhood acute lymphoblastic leukemia: comparison of fracture risk with the general practice research database. Pediatr Blood Cancer 48:21–27

Hughes C, Patterson K, Murray M (2007) Avascular necrosis of the femoral head in childhood chronic myeloid leukemia. Br J Haematol 139:1

Hwang S, Panicek DM (2007) Magnetic resonance imaging of bone marrow in oncology. Part 2. Skeletal Radiol 36:1017–1027

Jadvar H, Conti PS (2002) Diagnostic utility of FDG PET in multiple myeloma. Skeletal Radiol 31:690–694

Jaffe ES, Harris NL, Stein H, Varidman JW (eds) (2001) World Health Organization classification of tumours. Pathology and genetics. Tumours of haematopoietic and lymphoid tissues. IARC Press, Lyon

Kirsch J, Ilaslan H, Bauer TW, Sundaram M (2006) The incidence of imaging findings, and the distribution of skeletal lymphoma in a consecutive patient population seen over 5 years. Skeletal Radiol 35:590–594

Kobayashi D, Satsuma S, Kamegaya M et al. (2005) Musculoskeletal conditions of acute leukemia and malignant lymphoma in children. J Pediatr Orthop B 14:156–161

Krishnan A, Shirkhoda A, Tehranzadeh J, Armin AR, Irwin R, Les K (2003) Primary bone lymphoma: radiographic–MR imaging correlation. RadioGraphics 23:1371–1387

Linden A, Zankovich R, Theissen P, Diehl V, Schicha H (1989) Malignant lymphoma: bone marrow imaging versus biopsy. Radiology 173:335–339

Mahnken AH, Wildberger JE, Gehbauer G et al. (2002) Multidetector CT of the spine in multiple myeloma: comparison with MR imaging and radiography. Am J Roentgenol 178:1429–1436

Matuszewski L, Persigehi T, Wall A et al. (2006) Assessment of bone marrow angiogenesis in patients with acute myeloid leukemia by using contrast-enhanced MR imaging with clinically approved iron oxides: initial experience. Radiology 242:217–224

Mounasamy V, Berns S, Azouz EM, Giusti V, Knapp DR (2006) Anaplastic large cell lymphoma presenting as an epiphyseal lytic lesion: a case report with clinico-pathologic correlation. Skeletal Radiol 35:619–623

Muller-Hermelink HK, Catovsky D, Montserrat E, Harris NL (2001) Chronic lymphocytic leukaemia/small lymphocytic lymphoma. In: Jaffe ES, Harris NL, Stein H, Vardiman JW (eds) Pathology and genetics: tumours of haematopoietic and lymphoid tissues. IARC Press, Lyon, pp 127–130

Mulligan ME (2007) Myeloma update. Semin Musculoskelet Radiol 11:231–239

Mulligan ME, Badros AZ (2007) PET/CT and MR imaging in myeloma. Skeletal Radiol 36:5–16

Mulligan ME, McRae GA, Murphey MD (1999) Imaging features of primary lymphoma of bone. Am J Roentgenol 173:1691–1697

Nanni C, Zamagni E, Cavo M et al. (2007) 11C-choline vs. 18F-FDG PET/CT in assessing bone involvement in patients with multiple myeloma. World J Surg Oncol 5:68–75

Ostrowski M, Inwards C, Strickler JG et al. (1999) Osseous Hodgkin's disease. Cancer 85:1166–1178

Pierre R, Imbert M, Thiele J, Vardiman JW, Brunning RD, Flandrin G (2001) Polycythemia vera. In: Jaffe ES, Harris NL, Stein H, Vardiman JW (eds) Pathology and genetics: tumours of haematopoietic and lymphoid tissues. IARC Press, Lyon, pp 32–34

Resnick D, Haghighi P (2002) Myeloproliferative disorders. In: Resnick D (ed) Diagnosis of bone and joint disorders, 4th edn. Saunders, Philadelphia

Rahmouni A, Montazel JL, Divine M et al. (2003) Bone marrow with diffuse tumor infiltration in patients with lymphoproliferative diseases: dynamic gadolinium enhanced MR imaging. Radiology 229:710–717

Ruzek KA, Wenger DE (2004) The multiple faces of lymphoma of the musculoskeletal system. Skeletal Radiol 33:1–8

Taira AV, Herfkens RJ, Gambhir SS, Quon A (2007) Detection of bone metastases: assessment of integrated FDG PET/CT imaging. Radiology 243:204–211

Tragiannidis A, Athanassiadou F, Papageorgiou T (2006) Severe skeletal complications in a child with acute lymphoblastic leukemia. Pediatr Hematol Oncol 23:523–525

Vardiman JW, Pierre R, Thiele J, Imbert M, Brunning RD, Flandrin G (2001). Chronic myelogeneous leukemia. In: Jaffe ES, Harris NL, Stein H, Vardiman JW (eds) Pathology and genetics: tumours of haematopoietic and lymphoid tissues. IARC Press, Lyon, pp 20–26

Vijay A, Gertz MA (2007) Waldenstrom macroglobulinemia. Blood 109:5096–5103

Yasumoto M, Nonomura Y, Yoshimura R et al. (2002) MR detection of iliac bone marrow involvement by malignant lymphoma with various MR sequences including diffusion-weighted echo-planar imaging. Skeletal Radiol 31:263–269

Zajick DC Jr, Morrison WB, Schweitzer ME, Parellada JA, Carrino JA (2005) Benign and malignant processes: normal values and differentiation with chemical shift MR imaging in vertebral marrow. Radiology 237:590–596

Angiomatous Neoplasms of the Skeletal System

19

Agustinus S. Suhardja, Sophie Verbeke and Johan L. Bloem

CONTENTS

KEY POINTS

- For clinical classification purposes it suffices to recognize a benign (hemangioma) and malignant (angiosarcoma) side of the spectrum with hemangioendothelioma as a malignant intermediate form.
- A radiological diagnosis of angiosarcoma should be considered when multiple lesions are seen in one region.
- Histologically angiosarcoma looks like metastasis.
- A radiological suspicion for angiosarcoma should trigger the use of specific vascular markers by the pathologist.
- Angiosarcoma typically presents as an aggressive-looking osteolytic lesion, or lesions without periosteal reaction.
- Angiosarcma may present as a well-defined lesion with geographic destruction of bone, resembling fibrous dysplasia.
- Vertebral hemangiomas with a marked vascular component, as opposed to a marked fatty component, may cause severe symptoms.

A. S. Suhardja, MD, MSc
Department of Radiology, C2S, Leiden University Medical Center, Albinusdreef 2, P.O. Box 9600, 2300 RC Leiden, The Netherlands

S. Verbeke, MD
Department of Pathology, C2S, Leiden University Medical Center, Albinusdreef 2, P.O. Box 9600, 2300 RC Leiden, The Netherlands

J. L. Bloem, MD
Department of Radiology, C2S, Leiden University Medical Center, Albinusdreef 2, P.O. Box 9600, 2300 RC Leiden, The Netherlands

19.1 Introduction

The diversity of the radiological and pathological manifestations of skeletal angiomatous neoplasms has challenged radiologists and pathologists for decades to provide prognosis-based classifications, to understand their biological behavior, as well as to develop a simple but reliable method in establishing diagnosis of these protean lesions. These neoplasms, which range from the incidentally prevalent hemangiomas to the elusive but

clinically significant angiosarcomas, can have a seemingly innocuous appearance; however, their exclusion from differential diagnosis could potentially lead to deleterious or even catastrophic consequences for the patient. Although our understanding of the biological and clinical behavior of these neoplasms is still rudimentary, recent advancement in the classifications of these neoplasms can provide a better understanding of the radiological and pathological manifestations of these tumors which can lead to better diagnosis and treatment.

This chapter summarizes our current understanding of the classifications, biological and clinical behavior, as well as radiological and pathological manifestations of these neoplasms.

19.2 Classifications

While classification of hemangioma as the benign vascular tumor, and angiosarcoma as the malignant vascular tumor, is incontrovertible, considerable controversy exists concerning the classifications of the lesions from one end of the spectrum to the other. Tumors of this intermediate group are called, according to the WHO 2002 classification, hemangioendothelimas (Roessner and Boehling 2002).

Vascular tumors of skeletal systems have been historically referred to as epitheloid vascular neoplasms because of their possessing a high percentage of epithelioid-appearing cells manifesting as positive eosinophilic staining cytoplasm. Their positive eosinophilic staining is secondary to a large amount of keratin within the cells which is an inherent property of epithelial cells. Their designation as epitheloid cells emphasizes the importance of distinguishing these tumors from epithelial neoplasms. This is especially important since angiosarcoma has a propensity for multiplicity in addition to producing keratin and hence makes them prone to being confused with the much more prevalent metastatic carcinomas which could lead to an erroneous treatment and inadvertent prognosis.

In the pathology literature, a variant of hemangioendothelioma, the so-called epitheloid vascular tumor, has been described. Since there is no consensus that this is indeed a separate entity, in this chapter we only use the term hemangioendothelioma (Evans et al. 2003).

Characteristics of aggressive or malignant behavior of skeletal vascular tumors include loss of cohesive arrangements, vacuolated cells instead of vessel lumens, as well as pleomorphic and hyperchromatic nuclei which are not dissimilar from other malignant or aggressive tumors. The determination of endothelial cells is helped by vascular endothelial markers such as CD 31, CD 34, and factor-VIII-related antigen (MacLean et al. 2007).

19.3 Biological and Clinical Behavior

19.3.1 Hemangiomas

While there are no mitogens or inducers of cell proliferation required for maintenance of hemangiomas, there are anti-mitogenic agents, which specifically inhibit endothelial cell proliferations. The presence of angiostatin and endostatin inhibit endothelial proliferation and become an impediment for maintenance of hemangioma resulting in regression to dormancy in microscopic state (O'Reilly et al. 1997). The advancement of knock-out mice technology has enabled the identification of a family of tissue-specific DNA-binding protein transcription factors which have been proven to be an important determinant in the development and maintenance as well as growth of hemangiomas. FoxO transcription factors are a family of DNA-binding proteins that are the products of tissue- and cell-type-specific tumor suppressor genes, elimination of which produces activation of phosphoinositide-3 kinase (PI-3 kinase) signaling pathway leading to the development and maintenance of hemangiomas (Paik et al 2007).

While hemangiomas are most commonly discovered incidentally, they can sometimes cause nerve-compression-producing symptoms such as local or radicular pain (Chasi and Hide 2008). Hemangiomas in the skull are especially known for producing symptoms which may prompt the patient to seek medical treatment. Although skull hemangiomas are commonly symptomatic, they are not as prevalent as spinal hemangiomas.

Spinal hemangiomas can occur in any place but are found most commonly in the thoracic and lumbar vertebral bodies. Although spinal hemangiomas frequently display benign and indolent behaviors, they can sometimes extend to the posterior element leading to compressive symptoms. Only symptomatic hemangiomas require treatment.

While clinical presentation of back pain is probably as prevalent as radiological appearance of vertebral hemangiomas, their coexistence provides little indication about their causal relationship. Laredo et al. (1990) observed that the presence of fatty attenuation on CT studies and fatty high signal on T1-weighted MR im-

ages are more likely to be associated with asymptomatic patients. The presence of soft tissue attenuation on CT studies portends symptomatic lesion with potential for compression deformity (Laredo et al. 1990). This soft tissue attenuation has been ascribed to hypervascularity associated with growth of the lesion and hence symptoms, whereas fatty content has been correlated with indolent secondary fatty degeneration and asymptomatic clinical behavior (Laredo et al. 1990).

19.3.2 Angiosarcomas

While hemangiomas have been shown to be inhibited by tissue-specific transcription factors and anti-mitogens which lead to inhibition of PI-3 kinase pathways in endothelial cells, researchers have shown that activation of PI-3 kinase by overexpressing a specific activated subunit of protein in the pathway could lead to the development of angiosarcomas in vitro (Chang et al. 1997). In addition, mutation and activation of a serine–threonine kinase pathway (AKT kinase pathway) has also been found to lead to the development of angiosarcomas (Aoki et al. 1998). These researchers further deduced that AKT signaling pathway is downstream to the PI-3 signaling pathways (Aoki et al. 1998). These conclusions could indicate that the development and maintenance of both hemangiomas and angiosarcomas share at least two common pathways in the early stage of development which might later diverge to produce tumors with different biological and clinical behaviors.

The clinical behavior of angiosarcomas is similar to that of other bone sarcomas. The distinguishing features of angiosarcomas are their tendency for multifocality in approximately one third of cases, as well as for occurrence in older patient populations. The median age of patients with angiosarcomas is 47 years (range 11–82 years) with 75% prevalence between 30 and 75 years of age (Mulder et al. 1993). Although pain and soft tissue swelling are two of the most common presenting symptoms, their clinical presentations offer little indications to the ultimate diagnosis.

The most challenging differential diagnosis for angiosarcomas are metastatic carcinomas, multiple myelomas, and lymphomas. Although multiple myelomas can be easily recognized on pathology specimen, angiosarcomas and metastatic carcinomas may have similar appearance under the microscope (Lomasney et al. 1996). This is because both tumors have a tendency to produce keratin. Staining with molecular markers specific for vascular tissue may need to be performed to establish a diagnosis.

19.3.3 Hemangioendotheliomas

Although hemangioendotheliomas are classified as malignant neoplasms and may have aggressive clinical and radiological as well as pathological features, they range from indolent tumors mimicking hemangiomas to aggressive neoplasms similar to angiosarcomas. The biological and clinical prognosis of the patient sometimes can be predicted based on their histological appearance (Campanacci et al. 1980). Tumors with cytological atypia and mitotic activity are considered poorly differentiated and hence considered as undifferentiated versions of hemangioendotheliomas.

Tumors with epithelial component tend to be well differentiated and more indolent in their clinical progression. It is important to note that clinical presentation is not as reliable in predicting prognosis of these tumors as pathological appearance is (Larsson et al. 1975). Multiple lesions have been described as being low grade and as having good prognosis, whereas a single lesion may be high grade (Wenger and Wold 2000b). The reported better prognosis in cases of multiplicity could not be confirmed in the series by the Netherlands Committee on Bone Tumors (Mulder et al. 1993). It is therefore concluded that the degree of differentiation of the tumor as judged by the pathologist is the most reliable method of distinguishing well-differentiated tumor with better prognosis from poorly differentiated tumor with worse prognosis.

19.4 Radiological and Pathological Manifestation

19.4.1 Hemangiomas

The radiological description of benign hemangiomas is arguably the epitome of colloquialisms in musculoskeletal radiology, with terminologies such as “corduroy pattern” and “polka-dot pattern” acceptable in depicting these lesions in common practice. The conventional radiological characterization of corduroy pattern in benign vertebral hemangiomas originates from relative demineralization and fatty change of the vertebrae resulting in prominent vertical trabeculae (Wenger and Wold 2000a). These combined lytic and trabeculated appearances occur in approximately 40% of all skeletal hemangiomas (Mulder et al. 1993). Purely lytic lesions account for about 30% of all hemangiomas, but the majority of tumors display a combination of osteolysis with

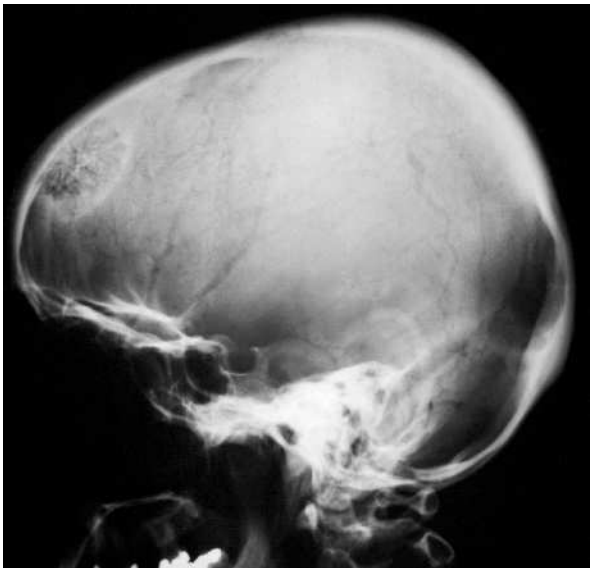

a

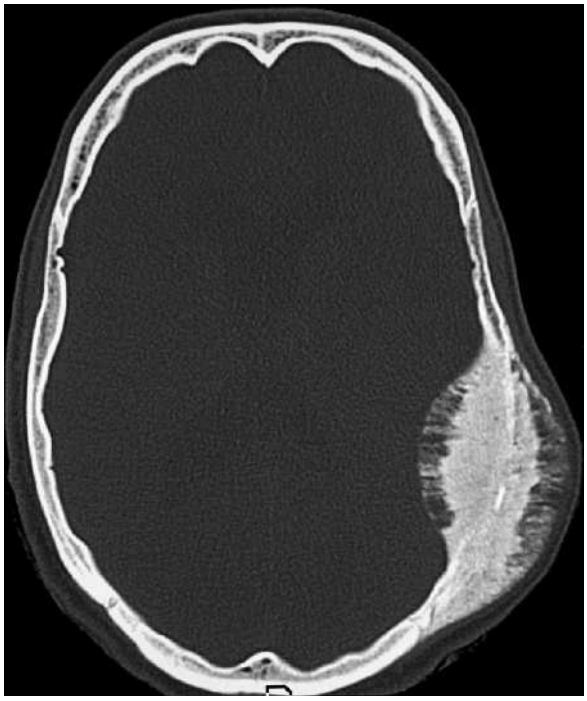

b

Fig. 19.1. **a** Classic hemangioma in the skull (frontal bone) demonstrates well-defined lytic lesion with prominent trabecular pattern. **b** Different patient with classic trabecular pattern of skull hemangioma on CT

ridges, trabeculae, and sclerosis (Mulder et al. 1993). In almost all cases, hemangiomas demonstrate sharply defined margins (Fig. 19.1) with a small minority demonstrating moth-eaten borders (Mulder et al. 1993). Involvement of the cortex can lead to the formation of a new cortex in the form of periosteal reaction.

The CT description of polka-dot pattern in vertebral hemangiomas arises from the presence of dense round foci of thickened vertical trabeculae in a cross-section, located within a well-defined lytic lesion containing fat (Fig. 19.2). Hemangiomas typically have low signal intensity on T1-weighted images secondary to the presence of fat. There may be cellular, well-vascularized components that have low signal on T1-, and high signal intensity on T2-weighted and Gd-enhanced images (Fig. 19.2). These cellular components are usually seen in soft tissue extension and symptomatic hemangiomas (Fig. 19.2; Laredo et al. 1990).

As described previously, it may be difficult to ascertain the relationship between symptoms and the presence of a hemangioma; however, certain radiological features have been proposed to indicate symptomatic tumors. While high signal intensity on T1-weighted MRI sequences is associated with asymptomatic neoplasms ascribed to the presence of fat within the tumor, low signal on T1-weighted sequences are correlated with symptomatic lesions secondary to the presence of cellular tissue including vascular tissue (Fig. 19.2; Resnick 2002). Other foreboding characteristics of symptomatic tumor include the presence of soft tissue component, especially with extension to extraosseous tissue compressing the spinal cord and nerve roots, loss of height of vertebral bodies, cortical expansion, as well as decreased polka-dot pattern on CT.

Pathologically, hemangiomas also pose little problem since they most often are composed of mature cells. Skeletal hemangiomas, like their soft tissue counterparts, are composed of cavernous, capillary, or venous subtypes with cavernous and capillary hemangiomas being the most prevalent varieties (Wenger and Wold 2000a). While cavernous hemangiomas are most prevalent in the skull, capillary hemangiomas commonly occur in the spine (Wenger and Wold 2000a). Lymphangiomas are distinguished from hemangiomas by the presence of lymphoid aggregates in the vicinity of vascular structures (Wenger and Wold 2000a). Although Gorham's disease may display hypervascular structures on pathological specimens similar to hemangiomas, radiological and clinical presentations of this disease seldom cause diagnostic dilemma.

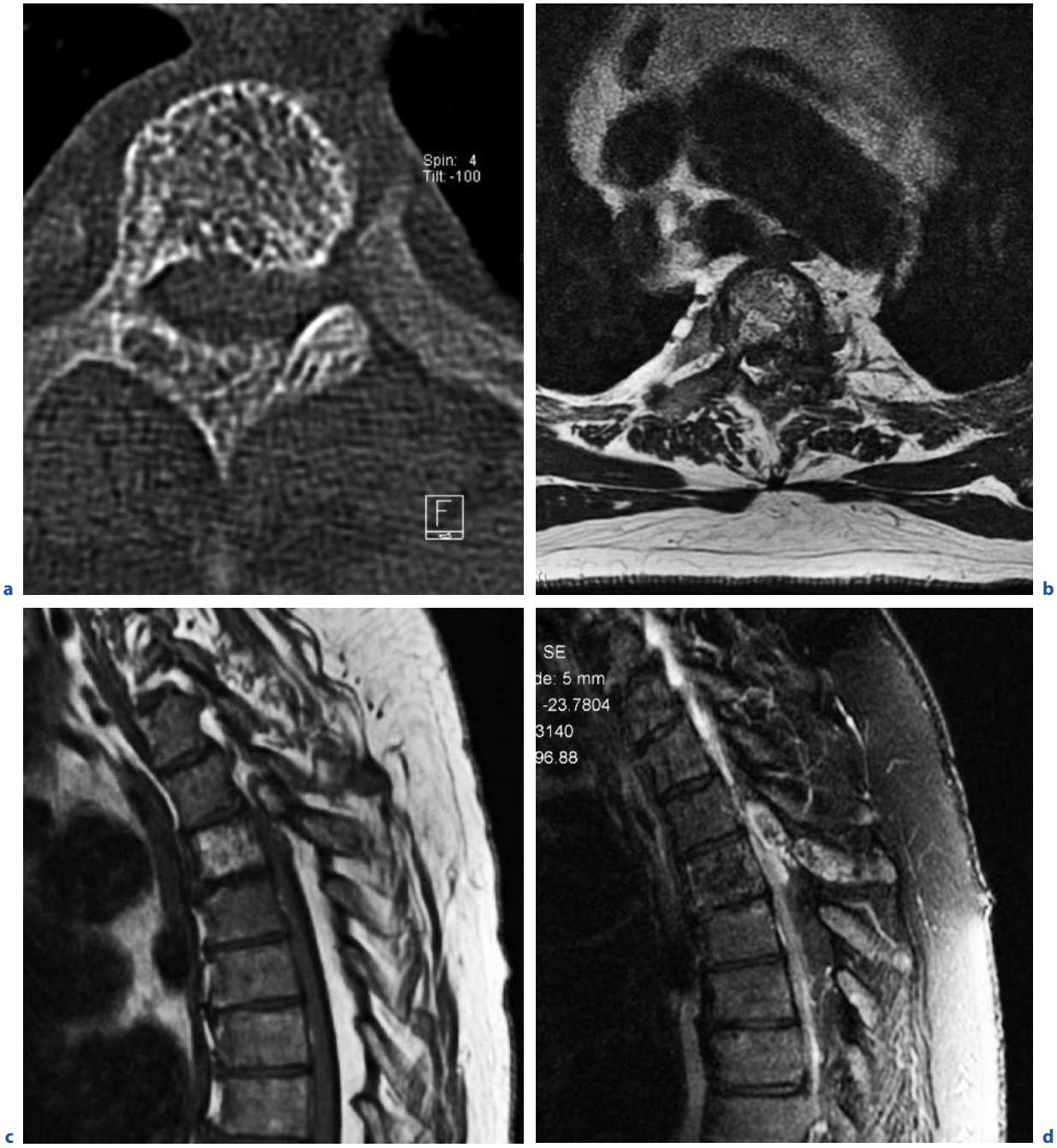

a b c d

Fig. 19.2a–d. Symptomatic hemangioma in the spine. **a** Axial CT scan image demonstrates "polka-dot" pattern representing vertical trabecular bone in cross section. **b** Axial T1-weighted MR image demonstrates high signal intensity secondary to fat and low signal secondary to trabecular bone and vessels. The low-signal component extends into the vertebral canal and neuroforamen causing symptoms. **c** Sagittal T1-weighted MR image demonstrates the same fatty and vascular components. **d** Sagittal T2 fat-suppressed image shows high signal intensity representing vascular component extending into the posterior elements

19.4.2 Angiosarcomas

Despite the relatively low prevalence of malignant vascular tumors of the bone, recognition and inclusion of angiosarcomas in the differential diagnoses can obviate the potential pitfall of recommending an inaccurate diagnosis or performing a biopsy on these lesions with possible deleterious or even ominous outcomes of diagnosis and treatment. Although they most likely present with an ill-defined lytic lesion, cortical destruction, or endosteal scalloping, they can appear as regional multiple foci (Fig. 19.3) with mixed lytic and sclerotic, or purely sclerotic, lesions (Fig. 19.4). These lesions are most commonly seen around the hip region, in the proximal femurs, as well as in the pelvic area. Their multitude of radiological appearances and the propensity for multiplicity makes them more prone to being confused with the much more prevalent metastatic carcinomas which could lead to an erroneous treatment and inadvertent prognosis (Wenger and Wold 2000b).

Radiologists play a crucial role in raising the diagnostic possibility of angiosarcoma when multiple lesions are discovered on imaging studies. The important role that the radiologist plays in diagnosing these lesions lies in the fact that without radiological suspicion for angiosarcoma, specific immunohistochemical stainings for vascular endothelium markers may not be performed by the pathologist. The specific staining of vascular markers, such as CD 31, CD 35, and factor VIII, are particularly useful in distinguishing angiosarcomas from other more common diagnoses due to their specificity for vascular tissues (Wenger and Wold 2000b). This specific vascular endothelial staining is required because the gross features as well as histological appearances of these lesions are non-specific and may resemble metastatic carcinomas.

As described previously, the gross morphology of these lesions is non-specific (Roessner and Boehling 2002). Necrosis is usually not observed on gross morphological specimens, except in poorly differentiated form. On histological specimen, angiosarcomas are generally vasoformative, although their tendency to form vascular spaces may be variable. In a well-differentiated angiosarcoma, the vascular channels are well formed; hence, well-differentiated angiosarcoma may mimic hemangiomas. In a poorly differentiated form, the vascular channels are not well established and the identification of these neoplasms as vascular tumors may be challenging.

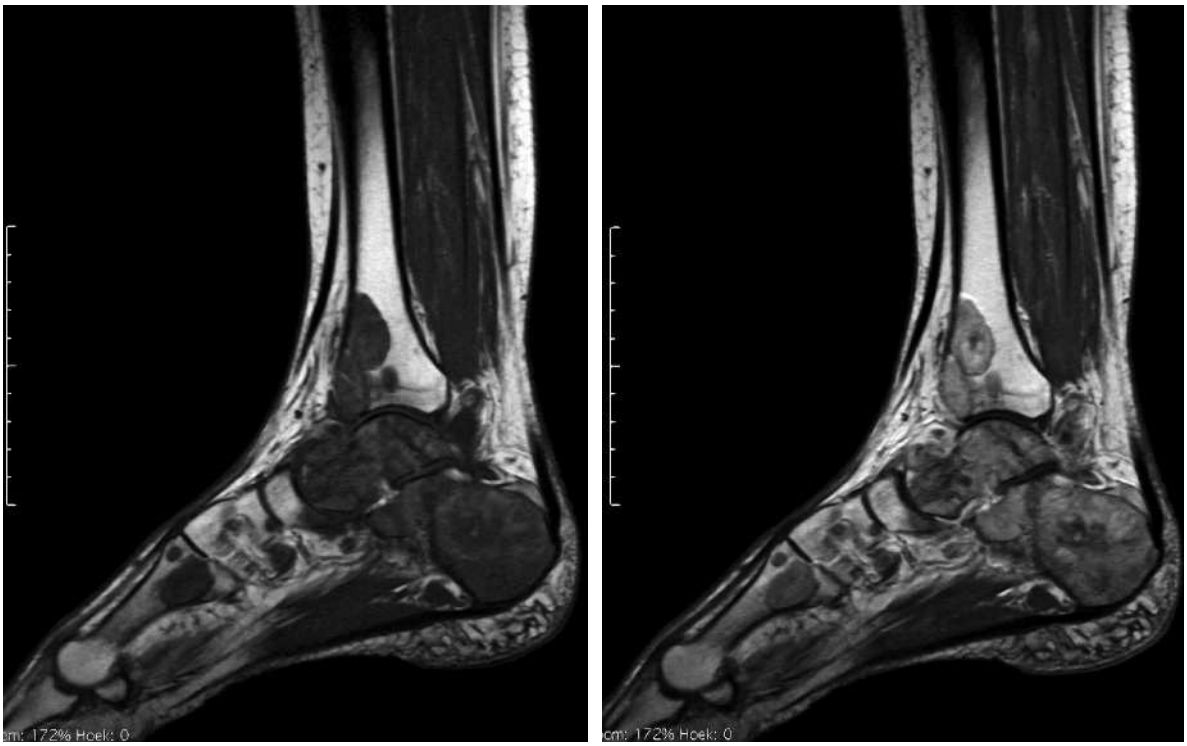

Fig. 19.3a,b. Angiosarcomas. T1- (**a**) and T2- (**b**) weighted images show multiple regional locations typical for angiosarcomas

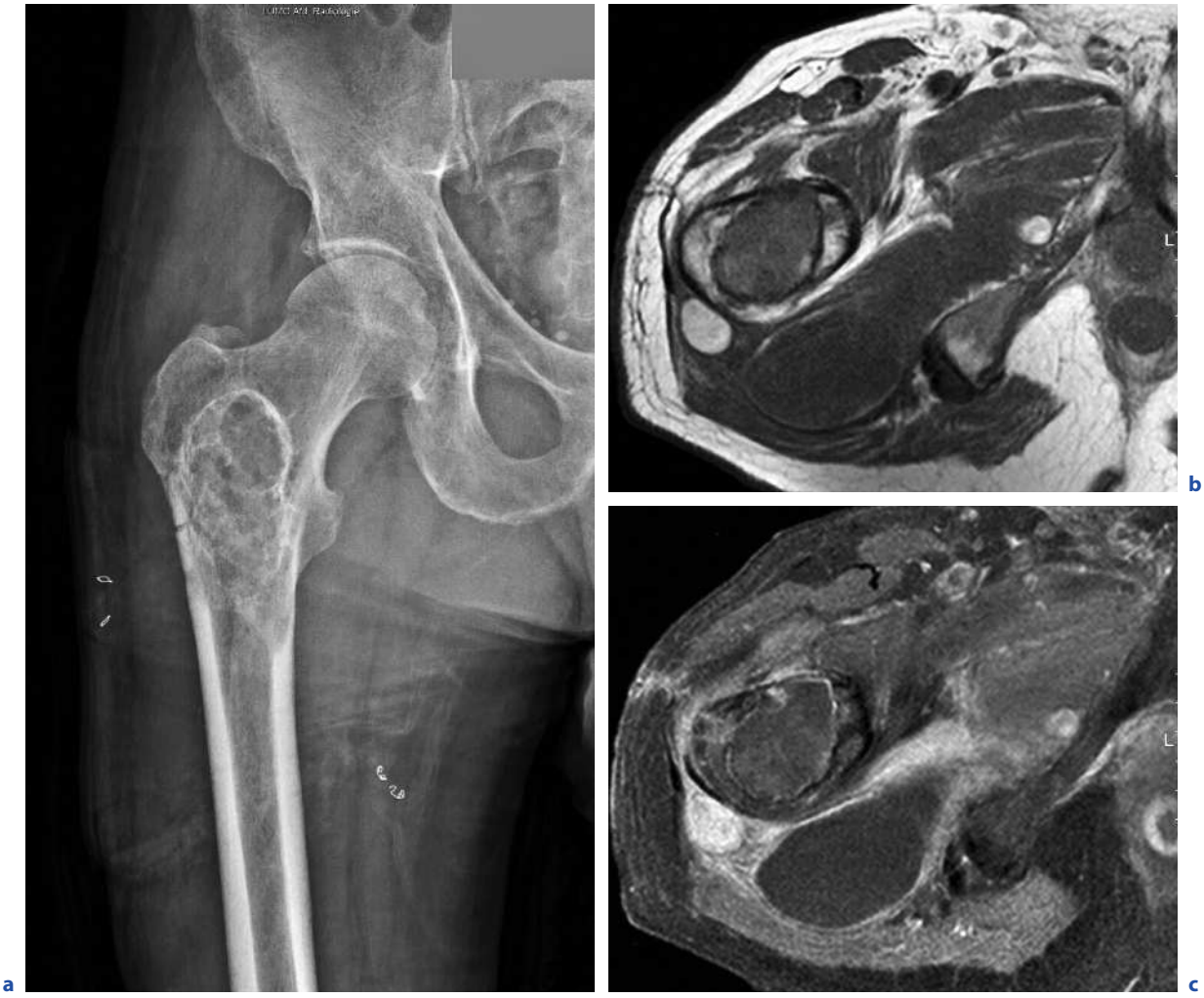

Fig. 19.4a–c. Angiosarcoma. **a** Radiograph of a well-defined, sclerotically marginated lesion with geographic type of destruction in proximal femur. Note biopsy track on the lateral side. The lesion has benign features resembling fibrous dysplasia. **b** The signal intensity of the osseous component is non-specifically low on this axial T1-weighted image. In the soft tissue region high-signal areas are appreciated representing hematomas. **c** Contrast-enhanced fat-suppressed T1-weighted image shows peripheral enhancement. At surgery, a large hematoma secondary to osseous angiosarcoma was found

The difficulty in establishing the diagnosis of poorly differentiated angiosarcomas is further confounded by the fact that they usually contain atypical cells, not readily identified as endothelial cells (Roessner and Boehling 2002). Nuclear atypia is abundantly observed with increased number of mitoses. As described previously, these neoplasms may display epithelial cellular features mimicking metastatic carcinomas, which complicates the diagnosis of these tumors even more. In addition, some of these tumors may demonstrate spindle cells and cytological features generally seen in other sarcomatous tumors of the bone (Roessner and Boehling 2002).

19.4.3 Hemangioendotheliomas

The radiological appearances of hemangioendotheliomas are non-specific. The predominant radiological features of these tumors are osteolytic lesions with sclerotic margins. These tumors may have well-defined or poorly defined margins with periosteal reaction. Bony expansion with cortical destruction is not rare, suggesting an underlying malignant etiology of these neoplasms.

The most important indication with hemangioendotheliomas is the presence of multifocal lesions (O'Connell et al. 2001); hence, differential diagnoses

for these neoplasms in adults include metastatic disease, multiple myeloma, and lymphomas (O'Connell et al. 2001), whereas in children, differential diagnoses includes Langerhans' cell histiocytoses, brown tumor, as well as multiple fibrous dysplasias.

The less commonly encountered solitary hemangioendothelioma should be differentiated from either benign or malignant bone tumors. Solitary hemangioendothelioma could mimic fibrous dysplasia or fibrous cortical defect. Malignant tumors, such as osteogenic sarcoma, Ewing's sarcoma, or fibrosarcoma, may resemble solitary hemangioendothelioma.

Pathological manifestation of this tumor includes the presence of soft and hemorrhagic lesion, which is composed of strands of cells with eosinophilic cytoplasms. The most important pathological features of these neoplasms include the presence of hyaloid or myxoid appearance of the stroma (O'Connell et al. 2001). Although the tumors may have well-formed vascular structures, the corded pattern of eosinophilic cytoplasms is the most important distinguishing feature in establishing pathological diagnosis of these tumors.

19.5 Conclusion

The heterogeneity of angiomatous skeletal neoplasms has been a challenge for radiologists and pathologists for decades in their effort to provide better diagnosis and to recommend better treatment for the patient. The inherent diversity of these neoplasms has also become an impediment in their efforts to better understand the tumors' biological and clinical behavior and to propose reliable prognostic-based classification systems. Although a variety of classification systems have been introduced, they have not been proven to provide significant improvement in the prognosis of the patient. The introduction of new classification systems has become a basis for hope that clinicians, radiologists, and pathologists will include some of these rare neoplasms in the differential diagnosis of multiple lesions. Being cognizant of the existence of these vascular neoplasms, especially when considering differential diagnosis of multiple lesions, is crucial to avoid rare, but potentially catastrophic, complications of diagnosis and treatment procedures.

Acknowledgement

We acknowledge the help of H. Kroon, J. Bovee, and M. Vermaat.

References

Aoki M, Batista O, Bellacosa A, Tsichlis P, Vogt PK (1998) The akt kinase: molecular determinants of oncogenicity. Proc Natl Acad Sci USA 95:14950–14955

Campanacci M, Boriani S, Giunti A (1980) Hemangioendothelioma of bone: a study of 29 cases. Cancer 46:804–814

Chang HW, Aoki M, Fruman D, Auger KR, Bellacosa A, Tsichlis PN, Cantley LC, Roberts TM, Vogt PK (1997) Transformation of chicken cells by the gene encoding the catalytic subunit of PI 3-kinase. Science 276:1848–1850

Chasi I, Hide G (2008) Hemangioma, bone. E-medicine, vol. 322

Evans HL, Raymond AK, Ayala AG (2003) Vascular tumors of bone: a study of 17 cases other than ordinary hemangioma, with an evaluation of the relationship of hemangioendothelioma of bone to epithelioid hemangioma, epithelioid hemangioendothelioma, and high-grade angiosarcoma. Hum Pathol 34:680–689

Laredo JD, Assouline E, Gelbert F, Wybier M, Merland JJ, Tubiana JM (1990) Vertebral hemangiomas: fat content as a sign of aggressiveness. Radiology 177:467–472

Larsson SE, Lorentzon R, Boquist L (1975) Malignant hemangioendothelioma of bone. J Bone Joint Surg Am 57:84–89

Lomasney LM, Martinez S, Demos TC, Harrelson JM (1996) Multifocal vascular lesions of bone: imaging characteristics. Skeletal Radiol 25:255–261

Maclean FM, Schatz J, McCarthy SW, Scolyer RA, Stalley P, Bonar SF (2007) Epithelioid and spindle cell haemangioma of bone. Skeletal Radiol 36 (Suppl 1):S50–S57

Mulder JD, Schütte HE, Kroon HM, Taconis WK (Netherlands Committee on Bone Tumors) (1993) The diagnosis of bone tumor. In: Radiologic atlas of bone tumors. Elsevier, Amsterdam, pp 9–16

O'Connell JX, Nielsen GP, Rosenberg AE (2001) Epithelioid vascular tumors of bone: a review and proposal of a classification scheme. Adv Anat Pathol 8:74–82

O'Reilly MS, Boehm T, Shing Y, Fukai N, Vasios G, Lane WS, Flynn E, Birkhead JR, Olsen BR, Folkman J (1997) Endostatin: an endogenous inhibitor of angiogenesis and tumor growth. Cell 88:277–285

Paik JH, Kollipara R, Chu G, Ji H, Xiao Y, Ding Z, Miao L, Tothova Z, Horner JW, Carrasco DR, Jiang S, Gilliland DG, Chin L, Wong WH, Castrillon DH, DePinho RA (2007) FoxOs are lineage-restricted redundant tumor suppressors and regulate endothelial cell homeostasis. Cell 128:309–323

Resnick D, Kyriakos M, Greenway GD (2002) Tumors and tumor-like lesions of bone: imaging and pathology of specific lesions. In: Resnick D (ed) Diagnosis of bone and joint disorders, 4th edn. Saunders, Philadelphia, pp 3983–3985

Roessner A, Boehling T (2002) Angiosarcoma. In: Fletcher C, Unni K, Mertens F (eds) Pathology and genetics of tumours of soft tissue and bone. IAC Press, Lyon, pp 322–323

Wenger DE, Wold LE (2000a) Benign vascular lesions of bone: radiologic and pathologic features. Skeletal Radiol 29:63–74

Wenger DE, Wold LE (2000b) Malignant vascular lesions of bone: radiologic and pathologic features. Skeletal Radiol 29:619–631

Notochordal Tumours

20

V. N. Cassar-Pullicino and D. C. Mangham

CONTENTS

Victor N. Cassar-Pullicino, MD
Consultant Radiologist
Department of Radiology
The Robert Jones & Agnes Hunt Orthopaedic and District Hospital NHS Trust
Gobowen, Oswestry, Shropshire SY10 7AG, UK

D. C. Mangham
Consultant Pathologist
Department of Musculoskeletal Pathology
The Robert Jones & Agnes Hunt Orthopaedic and District Hospital NHS Trust
Gobowen, Oswestry, Shropshire SY10 7AG, UK

KEY POINTS

- Notochordal tumors may be benign or malignant
- Notochordal tumors have a predilection for the spheno-occipital and sacral regions
- Benign notochordal tumors tend to be detected on MRI but demonstrate little or no abnormality on radiographs, CT or bone scintigraphy.
- Chordoma accounts for 50% of malignant sacral tumors.
- Sacral chordomas are predominently osteolytic with 90% showing varying degrees of calcification on CT, all showing an anterior soft tissue mass and 77% a posterior soft tissue mass on MRI.
- Biopsy identification of choirdoid tissue needs to be carefully correlated with MRI and CT appearances to decide if it represents BNCT or chordoma.

20.1 Introduction

The notochord is a posterior midline axial structure which plays a vital, albeit transient, role in human embryology, acting as the major structural organiser of spinal development. Before the second month it is surrounded by sclerotomes forming the ossification centres of the vertebral column lying anterior to the neural tube. As the embryonic spine develops, the notochord acts as an inducer of chondrification and segmentation of the mesenchymal elements. It involutes and fragments as development progresses, and by the second embryological month it persists in the intervertebral residues which later form the nucleus pulposus of the foetal and infant intervertebral disks up to three years of age (Salisbury 1993; Pazzaglia et al. 1989). Histologically the morphologically characteristic cell of noto-

chordal tissue is termed the physaliferous cell in which multiple cytoplasmic vacuoles indent the central nucleus, while immunohistochemically notochordal cells express the antigenic phenotype of cartilage and epithelial cells being strongly positive for S-100 protein, cytokeratin and epithelial membrane antigen (EMA). This morphology and immunophenotype of notochordal tissue is retained and manifested by notochordal tumours (Crapanzano et al. 2001).

Tumours of the notochord are unusual for a variety of reasons. Notochordal tissue has a purely embryonic role and is not present in the adult, and although the notochord is not an osseous tissue, tumours of the notochord are included as primary bone tumours because of their intimate relationship to bone. Intra-osseous cell remnants of the original notochord are believed to be the source of notochordal tumours. Prior to 1996 only chordoma , the malignant tumour of notochordal origin, was recognized. Since then it has become generally accepted that benign tumours of notochordal origin also exist, and there is increasing evidence of a causal relationship of these lesions with chordoma. The benign and malignant variants of notochordal tumours involve almost exclusively the midline axial skeleton. In embryogenesis, the notochord has a cartilaginous and osseous inductive effect, and in notochordal tumours there can be chondroid differentiation.

20.2 Notochordal Remnants

There are three introductory anatomical points which are helpful to understand this section. First, 3-D reconstruction studies have shown complex anatomical forking patterns of both the rostral and caudal ends of the developing notochord, which separate leaving chordal fragments during involution (Salisbury et al. 1993). Second, as the size of the notochord is small, reaching a peak in the fifth embryonal week, the anticipated size of notochordal remnants are bound to be very small. Third, notochordal vestiges are normally found in the intervertebral disks of neonates but disappear by the age of 3 years and do not materially contribute to the adult intervertebral disc (Pazzaglia et al. 1989). Recent autopsy experience on neonates and babies has shown that these intervertebral disk notochordal remnants are not associated with any notochordal tissue within the vertebral bodies. Although histologically these foetal notochordal vestiges are associated with myxoid matrix, they are immunoreactively negative for cytokeratin 18 (Yagamuchi et al. 2004a). It is therefore to be expected that the non-neoplastic remnants of the notochord would be microscopic in size and more likely located at the spheno-occipital and sacro-coccygeal areas.

Since 1856, multiple autopsy studies have shown the presence of non-neoplastic notochordal remnants in adults in an extraosseous location primarily around the spheno-occipital region. With an autopsy incidence of 2%, they take the form of small soft tissue nodules which are translucent and gelatinous in consistency, and histologically similar to the embryonal notochord containing physaliferous cells. They have been variously described as "ectopic notochordal rests", "ecchondrosis physaliphora spheno-occipitalis", "ecchordosis physaliphora spheno-occipitalis" and "benign chordoma" (Congdon 1952; Stewart and Burrow 1923; Howitz 1941; Virchow 1847; Luschka 1856; Muller 1858; Ribbert 1894). They have also been found in the sacro-coccygeal region, and very rarely in the vertebrae where they were given the designation of "ecchordosis physaliphora vertebralis". These intravertebral nodules are very small and microscopic measuring 0.18–0.86 mm in size (Ulich and Mirra 1982).

Since the advent of MRI, sporadic case reports have appeared in the radiology literature describing the imaging features (including CT) of small asymptomatic notochordal remnants in an extraosseous anatomical location in the cranio-cervical region (Ng et al. 1988). A retrospective review of 300 cranial MRI investigations identified five (1.7%) cases of retroclival ecchordosis physaliphora. All the lesions showed low T1 and high T2 signal, none of them showed contrast enhancement, four revealed signal intensity changes in the adjacent clivus, while three had a stalk connecting the notochordal remnant to the clivus (Mehnert et al. 2004). Up to 1996 it was generally accepted that notochordal remnants were precursors of chordoma enjoying similar location, distribution and relative incidence in the axial skeleton. The current thinking is that these intraosseous microscopic notochordal remnants are more likely to be the precursors of benign notochordal cell tumours, and it is the rare malignant transformation within these that gives rise to the classic chordoma.

20.3 Benign Notochordal Cell Tumours

20.3.1 Clinico-Pathological Considerations

At the Closed Meeting of the International Skeletal Society in 1996 held in Paris, Cassar-Pullicino and Darby

presented a unique case of a notochordal tumour without bone destruction or extra-osseous soft tissue component presumed to be a subset of chordoma treated by vertebrectomy. The solitary lesion was identified on MR imaging and occupied virtually the whole of the L5 vertebral body in a 39-year-old man (Fig. 20.1). Conventional radiographs and technetium scintigraphy were normal, while CT demonstrated mild sclerosis of the trabeculae without any bony destruction. This case generated a lot of debate and when published in 1999 (Darby et al. 1999), uncertainty still prevailed as to its exact nature which was reflected in the title chosen for the article – "Vertebral intraosseous chordoma or Giant notochordal rest?". Further case reports describing vertebral lesions of similar imaging and histological features were later published in 2001 (Mirra and Brien 2001) and 2003 (Kyriakos et al. 2003), with the pathological diagnoses of "Giant notochordal hamartoma of intraosseous origin" and "Giant vertebral notochordal rest", terms which are still currently in use (Chauvel

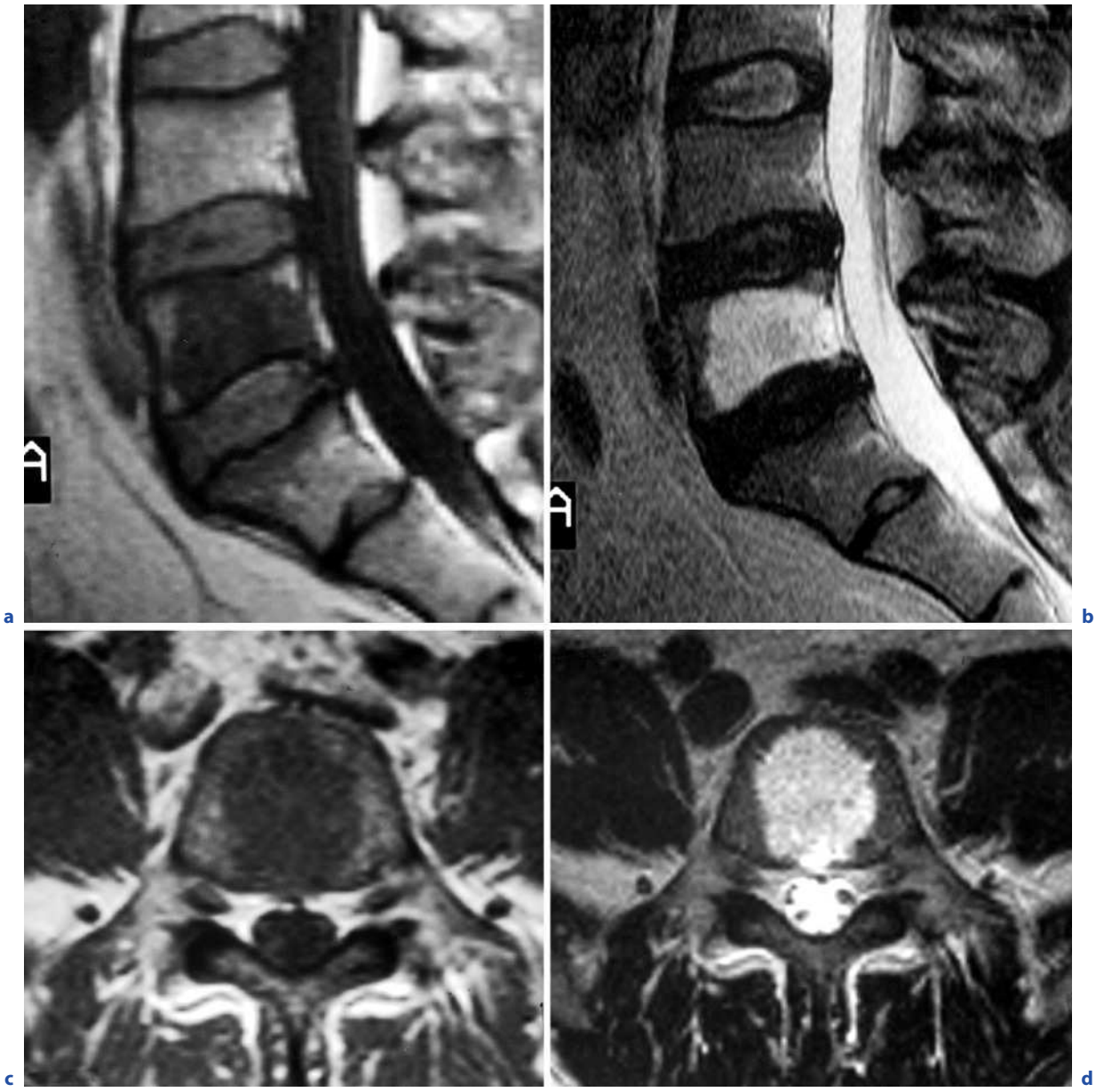

Fig. 20.1a–d. BNCT at L5 level. MR images in the sagittal plane T1 (**a**) and T2 (**b**) as well as in the axial plain T1 (**c**) and T2 (**d**). Note the high T2 signal, clear demarcation and preserved trabeculae in the lesion

et al. 2005; Oner et al. 2009). The three publications were essentially highlighting the same thing – a newly discovered benign notochordal tumoral entity detected since the advent of MRI which was distinct from the classic chordoma – and their authors equally struggled to find an acceptable terminology.

Yamaguchi and his colleagues coined the term "Benign Notochordal Cell Tumour (BNCT)" which is now the generally accepted terminology to describe this entity (Yagamuchi et al. 2004a, b). In the carefully conducted autopsy examinations, Yamaguchi et al. identified BNCT axial skeletal lesions in 20% of adult cadavers. In the 26 cases of intraosseous BNCT found in 20 autopsy cases, the mean age was 63 years, with a male to female ratio of 3:1. The results according to anatomical segments showed that 11.5% of the clivus, 5% of the cervical vertebrae, 0% of the thoracic vertebrae, 2% of the lumbar vertebrae and 12% of the sacrococcygeal segments were affected. This anatomic distribution of BNCT is similar to that of classical chordoma, supporting evidence that classical chordomas develop from intraosseous BNCT. BNCTs vary in size and are considered to develop as true benign tumours after birth presumably from notochordal remnants. An alternative mechanism has recently been postulated whereby notochordal cells in early life become dislodged from the nucleus pulposus through the endplate defect of a Schmorl's node, followed by proliferation in a supportive bone marrow micro environment (Corsi et al. 2008).

Pathologically BNCTs consist of small nodules, found predominantly at the cranial and caudal ends of the axial skeleton with a lesser incidence in the vertebrae of the mobile spine. Histologically BNCTs exhibit well demarcated intra-osseous sheets of adipocyte-like chordoid cells with a uni- or multivacuolated cytoplasm and bland nuclei. Virtually no mitotic activity is present. As the cells mimic adipocytes and lipoblasts the lesions can be wrongly diagnosed if thought to represent mature fatty marrow and necrotic bone trabeculae (Murakami et al. 2003, 2005). These authors initially published cases of presumed vertebral body osteonecrosis without vertebral collapse, and subsequently on review realised that the histology and allied imaging of these cases was typical of what is now known on BNCT. When multi-vacuolated with central nuclei these cells are termed physaliferous cells. The lesions are not lobulated, and lack any myxoid matrix. BNCT is totally intramedullary in location with no cortical involvement or soft tissue extension. The bony trabeculae within the lesion are undisturbed with no evidence of any lysis, but a mild reactive sclerosis is not uncommon (Fig. 20.2). The lesion permeates bone primarily by replacing the bone marrow and exhibits a sudden transition at the edge of the lesion when compared to the neighbouring normal haematopoietic marrow within normal medullary trabecular bone (Fig. 20.3). BNCT shows positive immunoreactivity for cytokeratin 18 unlike notochordal vestiges, with further positive immunostaining for vimentin, S-100, EMA and other cytokeratins (AE1/AE3) (Yamaguchi et al. 2008). This immunohistochemical panel is similar to chordoma and therefore cannot be used to differentiate benign from malignant notochordal tumours. Furthermore, BNCT stains positive for cytokeratin whereas fat cells do not, which is useful in the histological differentiation from fatty marrow lesions.

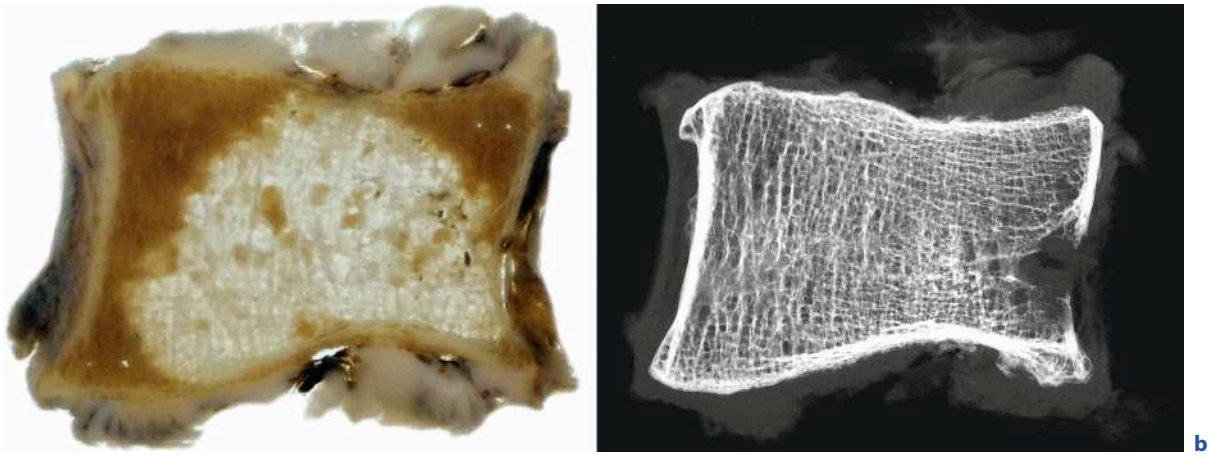

Fig. 20.2a,b. Thin sagittal slice of L5 vertebrectomy specimen (**a**) and radiograph (**b**). The BNCT lesion has a sharp demarcation from the normal marrow with intact intralesional trabecular bone

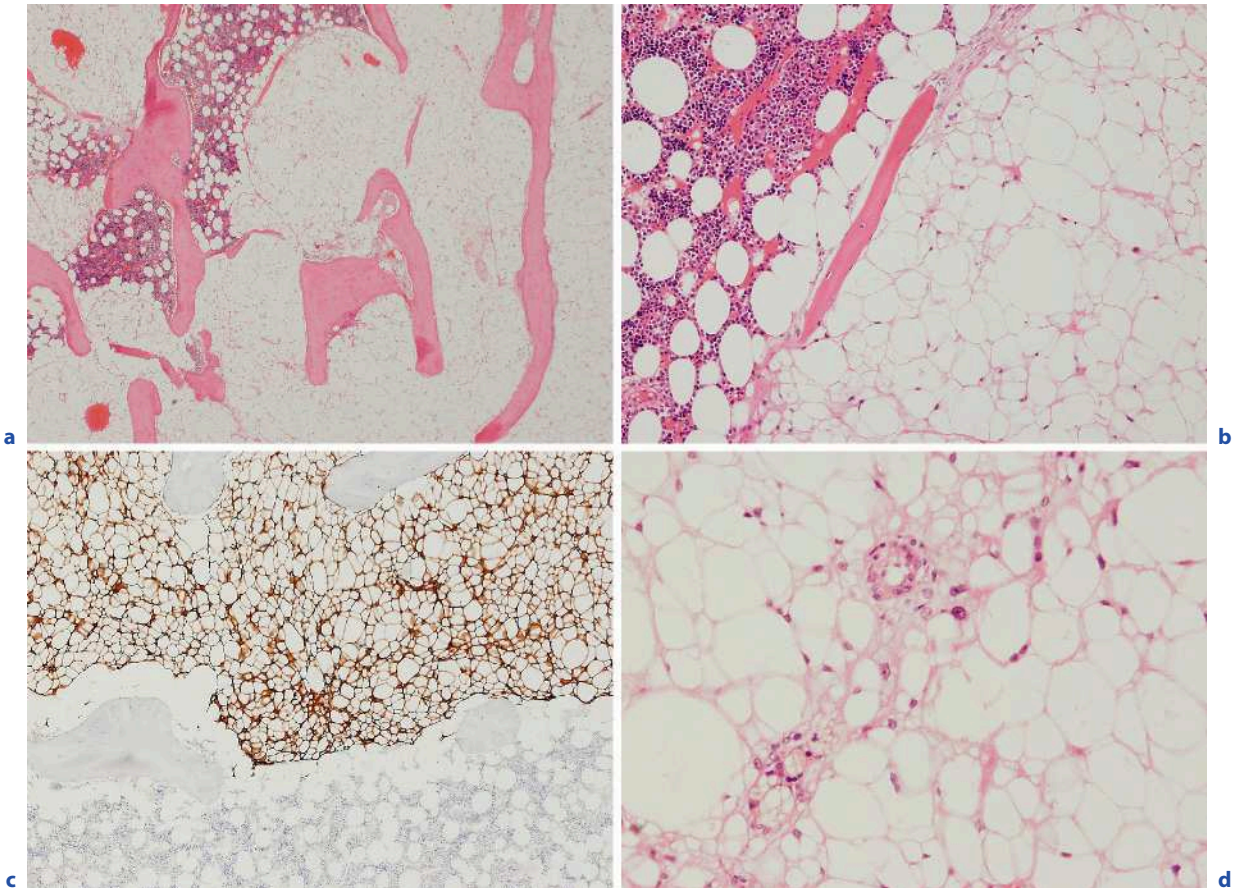

Fig. 20.3a–d. Microscopy of benign notochordal tumour (BNCT). **a** The tumour occupying the right two thirds of the picture. At this low power, the BNCT closely resembles fat, contains normal to mildly thickened bone trabeculae and has a sharp and harmonious interface with the adjacent haemopoietic tissue. **b** A higher power depiction of **a** showing the tumour cells to be composed of variably sized, clear vacuolated cells which are moulded to each other and possess small bland nuclei. There is a thin fibrous pseudocapsule at the tumour edge containing a contoured slither of bone. Tumour interfaces with undisturbed haemopoietic marrow containing true adipocytes. Note the complete lack of myxoid matrix production by the tumour. **c** A similar tumour/marrow interface immunostained (brown) for pan-cytokeratin. This dramatically demonstrates the true nature of the tumour cells contrasting with the complete lack of staining of the marrow adipocytes. **d** Occasional foci within the tumour where the nuclei display some degree of atypia. This, in itself, is not a sign of malignancy

20.3.2 Imaging Considerations

BNCT can be very small and easily overlooked, even at autopsy. Although indolent and predominantly asymptomatic, BNCT lesions can grow to a significant size, replacing virtually the entire bone marrow of a vertebral body. Large examples of BNCT, published in the 15 clinically identified cases, owe their detection to MR imaging. It is more than likely that on MR imaging, the smaller lesions are overlooked or possibly wrongly diagnosed as other benign entities such as atypical vertebral haemangiomas. In addition the anatomical distribution of BNCT in the autopsy study by Yamaguchi et al. is also different from the clinically published cases. In these 15 cases, 6 BNCTs were located in lumbar vertebrae, 5 in cervical vertebrae, 2 in the sacrum and 1 each in a thoracic vertebra and coccyx (Yamaguchi et al. 2008). Lesions in the clivus, sacrum and coccyx are overlooked as these anatomical areas are not routinely included in their entirety in MR examination protocols of the cervical and lumbar areas done for spinal pain.

The imaging features are consistently reproducible with a narrow variational spectrum (Fig. 20.4). In BNCT, radiographs and CT fail to identify a distinct lesion even when large. Radiographically the bone can appear normal or exhibit a variable degree of sclerosis which rarely results in an ivory vertebra. In the absence

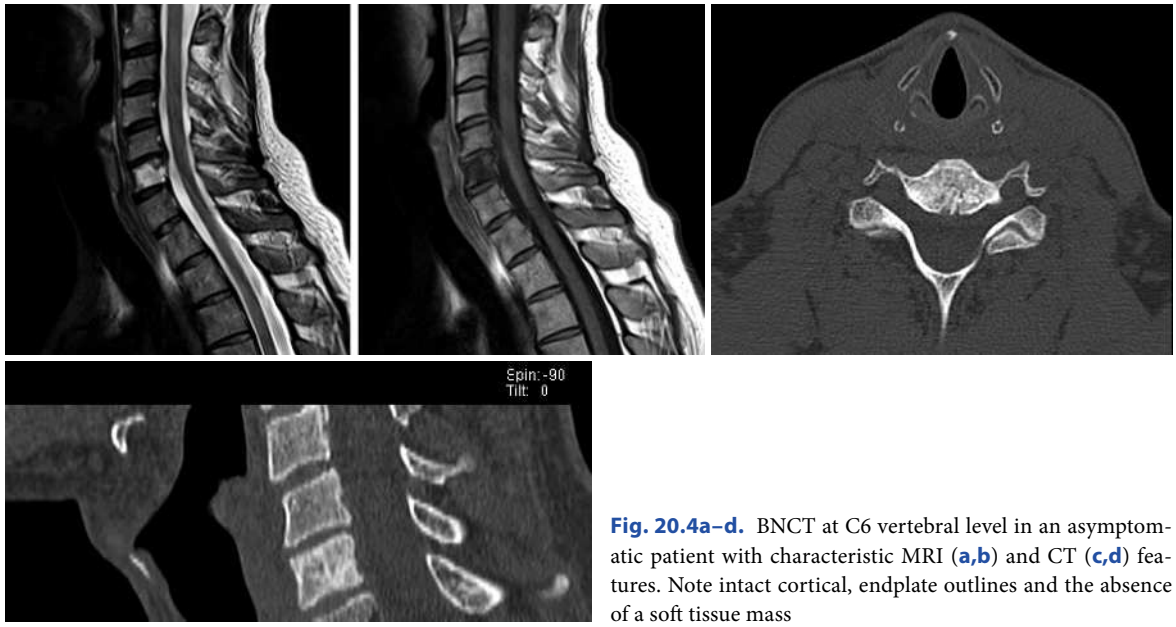

Fig. 20.4a–d. BNCT at C6 vertebral level in an asymptomatic patient with characteristic MRI (**a,b**) and CT (**c,d**) features. Note intact cortical, endplate outlines and the absence of a soft tissue mass

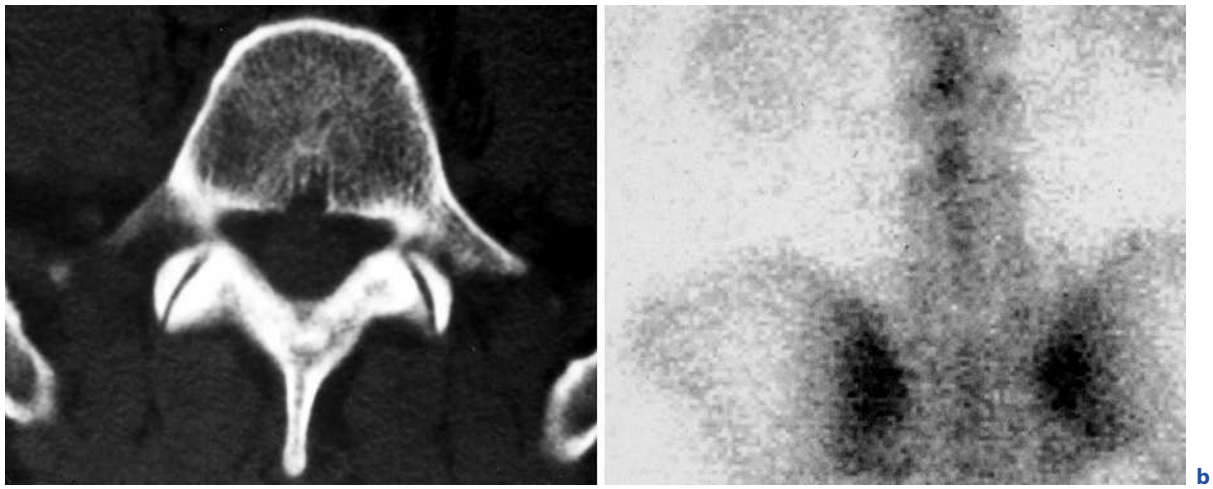

Fig. 20.5a,b. Axial CT (**a**) and 99-TcMDP scintigraphy (**b**) of L5 BNCT showing no osteolysis, mild trabecular sclerosis and normal radionuclide activity

of trabecular lysis (a defining characteristic of the entity), BNCT do not produce a CT detectable space-occupying effect but most lesions do excite a degree of CT detectable intralesional trabecular sclerosis. On MR imaging the lesions are very clear, sharply defined, and demarcated from the normal adjacent bone marrow. They are easily seen replacing the marrow space exhibiting low T1 signal with a very high T2 signal intensity, but no evidence of any enhancement following intravenous Gd-DTPA. There is no evidence of any cortical disruption or soft tissue mass. Technetium scintigraphy including SPECT is invariably negative when carried out (Yamaguchi et al. 2008) (Fig. 20.5).

20.4 Incipient Chordoma

The concept of "incipient chordoma" has been proposed by Yamaguchi et al. in 2005 as subclinical minute tumoral lesions with histologic features intermediate be-

tween BNCT and chordoma (Yamaguchi et al. 2005). This concept is essentially based on histopathological criteria and not supported by any corresponding imaging equivalence or reference. The essential histological features of incipient chordoma include small asymptomatic lesions exhibiting infiltrative sheets of cells with a uni-or multi vacuolated cytoplasm, bland nuclei and occasional cords of cells in a scanty myxoid matrix. The lesion is primarily intra-medullary with or without extension into and through the cortex. This lesion exhibits a delicate network of fibrous septae with barely discernible tumour lobularity. This concept is also strengthened by the fact that the autopsy distribution of BNCT also maps the relative axial distribution of chordoma. In addition, there are two retrospective histopathological reviews suggesting a causal link based on the identification of coexistent BNCT and chordoma (Yamaguchi et al. 2002; Deshpande et al. 2007).

Although there is growing evidence that BNCT does have the potential of malignant transformation to chordoma, there are still significant gaps in our knowledge of the true biological behaviour, risk and incidence of this rare event. In the first histologically confirmed case of classic chordoma arising in a precursor BNCT in the coccyx of a 57-year-old man, histology showed the BNCT was adjacent but separate, with a further two separate BNCT lesions seen in the sacrum (Yamaguchi et al. 2002). From the limited follow-up knowledge in the clinically published cases of BNCT, there is general agreement that once identified these lesions need to be carefully followed up by MRI and CT over the long term, and managed expectantly rather than surgically. Any imaging evidence of trabecular destruction, cortical invasion and growth beyond the confines of bone should intuitively suggest the development of chordoma. The guiding principle of screening the entire spine by MR imaging once a notochordal tumour (BNCT or chordoma) has been detected in one level of the spine is recommended.

20.5 Classic Chordoma

20.5.1 Clinico-Pathological Considerations

Chordoma is a rare tumour representing only 2–4% of all primary malignant bone tumours. It is rare below the age of 30 with a peak incidence in the fifth and sixth decades and shows a marked male predominance of 2/3:1. The tumour is exclusively observed in the axial skeleton with two sites of predilection in the spheno-occipital (35%) and sacrococcygeal (50%) regions. Vertebral involvement (15%) carries an equal male:female ratio and is most common in the cervical, followed by lumbar, levels with the thoracic spine the least common. A small number occur in children up to the second decade of life with typical involvement of the C2 vertebra. Cranial lesions tend to be smaller at presentation and occur in a younger age group compared with sacrococygeal lesions. Chordoma is the most frequent primary tumour of the sacrum accounting for 40% of all sacral tumours and 50% of all malignant sacral bone tumours. It has a tendency to involve the sacrum below the S 3 level. The tumour is rarely seen in the Afro-Caribbean population and is usually solitary rather than multicentric. Multilevel involvement due to direct craniocaudal spread to contiguous spinal levels via the epidural space, producing satellite lesions however is not uncommon. Apart from their exclusive involvement of the axial spine, chordomas also tend to involve the centre of the bone of origin in the clivus, sacrum, coccyx and vertebral body in the midline (York et al. 1999).

In the WHO tumour classification, "Chordoma is a low to intermediate grade malignant tumour that recapitulates notochord" (Fletcher et al. 2002). As it stands, this definition is insufficient as it does not differentiate chordoma from BNCT, lacking any descriptive features. Identification of chordoid tissue in a bone biopsy cannot be assumed to be due to chordoma. The pathological behaviour and presentation of chordoma is different from BNCT. Macroscopically chordomas appear as soft, white, multilobulated gelatinous masses contained by a fibrous pseudocapsule (Fig. 20.6). Although the appearances suggest a well demarcated lesion, there is no well developed pseudocapsule which explains why satellite tumour droplets and post-surgical recurrences are common. The tumours contain a fluid and mucoid matrix, old and recent haemorrhage, necrosis, calcification and sequestered bone fragments. Due to the low grade of malignancy and their inherent slow-growing nature, chordomas usually present late with advanced destruction of the bone they originate in. This also poses significant therapeutic challenges. There is almost invariably a large extraosseous soft tissue mass which, depending on the location of the tumour, initially compresses and later invades neighbouring structures, including the cranial nerves in spheno-occipital lesions, spinal canal contents in vertebral lesions, and the bladder and rectum in sacrococcygeal tumours. Bone destruction in some vertebral cases can be minimal as shown in 7 of 10 cervical vertebral chordomas which

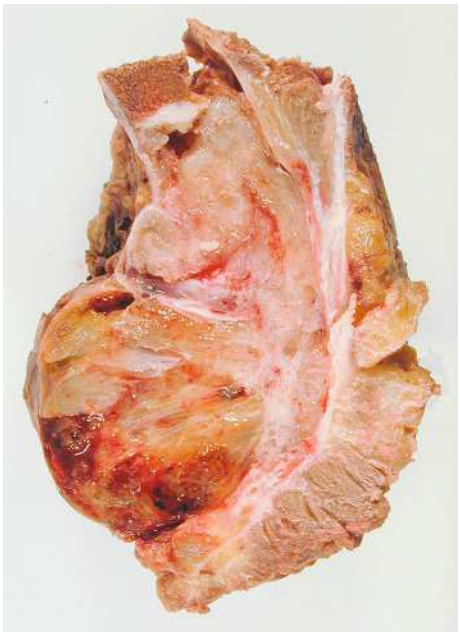

Fig. 20.6. Gross appearance of a sacrococcygeal chordoma. A sagittal section through the sacrum demonstrates the typical appearance of a chordoma. The lower sacral vertebrae have been completely destroyed by the tumour which has a lobular, gelatinous appearance. As is nearly always the case, extra-osseous chordoma is almost entirely positioned anterior to the destroyed sacrum, although later in the disease course the tumour will often push posteriorly as well

produced widening and destruction of neural foraminae simulating a neurogenic tumour (Wippold et al. 1999; Steenberghs et al. 2002; Wang et al. 1984).

Histologically the tumour is characterised by a pronounced lobular pattern with intersecting fibrous bands. The tumour lobules are composed of sheets and cords of cohesive vacuolated (including physaliferous cells) and non-vacuolated cells with atypical and/or pleomorphic nuclei which are infiltrative and destructive of the neighbouring trabecular and cortical bone. This bone resorption by virtue of lesional permeative growth is often largely due to recruited osteoclasts. There is a variable but usually abundant tumour cell production of a myxoid matrix. The interface between the lesion and adjacent marrow of the uninvolved bone is chronically inflamed exhibiting active osteoclastic recruitment. This latter feature contrasts with BNCT which exhibits a "harmonious" relationship with its normal surroundings (Fig. 20.7). BNCT co-exists with chordoma when specifically searched for, with an incidence of 7.3% in sacrococcygeal resections performed for primary classic chordoma (Deshpande et al. 2007).

20.5.2 Imaging Considerations

Chordoma is primarily an osteolytic lesion and due to the sites of involvement is easily overlooked radiographically especially in the sacrum (Firooznia et al. 1976). Osteosclerosis is rare in clival and sacral chordomas (Murphey et al. 1996) but it has been described in 64% (9 of 14) of spinal chordomas (De Bruine and Kroon 1988). However, five of the nine sclerotic cases did not have an associated soft tissue mass. It is difficult to know if some of these cases published before the

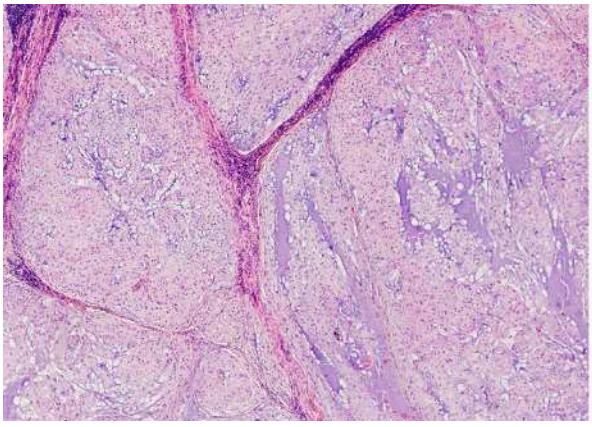

a

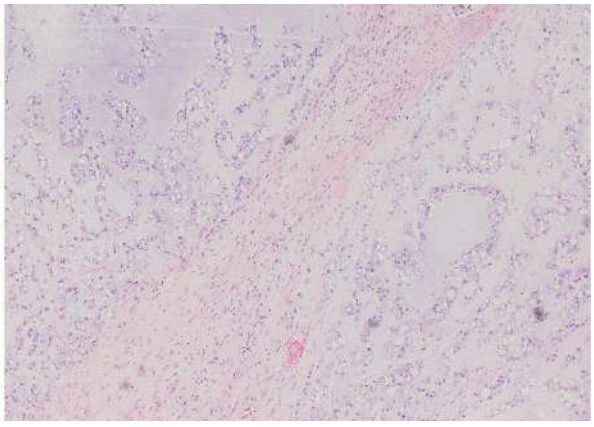

b

Fig. 20.7a–d. Microscopy of chordoma. **a** A low power view of a typical chordoma showing bone loss and intersecting fibrous septae, sometimes chronically inflamed, dividing the tumour lobules. Some of the tumour cells are vacuolated but many are not, rather possessing abundant pink cytoplasm. Note the presence of the flocculated myxoid matrix. **b** The fibrous septa divides lobules of tumour which are particularly rich in myxoid matrix. This matrix abundance serves to highlight the cord and island formations of the cohesive tumour cells. **c** *and* **d** *see next page*

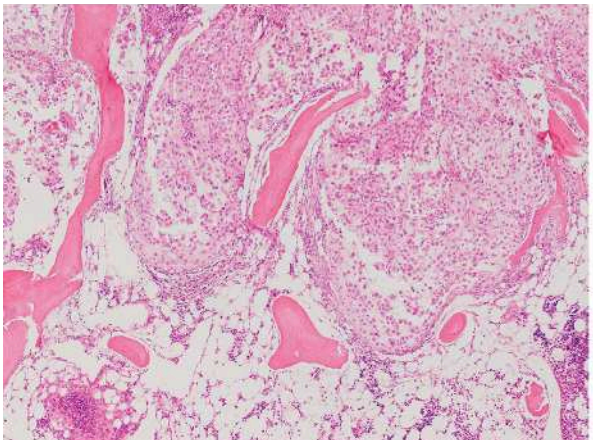

c

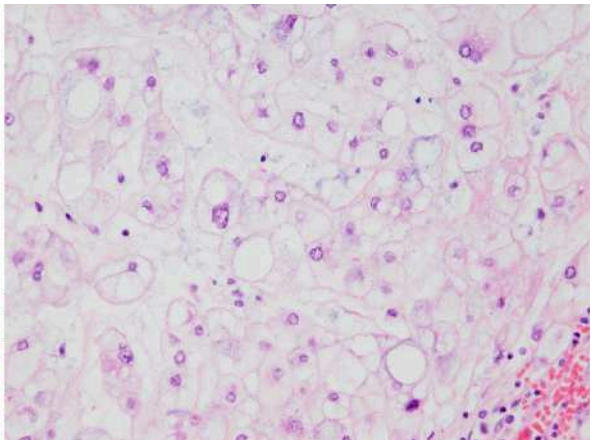

d

Fig. 20.7a–d. (*continued*) Microscopy of chordoma. **c** The edge of the permeative tumour, entrapping "moth-eaten" bone trabeculae. **d** A high power view of chordoma tumour cells: in contrast to Fig. 20.3b and d, the tumour cells are more often multivacuolated, show more atypical nuclei and have produced readily apparent extracellular myxoid matrix

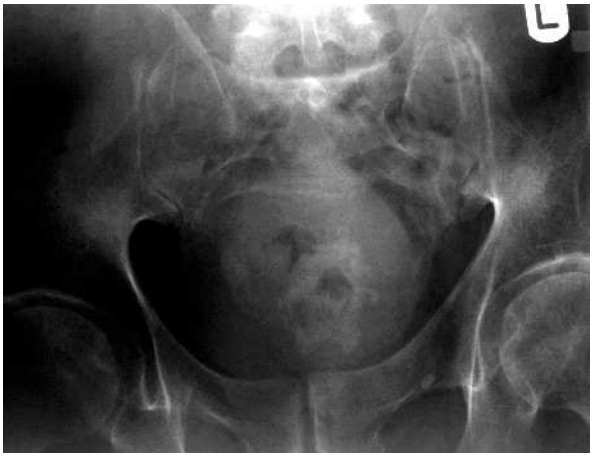

a

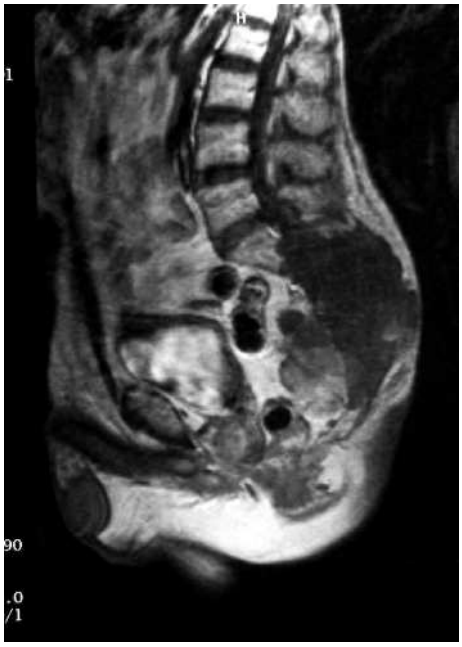

b

Fig. 20.8a–d. Sacro-coccygeal chordoma seen as an osteolytic lesion, cortical destruction with a large lobulated extraosseous soft tissue mass. Note the poor visibility on the plain radiograph (**a**), low T1 (**b**) and high T2 (**c**) MR signal and bone destruction (**d**). **c** *and* **d** *see next page*

recognition of BNCT represented true chordoma or alternatively chordoma arising in a sclerotic vertebra due to a BNCT. CT demonstrates the osteosclerosis mainly at the periphery of the destructive lesion. As presentation of this slow growing tumour is invariably delayed, the bone destruction is usually widespread, with variable bone expansion and almost invariably a large lobulated extraosseous soft tissue mass (Fig. 20.8). Within the tumour, calcification (90% in CT of sacral lesions, 15% of vertebral lesions) and residual bone fragments may be present, while the gelatinous myxoid content is highlighted as low attenuation on CT (Meyer et al. 1984), with low T1 and very high T2 signal on MR imaging (Rosenthal et al. 1985) (Fig. 20.9). The presence of haemorrhage and necrosis in the tumours produces increased cross-sectional imaging heterogeneity with areas of high T1 signal presumably due to blood products in 73% of cases (Sung et al. 2005). Contrast enhancement varies ranging from minimal, presumably as the myxoid containing lobules are hypo-vascular, to moderate enhancement which is prominent in the vascular fibrous internal septae which are easily delineated. In sacrococcygeal tumours these septae produce a characteristic criss-crossing pattern (Sung et al. 2005)

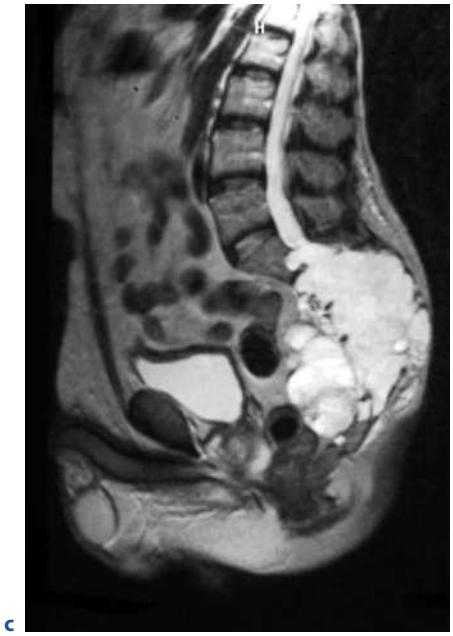

c

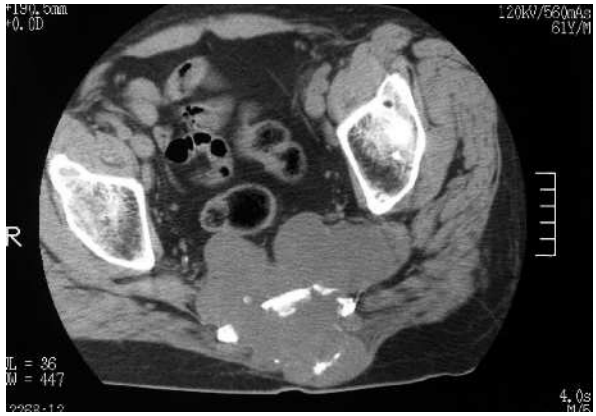

d

Fig. 20.8a–d. (*continued*) Sacro-coccygeal chordoma seen as an osteolytic lesion, cortical destruction with a large lobulated extraosseous soft tissue mass. Note the poor visibility on the plain radiograph (**a**), low T1 (**b**) and high T2 (**c**) MR signal and bone destruction (**d**)

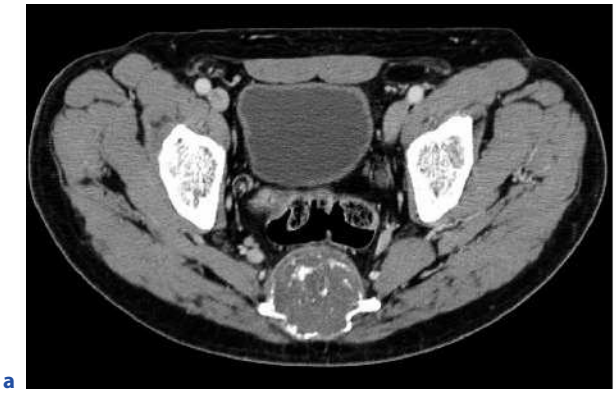

a

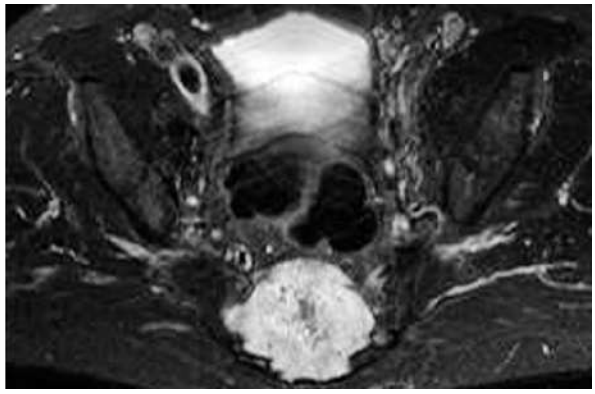

b

Fig. 20.9a,b. Sacral chordoma showing a soft tissue mass with calcification which is better seen on CT (**a**) than MR (**b**)

(Fig. 20.10). As sacrococcygeal chordoma excites little or no adjacent bone response, the scintigraphic appearances are often photopenic (Rossleigh et al. 1986).

In spheno-occipital lesions a retropharyngeal mass is common, while in sacrococcygeal lesions the anterior anatomical concavity harbours the soft tissue mass initially before spreading posteriorly. Using MR imaging, all sacrococcygeal chordomas were associated with an anterior soft tissue mass, while 77% had additional evidence of posterior extension (Sung et al. 2005). Vertebral lesions involve the centre of the vertebral body and produce an anterior and a posterior soft tissue mass with the propensity of craniocaudal spread involving contiguous vertebral bodies but sparing the intervertebral discs until late in the disease (Meyer et al. 1984; Smolders et al. 2003) (Fig. 20.11). When interpreting MRI scans of vertebral chordoma it is important to note that the MR signal of the intervertebral disc is virtually identical to chordoma tumour tissue. It is essential that the endplates are observed as being intact before declaring the absence of disc invasion. The presence of a concomitant soft tissue mass, spanning several vertebral levels is very characteristic of vertebral chordoma. Calcification is not a prominent feature. Extension into the soft tissues may occur anteriorly, laterally or posteriorly towards the epidural space producing the "curtain sign" and if it invades the posterior longitudinal ligament the "epidural tail sign" seen to enhance after Gd-DTPA (Smolders et al. 2003). Irrespective of location, once the epidural space is involved the tumour pro-

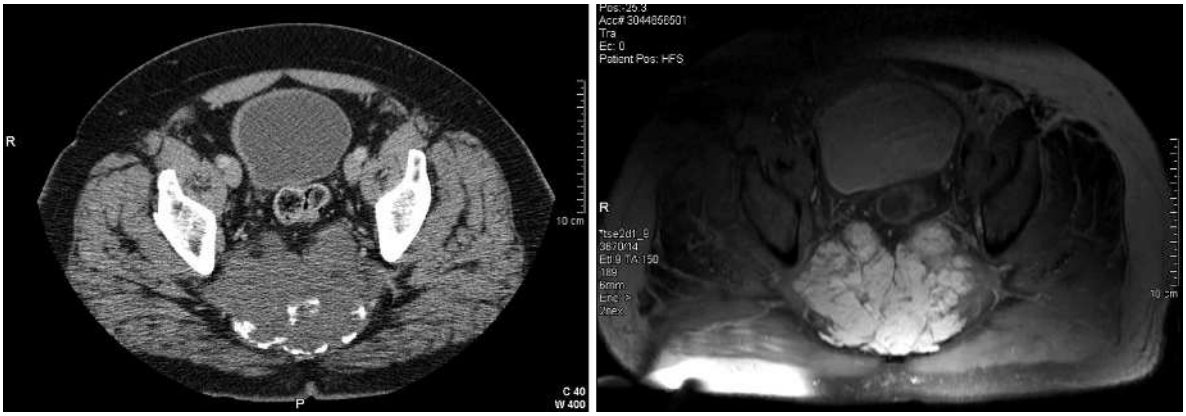

a b

Fig. 20.10a,b. Axial CT (**a**) and corresponding MR axial T2 image (**b**) demonstrating marked osteolysis and characteristic criss-cross MR pattern

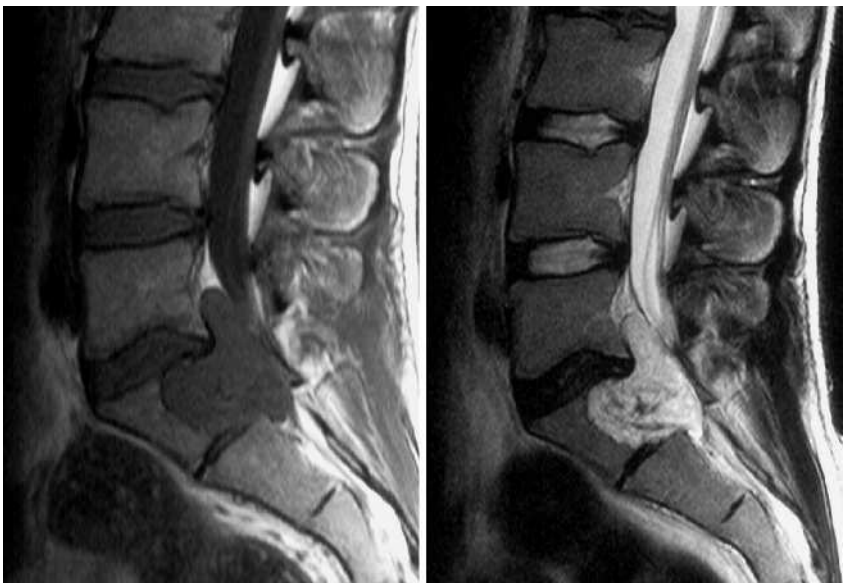

a,b

Fig. 20.11a,b. S1 chordoma located posteriorly extending into the epidural space with craniocaudal spread seen on sagittal T1 (**a**) and T2 (**b**) MRI with an intact L5-S1 intervertebral disc but destruction of S1-S2 rudimentary disc

duces craniocaudal migratory spread with a tendency for satellite lesions; this is why MR imaging is essential for accurate staging prior to surgical treatment (York et al. 1999) (Fig. 20.12).

In the preoperative assessment of sacrococcygeal chordomas, the identification of nerve root involvement by MRI is essential information. If the lesion can be removed with preservation of the upper three sacral nerves on one side and two on the other side, the patient will still be functionally continent. Loss of all but the first sacral roots bilaterally results in severe rectal, urinary and sexual dysfunction. Careful assessment of the anterior tumour relationship with the rectum is crucial as some patients will also need a colostomy. MR imaging reveals extension into the sacroiliac joints in 23% at presentation, as well as perineural spread along the spinal nerves and plexus with pseudopodia formation in the greater sciatic notch in 87% of chordomas (Sung et al. 2005). Involvement of the sacral nerve roots within the neural foramina is best seen in the coronal plane. MR imaging in the three planes is very useful in providing a 3-D representation of intraosseous and extraosseous spread and the tumour relationship to neural tissue, foramina, muscles, pelvic organs, etc. (Rosenthal et al. 1985) (Fig. 20.13). Although MRI is better in view of its superior resolution than CT in showing tumour soft tissue extent, it too probably cannot detect the exact tumour margin, and it is best still to employ a cautious surgical approach with a wide surgical margin to avoid tumour contamination and future recurrence (Hudson

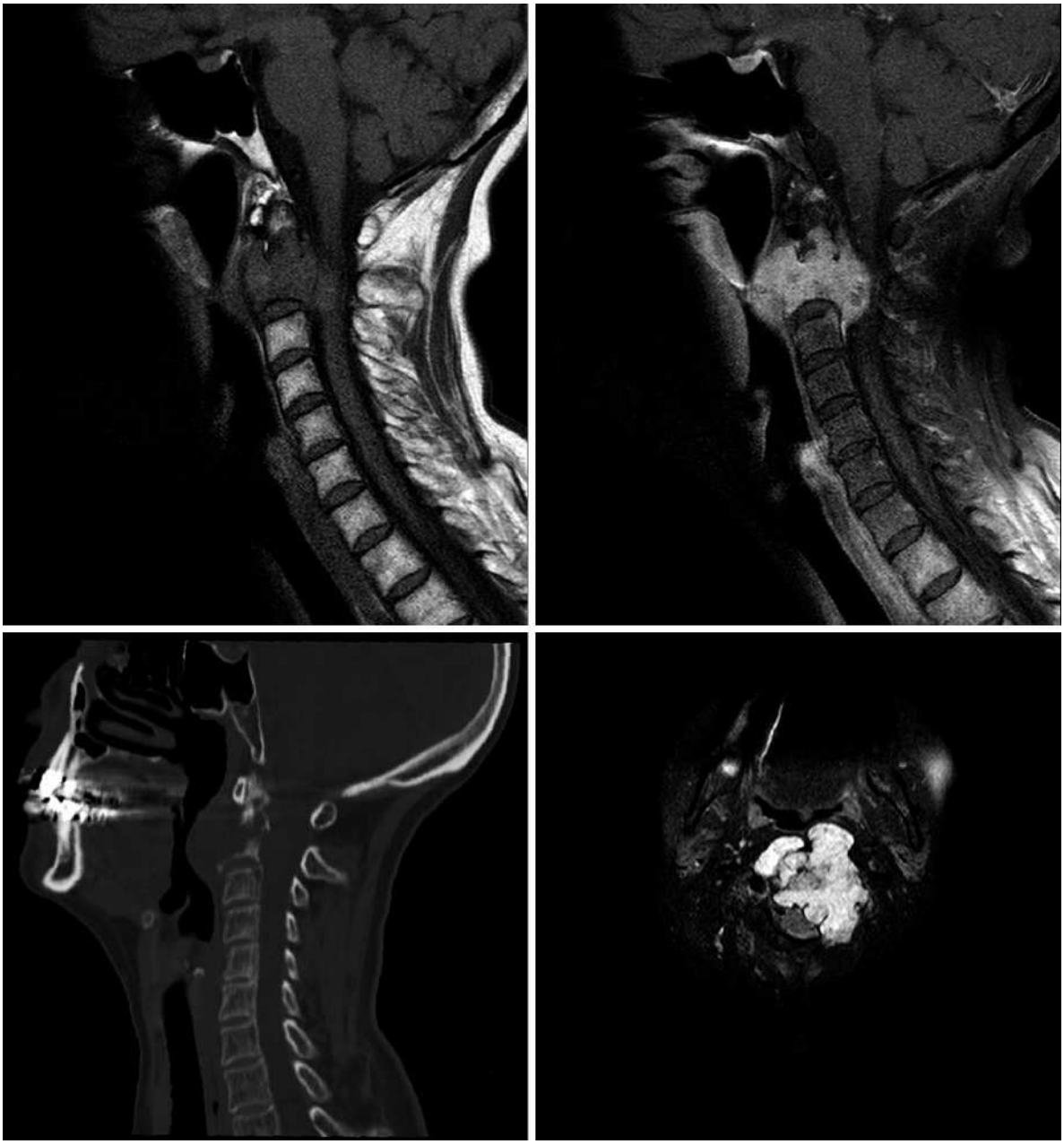

Fig. 20.12. Chordoma at C2 in a young female patient. Note the osteolysis cortical destruction, anterior and posterior soft tissue mass, spinal cord compression and intact C2/3 intervertebral disc

and Galceran 1983). The differential diagnosis based on the above imaging features would include spine tuberculosis, chondrosarcoma and renal adenocarcinoma metastases.

Tumour recurrence is highlighted by the presence of usually multiple soft tissue nodules of varying size seen locally at the resection site (Hudson and Galceran 1983). The imaging spectrum of the tumour recurrence is the same as the primary tumour (Fig. 20.14). MRI is more reliable in detecting and defining accurately the tissues involved by the recurrent tumour than CT because of the markedly prolonged T2 values of the tumour (Rosenthal et al. 1985). MRI is also helpful in monitoring a favourable response to proton therapy,

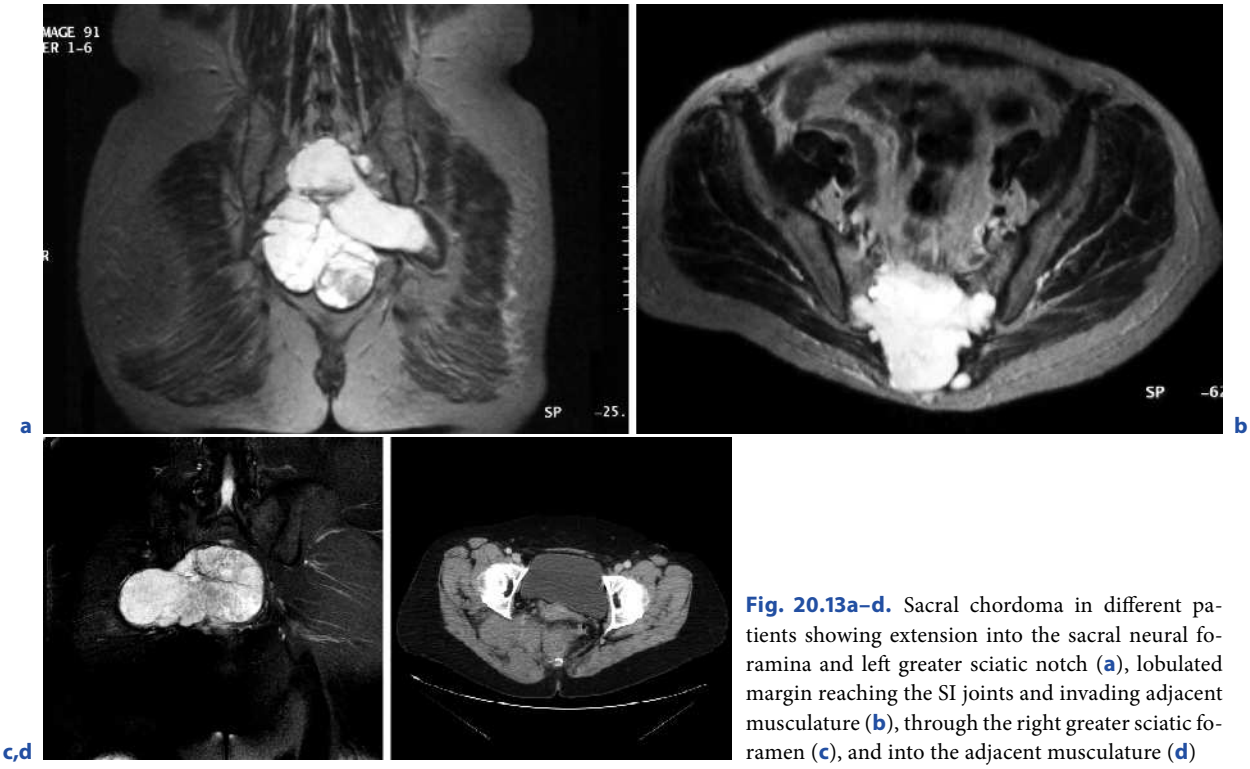

Fig. 20.13a–d. Sacral chordoma in different patients showing extension into the sacral neural foramina and left greater sciatic notch (**a**), lobulated margin reaching the SI joints and invading adjacent musculature (**b**), through the right greater sciatic foramen (**c**), and into the adjacent musculature (**d**)

while a limited number of nuclear medicine studies utilising PET–CT and SPECT show promise in assessing in vivo the therapeutic effects (Zhang et al. 2004; Di Girolamo et al. 2005). MR imaging is the modality of choice in excluding metastatic disease to musculoskeletal tissues. It is important that a baseline whole spine MRI is obtained at the time of the initial chordoma diagnosis to exclude the concomitant presence of other notochordal lesions elsewhere. This is to ensure that if present they in turn are managed appropriately, but also to avoid any confusion in future follow-up as they might inadvertently be considered as metastatic spread.

20.5.3 Prognosis

Compared with primary malignant bone tumours of the appendicular skeleton, staging of chordoma has not proven particularly valuable. This is due to multiple reasons including; delayed presentation, the rare and late nature of metastatic disease (Cheung et al. 1999). The survival rate from the onset of symptoms is 5.7 years which probably reflects their slow growing nature. Age at presentation is the single most important prognostic determinant, which is better in patients under rather than over 40 years. To a significant extent the prognosis in chordoma depends principally on the site of involvement and on the size at presentation, which in turn dictate the feasibility and success of radical surgical excision. Patients with sacrococcygeal lesions average 7–8 survival years compared with spheno-occipital lesion survival of 3–4 years. There is a clearly documented occurrence of spontaneous resolution without treatment in a cervical chordoma in a 24-year-old (Radl et al. 2005), but this must be exceptionally rare. Overall metastases are rare and usually occur late in the course of the disease. The declared improved prognosis in the chondroid variant of classic chordoma is controversial. Metastases are rarely seen in cranial chordoma as death occurs earlier from the primary tumour due to local invasion. In sacrococcygeal tumours metastasis to lungs, liver, bone, soft tissues and regional lymph nodes are seen in 10% of cases, while the vertebral tumours have a higher metastatic potential of 30–40%.

The only hope of cure is surgical resection with a wide surgical margin being the most important predictor of survival and local recurrence (Fuchs et al. 2005; Sciubba et al. 2008). Even after wide en bloc resection of sacrococcygeal tumours, the recurrence rate is of the order of 20%. Combined anterior and posterior surgical approaches in the operative management of sacrococ-

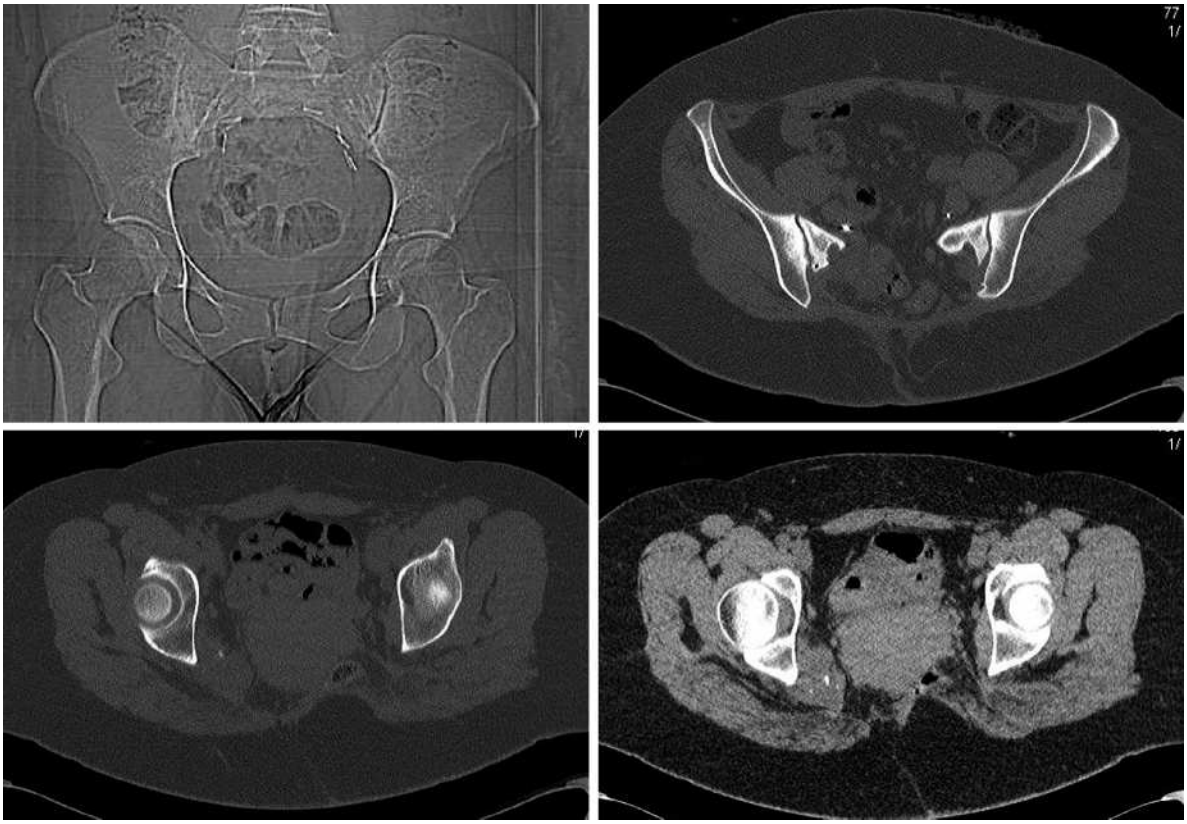

Fig. 20.14. Recurrent chordoma following partial sacro-coccygectomy with colostomy seen on the CT images as lobulated soft tissue masses with calcification and osteolysis

cygeal chordomas offer the best results. The recurrence rate is high in instances of intralesional, marginal or contaminated surgery (Hanna et al. 2008). Chordoma is well known to be resistant to radiotherapy, but is given in such instances in an attempt to reduce the recurrence rate. Proton and photon beam radiotherapy using high doses and therapeutic monoclonal antibodies are offered in selected cases especially in cranial and vertebral tumours as they carry a low risk of neural tissue damage. As mentioned later, dedifferentiated chordoma carries a very poor prognosis.

20.6 Chondroid Variant of Classic Chordoma

In 1973 Heffelfinger et al. described the chordoma variant that contains cartilaginous areas indistinguishable from hyaline type chondrosarcoma (Heffelfinger et al. 1973). The coexistence of chordoid and chondroid tumour components occurs in about 15% of chordomas and the majority of cases are spheno-occipital. The abundance of hyaline cartilaginous tissue may cause diagnostic difficulties in the histological interpretation of biopsy material. Chondroid chordoma behaves in a similar fashion to classic chordoma. On MR imaging this chordoma variant has shorter T1 and longer T2 signals because of its higher water content. Even post Gd-DTPA MR imaging of these chondroid variants can reveal a ring and arc enhancement pattern in common with chondrosarcoma.

Chondrosarcoma constitutes the main differential diagnosis of this chordoma variant. In adults chondrosarcoma is the second most common non-lymphoproliferative malignant bone tumour of the spine after chordoma. Chondrosarcoma does have similar imaging features. Radiographically it manifests itself as an osteolytic lesion, containing calcification with an extra-osseous soft tissue mass. In addition CT and MRI reveal a lobulated tumour, low CT attenuation areas with calcification, and a low T1 and high T2 signal characteristics.

However the post-contrast appearances are different with chordoma exhibiting no lobular enhancement and mild septal enhancement compared with the clear contrast enhancement of the tumour and intratumoral septae, producing a lobular, nodular or diffuse enhancement depending on the histological grade of chondrosarcoma. Histological distinction between chondroid chordoma and chondrosarcoma can be difficult. In a combined morphologic and immunohistochemical study Rosenberg et al. showed that chondroid chordoma exists as a variant of classic chordoma and can reliably be differentiated from chondrosarcoma. Immunohistochemical panels help in differentiating chondroid chordoma from chondrosarcoma which have positive S-100 protein in both tumours. All the chondroid and non-chondroid chordomas are positive for cytokeratin with the majority also positive for epithelial membrane antigen (EMA) and carcinoembryonic antigen (CEA) which contrasts with the lack of expression of all three antigens by chondrosarcoma (Rosenberg et al. 1994). Recently, the immunohistochemical detection of brachyury has proved highly specific for chordoma and has entered surgical pathology practice (Vujovic et al. 2006).

20.7 Dedifferentiated Chordoma

The emergence of a "histogenetically" distinct (i.e. different differentiation pathway) higher grade tumour arising in a pre-existing tumour is referred to as tumoral "dedifferentiation". The higher grade element has a higher growth rate and an increased risk of metastasis. The incidence of dedifferentiated chordoma is 6–9% of all chordomas with about 30 reported cases in the literature. It is more commonly reported in recurrences and following radiotherapy treatment. It can arise de novo and as chordoma is slow growing, any sudden increase in size or development of new symptoms should suggest the possibility of this usually lethal complication. The dedifferentiated element of the tumour is usually a high grade spindle cell/pleomorphic sarcoma (malignant fibrous histiocytoma-like) and is the element that dictates prognosis. Dedifferentiation can occur in either primary untreated cases or recurrent chordomas (Meis et al. 1987). It is more often seen in sacrococcygeal tumours with an average time delay of 5 years from initial chordoma diagnosis. It is postulated that radiation therapy increases the risk of chordoma dedifferentiation having been reported in about 65% of the published cases.

20.8 Extra-Axial Chordoma

Also known as chordoma periphericum, this very rare tumour involves the appendicular skeleton and is indistinguishable from classical chordoma. It has a similarly locally aggressive behaviour and low metastatic potential to classical chordoma, but the prognosis appears to be far better as it arises distant from vital structures, seems to present earlier and is generally amenable to complete resection (Tirabosco et al. 2008). Its occurrence far distant from notochordal tissue is currently a mystery and may prompt the search for ectopic notochordal rests and/or non-axial BNCT. So-called parachordoma (of soft tissue) is not related to true chordoma (Tirabosco et al. 2008).

20.9 Conclusion

There have been considerable advances in the understanding of these rare tumours over the last 10 years with a clearer role of MRI in the detection and management of these lesions. The emerging concept is that chordomas arise from a very small proportion of BNCT, (through an incipient chordoma phase) which in turn arise from microscopic notochordal remnants. Progression through these recognisable stages to classic chordoma is clearly an extremely rare event. Biopsy identification of chordoid tissue needs to be carefully correlated with MRI and CT appearances to decide if it represents BNCT or chordoma (Table 20.1). Currently the biological triggers of benign and malignant notochordal tumours are unclear. Future advances in molecular genetics and the roles that key molecules (e.g. brachyury) play in notochordal pathophysiology, will reduce the gaps in our knowledge and form the basis of future therapeutic advances.

Acknowledgements

Grateful thanks to Professor J. Bloem (Leiden) for images of Fig. 20.12 and to the Medical Photography Department at RJAH for their support with the illustrations.

Table 20.1. Distinguishing features of benign and malignant mortochordal tumours

	BNCT	CHORDOMA
Symptoms	Asymptomatic	Long history of pain
Presentation	Incidental MR finding	Compressive effect of tumour
Bone marrow	Tumour replacement	Tumour replacement
Zone of transition	Sharp delineation with normal marrow	Not sharply delineated with normal marrow
MRI	↓ T1, very ↑ T2	↓ T1, very ↑ T2
Gd-DTPA	No enhancement	Moderate enhancement
Trabecular bone	No osteolysis	Osteolysis
	Sclerosis – variable but common	Sclerosis – marginal, uncommon
Cortical bone	Intact	Osteolysis
Radiographs/CT	Normal/sclerosis	Osteolytic in sacrum/clivus
Scintigraphy	Normal	Variable – "cold" and "hot"
Soft tissues	Normal	Large mass invariable+ Ca++
Histology	Sheets of chordoid tissue	Sheets + cords of chordoid tissue
	No lobulation	Lobulation
	No extra cellular myxoid matrix	Abundant myxoid matrix
Immunoprofile	Positive S-100 protein, Vimentin	Positive S-100 protein, Vimentin
	Positive EMA	Positive EMA
	Positive cytokeratins (AE/1, AE/3, CK18)	Positive cytokeratins (AE/1, AE/3, CK18)
Management	Follow-up with MRI/CT	Wide surgical excision

References

Chauvel A, Taillat F, Gille O, et al. (2005) Giant vertebral notochordal rest: a new entity distinct from chordoma. Histopathology 47:643–652

Cheung EY, Ozerdemogle RA, Transfeldt EE, Thompson RC (1999) Lumbosacral chordoma: prognostic factors and treatment. Spine 24:1639–1645

Congdon CC (1952) Benign and malignant chordomas a clinico-anatomical study of twenty-two cases. Am J Surg Pathol 28:793–821

Corsi A, De Maio F, Mancini F, Ippolito E, Riminucci M, Bianco P (2008) Notochordal inclusions in the vertebral bone marrow. J Bone Miner Res 23:572–575

Crapanzano JP, Ali SZ, Ginsberg MS, Zakowski MF (2001) Chordoma; cytologic study with histologic and radiologic correlation. Cancer 93:40–51

Darby AJ, Cassar-Pullicino VN, McCall IW, Jaffray DC (1999) Vertebral intra-osseous chordoma or giant notochordal rest? Skeletal Radiol 28:342–346

De Bruine FT, Kroon HM (1988) Spinal chordoma: radiological features in 14 cases. AJR Am J Roentgenol 150:861–863

Deshpande V, Nielsen GP, Rosenthal DI, Rosenberg AE (2007) Intra-osseous benign notochord cell tumors (BNCT): further evidence supporting a relationship to chordoma. Am J Surg Pathol 31:1573–1577

Di Girolamo S, Ottoviani F, Floris R, Bruno E, Napolitano B, Schillaci O (2005) Indium III Pentetreotide single photon emission computed tomography (In III pentetreotide Spect) a new technique to evaluate sematostatin receptors in chordomas. J Laryngol OTOL 119:405–408

Firooznia H, Pinto RS, Baruch HH, Zausner J (1976) Chordoma: radiographic evaluation of 20 cases. Am J Roentgenol 127:797–805

Fletcher CDM, Unni KK, Mertens F (eds) (2002) WHO classification: Pathology and genetics of tumours of soft tissue and bone. IARC Press, Lyon

Fuchs B, Dickey ID, Yaczemski MJ, Inwards CY, Sims FH (2005) Operative management of sacral chordoma. J Bone Joint Surg Am 87:2211–2216

Hanna SA, Aston WJ, Briggs TW, Cannon SR, Saifuddin A (2008) Sacral chordoma: can local recurrence after sacrectomy be predicted? Clin Orthop Relat Res 466:2217–2223

Heffelfinger MJ, Dahlin DC, MacCarty CS, Beabout JW (1973) Chordomas and cartilaginous tumours at the skull base. Cancer 32:410–420

Howitz T (1941) Chordal ectopia and its possible relation to chordoma. Arch Path 31:354–362

Hudson TM, Galceran M (1983) Radiology of sacrococcygeal chordoma. Difficulties in detecting soft tissue extension. Clin Orthop Relat Res 175:237–242

Kyriakos M, Totty WG, Lenke LG (2003) Giant vertebral notochordal rest: a lesion distinct from chordoma: discussion of an evolving concept. Am J Surg Pathol 27:396–406

Luschka H (1856) Die Altersveränderungen der Zwischenwirbelknorpel. Virchows Arch Path Anat 9:311–327

Mehnert F, Beschorner R, Kuker W, Hahn U, Nagele T (2004) Retroclival ecchordosis physalphora: MR imaging and review of the literature. AJNR 25:1851–1855

Meis JM, Raymond AK, Evans HL, Charles RE, Giraldo AA (1987) "Dedifferentiated" chordoma. A clinico-pathologic and immunohistochemical study of three cases. Am J Surg Path 11:516–525

Meyer JE, Lepke RA, Undfors KK, Pagani JJ, Hirschy JC, Hayman LA, Momose KG, McGinnis B (1984) Chordomas: their CT appearances in the cervical thoracic and lumbar spine. Radiology 153:693–696

Mirra JM, Brien EW (2001) Giant notochordal hamartoma of intra-osseous origin: a newly reported benign entity to be distinguished from chordoma. Report of two cases. Skeletal Radiol 30:698–709

Müller H (1858) Über das Vorkommen von Resten der chorda dorsalis bei Menschen nach der Geburt und über ihr Verhältniss zu den Gallertgeschwulsten am Clivus Ztschr f. rat Med 2:202–229

Murakami H, Kawahara N, Gabata T, Nambu K, Tomita K (2003) Vertebral body osteonecrosis without vertebral collapse. Spine 28:E323–E328

Murakami H, Kawahara N, Tomita K, Yamaguchi T Re, Murakami H, Kawahara N, Gabata T et al. (2005) Vertebral body osteonecrosis without vertebral collapse (letter to the editor). Spine 30:593–594

Murphey MD, Andrews CL, Flemming DJ et al. (1996) Primary tumors of the spine: radiologic-pathologic correlation. Radiographics 16:1131–1158

Ng SH, Ko SK, Wan YL, Tang LM, Ho YS (1988) Cervical ecchordosis physaliphora: CT and MR features. BJR 171:329–331

Oner AY, Akpek S, Tali T, Ucar M (2009) Giant vertebral notochordal rest: magnetic resonance and diffusion weighted imaging. Korean J Radiol 10:303–306

Pazzaglia UE, Salisbury JR, Byers PD (1989) Development and involution of the notochord in the human spine. JRSM 82:413–415

Radl R, Leithner A, Kastner N, Bodo K, Nader A, Windhager R (2005) Disappearance of a cervical spine chordoma after non-operative treatment. A case report. J Bone Joint Surg Am 87:1822–1827

Ribbert H (1894) Ueber die Ecchondrosis physalifora spenooccipitalis. Zentralbl. F. allg. Path u path. Anat 5:457–461

Rosenberg AE, Brown GA, Bhan AK, Lee JM (1994) Chondroid chordoma – a variant of chordoma. A morphologic and immunohisto chemical study. Am J Clin Pathol 101:36–41

Rosenthal DI, Scott JA, Mankin HJ, Wismer GL, Brady TJ (1985) Sacrococcygeal chordoma: magnetic resonance imaging and computed tomography. AJR Am J Roentgenol 145:143–147

Rossleigh MA, Smith J, Yeh SD (1986) Scintigraphic features of primary sacral tumours. J Nuc Med 27:627–630

Salisbury JR (1993) The pathology of the human notochord. J Pathol 171:253–255

Salisbury JR, Deverell MH, Cookson MJ, Whimster WF (1993) Three-dimensional reconstruction of human embryonic notochords: clue to the pathogenesis of chordoma. J Pathology 171:59–62

Sciubba D, Chi J, Rhines L, Gokasian Z (2008) Chordoma of the spinal column. Neurosurg Clin North Am 19:5–15

Smolders D, Wang X, Drevelengas A, Vanhoenacker F, De Schepper AM (2003) Value of MRI in the diagnosis of non-clival, non-sacral chordoma. Skeletal Radiol 32:343–350

Steenberghs J, Kiekens C, Menten J, Monstrey J (2002) Intradural chordoma without bone involvement case report and review of the literature. J Neurosurg 97:94–97

Stewart MJ, Burrow J le F (1923) Ecchordosis physaliphora spheno-occipitalis. J Neurol Psychopath 4:218–220

Sung MS, Lee GK, Kang HS, Kwon ST, Park JG, Suh JS, Cho GH, Lee SM, Chung MH, Resnick D (2005) Sacrococcygeal chordoma: MR imaging in 30 patients. Skeletal Radiol 34:87–94

Tirabosco R, Mangham DC, Rosenberg AE, Vujovic S, Bousdras K, Pizzolitto S, De Maglio G, den Bakker MA, Di Francesco L, Kalil RK, Athanasou NA, O'Donnell P, McCarthy EF, Flanagan AM (2008) Brachyury expression in extra-axial skeletal and soft tissue chordomas: a marker that distinguishes chordoma from mixed tumor/myoepithelioma/parachordoma in soft tissue. Am J Surg Pathol 32(4):572–580

Ulich TR, Mirra JN (1982) Echordosis physaliphora vertebralis. Clin Orthop 163:282–289

Virchow R (1847) Untersuchungen über die Entwicklung des Schädelgrundes im gesunden und krankhaften Zustande und über den Einfluss derselben auf Schädelform, Gesichtsbildung und Gehirnbau. G Reimer, Berlin, p 47

Vujovic S, Henderson S, Presneau N, Odell E, Jacques TS, Tirabosco R, Boshoff C, Flanagan AM (2006) Brachyury, a crucial regulator of notochordal development, is a novel biomarker for chordomas. J Pathol 209(2):157–165

Wang AM, Joachim CL, Shillito J Jr, Morris JH, Zanani AA, Rumbaugh CL (1984) Cervical chordoma presenting with intervertebral foramen enlargement mimicking neurofibroma findings. J Comput Assist Tomogr 8:529–532

Wippold FJ, Koeller KK, Smirniotpoulos JG (1999) Clinical and imaging features of cervical chordoma. AJR AM J Roentgenol 172:1423–1426

Yamaguchi T, Yamato M, Saotome K (2002) First histologically confirmed case of a classic chordoma arising in a precursor benign botochodral lesion; differential diagnosis of benign and malignant notochordal lesions. Skeletal Radiol 31:413–418

Yagamuchi T, Suzuki S, Ishiiwa H, Shimizu K, Ueda Y (2004a) Benign notochordal cell tumors: a comparative histological study of benign notochordal cell tumors, classic chordomas and notochordal vestiges of fetal intervertebral disks. Am J Surg Pathol 28:756–761

Yamaguchi T, Suzuki S, Ishiiwa H, Ueda Y (2004b) Intraosseous benign notochordal cell tumors: overlooked precursors of classic chordomas? Histopathology 44:597–602

Yagamuchi T, Wannabe-Ishiiwa H, Suzuki S, Igarashi Y, Ueda Y (2005) Incipient chordoma: a report of two cases of early-stage chordoma. Mod Pathol 18:1005–1010

Yamaguchi T, Iwata J, Sugihara S, McCarthy EF Jr, Karita M, Murakami H, Kawahara N, Tsuchiya H, Tomita K (2008) Distinguishing benign notochordal cell tumours from vertebral chordoma. Skeletal Radiol 37:291–300

York JE, Kaczaraj A, Abi-Said D, Fuller GN, Skibber JM, Janjan NA, Gokaslan ZL (1999) Sacral chordoma: 40-year experience at a major cancer center. Neurosurgery 44:74–79

Zhang H, Yoshikawa K, Tamura K, Sagou K, Tian M, Suhara T, Kandatsu S, Suzuki K, Tanada S, Tsujii H (2004) Carbon 11-methionine emission tomography imaging of chordoma. Skeletal Radiol 33(9):524–530

Smooth Muscle Tumors

21

Claus Simpfendorfer and Murali Sundaram

CONTENTS

KEY POINTS

- Primary bone leiomyosarcoma is an exceedingly rare spindle cell tumor with smooth muscle differentiation.
- In all cases of leiomyosarcoma involving bone, metastatic disease must be excluded before being designated a primary bone leiomyosarcoma.
- Radiographs of primary bone leiomyosarcoma depict osteolytic lesions with aggressive features and ill-defined tumor margins.
- T2-weighted SE images of the tumor demonstrate areas of iso- and hypointensity relative to fat which may help distinguish primary bone leiomyosarcoma from other primary bone tumors.
- Primary bone leiomyoma and benign metastatic leiomyoma involving bone are exceptionally rare.

21.1 Introduction

Smooth muscle tumors of the bone include primary bone leiomyosarcoma and its benign counterpart, the leiomyoma of bone. They are defined as spindle cell tumors of bone with smooth muscle differentiation. Both neoplasms are exceedingly rare.

21.2 Primary Bone Leiomyosarcoma

Leiomyosarcomas are malignant smooth muscle cell tumors that usually involve the uterus, accounting for

C. Simpfendorfer, MD
Cleveland Clinic, Diagnostic Radiology/A21, 9500 Euclid Avenue, Cleveland, OH 44195, USA

M. Sundaram, MD, FRCR
Section of Musculoskeletal Radiology, Imaging Institute, Professor of Radiology, Cleveland Clinic Lerner School of Medicine of Case Western Reserve University, Cleveland Clinic, Diagnostic Radiology/A21, 9500 Euclid Avenue, Cleveland, OH 44195, USA

2% of uterine malignancies, or the gastrointestinal tract, where they constitute 1% of malignant neoplasms (Rubin and Farber 1994). Primary leiomyosarcoma of the bone is a rare spindle cell tumor with smooth muscle cell differentiation, introduced as such by the 1993 Histologic Tumor Classification of the World Health Organization (WHO) (Schajowicz 1993). Since its recognition as a distinct entity by Evans and Sanerkin in 1965 (Evans and Sanerkin 1965), there have been approximately 120 reported cases of primary extragnathic bone leiomyosarcoma in the English literature. The exclusion of a soft tissue tumor extending into adjacent bone and the absence of distant leiomyosarcoma are prerequisites for establishing the diagnosis of primary bone leiomyosarcoma. Therefore, most series exclude facial and skull bone leiomyosarcoma with extensive soft tissue involvement, as it is often difficult to determine which tissue the tumor was derived from. The cell of origin of osseous leiomyosarcoma is yet to be determined. It is thought to be either the smooth muscle cells of blood vessels or the mesenchymal myofibroblasts in bone (Antonescu et al. 1997).

21.2.1 Epidemiology

Leiomyosarcoma can affect all age groups, though it is mainly observed in the fourth through the seventh decade and rarely occurs under the age of 20 years (Berlin et al. 1987; Antonescu et al. 1997; Lopez-Barea et al. 1999; Sundaram et al. 1999). Earlier studies suggested a predilection for the later decades of life, but more recent series describe fairly equal representation among all ages, excluding the first two decades. Conflicting reports exist regarding gender predilection. Most studies suggest equal gender distribution, though some have found a 2:1 male predilection (Berlin et al. 1987; Antonescu et al. 1997; Sundaram et al. 1999). The discrepancies are mainly due to the small number of cases in series. The incidence of leiomyosarcoma is difficult to assess, though a Swedish study conducted in the late 1980s suggested an average annual incidence of 0.7 cases or 0.09 cases per million per year based on the review of the National Cancer Registry over a 15-year period (Berlin et al. 1987).

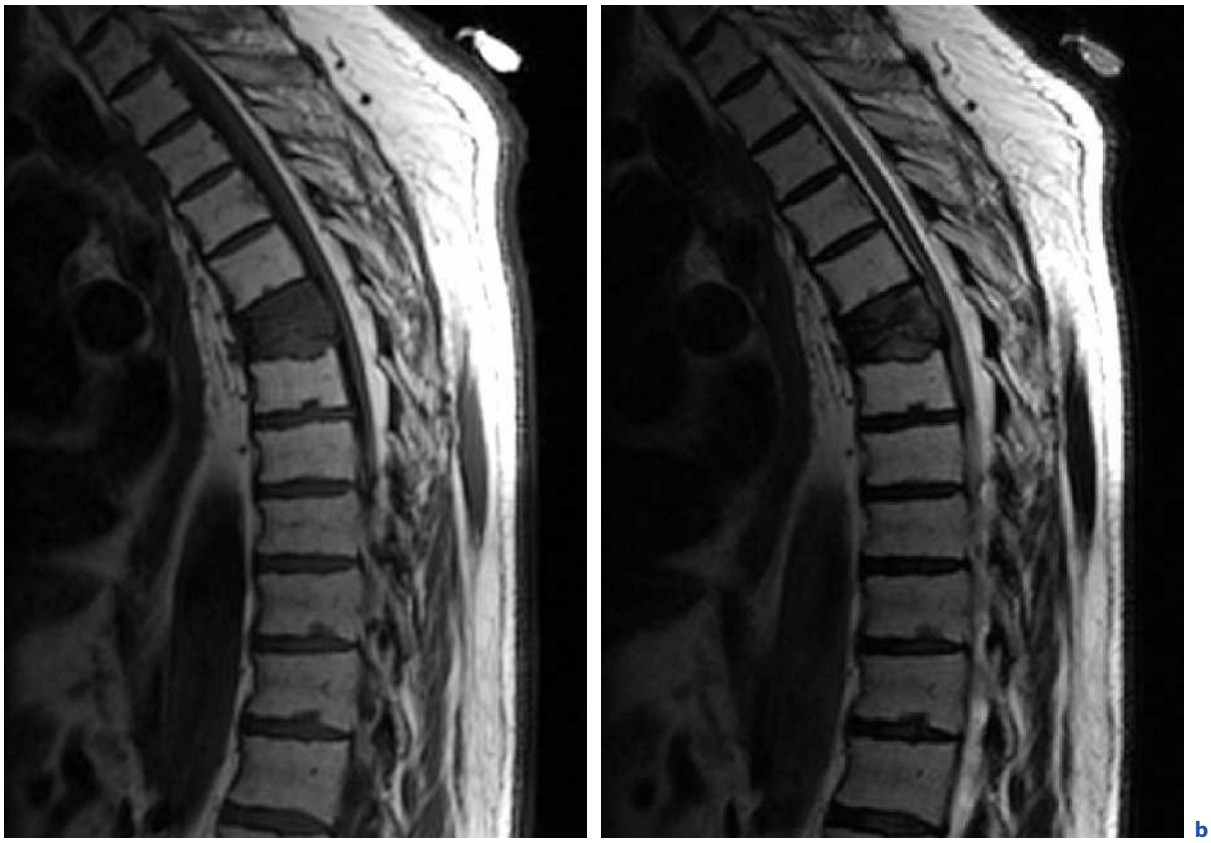

Fig. 21.1a,b. Primary bone leiomyosarcoma of the T6 vertebral body in a patient with previous lung cancer and radiation therapy. **a** The lesion is isointense to muscle on the sagittal T1-weighted SE (TR 637/TE 13). **b** On T2-weighted SE (TR 1710/TE 103) the lesion demonstrates areas of iso- and hypointensity relative to normal fat

21.2.2 Etiology

Little is known about the etiology of leiomyosarcoma. The mechanism of carcinogenesis, as is the case with the majority of common malignancies, remains obscure. The development of leiomyosarcoma has been related to radiation exposure, presence of a metal foreign body, a second primary malignancy, and Paget's disease (Antonescu et al. 1997; Jeanrot et al. 2000; Caron et al. 2004). Postirradiation sarcomas are a well-known long-term complication of cancer therapy (Wiklund et al. 1991). The majority of postirradiation sarcomas are osteosarcomas, fibrosarcomas, and malignant fibrous histiocytomas (MFH), however cases of primary bone leiomyosarcoma arising in a previous radiation field have been reported (Arlen et al. 1971; Antonescu et al. 1997; Aoki et al. 1998) (Fig. 21.1). Implant-associated sarcomas are a well-recognized but rare phenomenon pertaining to malignancies that arise in the vicinity of an orthopedic implant after a latency period of 2 years (McDonald et al. 2002). Cases of implant-associated primary bone leiomyosarcoma have been reported (Caron et al. 2004; Bouaziz et al. 2005). In patients with the hereditary form of bilateral retinoblastoma (RB), primary bone leiomyosarcoma can rarely arise as a second primary malignancy even in sites distant from the orbital radiation field (Guse and Weis 1994). The development of the second primary neoplasm in RB patients is believed to be related to abnormalities of the tumor suppressor genes, p53 and RB1. Neoplastic transformation is a known complication of Paget's disease (Rubin and Farber 1994). The majority of sarcomas arising in pagetoid bone are osteosarcomas and fibrosarcomas, though primary bone leiomyosarcoma has also been described (Young and Freemont 1991; Antonescu et al. 1997).

21.2.3 Clinical Presentation

The main presenting symptom of primary bone leiomyosarcoma is pain. In the case of extremity involvement the pain is usually localized to the anatomic site of the tumor, whereas pelvic bone leiomyosarcoma tends to present with vague lower back or groin pain. Swelling, limited range of motion, and a palpable mass are also associated with primary bone leiomyosarcoma. The mean interval from symptom onset to diagnosis varies from weeks to years.

21.2.4 Location

The vast majority of primary bone leiomyosarcomas affect long tubular bones, most commonly in the lower extremity around the knee joint. Apart from the distal femur and proximal tibia, primary bone leiomyosarcomas are found in facial bones, humerus, axial skeleton, and less frequently the fibula and phalanges.

21.2.5 Imaging Findings

Radiographs of primary bone leiomyosarcomas depict purely osteolytic lesions with aggressive features and ill-defined tumor margins (Fig. 21.2). Endosteal scalloping, permeation, cortical breaching, and lack of sclerosis are frequent findings. Periosteal new bone formation can occur in the form of cortical thickening, a single lamellar layer, or a Codman triangle. Pathologic fractures through the osteolytic lesion can be present in long bones. The lesions arise from the medullary cavity and are located predominantly in the metaphysis with epiphyseal or diaphyseal extension. Rarely primary bone leiomyosarcomas can be found subperiosteally, at the bone surface (Narvaez et al. 2005). A remarkable feature of primary bone leiomyosarcomas in tubular bones is their extraordinary length with a reported average of 11 cm (Sundaram et al. 1999). The marked vertical spread relative to the mediolateral expansion of the tumor in long bones distinguishes it in part from the typical metastatic lesion, but is reminiscent of lymphomatous bone lesions. Soft tissue extension can occur in long bone lesions but is distinctly more prominent in pelvic primary leiomyosarcoma where the bone is usually located in the center of large soft tissue extensions (Sundaram et al. 1999). Radiographs underestimate the size of the bone lesion and the extent of soft tissue expansion of the tumor. CT scan is helpful in determining the type and degree of bone destruction and is superior to radiographs in delineating the area of soft tissue involvement. Primary bone leiomyosarcoma contains hypervascular areas that enhance on contrast-enhanced CT (Goto et al. 2002). MR imaging is the modality of choice for evaluating primary bone leiomyosarcoma as it clearly demonstrates the lesion–tissue interface and tumor extension relative to adjacent structures. On T1-weighted images, the tumor appears isointense or hypointense compared to muscle. In contrast to most osteolytic lesions, T2-weighted SE images of the tumor demonstrate marked heterogeneity with areas of iso- and hypointensity relative to fat, a signal

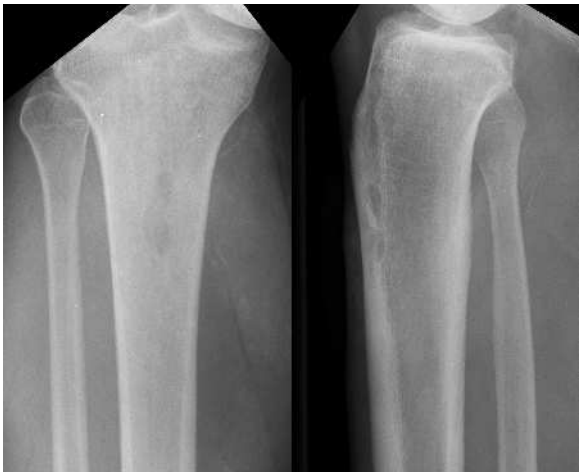

Fig. 21.2. AP and lateral radiographs demonstrate a nonspecific lytic lesion of the proximal tibia with nonsclerotic margins which turned out to be a primary bone leiomyosarcoma. The most common locations of primary bone leiomyosarcoma are the distal femur and proximal tibia

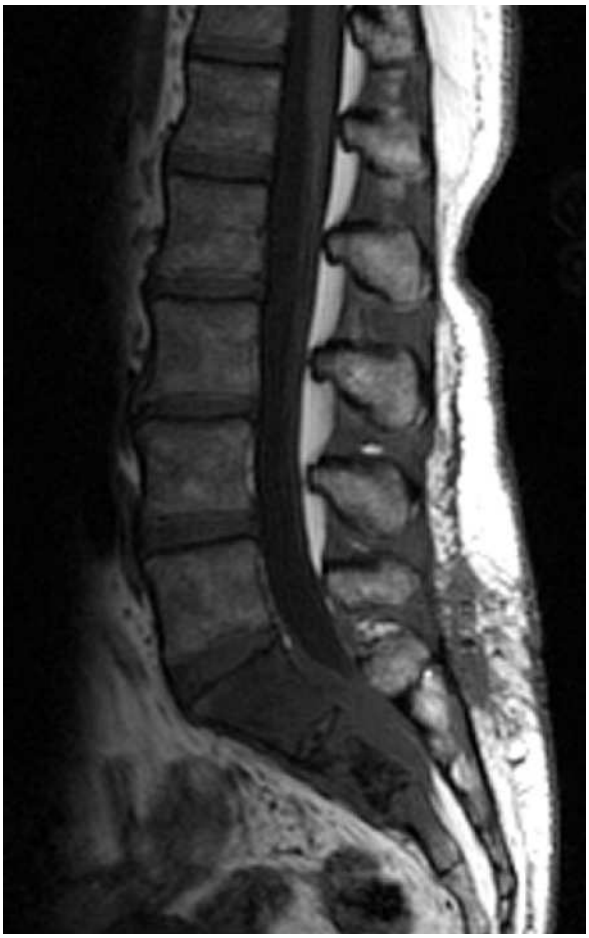

a

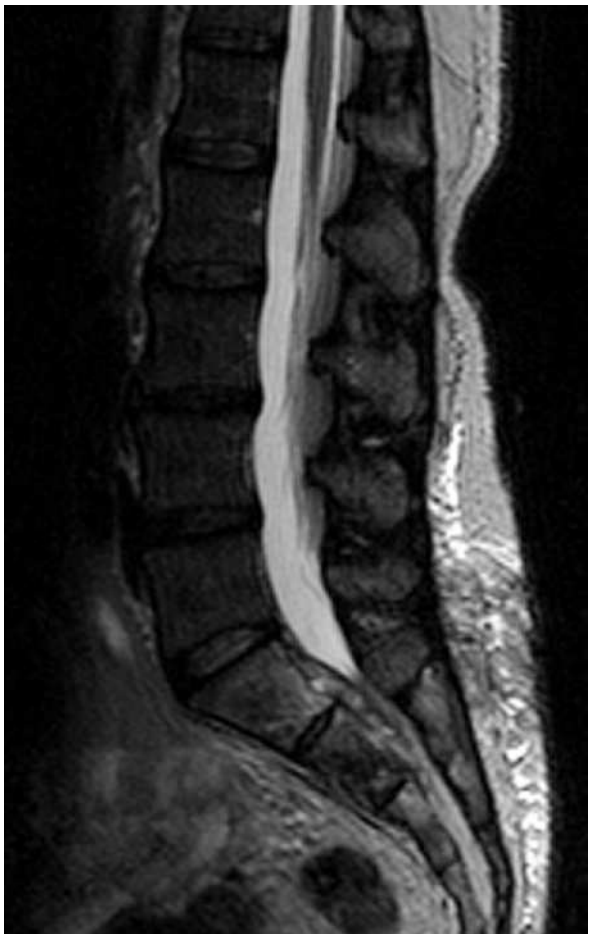

b

Fig. 21.3a,b. Primary bone leiomyosarcoma involving the S1, S2, and S3 segments. **a** The lesion is predominantly isointense to muscle on T1-weighted SE (TR 500/TE 12). **b** On the T2-weighted fast SE (TR 5080/TE 127) with fat saturation, the lesion demonstrates areas of iso- and hypointensity relative to fat

pattern that has been described in primary bone lymphomas (Sundaram et al. 1999) (Fig. 21.3). It is hypothesized that the muscle component of the tumor is responsible for the low signal intensity areas, since fibrosis and hypocellularity, thought to account for low signal intensity in lymphomas, are not characteristic of primary bone leiomyosarcoma (Shen et al. 2001). On T2-weighted SE with fat saturation the tumor is hyperintense, however this may not be a reflection of the histologic composition or cellularity but secondary to the suppressed signal of the surrounding normal tissue. Following intravenous gadolinium-chelate injection, primary bone leiomyosarcoma enhances as expected due to its vascular component (Slavikova-Boucher et al. 2001). As increased uptake on bone scintigraphy is typical for primary bone leiomyosarcoma, this modality can be helpful in tumor staging and metastatic work-up. Overall, primary bone leiomyosarcoma has no unique radiographic appearance and can mimic other primary and secondary malignant tumors.

21.2.6 Histopathology

Histologically, primary bone leiomyosarcoma is a spindle cell sarcoma similar to soft tissue leiomyosarcoma. Under light microscopy, the tumor is composed of interweaving cell bundles and fascicles intersecting at wide angles. The tumor cells are fusiform with elongated, blunt-ended cigar-shaped nuclei and prominent eosinophilic cytoplasm (Fig. 21.4). The stroma is composed of collagen with variable degrees of hyalinization and rare areas of necrosis. In contrast to soft tissue leiomyosarcoma, osteoclast-like giant cells are frequently interspersed in the neoplastic stroma (Dorfman and Czerniak 1998). The histologic grading of primary bone leiomyosarcoma is based on mitotic activity and presence of atypia. Immunohistochemistry is essential in diagnosing a primary bone leiomyosarcoma. The tumor cells always stain positive for smooth muscle actin (α-SMA) and frequently for common muscle actin (HHF-35), which is a less sensitive marker. Among the intermediary filaments, vimentin is present uniformly while desmin is positive in only 50% of cases (Antonescu et al. 1997). In equivocal cases, electron microscopy is mandatory in the diagnosis of primary bone leiomyosarcoma. Ultrastructural findings of actin myofilaments 6–80 nm thick with dense bodies, arranged in bundles parallel to the long axis of the cell, confirm the diagnosis. On electron microscopy, the cigar-shaped nuclei show multiple infoldings of the nuclear envelope and pinocytotic vesicles are abundant in the cytoplasm (Khoddami et al. 1996). The major differential diagnoses to be considered histologically include malignant fibrous histiocytoma, fibrosarcoma, and spindle cell carcinoma.

21.2.7 Therapy and Prognosis

Primary bone leiomyosarcoma is an aggressive malignancy with a median survival of 33 months and a mortality of 50% (Berlin et al. 1987; Antonescu et al. 1997). The histologic grading of the tumor is considered the best prognostic factor correlating with survival and metastatic potential. Primary bone leiomyosarcoma

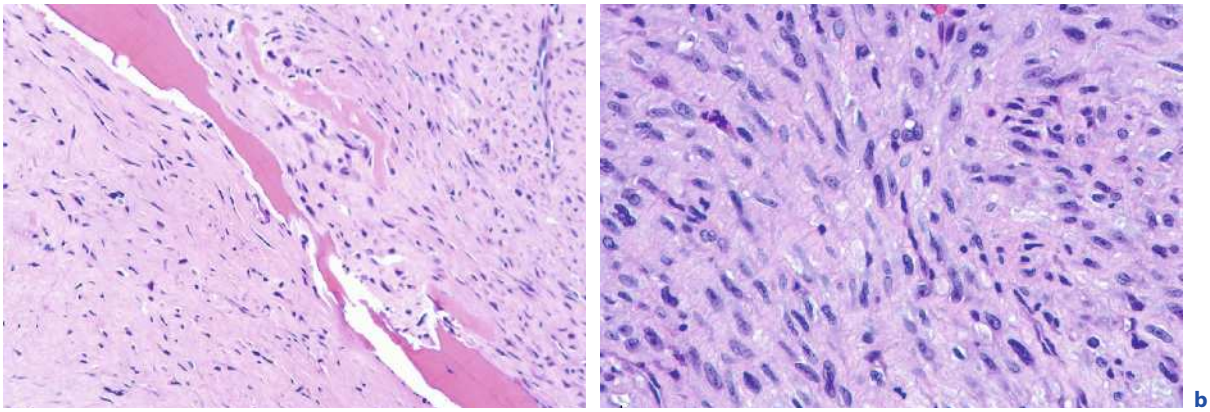

Fig. 21.4a,b. Microphotographs of T6 primary bone leiomyosarcoma in Fig. 21.1. **a** Low-power view (100×) shows a cellular spindle cell neoplasm infiltrating and engulfing spicules of lamellar/medullary bone. **b** High-power view (400×) shows fascicles of spindle-shaped cells with eosinophilic cytoplasm and elongated nuclei with tapering edges and clumpy chromatin. (Microphotographs courtesy of Brian Rubin, MD, PhD, Anatomic Pathology, Cleveland Clinic)

metastasizes to lung, lumbar spine, skin, and liver (Jeanrot et al. 2000). The treatment of choice in bone-confined cases is surgery, with extensive resection of the tumor, wide tumor-free margin, and appropriate normal tissue covering followed by reconstruction with an endoprosthesis. As surgical excision followed by limb salvage is generally not attempted in cases of metastatic bone involvement, it is essential to differentiate primary bone leiomyosarcoma from metastatic soft tissue leiomyosarcoma. Primary bone tumors tend to be larger compared to metastatic lesions, are more frequently located around the knee joint as opposed to the spine and proximal humerus, and affect men and women equally. The value of adjuvant chemotherapy is unclear, though intra-arterial preoperative chemotherapy has been used successfully for tumor debulking (Goto et al. 2002). Primary bone leiomyosarcoma is a radioresistant neoplasm. Radiation therapy is only of limited value as palliative treatment of painful metastatic bone lesions.

21.3 Bone Leiomyoma

Primary leiomyomas of bone occur even less frequently than primary bone leiomyosarcomas. Most cases occur in adults, but the age distribution ranges from infancy to the eighth decade of life. Men and women are equally affected (Balachandra et al. 2007). Primary bone leiomyoma shows a distinct predilection for facial bone involvement, with the mandible being the most common location followed by the maxilla (Huang and Antonescu 2003). The extragnathic skeleton is rarely affected, but among tubular long bones most cases are described in the tibia (Vaillo-Vinagre et al. 2000). The main presenting symptom, as in the case of primary bone leiomyosarcoma, is pain.

In women with a history of uterine leiomyomas, benign skeletal metastasis can occur. This is exceedingly rare and can occur with or without associated lung metastases (Pimentel et al. 2002). The metastatic lesions are most often found in the vertebrae, but have also been reported in the pelvis, femora, humeri, and skull base (Braun et al. 1994; Pimentel et al. 2002; Alessi et al. 2003). The pain associated with the metastatic lesions is usually related to cyclical premenstrual pain and treatment often includes hormonal therapy (Pimentel et al. 2002; Alessi et al. 2003).

On radiographs bone leiomyoma presents as a well-circumscribed osteolytic lesion. A sclerotic rim is frequently present and bone invasion is extremely rare. Unlike primary bone leiomyosarcomas, leiomyomas can appear multilocular on radiographs. Histologic findings of bone leiomyoma are identical to leiomyoma in soft tissue, with interlacing bundles of uniform spindle cells. Cellular atypia and mitotic figures are absent. The cells stain positive for α-SMA and desmin. If vascular structures are intermingled with the spindle cells, the tumor is histologically classified as angiomyolipoma (Vaillo-Vinagre et al. 2000). Surgical resection of leiomyoma of bone is curative.

References

Alessi G, Lemmerling M, et al. (2003) Benign metastasizing leiomyoma to skull base and spine: a report of two cases. Clin Neurol Neurosurg 105:170–174

Antonescu CR, Erlandson RA, et al. (1997) Primary leiomyosarcoma of bone: a clinicopathologic, immunohistochemical, and ultrastructural study of 33 patients and a literature review. Am J Surg Pathol 21:1281–1294

Aoki T, Ozeki Y, et al. (1998) Development of primary leiomyosarcoma of the sternum postirradiation: report of a case. Surg Today 28:1326–1328

Arlen M, Higinbotham NL, et al. (1971) Radiation-induced sarcoma of bone. Cancer 28:1087–1099

Balachandra B, Lee MW, et al. (2007) Leiomyoma of iliac bone. Can J Surg 50:E33–E34

Berlin O, Angervall L, et al. (1987) Primary leiomyosarcoma of bone. A clinical, radiographic, pathologic-anatomic, and prognostic study of 16 cases. Skeletal Radiol 16:364–376

Bouaziz MC, Chaabane S, et al. (2005) Primary leiomyosarcoma of bone: report of 4 cases. J Comput Assist Tomogr 29:254–259

Braun W, Kotter A, et al. (1994) Intraosseous leiomyoma of the neck of the femur. A case report. Int Orthop 18:47–49

Caron JJ, Pambuccian SE, et al. (2004) Leiomyosarcoma of the distal femur after anterior cruciate ligament reconstruction. Clin Orthop Relat Res 419:214–217

Dorfman H, Czerniak B (1998) Bone tumors, 1st edn. Mosby, St Louis

Evans DM, Sanerkin NG (1965) Primary leiomyosarcoma of bone. J Pathol Bacteriol 90:348–350

Goto T, Ishida T, et al. (2002) Primary leiomyosarcoma of the femur. J Orthop Sci 7:267–273

Guse TR, Weis LD (1994) Leiomyosarcoma of the femur in a patient with a history of retinoblastoma. A case report. J Bone Joint Surg Am 76:904–906

Huang HY, Antonescu CR (2003) Sinonasal smooth muscle cell tumors: a clinicopathologic and immunohistochemical analysis of 12 cases with emphasis on the low-grade end of the spectrum. Arch Pathol Lab Med 127:297–304

Jeanrot C, Ouaknine M, et al. (2000) Primary leiomyosarcoma of bone. Report of 5 anatomo-clinical cases and review of the literature. Rev Chir Orthop Reparatrice Appar Mot 86:63–73

Khoddami M, Bedard YC, et al. (1996) Primary leiomyosarcoma of bone: report of seven cases and review of the literature. Arch Pathol Lab Med 120:671–675

Lopez-Barea F, Rodriguez-Peralto JL, et al. (1999) Primary epithelioid leiomyosarcoma of bone. Case report and literature review. Virchows Arch 434:367–371

McDonald DJ, Enneking WF, et al. (2002) Metal-associated angiosarcoma of bone: report of two cases and review of the literature. Clin Orthop Relat Res 396:206–214

Narvaez JA, De Lama E, et al. (2005) Subperiosteal leiomyosarcoma of the tibia. Skeletal Radiol 34:42–46

Pimentel JR, de Almeida AL, et al. (2002) Metastatic skeletal leiomyomatosis (leiomyomatosis ossea). Skeletal Radiol 31:30–34

Rubin E, Farber J (1994) Pathology. Lippincott, Philadelphia

Schajowicz F (1993) World Health Organization International Histologic Classification of Tumors. Springer, Berlin

Shen SH, Steinbach LS, et al. (2001) Primary leiomyosarcoma of bone. Skeletal Radiol 30:600–603

Slavikova-Boucher L, Le Hir P, et al. (2001) MRI appearance of a primary leiomyosarcoma of bone with epiphyseal involvement. J Radiol 82:927–929

Sundaram M, Akduman I, et al. (1999) Primary leiomyosarcoma of bone. AJR Am J Roentgenol 172:771–776

Vaillo-Vinagre A, Ballestin-Carcavilla C, et al. (2000) Primary angioleiomyoma of the iliac bone: clinical pathological study of one case with flow cytometric DNA content and S-phase fraction analysis. Skeletal Radiol 29:181–185

Wiklund TA, Blomqvist CP, et al. (1991) Postirradiation sarcoma. Analysis of a nationwide cancer registry material. Cancer 68:524–531

Young MP, Freemont AJ (1991) Primary leiomyosarcoma of bone. Histopathology 19:257–262

Lipogenic Tumours of Bone

22

Robert S. D. Campbell

CONTENTS

R. S. D. Campbell, FRCR
Department of Radiology, Royal Liverpool University Hospital, Prescot Street, Liverpool L7 8XP, UK

KEY POINTS

- A lucent lesion with central calcification in the anterior os calcis is considered pathognomonic of an intraosseous lipoma.
- Confirmation of fat composition of a bone lesion by MR imaging or CT is usually sufficient to confirm the diagnosis of a lipogenic tumour of bone without the need to biopsy.
- Although other lesions may contain fat, they are nearly always benign lesions.
- Sinister features which merit biopsy include the presence of cortical destruction and an associated soft tissue mass.

22.1 Introduction

Lipogenic tumours are often considered to be the rarest of primary bone tumours, particularly the intraosseous liposarcoma (or osteoliposarcoma). Benign lipogenic tumours may be either intramedullary or parosteal in location. The intramedullary lipomas are a heterogeneous group of lesions, the most common of which is the intraosseous lipoma, although there are descriptions of lipoma variants including liposclerosing myxofibrous lesion of bone, angiolipoma, fibrolipoma and myelolipoma.

22.2 Intraosseous Lipoma

Intraosseous lipomas have been increasingly recognised with the advent of CT and MR imaging, which enable the identification of intralesional fat. Lipomas are com-

prised of mature fat cells, with variable small quantities of fibrous and vascular tissue (Barcelo et al. 1992), and are prone to varying degrees of fatty involution, with fat necrosis, cyst formation and dystrophic calcification. These features may resemble a bone infarct on histology, and careful radiological-pathological correlation is required to avoid misinterpretation. There are numerous published descriptions of intraosseous lipomas, with several large published series (Milgram 1988; Campbell et al. 2003; Radl et al. 2004).

22.2.1 Clinical Features

Intraosseous lipomas may be discovered as an incidental finding on radiographs. Occasionally there may be symptoms of pain or a palpable swelling if there is significant bony expansion. However, symptoms often resolve spontaneously or recur following surgery. This suggests that in some patients there may be an alternate unidentified cause of musculoskeletal pain. Pathological fractures and malignant transformation have been described but are rare (Milgram 1990; Campbell et al. 2003). Intraosseous lipomas are regarded by many as "leave me alone" lesions.

22.2.2 Age, Sex and Site Distribution

Age at presentation is very wide ranging from 4 to 85 years (mean 43 years), and sex distribution is roughly equal (M4:F3).

The commonest sites of involvement (derived from 206 published cases) include the os calcis (32%), femur (20%), tibia (13%), fibula (6%), upper limb (7%), skull and mandible (7%), spine and pelvis (12%) and rib (2.5%) (Campbell et al. 2003).

Lipomas are intramedullary in location with only a single reported case of an intracortical lipoma (Downey et al. 1983). Lesions of the calcaneum are always located within the critical angle of the anterior os calcis. In the long bones, lipomas are most typically located within

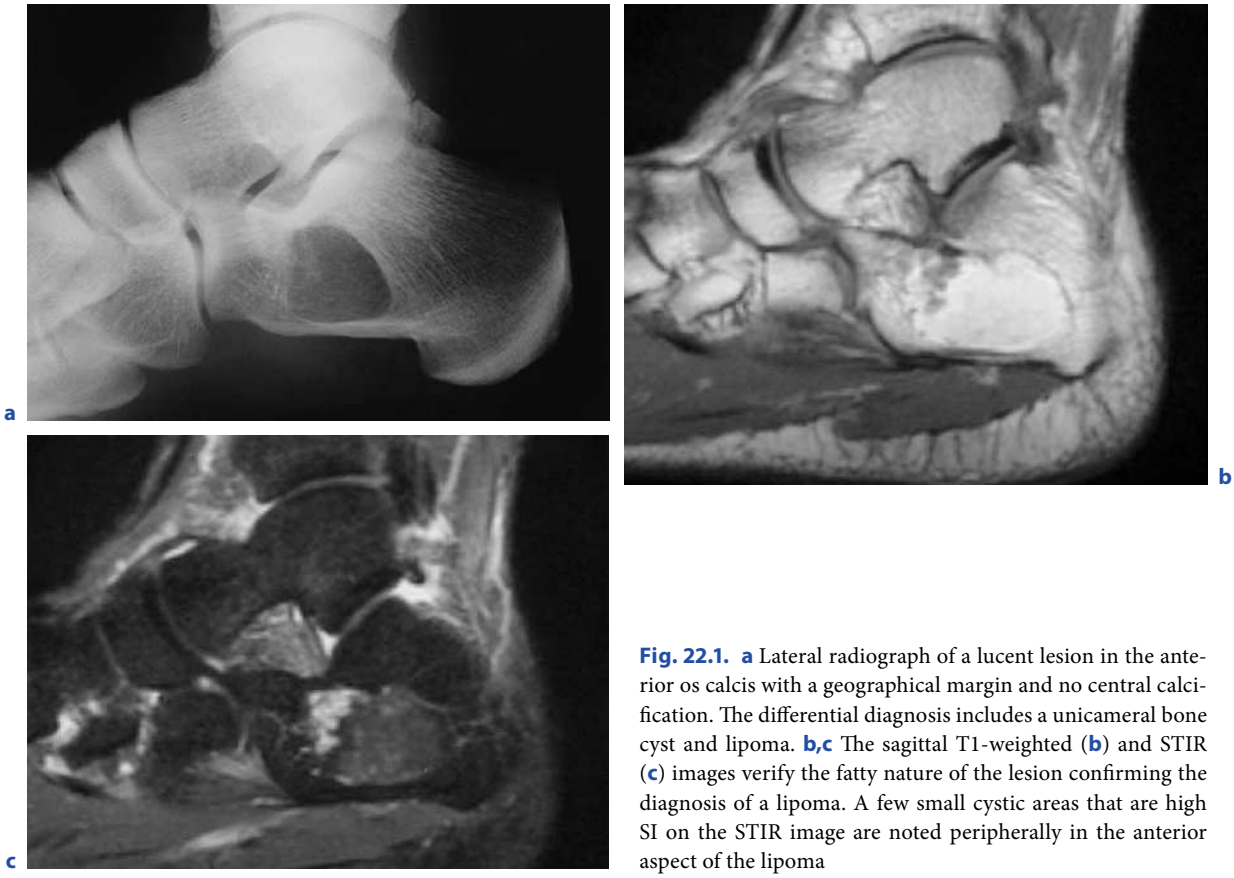

Fig. 22.1. **a** Lateral radiograph of a lucent lesion in the anterior os calcis with a geographical margin and no central calcification. The differential diagnosis includes a unicameral bone cyst and lipoma. **b,c** The sagittal T1-weighted (**b**) and STIR (**c**) images verify the fatty nature of the lesion confirming the diagnosis of a lipoma. A few small cystic areas that are high SI on the STIR image are noted peripherally in the anterior aspect of the lipoma

the metaphyseal regions. Isolated involvement of the epiphysis or diaphysis is unusual, although larger tumours may extend into the diaphysis.

22.2.3 Imaging

22.2.3.1 Radiographic Features

Lipomas are radiolucent lesions of bone, which demonstrate some variability in appearance with the exception of lesions of the os calcis, which have relatively constant features. Calcaneal lipomas vary in size from 10 to 41 mm (mean 30 mm), all occurring within the critical angle, with well-defined geographical margins (Fig. 22.1). Marginal sclerosis or a border of thickened trabecular bone is common (73%). However, it is the presence of central dystrophic calcification (73%) that is often considered pathognomonic of a lipoma (Fig. 22.2). These are usually focal aggregates of well-defined but irregular calcified masses. Bone expansion (5%) is uncommon in the os calcis.

Lipomas at other sites in the skeleton may show some areas of poorly defined margins in up to one third of cases, although some areas of marginal sclerosis are typically present (77%). Focal calcification is less frequent (31%), and may be peripheral as well as central in location (Fig. 22.3). Modelling deformity or bony expansion is more common (31%), but is usually not pronounced, although there are isolated case reports of marked bony expansion (Fig. 22.4). Internal bony trabeculation occurs in 15–18% of lipomas at all sites.

22.2.3.2 Cross-Sectional Imaging

If radiographs are non-specific, non-contrast enhanced imaging, either by CT or MR imaging is usually diagnostic for intraosseous lipomas.

Lipomas are composed entirely or partly of fatty tissue which is low attenuation (−40 to −60 HU) on

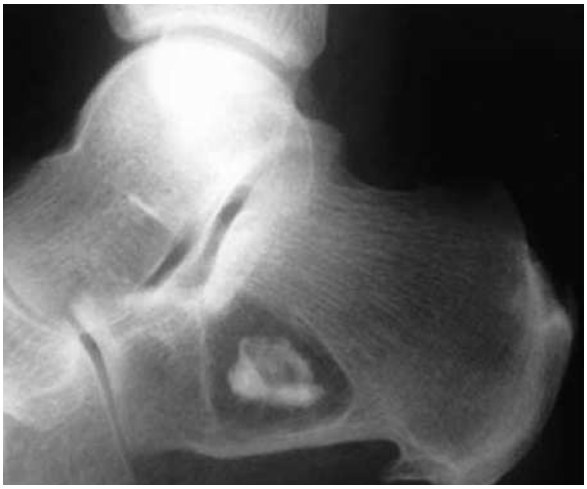

a

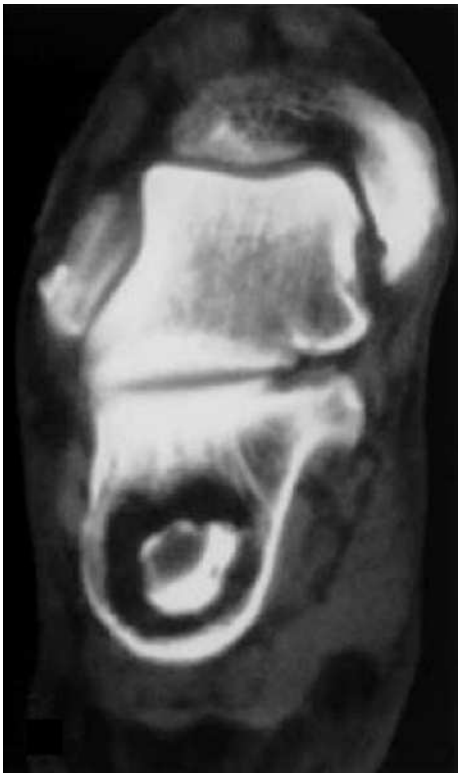

b

Fig. 22.2. **a** Lateral radiograph of a lucent lesion in the anterior os calcis with a large area of central dystrophic calcification. These features are pathognomonic of a lipoma. **b** The coronal CT image confirms the presence of low attenuation fat tissue. The dystrophic calcification is seen with a central area of fluid density. (Reproduced with permission from Campbell RS, Grainger AJ, Mangham DC, et al. (2003) Intraosseous lipoma: report of 35 new cases and a review of the literature. Skeletal Radiol 32:209–222, Fig. 5a,b)

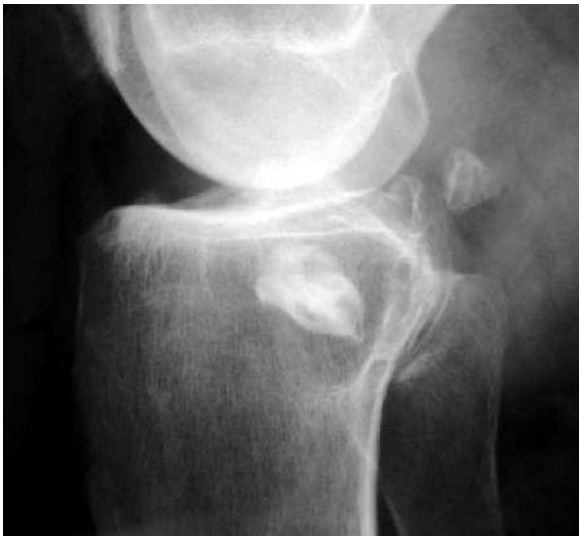

Fig. 22.3. Lateral radiograph of a typical lipoma in the proximal tibial epiphysis, with a geographical margin and central dystrophic calcification. There are areas of marginal sclerosis. (Reproduced with permission from Campbell RS, Grainger AJ, Mangham DC, et al. (2003) Intraosseous lipoma: report of 35 new cases and a review of the literature. Skeletal Radiol 32:209–222, Fig. 2a)

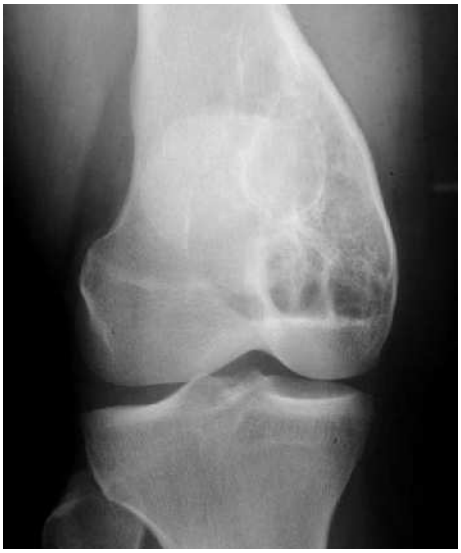

a

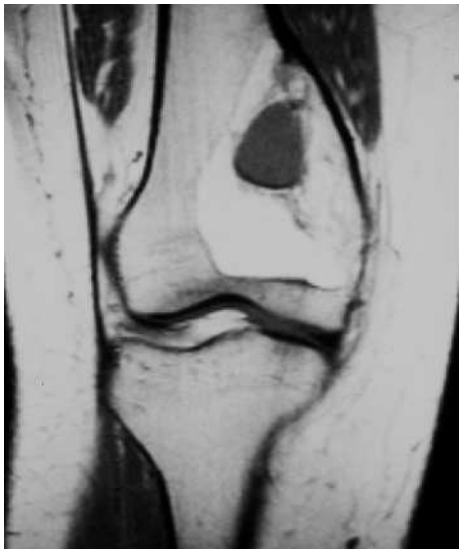

b

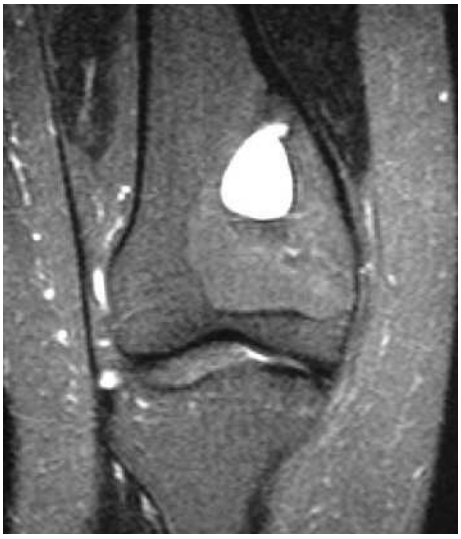

c

Fig. 22.4. **a** AP radiograph of a lipoma in the distal femoral metaphysis, which demonstrates areas of bony trabeculation and expansion. **b,c** The coronal T1-weighted (**b**) and STIR (**c**) images confirm the diagnosis of a lipoma. There is a prominent central cyst. (Reproduced with permission from Campbell RS, Grainger AJ, Mangham DC, et al. (2003) Intraosseous lipoma: report of 35 new cases and a review of the literature. Skeletal Radiol 32:209–222, Fig. 4a,c,d)

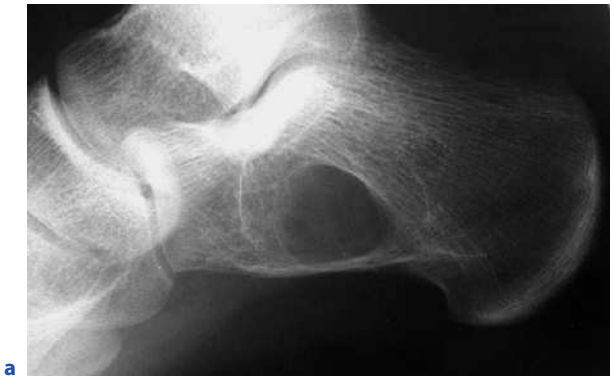

a

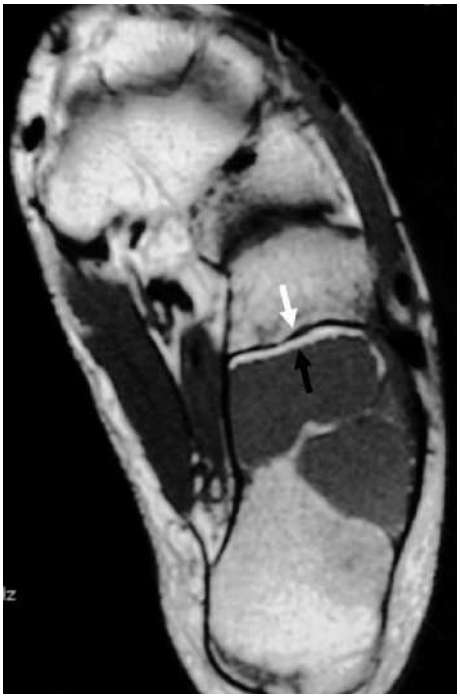

b

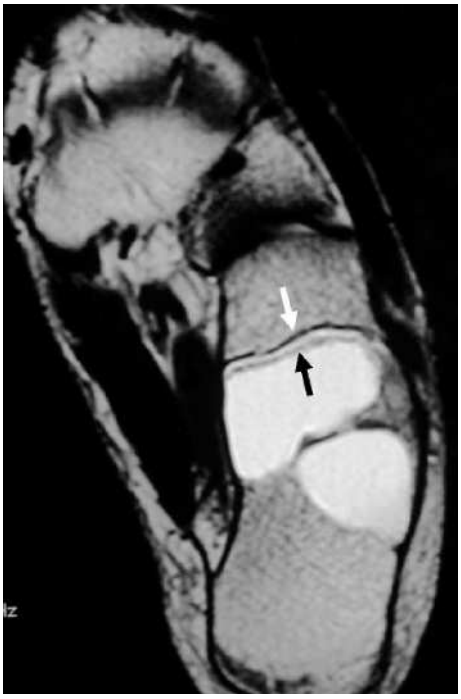

c

Fig. 22.5. **a** There is a well-defined lucent lesion in the os calcis. **b,c** The axial T1-weighted (**b**) and T2-weighted (**c**) images demonstrate a predominantly cystic lesion, with a distinct low SI sclerotic border (*white arrows*). There is also a thin layer of normal fat within the sclerotic border (*black arrows*). This could represent either a lipoma with pronounced cystic degeneration or perhaps a cyst undergoing fatty involution

CT imaging (Fig. 22.2b), and demonstrates increased SI on T1- and T2-weighted MR images, which suppresses on STIR or fat-saturated T2-weighted sequences (Figs. 22.1b,c, 22.4b,c). Intralesional cysts are common (67%), and may occur within areas of dystrophic calcification. Cysts are high SI on T2-weighted and STIR sequences, and are usually well defined. On CT images cysts are demonstrated as areas of increased attenuation within the fat tissue (0–20 HU). Occasionally more than one cystic area may be seen in a single lipoma. Areas of diffuse oedema on MR imaging are probably due to areas of early fat necrosis.

The presence of dystrophic calcification, internal trabeculation and marginal sclerosis is well demonstrated by CT (Fig. 22.2b), and identified on MR images as areas of low SI on all pulse sequences. Subtle bony expansion is more readily appreciated on cross-sectional imaging than on radiographs.

22.2.3.3 Differential Diagnosis

Lipomas in the os calcis without central calcification mimic simple unicameral bone cysts (Fig. 22.1). Elsewhere in the skeleton, the differential diagnosis may include non-ossifying fibroma, simple bone cyst, fibrous dysplasia, giant cell tumour, bone infarct and chondroid tumour.

Bone infarcts typically display peripheral calcification compared to the more common central calcification seen in lipomas. Cysts may occur in both fibrous

dysplasia and bone infarcts, and fat may also be seen within infarcts and fibrous dysplasia. Therefore careful analysis of the patterns of calcification, bony sclerosis as well as identification of fatty tissue may be required to make a specific diagnosis.

On cross-sectional imaging simple osteoporosis may be manifest as an area of predominantly fatty marrow with few internal trabeculae, which may mimic a lipoma. In a "lesion" without any discrete sclerotic or osseous margins, and which is composed wholly of fat, one should be cautious about making a diagnosis of lipoma.

22.2.4 Histology

Intraosseous lipomas are composed of mature fat cells devoid of medullary trabecular bone, and haematopoietic elements. Cellular atypia and mitoses are absent. Foci of fat necrosis associated with the presence of foamy histiocytes, cholesterol clefts, dystrophic calcification and focal reactive bone formation may be encountered. Lipomas are not typically encapsulated. Sparse areas of fibroblastic collagen formation are often present (Campbell et al. 2003).

Lipomas have been graded (stages I–III) dependent on the presence and degree of fat necrosis and infarction (Milgram 1988). These involutional changes may be due to ischaemia secondary to increased intramedullary pressure occurring with tumour growth, leading to a compromise of the blood supply at a capillary level (Chow and Lee 1992). However, the clinical utility of such a grading system remains to be proven.

Malignant transformation is rare, and may arise from areas of reactive ossification. Histological types include osteosarcoma and malignant fibrohistiocytoma.

22.2.5 Controversies

The classification of intraosseous lipomas as true benign tumours has been challenged, and the natural history of lipomas has not been well studied to date. It has been suggested that lipomas may result from areas of bone infarct, or are the end result of infection or other inflammatory lesions (Barker and Sloan 1986). There is no documented evidence of progressive growth of lipomas, despite descriptions of very expansile lesions. Some of these cases may be secondary to spontaneous involution of aneurysmal bone cysts (ABC) or other lesions (Coquerelle et al. 1995), and indeed a lesion with mixed features of lipoma and ABC has been reported (Michota et al. 1978). This process of involution leading to fatty replacement may also occur with simple bone cysts (Campbell et al. 2003; Wada and Lambert 2005) (Fig. 22.5). Finally the observation that lipomas are frequently located in areas of natural bony porosity, such as the critical angle of the os calcis, has led to the postulation that areas of bone devoid of trabeculae can become "walled off" by the laying down of trabecular bone peripherally through lines of biomechanical stress thus creating an apparent "lesion", which has limited blood supply and is prone to fat necrosis (Campbell et al. 2003).

Given the wide variety of radiological appearances and skeletal location, it is possible that multiple factors may be involved in the development of fat-containing lesions of bone. However, future cytogenetic studies may provide further insight into the nature of intraosseous lipomas. It has been shown that lipomatous tumours are characteristically associated with specific chromosomal abnormalities (Eyzaguirre et al. 2007).

22.2.6 Lipoma Variants

Benign fibro-osseous lesions of bone containing multiple histological elements including lipoma, fibroxanthoma, myxoma and myxofibroma have been termed variously as polymorphic fibro-osseous lesion of bone, polymorphic fibrocystic disease and liposclerosing myxofibrous tumour (LSMFT) (Ragsdale 1993; Kransdorf et al. 1999). LSMFTs nearly all occur in the proximal femur (85%) and the majority in the intertrochanteric region.

It is possible that all the histological changes are derived from intramedullary fat, and in this respect it has been argued that these lesions may represent involutional stages of intraosseous lipomas. However, there may also be features of fibrous dysplasia, with changes such as cyst formation, fat necrosis and reactive ossification. Fat tissue on CT and MR imaging is notably absent (Kransdorf et al. 1999), and it is now generally accepted that these lesions are in fact a variant of fibrous dysplasia, which is supported by the findings of recent genetic studies (Matsuba et al. 2003).

Other lipoma variants have been described, and include fibrolipoma, angiolipoma and myelolipoma (Newman 1957; Polte et al. 1976; Hall et al. 1986; Sundaram et al. 2007). All demonstrate fat on CT or MR imaging, and are otherwise indistinguishable from intraosseous lipomas.

22.3 Parosteal Lipoma

Parosteal lipomas are rare benign tumours composed of mature adipose tissue intimately related to the periosteum of the underlying bone. However, it may be difficult to distinguish a soft tissue lipoma that lies adjacent to bone from a lipoma that truly arises from the periosteum of bone. Recent cytogenetic studies have shown that parosteal lipomas and soft tissue lipomas may share similar genetic abnormalities including the translocation t(3;12)(q28;q14) (Bridge et al. 1995; Petit et al. 1998).

22.3.1 Clinical Features

Over 150 cases have been reported, but the overall incidence is probably less than 0.3% of all benign bone and soft tissue lipomas (Murphey 2007). There is no sex predilection, and cases are more frequent in the fifth to seventh decades. The tumours are almost invariably solitary, although a case of multiple parosteal lipomas has been reported in association with polyarthritis (Fernandez-Sueiro et al. 2006). There are no reports of malignant transformation.

The commonest sites of involvement are the in the metaphyseal and diaphyseal regions of long bones, particularly the femur, radius, humerus and tibia, although there are case reports at varying sites including the skull, mandible, ribs, sternum, scapula and pelvis.

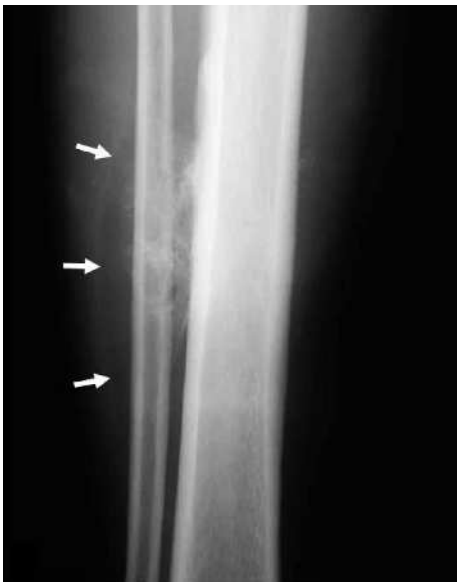

a

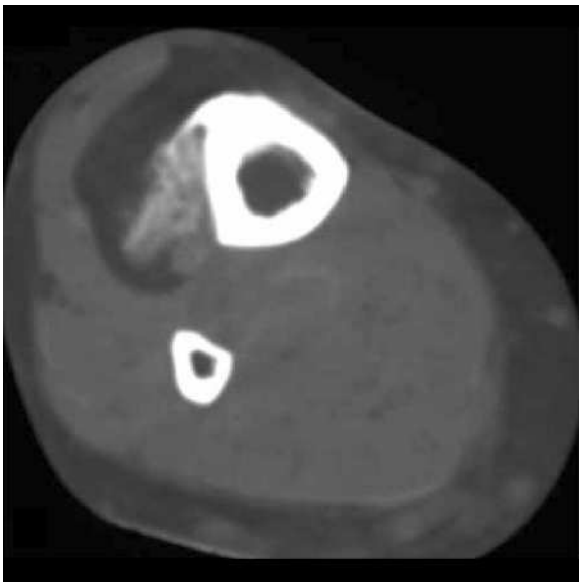

b

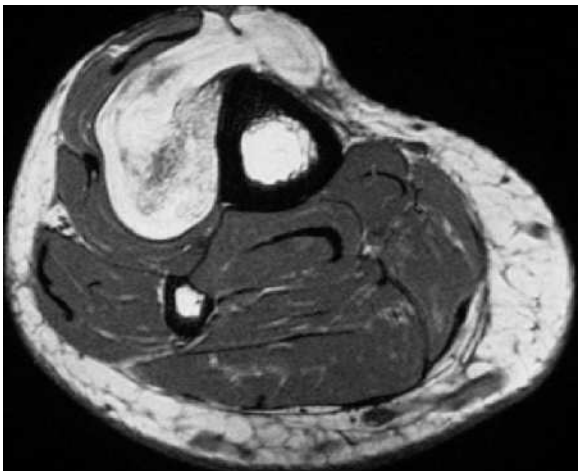

c

Fig. 22.6. a AP radiograph of the tibia with an area of periosteal bone proliferation arising from the lateral aspect of the tibia. There is an associated soft tissue mass of fat density (*white arrows*). **b,c** The axial CT (**b**) and MR (**c**) images clearly demonstrate the periosteal bone formation and the fatty component of the tumour, confirming the diagnosis of a parosteal lipoma. (**a,b** Reproduced with permission from Vanhoenacker FM, Snoeckx A, De Schepper AM, et al. (2006) Imaging of lipomatous soft tissue tumors. JBR-BTR 89:206–213, Fig. 3a,c)

Patients present with a painless, slow growing soft tissue mass which is non-tender and immobile but not fixed to the skin. Compression neuropathy (motor or sensory) is a relatively common complication reported to occur in over 50% of forearm lesions.

22.3.2 Imaging Features

Radiographs frequently demonstrate a radiolucent soft tissue mass adjacent to bone (Murphey et al. 1994), which may be lobulated or septated (Fig. 22.6). Underlying bony abnormalities, including cortical erosion or bowing (70%) and hypertrophic osseous reaction (50%), maybe present. The patterns of productive bone formation include cortical hyperostosis and periostitis which may give rise to large osseous excrescences (Figs. 22.6, 22.7). These represent the sites at which the lesion is most strongly attached to the underlying bone.

Cross-sectional imaging helps confirm the fatty nature of the tumour, if not apparent on radiographs, and is also used to document the relationship to adjacent neurovascular structures and muscle groups to aid surgical planning.

On T1-weighted images, MR imaging often demonstrates low signal intensity fibrovascular septation, which may be high signal on fat suppressed T2-weighted or STIR images. Minor enhancement of the fibrovascular septae may be seen after contrast administration. Heterogeneity within the fatty component represents other pathological tissues such as cartilage formation (Murphey et al. 1994). The osseous reaction is well demonstrated on both MR imaging and CT.

Muscle atrophy due to neural compression is best demonstrated by MR imaging, and individual nerves are best identified on axial images.

22.3.3 Differential Diagnosis

The osseous excrescence of a parosteal lipoma may be mistaken for an osteochondroma on radiographs, and there has been a single case report of a parosteal lipoma occurring in association with an osteochondroma. However, cross-sectional imaging will demonstrate a lack of cortical and medullary continuity with the lesion as well as the fatty nature of the tumour.

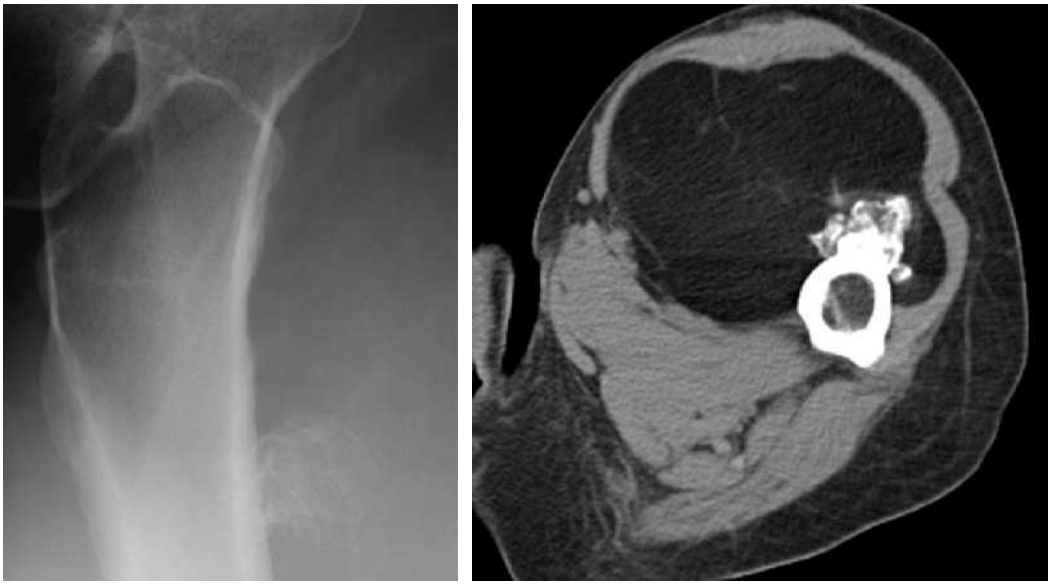

Fig. 22.7. **a** Lateral radiograph of the femur with an area of periosteal proliferation. **b** The CT confirms the diagnosis of a parosteal lipoma. There are a few areas of thin intermediate density fibrovascular septae running through the fatty component of the mass. (Images courtesy of Dr Laura Bancroft, Department of Radiology, University of Central Florida, Florida Hospital, Orlando, USA)

22.4 Intraosseous Liposarcoma

Although soft tissue liposarcomas are very common, primary intraosseous liposarcoma is an extremely rare tumour. Malignant transformation of a pre-existing fat-containing lesion of bone is far more common. In order to confirm the diagnosis of an intraosseous liposarcoma, there must be histological demonstration of liposarcoma with no other tumour elements present. Soft tissue origin and metastasis must also be excluded (Schwartz et al. 1970). Patients of all ages may be affected, and there may be a slight male predominance.

There are isolated reports of parosteal or juxtacortical liposarcoma, but again this diagnosis may be difficult to distinguish from a lesion of soft tissue origin.

22.4.1 Imaging Features

Intraosseous liposarcomas almost always arise in the long bones, and can affect the epiphysis, metaphysis or diaphysis. The femur and tibia are most commonly affected (Fig. 22.8). Radiographs demonstrate a non-specific lytic lesion of bone, which may be well defined or overtly destructive with cortical breakthrough (Figs. 22.8, 22.9). A fluid-fluid level has been described in an osteoliposarcoma, but this is a very non-specific feature and has been seen in many other bone tumours, both benign and malignant (O'Donnell and Saifuddin 2004). Areas of cortical breakthrough in an otherwise simple fatty lesion should prompt further analysis with contrast-enhanced MR imaging and consideration of biopsy of areas of concern.

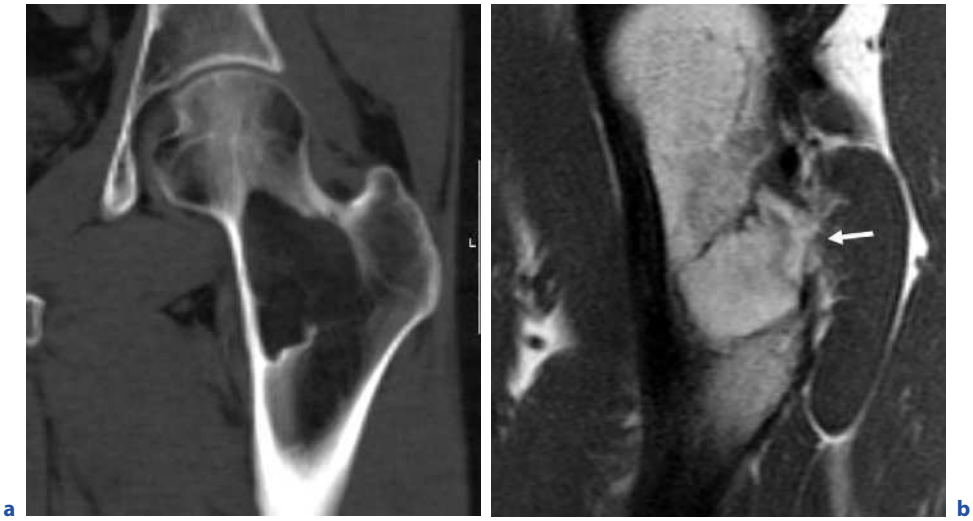

Fig. 22.8. **a** Coronal CT image demonstrates a lesion of fat density which appears typical of a benign lipoma. **b** However, the sagittal T1-weighted MR image shows an area of cortical breakthrough with fatty SI tissue extending beyond the cortical margin (*white arrow*). An osteoliposarcoma was proven on biopsy. (Images courtesy of Dr Asif Saifuddin, Department of Radiology, Royal National Orthopaedic Hospital, London, UK).

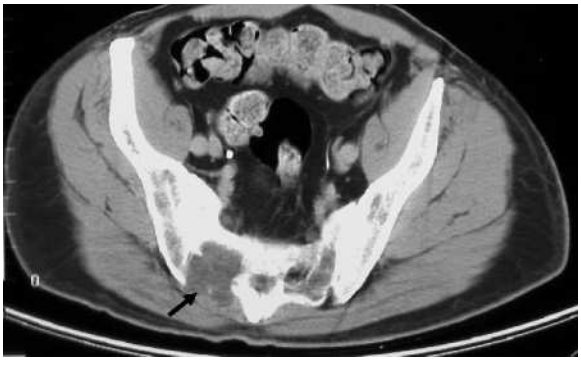

Fig. 22.9. Axial CT image of the sacrum with a focal destructive bone lesion (*black arrow*). The mass is lower density than normal soft tissue and muscle, but higher density than normal fat. Osteoliposarcoma was confirmed on histology. (Images courtesy of Dr H. Ilaslan, Department of Radiology, Cleveland Clinic Foundation, Ohio, USA)

References

Barcelo M, Pathria MN, Abdul-Karim FW (1992) Intraosseous lipoma. A clinicopathologic study of four cases. Arch Pathol Lab Med 116:947–950

Barker GR, Sloan P (1986) Intraosseous lipomas: clinical features of a mandibular case with possible aetiology. Br J Oral Maxillofac Surg 24:459–463

Bridge JA, DeBoer J, Walker CW, et al. (1995) Translocation t(3;12)(q28;q14) in parosteal lipoma. Genes Chromosomes Cancer 12:70–72

Campbell RS, Grainger AJ, Mangham DC, et al. (2003) Intraosseous lipoma: report of 35 new cases and a review of the literature. Skeletal Radiol 32:209–222

Chow LT, Lee KC (1992) Intraosseous lipoma. A clinicopathologic study of nine cases. Am J Surg Pathol 16:401–410

Coquerelle P, Cotten A, Flipo RM, et al. (1995) Intraosseous lipoma: role and limitations of modern imaging techniques. Rev Rhum Engl Ed 62:147–150

Downey EF Jr, Brower AC, Holt RB (1983) Case report 243. Cortical ossifying lipoma of femur. Skeletal Radiol 10:189–191

Eyzaguirre E, Liqiang W, Karla GM, et al. (2007) Intraosseous lipoma. A clinical, radiologic, and pathologic study of 5 cases. Ann Diagn Pathol 11:320–325

Fernandez-Sueiro JL, Pinto JA, Blanco FJ, et al. (2006) Multiple parosteal lipoma associated to polyarthritis. Joint Bone Spine 73:202–204

Hall FM, Cohen RB, Grumbach K (1986) Case report 377. Intraosseous lipoma (angiolipoma) of right third rib. Skeletal Radiol 15:401–403

Kransdorf MJ, Murphey MD, Sweet DE (1999) Liposclerosing myxofibrous tumor: a radiologic-pathologic-distinct fibro-osseous lesion of bone with a marked predilection for the intertrochanteric region of the femur. Radiology 212:693–698

Matsuba A, Ogose A, Tokunaga K, et al. (2003) Activating Gs alpha mutation at the Arg201 codon in liposclerosing myxofibrous tumor. Hum Pathol 34:1204–1209

Michota RS, Perdiue RL, McGee TP (1978) Aneurysmal bone cyst/lipoma of toe: case study and presentation. J Am Podiatry Assoc 68:725–731

Milgram JW (1988) Intraosseous lipomas. A clinicopathologic study of 66 cases. Clin Orthop Relat Res 231:277–302

Milgram JW (1990) Malignant transformation in bone lipomas. Skeletal Radiol 19:347–352

Murphey MD (2007) World Health Organization classification of bone and soft tissue tumors: modifications and implications for radiologists. Semin Musculoskelet Radiol 11:201–214

Murphey MD, Johnson DL, Bhatia PS, et al. (1994) Parosteal lipoma: MR imaging characteristics. AJR Am J Roentgenol 162:105–110

Newman CW (1957) Fibrolipoma of the mandible: report of case. J Oral Surg (Chic) 15:251–252

O'Donnell P, Saifuddin A (2004) The prevalence and diagnostic significance of fluid-fluid levels in focal lesions of bone. Skeletal Radiol 33:330–336

Petit MM, Swarts S, Bridge JA, et al. (1998) Expression of reciprocal fusion transcripts of the HMGIC and LPP genes in parosteal lipoma. Cancer Genet Cytogenet 106:18–23

Polte HW, Kolodny SC, Hooker SP (1976) Intraosseous angiolipoma of the mandible. Oral Surg Oral Med Oral Pathol 41:637–643

Radl R, Leithner A, Machacek F, et al. (2004) Intraosseous lipoma: retrospective analysis of 29 patients. Int Orthop 28:374–378

Ragsdale BD (1993) Polymorphic fibro-osseous lesions of bone: an almost site-specific diagnostic problem of the proximal femur. Hum Pathol 24:505–512

Schwartz A, Shuster M, Becker SM, et al. (1970) Liposarcoma of bone. Report of a case and review of the literature. J Bone Joint Surg Am 52:171–177

Sundaram M, Bauer T, von Hochstetter A, et al. (2007) Intraosseous myelolipoma. Skeletal Radiol 36:1181–1184

Wada R, Lambert RG (2005) Deposition of intraosseous fat in a degenerating simple bone cyst. Skeletal Radiol 34:415–418

Fibrous Dysplasia, Osteofibrous Dysplasia, and Adamantinoma

23

Sriram Mannava and Murali Sundaram

CONTENTS

S. Mannava, MD
Diagnostic Radiology/Hb6, The Cleveland Clinic Foundation, 9500 Euclid Avenue, Cleveland OH 44195, USA

M. Sundaram, MD, FRCR
Section of Musculoskeletal Radiology, Imaging Institute, Cleveland Clinic, Professor of Radiology, Cleveland Clinic Lerner School of Medicine, of Case Western Reserve University

KEY POINTS

- Monostotic fibrous dysplasia is more common than polyostotic fibrous dysplasia.
- Fibrous dysplasia can be encountered in any decade of life.
- Endocrine dysfunction and soft tissue myxoma are associated with fibrous dysplasia.
- A fibrous dysplasia-like lesion with cortical destruction suggests low-grade central osteosarcoma or malignant transformation.
- Osteofibrous dysplasia usually occurs in the first two decades of life.
- Osteofibrous dysplasia almost exclusively affects the tibia and fibula.
- Adamantinoma is a rare low-grade neoplasm that most commonly occurs in the second and third decades of life.
- Adamantinoma has a strong predilection for the tibia.

23.1 Introduction

Fibrous dysplasia is a benign disorder of bone. This fibroosseous lesion may affect one or several bones and may be encountered in any decade of life. Monostotic fibrous dysplasia is significantly more common than polyostotic disease. Rarely, endocrine dysfunction (i.e. McCune-Albright syndrome) or soft tissue myxoma (i.e. Mazabraud's syndrome) can be associated with fibrous dysplasia. A fibrous dysplasia-like lesion with radiographic features of cortical destruction suggests low-grade central osteosarcoma or malignant transformation. Osteofibrous dysplasia is a fibroosseous lesion with many pathologic features similar to those of fibrous dysplasia. Osteofibrous dysplasia is usually seen

in the first two decades of life and almost exclusively affects the tibia and fibula. The lesion characteristically and distinctively involves the cortex as multiple lytic lesions. Adamantinoma is a rare neoplasm with osteofibrous and epithelial elements. This rare low-grade malignancy has a predilection for the tibia, typically in the second and third decades of life.

23.2 Fibrous Dysplasia

23.2.1 Pathology

Fibrous dysplasia is a solitary or multifocal fibroosseous lesion composed of spindle cells with trabeculae of immature woven bone. The immature bone spicules lack osteoblastic rimming and are often described as resembling Chinese letters (Dorfman and Czerniak 1998; Fletcher et al. 2002). Fibrous dysplasia is associated with GNAS1 mutations and abnormal G-protein activation. The mosaic distribution of normal and mutated cells helps explain the variable appearance and manifestations of fibrous dysplasia (Weinstein 2006).

23.2.2 Manifestations

The lesions of fibrous dysplasia are intramedullary in origin. They may be entirely intracompartmental or they may expand and deform the bone without cortical destruction (Henry 1969; Kransdorf et al. 1990). The spectrum of fibrous dysplasia has distinct imaging patterns, primarily monostotic or polyostotic. The polyostotic variant can be further classified into monomelic (single extremity) or polymelic (multiple extremities) subtypes. Several syndromes are associated with fibrous dysplasia including the McCune-Albright syndrome and Mazabraud's syndrome. Rarely, fibrous dysplasia may undergo malignant transformation, with osteosarcoma being the most common tumor (Ruggieri et al. 1994).

In general, more extensive fibrous dysplasia is associated with an earlier onset of symptoms (Dorfman and Czerniak 1998). Although fibrous dysplasia can present at any age, the polyostotic form typically manifests during the first and second decades of life (Kransdorf et al. 1990). Monostotic disease is six to ten times more common than polyostotic fibrous dysplasia (Kransdorf et al. 1990; Fletcher et al. 2002; Dorfman and Czerniak 1998).

23.2.2.1 Monostotic Fibrous Dysplasia

Fibrous dysplasia, in particular monostotic fibrous dysplasia, is frequently encountered in adolescents and young adults. Henry (1969) reported that the peak incidence was 10–15 years, especially with long bone lesions. Initial lesions, particularly of the ribs, can be discovered as late as 60–70 years. This late presentation is likely due to the asymptomatic nature of lesions in non-weight-bearing bones. Monostotic fibrous dysplasia is equally distributed between the sexes (Harris et al. 1962; Henry 1969).

Asymptomatic monostotic fibrous dysplasia is often found incidentally on radiographic studies. When symptoms are present, they often are nonspecific, including pain, swelling, or pathologic fracture (Henry 1969; Harris et al. 1962; Kransdorf et al. 1990). Minimal bowing may be present, but severe deformities are unusual (Feldman 2002). Monostotic fibrous dysplasia does not convert to polyostotic fibrous dysplasia. Monostotic disease typically becomes inactive at the on-

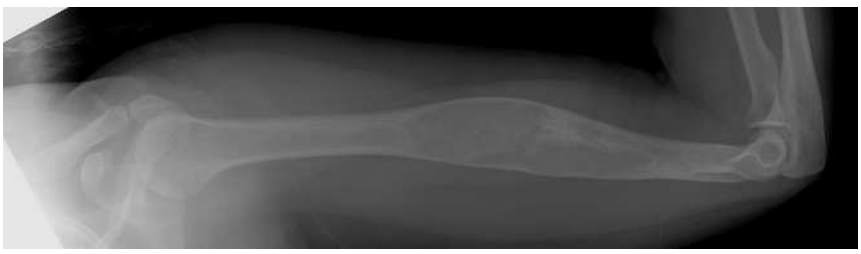

Fig. 23.1. Fibrous dysplasia. Lateral radiograph of the humerus in a young female shows an expansive, ground-glass-density, diaphyseal lesion consistent with fibrous dysplasia. The cortex is thinned but not disrupted. There is no periosteal reaction

set of puberty, with the exception of pregnancy-induced activity in the dysplastic tissue (Henry 1969).

In a review of 427 lesions of monostotic fibrous dysplasia, Kransdorf et al. (1990) reported that the most common sites of involvement were the ribs (28%), proximal femurs (23%), craniofacial bones (20%), and tibia (8%). The remaining lesions were distributed throughout the skeleton, including the upper extremities (Fig. 23.1), pelvis, and spine.

23.2.2.2 Polyostotic Fibrous Dysplasia

Polyostotic fibrous dysplasia frequently involves the pelvis (78%), femur (92%), tibia (82%), craniofacial bones (~50%), upper extremities, ribs, shoulder girdle, and spine (14%; Harris et al. 1962). Although findings can be unilateral, bilateral asymmetric involvement is also common. Harris et al. (1962) found that 25% of patients demonstrated 50% involvement of the skeleton at initial evaluation and 85% of patients sustained a fracture.

Polyostotic fibrous dysplasia represents approximately 20–30% of all cases of fibrous dysplasia (Feldman 2002). The monomelic variant typically affects the lower extremity and the ipsilateral hemipelvis. The polymelic variant demonstrates more widespread involvement (albeit asymmetric at times) including the extremities, axial skeleton, and craniofacial bones (Dorfman and Czerniak 1998). Polyostotic fibrous dysplasia typically presents during the first decade. In one series, two-thirds of patients developed symptoms before 10 years of age; however, some patients remained clinically silent into the seventh decade (Harris et al. 1962). The younger age distribution of polyostotic versus monostotic disease likely relates to the more severe clinical symptoms of polyostotic form (Feldman 2002); pathologic fracture often brings patients to medical attention earlier.

Lesions in polyostotic fibrous dysplasia are typically larger and are subsequently associated with greater deformity. When widespread fibrous dysplasia develops earlier in life, deformities are more severe, fracture incidence is increased, and disease progression is marked (Harris et al. 1962).

Greater than half of patients with polyostotic disease demonstrate abnormal cutaneous pigmentation, cafe-au-lait spots. These pigmented macules can be isolated or multiple. Multiple lesions tend to be arranged in the midline. The pigmentation is often found at birth and can increase during puberty (Albright et al. 1937; Feldman 2002).

23.2.2.3 McCune-Albright Syndrome

McCune-Albright syndrome consists of polyostotic fibrous dysplasia associated with endocrine abnormalities and cutaneous pigmentation. Initially, the syndrome was described in girls with precocious sexual development (Albright et al. 1937). Approximately 2–3% of all fibrous dysplasia is associated with endocrine dysfunction (Feldman 2002). Various endocrinopathies can occur including acromegaly, Cushing's disease, and hyperthyroidism. Patients can present with nonskeletal symptoms; vaginal bleeding was the initial abnormality in 25% of females studied by Harris et al. (1962). Hormonal disturbances can alter skeletal maturation and produce skeletal deformities.

23.2.2.4 Mazabraud's Syndrome

Mazabraud's syndrome is a rare association between benign soft tissue myxoma and fibrous dysplasia (Fig. 23.2). Although the myxomas occur more frequently in polyostotic fibrous dysplasia, myxoma may be encountered with monostotic disease. Primary myxomas are benign mesenchymal neoplasms with a tendency to recur. Zoccali et al. (2008) reviewed a total of 67 published cases and confirmed several conclusions regarding Mazabraud syndrome: (a) development of polyostotic fibrous dysplasia predates development of myxoma; (b) myxoma commonly develops in the fifth to sixth decades of life; and (c) myxomas are often multifocal. Awareness of the association between fibrous dysplasia and soft tissue myxoma can aid diagnosis and prevent the confusion of myxoma with malignant soft tissue sarcoma, malignancy with a soft tissue mass, or malignant transformation of fibrous dysplasia (Sundaram et al. 1989).

23.2.2.5 Malignancy in Fibrous Dysplasia

Malignant transformation in fibrous dysplasia is a rare occurrence; incidences are typically cited to be between 0.4 and 1% (Schwartz and Alpert 1964; Ruggieri et al. 1994). Clinically, patients present with increasing pain, swelling, and/or changes in the radiologic appearance of lesion (Schwartz and Alpert 1964; Yabut et al. 1988). Osteosarcoma is the most frequently occurring neoplasm, followed by fibrosarcoma. Approximately 50% of lesions in a series by Ruggieri et al.

Fig. 23.2. **a** Mazabraud's syndrome. Anteroposterior radiograph of the left hip demonstrates typical fibrous dysplasia of proximal femur. **b** Mazabraud's syndrome. Coronal T2-weighted MRI shows a hyperintense lesion of the bone and adjacent hyperintense soft tissue lesion. The diaphyseal cortex is intact. **c** Mazabraud's syndrome. Axial MRI demonstrates T1 hypointense and T2 heterogeneously hyperintense soft tissue myxoma. The soft tissue mass is separate from the bone

(1994) were associated with radiation therapy, but malignancies arise de novo as well. The craniofacial bones (especially the mandible and maxilla) and the femur are the most commonly affected; this finding correlates with the relative frequencies of fibrous dysplasia in the skeleton (Yabut et al. 1988; Ruggieri et al. 1994; Schwartz and Alpert 1964). Radiographic changes include osteolysis, cortical disruption, and soft tissue mass. Prognosis is poor and mean survival is approximately 3–4 years (Yabut et al. 1988); however, malignancy in fibrous dysplasia is a sporadic event. Fibrous dysplasia, unlike Paget's disease, is not considered a potentially premalignant disorder.

23.2.2.6 Low-Grade Central Osteosarcoma Mimicking Fibrous Dysplasia

A lesion that should be considered in the evaluation of fibrous dysplasia is low-grade central osteosarcoma (LGCOS). Low-grade central osteosarcoma represents

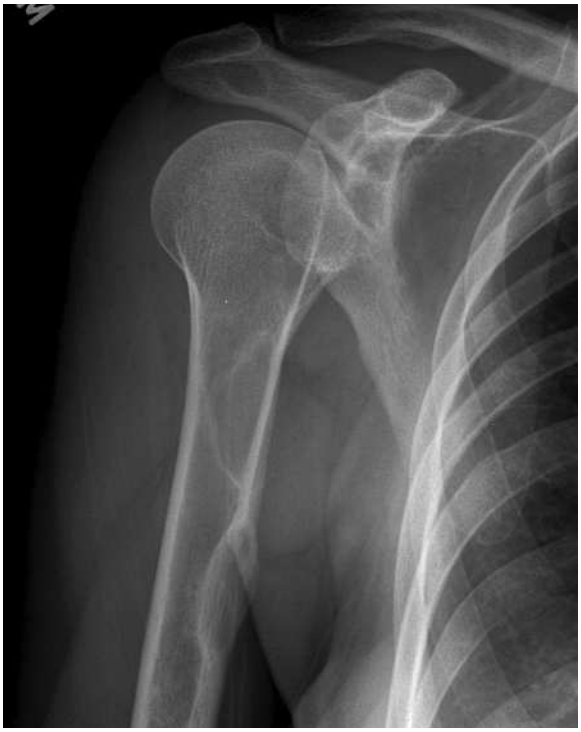

a

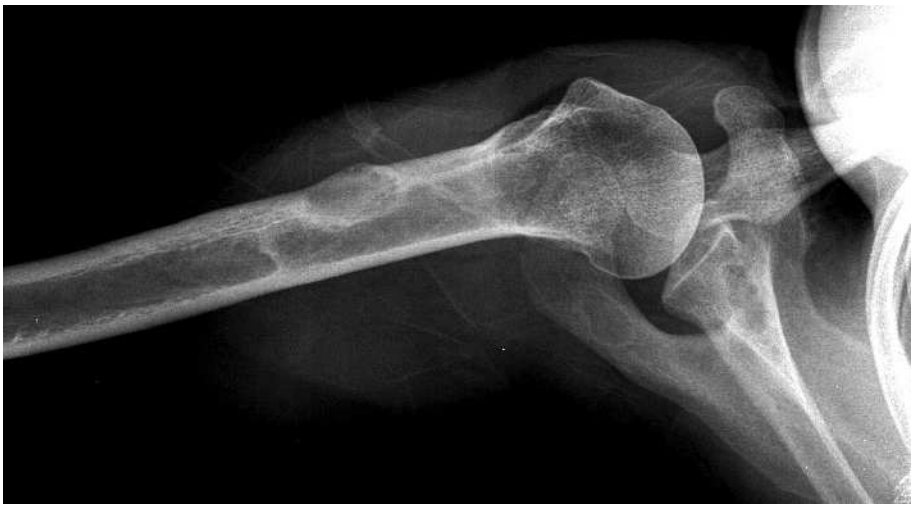

b

Fig. 23.3a–d. Cystic fibrous dysplasia. **a,b** Anteroposterior and axillary radiographs of the right shoulder show two eccentric lucent lesions in the proximal humerus. Additional lesions are noted in the glenoid and acromion. The lesions are corticated, without periosteal reaction or cortical disruption. **c,d** *see next page*

a small percentage of all osteosarcomas, but histologic differentiation from fibrous dysplasia can be difficult (Unni et al. 1977). Radiologically, the lytic pattern of LGCOS demonstrates cortical destruction with or without soft tissue mass, findings which are not present in fibrous dysplasia (Andresen et al. 2004; Sundaram 2006). If a radiographic appearance of fibrous dysplasia is present but with cortical disruption, the primary consideration must be LGCOS. In this scenario, if the rendered pathologic diagnosis is fibrous dysplasia, the microscopic appearances must be re-evaluated (Sundaram 2006).

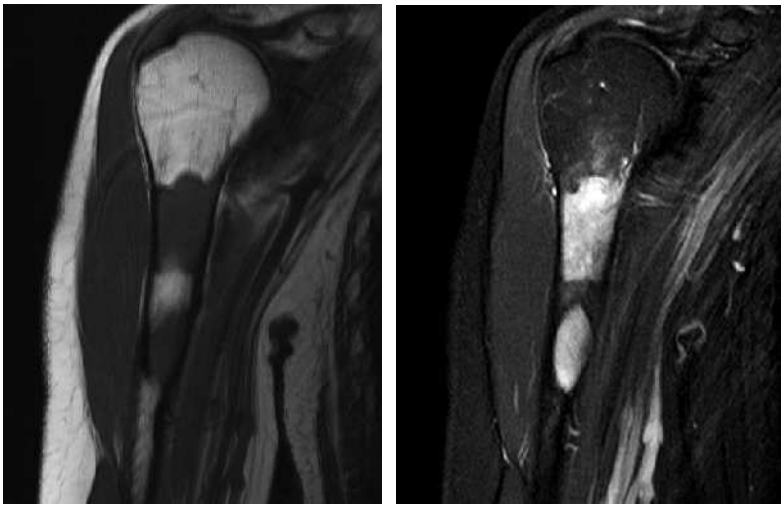

c,d

Fig. 23.3a–d. (*continued*) Cystic fibrous dysplasia. **c** Coronal T1 MR image (TR/TE: 613/16 ms shows that the lesions are isotense to muscle and longitudinally oriented to the humerus. **d** Coronal STIR MR image (TR/TE: 5040/39 ms) shows that the well-defined lesions are hyperintense to muscle

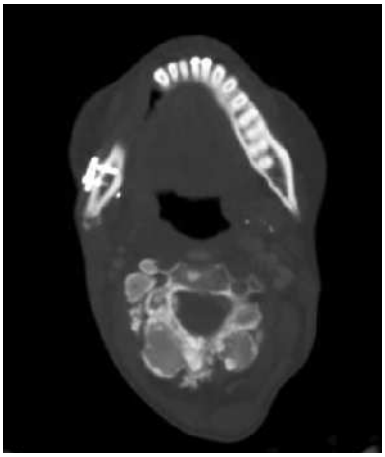

Fig. 23.4. Fibrous dysplasia protuberans. Axial CT of the neck shows well-circumscribed, exophytic masses with sclerotic margins arising from the posterior elements of the cervical vertebra

23.2.2.7 Cystic Fibrous Dysplasia

Osteolysis with cystic change is uncommon and may resemble formation of secondary aneurysmal bone cyst or malignancy; however, MRI can be used to help differentiate cystic degeneration of fibrous dysplasia from malignant transformation. On MRI cystic fibrous dysplasia demonstrates a well-defined margin with internal high T2 signal of fluid intensity (Fig. 23.3; Bahk et al. 2007; Simpson et al. 1989; Fisher et al. 1994).

23.2.2.8 Fibrous Dysplasia Protuberans

Fibrous dysplasia protuberans is an extremely rare variant of fibrous dysplasia. The lesions are eccentric, exophytic fibroosseous masses which extend beyond the cortical contour (Fig. 23.4). The intramedullary portions of the host bone are involved, suggesting medullary origin and eccentric growth. The appearance can resemble cortical disruption of malignant transformation (Dorfman et al. 1994; Hamadani et al. 2006).

23.2.3 Imaging Characteristics

Although fibrous dysplasia can demonstrate a wide spectrum of radiographic appearances, the typical lesions and locations are usually characteristic for the diagnosis; confirmatory imaging is rarely needed (Sundaram 2006). Classically, fibrous dysplasia is intramedullary (not cortical) with normal bone architecture replaced by ground-glass density (Kransdorf et al. 1990; Harris et al. 1962). The ground-glass pattern may be variably lucent or sclerotic depending on the amount of bone trabeculae and fibrous elements (Harris et al. 1962; Dorfman and Czerniak 1998). The lesions are locally expansive. Fibrous dysplasia is commonly well marginated and may have a rind of surrounding sclerotic reactive bone (Kransdorf et al. 1990). Endosteal scalloping and focal cortical thinning may be present but without cortical disruption. Periosteal reaction is absent, unless there is concomitant fracture (Harris et al. 1962).

Polyostotic disease usually presents with severe deformity, whereas monostotic lesions may demonstrate only mild bowing (Stewart et al. 1962; Kransdorf et al. 1990). Fractures are more common in polyostotic fibrous dysplasia. After fracture or surgery, the dysplastic lesion can contain multiple fluid-filled cysts (Harris et al. 1962). No strict criteria are present for identifying lesions at increased risk of pathologic fracture and intervention is based on individual scenario (DiCaprio and Enneking 2005).

23.2.3.1 Long Bones

Long bone lesions demonstrate the classic features of fibrous dysplasia: intramedullary, predominantly diaphyseal, ground-glass density; expansive, well-defined often sclerotic border (rind); endosteal erosions; intact cortex; and variable bone remodeling. Deformity, especially in the weight-bearing bones, is likely due to the weakened fibrous architecture (Dorfman and Czerniak 1998; Feldman 2002). Pathologic fractures are not infrequent, although usually only minimally displaced (Stewart et al. 1962). In the femur, the most common deformities are leg-length discrepancy and severe coxa vara ("Shepherd's crook"; Fig. 23.5a; Harris et al. 1962; Kransdorf et al. 1990; Fitzpatrick et al. 2004). Lesions of the femoral neck are prone to insufficiency fracture along the medial cortex. The fracture often demonstrates two foci of sclerosis divided by a radiolucent fracture line ("parrot's beak"; DiCaprio and Enneking 2005). A study by Ippolito et al. (2003) demonstrated significant fracture risk even in monostotic fibrous dysplasia affecting the proximal femur.

Besides femoral lesions, monostotic disease commonly affects the tibia with possible bowing deformity (Fig. 23.5b). Polyostotic disease affects numerous locations, including the tibia, humerus, and radius. Phalanges, metacarpal, and metatarsal bones can also be affected (Feldman 2002).

23.2.3.2 Craniofacial Bones

As previously mentioned, craniofacial involvement represents approximately 20% of monostotic and approximately 50% of polyostotic fibrous dysplasia. Craniofacial disease is slightly different from fibrous dysplasia in the rest of the skeleton. Skull base lesions typically involve the greater and lesser wings of the sphenoid bone and extend into the facial bones. They are often expansive and demonstrate increased sclerosis (Fig. 23.6). There is associated obliteration of the frontal/sphenoid sinuses and inferolateral displacement of the orbit. Findings are often unilateral, unlike Paget's disease which tends to be bilateral (Harris et al. 1962; Feldman 2002; Kransdorf et al. 1990). Clinically, the outward appearance of the deformities occasionally resembles a lion's face (*leonitiasis ossea*; Fitzpatrick et al. 2004). Lesions of the cranial vault are usually mixed radiolucent lesions, with expansion of the diploic space and intact inner and outer table (Harris et al. 1962; Fitzpatrick et al. 2004).

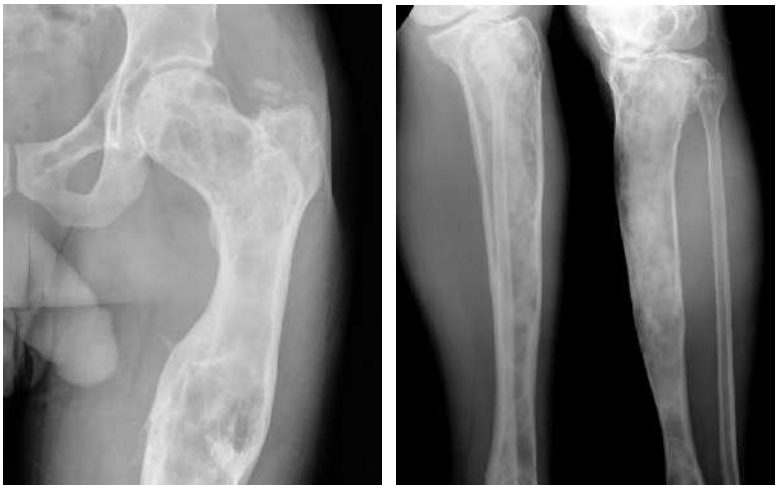

a,b

Fig. 23.5a,b. Fibrous dysplasia. **a** Anteroposterior radiograph of the hip shows a "Shepherd's crook" deformity with an expansive, ground-glass-opacity lesion centred within the medullary cavity of the femur. A similar lesion is present in the pubic ramus. **b** Anteroposterior and lateral radiographs of the leg show a similar intramedullary lesion of the tibia

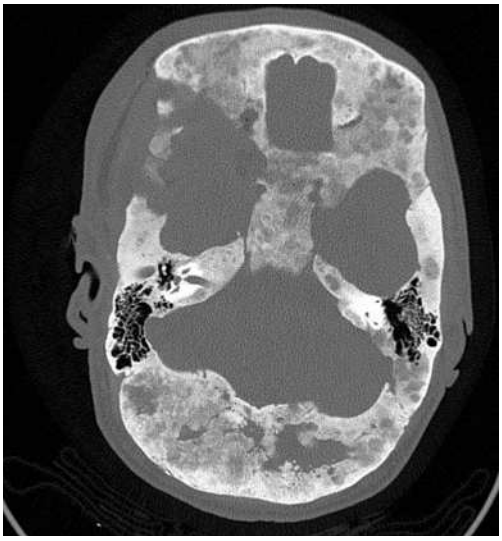

Fig. 23.6. Craniofacial fibrous dysplasia. Axial CT ground-glass-opacity matrix expanding the diploic space of the calvarium. There is cortical sparing, unlike the cortical thickening of Paget's disease

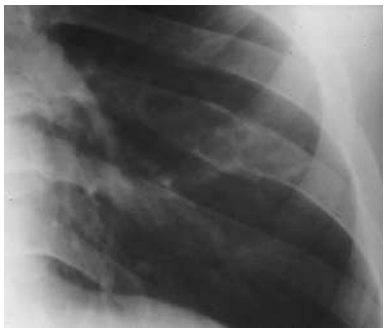

Fig. 23.7. Fibrous dysplasia. Anteroposterior chest radiograph shows a bubbly, well-defined expansive lesion of a lower posterior rib

23.2.3.3 Additional Skeletal Locations

The pelvis is commonly affected in polyostotic fibrous dysplasia, especially in the setting of a femoral lesion. Acetabular protrusion is often present (Harris et al. 1962). Because of the frequent association between femoral and pelvic lesions in polyostotic disease, when femoral fibrous dysplasia is detected, careful scrutiny for additional pathology on the pelvic radiograph is important (DiCaprio and Enneking 2005).

The ribs are a common site for monostotic and polyostotic fibrous dysplasia. In monostotic fibrous dysplasia, the ribs are often asymptomatic and are incidentally discovered on chest radiographs (Harris et al. 1962). Although usually asymptomatic, rib lesions are associated with osseous expansion and deformity (see Fig. 23.7; Fitzpatrick et al. 2004). Occasionally, a Harrison's groove deformity may be present (horizontal depression at the inferior border of the thorax, correlating to the costal insertion of diaphragm; Harris et al. 1962; DiCaprio and Enneking 2005). Unilateral distribution in the setting of polyostotic fibrous dysplasia helps differentiate this entity from other rib lesions such as metastatic disease (Feldman 2002).

Although rare in monostotic fibrous dysplasia, spinal disease is not uncommon in polyostotic fibrous dysplasia, especially in those patients with McCune-Albright syndrome (Harris et al. 1962). Spinal lesions can be well defined, expansive, and radiolucent with variable striations/septations (Fig. 23.8; Feldman 2002). Several publications have stressed the importance of vertebral fibrous dysplasia and its association with significant scoliosis (Leet et al. 2004; Ippolito et al. 2003). In patients with polyostotic fibrous dysplasia, Leet et al. (2004) reported a prevalence of spinal lesions as high as 63% (39 of 62 patients). Lumbar and thoracic vertebrae were more commonly affected than cervical and sacral levels.

23.2.3.4 Other Imaging Modalities

Although often not required for diagnosis, CT, bone scintigraphy, and MRI have been used as corollary imaging modalities. Computed tomography demonstrates characteristics similar to those of radiographs and can better characterize certain complex areas such as the spine, pelvis, and skull. In addition, CT may better exclude a malignant process, especially in the pelvis and vertebrae (Kransdorf et al. 1990).

Although not specific, increased uptake on delayed bone scintigraphy is sensitive for the early detection of fibrous dysplasia and for assessing the extent of polyostotic involvement (Johns et al. 1987; Leet et al. 2004). Because of the increased vascularity, fibrous dysplasia shows variably increased uptake on early scintigraphic

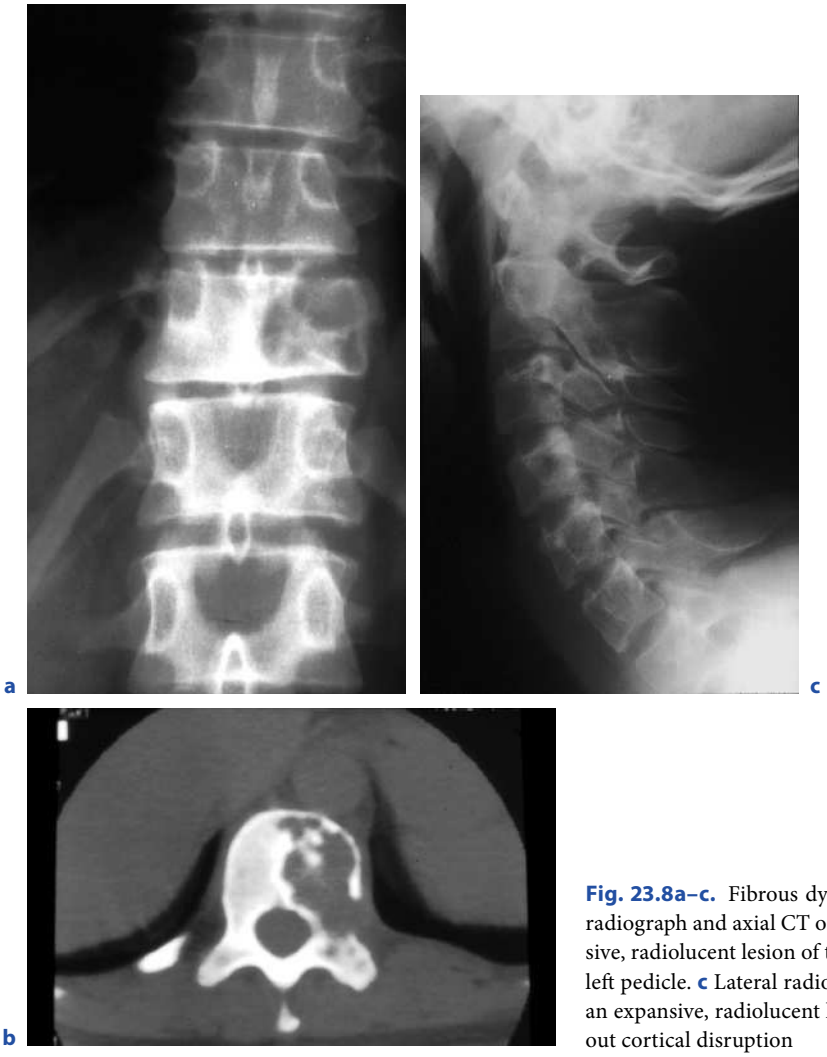

Fig. 23.8a–c. Fibrous dysplasia of the spine. **a,b** Anteroposterior radiograph and axial CT of the lower thoracic spine show an expansive, radiolucent lesion of the T11 vertebral body extending into the left pedicle. **c** Lateral radiograph of the cervical spine demonstrates an expansive, radiolucent lesion of the spinous process of C2, without cortical disruption

perfusion imaging. The scintigraphic and radiographic findings are complementary in assessing the extent of disease (Machida et al. 1986; Zhibin et al. 2004).

On MRI, fibrous dysplasia is typically isointense on T1 and heterogeneously hyperintense on T2 (in relation to skeletal muscle). A surrounding hypointense T1 and T2 rim is often present, corresponding to the sclerotic rind seen on radiographs. Enhancement after intravenous gadolinium is variable (Shah et al. 2005). Magnetic resonance imaging is also useful in detecting intralesional fat and fluid-fluid levels from secondary aneurysmal bone cysts (Sundaram 2006). Cartilage may be seen in 20% of patients with fibrous dysplasia and may be quite profound in some instances. These cartilage-containing lesions have been termed fibrocartilagenous dysplasia by pathologists; however, it is generally believed that these lesions with cartilage should be considered a part of the histologic spectrum of fibrous dysplasia and not sub-classified as fibrocartilagenous fibrous dysplasia (Kyriakos et al. 2004).

23.2.4 Treatment and Follow-up

For most incidentally discovered asymptomatic lesions, no treatment is warranted. With the exception of certain proximal femoral lesions, most asymptomatic fibrous dysplasia do not pose a risk for pathologic fracture (Ippolito et al. 2003; DiCaprio and Enneking 2005). Bisphosphonates have shown some success in providing pain relief and improving skeletal strength (DiCaprio and Enneking 2005).

23.3 Osteofibrous Dysplasia

23.3.1 Pathology

Osteofibrous dysplasia (occasionally referred to as ossifying fibroma of the tubular bones) is a benign fibroosseous lesion most commonly found in the anterior tibial cortex of young children (Kempson 1966; Campanacci and Laus 1981; Park et al. 1993). Pathologically, the lesion is similar to fibrous dysplasia in that bone trabecula are interspersed within a fibrous stroma; a key microscopic difference is osteoblastic rimming of the bone trabeculae in osteofibrous dysplasia (Fletcher et al. 2002; Kempson 1966). Osteofibrous dysplasia lacks epithelial elements, unlike adamantinoma.

23.3.2 Incidence and Clinical Presentation

Osteofibrous dysplasia is a rare tumor and incidence is uncertain. The tumor is usually identified in children during the first decade more often than the second decade of life. The lesion is rare after 15 years of age (Fletcher et al. 2002). Campanacci and Laus (1981) reported disease appearance during the first decade of life in 33 of 35 patients. Infants and neonates can also be affected (Campanacci and Laus 1981; Hindman et al. 1996). No significant gender predilection is present.

Osteofibrous dysplasia is almost exclusively found in the tibial diaphysis in approximately 90% of cases (Levine et al. 2003). Less commonly, de-novo fibular tumor, tibial and fibular tumors, or bilateral tibial tumors are present (Campanacci and Laus 1981; Park et al. 1993). Exceptional cases have also been reported in the upper extremities (Resnick et al. 2002; Wang et al. 1992).

Clinically, patients present with enlargement of the tibia and slight anterior bowing. The lesion is often painless but is prone to pathologic fracture. The bowing and deformity may be exaggerated following fracture and pseudoarthrosis (Campanacci and Laus 1981; Park et al. 1993; Wang et al. 1992).

23.3.3 Imaging Characteristics

Osteofibrous dysplasia is an intracortical, eccentrically expansive, predominantly lytic lesion often with a marginal band of sclerosis. The osteolysis may be a single focus or multiple bubble-like foci (Fig. 23.9). The peripheral sclerosis may be a thin rim or may be more extensive (Campanacci and Laus 1981; Campanacci 1976; Park et al. 1993; Campbell and Hawk 1982). In the tibia, the lesion classically involves the anterior tibial cortex. In the fibula, the whole cortical circumference is often involved. Anterior tibial bowing is often present and a helpful imaging sign.

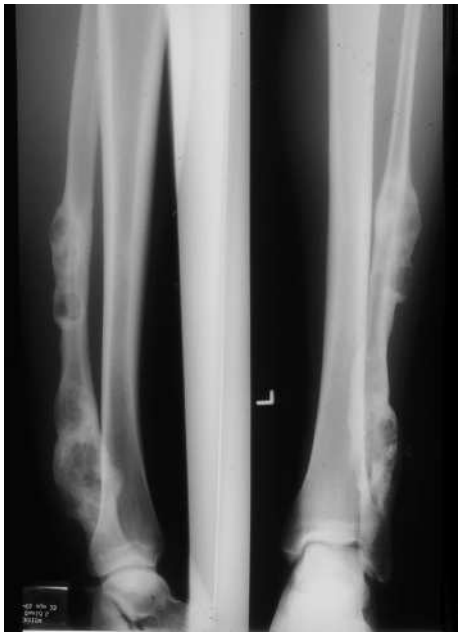

Fig. 23.9. Osteofibrous dysplasia. Anteroposterior and lateral radiographs of the fibula show multifocal, intracortical lesions. The lesions are expansive, with mixed osteolysis and sclerosis

Although the imaging appearance of osteofibrous dysplasia can mimic monostotic fibrous dysplasia and adamantinoma, certain distinguishing features are present. Osteofibrous dysplasia is most often found in patients less than 10 years of age, whereas adamantinoma often affects an older population. Monostotic fibrous dysplasia is usually intramedullary, whereas osteofibrous dysplasia is intracortical (Campanacci and Laus 1981; Wang et al. 1992; Levine et al. 2003).

23.3.4 Treatment and Follow-up

Osteofibrous dysplasia generally has a good prognosis. No consensus treatment has been developed. Lesions have a tendency to undergo spontaneous regression at

puberty (Kahn 2003). Campanacci and Laus (1981) recommended that excision be reserved for extensive disease and not attempted in patients under 15 years of age. Other authors suggest radical excision due to the possible association of osteofibrous dysplasia with differentiated adamantinoma (Lee et al. 2006). The lesion has a high recurrence rate following local therapy, especially when treated in skeletally immature patients. Pathologic fractures can respond to nonoperative treatment (Park et al. 1993; Campanacci and Laus 1981; Campbell and Hawk 1982).

23.4 Adamantinoma

23.4.1 Pathology

Adamantinoma is a rare, low-grade malignant neoplasm with several histologic patterns consisting of mixed osteofibrous and epithelial components. The pathogenesis of adamantinoma is unclear. The tumor has an exquisite predilection for the tibial diaphysis (Fletcher et al. 2002). A variant of adamantinoma, termed differentiated adamantinoma, has been described.

23.4.2 Incidence and Clinical Presentation

Adamantinoma is an uncommon tumor. Approximately 260 cases have been reported in the literature, representing only 0.4% of all primary bone tumors (Fletcher et al. 2002; Moon 1994; Hazelbag et al. 1994). The average age at initial presentation is approximately 30 years. The tumor is encountered in children (60 of 260 cases) and may arise into late adulthood (Moon 1994; Moon and Mori 1986; Hazelbag et al. 1994). There is no significant gender predilection.

Adamantinoma occurs in the tibial diaphysis in approximately 83% of cases. Tibial adamantinoma may be multifocal with ipsilateral fibular involvement in up to 10% of cases (Moon 1994). Less common primary sites include the fibula, humerus, and femur (Fletcher et al. 2002; Moon 1994).

Clinical presentation is usually painful or painless swelling. Symptoms may have a prolonged course, lasting for years before presentation. A history of preceding trauma is present in 25–60% of cases, although its role in pathogenesis is unclear (Hazelbag et al. 1994; Moon 1994). Pathologic fracture is a frequent presentation.

23.4.3 Imaging Characteristics

Adamantinoma is classically an anterior tibial, diaphyseal, eccentric, expansive, mixed osteolytic lesion (Fig. 23.10). The lesion is typically intracortical. Differentiation from osteofibrous dysplasia and fibrous dysplasia is sometimes difficult. Longitudinal intracortical extension or cortical destruction with medullary extension may be present. The presence of intramedullary extension aids in differentiation from osteofibrous dysplasia. Occasionally, periosteal reaction and soft tissue mass have been reported. Margins of the lesion are variable, ranging from ill-defined to sharply marginated. The tumor is often multilocular with thin walls around small cysts, simulating a "soap-bubble" appearance. Adamantinoma may be multifocal or simultaneously affect the tibia and fibula (Fig. 23.11; Bloem et al. 1991; Fletcher et al. 2002; Kahn 2003; Moon and Mori 1986; Resnick et al. 2002; Sweet et al. 1992; Van Der Woude et al. 2004).

A study by Bloem et al. (1991) analyzed multiple radiographic features to assist in accurately distinguishing fibrous dysplasia from adamantinoma. The most important signs indicating a diagnosis of fibrous dysplasia over adamantinoma were (a) young age, (b) ground-glass opacity with or without intralesional opacifications, (c) absence of periosteal reaction or moth-eaten bone destruction, and (d) anterior bowing. Despite these features, a significant overlap may be present and radiographic features are not always diagnostic.

The MRI findings are not specific but demonstrate low T1 signal, increased T2 signal, and intense post-contrast gadolinium enhancement. Magnetic resonance imaging is useful in assessing the extent of tumor, cortical disruption, and intramedullary extension (Van Der Woude et al. 2004). In addition, MRI can help delineate multifocal disease and guide preoperative planning.

23.4.4 Differentiated Adamantinoma

Many authors separate classic adamantinoma from differentiated adamantinoma (osteofibrous dysplasia-like adamantinoma) based on clinical and histologic features. Differentiated adamantinoma tends to have a more prolonged course similar to that of osteofibrous dysplasia and is treated less aggressively (Kahn 2003); however, accurate distinction between differentiated and classic adamantinoma cannot be made radiologically (Van Der Woude et al. 2004).

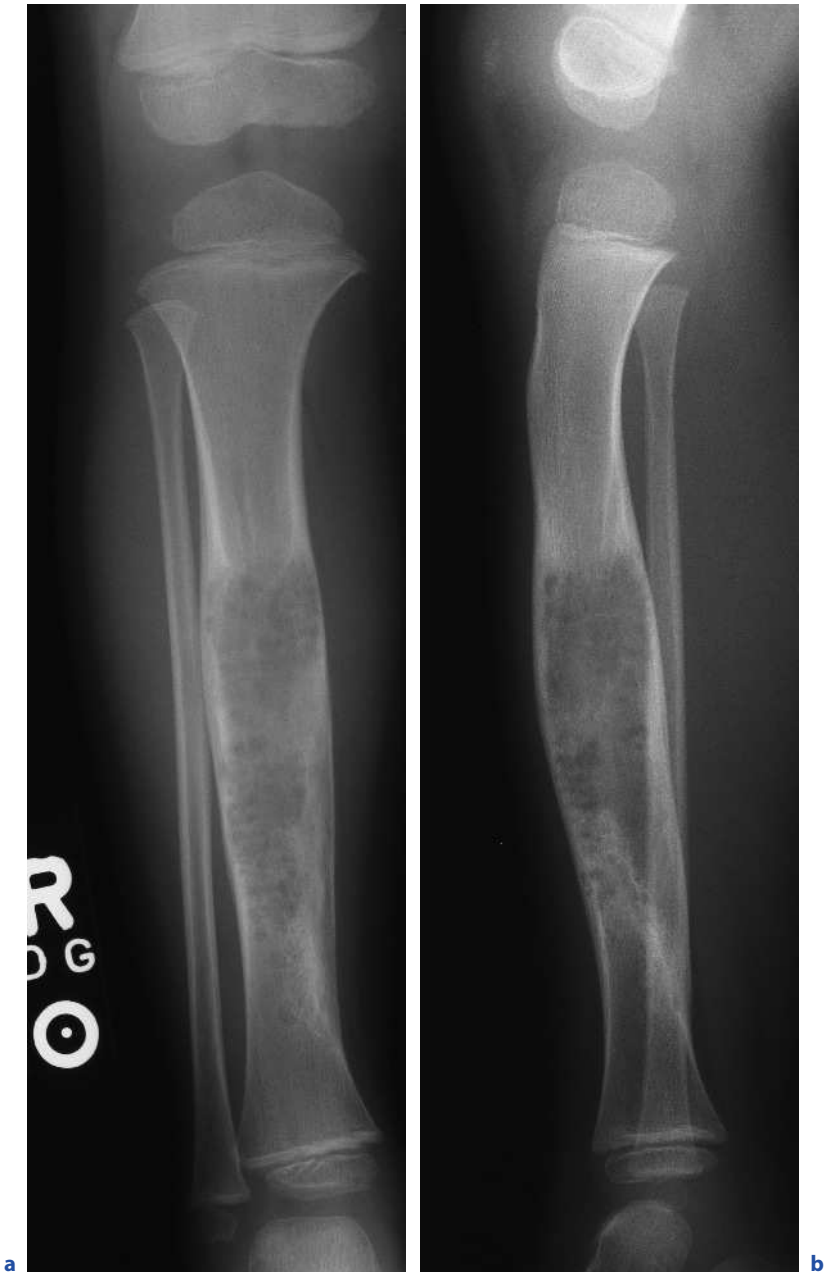

a b

Fig. 23.10a,b. Adamantinoma. **a,b** Anteroposterior and lateral radiographs of the tibia in a 4-year-old boy demonstrate an expansive, mixed osteolytic lesion with slightly ill-defined borders. The tumor appears multilocular, with multiple thin-walled cystic foci

23.4.5 Treatment and Follow-up

Current treatment for adamantinoma consists of en-bloc tumor resection with wide operative margins and limb salvage. Local excision has been associated with higher rates of local recurrence. Chemotherapy and radiation are ineffective. Ten-year survival is greater than 80%. Metastatic disease is often a late occurrence, affects between 10 and 30% of patients, and most frequently manifests in the lungs (Hazelbag et al. 1994; Moon 1994; Moon and Mori 1986; Qureshi et al. 2000).

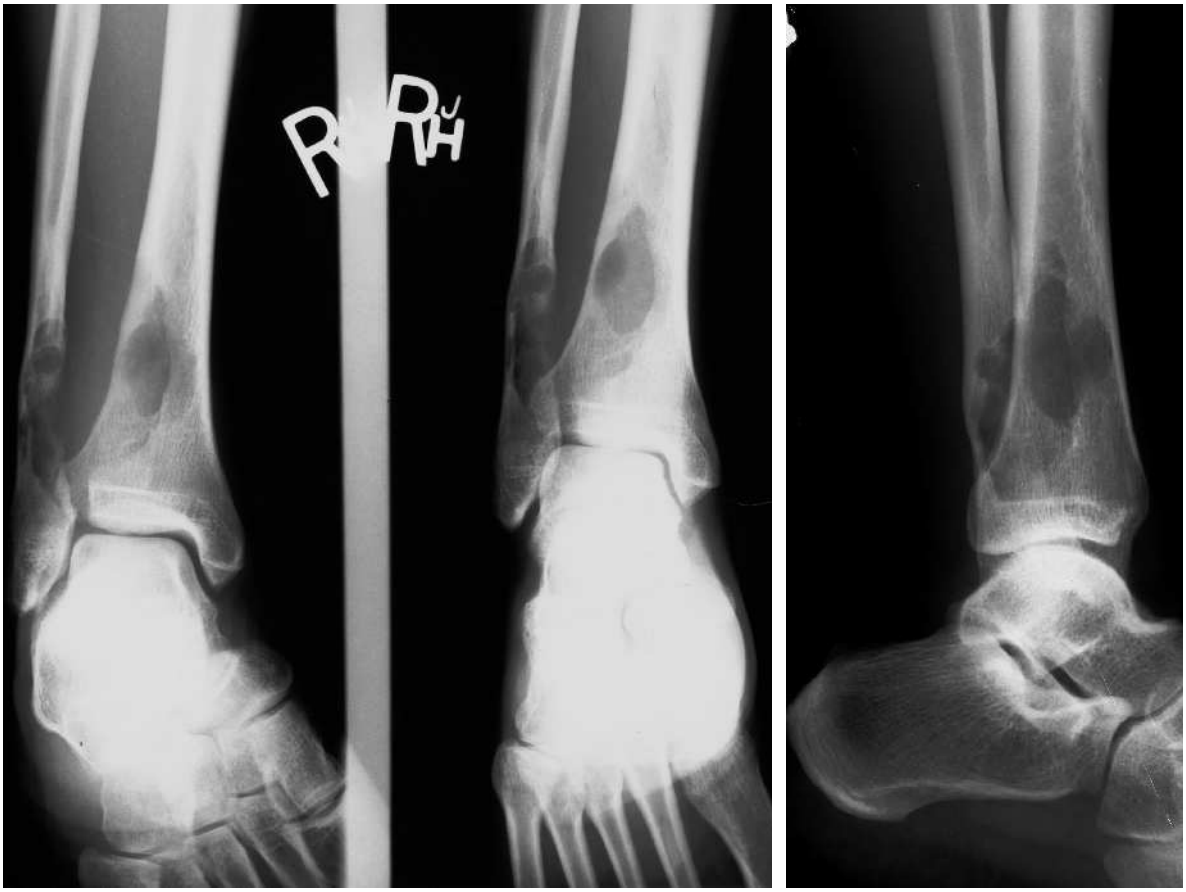

a b

Fig. 23.11a,b. Adamantinoma. **a,b** Anteroposterior, oblique, and lateral radiographs of the ankle in a 29-year-old man demonstrate a predominantly lytic lesion involving the distal tibia. There is synchronous involvement of the ipsilateral fibula, an unexpected finding at this age

References

Albright F, Butler AM, Hampton AO, Smith P (1937) Syndrome characterized by osteitis fibrosa disseminata, areas of pigmentation and endocrine dysfunction, with precocious puberty in females. N Engl J Med 216(17):727–746

Andresen KJ, Sundaram M, Unni KK, Sim FH (2004) Imaging features of low-grade central osteosarcoma of the long bones and pelvis. Skeletal Radiol 33:373–379

Bahk WJ, Kang YK, Rhee SK, Chung YG, Lee AH, Bahk YW (2007) Cystic fibrous dysplasia in the long bone. Orthopedics 30:871–873

Bloem JL, van der Heul RO, Schuttevaer HM, Kuipers D (1991) Fibrous dysplasia vs adamantinoma of the tibia: differentiation based on discriminant analysis of clinical and plain film findings. AJR 156:1017–1023

Campanacci M (1976) Osteofibrous dysplasia of long bones a new clinical entity. Ital J Orthop Traumatol 2:221–237

Campanacci M, Laus M (1981) Osteofibrous dysplasia of the tibia and fibula. J Bone Joint Surg Am 63:367–375

Campbell CJ, Hawk T (1982) A variant of fibrous dysplasia (osteofibrous dysplasia). J Bone Joint Surg 64:231–236

Caprio M di, Enneking W (2005) Fibrous dysplasia, pathophysiology, evaluation, and treatment. J Bone Joint Surg 87:1848–1864

Dorfman H, Czerniak B (1998) Bone tumors. Mosby, St. Louis

Dorfman H, Ishida T, Tsuneyoshi M (1994) Exophytic variant of fibrous dysplasia (fibrous dysplasia protuberans). Hum Pathol 25:1234–1237

Feldman F (2002) Tuberous sclerosis, neurofibromatosis and fibrous dysplasia. In: Resnick D (ed) Diagnosis of bone and joint disorders, 4th edn. Saunders, Philadelphia, pp 4792–4844

Fisher AJ, Totty WG, Kyriakos M (1994) MR appearance of cystic fibrous dysplasia. J Comput Assist Tomogr 18:315–318

Fitzpatrick K, Taljanovic M, Speer D et al. (2004) Imaging findings of fibrous dysplasia with histopathologic and intraoperative correlation. AJR 182:1389–1398

Fletcher CDM, Unni KK, Mertens F (eds) (2002) World Health Organization Classification of Tumours. Pathology and genetics of tumours of soft tissue and bone. IARC Press, Lyon

Hamadani M, Awab A, Rashid A et al. (2006) Fibrous dysplasia protuberans in a patient with McCune-Albright syndrome. J Coll Phys Surg Pak 16:376–377

Harris WH, Dudley R, Barry RJ (1962) The natural history of fibrous dysplasia: an orthopaedic, pathological, and roentgenographic study. J Bone Joint Surg 44:207–233

Hazelbag HM, Taminiau AH, Fleuren GJ et al. (1994) Adamantinoma of the long bones. A clinicopathologic study of thirty-two patients with emphasis on histological subtype, precursor lesion, and biological behavior. J Bone Joint Surg 76:1482–1499

Henry A (1969) Monostotic fibrous dysplasia. J Bone Joint Surg Br 51:300–306

Hindman BW, Bell S, Russo T et al. (1996) Neonatal osteofibrous dysplasia: report of two cases. Pediatr Radiol 26:303–306

Ippolito E, Bray E, Corsi A et al. (2003) Natural history and treatment of fibrous dysplasia of bone: a multicenter clinicopathologic study promoted by the European Pediatric Orthopaedic Society. J Pediatr Orthop 12(3):155–177

Johns WD, Gupta SM, Kayani N (1987) Scintigraphic evaluation of polyostotic fibrous dysplasia. Clin Nucl Med 12:627–631

Kahn L (2003) Adamantinoma, osteofibrous dysplasia and differentiated adamantinoma. Skeletal Radiol 32:245–258

Kempson RL (1966) Ossifying fibroma of the long bone: a light and electron microscopic study. Arch Pathol 82(3):218–233

Kransdorf M, Moser R Jr, Gilkey F (1990) Fibrous dysplasia. Radiographics 10:519–537

Kyriakos M, McDonald DJ, Sundaram M (2004) Fibrous dysplasia with cartilaginous differentiation ("fibrocartilaginous dysplasia"): a review, with an illustrative case followed for 18 years. Skeletal Radiol 33:51–62

Lee RS, Weitzel S, Eastwood DM et al. (2006) Osteofibrous dysplasia of the tibia: Is there a need for a radical surgical approach? J Bone Joint Surg Br 88:658–664

Leet AI, Magur E, Lee JS et al. (2004) Fibrous dysplasia in the spine: prevalence of lesions and association with scoliosis. J Bone Joint Surg 86:531–537

Levine S, Lambiase R, Petchprapa C (2003) Cortical lesions of the tibia: characteristic appearances at conventional radiography. Radiographics 23:157–177

Machida K, Makita K, Nishikawa J et al. (1986) Scintigraphic manifestation of fibrous dysplasia. Clin Nucl Med 11:426–429

Moon NF (1994) Adamantinoma of the appendicular skeleton in children. Int Orthop 18:379–388

Moon NF, Mori H (1986) Adamantinoma of the appendicular skeleton: updated. Clin Orthop Relat Res 204:215–237

Park YK, Unni KK, McLeod RA et al. (1993) Osteofibrous dysplasia: clinicopathologic study of 80 cases. Hum Pathol 24(12):1339–1347

Qureshi AA, Shott S, Mallin BA et al. (2000) Current trends in the management of adamantinoma of long bones. J Bone Joint Surg 82:1122–1131

Resnick D, Kyriakos M, Greenway GD (2002) Tumors and tumor-like lesions of bone: imaging and pathology of specific lesions. In: Resnick D (ed) Diagnosis of bone and joint disorders, 4th edn. Saunders, Philadelphia, 4:3763–4128

Ruggieri P, Sim F, Bond J et al. (1994) Malignancies in fibrous dysplasia. Cancer 73:1411–1424

Schwartz D, Alpert M (1964) The malignant transformation of fibrous dysplasia. Am J Med Sci 247:1–20

Shah Z, Peh W, Koh W et al. (2005) Magnetic resonance imaging appearances of fibrous dysplasia. Br J Radiol 78:1104–1115

Simpson AHR, Creasy TS, Williamson DM et al. (1989) Cystic degeneration of fibrous dysplasia masquerading as sarcoma. J Bone Joint Surg Br 71:434–436

Stewart M, Gilmer WS, Edmonson A (1962) Fibrous dysplasia of bone. J Bone Joint Surg 44:302–318

Sundaram M (2006) Imaging of Paget's disease and fibrous dysplasia of bone. J Bone Miner Res 21:28–30

Sundaram M, McDonald D, Merenda G (1989) Intramuscular myxoma: a rare but important association with fibrous dysplasia of bone. AJR 153:107–108

Sweet D, Vinh T, Devaney K (1992) Cortical osteofibrous dysplasia of long bone and its relationship to adamantinoma: a clinicopathologic study of 30 cases. Am J Surg Pathol 16(3):282–290

Unni KK, Dahlin DC, McLeod RA et al. (1977) Intraosseous well-differentiated osteosarcoma. Cancer 40:1337–1347

Van der Woude H, Hazelbag H, Bloem J et al. (2004) MRI of adamantinoma of long bones in correlation with histopathology. AJR 183:1737–1744

Wang J, Shih C, Chen W (1992) Osteofibrous dysplasia (ossifying fibroma of long bones): a report of four cases and review of the literature. Clin Orthop Relat Res 278:235–243

Weinstein L (2006) G_s mutations in fibrous dysplasia and McCune-Albright syndrome. J Bone Miner Res 21:120–124

Yabut S, Kenan S, Sissons H et al. (1988) Malignant transformation of fibrous dysplasia: a case report and review of the literature. Clin Orthop Relat Research 228:281–289

Zhibin Y, Quanyong L, Libo C et al. (2004) The role of radionuclide bone scintigraphy in fibrous dysplasia of bone. Clin Nucl Med 29:177–180

Zoccali C, Teori G, Prencipe U et al. (2008) Mazabraud's syndrome: a new case and review of the literature. Int Orthop [Epub ahead of print]

Cystic Lesions of Bone

24

Paul G. O'Donnell

CONTENTS

KEY POINTS

- There are several unrelated types of bone cyst. Simple (unicameral) bone cysts (SBCs) are most commonly found in the proximal humerus and proximal femur in children, and also occur in the calcaneum in adults.
- They tend to present with pathological fracture, which may lead to healing of the lesion. Aneurysmal bone cysts (ABC) are often markedly expansile lesions, which may grow rapidly.
- They occur in the appendicular, axial and craniofacial skeleton, typically in children and adolescents and contain multiple blood-filled cysts.

P. G. O'Donnell, FRCR
Department of Radiology, Royal National Orthopaedic Hospital, Brockley Hill, Stanmore Middlesex HA7 4LP, UK

A proportion occurs in association with other bone lesions (secondary ABC).

- SBC and primary ABC have long been considered non-neoplastic, but cytogenetic abnormalities found in primary ABCs have suggested that they do represent neoplasms.
- Intraosseous ganglia and geodes are lesions which generally occur in subarticular bone, showing similar imaging and pathological features.
- The distinction is based on the presence of arthropathy, but they probably represent manifestations of the same process.

24.1 Simple Bone cyst

24.1.1 Synonyms

Synonyms for simple bone cyst (SBC) are unicameral bone cyst and benign bone cyst (Kaelin and MacEwen 1989).

24.1.2 Aetiology

A number of aetiologies have been proposed to explain SBC:

1. Venous obstruction in a pre-existing lesion (non-ossifying fibroma or cartilage rest; Broder 1968). Re-establishing connection between the cyst and the venous system by pressure injection of saline and mechanical intervention leads to cyst healing (Gebhart and Blaimont 1996).
2. Blocked drainage of interstitial fluid in an area of rapidly remodelling bone: cyst fluid resembles plasma or blood (Cohen 1960).
3. Congenital rest of synovial tissue or invagination of the synovial membrane of a large joint via the growth plate into the metaphysis, thought to occur at the synovial reflection during fetal or early infant growth (Mirra et al. 1978).
4. Remodelling out of control (Garceau and Gregory 1954).
5. Traumatic haematoma with cystic resorption (Pommer 1920).
6. Mild osteomyelitis analogous to a Brodie's abscess (Phemister and Gordon 1926).
7. Faulty local calcium metabolism or osteoclast function (James et al. 1948).

Occurrence in monozygotic twins suggests a genetic basis (Goto et al. 2007). There have been two case reports of differing cytogenetic abnormalities in SBCs (Richkind et al. 2002; Vayego et al. 1996). Despite these reports, the lesion is generally thought to be non-neoplastic and its aetiology is debated. Once formed, cyst pressure may be important for enlargement; bone-resorptive factors in cyst fluid, such as prostaglandins, interleukins, proteolytic enzymes (Komiya et al. 1993) and oxygen radicals (Komiya et al. 1994), may be responsible for further destruction of the bone matrix.

24.1.3 Incidence

The exact incidence is difficult to determine as many lesions are silent prior to fracture. Simple bone cyst is estimated to account for 3–5% (Baig and Eady 2006; Mirra et al. 1989a) of primary bone lesions (excluding multiple myeloma). The calculated annual prevalence is 0.30 per 100,000 people (Zehetgruber et al. 2005).

24.1.4 Age

The average age at discovery is 9–11 years (Boseker et al. 1968; Zehetgruber et al. 2005), with most SBCs presenting between the ages of 5 and 15 years (Parman and Murphey 2000; Margau et al. 2000). 85% of patients are less than 20 years old (Mirra et al. 1989a). They can occur in adults, but usually only in certain sites (see Sect. 24.1.6).

24.1.5 Gender

There is a male preponderance, with a male-to-female ratio of approximately 2–2.5 to 1 (Margau et al. 2000).

24.1.6 Site

Over 90% of SBCs occur in two locations. Approximately 60% of lesions occur in the proximal humeral

metaphysis and 30% in the proximal femoral metaphysis (Baig and Eady 2006). In childhood, other locations are rare, but SBCs have been reported in a wide variety of locations, including the ischium, pubic rami (Baig and Eady 2006), forearm bones (Stürz and Witt 1999), the craniofacial skeleton (Chang et al. 2003) and spine (Coskun et al. 2004). They occur with equal frequency in the proximal and distal aspects of the tibia (Garceau and Gregory 1954). In adults, SBCs tend to occur in the distal calcaneum and the ilium adjacent to the sacroiliac joint (Parman and Murphey 2000). For lesions in the pelvis, the average age of patients is 32 years (Boseker et al. 1968).

24.1.7 Skeletal Distribution

In the typical long bone location, SBCs are metaphyseal, usually located adjacent to an open physis. Several authors differentiate active (metaphyseal, in contact with the growth plate) and inactive (diaphyseal) SBCs. When bone growth exceeds cyst growth, the physis moves away from the cyst, the latter becoming diaphyseal. Active lesions tend to occur in patients less than 10 years old, who have been suggested to have a higher recurrence rate following surgery, a fact not confirmed by Neer et al. (1973). There are reported examples of epiphyseal/apophyseal cysts, usually resulting from extension of a metaphyseal cyst across the physis (Gupta and Crawford 1996), and multifocal lesions (Chigera et al. 1987).

24.1.8 Clinical Features

Patients often present with acute pain due to pathological fracture (Baig and Eady 2006). Lesions are frequently asymptomatic before this time.

24.1.9 Imaging

24.1.9.1 Radiographs

An SBC is usually a well-defined area of osteolysis, located centrally within the metaphysis of the proximal humerus (Fig. 24.1) or proximal femur (Fig. 24.2; Parman and Murphey 2000; Baig and Eady 2006; Gar-

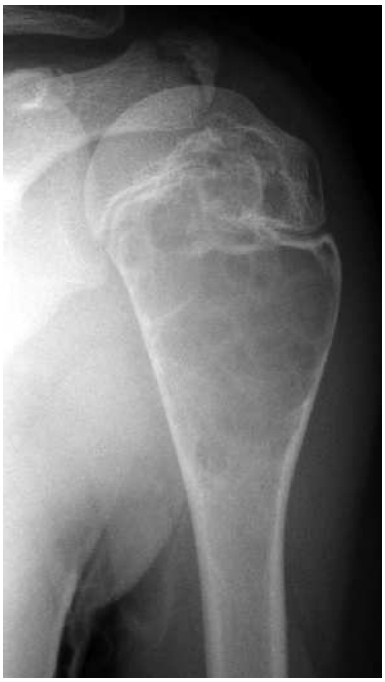

Fig. 24.1. Simple bone cyst. Anteroposterior radiograph of the left humerus: typical appearances of a simple bone cyst, with extension into the epiphysis

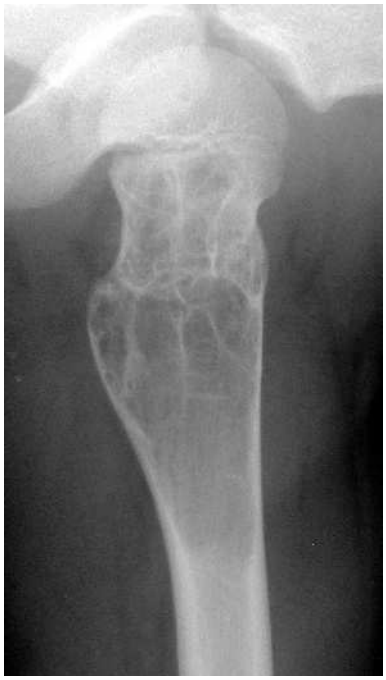

Fig. 24.2. Simple bone cyst (SBC). Lateral radiograph of the left femur: uncomplicated proximal femoral SBC, showing marked trabeculation

ceau and Gregory 1954; Mirra et al. 1989a). Unless migrated, it normally abuts the open growth plate with its longitudinal dimensions usually greater than transverse. The inferior margin may occasionally be difficult to identify but can be indicated by the presence of a fallen fragment. There is usually a geographic pattern of bone destruction with a well-defined sclerotic edge and a narrow zone of transition. Endosteal scalloping causes cortical thinning. Subperiosteal new bone formation occurring simultaneously results in mild bone expansion. Apparent trabeculation is common but represents ridging – "scroll-like elevations" (Garceau and Gregory 1954) – of the walls of the cyst (Fig. 24.2). There is usually no periosteal reaction visible unless a pathological fracture has occurred. Matrix mineralization is very uncommon but can be seen following fracture or due to the production of an acellular material resembling dental cementum (Mirra et al. 1978, 1989a), which is rarely radiographically visible. Foci of calcification can be seen in mature cysts (Sanerkin 1979).

The fallen-fragment sign (Fig. 24.3) is seen in 5–20% of SBCs (Parman and Murphey 2000; Struhl et al. 1989). It is thought to be pathognomonic of an SBC, although it has recently been described in Langerhans' cell histiocytosis (Alyas et al. 2008) and is theoretically also possible in other cystic lesions. Following typically minor trauma, the surrounding periosteum remains intact preventing outward displacement of the bone fragment. A fragment of cortex is seen within the cyst, either "hinged", still attached to periosteum or lying dependently, where it may be helpful to identify the inferior aspect of the lesion. Single or multiple, fallen and hinged fragments may coexist. Gravitational displacement of the fragment implies a cystic, unicameral lesion and would not be seen with solid lesions or septated cysts such as aneurysmal bone cyst (ABC). The fallen-fragment sign may be helpful in the diagnosis of SBC in atypical locations. Struhl et al. (1989) observed the fallen-fragment sign only in active SBCs (metaphyseal lesions with open physes). Following fracture, haematoma within the cyst can prevent displacement.

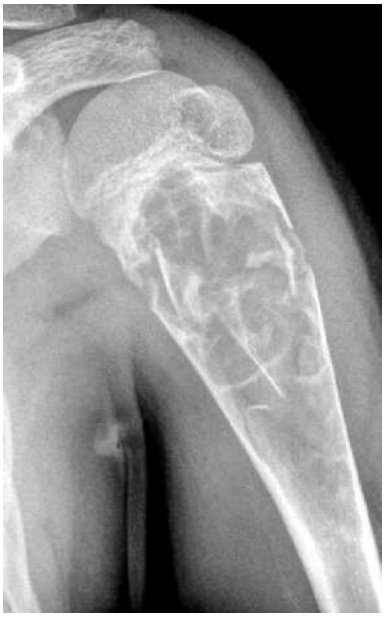

Fig. 24.3. Simple bone cyst. Anteroposterior radiograph of the left humerus: SBC with pathological fracture and multiple fallen fragments

24.1.9.2 CT

Features noted on plain radiographs may be seen more clearly using CT. It can demonstrate the presence of a fracture, trabeculation in the walls of, but not traversing, the lesion, cortical thinning and lack of periosteal reaction. The attenuation of the cyst may be slightly higher than water in keeping with a proteinaceous content (Parman and Murphey 2000).

24.1.9.3 MR Imaging

Prolonged T1 and T2 relaxation times suggest a cyst, although T1 shortening (Fig. 24.4) may reflect proteinaceous content resulting in signal which is higher than water (Parman and Murphey 2000). Fluid-fluid levels are usually only seen following fracture, but as most cysts will have fractured by the time of presentation, fluid-fluid levels are frequent. In a series of 20 SBCs studied with MRI, only 10% were classified as uncomplicated by acute or remote fracture; one of these showed fluid-fluid levels (Margau et al. 2000). Following intravenous injection of gadolinium chelate in uncomplicated cysts, a thin rim of peripheral enhancement is seen. After a fracture, there may be evidence of haemorrhage. Other changes following fracture include heterogeneous internal signal, apparently solid areas and a variety of enhancement patterns, including focal nodular, heterogeneous central, a thick peripheral rim and subcortical with adjacent soft tissue enhancement (Fig. 24.5); however, even following fracture, some of the lesion will resemble a simple a cyst containing homogeneous fluid signal and thin rim or septal enhancement.

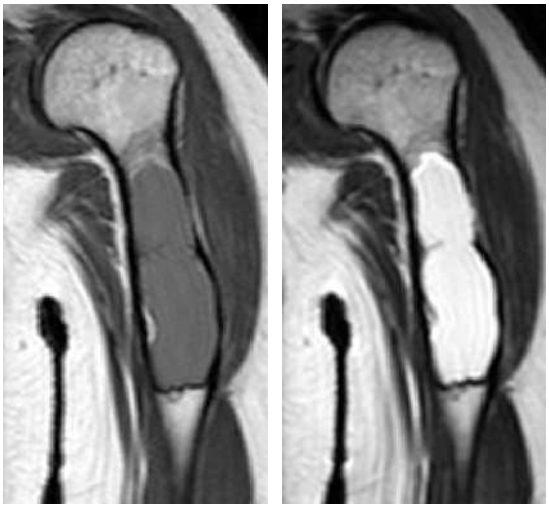

a,b

Fig. 24.4a,b. Simple bone cyst. Coronal T1- (**a**) and T2- (**b**) weighted MR images of a migrated SBC. The lesion returns fluid signal but shows relative T1 hyperintensity

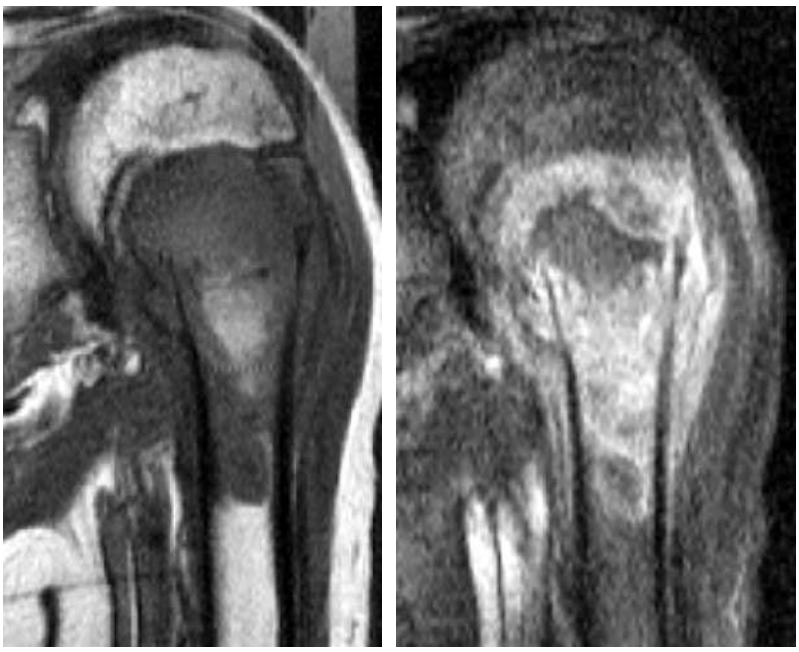

a,b

Fig. 24.5a,b. Simple bone cyst. Coronal T1- (**a**) and post-gadolinium-chelate fat-saturated T1- (**b**) MR images of a left humeral SBC following fracture. Pre-contrast images show high T1 signal due to haemorrhage in the medulla; following contrast, enhancement is seen diffusely within the cyst and in adjacent extraosseous tissues

24.1.9.4 Bone Scintigraphy

There may be mildly increased uptake in the margin of uncomplicated cysts with central photopaenia, and increased activity at the site of a fracture (Parman and Murphey 2000).

24.1.10 Differential Diagnosis

The major differential diagnoses include aneurysmal bone cysts, fibrous dysplasia, particularly when showing cystic change (fibrous dysplastic cysts), which can be difficult to differentiate from diaphyseal cysts, and lytic sarcomas. Small cysts may be mistaken for non-ossifying fibromata and following fracture, SBC may resemble osteoblastoma radiologically and pathologically (Mirra et al. 1989a). Calcaneal cysts show some overlapping appearances with intraosseous lipoma.

24.1.10.1 Aneurysmal Bone Cyst

The degree of bone expansion and cortical thinning, and the location, may help differentiation. The presence of multiple septations and fluid-fluid levels on MRI also suggests ABC rather than SBC.

24.1.10.2 Fibrous Dysplasia

Cysts in fibrous dysplasia (FD) not uncommonly occur in the femoral neck and also in the proximal humerus. Ground-glass density in adjacent bone may abut the cyst and an extensive abnormality is often seen in long bones. The FD typically shows a thick surrounding rind of sclerosis and other bones may be involved. If presenting in a child, the disease is likely to be polyostotic.

24.1.10.3 Sarcoma

Purely lytic sarcomas can be mistaken for cysts. In particular, an osteosarcoma (OS) variant, the pseudocystic OS, may show indolent clinical behaviour and similar radiographic appearances (Sundaram et al. 2001). Occasionally, telangiectatic OS can resemble SBC (Mirra et al. 1989a). Two cases of Ewing's sarcoma with the radiographic appearances of SBC (Bhagia et al. 1997; Hammoud et al. 2006) have been reported. These lesions may occur at an unusual age and location for SBC and show a more aggressive margin than would be typical for SBC.

24.1.11 Modern Management

There are open and closed techniques for the treatment of SBC. Closed methods include percutaneous injection with steroids (Scaglietti et al. 1982), bone marrow (Lokiec et al. 1996) and demineralized bone matrix (Killian et al. 1998). Injection of a fibrosing agent (Ethibloc; Adamsbaum et al. 1993) and alcohol (Wada and Lambert 2005) have been described and recently botulinum toxin has also been suggested (Namazi 2008). Intralesional steroid injections can lead to successful healing, but multiple injections are usually required, and the success depends on loculation, the age of the patient (activity of the cyst) and the size (Capanna et al. 1982). Although the overall success of steroid and bone marrow injections is similar, there is a higher recurrence rate after a single treatment with steroids (methylprednisolone) and more injections are required to achieve healing (Cho et al. 2007). One third of cysts in the femur or tibia showed an unsatisfactory clinical outcome after a median of 5 years following steroid injection (Hashemi-Nejad and Cole 1997), suggesting the site of the lesion is also important. Procedures aimed at reducing cyst pressure, either by drilling (Shinozaki et al. 1996) or re-establishing venous drainage with high-pressure saline injection and reaming of the medullary cavity (Gebhart and Blaimont 1996) have also been used; however, there is a continued risk of pathological fracture following injection therapy and drilling despite appropriate medical management. This is reduced by insertion of a flexible intramedullary nail (Roposch et al. 2000), which has been recommended as the treatment of choice as it provides stability to bone and allows early mobilization (de Sanctis and Andreacchio 2006).

Open procedures are not usually indicated as primary treatment. Curettage and bone grafting is associated with a high recurrence rate, high intraoperative blood loss, the need for a large cortical window to remove the cyst lining, problems with graft incorporation and donor-site morbidity (Roposch et al. 2004).

Many cysts heal following fracture, possibly due to reduced cyst pressure. Growth arrest may result in limb shortening or deformity in 6–20% of cases, due to damage of the physis at surgery, repeated pathological fractures, steroid injection or cyst extension through the growth plate (Violas et al. 2004).

24.2 Aneurysmal Bone Cyst

24.2.1 Aetiology

Aneurysmal bone cyst (ABC) has long been considered non-neoplastic, occurring as either a reactive vascular phenomenon or secondary to another lesion or trauma. The aetiology remains uncertain in a large number of cases, although there is increasing evidence of cytogenetic abnormalities in primary ABCs, suggesting that they do represent neoplasms. The haemodynamic hypothesis suggested either an arteriovenous malformation or intramedullary venous engorgement secondary to thrombosis of a large vein (Lichtenstein 1950). Biesecker et al. (1970) concluded that the thrombosis was secondary to an underlying primary benign bone

tumour. Intramedullary ABC following fracture has also been documented (Dabezies et al. 1982; Ratcliffe and Grimer 1993) and trauma is thought to be the cause of the majority of surface lesions (Burnstein et al. 1990).

Recently, a genetic basis has been suggested, contradicting the reactive vascular theory:

1. Gene rearrangements involving the USP6 and CDH11 oncogenes have been identified in primary but not secondary ABC (Oliveira et al. 2004).
2. Clonal aberrations have been found on chromosomes 16 and 17 (Panoutsakopoulos et al. 1999), and subsequently in soft-tissue and surface ABCs (Dal Cin et al. 2000).

Aneurysmal cystic changes superimposed on pre-existing bone lesions (secondary ABC) account for approximately one third of cases. The remainder, approximately 70% of cases, are referred to as primary ABCs.

24.2.2 Incidence

The annual incidence of primary ABC is 0.14×10^5 (Leithner et al. 1999). They account for 1–2% of primary bone tumours (Mirra et al. 1989b; Parman and Murphey 2000).

24.2.3 Age

Most patients are less than 20 years of age at presentation, with an average of 13–17.7 years (Leithner et al. 1999; Martinez et al. 1988). In a large study of 246 primary ABCs, 5.3% of patients were less than 5 years old and 2.8% over 50 years (Vergel de Dios et al. 1992). Secondary ABC occurs at an age determined by the primary tumour.

24.2.4 Gender

A slight female preponderance has been noted (Leithner et al. 1999; Vergel de Dios 1992).

24.2.5 Site

Primary ABCs are found in long and short tubular bones, the pelvis, and the axial and craniofacial skeleton (Vergel de Dios 1992).

24.2.5.1 Appendicular Skeleton

ABCs occur in the long bones of the lower limb, particularly the distal femur, proximal and distal tibia, and the short tubular of the hands and feet and tarsal bones (also a frequent site for secondary ABC). ABCs can occur anywhere in the pelvis which accounts for 50% of flat bone lesions.

24.2.5.2 Axial Skeleton

Twenty to 30% of primary ABCs occur in the spine. Any location in the fixed or mobile spine can be affected with the cervical and thoracic spines more commonly affected than the lumbar spine and sacrum (Vergel de Dios et al. 1992); however, a predilection for the lumbar spine has been reported in other series (Turker et al. 1998; Boriani et al. 2001), with the lumbar spine showing more cases per vertebra (Hay et al. 1978).

24.2.6 Skeletal Distribution

24.2.6.1 Appendicular Skeleton

In tubular bones, ABCs are metaphyseal, although the site of origin is difficult to determine in short tubular bones, when the entire bone is often involved, and also in carpal/tarsal bones. Larger lesions extend to the diaphysis. The frequency of epiphyseal involvement across the open growth plate is variable (15–23%), rising to 68% when the physis is fused (Biesecker et al. 1970; Vergel de Dios et al. 1992). Capanna et al. (1985b) described five morphological types based largely on location in long bones (Fig. 24.6): type 1, central with little expansion; type 2, central with expansion and cortical thinning; type 3, eccentric with involvement of only one cortex; type 4, subperiosteal extending "outwards" with intact or only superficially eroded cortex; and type 5, subperiosteal with growth both outwards and

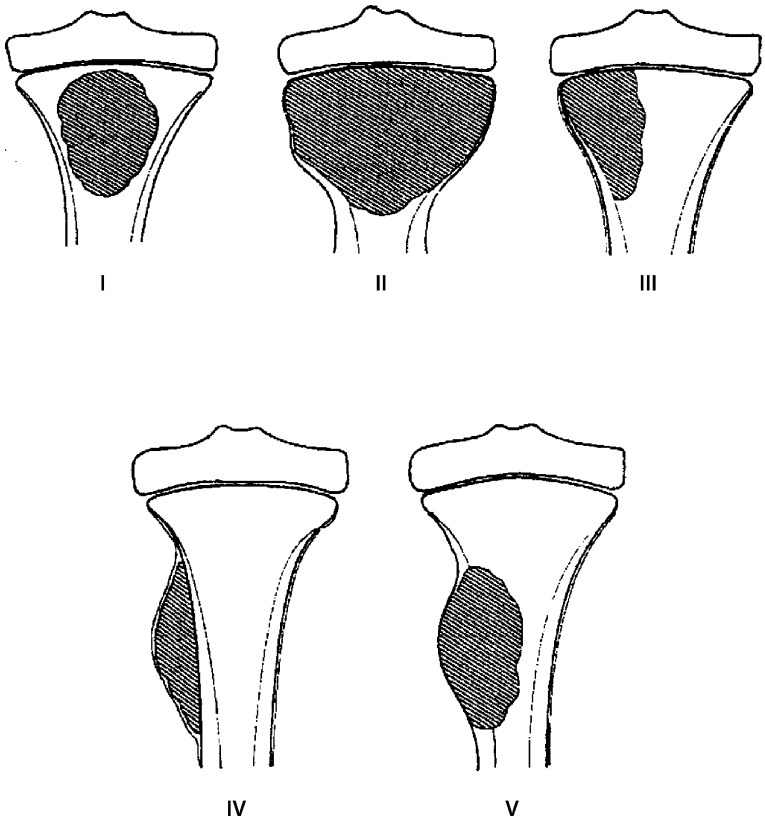

Fig. 24.6. Classification of morphological types of ABC. (After Capanna et al. 1985b. With kind permission of Springer Science + Business Media)

centrally towards the medulla, with cortical destruction (see Sect. 24.2.8.6). Central lesions (types 1 and 2) accounted for 42% and eccentric (type 3) 37% of the total; other series have suggested that most lesions are eccentric (Vergel de Dios et al. 1992). The radiographic appearance depends on the diameter of the bone affected. Surface lesions generally occur in the diaphysis (Maiya et al. 2002) and account for 16–27% of primary ABCs (Vergel de Dios et al. 1992; Capanna et al. 1985b). Contiguous bone involvement is extremely rare in the appendicular skeleton (a case of contiguous medial malleolar and talar involvement has been reported (Tillman et al. 1968). The skeletal distribution of secondary ABC is determined by the primary tumour, suggesting that the ABC component is a secondary phenomenon (Martinez et al. 1988).

In the pelvis, lesions are typically peri-acetabular but rarely cross the triradiate cartilage unless it is fused (Vergel de Dios et al. 1992).

24.2.6.2 Axial Skeleton

Both the vertebral body and neural arch are involved in the majority of cases (up to 90%; Vergel de Dios et al. 1992); however, there appears to be a predilection for the neural arch, with anterior extension to the vertebral body occurring commonly (Boriani et al. 2001). Solitary neural arch involvement occurred in 40% of spine ABCs in one series, always affecting the spinous process and lamina (Capanna et al. 1985a), while vertebral body involvement in isolation was not seen. Contiguous vertebral involvement is not infrequent.

24.2.7 Clinical Features

There is typically a short history, consisting of pain and swelling of less than 6 months' duration (Ver-

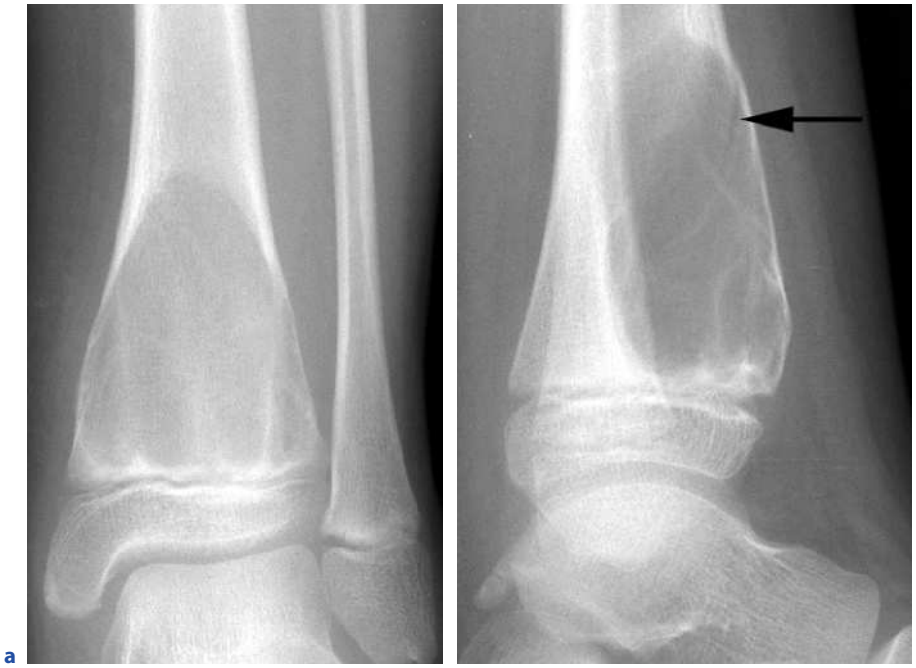

Fig. 24.7a,b. Aneurysmal bone cyst. Anteroposterior (**a**) and lateral (**b**) radiographs of left distal tibia in a 9-year-old child: centrally located lucency with slight bone expansion. A lucent line consistent with a fracture is seen anteriorly (*arrow* in **b**)

GEL DE DIOS et al. 1992); only one patient in a series of 66 ABCs had symptoms for greater than 1 year (BIESECKER et al. 1970). Occasionally, the lesion is pulsatile (BIESECKER et al. 1970). Acute pain is suggestive of pathological fracture, which is more common in the spine, found in 8% of ABCs at presentation (VERGEL DE DIOS et al. 1992).

In the spine, a mass may be palpable with neural arch and cervical lesions. Nerve root or spinal cord compression may result from a mass or pathological fracture and deformity (scoliosis and torticollis) may be presenting features (CAPANNA et al. 1985a; BORIANI et al. 2001; OZAKI et al. 1999). Of spine ABCs, 21% show evidence of fracture at presentation (VERGEL DE DIOS et al. 1992).

24.2.8 Imaging: Long Bones

24.2.8.1 Radiographs

The radiographic appearances are variable as the lesion evolves through discrete phases (Fig. 24.7; DABSKA and BURACZEWSKI 1969):

1. Initial phase: osteolysis and periosteal elevation.
2. Active/growth phase: rapid enlargement of the tumour with progressive bone destruction and poor demarcation. Aneurysmal expansion may occur to the extent that the external border is radiographically invisible, but there may be less aggressive features at the interface with host bone (a dichotomous border; PARMAN and MURPHEY 2000). Most patients become symptomatic at this time. An aggressive, lamellated periosteal reaction with Codman's triangles contributes to the appearances of an aggressive bone tumour.
3. Stabilization phase: development of the classical appearances of an ABC with a thin shell of periosteal bone and septal ossification. Periosteal reaction at the margin of the lesion matures to form a periosteal/cortical buttress at the interface with normal bone.
4. Healing phase: gradual ossification of the lesion.

The pattern of bone destruction is usually geographic. The margin is usually well-defined, except in the growth phase, and the edge variable [sclerotic (32%), sharp but not sclerotic (54%) or indistinct (14%)]. The zone of transition with host bone is usually narrow. A range of cortical reactions are possible: scalloped, expanded

or destroyed and cortical thinning may be so marked that it is not visible radiographically (but may be visible on CT). A complete, but thin, shell is visible in 63% radiographically. Matrix mineralization is rare, but in the later stages, trabeculation occurs. Periosteal reaction is common, as is the *appearance* of an extraosseous mass beyond the destroyed cortex (Vergel de Dios et al. 1992).

In the pelvis some of these features are difficult to assess due to complex anatomy.

24.2.8.2 CT

The features of the lesion are more clearly demonstrated, including a thin surrounding shell of bone or soft tissue attenuation, the latter corresponding to the fibrous periosteum (Parman and Murphey 2000), which can be helpful diagnostically, showing an extraosseous mass to be rare. Fluid-fluid levels (FFLs) were first described in ABCs using CT (Hudson 1984) and are clearly seen assuming the patient has been recumbent and stationary for sufficient time, with higher attenuation in the more dependent part. Approximately 35% of ABCs will show FFLs on CT (Parman and Murphey 2000).

24.2.8.3 MR Imaging

The FFLs within the lesion are more clearly demonstrated on MRI (Fig. 24.8), but are not unique to ABCs. They have been described in a large number of other benign and malignant bone lesions (reviewed in Alyas and Saifuddin 2008) and may not always indicate aneurysmal cystic changes. MR imaging, in combination with other imaging techniques, may be useful to exclude a secondary ABC and indicate whether the lesion is likely to be benign or malignant.

Primary ABCs consist of blood-filled spaces with thin septae and usually no or minimal solid component. A significant solid component increases the chances of an underlying lesion (and therefore a secondary ABC). In a study of 83 patients with bone lesions showing FFLs on T2-weighted or STIR images, the chance of an underlying malignant lesion was inversely related to the degree of cystic change (or directly related to the amount of solid tissue within the lesion). When the cystic spaces (FFLs) occupied less than one third of the lesion, almost 70% were malignant and half of these were conventional intramedullary osteosarcomas. With an increasing proportion of FFLs there was a greater chance of benignity: if over two thirds of the lesion contained FFLs, 89% of diagnoses were benign, and if the entire lesion was occupied by FFLs, diagnoses were benign in 100% (O'Donnell and Saifuddin 2004). The majority of predominantly cystic lesions were primary ABCs. Targeted biopsy should aim to sample any solid component.

Other MR imaging features include visualization of a low-signal peripheral rim (periosteum; Fig. 24.9) and perilesional oedema (Woertler et al. 2000); 18% of the ABCs in this study, which were primary, contained solid components. Following gadolinium-chelate, there is rim and thin septal enhancement with primary ABCs.

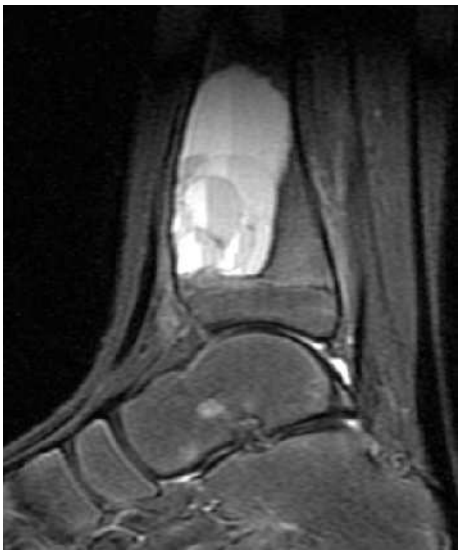

a

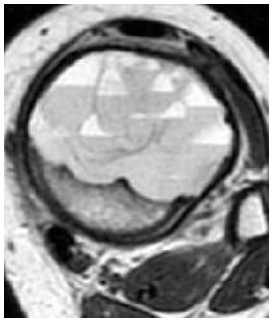

b

Fig. 24.8a,b. Aneurysmal bone cyst. Sagittal intermediate-weighted MR image with fat saturation (**a**) and transverse T2-weighted MR image (**b**) of the distal left tibia (same patient as in Fig. 24.7): there are multiple fluid-fluid levels (FFLs), no solid component and the lesion is demarcated by a low-signal margin (cortical bone)

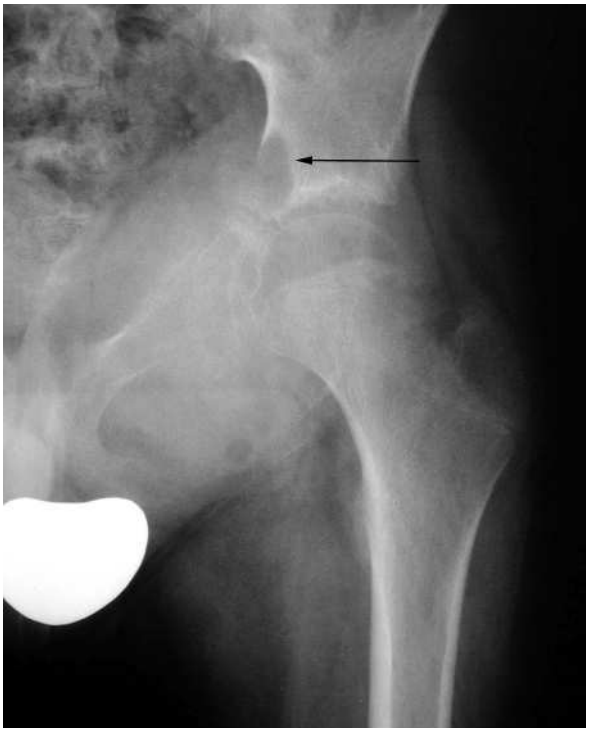

a

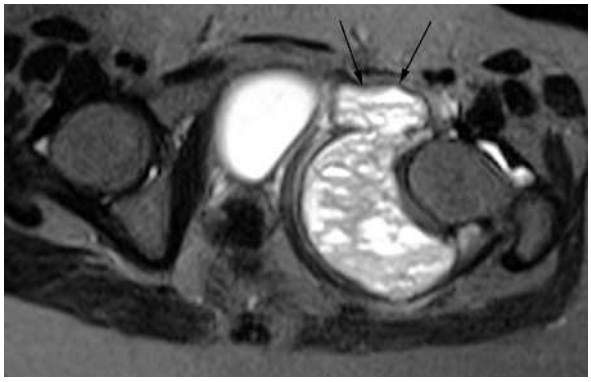

b

Fig. 24.9a,b. Aneurysmal bone cyst. Anteroposterior radiograph (**a**) and transverse T2-weighted MR image (**b**) of left acetabular ABC. The lesion involves the pubis, ischium and ilium, and shows aggressive appearances; however, the proximal (iliac) margin shows a well-defined border (*arrow*). Multiple FFLs are again seen (**b**) and the "extraosseous" mass anteriorly is shown to be enclosed by a low-signal margin (periosteum, *arrows*)

Enhancement of nodular septae, a thick peripheral rim of tissue or a significant solid component suggests secondary ABC (Parman and Murphey 2000).

Recent interest has focused on the signal characteristics of the cystic spaces and has found a greater chance of the lesion being malignant if the superior layer shows increased signal intensity on T1-weighted images compared with muscle (Van Dyck et al. 2006; Alyas and Saifuddin 2008). This may reflect recent haemorrhage and liquefied, necrotic tumour rather than serous fluid and old blood in benign lesions.

The combination of MRI with radiographs (Mahnken et al. 2003) and/or CT is essential for complete assessment, but especially for the exclusion of secondary ABC and aggressive, necrotic tumours.

24.2.8.4 Bone Scintigraphy

Isotope uptake is usually peripheral, and occasionally diffuse, but there are no specific diagnostically helpful features (Parman and Murphey 2000).

24.2.8.5 Imaging: Axial Skeleton

The imaging features are similar in the axial skeleton. Radiographs may show an expansile lesion commonly centered on the neural arch. It may be located in the concavity of a scoliosis. The thin peripheral shell of bone is best demonstrated using CT, and MRI shows similar imaging features to those in the appendicular skeleton. Involvement of more than one vertebra is not infrequent (up to 43% of lesions in one small series; Hay et al. 1978) and involvement of an adjacent rib can be seen with thoracic lesions. Vertebra plana has been reported but is rare (Turker et al. 1998).

24.2.8.6 Imaging: Surface ABC

These correspond to types 4 and 5 of Capanna's classification (Capanna et al. 1985b) and may be classified as subperiosteal, cortical or mixed, the last category containing lesions where the origin is uncertain. Surface

lesions account for 16–27% of all ABCs (Maiya et al. 2002; Capanna et al. 1985b), and show identical mean age to medullary ABCs but a 3:1 female:male ratio. There is a slightly different skeletal distribution, in that surface lesions do not appear to arise from flat bones. The histological appearance is identical to intramedullary ABC and the distinction is radiological.

Subperiosteal ABCs tend to be metadiaphyseal or diaphyseal, and show predominantly "extraosseous" extension (although surrounded by periosteum) with varying amounts of preservation of the inner cortex. Typically, a thin layer of inner cortex remains and the lesion is surrounded by a radiographically visible shell of periosteal new bone in most cases.

Cortical lesions are usually metaphyseal, showing fairly symmetrical extension into and out of bone. A peripheral shell of bone is visible less frequently than with subperiosteal lesions, but MR imaging can demonstrate low-signal margins, representing periosteum/periosteal new bone formation and endosteum. They may show more aggressive radiographic appearance (Fig. 24.10).

"Mixed" lesions show features of both cortical and subperiosteal ABCs and their site of origin is unclear.

24.2.8.7 Imaging: Solid ABC

This uncommon variant of ABC (extragnathic giant cell reparative granuloma; Oda et al. 1992) is similar to lesions found in the craniofacial skeleton and short tubular bones in the hands and feet (Ilaslan et al. 2003). Histologically, it is identical to the solid components of ABC, but there are no blood-filled cavities and this is reflected in its MRI appearances. It affects a similar age group to intramedullary ABCs (average age 18 years) and shows similar skeletal appearances with minor differences: one third of cases are not aneurysmal and in long bones, there is more variable distribution; metaphyseal and diaphyseal cases occur with almost equal frequency, and lesions are also seen in a juxta-articular, intracortical and surface location. The spine is also affected. Magnetic resonance imaging shows a predominantly solid tumour exhibiting relative hyperintensity on T1- and T2-weighted images. Oedema is common in the adjacent marrow and often striking: the appearances may mimic other benign tumours typically associated with marrow oedema, such as osteoblastoma and chondroblastoma. Cystic foci may be present within solid lesions. Histology suggests that both lesions are related to intraosseous haemorrhage, and solid ABC may represent the healing stage of conventional ABC. Secondary solid ABC has also been reported (Yamaguchi and Dorfman 2001; De Smet et al. 1982).

24.2.8.8 Imaging: Secondary ABC

Approximately 30% of ABCs occur in association with another bone lesion (Biesecker et al. 1970; Martinez and Sissons 1988), with evidence of both lesions

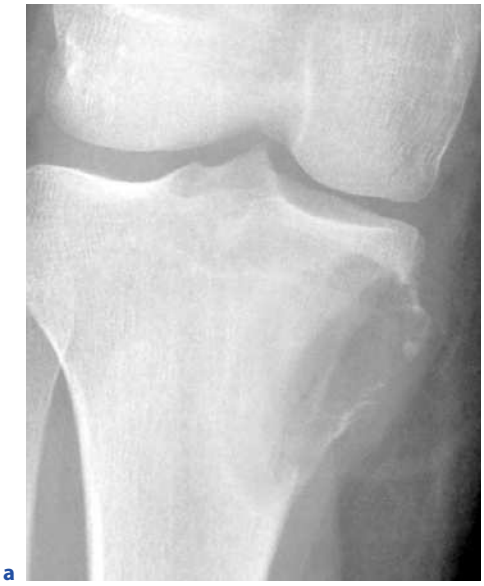

a

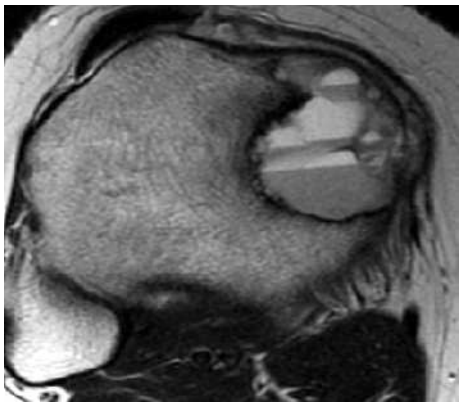

b

Fig. 24.10a,b. Surface aneurysmal bone cyst. Anteroposterior radiograph (**a**) and transverse T2-weighted MR image (**b**) of right proximal tibia: cortical ABC with aggressive bone destruction and symmetrical intra- and extraosseous extension

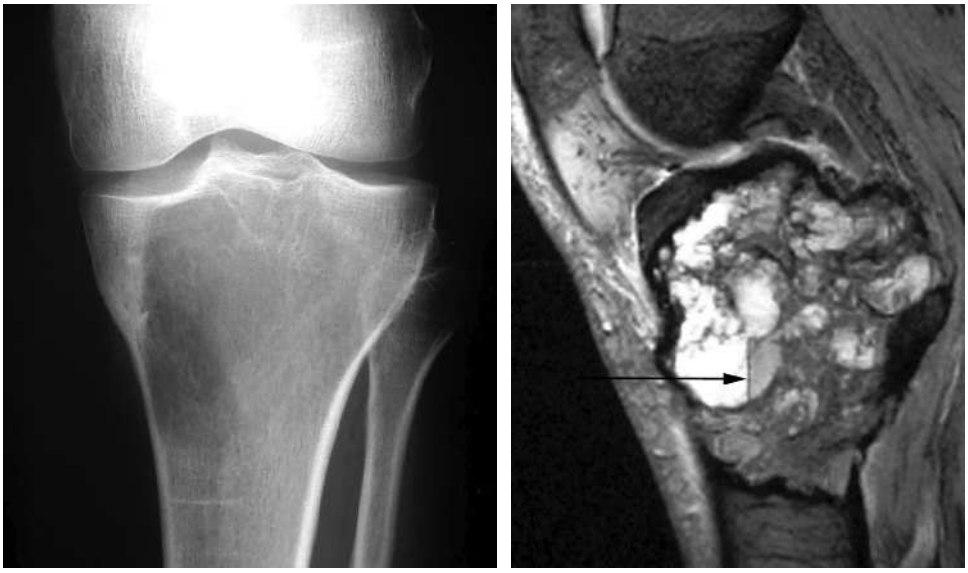

Fig. 24.11a,b. Secondary aneurysmal bone cyst. Anteroposterior radiograph (**a**) and sagittal T2GE MR image (**b**) of the left knee: the radiographic appearances are those of a giant cell tumour (GCT) in the proximal tibia. MR imaging appearances are consistent with GCT with additional aneurysmal changes anteriorly (*arrow* in **b** indicates a fluid-fluid level)

pathologically. As the radiographic appearances, patient age and skeletal site are usually those associated with the primary lesion, the ABC component has been assumed to be a secondary phenomenon. A large number of lesions may show secondary ABC formation, but the commonest include giant cell tumour (Fig. 24.11) and chondroblastoma: approximately 15% of these tumours show secondary aneurysmal changes (Martinez and Sissons 1988). Other benign lesions include non-ossifying fibroma, fibrous dysplasia, SBC, osteoblastoma and chondromyxoid fibroma (Martinez and Sissons 1988; Levy et al. 1975). Of the malignant lesions showing secondary ABC formation, osteosarcoma (OS) is the commonest, but differentiating telangiectatic OS, where the cysts are lined by sarcomatous tissue, and conventional intramedullary OS with secondary ABC, can be impossible on imaging. Occasionally, non-neoplastic lesions, such as osteomyelitis (O'Donnell and Saifuddin 2004), intraosseous ganglia (Grey et al. 1997) and brown tumours (Davies et al. 2001), show FFLs, but this finding is non-specific and usually does not reflect secondary ABC. The nature of the tissue submitted for pathological examination determines the sensitivity for detection of small foci of ABC, the diagnosis made approximately twice as frequently with resection specimens as with curettage (Martinez and Sissons 1988). There may be little radiographic suspicion of aneurysmal changes – the lesion may appear slightly more expansile than usual and MR imaging may reveal FFLs – and the ABC component may only been identified histologically.

24.2.9 Radiological Differential Diagnosis

The major differential diagnosis is telangiectatic osteosarcoma (tOS), which may resemble ABC both radiologically and histologically (Mirra et al. 1989b). TOS usually shows geographic bone destruction, metaphyseal location and expansion; however, the expansion is rarely aneurysmal, the majority has a wide zone of transition, periosteal reaction is aggressive and the cortex is destroyed with evidence of an extraosseous mass. Intravenous contrast material helps differentiate the thick, nodular septae of tOS, representing high-grade sarcomatous tissue, from the peripheral enhancement and thin septae of ABC without nodularity. The more aggressive radiographic appearance and matrix mineralization, seen in viable tumour lining the cystic spaces in up to 85% on CT, may also help differentiate tOS (Murphey et al. 2003).

Pseudocystic osteosarcoma (Sundaram et al. 2001) is a rare subgroup which on imaging is usually diagnosed as either simple or aneurysmal bone cyst. They may show slow growth without periosteal reaction or extraosseous mass, but histologically are conventional osteosarcomas. One of the cases in the series of Sundaram et al. (2001) was diagnosed originally has ABC on the basis of histology but subsequently presented with metastases. The age range in this small series was wide (3–34 years) and clinical course variable.

Low-grade central osteosarcomas (Andresen et al. 2004) are more frequently mistaken for fibrous dysplasia, but the predominantly lytic form may resemble ABC on plain radiographs. Patients are usually older (third or fourth decade) and despite the histology, there is usually an extraosseous mass. Giant cell tumours (GCT) in adults are usually subarticular, but in children they arise in the metaphysis. Distinction of SBC from ABC may also be difficult using plain radiographs: in these cases, MRI can identify a "double-density" fluid level, septations and a signal pattern suggesting ABC (low T1 signal compared with intermediate T1 signal in SBC; Sullivan et al. 1999). Other lesions often included in the radiological differential diagnosis are fibrous dysplasia and malignant lesions showing expansile bone destruction, but tending to occur in an older age group (thyroid and renal metastases; Dabska and Buraczewski 1969). Myositis ossificans may resemble a surface ABC.

24.2.10 Difficulties in Obtaining Histological Diagnosis

As both tOS and ABC contain blood-filled cavities, interpretation of small biopsy specimens, which may contain little solid material, is difficult. Viable tumour may only be present at the periphery of the lesion, surrounding cystic spaces in a thick or nodular rind (Murphey et al. 2003). Even if these areas are successfully sampled, tOS may exhibit only subtle atypia. The situation is further complicated by the rare possibility of malignant transformation of primary ABC, even those not treated with radiotherapy (Kyriakos and Hardy 1991). The question often asked in such cases is whether a small focus of tOS was missed at the time of initial diagnosis.

Needle biopsy of ABC and GCT yields osteoclast rich tissue and careful radiological/pathological correlation is needed. In the case of secondary ABC, sampling error at biopsy may miss either the ABC component or associated lesion.

24.2.11 Modern Management

Standard treatment is curettage with thorough removal of the cyst lining, followed by grafting (Green et al. 1997). Recurrence occurs in approximately 20% of cases, usually within 2 years (Vergel de Dios et al. 1992). Application of phenol to the walls of the ABC (to "sterilize" the cyst cavity) can reduce recurrence but has been associated with a number of complications (neurovascular damage, fracture, flap necrosis, osteonecrosis and growth arrest). Injection of a fibrosing agent ("Ethibloc") has been advocated as therapy for ABC but is again not without complications (transient inflammatory reaction, aseptic osteitis/abscess), and the unacceptably high rate of major complications, including pulmonary embolus and chronic fistula formation, has led one group to abandon its use (Topouchian et al. 2004). Selective arterial embolization (SAE) using gelfoam pellets (biodegradable and therefore temporary), polyvinyl alcohol (PVA) particles or coils can lead to reduction in the size of the lesion, reduced pain and occasionally bone reconstitution. This technique has been used for rapidly enlarging lesions, recurrent lesions and surgically inaccessible sites, and may be a useful adjunct to surgery, reducing intraoperative blood loss. PVA particles have been used safely to treat an ABC in the atlas (Mohit et al. 2004).

24.3 Intraosseous Ganglion

24.3.1 Synonyms

Synonyms for intraosseous ganglion (IOG) are juxtaarticular bone cyst, subchondral/synovial bone cyst, ganglionic cystic defect of bone and capsulo-synovial intraosseous inclusion (Schajowicz et al. 1979).

24.3.2 Introduction

Intraosseous ganglia are cystic lesions that usually occur in a subarticular location and show histology similar to that of soft tissue ganglia. They may be lined by a fibrous membrane and filled with mucoid, jelly-like material but do not show a continuous layer of synovium (Schajowicz et al. 1979).

Several theories have tried to explain their existence

(Helwig et al. 1994), suggesting two basic types: primary or idiopathic; and secondary to an extraosseous ganglion cyst which penetrates bone. The latter was originally thought an important cause, explaining up to half of lesions (Kambolis et al. 1973), but was subsequently shown to explain only the minority (Schajowicz et al. 1979). Theories for the aetiology of primary IOG include:

1. Intramedullary metaplasia: cellular (synoviocytic) hyperplasia within bone (stimulus uncertain, but possibly post-traumatic) is followed by differentiation to fibroblasts. These cells produce hyaluronic acid and mucoid material, which accumulates between connective tissue fibres (Goldman and Friedman 1969). There follows a degenerative phase when the enlarging cyst causes pressure atrophy of bone trabecula, resulting in the formation of an IOG.
2. Chronic trauma: either through initiation of intramedullary metaplasia, or via avascular necrosis/local vascular disturbance following repetitive micro-trauma. This results in fibrous tissue proliferation. There is usually no evidence of cystic bone necrosis histologically, but it has been suggested that this is because only mature cysts are resected or curetted, and that necrotic foci have, by this stage, been resorbed or remodelled (Schajowicz et al. 1979).
3. Acute trauma: communication with the joint has suggested a traumatic cause due to intra-articular fracture, but there is rarely a history of acute trauma (Kambolis et al. 1973).
4. Synovial herniation: in view of the peripheral location close to capsule and ligamentous insertions, herniation of synovium has been suggested particularly for carpal lesions (Crane and Scarano 1949). A closely related theory suggests synovial rests, periarticular remnants of synovial tissue, invaginate into bone. There is little histological or embryological evidence for this (Feldman and Johnston 1973).

Traditionally, IOG have been differentiated from cysts occurring in the context of degenerative or inflammatory arthritis (geode), particularly in young patients and those without radiographic evidence of arthritis. A number of features have been used to differentiate IOG from geode: age (IOG occurring in patients less than 30 years of age), presence of joint disease (patients with IOG showing no evidence of joint disease, or abnormality restricted to the site of the cyst) or a cyst which is disproportionately large relative to the degree of arthropathy (Schajowicz et al. 1979). The location of the cyst has also been suggested as an important distinguishing feature: in the hip, degenerative cysts are found in the weight-bearing regions of the acetabulum (anterosuperior location, near the anterior inferior iliac spine or acetabular–labral junction; Eggers et al. 1963) and IOG more medially in the acetabulum and in the femoral head, often extending into the neck. In other joints, IOG are identified at non- or minimal weight-bearing areas or at capsular insertions. Geodes have been considered features of joint disease that occur at a late stage when other features are usually visible (joint-space narrowing, sclerosis, osteophyte and deformity; Feldman and Johnston 1973). Communication with the joint via a disrupted articular surface has also been suggested to be common with geodes and rare with IOG, but has been shown in 57% of IOG using conventional tomography (Menges et al. 1977), and will probably be found even more frequently using multi-detector CT. Some authors have suggested that intraosseous ganglion may even be a precursor to degenerative joint disease (Eggers et al. 1963); excision of the cyst in young patients was not associated with progressive arthropathy (Schajowicz et al. 1979). However, several large series of IOG, which have attempted to differentiate these entities, included patients with radiographic evidence of osteoarthritis. The terms geode and IOG are currently used interchangeably at the discretion of the clinician, with geode more often utilized if there is radiographically visible inflammatory or degenerative arthritis. The imaging and histology of geode and IOG are, however, identical. They are likely to have a similar aetiology and the distinction, based on the degree of radiographic joint disease, may well be spurious (Williams et al. 2004); however, it is likely that use of both terms will continue, with IOG describing cysts in younger patients without evidence of arthropathy (May et al. 1997) and geode indicating subarticular cysts associated with joint disease.

24.3.3 Incidence

The exact incidence is unknown. It is a common but infrequently biopsied lesion.

24.3.4 Age

There is a wide age range. The largest series contained patients from 14 to 91 years old (Schajowicz et al. 1979; Williams et al. 2004) with a peak age in the fourth and fifth decades. Lesions occasionally have been reported in children (May et al. 1997) and in certain

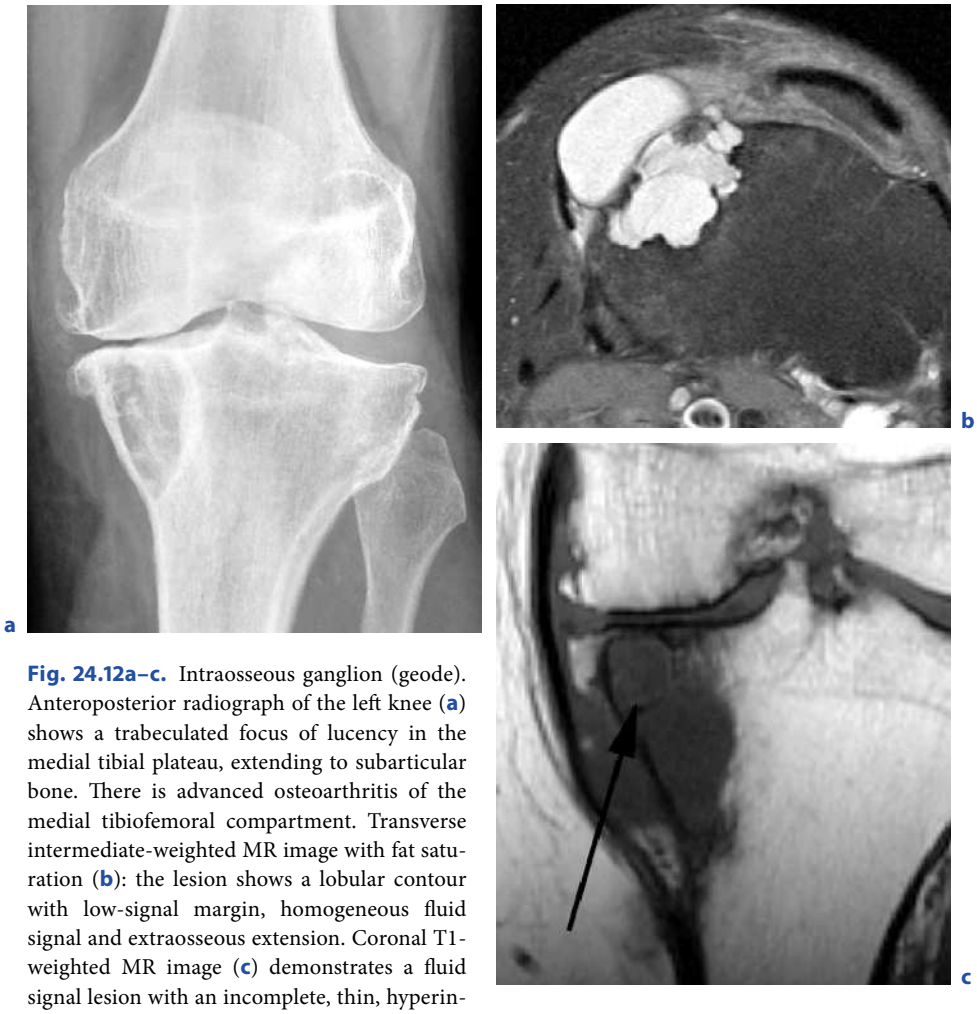

Fig. 24.12a–c. Intraosseous ganglion (geode). Anteroposterior radiograph of the left knee (**a**) shows a trabeculated focus of lucency in the medial tibial plateau, extending to subarticular bone. There is advanced osteoarthritis of the medial tibiofemoral compartment. Transverse intermediate-weighted MR image with fat saturation (**b**): the lesion shows a lobular contour with low-signal margin, homogeneous fluid signal and extraosseous extension. Coronal T1-weighted MR image (**c**) demonstrates a fluid signal lesion with an incomplete, thin, hyperintense internal margin (*arrow*)

locations (tarsal and carpal bones) tend to occur in younger patients (Schajowicz et al. 1979).

24.3.5 Gender

There is a slight male predilection (56% male; Williams et al. 2004).

24.3.6 Site

The majority of IOGs are subarticular, in long bones often extending to the metaphysis. The lesion is frequently eccentrically located.

24.3.7 Distribution

76% of IOG are related to the weight-bearing surfaces of lower limb joints (Fig. 24.12; Schajowicz et al. 1979; Williams et al. 2004.). Two thirds of lesions are found around the knee. Other common sites include locations in the lower limb (medial malleolus, hip, tarsal bones). Lesions are frequently found on both sides of a joint but are often asymmetrical in size. They may also be found in non-weight-bearing locations, for example, the glenoid (Fig. 24.13) and carpal bones. Small, apparently cystic lesions which may be multiple and symmetrical (Pablos et al. 1998) can be found in the carpus and have been found in 3.7% of patients with unexplained chronic wrist pain (Magee et al. 1995). They may also be multiple outside the wrist (Schajowicz et al. 1979,

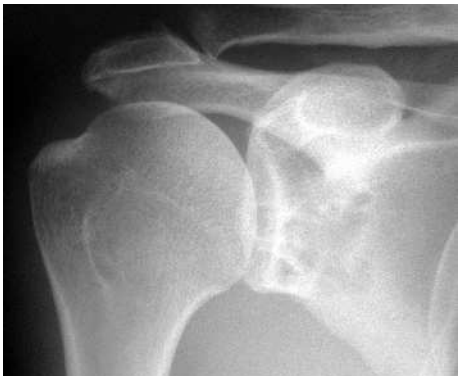
a

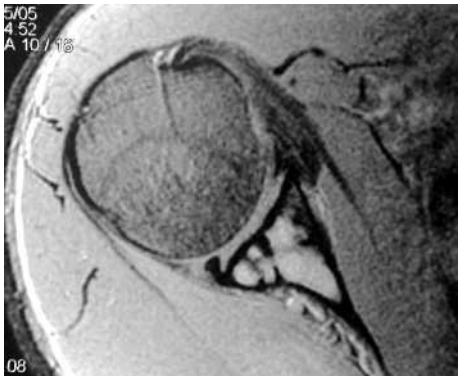
b

Fig. 24.13a,b. Intraosseous ganglion. Anteroposterior radiograph of the right shoulder (**a**): there is a well-defined, multi-locular lucent lesion with a sclerotic margin. There is no evidence of arthropathy. Axial T2GE MR image (**b**) shows the typical septated, fluid signal appearances of an IOG in subarticular bone

Feldman and Johnston 1973). Rarer sites include the ischial tuberosity, lumbar spinous process (Helwig et al. 1994), the patella (Tam et al. 1996) and first metacarpal (Nakano et al. 2001).

24.3.8 Clinical Features

IOG may be identified incidentally, but are often associated with pain (60–100% of cases; Williams et al. 2004; Schajowicz et al. 1979). It is difficult to determine the cause of pain if there is concomitant joint disease. The pain is often chronic (up to 5 years' duration; Helwig et al. 1994). If there is extraosseous extension, a mass may be palpable and may cause pressure on neurovascular structures; compression of the common peroneal nerve has been reported (Donahue et al. 1996).

24.3.9 Imaging

Imaging features have been described in detail in a series of 45 patients (Williams et al. 2004).

24.3.9.1 Radiographs

IOG are typically osteolytic, septated or trabeculated lesions located eccentrically in juxta-articular bone. Lesions range from a minimum diameter of 6 mm to a maximum of 120 mm and are elongated in the long axis of the bone. A small lesion is seen on the other side of the joint in approximately 20% of cases. About half of patients show no evidence of degenerative joint disease. A geographic pattern of bone destruction is usual with the vast majority (80%) showing a sclerotic margin (Lodwick type 1A). The zone of transition with normal bone is narrow. There is a range of cortical responses (expansion, destruction, endosteal scalloping), and fracture may occur, but there is rarely periosteal reaction. No matrix mineralization is identified. A soft tissue mass is rarely seen (4%) on plain radiographs.

24.3.9.2 CT

Computed tomography demonstrates the lobular, sclerotic border and excludes matrix mineralization. There may be cortical thinning or deficiency. Gas can be seen within the lesion if there is communication with the joint and the latter can also be shown by CT arthrography (Fig. 24.14).

24.3.9.3 MR Imaging

An IOG appears lobular and well defined. Internal signal is often slightly heterogeneous but predominately of fluid signal intensity. The majority of IOG demonstrate T1 signal intensity which is isointense to muscle, but there is occasional hyperintensity, suggesting increased

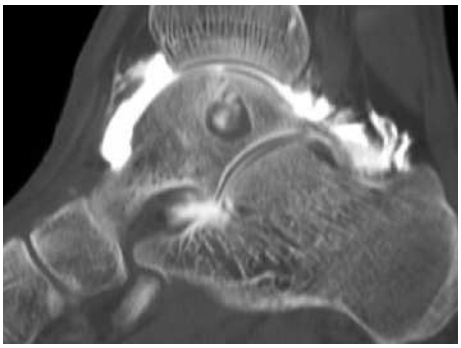

Fig. 24.14. Intraosseous ganglion. Sagittal CT arthrogram of the ankle. Contrast extends through a defect in the articular surface of the talar dome into the body

protein content. There may also be a rim of a relatively hyperintense tissue in the margin of the lesion on unenhanced images, corresponding to a fibrous membrane; most show homogeneous fluid signal intensity on T2-weighted and STIR images. A fluid-fluid level may be demonstrated, even in the absence of trauma or surgery (Grey et al. 1997). Extraosseous extension and communication with the articular surface may be demonstrated. Small cysts on the other side of the joint are more clearly seen with MRI. Following intravenous gadolinium chelate injection, there may be enhancement in the rim or occasionally heterogeneous enhancement throughout the lesion.

24.3.9.4 Bone Scintigraphy

Non-specific increased activity is seen in the region of the IOG. Large lesions may show a "doughnut" pattern with peripheral increased activity surrounding the cyst. Occasionally there is increased activity on the opposing side of the joint, even in the absence of joint disease.

24.3.10 Differential Diagnosis

Most lesions arise in a fused skeleton, and the differential diagnosis of subarticular lesions includes GCT, chondrosarcoma (particularly the clear cell type) and chondroblastoma. Cysts related to inflammatory joint disease or pigmented villonodular synovitis can usually be differentiated from intraosseous ganglia clinically and with the help of MR imaging. Brodie's abscess, which in adults can occur at the articular end of the bone, may show similar imaging features, with a sclerotic edge, a "penumbra sign" on unenhanced T1-weighted images and marrow oedema. Other lesions which may occur in this site, but which usually demonstrate more aggressive features include metastasis, malignant fibrous histiocytoma and plasmacytoma. In a child, chondroblastoma is the major differential consideration.

24.3.11 Difficulties Obtaining Histological Diagnosis

Biopsy of these lesions is infrequent, as they are usually diagnosed on imaging.

24.3.12 Modern Management

Management involves curettage and grafting with cement or bone (Helwig et al. 1994) and treatment of associated joint disease.

24.4 Miscellaneous Bone Cysts

24.4.1 Post-traumatic Cystic Defect

Small lucencies occurring after fracture have been incorrectly described as post-traumatic cysts but appear to represent foci of fat extruded from the medulla in a process comparable to lipohaemarthrosis (Roach et al. 2002). They are typically seen following greenstick or torus fractures of the distal radius but have also been described in the tibia (Malghem and Maldague 1986). On the compressive (usually dorsal) side of the fracture, fat cells originating from bone marrow are expelled into the subperiosteal space with subsequent ossification of the surrounding haematoma. These lesions

take some weeks to become radiographically visible, are usually seen just proximal to the fracture and are often solitary on radiographs but multiple on MR imaging (Durr et al. 1997). Signal on MR imaging and density on CT suggest that they consist of fat, although some groups suggest they are haematomas (Durr et al. 1997). With bone growth they migrate into the diaphysis and usually resolve spontaneously without impeding fracture healing. Post-traumatic cystic defects (which are transient) should be differentiated from other entities which continue to enlarge following fracture (which are progressive) and are either caused by, or result from, the trauma (Davids et al. 1993). Aneurysmal bone cyst following fracture has been reported, as has a case of SBC, which showed atypical imaging but compatible histology (Moore et al. 1989).

24.4.2 Cystic Fibrous Dysplasia

Cystic areas are commonly found within bones affected by FD. They were reported in 8.2% of 98 patients with FD, most commonly in the femur (Bahk et al. 2007). In every case, radiographs showed lucency next to an area of ground-glass density and MR imaging revealed corresponding signal abnormalities in keeping with fluid and fibrous areas. The cystic component was non-specific histologically and showed no epithelial lining. Cystic changes were so excessive that in one case the fibrous component was almost undetectable pathologically. The average age at presentation of cystic FD was 36.7 years.

Cystic change in FD is a cause of a progressive bone lesion following puberty. Occasionally, enlargement can be extremely rapid with superimposed cystic/haemorrhagic changes. Biopsy may be required to differentiate from secondary ABC, as the cyst may contain FFLs in the absence of aneurysmal change (Fisher et al. 1994), and also to exclude malignant transformation (Schlesinger et al. 1949).

References

Adamsbaum C, Kalifa G, Seringe R et al. (1993) Direct Ethibloc injection in benign bone cysts: preliminary report of 4 patients. Skeletal Radiol 22:317–320

Alyas F, Saifuddin A (2008) Fluid-fluid levels in bone neoplasms: variation of T1-weighted signal intensity of the superior to inferior layers: diagnostic significance on magnetic resonance imaging. Eur Radiol (Epub ahead of print)

Alyas F, Tirabosco R, Cannon S et al. (2008) "Fallen fragment sign" in Langerhans' cell histiocytosis. Clin Radiol 63:92–96

Andresen K, Sundaram M, Unni K (2004) Imaging features of low-grade central osteosarcoma of the long bones and pelvis. Skeletal Radiol 33:373–379

Bahk W, Kang Y, Rhee S et al. (2007) Cystic fibrous dysplasia in the long bone. Orthopedics 30:871–873

Baig R, Eady J (2006) Unicameral (simple) bone cysts. South Med J 99:966–976

Bhagia S, Grimer R, Davies AM et al. (1997) Ewing's sarcoma presenting as a solitary bone cyst. Skeletal Radiol 26:722–724

Biesecker J, Marcove R, Huvos A et al. (1970) Aneurysmal bone cysts. A clinicopathologic study of 66 cases. Cancer 26:615–625

Boriani S, De Iure F, Campanacci L et al. (2001) Aneurysmal bone cyst of the mobile spine. Report on 41 cases. Spine 26:27–35

Boseker E, Bickel W, Dahlin D (1968) A clinicopathologic study of simple unicameral bone cysts. Surg Gynecol Obstet 127:550–560

Broder H (1968) Possible precursor of unicameral bone cysts. J Bone Joint Surg [Am] 50-A:503–507

Burnstein M, De Smet A, Hafez G et al. (1990) Case report 611. Skeletal Radiol 19:294–297

Campanacci M, Capanna R, Picci P (1986) Unicameral and aneurysmal bone cysts. Clin Orthop Relat Res 204:25–36

Capanna R, Dal Monte A, Gitelis S et al. (1982) The natural history of unicameral bone cyst after steroid injection. Clin Orthop Relat Res 166:204–211

Capanna R, Albisinni U, Picci P et al. (1985a) Aneurysmal bone cyst of the spine. J Bone Joint Surg [Am] 67-A:527–531

Capanna R, Bettelli G, Biagini P et al. (1985b) Aneurysmal bone cysts of long bones. Ital J Orthop Traumatol 11:409–417

Chang JH, Chang JW, Park Y et al. (2003) Simple bone cyst occurring in calvarium. Acta Neurochir (Wien) 145:927–928

Chigera M, Takehi Y, Nagase M et al. (1987) A case of multiple simple bone cysts with special reference to their etiology and treatment. Arch Orthop Trauma Surg 106:390–393

Cho H, Oh J, Kim H et al. (2007) Unicameral bone cysts. A comparison of injection of steroid and grafting with autologous bone marrow. J Bone Joint Surg [Br] 89-B:222–226

Cohen J (1960) Simple bone cysts:studies of cyst fluid in six cases with a theory of pathogenesis. J Bone Joint Surg [Am] 42-A:609–616

Coskun B, Akpek S, Dogulu F et al. (2004) Simple bone cyst in spinous process of the C4 vertebra. Am J Neuroradiol 25:1291–1293

Crane A, Scarano J (1949) Synovial cysts (ganglia) of bone. Report of 2 cases. J Bone Joint Surg [Am] 49-A:355–361

Dabezies E, D'Ambrosia R, Chuinard R et al. (1982) Aneurysmal bone cyst after fracture. A report of three cases. J Bone Joint Surg [Am] 64A:617–621

Dabska M, Buraczewski J (1969) Aneurysmal bone cyst. Pathology, clinical course and radiologic appearances. Cancer 23:371–389

Dal Cin P, Kozakewich H, Goumnerova L et al. (2000) Variant translocations involving 16q22 and 17p13 in solid variant and extraosseous forms of aneurysmal bone cyst. Genes Chromosomes Cancer 28:233–234

Davids J, Graner K, Mubarak S (1993) Post-fracture lipid inclusion cyst. A case report. J Bone Joint Surg [Am] 75-A:1528–1532

Davies AM, Evans N, Mangham D et al. (2001) MR imaging of brown tumour with fluid-fluid levels: a report of three cases. Eur Radiol 11:1445–1449

De Sanctis N, Andreacchio A (2000) Elastic stable intramedullary nailing is the best treatment of unicameral bone cysts of the long bones in children? Prospective long-term follow-up study. J Pediatr Orthop 26:520–525

De Smet A, Travers H, Neff J (1982) Case report 207. Skeletal Radiol 8:314–318

Donahue F, Turkel D, Mnaymneh W et al. (1996) Intraosseous ganglion cyst associated with neuropathy. Skeletal Radiol 25:675–678

Durr H, Lienemann A, Stabler A et al. (1997) MRI of posttraumatic cyst-like lesions of bone after a greenstick fracture. Eur Radiol 7:1218–1220

Eggers G, Evans E, Blumel J et al. (1963) Cystic change in the iliac acetabulum. J Bone Joint Surg [Am] 45-A:669–722

Feldman F, Johnston A (1973) Intraosseous ganglion. Am J Roentgenol 118:328–343

Fisher A, Totty W, Kyriakos M (1994) Case report. MR appearance of cystic fibrous dysplasia. J Comput Assist Tomogr 18:315–318

Garceau G, Gregory C (1954) Solitary unicameral bone cyst. J Bone Joint Surg [Am] 36-A:267–280

Gebhart M, Blaimont P (1996) Contribution to the vascular origin of the unicameral bone cyst. Acta Orthop Belg 62:137–143

Goldman R, Friedman N (1969) Ganglia ("synovial" cysts) arising in unusual locations. Clin Orthop Relat Res 63:184–189

Goto T, Nemoto T, Okuma T et al. (2007) Mirror-image solitary bone cyst of the humerus in a pair of mirror-image monozygotic twins. Arch Orthop Trauma Surg (Epub ahead of print)

Green J, Bellemore M, Marsden F (1997) Embolization in the treatment of aneurysmal bone cysts. J Pediatr Orthop 17:440–443

Grey A, Mangham D, Davies AM et al. (1997) Fluid-fluid level in an intraosseous ganglion. Skeletal Radiol 26:667–670

Gupta A, Crawford A (1996) Solitary bone cysts with epiphyseal involvement: confirmation with magnetic resonance imaging: a case report and review of the literature. J Bone Joint Surg [Am] 78-A:911–915

Hammoud S, Frassica F, McCarthy E (2006) Ewing's sarcoma presenting as a solitary cyst. Skeletal Radiol 35:533–535

Hashemi-Nejad A, Cole W (1997) Incomplete healing of simple bone cysts after steroid injections. J Bone Joint Surg [Br] 79-B:727–730

Hay M, Paterson D, Taylor T (1978) Aneurysmal bone cysts of the spine. J Bone Joint Surg [Br] 60-B:406–411

Helwig U, Lang S, Baczynski M et al. (1994) The intraosseous ganglion. A clinical–pathological report on 42 cases. Arch Orthop Trauma Surg 114:14–17

Hudson T (1984) Fluid levels in aneurysmal bone cysts: a CT feature. Am J Roentgenol 141:1001–1004

Ilaslan H, Sundaram M, Unni K (2003) Solid variant of aneurysmal bone cysts in long tubular bones: giant cell reparative granuloma. Am J Roentgenol 180:1681–1687

James A, Coley B, Higinbotham N (1948) Solitary unicameral bone cyst. Arch Surg 57:137–147

Kaelin A, MacEwen G (1989) Unicameral bone cysts. Natural history and the risk of fracture. Int Orthop 13:275–282

Kambolis C, Bullough P, Jaffe H (1973) Ganglionic cystic defects of bone. J Bone Joint Surg [Am] 55-A:496–505

Killian J, Wilkinson L, White S et al. (1998) Treatment of unicameral bone cyst with demineralised bone matrix. J Pediatr Orthop 18:621–624

Komiya S, Minamitani K, Sasaguri Y et al. (1993) Simple bone cyst treatment by trepanation and studies on bone resorptive factors in cyst fluid with a theory of its pathogenesis. Clin Orthop Relat Res 287:204–211

Komiya S, Tsuzuki K, Mangham D et al. (1994) Oxygen scavengers in simple bone cysts. Clin Orthop Relat Res 308:199–206

Kyriakos M, Hardy D (1991) Malignant transformation of aneurysmal bone cyst, with an analysis of the literature. Cancer 68:1770–1780

Leithner A, Windhager R, Lang S et al. (1999) Aneurysmal bone cyst. A population based epidemiologic study and literature review. Clin Orthop Relat Res 363:176–179

Levy W, Miller A, Bonakdapour A et al. (1975) Aneurysmal bone cyst secondary to other osseous lesions: report of 57 cases. Am J Clin Pathol 63:1–8

Lichtenstein L (1950) Aneurysmal bone cyst. A pathological entity commonly mistaken for giant-cell tumor and occasionally for hemangioma and osteogenic sarcoma. Cancer 3:279–289

Lokiec F, Ezra E, Khermosh O et al. (1996) Simple bone cysts treated by percutaneous autologous marrow grafting: a preliminary report. J Bone Joint Surg [Br] 78-B:934–937

Magee T, Rowedder A, Degnan G (1995) Intraosseous ganglia of the wrist. Radiology 195:517–520

Mahnken A, Nolte-Ernsting C, Wildberger J et al. (2003) Aneurysmal bone cyst: value of MR imaging and conventional radiography. Eur Radiol 13:1118–1124

Maiya S, Davies AM, Evans N et al. (2002) Surface aneurysmal bone cysts: a pictorial review. Eur Radiol 12:99–108

Malghem J, Maldague B (1986) Transient fatty cortical defects following fractures in children. Skeletal Radiol 15:369–371

Margau R, Babyn P, Cole W et al. (2000) MR imaging of simple bone cysts in children: not so simple. Pediatr Radiol 30:551–557

Martinez V, Sissons H (1988) Aneurysmal bone cyst. A review of 123 cases including primary lesions and those secondary to other bone pathology. Cancer 61:2291–2304

May D, McCabe K, Kuivila T (1997) Intraosseous ganglion in a 6-year-old boy. Skeletal Radiol 26:67–9

Menges V, Prager P, Cserhati M et al. (1977) Das intraossäre Ganglion. Z Orthop 115:67–75

Mirra J (1989a) Simple bone cyst. In: Mirra J, Picci P, Gold R (eds) Bone tumors. Clinical, radiologic and pathologic correlations. Lea and Febiger, Philadelphia pp 1235–1267

Mirra J (1989b) Aneurysmal bone cyst. In: Mirra J, Picci P, Gold R (eds) Bone tumors. Clinical, radiologic and pathologic correlations. Lea and Febiger, Philadelphia, pp 1267–1309

Mirra J, Bernard G, Bullough P et al. (1978) Cementum-like bone production in solitary bone cysts (so-called "cementoma" of long bones). Report of three cases. Electron microscopic observations supporting a synovial origin to the simple bone cyst. Clin Orthop Relat Res 135:295–307

Mohit A, Eskridge J, Ellenbogen R et al. (2004) Aneurysmal bone cyst of the atlas: successful treatment through selective arterial embolization: case report. Neurosurgery 55:1001–1005

Moore T, King A, Travis R et al. (1989) Post-traumatic cysts and cyst-like lesions of bone. Skeletal Radiol 18:93–97

Murphey M, Jaovisidha S, Temple T et al. (2003) Telangiectatic osteosarcoma:radiologic–pathologic correlation. Radiology 229:545–553

Nakano H, Itoh T, Katoh Y et al. (2001) Intraosseous ganglion of the first metacarpal bone. Skeletal Radiol 30:596–599

Namazi H (2008) Practice pearl: a novel use of Botulinum toxin for unicameral bone cyst ablation. Ann Surg Oncol 15:657–658

Neer C, Francis K, Johnston A et al. (1973) Current concepts on the treatment of solitary unicameral bone cyst. Clin Orthop 97:40–51

O'Donnell P, Saifuddin S (2004) The prevalence and diagnostic significance of fluid-fluid levels in focal lesions of bone. Clin Radiol 33:330–336

Oda Y, Tsuneyoshi M, Shinohara N (1992) "Solid" variant of aneurysmal bone cyst (extragnathic giant cell reparative granuloma) in the axial skeleton and long bones. A study of its morphologic spectrum and distinction from allied giant cell lesions. Cancer 70:2642–2649

Oliveira A, Perez-Atayde A, Inwards C et al. (2004) USP6 and CDH11 oncogenes identify the neoplastic cell in primary aneurysmal bone cysts and are absent in so-called secondary aneurysmal bone cysts. Am J Pathol 165:1773–1780

Ozaki T, Halm H, Hillman A et al. (1999) Aneurysmal bone cysts of the spine. Arch Orthop Trauma Surg 119:159–162

Pablos J, Valdes J, Gavilan F (1998) Bilateral lunate intraosseous ganglia. Skeletal Radiol 27:708–710

Panoutsakopoulos G, Pandis N, Kyriazoglu I et al. (1999) Recurrent t(16;17)(q22;p13) in aneurysmal bone cysts. Genes Chromosomes Cancer 26:265–266

Parman L, Murphey M (2000) Alphabet soup: cystic lesions of bone. Semin Musculoskelet Radiol 4:89–101

Phemister D, Gordon J (1926) The etiology of solitary bone cyst. J Am Med Assoc 87:1429–1433

Pommer G (1920) Zur Kenntnis der progressiven Hämatom- und Phlegmasieveränderungen der Röhrenknochen auf Grund der mikroskopischen Befunde im neuen Knochenzystenfalle. H. v. Haberers. Arch Orthop Unfallchir 17:17–69

Ratcliffe P, Grimer R (1993) Aneurysmal bone cyst arising after tibial fracture. A case report. J Bone Joint Surg [Am] 75A:1225–1227

Richkind K, Mortimer E, Mowery-Rushton P et al. (2002) Translocation (16;20)(p11.2;q13): sole cytogenetic abnormality in a unicameral bone cyst. Cancer Genet Cytogenet 137:153–155

Roach R, Cassar-Pullicino V, Summers B (2002) Paediatric post-traumatic cortical defects of the distal radius. Pediatr Radiol 32:333–339

Roposch A, Saraph V, Linhart W (2000) Flexible intramedullary nailing for the treatment of unicameral bone cysts in long bones. J Bone Joint Surg [Am] 82-A:1447–1453

Roposch A, Saraph V, Linhart W (2004) Treatment of femoral neck and trochanteric simple bone cysts. Arch Orthop Trauma Surg 124:437–442

Sanerkin N (1979) Old fibrin coagula and their ossification in simple bone cysts. J Bone Joint Surg [Br] 61-B:194–199

Scaglietti O, Marchetti P, Bartolozzi P (1982) Final results obtained in the treatment of bone cysts with methylprednisolone acetate (depo-medrol) and a discussion of the results achieved in other bone lesions. Clin Orthop Relat Res 165:33–42

Schajowicz F, Sainz M, Slullitel J (1979) Juxta-articular bone cysts (intra-osseous ganglia). A clinicopathological study of eighty-eight cases. J Bone Joint Surg [Br] 61-B:107–116

Schlesinger P, Keats S, Ruoff A (1949) Fibrous dysplasia: report of a case. J Bone Joint Surg [Am] 31-A:187–191

Shinozaki T, Arita S, Watanabe H et al. (1996) Simple bone cysts treated by multiple drill-holes: 23 cysts followed 2–10 years. Acta Orthop Scand 67:288–290

Struhl S, Edelson C, Pritzker H et al. (1989) Solitary (unicameral) bone cyst. The fallen-fragment sign revisited. Skeletal Radiol 18:261–265

Stürz H, Witt A (1979) Solitary bone cysts of the ulna. Arch Orthop Trauma Surg 31:105–108

Sullivan R, Meyer J, Dormans J et al. (1999) Diagnosing aneurysmal and unicameral bone cysts with magnetic resonance imaging. Clin Orthop Relat Res 366:186–190

Sundaram M, Totty W, Kyriakos M et al. (2001) Imaging findings in pseudocystic osteosarcoma. Am J Roentgenol 176:783–788

Tam W, Resnick D, Haghighi P et al. (1996) Intraosseous ganglion of the patella. Skeletal Radiol 25:588–591

Tillman B, Dahlin D, Lipscomb P et al. (1968) Aneurysmal bone cyst: an analysis of ninety-five cases. Mayo Clin Proc 43:478–495

Topouchian V, Mazda K, Hamze B et al. (2004) Aneurysmal bone cysts in children: complications of fibrosing agent injection. Radiology 232:522–526

Turker R, Mardjetko S, Lubicky S (1998) Aneurysmal bone cysts of the spine: excision and stabilization. J Pediatr Orthop 18:209–213

Van Dyck P, Vanhoenacker P, Vogel J et al. (2006) Prevalence, extension and characteristics of fluid-fluid levels in bone and soft tissue tumors. Eur Radiol 16:2644–2651

Vayego S, de Conti O, Varella-Garcia M (1996) Complex cytogenetic rearrangement in a case of unicameral bone cyst. Cancer Genet Cytogenet 86:46–49

Vergel de Dios A, Bond J, Shives T et al. (1992) Aneurysmal bone cyst. A clinicopathologic study of 238 cases. Cancer 69:2921–2931

Violas P, Salmeron F, Chapuis M et al. (2004) Simple bone cysts of the proximal humerus complicated with growth arrest. Acta Orthop Belg 70:166–170

Wada R, Lambert R (2005) Deposition of intraosseous fat in a degenerating simple bone cyst. Skeletal Radiol 34:415–418

Williams H, Davies AM, Allen G et al. (2004) Imaging features of intraosseous ganglia: a report of 45 cases. Eur Radiol 14:1761–1769

Woertler K, Blasius S, Hillmann A et al. (2000) MR morphology of primary aneurysmal bone cysts: a retrospective analysis of 38 cases. Rofo 172:591–596

Yamaguchi T, Dorfman H (2001) Giant cell reparative granuloma. A comparative clinicopathologic study of lesions in gnathic and extragnathic sites. Int J Surg Pathol 9:189–200

Zehetgruber H, Bittner B, Gruber D et al. (2005) Prevalence of aneurysmal and solitary bone cysts in young patients. Clin Orthop Relant Res 439:136–143

Langerhans Cell Histiocytosis

25

Karl Johnson and David Hobin

CONTENTS

K. Johnson, MB Bch, MRCP, FRCR
Birmingham Children's Hospital, Steelhouse Lane, Birmingham, B4 6NH, UK

D. Hobin, MB Bch, MRCPCH
Birmingham Children's Hospital, Steelhouse Lane, Birmingham, B4 6NH, UK

KEY POINTS

- Langerhans cell histiocytosis replaces the other descriptive terms for this idiopathic disorder that included histiocytosis X and eosinophilic granuloma.
- LCH is a multisystemic disorder that can affect any organ. Prognosis depends on age of onset and extent of disease involvement.
- Skeletal involvement is common.
- Typically skeletal lesions are well defined. The presence of sclerotic margin is variable.
- Flat bones often have a central button sequestrum.
- A radiographic skeletal survey is the current screening examination of choice, but the use of whole body MR imaging is being increasingly used.

25.1 Introduction

Since its first description over a century ago (Hand 1893), there has been relatively little improvement in our understanding of Langerhans Cell Histiocytosis (LCH); it remains an enigmatic disease entity. There have been a number of different descriptions of LCH, all of which were initially thought to represent different disease types; however, over more recent times it has become clear that conditions such as Hand-Schueller-Christian disease, Letterer-Siwe disease, Histiocytosis X and eosinophilic granuloma, for example, are all "variations on a theme". Indeed all of these and similar entities have been brought together as LCH following the work of the Histiocyte Society who, in addition, have done much to try to add clarity to the classification of Histiocyte-derived disorders recognising the pathological role

of Langerhans cells in all aspects of LCH (Stull et al. 1992; Favara 1991; Favara et al. 1997; Chu et al. 1987; Coppes-Zantinga and Egeler 2002; Komp 1987; Writing Group of the Histiocyte Society 1987).

25.2 Nomenclature and History

The first description of this disorder was by Dr. Thomas Smith in 1865. In 1868, Paul Langerhans described a non-pigmentary dendritic cell in the epidermis which is the hallmark of the disorder (Hoover et al. 2007).

In 1893 Alfred Hand described a child with exophthalmos polyuria and polydipsia, in 1915 Arthur Schueller described two further children with similar findings, and in 1920 Henry Christian described a child with skull lesions, diabetes insipidus and exophthalmos. This led to the use of the term Hand-Schueller-Christian disease, which is a chronic disseminated form of LCH associated with skeletal involvement, retarded growth and development, exophthalmos, blindness, hearing loss, progressive ataxia, diabetes insipidus, hepatosplenomegaly, and dermatological changes. This form of the disease is most commonly seen in children of 10–14 years of age (Komp 1987; Coppes-Zantinga and Egeler 2002; Hoover et al. 2007).

In 1924 Erich Letterer described an acute disorder of the reticuloendothelial system in a 6-month-old child, followed in 1933 by Sture Siwe who described a similar case of splenomegaly, hepatomegaly, bone lesions and lymphadenopathy, with histocytic hyperplasia in a young child. Further children with similar disorders have subsequently been described. This led to the use of the description Letterer-Siwe disease, which typically occurs in children under 1 year of age who have an acute onset of hepatosplenomegaly, rash, lymphadenopathy, and pulmonary involvement. Skeletal involvement may not be present (Grundy and Ellis 1986; Oberman 1961; Avery et al. 1957; Lichtenstein 1953).

A number of authors have described solitary granulomatous histiocytic lesions of the bone which are termed eosinophilic granuloma. These lesions are confined to the bone and relatively benign in nature and are most common in children of 10–14 years of age.

Histological observation of Hand-Schuller-Christian disease, Letterer Siwe disease and eosinophilic granuloma has shown identical histological patterns and it was suggested that all three conditions should be named Histiocytosis X, the X as a consequence of the unknown aetiology. While the histological features in all three conditions are similar, the clinical presentation, severity degree of symptoms and outcome is very different.

Further research suggested that the cells which appeared in all three forms were Langerhans granuloma cells and it was therefore proposed that the name should be changed to Langerhans Cell Histiocytosis. The Writing Group of the Histiocyte Society has established a histiocytosis classification system based on distinct pathologic criteria and on the clinical evolution of disease. Langerhans cell histiocytosis was designated as class I of these histiocytic disorders (Table 25.1) (Writing Group of the Histiocyte Society 1987; Osband and Pochedly 1987; Scmidt et al. 2004; Hoover et al. 2007).

25.3 Pathogenesis

Langerhans cells are part of a family of bone marrow-derived cells whose role is that of antigen presentation (dendritic cells and Langerhans cells) and antigen processing (monocytes and tissue macrophages). Although clonality has been described of the lesional Langerhans cells in LCH, the disease is not regarded as a malignant

Table 25.1. Classification of histiocytoses

Class I	Class II	Class III
• Langerhans cell histiocytosis • Secondary dendritic processes • Juvenile Xanthogranuloma • Solitary dendritic histiocytoma	• Haemophagocytic lymphohistiocytosis (HLH) • Sinus histiocytosis with massive lymphadenopathy (Rosai-Dorfman disease) • Multicentric reticulohistiocytosis	• Acute monocytic leukaemia • True histiocytic lymphoma

It should be noted that malignant histiocytosis, originally regarded as Class III histiocytosis, has subsequently been recognised and reclassified as anaplastic large cell lymphoma (ALCL)

Table 25.2. The current treatment recommendations for LCH according to patient risk of reactivation/mortality

Group 1	Multi-system "Risk" Patients: Multi-system patients WITH involvement of one or more "RISK" organs, i.e. haemopoietic system, liver, spleen or lungs
Group 2	Multi-system "Low Risk" Patients: Multi-system patients with multiple organs involved but WITHOUT involvement of "RISK" organs
Group 3	Single system "Multifocal bone disease" and localized "Special site" involvement: Patients with multifocal bone disease, i.e. lesions in 2 or more different bones Patients with localised special site involvement, like "CNS-RISK" lesions with intracranial soft tissue extension or vertebral lesions with intraspinal soft tissue Extension

process, but more that of a reactive one (Favara et al. 1997; Willman et al. 1994; Dreyer et al. 1991). As these cells progress through a maturation process they migrate from the marrow via peripheral blood to reside within most organs (e.g. Kupffer cells within the liver, Langerhans cells within the epidermis). The differing roles of such cells, i.e. antigen presentation and processing, has lead to a proposed classification system for the histiocytoses. Class I relate to a primary proliferation of the dendritic/Langerhans cells; Class II includes disorders primarily related to mononuclear cells (macrophages) and Class III histiocytoses represent the truly malignant disorders (Table 25.1).

LCH is the commonest of the histiocytic disorders and although it can occur at any age there is a predominance in young children (first 5 years of life) with a male:female ratio of 2:1 (Carstensen and Ornvold 1993). The aetiology of LCH remains unclear (Nesbit et al. 1981; Weitzman and Egeler 2008). A variety of immunological anomalies have been described in patients with LCH, but none of these have allowed the identification of an underlying aetiological agent or process. The clinical presentation of LCH is extremely diverse ranging from an isolated "single system" lesion, usually bone or skin, to that of widespread multiple organ involvement often with evidence of significant organ dysfunction. The course of the disease is equally diverse from a lesion with the potential to undergo spontaneous regressions, through a rapidly progressive disease process with an associated mortality to a more chronic resolving and recurring pattern with the ability to cause permanent end-organ damage. A definitive diagnosis of LCH can only be made on histological examination of the lesion of concern. This requires the demonstration of CD1a positivity on immunohistochemistry or the presence of Birbeck granules on electron microscopy (Broadbent et al. 1989; Refabert et al. 1996; Betts et al. 1998).

25.4 Incidence

LCH is a rare disease and its estimated annual incidence is 0.05–0.5 per 100,000 children in the United States. Males are slightly more commonly affected than females (2:1) and it is commoner in Caucasians. Cases usually present under 30 years of age, with the mean age being 5–7 years. It can present from the neonatal period up to old age.

The age of onset typically varies according to the type of disease presentation, multifocal disease often occurs before 10 years of age and non-osseous manifestations usually predominate. The more localised osseous most commonly presents around 5–15 years (Scmidt et al. 2004; Hoover et al. 2007).

25.5 Clinical Presentation

Clinical features will be determined by the age of the patient, the exact localisation and the extent of the disease. Signs and symptoms therefore cover a broad clinical spectrum and individual cases may only have a few features whereas some cases may have a considerable number. For example, very young children can present with life threatening LCH involving all organs (often sparing the kidney and gonads), while in the older patient there may just be a single organ (often bone) involved with a 100% survival rate and no residual symptoms. Some patients can have a chronic relapsing course which may leave them with residual disability.

The commonest signs and symptoms are those localised to the musculoskeletal system which includes bone pain, limb tenderness and soft tissue swelling.

Often sites of bone involvement are asymptomatic and their frequency may be underestimated. New bone lesions typically develop in within 1–2 years, but it can be longer. Bone lesions can cause deformity and result in pathological fractures. In the skull, lesions can cause otitis media with destruction of the temporal and mastoid bones, resulting in deafness and loose teeth (so-called 'floating teeth'). Spinal cord compression has been described as has extension into the nervous system.

In the multifocal forms, the classical symptoms are diabetes insipidus, exophthalmos. Other extra-skeletal features include hepatosplenomegaly, lymphadenopathy, exophthalmos, skin rash, an enlarged thymus, acute mastoiditis and gingivitis. Pulmonary involvement can cause lung fibrosis which may lead to tachypnoea, dyspnoea and cough.

25.6 Treatment

The treatment for LCH has evolved somewhat over recent decades. The relative rarity of this condition and the wide spectrum of clinical manifestations have required a standardised approach to the stratification of the disease and the treatment applied. The Histiocyte Society has driven the establishment of international multicentre clinical trials for the treatment of LCH, the first of which opened to recruitment in 1991. It has become clear that those individuals with "Single system" disease have a good prognosis and require minimal therapy. In contrast, however, those with "Multi-system" disease, more frequent in the younger patients (<2 years), have a significantly worse prognosis and an associated risk of death and require therapy with cytotoxic agents (Ceci et al. 1988; Gadner et al. 1994). Within this latter group, it has also been possible to identify further prognostic factors by determining involvement of so-called "Risk" organs; these includes liver, spleen, lungs and haemopoetic system. Early clinical trials also indicated that response to treatment with chemotherapy and steroids at 6 and 12 weeks in this group of patients is important and showed a 75% mortality if the disease was still active or had progressed at such time points in this cohort of patients. In addition, protracted therapy over a period of 12 months also showed a benefit (Gadner et al. 1994; Minkov et al. 2001).

Thus the current treatment recommendations for LCH aims to stratify patients according to their risk of reactivation/mortality and categorises patients into three groups (Table 25.2).

Groups 1 and 2 receive a total of 12 months therapy whilst Group 3 receives only 6-months total therapy. Therapy for LCH includes the use of prednisolone, vinblastine and 6-mercaptopurine. Figure 25.1 summarises the current recommended treatment for LCH.

Treatment for patients with refractory disease remains a major challenge with little overwhelming evidence to support any particular regimen. Some have looked at the addition of cyclosporin A (CSA) to vinblastine and steroids, sustained response was rarely seen (Ceci et al. 1988). Monoclonal antibody therapy directed against CD1a may provide a possible therapeutic strategy (Ceci et al. 1988). More recent interest has focused on 2-chlorodeoxyadenosine (2-CdA); this is a deoxyadenosine analogue resistant to deoxyadenosine aminase when phosphorylated, resulting in accumulation and subsequent inhibition of DNA synthesis and cell death. There is no evidence to support highly immunosuppressive therapy along with stem cell transplantation for resistant LCH, although with new reduced intensity conditioning regimens and improvements in transplant-related mortality, this debate may re-open (Mahmoud et al. 1991; Kelly and Pritchard 1994).

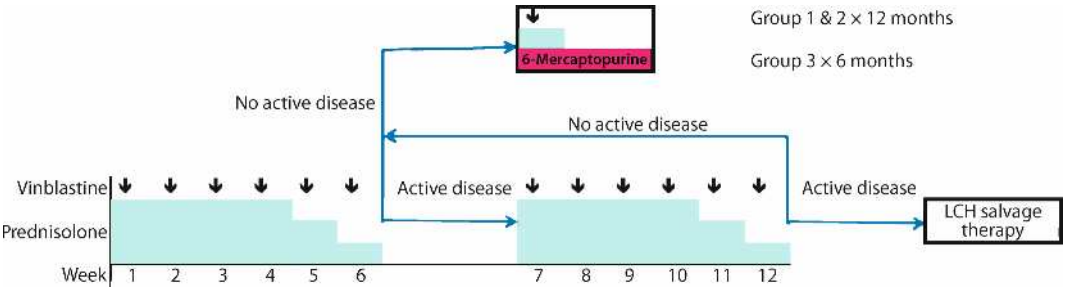

Fig. 25.1. Summary of treatment for LCH

25.7 Skeletal Disease

Any site in the skeleton can be involved, the commonest being the skull, mandible, spine, ribs, pelvis, and long bones. Lesions in the sternum and clavicle are less frequently seen, while hand and feet involvement is rare. Flat bone involvement is commoner in adults. Solitary lesions are more common than multiple lesions, but multifocal disease may develop in up to 10% of cases (Stull et al. 1992).

25.7.1 Radiographic Features

The radiographic features of LCH will vary depending on the location and stage of the disease. Generally lesions are lytic, but the margins may be ill defined or well demarcated and sclerosis may or may not be present. In the early phase of the disease lesions appear more lytic and aggressive; later they become more demarcated with increase sclerosis. Remodelling, bone expansion, periosteal reaction and soft tissue extension can occur. Lesion can resolve completely (Hoover et al. 2007; Ghanem et al. 2003; Kilpatrick et al. 1995; Stull et al. 1992).

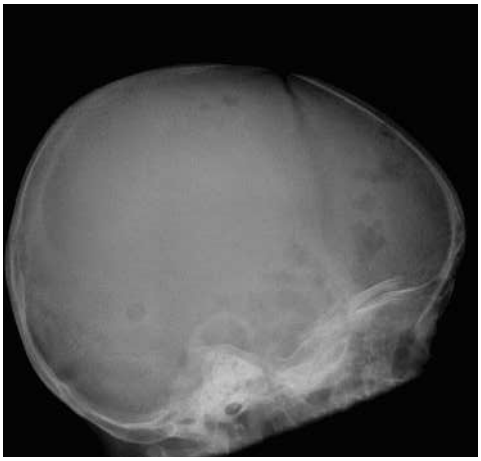

Fig. 25.2. Lateral skull radiograph shows multiple lytic skull lesions which have well defined but bevelled margins

25.7.1.1 Skull and Mandible

There are single or multiple well defined round or oval lytic defects which initially do not have a sclerotic rim ('punched out' appearance). As the lesion heals, a sclerotic rim may occur. There is no periosteal reaction. In the centre of some of the lesions there may be a small radiodense focus, the so-called 'button sequestrum' or 'bulls-eye' appearance. The edge of the lesion often has a slightly bevelled appearance, due to differential involvement of the outer and inner skull tables (Fig. 25.2). Multiple lesions can coalesce, creating a larger 'geographic' appearance; this is typically associated with chronic disease. Confluent lesions may create a 'hole within a hole' appearance (Stull et al. 1992; Kilborn et al. 2003; Berry and Brecon 1987; Ochsner 1966; David et al. 1989).

Vault lesions are commoner in the parietal and frontal bones and they rarely cross suture lines. Soft tissue masses can accompany skull lesions, with extension to dura and brain being described.

At the skull base the temporal bone, petrous ridge and mastoids can be affected. Involvement of the alveolar portion of the mandible causes a loss of supporting structure around the teeth, the so-called a 'floating teeth' appearance. A similar finding can occur in the maxilla.

25.7.1.2 Other Flat Bones

Pelvic lesions are initially poorly defined osteolytic lesions which gradually become better defined with surrounding sclerosis. The appearances can resemble those seen in the skull with a multiloculated scalloped border (Fig. 25.3). Rib involvement can create a geographic, moth eaten or permeative pattern. Any periosteal reaction is typically related to a pathological fracture and, there may be an accompanying soft tissue mass. Clavicular lesions are more varied and periosteal reaction is more common. Scapula lesions are similar to those in the pelvis and skull (Schlesinger et al. 1986; Stull et al. 1992; Hoover et al. 2007).

25.7.1.3 Spine

The classic spinal lesion is vertebral plana, which is complete collapse and flattening of the vertebral body (so-called 'coin on edge' appearance) but the vertebral disc

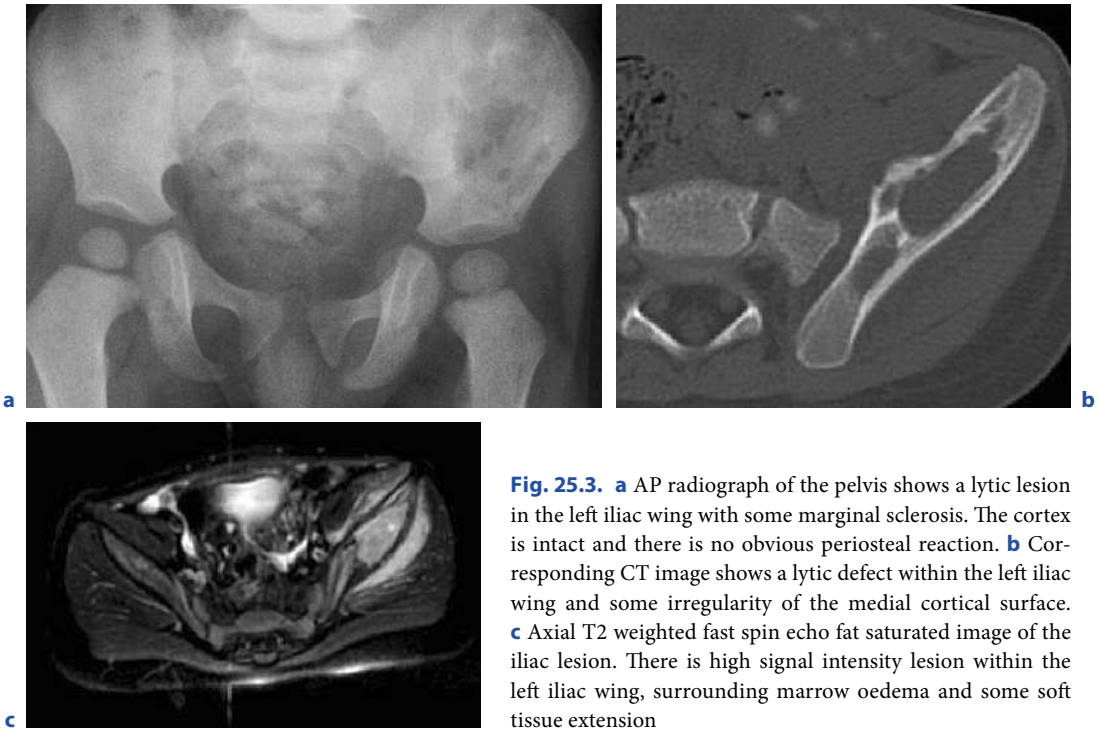

Fig. 25.3. **a** AP radiograph of the pelvis shows a lytic lesion in the left iliac wing with some marginal sclerosis. The cortex is intact and there is no obvious periosteal reaction. **b** Corresponding CT image shows a lytic defect within the left iliac wing and some irregularity of the medial cortical surface. **c** Axial T2 weighted fast spin echo fat saturated image of the iliac lesion. There is high signal intensity lesion within the left iliac wing, surrounding marrow oedema and some soft tissue extension

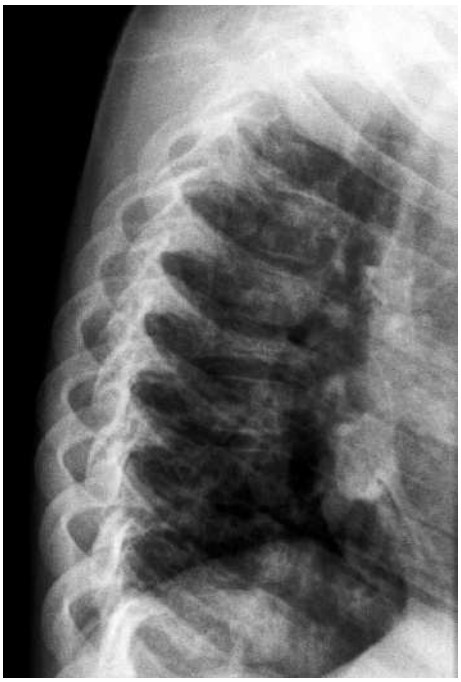

Fig. 25.4. Vertebra plana of the thoracic 6th vertebrae. There is loss of vertebral body height but preservation of disc height

height is often preserved and can be widened (David et al. 1989). This is commoner in children than adults (Fig. 25.4). There may also be anterior or lateral compression of the vertebral body. A less common appearance is a bubbly, lytic and expansible lesion in the vertebral body. The healing response to the spinal lesions can result in an improvement in vertebral body height, increased sclerosis and occasional a bone within a bone appearance. The thoracic and lumbar vertebrae are typical sites for vertebral involvement and often there are more than one vertebral body involved. Paraspinal, intradural and extradural masses can occur which can result in significant neurological symptoms (Kilpatrick et al. 1995; Stull et al. 1992; Hoover et al. 2007).

25.7.1.4 Long Bones

Initially, lesions are ill defined medually based lytic defects, typically within the diaphyses and metaphyses, but in children epiphyseal lesions that cross the physis can occur. In the early stages of the disease the appearances are more aggressive and can appear moth-eaten

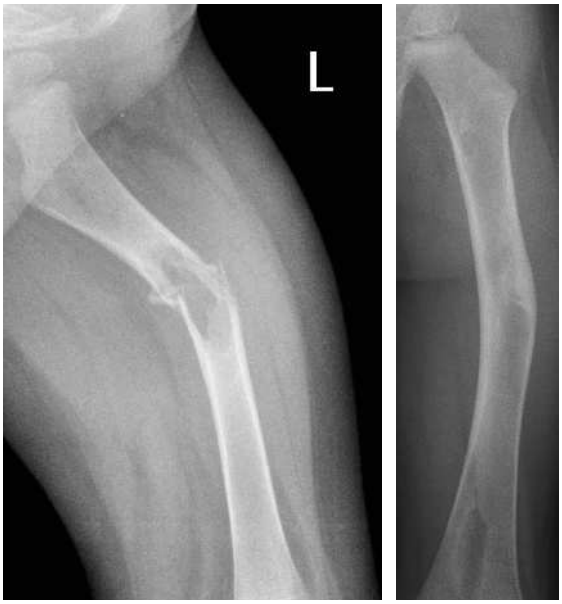

a,b

Fig. 25.5. **a** Pathological fracture in the mid shaft of the left femur, through a acute lesion. It is well defined lytic lesion but no marginal sclerosis. **b** The same patient one year later. The pathological fracture of the mid shaft of left femur shows remodelling. There is a further lesion in the distal left femur which has a more sclerotic margin, which has developed in the previous year from the time of the radiograph in **a**

or permeative. As they enlarge, the lesions become better defined and they can encroach on the cortex, causing endosteal erosions and scalloping. Cortical expansion can occur with extension into the surrounding soft tissues. Bone remodelling and deformity can occur. Lesions may coalesce and create a 'hole in a hole' appearance. A sclerotic margin is a later feature. As the lesion continues to heal it appears more sclerotic and it may completely disappear with no residual defect (Stull et al. 1992; Ochsner 1966) (Fig. 25.5).

Periosteal reaction can occur, but is more prominent with pathological fracturing, Soft tissue masses can also occur rarely without any bone involvement (Kilpatrick et al. 1995; Stull et al. 1992; Hoover et al. 2007; David et al. 1989).

25.7.2 MR Imaging Findings

The infiltration of the normal marrow by LCH is readily detectable on MR imaging. On T1 weighted spin echo (SE) images, the lesions are of hypointense signal intensity compared with the surrounding marrow fat. In a younger child, these lesions may be slightly less discernible if the marrow is haemopoietic. On T2 weighted SE images, the lesions are of increased signal intensity but the margins may be less well defined due to the surrounding high signal intensity of the marrow oedema. The amount of peri-lesional oedema is thought to be less when compared with more malignant lesions such as Ewings sarcoma (Davies et al. 1994). As they heal, the lesions there is often a general reduction in the T2 signal intensity. Lesions show contrast enhancement (Beltran et al. 1993; Hoover et al. 2007; Azouz et al. 2005; Kilborn et al. 2003).

MR imaging will also detect cortical changes, periosteal reactions and any soft tissue extension. Periarticular lesions may be associated synovial hypertrophy (Glajchen et al. 1997) (Fig. 25.6).

Whole body MR imaging, typically using T1 and STIR sequences, is an increasing useful investigation to asses the extent of disease and in the follow-up of LCH (Fig. 25.7). Whole body MR imaging identifies more skeletal lesions of the disease, than either radiographs or bone scintigraphy, and is more sensitive in detecting extra-skeletal lesions. In one study whole body MRI identified additional skeletal lesions in 38% and 25% of patients, compared with radiographs and bone scintigraphy, respectively. In addition it detected extra-skeletal lesions in 56% of the cases; however, in one patient the lung lesions were detected on radiographs. MR imaging has the advantage of not involving any ionising radiation, which is particularly relevant in paediatrics (Steinborn et al. 2008, Goo et al. 2006).

25.7.3 Nuclear Medicine

The use of bone scintigraphy ($Tc99^{m}$) in the detection of lesions in LCH is open to debate. Nuclear scintigraphy is less sensitive than radiographs in the detection of osseous lesions. While in the majority of cases there is increased uptake there may be areas of reduced uptake with a surrounding halo of increased activity. In children the normal physeal activity may mask the presence of some metaphyseal lesions. In some cases the uptake may be normal. Conversely areas of abnormal uptake may have no corresponding radiographic changes. Consequently radiographs and scintigraphy should be regarded as complementary imaging modalities. The use of other radiopharmaceuticals offers no advantage (Stull et al. 1992; Kumar and Balachandran 1980).

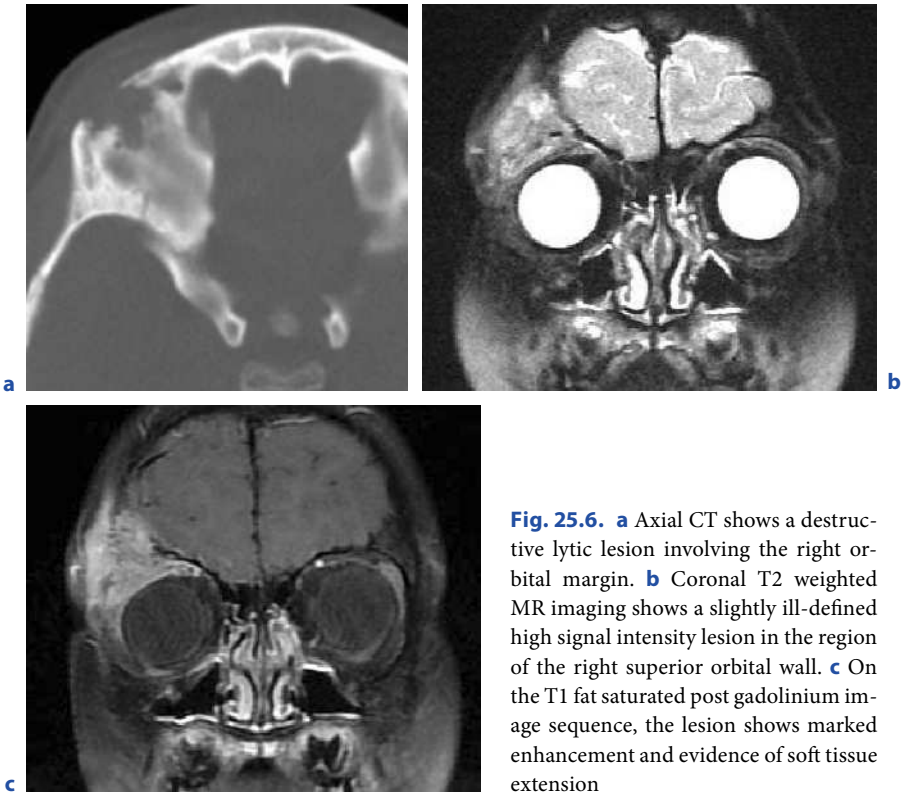

Fig. 25.6. **a** Axial CT shows a destructive lytic lesion involving the right orbital margin. **b** Coronal T2 weighted MR imaging shows a slightly ill-defined high signal intensity lesion in the region of the right superior orbital wall. **c** On the T1 fat saturated post gadolinium image sequence, the lesion shows marked enhancement and evidence of soft tissue extension

25.7.4 FDG PET

The use of FDG PET to assess osseous lesions in LCH is limited and still predominantly in the research phase. Initial reports suggest that FDG PET is sensitive in detecting lesions and may be useful in determining the stage of the lesion, with activity returning to normal in healed lesions. It is possible that FDG PET may be able to detect response to chemotherapy (Kaste et al. 2007; Blum et al. 2002; Binkovitz et al. 2003).

25.7.5 CT

CT is not routinely used in the assessment of LCH but can be useful to asses the extent of lesions in specific locations. It is helpful in determining for the presence of pathological fractures, periosteal reactions, reactive sclerosis and detailing the bevelled nature of lesions. It useful in guiding biopsies,

For extraskeletal disease it is most commonly used in the evaluation of pulmonary involvement and the assessment of interstitial changes.

25.8 Extraosseous Involvement

Extraosseous involvement in LCH occurs less frequently than skeletal disease. It can affect nearly any anatomic site and involvement of any organ can occur with a very diverse combinations of clinical manifestations. The imaging features cover a broad and varied spectrum none of which can be considered pathognomonic (Schmidt et al. 2004).

25.8.1 Chest

The early feature of chest involvement is bilateral, symmetrical interstitial disease, which on a chest radiograph will show as a diffuse reticulonodular pattern. This is a result of the summation of lung nodules and the thin walls of small cysts (Smets et al. 1997; Kulwiec et al. 1992; Moore et al. 1989). Unlike many other interstitial diseases processes, the lung volume mostly remains normal or may even be increased (Abbot et al. 2004; Kulwiec et al. 1992). As the disease progresses, the

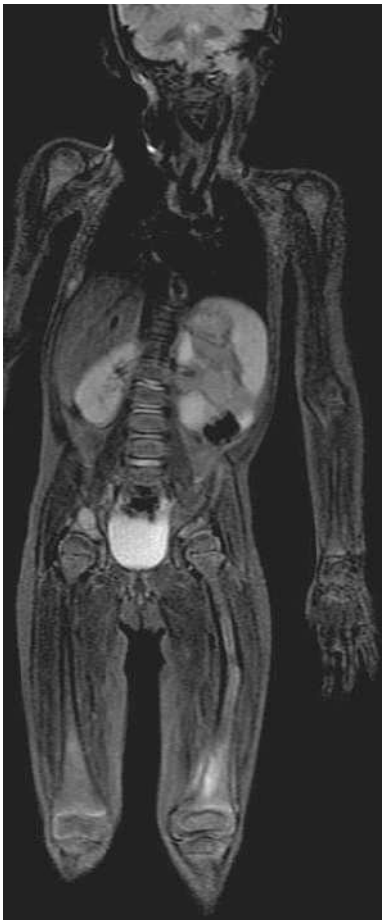

a

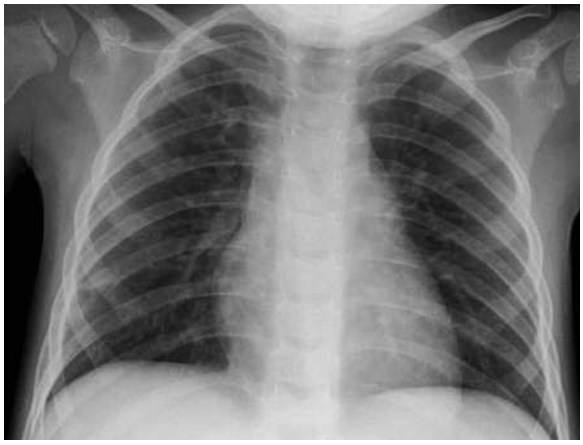

b

Fig. 25.7. **a** Same patient as in Fig. 25.5. Section of a whole body STIR shows the lytic lesion in the distal left femur and a further high signal area over the right thoracic cavity. **b** Corresponding chest radiograph shows an expansile lytic lesion within the lateral right 7th rib

radiographic features gradually change from a reticulonodular pattern to a honeycomb like pattern due to the coalescing of these air-filled cysts. Less frequently pleural effusions, mediastinal and hilar lymphadenopathy occur (Schmidt et al. 2004).

With chronic disease there is usually fibrosis (e.g. stellate scars and surrounding cystic spaces of variable diameter), emphysema with pulmonary hypertension resulting from the extensive parenchymal destruction.

High resolution CT can detect early changes even in asymptomatic patients. Findings include multiple bilateral small nodules, with cysts of varied wall thickness, typically in the upper and middle lobes with sparing of the costophrenic angles are suggestive of LCH (Abbot et al. 2004; Brauner et al. 1989).

25.8.2 Hepatobiliary Involvement

Hepatobiliary involvement occurs in 50%–60% of children with multisystem disease (Schmidt et al. 2004; Jaffe 2004). Langerhans cells directly infiltrate the periportal regions of the liver, particularly the bile ducts (Jaffe 2004). The radiological findings reflect the underlying histopathologic process, which consists of four phases; an initial proliferative phase followed by granulomatous, xanthomatous and eventually fibrous stages. Progression or regression may occur with treatment (Jaffe 2004; Kilborn et al. 2003; Parker and Lichtenstein 1963).

In children who have direct liver infiltration by Langerhans cells initially present with hepatomegaly, jaundice or biologic signs of liver dysfunction. Associated splenomegaly, either caused by portal hypertension

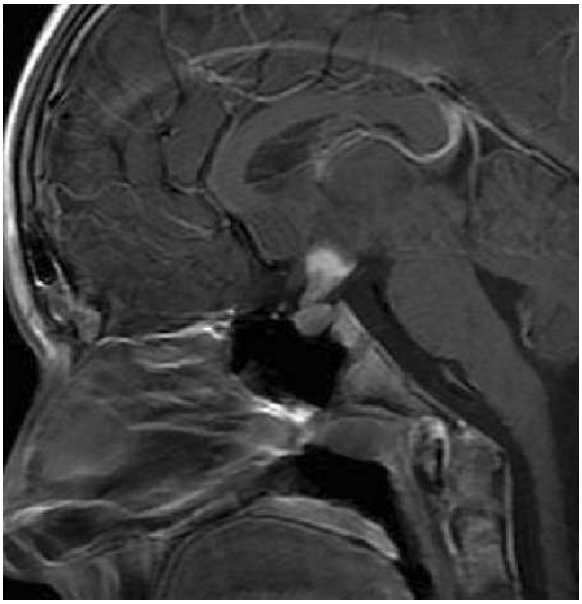

Fig. 25.8. Coronal T1 post gadolinium images shows thickening and enhancement of the pituitary stalk

resulting from periportal fibrosis or secondary to direct histiocytic infiltration can occur (Schmidt et al. 2004; Jaffe 2004).

During the proliferative and granulomatous phases, there is infiltration of Langerhans cells that causes periportal inflammation and oedema. On ultrasound this is relatively hypoechoic which can be band-like or nodular. On MR imaging there is increased signal intensity on T2 weighted images and contrast enhancement (Kim et al. 1999; Chan et al. 1997; Schmidt et al. 2004). Progression to the xanthomatous phase is characterized by linear periportal abnormalities and the formation of lipid-laden nodules in the liver parenchyma, which are hyperechoic on US and show increased signal intensity on unenhanced T1-weighted MR imaging (Chan et al. 1997). The final fibrous phase creates a dysmorphic and nodular appearance to the liver parenchyma, with periductal fibrosis and micronodular biliary cirrhosis with secondary portal hypertension (Schmidt et al. 2004; Kilborn et al. 2003). Associated sclerosing cholangitis can cause extra- and intrahepatic biliary irregularities with a beaded appearance of the bile ducts on MRCP. Liver failure can occur.

25.8.3 Gastrointestinal Tract Involvement

Gastrointestinal involvement is rare, occurring in only 2%–6% of children with multisystem disease. The mean age at diagnosis is 6 months. (Schmidt et al. 2004; Geissmann et al. 1996). The clinical symptoms are non-specific and include vomiting, diarrhoea, bloody stools, malabsorption, and a failure to thrive.

Radiological findings on barium studies are non-specific. They include loss of the normal mucosal pattern, coarsening and cobble stoning of the mucosa, segmental narrowing with areas of focal dilation and bowel loop separation due to oedematous inflammation. These features can be seen in other enteropathies, inflammatory bowel diseases, lymphoma and infection (Geissman et al. 1996; Schmidt et al. 2004).

On CT and MR imaging there is bowel wall thickening, mucosal contrast enhancement, segmental narrowing and dilatation of the lumen, infiltration of the mesenteric fat and free intraabdominal fluid, features which again are non-specific (Schmidt et al. 2004).

25.8.4 Central Nervous System Involvement

Involvement of the central nervous system occurs in 23%–35% of children with LCH, mostly in those affected by multisystem disease (Schmidt et al. 2004). Diabetes insipidus occurs in 24% of cases and is the most frequent initial manifestation of CNS involvement and can be considered a clinical hallmark of LCH (Schmidt et al. 2004). The neuropathologic patterns in simple terms can be separated into those that show either space-occupying or degenerative features on MR imaging.

Space-occupying lesions most commonly affect the hypothalamic-neurohypophyseal axis (Maghnie et al. 1992) often with symptoms of diabetes insipidus and other hormonal deficiencies. Involvement can occur from direct extension from the sphenoid bone, or due to histiocytic proliferation forming granulomatous masses primarily within the brain, but they can occur at any site in the CNS, including the spinal cord (Schmidt et al. 2004). The formation of granulomas causes a reduction in the normally high signal intensity of the posterior neurohypophysis on T1-weighted MR images. As a result of the infiltration, the hypothalamus and pituitary stalk are often enlarged and show increased homogeneous gadolinium enhancement (Fig. 25.8) (Schmidt et al. 2004; Maghnie et al. 1992; Prayer et al. 2004).

The second most frequent pattern of CNS involvement is intraaxial inflammatory and degenerative changes, which are typically seen as bilateral symmetrical lesions in the cerebellum, the dentate nucleus, basal ganglia, and brainstem. The degeneration leads to atrophy of the cerebellar cortex and the white matter. These areas show variable signal intensity on MR images, depending on the site and stage of disease (Schmidt et al. 2004; Prayer et al. 2004). As demyelination and gliosis occur, the lesions appear as poorly defined patchy areas of high signal intensity on T2-weighted images and low signal intensity on unenhanced T1-weighted images. Typically they do not enhance (Schmidt et al. 2004; Maghnie et al. 1992; Prayer et al. 2004).

25.8.5 Craniofacial and Neck Involvement

Head and neck involvement is common and has been reported to occur in 60%–82% of patients, either as primary or secondary disease. Disease manifestations include bone and soft-tissue lesions, cervical lymphadenopathy, skin rash (Cochrane et al. 2003; Prayer et al. 2004), the thymus and rarely the salivary glands (Junewick and Fitzgerald 1999; Sumner et al. 1993).

Due to the various anatomic structures in the head and neck, lesions are often complex, and can involve multiple structures simultaneously. Craniofacial osseous destruction can occur in association with adjacent soft-tissue infiltration. Soft-tissue involvement may involve the cavernous sinus, orbits, the paranasal sinuses, the naso- and oropharynx, the temporal region, the ear, larynx, hypopharynx, thyroid, the salivary glands and adjacent muscles (Buchmann et al. 2006).

CT is typically performed to evaluate the extent of osseous erosion or destruction, and MR imaging to assess the soft tissues. Compared with the surrounding muscles, soft-tissue masses are of high signal intensity on T2-weighted sequences and isointense to hypointense signal on T1-weighted images. They enhance following gadolinium administration (Fernandez-Latorre et al. 2000; Buchmann et al. 2006; Hurley et al. 2004).

25.8.6 Skin Involvement

After bone, the skin is the most frequently affected organ, and occurs in 50%–55% of all cases of LCH (Schmidt et al. 2004). The commonest presentation is with seborrhoea-like eruptions; other features are papules, vesicles, crusted plaques and nodules. Patients with skin LCH may show disease progression, spontaneous regression, and reactivation, and in rare cases it can be fatal.

25.9 Investigation of Patients

Once the initial diagnosis has been made, there are a number of investigations that are mandatory to fully assess the extent of disease. A further set of investigations are required depending on the specific indications and those organs which are involved.

A full skeletal survey including and AP and lateral chest radiograph is the standard imaging investigation. As has been previously discussed the role of whole body MRI is increasingly used and this may eventually replace the skeletal a survey. Nuclear scintigraphy is not recommended as first line screening investigation. In addition the radiological investigations patients undergo a series of laboratory test to assess full blood count, creatinine clearance, liver function, coagulation and urine osmolarity. If a patient has multisystem disease at presentation they require bone marrow aspiration.

Depending on clinical signs and symptoms, and the result of the laboratory investigations, the imaging studies required include abdominal ultrasound if there is suspicion of organ enlargement. If there are respiratory symptoms then a high resolution CT should be considered, even if the chest radiograph is normal. Any visual, otolaryngeal or neurological signs as well as symptoms of pituarity dysfunction (polyuria, polydipsia, short stature, precocious puberty, etc.), requires an MRI with post gadolinium sequences.

References

Abbott GF, Rosado-de-Christenson ML, Franks TJ, Frazier AA, Galvin JR (2004) From the archives of the AFIP: pulmonary Langerhans cell histiocytosis. Radiographics 24(3):821–841

Avery ME, McAfee JG, Guild HG (1957) The course and prognosis of reticuloendotheliosis (eosinophilic granuloma, Schuller-Christian disease and Letterer-Siwe disease); a study of forty cases. Am J Med 22(4):636–652

Azouz EM, Saigal G, Rodriguez MM, Podda A (2005) Langerhans' cell histiocytosis: pathology, imaging and treatment of skeletal involvement. Pediatr Radiol 35(2):103–115

Beltran J, Aparisi F, Bonmati LM, Rosenberg ZS, Present D, Steiner GC (1993) Eosinophilic granuloma: MRI manifestations. Skeletal Radiol 22:157–161

Berry DH, Brecon DL (1987) Natural history of hitiocytosis X. Hematol Oncol Clin North Am 1:23–34

Betts DR, Leibundgut KE, Feldges A, Pluss HJ, Niggli FK (1998) Cytogenetic abnormalities in Langerhans cell histiocytosis. Br J Cancer 77(4):552–555

Binkovitz LA, Olshefski RS, Adler BH (2003) Coincidence FDG-PET in the evaluation of Langerhans' cell histiocytosis: preliminary findings. Pediatr Radiol 33(9):598–602

Blum R, Seymour JF, Hicks RJ (2002) Role of 18FDG-positron emission tomography scanning in the management of histiocytosis. *Leuk Lymphoma*. 43(11):2155–2157

Brauner MW, Grenier P, Mouelhi MM, Mompoint D, Lenoir S (1989) Pulmonary histiocytosis X: evaluation with high-resolution CT. Radiology 172(1):255–258

Broadbent V, Gadner H, Komp DM, Ladisch S (1989) Histiocytosis syndromes in children: II. Approach to the clinical and laboratory evaluation of children with Langerhans cell histiocytosis. Clinical Writing Group of the Histiocyte Society. Med Pediatr Oncol 17:492–495

Buchmann L, Emami A, Wei JL (2006) Primary head and neck Langerhans cell histiocytosis in children. Otolaryngol Head Neck Surg 135:312–317

Carstensen H, Ornvold K (1993) The epidemiology of Langerhans cell histiocytosis in children in Denmark, 1975–1989. Med Pediatr Oncol 21:387–388

Ceci A et al. (1988) Etoposide in recurrent childhood Langerhans' cell histiocytosis: an Italian co-sperative Study. Cancer 62:2528–2531

Chan YL, Li CK, Lee CY (1997) Sonographic appearance of hepatic Langerhans cell histiocytosis. Clin Radiol 52(10):761–763

Chu T, D'Angio GJ, Favara BE, Ladisch S, Nesbit M, Pritchard J (1987) Histiocytosis syndromes in children. Lancet 2(8549):41–42

Cochrane LA, Prince M, Clarke K (2003) Langerhans' cell histiocytosis in the paediatric population: presentation and treatment of head and neck manifestations. J Otolaryngol 1:33–37

Coppes-Zantinga A, Egeler RM (2002) The Langerhans cell histiocytosis X files revealed. Br J Haematol 116(1):3–9

David R, Oria RA, Kumar R, Singleton EB, Lindell MM, Shirkhoda A et al. (1989) Radiologic features of eosinophilic granuloma of bone. AJR Am J Roentgenol 153(5):1021–1026

Davies AM, Pikoulas C, Griffith J (1994) MRI of eosinophilic granuloma. Eur J Radiol 18:205–209

Dreyer ZE, Dowell BL, Chen H, Hawkins E, McClain KL (1991) Infection-associated hemophagocytic syndrome. Evidence for Epstein-Barr virus gene expression. Am J Pediatr Hematol Oncol 13(4):476–481

Favara BE (1991) Langerhans' cell histiocytosis pathobiology and pathogenesis. Semin Oncol 18(1):3–7

Favara BE, Feller AC, Pauli M et al. (1997) A contemporary classification of histiocytic disorders. The WHO Committee on Histiocytic/Reticulum Cell Proliferations. Reclassification Working Group of the Histiocytic Society. Med Pediatr Oncol 29:157–166

Fernández-Latorre F, Menor-Serrano F, Alonso-Charterina S, Arenas-Jiménez J (2000) Langerhans' cell histiocytosis of the temporal bone in pediatric patients: imaging and follow-up. AJR Am J Roentgenol 174:217–221

Gadner H, Heitger A, Grois N, Gatterer-Menz I, Ladisch S (1994) Treatment strategy for disseminated Langerhans cell histiocytosis. Med Ped Oncol 23:72–80

Geissmann F, Thomas C, Emile JF, Micheau M, Canioni D, Cerf-Bensussan N et al. (1996) Digestive tract involvement in Langerhans cell histiocytosis. The French Langerhans Cell Histiocytosis Study Group. J Pediatr 129(6):836–845

Ghanem I, Tolo VT, D'Ambra P, Malogalowkin MH (2003) Langerhans cell histiocytosis of bone in children and adolescents. J Pediatr Orthop 23(1):124–130

Glajchen N, Springfield DA, Lipton JM (1997) Langerhans' cell histiocytosis of the synovium. AJR Am J Roentgenol 169(6):1751–1752

Goo HW, Yang DH, Ra YS, Song JS, Im HJ, Seo JJ, Ghim T, Moon HN (2006) Whole-body MRI of Langerhans cell histiocytosis: comparison with radiography and bone scintigraphy. Pediatr Radiol 36:1019–1031

Grundy P, Ellis R (1986) Histiocytosis X: a review of the etiology, pathology, staging, and therapy. Med Pediatr Oncol 14(1):45–50

Hand A (1893) Polyuria and tuberculosis. Arch Pediatric 10:673–675

Hoover KB, Rosenthal DI, Mankin H (2007) Langerhans cell histiocytosis. Skeletal Radiol 36:95–104

Hurley ME, O'Meara A, Fogarty E, Hayes R (2004) Langerhans' cell histiocytosis of the clivus: case report and literature review. Pediatr Radiol 34:267–270

Jaffe R (2004) Liver involvement in the histiocytic disorders of childhood. Pediatr Dev Pathol 7(3):214–225

Junewick JJ, Fitzgerald NE (1999) The thymus in Langerhans' cell histiocytosis. Pediatr Radiol 29:904–907

Kaste SC, Rodriguez-Galindo C, McCarville ME, Shulkin BL (2007) PET-CT in pediatric Langerhans cell histiocytosis. Pediatr Radiol 37:615–622

Kelly KM, Pritchard J (1994) Monoclonal antibody therapy in Langerhans cell histiocytosis – feasible and reasonable? Br J Cancer 70(Suppl.XXIII):54–55

Kilborn TN, Teh J, Goodman TR (2003) Paediatric manifestations of Langerhans cell histiocytosis: a review of the clinical and radiological findings. Clin Radiol 58(4):269–278

Kilpatrick SE, Wenger DE, Gilchrist GS, Shives TC, Wollan PC, Unni KK (1995) Langerhans' cell histiocytosis (histiocytosis X) of bone. A clinicopathologic analysis of 263 pediatric and adult cases. Cancer 76(12):2471–2484

Kim M, Lyu C, Jin Y, Yoo H (1999) Langerhans' cell histiocytosis as a cause of periportal abnormal signal intensity on MRI. Abdom Imaging 24(4):373–377

Komp DM (1987) Historical perspectives of Langerhans cell histiocytosis. Hematol Oncol Clin North Am 1:9–21

Kulwiec EL, Lynch DA, Aguayo SM, Schwarz MI, King TE Jr (1992) Imaging of pulmonary histiocytosis X. Radiographics 12(3):515–526

Kumar R, Balachandran S (1980) Relative roles of radionuclide scanning and radiographic imaging in eosinophilic granuloma. Clin Nucl Med.5:538–542

Lichtenstein L (1953) Histiocytosis X; integration of eosinophilic granuloma of bone, Letterer-Siwe disease, and Schuller-Christian disease as related manifestations of a single nosologic entity. AMA Arch Pathol 56(1):84–102

Maghnie M, Arico M, Villa A, Genovese E, Beluffi G, Severi F (1992) MR of the hypothalamic-pituitary axis in Langerhans cell histiocytosis. AJNR Am J Neuroradiol 13(5):1365–1371

Mahmoud HH, Wang WC, Murphy SB (1991) Cyclosporine therapy for advanced Langerhans cell histiocytosis. Blood 77:721–725

Minkov M, Grois N, Heitger A (2001) Response to initial treatment: an important prognostic predictor in multisystem Langerhans cell histiocytosis. J Pediatr 138:728–734

Moore AD, Godwin JD, Muller NL, Naidich DP, Hammar SP, Buschman DL et al. (1989) Pulmonary histiocytosis X: comparison of radiographic and CT findings. Radiology 172(1):249–254

Nesbit ME Jr, O'Leary M, Dehner LP, Ramsay NK (1981) The immune system and the histiocytosis syndromes. Am J Pediatr Hematol Oncol 3:141–149

Oberman HA (1961) A clinicopathologic study of 40 cases and review of the literature on eosinophilic granuloma of bone. Hand-Schuller-Christian disease and Letterer-Siwe disease. Pediatrics 28:307–327

Osband ME, Pochedly C (1987) Histiocytosis-X: an overview. Hematol Oncol Clin North Am 1(1):1–7

Ochsner SF (1966) Eosinophilic granuloma of bone: experience with 20 cases. AJR Am J Roentgenol 97:719–726

Parker JW, Lichtenstein L (1963) Severe hepatic involvement in chronic disseminated histiocytosis X. Report of a case with necropsy. Am J Clin Pathol 40:624–632

Prayer D, Grois N, Prosch H, Gadner H, Barkovich AJ (2004) MR imaging presentation of intracranial disease associated with Langerhans cell histiocytosis. AJNR Am J Neuroradiol 25(5):880–891

Refabert L, Rambaud C, Mamou-Mani T, Scheinmann P, de Blic J (1996) Cd1a-positive cells in bronchoalveolar lavage samples from children with Langerhans cell histiocytosis. J Pediatr 129(6):913–915

Schlesinger AE, Glass RB, Young S, Fernbach SK (1986) Case report 342: eosinophilic granuloma of the right iliac wing. Skeletal Radiol 15:57–59

Schmidt S, Eich G, Hanquinet S, Tschappeler H, Waibel P, Gudinchet F (2004) Extra-osseous involvement of Langerhans' cell histiocytosis in children. Pediatr Radiol 34(4):313–321

Smets A, Mortele K, de Praeter G, Francois O, Benoit Y, Kunnen M (1997) Pulmonary and mediastinal lesions in children with Langerhans cell histiocytosis. Pediatr Radiol 27(11):873–876

Steinborn M, Wörtler K, Nathrath M, Schöniger M, Hahn H, Rummeny EJ (2008) Whole-body MRI in children with langerhans cell histiocytosis for the evaluation of the skeletal system. Rofo 180(7):646-53

Stull MA, Kransdorf MJ, Devaney KO (1992) Langerhans cell histiocytosis of bone. Radiographics 12(4):801–823

Sumner TE, Auringer ST, Preston AA (1993) Thymic calcifications in histiocytosis X. Pediatr Radiol 23:204–205

Weitzman S, Egeler RM (2008) Langerhans cell histiocytosis: update for the pediatrician. Curr Opin Pediatr 20(1):23–29

Willman C, Busque L, Griffith B et al. (1994) Langerhans cell histiocytosis (Histiocytosis X) – a clonal proliferative disease. N Engl J Med 331:154–160

Writing Group of the Histiocyte Society (1987) Histiocytosis syndromes in children. Lancet 1:208–209

Bone Metastases 1: Spine

26

Prudencia N. M. Tyrrell, Victor N. Cassar-Pullicino, Radhesh K. Lalam and Bernhard J. Tins

CONTENTS

KEY POINTS

- The radiograph is insensitive in terms of identifying metastases which have involvement of <50% of the vertebral body.
- Sagittal T1-weighted and STIR MR imaging sequences are useful screening approaches in assessment of the presence of spinal metastases.
- In the presence of "red flag" symptoms, MRI should be carried out as soon as is reasonably practical.
- Classically the intervertebral disc is not involved in metastatic disease which is helpful in trying to differentiate between metastasis and infection.
- In differentiating malignant from benign vertebral collapse using MRI, the presence of posterior bowing of the vertebral body, heterogeneous abnormal signal throughout the body with signal extension into the pedicle and posterior elements, and paravertebral and epidural soft tissue extension all favour a malignant aetiology.

26.1 Introduction

A metastasis is the spread of cells from one site in the body to another. Usually it is used in the context of malignant disease where there has been spread of cells from the site of origin of the tumour (primary site) to other (distant) sites. Metastases are the commonest malignant tumour in all age groups. As a group, the most common sites for metastases are lung, liver and bone. The most common malignancies to metastasise to bone are breast, lung, prostate, thyroid and renal carcinoma. This may be due to specific characteristics of the tumour

P. N. M. Tyrrell, MD
V. N. Cassar-Pullicino, MD
R. K. Lalam, MD
B. J. Tins, MD
Department of Radiology, The Robert Jones and Agnes Hunt Orthopaedic and District Hospital NHS Trust, Oswestry, Shropshire SY10 7AG, UK

cells and in turn the bone reacts in different ways to different types of primary tumour cells producing different responses in the bone, to produce a lytic, sclerotic or mixed response. Certain tumour types have a predilection for spread to the spine and this is seen especially with primary carcinoma of the breast and prostate. Late in the disease, however, skeletal involvement may be widespread.

This chapter focuses on metastatic disease of the spine and addresses the issue of why some tumours preferentially spread to that region and the peculiar patho-anatomy which lends itself to that spread. It also discusses clinical and imaging features, an algorithmic approach to determination of the solitary spinal lesion, fracture risk assessment, surgical management and finally addresses imaging following treatment of spinal metastases.

26.2 Pathophysiology of Spinal Metastases

The vertebral body is rich in red marrow and undergoes haematopoietic change as in other areas of the skeleton particularly the proximal humeri and femora. This contrasts with the more peripheral skeleton where there is relatively avascular yellow or fatty marrow. The pedicles, and to a lesser extent the posterior neural arch of the vertebral body, also contain red marrow. Early studies by Batson (1942), using injections of radiographic-opaque material into cadavers, through the dorsal vein of the penis, demonstrated spread into the veins of the bones of the pelvic girdle and the veins in the vertebrae and those about the vertebral column. These veins had first been described by Breschet in the nineteenth century (Breschet 1832). The basivertebral vein enters the back of the vertebral body and bifurcates to drain the body. The basivertebral vein communicates with Batson's vertebral venous plexus, a set of valveless, plexiform, longitudinal venous channels that join the cranial venous sinuses to the pelvic veins without the intermediation of the lungs. This plexus forms an extensive intercommunicating valveless network of veins with the intercostal and lumbar veins. Batson (1942) demonstrated that the prostatic and breast venous systems drain directly into this vertebral plexus. In the absence of valves, blood is able to drain in any direction; hence, the basivertebral vein may be considered to enter the back of the vertebral body and bifurcate to drain the body, but equally it may be considered to join by the union of two tributaries and leave the body posteriorly. Although spread of tumour cells via the inferior vena cava (IVC) is the normal course of flow, when the intra-abdominal pressure is raised, e.g. through straining, and there is associated resistance to flow through the IVC, then flow can occur freely via the bone protected vertebral vein plexus and from there spread into the intercostal vessels bypassing the caval and portal systems. A similar valveless network from the breast, bypassing the portal, caval and pulmonary vein systems, was demonstrated by Batson (1942). The direction of flow is determined by simple changes in posture and alterations in intrathoracic and intra-abdominal pressures. Because of the variable direction of flow through this plexus, the vertebral bodies can be exposed to tumour microemboli from almost anywhere in the body. This system favours deposition of metastases within the spine from particular sites such as breast and prostate.

Metastases to the spine are determined not only by the rich vertebral capillary network but also by a variety of local factors including chemotactic factors released by the bone attracting tumour cells to the bone surface. Some tumours have chemical responses to bone. Paget (1889) hypothesised that a metastasis is dependent upon provision of a fertile environment (the soil) in which compatible tumour cells (the seed) could proliferate. Humoral factors secreted by the tumour cells play an important role in deposition and growth of metastases in bone (Galasko 1972). Bone can respond in a variety of ways to metastatic tumour deposition and variations in stimulation of osteoblasts and osteoclasts largely determines how the lesion will appear in imaging studies. There may be loss of bone (destruction, lysis), production of new bone (sclerosis, periosteal new bone) or a combination of bone destruction and bone formation to produce a mixed lesion. Resorption of bone may be due to the role of osteoclasts, tumour cells, macrophages and monocytes. Osteoclast-mediated osteolysis can occur in myeloma where, for example, the leucocytes produce an osteoclast-activating factor (Mundy et al. 1974a,b; Mundy et al. 1977). Bone resorption may also be due to immobilisation or other humoral factors such as vascular endothelial growth factor and interleukins 8+11, parathormone or prostaglandins contributing to bone loss (Guise et al. 2005). Tumour-produced parathormone related protein (PTHrP) stimulates osteoclasts that secrete tumour-activating transforming growth factor β that further stimulates local cancer cells. This in turn may stimulate further PTHrP production by tumour cells leading to further osteolysis (Guise 2000; Clines and Guise 2005). Malignant cells may be attracted to the bone surface by a chemotactic factor released by the bone (Mundy and Spiro 1981), and that once there, the malignant cells secrete lytic enzymes which

contribute to continued bone destruction (Galasko 1982; Manishen et al. 1986). Osteolytic bone destruction can also give rise to hypercalcaemia.

Bone may also respond to tumour cells by the formation of bone. Osteoblastic metastases can be caused by tumour-secreted endothelin-1 (ET-1), but there are other potentially osteoblastic factors. Stimulation of osteoblasts can increase osteoclast function, as bone-synthesising osteoblasts are the main regulators of bone-destroying osteoclasts. Bone resorption can result in the release of bone growth factors which may in turn increase the formation of bone metastases and activate a vicious circle (Guise et al. 2005). Clinically approved bisphosphonates prevent bone resorption and reduce the release of bone growth factors. Stromal new bone formation occurs only in the skeletal metastases that are associated with the development of fibrous stroma, particularly from those arising from carcinoma of the prostate. Highly cellular tumours possess little or no stroma and are not accompanied by this type of bone formation (Galasko 1982). Reactive new bone formation occurs as a response to bone destruction (Galasko 1982). This process is seen to a variable extent in all malignant tumours but may be minor in highly anaplastic rapidly growing tumours. The rate of bone destruction may exceed the rate of reactive new bone formation and thus new bone formation may not be appreciable on imaging studies.

Although the distribution of skeletal metastases is influenced by the specific type of primary malignant tumour, predominant involvement of the axial skeleton, rich in red marrow, is well known. Factors favouring the development of metastases in red marrow is the rich capillary network, sluggish blood flow and the suitability of this type of tissue for the growth of tumour emboli (Galasko 1981).

26.3 Clinical Features of Spinal Metastases

Spinal metastases may be completely asymptomatic and detected purely as a seemingly incidental finding during imaging for unrelated symptomatology. They may present as back pain which may be due to vertebral collapse secondary to metastatic infiltration. They may present with symptoms such as sciatica or bilateral leg weakness culminating in cauda equina syndrome due to pressure effects on neural structures from the growing tumour mass, resulting in nerve root or cord compression. Metastatic tumour may be far advanced at this stage, involving the entire vertebral body and posterior elements infiltrating into the spinal canal to surround and compress the cord. Metastatic disease of the spine is often found together with evidence of degenerative disc disease as the latter is a common finding in the older population.

Back pain is a common symptom, so in which patients does one suspect malignancy and proceed to imaging beyond radiographs? During clinical history taking, enquiry about systemic symptoms, e.g. appetite, weight loss and night pain, as well as more general enquiry including cough, smoking history and relevant past medical history such as previous malignancy, is important. Positive findings are likely to raise an index of suspicion and lead to more detailed assessment. The radiograph is a good starting point in imaging but is relatively insensitive as more than 50% of the vertebral body can be destroyed before this becomes radiologically apparent (Fig. 26.1; Edelstyn et al. 1967). Large lesions occupying more than 40% of the vertebral body diameter are much better detected than small ones <26% (Haller et al. 1990a,b). There are certain "red flag" features of back pain which indicate that MRI should be carried out as the imaging investigation of choice as it has a stronger negative predictive value than radiographs (Royal College of Radiologists 2007). Such red flags include pain lasting more than 6 weeks, age more than 60 years, pain at night and pain aggravated by lying down. Aggravation of pain when lying down is due to blood pooling. If the radiograph is normal, then further imaging with CT, MRI or scintigraphy is indicated. The presence of neurological symptoms dictates that MRI be performed urgently which will allow assessment of the bone, bone marrow, the intervertebral discs, the facet joints, the contents of the spinal canal and paravertebral soft tissues. Symptoms of spinal cord compression include back pain, especially at night and increased with movement, with or without radicular pain. Over time this can progress to motor weakness which may proceed to paraplegia. Not invariably, there will be symptoms of numbness and a sensory level may be identified. Bladder and bowel disturbances are late features. Cord compression may be due to extension of tumour mass from the vertebral body, to surround and compress the cord, but it may also be due to pathological fracture, dislocation, severe spinal angulation due to vertebral collapse or pressure due to intradural metastases; the latter tends to be rare as the dura acts as a barrier to tumour invasion.

In evaluating the patient clinically, the erythrocyte sedimentation rate (ESR), C-reactive protein, serum bone biochemistry (serum calcium, serum phosphate, alkaline phosphatase), serum prostate surface antigen (PSA) and haematological parameters are all valuable.

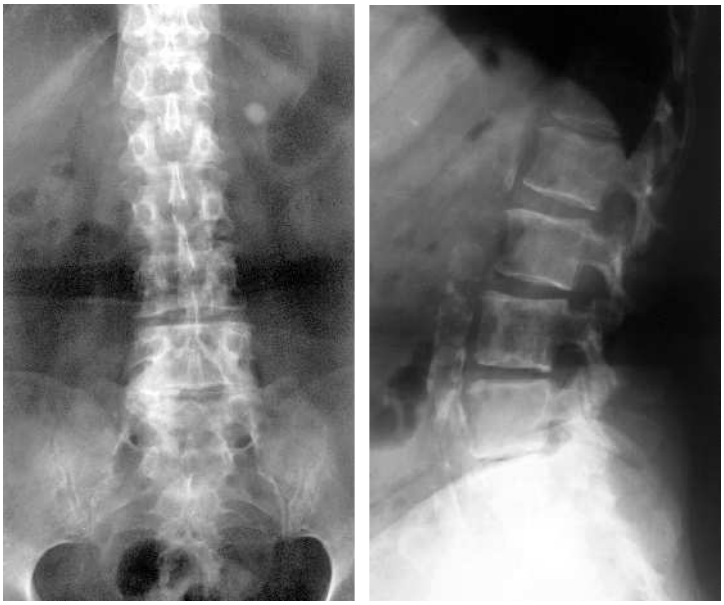

a,b

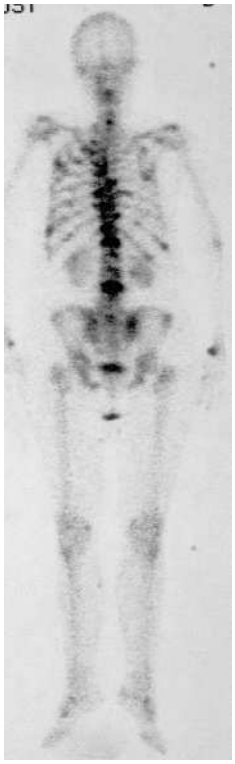

c

Fig. 26.1. **a** Anteroposterior and **b** lateral radiographs of the lumbar spine demonstrate abnormal texture of the body of L3 with a predominant lucent pattern. There are no radiographic soft tissue signs. **c** Whole-body scintigram of the same patient shows abnormal increased uptake in multiple vertebrae, which appear normal on radiography

In the emergency setting, MRI may be the first imaging investigation, but the radiograph still plays a valuable role because it is readily available, cheap and acts as a baseline. In some instances it may be the radiograph by which treatment, and response to that treatment, is followed, for example, by monitoring the degree of collapse or deformity.

26.4 Imaging Features of Spinal Metastases

Spinal metastases are more common in the lumbosacral and thoracic areas than in the cervical region. The frequency and distribution of spinal metastases may relate to whether the primary site is a pelvic organ or a non-pelvic site (Batson 1942, 1957). Osteolytic lesions are more common than osteoblastic lesions. Some lesions may be mixed sclerotic and lytic. Some slow-growing metastases may mimic a primary tumour with a sclerotic margin and internal mineralisation (Rodallec et al. 2008).

Metastatic foci are more common in the vertebral bodies than the posterior elements. Pedicle destruction in skeletal metastases is common but is rare in multiple myeloma. In the spine a large amount of bone destruction is required before the lesion is detected by radiography (Edelstyn et al. 1967; Haller et al. 1990a,b). This problem is accentuated if a lesion is confined to the medullary space in which relatively few trabeculae are found. Destruction of the cortex is more readily apparent owing to the presence of larger amounts of bone that are compact in nature. Early studies suggested that pedicle destruction was an early sign of metastatic disease on radiography. The development of cross-sectional imaging with CT and MRI has demonstrated that metastatic involvement of a pedicle does not occur in the absence of vertebral body involvement and that involvement of the pedicles usually occurs as a result of further extension of a tumorous deposit within the posterior portion of the vertebral body (Asdourian et al. 1990; Algra et al. 1992).

In metastatic disease, the intervertebral disc is relatively resistant to the spread of tumour, as it is usually avascular. Disc destruction, however, has been reported with cases of plasma cell myeloma, chordoma (Firooznia et al. 1976) and some vertebral metastases (Hubbard and Gunn 1972); however, different pathways of the tumour into the disc have been observed, including (a) direct infiltration from the rim of the vertebral body not covered by the cartilaginous plate; (b)

infiltration into the outer layer of the annulus fibrosus through the subspace beneath the longitudinal ligament from the side of the vertebral body; and (c) via small vessels in the subspace beneath the longitudinal ligament (Yasuma et al. 1989). Vascularisation of the disc can occur with normal aging from the vertebral body though a rupture in the cartilaginous plate. In general, however, discal invasion is rare, as the cartilaginous plate and the intradiscal pressure act as a barrier against tumour invasion into the disc (Yasuma et al. 1989). Abnormalities of the disc are most frequently related to metastases from the prostate (Resnick and Niwayama 1978) but may be associated with metastases from other primary sites.

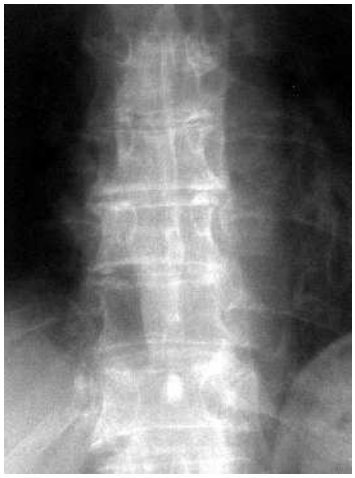

Fig. 26.2. Anteroposterior radiograph shows complete absence of the pedicles at T11

26.4.1 Radiography

Radiographs are readily available, cheap and usually easy for the patient to undergo. Anteroposterior and lateral views are required in order to increase the chance of lesion detection. Reliance on one view only will lead to pathology being missed (Tyrrell et al. 1995). Experimental studies have shown that 50–60% of the trabecular bone must be destroyed before osseous destruction is detectable on the radiograph. Early disruption of cortical outlines and margins can, however, be detected more readily. Although not particularly sensitive, the radiograph does give an overview of the status of the spine, and in the absence of red flag symptoms it is a good preliminary investigation. It is helpful to adopt a regular method for interrogation of the spine radiograph. A suggested approach might be evaluation of bone density and observation of bone texture, assessment of paravertebral soft tissues (to check for the possibility of swelling), then to assess the vertebral body outline including the posterior vertebral body line on the lateral view together with the vertebral end-plate margin, vertebral body height, the disc margins and disc height, and also the pedicle and spinous process outlines (Fig. 26.2). Spinal metastases as with metastases elsewhere in the skeleton may be lucent presenting with lysis/destruction due to replacement of bone by a tumorous deposit (Fig. 26.3). Metastases may also be sclerotic due to malignant new bone formation, or maybe mixed (Table 26.1). Sclerosis of a vertebral body or multiple sclerotic deposits may be due to metastases from carcinoma of the prostate most commonly but

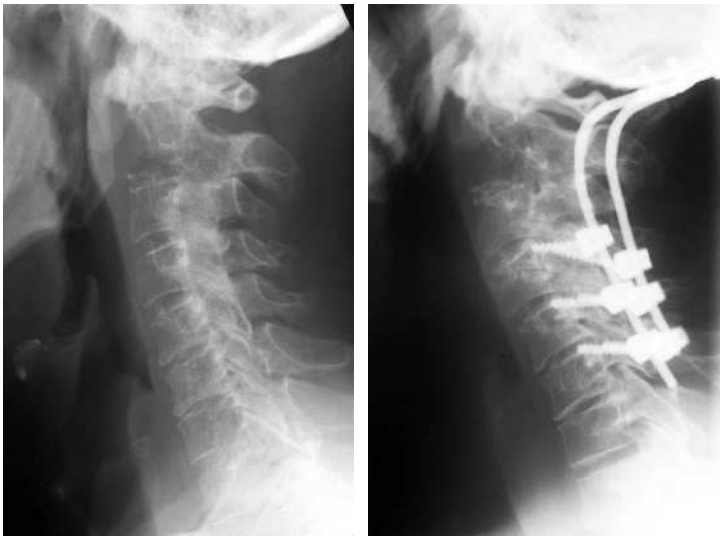

a,b

Fig. 26.3. **a** Lateral radiograph of the cervical spine shows pre-vertebral soft tissue swelling resulting in a posterior impression on the airway. The body and pedicles of C2 are destroyed. Vertebral support is greatly diminished and fracture risk is high. **b** Same patient post-surgical stabilisation

Table 26.1. Skeletal metastases: most common radiological appearances

Lytic	
Carcinoma of lung	Testis
Breast	Colon
Renal cell	Melanoma
Bladder	Squamous cell carcinoma of skin
Cervix	Phaeochromocytoma
Uterus	Adrenal
Ovary	Neuroblastoma
Sclerotic	
Prostate	Carcinoid
Breast (post-treatment)	Medulloblastoma
Lymphoma	Bladder (occasionally)
Mucoid adenocarcinoma	Testis (occasionally)
Stomach	Neuroblastoma (occasionally)
Colon (occasionally)	
Expansile metastases	
Renal	Melanoma
Thyroid	Phaeochromocytoma
Metastases associated with tumour bone formation	
Osteosarcoma	Transitional cell carcinoma (kidney or bladder)
Liposarcoma	Adenocarcinoma of colon (sometimes)

may also be secondary to colonic and other neoplasms (Figs. 26.4, 26.5). Lymphoma and also occasionally plasma cell myeloma may result in a sclerotic vertebral body. The differential diagnosis of sclerosis within a vertebral body is wide and includes chronic infection, mastocytosis, tuberous sclerosis, myelofibrosis, Paget's disease and degenerative discogenic abnormalities.

Generalised reduction in bone density may reflect underlying osteoporosis which may be uncomplicated but, when seen in a male, should suggest possible underlying multiple myeloma requiring prompt baseline serological/immunological assessment. An expansile lucent lesion may suggest myeloma/plasmacytoma or metastasis especially of renal or thyroid origin. Bone texture may appear inhomogeneous – patchily lucent or sclerotic – which requires explanation. Lodwick (1964) described three patterns of osteolytic involvement including a geographical appearance due to focal destruction, moth eaten and permeative. A blurred or fuzzy outline to the vertebral body margin suggests

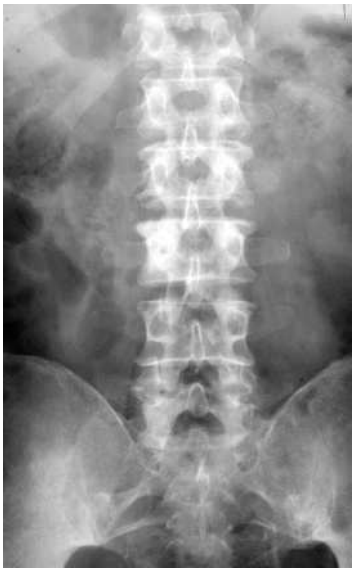

a

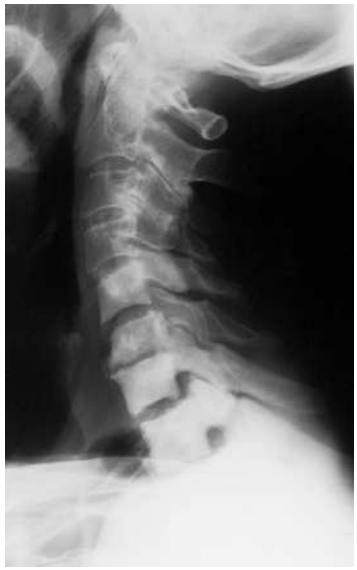

b

Fig. 26.4a,b. Patterns of osteoblastic metastases. **a** Anteroposterior radiograph of the lumbar spine. Sclerosis of the right pedicle of L3 extending into the right lateral margin of the vertebral body. The vertebral body outline on the right side is fuzzy and indistinct indicative of cortical involvement, and **b** in another case, diffuse involvement of vertebral bodies

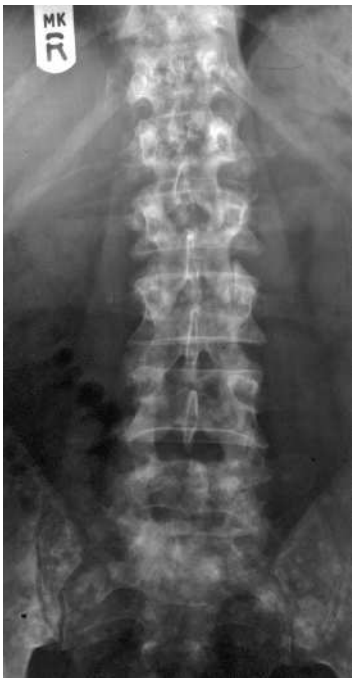

a

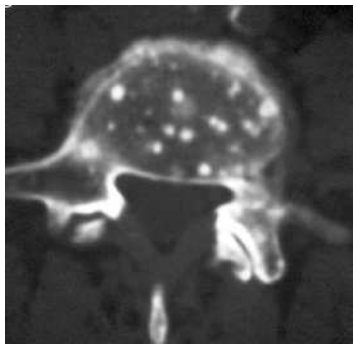

b

Fig. 26.5. **a** Anteroposterior radiograph of the lumbo-sacral spine showing multiple sclerotic metastases. **b** Multiple small sclerotic deposits are also demonstrated on axial CT

cortical involvement possibly due to infiltrative disease. Cortical thickening may occur with a slightly irregular margin. The possibility of Paget's disease needs consideration and other features of trabecular thickening and bony expansion should be sought. Loss of the posterior vertebral body cortex as well as posterior convexity are highly specific signs of malignancy (Guillevan et al. 2007). Destruction of the pedicle was described as an early sign of vertebral metastases (Jacobson et al. 1958), but subsequent studies using CT have shown that pedicle involvement is always associated with vertebral body involvement and is essentially a sign of fairly advanced metastatic infiltration (Algra et al. 1991). Loss of a pedicle has been described as the "winking owl's eye" when seen on the AP radiograph. A pedicle may also appear sclerotic when involved by an osteoblastic metastasis. The absence of a pedicle on radiography clearly requires further assessment by CT or MRI. Similarly, a sclerotic pedicle also requires further assessment.

Traditional teaching indicates that the intervertebral disc is preserved in cases of malignancy, whereas in infection the disc is more usually involved. "Good disc, bad news; bad disc good news" helps remind that the vertebral lesion with a preserved disc more likely represents malignancy, whereas the destroyed disc with a vertebral lesion or vertebral abnormality is more likely to represent treatable disease in the form of infection. There are exceptions to this "rule of thumb" (Hubbard and Gunn 1972; Firooznia et al. 1976). In addition, one of the modes of spread of tuberculous disease is via subligamentous spread, in which case the disc may be spared (Jung et al. 2004; Khattry et al. 2007). Tuberculous infection, however, is often associated with large soft tissue masses and associated calcification, features which help to narrow the differential diagnosis.

Vertebral body collapse is often found in metastatic disease and when present is often one of flattening rather than wedging. If there is generalised osteopaenia, this type of collapse may need to be differentiated from benign osteoporotic collapse. Radiographic features suggestive of osteoporotic versus malignant collapse include visualisation of both pedicles, a vacuum phenomenon (gas) within the adjacent disc space and absence of a paravertebral soft tissue mass (although this latter feature may be difficult to appreciate on plain radiographs). Cross-sectional imaging may be required and even then differentiation may be difficult. The pattern of radiographic abnormality includes destruction (lysis), sclerosis and also mixed lysis sclerosis. The pattern may be diagnostic of metastatic disease if there are multiple lesions, but further imaging may be warranted to confirm the nature of the disease and/or to determine the extent. The presenting solitary bone lesion on the spine radiograph will need confirmation that it is indeed not only a solitary spine lesion but also a solitary lesion in the skeleton. Whole-body bone scintigraphy using technetium-labelled methylene diphosphonate (Tc99m-MDP) may be the simplest method, but others will argue for a whole-body MRI scan. Computed tomography is often indicated especially in assessment of the apparently solitary spinal lesion. There is a wide differential diagnosis of a solitary spine lesion (Rodallec et al. 2008).

The radiograph has a particular role in the follow-up of cases of spinal metastases to assess the degree of collapse and deformity. Weight bearing views of the spine allow assessment of spinal balance and need for spinal stabilisation (Rodallec et al. 2008). They are also valuable in follow up after spinal surgery or radiotherapy. Often MRI may be used additionally in the follow-up.

26.4.2 Computed Tomography

The availability of CT has increased greatly in recent years and the speed and quality of image reconstruction has been greatly enhanced. Computed tomography allows fine detail assessment of osseous architecture, including the cortex and the trabecular framework, and detects much smaller areas of trabecular destruction/invasion than that appreciated on radiography alone. The pattern of destruction and the location within the vertebra indicates the infiltrative nature of the process (Fig. 26.6). The normal trabecular bone may be replaced by material of amorphous density and variable mineralisation in osteoblastic metastases. It helps evaluate the

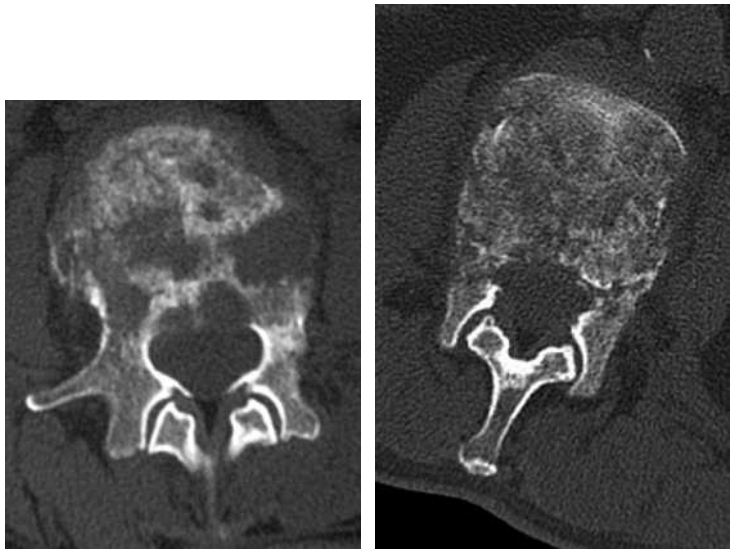

a,b

Fig. 26.6. **a** Axial CT scan demonstrates focal destructive change including destruction of the anterolateral margin of the body with paravertebral and epidural soft tissue extension and **b** diffuse destructive change of the vertebral body with paravertebral and epidural soft tissue extension

risk for vertebral body collapse (Taneichi et al. 1997). The extent of marrow involvement is well appreciated and early cortical invasion may be manifest by fine erosion of the inner margin. Image interrogation on the console allows the spine to be viewed with appropriate windowing even after thorax or abdominal imaging when unexpected spinal metastases may be detected. It is noteworthy, however, that if the scan was performed to specifically look at the thorax or abdomen using a soft tissue algorithm, then the images should be viewed with a bony algorithm on appropriate windows in order to avoid overlooking a subtle lesion. Computed tomography is also particularly helpful in assessing those areas which can be difficult to appreciate on radiography such as the sacrum (Fig. 26.7). Radiation dose with CT is significantly higher than with radiography, but as long as the ALARA principle is employed this should not be an issue. Some authors have suggested using low-dose CT instead of conventional radiography in patients affected by myeloma, bone metastases or fractures secondary to osteoporosis (Chassang et al. 2007; Horger et al. 2005). Computed tomography does have its merits in that it is quick to perform and from the patient's perspective there is minimal movement once the patient is positioned comfortably on the table. Additional unexpected lesions may also sometimes be detected; however, it is not always readily available, and although the patient may ultimately undergo CT, this is usually as part of the diagnostic work-up rather than being the preliminary imaging investigation (Fig. 26.8).

Some tumours exhibit a very characteristic CT pattern. Plasmacytoma, for example, is usually predominantly lytic. The tumour preferentially replaces the cancellous bone with preservation of the cortical bone which may result in an expansile, hollow vertebral body (Laredo et al. 2001). The cortex may then thicken, resulting in a "mini-brain" appearance on axial CT images (Major et al. 2000). Plasmacytoma may rarely be sclerotic (Voss et al. 2001). Similar to radiography, lesions on CT may be lytic, sclerotic or mixed. The axial cross-sectional nature allows assessment of the degree of soft tissue tumour encroachment on the spinal canal and cord and the degree of invasion of adjacent tissues. Magnetic resonance imaging is usually the preferred modal-

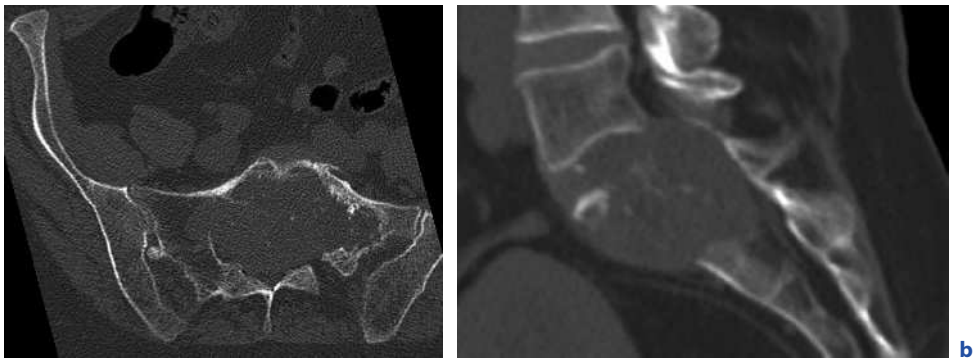

Fig. 26.7. **a** Axial and **b** sagittal CT images of a sacral metastasis

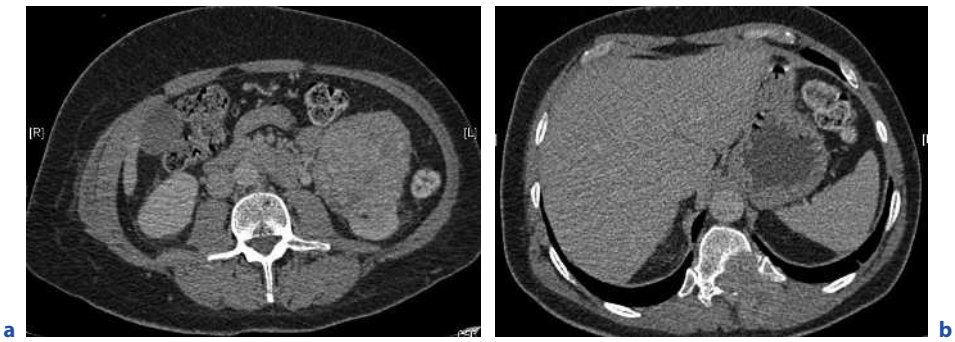

Fig. 26.8. **a** Axial CT scan of the abdomen demonstrates carcinoma of the left kidney. **b** The same CT scan also demonstrates a focal destructive lesion involving a thoracic vertebral body, left pedicle and adjacent soft tissues with infiltration of the spinal canal

ity in evaluation of malignant or indeed any spinal cord compression. In those instances, however, where MRI is contra-indicated, CT is an acceptable alternative, albeit with some limitations. The newer 64-slice multi-detector CT scanners allow rapid reconstruction of axial images with superb contrast and spatial resolution.

The multiplicity of lesions is the usual indication that lesions are metastases rather than other pathology. The presence of a single lesion will require a more studied approach to the investigation. Depending on the area covered, one may be able to view other structures, for example, thorax or abdomen, to seek a primary or evidence of other distant (soft tissue) metastases. A solitary expansile lesion, with or without soft tissue extension, may suggest myeloma or plasmacytoma as the underlying pathology. A single metastatic deposit from a renal cell carcinoma, however, would also need consideration and in this instance an ultrasound examination of the kidneys (if not already visible on the CT) would be helpful. Serum biochemistry and electrophoresis, however, together with a check on serum calcium would also help in such an instance, differentiating between myeloma and renal cell carcinoma metastasis. High-resolution CT can help differentiate between benign and malignant vertebral compression fractures. Kubota et al. (2005) demonstrated that the most reliable signs for malignant fractures included destruction of the anterolateral and/or posterior cortex of the vertebral body (100% accuracy) and destruction of the cancellous bone of the vertebral body (97.4% accuracy). Other features favouring malignancy included destruction of the end plate, destruction of the pedicle, a focal paraspinal soft tissue mass, a paraspinal soft tissue mass >5 mm and an epidural mass (Kubota et al. 2005).

26.4.3 Nuclear Medicine/Scintigraphy

The whole-body isotope bone scan utilising technetium-labelled methylene diphosphonate (Tc99m-MDP) is a very sensitive test for abnormal uptake, particularly increased uptake, but it is not very specific. Scintigraphy is also extremely limited as regards detailed anatomy (Wang et al. 2005) due in part to its very poor spatial resolution. Cold lesions are particularly common with multiple myeloma and can be difficult to appreciate. Whole-body MRI has been advocated by some centres in preference to whole-body bone scintigraphy due to its superiority in depicting bone metastases (Eustace et al. 1997; Steinborn et al. 1999; Ghanem et al. 2004). Uptake within the axial skeleton is particularly common in carcinoma of the breast or prostate (Fig. 26.1c). The "super scan" in cases of florid bone metastases occurs when there is so much uptake within the skeleton that none is visibly seen being excreted through the kidneys, which therefore are not readily appreciated. In cases of a known primary carcinoma, a whole-body bone scan is sometimes used as a screening tool for bone metastases. Correlating radiographs are often performed in conjunction. Again the pattern of uptake can help identify whether the pathology is most likely due to metastases or may be related to widespread arthropathy.

26.4.4 Magnetic Resonance Imaging

Magnetic resonance imaging is probably the most sensitive technique for detection of spinal metastases. The imaging protocol will be determined by whether one is simply using it as a screening tool or investigating specific symptomatology. A sagittal T1 and STIR sequence may be sufficient as a screening tool. The MRI appearance of metastatic deposits is variable depending on the repetition time (TR) and echo time (TE) of the sequence employed. Metastatic foci are often of low signal intensity on T1, and are well appreciated due to the mildly hyperintense marrow seen in adults (Daffner et al. 1986); however, high signal intensity on T1 can be due to the presence of blood (methaemoglobin), calcium, fat or melanin. Haemorrhage within a deposit may be indicative of a very vascular lesion such as can be found with renal cell carcinoma metastases; however, low signal due to flow voids can also occur in highly vascular renal metastases. High signal intensity on T1, in the appropriate setting, may also be reflective of metastases from melanoma (McMenamin et al. 2007). Other lesions are usually of low signal intensity on T1. Lesions are often of high signal intensity on fat-suppressed short tau inversion recovery (STIR) sequences, but if they contain fat or calcium, or are sclerotic in nature, they may not be so well appreciated. Short tau inversion recovery is a very sensitive sequence but has decreased spatial resolution compared with T1. Lesions which have low signal on T1 and high signal on STIR often have high or intermediate to high signal intensity on T2 but are often not so well appreciated. Osteoblastic metastases may have low signal intensity on both T1- and T2-weighted images. The T2-weighted study demonstrates the effect of the deposit on the subarachnoid and epidural space to particular advantage due its "myelographic" effect. A sagittal study alone may be a useful screening tool; however axial images through focal areas of abnormality seen in the sagittal study will be valuable. The value of the axial study is that it facili-

tates evaluation of the degree of encroachment on the spinal canal and epidural space and the effects of that encroachment on the spinal cord. The degree of cord compression can be evaluated, areas of osseous infiltration accurately identified and signal change within the cord indicative of myelomalacic change secondary to cord compression can be assessed. Coronal images are not routinely required but may play a role when focal pathology or extension of pathology into the paraspinal musculature is seen. Contrast enhancement is rarely required; however, it may be used if a single lesion only is identified in order to gather as much information as possible about the lesion. In cases of spinal metastases, whether picked up as an incidental lesion or in the presence of multiple lesions, it is very helpful to perform whole-spine MRI also including the sacrum. This may detect further unsuspected metastases, the presence of which may have an effect on management.

Magnetic resonance imaging not only of the whole spine, but also of the whole body, is becoming an increasingly valuable investigation in the assessment of metastatic disease. Improvements in table and coil design led to the introduction of a dedicated rolling table platform with a fixed surface coil and subsequent introduction of parallel imaging techniques have resulted in significant reduction of examination time and increase in patient comfort (Schmidt et al. 2005).

Different patterns of metastatic infiltration are described. There may be diffuse infiltration involving an entire vertebral body, with extension into the pedicles and possibly also the posterior elements (Fig. 26.9). Discrete focal deposits may affect isolated areas of the posterior neural arch, including the spinous process. There may be varying degrees of vertebral body collapse, contiguous vertebral and/or posterior element involvement, very often with sparing of the intervertebral disc (Fig. 26.10). This is a useful pointer in differentiating from spinal infection. There may be associated paravertebral soft tissue swelling or lymphadenopathy. Classically infection will be associated with loss of definition of the end plates and involvement of the disc, but this is not always the case. In tuberculosis, for example, very often the disc is spared and the mode of spread is subligamentous. In tuberculosis there is often quite extensive soft tissue swelling. Clinical details, basic blood tests, including a full blood count, ESR and C-reactive protein, can all be helpful in giving more weight to one or other diagnosis, but in the majority of cases, biopsy and histological assessment will be required. Medullary involvement with an adjacent soft tissue mass and intact cortex may be suggestive of lymphoma. Contiguous vertebral involvement may occur (Mulligan et al. 1999). Lymphoma, as the primary lesion, may be suspected by the presence of para-aortic or paracaval lymphade-

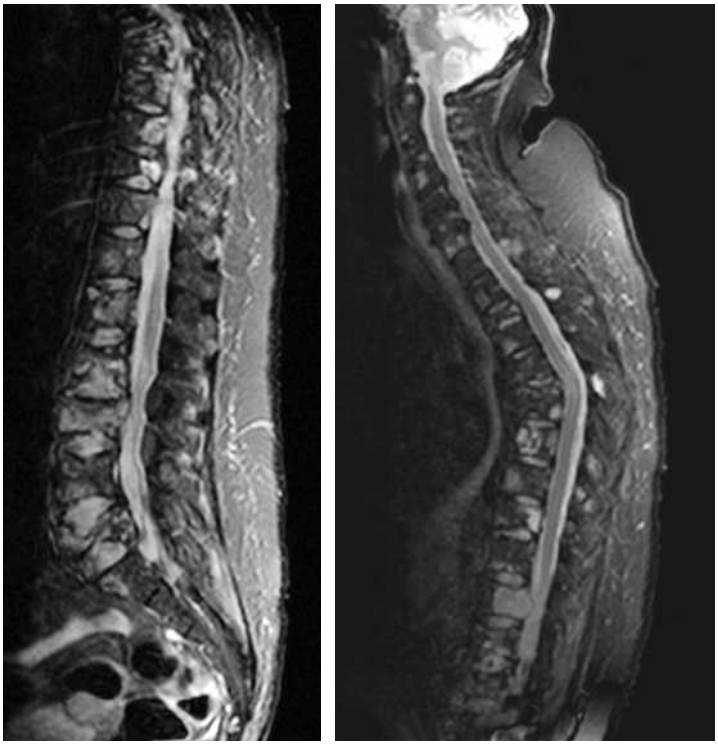

a,b

Fig. 26.9a,b. Pattern of vertebral involvement. **a** Sagittal STIR image of the thoracolumbar spine shows multiple metastases in vertebral bodies with varying degrees of vertebral collapse. There are deposits within the vertebral body and at the corners of the bodies deep to the vertebral end plates at sites of maximum blood supply. **b** Sagittal STIR image of the cervicothoracic spine with multiple deposits in vertebral bodies, and within the posterior neural arch. Note posterior bowing of a lower thoracic vertebral body due to tumour extension

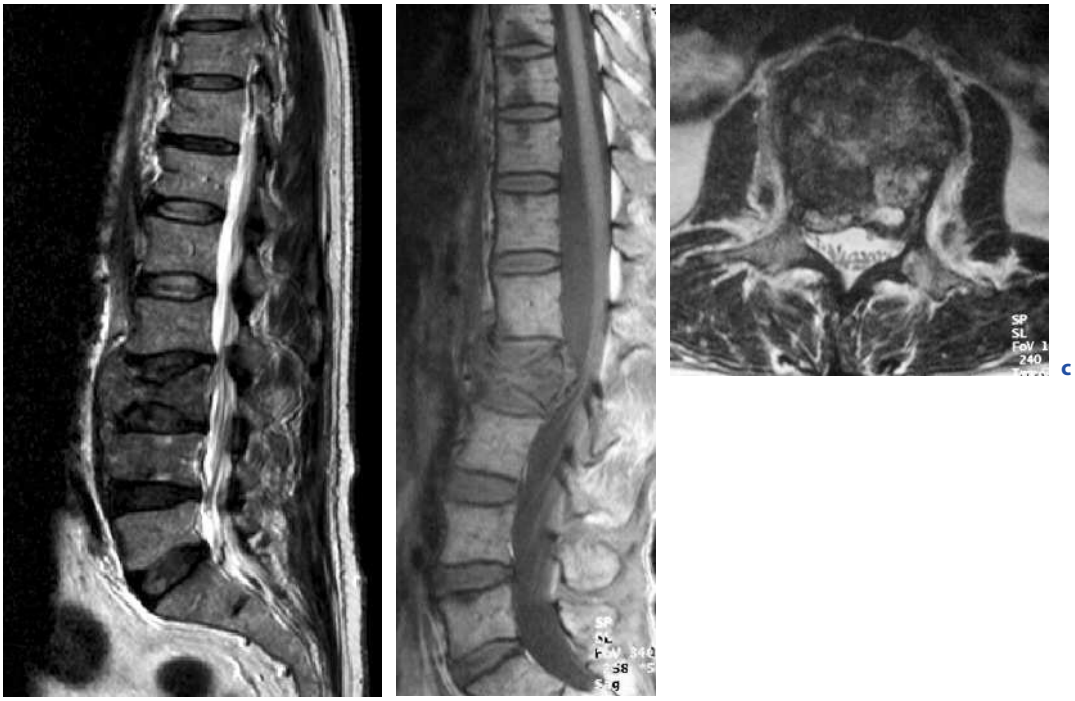

a,b c

Fig. 26.10. **a** Sagittal T2-weighted image shows contiguous metastases (L3 and L4) with anterior bowing of L3 due to tumour extension. **b** Midline sagittal T1-weighted MR image in another patient. Tumour infiltrative collapse of L2. Note the posterior bowing of the vertebral body, the prevertebral and epidural soft tissue extension. Marked compromise of the central spinal canal. Note a further deposit in the antero-inferior corner of L1 which has likely developed due to direct spread. Note further deposits principally in a subchondral location adjacent to the end plates, sites of particular vascularity. **c** Axial MR image through L2. Note the posterior bowing of the vertebral body, diffuse heterogeneous abnormal signal within the body, with cortical breakthrough in a left lateral location and extension posteriorly into the left pedicle. Tumour encroachment on the epidural space

nopathy. This occurs more usually from haematogenous spread than from direct bone invasion from adjacent lymph nodes. It may occur with osseous, paravertebral or epidural involvement in isolation or in combination (Laredo et al. 2001).

On MRI, vertebral body collapse as a cause of symptoms will need to be differentiated between benign osteoporotic collapse and metastatic infiltration (Fig 26.10). The use of other complimentary imaging modalities, for example, CT, will be helpful. Certain features help to differentiate between the two conditions including the presence or absence of paravertebral soft tissue swelling, an epidural mass, as well as cortical and cancellous bone destruction (Fig. 26.10; Kubato et al. 2005). Diffusion-weighted imaging on MR has been advocated as being helpful in differentiating between the two. Baur et al. (1998, 2001, 2003) has shown that benign compression fractures are hypo- to iso-intense relative to normal vertebral bodies on DWI, whereas pathological compression fractures are hyperintense. Another study, however, has shown that benign and malignant compression fractures show considerable overlap on diffusion-weighted MR images even in quantitative assessment with apparent diffusion coefficient maps. Another study found DWI to be useful in differentiating sacral insufficiency fractures from metastases of the sacrum (Byun et al. 2007).

In the case of a limited area of the spine initially being scanned to investigate symptoms, should this demonstrate probable metastases then it is advisable to scan the whole spine for full assessment and to allow optimum patient management. In particular, in those patients being scanned to investigate cord compression, if a level has been identified, then it is mandatory to scan the whole spine to ensure that there is no other level of impending compression prior to surgery. The surgeon will also wish to know the status of the vertebrae at levels adjacent to the level for decompression to ensure that there will be adequate purchase for any surgical stabilisation (Fig. 26.11).

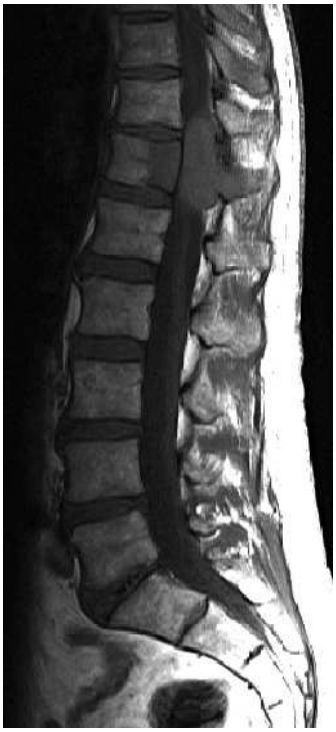

a

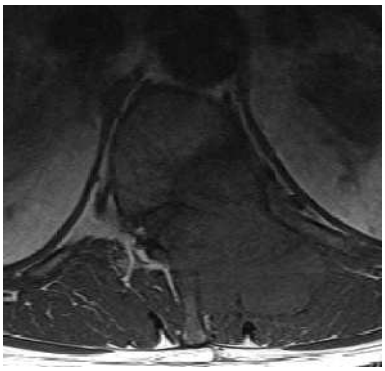

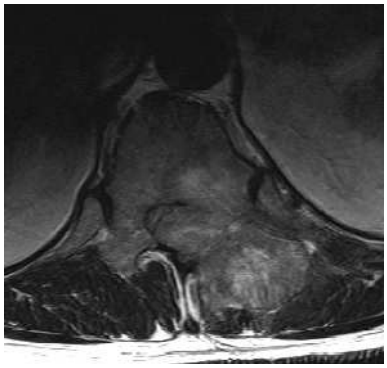

b,c

Fig. 26.11a–c. Patient presents with red-flag symptoms of spinal cord compression (**a**). Sagittal T1-weighted MR image demonstrates extensive tumour infiltration of the body of T12, extending into the pedicle and adjacent soft tissues including the spinal canal. **b** Axial T1-weighted MR image demonstrates the extensive tumour infiltration into the spinal canal with marked compression of the cord and **c** axial T2-weighted MR image shows compression of the cord with complete effacement of the cerebrospinal fluid in the thecal sac

Surgical instrumentation used in spinal stabilisation procedures after decompression is usually made of titanium which is associated with fairly minimal artefact and usually a reasonable view of the spinal canal and cord can be obtained. Magnetic resonance imaging plays a role in differentiating post-operative change from tumour recurrence. Intravenous gadolinium chelate is valuable in this situation. Post-operative fibrosis usually results in fairly diffuse enhancement of the tissues, whereas recurrent tumour will usually demonstrate a fairly inhomogeneous enhancement pattern depending on the nature of the primary tumour, its degree of vascularity and/or necrosis. Tumour recurrence is usually associated with mass effect and likely demonstrates a signal pattern similar to that seen on pre-operative imaging. Magnetic resonance imaging also clearly demonstrates post-radiotherapy change, which is usually manifest as fatty change in vertebral bodies. A sharp zone of transition between those vertebrae previously subjected to radiotherapy and non-irradiated vertebrae is usually apparent.

In the context of metastases affecting not only the spine but other areas of the body, whole-body MRI has been advocated as superior to whole-body isotope scintigraphy.

26.4.5 Positron Emission Tomography

The FDG positron emission tomography (PET) technique is not used greatly for the diagnosis of spinal metastases. Occasionally, however, it may play a role, for example, in a situation where a single spinal lesion is identified whose differential diagnosis could include benign aetiology. PET may play a role in this instance by assessing the metabolic activity of the lesion, but currently it is not used routinely. PET plays a role more in evaluation of soft tissue metastases from breast or lung.

26.5 Algorithmic Approach

Each imaging modality has particular advantages. It would be inappropriate to perform all modalities on all patients and in practice it is not uncommon for a combination of modalities to be used to arrive at a differential diagnosis. A suggested algorithm for the investigation of a patient with suspected spinal metastases is shown in Table 26.2.

Table 26.2. Algorithm: No known primary lesion. *LBP* lower back pain

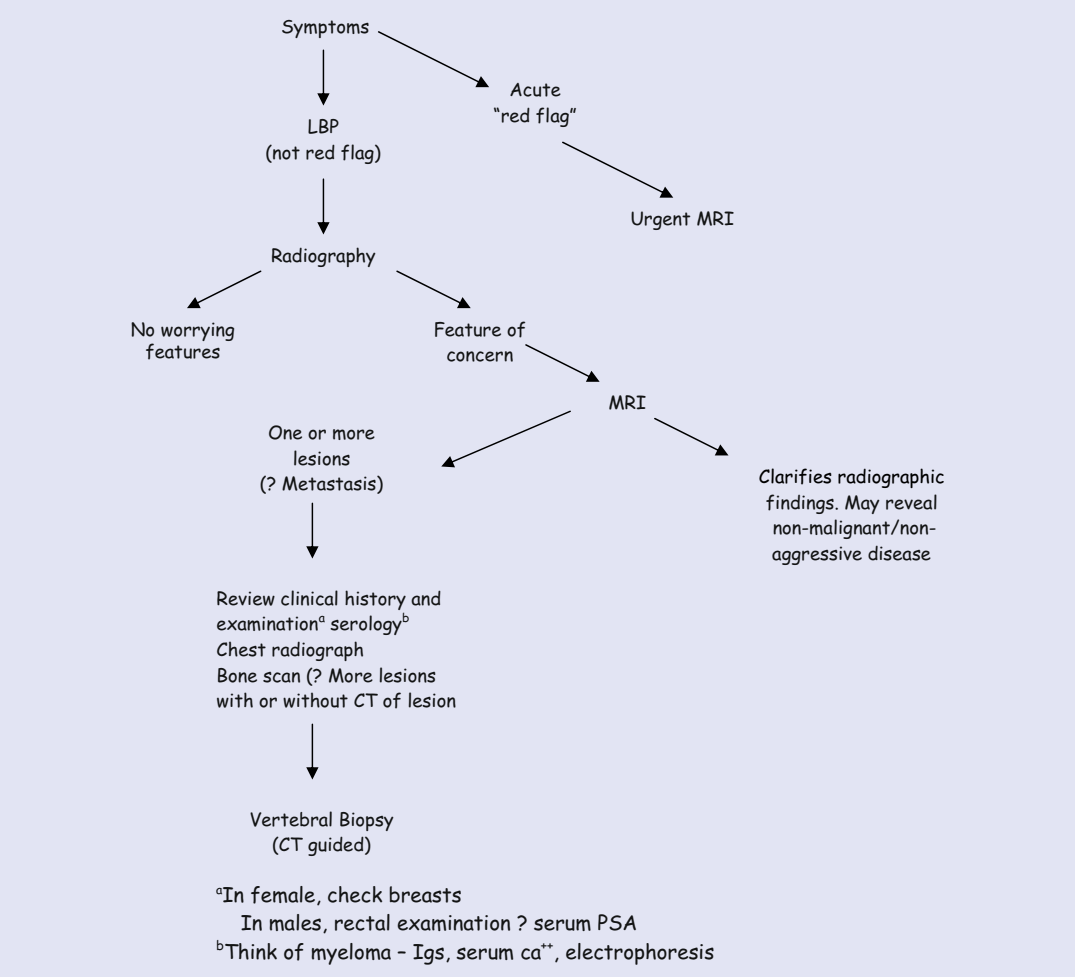

[a]In female, check breasts. In males, rectal examination? serum PSA. [b]Think of myeloma–Igs, serum ca^{++}, electrophoresis

26.6 Differential Diagnosis

The differential diagnoses to be considered in the imaging of spinal metastases will very often depend on the number of lesions, the extent of involvement and the area of involvement of the vertebrae (whether it is the vertebral body, the pedicle or part of the neural arch). There can sometimes be particular difficulties in differential diagnosis when either the intervertebral disc or a facet joint is involved. Clearly the age of the patient will have a bearing on consideration as well as the clinical presentation. The presence of multiple lesions will raise one set of differential diagnoses. The presence of an apparently solitary lesion will suggest a different range of differentials. In the older patient one or more lucent lesions or focal areas of destruction will raise the possibility of multiple myeloma. This is particularly the case where the bone may appear slightly expanded. Both renal and thyroid metastases, however, can also appear expansile in nature. With expansile lucent lesions, prior to consideration of biopsy, it is always valuable to do an ultrasound examination of the kidneys to ensure that there is no obvious renal tumour present. Renal cell metastases can be particularly vascular. If there is involvement of the intervertebral disc, infection (pyogenic or granulomatous, including tuberculosis) needs to be considered (Ross and Fleming 1976; Modic et al. 1985; Dagirmanjian et al. 1996). Contiguous vertebral involvement with discal sparing may also raise the suggestion of infection in the appropriate setting as some infections, particularly tuberculosis, can spread subligamentously. The phrase "good disc, bad news; bad disc, good news" is not always true. The meaning of this is that if the disc is destroyed with vertebral end-plate

destruction, in the majority of cases this is likely due to infection; however, if there is destructive change within two adjacent vertebral bodies but the end plates remain intact and the disc preserved, then this is more likely to mean malignancy. This is not exclusive, however. Intervertebral disc involvement by metastatic disease is well described but is relatively rare (Hubbard and Gunn 1972; Resnick and Niwayama 1978) and spinal infection does not always involve the disc (Hsu et al. 2008). Sclerotic foci within the vertebrae may represent metastatic deposits but, if solitary, may represent a bone island. A sclerotic pedicle may be due to the presence of a sclerotic metastasis, but other causes of sclerosis in this location can occur including pedicle hypertrophy in association with a contra-lateral spondylolysis or congenital hypoplasia of the neural arch (Fig. 26.12; Yochum et al. 1990). Other very unusual causes would include mastocystosis. Multiple osteomata can occur in Gardner's syndrome. Paget's disease is usually diagnostically obvious, but again, particularly when involving a single vertebra, may give rise to confusion and enter the differential diagnosis.

Osteoporosis when associated with vertebral body collapse may raise the suspicion of metastatic involvement, particularly when there is difficultly in appreciating the pedicles. Difficulty in appreciation of the pedicles may be due to poor radiographic technique or due to the very intense osteopaenia rendering the pedicular margin difficult to appreciate. Multiple levels and variable degrees of vertebral collapse together with altered signal on MRI can be confusing; however, often the pattern of signal intensity on MRI will assist. In osteoporotic collapse the signal intensity is often high in a linear distribution just inferior to the end plate. There is no paravertebral soft tissue swelling and no epidural encroachment. There may also be foci of fatty change within vertebral bodies, manifest as high signal intensity on both T1- and T2-weighted images, which suppress completely on fat-suppressed or STIR images.

On scanning of the lumbar spine careful attention should be paid to the sacrum as this is a site where lesions can often be overlooked as the area sometimes rests at the very edge of the scan field and slightly altered signal here may be misinterpreted as being due to artefact. The sacrum is a not uncommon site for metastases. It is also a common site for insufficiency fractures, which can occur in association with osteoporotic fractures in the lumbar and thoracic spine. They can

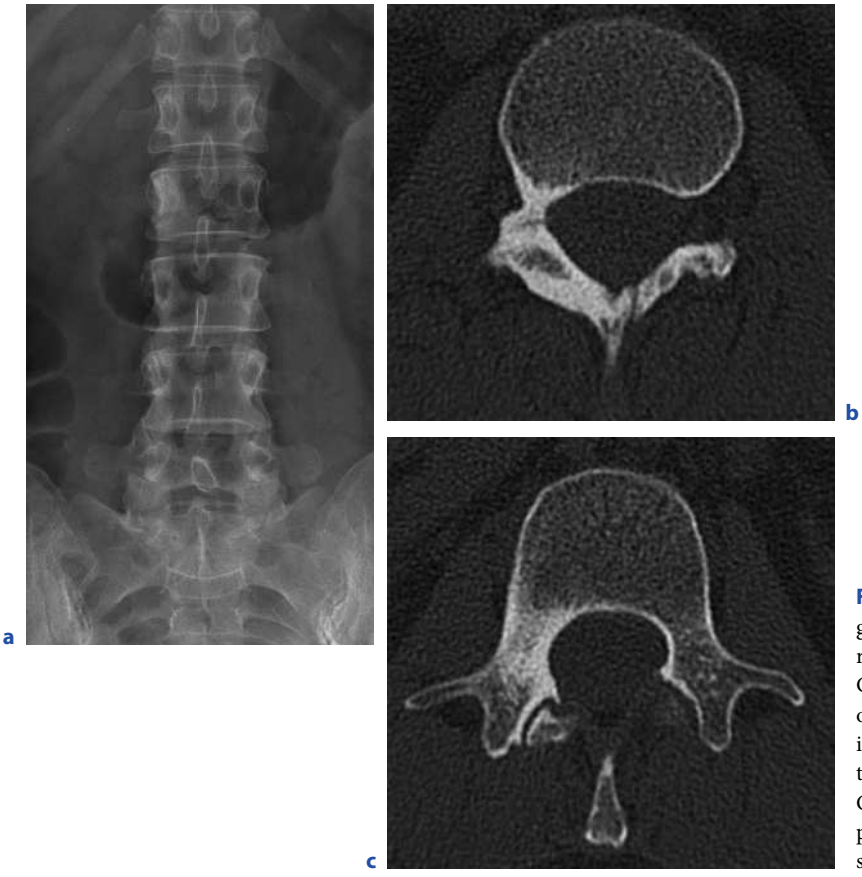

Fig. 26.12. **a** Anteroposterior radiograph demonstrates sclerosis of the right pedicle of L2. **b** A subsequent CT scan demonstrates a spondylolysis of the left lamina with a corresponding stress reaction and fracture of the right pedicle. **c** On a further axial CT image hypertrophy of the right pedicle with associated sclerosis is seen

also occur secondary to radiotherapy given in cases of gynaecological malignancy, especially for carcinoma of the cervix, and also in carcinoma of the prostate. Sacral insufficiency fractures may present with pain but may present in other ways and be an unsuspected finding. On MRI they may present with very florid oedema.

Spondyloarthropathy as seen on MRI may also be a potential source of confusion in differentiating it from metastases. Multiple lesions of varying signal intensity, representative of variable activity at sites of entheses, are seen. The very characteristic location of these foci, related to the entheses and also to costovertebral articulations, should obviate misinterpretation.

Modic signal changes of degenerative disc disease (Modic et al. 1988) should be readily recognisable from their characteristic location adjacent to the end plates and almost invariable association with other signs of degeneration in relation to the intervertebral disc with loss of disc hydration and variable reduction of disc height, with or without disc bulging or prolapse.

Haemotopoietic bone islands can be a source of confusion often resulting in a patient undergoing a variety of imaging investigations with subsequent follow-up. On MRI these bone islands may present as areas of subtle low signal on T1-weighted images (Gupta et al. 2007).

Assessment of the solitary spinal bone lesion presents a wide differential diagnosis (Rodallec et al. 2008). An isolated bone lesion involving the vertebral body or the posterior elements in the older age group is still more likely to represent a metastasis. In the younger age group, other benign lesions, including aneurysmal bone cyst and osteoblastoma, will need consideration. Often, following consideration of the age, clinical presentation and review of the clinical findings, the diagnosis may be clear; however, it is only following biopsy and histological evaluation that the diagnosis is confirmed. Although biopsy of these lesions is not always indicated, certainly if it is in any way likely to alter patient management such biopsy will be required.

26.7 Biopsy

Histological confirmation of metastasis is only achieved by biopsy. If infection has been a consideration in the differential diagnosis, then a sample of the biopsy material should also be sent to microbiology for culture and sensitivity. The relevant departments will be able to advise on the particular medium in which the specimens should be sent. Radiology departments will vary as regards what facilities they are able to provide for biopsy. Utilising CT guidance is probably the optimum modality allowing the radiologist to target specific areas of involvement. Ideally biopsy samples should be obtained from the margin of the lesion and the lesion/bone interface. This is usually the site of active invasion/destruction and will provide the histopathologist with the best opportunity for making a definitive diagnosis. Tissue taken from the very centre of a lesion may simply yield blood and necrosis. Biopsy material obtained too peripheral to the lesion may simply reveal reactive bone rather than frank pathological lesional tissue (McCarthy 2007). Biopsy in the thoracic and lumbar region is via a postero-lateral approach. Biopsy of a cervical vertebral body will more usually be done by an antero-lateral approach. If the lesion to be biopsied has features which might suggest a metastasis from a renal cell carcinoma (lucent, expansile, hypervascular on post-contrast imaging studies), then it is prudent to carry out an ultrasound or other imaging of the kidneys prior to biopsy. Metastases from renal cell tumours can be particularly vascular and haemorrhagic and "forewarned is forearmed!"

Once the biopsy samples have been sent to pathology, the samples will usually undergo a process of decalcification prior to examination of the tissue. Histological assessment has advanced significantly in recent years with the development of multiple stains as well as immunological and tissue markers which in many cases can produce a highly accurate and confirmatory diagnosis. Even where a single diagnosis is not obtained, the differential diagnosis list is usually narrow and if a primary lesion is not already known clinically, then the histology results can direct further investigation.

26.8 Management/Therapy

Management of spinal metastases varies depending on a number of factors. The presence of a single isolated spinal metastasis may be treated quite differently compared with a situation where there are multiple spinal lesions. The nature of the primary lesion can also have a significant effect on further management. Patients with primary carcinoma of the lung and secondary spread to the spine tend not to do well and have a very poor prognosis, although there are occasional exceptions. The principal indications for surgery in spinal metastatic disease include decompression of the cord in those situations where the patient presents with symptoms due to

neurological compromise from spinal cord compression due to metastatic infiltration of the spine and spinal canal. This is usually undertaken for palliative purposes rather than as a curative procedure. Even if a patient has only a very limited prognosis in terms of months, quality of life can be improved greatly by spinal decompression relieving the patient of final days as a paraplegic with associated bowel and urine problems. If the compressing tumour is radiosensitive, then radiotherapy may be a preferred option, particularly in those cases where the patient has multiple spinal metastases and gaining purchase with stabilising metalwork may prove difficult. Other indications for surgery include fixation/instrumentation to stabilise the spine in order to avoid deformity and to reduce the risk of fracture with its associated complications. Taneichi et al. (1997) showed that the most important risk factor leading to vertebral collapse in the thoracic region (T1–T10) was involvement of the costovertebral joint. Tumour size within the vertebral body was the second most important risk factor. Impending collapse exists when 50–60% of the thoracic vertebral body alone is involved, or 25–30% with costovertebral joint involvement. In the thoracolumbar and lumbar spine, the most important factor for collapse is the size of the tumour within the vertebral body. The second most important factor is destruction of the pedicle. The criteria for impending collapse are 35–40% involvement of the vertebral body alone, reducing to 20–25% involvement when the pedicle or posterior elements are also involved (Figs. 26.8, 26.11). Following instrumentation, radiographs are employed to check position (Fig. 26.13) and thereafter may be obtained should new symptoms develop to check that the instrumentation has not loosened or slipped due to progressive tumour infiltration.

Newer techniques involving radiofrequency thermoablation have been used in some cases of spinal metastases. Vertebral body collapse due to metastatic infiltration has been treated by vertebroplasty with variable success. Again, this is a palliative procedure more to help alleviate symptoms than anything else.

Follow-up imaging of spinal metastases is not carried out as a routine. When patients develop symptoms related to the spine, then clearly follow-up imaging is indicated. This is usually with MRI. Even in the presence of metalwork, reasonable and diagnostic views of the spinal canal and cord can usually be obtained utilising appropriate sequences. Following radiotherapy, the treated marrow undergoes fatty change and evidence of this may be clearly visible on follow-up MR imaging. The horizontal line of the edge of the radiotherapy field clearly delineates treated from untreated areas.

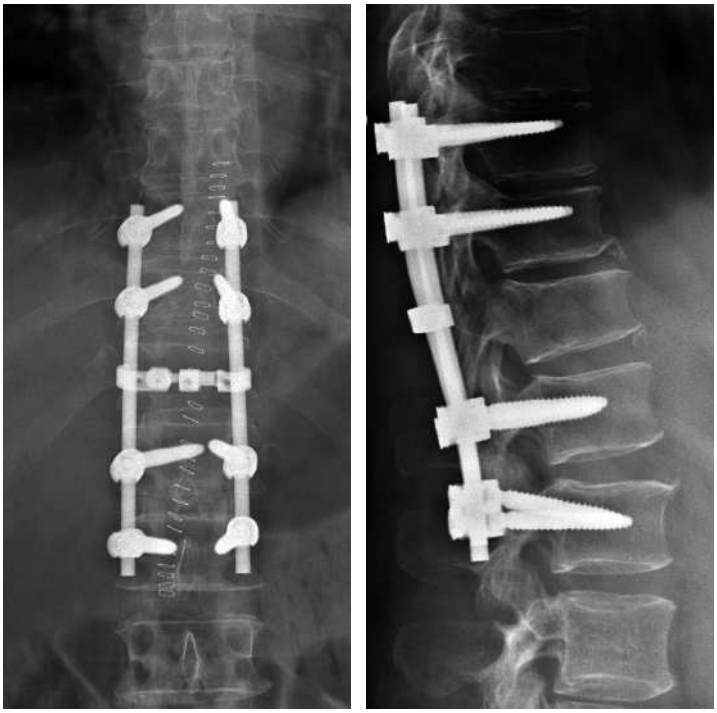

a,b

Fig. 26.13. **a** Anteroposterior and **b** lateral radiographs of the thoraco-lumbar spine following surgical stabilisation of T12 (same patient as in Fig. 26.11)

References

Algra P, Heimans JJ, Valk J, Nauta JJ, Lachniet M, Van Kooten B (1992) Do metastases in vertebrae begin in the body or in the pedicles? Imaging study in 45 patients. AJR 158:1275–1279

Asdourian PL, Weidenbaum M, DeWald RL, Hammerberg KW, Ramsey RG (1990) The pattern of vertebral involvement in metastatic vertebral breast cancer. Clin Orthop 250:164–170

Batson OV (1942) The role of the vertebral veins in metastatic processes. Ann Intern Med 16:38–45

Batson OV (1957) The vertebral vein system. AJR 78(2):195–212

Baur A, Stabler A, Bruning R et al. (1998) Diffusion weighted MR imaging of bone marrow. Differentiation of benign versus pathologic compression fractures. Radiology 207:349–356

Baur A, Huber A, Ertl-Wagner B et al. (2001) Diagnostic value of increased diffusion weighting of a steady-state free precession sequence for differentiating acute benign osteoporotic fractures from pathologic vertebral compression fractures. AJNR 22:366–372

Baur A, Dietrich O, Reiser M (2003) Diffusion-weighted imaging of bone marrow: current status. Eur Radiol 13:1699–1708

Breschet G (1832) Récherches anatomiques, physiologiques et pathologiques sur le système veineux et voie anatomiques. Masson, Paris

Byun WM, Jang HW, Kim SW, Jang SH, Ahn SH, Ahn MW (2007) Diffusion weighted magnetic resonance imaging of sacral insufficiency fractures; comparison with metastases of the sacrum. Spine 32(26):E820–E824

Chassang M, Grimaud A, Cucchi JM, Novellas S, Amoretti N, Chevallier P, Brunton JN (2007) Can low dose computed tomographic scan of the spine replace conventional radiography? An evaluation basd on imaging myelomas, bone metastases, and fractures from osteoporosis. Clin Imaging 31:225–227

Clines GA, Guise TA (2005) Hypercalcaemia of malignancy and basic research on mechanisms responsible for osteolytic and osteoblastic metastasis to bone. Endocrinol Relat Cancer 12(3):549–583

Daffner RH, Lupetin AR, Dash N et al. (1986) MRI in the detection of malignant infiltration of bone marrow. AJR 146:353–358

Dagirmanjian A, Schils J, McHenry M, Modic MT (1996) MR imaging of vertebral osteomyelitis revisited. AJR 167:1539–1543

Edelstyn GA, Gillespie PJ, Grebbell FS (1967) The radiological demonstration of osseous metastases. Experimental observations. Clin Radiol 18:158–162

Eustace S, Tello R, DeCarvalho V et al. (1997) A comparison of whole body turbo STIR MR imaging and planar 99mTC-methylene diphosphonate scintigraphy in the examination of patients with suspected skeletal metastases. AJR 169:1655–1661

Firooznia H, Pinto RS, Lin JP, Baruch HH, Zausner J (1976) Chordoma: radiologic evaluation of 20 cases. AJR 127:979–805

Galasko CSB (1972) Skeletal metastases and mammary cancer. Ann R Coll Engl 50(1):3–28

Galasko CSB (1981) The anatomy and pathways of skeletal metastases. In: Weiss L, Gilbert HA (eds) Bone metastasis. Hall, Boston, p 49

Galasko CSB (1982) Mechanisms of lytic and blastic metastatic disease of bone. Clin Orthop 169:20–27

Ghanem N, Kelly T, Altehoefer C et al. (2004) Whole body MRI in comparison to skeletal scintigraphy for detection of skeletal metastases in patients with solid tumours. Radiology 44:864–873

Guillevan R, Vallee J-N, Lafitte F, Menuel C, Duverneuil N-M, Chiras J (2007) Spine metastasis imaging: review of the literature. J Neuroradiol 34:311–321

Guise TA (2000) Molecular mechanisms of osteolytic bone metastases. Cancer 88 (12 Suppl):2892–2898

Guise TA, Kozlow WM, Heras-Herzig A, Padalecki SS, Yin JJ, Chirgwin JM (2005) Molecular mechanisms of breast cancer metastases to bone. Clin Breast Cancer 2 (5 Suppl):546–553

Gupta G, Robertson P, Szer J (2007) Focal lesions on magnetic resonance imaging in aplastic anaemia: multiple metastases or haemopoetic marrow. Austral Radiol 51:8110–8114

Haller J, André P, Resnick D, Miller C, Howard BA, Mitchell MJ, Schils JP, Sartoris DJ, Trudell D (1990a) Detection of thoracolumbar vertebral body destruction with lateral spine radiography. Part 1: Investigation in cadavers. Invest Radiol 25:517–522

Haller J, André P, Resnick D, Miller C, Howard BA, Mitchell MJ, Schils JP, Sartoris DJ, Trudell D (1990b) Detection of thoracolumbar vertebral body destruction with lateral spine radiography. Part 2: Clinical investigation with computed tomography. Invest Radiol 25:523–531

Horger M, Claussen CD, Bross-Bach U, Vonthein R, Trabold T, Heuschmid M, Pfannenberg C (2005) Whole body low dose multidetector row-CT in the diagnosis of multiple myeloma: an alternative to conventional radiography. Eur J Radiol 54:289–297

Hsu CY, Yu CW, Wu MZ, Chen BB, Huang KM, Shih TTF (2008) Unusual manifestations of vertebral osteomyelitis: intraosseous lesions mimicking metastases. AJNR 29:1104–1110

Hubbard DD, Gunn DR (1972) Secondary carcinoma of the spine with destruction of the intervertebral disk. Clin Orthop 88:86–88

Jacobson HG, Poppel MH, Shapiro JH, Grossberger S (1958) The vertebral pedicle sign: a roentgen finding to differentiate metastatic carcinoma from multiple myeloma. AJR 80:817–821

Jung N-Y, Jee W-H, Ha K-Y, Park C-K, Byun J-Y (2004) Discrimination of tuberculous spondylitis from pyogenic spondylitis on MRI. AJR 182:1405–1410

Khattry N, Thulkar S, Das A, Khan SA, Bakhshi S (2007) Spinal tuberculosis mimicking malignancy; aptypical imaging features. Indian J Paediatr 74:297–298

Kubota T, Yamada K, Ito H, Kizu O, Nishimura T (2005) High resolution imaging of the spine using multidetector non-computed tomography: differentiation between benign and malignant vertebral compression fractures. J Comput Assist Tomogr 29(5):712–718

Laredo JD, el Quessar A, Bossard P, Vuillemin-Bodaghi V (2001) Vertebral tumours and pseudotumours. Radiol Clin North Am 39 (1):137–163, vi

Lodwick GS (1964) Reactive response to local injury in bone. Radiol Clin North Am 50:209–219

Major NM, Helms CA, Richardson WJ (2000) The "mini brain": plasmacytoma in a vertebral body on MR imaging. AJR 175(1):261–263

Manishen WJ, Sivananthan K, Orr FW (1986) Resorbing bone stimulates tumour cell growth. A role for the host microenvironment in bone metastasis. Am J Pathol 123:39

McCarthy EF (2007) CT-guided needle biopsies of bone and soft tissue tumours: a pathologist's perspective. Skeletal Radiol 36:181–182

McMenamin DS, Stuckey SL, Potgleter GJ (2007) T1 hyperintense vertebral column melanoma metastases. AJNR 28:1817–1818

Modic MT, Feiglin DH, Piralno DW et al. (1985) Vertebral osteomyelitis: assessment using MR. Radiology 157:157–166

Modic MT, Steinberg PM, Ross JS, Masaryk TJ, Carter JR (1988) Degenerative disc disease: assessment of changes in vertebral body marrow with MR imaging. Radiology 166:193–199

Mulligan ME, McRae GA, Murphey MD (1999) Imaging features of primary lymphoma of bone. AJR 173(6):1691–1697

Mundy GR, Spiro TP (1981) The mechanism of bone metastasis and bone destruction by tumour cells. In: Weiss L, Gilbert HA (eds) Bone metastasis. Hall, Boston, p 64

Mundy GR, Luben RA, Raisz LG, Oppenheim JJ, Buell DN (1974a) Bone resorbing activity in supernatants from lymphoid cell lines. N Engl J Med 290:867–871

Mundy GR, Raisz LG, Cooper RA, Schechter GP, Salmon SE (1974b) Evidence for the secretion of an osteoclast stimulating factor in myeloma. N Engl J Med 291:1041–1046

Mundy GR, Raisz LG, Shapiro JL, Bandelin JG, Turcotte RJ (1977) Big and little forms of osteoclast activating factor. J Clin Invest 60:122–128

Paget S (1889) The distribution of secondary growths in cancer of the breast. Lancet 1:571–573

Resnick D, Niwayama G (1978) Intervertebral disc abnormalities associated with vertebral metastasis: observations in patients and cadavers with prostatic cancer. Invest Radiol 13:182–190

Rodallec MH, Feydy A, Larousserie F, Anract P, Campagna R, Babinet A, Zins M, Drape J-L (2008) Diagnostic imaging of solitary tumours of the spine: what to do and say. Radiographics 28:1019–1041

Ross PM, Fleming JL (1976) Vertebral body osteomyelitis. Spectrum and natural history. A retrospective analysis of 37 cases. Clin Orthop 118:190–198

Royal College of Radiologists, London (2007) Making the best use of clinical radiology services. Referral guidelines, 6th edn

Schmidt GP, Schoenberg SO, Reiser, Baur-Melnyk A (2005) Whole body MR imaging of bone marrow. Eur J Radiol 55:33–40

Steinborn M, Heuch AF, Tiling R, Bruegel M, Gauger L, Reiser MF (1999) Whole body bone marrow MRI in patients with metastatic disease to the skeletal system. J Comput Assist Tomogr 23:123–129

Taneichi H, Kaneda K, Takeda N, Abumi K, Satoh S (1997) Risk factors and probability of vertebral body collapse in metastases of the thoracic and lumbar spine. Spine 22(3):239–245

Tyrrell PNM, Cassar-Pullicino V, McCall IW (1995) Short communication. A lateral will do. Br J Radiol 68:1371

Voss SD, Murphey MD, Hall FM (2001) Solitary osteosclerotic plasmacytoma: association with demyelinating polyneuropathy and amyloid deposition. Skeletal Radiol 30(9):527–529

Wang K, Allen L, Fung E, Chan CC, Chan JC, Griffith JF (2005) Bone scintigraphy in common tumours with osteolytic components. Clin Nucl Med 30(10):655–671

Yasuma T, Yamauchi Y, Arai K, Makino E (1989) Histopathologic study on tumor infiltration into the intervertebral disc. Spine 14(11):1245–1248

Yochum TR, Sellers LT, Oppenheimer DA, Peterson CK, Kirton CW, Dal Mas EC, Anderson AL (1990) The sclerotic pedicle: How many causes are there? Skeletal Radiol 19:411–417

Bone Metastases 2: Pelvis and Appendicular Skeleton

27

Bernhard J. Tins, Radhesh K. Lalam, Victor M. Cassar-Pullicino and Prudencia N. M. Tyrrell

CONTENTS

B. J. Tins, MD
R. K. Lalam, MD
V. N. Cassar-Pullicino, MD
P. N. M. Tyrrell, MD
Department of Radiology, The Robert Jones and Agnes Hunt Orthopaedic and District Hospital NHS Trust, Oswestry, Shropshire SY10 7AG, UK

KEY POINTS

- Metastatic bone disease is the commonest bone malignancy in the adult ≥40 years of age.
- The occurrence of bone metastases is a sign of poor prognosis, and major complications due to bone metastases are common and include hypercalcaemia and pathological fracture.
- Fracture risk can be assessed utilising clinical criteria and radiographs using the Mirels score.
- Bone lesions, especially if solitary, cannot be assumed to be metastases even in patients with a known primary malignancy.
- Biopsies should be performed in a dedicated bone tumour centre.
- The main aim of all treatments must be to relieve pain and restore function; patient management benefits from a multidisciplinary approach.
- Follow-up imaging after treatment is challenging for the radiologist and requires detailed knowledge about the treatment and possible outcomes and complications.
- Bone metastases can occur within any bone in any location.
- The morphology of bone metastases is extremely varied and unspecific; in many cases histological confirmation is indicated.
- Radiographs are relatively insensitive and unspecific but still a valuable first-line investigation for focal pain.
- Bone scintigraphy is a simple and inexpensive screening test for bone metastases, but specificity and less so sensitivity are limited.
- PET–CT and whole-body MRI offer good sensitivity and specificity but are expensive and not universally available.

27.1 Introduction

Bone metastases to the appendicular skeleton are less frequent than those to spine and pelvis. They can be the first manifestation of the underlying primary malignancy or be "just" another complication in a patient with known metastatic disease. Their morphological and clinical spectrum is vast and this can make the diagnosis difficult. Failing to make the diagnosis and failing to act appropriately can make the difference between life and death or, more frequently, between a reasonably active and pain-free end of life to misery and pain. Imaging is at the forefront of assessing the patient's disease status and should be part of a multidisciplinary approach to these patients.

This chapter discusses the most important issues facing the radiologist, the choice of imaging modality, the morphology of metastatic bone lesions and biopsy and treatment.

27.2 Definition

Metastasis describes the spread of a disease process away from its site of origin. Metastatic disease of the skeleton is commonly taken as spread of a neoplastic disease process to bone, but strictly speaking it describes seeding of any disease process and would, for example, include infectious seeding. In the context of this chapter metastatic disease of the appendicular skeleton is seen as spread of a primary malignancy to bone other than the spine. Myeloproliferative diseases, including multiple myeloma, are not included in the discussion.

27.3 Epidemiology

Metastatic bone disease is important because it is so common and usually leads to severe complications. It has been estimated that in the U.S.A. alone 350,000 people die each year from bone metastases. In autopsy series bone was the third most common site of metastatic spread, after lung and liver, and occurs overall in about 60% of patients dying from a malignancy (Berrettoni and Carter 1986; Yuh et al. 1996; Roodman 2004). In the adult metastases are the commonest malignancy of bone and more common than primary bone tumours (Berrettoni and Carter 1986; Yuh et al. 1996).

The incidence of metastatic bone disease depends on the propensity of a tumour to spread to bone and the overall incidence of the primary tumour. In combination with the prevalence of the tumour it determines the prevalence of bone metastases.

In autopsy series more than 80% of all patients with bone metastases suffered from cancer of the breast, prostate, lung, thyroid and kidney (Berrettoni and Carter 1986). It has been estimated that breast and prostate cancer alone are responsible for up to 80% of all patients with bone metastases (Coleman 2004).

The prevalence of bone metastases at the patient's death is about 80–85% for breast and prostate cancer. The numbers for lung cancer vary between 30–40% and 80–85%, for cancer of the thyroid between 50–60% and for renal cancer between 20–37% (Berrettoni and Carter 1986; Tillman et al. 2002; Coleman 2004; Even-Sapir 2005; Martinez-Zapata et al. 2006).

For the U.K., with about 60 million population, this equates to >20,000 new cases of bone metastases per year. Functional disability and pain occur in 45–75% of these and major complications can be expected in one third of patients whose first major relapse after treatment is in bone. Of this group, 10–15% will develop hypercalcaemia and 10–20% will develop pathological fractures (Figs. 27.1, 27.2); (Martinez-Zapata et al. 2006).

27.4 Pathophysiology

Metastatic spread to bone can occur by direct extension, lymphatic or haematogenous spread. Haematogenous spread is the most common and uses the arterial and venous route. The reasons for the high frequency of bone metastases are not quite understood. Considering that bone receives only 5–10% of the cardiac output, bone metastases are overrepresented. It has been proposed that certain mediators and cell receptors favour the development of bone metastases (Berrettoni and Carter 1986; Yuh et al. 1996; Taoka et al. 2001; Nakamura et al. 2003; Roodman 2004).

Most bone metastases occur in areas of red marrow and therefore in the adult in spine, ribs, pelvis, the proximal ends of long bones, the sternum and the skull (Figs. 27.1, 27.3). The role of Batson's venous plexus is often mentioned in the literature, but this concept is not

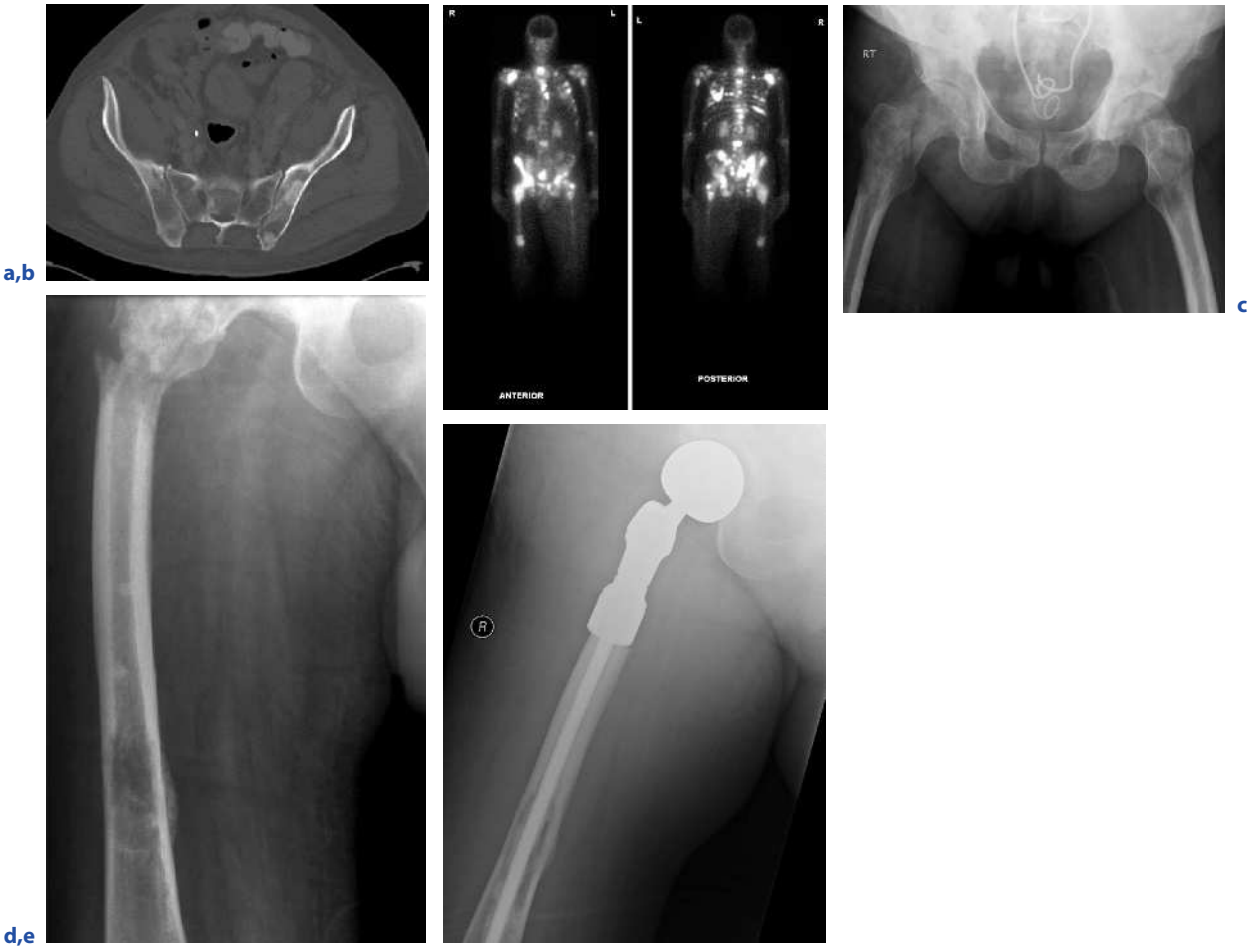

Fig. 27.1a–e. A 60-year-old man with known prostate metastases. CT (**a**) shows multiple lytic and sclerotic lesions in the pelvis. An isotope bone scan shows lesions particularly in pelvis and spine but also in the scapulae and multiple ribs and the proximal femora (**b**). Additional lesion in the right femur shaft. **c,d** Radiographs show lytic/sclerotic bone lesions of the pelvis and proximal femora (**c**) and a pathological neck of femur fracture. There is also a lytic lesion with periosteal reaction indicating fracture of the femur shaft (**d**). This led to the choice of a long-stemmed femoral replacement (**e**). Careful review of imaging and multidisciplinary discussion optimises patient treatment

without critics and certainly not the sole main factor for metastatic spread. Bone metastases can occur literally in any bone and anywhere within this bone (Berrettoni and Carter 1986; Taoka et al. 2001; Roodman 2004; Even-Sapir 2005; Martinez-Zapata et al. 2006).

Lung, kidney and possibly breast cancer are said to have a propensity for cortical metastases. Generally the incidence of cortical metastases has probably been underestimated. It can be difficult to diagnose on single-projection radiographs (Fig. 27.4). The location of cortical metastases is often the diaphysis of long bones, especially the femur, and this site is not typical for medullary metastases (Coerkamp and Kroon 1988; Hendrix et al. 1991; Miric et al. 1998). The relevance of cortical metastases lies in the increased risk of pathological fracture with early cortical involvement particularly in the weight-bearing bones (Fig. 27.2; Hendrix et al. 1991). The risk of pathological fracture is multifactorial and prediction of fracture risk is difficult. This is discussed in more detail below.

Bone metastases can be lytic, sclerotic or mixed. This description can be applied to a particular bone lesion but also to the totality of all bone lesions in a patient (Figs. 27.1, 27.3, 27.5). These are descriptive terms for the overall appearance of the bone lesions as in fact all metastatic lesions show bone lysis histologically and of-

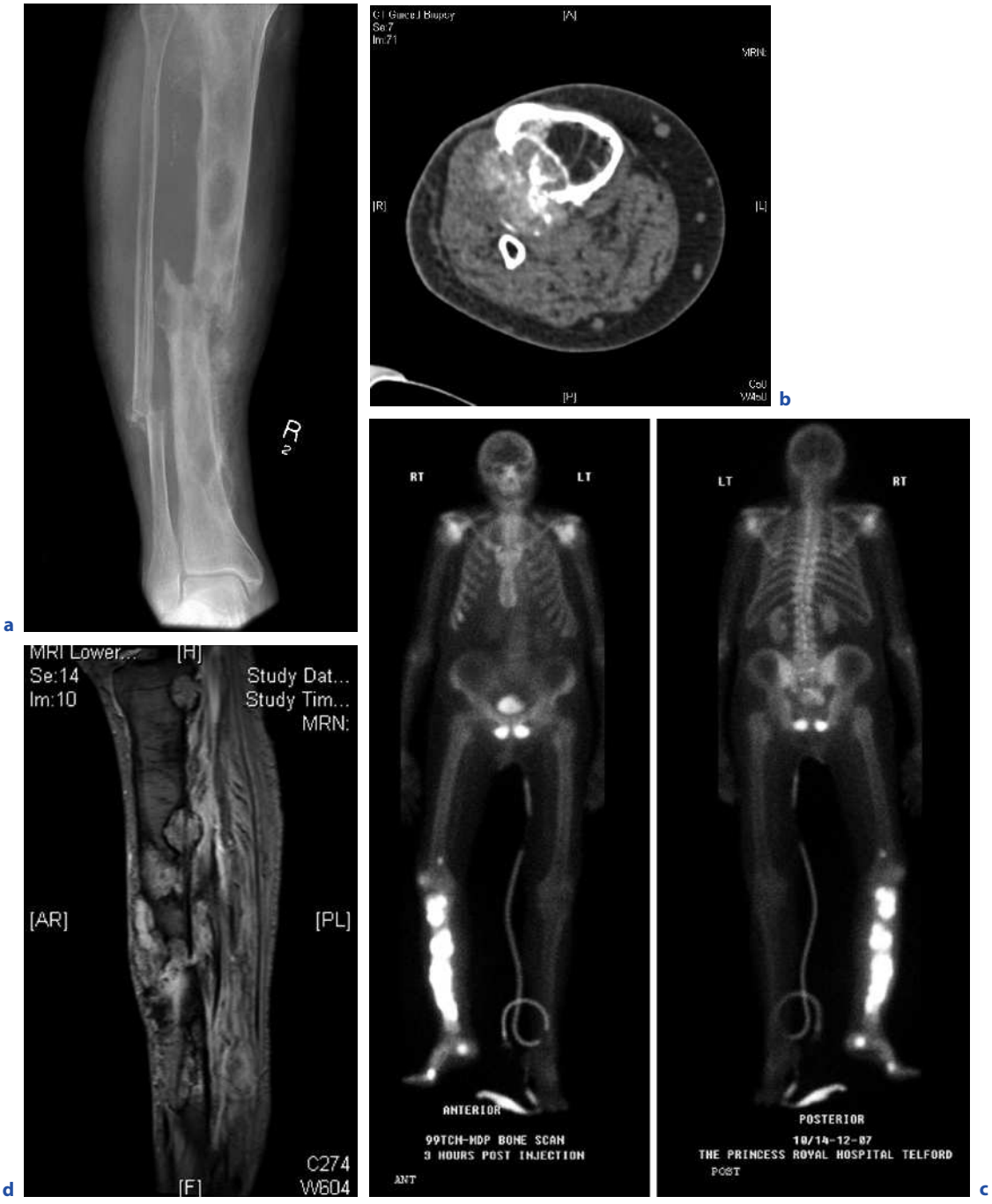

Fig. 27.2a–d. An 82-year-old man with a history of calf pain and pathological tibia fracture shortly after presentation. Previous history of transitional cell cancer of the urinary bladder. An AP radiograph (**a**) demonstrates multiple bone metastases with new bone formation best appreciated on CT (**b**). Bone scintigraphy (**c**) shows bone lesions to be limited to the right tibia and the adjacent distal femur (foot uptake degenerative). MR imaging (**d**) shows most metastases to be cortically based. Biopsy confirmed metastases from the bladder carcinoma. Cortical metastases are at higher risk of fracture. The tibial uptake pattern of the bone scintigraphy is unusual for metastatic disease.

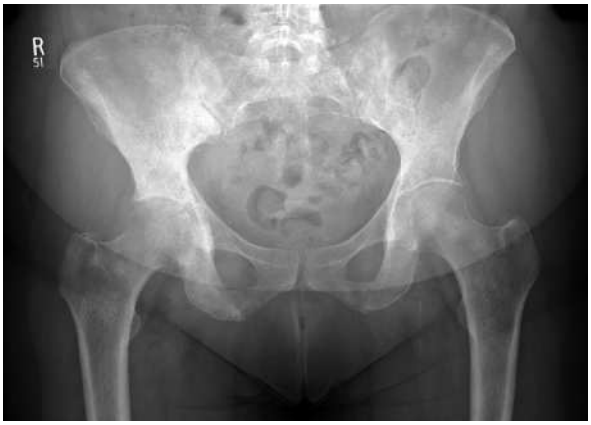

a

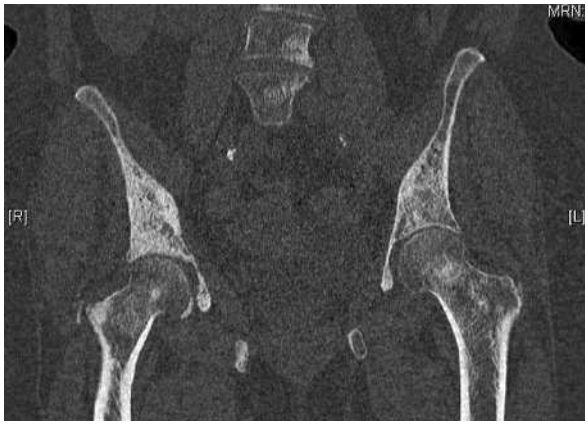

b

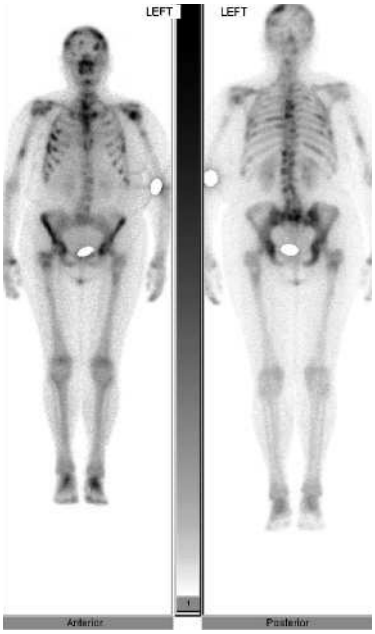

c

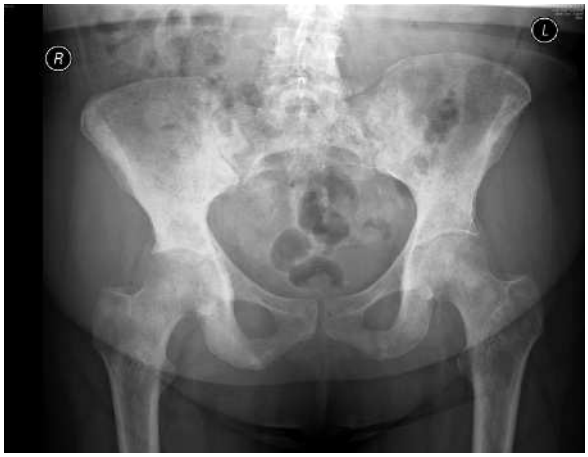

d

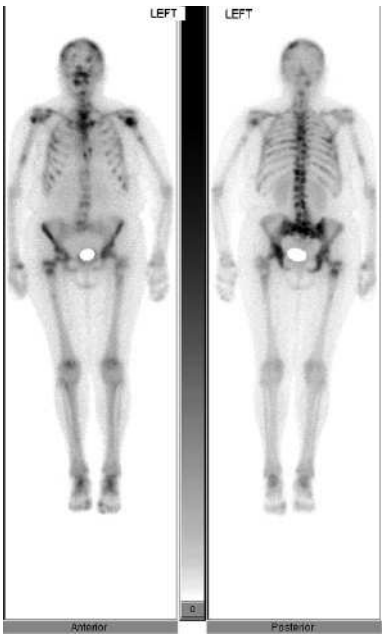

e

Fig. 27.3a–e. A 73-year-old woman with a history of breast cancer 10 years prior, now presenting with ill-defined pain for several years. Radiograph (**a**) and CT (**b**) show mainly osteoblastic bone lesions. Bone scintigraphy shows an activity pattern typical for metastatic spread, though compared with CT it underestimates the amount of bone change. **c** Biopsy confirmed breast cancer metastases, oestrogen receptor positive. Anti-hormonal treatment and bisphosphonates were commenced. **d,e** Three months after the commencement of treatment repeat pelvic radiograph (**d**) and bone scintigraphy (**e**) show no new bone lesions and increased sclerosis on the radiograph. The clinical symptoms were much diminished. Persistent increased scintigraphic uptake after treatment can be normal and due to osteoblastic healing. In sclerotic metastases this leads to diagnostic difficulties. The absence of new lesions is reassuring; however, apparently new lesions can be due to blastic repair of previously lytic lesions

Fig. 27.4a–e. A 62-year-old woman with known lung cancer with lung and liver metastases presenting with left femur pain. An AP radiograph of the femur (**a**) shows no obvious destructive lesion, and a lateral radiograph (**b**) does demonstrate a cortically based destructive lesion. This is much better shown on a repeat view taken a few days later (**c**). Axial MR imaging (**d**) confirms that this lesion is likely to have arisen from the cortex and shows the extensive soft tissue involvement not appreciated on the radiographs. A sagittal MR imaging sequence (**e**) shows the spread within the marrow cavity not appreciated on the radiographs. Unless very large, cortical metastases are only appreciated radiographically if imaged tangentially. Cortical involvement increases the fracture risk and this is important for patient management

ten also show some bone formation. In metastatic prostate cancer the rate of lysis is very high and much higher than in breast cancer but is often exceeded by the rate of new bone formation resulting in mainly sclerotic bone lesions (Fig. 27.6; Coleman 2004; Roodman 2004).

Metastatic bone disease in breast cancer, despite frequently being mixed lytic/sclerotic and having less osteolysis than prostate cancer bone metastases, is generally the most aggressive in its biological behaviour. The rate of significant bone-related episodes is highest for this tumour compared with other tumours with frequent bone metastases (Coleman 2004). A brief guide to the typical appearance of bone metastases of more common primary malignancies is given in Table 27.1.

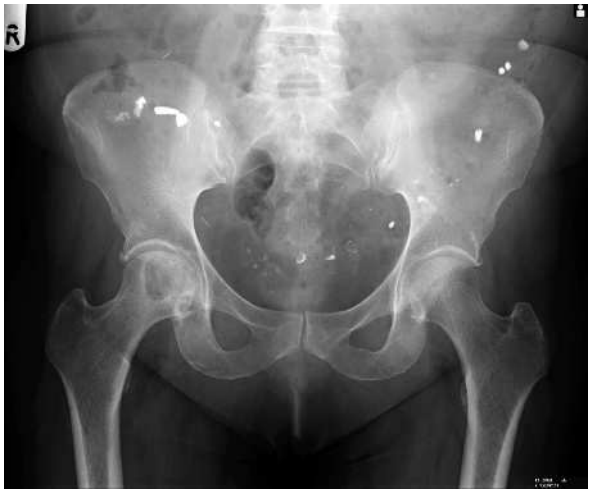

a

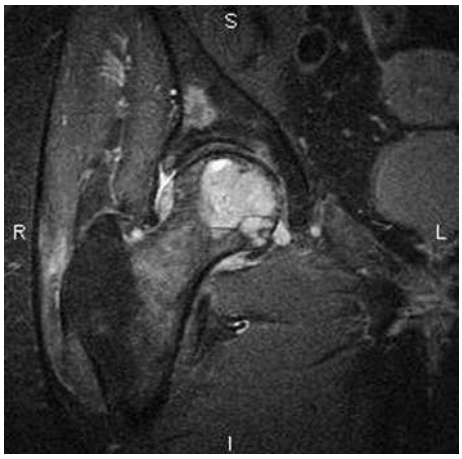

c

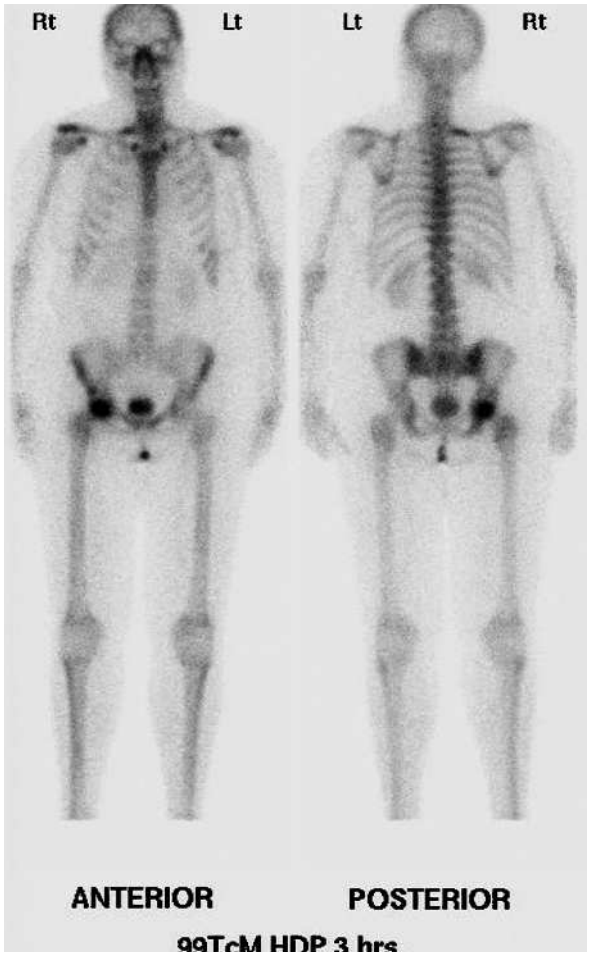

b

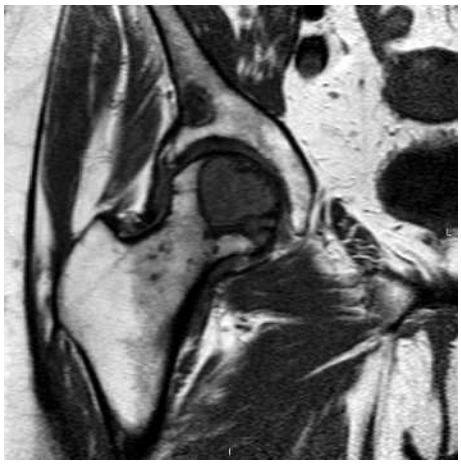

d

Fig. 27.5a–d. A 64-year-old woman with right hip pain. She had breast cancer 15 years prior but no problems since. A radiograph (**a**) shows a well-defined lytic lesion in the right femoral head with a sclerotic rim. Appearances are unspecific and could even be benign. There is also a small area of sclerosis in the adjacent acetabulum, laterally. A bone scintigraph (**b**) shows marked increased uptake in the right femoral head and a small focus of increased uptake in the right lateral acetabulum. Also increased uptake of the right first posterior rib. MRI (**c** T2 fat saturation, **d** T1-weighted) shows mixed high and low signal in the acetabular lesion on T2 fat saturation and low signal on T1-weighting indicating at least partial sclerosis. MR imaging shows tumour extension into the hip joint. Biopsy confirmed metastatic breast cancer. Lysis, sclerosis and mixed lesions frequently occur in the same patient. Radiographs have limited sensitivity and are unspecific

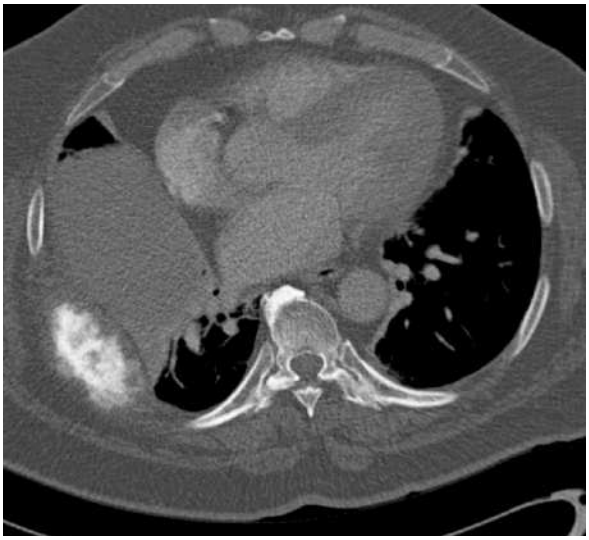

a

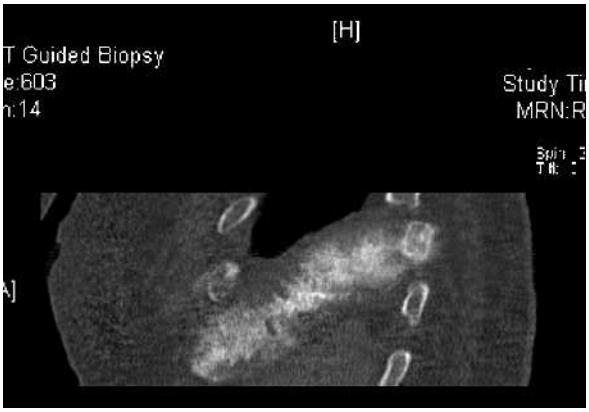

b

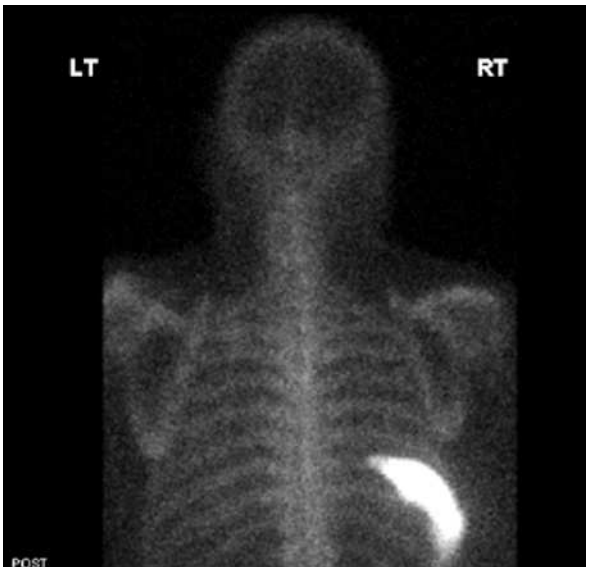

c

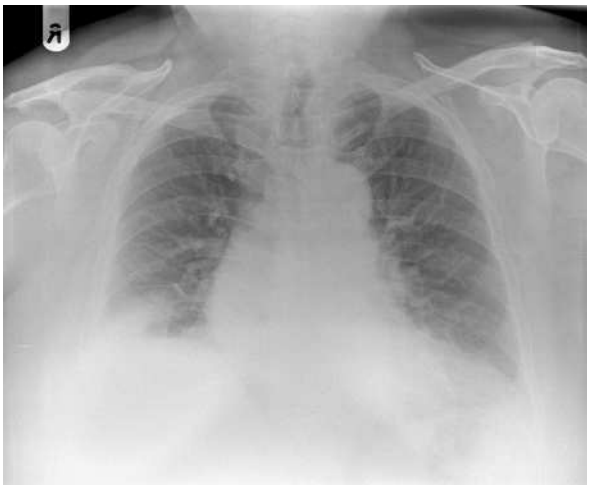

d

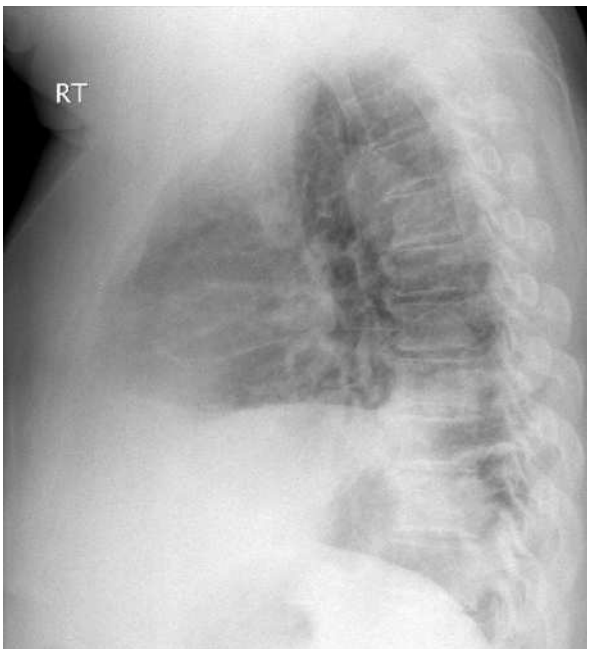

e

Fig. 27.6a–e. A 72-year-old man presenting with shortness of breath. CT pulmonary angiogram demonstrates a sclerotic expansile rib lesion (**a,b**). Bone scan shows an isolated lesion which, for example, could be related to Paget's disease (**c**). Despite its size, this was not appreciated on PA and lateral (**d,e**) chest radiographs 2 days prior to the CT-PA exam. On biopsy the lesion was soft and bled profusely. Histology found prostate cancer metastasis. Prostate cancer more typically presents with multiple sclerotic lesions in pelvis and spine. New bone formed by metastases is often abnormally soft compared with normal bone and can bleed markedly

Table 27.1. Primary cancer vs typical appearance of its bone metastases

Primary cancer	Radiographic appearance of metastases
Breast cancer	Usually mixed lytic and sclerotic
Prostate cancer	Usually markedly sclerotic or mixed but can be entirely lytic
Lung cancer	Usually lytic, relatively common in periphery and cortex
Renal cell carcinoma	Almost always lytic, can be expansile
Thyroid cancer	Almost always lytic, can be expansile
Gastrointestinal cancer	Bone lesions uncommon, usually lytic but not rarely sclerotic
Transitional cell cancer	Usually lytic, but not uncommonly sclerotic
Melanoma	Bone metastases uncommon, usually lytic, can be sclerotic
Soft tissue sarcoma	Lytic
Bone sarcoma	Usually like primary sarcoma

27.5 Imaging Modalities

Although the classification into lytic, mixed or sclerotic typically describes the pathological presentation, it frequently is used synonymously to describe the imaging presentation on radiographs or computed tomography (CT).

The following discussions of imaging modalities are to be seen as a guide only. The individual variability of bone metastases is huge and they can literally mimic any bone lesion (Figs. 27.1, 27.2, 27.5, 27.7). The area of transition can be well defined, sclerotic or permeative and moth-eaten. Periosteal reaction (Fig. 27.7) and fluid-fluid levels can occur. For this reason bone metastasis has to be in the differential diagnosis of most bone lesions.

27.5.1 Radiographs

Radiographs were historically the first imaging modality available to assess bone and there is a large body of experience regarding their use. The main problem of

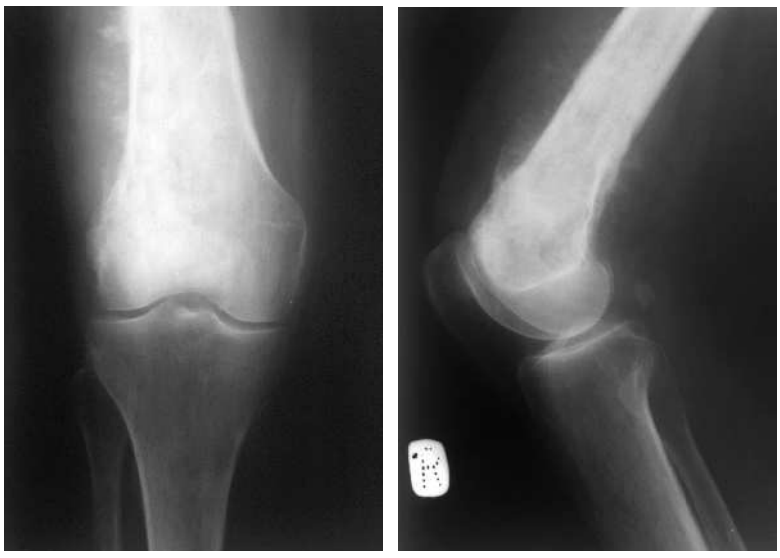

a,b

Fig. 27.7a,b. A 45-year-old woman with a history of colon carcinoma in the past now presenting with knee pain. AP and lateral radiographs (**a,b**) show an aggressive bone lesion with sclerosis indicating bone formation and sunburst spiculation. Findings are typical for osteosarcoma. Biopsy, however, showed metastasis from colon carcinoma. Gastrointestinal metastases can be osteoblastic. Radiographic appearances of metastases are unspecific and can mimic virtually any bone pathology

radiography is the poor sensitivity for bone destruction (Figs. 27.1, 27.3, 27.4, 27.8, 27.9). About 30–75% of bone mass must be destroyed to become radiographically apparent. This results in a very poor sensitivity for processes affecting only medullary bone (Taoka et al. 2001; Even-Sapir 2005). Advantages of radiographs are universal and easy access, relatively low cost and familiarity of all health professionals with this technique; however, familiarity does not equal expertise, careful assessment and a sufficient knowledge base are prerequisites for the safe and accurate assessment of radiographs. Assessment of fracture risk is not easily based on radiographs alone; fracture risk is discussed further below.

27.5.2 Computed Tomography

Computed tomography is well suited to image bone. It easily differentiates areas of lysis, erosion, sclerosis, calcification and bone remodelling (Figs. 27.1, 27.3, 27.10). It is therefore well suited for the assessment of established bone lesions with cortical and medullary destruction (Even-Sapir 2005; Liu et al. 2007). It struggles, however, to demonstrate bone marrow lesions and the radiologist frequently will see abnormalities on nuclear medicine studies or MR imaging not visualised on CT (Fig. 27.8). Computed tomography on its own has never established itself as a screening tool for bone metastases; however, the spine and pelvis are routinely imaged on staging CT examinations including CT chest, abdo-

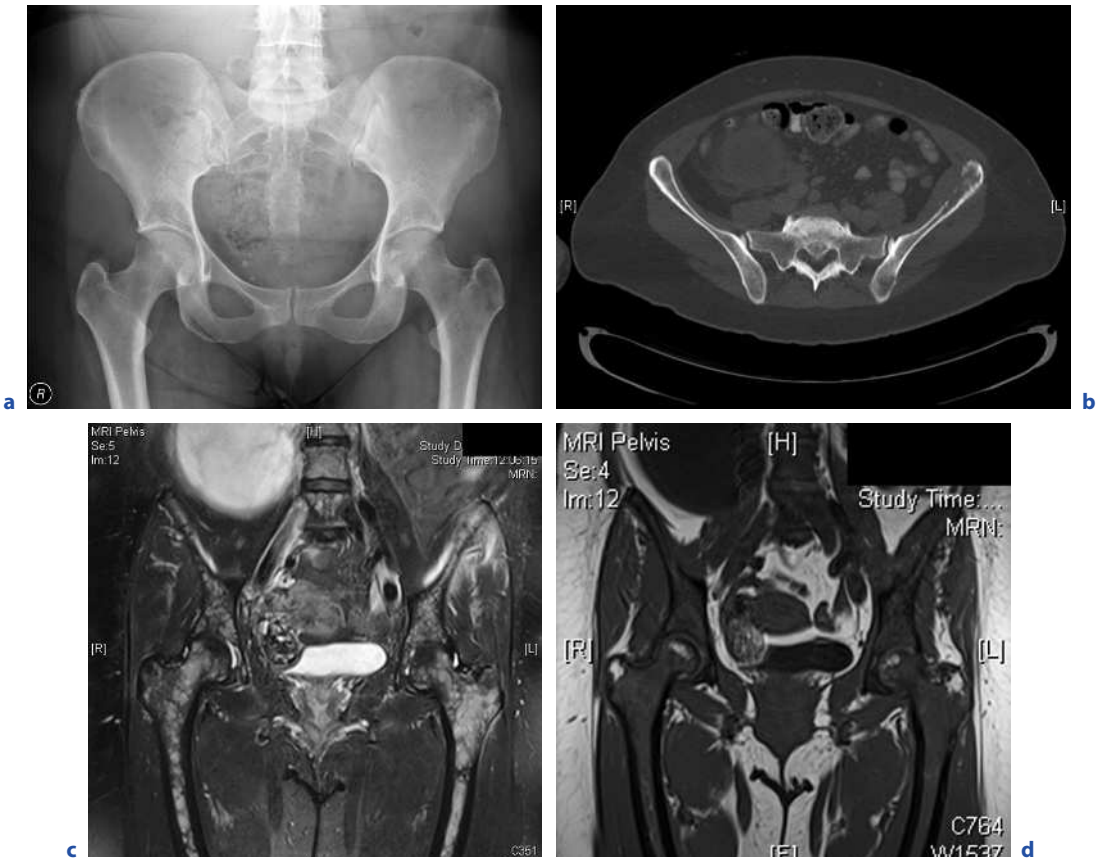

Fig. 27.8a–d. A 41-year-old woman presenting with low back, pelvic and hip pain. A radiograph of the pelvis (**a**) shows bony destruction of the left ilium which might be confused with bowel markings and a radiopacity in the right-sided abdomen. CT (**b**) confirms the destructive lesion in the left ilium and a mass extending into the right iliac fossa due to a large right-sided renal cell carcinoma. MR imaging of the pelvis (**c** STIR, **d** T1-weighted) shows extensive bone marrow seeding in the entire imaged marrow space more suggestive of a haematological disorder. No expansile bone lesion typical of renal cell carcinoma. Morphology is no reliable predictor for histology. Radiographs and even CT can markedly underestimate tumour load due to the inability to assess the bone marrow

men and pelvis. Computed tomography has also gained popularity as part of positron emission tomography (PET)–CT examinations. The PET overcomes the poor sensitivity of CT for bone marrow involvement in lesions without significant bone reaction (Even-Sapir 2005; Taira et al. 2007).

27.5.3 MR imaging

Magnet resonance imaging (MR imaging) is often the examination of choice in musculoskeletal imaging and presently competes with nuclear medicine techniques in the screening for bone metastases (Fig. 27.9). While the bony cortex and matrix calcification are not as well demonstrated as on CT, it is far superior for the assessment of bone marrow and the soft tissues adjacent to bone lesions (Fig. 27.8). When screening for bone metastases one might decide to image only the axial skeleton with the red marrow, as the incidence of bone metastases is highest here or one might image the whole body. Typically used screening protocols combine T1-weighted and STIR sequences. T1-weighted sequences allow the identification of osteoblastic lesions with little STIR signal increase. The STIR sequences are, of course, very sensitive for oedema-like changes (Even-Sapir 2005; Ketelsen et al. 2008).

The imaging parameters need to be chosen carefully. Slice thickness and choice of imaging plane influence the sensitivity and accuracy of any chosen imaging protocol. Protocols limited to only coronal images struggle

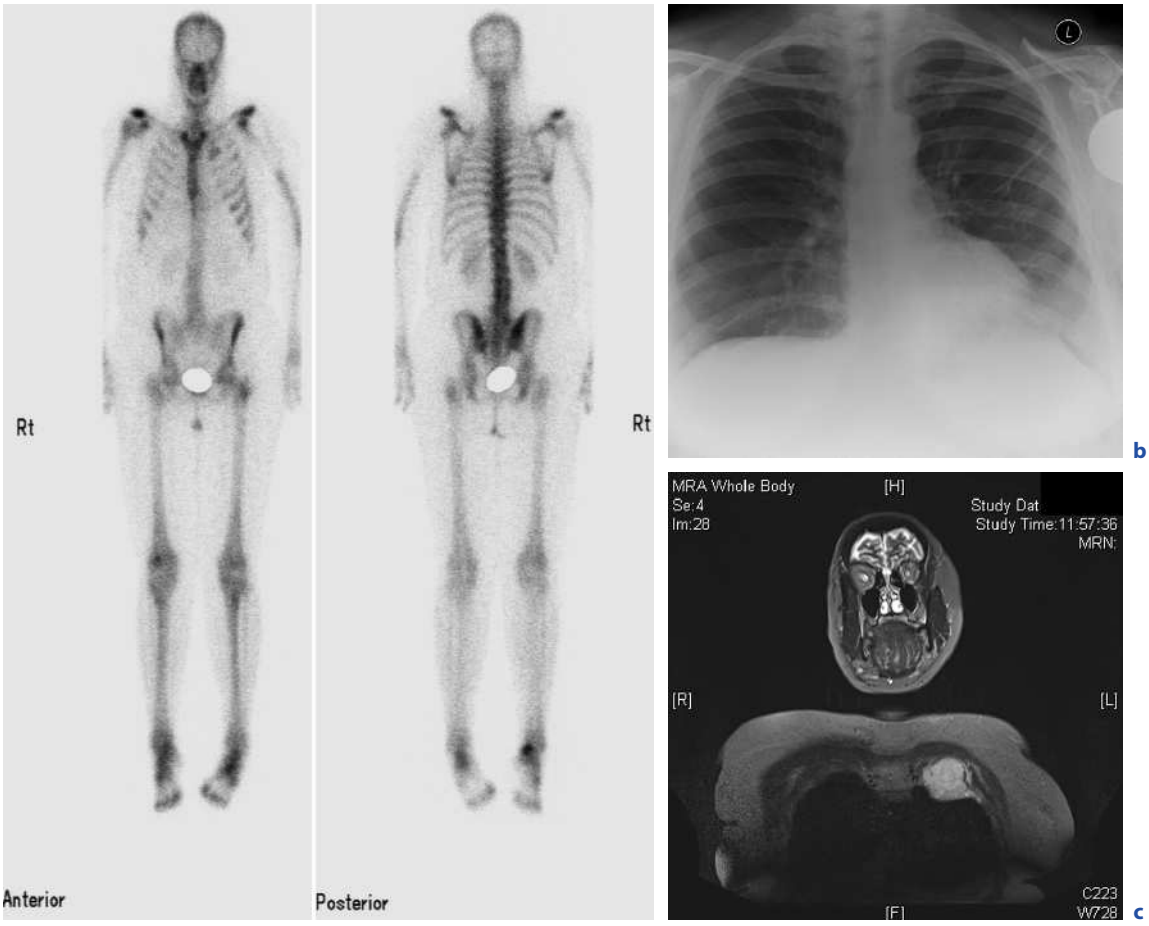

Fig. 27.9a–g. A 52-year-old woman with a history of malignant meningioma with left humeral metastasis treated with humeral replacement. Two years after this, she presented with left chest wall pain. Bone scintigraphy (**a**) shows mild increased activity in the anterior left upper chest wall and the left proximal femur. Note the absent uptake in the left proximal humerus after humeral replacement. **b** A PA chest radiograph shows subtle decreased radiopacity of the left anterior second and third ribs but no definite lesion. Whole-body MR imaging (the STIR images shown here) show a large (**c**) and adjacent smaller chest wall lesion (**d**). **d–g** *see next page*

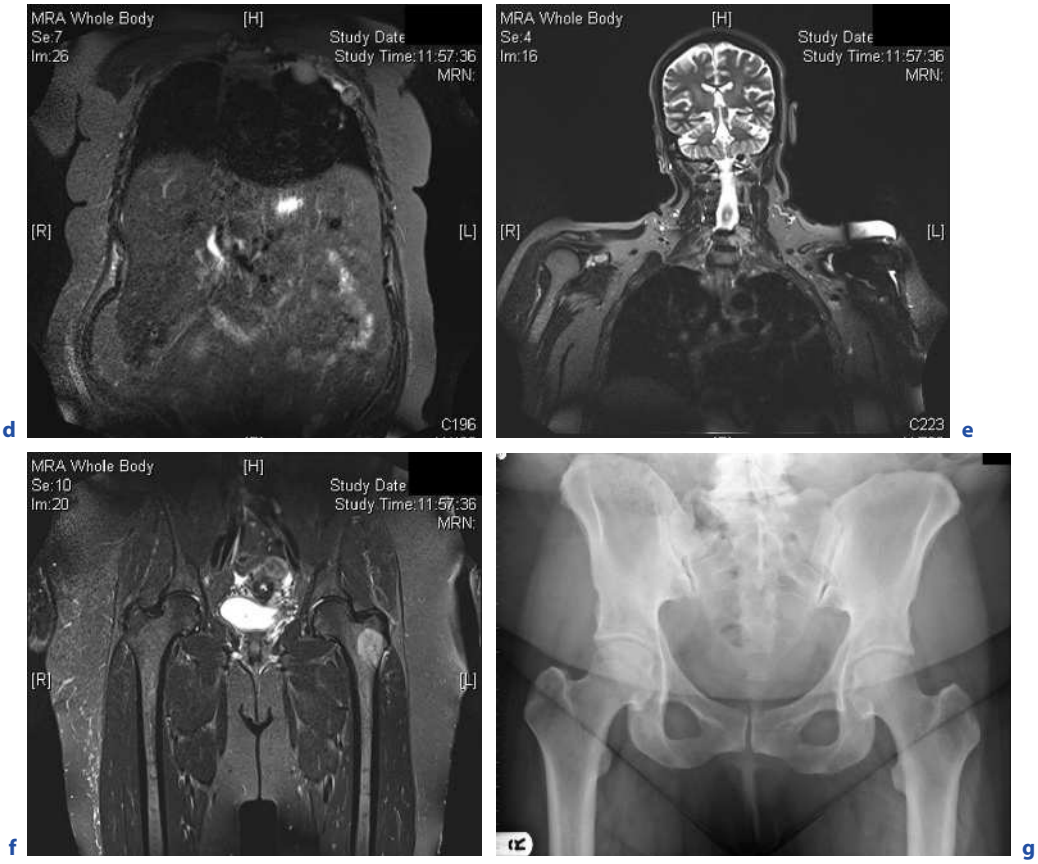

Fig. 27.9a–g. (*continued*) There is also a lesion in the right coracoid (**e**) There is also a lesion in the left proximal femur on the whole-body MRI (**f**) which could easily be overlooked on an AP radiograph of the pelvis (**g**). MR imaging is superior to bone scintigraphy and radiographs in sensitivity and specificity

to visualise the entire ribs adequately. The spine is better imaged with sagittally aligned sequences (Taoka et al. 2001). The combination with diffusion-weighted sequences increases the sensitivity of MR imaging for bone lesions (Nakanishi et al. 2007). Use of contrast agents can be of help in some cases and apart from gadolinium-containing contrast agents there is increasing interest in the use of superparamagnetic iron oxide particles (SPIOs), for example to differentiate inflammation from tumour (Fukuda et al. 2006).

High-field scanners (3 T or higher) can reduce imaging times or increase spatial or contrast resolution but are probably not necessary for routine screening.

27.5.4 Nuclear Medicine

Nuclear medicine techniques comprise particularly Tc99m methylene diphosphonate (MDP) bone scintigraphy and F18 PET or PET–CT. There are other techniques using other isotopes, e. g. iodine, and special labelling techniques with increased sensitivity to either certain tumours or inflammatory states (Inoue et al. 2007); however, Tc99m MDP scintigraphy still forms the mainstay of isotope scintigraphy. Over the past decade PET and PET–CT have gained importance.

Nuclear medicine techniques have in common that they image a metabolic status rather than anatomy as other imaging techniques do. The isotopes circulate in the body and accumulate wherever the conditions are right; therefore, nuclear medicine techniques are by their nature whole-body examinations. Common to these techniques is also their relative lack in specificity (Even-Sapir 2005).

For Tc-MDP scintigraphy the particular strengths and weaknesses are well known. Its strength is relatively low cost, whole-body imaging and decent sensitivity; increased activity by about 5–10% compared with normal bone is identifiable (Even-Sapir 2005). One of the

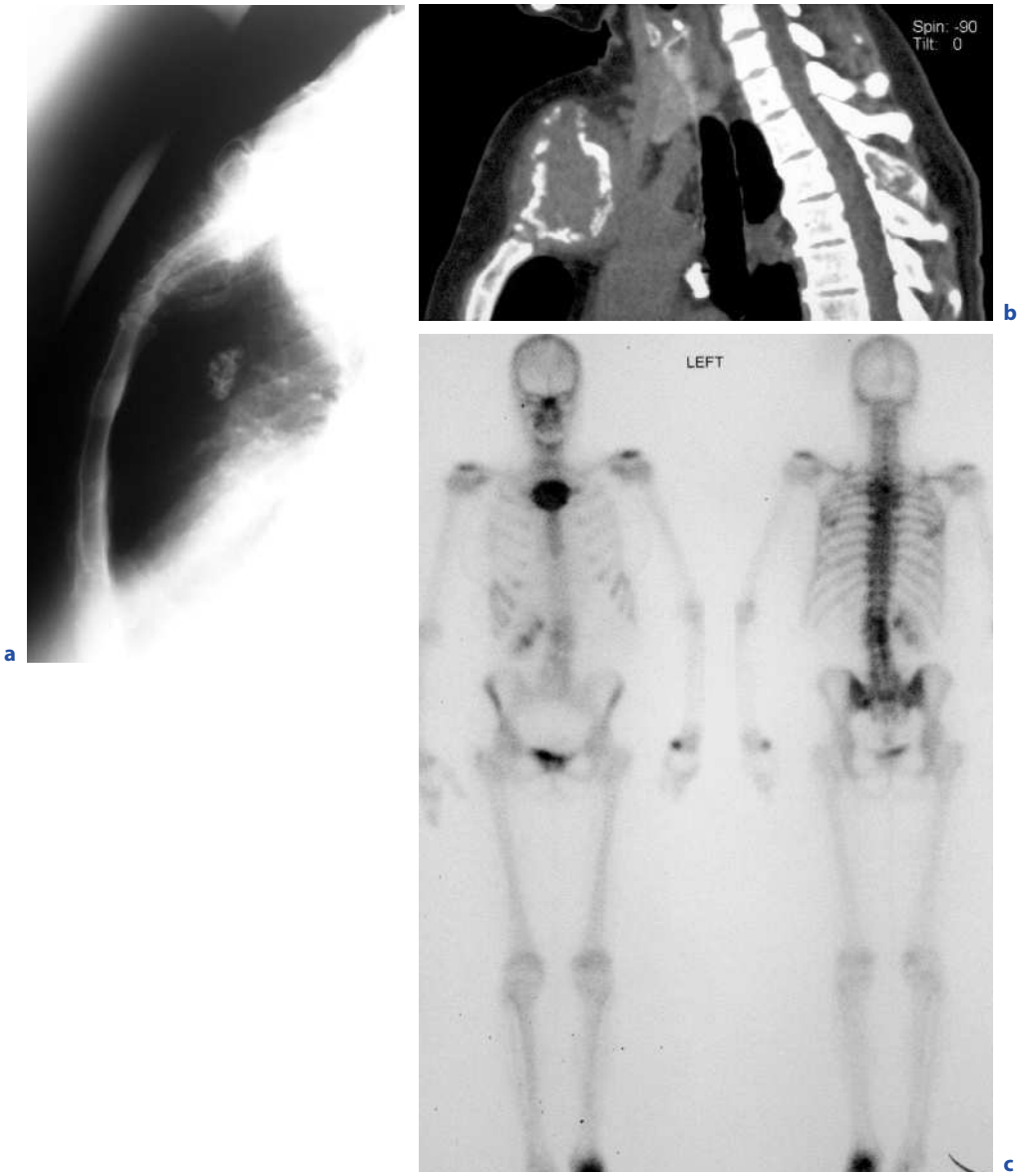

Fig. 27.10a–c. A 66-year-old woman with known renal cell carcinoma, presenting with sternal pain. A lateral radiograph (**a**) shows an expansile sternal mass, much better appreciated on CT (**b**), which shows also a spinous process lesion at the same level. **b,c** The spinous process lesion could not be appreciated on a bone scan (**c**) due to superimposition with the sternal lesion. Note the absent left kidney after previous nephrectomy. The uptake in the left ankle was due to degenerative disease. The anatomical resolution of a standard bone scan is not sufficient to differentiate lesions in the same plane, although this can be improved with SPECT. The same patient can have expansile and non-expansile metastases. For a single metastasis curative treatment is often attempted; accurate staging is therefore essential

main problems of Tc-MDP scintigraphy is the limited sensitivity for bone lesions which limits its reliability as a screening tool for bone metastases. It has been reported that medullary lesions <1 cm diameter and lesions not involving the cortex are poorly visualised (Taoka et al. 2001; Abe et al. 2005; Chen et al. 2007; Ketelsen et al. 2008).

Increased uptake is not limited to bone but can occur at any location of increased phosphate turnover, in soft tissue or bone. If a bone lesion is strictly lytic without any bone formation, there will be no marker accumulation and therefore no increased activity. Multiple myeloma is notorious for this; this pathology is beyond the scope of this chapter. Lesions might be visible as a "cold" area due to lack of activity compared with normal bone. Generally, though, there is some activation of new bone formation even in lytic bone metastases (Roodman 2004).

In reverse, generalised increased activity (the so-called superscan) can also be hard to spot as there is no focal change. Lack of renal or other soft tissue activity is usually the clue, but this is not 100% reliable (Even-Sapir 2005; Chen et al. 2007).

Increased activity is not limited to tumour but can, for example, be due to fractures or metabolic problems such as hyperparathyroidism or degenerative change. The location and pattern of multiple foci of activity are often helpful in narrowing the differential diagnosis, but correlation with anatomical imaging is usually required.

Positron emission tomography imaging depicts glucose metabolism and again is unspecific. The combination with CT enables excellent anatomical correlation of lesions and CT is particularly well suited to imaging the skeleton. Attempts at combining PET imaging with MR imaging are also being undertaken but are currently more of research interest (Even-Sapir 2005).

F18-PET imaging can struggle with the detection of osteoblastic lesions (Abe et al. 2005; Even-Sapir 2005) and the minimal detectable size for bone metastases is 2 mm for MR imaging and 5 mm for PET–CT (Schmidt et al. 2007).

Comparative studies of conventional bone scintigraphy, bone scintigraphy with planar reconstruction, such as single photon emission computed tomography (SPECT), PET, PET–CT and MR imaging, have consistently found limited sensitivity of bone scintigraphy, improved sensitivity for scintigraphy with SPECT, good sensitivity for PET and best sensitivity and accuracy for PET–CT and MR imaging (Taoka et al. 2001; Abe et al. 2005; Even-Sapir et al. 2006; Fujimoto et al. 2006; Du et al. 2007; Schmidt et al. 2007a,b; Beheshti et al. 2008; Ketelsen et al. 2008; Kumar et al. 2008). The numbers vary between studies; sensitivity of bone scintigraphy is about 46–70%, with SPECT up to 92%, PET up to 100%, PET–CT 78–100% and MR imaging 94–100%. Specificity and accuracy of MR imaging and PET–CT were markedly higher than any other modality and were 100% or near to it. Specificities for bone scintigraphy or PET imaging alone are relatively poor due to their unspecific nature (Even-Sapir 2005; Even-Sapir et al. 2006; Fujimoto et al. 2006; Du et al. 2007; Lecouvet et al. 2007; Schmidt et al. 2007a,b; Yilmaz et al. 2008; Ketelsen et al. 2008; Kumar et al. 2008).

27.6 Clinical Considerations

27.6.1 Implications for the Radiologist

The clinical presentation of bone metastases is often unspecific and making the diagnosis often falls to the radiologist (Spencer 2008). A patient with known primary disease, known bone metastases and presenting with further typical bone lesions, will not present diagnostic challenges. All other scenarios require considerably more thought.

A patient with known primary malignancy but no known metastatic disease presenting with musculoskeletal pain is difficult to assess. Typically radiographs are obtained as first-line investigation. If they show multiple bone lesions consistent with metastases of the primary disease, further diagnostic measures are often not taken and symptomatic treatment is instituted assuming metastatic disease from the known primary; however sometimes this assumption will be wrong (Fig. 27.11), and the bone lesions might be due to a second primary disease or have a benign cause, e. g. hyperparathyroidism. The authors are not aware of studies assessing the incidence of this but have come across this scenario repeatedly in their own practice at a tertiary referral centre. These cases are diagnosed retrospectively if at all. The reason for review is usually a clinical course inconsistent with the assumed diagnosis. For this reason the authors advocate to always send material for histopathology even if the diagnosis seems clear.

In the scenario of hitherto unknown metastatic disease, localised imaging of the clinically suspicious area or screening imaging tests can be employed. Radiographs are often the first imaging examination of choice, but their sensitivity is limited. If symptoms are

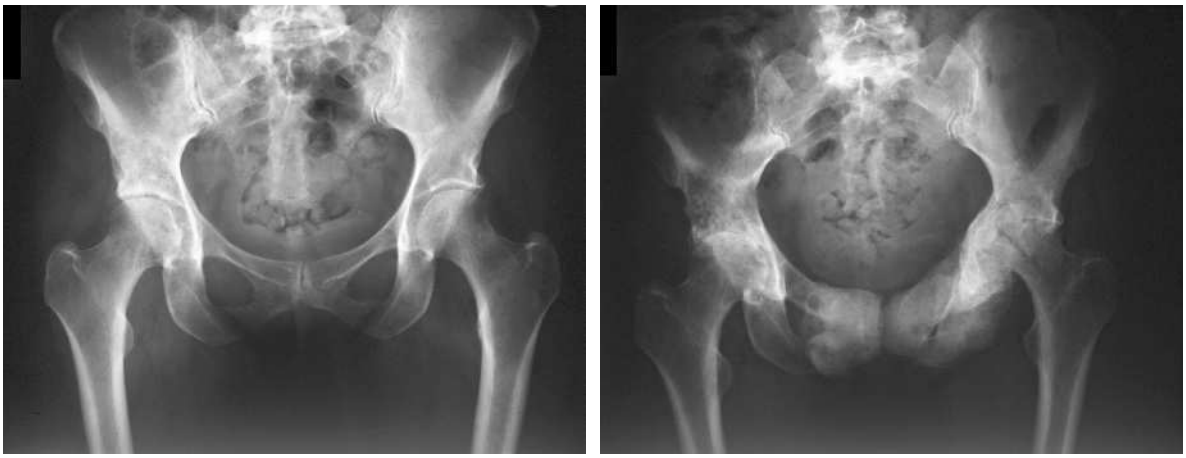

a b

Fig. 27.11a,b. A 54-year-old woman presenting with right hip pain. Previous history of breast cancer. Ill-defined lytic/sclerotic changes in the right acetabulum (**a**). Biopsy demonstrated abnormal bone but no metastasis. The patient was diagnosed with osteomalacia. A follow-up radiograph 2 years later demonstrates persistence of radiographic changes in the right acetabulum, healed insufficiency fractures of the pubic bones, protrusion of the left hip joint with femoral collapse due to osteopenia and a lytic lesion in the right femur at the edge of the film, a brown tumour (**b**). The occurrence of bone lesions in a patient with a history of cancer does not necessarily mean metastatic disease. Biopsy can prevent misdiagnosis and mistreatment

localised, MR imaging is often useful; otherwise, a Tc-MDP bone scintigraphy is still a good screening test. Routine blood tests are also indicated.

If there is a known primary malignancy, hitherto no known metastatic disease and a *single* bone lesion is seen, increased caution is advised. It has to be ascertained whether there is indeed a single lesion or whether there are more (Figs. 27.10, 27.12). A single metastasis might still be treated with a curative approach if the primary tumour has been treated successfully. Repeat staging examination is advised in these cases. Furthermore, the occurrence of a lesion that resembles a metastasis from a known primary does not mean it is a metastasis and other diagnoses need to be considered in particular primary bone tumours.

Metastatic bone disease might be the first presenting sign of a malignancy and this might be by pathological fracture. It is not always easy to differentiate a pathological from a simply traumatic fracture. Preoperative imaging might therefore include MR imaging to assess the adjacent bone and bone marrow.

If a bone lesion of unclear nature is seen and there is no known primary tumour, a diagnosis has to be established and the easiest way to do this is by biopsy. Biopsy is more economical than performing staging examinations at this initial stage; however, if the only known lesion is in a difficult location, it can be worthwhile to try to establish whether further lesions are present which might be easier to access.

The biopsy approach must take any eventual further treatment into account. A primary bone tumour biopsied by the wrong path can mean losing a limb or even the life for the patient (Liu et al. 2007; Espinosa et al. 2008). For this reason biopsies are ideally performed at or after discussion with the centre providing treatment if the lesion turns out to be a primary bone tumour.

As mentioned in several scenarios above there is often an assumption that a lesion is a metastasis, but it might not be. This is a perennial problem for all doctors involved in patient care. The patient's views and economic factors have to be considered. If a primary tumour is known, tumour-specific guidelines can be of help.

The clinical presentation is often unspecific with musculoskeletal pain. The patient might present to any health care professional. As discussed before the clinical history will often determine the clinician's thoughts and actions and where available guidelines can be useful.

The pain in metastatic disease can vary from a dull ache to a very intensive pain. It is often exacerbated by weight bearing and is sometimes worse at night. It often involves release of chemical mediators (Tillman et al. 2002; Coleman 2004; Martinez-Zapata et al. 2006).

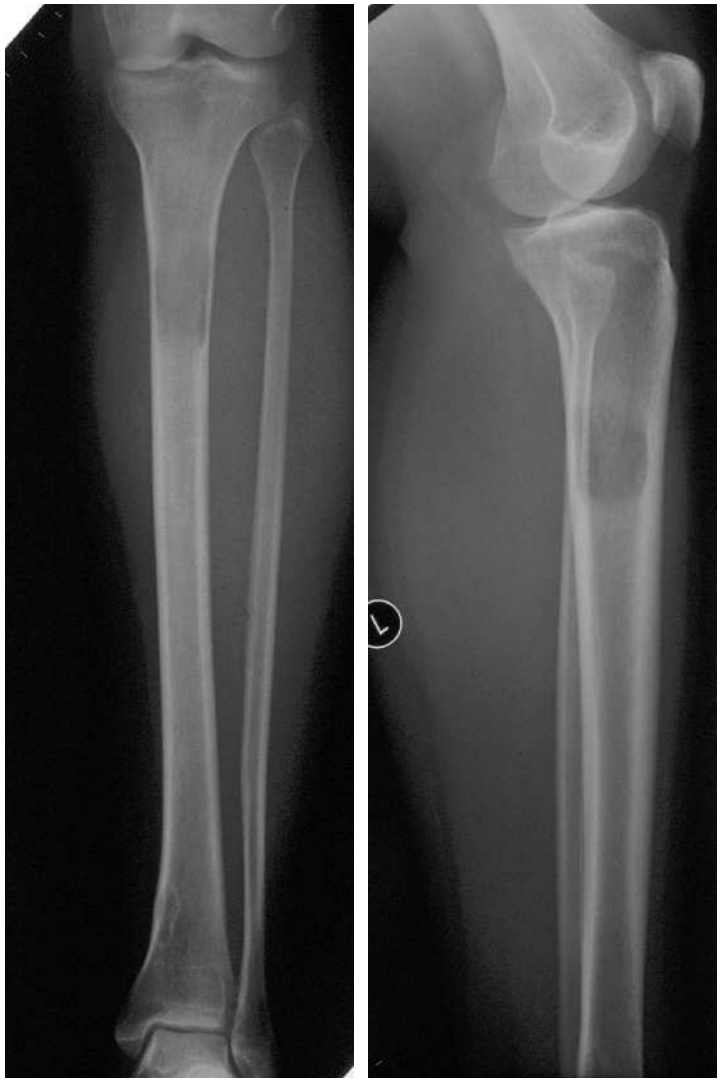

a b

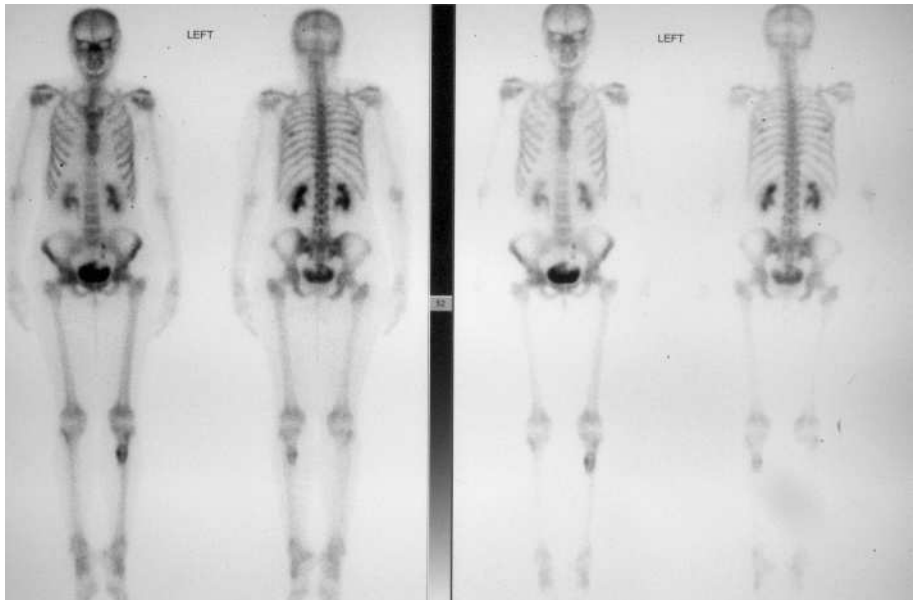

c

Fig. 27.12a–d. A 39-year-old woman presenting with tibia pain. AP (**a**) and lateral (**b**) radiographs show an osteolytic reasonably well-defined tibia lesion centred in the medullary space. Bone scan (**c**) demonstrated this to be an isolated lesion. **d** *see next page*

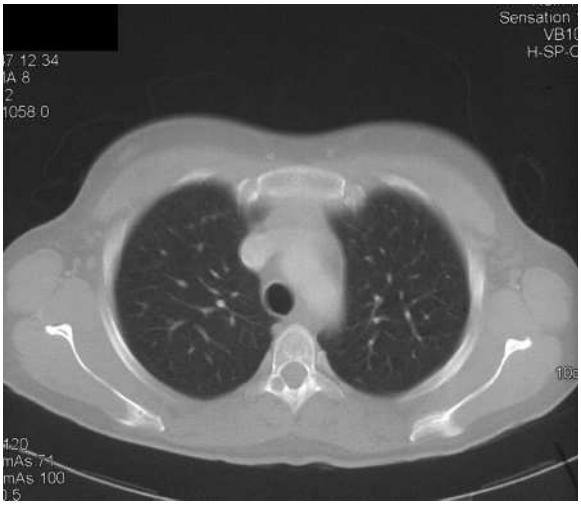

d

Fig. 27.12a–d. (*continued*) Biopsy and further imaging established leiomyosarcoma of the uterus as source. Staging CT of the thorax (**d**) demonstrates a lytic lesion in the right pedicle of an upper thoracic vertebra. This was not appreciated on the bone scan (though in retrospect there is subtle increased uptake in the upper thoracic spine to the right of the midline). The radiographic appearances were unspecific

27.6.2 Diagnostic Approach to Bone Lesions

Before imaging investigations are obtained, full blood count, renal and liver function, ESR and CRP are frequently obtained. If bone lesions are considered, serum calcium and phosphate and alkaline phosphatase are usually added. Hypercalcaemia in particular has to be excluded or, if present, treated (Tillman et al. 2002; Coleman 2004; Martinez-Zapata et al. 2006).

Radiographs are usually obtained first. If they are abnormal, whole-body screening with nuclear medicine techniques or MR imaging can evaluate whether there are multiple lesions. If the radiographs are normal, bone scintigraphy or focal MR imaging can determine whether a local bone lesion is present.

The morphology of a bone lesion is not reliable for determining the underlying pathology. In particular, metastatic disease can mimic most benign and malignant bone lesions. While, for example, bone metastases of prostate cancer are often sclerotic, they might be completely lytic. Expansile destructive lesions are associated with thyroid or renal cancer but also occur with other primary lesions. Furthermore, while expansile lytic lesions can bleed significantly, one might encounter a largely sclerotic bone lesion with significant haemorrhage at biopsy or surgery.

Screening for bone metastases in patients with an established primary tumour is a complex subject. In the section on the imaging modalities some technical aspects are discussed. Bone scintigraphy has reasonable sensitivity but needs to be correlated to other imaging modalities where positive. Certain types of metastases are poorly visualised with this technique (Figs. 27.9, 27.10, 27.12). Whole-body MR imaging and PET–CT are superior in sensitivity and specificity. Radiation burden is only an issue for PET–CT; however, for all modalities economic considerations are important.

Without a clear clinical consequence, screening for bone metastases is not indicated. The likelihood of bone metastases depends on the type and aggressiveness of the tumour. Factors such as local tumour stage and blood test results can partially predict the likelihood of metastases.

Special-interest societies give advice on appropriateness on screening and national or regional guidelines might be available.

27.7 Differential Diagnosis

Metastases can mimic almost any bone lesion (Figs. 27.5–27.7). For bone lesions with distinct margins fibrous cortical defect, brown tumour/hyperparathyroidism, eosinophilic granuloma, giant cell tumour, aneurysmal bone cyst, enchondroma, fibrous dysplasia, infection with Brodie abscess, plasmacytoma/multiple myeloma, lymphoma and primary malignant bone lesions and many others have to be considered (Fig. 27.12).

For more complex lesions giant bone island, osteoblastoma/osteoid osteoma, calcified or ossified enchondroma, bone infarct, fibrous dysplasia, chondromyxoid fibroma, fibro-osseous dysplasia, adamantinoma, lymphoma, healing bone lesions and primary bone neoplasms, such as osteosarcoma and chondrosarcoma, have to be considered.

Some drugs, such as corticosteroids, cytotoxic drugs for chemotherapy or for treatment of autoimmune disorders such as rheumatoid arthritis, can cause bone marrow necrosis mimicking bone metastases (Vanel et al. 2007).

The patient's age, the location of the lesion, the clinical history and the radiological appearance are all useful contributors for the differential diagnosis (Coerkamp and Kroon 1988).

27.8 Biopsy

The only definitive way of making a diagnosis is by histopathology. Image-guided biopsy frequently is the method of choice for obtaining tissue. Compared with open biopsy, cost and morbidity are lower, and if performed technically adequately image-guided biopsy has good sensitivity and accuracy (Harish et al. 2006; Liu et al. 2007; Wu et al. 2008). The complication rate of percutaneous needle biopsy is about 1% and therefore much lower than that of open biopsy (up to 16%) Liu et al. 2007; Espinosa et al. 2008).

Fine-needle aspiration is not an appropriate method for the biopsy of bone lesions. The histological diagnosis is frequently not based just on single cells but on the tissue architecture and the interface between normal and abnormal tissue. For this reason it is important to include the interface with normal tissue in the biopsy sample. It is obvious that advance planning of a biopsy results in better samples and higher accuracy. The larger and the more representative the sample, the more confident the pathologist. Necrotic tissue is not particularly useful. If possible, viable soft tissue or bone should be obtained. If only blood can be aspirated, this should still be sent for histopathology as this often contains clumps of the underlying tumour (Harish et al. 2006). Generally samples should be sent for microbiology (Liu et al. 2007; Espinosa et al. 2008; Wu et al. 2008).

Studies looking at the diagnostic yield of biopsies vary widely with yields from 76 to 99%. This seems to be due to the techniques used (Diederich et al. 2006; Harish et al. 2006; Liu et al. 2007; Espinosa et al. 2008; Wu et al. 2008).

The choice of biopsy equipment contributes significantly to the diagnostic yield. For non-sclerotic lesions simple bone biopsy sets can be used. These sets typically have a bevelled or serrated end on an outer trochar and a sharp inner stylet. The stylet remains in place until the needle is in a position where the biopsy is to be taken. After removal of the stylet, the outer trochar is advanced further to take a sample. To aid retention of the sample on withdrawal of the trochar a number of techniques are used. Some biopsy sets use a trap that is advanced into the trochar after it has been advanced. The aim is to compress and "trap" the sample in the trochar. Many trochars have a tapering, smaller end hole aiding sample retention. Many systems have luer-lock adapters to apply suction during trochar withdrawal. While typically most of these systems are designed for bone marrow biopsies, they usually work well for bone biopsies, too. This applies to many radiographically sclerotic bone lesions. While truly hard lesions are not suitable for the systems described above, many radiologically sclerotic lesions are actually fairly soft due to the formation of abnormal bone.

The biopsy of truly hard lesions is more challenging. The systems described above are difficult to advance into these lesions. If one does succeed, the obtained sample often displays severe crush artefact making histological interpretation difficult.

Some biopsy kits offer a drill to access a lesion but not to take the biopsy, which can result in the same problem as discussed above. One of the advantages of this type of device, however, is that the outer trochar stays in place and multiple samples can be taken with the biopsy needle through the outer trochar.

Better suited are systems that utilise a drill-like biopsy needle to obtain the sample after placing the outer trochar making it ideal for very hard lesions.

Some publications advocate using spring-loaded soft tissue biopsy needles for the biopsy of non-sclerotic bone lesions. The authors of this chapter do use spring-loaded systems for soft tissue biopsies but find them not routinely useful for bone biopsies.

Apart form the frequently used true-cut-type devices, which are sidecutting, in some circumstances endcutting devices can be useful and excellent results have been reported (Diederich et al. 2006).

If there is any doubt regarding further treatment, the route of percutaneous biopsy should be discussed with the surgeon in charge. Inappropriate biopsy access can result in loss of limb or life for a patient. This is mainly an issue in primary bone tumours, but they can mimic metastases morphologically and therefore deliberated planning of biopsies is good practice.

Generally, one should aim not to contaminate compartments so far not affected by tumour, the physis should not be crossed and if curative surgery is considered the biopsy track should be resectable; otherwise, the lesion easiest to sample should be chosen. Paraosseous soft tissue masses have a higher diagnostic yield than bone lesions (Harish et al. 2006).

If non-diagnostic biopsies are recorded, despite adequate needle position and viable tissue in the biopsy sample, the underlying lesion is frequently benign and commonly a haemangioma. Non-diagnostic biopsies warrant detailed discussion between surgeon, radiologist and pathologist. It needs to be ascertained as to whether representative tissue was obtained; if so, a repeat biopsy might not be necessary; if not, then either repeat biopsy, image guided or open, or more definite treatment have to be considered.

The imaging modality chosen for biopsy depends on local expertise and availability. For bone lesions CT and fluoroscopy-guided intervention is ideal. Fluoroscopy should allow imaging in multiple planes, i.e. biplanar or by using a C-arm. Computed tomography is particularly useful when special consideration must be given to overlying soft tissue, e.g. to stay within a particular soft tissue compartment. Computed tomography is also superior for small lesions. In rare cases large, expansile, destructive bone lesions can be biopsied under ultrasound guidance.

Some form of anaesthesia is usually required. Superficial destructive lesions can usually be biopsied under local anaesthesia. Deeper lesions with normal overlying soft tissue and periosteum can be more difficult to biopsy under local anaesthesia. Conscious sedation often still results in some patient movement and fluoroscopy-guided biopsies are generally less sensitive for movement than CT-guided intervention. Conscious sedation can also lead to problems with the patient's protective reflexes and careful supervision is required. For these reasons the authors favour general anaesthesia. If an anaesthetist is available, the form of anaesthesia should be discussed between all parties involved, including the patient.

27.9 Tumour-Specific Considerations

27.9.1 Prostate cancer

Prostate cancer is a particularly frequent malignancy with a high incidence of bone involvement. The recommendations regarding staging for bone metastases after the diagnosis of prostate cancer vary, but all published guidelines suggest that it is not indicated if PSA <10 ng/ml. The chances of a positive bone scintigraphy are <1% here. When the PSA level is 10–50 ng/ml, the incidence of a positive bone scintigraphy increases to about 10%, and with PSA levels above 50 ng/ml, it increases to about 50% (Hricak et al. 2007). As discussed before, small metastatic lesions to bone without cortical involvement are not well visualised with bone scintigraphy; MR imaging is more sensitive for them (Hricak et al. 2007).

For the imaging in recurrent disease nomograms are used. They predict whether recurrence is local or by distant metastasis using tumour stage, tumour grade and PSA doubling time. Distant metastases usually show short PSA doubling time (10 months) and high-grade cancer. Despite this, the bone scintigraphy stays usually normal until PSA levels are high (≥30 ng/ml). FDG-PET is emerging as modality of choice in the follow-up of bone metastasis after treatment in patients with aggressive disease. Positron emission tomography is better than either bone scintigraphy or CT for the differentiation between "active" bone metastasis and healing bone (Hricak et al. 2007).

27.9.2 Breast Cancer

Breast cancer along with prostate cancer is responsible for the bulk of bone metastases and is usually more aggressive in its clinical course once bone metastases have occurred; however, primary screening for bone metastases is not usually recommended. Screening is advised when clinical or laboratory parameters are suggestive or suspicious (Hamaoka et al. 2004; Even-Sapir 2005). Bone scintigraphy is frequently still the first investigation of choice. This technique has limitations in its sensitivity and some authors suggest PET–CT (Chen et al. 2007). The approach to screening for bone metastases is dictated by local guidelines. There are also a host of guidelines available online, e.g. from the National Comprehensive Cancer Network in the United States.

27.10 Treatment Options

The basis of treatment considerations is formed by tumour staging. In the case of metastatic disease curative treatment attempts are rarely indicated; however, in exceptional cases, such as treated renal cancer with a single bone metastasis, it might be attempted. In the vast majority of cases treatment is palliative.

The aim of treatment is to avert immediate threat to life, e. g. by hypercalcaemia, to avert complications such as fractures, to relieve pain and to restore function. Multidisciplinary teams play a valuable role in the management of these patients (Macklis et al. 1998; Tillman et al. 2002; Ross et al. 2003; Coleman 2004; Martinez-Zapata et al. 2006; Inoue et al. 2007).

Surgical intervention is usually indicated to treat or prevent a pathological fracture. Ideally the surgery should provide immediate stability, allow weight-bearing and should last the lifetime of the patient even as-

suming a fracture will not unite (see Fig. 27.1; Tillman et al. 2002).

Palliative radiotherapy can also be used in an attempt to prevent a fracture and to treat certain fractures. About 30–40% of pathological fractures unite after palliative radiotherapy. Clearly this is not an option for weight-bearing fractures such as neck of femur fractures. Radiotherapy can address some pain but will not cure mechanically induced pain. Radiotherapy can be cost-effective compared with intense drug treatment for pain (Macklis et al. 1998; Tillman et al. 2002).

Drug treatment is not limited to analgesic drugs only. Bisphosponates have been shown to significantly reduce skeletal morbidity in all patients with malignant involvement of the skeleton. They reduce the time to onset of skeletal symptoms and complications. They should probably be prescribed from the first diagnosis of bone involvement; however, they do not prolong life and do not reduce spinal cord compressions (Tillman et al. 2002; Ross et al. 2003; Coleman 2004; Martinez-Zapata et al. 2006).

Radioisotopes can be used to attempt treatment of some tumours with bone metastases (Martinez-Zapata et al. 2006; Inoue et al. 2007).

Cementoplasty with or without preceding radiofrequency ablation can be a useful tool to address painful bone metastases with mechanical pain and risk of fracture, e.g. in the pelvis and spine (Cotten et al. 1995, 1999; Hodge 2000; Nakatsuka et al. 2004).

27.11 Fracture Risk

Pathological fractures due to bone metastases in the appendicular skeleton are most common around the hip but can occur anywhere. It is difficult to assess the fracture risk based on radiographs alone, and a scoring system incorporating the radiographic appearance of size and lytic or sclerotic nature, the location and severity of pain has been proposed and been named after the surgeon, Mirels (Mirels 1989). This fairly simple system (Table 27.2) is widely used by surgeons and has been validated (Evans et al. 2008).

The fracture risk for the neck of femur can also be assessed by measuring the bone mineral density. With cortical destruction rotational forces are more dangerous to the osseous integrity than axial loading (Michaeli et al. 1999). Once more than 50% of cortical bone is destroyed, a fracture is probably inevitable and can occur after minimal or even without trauma (Tillman et al. 2002).

Pathological fractures of the appendicular skeleton occur most frequently around the hip (Fig. 27.1). Full assessment prior to any intervention is more important than speed of surgery, and mistaking a primary bone tumour for metastasis and instigating inappropriate treatment can be a catastrophe for the patient (Tillman et al. 2002).

27.12 Further Imaging/Follow-up

Follow-up imaging of bone metastases after treatment can be difficult to interpret (see Fig. 27.3). Obvious disease progression with increase in lesion size poses no diagnostic challenge; however, not every new bone lesion is necessarily a new metastasis. Bone marrow necrosis due to chemotherapy or steroid administration can lead to the appearance of new bone lesions which are not metastatic (Du et al. 2007; Vanel et al. 2007).

Table 27.2. Mirels' scoring system for metastatic bone disease

Score	1	2	3
Site	Upper limb	Lower limb	Peritrochanteric
Pain	Mild	Moderate	Functional
Lesion morphology on X-ray	Blastic	Mixed blastic/lytic	Lytic
Size as seen on X-ray, maximum cortical destruction on any view	<1/3	1/3–2/3	>2/3

Maximum possible score is 12. For scores ≥8, prophylactic fixation is recommended prior to radiotherapy

Newly appeared sclerotic bone lesions can be due to healing reaction or represent new tumour. Bone scintigraphy is not helpful for the differentiation because increased uptake within the few months after treatment can be a normal flare phenomenon, the normal healing response of bone. This peaks at about 6 weeks and is not indicative of tumour. Lesions that might have shown minimal or no increased uptake before treatment can show marked uptake after (Even-Sapir 2005; Hricak et al. 2007; Stattaus et al. 2008). This effect might also be visible on radiographs, CT or MR imaging with the appearance of sclerotic bone lesions which are simply a healing bone response after tumour treatment (Stattaus et al. 2008). The FDG-PET technique is a more reliable imaging method; increased activity means unsuccessful treatment (Even-Sapir 2005; Specht et al. 2007; Taira et al. 2007).

27.13 Conclusion

Metastatic bone disease to the skeleton is an extremely varied and often challenging disease process. Patients with metastatic bone disease often benefit from a multidisciplinary approach. Critical reflection and considered treatment, rather than complacent assumption, can make a huge difference for the clinical outcome.

References

Abe K, Sasaki M et al. (2005) Comparison of 18FDG-PET with 99mTc-HMDP scintigraphy for the detection of bone metastases in patients with breast cancer. Ann Nucl Med 19(7):573–579

Beheshti M, Vali R et al. (2008) Detection of bone metastases in patients with prostate cancer by F-18 fluorocholine and F-18 fluoride PET-CT: a comparative study. Eur J Nucl Med Mol Imaging [Epub ahead of print]

Berrettoni BA, Carter JR (1986) Mechanisms of cancer metastasis to bone. J Bone Joint Surg Am 68(2):308–312

Chen YW, Huang MY et al. (2007) Discordant findings of skeletal metastasis between tc 99M MDP bone scans and F18 FDG PET/CT imaging for advanced breast and lung cancers: two case reports and literature review. Kaohsiung J Med Sci 23(12):639–646

Coerkamp EG, Kroon HM (1988) Cortical bone metastases. Radiology 169(2):525–528

Coleman RE (2004) Bisphosphonates: clinical experience. Oncologist 9 (Suppl 4):14–27

Cotten A, Deprez X et al. (1995) Malignant acetabular osteolyses: percutaneous injection of acrylic bone cement. Radiology 197(1):307–310

Cotten A, Demondion X et al. (1999) Therapeutic percutaneous injections in the treatment of malignant acetabular osteolyses. Radiographics 19(3):647–653

Diederich S, Padge B et al. (2006) Application of a single needle type for all image-guided biopsies:results of 100 consecutive core biopsies in various organs using a novel tri-axial, end-cut needle. Cancer Imaging 6:43–50

Du Y, Cullum I et al. (2007) Fusion of metabolic function and morphology:sequential [18F]fluorodeoxyglucose positron-emission tomography/computed tomography studies yield new insights into the natural history of bone metastases in breast cancer. J Clin Oncol 25(23):3440–3447

Espinosa LA, Jamadar DA et al. (2008) CT-guided biopsy of bone: a radiologist's perspective. Am J Roentgenol 190(5):W283–W289

Evans AR, Bottros J et al. (2008) Mirels' rating for humerus lesions is both reproducible and valid. Clin Orthop Relat Res 466(6):1279–1284

Even-Sapir E (2005) Imaging of malignant bone involvement by morphologic, scintigraphic, and hybrid modalities. J Nucl Med 46(8):1356–1367

Even-Sapir E, Metser U et al. (2006) The detection of bone metastases in patients with high-risk prostate cancer: 99mTc-MDP Planar bone scintigraphy, single- and multi-field-of-view SPECT, 18F-fluoride PET, and 18F-fluoride PET/CT. J Nucl Med 47(2):287–297

Fujimoto R, Higashi T et al. (2006) Diagnostic accuracy of bone metastases detection in cancer patients: comparison between bone scintigraphy and whole-body FDG-PET. Ann Nucl Med 20(6):399–408

Fukuda Y, Ando K et al. (2006) Superparamagnetic iron oxide (SPIO) MRI contrast agent for bone marrow imaging: differentiating bone metastasis and osteomyelitis. Magn Reson Med Sci 5(4):191–196

Hamaoka T, Madewell JE et al. (2004) Bone imaging in metastatic breast cancer. J Clin Oncol 22(14):2942–2953

Harish S, Hughes RJ et al. (2006) Image-guided percutaneous biopsy of intramedullary lytic bone lesions: utility of aspirated blood clots. Eur Radiol 16(9):2120–2125

Hendrix RW, Rogers LF et al. (1991) Cortical bone metastases. Radiology 181(2):409–413

Hodge JC (2000) Cementoplasty and the oncologic population. Singapore Med J 41(8):407–409

Hricak H, Choyke PL et al. (2007) Imaging prostate cancer: a multidisciplinary perspective. Radiology 243(1):28–53

Inoue T, Yoshinaga K et al. (2007) Whole-body iodine-131 metaiodobenzylguanidine imaging for detection of bone metastases in patients with paraganglioma: comparison with bone scintigraphy. Ann Nucl Med 21(5):307–310

Ketelsen D, Rothke M et al. (2008) Detection of bone metastasis of prostate cancer: comparison of whole-body MRI and bone scintigraphy. Rofo 180(8):746–752 [in German]

Kumar J, Seith A et al. (2008) Whole-body MR imaging with the use of parallel imaging for detection of skeletal metastases in pediatric patients with small-cell neoplasms: comparison with skeletal scintigraphy and FDG PET/CT. Pediatr Radiol 38(9):953–962

Lecouvet F, Geukens ED et al. (2007) Magnetic resonance imaging of the axial skeleton for detecting bone metastases in patients with high-risk prostate cancer: diagnostic and cost-effectiveness and comparison with current detection strategies. J Clin Oncol 25(22):3281–3287

Liu PT, Valadez SD et al. (2007) Anatomically based guidelines for core needle biopsy of bone tumors: implications for limb-sparing surgery. Radiographics 27(1):189–206

Macklis R, Cornelli MH et al. (1998) Brief courses of palliative radiotherapy for metastatic bone pain: a pilot cost-minimization comparison with narcotic analgesics. Am J Clin Oncol 21(6):617–622

Martinez-Zapata MJ, Roque M et al. (2006) Calcitonin for metastatic bone pain. Cochrane Database Syst Rev 3:CD003223

Michaeli DA, Inoue K et al. (1999) Density predicts the activity-dependent failure load of proximal femora with defects. Skeletal Radiol 28(2):90–95

Mirels H (1989) Metastatic disease in long bones. A proposed scoring system for diagnosing impending pathologic fractures. Clin Orthop Relat Res(249):256–264

Miric A, Banks M et al. (1998) Cortical metastatic lesions of the appendicular skeleton from tumors of known primary origin. J Surg Oncol 67(4):255–260

Nakamura T, Kusuzaki K et al. (2003) Case report: recurrence of soft tissue MFH in bone due to minute intravenous tumor emboli detected by MRI. Oncol Rep 10(6):1957–1960

Nakanishi K, Kobayashi M et al. (2007) Whole-body MRI for detecting metastatic bone tumor: diagnostic value of diffusion-weighted images. Magn Reson Med Sci 6(3):147–155

Nakatsuka A, Yamakado K et al. (2004) Radiofrequency ablation combined with bone cement injection for the treatment of bone malignancies. J Vasc Interv Radiol 15(7):707–712

Roodman GD (2004) Mechanisms of bone metastasis. N Engl J Med 350(16):1655–1664

Ross J, Saunders RY et al. (2003) Systematic review of role of bisphosphonates on skeletal morbidity in metastatic cancer. Br Med J 327(7413):469

Schmidt GP, Kramer H et al. (2007a) Whole-body magnetic resonance imaging and positron emission tomography–computed tomography in oncology. Top Magn Reson Imaging 18(3):193–202

Schmidt GP, Schoenberg SO et al. (2007b) Screening for bone metastases: whole-body MRI using a 32-channel system versus dual-modality PET–CT. Eur Radiol 17(4):939–949

Specht JM, Tam SL et al. (2007) Serial 2-[18F] fluoro-2-deoxy-D-glucose positron emission tomography (FDG-PET) to monitor treatment of bone-dominant metastatic breast cancer predicts time to progression (TTP). Breast Cancer Res Treat 105(1):87–94

Spencer JA (2008) Indeterminate lesions in cancer imaging. Clin Radiol 63(8):843–852

Stattaus J, Hahn S et al. (2008) Osteoblastic response as a healing reaction to chemotherapy mimicking progressive disease in patients with small cell lung cancer. Eur Radiol [Epub ahead of print]

Taira AV, Herfkens RJ et al. (2007) Detection of bone metastases: assessment of integrated FDG PET/CT imaging. Radiology 243(1):204–211

Taoka T, Mayr NA et al. (2001) Factors influencing visualization of vertebral metastases on MR imaging versus bone scintigraphy. Am J Roentgenol 176(6):1525–1530

Tillman R, Jane M et al. (2002) Metastatic bone disease: a guide to good practice. British Orthopaedic Association, UK

Vanel D, Bonvalot S et al. (2007) Imatimid-induced bone marrow necrosis detected on MRI examination and mimicking bone metastases. Skeletal Radiol 36(9):895–898

Wu JS, Goldsmith JD et al. (2008) Bone and soft-tissue lesions: What factors affect diagnostic yield of image-guided core-needle biopsy? Radiology 248(3):962–970

Yilmaz MH, Ozguroglu M et al. (2008) Diagnostic value of magnetic resonance imaging and scintigraphy in patients with metastatic breast cancer of the axial skeleton: a comparative study. Med Oncol 25(3):257–263

Yuh WT, Quets JP et al. (1996) Anatomic distribution of metastases in the vertebral body and modes of hematogenous spread. Spine 21(19):2243–2250

Radiation-Induced Tumours

28

A. Mark Davies and Steven L. J. James

CONTENTS

KEY POINTS

- Radiation-induced bone tumours include osteochondroma and sarcoma, most commonly osteosarcoma.
- Radiation-induced osteochondromas arise in patients who have undergone radiation therapy under the age of 5 years. The incidence is up to 29% of young children undergoing total body irradiation.
- The incidence of radiation-induced sarcoma is approximately 0.2% of patients who have survived the subsequent 5 years.
- The latent period for development of a radiation-induced sarcoma is 4–55 years (mean 11–14 years).
- Most radiation-induced sarcomas arise in the periphery of the former radiation therapy field.
- Cortical destruction and soft tissue extension on CT and/or MR imaging within the radiation field is highly suggestive of malignant transformation to a sarcoma.
- Multiple radiation-induced insufficiency-type stress fractures, particularly when arising in the pelvis, should not be mistaken for metastases.

A. M. Davies, MBChB, FRCR
Consultant Radiologist, Department of Radiology, Royal Orthopaedic Hospital, NHS Foundation Trust, Bristol Road South, Northfield, Birmingham B31 2AP, UK

S. L. J. James, MD
Consultant Radiologist, Department of Radiology, Royal Orthopaedic Hospital, NHS Foundation Trust, Bristol Road South, Northfield, Birmingham B31 2AP, UK

28.1 Introduction

Radiation damage to bone is as much an issue today as it was when X-rays were first discovered. X-rays continue to be routinely used for diagnostic and interventional purposes as well as in the treatment of many malignancies. Even when the target is non-osseous, bones within the radiation field may be affected. Advances in

oncological treatments have resulted in improved survival rates, particularly in paediatric cancers, so that it is not unusual to see the late effects of radiotherapy. It is important to recognize the skeletal complications of radiation as they can cause diagnostic problems and some, such as sarcomatous transformation, are associated with significant morbidity and/or mortality. The purpose of this chapter is to review the imaging features of radiation-induced tumours of bone and other radiation-associated complications that can simulate a bone tumour. While it is recognized that radiation can also induce non-osseous malignancies, this chapter is confined to osseous lesions.

28.2 Historical Perspective

The enthusiasm with which Wilhelm Roentgen's discovery of X-rays in 1895 was embraced by both the medical community and the general population has rarely been paralleled. Diagnostic radiography was rapidly introduced but within 6 months the first deleterious effects were being reported, including hair loss, skin reddening and desquamation, and systemic effects such as pyrexia, diarrhoea and vomiting (Hawks 1896; Kolle 1897; Walsh 1897). It took several years before it was realized that prolonged exposure of both the patient and the operator to diagnostic X-rays could cause serious damage. At the same time X-ray therapy was being used indiscriminately for what are now recognized as inappropriate indications. In 1902 a radiation-induced skin neoplasm was reported in a 33-year-old man who had been demonstrating X-rays for 4 years (Frieben 1902). A British radiologist, John Hall-Edwards, was one of the first to give a comprehensive description of the effects of X-rays on the bones of the hands – using his own hands for case material (Hall-Edwards 1908)! The realization of the harmful effects was reinforced by the death of early X-ray pioneers, including Hall-Edwards, over the next 25 years. Cases of osteosarcoma were reported in workers who ingested radium and mesothorium in the fluorescent paint used to paint clock faces by pointing the brushes with their teeth (Maitland and Humphries 1929) and in patients who had received radiation treatment for tuberculous arthritis (Beck 1922). Today, the harmful effects of both diagnostic and therapeutic radiation on organ systems are increasingly better understood. Radiation protection continues to be an important issue as reports of the potential increased risk of developing solid cancers following diagnostic and interventional procedures are highlighted in the scientific literature and the popular press (Berrington de González and Darby 2004; Penman 2004). The burgeoning collective radiation dose from computed tomography (CT) remains a particular cause for concern (Hall and Brenner 2008).

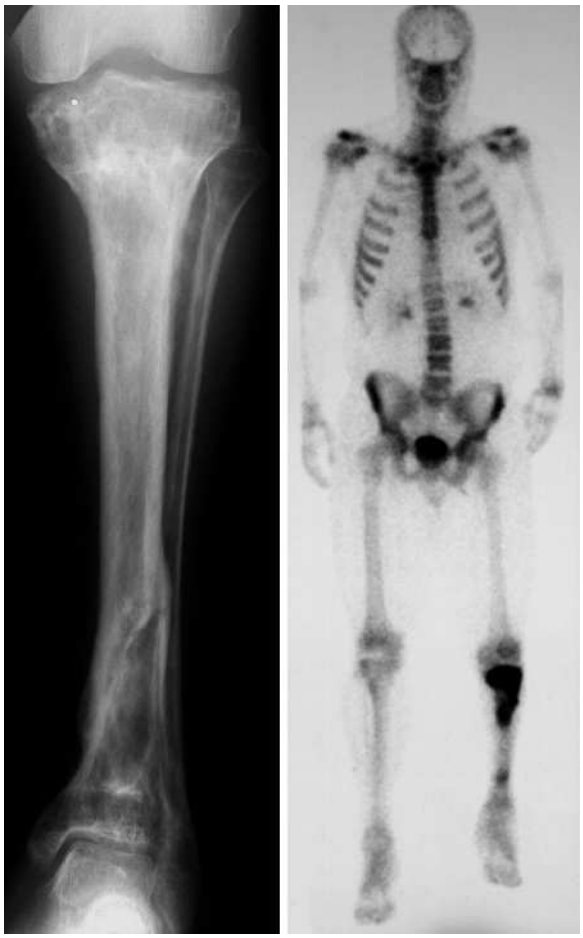

Fig. 28.1. **a** AP radiograph of the tibia showing a radiation osteosarcoma arising in the proximal tibial metadiaphysis 20 years after radiotherapy for a Ewing's sarcoma and 5 years after sustaining a fracture following minor trauma. There is shortening of the tibia with the ghost of the original tumour and a healed spiral fracture of the distal tibia. **b** Whole body bone scintigraphy showing marked increased activity from the radiation sarcoma and minor increased activity at the site of the healed fracture. The degree of radiation-induced shortening can be appreciated by comparison with the contralateral tibia

28.3 Microscopic Effects of Radiation on Bone

Irradiation of tissues may cause: (1) immediate or delayed cell death, (2) cellular injury with recovery, (3) arrest of cellular division and (4) abnormal repair with neoplasia. Although the pathological effects of radiation are independent of their method of production, the effects differ in the immature (growing) and mature (adult) skeleton. The bony changes follow (Dalinka and Haygood 2002). Radiation affects the immature skeleton by interfering with chondrogenesis and reabsorption of calcified cartilage and bone at the growth plate (Rubin et al. 1959). The greater the growth potential of an individual at the time of irradiation, the more growth is affected, hence radiation has a greater effect in younger patients (Fig. 28.1). Severe changes are also common when irradiation occurs during the pubertal growth spurt, when the zone of provisional calcification is hypertrophied (Probert and Parker 1975). In the mature skeleton the effect is mainly on the osteoblasts, primarily resulting in decreased matrix formation and in severe cases malignant transformation (Howland et al. 1975; Ergun and Howland 1980).

28.4 Radiation-Induced Bone Tumours

28.4.1 Benign Tumours

Osteochondroma is a manifestation of abnormal enchondral bone growth, with disturbance of orderly chondrogenesis as a response to injury, which includes irradiation (Murphy and Blount 1962; Cole and Darte 1963). It is thought that any irradiated epiphysis or enchondral bone is at risk of osteochondroma development until growth ceases. In the past most reports of radiation-induced osteochondromas were in children who received radiotherapy for Wilms' tumour or neuroblastoma, with an incidence of 4.8% (Fig. 28.2) (Paulino et al. 2000). The use of total body irradiation (TBI) prior to haematopoietic stem cell transplantation has resulted in an increased incidence of osteochondroma ranging from 10% to 29% (Harper et al. 1998; Bordigoni et al. 2002; Taitz et al. 2004; Faraci et al. 2005). Most cases occur in those who have received TBI in the first 5 years of life (Taitz et al. 2004; Faraci et al. 2005). The time interval between radiotherapy and onset is extremely variable and largely dependent on the site of the lesion, any associated pressure or mass effects or if it is discovered incidentally on follow-up imaging (Fig. 28.2). Lesions may be multiple and development is reported between 3 and 18 years after radiotherapy (Ra-

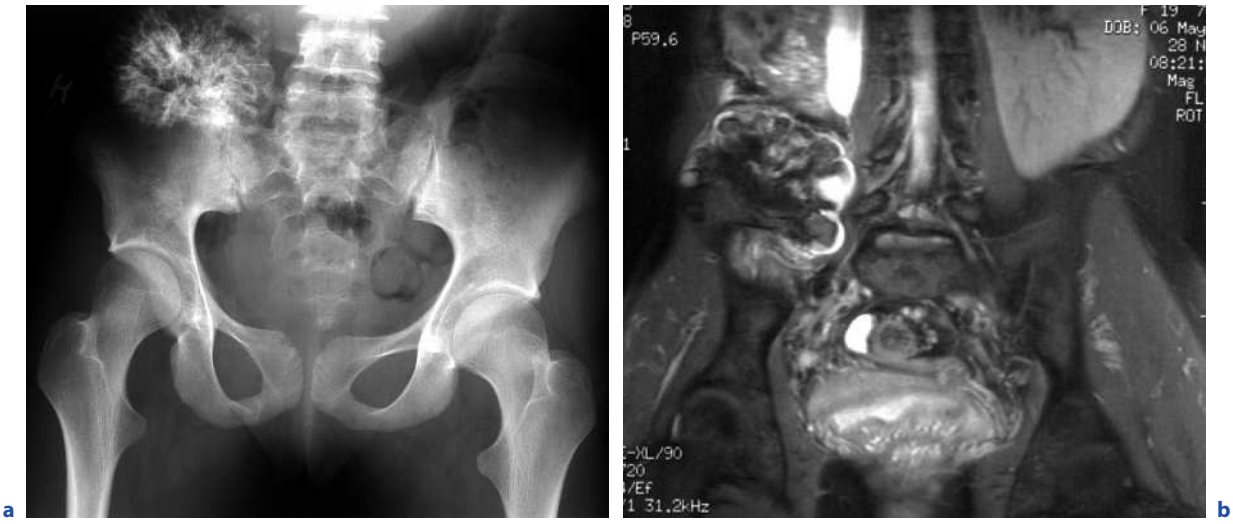

Fig. 28.2. **a** AP radiograph showing a large radiation-induced osteochondroma arising from the right ilium first detected 19 years after surgery and radiotherapy for a Wilms' tumour. There is also hypoplasia of the right hemipelvis. **b** Coronal T2-weighted fat suppressed image showing the thin cartilage cap to the osteochondroma and the compensatory hypertrophy of the remaining left kidney

jah et al. 1975; Libshitz and Cohen 1982; DiSimone et al. 1993; Bordigoni et al. 2002; Taitz et al. 2004; Harish et al. 2006). The dose of radiation required to induce osteochondroma development varies between 1,500 and 5,000 cGy, although doses as low as 125 cGy have been reported (Neuhauser et al. 1952). The imaging and pathological features, surgical treatment and prognosis are identical to those for a spontaneous osteochondroma (Mitchell and Logan 1998). Malignant transformation is rare with only two reported cases in the literature (Perez et al. 1967; Mahboubi et al. 1997). The simultaneous occurrence of a separate radiation-induced osteosarcoma and an osteochondroma has been described (Poustchi et al. 1996). Other benign radiation-induced tumours, such as osteoblastoma, have rarely been reported (Cohen and D'Angio 1962).

28.4.2 Malignant Tumours

There is some controversy as to whether malignant transformation following radiation treatment should be called radiation-induced sarcoma or postradiation sarcoma (Patel 2000; Sheppard and Libshitz 2001). Radiation-induced may not be appropriate for, despite overwhelming evidence, an absolute causal relationship has not been established (Sheppard and Libshitz 2001). In addition there may be other contributory factors such as carcinogenic alkylating chemotherapy (Patel 2000).

Postradiation sarcomas of bone are rare, accounting for approximately 1.5% of all bone sarcomas (Weatherby et al. 1981). The reported incidence was thought to range between 0.1% and 0.2% of breast cancer survivors, but may actually be higher due to longer survival of these patients (Kim et al. 1978; Smith 1987). The reported risk at 5 years in patients following treatment for Hodgkin's disease is 0.9% (Halperin et al. 1984). One estimate of the overall incidence ranges from 0.03% (of patients who receive radiation) to 0.2% (of patients who received radiation and survived 5 years) (Patel 2000).

Sarcomas can develop in any bone exposed to either internal or external radiation sources (Fig. 28.3). They may arise at the site of pre-existing bone lesions or in bones that were normal at the time of irradiation, for example, when radiation has been used to treat malignancy in adjacent soft tissue tumours without bony involvement (Fig. 28.4). Approximately one third of postradiation sarcomas arise in association with pre-existing bone lesions such as giant cell tumour, lymphoma, osteosarcoma or round cell tumours such as Ewing's sarcoma (Huvos et al. 1985; Kuttesch et al. 1996; Koshy et al. 2005). There was a vogue in the mid-twentieth century, long since ceased, to treat fibrous dysplasia with radiotherapy. As a result radiation sarcomas were seen in the past in association with fibrous dysplasia (Fig. 28.5).

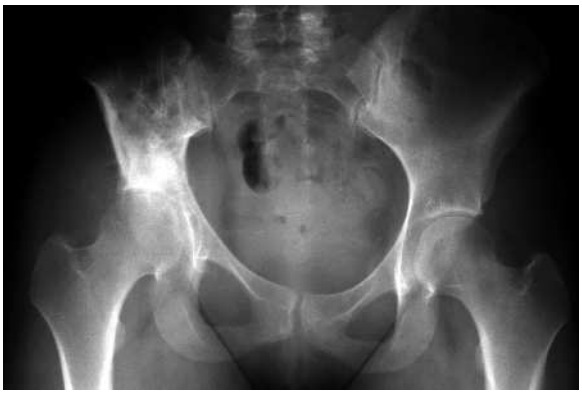

a

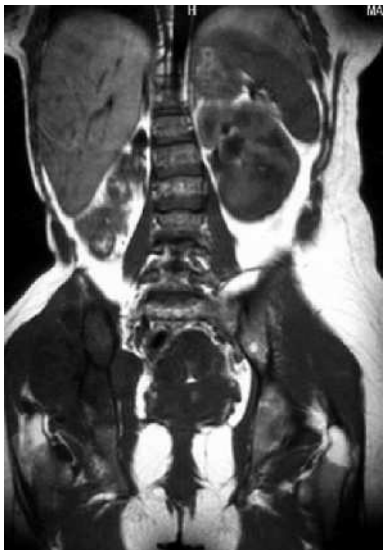

b

Fig. 28.3. **a** AP radiograph of the pelvis showing a right iliac radiation osteosarcoma 23 years after surgery and radiotherapy for a Wilms' tumour. The sarcoma is indicated by the sclerosis of the malignant osteoid, the spiculated periosteal new bone formation and the faint outline of a soft tissue mass. There is radiation-induced hypoplasia of the right hemipelvis. **b** Coronal T1-weighted image of the abdomen and pelvis showing tumour infiltration of the right ilium, an absent right kidney and a minor scoliosis to the operated side

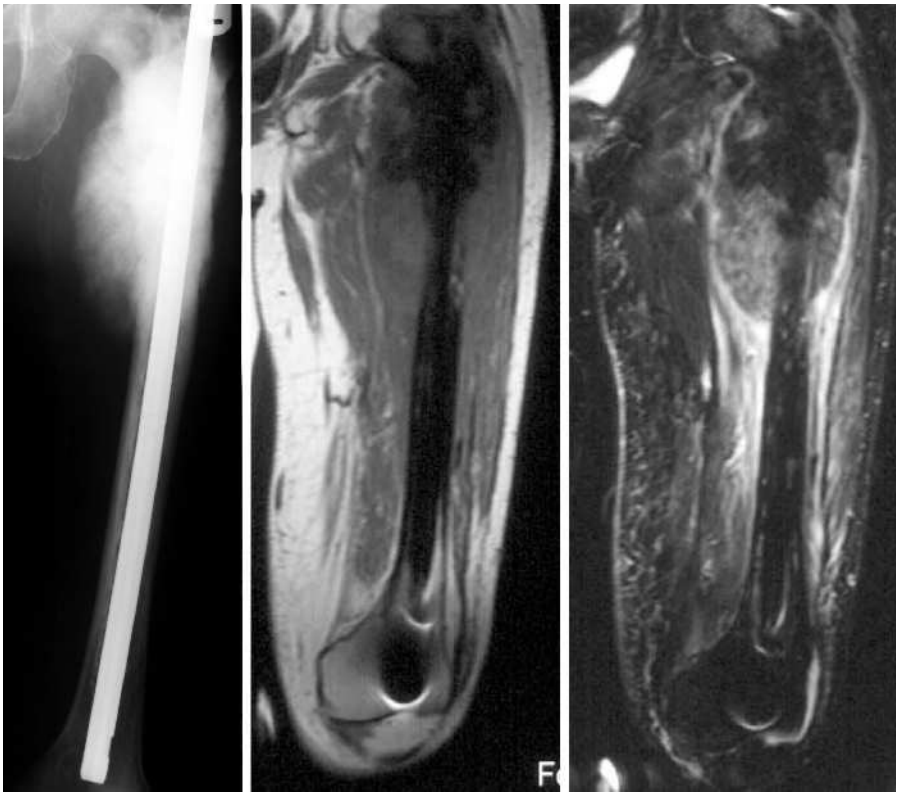

a,b c

Fig. 28.4. **a** AP radiograph showing an extensive osteosarcoma arising in the proximal femur 30 years after radiotherapy for a soft tissue sarcoma. An intramedullary nail had been inserted some years before for a radiation-associated fracture. **b, c** Coronal T1-weighted image (**b**) and coronal STIR image (**c**) showing the sarcoma to be predominantly low signal due to the mineralization with a heterogeneous soft tissue component distally. There is a linear signal void with minor artefact from the intramedullary nail

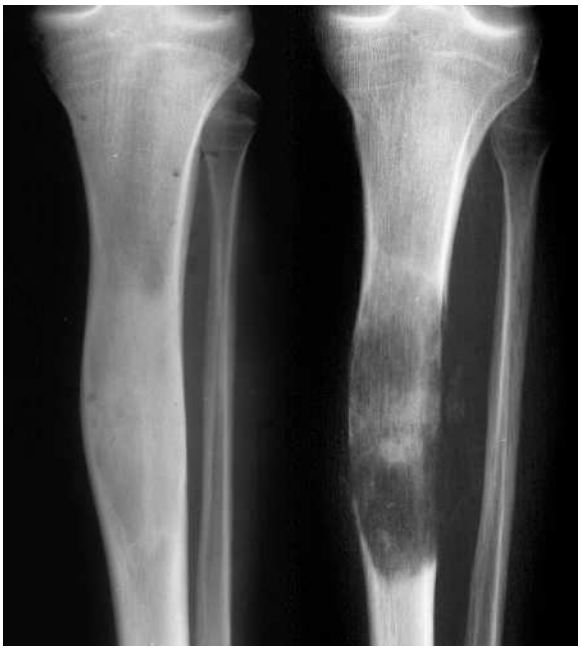

Fig. 28.5. **a** AP radiograph of the tibia obtained in 1947 showing monostotic fibrous dysplasia which was "treated" with radiotherapy. **b** AP radiograph obtained 38 years later when the patient re-presented with a radiation-induced osteosarcoma showing a predominantly lytic appearance

Although sarcomas have been reported with doses as low as 800 cGy, postradiation sarcomas usually require a dose of 3,000 cGy over a period of 3 weeks, with a threshold of about 1,000 cGy (Kim et al. 1978). They do not usually occur in heavily damaged areas of bone because these lack the ability to regenerate but develop in areas where the dose has been sufficient to cause cell mutation, but not complete sterilization. For this reason, postradiation sarcomas tend to occur in the periphery of the radiation field, arising some distance from the primary tumour (Fig. 28.6). It is, therefore, unusual for a postradiation sarcoma to arise within an old sarcoma as that was usually in the centre of the radiation field. Histologically, postradiation sarcomas are identical to those arising spontaneously. Osteosarcoma and spindle cell sarcoma (fibrosarcoma, malignant fibrous histiocytoma) account for over 90% of radiation-induced sarcomas (Kalra et al. 2007). Chondrosarcomas account for less than 10% of the total (Smith 1987).

Established diagnostic criteria for postradiation sarcoma are: (1) malignancy arising within the irradiated field, (2) histological proof of sarcoma, distinct from

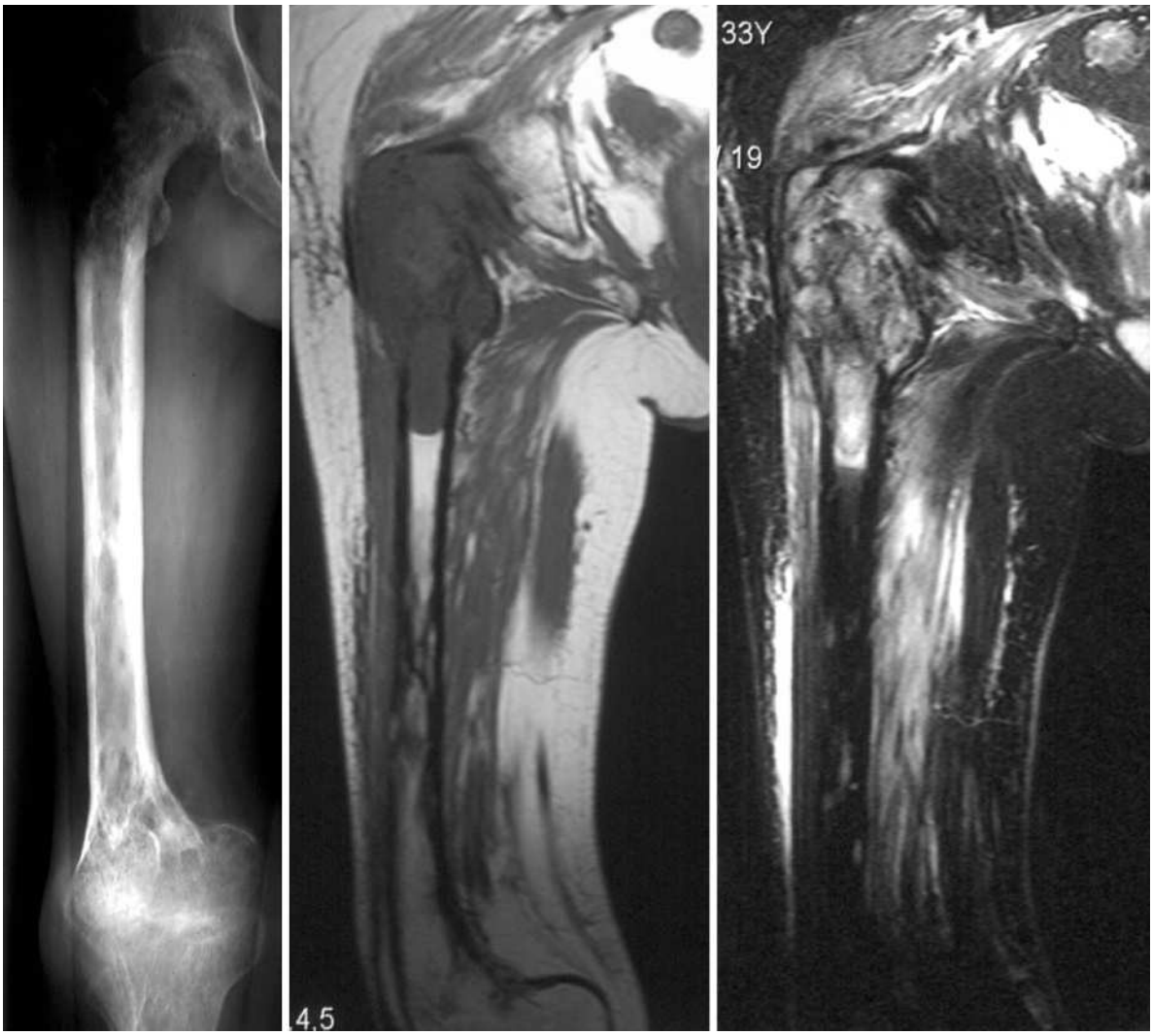

Fig. 28.6. **a** AP radiograph of the femur showing a lytic radiation-induced spindle cell sarcoma of the proximal femur. The patient had received radiotherapy for a distal femoral Ewing's sarcoma 23 years before. The distorted bony architecture of the distal femur represents the treated primary sarcoma and radiation change. The patchy lucencies in the diaphysis are secondary to the radiotherapy and not due to further tumour. **b** Coronal T1-weighted image showing the radiation sarcoma as hypointense. The radiation changes in the femoral diaphysis resemble pagetic bone without expansion. **c** Coronal STIR image showing the radiation sarcoma to be heterogeneous but predominantly hyperintense. The patchy diaphyseal lucencies are mildly hyperintense

the original lesion, and (3) a long latent period of at least 4 years following irradiation (Cahan et al. 1948; Arlen et al. 1971). The latent period ranges from 4 to 55 years with an average of 11–14 years (Weatherby et al. 1981; Wiklund et al. 1991; Kalra et al. 2007; Makimoto et al. 2007). It does not differ between children and adults, but in children a higher prevalence of radiation-induced sarcoma can be expected because the immature skeleton is more susceptible to radiation-induced induction of malignancy, and they have a longer period over which they are at risk and have the potential to develop malignancy. Latency may be inversely proportional to radiation dose, with shorter latent periods often seen following administration of higher doses (Vázquez et al. 2003).

Typical presentation is with pain, swelling or a palpable soft tissue mass. Radiographically an aggressive lytic lesion is present often with soft tissue extension (Figs. 28.3, 28.5, 28.6) (Mitchell and Logan 1998; Roebuck 1999; Sheppard and Libshitz 2001). Malignant osteoid formation with dense sclerosis is a feature of radiation-induced osteosarcoma (Fig. 28.3). Coexisting radiation bone changes are seen in up to 50% of patients. The cardinal features of cortical destruction and soft tissue extension are optimally demonstrated with MR imaging but CT can also be used (Figs. 28.3b, 28.4b, c, 28.6b, c, 28.7b) (Lorigan et al. 1989; Roebuck 1999).

Bone healing and remodelling in the development of the imaging features of radiation osteonecrosis are dynamic and it can be difficult to exclude malignancy radiographically. This is particularly a problem in cases where radiotherapy was administered for a pre-existing bone lesion. The bony architecture may be greatly distorted by the coexisting ghost of the original lesion and radiation bone changes. Relative lack of change on serial radiographs favours radiation change, whereas pain, presence of a soft tissue mass and increasing lysis favour the diagnosis of recurrent tumour or radiation-associated sarcoma. If, as is frequently the case, there is a long latent period, previous imaging may not be available for comparison. MR imaging is particularly useful in this situation. The absence of true bone destruction, soft tissue mass and lack of enhancement with a gadolinium-chelate suggests that there is no tumour present (Fig. 28.8). Conversely, bone destruction, soft tissue mass and active enhancement are suggestive of tumour (Fig. 28.7). Most primary tumours, including giant cell tumour of bone and sarcoma, will tend to recur within 5 years of initial treatment with radiotherapy. Therefore,

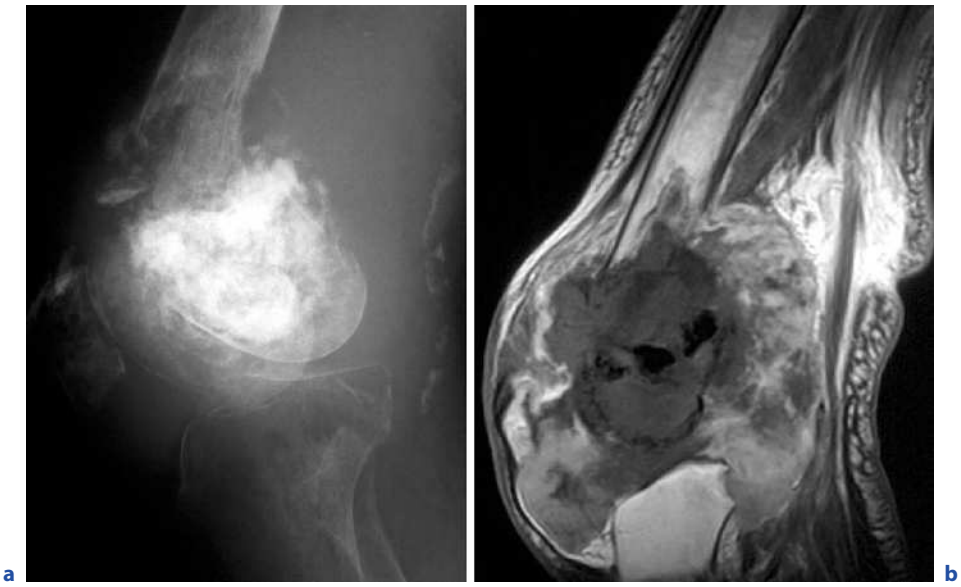

Fig. 28.7. **a** Lateral radiograph showing an extensive radiation osteosarcoma presenting with a pathological fracture at the site of a giant cell tumour of bone treated 50 years before with radiotherapy. The sclerosis may be due in part to the ghost of the original tumour, malignant osteoid from the radiation sarcoma and disordered bone repair in response to the radiotherapy. **b** Sagittal T1-weighted contrast-enhanced image showing tumour infiltrating the distal femur, invading the knee and extending into the popliteal fossa

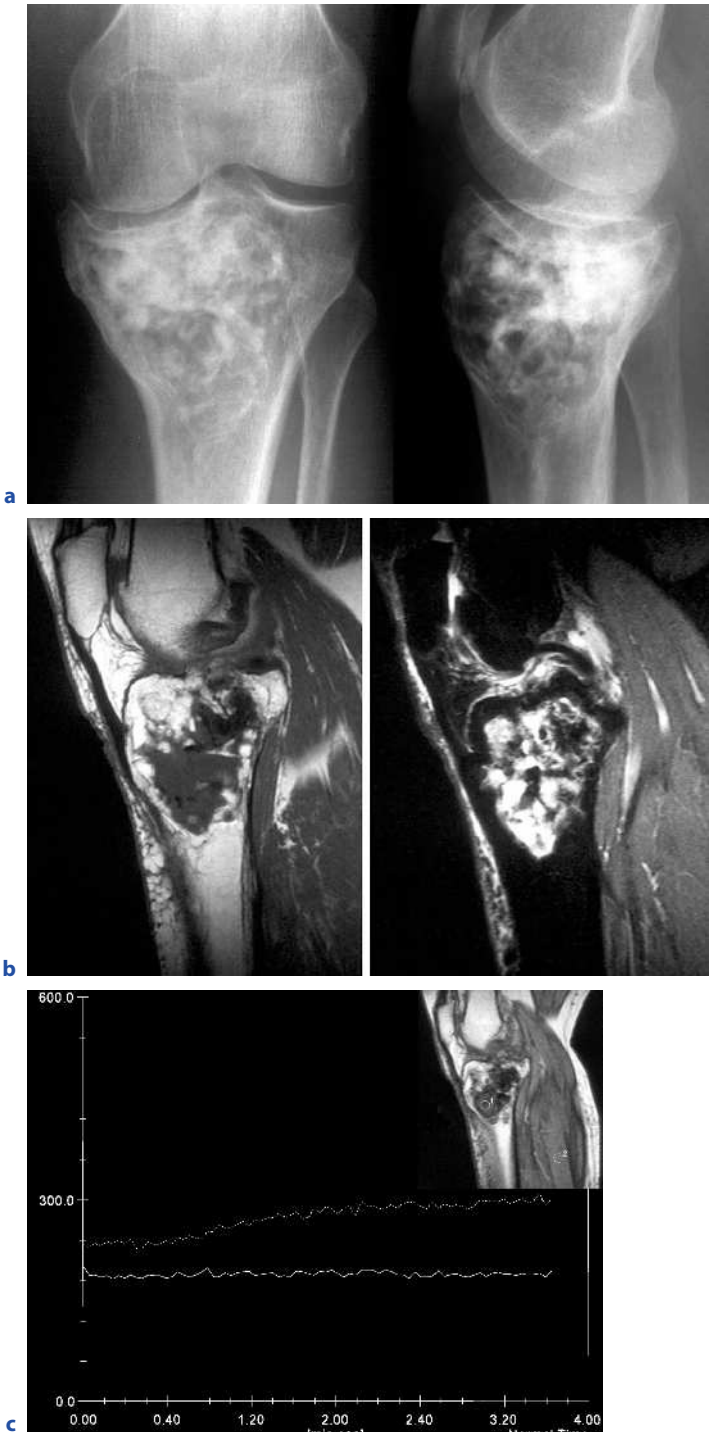

Fig. 28.8. **a** AP and lateral radiographs of the knee in a patient presenting with pain 45 years after surgery for primary and then radiotherapy for recurrent giant cell tumour of the proximal tibia. The possibility of malignant transformation was queried and there were no previous radiographs available for comparison due to the long period since initial treatment. **b** Sagittal T1-weighted and STIR images showing a heterogeneous lesion at the site of the old tumour. There is no cortical breaching evident. **c** Time-intensity curve plotted after performing a dynamic contrast-enhanced sequence. Regions of interest were placed over the main lesion (*bottom line*) showing no enhancement and a control on the posterior calf muscles (*top line*) showing minor progressive enhancement. This effectively excludes malignant transformation as a sarcoma would typically show a very rapid enhancement pattern

the longer the period over 5 years between treatment and development of an aggressive tumour the more likely the tumour is to be radiation-associated. Occasionally, differentiation of tumour from radiation bone changes complicated by infection may also be difficult. Biopsy is advised to establish the histological nature of any aggressive lesion and distinguish between tumour and infection. As many radiation-associated sarcomas develop in those treated for a prior malignancy or in the elderly the differential diagnosis of an aggressive lesion has to also include metastatic disease. Metastases, however, usually involve multiple sites and are also found outside the radiation field. Multifocal radiation sarcoma would appear to be remarkably rare (Matsuo et al. 2005). It is worth noting that childhood retinoblastoma increases the risk of de novo osteosarcoma but also potentiates the sarcoma-inducing ability of radiation therapy. Seventy per cent of second malignant neoplasms in these cases arise within the field of therapeutic radiation (Abramson et al. 1984; Chan et al. 2000).

28.5 Tumour-Like Complications of Radiation

The non-neoplastic effects of radiation on mature bone can be regarded as a spectrum ranging from mild osteopenia to osteonecrosis (Williams and Davies 2006). Radiographically, the bone appears osteopenic approximately 1 year after irradiation (Howland et al. 1975).

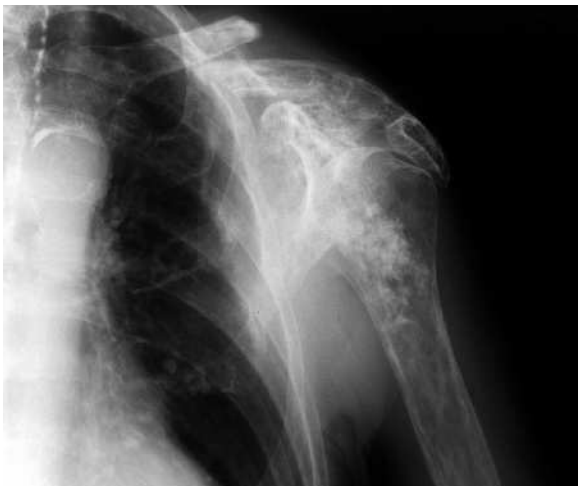

Fig. 28.9. AP radiograph of the shoulder 19 years after radiotherapy in a patient with a history of breast carcinoma. There is radiation-induced osteopenia, coarsening of the trabeculae, dystrophic calcification in the proximal humerus and a displaced ununited fracture of the clavicle

This long latent period between irradiation and recognition of its effects is due to the slow metabolic turnover rate of adult bone, and the relative insensitivity of conventional radiographs for the detection of osteopenia. Following this period of bone atrophy, repair occurs with the deposition of bone on unresorbed trabeculae. Radiographs obtained 2–3 years after irradiation demonstrate mottled areas of bone with osteopenia, coarse trabeculation and focal areas of increased bone density mimicking marrow infiltration (Fig. 28.9). There is a narrow zone of transition between the affected area and normal bone and the changes are confined to the radiation field. *Radiation osteitis* was the term first used to describe radiation-induced bony changes (Ewing 1926). *Radiation osteonecrosis* or *osteoradionecrosis* are also used interchangeably in the literature, but both terms imply greater damage to bone resulting in cell death and, in turn, more severe changes on imaging (Fig. 28.9).

The classic radiation-associated complication is the development of insufficiency-type stress fractures. They are a common and significant complication of pelvic irradiation typically seen in women (Fu et al. 1994; Bliss et al. 1996; Mumber et al. 1997; Moreno et al. 1999). Frequently symptomatic, these fractures are often multiple and bilateral. They usually occur within 12 months of treatment, and vertical fractures of the sacral ala are the most common type (Fig. 28.10) (Blomlie et al. 1996). Sacral insufficiency fractures may be detected using CT, bone scintigraphy and MR imaging (Fig. 28.10) (Mammone and Schweitzer 1995). Pubic fractures are less common and this may be attributed to reduced compressive forces on the anterior pelvic ring with standing because most of the load is distributed to the acetabula. Hence medial acetabular wall insufficiency fractures are fairly common (Fig. 28.11). Femoral neck fractures may also occur (McCrorie 1950; Bonfiglio 1953; Epps et al. 2004). As these days many female patients treated for a gynaecological malignancy are long-term survivors it is not unusual to see rapidly progressive insufficiency fracture formation developing many years after radiotherapy when pre-existing radiation changes are associated with the onset of osteoporosis. The diagnosis of metastatic disease is often considered particularly when multiple insufficiency fractures are detected on bone scintigraphy. It is self-evident that combined radiation- and osteoporosis-associated insufficiency fractures do not respond well to further radiotherapy! Imaging, in particular CT, will elegantly demonstrate the fractures in the absence of bone destruction and a soft tissue mass. It should be stressed that radiation changes in bone may coexist with recurrent or metastatic tumour (Fig. 28.10b) (Williams and Davies 2006).

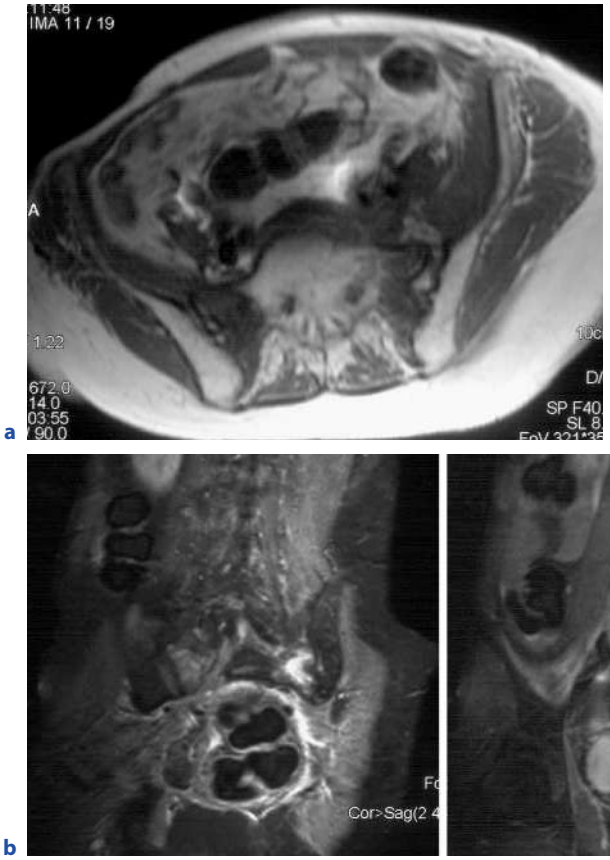

a

b

Fig. 28.10. **a** Axial T1-weighted image showing bilateral sacral insufficiency fractures as hypointense zones in the sacral ala in a patient treated with radiotherapy for carcinoma of the cervix. **b** Coronal STIR images showing the sacral insufficiency fractures to be hyperintense. In addition, there is metastatic infiltration of the body of L5 evident in the right-hand image. This highlights the fact that radiotherapy changes can coexist with recurrent and/or metastatic disease

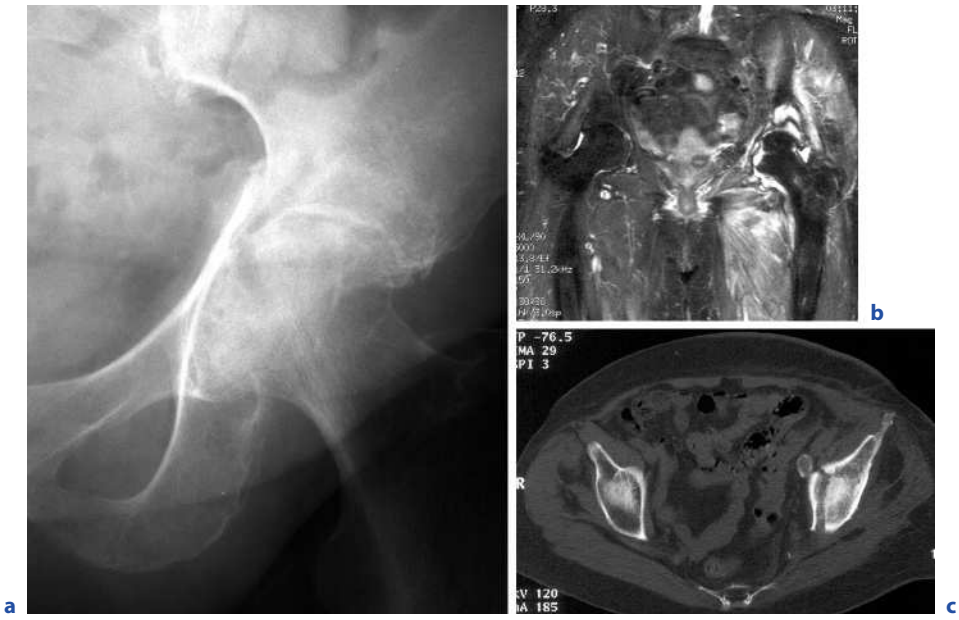

a

b

c

Fig. 28.11. **a** AP radiograph showing an insufficiency fracture of the medial wall of the acetabulum with surrounding bony sclerosis and narrowing of the hip joint 4 years after radiotherapy for squamous cell carcinoma of the vulva. **b** Coronal T2-weighted fat-suppressed image showing a hip joint effusion, oedema in the acetabulum and soft tissue oedema in the buttock and adductor muscles. **c** Axial CT showing the acetabular fracture and absence of bone destruction and a soft tissue mass

28.6 Conclusion

A century ago the harmful effects of radiation were seen initially due to excessive and uncontrolled use of diagnostic X-rays. Subsequently, problems arose principally with the use of radiotherapy for benign and malignant conditions and this remains the most common reason for seeing radiation changes in tissues on imaging studies. The fact that radiation-induced bone changes are arguably as common today as they were 50 years ago is not due to the indiscriminate use of radiotherapy but the fact that many patients are now long-term survivors of their first malignancy. It is important to recognize the spectrum of bone changes secondary to radiation and to be able to differentiate, using imaging, malignant transformation from other less serious complications.

References

Abramson DH, Ellsworth RM, Kitchin FD, Tung G (1984) Second nonocular tumors in retinoblastoma survivors: are they radiation induced? Ophthalmology 91:1351–1355

Arlen M, Higginbotham NL, Huvos AG (1971) Radiation-induced sarcoma of bone. Cancer 28:1087–1099

Beck A (1922) Zur Frage des Rontgensarcoms, Zugleich ein Beitrag zur Patholgenese des Sarcoms. Munchen Med Wschr 69:623–625

Berrington de Gonzàlez A, Darby S (2004) Risk of cancer from diagnostic x-rays: estimates for the UK and 14 other countries. Lancet 363:345–351

Bliss P, Parsons CA, Blake PR (1996) Incidence and possible aetiological factors in the development of pelvic insufficiency fractures following radical radiotherapy. Br J Radiol 69:548–554

Blomlie V, Rofstat EK, Talle K, Sundfor K, Winderen M, Lein HH (1996) Incidence of radiation-induced insufficiency fractures of the female pelvis: evaluation with MR imaging. AJR Am J Roentgenol 167:1205–1210

Bonfiglio M (1953) The pathology of fractures of the femoral neck following irradiation. AJR Am J Roentgenol 70:449–459

Bordigoni P, Turello R, Clement L, Lascombes P, Leheup B, Galloy MA, Plenat F (2002) Osteochondroma after pediatric hematopoietic stem cell transplantation: report of eight cases. Bone Marrow Transplant 7:611–614

Cahan WG, Woodard HQ, Higinbotham NL, Stewart FW, Coley BL (1948) Sarcoma arising in irradiated bone. Cancer 1:3–29

Chan LL, Czerniak BA, Ginsberg LE (2000) Radiation-induced osteosarcoma after bilateral childhood retinoblastoma: radiologic-pathologic conferences of the University of Texas MD Anderson Cancer Centre. AJR Am J Roentgenol 174:1288

Cohen J, D'Angio GJ (1962) Unusual bone tumors after roentgen therapy of children. AJR Am J Roentgenol 86:502–512

Cole ARC, Darte JMM (1963) Osteochondromata following irradiation in children. Pediatrics 32:285–288

Dalinka MK, Haygood TM (2002) Radiation changes. In: Resnick D (ed) Diagnosis of bone and joint disorders, 5th edn. Saunders, Philadelphia, pp 3393–3422

DiSimone DP, Abdelwahab IF, Kenan S, Klein MJ, Lewis MM (1993) Radiation-induced osteochondroma of the ilium. Skeletal Radiol 22:289–291

Epps HR, Brinker MR, O'Connor DP (2004) Bilateral femoral neck fractures after pelvic irradiation. Am J Orthop 33:457–460

Ergun H, Howland WJ (1980) Postradiation atrophy of mature bone. Crit Rev Diagn Imaging 12:225–243

Ewing J (1926) Radiation osteitis. Acta Radiol 6:399–412

Faraci M, Barra S, Cohen A, et al. (2005) Very late nonfatal consequences of fractionated TBI in children undergoing bone marrow transplant. Int J Radiat Oncol Biol Phys 63:1568–1575

Frieben A (1902) Cancroid des Handruckens nach Langdauernder Einwirkung von Röntgenstrahlen. Fortschr Rontgenstr 6:106–112

Fu AL, Greven KM, Maruyama Y (1994) Radiation osteitis and insufficiency fractures after pelvic irradiation for gynaecological malignancies. Am J Clin Oncol 17:248–254

Hall EJ, Brenner DJ (2008) Cancer risks from diagnostic radiology. Br J Radiol 81:362–378

Hall-Edwards J (1908) The effects upon bone due to prolonged exposure to the X-ray. Arch Roentgen Ray 13:44

Halperin EC, Greenberg MS, Suite HD (1984) Sarcoma of bone and soft tissue following treatment of Hodgkin's disease. Cancer 53:232–236

Harish S, Rehm A, Bearcroft PWP (2006) Case of the month: an unusual cause and presentation of a pelvic mass. Br J Radiol 79:177–178

Harper GD, Dicks-Mireaux C, Leiper AD (1998) Total body irradiation-induced osteochondromata. J Pediatr Orthop 18:356–358

Hawks HD (1896) The physiologic effects of the Roentgen rays. Elect Engineer 22:276

Howland WJ, Loeffler RK, Starchman DE, Johnson RB (1975) Post-irradiation atrophic changes of bone and related complications. Radiology 117:677–685

Huvos AG, Woodard HQ, Cahan WG (1985) Postradiation osteogenic sarcoma of bone and soft tissues. Cancer 55:1244–1255

Kalra S, Grimer RJ, Spooner D, Carter SR, Tillman RM, Abudu A (2007) Radiation-induced sarcomas of bone: factors that effect outcome. J Bone Joint Surg Br 89B:808–813

Kim JH, Chu FCH, Woodard HQ, Melamed MR, Huvos A, Cantin J (1978) Radiation induced soft tissue and bone sarcoma. Radiology 129:501–508

Kolle FS (1897) The effect of x-rays on the hair. Elect Engineer 23:267

Koshy M, Paulino AC, Mai W, The BS (2005) Radiation-induced osteosarcomas in the pediatric population. Int J Radiat Oncol Biol Phys 63:1169–1174

Kuttesch JF, Wexler LH, Marcus RB (1996) Second malignancies after Ewing's sarcoma: radiation dose-dependency of secondary sarcomas. J Clin Oncol 14:2818–2825

Libshitz HI, Cohen MA (1982) Radiation-induced osteochondromas. Radiology 142:643–647

Lorigan JG, Libshitz HI, Peuchot M (1989) Radiation-induced sarcoma of bone: CT findings in 19 cases. AJR Am J Roentgenol 153:791–794

Mahboubi S, Dormans JP, D'Angio G (1997) Malignant degeneration of radiation-induced osteochondroma. Skeletal Radiol 26:195–198

Maitland HS, Humphries RE (1929) Osteogenic sarcoma in dial pointers using luminous paint. Arch Pathol 7:406

Makimoto Y, Yamamoto S, Takano H, et al. (2007) Imaging findings of radiation-induced sarcoma of the head and neck. Br J Radiol 80:790–797

Mammone JF, Schweitzer ME (1995) MRI of occult sacral insufficiency fractures following radiotherapy. Skeletal Radiol 24:101–104

Matsuo T, Sugita T, Shimose S, Kubo T, Yasunaga Y, Hiyama E, Ochi M (2005) Postradiation malignant fibrous histiocytoma and osteosarcoma of a patient with high telomerase activities. Anticancer Res 25:2951–2955

McCrorie W (1950) Fractures of the femoral neck following pelvic irradiation. Br J Radiol 23:587–592

Mitchell MJ, Logan PM (1998) Radiation-induced changes in bone. Radiographics 18:1125–1136

Moreno A, Clemente J, Crespo C (1999) Pelvic insufficiency fractures in patients with pelvic irradiation. Int J Radiat Oncol Biol Phys 44:61–66

Mumber MP, Greven KM, Haygood TM (1997) Pelvic insufficiency fractures associated with radiation atrophy: clinical recognition and diagnostic evaluation. Skeletal Radiol 26:94–99

Murphy FD, Blount WP (1962) Cartilaginous exostoses following irradiation. J Bone Joint Surg Am 44:662–628

Neuhauser EBD, Wittenborg MH, Berman CZ, Cohen J (1952) Irradiation effects of roentgen therapy on the growing spine. Radiology 59:637–650

Patel SR (2000) Radiation-induced sarcoma. Curr Treat Options Oncol 1:258–261

Paulino AC, Wen BC, Brown CK, Tannous R, Mayr NA, Zehn WK, Weidner GJ, Hussey DH (2000) Late effects in children treated with radiation therapy for Wilms' tumour. Int J Radiat Oncol Biol Phys 46:1239–1246

Penman D (2004) Medical x-rays cause thousands of cancers. NewScientist.com news service 30 January 2004

Perez CA, Vietti T, Ackerman LV, Eagleton J, Powers WE (1967) Tumors of the sympathetic nervous system in children: an appraisal of treatment and results. Radiology 88:750–760

Poustchi AM, Leonidas JC, Elkowitz SS (1996) Simultaneous occurrence of osteosarcoma and osteochondroma following treatment of neuroblastoma with chemotherapy, radiotherapy and bone marrow transplantation. Pediatr Radiol 26:155–157

Probert JC, Parker BR (1975) The effects of radiation therapy on bone growth. Radiology 114:155–162

Rajah R, Tinkler SA, Conway WF (1975) General case of the day. RadioGraphics 15:1510–1512

Roebuck DJ (1999) Skeletal complications in pediatric oncology patients. RadioGraphics 19:873–885

Rubin P, Andrews JR, Swarm JR, Gump H (1959) Radiation induced dysplasia of bone. AJR Am J Roentgenol 82:206–216

Sheppard DG, Libshitz HI (2001) Post-radiation sarcomas: a review of the clinical and imaging features in 63 cases. Clin Radiol 56:22–29

Smith J (1987) Postradiation sarcoma of bone and soft tissues. Skeletal Radiol 16:524–532

Taitz J, Cohn RJ, White L, Russell SJ, Vowels MR (2004) Osteochondroma after total body irradiation: an age related complication. Pediatr Blood Cancer 42:225–222

Vázquez E, Castellote A, Piqueras J, Ortuño P, Sánchez-Toledo J, Nogués PO, Lucaya J (2003) Second malignancies in pediatric patients: imaging findings and differential diagnosis. RadioGraphics 23:1155–1172

Walsh D (1897) Deep tissue traumatism from Roentgen ray exposure. BMJ 2:272–273

Weatherby RP, Dahlin DC, Irvins JC (1981) Post radiation sarcoma of bone: review of 78 Mayo Clinic cases. Mayo Clin Proc 56:294–306

Wiklund TA, Blomqvist CP, Raty J, Elomaa I, Rissanen P, Miettinen M (1991) Postirradiation sarcoma: analysis of a nationwide cancer registry material. Cancer 68:524–531

Williams HJ, Davies AM (2006) The effect of X-rays on bone: a pictorial review. Eur Radiol 16:619–633

Tumour and Tumour-like Conditions Associated with Paget's Disease of Bone

29

A. Mark Davies, Etienne Pluot and Steven L. J. James

CONTENTS

KEY POINTS

- Fewer than 5% of patients with Paget's disease will undergo malignant transformation to a sarcoma.
- The risk of a patient developing a sarcoma is greater the more extensive the Paget's disease and the longer the patient has been affected.
- Paget's sarcoma may appear photopenic ("cold") on bone scintigraphy against a background of increased activity from the surrounding pagetic bone.
- Not all malignancies arising in Paget's disease are a sarcoma. Metastases, myeloma and lymphoma should be considered in the differential diagnosis.
- There is a rare recognised association between Paget's disease and giant cell tumour of bone typically involving the skull and facial bones.
- The preservation of the normal hyperintense signal of marrow fat on T1-weighted MR images is typical of uncomplicated Paget's disease in all its stages. The loss of this hyperintense signal is seen when complications arise, including tumour, occult fractures, etc.
- The worldwide prevalence of Paget's disease in the population appears to be decreasing.

A. M. Davies, MBChB, FRCR
Consultant Radiologist, Department of Radiology, Royal Orthopaedic Hospital, Birmingham B31 2AP, UK

Etienne Pluot, MD
Musculoskeletal Fellow, Service de Radiologie B, Hôpital Cochin, 27 rue du Faubourg Saint Jacques, 75679 Paris Cedex 14, France

S. L. J. James, MD
Consultant Radiologist, Department of Radiology, Royal Orthopaedic Hospital, Birmingham B31 2AP, UK

29.1 Introduction

Paget's disease of bone, named after the nineteenth century British surgeon, Sir James Paget, is a localised or multifocal disorder of bone characterised by abnormal bone turnover with increased osteoclastic bone resorption and compensatory increased osteoblastic activity. Although Paget was arguably the sixth to describe the

condition also previously known as osteitis deformans, he was the first to recognise the dreaded association with osseous malignancy (Hamdy 1981). By the time he published his life's experience, 12 years after his original seminal description, he had seen no less than five patients die of malignancy out of a total series of 23 cases (Paget 1877, 1889). The development of a bone sarcoma is by far and away the most serious of the numerous complications that can occur in Paget's disease of bone. However, referring to tumour in the strict literal sense as a mass, not all tumours arising in Paget's disease are malignant or, for that matter, neoplastic (López et al. 2003). This chapter reviews the imaging features and differential diagnosis of neoplastic transformation and tumour-like lesions in Paget's disease.

29.2 Malignant Tumours

29.2.1 Sarcoma

Sarcoma is claimed to be the most common histologically proven malignancy arising in Paget's disease, and the term Paget's sarcoma is frequently used to encompass all the histological subtypes. It must be recognised, however, that elderly patients developing other malignancies in bone such as metastases, myeloma and lymphoma may also have pre-existing Paget's disease (see below).

29.2.1.1 Incidence

The likelihood of an imaging department seeing a case of Paget's sarcoma depends primarily on the prevalence of Paget's disease in the population. It affects approximately 3–4% of the Caucasian population, particularly those of English descent, being less common in other European countries and rare among the Asian and African races. Theoretically, all those factors that influence life expectancy, quality of health care, sanitation, etc., may also be relevant as Paget's is a disease of ageing. The literature quotes an incidence of sarcoma arising in patients with Paget's disease ranging from 0.7% to 6.3% (Hadjipavlou et al. 1992; Greditzer et al. 1983; Wick et al. 1981; Schajowicz et al. 1983). Such variation is likely to be explained by referral bias among different series with tertiary treatment centres artificially concentrating sarcomas and, in comparison, seeing relatively few cases of uncomplicated Paget's disease. One needs look no further than Paget's own series to see how a single factor can influence the apparent incidence. His remarkably high incidence of malignant change of 22% can be attributed to the fact that his cases were all collected before the discovery of X-rays, so that only those patients with the most serious complications of the disease would be identified.

Paget's sarcoma is twice as common in males as females. Although women tend to live longer than men in those countries with a higher incidence of Paget's disease, the uncomplicated disease is also commoner in men. The majority of cases of Paget's sarcoma present in the 6th and 7th decades. Rarely, cases have been described as early as the 3rd decade. Sarcomas are also more common in patients with multifocal Paget's disease. Studies of patients with Paget's sarcoma in which skeletal surveys were available have shown 79-87% cases with multifocal Paget's disease (Huvos et al. 1983; Haibach et al. 1985). Undoubtedly, the risk of a patient developing a sarcoma is greater the more extensive the Paget's disease and the longer they are affected.

29.2.1.2 Aetiology

Recent studies analysing Paget's disease, Paget's osteosarcoma and sporadic osteosarcoma have all shown loss of constitutional heterozygosity for all or part of the distal portion of chromosome 18q (Hansen et al. 1999; Damron et al. 2001). A tumour suppressor locus has been found at the same region on this chromosome as the Paget's predisposition locus. This genetic theory may explain the racial variation in incidence of Paget's disease and is currently favoured over the viral aetiology previously postulated. On occasion a Paget's sarcoma may develop at the site of a previous fracture through Pagetic bone (Hadjipavlou et al. 1992; Mckenna et al. 1964; Porretta et al. 1957; Price and Goldie 1969; Smith et al. 1984). It is unclear whether the fracture represents the earliest subtle manifestation of the sarcoma or whether it subsequently arises within the primitive callus around the healing fracture.

29.2.1.3 Site

The commonest sites of Paget's sarcoma, in descending order of frequency, are the femur, pelvis and humerus (Fig. 29.1). Why the humerus, a bone less commonly affected by uncomplicated Paget's disease, has such a

high incidence of malignant transformation (18–24%) is unknown. It is also not understood why Paget's sarcoma is so infrequent in the spine (2%), which is one of the commonest sites for Paget's disease (Sharma et al. 2006). A simplistic explanation may be that, although the spine is a common site for Paget's disease, the actual volume of bone involved in the vertebra can be relatively little as compared with the pelvis and, as explained above, the risks of malignant transformation are related to both extent and duration of disease. Multifocal sarcoma has been reported to account for 2.4–17% of all Paget's sarcoma, although there would appear to be less than 30 documented cases in the world literature (Wick et al. 1981; Choquette et al. 1982; Greditzer et al. 1982; Schajowicz et al. 1983; Huvos et al. 1983; Haibach et al. 1985; Moore et al. 1990; Erlich et al. 1999). A report of two patients queried whether these cases are due to the simultaneous development of two or more primaries or to metastases from a single primary (Vuillemin-Bodaghi et al. 2000).

29.2.1.4 Histology

By far and away the most frequent histology of Paget's sarcoma is osteosarcoma. In those parts of the world where Paget's disease is common, 20% of patients with osteosarcoma who are older than 40 years of age and as high as 50% of patients with osteosarcoma over the age of 60 have Paget's as the predisposing condition (Wick et al. 1981; Huvos 1986). In the older literature, the second commonest histology in Paget's sarcoma is fibrosarcoma. More recent pathological redefinition of spindle cell sarcomas means that other diagnoses, such as malignant fibrous histiocytoma, leiomyosarcoma and pleomorphic sarcoma, tend to be favoured over fibrosarcoma. Chondrosarcoma figures prominently in some series and is absent from others. Mirra and colleagues (1995b) query whether some are classifying chondroblastic osteosarcoma with minimal osteoid as chondrosarcoma. The nature of the histology does not appear to influence the prognosis in individual cases.

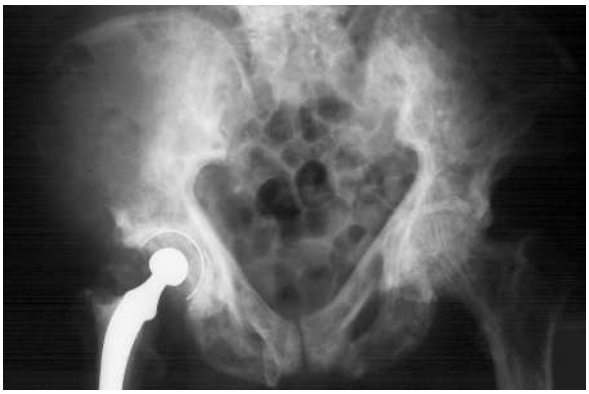

a

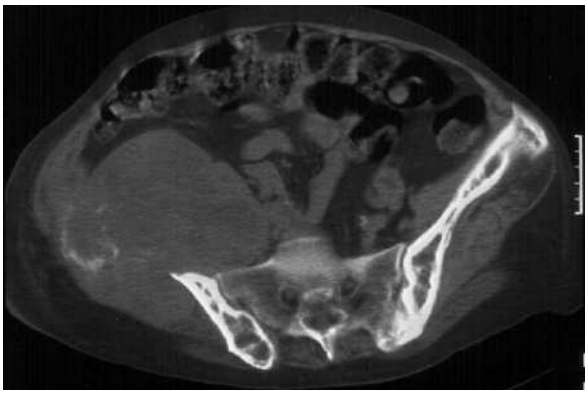

b

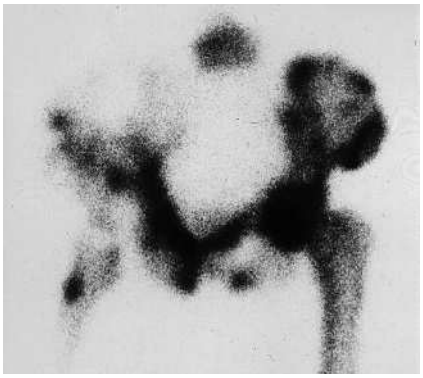

c

Fig. 29.1. **a** AP radiograph of the pelvis showing extensive Paget's disease and a lytic Paget's sarcoma destroying the right ilium. **b** CT scan showing the destruction of the ilium and a large soft tissue mass. **c** Anterior 3-h scintigram showing pelvic deformity and multiple areas of increased activity due to the underlying Paget's disease. The Paget's sarcoma in the right ilium appears relatively photopenic

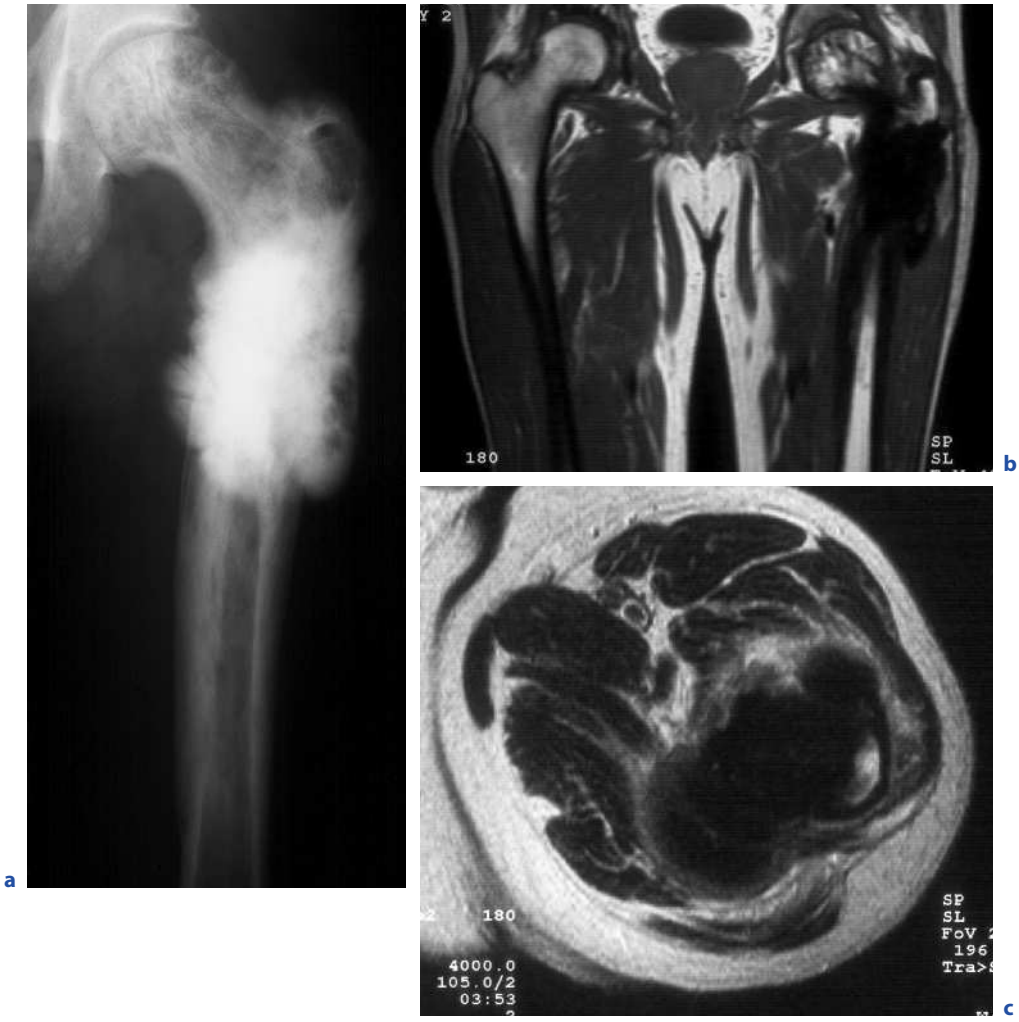

Fig. 29.2. **a** AP radiograph showing sclerotic Paget's disease of the proximal femur and a Paget's sarcoma arising from the proximal diaphysis. **b,c** Coronal T1-weighted image and axial intermediate-weighted fast spin echo images showing the sarcoma to be low signal intensity due to the dense mineralisation

29.2.1.5 Radiographic and Computed Tomographic Features

The majority of Paget's sarcomas are predominantly lytic, in the mixed or sclerotic phase of the underlying disease, with cortical destruction and a soft tissue mass (Fig. 29.1). Expansion of bone and presentation with a pathological fracture occur in approximately one third of patients, respectively. Periosteal new bone formation is uncommon presumably due to the highly aggressive nature of the tumour (Greditzer et al. 1983; Smith et al. 1984; Haibach et al. 1985). A minority of cases with heavy malignant osteoid production will exhibit a predominantly sclerotic appearance (Fig. 29.2). Serial radiographs show the sarcomas to be rapidly progressive (Fig. 29.3). Although largely superseded by MR imaging for staging sarcomas, CT readily reveals obliteration of normal marrow fat by tumour, cortical breaching and soft tissue extension, all features suggestive of malignant transformation (Fig. 29.1bc) (Mirra et al. 1995a).

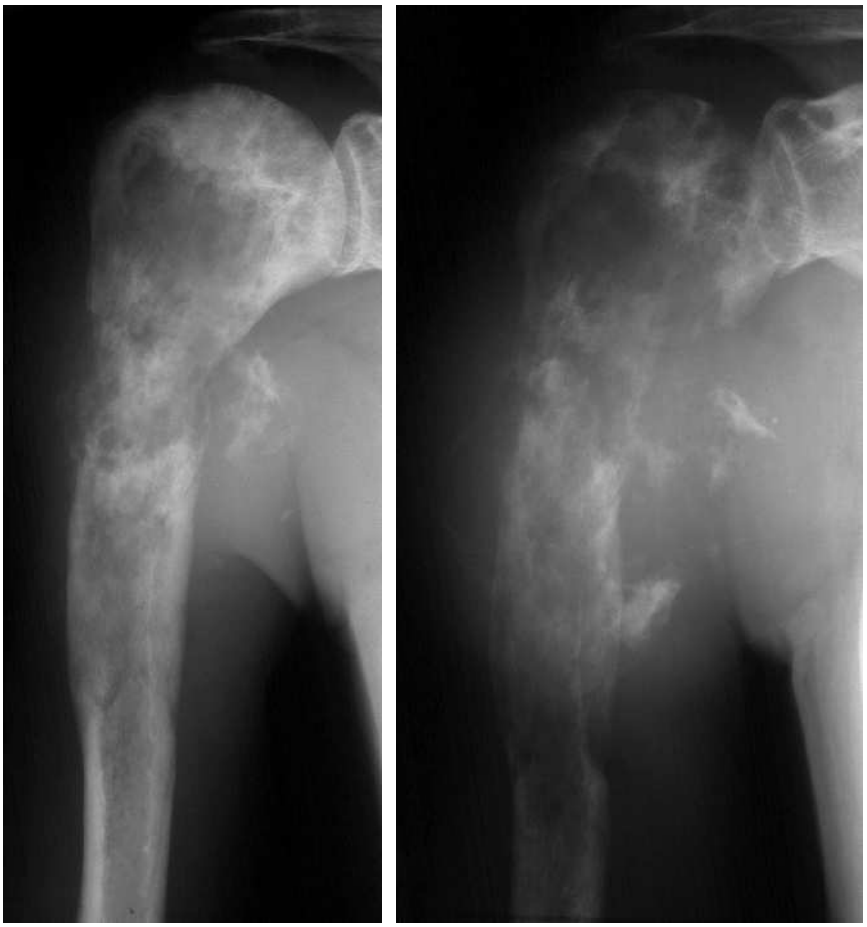

a b

Fig. 29.3a,b. AP radiographs of the upper humerus obtained 6 weeks apart. Typical features of a Paget's sarcoma presenting with a pathological fracture. There has been rapid progression in the intervening period

29.2.1.6 Scintigraphic Features

Bone scintigraphy with Tc-99m MDP invariably reveals increased activity in Paget's disease due to the hypervascularity and active bone remodelling. It can be used to make the diagnosis, identify the extent of disease and monitor response to bisphosphonates (Hain and Fogelmann 2002). Yeh and coworkers (1982) found that Tc-99m MDP bone scans showed decreased activity at the site of Paget's sarcoma, whereas they found increased activity with Ga-67 scanning. They concluded that an area of decreased Tc-99m MDP uptake with corresponding increased uptake of Ga-67 in an area of Paget's disease was probably pathognomonic of a sarcoma. Unfortunately, cases of failure of Ga-67 to show increased activity at the site of the tumour have been reported (Smith et al. 1984). Increased uptake with thallium-201 has also been observed in Paget's sarcoma (Colarinha et al. 1996). The authors of this chapter have no experience of either gallium or thallium scanning in this context, but can confirm that Paget's sarcoma may appear as a relatively photopenic area on Tc-99m MDP scans (Fig. 29.1b). It is, however, a non-specific finding in that this phenomenon may occur in cases of a metastasis arising within pagetic bone (Fig. 29.4) (López et al. 2003).

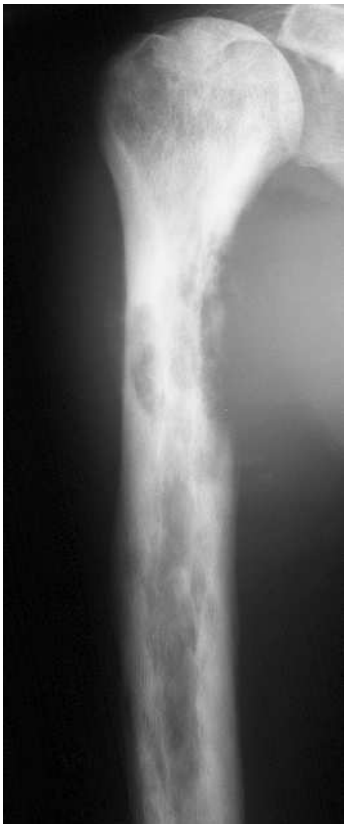

a

b

Fig. 29.4. **a** AP radiograph of the humerus in the sclerotic phase of Paget's disease. There is a destructive lesion arising medially within the proximal diaphysis with a soft tissue mass. **b** Anterior image of upper arm from a 3-h bone scintigram showing a relatively photopenic area at the site of the lytic lesion with generalised increased activity in the humerus from the Paget's disease. Biopsy revealed a metastasis from a bronchial carcinoma

29.2.1.7 Magnetic Resonance Features

Magnetic resonance (MR) imaging is infrequently required in the management of the patient with uncomplicated Paget's disease. Several reports have stressed that the signal from marrow fat is typically preserved in all phases of the disease, seen as high signal intensity on both T1- and T2-weighted sequences (Fig. 29.5) (Kaufmann et al. 1991; Sundaram et al. 2001; Vande Berg et al. 2001). In complicated Paget's disease, such as in the presence of a neoplasm, the normal marrow fat signal is absent. Boutin and colleagues (1998), in their study of 33 patients, concluded that, if the high signal intensity of the bone marrow within the pagetic bone was preserved, the negative predictive value for MR imaging in excluding a sarcoma or other neoplasm was high. Most Paget's sarcomas showed replacement of the marrow fat by intermediate or low signal intensity tumour tissue on T1-weighted images, usually with correspondingly high signal intensity on T2-weighted and short tau inversion recovery (STIR) images (Fig. 29.6). The exception is if the sarcoma is densely mineralised, thereby exhibiting low signal intensity on all sequences (Fig. 29.2). Coarsening of the trabeculae with cortical thickening is typically seen in the pagetic bone adjacent to the tumour (Fig. 29.6). Most Paget's sarcoma will show cortical destruction with a moderate or large soft tissue mass (Fig. 29.6). It is important to stress, therefore, that an intact cortex and absence of a soft tissue mass do not conclusively exclude a sarcoma. It should be noted that both active Paget's disease and sarcoma will show hypervascularity on dynamic contrast-enhanced MR imaging (Libicher et al. 2008a), and so this technique is unlikely to be helpful in diagnosing malignant transformation. It may, however, prove to have a role in monitoring response to bisphosphonate therapy (Libicher et al. 2008b).

29.2.1.8 Prognosis

Despite significant improvements in the investigation and more aggressive management of osseous malignancies, the prognosis of Paget's sarcoma, irrespective of the histological subtype, remains dismal (Mankin and Hornicek 2005). A study from the authors' own unit

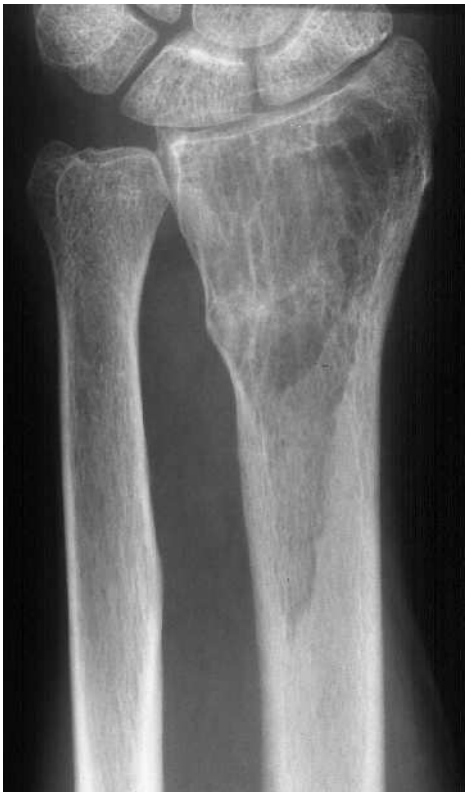

a

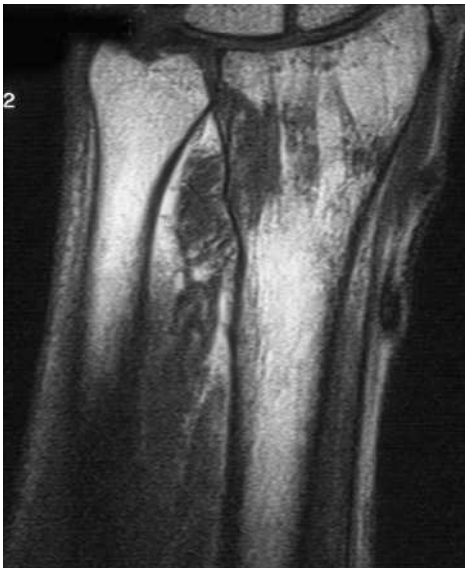

b

Fig. 29.5. **a** PA radiograph of distal forearm showing extensive lytic Paget's disease of the radius initially misinterpreted as malignant infiltration. **b** Coronal T1-weighted image showing coarsening of the trabeculae with the high signal intensity of the marrow fat largely preserved

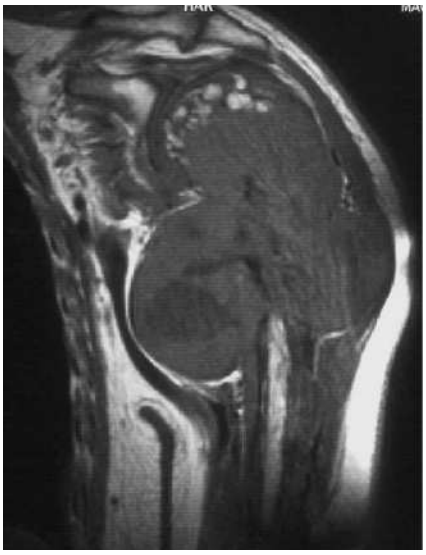

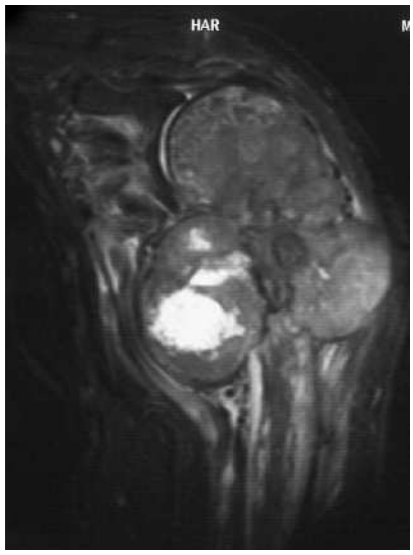

a,b

Fig. 29.6. **a** Coronal T1-weighted and (**b**) STIR images showing a large Paget's sarcoma arising in the proximal humeral metaphysis. The soft tissue extension medially is displacing, but not involving, the axillary vessels. There is a little Paget's disease remaining in the femoral head seen as nests of high signal intensity in (**a**). The cortical high signal intensity distal to the tumour in (**b**) indicates hypervascular Paget's disease and not extension of the tumour

showed 53% of patients alive at 1 year, 25% at 2 years and none surviving beyond 5 years (Shaylor et al. 1999). Similar results have been reported by other large studies, where the overall 5-year survival is consistently less than 10% (Deyrup et al. 2007). This contrasts poorly with the 5-year survival for conventional high-grade osteosarcoma of approximately 65%. There are a number of reasons to explain this enormous difference. The single factor that has most significantly improved the prognosis for conventional osteoasarcoma has been

the introduction of adjuvant chemotherapy. Unfortunately, most patients developing a Paget's sarcoma are elderly and often too frail to undergo chemotherapy. In addition, it is postulated that the increased vascularity in Paget's disease predisposes to early metastasis with an increased incidence of pulmonary metastases at presentation of 29% (Smith et al. 1984).

29.2.2 Metastases

If the literature is to be taken factually, then the commonest malignancy arising in association with Paget's disease is a sarcoma. This is arguably true for solitary malignancies and, again, reflects referral bias to specialist orthopaedic oncology centres. There are a handful of reports of metastatic carcinoma being identified in pagetic bone (Burgener and Perry 1977; Roberts 1986; Fenton and Resnick 1991; Roblot et al. 1987; Schajowicz et al. 1988; Nicholas et al. 1987; Conrad and Johnson 1997; Boutin et al. 1998). However, in countries where Paget's disease is common, the concurrence with metastatic bone disease in the ageing population must not be that unusual. Indeed, it has been suggested malignant neoplasms associated with Paget's disease are most likely to be metastatic carcinoma, presumably related to hypervascularity of the bone (Jacobson and Siegelmann 1966; Moore et al. 1994). The identification of Paget's disease in a patient with multiple bone metastases is hardly a cause for additional concern as it is unlikely to influence management or the ultimate prognosis. Problems may arise in distinguishing the two conditions in patients with a sclerotic bone lesion and a history of a previous primary malignancy, such as breast or prostatic carcinoma (Fig. 29.7). In this situation close correlation of all the imaging investigations is important. The all too familiar trap of assuming multiple foci of increased activity, when reporting on a bone scan in isolation, as indicative of metastases should be avoided. For the solitary aggressive lesion where the differential diagnosis includes both sarcoma and metastasis, biopsy is required. The authors note that, in the three cases of solitary metastasis in pagetic bone they have seen, all were diaphyseal and eccentric in origin (Fig. 29.4). This differs from Paget's sarcomas that tend to be epimetaphyseal or meta-diaphyseal and central in location (López et al. 2003). These observations have to be considered anecdotal in view of the small number of cases involved.

29.2.3 Myeloma

Tumours that arise from the bone marrow elements not involved in osteoblastic or osteclastic activity comprise only a small percentage of the malignancies in Paget's disease. Possibly the most common is multiple myeloma (Singer 1977). Again, this is likely to be an incidental occurrence with myeloma the more significant condition with respect to long-term prognosis (Rosenkrantz and Gluckman 1957). Diffuse infiltration with myeloma may be difficult to detect radiographically against a background of Paget's disease (Fig. 29.8). Lymphatic leukaemia has also been described in association with Paget's disease (Cazeilles et al. 1953).

29.2.4 Lymphoma

Only ten cases of lymphoma of bone associated with Paget's disease had been reported in the literature up to 1994 (Stephens et al. 1994). This is likely to be a coincidental occurrence, but it is notable that it has a better prognosis than Paget's sarcoma (Hadjipavlou et al. 1992; Price et al. 1969; Molle et al. 1983; Lauchlan and Walsh 1963). The author has seen one such case whose imaging features were indistinguishable from Paget's sarcoma (Fig. 29.9).

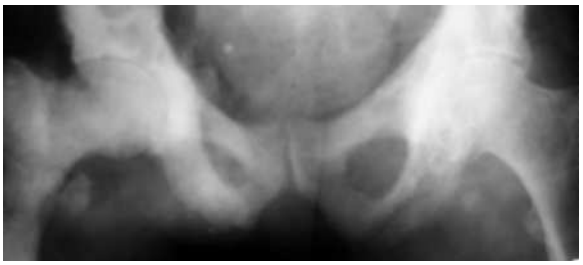

Fig. 29.7. AP radiograph of the pubis in an elderly male with multiple sclerotic prostatic metastases. There is coincidental Paget's disease of the left ischium

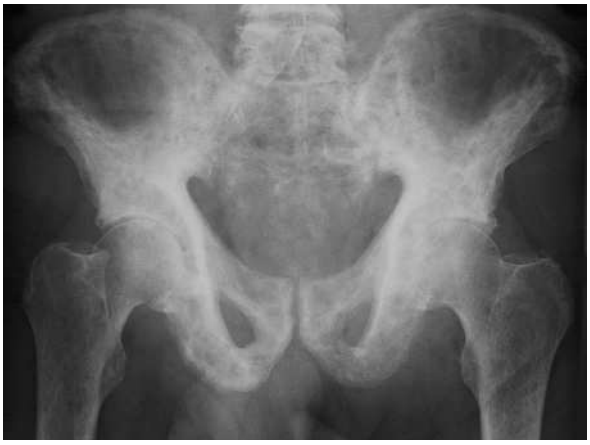

a

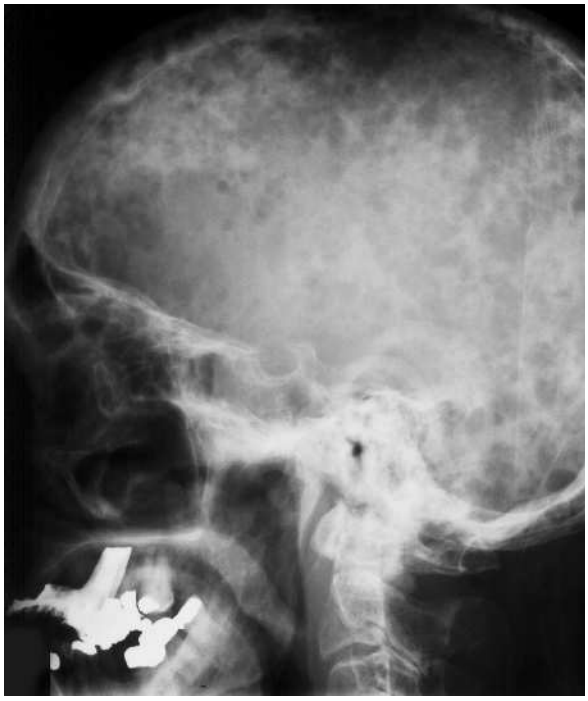

b

Fig. 29.8. **a** AP radiograph of the pelvis and (**b**) lateral radiograph of the skull in a patient with multiple myeloma and Paget's disease. Note how the pagetic bone in the pelvis tends to obscure the myeloma

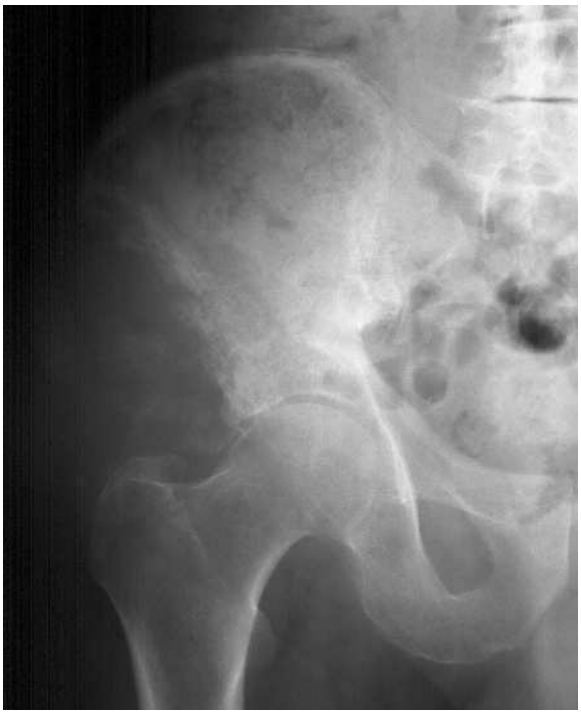

Fig. 29.9. Extensive infiltration of the ilium, cortical destruction and a soft tissue mass superimposed on Paget's disease. The appearances were assumed to be those of a Paget's sarcoma, but biopsy revealed lymphoma

29.3 Benign Tumours

29.3.1 Giant Cell Tumour

Giant cell tumour (GCT) of bone is a well-recognised, but rare association of Paget's disease with approximately 40 cases published in the literature since 1945 (Fig. 29.10) (Gebhart et al. 1998). The vast majority of tumours occur in patients with polystotic Paget's disease (Dixon et al. 1995; Ueda et al. 1996), although involvement with monostotic disease has been reported (Hoch et al. 2007). Certain differences have been observed between these tumours and conventional GCT of bone. GCT in Paget's occurs in an older age group and is more commonly found in the skull and facial bones. These tumours may be multifocal and have also been reported to be responsive to steroid therapy (Jacobs et al. 1979; Potter et al. 1991; De Chari et al., 1998). A unique feature is that five of the affected patients all originated from Avellino, a small Italian town, suggesting a hereditary influence (Jacobs et al. 1979; Rendina et al. 2004).

29.3.2 Enchondroma

A case of an enchondroma arising within an area of Paget's disease has been reported (Zehr et al. 2000). It is unlikely that there is a causal relationship, and it seems reasonable to assume that two such common conditions

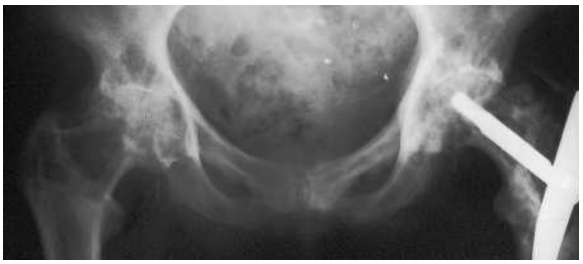

Fig. 29.10. AP radiograph of the hips in a patient with extensive polyostotic Paget's disease. Biopsy of the lytic lesion in the right femoral neck revealed a giant cell tumour (case courtesy of Dr. David Ritchie)

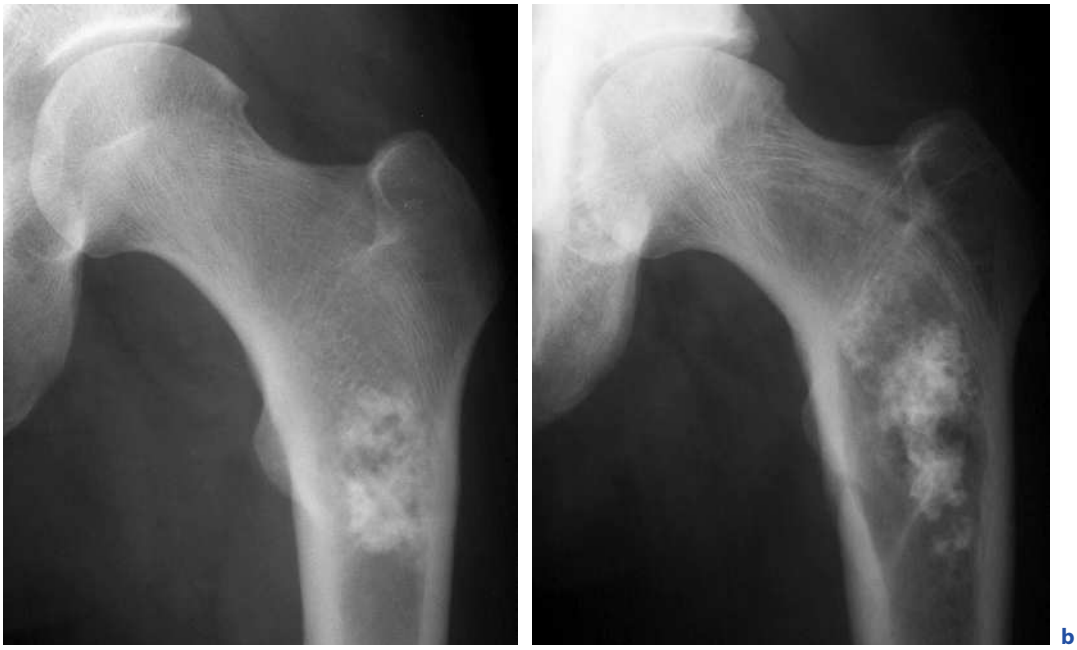

a **b**

Fig. 29.11. **a** A 35-year-old male with a biopsy-proven enchondroma of the proximal femoral diaphysis. **b** Eighteen years later, there is co-existing Paget's disease of the acetabulum and proximal femur

would inevitably occur coincidentally. There is little diagnostic difficulty if the enchondroma is identified radiographically before the development of Paget's disease (Fig. 29.11). Diagnosis in the reported case was more problematic as the enchondroma had not been previously identified, and there was the additional problem of severe osteomalacia secondary to the medical treatment (Zehr et al. 2000). It seems probable that other benign neoplasms reported in association with Paget's disease, such as pigmented villonodular synovitis and desmoplastic fibroma, were also coincidental (Marsal et al. 1993; Mirra et al. 1980; Hillmann et al. 1988).

29.4 Tumour-Like Conditions

The characteristic imaging features of uncomplicated Paget's disease are extremely well known (Mirra et al. 1995). What constitutes a tumour-like lesion in Paget's disease of bone largely depends on the experience of the individual reviewing the imaging. It is not unusual for the lytic phase, particularly if identified at an unusual site or age, to be mistaken for malignant infiltration (Fig. 29.5) (Bowerman et al. 1975; Marin et al. 1996). For the purposes of this chapter, those situations where the aspects of imaging have been previously described as aberrant or unusual have been included (Moore et al. 1994; Mirra et al. 1995b; Boutin et al. 1998).

29.4.1 Active Paget's Disease and Occult Fractures

Single or multiple foci of lysis in Paget's disease, termed pseudotumourous lysis by Mirra and colleagues (1995b), may easily be mistaken for neoplasm (Eisman and Martin 1986). Larger lesions are a feature of the early lytic phase of the disease and are usually not a diagnostic problem. Smaller, typically cortically based lesions may be a cause of confusion in the mixed or late phases (Fig 29.12). These are likely to represent locally hypervascular disease or resorption at the site of an

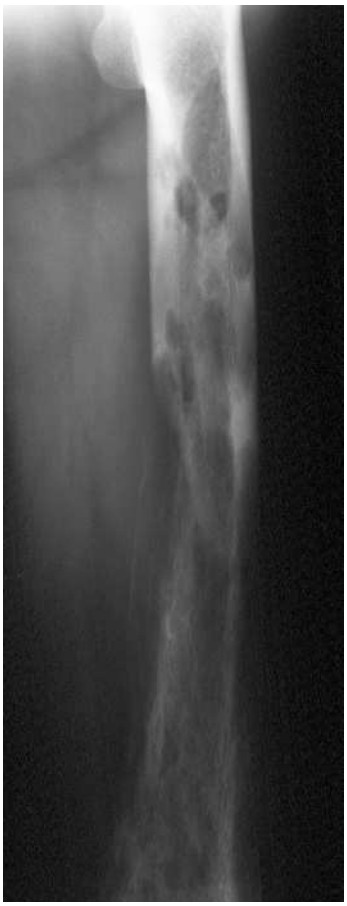

a,b

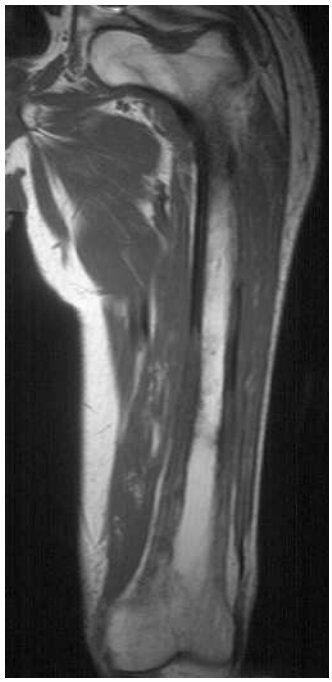

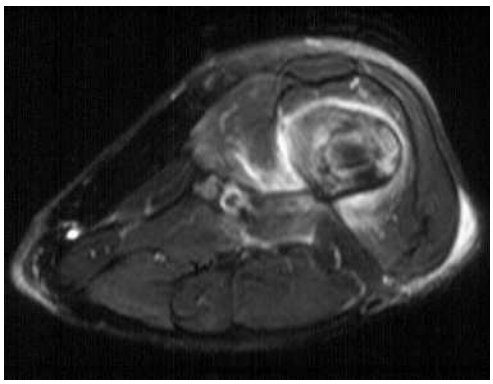

c

Fig. 29.12. **a** AP radiograph of the femur showing extensive Paget's disease with demineralisation of the mid and distal diaphyseal cortex and multiple cortical lucencies proximally simulating malignancy. **b** Coronal T1-weighted image shows intermediate signal intensity within the thickened cortex and relative preservation of the high signal intensity marrow fat. **c** Axial STIR image reveals extensive cortical and juxtacortical oedema. Biopsy-confirmed hypervascular Paget's disease with no evidence of malignant transformation

occult fracture (Kumar et al. 1993). Boutry and colleagues (2000) described a series of patients with "inflammatory changes" on MR imaging that correlated with histological appearances of hypercellularity, hypervascularity and/or fibrosis. Fat-saturated T2-weighted images revealed focal or extensive cortical and medullary oedema that enhanced following administration of a gadolinium chelate (Fig. 29.12). Only one case showed oedema within the adjacent soft tissues. In none of the cases was there a true soft tissue mass (Boutry et al. 2000). Hypervascular Paget's disease and sarcoma may be present in the same patient (Fig. 29.6). Similar MR imaging features might be expected with an occult fracture.

29.4.2 Pseudosarcoma

The term pseudosarcoma might be applied to any situation in which the imaging features of Paget's disease are mistaken for malignancy (Tins et al. 2001). In the literature this term has been reserved for those rare cases in which there is focal proliferation of pagetic periosteal new bone. To date, fewer than 20 cases have been reported, the majority arising from the lower limb long bones (Tins et al. 2001; Greditzer et al. 1983; Lamovec et al. 1999; Donáth et al. 2000; Golding 1960; Resnick et al. 1982; Monson et al. 1989; Khraishi et al. 1991; Resnick 1995; Milgram 1977; Mcnairn et al. 2001). The typical imaging features show chronic Paget's disease with a periosteal-based soft tissue mass. The underlying cortex may be intact or destroyed, and the mass shows amorphous mineralisation ("pumice bone") or coarse spiculations (Fig. 29.13). These findings are indistinguishable from malignant transformation and are much more likely to represent sarcoma than pseudosarcoma (Tins et al. 2001). The presence of high signal intensity fat within the mass on MR imaging is suggestive of pseudosarcoma, but at least three cases have shown signal characteristics similar to a sarcoma (Donáth et al. 2000; Mcnairn et al. 2001; Tins et al. 2001). Clearly, if there remains any doubt as to the diagnosis, biopsy is indicated (Lamovec et al. 1999; Monson et al. 1989; Khraishi et al. 1991; Tins et al. 2001). A single case report has been published describing a subperiosteal ganglion of the obturator rim associated with Paget's disease simulating a tumour (Mansour et al. 2005).

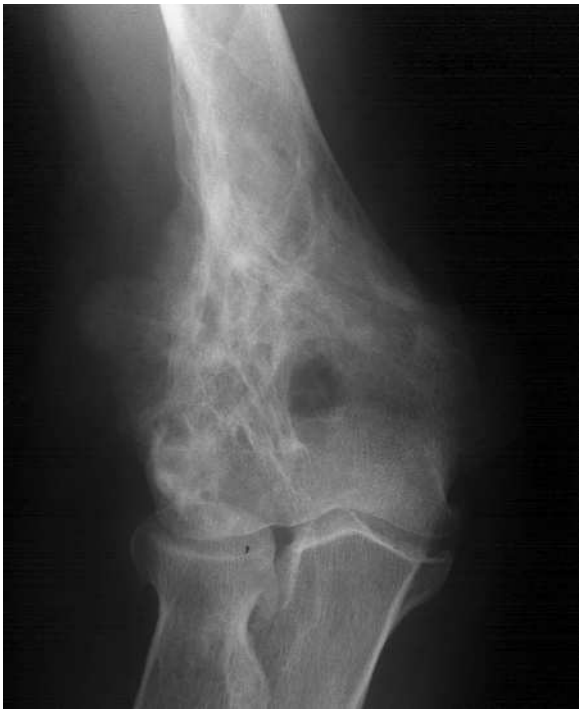

Fig. 29.13. AP radiograph of the distal humerus showing sclerotic Paget's disease with a mineralised soft tissue mass arising from the lateral supracondylar ridge. Although suspected to be a Paget's sarcoma, repeated biopsies proved this to be "pumice bone" typical of Paget's pseudosarcoma

29.4.3 Post-Immobilisation Lysis

Following fractures or prolonged immobilisation, there may be a dramatic increase in bone resorption, which has been termed "accelerated disuse osteoporosis" and can simulate malignancy (Sear 1949; Mitchell et al. 1987; Moore et al. 1994; Wallace et al. 1996). Again, the preservation of predominantly high signal intensity fat within the affected bone on MR imaging and the absence of true bone destruction or a soft tissue mass are useful indicators of a benign aetiology. Rapid osteolysis may also occur after revision hip arthroplasty (Fig. 29.14) (Oakley and Matheson 2003).

29.4.4 Bisphosphonate-Induced Bone Disease

Bisphosphonates have been used in the medical management of Paget's disease for over 30 years (Smith et al. 1971). The complex action of these drugs reduces both bone resorption and formation (Hadjipavlou

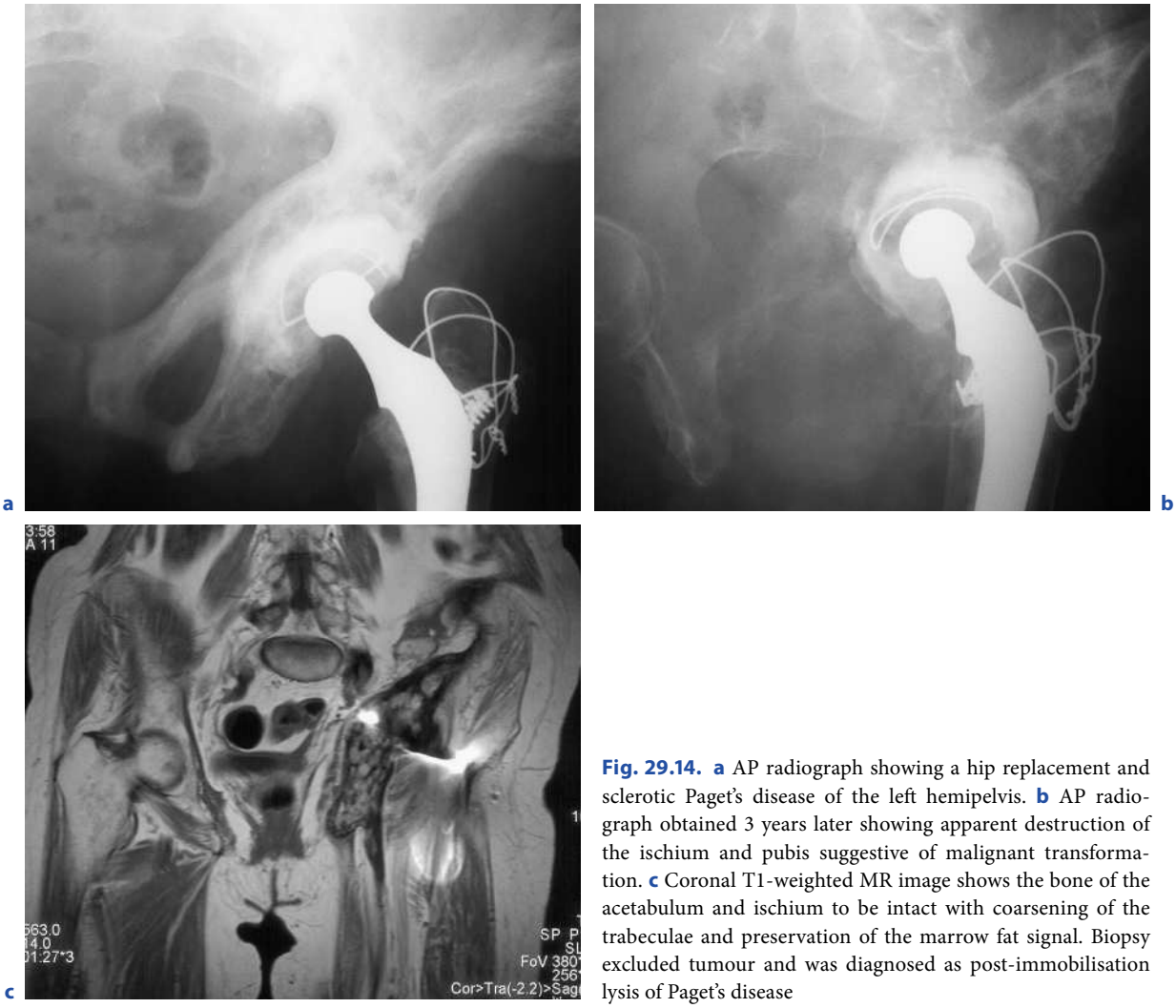

Fig. 29.14. **a** AP radiograph showing a hip replacement and sclerotic Paget's disease of the left hemipelvis. **b** AP radiograph obtained 3 years later showing apparent destruction of the ischium and pubis suggestive of malignant transformation. **c** Coronal T1-weighted MR image shows the bone of the acetabulum and ischium to be intact with coarsening of the trabeculae and preservation of the marrow fat signal. Biopsy excluded tumour and was diagnosed as post-immobilisation lysis of Paget's disease

et al. 2002). This inhibition of skeletal mineralisation can lead to osteomalacia, a recognised complication particularly of the use of disodium etidronate in Paget's disease (Macgowan et al. 2000). As a result, the radiographic appearances of osteomalacia, superimposed on Paget's disease, may simulate marrow infiltration with malignancy (Marin et al. 1996). Another bisphosphonate-associated condition that might cause confusion is bone necrosis of the maxilla and mandible (Merigo et al. 2006). If used in the treatment of Paget's disease, the bone destruction might be mistaken for malignant transformation.

29.5 Conclusion

The identification of an ill-defined or permeative lytic lesion, with cortical destruction and a soft tissue mass, developing within Paget's disease should always raise the question of a sarcoma. However, not all malignant lesions arising in Paget's are sarcomas. Metastases, myeloma and lymphoma need to be considered and cannot be distinguished from a sarcoma on imaging features alone. Also, benign bone tumours, such as giant cell

tumour, and several tumour-like conditions may also mimic a sarcoma. The imaging investigations of choice are radiography and MRI. Scintigraphy is of limited value as it typically shows increased activity in uncomplicated Paget's disease and may show reduced activity in the presence of malignancy. Preservation of the fatty marrow signal on MR imaging is useful as it tends to exclude malignant infiltration or other complications of Paget's disease. Where any doubt remains as to the presence or absence of malignancy and whether the tumour is a sarcoma or not, biopsy is mandatory. Finally, it is interesting to speculate as to whether these complications of Paget's disease are likely to become all the more rare as there is increasing evidence that the prevalence of the disease itself is declining (Van Staa et al. 2002; Cundy 2006).

References

Boutin RD, Spitz DJ, Newman JS, Lenchik L, Steinbach LS (1998) Complications in Paget's disease at MR imaging. Radiology 209:641–651

Boutry N, Moisan-Lemanissier S, Leroy X, Paul C, Lecomte-Houcke M, Cotton A (2000) "Inflammatory changes" in Paget's disease of bone: a frequent MR finding on fat suppression techniques. Radiology 217 (Suppl):269–270

Bowerman JW, Altman J, Hughes JL, Zadek RE (1975) Pseudomalignant lesions in Paget's disease of bone. AJR 124:57–61

Burgener FA, Perry PE (1977) Solitary renal metastasis in Paget's disease simulating sarcomatous degeneration. AJR 128:853–855

Cazeilles M, Cornet L, Javel R, Pene J (1953) Leucémie lymphoide et ostéopathia à type de maladie de Paget avec ostéoporose circonstrite du crane de Schüller. J Med Bordeaux 130:1012–1015

De Chiari A, Apice U, Fazioli F et al. (1998) Multicentric giant cell tumour with viral-like inclusions associated with Paget's disease of bone: a case treated with steroid therapy. Oncol Rep 5:317–320

Choquette D, Haraoui B, Altman RD, Pelletier JP (1983) Multifocal sarcoma in Paget's disease: a hypothesis. Clin Orthop 179:308–311

Colarinha P, Fonseca AT, Salgado L, Vieira MR (1996) Diagnosis of malignant change in Paget's disease by Tl-201. Clin Nucl Med 21:299–301

Conrad GR, Johnson AW (1997) Solitary adenocarcinoma metastasis mimicking sarcomatous degeneration in Paget's disease. Clin Nucl Med 22:300–302

Cundy T (2006) Is Paget's disease of bone disappearing? Skeletal Radiol 35:350–351

Damron TA, McNairn J, Landas S, Shrimpton A (2001) Inheritance of Paget's osteosarcoma of bone: a familial linkage study. Proceedings 11th International Symposium on Limb Salvage Birmingham, UK, pp 66–67

Deyrup AT, Montag AG, Inwards CY, Xu Z, Swee R, Unni KK (2007) Sarcomas arising in Paget's disease of bone: a clinicopathologic analysis of 70 cases. Arch Pathol Lab Med 131:942–946

Dixon GR, Ritchie DA, Myskow MW (1995) Case report: Benign giant cell tumour associated with Paget's disease of bone. Clin Radiol 50:269–271

Donáth J, Szilágyi M, Fornet B, Bély M, Poór G (2000) Pseudosarcoma in Paget's disease: case report. Eur Radiol 10:1664–1668

Eisman JA, Martin T (1986) Osteolytic Paget's disease. J Bone Joint Surg (Br) 68:112–117

Erlich RB, Romano S, Meohas W, Smith J (1999) Synchronous Paget's sarcoma of tibiae in which Paget's disease was limited to these bones. Skel Radiol 28:599–603

Fenton P, Resnick D (1991) Metastases to bone affected by Paget's disease. A report of three cases. Int Orthop 15:397–399

Gebhart M, Vandeweyer E, Nemec E (1998) Paget's disease of bone complicated by giant cell tumor. Clin Orthop 352:187–193

Golding C (1960) Museum pages: IV. On the differential diagnosis of Paget's disease. J Bone Joint Surg (Br) 42:641–643

Greditzer HG, McLeod RA, Unni KK, Beabout JW (1983) Bone sarcomas in Paget's disease. Radiology 146:327–333

Hadjipavlou A, Lander P, Srolovitz H, Enker P (1992) Malignant transformation in Paget's disease of bone. Cancer 70:802–808

Hadjipavlou AG, Gaitanis IN, Kontakis GM (2002) Review article: Paget's disease of bone and its management. J Bone Joint Surg (Br) 84:160–169

Haibach H, Farrell C, Dittrich FJ (1985) Neoplasm arising in Paget's disease of bone: a study of 82 cases. Am J Clin Pathol 83:594–600

Hain SF, Fogelmann I (2002) Nuclear medicine studies in metabolic bone disease. Semin Muscul Radiol 6:323–329

Hamdy RC (1981) Paget's disease of bone: assessment and management. Praeger Publishers, UK, pp 1–2

Hansen MF, Nellissery MJ, Bhatia P (1999) Common mechanisms of osteosarcoma and Paget's disease. J Bone Min Res 14:39–44

Hillmann JS, Mesgarzadeh M, Tang CK, Bonakdapour A, Reyes TG (1988) Case report 481: Benign intraosseous fibroma (desmoplastic fibroma) associated with Paget's disease of the iliac bone. Skeletal Radiol 17:356–359

Hoch B, Hermann G, Klein MJ, Abdelwahab IF, Springfield D (2007) Giant cell tumor complicating Paget disease of long bone. Skel Radiol 36:973–978

Huvos AG, Butler A, Bretsky SS (1983) Osteogenic sarcoma associated with Paget's disease of bone: a clinicopathologic study of 65 cases. Cancer 52:1489–1495

Huvos AG (1986) Osteogenic sarcoma of bones and soft tissues in older persons. A clinico pathologic analysis of 117 patients older than 60 years. Cancer 57:1442–1449

Jacobs TP, MichelsonJ, Polay JS, d'Adamo AC, Canfield RE (1979) Giant cell tumor in Paget's disease of bone: familial and geographical clustering. Cancer 44:742–747

Jacobson HG, Siegelmann SS (1966) Some miscellaneous solitary bone lesions. Semin Roentgenol 1:314–335

Kaufmann GA, Sundaram M, McDonald DJ (1991) MR imaging in symptomatic Paget's disease. Skeletal Radiol 20:413–418

Khraishi M, Howard B, Fam AG (1991) Paget's pseudosarcoma. Arthritis Rheum 34:241–24

Kumar A, Poon PY, Aggarwal S (1993) Value of CT in diagnosing nonneoplastic osteolysis in Paget's disease. J Comput Assist Tomogr 17:144–146

Lamovec J, Renner M, Spiler M (1999) Pseudosarcoma in Paget's disease of bone. Ann Diagn Pathol 3:99–103

Lauchlan SC, Walsh MJ (1963) Reticulum cell sarcoma complicating Paget's disease. Can Med Assoc 88:891–892

Libicher M, Kasperk C, Hosch W, Kauczor H, Delorme S (2008a) Dynamic contrast-enhanced MRI in Paget's disease of bone: correlation of regional microcirculation and bone turnover. European Society Musculoskeletal Radiology 15th Annual Meeting 2008, Galway, Ireland (Abstract). Skel Radiol 37:594

Libicher M, Delorme W, Hosch W, Kauczor H, Kasperk C (2008b) Dynamic contrast-enhanced MRI for monitoring bone perfusion in Paget's disease during bisphophonate therapy. European Society Musculoskeletal Radiology 15th Annual Meeting 2008, Galway, Ireland (Abstract). Skel Radiol 37:595

López C, Thomas DV, Davies AM (2003) Neoplastic transformation and tumour-like lesions in Paget's disease of bone: a pictorial review. Eur Radiol 13:L151–L163

Marsal S, Arnal C, Garcia F, Azorin L, Lience E (1993) Pigmented villonodular synovitis of the knee in a patient with Paget's disease of the adjacent femoral bone. Br J Rheum 32:166–168

MacGowan JR, Pringle J, Morris VH, Stamp TCB (2000) Gross vertebral collapse associated with long-term disodium etidronate treatment for pelvic Paget's disease. Skeletal Radiol 29:279–282

McKenna RJ, Schwinn CP, Soongy KY, Higinbotham NL (1964) Osteogenic sarcoma arising in Paget's disease. Cancer 17:42–66

McNairn JDK, Damron TA, Landa SK, Ambrose JL (2001) Benign tumefactive soft tissue extension from Paget's disease of bone simulating malignancy. Skeletal Radiol 30:157–160

Mankin HJ, Hornicek FJ (2005) Paget's sarcoma: a historical and outcome review. Clin Orthop Relat Res 438:97–102

Mansour R, Nanni M, Muthukumar T, Butt SH, Cassar-Pullicino VN (2005) Subperiosteal ganglion associated with Paget's disease. Skel Radiol 34:419–423

Marin F, Billey T, Lassoued S (1996) Ostéolyse pseudosarcomateuse du femur chez un pagétique traité au long cours par étidronate disodique: à propos d'une nouvelle observation. Rev Méd Interne 17:856–858

Merigo E, Manfredi M, Meleti M, Guidotti R, Ripasarti A, Zanzucchi E, Aleo P, Corradi D, Corcione L, Sesenna E, Ferrari S, Poli T, Bonaninil M, Vescovi P (2006) Bone necrosis of the jaws associated with bisphosphonate treatment: a report of 29 cases. Acta Biomed 77:109–117

Milgram JW (1977) Radiographical and pathological assessment of the activity of Paget's disease of bone. Clin Orthop 127:43–5

Mirra JM, Finerman G, Lindholm S (1980) Diffuse pigmented villonodular synovitis in association with Paget's disease of bone: a report of a case. Clin Orthop 149:305–309

Mirra JM, Brien EW, Tehranzadeh J (1995a) Paget's disease of bone: review with emphasis on radiologic features, part II. Skeletal Radiol 24:173–184

Mirra JM, Brien EW, Tehranzadeh J (1995b) Paget's disease of bone: review with emphasis on radiologic features, part I. Skeletal Radiol 24:163–171

Mitchell ML, Ackerman LV, Tsutsumi A (1987) Case report 438: osteolytic phase of Paget's disease. Skeletal Radiol 16:498–503

Molle D, Bard H, Kuntz D et al. (1983) Osteolyse relatrice d'un lymphome developpe sur un os pagetique. Rev Rhum Mal Osteoartic 50:217–221

Monson DK, Finn HA, Dawson PJ, Simon MA (1989) Pseudosarcoma in Paget's disease of bone. J Bone Joint Surg (Am) 71:453–455

Moore TE, King AR, Kathol MH, El-Khoury GY, Palmer R, Downey PR (1991) Sarcoma in Paget's disease of bone: clinical radiologic and pathologic features in 22 cases. AJR 156:1199–1203

Moore TE, Kathol MH, El-Khoury GY, Walker CW, Gendall PW, Whitten CG (1994) Unusual radiological features in Paget's disease of bone. Skeletal Radiol 23:257–260

Nicholas JJ, Srodes CH, Herbert D, Hoy RJ, Peel RL, Goodman MA (1987) Metastatic cancer in Paget's disease of bone: a case report. Orthopedics 10:725–729

Oakley AP, Matheson JA (2003) Rapid osteolysis after revision hip arthroplasty in Paget's disease. J Arthroplasty 18:204–207

Paget J (1877) On a form of chronic inflammation of bones (osteitis deformans). Trans R Med Chir Soc (Lond) 60:37–63

Paget J (1889) Remarks on osteitis deformans. Illust Med News 2:181–185

Porretta CA, Dahlin DC, James JM (1957) Sarcoma in Paget's disease of bone. J Bone Joint Surg (Am) 39:1314–1329

Potter HG, Schneider R, Ghelman B, Healey JH, Lane JM (1991) Multiple giant cell tumors and Paget's disease of bone: radiographic and clinical correlations. Radiology 180:261–264

Price CHG, Goldie W (1969) Paget's sarcoma of bone: a study of 80 cases from the Bristol and Leeds Bone Tumour Register. J Bone Joint Surg (Br) 51:205–224

Rendina D, Mossetti G, Soscia E, Sirignano C, Insabato L, Viceconti R, Ignarra R, Salvatore M, Nunziata V (2004) Giant cell tumor and Paget's disease of bone in one family: Geographic clustering. Clin Orthop Relat Res 421:218–224

Resnick CS, Walter RD, Haghighi P, Resnick D (1982) Paget's disease with soft tissue extension. Case report 218. Skeletal Radiol 9:145–14

Resnick D (1995) Diagnosis of bone and joint disorders, 3rd edn. Philadelphia: WB Saunders p1953

Roberts JA (1986) Paget's disease and metastatic carcinoma. JBJS (Br) 68:22–23

Roblot P, Alcay M, Payen J, Clarac JP, Fontanel JP, Bontoux D (1987) Metastases of a lingual epidermoid carcinoma in a femur affected by Paget's disease. Report of a case. J Bone Joint Surg (Am) 69:1440–1441

Rosenkrantz JA, Gluckman EC (1957) Co–existence of Paget's disease of bone and multiple myeloma. AJR 78:30–38

Schajowicz F, Santini AE, Berenstein M (1983) Sarcoma complicating Paget's disease of bone: a clinicopathological study of 62 cases. J Bone Joint Surg (Br) 65:299–306

Schajowicz F, Velan O, Santini AE et al. (1988) Metastases of carcinoma in the pagetic bone. A report of two cases. Clin Orthop 228:290–296

Sear HR (1949) Osteogenic sarcoma as a complication of osteitis deformans. Some personal experiences and reflections. Br J Radiol 22:580–587

Sharma H, Mehdi SA, MacDuff E, Reece AT, Jane MJ, Reid R (2006) Paget sarcoma of the spine: Scottish bone tumor registry experience. Spine 31:1344–1350

Shaylor PJ, Peake D, Grimer RJ, Carter SR, Tillman RM, Spooner D (1999) Paget's osteosarcoma – no cure in sight. Sarcoma 3:191–192

Singer FR (1977) Paget's disease of bone. Plenum Medical Book Co, New York, pp 99–102

Smith R, Russell RGG, Bishop M (1971) Diphosphonates and Paget's disease of bone. Lancet 1:945–947

Smith J, Botet JF, Yeh DJ (1984) Bone sarcomas in Paget's disease: a study of 85 patients. Radiology 152:583–590

Van Staa TP, Seby P, Leufkens HGM, Lyles K, Sprafka JM (2002) Incidence and natural history of Paget's disease of bone in England and Wales. J Bone Min Res 17:465–471

Stephens GC, Lennington WJ, Schwartz HS (1994) Primary lymphoma and Paget's disease of the femur. Am J Clin Pathol 101:783–786

Sundaram M, Khanna G, El-Khoury GY (2001) T1-weighted MR imaging for distinguishing large osteolysis of Paget's disease from sarcomatous degeneration. Skeletal Radiol 30:378–383

Tins BJ, Davies AM, Mangham DC (2001) MR imaging of pseudosarcoma in Paget's disease of bone: a report of two cases. Skeletal Radiol 30:161–165

Ueda T, Healey JH, Huvos AG, Panicek DM (1996) Orthopaedic, radiology, pathology conference: Scapular pain and swelling in a 60-year-old man with Paget's disease. Clin Orthop 326:284–286, 310–312

Vande Berg BC, Malghem J, Lecouvet FE, Maldague B (2001) MR appearance of uncomplicated Paget's disease of Bone. Semin Musculoskel Radiol 5:69–77

Vuillemin-Bodaghi V, Parlier-Cuau C, Cywiner-Golenzer C, Quillard A, Kaplan G, Laredo JD (2000) Multifocal osteogenic sarcoma in Paget's disease. Skeletal Radiol 29:349–353

Wallace K, Haddad JG, Gannon FH, Esterhai J, Kaplan FS (1996) Skeletal response to immobilization in Paget's disease of bone: a case report. Clin Orthop 328:236–240

Wick MR, Siegal GP, Unni KK, McLeod RA, Greditzer G (1981) Sarcomas of bone complicating osteitis deformans (Paget's disease): 50 years experience. Am J Surg Pathol 5:47–57

Yeh DJ, Rosen G, Benua RS (1982) Gallium scans in Paget's sarcoma. Clin Nucl Med 7:546–552

Zehr RJ, Bauer TW, Recht MP (2000) Enchondroma associated with Paget's disease. Orthopedics 23:1287–1290

Reactive, Metabolic, and Tumor-Like Lesions of Bone

30

Darshana Sanghvi and Murali Sundaram

CONTENTS

D. Sanghvi, MD,DNB
Department of Radiology, KEM Hospital and Seth GS Medical College, Parel, Mumbai 400 012, Maharashtra, India

M. Sundaram, MD, FRCR
Section of Musculoskeletal Radiology, Imaging Institute, Cleveland Clinic, Professor of Radiology, Cleveland Clinic Lerner School of Medicine of Case Western Reserve University, Diagnostic Radiology/A21, The Cleveland Clinic Foundation, 9500 Euclid Avenue, Cleveland, OH 44195, USA

KEY POINTS

- Metabolic bone diseases are not included in the WHO classification of bone tumors. Metabolic bone disease conventionally includes osteoporosis, osteomalacia, hyperparathyroidism, and Paget's disease.
- Osteoporosis is characterized by fractures that in the vertebrae and pelvis could be mistaken for a more sinister disease, such as metastases. Recognizing their patterns on the different imaging modalities would permit the correct diagnosis to be made and prevent the patient from being overstaged and inappropriately investigated. Exuberant callus formation in OI type V should not be mistaken for sarcoma.
- Oncogenic osteomalacia is a rare clinicopathological syndrome characterized by a triad of severe hypophosphatemia, hyperphosphaturia, and osteomalacia secondary to a neoplasm. The condition is challenging to diagnose, as the patient most often presents with symptoms of osteomalacia, and the primary mesenchymal tumor may be small and often asymptomatic. However, correct diagnosis is particularly gratifying as surgical removal of the offending tumor can lead to a dramatic reversal of osteomalacia. Amyloid deposition in patients on long-term hemodialysis can lead to periarticular osteolytic lesions, and these tumor-like osseous lesions are called amyloidomas of the bone. With the increased life span of hemodialysis patients, radiologists are more likely to encounter brown tumors as well as musculoskeletal manifestations of β_2-microglobulin-associated amyloidosis, including lytic osseous lesions (amyloidomas) and renal spondyloarthropathy, and these conditions should not be

mistaken for primary or secondary bone neoplasms.

- Florid reactive periostitis (FRP) and bizarre parosteal osteochondromatous proliferation (BPOP) represent opposing ends of a spectrum of reactive lesions that mimic sarcoma. BPOP, also called Nora's lesion, has been defined as a "well-marginated mass of heterotopic mineralization arising from the periosteal aspect of an intact cortex, without medullary changes." The radiological appearances of these benign entities are often mistaken for more ominous pathologies, most commonly osteogenic osteosarcoma and chondrosarcoma and also osteomyelitis. Familiarity with the entity of FRP will allow radiologists to provide the correct diagnosis and prevent unnecessary antibiotic therapy or aggressive, early surgery. Close clinical and radiological follow-up of FRP usually shows conversion to BPOP.
- SAPHO is an acronym for a syndrome comprising synovitis, acne, pustulosis, hyperostosis, and osteitis. The radiologist plays a central role in the early, accurate, and definitive diagnosis of SAPHO syndrome. Awareness of SAPHO syndrome is important to facilitate differentiation from other entities with similar radiological presentation, but dramatically different progression, treatment, and prognosis. These entities include malignancies such as round cell tumors like lymphoma and Ewing's sarcoma, metastases, and also osteomyelitis and Paget's disease.

30.1 Metabolic Bone Diseases

Metabolic bone diseases are not included in the WHO classification of bone tumors. Metabolic bone disease conventionally includes osteoporosis, osteomalacia, hyperparathyroidism, and Paget's disease. Paget's disease will be discussed in another chapter (see Chap. 29). The three other entities will be discussed as they pertain to tumor or tumor-like lesions of bone.

30.1.1 Osteoporosis

Osteoporosis, which refers to a decrease in bone mass, is the most common metabolic bone disease across the globe. Its most frequent etiology is senile and post-menopausal osteoporosis.

30.1.1.1 'Benign' versus 'Malignant' Vertebral Fractures

The most common cause of vertebral compression fractures in the elderly is osteoporosis. However, up to 39% of bone metastases occur in the vertebrae and may often result in pathological fractures (Yuh et al. 1989). Since both solitary and multiple vertebral fractures occur frequently in senile and post-menopausal osteoporosis, it is often perplexing to distinguish them from pathological vertebral fractures that occur in the elderly due to metastases and multiple myeloma. Osteoporotic vertebral fractures are termed "benign," whereas pathological vertebral fractures as a result of aggressive tumor are labeled "malignant."

Radiographs and CT

Radiographic absence of discrete, focal osteolytic lesions, significant cortical disruption, pedicular involvement, and paravertebral soft tissue mass can be reassuring evidence of the absence of tumor. CT differentiates cortical bone comminution and burst fragments from cortical destruction, whereas on radiographs both appear as bone destruction. Therefore, radiographs overdiagnose cortical destruction. Presence of an intravertebral vacuum phenomenon on radiographs or CT is further evidence of a benign fracture. Fracture lines in the cortical and cancellous bone of the vertebral body depicted at CT are again suggestive of a benign process (Sattari et al. 2008).

Conventional MR Imaging

However, radiographic features are often equivocal in distinguishing benign from malignant vertebral collapse. The inability of radiographs to demonstrate medullary lesions contributes to poor specificity in this situation (Vogler and Murphy 1988). Thus, MR imaging is the modality of choice. The superiority of MR

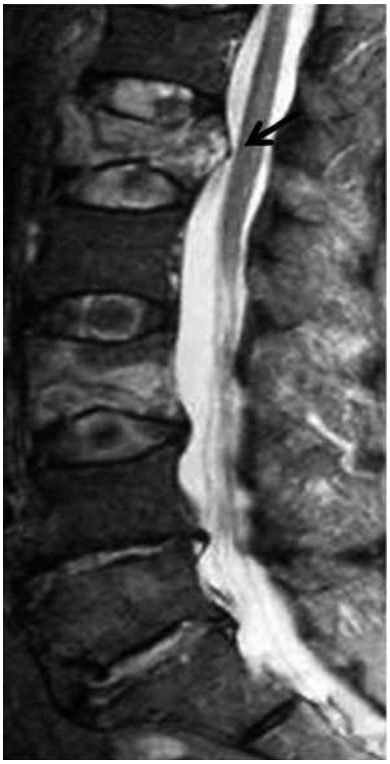

Fig. 30.1. Malignant vertebral collapse. Sagittal STIR MR image of the lumbar spine shows abnormal marrow signal intensity in the L1 and L3 vertebral bodies. Convex posterior border (*arrow*) of the collapsed L1 vertebra favors a diagnosis of metastases. (Courtesy of A. Anbarasu, MD, FRCR, Coimbatore, India)

a,b

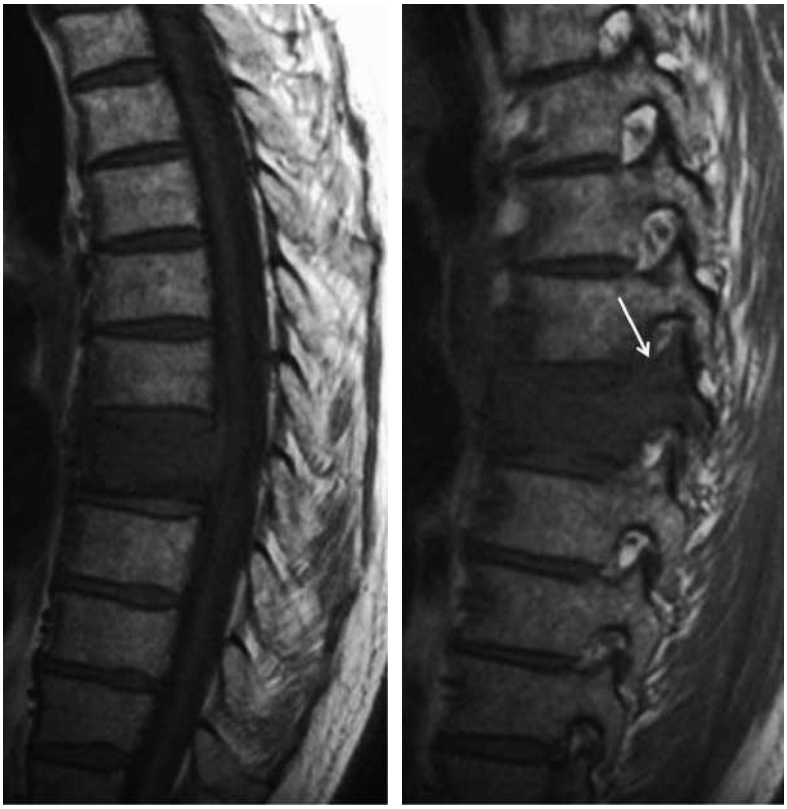

Fig. 30.2a,b. Malignant vertebral collapse. **a** Sagittal T1-weighted MR image of the dorsal spine shows minimal collapse of a solitary dorsal vertebra. Diffuse low marrow signal abnormality involving the entire body is suggestive of malignant collapse. **b** Parasagittal T1-weighted MR image shows the abnormal marrow signal extends into the pedicle (*arrow*), which is characteristic of a malignant pathology. (Courtesy of A. Anbarasu, MD, FRCR, Coimbatore, India)

imaging is due to its exquisite sensitivity to alterations in bone marrow signal intensity. In elderly individuals, the dominant type of marrow in the spinal column is fatty marrow, which normally appears hyperintense on T1-weighted images and shows intermediate signal intensity on T2-weighted images. The presence of tumor in the vertebrae results in low signal on T1-weighted images with variable signal on T2-weighted images depending on the histopathological variety of the tumor. In most instances, however, the infiltrated marrow appears hyperintense on T2-weighted images.

Distinction between metastatic and acute osteoporotic compression fractures can be made on the basis of MR imaging findings. The sensitivity, specificity, and accuracy for metastatic compression fractures was 100%, 93%, and 95%, respectively, in a study by Jung et al. (2003). MR imaging findings suggestive of metastatic compression fractures are as follows: a convex posterior border of the vertebral body (Fig. 30.1), diffuse low signal intensity of the vertebra on T1-weighted images (Fig. 30.2a), abnormal signal intensity of the pedicle or posterior element (Fig. 30.2b), an epidural mass, a focal paraspinal mass, and other spinal metastases. MR imaging findings suggestive of acute osteoporotic compression fractures are as follows: a low-signal-intensity (SI) band on T1- and T2-weighted images (Fig. 30.3), spared normal bone marrow signal intensity of the vertebral body (Fig. 30.4), retropulsion of a posterior bone fragment (Fig. 30.5), and multiple compression fractures. In malignant vertebral collapse, the low SI area involves the entire vertebral body in 77–88% of cases, while some areas of normal fatty SI are preserved within the vertebral body in 68% of acute benign vertebral collapse (Cuenod et al. 1996; Moulopoulos et al. 1996; Yuh et al. 1989; Jung et al. 2003). Another sign that is highly specific for benign osteoporotic vertebral collapse is the fluid sign described by Baur et al. (2002). The fluid sign is defined as a focal, linear, or triangular area of strong hyperintensity on T2-weighted or STIR images on a background of diffuse hyperintensity in the vertebral body because of acute collapse (Fig. 30.6). The signal intensity of the fluid sign is equivalent to that of cerebrospinal fluid. Baur et al. (2002) proposed that in acute osteoporotic fractures with bone marrow edema, the cause of the fluid sign on MRI is fluid pressed into the space of osteonecrosis. Osteonecrosis develops at the site of the fractured end plate because of strong compression of the trabecular network in that area. The fluid sign also always occurs at the site of the fractured end plate, where compression of the spongiosa is most severe. On gadolinium-enhanced T1-weighted images, in 85% of benign cases from a recent series (Sattari et al. 2008), the enhancement resulted in a "return to normal SI" in the collapse, with additional bands of low and/or high SI below or parallel to the fractured endplates, a pattern suggestive of benign vertebral collapse. In malignancy, on the contrary, there is heterogeneous enhancement with no tendency to linear arrangement (Cuenod et al. 1996; Moulopoulos et al. 1996). Low SI bands may correspond to fracture lines, whereas high SI lines may be due to a vascular repair process along the fracture line.

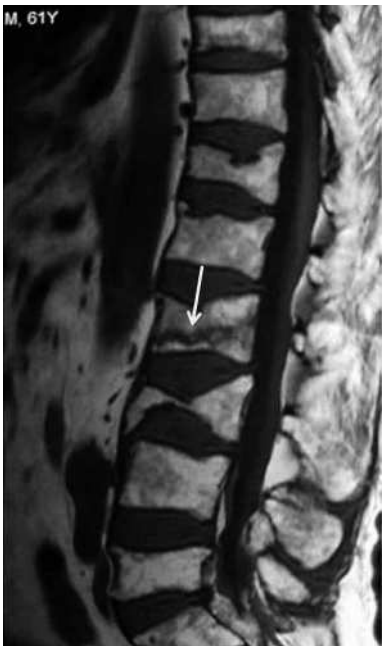

Fig. 30.3. Benign vertebral collapse. Sagittal T1-weighted MR image of the spine shows a linear hypointense fracture line (*arrow*) in the collapsed vertebra characteristic of benign vertebral collapse. (Courtesy of A. Anbarasu MD, FRCR, Coimbatore, India)

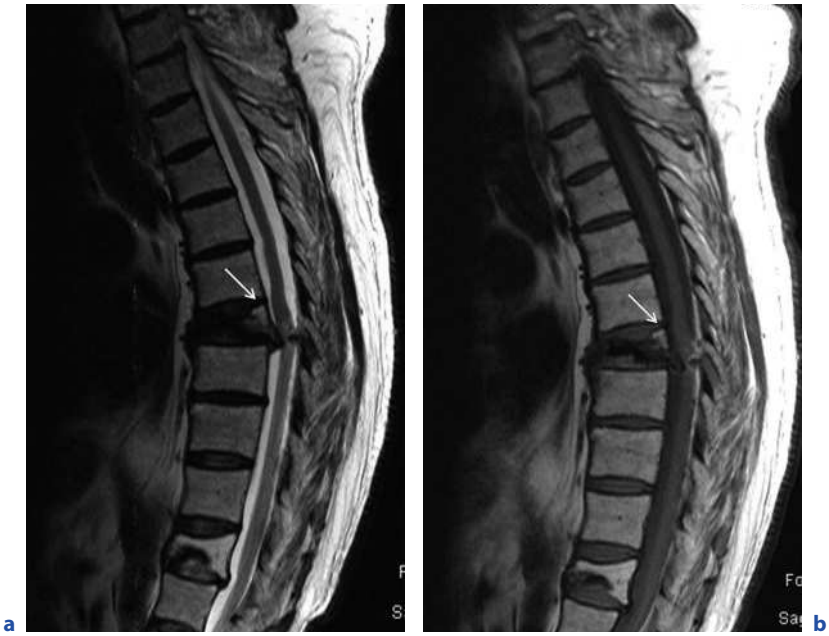

Fig. 30.4a,b. Benign vertebral collapse. **a** T1-weighted and **b** T2-weighted sagittal MR images show focal sparing of normal marrow signal intensity (*arrows*) in a collapsed vertebra indicative of osteoporotic collapse. (Courtesy of B. Jankharia, MD, Mumbai, India)

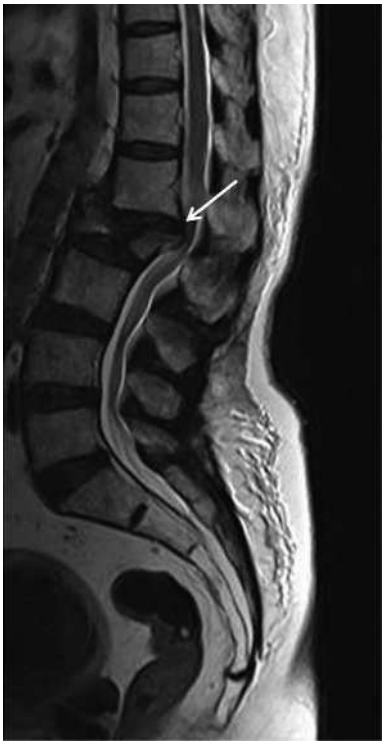

Fig. 30.5. Benign vertebral collapse. Sagittal T2-weighted MR image of the lumbar spine shows retropulsion of the posterosuperior corner of a collapsed vertebral body (*arrow*) typical of a benign osteoporotic collapse

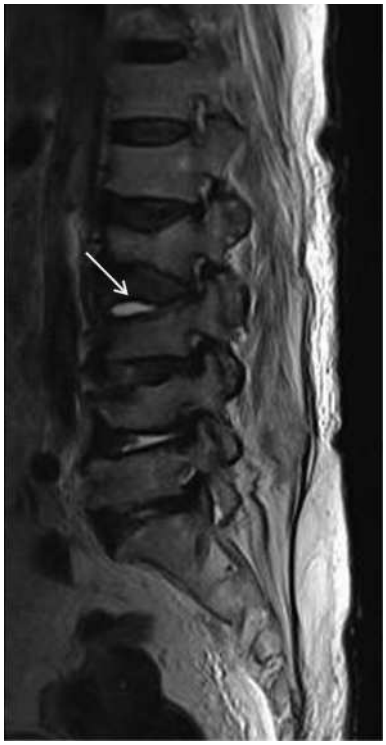

Fig. 30.6. Benign vertebral collapse: Fluid sign. Parasagittal T2-weighted MR image of the lumbar spine shows linear hyperintense signal corresponding to fluid (*arrow*) along the superior endplate of L3 vertebra

Diffusion MR Imaging

There have been many conflicting papers in the literature alluding to the utility of diffusion MR imaging in distinguishing benign from malignant vertebral compression fractures. Signal enhancement in tumor masses on T2-weighted images reflects mainly intracellular water, whereas fracture edema reflects interstitial water. The two bone marrow edema entities cannot be differentiated with conventional MR imaging because of similar signal intensities (Spuentrup et al. 2001). Diffusion-weighted imaging allows for differentiation between intracellular and interstitial edema in the brain. Differences in diffusion effects may be responsible for the differences observed between benign and malignant vertebral compression fractures in that, theoretically, more restricted diffusion is present in malignant compression fractures (Fig. 30.7) with packed tumor cells than in benign compression fractures (Fig. 30.8) with more mobile water in the extracellular volume fraction. Bauer et al. (1998) published the first major article on diffusion imaging in the bony spine and showed that on diffusion-weighted images malignant pathologic fractures are high in signal intensity compared to normal bone marrow, while benign osteoporotic and traumatic fractures are low in signal intensity. However, a subsequent paper by Castillo et al. (2000) demonstrated no advantage of diffusion-weighted scanning in the detection or characterization of vertebral metastases. They noted that all the metastatic lesions that were hyperintense on diffusion scans were also hyperintense on T2-weighted scans, and they suggested that T2 shine-through may be playing a prominent role in the appearance of the metastatic lesions. Subsequently, Zhou et al. (2002) used quantitative apparent diffusion coefficient (ADC) mapping to improve accuracy by eliminating this T2 effect

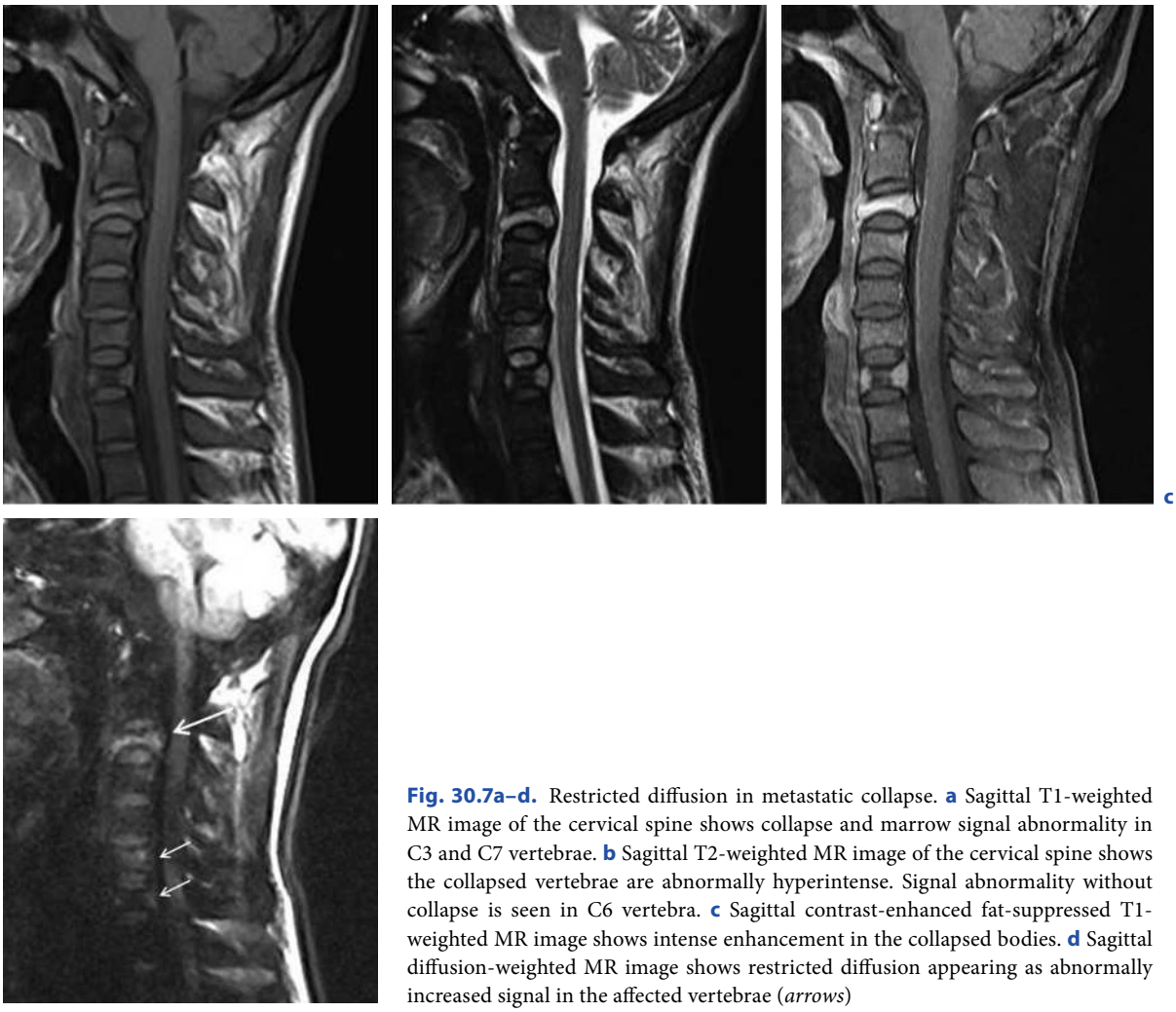

Fig. 30.7a–d. Restricted diffusion in metastatic collapse. **a** Sagittal T1-weighted MR image of the cervical spine shows collapse and marrow signal abnormality in C3 and C7 vertebrae. **b** Sagittal T2-weighted MR image of the cervical spine shows the collapsed vertebrae are abnormally hyperintense. Signal abnormality without collapse is seen in C6 vertebra. **c** Sagittal contrast-enhanced fat-suppressed T1-weighted MR image shows intense enhancement in the collapsed bodies. **d** Sagittal diffusion-weighted MR image shows restricted diffusion appearing as abnormally increased signal in the affected vertebrae (*arrows*)

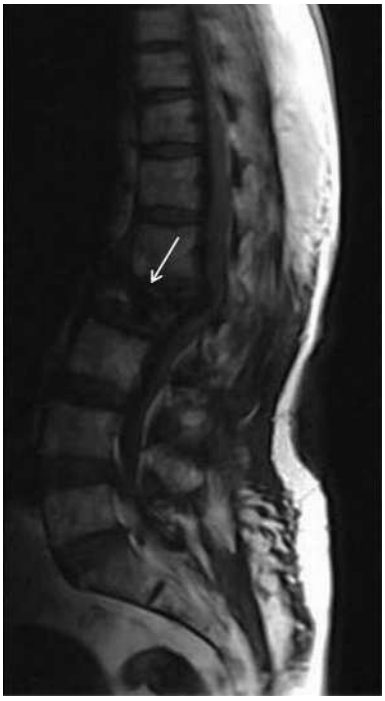

Fig. 30.8. Diffusion-weighted MR image in benign collapse. Sagittal diffusion-weighted MR image of the lumbar spine in a benign collapse (*arrow*) shows no restriction of diffusion

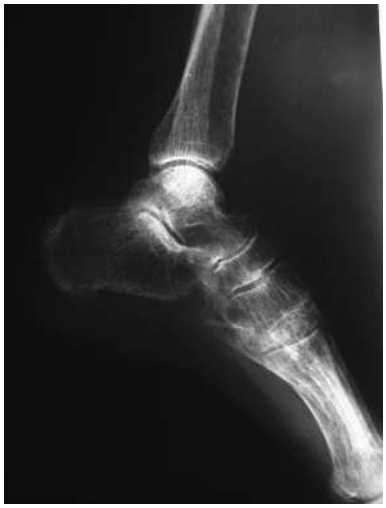

Fig. 30.9. Disuse osteoporosis following trauma. Lateral radiograph of the ankle following prolonged immobilization for a femoral fracture shows patchy osteopenia of all the visualized bones, mimicking multiple myeloma

from the diffusion-weighted images. The rationale for measuring ADC is that in metastatic lesions, the cellularity is high, especially in actively growing tumors, and this is thought to reflect as lower ADC values. However, the cellularity in benign fractures is lower than that of metastatic lesions because of the increased interstitial space associated with edema in the acute phase. This would lead to higher ADC values in metastatic collapse. However, again, a later study (Maeda et al. 2003) concluded that even ADC values did not always permit a clear distinction between benign and malignant compression fractures due to considerable overlap between the measurements in the two groups. Finally, a recent paper (Tang et al. 2007) has suggested that optimizing the B values within the range of around 300 s/mm contributes to making the ADC values more reliable in differentiating benign from malignant vertebral collapses. Thus, in view of the overall contradictions between various published studies, as stated by Finelli (2001) in his editorial in AJNR on the same subject, the value of unique diagnostic information from diffusion scans that may influence management is questionable.

30.1.1.2 Disuse Osteoporosis versus Neoplasm

Regional osteoporosis may develop rapidly after disuse and immobilization of a limb as occurs after paralysis (Leslie and Nance 1993; Iversen et al. 1989), prolonged therapeutic bed rest, or following trauma. Lack of normal biomechanical stress on bone decreases osteoblast-mediated bone formation and encourages osteoclast-mediated bone resorption. Patchy lucent areas of disuse osteoporosis (Fig. 30.9) due to post-traumatic demineralization or disuse due to paralysis may mimic the permeative lysis of neoplasms like metastases and myeloma (Joyce and Keats 1986). Recognition of the regional distribution of osteopenia in the characteristic clinical setting is the key to correct diagnosis. If function of the involved extremity is recovered, the radiographic abnormalities of regional osteoporosis may completely reverse.

30.1.1.3 Insufficiency Fractures and Pubic Osteolysis: Mimics of Malignancy

An insufficiency type of stress fracture is an important sequela of generalized osteoporosis. Normal physiological or abnormal amounts of biomechanical stress placed on bones that are structurally weak lead to osseous failure. Insufficiency fractures can be difficult to diagnose, and the imaging appearance may be misleading for malignancy. Patients with previous pelvic malignancy are at increased risk for sacral insufficiency fractures, and metastatic disease can be incorrectly diagnosed, potentially leading to distress, prolonged symptoms, and delayed or inappropriate treatment (Blake and Connors 1994). Radiographs, scintigraphy, MR imaging, and CT establish the diagnosis of insufficiency fractures with varying success. Recently, PET has been used with increasing frequency as a diagnostic tool in oncology; insufficiency fractures may be mistakenly diagnosed as tumor on PET as increased uptake of FDG may be seen in both situations. Bilaterality and typical sites of involvement, such as the sacrum and pubis, are the keys to diagnosis. If the diagnosis is not certain, or if there is concern regarding healing, follow-up CT or MRI is advocated. Some patients who had unilateral fractures at first presentation develop a classical bilateral appearance at follow-up, thereby further establishing the diagnosis.

Pubic osteolysis is a rare destructive condition affecting the pubic bone (McCarthy and Dorfman 1990). It is seen in postmenopausal women with osteoporosis and often with a history of trauma. On radiographs, lytic bone abnormality is seen in the body or rami of the pubic bone. Involvement of the symphysis pubis has been reported. Histological features may suggest chondrosarcoma or other primary bone malignancy, compounding erroneous radiological interpretation. Symptoms improve with conservative management, and sclerotic interval change may be seen radiographically (O'Connor and Whittaker 2006).

Radiographs

On radiographs, pelvic insufficiency fractures can be categorized into occult and aggressive types (Peh et al. 1996). Occult fractures occur in the sacrum and appear as sclerotic bands, cortical disruptions, and even visible fracture lines may be seen in the ala. However, the sacrum is often obscured by bowel gas, and the subtle findings are not usually identifiable or diagnostic.

On the other hand, fractures of the para-symphysis and pubic rami often have an aggressive appearance that depends on the stage of fracture development at which radiography is performed. Initially radiographs show a fracture line in the os pubis. An exuberant lesion may be seen with healing and callus formation. If healing is prolonged or delayed, increased lysis and bone fragmentation may be seen. Both the latter two stages of fractures often have an aggressive radiographic appearance, which may resemble those of malignant neoplasms (Peh et al. 1996). These aggressive parasymphyseal fractures may be misdiagnosed as neoplasm and inappropriately subjected to biopsy. Biopsy specimens of primary callus can be difficult to interpret with the added histopathological uncertainty compounding the error made at radiographic diagnosis. Thus, further imaging is often required for the diagnosis of both occult and aggressive insufficiency fractures.

MR Imaging

The sensitivity of MR imaging in the diagnosis of insufficiency fractures relates to the occurrence of bone marrow edema as an early manifestation of the fracture. The MR imaging characteristics of traumatic edema include low signal intensity on T_1-weighted and high signal intensity on T_2-weighted images. T_2-weighted short tau inversion recovery (STIR) images are particularly sensitive. Coronal imaging in the plane of the sacrum is helpful, often showing a horizontal component of the fracture, and T_2-weighted images can also be useful,

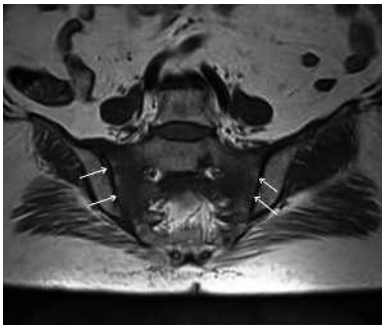

Fig. 30.10. Sacral insufficiency fractures. Coronal T1-weighted MR image shows bilaterally symmetric low signal in the sacrum of a middle-aged patient with low back pain and prior history of pelvic malignancy. Although the fracture lines are not obvious, the characteristic location, symmetric appearance, and lack of associated abnormal soft tissue masses suggest the diagnosis of insufficiency fractures

particularly if fat suppression is used. Usually a fracture line will be demonstrated, but even if one cannot be seen, the combination of edema-like signal, location, and the absence of a soft tissue mass should suggest a stress reaction (Fig. 30.10).

Bone Scintigraphy

Bone scintigraphy is a sensitive technique for suspected insufficiency fractures of the sacrum. The classic "H" pattern is considered diagnostic in the right clinical setting and is produced when there are fractures of both the sacral ala and a horizontal component involving the sacral body. However, the H-sign is often absent, and if there are other pelvic insufficiency fractures, this may lead to misinterpretation as metastatic disease (Blake and Connors 1994). In a meta-analysis by Finiels et al. (1997), the classical H-sign was documented in just 40% of cases.

Computed Tomography (CT)

CT of insufficiency fractures of the pelvis will show fracture lines or linear sclerosis. If there is doubt regarding the diagnosis of insufficiency fractures versus bony metastases on MRI and scintigraphy, the demonstration of normal, intact trabeculae adjacent to the fracture lines on CT rules out malignancy.

30.1.1.4 Osteogenesis Imperfecta Type V

Osteogenesis imperfecta (OI) is a heritable disorder characterized by bone fragility, fractures, and deformity. Since Battle and Shattock's original description in 1908 of three members of one family in whom sarcoma-like swellings of the femur developed following fractures, hyperplastic callus formation (HPC) in osteogenesis imperfecta has become well recognized.

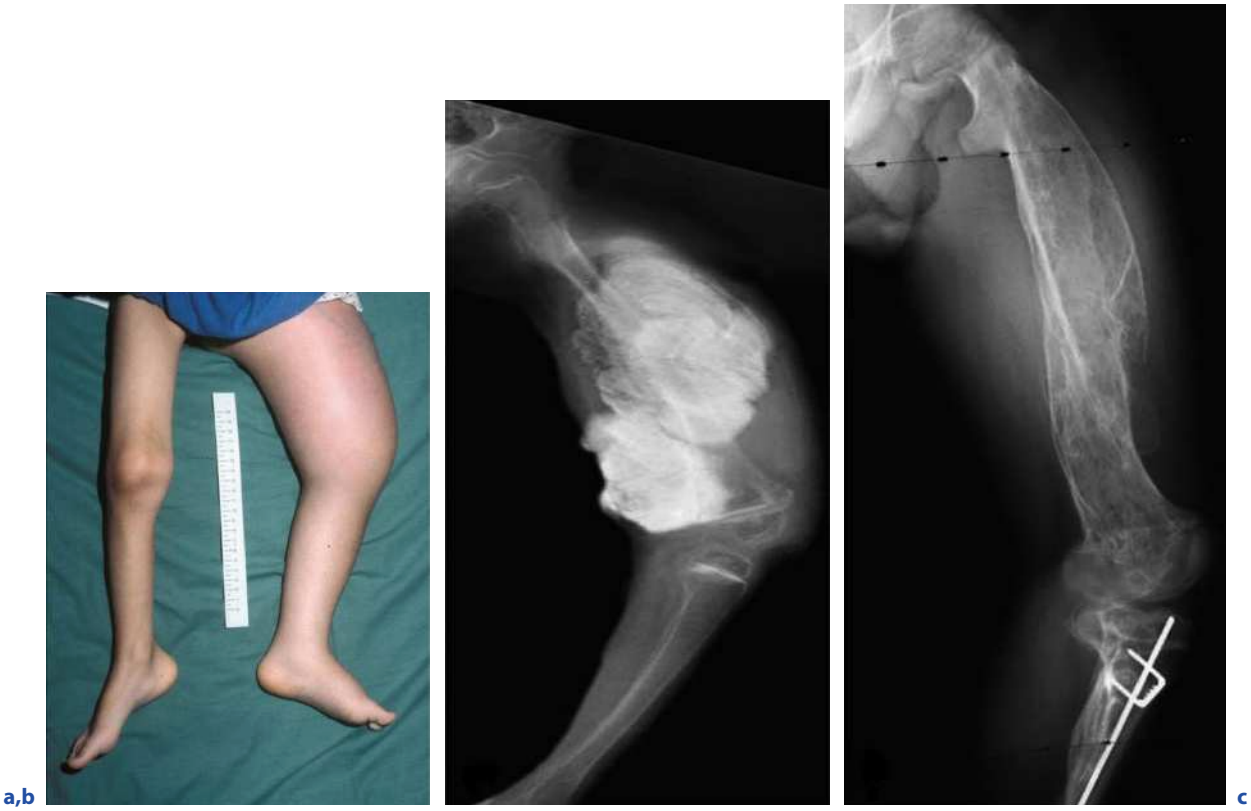

Fig. 30.11a–c. Hyperplastic callus formation in osteogenesis imperfecta type V. **a** A 4-year-old boy presented with suspected osteosarcoma after a short history of a rapidly enlarging swelling of his left thigh, arising after a fracture. **b** Radiograph shows an exuberant lobulated radio-dense mass arising from the left femur representing hyperplastic callus. **c** Nine years later, there is internal reorganization with smooth contours. [Reprinted from Cheung et al. (2008); permission to reproduce granted by Skeletal Radiology, International Skeletal Society]

More recently, Glorieux et al. (2000) classified OI with a propensity to produce exuberant, hyperplastic callus as a separate entity – type V.

Exuberant callus formation in OI type V (Fig. 30.11a and b) should not be mistaken for sarcoma. The main differential diagnoses of HPC are intraosseous osteosarcoma with aggressive periosteal reaction, parosteal osteosarcoma, juxtacortical myositis ossificans, and large osteochondromas (Dobrocky et al. 1999). The hyperplastic callus appears after fractures or corrective surgery and typically presents as a hard, painful, and warm swelling over the affected bone that may initially suggest inflammation or sarcoma. Microscopically, there is exuberant production of poorly organized, partly mineralized extracellular matrix (Brenner et al. 1989). After a rapid growth period, the size and shape of the callus may remain stable for many years (Fig. 30.11c) (Cheung et al. 2008).

30.1.2 Osteomalacia

Osteomalacia is a disorder of inadequate mineralization of osteoid, organic bone matrix. Since osteoid is mineralized to bone through deposition of crystals composed of calcium and phosphate, long-standing deficiency of phosphate, calcium, or both can lead to osteomalacia. Chronic hypophosphatemia results from inadequate intake or excessive loss and presents in inherited or acquired forms. Inadequate phosphate intake can be the result of extensive intestinal disease, the presence of phosphate binders in the diet, or secondary to vitamin D deficiency (due to low dietary intake, lack of sun exposure, renal or hepatic disease, and inherited disorders of vitamin D metabolism). Excessive urinary loss due to renal tubular dysfunction can be inherited (e.g., autosomal-recessive and X-linked hypophosphatemic rickets, Fanconi syndrome) or acquired (e.g., renal tubular acidosis, toxic damage by heavy metals or certain chemotherapeutic agents, and tumor-induced osteomalacia). In the presence of low serum phosphate, the differential diagnosis of oncogenic osteomalacia is X-linked hypophosphatemia. Enthesitis, ligament ossification, and periostitis are some of the imaging features encountered in X-linked hypophosphatemia that help to distinguish it from oncogenic osteomalacia. In X-linked hypophosphatemia, the patients are usually short with bowed legs.

Chronic hypocalcemia as a result of intestinal disease, abnormalities of vitamin D and parathyroid hormone, or systemic acidosis is an unusual cause of osteomalacia since symptoms of hypocalcemia often result in earlier medical attention and are only rarely seen in hypoparathyroidism and pseudohypoparathyroidism (Lamont et al. 1999).

30.1.2.1 The Radiologist and Oncogenic Osteomalacia

Oncogenic osteomalacia is a rare clinicopathological syndrome characterized by a triad of severe hypophosphatemia, hyperphosphaturia, and osteomalacia secondary to a neoplasm (Sundaram and Mccarthy 2000; Folpe et al. 2004). Serum calcium is often normal. The cause is usually a mesenchymal tumor with prominent vascularity and giant primitive stromal cells (Clunie et al. 2000; Schapira et al. 1995). Although often classified as a paraneoplastic syndrome, paradoxically, the neoplasm may be of limited clinical significance, whereas generalized, debilitating osteomalacia and rickets are the important clinical problems for the patient (Carpenter 2003). Typically patients present with signs and symptoms of osteomalacia, such as muscle weakness, bone pain, waddling gait, and joint deformities with anorexia and fatigue. The condition is challenging to diagnose, as the patient most often presents with symptoms of osteomalacia, and the primary mesenchymal tumor may be small and often asymptomatic. However, correct diagnosis is particularly gratifying as surgical removal of the offending tumor can lead to a dramatic reversal of osteomalacia.

Etiopathogenesis

A review of the literature shows that most cases of oncogenic osteomalacia are caused by benign bone and soft tissue tumors, which include hemangiopericytomas, benign giant cell tumors, non-ossifying fibromas, fibrous dysplasia, neurofibromas, and some benign osteoid and cartilage-forming tumors (Pollack et al. 1973; Martini et al. 1983; Spargana 1987). The most common causative tumor reported is hemangiopericytoma. There are a few isolated reports of malignant mesenchymal tumors such as osteosarcoma causing oncogenic osteomalacia (Nomura et al. 1981; Park et al. 1994; Wyman et al. 1997; Hasegawa et al. 1999). Finally, rarely, oncogenic osteomalacia is associated with lymphoproliferative disorders, including multiple myeloma, lymphoma, leukemia, and plasmacytoma (Narvaez et al. 2005; Rao et al. 1987; Messiaen et al. 2000; Minemura et al. 2004; Ma et al. 2004; Chua et al. 2008). The term phosphaturic mesenchymal tumor, mixed connec-

tive tissue variant (PMTMCT) has long been used to describe a distinct subset of these tumors; however, it has not been widely accepted by histopathologists until recently (Folpe et al. 2004).

Although the pathophysiology has not yet been clearly delineated, a humoral factor produced by the tumor is suspected to be the cause of defective bone mineralization from renal phosphate loss. Thus, tumor elaboration of a phosphaturic factor is the putative mechanism. The underlying humoral phosphaturic factor, overproduction of fibroblast growth factor 23 (FGF23), has been identified and utilized in serology and immunohistochemical tests in suspect cases (Takeuchi et al. 2004). Studies have shown phosphaturia in dogs and rats injected with tumor extracts (Aschinberg et al. 1977; Popotvtzer 1981) and in athymic mice transplanted with tumor (Cai Qiang et al. 1994). The pathophysiological mechanism of lymphoproliferative disorders leading to osteomalacia is believed to be tubular dysfunction secondary to accumulation of immunoglobulin light chain fragments within lysosomes of tubular epithelial cells.

Imaging

At the initial presentation, radiographs may demonstrate significant osteopenia, Looser's zones (pseudofractures), and fractures (Fig. 30.12), but frequently fail to detect an associated tumor. In suspected cases of oncogenic osteomalacia, the search for the primary tumor starts with clinically looking for innocuous 'lumps' and 'bumps,' especially in the extremities and head and neck regions. The search should continue with radiological studies and useful modalities for demonstration of the causative phosphaturic mesenchymal tumor, which is often subcentimeter sized, including radiographic or MR skeletal survey and PET CT. Due to the vascular nature of the tumor, a blood pool scan maybe helpful. Case reports of the use of octreotide scanning using In-

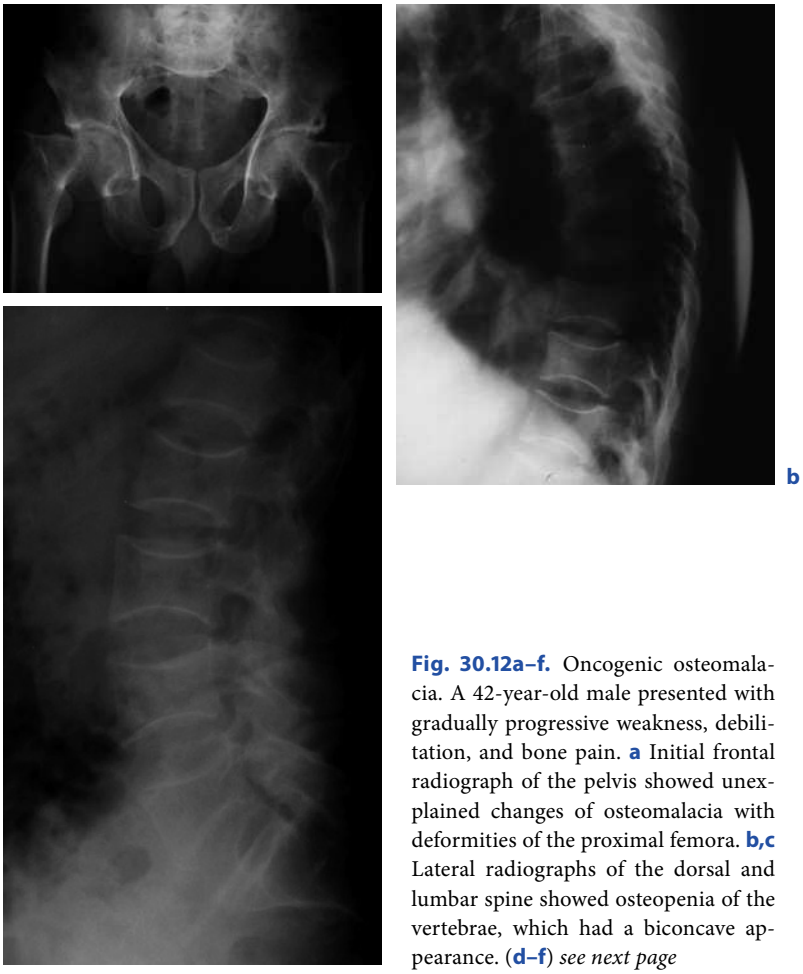

Fig. 30.12a–f. Oncogenic osteomalacia. A 42-year-old male presented with gradually progressive weakness, debilitation, and bone pain. **a** Initial frontal radiograph of the pelvis showed unexplained changes of osteomalacia with deformities of the proximal femora. **b,c** Lateral radiographs of the dorsal and lumbar spine showed osteopenia of the vertebrae, which had a biconcave appearance. (**d–f**) *see next page*

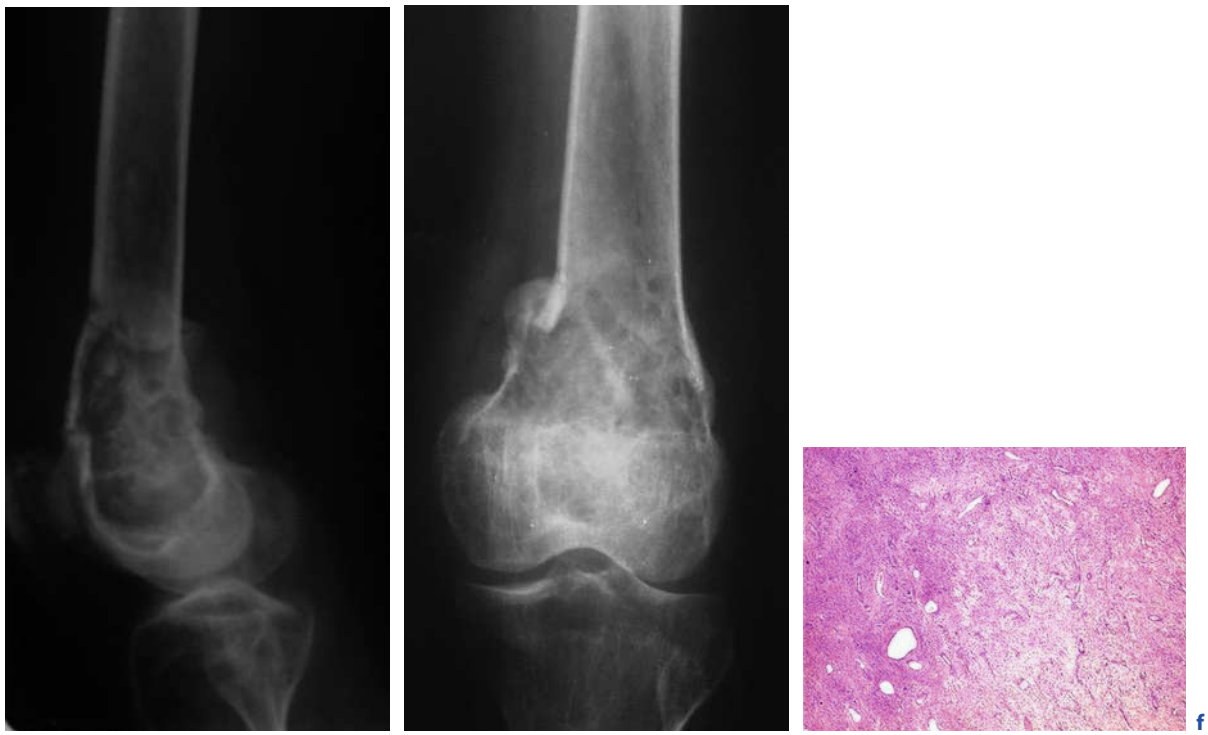

d,e f

Fig. 30.12a–f. (*continued*) **d,e** A few months later, the patient developed severe pain in the left lower limb. Lateral and frontal radiographs of the femur showed a primary bone tumor in the lower end of the femur with a pathological fracture. The tumor was curetted, and bone grafting was done. Histopathology showed a phosphaturic mesenchymal tumor. In the immediate postoperative period, the phosphate requirement was reduced. **f** Histopathology of the femoral tumor revealed moderately cellular spindle cell tumor showing hemangiopericytomatous areas admixed with scattered osteoclast-like giant cells (hematoxylin and eosin; original magnification: ×40). (Courtesy N.A. Jambhekar, MD, Mumbai, India)

111-labeled octreotide have been reported as a valuable diagnostic tool (Auethavekiat et al. 2005).

Venous sampling for systemic survey of regional sera FGF-23 levels has been found to be useful for the diagnosis of oncogenic osteomalacia and localization of the responsible tumor. Takeuchi et al. (2004) reported a case of tumor-induced osteomalacia due to a right inguinal tumor that was diagnosed by selective venous sampling and MRI, suggesting that this combination procedure is clinically useful for identifying the tumor responsible. However, while selective venous sampling is accurate and produces higher quality images, it is an invasive technique, which can sometimes cause complications such as blood loss and embolism (Ogura et al. 2008).

Treatment and Prognosis

A high index of suspicion is warranted for the presence of a tumor in any adult patient with osteomalacia and acquired hypophosphatemia. A thorough search for a tumor must be initiated without delay, as its surgical removal in most cases results in normalization of the metabolic disturbances. There is an impressive improvement in the clinical course of oncogenic osteomalacia when the aberrant tumor is correctly recognized and completely excised. The serum phosphate levels normalize within hours to days after the removal of the tumor. However, clinical resolution of symptoms and serum biochemical markers of bone turnover, such as the osteocalcin level and alkaline phosphatase activity, tend to take longer to normalize. Therapy may be aided by short-term replacement of phosphate orally and the addition of vitamin D and calcium (Jacob et al. 2007). Since the condition is usually associated with localized benign tumors and not metastatic malignant disease, this approach is usually successful. In the presence of hypophosphatemia, radiologists need to be aware that any lesion of the bone and soft tissue, however innocuous histologically or biologically, should be considered significant and causative of oncogenic osteomalacia.

30.1.3 Hyperparathyroidism

Hyperparathyroidism is a general term applied to overfunctioning of the parathyroid gland, for which there are diverse causes. Histopathologically, over-excretion of parathyroid hormone leads to an imbalance of osteoclastic and osteoblastic activity in the fibrous stromal matrix in multiple skeletal lesions. Hyperparathyroidism has striking and multifaceted musculoskeletal manifestations. In this section, we discuss how certain manifestations of hyperparathyroidism may masquerade as primary or secondary bone tumors.

30.1.3.1 Brown Tumors

Hyperparathyroidism is an uncommon diagnosis in the West because of the routine use of serum autoanalyzers, but in developing countries, the disease may occasionally present with a brown tumor that may be indistinguishable from a more sinister disease process. Brown tumors are usually noted in conjunction with primary hyperparathyroidism, but are being reported more recently with increasing frequency in secondary hyperparathyroidism. The incidence of brown tumor has been reported to be 3% in patients with primary hyperparathyroidism, in contrast to 1.5–1.7% in patients with secondary hyperparathyroidism (Grulois et al. 2005).

In primary hyperparathyroidism, bone lysis occurs partly due to the destruction of hydroxyapatite crystals, but more significantly due to the osteoclastic resorption. The bone resorption results in holes in the bone (Hsieh et al. 2004). The holes are then filled in with fibrous tissue (osteitis fibrosa) or become confluent to result in a large defect, known as a brown tumor (osteitis fibrosa cystic). Therefore, the histopathological findings of osteitis fibrosa cystica consist of osteoclastic resorption of the bone, irregularly thickened woven trabecular bone surrounded by loose fibrous tissue, increased numbers of osteoblasts and osteoclasts, and areas of granulation tissue, inflammatory cells, giant cells, and hemosiderin deposition with virtually no bone at all.

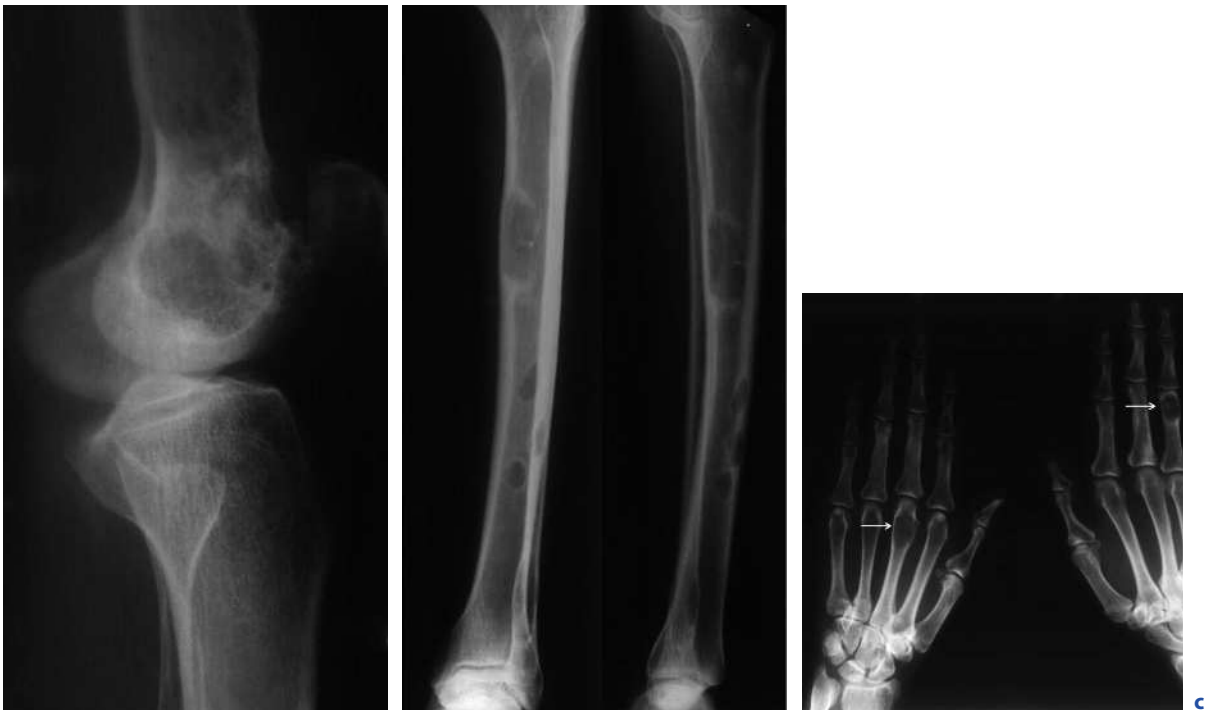

a,b c

Fig. 30.13a–c. Multiple brown tumors. **a** Initial lateral radiograph of the knee following pain shows an expansive osteolytic lesion in the distal metadiaphysis of the distal femur mimicking an aggressive primary bone tumor. **b** Frontal and lateral radiographs of the leg show multiple well-marginated, expansive osteolytic lesions in the tibial shaft. **c** Radiographs of the hands show similar lesions in the right third metacarpal and proximal phalanx of the left ring finger (*arrows*), which along with subperiosteal resorption suggests that all lesions are brown tumors of hyperparathyroidism

The name "brown tumor" relates to the gross findings of abundant vascularized fibrous tissue with a brownish color of hemorrhage and hemosiderin on biopsy. Thus, brown tumors, often termed osteoclastoma, are not true neoplasms, but represent localized accumulations of fibrous tissue and giant cells that can replace bone and even produce osseous expansion.

On radiographs, brown tumors appear as central, slightly expansive, lightly septated, and distinct geographic radiolucencies (Fig. 30.13). Commonly affected sites include the metacarpals, phalanges, jaw, skull, pelvis, clavicle, ribs, femur, and spine. The destructive skeletal lesions heal spontaneously after treatment of the parathyroid disorders. Surgical curettage, bone grafting, or prophylactic stabilization are only recommended for unrelenting symptomatic bone lesions, persistent osteolytic lesions at high-stress anatomical sites, as well as pathologic fractures.

Radiologically, multiple bone lesions of brown tumor may be misdiagnosed as multiple myeloma, metastatic carcinoma, lymphangiomatosis, leukemia, Langerhans' cell histiocytosis, multiple bone cysts, or multiple non-ossifyng fibromas (Kocher et al. 2000). Bone scintigraphy is a valuable technique for distinguishing hyperparathyroidism from multiple bone metastases (Jordan et al. 1993). The former demonstrates systemic generalized hypermetabolism of whole bones, whereas the latter shows multiple focal uptakes, reflecting local elevation of bone turnover over caused by metastasis (Hoshi et al. 2008). Solitary brown tumor may be confused with giant cell tumor and giant cell reparative granuloma, and the differential diagnosis may be problematic without knowledge of the clinical features and laboratory results. Serum calcium, phosphorus, and PTH levels are valuable in differentiating brown tumors from giant-cell-rich reparative granuloma and giant cell tumor.

30.1.3.2 Amyloidomas of the Bone and Renal Spondyloarthropathy

Renal osteodystrophy is the term applied to bone disease that is apparent in patients with chronic renal failure. The pathologic and radiological findings in renal osteodystrophy include hyperparathyroidism, rickets, and osteomalacia, osteoporosis, soft tissue and vascular calcification, and musculoskeletal abnormalities occurring after dialysis, such as amyloid deposition.

Amyloidosis accompanying chronic hemodialysis is related to the accumulation of β_2-microglobulin, a low-molecular-weight serum protein that is not filtered by standard dialysis membranes. The serum concentrations of β_2-microglobulin are 40 to 50 times higher in patients undergoing hemodialysis as compared to those with normal renal function. β_2-Microglobulin-associated amyloidosis accompanying chronic hemodialysis appears to predominantly involve the musculoskeletal system, and the prevalence of such amyloid deposition increases progressively with the duration of dialysis therapy (Campistol and Skinner 1993).

Amyloid deposition can lead to periarticular osteolytic lesions, and these tumor-like osseous lesions are called amyloidomas of the bone. Amyloidomas are the rarest form in the group of amyloidosis-related pathologic abnormalities. They are frequently multiple, may be bilateral, and can increase in size and number. On radiographs and CT, the osseous lesions are well defined with geographic bone destruction and may be septated with a sclerotic margin. Pathological fractures may occur through these cystic lesions. They affect both central and marginal regions of periarticular bone and, when large, may lead to collapse of the articular surface (Resnick 2002). It has been reported (Simoens et al. 2000) that the signal characteristics of amyloid on MR images closely resemble those of skeletal muscle, the structure of amyloid being akin in many ways to the highly organized multilayered, myofibrillar ultrastructure of skeletal muscle (Banker and Girvin 1971). The lesions grow slowly, and the significant local destruction of bone and associated soft tissue component give them a tumor-like appearance (Fig. 30.14) and behavior that makes the diagnosis difficult to establish on imaging studies.

The differential diagnosis of multiple lytic bone lesions includes, foremost, metastatic disease and multiple myeloma (Ross et al. 1991). Neither of these entities demonstrates a juxta-articular predilection, and a diagnosis of myeloma can be made with laboratory studies. Lytic bone lesions in a patient who has undergone long-term hemodialysis should also suggest the diagnosis of secondary hyperparathyroidism and brown tumor. Other stigmata of secondary hyperparathyroidism, such as subperiosteal and subchondral bone resorption, should be present, as well as characteristic blood chemistry abnormalities. Also, brown tumors do not occur in a para-articular location (Ross et al. 1991). Some solitary amyloidomas reported in the literature are calcified (Cloft et al. 1995; Pawar et al. 1982), and in such cases, the differential diagnosis includes chondrosarcoma, osteosarcoma, and a calcified metastatic tumor, such as mucinous adenocarcinoma of the colon.

In addition to amyloidomas of the bone, patients on long-term dialysis may also develop disco-vertebral lesions mimicking either neoplasm (Fig. 30.15) or infec-

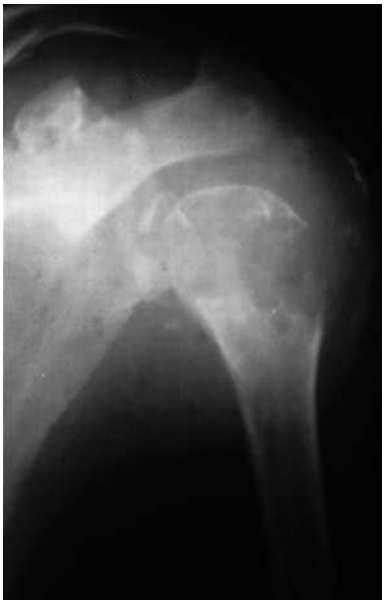

Fig. 30.14. Amyloidoma of the bone. Frontal radiograph of the left shoulder shows an osteolytic lesion with geographic margins in the head of the humerus mimicking a primary bone tumor

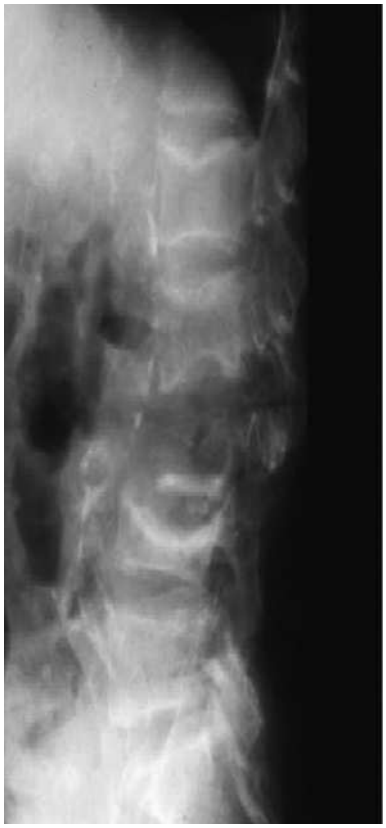

Fig. 30.15. Renal spondyloarthropathy in a 67-year-old woman who had been on maintenance hemodialysis for 14 years. Lateral radiograph of the lumbar spine shows destruction of L3 vertebral body and resorption of the superior endplate of L4 vertebra mimicking malignancy

tion. In such a clinical setting, renal spondyloarthropathy should be the primary consideration (Sundaram et al. 1987; Leone et al. 2001). Histological examination of excised tissue in renal spondyloarthropathy shows ß$_2$-microglobulin amyloidal deposits in the intervertebral disk, the synovium of apophyseal joints, and the ligamentum flavum (Marcelli et al. 1996).

With the increased life span of hemodialysis patients, radiologists are more likely to encounter musculoskeletal manifestations of β_2-microglobulin-associated amyloidosis, including lytic osseous lesions. The presence of multiple juxta-articular osteolytic lesions in a long-term hemodialysis recipient should suggest the diagnosis. In addition, one should look for the associated features of hemodialysis-associated amyloidosis, such as carpal tunnel syndrome and spondyloarthropathy. However, in patients with a primary malignancy or lytic lesions that are symptomatic, solitary, rapidly progressive, or not in a para-articular location, biopsy may be unavoidable so that other causes can be ruled out (Ross et al. 1991).

30.2 Reactive and Tumor-Like Lesions of the Bone

Reactive lesions, such as florid reactive periostitis (FRP) and bizarre parosteal osteochondromatous proliferation (BPOP), may simulate aggressive malignant pathologies, chiefly osteosarcoma and also chondrosarcoma. Correct radiological diagnosis is imperative as these lesions do not require immediate biopsy unless the natural evolution is unspecific.

SAPHO is an acronym for a syndrome comprised of synovitis, acne, pustulosis, hyperostosis, and osteitis. Awareness of the SAPHO syndrome is important to facilitate differentiation of the tumor-like osteoarticular

manifestations of this entity from true bone neoplasms with similar radiological presentation, but dramatically different progression, treatment, and prognosis. These entities include malignancies such as round-cell tumors like lymphoma and Ewing's sarcoma, metastases, and also osteomyelitis and Paget's disease.

30.2.1 Florid Reactive Periostitis (FRP) and Bizarre Parosteal Osteochondromatous Proliferation (BPOP)

Florid reactive periostitis (FRP) and bizarre parosteal osteochondromatous proliferation (BPOP) are reactive lesions that are believed to represent entities from opposing ends of a spectrum. In other words, FRP most likely naturally progresses to BPOP. BPOP is also referred to as Nora's lesion since it was first described by Nora et al. in 1983. Nora's lesion or BPOP is defined as a "well-marginated mass of heterotopic mineralization arising from the periosteal aspect of an intact cortex, without medullary changes" (Dhondt et al. 2006) (Fig. 30.16). The radiological appearances of these benign entities are often mistaken for more ominous pathologies, most commonly osteogenic sarcoma and chondrosarcoma, and also osteomyelitis.

Etiopathogenesis

Although the natural history and radiological features of FRP and BPOP are well established in numerous studies in the literature, there is limited insight into the etiopathogenesis of these unique entities. Thus, the inciting factor for the soft tissue mass, associated periosteal reaction, and ossification remains unknown. Both lesions are likely reactive, and a relationship to trauma has been suggested, but not proved. Some authors (Ouri et al. 2002) have suggested that a possible relationship between systemic or local inflammatory processes and development of Nora's lesion may exist. Finally, cytogenetic studies (Nilsson et al. 2004) have indicated that t(1;17)(q32;q21) and variant translocations involving 1q32 are unique and common to the lesion.

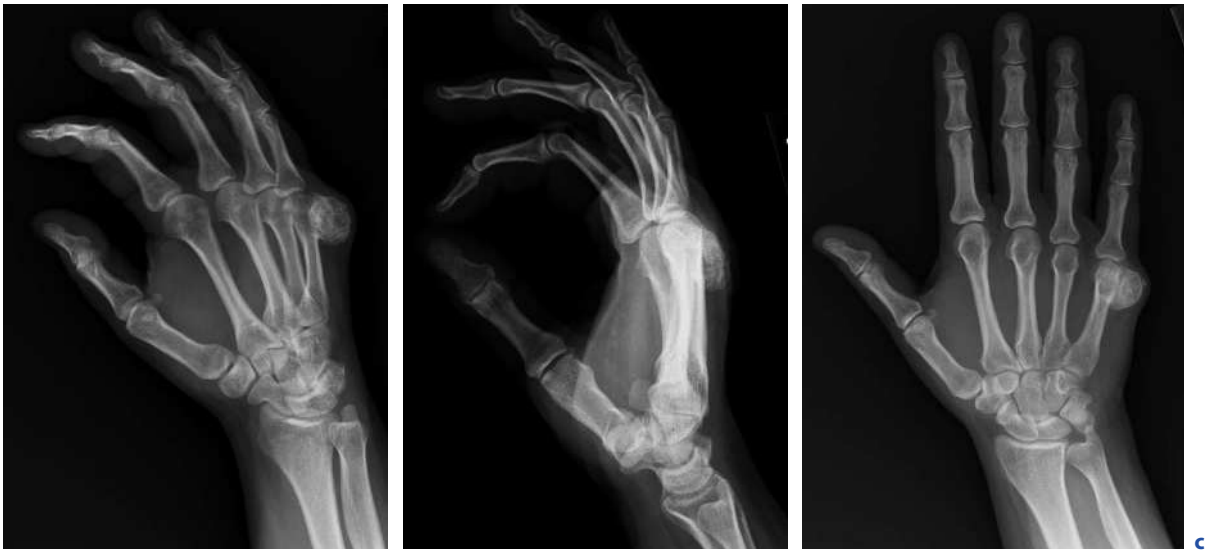

Fig. 30.16a–c. Bizarre parosteal osteochondromatous proliferation (*BPOP*). **a** Oblique, **b** lateral, and **c** frontal radiographs of the hand show a bulky ossified "osteochondromatous" lesion adherent to the lateral cortex of the fifth metacarpal. The cortex adjacent to the lesion is intact

Radiological Diagnosis

The radiological hallmarks of FRP and BPOP are soft tissue masses associated with exuberant periosteal reaction and ossification. FRP presents on radiographs as a soft tissue swelling that is disproportionate to the extent of periosteal reaction. The medullary bone is uninvolved, and cortex adjacent to the periosteal reaction is intact, a feature that permits distinction from both a bone tumor and osteomyelitis and suggests a reactive lesion such as FRP. Rapid progression of the periosteal bone production is another feature of these lesions. Initially, in FRP, there is immature laminated periostitis that often progresses to broad-based osseous excrescences characteristic of BPOP (Fig. 30.17). These entities commonly affect the small bones of the hands and feet. Radiographs can conclusively establish the diagnosis of FRP and BPOP, and further imaging with CT or MRI does not provide supplementary information.

The two major radiological differential diagnoses of FRP and BPOP are sarcomas and infection. BPOP may be mistaken for both benign and malignant conditions involving the periosteum, including juxtacortical chondroma, periosteal/parosteal chondrosarcoma, and most commonly osteosarcoma. In spite of its relative rarity, FRP is, on a statistical basis, a more common lesion of

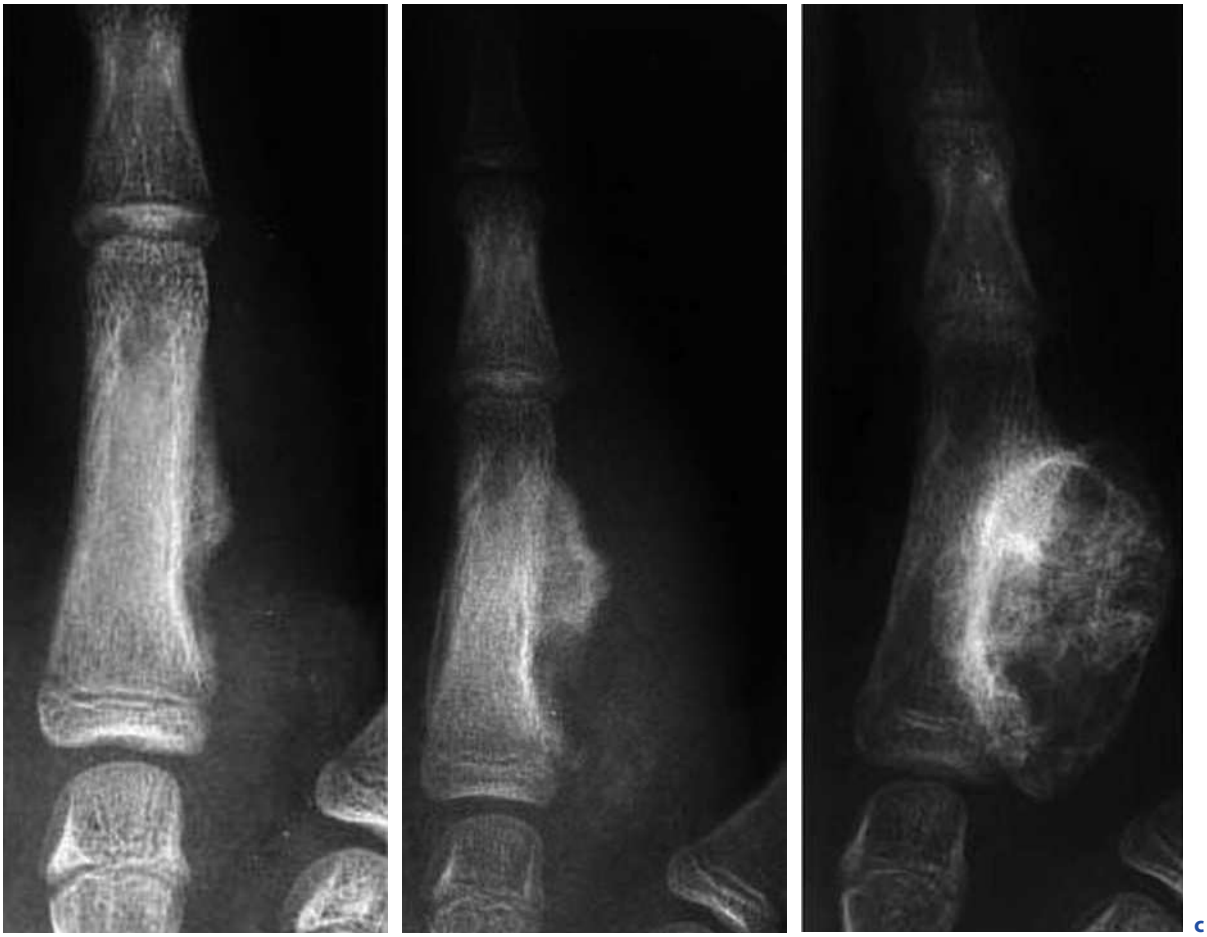

a,b c

Fig. 30.17a–c. Rapid progression of florrid reactive periostitis (*FRP*) to bizarre parosteal osteochondromatous proliferation (*BPOP*). An 11-year-old female with a swollen right fourth digit referred for confirmation of osteomyelitis and intravenous antibiotic treatment. **a** Initial frontal radiograph of the phalanx shows periosteal reaction adjacent to the medial cortex of the proximal phalanx. The cortex is intact. A diagnosis of FRP was made and close follow-up recommended. **b** Radiograph 3 weeks later shows soft tissue swelling and more profound bone medially conforming to bizarre parosteal osteochondromatous proliferation (*BPOP*) with periosteal reaction laterally, but no bone destruction. **c** Radiograph 2 months later shows large, bulky, ossified "osteochondromatous" lesion adherent to the medial cortex, which it has scalloped. Periosteal reaction laterally is solid. The radiographic appearance is that of BPOP. [Reprinted from Sundaram et al. (2001); permission to reproduce granted by Skeletal Radiology, International Skeletal Society]

the small bones of the hands than osteosarcoma and is a diagnosis that should be considered when a patient presents with a large soft tissue mass, an intact phalanx, and an aggressive periosteal reaction. An intact cortex and lack of soft tissue infiltration permits further distinction of BPOP from parosteal osteosarcoma. An early follow-up radiograph within 7–10 days, viewed in conjunction with the clinical findings, separates FRP and BPOP from osteomyelitis and soft tissue infection, which are the other important differential diagnoses (Sundaram et al. 2001).

These reactive lesions may be monitored radiologically or surgically excised if overtly symptomatic. The exact timing for surgical excision has not been established. Recurrence after surgery is common and reported in one series to be 29% after excision (Dhondt et al. 2006). Familiarity with the entity of FRP will allow radiologists to provide the correct diagnosis and prevent unnecessary antibiotic therapy or aggressive, early surgery. Close clinical and radiological follow-up of FRP usually shows conversion to BPOP.

30.2.2 SAPHO Syndrome

SAPHO is an acronym for a syndrome comprised of synovitis, acne, pustulosis, hyperostosis, and osteitis. The radiologist plays a central role in the early, accurate, and definitive diagnosis of the SAPHO syndrome. Awareness of the SAPHO syndrome is important to facilitate differentiation from other entities with similar radiological presentation, but dramatically different progression, treatment, and prognosis. These entities include malignancies such as round cell tumors like lymphoma and Ewing's sarcoma, metastases, and also osteomyelitis and Paget's disease.

The osteoarticular manifestations of SAPHO syndrome comprise synovitis, hyperostitis, and aseptic osteitis (Fig. 30.18). Synovitis is encountered most often in the upper anterior chest wall in the sternoclavicular, manubriosternal, and costoclavicular joints and less commonly in an extrathoracic location such as the sacroiliac joints. However, it is the discovery of hyperostosis

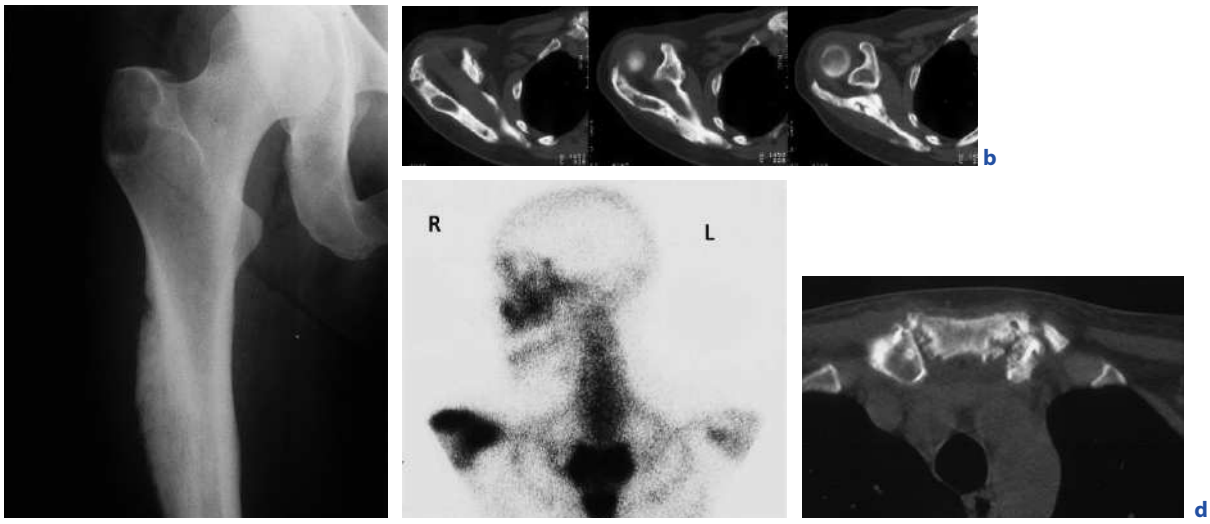

a,c b d

Fig. 30.18a–d. SAPHO syndrome. A 30-year-old woman presented with intermittent pain in the right thigh. About 1 year prior to referral, the patient had received oral steroid therapy for a skin eruption on the hands and feet and had also been investigated by a rheumatologist for neck and bilateral shoulder girdle pain. **a** Anteroposterior radiograph of the femur showed a hyperostotic lesion arising on the outer cortex of the proximal femoral diaphysis, interpreted at the time radiologically and pathologically as a low-grade parosteal osteosarcoma and surgically resected; 19 years later, she presented with right shoulder pain and was investigated for the same. **b** CT scan of the scapula showed a mixed pattern of lysis and sclerosis. **c** Three-hour anterior bone scintigraphy of the upper trunk showed increased activity over the right superior scapula and symmetrically over the sternoclavicular joints ("bull's head" sign). **d** CT scan of the sternoclavicular joints showed the typical sclerotic and erosive changes of SAPHO syndrome. The combination of skin lesions, hyperostosis of the femur, scapular, and sternoclavicular lesions leads to the correct diagnosis of SAPHO syndrome. Retrospective review of the histology of the old femoral lesion showed bone remodeling, marrow fibrosis with acute and chronic inflammation, and prominent periosteal new bone formation. The latter feature was originally mistaken for a parosteal osteosarcoma. [Reprinted from Davies et al. (1999); permission to reproduce granted by Skeletal Radiology, International Skeletal Society]

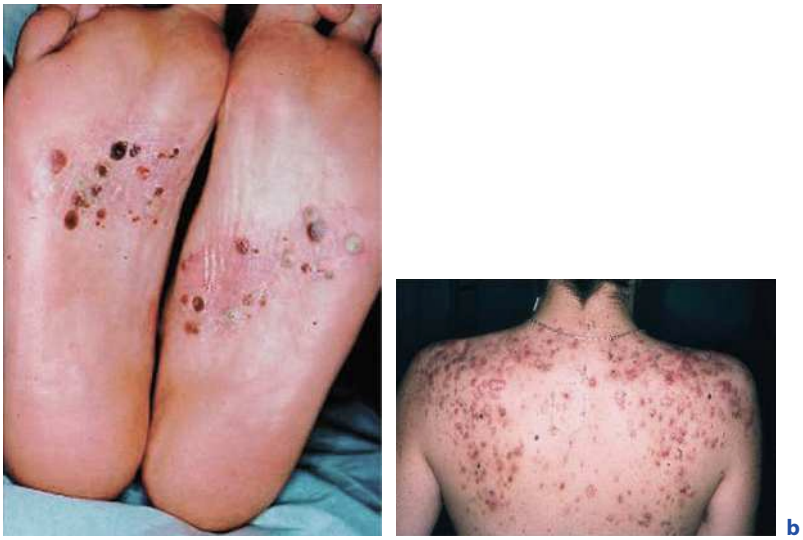

Fig. 30.19a,b. Dermatological manifestations of SAPHO syndrome. **a** Palmoplantar pustulosis (*PPP*). Sterile pustules on the soles of the feet surrounded by a mild inflammatory reaction. **b** Acne conglobata. Extensive involvement of the back with multiple papules, pustules, and hemorrhagic crusts. [Reprinted from Earwaker et al. (2003); permission to reproduce granted by Skeletal Radiology, International Skeletal Society]

and osteitis that leads the radiologist to the correct diagnosis. "Hyperostosis" refers to excessive osteogenesis. "Osteitis" refers to inflammation of bone. Hyperostosis and osteitis are manifestations of a chronic inflammatory reaction involving both the cortex and the medullary canal with associated endosteal and periosteal thickening. This results in diffuse cortical thickening and narrowing of the medullary canal with or without areas of osteolysis. Bone sclerosis may be homogeneous, but may also include areas of osteolysis within it (Earwaker and Cotten 2003). Clinically, the patient typically complains that the involved bone is painful and tender.

On histopathological examination, infiltrates of inflammatory cells – usually without causative organisms – are found at these sites (Boutin and Resnick 1998). Although *Propionibacterium acnes,* the microorganism responsible for acne, has been recovered at bone biopsy in some cases, a causal relationship has not been definitively established since *P. acnes* is an anaerobic saprophyte that is frequent found in the skin and is a common contaminant of specimens obtained via a transcutaneous route. Moreover, trials of antibiotics have generally been unhelpful (Wagner et al. 1997), although there are case reports of dramatic responses to prolonged courses of doxycycline (Ballara et al. 1999). A link with seronegative spondyloarthropathies has also been suggested due to the common occurrence of sacroiliitis and spinal lesions, paravertebral ossifications, and association with inflammatory bowel disease and psoriasis (Earwaker and Cotten 2003).

The predominance of sclerotic changes in the bone lesions with lack of significant bone destruction and associated soft tissue abnormality helps in distinguishing the SAPHO syndrome from malignant tumors of the bone, such as lymphoma, Ewing's sarcoma, and metastases. An association of the characteristic osteoarticular lesions with dermatological manifestations of palmoplantar pustulosis and acne (Fig. 30.19) usually clinches the diagnosis. Unfortunately, the dermatological (acne and pustulosis) and osteoarticular (synovitis, hyperostitis, and osteitis) manifestations of the syndrome do not always have a synchronous appearance, often leading to delay in the correct diagnosis. The acne and pustulosis seen with this entity may precede the bone lesion (and the patient may have forgotten about them), be concurrent with the bone lesion (the patient may not mention them because of chronicity), or appear subsequent to the bone lesion. Hence, familiarity with this condition, a high index of suspicion, and careful history-taking are essential to establish the diagnosis and avoid biopsy.

The clinical course of SAPHO syndrome is chronic, indolent, and self limiting. Treatment is conservative and consists of a course of non-steroidal anti-inflammatory drugs that is usually effective for the relief of pain. In cases of severe pain, a low dose of corticosteroids with analgesics is prescribed.

30.3 Conclusions

A vast array of metabolic bone conditions, including 'benign' osteoporotic vertebral collapse, patchy disuse osteoporosis, brown tumors, and amyloidomas, may mimic primary or secondary malignant bone tumors. Therefore, knowledge of their specific imaging appearances is useful to avoid unnecessary biopsies. Most of these lesions respond to conservative therapy. Similarly, reactive and tumor-like lesions, such as florid reactive periostitis (FRP)/bizarre parosteal osteochondromatous proliferation (BPOP) and the osteo-articular manifestations of the SAPHO syndrome, may be mistaken for bone tumor. However, their characteristic clinical and radiological presentation should allow for a specific diagnosis to be made in most instances, obviating further investigations and unnecessary anxiety.

References

Aschinberg LC, Solomon LM, Zeis PM et al. (1977) Vitamin D-resistant rickets associated with epidermal nevus syndrome: demonstration of a phosphaturic substance in the dermal lesions. J Pediatr 91:56– 60

Auethavekiat P, Roberts JR, Biega TJ et al. (2005) CASE 3. Oncogenic osteomalacia associated with hemangiopericytoma localized by octreotide scan. J Clin Oncol 23:3626–3628

Ballara SC, Siraj QH, Maini RN et al. (1999) Sustained response to doxycycline therapy in two patients with SAPHO syndrome. Arthritis Rheum 42:819–821

Banker BQ, Girvin JP (1971) The ultrastructural features of the mammalian muscle spindle. J Neuropathol Exp Neurol 30:155–195

Battle WH, Shattock HG (1908) A remarkable case of diffuse cancellous osteoma of the femur following a fracture. Proc Roy Soc Med 1:82–102

Baur A, Stabler A, Arbogast S et al. (2002) Acute osteoporotic and neoplastic vertebral compression fractures: Fluid sign at MR Imaging. Radiology 225:730–735

Baur A, Stabler A, Bruning R et al. (1998) Diffusion-weighted MR imaging of bone marrow: differentiation of benign versus pathologic compression fractures. Radiology 207:349–356

Blake SP, Connors AM (2004) Sacral insufficiency fracture. BJR 77:891–896

Boutin RD, Renick D (1998) The SAPHO syndrome: An evolving concept for unifying several idiopathic disorders of bone and skin. AJR 170:585–594

Brenner RE, Vetter U, Nerlich A et al. (1989) Biochemical analysis of callus tissue in osteogenesis imperfecta type IV. Evidence for transient overmodification in collagen types I and III. J Clin Invest 84:915–921

Cai Qiang, Hodgson SF, Kao PC et al. (1994) Brief report: inhibition of renal phosphate transport by a tumor product in a patient with oncogenic osteomalacia. New Engl J Med 330(23):1645–1649

Campistol JM, Skinner M (1993) β_2-Microglobulin amyloidosis: An overview. Semin Dialysis 6:117

Carpenter TO (2003) Oncogenic osteomalacia–A complex dance of factors. NEJM 348:1705–1708

Castillo M, Arbelaez A, Smith JK et al. (2000) Diffusion-weighted MR imaging offers no advantage over routine noncontrast MR imaging in the detection of vertebral metastases. AJNR Am J Neuroradiol 21:948–953

Cheung MS, Michel Azouz E, Glorieux FH et al. (2008) Hyperplastic callus formation in osteogenesis imperfecta type V: follow-up of three generations over 10 years. Skeletal Radiol 37:465–467

Chua SC, O'Connor SR, Wang WL et al. (2008) Solitary plasmacytoma of bone with oncogenic osteomalacia: recurrence of tumour confirmed by PET/CT. BJR 81:e110–e114

Cloft HJ, Quint DJ, Markert JM et al. (1994) Primary osseous amyloidoma causing spinal cord compression. AJNR Am J Neuroradiol 16:1152–1154

Clunie GPR, Fox PE, Stamp TCB (2000) Four cases of acquired hypophosphataemic ("oncogenic") osteomalacia. Problems of diagnosis, treatment and long-term management. Rheumatol 39:1415–1421

Cuénod CA, Laredo JD, Chevret S et al. (1996) Acute vertebral collapse due to osteoporosis or malignancy: appearance on unenhanced and gadolinium-enhanced MR images. Radiology 199:541–549

Davies AM, Marino AJ, Evans N et al. (1999) SAPHO syndrome: 20-year follow-up. Skeletal Radiol 28:159–162

Dhondt E, Oudenhoven L, Khan S et al. (2006) Nora's lesion, a distinct radiological entity? Skeletal Radiol 35:497–502

Dobrocky I, Seidl G, Grill F (1999) MRI and CT features of hyperplastic callus in osteogenesis imperfecta tarda. Eur Radiol 9:665–668

Earwaker JWS, Cotten A (2003) SAPHO: syndrome or concept? Imaging findings. Skeletal Radiol 32:311–327

Finelli DA (2001) Diffusion-weighted imaging of acute vertebral compressions: Specific diagnosis of benign versus malignant pathologic fractures. AJNR Am J Neuroradiol 22(2):366–372

Finiels H, Finiels PJ, Jacquot JM et al. (1997) Fractures of the sacrum caused by bone insufficiency. Meta-analysis of 508 cases. Presse Med 26:1568–1573 (English abstract)

Folpe AL, Fanburg-Smith JC, Billings SD et al. (2004) Most osteomalacia-associated mesenchymal tumours are a single histopathologic entity: an analysis of 32 cases and a comprehensive review of the literature. Am J Surg Pathol 28:1–30

Glorieux FH, Rauch F,Plotkin H et al. (2000) Type V osteogenesis imperfecta: A new form of brittle bone disease. J Bone Miner Res 15:1650–1658

Grulois V, Buysschaert I, Schoenaers J, Debruyne F, Delaere P, Vander Poorten V (2005) Brown tumour: presenting symptom of primary hyperparathyroidism. B-ENT 1:191–195

Hasegawa T, Shimoda T, Yokkoyama R et al. (1999) Intracortical osteoblastic osteosarcoma with oncogenic rickets. Skeletal Radiol 28:41–45

Hoshi M, Takami M, Kajikawa M et al. (2008) A case of multiple skeletal lesions of brown tumors, mimicking carcinoma metastases. Arch Orthop Trauma Surg 128:149–154

Iversen E, Hassager C, Christiansen C (1989) The effect of hemiplegia on bone mass and soft tissue body composition. Acta Neurol Scand 79:155–159

Jordan KG, Telepak RJ, Spaeth J (1993) Detection of hypervascular brown tumors on three-phase bone scan. J Nucl Med 34:2188–2190

Jacob JJ, Finny P, Thomas M et al. (2007) Oncogenic osteomalacia. JAPI 55:231–233

Joyce JM, Keats TE (1986) Disuse osteoporosis: Mimic of neoplastic disease. Skeletal Radiol 15(2):129–132

Jung HS, Jee WH, Mc Cauley TR et al. (2003) Discrimination of metastatic from acute osteoporotic compression spinal fractures with MR imaging. Radiographics 23:179–187

Kocher MS, Gebhardt MC, Jaramillo D et al. (2000) Multiple lytic skeletal lesions and hypercalcemia in a 13-year-old girl. Clin Orthop Relat Res 374:298–302

Lamont EB, Cavaghan MK, Brockstein BE (1999) Oncogenic osteomalacia as a harbinger of recurrent osteosarcoma. Sarcoma 3:95–99

Leone A, Sundaram M, Cerase A et al. (2001) Destructive spondyloarthropathy of the cervical spine in long-term hemodialyzed patients: a 5-year clinical radiological prospective study. Skeletal Radiol 30:431–441

Leslie W, Nance P (1993) Dissociated hip and spine demineralization: A specific finding in spinal cord injury. Arch Phys Med Rehabil 74:960–964

Ma CX, Lacy MQ, Rompala JF, Dispenzieri A et al. (2004) Acquired Fanconi syndrome is an indolent disorder in the absence of overt multiple myeloma. Blood 104:40–42

Maeda M, Sakuma H, Maier SE et al. (2003) Quantitative assessment of diffusion abnormalities in benign and malignant vertebral compression fractures by line scan diffusion-weighted imaging. AJR 181:1203–1209

Marcelli C, Pérennou D, Cyteval C et al. (1996) Amyloidosis-related cauda equina compression in long-term hemodialysis patients. Three case reports. Spine 21:381–385

Martini A, Notarangeleno LD, Barberis L et al. (1983) Acquired vitamin-D resistance rickets caused by prolonged latency in appearance of bone tumour. Am J Dis Child 137:1025–1026

McCarthy B, Dorfman HD (1990) Pubic osteolysis: a benign lesion of the pelvis closely mimicking a malignant neoplasm. Clin Orthop Relat Res 251:300–307

Messiaen T, Deret S, Mougenot B et al. (2000) Adult Fanconi syndrome secondary to light chain gammopathy. Clinicopathologic heterogeneity and unusual features in 11 patients. Medicine (Baltimore) 79:135–154

Minemura K, Ichikawa K, Itoh N et al. (2001) IgA-kappa type multiple myeloma affecting proximal and distal renal tubules. Intern Med 40:931–935

Moulopoulos LA, Yoshimistu K, Johnston DA et al. (1996) MR prediction of benign and malignant vertebral compression fractures. J Magn Reson Imaging 6:667–674

Narvaez J, Domingo-Domenech E, Narvaez JA et al. (2005) Acquired hypophosphatemic osteomalacia associated with multiple myeloma. Joint Bone Spine 72:424–426

Nilsson M,Domanski HA,Mertens F et al. (2004).Molecular cytogenetic characterization of recurrent translocation breakpoints in bizarre arosteal osteochondromatous proliferation. Hum Pathol 35:1063–1069

Nomura G, Koshino Y, Morimoto H et al. (1981) Vitamin D resistant hypophosphatemic osteomalacia associated with osteosarcoma of the mandible: report of a case. Jpn J Med 21:35–39

Nora Dahlin DC, Beabout JW (1983) Bizarre parosteal osteochondromatous proliferations of hand and feet. Am J Surg Pathol 7:245–250

O'Connor AR, Whittaker C (2006) Radiologic findings that mimic malignancy. AJR 187:W357–W364

Ogura E, Kageyama K, Fukumoto S et al. (2008) Development of tumor-induced osteomalacia in a subcutaneous tumor, defined by venous blood sampling of fibroblast growth factor-23. Intern Med 47:637–641

Ouri H, Ishikawa A, Tsuchiya T, Ogino T (2002) Magnetic resonance imaging characteristics of bizarre parosteal osteochondromatous proliferation of the hand. A case report. J Hand Surg 27:1104–1108

Park YK, Unni KK, Beabout JW et al. (1994) Oncogenic osteomalacia: a clinicopathologic study of 17 bone lesions. J Korean Med Sci 9:289–98

Pawar S, Kay CJ, Anderson HH et al. (1982) Primary amyloidoma of the spine. J Comput Assist Tomogr 6:1175–1177

Peh WC, Khong PL, Yin Y et al. (1996) Imaging of pelvic insufficiency fractures. Radiographics 16:335–348

Pollack JA, Schiller AL, Crawford JD (1973) Rickets and myopathy cured by removal of a non-ossifying fibroma of bone. Pediatrics 52:364–372

Popotvtzer MM (1981) Tumor-induced hypophosphatemic osteomalacia: evidence for a phosphatur ic cyclic AMP-independent action of tumor extract. Clin Res 29:418A

Rao DS, Parfitt AM, Villanueva AR et al. (1987) Hypophosphatemic osteomalacia and adult Fanconi syndrome due to light-chain nephropathy. Another form of oncogenous osteomalacia. Am J Med 82:333–338

Resnick D (2002) Parathyroid disorders and renal osteodystrophy. In: Resnick D (ed) Diagnosis of bone and joint disorders. WB Saunders, Philadelphia, pp 2043–2111

Ross LV, Ross GJ, Mesgarzadeh M et al. (1991) Hemodialysis related amyloidomas of the bone. Radiology 178:263–265

Sattari A, Quillard A, Laredo J et al. (2008) Benign nontraumatic osteolytic vertebral collapse simulating malignancy. Eur Radiol 18: 631–638

Schapira D, Ben Izhak O, Nachtigal A et al. (1995) Tumour-induced osteomalacia. Semin Arthritis Rheum 25:35–46

Simoens WA, Van den Hauwe L, Van Hedent et al. (2000) Amyloidoma of the skull base. AJNR Am J Neuroradiol 21:1559–1562

Sparagana M (1987) Tumour-induced osteomalacia: long-term follow-up of two patients cured by removal of their tumours. J Surg Oncol 36:198–205

Spuentrup E, Buecker A, Adam G et al. (2001) Diffusion-weighted MR imaging for differentiation of benign fracture edema and tumor infiltration of the vertebral body. AJR 176:351–358

Sundaram M, McCarthy EF (2000) Oncogenic osteomalacia. Skeletal Radiol 29:117–124

Sundaram M, Seelig R, Pohl D (1987) Vertebral erosions in patients undergoing maintenance hemodialysis for chronic renal failure. AJR 149:323–327

Sundaram M, Wang L, Rotman L (2001) Florid reactive periostitis and bizarre parosteal osteochondromatous proliferation: pre-biopsy imaging evolution, treatment and outcome. Skeletal Radiol 30:192–198

Takeuchi Y, Suzuki H, Ogura S et al. (2004) Venous sampling for fibroblast growth factor-23 confirms preoperative diagnosis of tumor-induced osteomalacia. J Clin Endocrinol Metab 89:3979–3982

Tang G, Liu Y, Li W et al. (2007) Optimization of b value in diffusion-weighted MRI for the differential diagnosis of benign and malignant vertebral fractures. Skeletal Radiol 36:1035–1041

Vogler JB III, Murphy WA (1988) Bone marrow imaging. Radiology 168:679

Wagner AD, Mai U, Hammer M et al. (1997) Long–term antibiotic therapy in patients with SAPHO syndrome (abstract). Arthritis Rheum 40:562

Wyman AL, Paratinas FJ, Daly JR (1997) Hypophosphatemic osteomalacia associated with a malignant tumour of the tibia: report of a case. J Clin Pathol 30:328–335

Yuh WT, Zachar CK, Barloon TJ et al. (1989) Vertebral compression fractures: distinction between benign and malignant causes with MR imaging. Radiology 172:215–218

Zhou XJ, Leeds NE, McKinnon GC (2002) Characterization of benign and metastatic vertebral compression fractures with quantitative diffusion MR imaging. AJNR Am J Neuroradiol 23:165–170

Tumours of the Ribs and Clavicle

31

David Malfair and Peter L. Munk

CONTENTS

KEY POINTS

- Primary bone tumours of the ribs, clavicle and sternum are uncommon.
- Infection and stress-related injuries often present as clavicle pseudotumours.
- The majority of tumours of the clavicle are malignant and the most common are plasmacytoma, osteosarcoma and Ewing's sarcoma.
- Aneurysmal bone cysts and eosinophilic granuloma are the most common benign lesions of the clavicle.
- Myeloma, chondrosarcomas and Ewing's sarcoma are the most common primary bone tumours that involve the ribs.
- Enchondromas and fibrous dysplasia are the most common benign rib lesions.
- The majority of tumours of the sternum are malignant, and the most common are chondrosarcoma, myeloma and osteosarcoma.

31.1 Tumours of the Clavicle

Primary tumours of the clavicle are uncommon. In one literature review, 0.45% of 13,000 primary bone tumours involved the clavicle. The majority of these lesions were malignant (Klein et al. 1979). Due to their rarity, most reports on tumours involving the clavicle are case reports or small case series. Several non-tumoral lesions particular to the clavicle, such as osteitis condensans and SAPHO (synovitis, acne, pustulosis, hyperostosis and osteitis), have a characteristic imaging appearance that may obviate biopsy. An approach to forming a differential in these patients that includes the imaging appearance and the age of the patient is discussed herein. Previous chapters provide a more detailed description of each entity.

D. Malfair, MD
Department of Radiology, Vancouver General Hospital, University of British Columbia, 899 West 12th Avenue, Vancouver, BC, V5Z 4E3, Canada

P. L. Munk, MD
Professor and Head, Musculoskeletal Division, Department of Radiology, Vancouver Hospital and Health Sciences Centre, 855 West 12th Avenue, Vancouver, B C V5Z 1M9, Canada

31.1.1 Non-aggressive Sclerotic Lesions of the Clavicle

Several malignant tumours may present with extensive sclerosis and expansion of a clavicle without destruction. These tumours include osteoblastic metastases, lymphoma, Ewing's sarcoma and osteosarcoma; however, this gamut includes a large number of non-tumoral entities. Examples of benign sclerotic lesions referred for biopsy include degenerative change of the sternoclavicular joint, osteitis condensans, SAPHO, radiation, osteomyelitis and Paget's disease. Most of these benign pseudotumours occur in older patients. Osteomyelitis and SAPHO are the exceptions to this rule and may occur at any age.

Degenerative change of the sternoclavicular joint sometimes manifests as a palpable abnormality and presents to the radiologist with a request for biopsy. These pseudotumours are more common after resection of the sternocleidomastoid muscle in a modified radical neck dissection for head and neck cancer (Islam et al. 2006). Significant sclerosis and irregularity of the medial clavicle may occur. The identification of similar changes on the sternal side of the articulation confirms the diagnosis of an arthropathy.

Osteitis condensans is a rare disorder of the clavicle that classically occurs in females older than 30 years. It is characterized by pain with the absence of local or systemic inflammatory symptoms. Sclerosis and enlargement of the medial clavicle is present on radiographs. It tends to affect the inferior aspect of the medial clavicle in most cases. Absence of sternoclavicular joint arthritis and lack of associated soft tissue mass on cross-sectional imaging are important findings (Fig. 31.1). The hypothesized mechanical aetiology of this disorder is supported by the classic history of lifting heavy weights and reinforcement of trabeculae seen on histology (Brower et al. 1974). Some authors recommend histological confirmation in every case; others advocate close follow-up if characteristic clinical and imaging features are present (Kruger et al. 1987).

SAPHO is an acronym referring to a syndrome characterized by synovitis, acne, pustulosis, hyperostosis and osteitis. SAPHO is an incompletely understood entity that involves a spectrum of disorders with similar clinical, radiological and pathological characteristics. These characteristics include sternocostoclavicular hyperostosis, acne-associated spondyloathropathy and chronic recurrent multifocal osteomyelitis (Sugimoto et al. 1998). The aetiology is debated. Hypotheses include a direct infection/autoimmune response to a low-grade pathogen vs a manifestation of a seronegative spondyloarthropathy (Earwalker and Cotton 2003). In adults, the sternocostoclavicular region is the most frequent site of involvement. Radiographic hallmarks include sclerosis and expansion of the involved bone. Anklyosis and osseous erosions are frequently seen. If confined mainly to the medial clavicle, soft tissue changes are helpful in distinguishing this entity from osteitis condensans of the clavicle. A confident imaging diagnosis can be made if the manubrium is involved. The bull's-head appearance on bone scintigraphy is highly characteristic of this entity and may obviate biopsy (Freyschmidt and Sternberg 1998). *Proprionibacterium acnes* has been repeatedly isolated in these lesions in both open and needle biopsies with various ranges of sensitivities to antibiotics (Kirchoff et al. 2003). Some authors describe clinical improvement with antibiotic treatment in *P. acnes*-positive cases rather than those with negative culture (Wagner et al. 1997). Biopsy for culture and sensitivity may be required on this basis. Pre-procedure MR imaging improves biopsy yield by targeting areas of T2 prolongation.

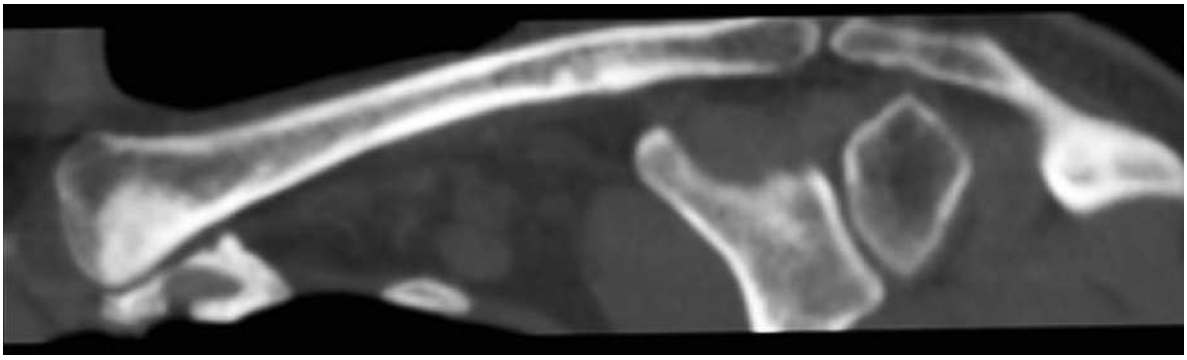

Fig. 31.1. Osteitis condensans of the clavicle. Coronal curved multiplanar reformatted CT image demonstrates characteristic sclerosis of the inferior aspect of the clavicle. Mild periosteal reaction without soft tissue mass was noted on transverse images

Osteomyelitis has a protean appearance in the clavicle and may be characterized by lytic, sclerotic or mixed changes. The medial aspect of the clavicle is most commonly involved, often in concert with sternoclavicular septic arthritis (Gerscovich and Greenspan 1994). Abnormalities are generally extensive. It would be unusual for osteomyelitis to involve less than 2 cm of the clavicle. In most cases, the lesions are painful and systemic symptoms are present. Biopsy is often required for confirmation and culture and sensitivity, and acute infections are treated aggressively (Robinson et al. 2008).

Radiation changes may result in diffuse or partial sclerosis of the clavicle. When present, radiation changes in the subjacent lung apex are a helpful imaging finding. Clinical history is the key to diagnosis. Approximately 13% of those patients with Paget's disease have clavicular involvement. It is usually asymptomatic and tends to involve the medial clavicle. Hallmark radiographic features include cortical thickening and coarsened trabeculae often involving the majority of the clavicle (Mirra et al. 1995).

Lymphoma, Ewing's sarcoma, eosinophilic granuloma and osteosarcoma are considerations when a young patient presents with sclerosis of the clavicle. Although cortical destruction and an associated soft tissue mass are usually present, they may mimic benign lesions. Metastatic disease should be a strong consideration in the older patient with a sclerotic lesion in the clavicle. A history of primary, especially breast or prostate, carcinoma is usually present. Bone scintigraphy can be helpful to identify additional lesions.

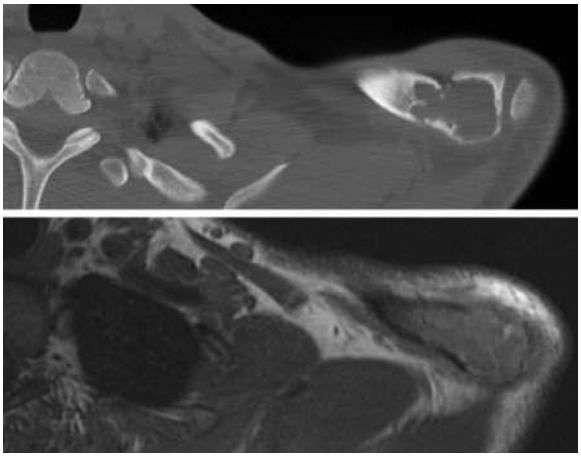

Fig. 31.2. Ewing's sarcoma of clavicle. Transverse CT image demonstrates a pathological fracture through a well-defined, non-aggressive-appearing lesion of the distal clavicle. Transverse T1-weighted MR image demonstrates no significant soft tissue mass

31.1.2 Non-aggressive Lucent Lesions of the Clavicle

Most tumours of the clavicle are malignant and masses with a non-aggressive appearance should be treated with suspicion. Metastases and myeloma are the most common cause of lucent clavicular lesions in patients over 40 years. Other primary sarcomas of the clavicle may present with a non-aggressive appearance (Fig. 31.2). In younger patients, eosinophilic granuloma and aneurysmal bone cysts have a predilection for the clavicle. Most other benign lesions, including giant cell tumour, osteoblastoma, unicameral bone cyst and fibrous dysplasia, are seldom found in the clavicle. In general, cartilage-forming tumours are rarely found in the clavicle. This is likely on the basis that the clavicle is largely formed from membranous ossification. Endochondral ossification does occur at the sternal and acromial ends.

Several pseudotumours may present as a lucent lesion of the clavicle. The rhomboid fossa is a normal variant consisting of a prominent lucency along the inferior aspect of the medial clavicle at the attachment site of the costoclavicular ligament. When large and asymmetric it may be mistaken for a destructive neoplasm (De Wilde et al. 2003). Post-traumatic osteolysis of the distal clavicle may occur as an acute traumatic event or secondary to chronic stress (Cahill 1982). Characteristic radiographic features include erosions, resorption of the subchondral bone of the distal clavicle and widening of the AC joint. On MR imaging prominent T2 prolongation of the distal clavicle may simulate a mass lesion. The presence of low signal intensity lines adjacent to the acromioclavicular joint likely represent subchondral fractures and allow accurate diagnosis (Kassarjian et al. 2006).

Aneurysmal bone cysts are not uncommon in the clavicle, with involvement between 3 and 4% in most series (Sabanathan et al. 1984); the majority occur in patients under 20 years. In one series of six cases, all cysts occurred in the distal clavicle with eccentric expansion (Smith et al. 1988). Eosinophilic granuloma involves the clavicle in approximately 4% of cases. The appearance is variable as in other sites of the body, but a well-defined lucent lesion is the most common manifestation. Prominent periosteal reaction and aggressive appearance may be seen, particularly when cortical destruction is present (Stull et al. 1992). A predilection for the distal clavicle has been noted (Smith et al. 1988). Brown tumours of hyperthyroidism may also be occasionally found.

31.1.3 Aggressive-Appearing Clavicular Lesions

The three most common primary tumours of the clavicle are myeloma, osteosarcoma and Ewing's sarcoma (Dahlin and Unni 1986). The literature provides little insight into their particular behaviour within the clavicle. Metastatic lesions are a prime consideration in older patients with a clavicular lesion. Multiple myeloma is the most common primary bone tumour of the clavicle. These lesions are usually purely lytic, medullary based and demonstrate endosteal scalloping. Findings may be very subtle on radiography and are better characterized on CT and MR imaging. Plasmacytomas occur in the clavicle in 5% of cases. Solitary plasmacytomas may have a benign or aggressive appearance and the diagnosis can be difficult without biopsy. Approximately 3% of primary bone lymphoma involves the clavicle and may occur at any age. In young children, periosteal reaction is often the dominant feature. A permeative lytic pattern is most common in older patients. A soft tissue mass is less common than in Ewing's sarcoma, a potential differentiating feature.

Primary osteosarcomas tend to involve the distal clavicle (Smith et al. 1988). An unusual feature of osteosarcomas at this location is their presentation as a lytic destructive mass. Osteoid matrix is less common than at other sites. Secondary osteosarcoma occurs in an older population. Underlying Paget's disease or a history of radiation is usually present. These secondary osteosarcomas often involve the entire clavicle.

The clavicle is involved in approximately 1% of Ewing's sarcoma (Cotterill et al. 2000). Patients with clavicular involvement may be slightly older than typical for Ewing's sarcoma, but nearly all patients are under 35 years. Permeative destruction, periosteal reaction and soft tissue mass are common; however, some Ewing's sarcomas have a non-aggressive appearance (Fig. 31.2). The most common differential is chronic osteomyelitis. In a recent series of 59 patients referred for clavicular tumors, all 17 patients referred for Ewing's sarcoma were eventually diagnosed with chronic recurrent multifocal osteomyelitis (CRMO; Suresh and Saifuddin 2008). Eleven of these cases were biopsied, all of which were culture negative. In contradistinction to Ewing's sarcoma, soft tissue masses are uncommon in CRMO, occurring in only one case in this series. Bone scintigraphy often demonstrates additional areas of radiotracer uptake in these cases and may assist a preoperative diagnosis of infection.

Chondrosarcomas are rare in the clavicle. When present, they are generally found in the ends of the clavicle (where endochondral ossification occurs) or secondary to malignant degeneration of an osteochondroma. In one series of five clavicular chondrosarcomas, four involved the distal clavicle. Patients were younger is this series than typical for chondrosarcoma, with all four being in the third or fourth decade of life. MFH or fibrosarcoma of bone may also affect the clavicle. A history of radiation is often present and a medial location was noted in one case series (Smith et al. 1988).

31.2 Ribs

Primary tumours of the rib are uncommon, comprising 3.5–8% of primary bone tumours in most series (Barrett 1955; Dahlin and Unni 1986). Metastases and myeloma are the first and second most common tumours of the ribs, respectively, and should be considered in the differential in most rib masses. Other primary tumours are rare. In a review of 325,000 chest radiographs only 10 cases of incidental primary rib tumours were discovered (Condon and Harper 1950). Location of a tumour within the rib may aid in forming a differential. Cartilaginous tumours tend to occur near the costochondral junction (68%) or posteriorly (26%), rather than within the shaft of the rib (6%; Marcove and Huvos 1971) Myeloma, metastatic disease and fi-

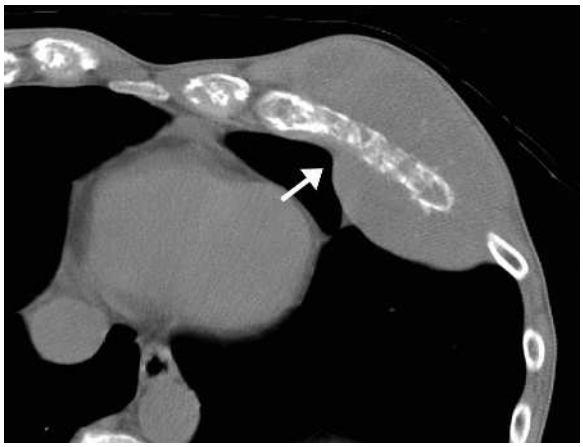

Fig 31.3. Chondrosarcoma of rib. Transverse CT imaging demonstrates an aggressive lesion of the anterior rib with an associated soft tissue mass. Minimal calcified matrix is present. Rib lesions generally have a smooth interface with the lung displaced the subpleural fat towards the lung (*arrow*)

brous dysplasia are more likely to affect the shaft of the rib.

Rib lesions may grow quite large before presenting as a chest wall mass. Rib sarcomas more commonly present with pain; over 60% in one series (Walsh and Putnam 2001). When large, it may prove challenging to differentiate a primary rib lesion from a lesion arising from the lung and involving the rib. Primary rib lesions tend to be centered on the rib, have a smooth interface with the lung and deviate the pleural and extrapleural fat towards the lung (Fig. 31.3).

31.2.1 Sclerotic, Intramedullary Lesions of the Rib

The differential diagnosis for a sclerotic, intramedullary lesion of the ribs includes osteoblastic metastases, osteoblastoma, osteosarcoma, osteoid osteoma, Paget's disease, calcifying enchondroma and ossifying fibroxanthoma; of these, osteoblastic metastases are the most common and should always be the primary consideration in patients over 40 years. Prostate, breast, neuroendocrine and bladder primaries are common primaries that lead to sclerotic metastases. Healing rib fractures are common mimics of osteoblastic metastases and have a characteristic imaging appearance. The sclerotic abnormality tends to be oriented perpendicular to the long axis of the rib, occurs at multiple locations and may be associated with deformity. Enostoses are common in the ribs (second only to the pelvis) with a 0.4% prevalence in the population. They characteristically demonstrate homogenous density similar to cortical bone with feathered, radiating bony margins on radiographs and computed tomography (Greenspan 1995). This characteristic appearance coupled with negative bone scintigraphy in an asymptomatic patient can reliably diagnose an enostosis even in the circumstance of a known primary tumour. Occasionally, scintigraphy may be positive which can make evaluation more challenging. In these difficult cases, biopsy may be necessary if the growth rate exceeds 25% increase in diameter in 6 months or 50% increase in 1 year (Brien 1995).

Less than 1% of osteoid osteomas involve the ribs. When present, they tend to involve the posterior or posterolateral shaft of the rib. They present with similar imaging features in the ribs as elsewhere in the body, with prominent sclerosis surrounding a central radiolucent nidus. Patients may present with a painful scoliosis or a pleural effusion (Mehdian 1988). Computed tomography is the best modality for assessing these lesions due to their accuracy in detecting the nidus. Reports of lesions with an identical imaging appearance and histology, but different clinical manifestations, have been reported. These lesions are asymptomatic and often incidentally detected on bone scintigraphy. Some propose that these lesions represent a distinct clinicopathological entity (McCarthy et al. 1985). Osteoblastomas occur commonly in the ribs, as much as 5–10% in some series (McLeod et al. 1976). These tumours also tend to occur posteriorly in the ribs but are larger, often associated with a soft tissue mass, often have osseous matrix and are seldom painful – in contradistinction to osteoid osteomas.

Approximately 2% of Paget's disease involves the ribs (Mirra 1995). Paget's disease of the rib appears similar to other sites with coarsening of the trabeculae and cortex, sclerosis and expansion of the rib. Lymphoma, osteosarcoma, infection and other primary malignancies of the rib may also present with ill-defined sclerosis of a rib; however, these other entities are usually associated with some element of cortical destruction and associated soft tissue mass.

31.2.2 Rib Lesions with Aggressive Appearance in Young Patient

Aggressive-appearing rib lesions in patients under 30 years are most commonly secondary to infection, lymphoma, Ewing's sarcoma, eosinophilic granuloma and osteosarcoma. Ewing's sarcoma is common in the ribs, accounting for 6–12% of cases (Paulussen et al. 2001). It usually presents with lytic destruction of a rib (80%), although a partially sclerotic (10%) or dominantly sclerotic appearance may also occur (Moser et al. 1990). Extensive periosteal reaction related to Ewing's sarcoma is less common in the rib than in other sites. An associated soft tissue mass is a helpful differentiating feature. A large soft tissue mass was noted in 32 of 34 cases in one series (Moser et al. 1990), averaging 11 cm in diameter and engulfing the rib. The lateral aspect of the rib is involved most commonly. Unfortunately, location is not helpful in ordering a differential, as it can occur anywhere. A solitary eosinophilic granuloma may mimic this appearance in young patients. Eosinophilic granulomas are less common and tend to have a smaller soft tissue component (Jabra and Fishman 1992). Primary lymphoma of rib presents in a similar fashion.

Osteosarcoma involves the ribs in 1–3% of cases (Deitch et al. 2003). There is a higher tendency for these tumours to occur in older patients as a secondary phenomenon in patients with Paget's disease or history

of radiation. Primary osteosarcomas are rare but do occur in younger patients (Abdulrahman et al. 1995). They classically present as a large calcified mass engulfing the rib. The characteristic cloudy osseous matrix is strongly suggestive of this diagnosis, although osteoblastomas may have a similar appearance. MFH of bone may occur in this age group but more commonly affects older patients.

Pyogenic and tuberculous osteomyelitis accounts for less than 1% of osteomyelitis in children and is rare in adults. In the past, it usually occurred via hematogenous spread (Dich et al. 1975), but more recent studies show a higher prevalence of contiguous spread from the lung, especially in cases of trauma or empyema (Bishara et al. 2000). Although hematogenous osteomyelitis presenting as a rib or sternal tumour is rare, it does occur and biopsy should be routinely sent for culture and sensitivity (Levinsohn et al. 1982). Acute osteomyelitis is usually characterized by periosteal reaction and cortical destruction. Soft tissue changes are almost always present. Sclerosis and expansion of the rib may occur in chronic osteomyelitis; however, mild sclerosis and expansion of the ribs may occur in the setting of chronic pleural and lung inflammatory disease, such as tuberculosis, in the absence of osteomyelitis. This likely occurs on the basis of chronic hyperemia (Eyler et al. 1996).

31.2.3 Rib Lesions with an Aggressive Appearance in the Older Patient

Metastases and myeloma are by far the most common cause of lesions in the older patient and should be at the top of any differential. Approximately 70% of malignant bone tumours are metastases, generally found in older patients. Metastases have a protean appearance and can mimic both benign and aggressive lesions. In most cases, a history of a primary malignancy is offered or multiple lesions are present. Scintigraphy may be valuable in this respect to show additional lesions that support a diagnosis of metastatic disease. A lesion in a safer location to biopsy may be also be identified. Rib metastases tend to be focal. It is unusual for a metastatic deposit to involve more than 5 cm of rib in a longitudinal fashion.

Multiple myeloma generally occurs in patients older than 40 years. Rib involvement is common, seen in 50% of patients. Multiple lesions are helpful in the diagnosis. Solitary plasmacytomas are uncommon in the rib (Fig. 31.4). Punched-out lytic lesions, often with associated soft tissue masses, are commonly observed. Lymphoma has a similar appearance. These lesions may occur anywhere but the mid-portion of the rib is characteristic.

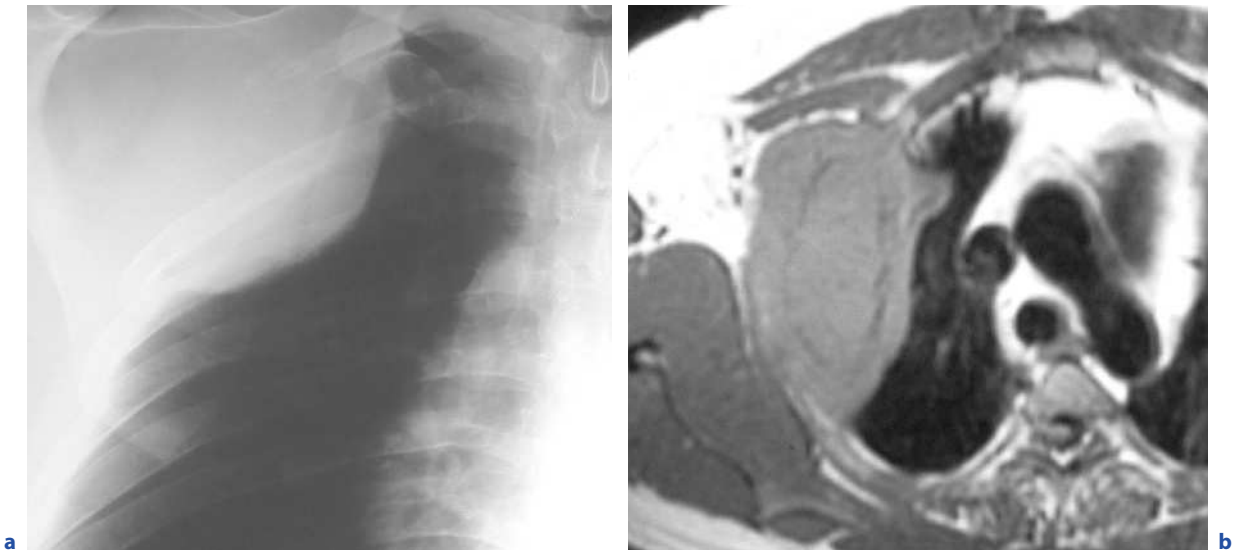

a b

Fig. 31.4a,b. Plasmacytoma of rib. Coned chest radiograph demonstrates an extra-pleural soft tissue mass associated with destruction of the lateral aspect of the second rib. Transverse T1-weighted image demonstrates marked expansion of the rib with surrounding soft tissue mass

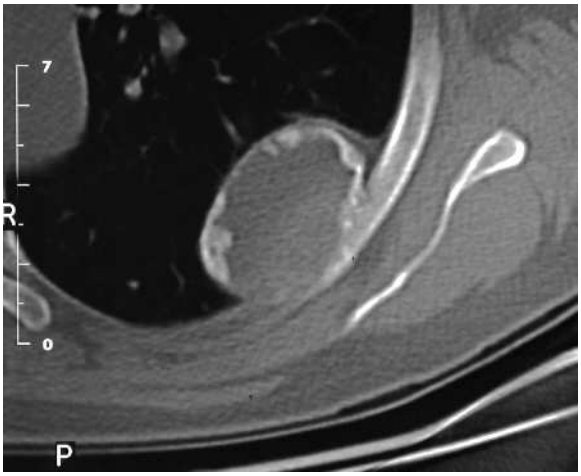

Fig. 31.5. Chondromxyoid fibroma of rib. Transverse CT demonstrates eccentric, peripherally calcified mass arising from the inner aspect of the posterolateral rib. The underlying rib is minimally affected

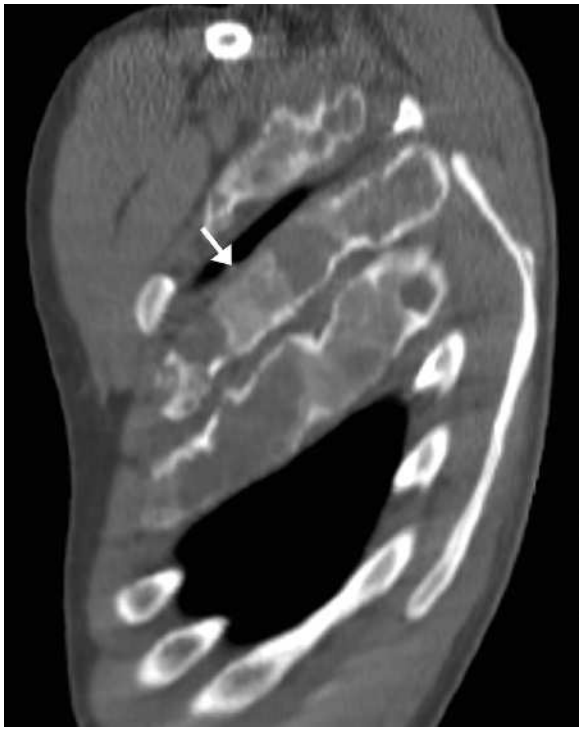

Fig. 31.6. Polyostotic fibrous dysplasia of ribs. Oblique sagittal multiplanar reformatted CT image demonstrates extensive involvement of the ribs with fibrous dysplasia. Note the length of the rib involvement and the ground-glass matrix (*arrow*)

Approximately 9% of chondrosarcomas occur in the ribs making this the most common primary malignancy, other than myeloma, to affect this location. They typically occur in the anterior aspect or posterior aspect of the rib, and are usually associated with a soft tissue mass (Fig. 31.3). Chondroid calcification can strongly suggest the diagnosis. Other chondroid forming tumours, such as chondroma, chondromyxoid fibroma and chondroblastoma of the ribs, may occur but are rare (Fig. 31.5). MFH of bone is an uncommon lesion that has a predilection for the ribs in 5% of cases. In one series of 51 patients with chest wall sarcomas, 15 presented with chondrosarcoma and 9 with MFH of bone (Walsh and Putnam 2001). It has a non-specific appearance with destruction and soft tissue mass. Osteogenic sarcomas usually occur secondary to underlying Paget's disease or as a sequelae of radiation in older patients.

31.2.4 Rib Lesions with Non-aggressive Appearance in a Young Patient

Fibrous dysplasia represents the most common benign neoplasm of the ribs (Anderson and Burt 1994). Monostotic fibrous dysplasia involves the ribs in 5–20% in most series, with a predilection for the second rib (Henry 1969). Approximately half of patients with polyostotic fibrous dysplasia have rib involvement. Radiologically, the lesions are centrally located within the rib and may be mildly expansile. Soft tissue changes are uncommon in the absence of pathological fracture or malignant degeneration. In general, they occur posterior and lateral in the ribs, although in some cases the abnormality may extend the length of the rib, unusual for most other entities. A ground-glass matrix is frequently present, although the lesions are lucent or sclerotic in other cases (Fig. 31.6).

Enchondromas are the second most common rib tumour, accounting for 2–12% of primary rib tumours not

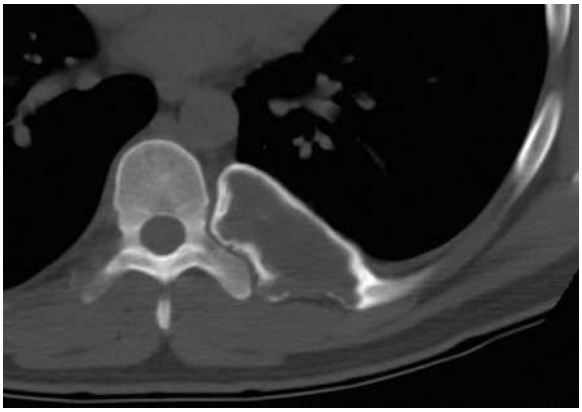

Fig. 31.7. Enchondroma of rib. Transverse CT image demonstrates lucent, well-defined, mildly expansile lesion of posterior rib. No evidence of matrix calcification is present in this example

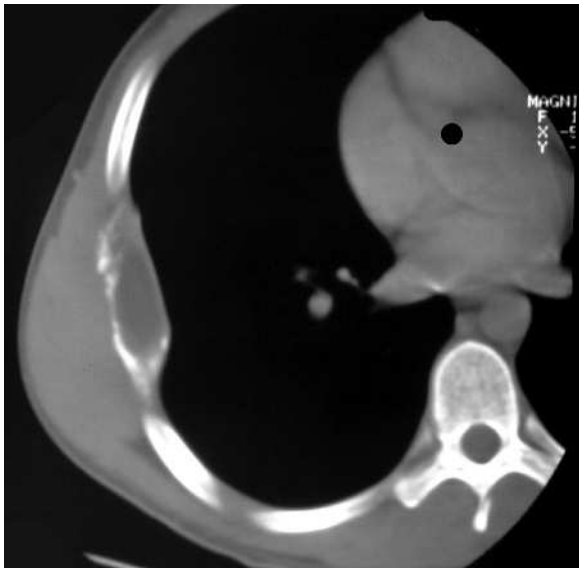

Fig. 31.8. Unicameral bone cyst of rib. Transverse CT demonstrates moderately expansile, non-aggressive lesion of the lateral rib

including myeloma (Hughes et al. 2006). As previously mentioned it has a predilection for the anterior and posterior aspects of the ribs. Enchondromas are usually well defined, under 4 cm and mildly expand the rib (Fig 31.7). Prominent expansion can be more common in the ribs and is termed enchondroma protuberans. CT can be helpful to identify calcified chondroid matrix. On MR imaging, these lesions have high signal on T2 and low signal on T2 due to the high water content of cartilage is present. When heavily calcified, susceptibility artefact reduces signal intensity on all sequences. Osteochondromas may simulate the appearance of enchondroma protuberans. Solitary osteochondromas are seldom found in the ribs, accounting for 1–4% of cases (Barrett 1955). They are more commonly found in patients with diaphyseal aclasia with a prevalence of around 50%. They may occur at any location but most commonly are seen anteriorly. Cross-sectional imaging is diagnostic, demonstrating communication of the lesion with the medullary cavity and presence of cartilaginous matrix in a cartilage cap. Chondroblastomas and chondromyxoid fibromas are very rare in the ribs but are included in the differential diagnosis when cartilaginous matrix is identified.

The ribs are the location of aneurysmal bone cysts in 2–3% of cases, generally occurring in younger patients (Sabanathan et al. 1984). The posterior and lateral ribs are most commonly affected. They are frequently expansile with fluid-fluid levels noted on cross-sectional imaging. A soft tissue component is unusual. Osteoblastomas may present in a similar fashion and may also demonstrate fluid-fluid levels. Most other expansile osseous lesions without cortical destruction (giant cell tumour, unicameral bone cysts) are rarely found in the ribs but may occur (Fig. 31.8; Marsh et al. 1982).

31.2.5 Rib Lesions with Non-aggressive Appearance in the Older Patient

Most of these lesions have been discussed previously. Again, the most common non-aggressive lesions in older patients are metastases and myeloma. Fibrous dysplasia and enchondromas less commonly present in older patients but remain considerations. Brown tumours of hyperparathyroidism may also occur and are generally multiple. Most other benign lesions tend to be unusual in older patients.

31.3 Sternal Tumours

The most common sternal tumours are metastases – most commonly from the malignant tumours of breast, lung, kidney and thyroid (Fig. 31.9). The large

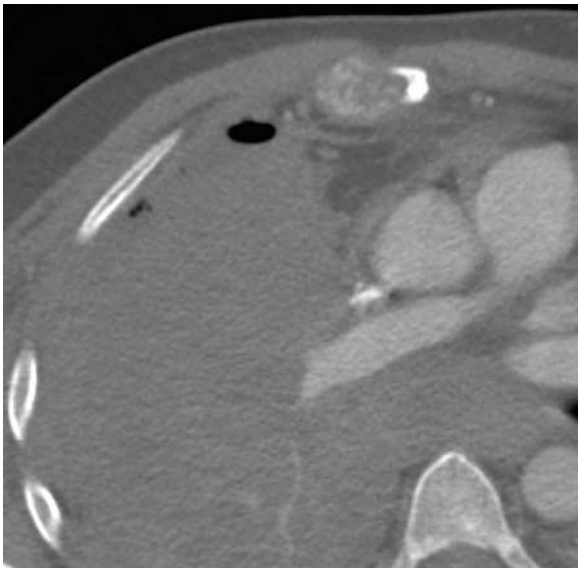

Fig. 31.9. Lung metastasis to sternum. Aggressive, destructive lesion along the lateral body of the sternum. Note large adjacent malignant pleural effusion from primary bronchogenic cancer

majority of primary sternal lesions are malignant and should be considered so until proven otherwise. Chondrosarcoma is the most common primary, followed by myeloma, lymphoma and osteosarcoma. Computed tomography is valuable in characterizing tumour matrix and aiding in the differential. Chondrosarcomas are usually found at the junction of the ribs. A lobulated contour and chondroid calcification suggest the diagnosis. Solitary plasmacytomas are relatively common in the sternum comprising 5–25% of primary sternal tumours. (Dahlin and Uhni 1986) Osteosarcomas of the sternum usually occur secondary to radiation.

References

Abdulrahman RE, White CS, Templeton PA (1995) Primary osteosarcoma of the ribs: CT findings. Skeletal Radiol 24:127–129

Anderson BO, Burt ME (1994) Chest wall neoplasms and their management. Ann Thorac Surg 58:1774–1781

Barrett NR (1955) Primary tumours of the rib. Br J Surg 43:13–132

Bishara J, Gartman-Israel D, Weinberger M et al. (2000) Osteomyelitis of the ribs in the antibiotic era. Scand J Infect Dis 32(3):223–227

Brien EW, Mirra JM, Lotanza L et al. (1995) Giant bone island of femur. Skeletal Radiol 24:546–550

Brower A, Sweet DE, Keats TE (1974) Condensing osteitis of the clavicle. A new entity. Am J Roentgenol 121:17–21

Cahill BR (1982) Osteolysis of the distal part of the clavicle in male athletes. J Bone Joint Surg (Am) 64(7):1053–1058

Condon WB, Harper FR (1950) Tumors of the chest wall. Dis Chest 17:741–755

Cotterill SJ, Ahrens S, Paulussen M (2000) Prognostic factors in Ewing's tumor of bone: analysis of 975 patients from the European Intergroup Cooperative Ewing's Sarcoma Study Group. J Clin Oncol 18(17):3108–3114

Dahlin DC, Unni KK (1986) Bone tumors: general aspects and data on 8542 cases, 4th edn. Thomas, Springfield, p 12

De Wilde V, De Maesesneer M, Lenchik L et al. (2004) Normal osseous variants presenting as cystic or lucent areas on radiography and CT imaging. Eur J Radiol 51(1):77–84

Deitch J, Crawford AH, Choudhury S (2003) Osteogenic sarcoma of the rib. Spine 28(4):274–277

Dich VQ, Nelson JD, Haltalin KC (1975) Osteomyelitis in infants and children. A review of 163 cases. Am J Dis Child 129:1273–1278

Earwalker JWS, Cotton A (2003) SAPHO: Syndrome or concept? Imaging findings. Skeletal Radiol 32:311–327

Eyler JL, Monsein LH, Beute GH et al. (1996) Rib enlargement in patients with chronic pleural disease. AJR 167:921–926

Freyschmidt J, Sternberg A (1998) The bull's head sign: scintigraphy pattern of sternoclavicular hyperostosis and pustulotic arthrosclerosis. Eur Radiol 8:807–812

Gerscovich EO, Greenspan A (1994) Osteomyelitis of the clavicle, clinical, radiologic and bacteriologic findings in ten patients. Skeletal Radiol 23(3):205–210

Greenspan A (1995) Bone island (enostosis): current concept – a review. Skeletal Radiol 24:111–115

Henry A (1969) Monostotic fibrous dysplasia. J Bone Joint Surg (Br) 51(2):300–306

Hughes EK, James SLJ, Butt S et al. (2006) Benign primary tumours of the ribs. Clin Radiol 61:314–322

Islam S, Walton GM, Hoffman GR (2006) Sternoclavicular joint pseudo-tumor: a case report and literature review. J Laryngol Otol 120(11):e39

Jabra AA, EK Fishman (1992) Eosinophilic granuloma simulating an aggressive rib neoplasm: CT evaluation. Pediatr Radiol 22(6):447–448

Kassarjian A, LLopis E, Palmer WE (2006) Distal clavicular osteolysis: MR evidence for subchondral fracture. Skeletal Radiol 36:17–22

Kirchhoff T, Merkesdal S, Rosenthal H et al. (2003) Diagnostic management of patients with SAPHO syndrome: use of MR imaging to guide bone biopsy at CT for microbiological and histological work-up. Eur Radiol 13:2304–2308

Klein MJ, Lusskin R, Becket MH et al. (1979) Osteoid osteoma of the clavicle. Clin Orthop 143:162–164

Kruger GD, Rock MG, Munor TG (1987) Condensing osteitis of the clavicle. A review of the literature and report of three cases. J Bone Joint Surg (Am) 69:550-557

Levinsohn EM, Sternick A, Echeverria TS et al. (1982) Acute hematogenous osteomyelitis of the rib. Skeletal Radiol 8(4):291–293

Marcove RC, Huvos AC (1971) Cartilaginous tumours of the ribs. Cancer 27:794–801

Marsh JI, Munk PL, Muller NL (1982) CT of a unicameral bone cyst of rib. Br J Radiol 65(769):74–75

McCarthy EF, Moses DC, Zibreg JW et al. (1985) Painless fibro-osseous lesion of the rib resembling osteiod osteoma: a report of six cases. Skeletal Radiol 13:263–266

McLeod RA, Dahlin DC, Beabout JW (1976) The spectrum of osteoblastoma. AJR 126:321–335

Mehdian H, Summers B, Eisenstein S (1988) Painful scoliosis secondary to an osteoid osteoma of the rib. Clin Orthop 230:273–276

Mirra JM, Brien EW, Tehranzadeh (1995) Paget's disease of bone: review with emphasis on radiologic features, part I. Skeletal Radiol 24:163–171

Moser RP, David MJ, Gilkey FW et al. (1990) Primary Ewing sarcoma of rib. Radiographics 10:899–914

Paulussen M, Ahrens S, Dunst J (2001) Localized ewing tumor of bone: final results of the cooperative Ewing's sarcoma study CESS 86. J Clin Oncol 19:1818–1829

Robinson CM, Jenkins PJ, Markam PE (2008) Disorders of the sternoclavicular joint. J Bone Joint Surg (Br) 90-B(6):685–696

Sabanathan S, Chen K, Robertson CS et al. (1984) Aneurysmal bone cyst of the rib. Thorax 39:125–130

Smith J, Yuppa F, Watson RC (1988) Primary tumors and tumor-like lesions of the clavicle. Skeletal Radiol 17:235–246

Stull MA, Kransdorf MJ, Devaney KO (1992) Langerhans cell histiocytosis of bone. Radiographics 12:801–823

Sugimoto H, Tamura K, Fujii T (1998) The SAPHO syndrome: defining the radiologic spectrum of diseases comprising the syndrome. Eur Radiol 8:800–806

Suresh S, Saifuddin A (2008) Unveiling the "unique bone": a study of the unique distribution of clavicular lesions. Skeletal Radiol 37(8):749–756

Wagner AD, Mai U, Hammer M, Zeidler H (1997) Longterm antibiotic therapy successful in patients with SAPHO syndrome. Arthritis Rheum 40(S9):S62

Walsh GL, Putnam JB (2001) A single-institutional, multidisciplinary approach to primary sarcomas involving the chest wall requiring full-thickness resections. J Thorac Cardiovasc Surg 121:48–60

Scapula

32

Suzanne E. Anderson-Sembach, Rainer Erlemann, Peter Choong and Gernot Jundt

CONTENTS

S. E. Anderson-Sembach, MD, PD, CH
School of Medical Imaging, School of Medicine Sydney, The University of Notre Dame Australia, 160 Oxford Street Darlinghurst, Sydney NSW 2010, Australia *and* Department of Diagnostic, Pediatric and Interventional Radiology, Inselspital, University of Bern, 3010 Bern, Switzerland

R. Erlemann, MD
Department of Radiology, St. Johannes Hospital, Katholisches Klinikum Duisburg, An der Abtei 7–11, 47166 Duisburg, Germany

P. Choong, MD
Department of Orthopaedics, University of Melbourne, Department of Surgery St. Vincent´s Hospital, 41 Victoria Parade, Fitzroy 3065, Victoria Australia. Bone and Soft Tissue Tumour Service, Peter MacCallum Cancer Centre, St. Andrew´s Place, East Melbourne 3002, Victoria Australia

G. Jundt, MD
Bone Tumor Reference Center at the University Institute of Pathology, University Hospital Basel, Schoenbeinstrasse 40, 4031 Basel, Switzerland

32.1 Introduction and Background

Bone tumors are infrequent within the scapula. Lesions are reported with varying frequency between 0 and 8% (Erlemann et al. 1988; Resnick 1997; Brtvoka et al. 1999). A review of the Netherlands Bone Tumor Registry is summarized in Table 32.1. As it is a flat bone with complex anatomy, diagnosis and staging of tumors may be more difficult compared with long bones; therefore, use of a combination of imaging modalities is recommended.

A variety of malignant and benign tumors may occur within the scapula. Cartilaginous tumors are the most frequent, with benign osteochondroma having a more characteristic imaging appearance, and malignant chondrosarcoma which may have a more varied imaging appearance making them diagnostically more difficult (Erlemann et al. 1988; Brtkova et al. 1999). Regarding benign and malignant tumors in the pediatric age group, osteochondroma and Ewing's sarcoma, respectively, and in the adult age group, osteochondroma, chondrosarcoma, multiple myeloma, and metastases respectively, should be considered. The radiological findings and features of the tumors, and important information the tumor orthopedic surgeon needs to know, are discussed.

KEY POINTS

- Bone tumors are less common within the scapula.
- Characteristic imaging features may be present or absent.
- Being a flat bone with complex anatomy, diagnosis and staging of tumors may be more difficult compared with long bones.
- A combination of imaging modalities is best to characterize, stage, and preoperatively image these lesions.

32.1.1 Surgical and Treatment Options

Primary malignancies of the scapular present particular challenges for management. Not only do scapular tumors mimic benign conditions and may lead to misdiagnosis (Quan 2005), but their anatomic location also requires special considerations when contemplating surgical excision. These considerations include (1) the presence of adjacent vital neurovascular structures, (2) the early involvement of the glenohumeral joint, (3) involvement of the chest wall as a feature of late presentation of disease, and (4) location of the biopsy site. For these reasons, anatomic imaging is critical in delineating the extent of disease (Choong and Sim 2000).

32.1.1.1 Investigations

The key features that are important in the preoperative imaging of disease include the extent of the tumor, its soft tissue component and the capsule that invests the growth. It is vital to identify whether the tumor involves the supra- or infraspinous portions of the scapular, or both, and whether any soft tissue component is limited by the spinatus or subscapularis musculature. Furthermore, it is important to assess whether the glenohumeral joint is involved and this may be indicated by involvement of the biceps tendon, subscapular bursa, or if a joint effusion is present. Extension of the tumor through the subscapular fascia potentially endangers the axillary neurovascular structures and the radial nerve and profunda humerus vessels may be involved with tumors of the scapular that are close to the inferior

Table 32.1. Percentages of malignant and benign bone tumors and tumor-like lesions of the scapula compared to those of long bones (in %)

	n	OS	POS	ChSa	pChSa	Ewing	FibSa	MFH	Adam	Plasm	NHL
Malignant bone tumors											
Skapula	95	7		**24**	**17**	**17**	5	4		4	3
Humerus	542	**15**	2	8	1	7	3	3		1	1
Femur	1534	**31**	2	8	1	4	5	5		1	1
Tibia	862	**23**	1	4	2	4	1	3	2		

OS: osteosarcoma, *POS*: parosteal osteosarcoma, *ChSa*: chondrosarcoma, *pChSa*: peripheral chondrosarcoma, *FibSa*: fibrosarcoma *MFH*. malignant fibrous histiocytoma, Adam: adamantinoma, Plasm: plasmocytoma, *NHL*: Non-Hodgkin Lymphoma of bone

	O-O	OB	Ench	Och	Chbl	CMF	GCT	AKZ	SKZ	FD	NOF	EG
Benign bone tumors and tumor-like lesions												
Skapula		1		9				3		1		3
Humerus	2	1	4	8	6		6	4	**19**	4	2	2
Femur	3	1	3	3	3	1	8	2	3	6	7	2
Tibia	5	1	2	3	4	2	**14**	5	1	6	**16**	1

O-O: osteoid-osteoma, *OB*: osteoblastoma, *Ench*: enchondroma, *Och*: osteochondroma, *Chbl*: chondroblastoma, *CMF*: chondromyxoidfibroma, *GCT*: giant cell tumor, AKZ: aneurysmal bone cyst, SKZ.: solitary bone cyst, FD. fibrous dysplasa, NOF: non-ossifying fibroma, EG: eosinophilic granuloma

Calculated from Daten: Mulder JD, Schütte HE, Kron HM, Taconis WK. Radiological Atlas of Bone tumors. Elsevier, Amsterdam, 1993, S. 20–21

aspect of the glenoid. Supraspinous tumors may endanger the suprascapular vessels and nerves. Understanding the relationship of the tumor to the aforementioned structures is critical for planning the appropriate resection margin and biopsy path.

32.1.1.2 Biopsy

All primary tumors must be biopsied prior to definitive treatment. All imaging should be completed prior to biopsy as biopsy artifact may confound the interpretation of anatomic imaging, particularly MRI. Functional nuclear imaging with PET or thallium scanning is ideal for targeting areas of high metabolic activity and can accurately guide needle biopsy when combined with co-registration of CT or MRI images. More importantly, functional nuclear scans assist in identifying areas of tumor necrosis which are to be avoided when undertaking biopsy.

In principle, biopsy should be conducted only after close consultation with centers expert in the management of primary bone and soft tissue tumors. The location of the biopsy tract must be carefully planned as inappropriate biopsy may jeopardize the potential for limb-sparing surgery and lead to unnecessary amputation. Whether an incisional or percutaneous biopsy is chosen, the biopsy path must be placed in line with the planned incision to allow excision of the biopsy tract (Fig. 32.1). Computer-guided needle biopsy is the preferred technique and is associated with fewer biopsy-related complications (Altuntas et al. 2005). Most scapular biopsies should be performed from a posterior approach in line with an incision that passes from the inferior angle of the scapular to the midpoint of the scapular spine then laterally along the scapular spine to the posterior then anterior aspect of the acro-

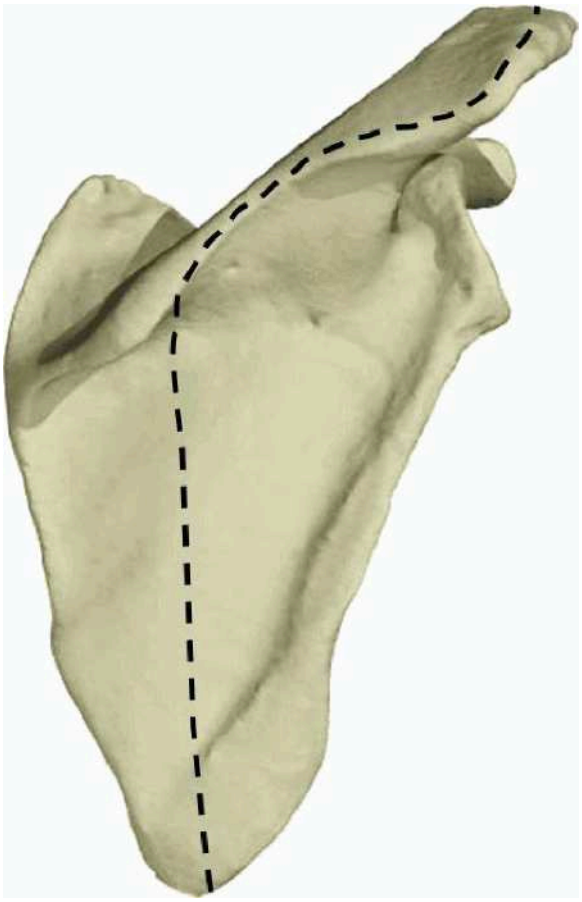

Fig. 32.1. Standard incision for posterior approach to scapula. Biopsy sites should be located along this incision

mion. Transaxillary approaches to the scapular should be avoided as injury or contamination of the contents of the axilla may lead to unacceptably high rates of local recurrence of tumor. An anterior approach to the scapular should only be reserved for corocoid process lesions.

32.1.1.3 Surgery

The main aim of surgery is to resect the tumor with wide surgical margins (Choong and Sim 2000). A wide margin is defined as a resection margin that is separated from the tumor by at least one normal anatomic layer or by at least one normal-named fascia. The subscapularis, infraspinatus, and supraspinatus fasciae are examples of such named fascial boundaries. Magnetic resonance imaging scans are ideal for demonstrating this fascial layer (Fig. 32.2); therefore, a tumor of the scapular which has as a layer the subscapularis, infraspinatus, or supraspinatus muscle is said to be excised with wide margins if the fascia surrounding the aforementioned muscles is included as part of the resection specimen. If the tumor engages any of these fasciae, then inclusion only of these fasciae is referred to as a marginal resection. Marginal resections are associated with a higher local recurrence rate than wide resections and should be avoided where possible. If avoidance of a marginal resection is not possible, then inclusion of neoadjuvant therapy, such as chemotherapy or radiotherapy, can improve or enhance the margin. Radiotherapy is specifically associated with the development of a rind of fibrous tissue around the tumor which is more resistant to recurrence than the inflammatory areolar tissue around a tumor.

Intra-articular extension of the glenohumeral joint is an early feature of scapular tumors (Fig. 32.3). Features that raise suspicion of this include involvement of the biceps tendon, which is an intra-articular structure, and involvement of the subscapularis bursa, which is frequently in continuity with the shoulder joint.

Chest wall extension of scapular tumors is a late feature of disease. This is because the soft tissue component of the tumor is usually a pushing rather than an invading structure and the subscapularis muscle and fascia and the chest wall muscles are good barriers to extension of disease. Involvement of the chest wall mandates resection of the latter. Passage of tumor through the

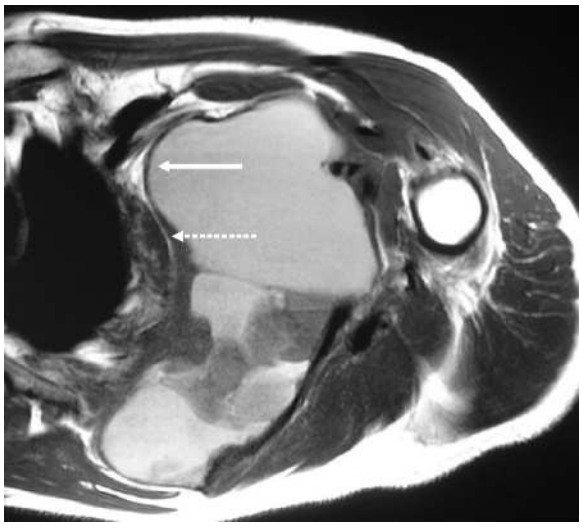

Fig. 32.2. Subscapularis cystic soft tissue sarcoma. Note the clear fascial margin of subscapularis (*solid arrow*) and the excellent soft tissue contrast afforded by proton-density MRI which allows delineation of fat plane and potential surgical margin (*dotted arrow*)

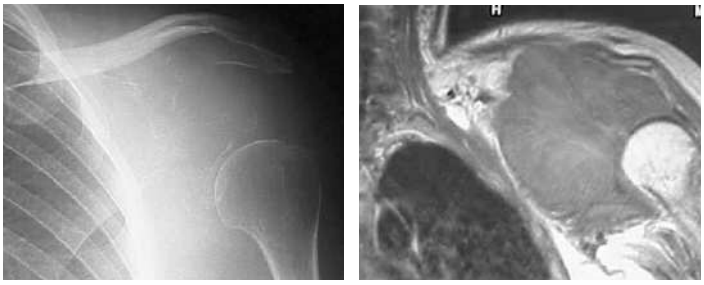

a,b

Fig. 32.3. **a** Radiograph of destructive scapular sarcoma. **b** Prominent soft tissue component clearly demonstrated on T1-weighted MRI with encirclement and involvement of glenohumeral joint. Involvement of the superior glenoid region potentially implicates biceps tendon as route for intracapsular extension of tumor

chest wall, however, is difficult to cure because seeding frequently occurs between the parietal and visceral pleurae.

Imaging of the humerus should always be performed because of the potential for skip metastases (Fig. 32.4). Although uncommon, skip metastases alter the prognosis and surgical management of scapular tumors.

The surgical options for primary tumors of the scapular include (Nakamura et al. 1999; Rodriguez et al. 1999; Mayil et al. 2007):

1. Partial scapulectomy
2. Total scapulectomy ± prosthetic scapular reconstruction
3. Partial scapulectomy and proximal humeral resection ± prosthetic humeral reconstruction
4. Transcapulo-thoracic amputation
5. Extended transcapulo-thoracic amputation (includes chest wall)

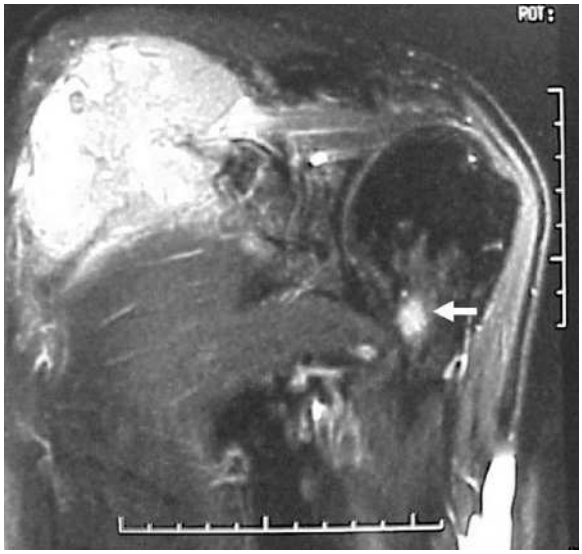

Fig. 32.4. Fat suppressed T2 weighted contrast enhanced MRI demonstrating large scapular sarcoma with skip lesion in the surgical neck of humerus (*arrow*)

32.1.1.4 Post-operative Surveillance

Regular post-operative imaging is recommended to determine the presence of local recurrence of disease. The presence of a metallic prosthesis will create image artifact that will render MRI imaging of the scapular less than satisfactory. If a prosthesis is employed, it is recommended that CT scans utilizing bone windows be used to suppress the metal artifact or specific software for this purpose. If there is a suspicion of local recurrence, then the CT scan should be supplemented with functional nuclear imaging. Any suspicious area with tracer avidity should be subjected to CT-guided biopsy. Pulmonary imaging should always be included as part of the post-operative surveillance. While CT scans are the preferred technique for pulmonary imaging, metal artifact may degrade the image. If image degradation is sufficient to contraindicate the use of CT, then orthogonal radiography should be performed while recognizing the potential for missing small pulmonary lesions.

32.1.2 Demographics and Clinical

Isolated scapula lesions are rare. Of the primary bone tumors in the shoulder region reviewed by Link et al. (1999), 602 were isolated to the humerus, 90 to the scapula, and 19 to the clavicle. The acromion and coracoid processes (Ogose et al. 1999) appear more likely to be involved by some tumors including chondrosarcoma and aneurysmal bone cyst (Brtkova et al. 1999).

Within the pediatric age group lesions of the shoulder girdle involve more commonly the proximal humerus and clavicle, then the scapula. A 25-year-period review from the St. Jude's Children Research Hospital (Memphis, Tenn.), for flat bone sarcomas (other than Ewing's sarcoma), isolated 28 patients with a median age of 15 years, with tumor types being mostly osteosar-

coma or malignant fibrous histiosarcoma (Kellie et al. 1990). Of the flat bones, the scapula was the third most common site, after the craniofacial region and the pelvis (Kellie et al. 1990). All bone lesions had large soft tissue extensions at the time of presentation (Kellie et al. 1990).

In the adult, however, the upper extremity, the shoulder girdle region, is the third most common site for primary bone and soft tissue tumors (Cleeman et al. 2005). Benign lesions are more common than malignant lesions. Interestingly, Cleeman et al. (2005), on review of 194 shoulder girdle tumor cases, found that the presence of pain or a mass lesion generally was not a risk factor for diagnosis of a malignant tumor; however, they found three significant risk factors for a malignant tumor of the shoulder girdle: (1) older age group; (2) pain or tenderness to palpation; and (3) a lesion within the scapula.

From a 28-year period, 68 cases of scapula tumors, studied using radiological and histological techniques, were reviewed at the Swiss Bone Tumor Reference Centre, Institute of Pathology, University Clinic in Basel where there was a dominance of cartilaginous tumors (27 osteochondromas, 16 chondrosarcomas, and 3 chondromas; Brtkova et al. 1999). Most tumors (68%) were cartilaginous in origin, either benign osteochondromas (one third) or malignant chondrosarcomas (one quarter; Brtkova et al. 1999). The next group (3 of 68) was non-Hodgkin's lymphoma, then two cases each of aneurysmal bone cyst, eosinophylic granuloma, Ewing's sarcoma, and chronic osteomyelitis. The remainder from this series included one each of plasmacytoma, round cell sarcoma, chondroblastoma, desmoplastic fibroma, metastasis, osteoblastoma, traumatic dysplasia, osteosarcoma, simple bone cyst, and secondary involvement of scapula by one each of synovial sarcoma and myositis ossificans.

Other, smaller series present similar diagnoses and breakdown with one series of 18 primary bone lesions having, 11 being either chondrosarcoma or dedifferentiated chondrosarcoma, 2 osteoid osteomas, and 1 each of osteosarcoma, plasmacytoma, lymphoma, giant cell tumor of bone, and aneurysmal bone cyst (OGOSE et al. 1999).

32.1.3 Important Anatomical and Embryological Features

Through enchondral ossification the scapula develops from seven ossification centers (Fig. 32.5; Brtvoka et al. 1999). This gives a total length of physes, if combined, to exceed any tubular bone. Glenoid, acromion, and coracoid processes correspond with the distal end of a long bone (Aoki et al. 1989), whereas the medial margin and inferior angle represent the site of highest growth potential (Crocco 1977). These embryological and anatomical features explain why cartilaginous tumors are more frequent within the scapula.

The location of osteochondroma and chondrosarcoma within the scapula is strikingly different (Erlemann et al. 1988; Brtvoka et al. 1999). Osteochondromas are mostly located within the body of scapula, whereas chondrosarcomas are mostly located at the lateral scapula margin over the inferior angle and within the acromion and coracoid process (Erlemann et al. 1988; Brtvoka et al. 1999). All other lesions, whether benign or malignant, are evenly distributed throughout the scapula with a slight prevalence for the upper half.

32.1.4 Imaging Investigations

Given the complex anatomy of the scapula flat bone, adjacent glenohumeral and acromioclavicular joints, and nearby neurovascular bundles, a combination of imaging is recommended. For primary characterization and local staging, conventional radiographs in two plains may be performed or computed tomography (CT) with reconstructions. Radiographs of the glenohumeral joint may include an anterior–posterior view, transthoracic view, axillary view, true lateral projection of the scapula (patient is in a 60° anterior oblique position) or with additional oblique lateral (Resnick 1995). Radiographs may be used as baseline studies for follow-up studies; however, CT and MRI have over taken this role and give more accurate information. Computed tomography with bone and soft tissue windows and reconstructions are used to define both bone and soft tissue extent. Magnetic resonance imaging is usually performed as part of routine workup to characterize the tumor type prior to histological diagnosis and for bone and soft tissue extent prior to surgery. Review for unusual involvement of the nearby joints or the neurovascular bundles should be performed. The MR imaging protocol usually includes standard T1- and T2-weighted sequences and short-tau inversion recovery (STIR), and the administration of an intravenous contrast agent is helpful. Usually the use of contrast is performed with fat-suppression technique recommended for optimal differentiation between tumor and adjacent

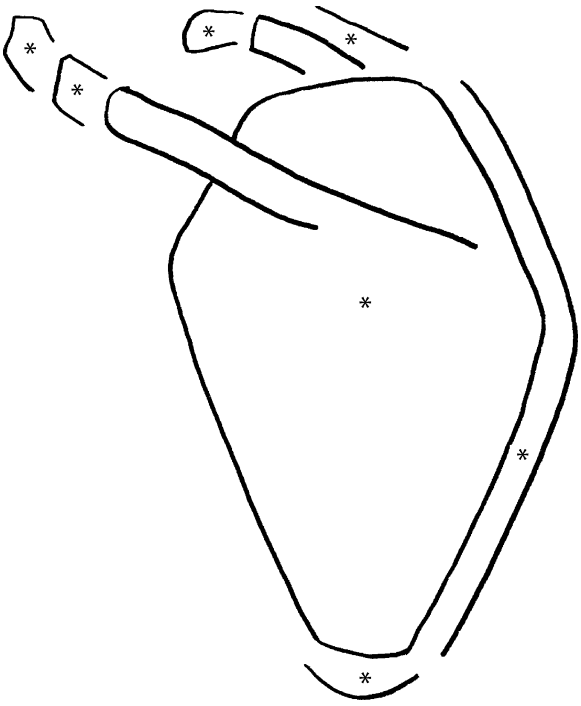

Fig. 32.5. The seven ossification centers of the scapula. (Adapted from Brtkova et al. 1999)

fat, which otherwise have a similar signal intensity on T1-weighting. Contrast administration is performed to help distinguish solid and viable tumor components from degenerative or hemorrhagic tumor components, to aid in tumor characterization (a chondroid matrix will enhance peripherally like a water-color painting and fill over time centrally, if there is not too large a calcified matrix component) and extent, and in defining an appropriate biopsy site. When performing an MRI, the whole shoulder joint and full rotator cuff muscles, acromioclavicular joint, axilla, and the adjacent chest wall should be included in the field. The whole humerus should also be reviewed with MR to exclude any skip lesions, which, if present, change the diagnosis from a primary tumor to that with metastatic disease. Additional MR angiography sequences, with early and late phase, for arterial and venous vascular anatomy and tumor vascularity can be useful.

Positron emission tomography (PET) and thallium scanning for local tumor activity may also be performed as a frontline modality of investigation for staging and biopsy planning as well as post-therapy review. Systemic staging is also performed with whole-body CT and nuclear medicine technetium bone scan.

If initial radiographs are normal, as the acromion and coracoid processes are particularly difficult to image with radiographs if there is persistent pain, combined CT and MRI are recommended (Ogose et al. 1999).

32.1.5 Imaging Diagnosis and Differential Diagnosis

In the reported radiology scapula series available (Erlemann et al. 1988; Brtvoka et al. 1999), with 38 and 68 cases, two thirds of all tumors were cartilaginous in origin. In both series typical radiological features read by musculoskeletal specialized radiologists, allowed for the correct diagnosis or correct differentiation between malignant and benign in 63 and 83%, respectively (Erlemann et al. 1988; Brtvoka et al. 1999). More characteristic imaging appearances were present for the most frequent benign tumor, the osteochondroma in the younger age group (first three decades) and chondrosarcomas were more frequent in the older age group (fourth to seventh decades) with more varied imaging appearances being present, either characteristically malignant or with apparent benign features such as focal expansion with sclerotic rims and no overt calcified cartilaginous matrix. Other authors comment on the lack of typical imaging features in tumors within the scapula (Aoki et al. 1989; Gold and Mirra 1983; Moyer et al. 1987).

In approximately one third of cases (Brtvoka et al. 1999), the radiological differential diagnosis for a scapula lesion remains broad including benign and malignant lesions. In children a malignant or even less aggressive expansile lesion should raise the possibility of Ewing's sarcoma (Coombs et al. 1986), or even chondrosarcoma (Brtvoka et al. 1999) or eosinophilic granuloma (Moyer et al. 1987). A further differential in this age group is an aneurysmal bone cyst (Kaila et al. 2007). Sharply marginated lesions in children include a differential of occasionally a unicameral bone cyst, or if calcified an osteoid osteoma, osteoblastoma, or chondroblastoma. In the adult, chondrosarcoma or another malignant tumor and metastases or plasmacytoma should be considered. Renal metastases are reported as the most common metastasis to involve the scapula (Brtvoka et al. 1999). Non-Hodgkin's lymphoma can occur in any age group.

32.2 Benign Bone Tumor of Scapula

32.2.1 Aneurysmal Bone Cyst

These expansile multiloculated lytic lesions may very occasionally involve the scapula (Kaila et al. 2007; Tateishi et al. 2003a). In the shoulder girdle, the proximal humerus and distal clavicle are more frequently involved, whereas the scapula is rarely involved (Kaila et al. 2007). Of all ABCs approximately only 2% may involve the scapula (Resnick 1995). They have been also described to occur with other lesions such as chondroblastoma within the scapula, which is usually a diagnosis made at histology. As at other sites, they have multiple fluid levels and in the scapula soft tissue extension may be evident (Gold 1983). The literature suggests a combination of modalities for diagnosis and preoperative imaging with radiographs, computer tomography and MRI. Some tumor centers report that sole curettage of scapular ABC lesions are appropriate with low recurrence rates (Kaila et al. 2007).

32.2.2 Unicameral Bone Cyst

Unicameral bone cysts have been rarely described within the scapula (Ruggieri et al. 1987; Hreslco et al. 1988).

32.2.3 Ganglion

Ganglion cysts within the glenoid are usually focal lesions with a well-defined wall with central fluid. Their etiology may be developmental or related to post-traumatic or degenerative joint findings (Fig. 32.6). On MRI the lesion's fluid is decreased in signal intensity on T1- and increased on T2-weighted images with only a fine peripheral rim of contrast enhancement.

32.2.4 Osteoid Osteoma and Osteoblastoma

Osteoid osteomas with central nidus calcification may occur rarely in the scapula. They have been described as occurring at the anterior surface of scapula at the base of the coracoid process and within the spine of scapula at its base and can be successfully treated with percutaneous electrocoagulation (Rosenthal et al. 1992). Osteoblastoma, being over 1.5 cm in size, has been rarely described within the scapula and may be associated with systemic features (Theologis et al. 2007).

32.2.5 Chondroblastoma

Chondroblastoma have been described within the glenoid region of the scapula (Weatherall et al. 1994) and the acromion (Gebert et al. 2004; Holt et al. 1995). The predominance for these sites is explained by the fact that they are epiphyseal/apophyseal in origin. As at other anatomic sites there is a small sclerotic rim with matrix chondroid calcification and on MRI they are usually associated with large areas of altered bone marrow and soft tissue signal intensities due to the inflammatory component related to this benign tumor. This may give a falsely aggressive-looking appearance.

32.2.6 Giant Cell Tumor

Flat bone involvement with giant cell tumor (GCT) is extremely rare. Case reports (e.g., Park et al. 1991) and small series (Aoki et al. 1989) describe GCT of bone within the scapula with and without ABC components. In a review of 13 cases within the scapula Aoki et al. (1989) describe cases which presented 20 years earlier than the typical distribution (between 20 and 40 years) compared with GCT of long bones. Scapula sites involved were coracoid process, acromion, and scapula body (3 cases each), glenoid (2 cases), and superior and inferior angles (1 case each; Aoki et al. 1989). The tumors had an appearance similar to that of other, more typical sites within long bones, with well-defined margins, occasional delicate sclerotic rim, prominent trabeculae, expanded bony contour, frequent extension to subchondral plate, and absence of matrix mineralization, and cystic blood-filled clefts are possible (Aoki et al. 1989).

32.2.7 Hemangioma

Hemangioma is rarely reported as involving the scapula (Resnick 1995), and this may be incidentally found at

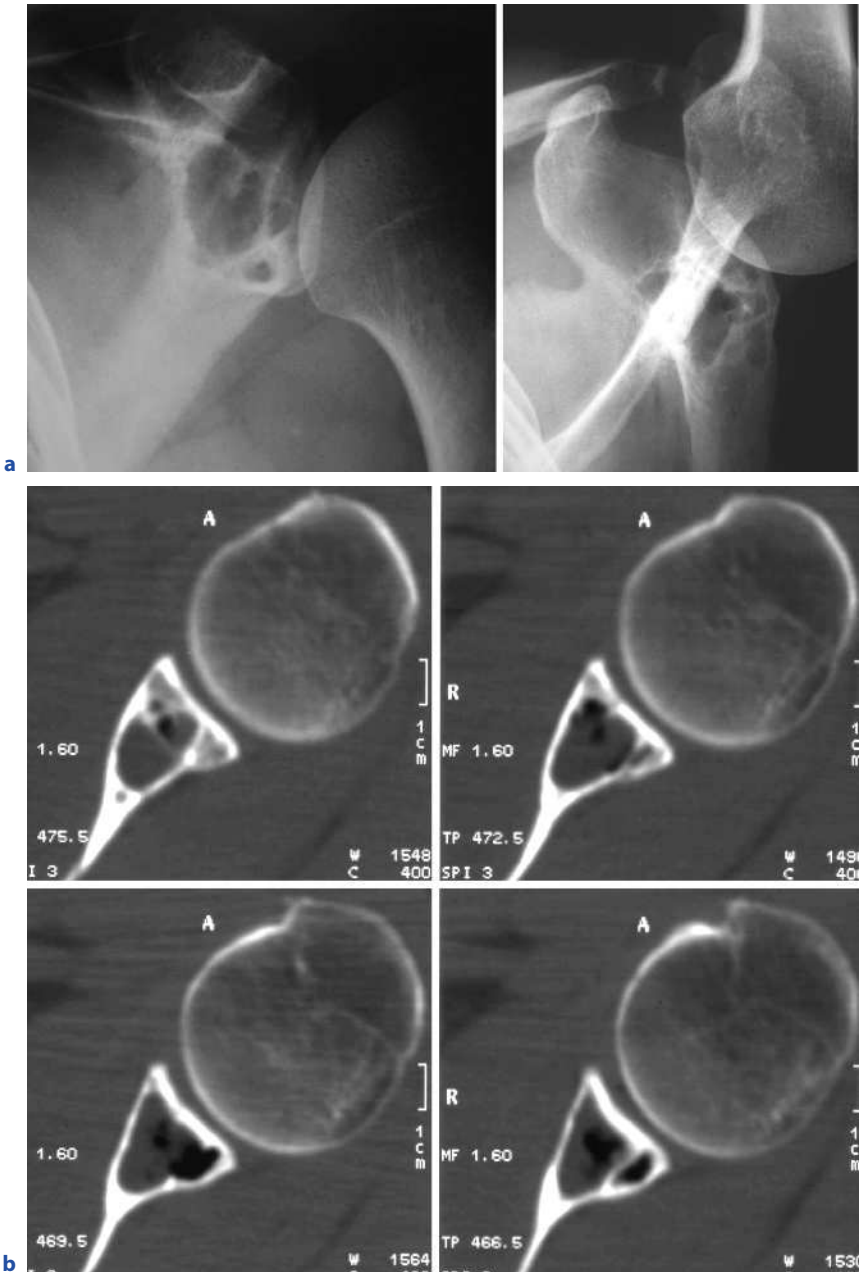

Fig. 32.6a–d. Benign ganglion of the glenoid of scapula. **a** Radiographs show a focal lytic process within the glenoid with some partial septation. **b** Computed tomography images show some gas evident within the lesion. **c,d** *see next page*

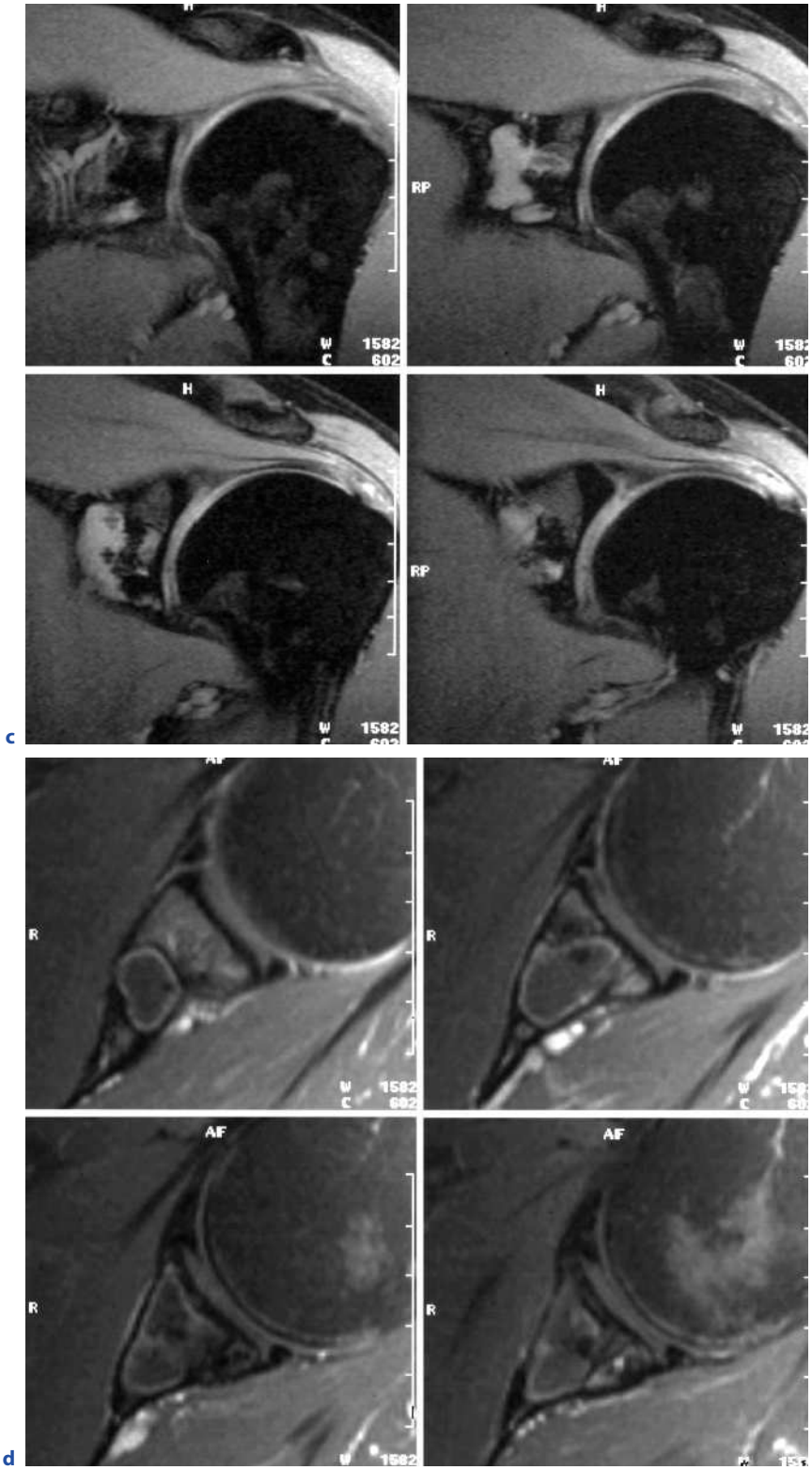

Fig. 32.6a–d. (*continued*) Benign ganglion of the glenoid of scapula. **c** Coronal plane, MRI images with T2* gradient echo (GE) with fat saturation, show the focal glenoid lesion involving the subarticular zone. T2*-weighted GE with fat saturation. **d** Axial-plane T1-weighted MRI after intravenous contrast administration with fat saturation shows a thin peripheral rim of contrast enhancement and absence of any nodular contrast enhancement

the time of imaging for trauma review (Ogose et al. 2000). These lesions, as at other sites, have focal linear decreased and increased signal intensities on T1- and T2-weighted MR images, respectively, with a well-defined intraosseous component and radiating-like pattern which may suggest the diagnosis , and radiographically there is the distinctive trabecular pattern (Resnick 1995).

32.2.8 Osteochondroma and Hereditary Multiple Exostoses

Solitary osteochondromas of the under surface of the scapula wing are a well-known entity (Figs. 32.7, 32.8) often presenting in the young adult due to an inflamed adjacent soft tissue bursa between the osteochondroma and chest wall. There is a 4% incidence of solitary osteochondroma involving the scapula, and an approximately 40% involvement of the scapula and ribs with hereditary multiple exostoses (Murphey et al. 2000). In the Swiss Tumor Registry Scapula Review (Brtkova et al. 1999), one third from this series (27 of 68) were osteochondroma occurring in the first three decades of life in males and mostly within the body of scapula. Osteochondromas (Brtkova et al. 1999) were located mostly arising from the body of the scapula (14/27/68) with nearly half of these arising from the spine of the scapula, then two equally arose from the superior, medial, and inferior margin with one at the superior angle. They were found to involve both the dorsal and ventral scapular surfaces (Brtkova et al. 1999). The sites are summarized in Fig. 32.9.

Scapular osteochondromas may be difficult to diagnose as with other flat bones, particularly if they are sessile or have small pedicles and are complicated by large bursae. Often a combination of radiographs, computed tomography with MRI, is necessary to confirm continuity of intraosseous bone into the pedunculated stalk, and to diagnose bursae and cartilage caps (Murphey 2000). Over 50% of scapula osteochondroma are associated with a bursa (Murphey 2000). As the bursa has a synovial lining, this may become inflamed, infected, or even hemorrhagic, and become enlarged, causing concern for possible cartilage cap enlargement and sarcoma development. If the bursa is long-standing occasionally fibrin debris or pearls may develop or more unusually synovial osteochondromatosis; however, MRI allows a fluid-filled bursa to be distinguished from the cartilage cap. The scapula solitary osteochondroma may also be associated clinically with snapping tendons. The osteochondroma and bursa can be treated with open or arthroscopic surgery (Van Riet and Van Glabbeek 2007). Malignant transformation of the cartilage cap with development of secondary chondrosarcoma is reported as being generally for all solitary osteochondromas 1% and for hereditary multiple exostoses 3–5% (Murphey 2000).

32.2.9 Dysplasia Epiphysealis Hemimelia

Dysplasia epiphysealis hemimelia is a benign cartilaginous overgrowth tumor of one or multiple epiphyses or centers of ossification. It has been most rarely reported in the scapula (Azouz et al. 1985).

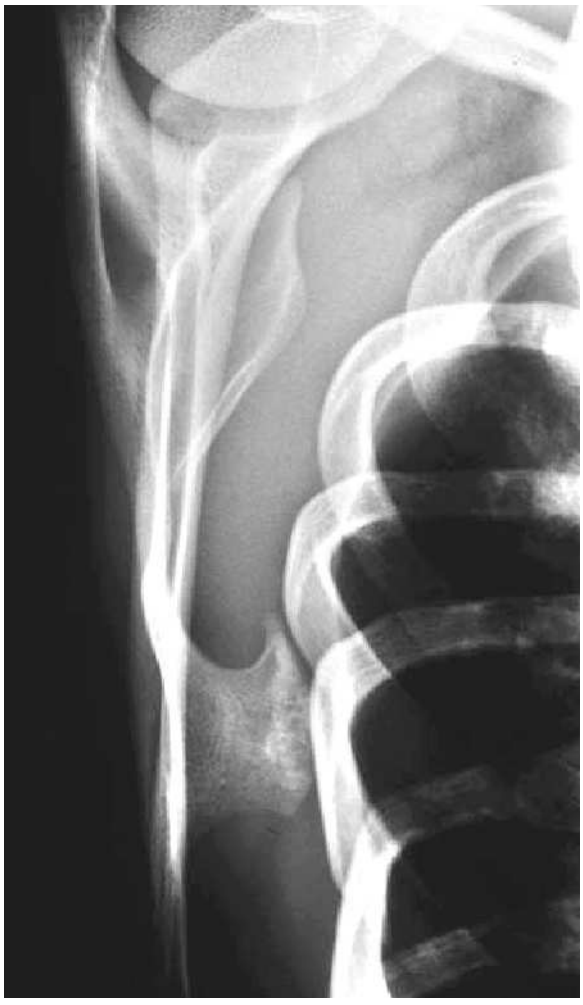

Fig. 32.7. Benign osteochondroma of the inferior border of scapula. Oblique radiograph shows inferior medial osteochondroma. The radiograph clearly demonstrates that the stalk of the lesion is continuous with the scapula intramedullary bone

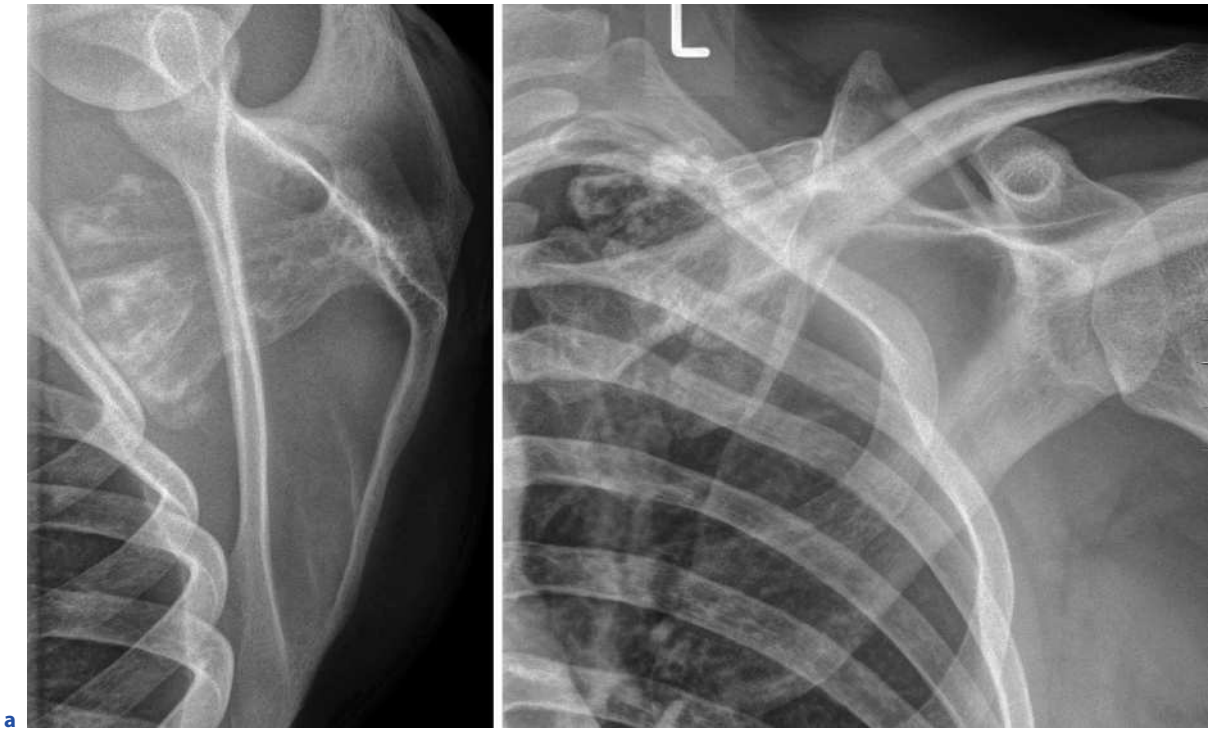

a

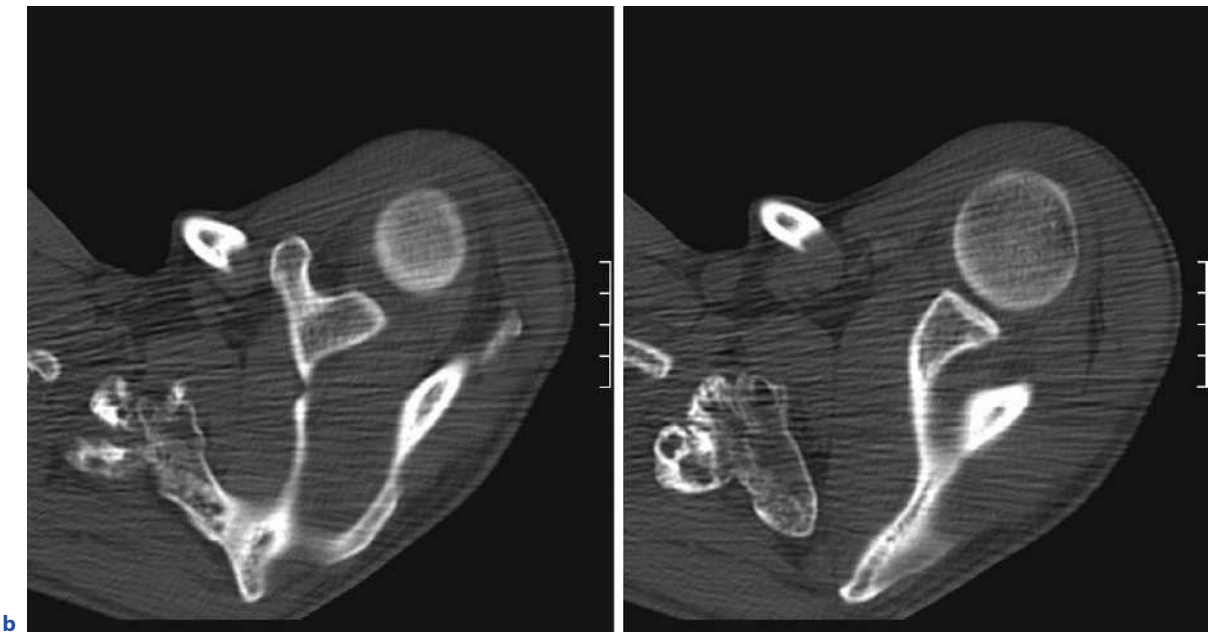

b

Fig. 32.8a–f. Benign osteochondroma. **a** Radiographs oblique and frontal show the large osteochondroma clearly arising with stalk from the scapula. **b** Computed tomography images show the osteochondroma. **c–f** *see next page*

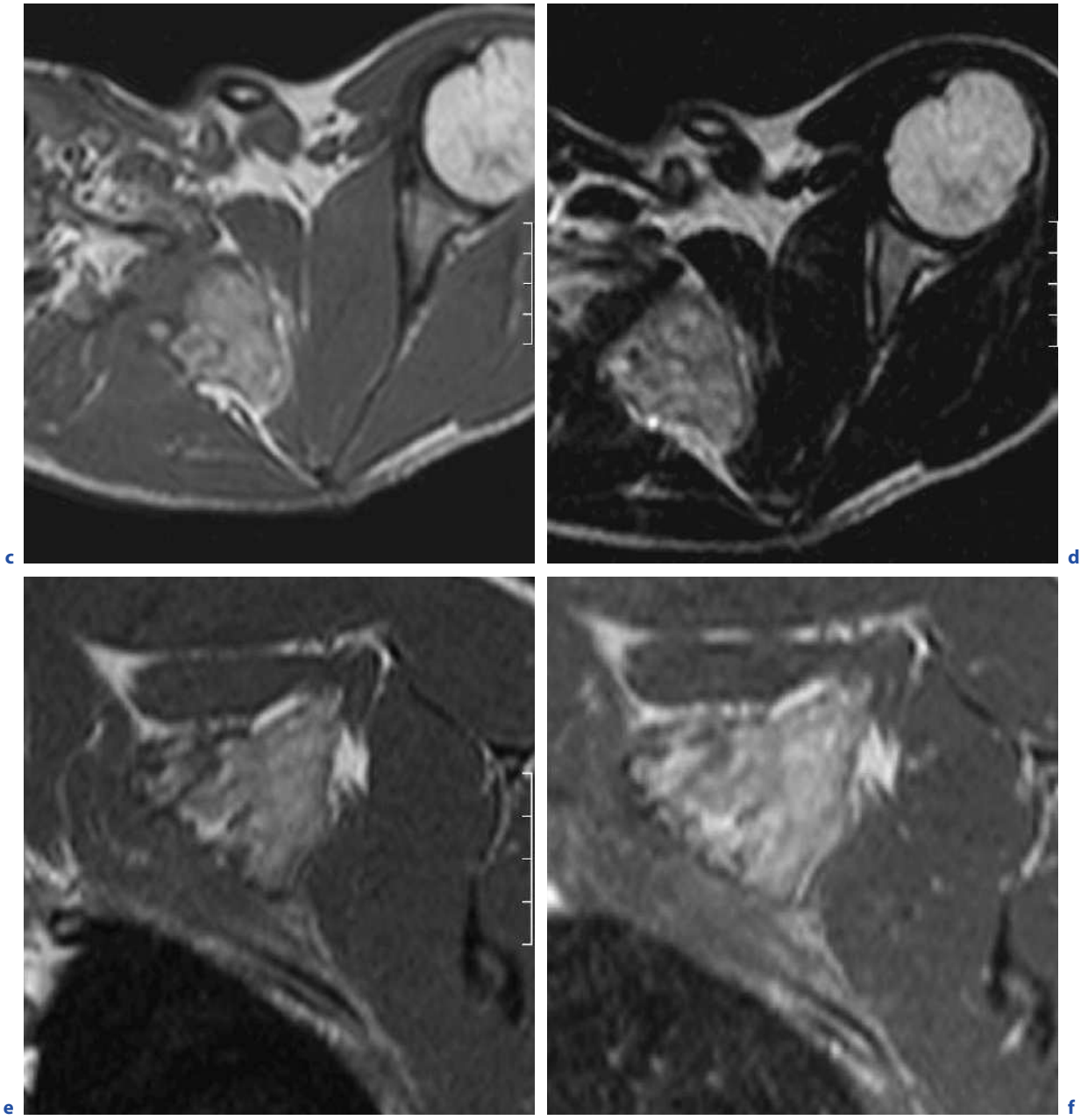

Fig. 32.8a–f. (*continued*) Axial-plane MRI with **c** T1- and corresponding **d** T2-weighted images of the distal aspect of the large osteochondroma. **e** Coronal T1 and **f** corresponding image after contrast administration again shows the large osteochondroma. No large cartilage cap or bursa are present

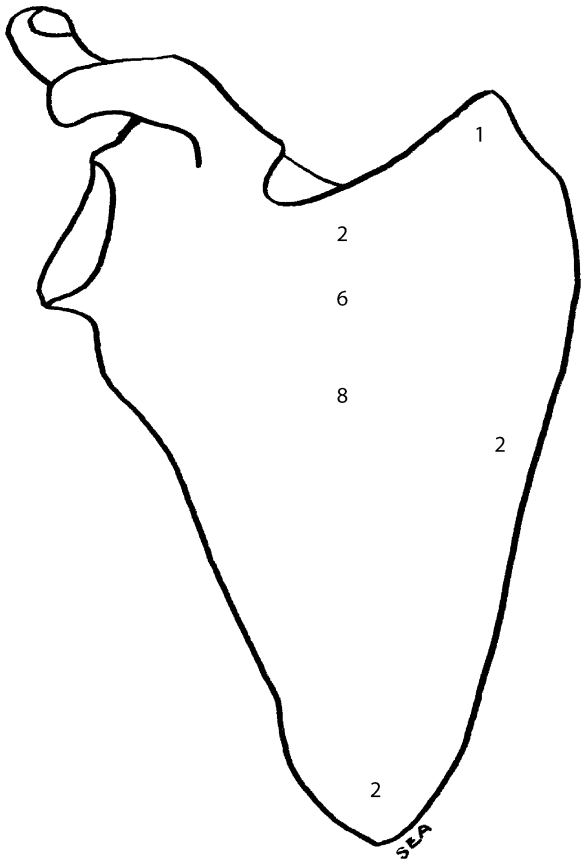

Fig. 32.9. Localization of osteochondroma from the Swiss Tumor Registry series of 68 cases. *Numbers* represent recorded cases and sites of pathology from the Swiss Tumor Register series. (Adapted from Brtkova et al. 1999)

32.2.10 Non-ossifying Fibroma

Very rarely is the scapula involved in cases of non-ossifying Fibroma (Resnick 1995), and radiologically this lesion may be similar in appearance to ABCs or chondroblastoma, and the diagnosis is usually made with histology.

32.2.11 Fibrous Dysplasia

Monostotic involvement of the scapula is very rare, as compared with polyostotic fibrous dysplasia. Some case reports describe isolated cases or similar cases where these may be related to post-traumatic reactive changes, the "fibro-osseous reparative pseudotumor" of the scapula analogous to the rib (Kessler et al. 1994).

32.2.12 Paget's Disease of Bone

Scapula involvement by Paget's disease of bone is not uncommon, particularly with polyostotic Paget's involvement with 13 cases of scapula involvement described in a total of 107 patients (Vellenga et al. 1984). There is scapular expansion with intraosseous and cortical expansion (Boutin et al. 1998). Usually the normal yellow fatty marrow is maintained on MRI in uncomplicated Paget's disease of bone, with fatty marrow signal intensity being maintained on T1-weighted imaging (Smith et al. 2002). Rarely, as at other Paget sites of involvement, benign GCTs of bone may develop within the scapula (Potter et al. 1991). Giant cell tumor complicating Paget's disease of bone can have decreased to intermediate signal intensities on T1- and T2-weighted images thought to be due to higher cellularity and fibrous content, plus or minus the presence of cystic or hemorrhagic components (see below for development of malignant secondary Paget's-related sarcoma; Smith et al. 2002).

32.2.13 Melorheostosis

If the "candle-wax dripping" cortical thickened bone is present involving the scapula, it is usually present in combination with proximal humerus involvement, and is described in the occasional case report (Kalbermattan 2001; Subhas 2008). If the upper limb is involved, usually there is a combination of characteristic calcifications, i.e., cortical hyperostoses, which may be small or involve large regions of bone of the clavicles, scapula, and proximal humerus in a sclerotome (the zones of the skeleton supplied by individual spinal sensory nerves) distribution (Murray and McCredie 1979). There is also commonly endosteal hyperostoses which may partially or completely obliterate the medullary cavity. If the scapula is involved as in the pelvis, there can be radiating or focal sclerotic patches (Resnick 1995). There may also be a combination of more large bone-like masses and/or some soft tissue calcifications near the shoulder joint.

32.2.14 Extra-axial Meningioma of the Scapula

This is extremely rare with extradural meningiomas accounting for only 1–2% of all meningiomas and only isolated case reports describe meningioma of the scapula (Llauger et al. 2008).

32.2.15 Osteopoikilosis and Osteopathia Striata

Multiple focal or linear dense sclerotic bone islands may be evident within the medial aspect of the scapula near the joint surface; however, with multiple findings near the joints this diagnosis, although rare, is usually obvious. These findings are usually present in adolescence and do not develop in adults, as opposed to breast metastatic disease. In these entities there is usually no associated increased technetium uptake on nuclear medicine bone scans as opposed to metastatic disease.

32.2.16 Gorham's Disease

Very rarely can there be bone loss of the scapula with radiographic progressive osteolysis related to involvement of Gorhams's vanishing bone disease (Damron et al. 1993). The etiology remains debated. Usually the diagnosis is made with histology.

32.2.17 Diaphyseal Dysplasia

Occasionally there may be increased radiographic density and scintigraphic uptake within the lateral borders of the scapula and more medial glenoid region in the adolescent and child with Engelmann's disease (diaphyseal dysplasia; Kumar et al. 1981); however, with overriding marked diaphyseal long bone widening and sclerosis, the diagnosis should remain overt.

32.3 Malignant Bone Tumors of Scapula

32.3.1 Chondrosarcoma (Conventional, Mesenchymal)

After the pelvis (25% all cases), the scapula (5%) is the second most frequently involved flat bone with chondrosarcoma (Fig. 32.10; Dorfmann and Czerniak 1998). Benign enchondromas are extremely rare in this site and therefore any cartilaginous lesion in this region should be treated as neoplastic in nature and not reactive (Dorfmann and Czerniak 1998; Brtkova et al. 1999). Occasionally secondary malignant change may occur with enchondromatosis (Ollier's disease) or secondary to an osteochondroma (Brtkova et al. 1999). All types of chondrosarcoma have been described within the scapula as well as the central, peripheral, and periosteal bone formation (Brtkova et al. 1999).

Peak incidence is during the sixth and seventh decades, and chondrosarcomas in people younger than 45 years are rare, although this may be under-reported within the scapula. Cases as young as in 6- and 20-year-olds have been described (Brtkova et al. 1999). In the Swiss Tumor Registry collective paper, chondrosarcoma was the commonest malignant tumor (16 of 68; Brtkova et al. 1999). Chondrosarcomas were present in approximately 25% of total cases, between the fourth and seventh decades, but also occasionally in a younger age group. Chondrosarcomas are located mainly at the medial scapula margin, and over the inferior angle, corresponding to the sites of highest growth potential within the scapula during enchondral ossification, and in the acromion and coracoid process, the secondary ossification centers with physes (Brtkova et al. 1999). The sites of involvement are summarized in Fig. 32.11.

Chondrosarcomas within the scapula may have classically malignant appearances with large size, bone destruction, and clearly evident calcified cartilaginous matrix associated with cortical breach and extraosseous tumor extension, or they may be poorly circumscribed or "bubbly" lytic expansile lesions and may mimic apparent benign lesions (Erlemann et al. 1988; Brtvoka et al. 1999). They often have thinned cortex with some possible regions of destruction and thick septation, with scarce or variable intralesional matrix calcification being present. Of primary bone lesions involving the coracoid, chondrosarcoma is most likely to be the diagnosis

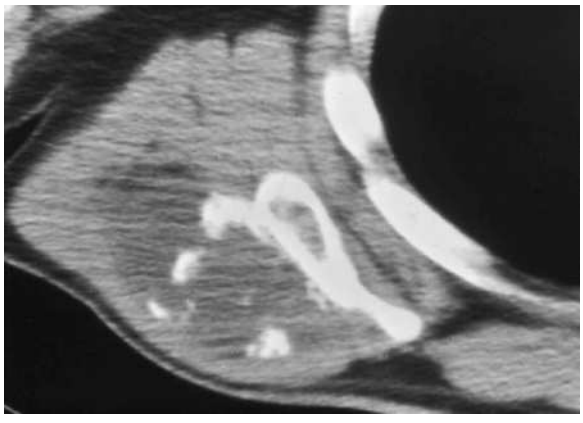

Fig. 32.10. Malignant secondary chondrosarcoma, arising in an osteochondroma. Computed tomography shows >2-cm irregular cartilage cap with irregular matric calcification consistent with chondrosarcoma

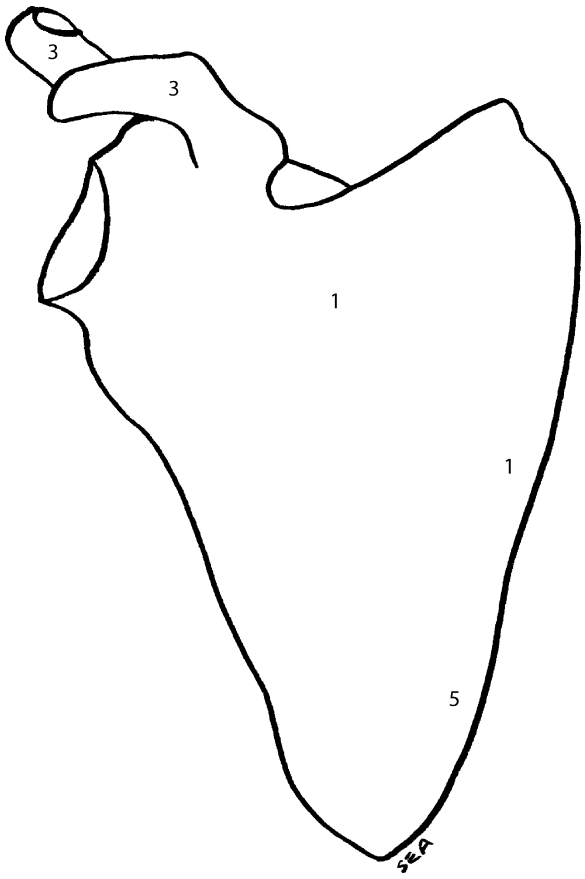

Fig. 32.11. Localization of chondrosarcoma from the Swiss Tumor Registry series of 68 cases. *Numbers* represent recorded cases and sites of pathology from the Swiss Tumor Register series. (Adapted from Brtkova et al. 1999)

(Ogose et al. 1999). The cortex typically has regions of thinning and associated with the outer cortical surface there may be parallel periosteal new bone formation. As with the involvement in other flat bones (e.g., pelvis and cranium), at the time of presentation within the scapula it is more likely that there will be cortical disruption and significant soft tissue extension. Typically there will be larger masses at presentation than occurs associated with long bone involvement. The prognosis is therefore often significantly worse, with complete surgical removal being more complicated compared with that of long bones. A chondroid calcified matrix may or may not be evident within the lesion, and CT is important for review in this case and for cortical breach (Brtkova et al. 1999). Imaging, particularly MRI, is needed to determine the intramedullary and extramedullary tumor extent.

32.3.2 Osteosarcoma

The scapula is rarely involved with primary osteosarcoma, with an incidence of less than 2% of all osteosarcomas occurring at this site (Dorfmann and Czerniak 1998; Resnick 1995). Patients present in the second or third decades or later, after the sixth decade. The latter case usually relates to secondary forms of osteosarcoma due to pre-existing disorders such as Paget's disease of bone or related to previous therapy, such as with radiotherapy. Histological types are similar to long bone types. Although rare within the scapula, they are usually of high histological grade. Magnetic resonance imaging, with CT and reconstructions, are essential for determining pre-operative intra- and extraosseous tumor extent. Telangiectatic osteosarcoma, being very destructive and expansile, occasionally may replace the scapula with large areas of hemorrhage and necrosis and small foci of mineralized matrix (Murphey et al. 2003). The evidence of contrast-enhancing solid viable sarcomatous tumor, giving a diagnosis of telangiectatic osteosarcoma, allows for distinction from a benign ABC (Murphey et al. 2003) and for biopsy site.

Extramedullary tumor extent is frequent in these lesions at presentation. As these lesions can be extensively sclerotic, CT can aid in defining the bony extent and soft tissue extension of the lesion. Magnetic resonance imaging also defines intramedullary and soft tissue tumor extent. Use of intravenous contrast is recommended for MRI to review for viable tumor components and aid with planning the optimal biopsy site.

Osteosarcoma development within the scapula may be primary or relate to previous radiation or Paget's disease of bone (Sharma et al. 2005).

Sarcomatous degeneration within Paget's disease of bone usually is evident with aggressive focal bone destruction with intermediate to focal high signal intensity on T2-weighting associated with a mass which shows contrast enhancement (Smith et al. 2002), differentiating solid versus necrotic tumor components. From the Scottish Bone Tumor Registry experience between 1950 and 2000, with a mean age of 61 years, there were 13 humeral and 3 scapular Paget's sarcomas (Sharma et al. 2005), and interestingly the humeral lesions were predominantly lytic radiologically and the scapula lesions purely sclerotic. The Paget's sarcomas were osteosarcoma predominant and presented with progressive pain and mass formation and possible pathological fracture (Sharma et al. 2005).

32.3.3 Post-radiation Sarcoma

Post-radiation sarcoma is a sarcoma that develops in the field of previous radiotherapy. This has been described in the scapula occurring after radiation for breast cancer (Dorfmann and Czerniak 1998; Hatfield and Schulz 1970). Post-radiation sarcomas of the scapula have also been described after radiation therapy for non-Hodgkin's lymphoma (Lagrange et al. 2000) and bronchogenic carcinoma (Logan et al. 1996). There may be an overt destructive mass, or bone necrosis with fracture and mass. Histological tumor types of induced sarcomas include osteosarcoma, chondrosarcoma, and malignant fibrous histiocytoma.

32.3.4 Ewing's and PNET Sarcoma

Involving the scapula Ewing's and primitive neuroectodermal tumor (Pnet) sarcomas occur in the young age group, often destroying a large component of the body (Fig. 32.12) and glenoid regions, and are associated with large soft tissue masses. Sclerotic features of parent bone thickening and enlargement or focal cloud-like opacities may be evident more often when the scapula, a flat bone, is involved as opposed to a long bone (Dorfmann and Czerniak 1998; Brtkova et al. 1999), or the intramedullary bone is replaced with little destruction if the lesion presents early. Regardless of frequency, the lesions are larger at presentation and have a large associated soft tissue component, and are more difficult to resect (Dorfmann and Czerniak 1998); thus, the prognosis is poorer with a scapula primary site compared with a peripheral long bone. Occasionally primary Ewing's sarcoma of the scapula clinically may have suprascapular nerve compression due to extra-osseous tumor components (Fritz et al. 1992). This entity is most commonly associated with benign ganglion cysts related to labral tears of the glenohumeral joint; however, sometimes it may be associated with tumors of the scapula, such as with chondrosarcoma and metastatic renal cell carcinoma (Fritz et al. 1992).

32.3.5 Malignant Fibrous Histiocytoma

Malignant fibrous histiocytoma (MFH) occurs very seldom in the flat-bone scapula (Resnick 1995) and may be associated with osseous expansion and lysis. There are no specific tumor MRI characteristics. Rare case reports describe MFH within the acromion of the scapula (Johnson et al. 1978).

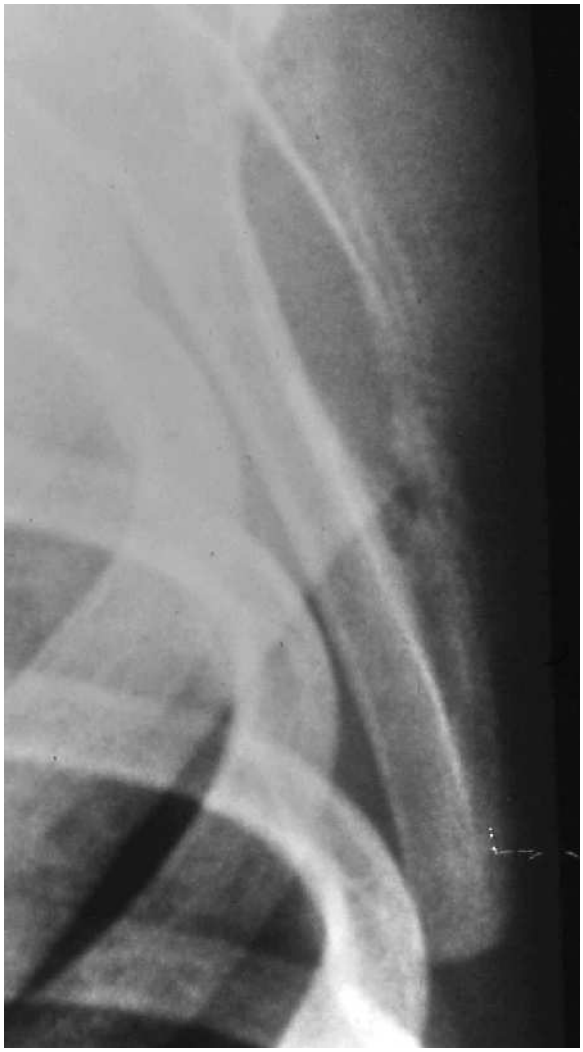

Fig. 32.12. Malignant peripheral neuroectodermal tumor. Oblique radiograph shows the irregular bone destruction over a broad area and suggestion of an associated mass

32.3.6 Hemangiopericytoma

Rare cases of vascular malignant tumors have been reported within the scapula, particularly the acromion or corocoid processes (Fig. 32.13), including hemangiopericytoma and hemangioendothelioma (Lye et al. 1988).

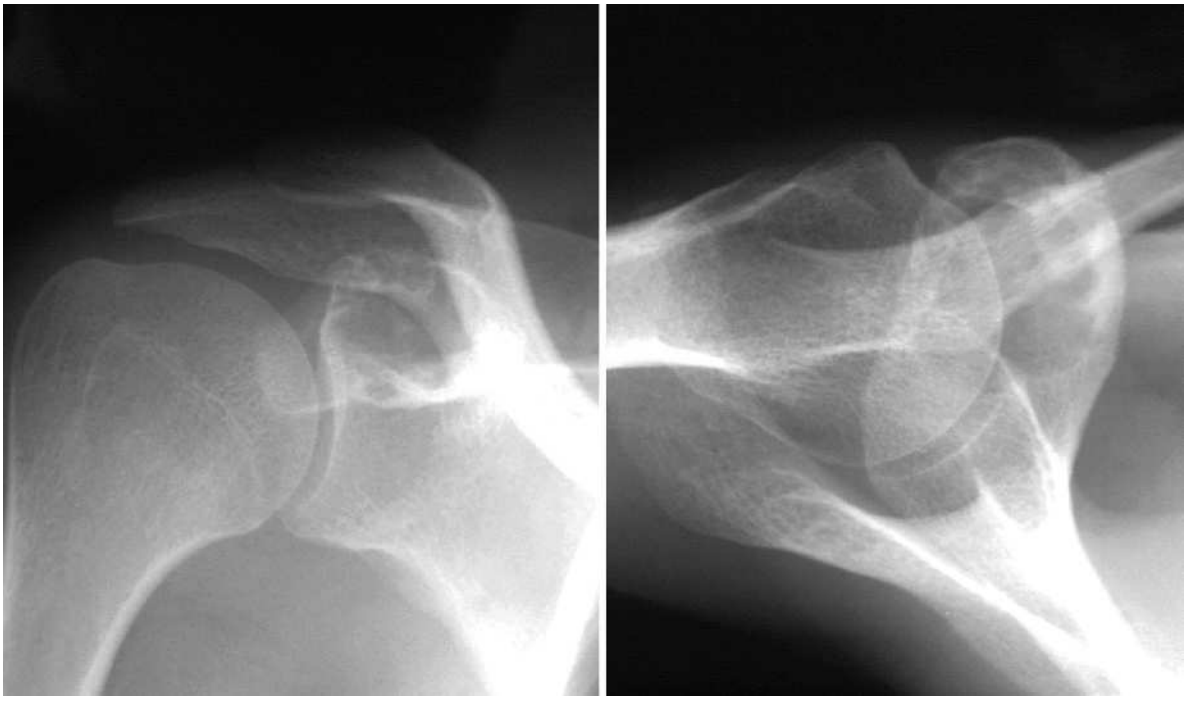

Fig. 32.13. Malignant hemangioendothelioma of scapula. Radiographs show focal bone lysis/destruction with partial septation and expansion within the coracoid process

32.3.7 Non-Hodgkin's Lymphoma

As with all other bones, the scapula can be involved with non-Hodgkin's lymphoma (Bloem 1985), although it only rarely presents initially there or with sparse synchronous lesions (Malde et al. 2004). These lesions within the scapula may be very sclerotic with expansion, possible thick septations, or permeative and lytic, with possible pathological fractures (Brtkova et al. 1999).

32.3.8 Plasmacytoma and Multiple Myeloma

A common hematopoietic malignancy with a peak age in the eighth decade, multiple myeloma is not uncommon within the scapula; however, if present, it is usually associated with multifocal disease (Dorfmann and Czerniak 1998). These lesions are usually sharply punched-out lytic cortical ones with some intraosseous expansion if thinner parts of the bone are involved. Lesions are rarely sclerotic and this is usually in association with the Poems systemic syndrome, which consists of polyneuropathy, organomegaly, endocrinopathy, M-component spike in blood serum, and skin changes (Bardwick et al. 1980; Hall and Gore 1988). Occasionally, in approximately 10–15% of patients with multiple myeloma (Grogan and Spier 1992), amyloidosis may be deposited within the bone marrow, sometimes adjacent to joints. Plasmacytoma is a solitary myeloma seen at radiographic screening with a skeletal survey and there is no M component within the serum, although approximately 25% of patients may have low-level gammopathies (Dorfmann and Czerniak 1998). They are usually lytic focal bone lesions with final diagnosis made at biopsy.

32.3.9 Eosinophilic Granuloma, Langerhans Cell Histiocytosis

These lesions may sometimes involve the scapula and can have an apparent benign appearance with marked focal expansion (Brtkova et al. 1999), and have been described within the acromion (Moyer et al. 1987).

32.3.10 Metastases and Malignant Systemic Entities

Metastases of many tumor primaries may involve the scapula. Renal metastases have rarely been reported to present within the scapula (Cheng et al. 2007). Other malignant systemic disorders, such as the Erdheim–Chester disease, may also involve the scapula.

32.4 Extraosseous Tumor with Overt Secondary Bone Destruction of Scapula

A variety of chest wall tumors can secondarily invade the scapula (Tateishi et al. 2003b). The epicenter of the tumor is usually associated with a larger mass outside of the scapula.

32.5 Bone Pseudotumors of Scapula

32.5.1 Variations of Central Ossification

These variants may mimic trauma or simulate tumor. There is variation of the ossification of the acromial process of the scapula and pseudoepiphysis; these may be symmetric bilaterally and occur age specifically (Kleinman and Spevak 1991). Ossification of the acromion process occurs by age 15 years, as opposed to the coracoid-process secondary ossification center which occurs around 3 months (Kleinman and Spevak 1991). The ossification of the scapula begins at the central nutrient artery nearer the glenoid than the vertebral margin. Endochondral bone formation progresses from this region of central ossification (Kleinman and Spevak 1991), as opposed to a real post-traumatic fracture line passing through the middle of the scapula with a horizontal path.

32.5.2 Normal Bone Marrow and Foramina

Normal age-related variations of red and yellow marrow, especially of the red marrow within the epiphysis more adjacent to near the glenoid margin, within the intraosseous bone of the scapula occur (Richardson and Patten 1994; Anderson et al. 2007, 2008). This is usually less patchy than seen in the marrow of the sacrum with aging. A combination of standard MR sequences, particularly a T1-weighted sequence, usually allows for recognition of normal marrow.

Although rare, 29% of scapulae may have normal foramina which may produce radiolucent defects potentially mimicking metastases and myeloma (Pate et al. 1985). The four main sites of well-punched-out foraminae occur at the superior border of the scapula at the junction with the coracoid process, in the body at the inferior scapula spine, in the superior fossa and superomedial border above the scapular spine (Pate et al. 1985; Resnick 1995).

32.5.3 Scapular Thinning

Scapula normal foramina should be differentiated from scapula thinning, which is evident in the body of the bone of the scapula and may result in large regions of radiographic radiolucency of variable shapes and size (Resnick 1995).

32.5.4 Congenital or Developmental Anomalies/ Variants that May Mimic Tumors

Usually present at birth or in association with a combination of radiological and clinical features, these entities should not be confused with tumors. Developmental processes may be associated with scapula irregularities or apparent pseudotumor formation, e.g., partial or complete duplication of the scapula, which very rarely presents in newborns (Sanches et al. 2003; Simanovsky et al. 2006), and of components such as the coracoid process (Sharma 2003). These very rare additional scapulae may occur lateral and above the humerus as accessory or anomalous ossicles. Other focal congenital anomalies include Sprengel's deformity of the scapula (Ogden et al. 1979), shoulder girdle and secondary to brachial plexus birth palsies (Kon et al. 2004), or systemic disorders such as with Erb–Duchenne paralysis. Hypoplasia of the glenoid and scapula neck have been described in small series (Theodorous et al. 2006) and may be associated with humeral head subluxation and labral enlargement. Around the hypoplasia regions there can be a replacement of abnormal tissue with inhomogeneous MR signal intensities reflecting fibrocartilage and fat, each in approximately half of cases (Theodorous et al. 2006); however, there is hypoplasia or a bone deficit with a combination of findings such

as glenohumeral subluxation and no destructive mass present.

Ossification of the superior transverse ligament above the scapula notch may occur leading to compression of the suprascapular nerve as it passes through this canal, especially associated with active rotational movements of the shoulder joint. Weakness and atrophy of the supraspinatus and infraspinatus muscle may develop and is known as the scapular notch syndrome.

32.5.5 Post-traumatic Bone Pseudotumors of Scapula

Deformities may be due to focal trauma such as posterior or anterior glenohumeral dislocation with fractures, Bankart lesions within the inferior glenoid rim, or a more rare osteochondral defect/avascular necrosis of the glenoid fossa (OCD). The OCD of the glenoid fossa of the scapula (Yu et al. 1998) may be associated with a single trauma or arise from low-grade repetitive microtrauma. It is usually associated with a history of anterior dislocation and shoulder instability, and may be associated with a heavy work load or occupation involving heavy lifting. There is a bony defect within the anterior inferior and middle glenoid fossa, but if extensive this finding may continue to involve superior and posterior glenoid fossa surfaces (Yu et al. 1998). The bony defect is a subchondral cystic one with sclerotic rim and typically there is an absence of cortical articular surface bone in the involved region (Yu et al. 1998).

Regarding stress and fracture pseudotumors, fractures of the scapula may occasionally present as bony pseudotumors. Usually the appearances and clinical history are diagnostic; however, delay in the initial diagnosis may make the appearances more complex and diagnosis difficult. Subglenoid scapular transverse fractures may sometimes occur in some sports, such as ice hockey, and delayed diagnosis with pseudoarthrosis may be difficult. Fractures may occur within the scapula, e.g., scapula neck with dysplasias/hypoplasias or related to osteogenesis imperfecta, or coracoid process associated with acromioclavicular separation (Protass 1975), or related to the abused child syndrome.

Scapula stress injury (Sandrock 1975; Herick-Hoff et al. 2007) or stress fractures (Bowerman and McDonnell 1975) may relate to acute or repetitive sporting injuries with throwing sports such as baseball or trap shooting and golf (Resnick 1995).

32.6 Benign Systemic Disorders which May Involve the Scapula

32.6.1 SAPHO Syndrome and Associated Entities

The scapula may become sclerotic with variable density (Kasperczyk and Freyschmidt 1994), although usually there is a diagnostic constellation of features and sites of involvement, such as with sternoclavicular, sacroiliac joint, and spine. Very rarely these may present or occur at different time points (Davies et al. 1999).

32.6.2 Myelofibrosis

Myelofibrosis may have associated scapula osteosclerosis. Other systemic sclerotic-forming bone systemic disorders may also be associated with increased scapula density, although this is usually associated with multiple anatomic sites.

32.6.3 Cystic Angiomatosis

The scapula may be involved with rare benign systemic disorders such as the diffuse angiomatous disorder cystic angiomatosis (Resnick 1995). The vascular bone lesions may be single or multiple at the time of presentation and there may also be visceral involvement. This entity may mimic malignant disorders with its expansile multiple bone lesions which may resemble malignant vascular tumors. The diagnosis is usually made by histology.

32.6.4 Post Therapy, Post Radiation

Bone damage after ionizing radiation, radiation necrosis, may occur due to the dose range used in modern radiotherapy. On radiographs lytic or sclerotic changes are evident usually involving both the glenoid of the scapula and the humeral head and the appearances can mimic a neuropathic joint (Bluemke et al. 1994; Anderson et al. 2008). On MRI there is a patchy increase in signal intensity within the bone marrow, skin, and soft tissue, and the absence of a mass-like focal or destructive lesion. Stress fractures may be associated with

these findings and occur in this setting in the midscapula region (Bluemke et al. 1994).

32.6.5 Joint-Related Processes

32.6.5.1 Synovial Chondromatosis

Synovial chondromatosis, if extensive, may partially erode the scaphoid and may be misdiagnosed as a cartilaginous tumor; however, correct use and correlation between radiographs and/or CT with MRI is usually diagnostic.

32.6.5.2 Rheumatological and Degenerative

Rheumatoid arthritis may be more largely monoarticular at presentation with large regions of pannus soft tissues eroding the glenoid and scapula neck region, and present as a diagnostic difficulty to the unsuspecting (Resnick 1995). The presence of fibrin pearls and joint effusion with more rim-like pannus contrast enhancement is usually enough to make the correct diagnosis with supporting hematological screens (Anderson 2008). Amyloidosis may also involve the glenohumeral joint eroding bone of the neck of scapula, although it is unusual. This latter situation has the unusual, but diagnostically supportive, signal characteristics of decreased signal intensity on both T1- and T2-weighted images.

Glenoid synovial cysts, multiple or single, due to overuse or degeneration may be problematic for diagnosis particularly if there is monoarticular joint presentation; however, there is usually a combination of features which make the diagnosis possible (Resnick 1995; Anderson et al. 2008).

32.6.5.3 Crystal Arthropathies

Extensive monoarticular tophaceous gout, hydroxyapatite deposition disease (HADD), and calcium pyrophosphate deposition disease (CPPD), continue to occasionally be misdiagnosed as tumor. Correlation of radiographs and/or CT with MRI is usually diagnostic if the diagnosis is considered to be within the radiological differential list for exclusion (Anderson et al. 2008). Extensive and rapid chondrolysis may be associated with some scapula destruction; however, usually there is concern for infection, not tumor, and aspiration may diagnose a crystal arthropathy.

32.6.6 Infection

Scapula infection is rare unless associated with direct penetrating injuries or with immune compromise where there may be shoulder joint and scapula destruction (Steinbach et al. 1993). In the pediatric age group infection within the scapula is very rare and made difficult as the scapula is anatomically difficult to image; therefore, a combination of computed tomography and MRI is recommended in this age group specifically (Azoulay et al. 2007). In the adult, atypical infections, such as *Brucellosis,* may affect the scapula (Karsen et al. 2007) and there may be a diffusely sclerotic appearance (Brtkova et al. 1999). Tuberculosis should be considered in the pseudotumor diagnostic list involving the scapula. It may be primarily of bone described within the acromion and body of the scapula, or secondarily involve the scapula from the surrounding soft tissues (Kam et al. 2000; Greenhow and Weintrub 2004; Husen et al. 2006). Hydatid involvement of the scapula may occur in endemic regions (Herrera and Martinez 2003).

32.7 Extraosseous Tumors Related to/with Impact on the Scapula

Myositis ossificans involving deep muscles adjacent to bone may incite a periosteal new bone formation that is typically multilayered and has been described adjacent to the scapula (Dorfmann and Czerniak 1998). Usually there is a cleft between the scapula and pseudotumor soft-tissue-centered zonal calcification on radiographs and/or computed tomography, allowing for diagnosis; however, given the uncommon location, follow-up imaging and also biopsy may be required. Different from this appearance (Brtkova et al. 1999), myositis ossificans may be indistinguishable from an osteochondroma due to superimposition of nearby bony structures.

32.8 Conclusion

Scapular bone tumors are rare. Due to flat-bone complex anatomy and potential lack of characteristic im-

aging features, a combination of imaging modalities is recommended to determine diagnostic features and for local staging. Benign tumors, such as osteochondroma and tumor-like lesions, are more frequent in the first three decades of life, as opposed to malignant tumors, which occur mainly in the fourth to seventh decades, with chondrosarcoma being the most frequently reported lesion. Special concern should be raised by the presence of apparently benign-appearing lesions over the lateral scapular margin or within the acromion or coracoid processes in the adult, as this may be a chondrosarcoma. Prior to biopsy, a surgical oncology opinion should be sought.

References

Altuntas AO, Slavin J, Smith PJ et al. (2005) Accuracy of computed tomography guided core needle biopsy of musculoskeletal tumours. Aust N Z J Surg 75(4):187–191

Anderson SE, Davies AM, Vanhoenacker FM, Maas M, Gielen JL (2007) Imaging of orthopedic sports injuries, 1st edn. Springer, Berlin Heidelberg New York

Anderson SE, Johnstom JO, Steinbach LS (2008) Invited review: Pseudotumors of the shoulder. Eur J Radiol:68:147–158

Aoki J, Moser RP, Vinh TN (1989) Giant cell tumor of the scapula. A review of 13 cases. Skeletal Radiol 18(6):427–434

Azoulay R, Alison M, Sekkel A et al. (2007) Imaging of child osteoarticular infections. 14 (Suppl 2):S112–S121

Azouz EM, Slomic AM, Marton D et al. (1985) The variable manifestations of dysplasia epiphysealis hemimelica. Pediatr Radiol 15:44–49

Bardwick PA, Zvaifler NJ, Gill GN et al. (1980) Plasma cell dyscrazia with polyneuropathy, organomegaly, endocrinopathy, M protein and skin changes: the POEMS syndrome–report on two cases and a review of the literature. Medicine 59:311–322

Bloem JL, Falke TH, Taminiau AH et al. (1985) Magnetic resonance imaging of primary malignant bone tumors. RadioGraphics 5: 853–886

Bluemke DA, Fishman EK, Scott WW (1994) Skeletal complications of radiation therapy. RadioGraphics 14:111–121

Boutin RD, Spitz DJ, Newman JS et al. (1998) Complications in Paget's disease at MR imaging. Radiology 209:641–651

Bowerman JW, McDonnell EJ (1975) Radiology of athletics injuries: baseball. Radiology 116:611–615

Brtkova J, Nidecker A, Ziakova et al. (1999) Tumors and tumor-like lesions of scapula. Acta Med (Hradec Kralove) 42:103–110

Cheng MF, Peng YJ, Huang GS (2007) Unusual scapular metastases as initial manifestation of advanced nonseminomatous germ cell tumor of the mediastinum. Heart Lung 36(1):79–84

Choong P, Sim F (2000) Tumours: masterclass. Curr Orthop 14(2):117–132

Cleeman E, Auerbach JD, Springfield DS (2005) Tumors of the shoulder girdle: a review of 194 cases. J Shoulder Elbow Surg 14(5):460–465

Coombs RJ, Zeiss J, McCann K et al. (1986) Case report 360: multifocal Ewing tumor of the skeletal system. Skeletal Radiol 15:254–257

Crocco JA (1977) The Scapula. In: Gray H (ed) Anatomy descriptive and surgical. Bounty Books, Crown Publishers, New York

Damron TA, Brodke DS, Hecher JP et al. (1993) Case report 803: Gorhmas disease (Gorham Stout syndrome). Skeletal Radiol 22(6):464–467

Davies AM, Marino JA, Evans N et al. (1999) Sapho syndrome: 20-year follow-up. Skeletal Radiol 28(3):159–162

Dorfmann HD, Czerniak B (1998) Bone tumors, Mosby, St. Louis

Erlemann R, Davies AM, Edel G et al. (1988) Tumoroese Raumforderungen der Skapula. Radiologe 28:87–93

Fritz RC, Helm CA, Steinbach LS et al. (1992) Suprascapular nerve entrapment: evaluation with MR imaging. Radiology 182:437–444

Gebert C, Hardes J, Streitbuerger A et al. (2004) Chondroblastoma of the acromion mimicking fibrous dysplasia. Acta Orthp Belg 70(6):616–618

Gold RH, Mirra JM(1983) Case report 234. Skeletal Radiol 10:57

Greenhow TL, Weintrub PS (2004) Scapular mass in an adolescent. Pediatr Infect Dis J 23(1):84–85, 89–90

Grogan TM, Spier CM (1992) The B-cell immunoproliferative disorders, including multiple myeloma and amyloidosis. In: Knowles DM (ed) Neoplastic hematology. Williams and Wilkins, Baltimore

Hall FM, Gore SM (1988) Osteosclerotic myeloma, and other lymphoreticular neoplasms. Skeletal Radiol 17:101–105

Hatfield PM, Schulz MD (1970) Postirradiation sarcoma. Including 5 cases after X-ray therapy of breast carcinoma. Radiology 96:593

Herickhoff PK, Keyurapan E, Fayad LM et al. (2007) Scapular stress fracture in a professional baseball player: a case report and review of the literature. Am J Sports Med 35(7):1193–1196

Herrera A, Martinez AA (2003) Extraspinal bone hydatidosis. J Bone Joint Surg Am 85-A(9):1790–1794

Holt EM, Murphy GJ, Al-Jafari M (1995) Chondroblastoma of the acromion. Skeletal Radiol 24(3):223–224

Hreslco MT, Miele JF, Goldberg MJ (1988) Unicameral bone cyst in the scapula of an adolescent. Clin Orthop Relat Res 236:141–144

Husen YA, Nadeem N, Aslam F et al. (2006) Tuberculosis of the scapula. J Pak Med Assoc 56(7):336–338

Johnson WW, Coburn TP, Pratt CB et al. (1978) Ultrstructure of malignant fibrous histiocytoma arising in the acromion. Human Pathol 9:199

Kaila R, Ropars M, Briggs TW et al. (2007) Aneurysmal bone cyst of the paediatric shoulder girdle: a case series and literature review. J Pediatr Orthop B 16(6):429–436

Kalbermatten NT, Vock P, Rufenacht D et al. (2001) Progressive melorheostosis in the peripheral and axial skeleton with associated vascular malformation: imaging findings over three decades. Skeletal Radiol 30(1):48–52

Kam WL, Leung YF, Chung DM et al. (2000) Tuberculous osteomyelitis of the scapula. Int Orthop 24(5):301–302

Karsen H, Akdeniz H, Irmak H et al. (2007) A *Brucellosis* case presenting with mass formation suggestive for tumor in soft tissue. South Med J 100(11):1074

Kasperczyk A, Freyschmidt J (1994) Pustulotic arthroosteitis: spectrum of bone lesions with palmoplantar pustulosis. Radiology 191:207–211

Kellie SJ, Pratt CB, Parham DM et al. (1990) Sarcoma (other than Ewing's) of flat bones in children and adolescents. A clinicopathologic study. Cancer 6s(4):1011–1016

Kessler S, Mirra JM, Gordon O (1994) Case report 823: fibro-osseous pseudotumor of the scapula. Skeletal radiol 23(1):73–77

Kleinman PK, Spevak MR (1991) Variations in acromial ossification simulating infant abuse in victims of sudden infant death syndrome. Radiology 180(1):185–187

Kon DS, Darakjian AB, Pearl ML et al. (2004) Glenohumeral deformity in children with internal rotation contractures secondary to brachial plexus birth palsy: intraoperative arthrographic classification. Radiology 231:791–795

Kumar B, Murphy WA, Whyle MP (1981) Progressive diaphyseal dysplasia (Engelmann's disease): scintigraphic–radiographic–clinical correlations. Radiology 140:87–92

LaGrange JE, Ramaioli A, Chateau MC et al. (2000) Sarcoma after radiation therapy: retrospective multiinstitutional study of 80 histological confirmed cases. Radiology 216:197–205

Link TM, Brinkschmidt C, Lindner N et al. (1999) Primary bone tumors and "tumor-like lesions" of the shoulder. Their histopathology and imaging. Rofo170(5):507–513

Llauger J, Aixut S, Canete N et al. (2008) Meningioma of the scapula. Skeletal Radiol 37(2):169–171

Logan PM, Munk PL, O'Connel JX et al. (1996) Post-irradiation osteosarcoma of the scapula. Skeletal Radiol 25(6):596–601

Lye DJ, Wepfer JF, Haskell DS (1988) Case report 458: low grade hemangioendothelioma of the clavicle and acromion. Skeletal Radiol 17(1):57–59

Malde R, Laskar S, Muckaden MA et al. (2004) Primary, multifocal extranodal lymphoma presenting with multiple cranial nerve palsies: an unusual presentation of an uncommon entity. Leuk Lymphoma 45(2):389–391

Mayil Vahanan N, Mohanlal P, Bose JC et al. (2007) The functional and oncological results after scapulectomy for scapular tumours: 2- to 16-year results. Int Orthop 31(6):831–836

Moyer RA, Betz RR, Bonakdarpour A (1987) Case report 424: Eosinophilic granuloma of the acromion. Skeletal Radiol 16:333–335

Mulder JD, Schütte HE, Kron HM, Taconis WK (1993) Radiological atlas of bone tumors. Elsevier, Amsterdam, S20–S21

Murphey MD, Choi JJ, Kransdorf MJ et al. (2000) Imaging of osteochondroma: variants and complications with radiologic–pathologic correlation. RadioGraphics 20:1407–1434

Murphey MD, Jaovisidha S, Temple T et al. (2003) Telangiectatic osteosarcoma: radiological pathological comparison. Radiology 229:545–553

Murray RO, McCredie J (1979) Melorheostosis and the sclerotomes: a radiological correlation. Skeletal Radiol 4:57

Nakamura S, Kusuzaki K, Murata H et al. (1999) Clinical outcome of total scapulectomy in 10 patients with primary malignant bone and soft-tissue tumors. J Surg Oncol 72(3):130–135

Ogden JA, Conlogue GJ Phillips MS et al. (1979) Sprengel's deformity. Radiology of the pathologic deformation. Skeletal Radiol 4(4):204–211

Ogose A, Sim FH, O'Connor MI et al. (1999) Bone tumors of the coracoid process of scapula. Clin Orthop Relat Res (358):205–214

Ogose A, Hotta T, Morita T et al. (2000) Solitary osseous hemangioma outside the spinal and craniofascial bones. Arch Orthop Trauma Surg 120(5–6):262–266

Park YN, Ryu KN, Han CS et al. (1991) Giant cell tumor of scapula associated with aneurysmal bone cyst. J Korean Med Soc 6(1):69–73

Pate D, Kusunoglu S, Resnick D (1985) Scapula foramina. Skeletal Radiol 14(4):270–275

Potter HG, Schneider R, Ghelman B et al. (1991) Multiple giant cell tumors and Paget's disease of bone: radiographic and clinical correlation. Radiology 180:261–264

Protass JJ, Stampfli FV, Osmer JC (1975) Coracoid process fracture diagnosis in acromioclavicular separation. Radiology 116:61–64

Quan GM, Carr D, Schlicht S et al. (2005) Lessons learnt from the painful shoulder; a case series of malignant shoulder girdle tumours misdiagnosed as frozen shoulder. Int Semin Surg Oncol 2(1):2

Resnick D (1995) Diagnosis of bone and joint disorders, 3rd edn. Saunders, Philadelphia

Richardson ML, Patten RM (1994) Age-related changes in marrow distribution in the shoulder: MR changes in imaging findings. Radiology 192:209–215

Rodriguez JA, Craven JE, Heinrich S et al. (1999) Current role of scapulectomy. Am Surg 65(12):1167–1170

Rosenthal DI, Alexander A, Rosenberg AE et al. (1992) Ablation of osteoid osteoma with percutaneous placed electrode: a new procedure. Radiology 183:29–33

Ruggieri P, Biagnini B, Picci P (1987) Case report 437: Solitary (unicameral simple) bone cyst of the scapula. Skeletal Radiol 16(6):493–497

Sanches Alegre MC, Maria C, Mardonnes GG (2003) Duplication of the scapula. Skeletal Radiol 32(12):728–730

Sandrock AR (1975) Another sports fatigue fracture. Stress fracture of the coracoid process of the scapula. Radiology 117:274

Sharma BG (2003) Duplication of the clavicle with triplication of the coracoid process. Skeletal Radiol 32(11):661–664

Sharma H, Jane MJ, Reid R (2005) Scapulo-humeral Paget's sarcoma: Scottish Bone Tumor Regsitry experience. Eur J Cancer Care (Engl) 14(4):367–372

Simanovsky N, Hiller N, Simanovsky N (2006) Partial duplication of the scapula 35(9):696–698

Smith SE, Murphey MD, Motamedi K et al. (2002) From the archives of the AFIP. Radiologic spectrum of Paget's disease of bone and its complications with pathologic correlation. RadioGraphics 22:1191–1216

Steinbach LS, Tehranzadeh J, Fleckenstein J et al. (1993) Human immunodeficiency virus infection: musculoskeletal manifestations Radiology 186:833

Subhas N, Sundaram M, Bauer TW et al. (2008) Glenoid labrum ossification and mechanical restriction of joint motion: extraosseous manifestations of melorheostosis. Skeletal Radiol 37(2):177–181

Tateishi U, Gladish GW, Kusumoto M et al. (2003a) Chest wall tumors: radiologic findings and pathologic correlation: Part 1. Benign tumors. RadioGraphics 23:1477–1490

Tateishi U, Gladish W, Kusumoto M et al. (2003b) Chest wall tumors: radiologic findings and pathologic correlation: Part 2. Malignant tumors. RadioGraphics 23:1491–1508

Theodorous JJ, Theodorous DJ, Resnick D (2006) Hypoplasia of the glenoid neck of the scapula: imaging findings and report of 16 cases. J Comput Assist Tomogr 30(3):535–542

Theologis T, Osterlere S, Gibbons CL et al. (2007) Toxic osteoblastoma of the scapula. Skeletal Radiol 36(3):253–257

Van Riet RP, Van Glabbeek F (2007) Arthroscopic resection of a symptomatic snapping subscapular osteochondroma. Acta Orthop Belg 73(2):252–254

Vellenga CJR, Puawels EKJ, Bijvoet OL et al. (1984) Untreated Paget's disease bone studied with scintigraphy. Radiology 153:799–805

Weatherall PT, Maale GE, Mendelsohn DB et al. (1994) Chondroblastoma: classic and confusing appearance at MR imaging. Radiology 190:467–474

Yu JS, Greenway G, Resnick D (1998) Osteochondral defect of glenoid fossa. Radiology 206:35–40

Anatomical Considerations: Spine and Sacrum

33

Amy W. Kao and Hakan Ilaslan

CONTENTS

KEY POINTS

- In children and adults, metastases are both the most frequent tumor of bone and the most frequent tumor of the axial skeleton
- The age of the patient, favored location of specific tumors in the axial skeleton, and its relative frequency is essential to evaluating a vertebral tumor
- On the basis of location within the vertebrae, lesions with a predilection for the posterior elements include aneurysmal bone cyst, osteoid osteoma, osteoblastoma, osteochondroma, Ewing sarcoma, osteosarcoma, chondrosarcoma
- On the basis of location within the vertebrae, lesions with a predilection for the vertebral body include metastases, Langerhans cell histiocytosis of the spine, giant cell tumor, hemangioma, plasmacytoma, myeloma and lymphoma
- Lesions with a predilection for the sacrum include Paget's disease, chordoma, giant cell tumor and benign notochordal cell tumors

A. W. Kao, MD
Diagnostic Radiology/Hb6, Cleveland Clinic Foundation, 9500 Euclid Avenue, Cleveland OH 44195, USA

H. Ilaslan, MD
Section of Musculoskeletal Radiology, Imaging Institute, Cleveland Clinic, Assistant Professor of Radiology, Cleveland Clinic Lerner School of Medicine of Case Western Reserve University, Diagnostic Radiology/A21, Cleveland Clinic Foundation, 9500 Euclid Avenue, Cleveland OH 44195, USA

33.1 Introduction

Primary tumors of the vertebral column are far less common than metastatic lesions. Often, one can arrive at an accurate pre-histologic diagnosis, with patient age, history and an understanding of imaging characteristics of a lesion with a predilection for the vertebrae and sacrum.

33.2 Metastases

The axial skeleton is the most common site for osseous metastases. The thoracic spine is the most commonly affected. In the pediatric population, neuroblastoma and leukemia are the most common primary malignancies to metastasize. In the adult population, breast, prostate, and lung carcinomas are the most common primary malignancies to metastasize. The vertebral body, the subchondral regions, anterior margins and pedicles are the earliest sites of involvement due to the rich vascular supply. Metastatic lesions are variable in appearance ranging from osteolytic, sclerotic, or mixed. Up to 70% of cancellous bone is destroyed before a lesion is detectable radiographically (Sundaram 1996). Bronchogenic carcinoma and breast carcinoma are the most common lytic metastases. The most common sclerotic metastases are of prostate and breast origin. Less frequently seen are gastrointestinal and lymphoma metastases. Expanded vertebral sclerotic metastases may have a patchy or diffuse appearance. Diffuse sclerotic metastases give rise to the appearance of the "ivory vertebra".

33.3 Overview of Primary Pediatric Bone Tumors

In the pediatric population, age can help narrow a list of possible diagnoses. Average age ranges at the time of diagnosis for tumors in the axial skeleton are as follows: in the 0–5 age range, Langerhans cell histiocytosis is the main benign consideration, whereas in the malignant category, Ewing Sarcoma, leukemia and metastatic neuroblastoma and Wilms tumor are the primary considerations. In the 5–10 age range, benign lesions include aneurysmal bone cyst, Langerhans cell histiocytosis, non ossifying fibroma, osteoblastoma, and osteoid osteoma. Ewing sarcoma and osteosarcoma are the malignant considerations. In the 10–20 age range, aneurysmal bone cyst, osteochondroma, and osteoid osteoma are the most common benign lesions, and chondrosarcoma joins the list of malignant considerations considered in the previous age range (Dormans and Moroz 2007).

33.4 Benign Lesions in the Pediatric Population

33.4.1 Langerhans Cell Histiocytosis of the Spine

Langerhans cell histiocytosis (LCH), also known as eosinophilic granuloma of the bone, is seen most frequently in the first three decades with a peak incidence between ages 5 and 10. Appendicular skeleton involvement is more common than axial involvement; only up to 15% of children with LCH have vertebral involvement. Although they are often discovered in asymptomatic patients, the most common presenting complaint is pain, rarely accompanied by neurological symptoms.

LCH typically involves the vertebral body and is an aggressive-appearing osteolytic lesion leading to vertebral collapse, with complete collapse giving the characteristic appearance of vertebra plana (Fig. 33.1a–c). In older children, the degree of destruction is less severe, and vertebra plana is less common. A grading system has been suggested with Grade I lesions reflecting 0%–50% collapse and Grade II lesions having 51%–100% collapse. Lesions are further classified as A or B according to symmetric or asymmetric collapse, respectively. There is contradicting evidence about the predilection of LCH for particular regions of the spine: some have suggested LCH is more common in the thoracic spine, while others have indicated higher prevalence in the cervical spine. Since LCH is multifocal in half of patients, a skeletal survey or bone scan can be done to identify other lesions. Most patients with LCH have a favorable course, as LCH may spontaneously regress with osseous reconstitution and partial restoration of vertebral height.

33.4.2 Aneurysmal Bone Cyst

Aneurysmal bone cysts account for only 1% of primary bone tumors; however, of these, up to 20% are located in the spine (Boriani et al. 2001). Approximately 80% present in patients in the first two decades of life (Sundaram 1996) with a slight female predominance. They

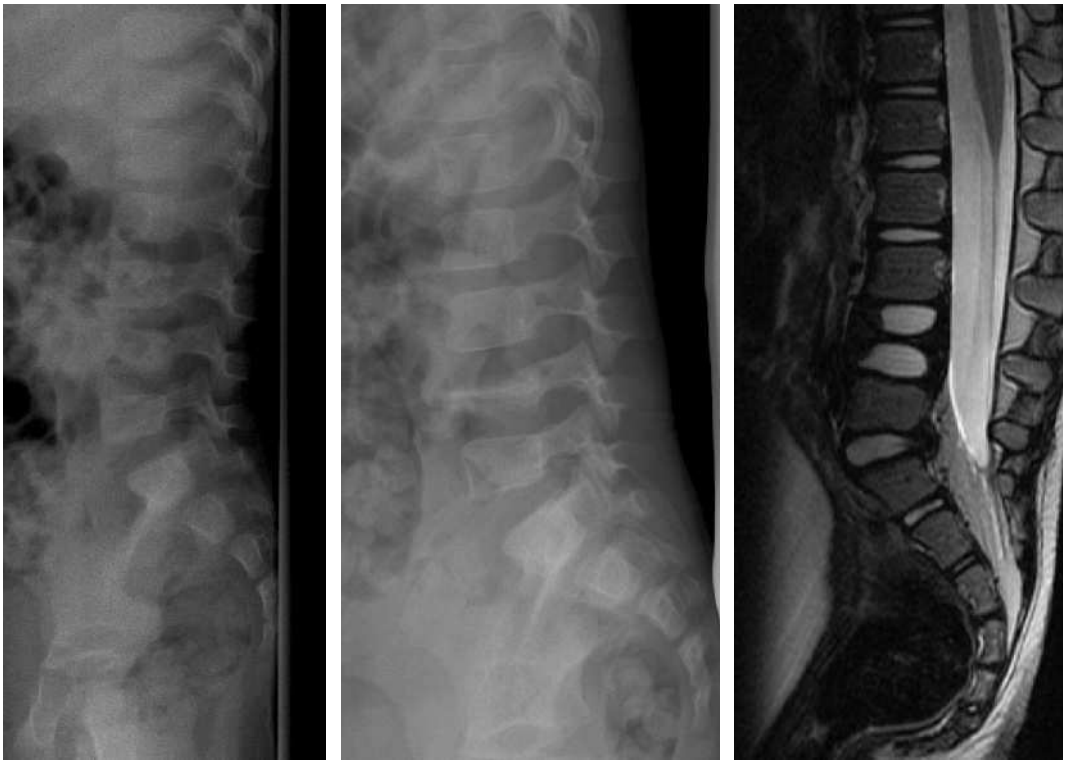

a b,c

Fig. 33.1a–c. Langerhans cell histiocytosis. **a** Initial lateral lumbar radiograph in a child demonstrates preservation of vertebral body height at all levels. **b** Follow-up imaging one year later demonstrates vertebra plana deformity of the L4 vertebral body. **c** Sagittal T2 image of the same patient demonstrates collapse of the L4 vertebral body with preservation of the adjacent intervertebral disc height

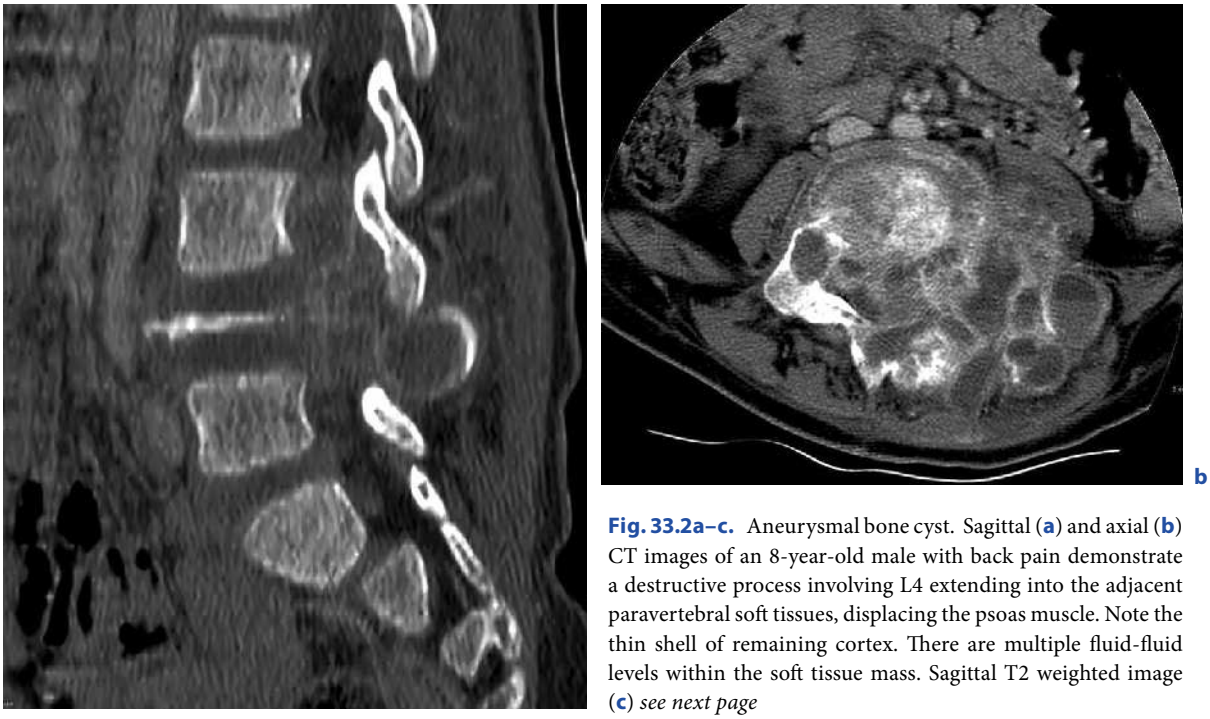

a b

Fig. 33.2a–c. Aneurysmal bone cyst. Sagittal (**a**) and axial (**b**) CT images of an 8-year-old male with back pain demonstrate a destructive process involving L4 extending into the adjacent paravertebral soft tissues, displacing the psoas muscle. Note the thin shell of remaining cortex. There are multiple fluid-fluid levels within the soft tissue mass. Sagittal T2 weighted image (**c**) *see next page*

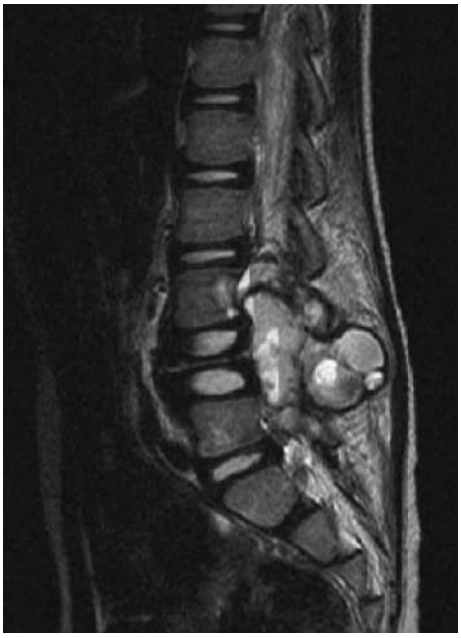

c

Fig. 33.2a–c. (*continued*) (**c**) demonstrates associated vertebral body involvement seen as vertebra plana, an uncommon manifestation of ABC. The MR images confirm the presence of multiple fluid-fluid levels within the adjacent soft tissue mass

involve all regions of the axial skeleton with slightly increased frequency in the lumbar spine (Akbarnia and Merenda 1996) and thoracic spine. Either the posterior elements alone, or the vertebral body in addition to the posterior elements, are involved. Aneurysmal bone cysts do not usually involve the vertebral body without extending into posterior elements. The lesion is usually purely lytic with expansion leading to a thin shell of bone seen at the periphery, which is a defining feature of an aneurysmal bone cyst (Fig. 33.2a). Lesions can span two and even three adjacent vertebrae which is a distinguishing feature of an aneurysmal bone cyst. Cross-sectional imaging with MR and CT demonstrates a well-defined cavity with multiple fluid–fluid levels reflecting hemorrhage with sedimentation which is a hallmark of this lesion (Fig. 33.2b,c). The differential diagnosis of an aneurysmal bone cyst varies on the location in the vertebral column and the age of the patient. Aneurysmal bone cysts in the sacrum may be difficult to distinguish from giant cell tumor in young adults. Aneurysmal bone cysts without an identifiable rim may be difficult if not impossible to distinguish from osteoblastoma. Only rarely do metastases or plasmacytoma enter the differential diagnosis due to the typical age of the patient with aneurysmal bone cyst.

33.4.3 Osteoblastoma and Osteoid Osteoma

Osteoid osteoma may be histologically indistinguishable from osteoblastoma. The vertebral column is the preferred site of osteoblastomas when compared to the appendicular skeleton. The opposite is true for osteoid osteoma. Lesions less than 1.5–2 cm in diameter are called osteoid osteomas, whereas those larger than 2 cm are called osteoblastomas. The majority of patients with osteoblastomas and osteoid osteomas present in the second and third decades of life.

Approximately 40% of all osteoblastomas are located in the spine (Llauger et al. 2000) and more than half are associated with scoliosis. Most osteoblastomas are localized to the posterior element, with vertebral body involvement following posterior element involvement (Fig. 33.3a). These lesions may demonstrate expansion, an osteoid matrix, and measure greater than 2 cm in diameters. More aggressive lesions demonstrate extension into the adjacent soft tissue and cortical destruction. MR appearance is variable depending on the proportion of matrix mineralization, T2-weighted sequences may show areas of mixed low and high signal intensity or may be mainly of low signal intensity (Shaikh et al. 1999) (Fig. 33.3b,c). A lesion with intense sclerosis without bony expansion favors osteoid osteoma over osteoblastoma. If the lesion is completely radiolucent, as are some osteoblastomas, it may be impossible to distinguish from an aneurysmal bone cyst.

Osteoid osteoma of the spine accounts for 10% of all osteoid osteomas. Patients with osteoid osteoma sometimes present with painful scoliosis with lesions located within two vertebrae of the apex of the spinal deformity (Akbarnia and Merenda 1996). Lesions can be difficult to identify on radiographs due to the small size. The classic CT appearance demonstrates sclerosis adjacent to a lytic lesion with a central calcified nidus. Bone scintigraphy is a useful method for evaluation of the axial skeleton when an osteoid osteoma is suspected and will demonstrate a focus of marked increased radiotracer uptake.

33.4.4 Osteochondroma

Although osteochondromas are uncommon in the spine, they are the most common benign tumors in the pediatric population. Spinal involvement is seen in 3% of cases, with the cervical spine the most common site in the axial skeleton (Albrecht et al. 1992). There is a

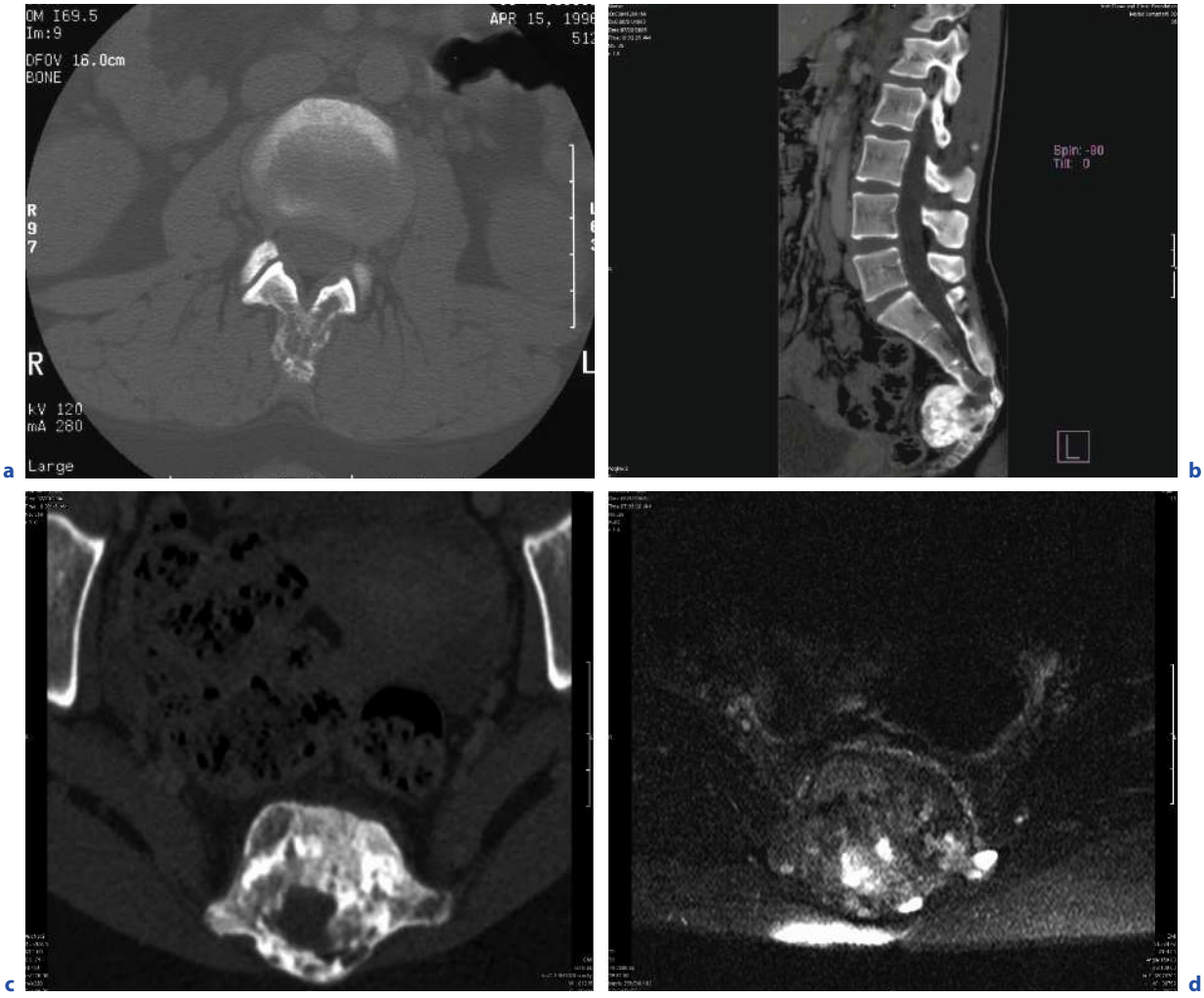

Fig. 33.3a–d. Osteoblastoma. Axial CT image (**a**) of in a young adult demonstrates an expansive lesion with diffuse osteoid matrix arising from the spinous process. This location and appearance in a young adult favors osteoblastoma. Sagittal (**b**) and axial (**c**) CT images demonstrate unexpected location of an osteoblastoma in a 21-year-old woman. There is an expansive sacrococcygeal lesion with extraosseous extension into the pelvis and diffuse osteoid matrix. Axial T2 weighted image (**d**) demonstrates corresponding low T2 intensity likely representing osteoid matrix and areas of increased T2 intensity representing secondary aneurysmal bone cysts

debate regarding its association with multiple hereditary exostoses. Osteochondromas most commonly involve the posterior elements, in particular the spinous processes. Association with prior radiation treatment has been reported in patients previously treated for neuroblastoma or Wilms tumor with a latent period between 17 months and 17 years (Murphey et al. 2000). Lesions are usually asymptomatic unless there is impingement on the spinal canal or neuroforamina. Radiographically, the hallmark of an osteochondroma is the continuity of the cortex between normal bone and the lesion. A cartilaginous cap may be present in the skeletally immature patient. CT is helpful for identifying cortical continuity with the affected vertebrae. Lesions that increase in size after skeletal maturity with a thick cartilaginous cap should raise suspicion of malignant degeneration (Rodallec et al. 2008).

33.5 Malignant Lesions in the Pediatric Population

33.5.1 Ewing Sarcoma

Ewing sarcoma is the most common primary malignant bone lesion in the pediatric population up to age ten (Bernstein et al. 2006). Mean age at presentation is in the second decade. There is a male predominance, 62% in a large series with 125 cases of primary vertebral Ewing sarcoma. Although it has a predilection for the appendicular skeleton primary axial involvement is seen in 3%–10% of cases (Ahlgren et al. 1996). Of the axial skeleton, the sacrum is the most frequent site of involvement followed by the thoracic and lumbar spine (Ilaslan et al. 2004a). Radiographs and CT appearance range from lytic, most commonly, to mixed, or the rare sclerotic lesion. Typical radiographic appearance is that of a permeative destruction with periosteal reaction and adjacent soft tissue mass and spinal canal invasion (Fig. 33.4). In the majority of lesions in the nonsacral spine, there was involvement of the posterior elements with extension into the vertebral body. The ala was the most frequently affected site in the sacrum. Other less common findings include vertebra plana, ivory vertebra, and pseudohemangioma (Ilaslan et al. 2004a). The reactive bone in Ewing sarcoma is typically not in the adjacent soft tissue mass, which is a distinguishing feature from osteosarcoma. Ewing sarcoma frequently metastasizes to bone, and lung. Metastatic Ewing sarcoma to the vertebrae is more common than a primary vertebral Ewing sarcoma. MR imaging features are nonspecific.

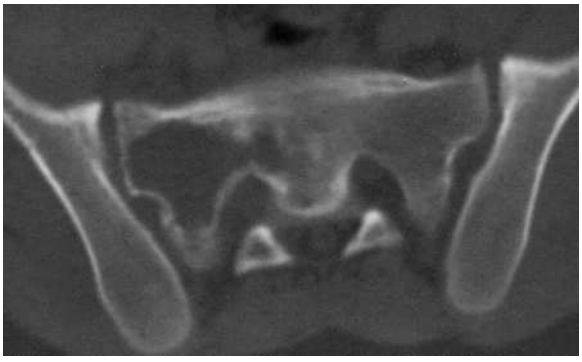

Fig. 33.4. Ewing sarcoma. Axial CT image of the sacrum demonstrates lytic lesion within the sacral ala. Such an appearance renders consideration of Ewing sarcoma from lymphoma as influenced by age

33.5.2 Leukemia

According to the Leukemia and Lymphoma society, leukemia represent 33% of all cancers occurring among children younger than 20 years of age. Radiographic findings of leukemic involvement in the axial skeleton are nonspecific and variable in appearance. Diffuse osteopenia, osteolysis, osteosclerosis, periosteal bone formation and permeative destruction, and pathologic vertebral fractures have all been observed. MR imaging is much more sensitive for demonstrating bone marrow changes in patients with leukemia but is nonspecific as well. The bone marrow is completely replaced by leukemic cells resulting in diffuse signal changes. On T1 weighted images, the signal intensity of the diseased marrow is hypointense compared to the intervertebral discs. This may sometimes be difficult to distinguish from the normal hematopoietic marrow in young adults. On T2-weighted images, there is variable increase in intensity. In addition, the abnormal marrow is enhanced after the intravenous administration of gadolinium chelate (Moulopoulos and Dimopoulos 1997).

33.5.3 Osteosarcoma

Osteosarcoma is the most common non hematological primary malignant lesion of bone. Osteosarcoma has a bimodal distribution with a peak incidence in the second decade of life. However, the mean age of incidence of vertebral osteosarcoma in the fourth decade is two decades later than the mean age of its appendicular counterpart (Llauger et al. 2000). Only 5% of osteosarcomas have primary lesions in the spine. In the largest series on primary vertebral osteosarcoma involving 198 cases, there was a predilection for the thoracic and lumbar spine followed by the sacrum and the cervical vertebral column (Ilaslan et al. 2004b). The most common histologic subtype was osteoblastic, followed by chondroblastic, then telangiectatic, fibroblastic, small cell and epithelioid (Ilaslan et al. 2004b). The lesions most often involve the posterior elements with extension through the pedicles to the vertebral body (Fig. 33.5a,b). Sacral tumors usually involve the body and sacral ala. Frequently, there is an associated soft tissue mass invading the spinal canal. Radiographic and CT appearance vary according to lesion type and grade but often show extensive cortical destruction and a soft tissue mass with calcification. In the Ilaslan et al. series, the majority

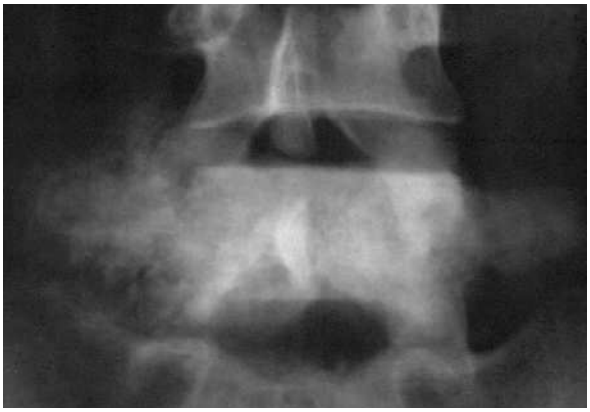

a

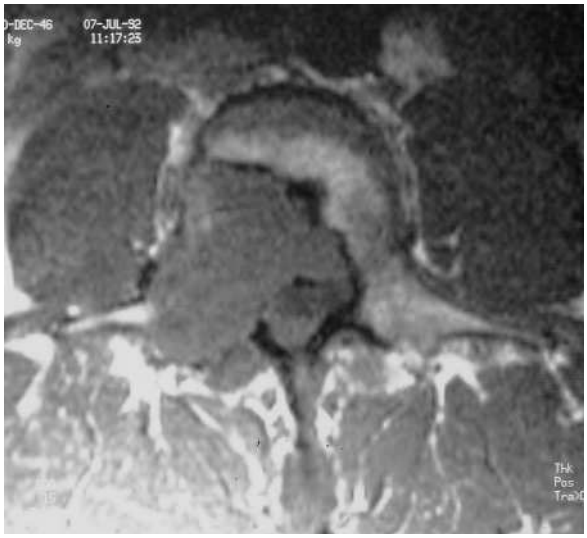

b

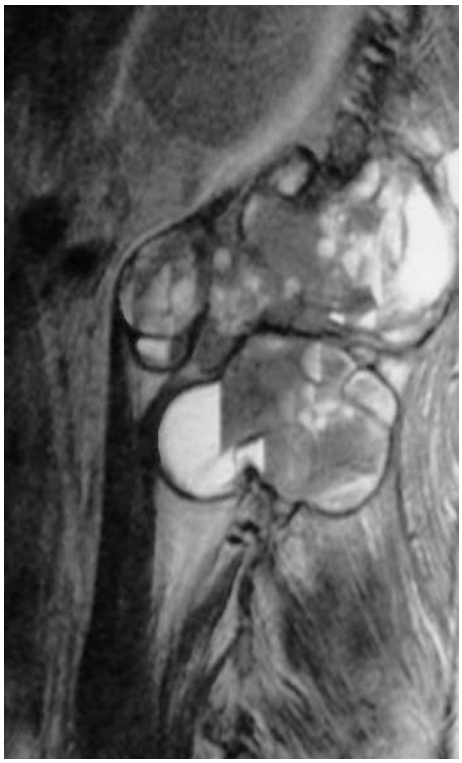

c

Fig. 33.5a–c. Spectrum of osteosarcoma. **a** Osteoblastic osteosarcoma. Frontal radiograph demonstrates sclerosis of the right transverse process in a 29-year-old male with associated diffuse sclerosis of the vertebral body and right transverse process which obscures the normal bony outlines. **b** Osteosarcoma. Axial T1 through the spine in a 48-year-old female demonstrates a large low signal mass centered on the right pedicle which invades the central canal and the vertebral body posteriorly. **c** Telangiectatic osteosarcoma. Sagittal T2-weighted MR of the spine in a 37-year-old female demonstrates replacement of the posterior elements by an expansive mass containing large and small fluid-fluid levels

of cases demonstrated mineralized matrix. Purely lytic lesions were less commonly seen but were identified in all patients with telangiectatic osteosarcoma. Fluid-fluid levels were also seen in telangiectatic osteosarcoma (Fig. 33.5c). In a minority of cases marked mineralization was observed to be confined to the vertebrae with an ivory appearance. MR characteristics are nonspecific in non-mineralized areas of involvement (Rodallec et al. 2008).

33.5.4 Chondrosarcoma

In the axial skeleton, chondrosarcomas are more common than osteosarcomas, and the opposite is true for the appendicular skeleton. Chondrosarcomas may arise as primary lesions or may develop secondarily from enchondromas or osteochondromas. There is a predilection for the thoracic spine. The sacrum is seldom

a primary site. As many as 40% of lesions arise from the posterior elements of the spine. More commonly, however, both vertebral body and posterior elements are involved at presentation when there is appearance of neurologic compromise. Radiographically, vertebral chondrosarcomas appear lytic with chondroid matrix mineralization and associated soft tissue mass. Calcifications are usually rounded or curvilinear and are best evaluated on CT. Calcified matrix is seen as signal voids on MR imaging. In contrast enhanced MR imaging, characteristic ring and arcs signify vascular septation between cartilaginous lobules (Murphey et al. 1996).

33.6 Benign Lesions in Adults

33.6.1 Giant Cell Tumor

Giant cell tumors are usually seen in patients in the second to fourth decade of life. Giant cell tumors are the most frequently encountered sacral tumor after chordoma (Diel et al. 2001). In the sacrum, the lesion is well defined, lytic, with expansion and no surrounding sclerosis (Hart et al. 1997). Vertebral lesions are rare, but when present the lesion usually affects the vertebral body and on occasion, with an associated pathologic fracture. Sacral giant cell tumors – not uncommonly – extend across the sacroiliac joint (Fig. 33.6d–f). Most lesions have an extraosseous component. Solid components of giant cell tumors demonstrate low to intermediate signal intensity on T1- and T2-weighted imaging. The low to intermediate signal intensity on T2-weighted images is due to the presence of hemosiderin (Fig. 33.6a–f). There is usually no sclerotic rim at the margin of the tumor on CT (Murphey et al. 2001). Thus, in younger patients, the differential diagnosis includes aneurysmal bone cyst.

33.6.2 Hemangioma

Hemangiomas are usually found after the fourth decade of life. There is a predilection for the thoracolumbar spine; usually only the vertebral body is involved. Vertebral hemangiomas are the most common benign spinal neoplasm. Large hemangiomas are seen on radiographs as coarse striated or honeycomb appearance of the involved vertebral body. On CT, vertebral hemangiomas produce a polka-dot appearance. Hemangiomas can have a wide range of appearances on MR depending on the ratio of vascular vs fatty stroma (Akbarnia and Merenda 1996).

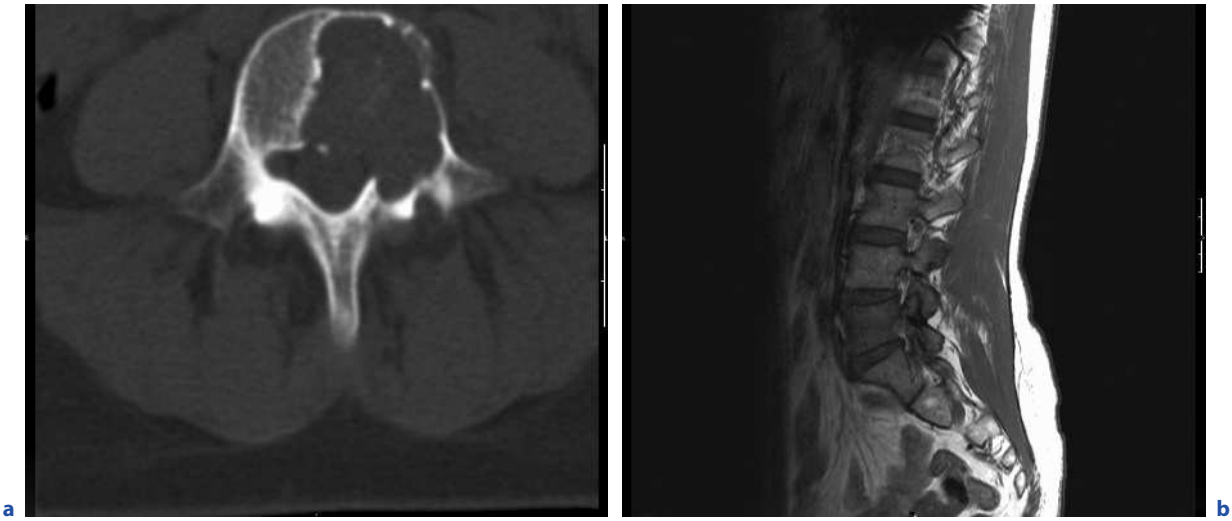

a b

Fig. 33.6a–f. Giant cell tumor. **a** Axial CT image of L5 in a 38-year-old female demonstrates eccentric osteolytic lesion in the vertebral body with extension into the left pedicle. Vertebral giant cell tumor as in the appendicular skeleton can appear aggressive and in addition to Langerhans cell histiocytosis are the two benign lesions with a predilection for the vertebral body. **b** Sagittal T1-weighted image in the same patient demonstrates low T1 intensity in the affected vertebral body. (**c–f**) *see next page*

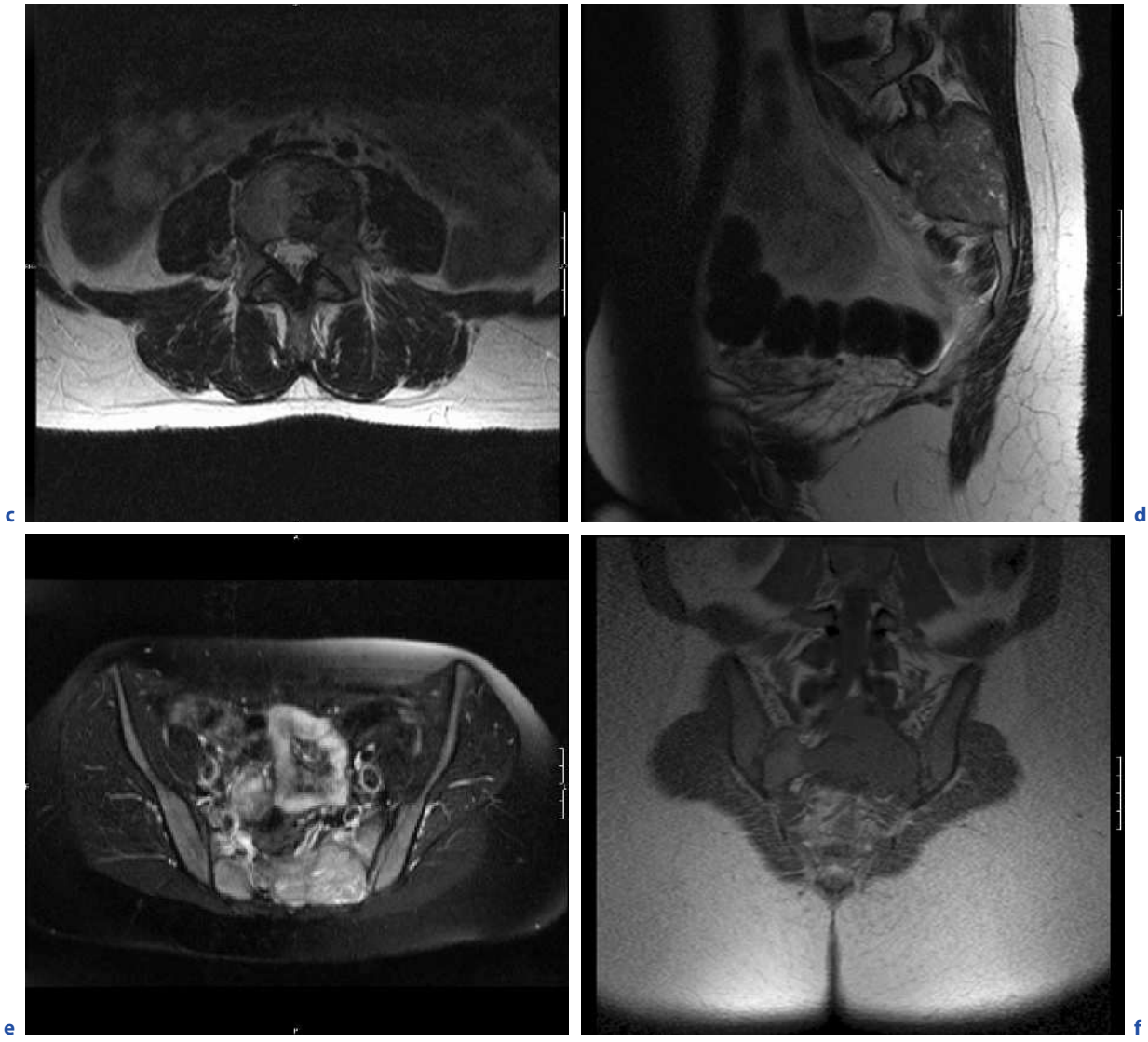

Fig. 33.6a–f. (*continued*) **c** Corresponding axial T2-weighted image demonstrates low signal intensity within the lesion. Giant cell tumor is one of those rare osteolytic tumors that may show low to intermediate signal on T2 weighted MR images due to the presence of hemosiderin. **d** Sagittal non-fat saturated T2-weighted image demonstrates a sacral giant cell tumor in a 21-year-old female with characteristic low signal intensity within the lesion. **e** The lesion extends across the left sacroiliac joint, and increases in signal intensity on fat-saturated T2-weighted imaging. **f** Corresponding coronal T1-weighted image demonstrates the lesion extending across superiorly and across the midline in addition to involvement of the left sacroiliac joint

33.6.3 Paget's Disease

Paget's disease is relatively common disease affecting up to 10% of persons more than 80 years old; it is rare in patients less than 40 years old (Rodallec et al. 2008). It occurs more frequently in Caucasians of Northern European descent and is rare in persons of African and Asian descent. Paget's disease has a predilection for the pelvis, sacrum and femur. The disease has three radiographically distinct phases: lytic, intermediate, and sclerotic. Due to the age of affected individuals, the purely lytic phase of Paget's disease provokes the differential diagnosis of metastasis or lymphoma. Fortunately, it is

the rarest clinical manifestation of Paget's disease. Radiographically, axial involvement in the intermediate phase manifests as expansion of the vertebra with coarse mixed lytic and sclerotic thickened trabeculae and cortices. When the sclerotic phase of Paget's occurs without bony expansion, it may be difficult to distinguish from osseous metastases in patients with known prostatic or breast carcinoma. In such situations, there are anecdotal cases where PET scanning may be helpful in differentiating osseous metastases, which are hypermetabolic, from sclerotic Paget's disease lesions, which are not. There may also be large associated soft tissue masses. Other patterns of involvement include the "ivory vertebra" and isolated posterior arch involvement. Sarcomatous degeneration to osteosarcoma or less commonly chondrosarcoma and malignant fibrous histiocytoma is a rare complication of the disease affecting less than 1% of patients (Sundaram 2006).

33.6.4 Chondroblastoma and Other Benign Cartilaginous Tumors

Chondroblastoma is a benign cartilaginous neoplasm with a predilection for the epiphysis of the growing skeleton. Less than 1% of benign primary bone tumors are chondroblastoma. In a study by Ilaslan et al., the largest known series on vertebral chondroblastoma, less than 1.4% of all cases of chondroblastoma arose from the vertebrae. Median age was 28 years which is a decade later than its appendicular counterpart. Radiographs were nonspecific; lesions were detectable but without enough detail for characterization. In Ilaslan's series, seven cases with adequate imaging, four arose from the posterior elements, and three from the vertebral body. On CT and MR, all lesions were expansive and most demonstrate aggressive features with soft tissue mass and bone destruction. Calcification was seen in seven of nine patients reflective of its cartilaginous origin (Fig. 33.7a–c). Bone marrow edema and sec-

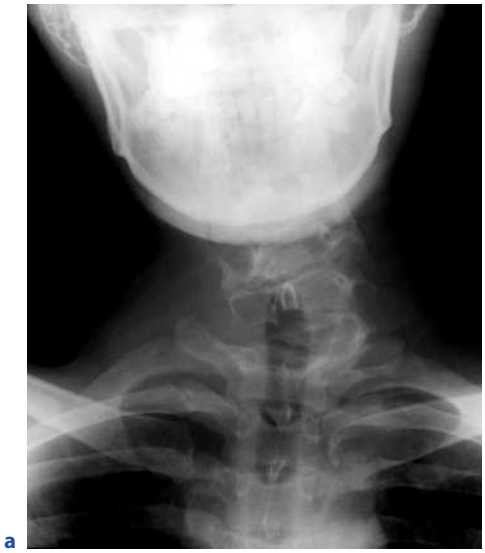

a

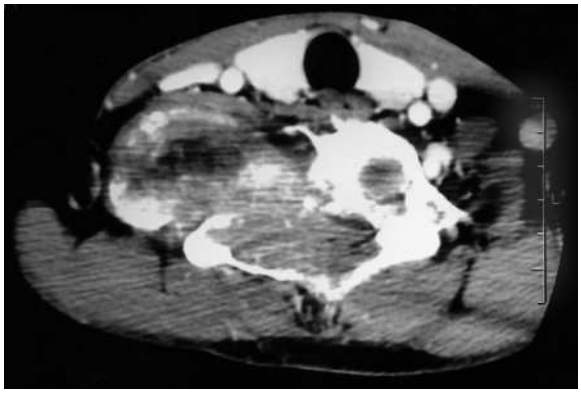

b

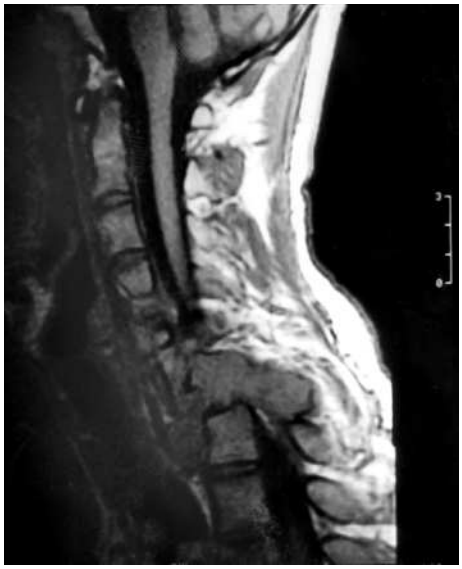

c

Fig. 33.7a–c. Vertebral chondroblastoma. **a** AP radiograph demonstrates collapse of the C7 vertebral body. **b** Axial CT demonstrates an expansive mass centered on the right pedicle containing calcification and large soft tissue involvement. **c** Sagittal T1 weighted MR image at the same level demonstrates a large low signal exophytic mass with destruction of the vertebrae and extension into the central canal and paraspinal soft tissue. This rare vertebral tumor, despite its histology almost always has a malignant appearance on imaging

ondary aneurysmal bone cysts were not seen. The aggressive appearance of vertebral chondroblastoma, as an expansive tumor with extension into the spinal canal and mineralization, renders it nearly impossible to distinguish vertebral chondroblastoma from vertebral chondrosarcoma, osteoblastoma, or osteosarcoma on the basis of imaging (Ilaslan 2003 et al.). The other benign cartilaginous tumors such as chondromyxoid fibroma and chondroma are rare in the vertebra and have nonspecific imaging features.

33.7 Malignant Tumors in Adults

33.7.1 Chordoma and Benign Notochordal Cell Tumors

Chordomas comprise only 2%–4% of all primary malignant bone tumors. However, chordoma is the most common primary malignant sacral neoplasm. This malignancy is found in all ages but peaks in the fifth to sixth decade. Chordomas are rare outside of the axial skeleton. Radiographically, chordomas present as an expansive lesion with a central area of bone destruction with a soft tissue mass that may contain calcification (Fig. 33.8a,b). About half of chordomas occur in the sacrum, another 35% occurs in the suboccipital region (Llauger et al. 2000). They can also metastasize. Sacrococcygeal chordomas may attain a large size due to the capaciousness of the pelvic cavity. The differential diagnosis of sacrococcygeal chordomas includes chondrosarcoma and giant cell tumor. However, chondrosarcoma usually affects the upper two sacral segments whereas chordomas usually originate from the lower sacral segments or the coccyx. MR demonstrates enhancement with intravenous contrast (Fig. 33.8c–e).

Chordomas are believed to arise from the vertebral remnants of the embryonic notochord. Histologically it is characterized by lobulation, abundant mucoid matrix with cords of epitheloid cells with some degree of nuclear atypia. Recent studies have described retained benign notochordal tissue that grows to produce symptomatic benign vertebral lesions. Mirra and Brien (2001) were the first to introduce this concept as giant notochordal hamartoma, or more recently, benign notochordal cell tumors (BNCTs); these lesions are usually non-destructive vertebral lesions which are often mistaken for a chordoma. These benign notochordal cell tumors have also been thought to represent precursors to chordomas (Yamaguchi et al. 2005). However, long term follow up on a few cases has not shown benign notochordal cell tumors to evolve into chordomas. Like the chordoma, there is a predilection for the sacrum, followed by the cervical and lumbar vertebrae. Most benign notochordal cell tumors are small, as-

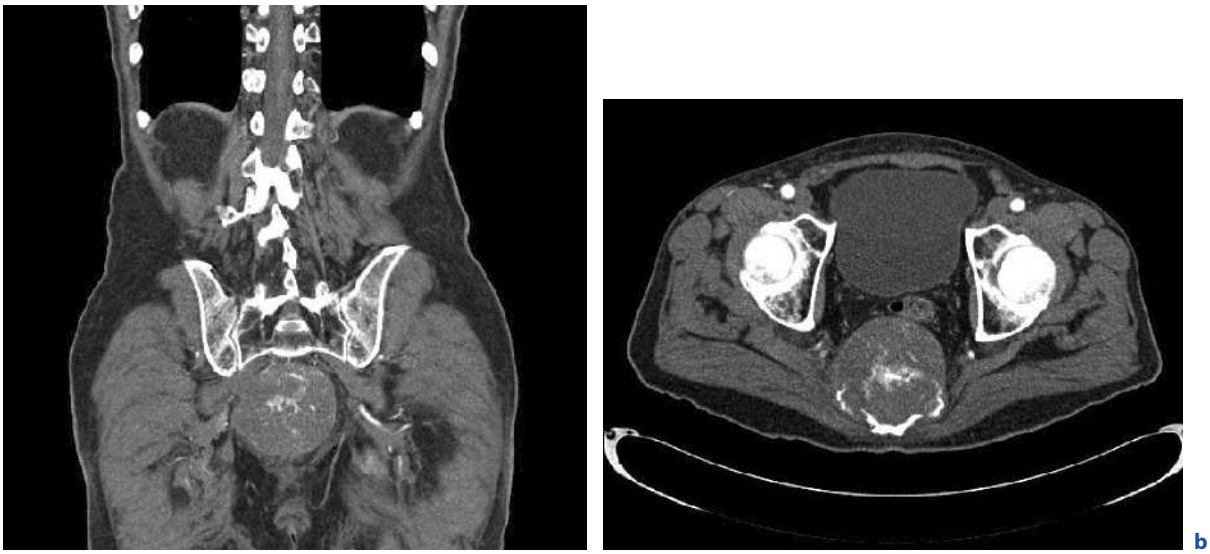

Fig. 33.8a–e. Chordoma. Coronal (**a**) and axial (**b**) CT images of a 70-year-old male demonstrate a large midline sacrococcygeal soft tissue mass with scattered amorphous calcifications which are virtually pathognomonic for chordoma. Sagittal T1 weighted image (**c–e**) *see next page*

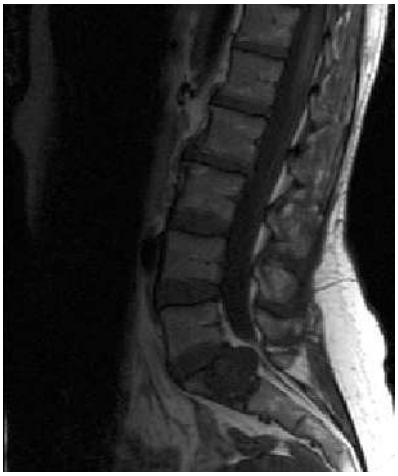

c

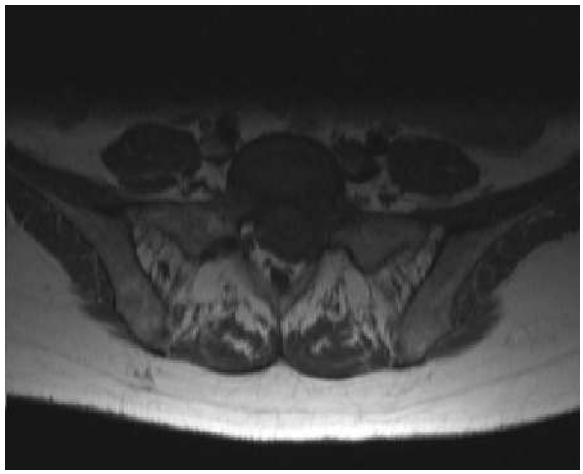

d

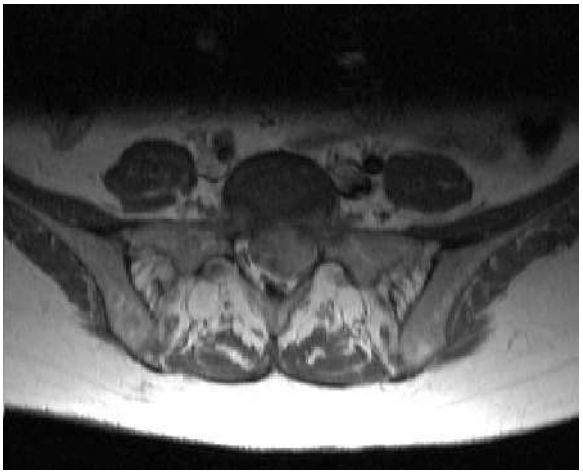

e

Fig. 33.8a–e. (*continued*) (**c**) from another patient demonstrates an expansive mass arising from the sacrum which extends posteriorly into the central canal with associated osseous destruction. Pre-contrast axial T1-weighted (**d**) and post-contrast axial T1-weighted (**e**) images demonstrate nearly homogenous enhancement of the lesion, typical of chordomas

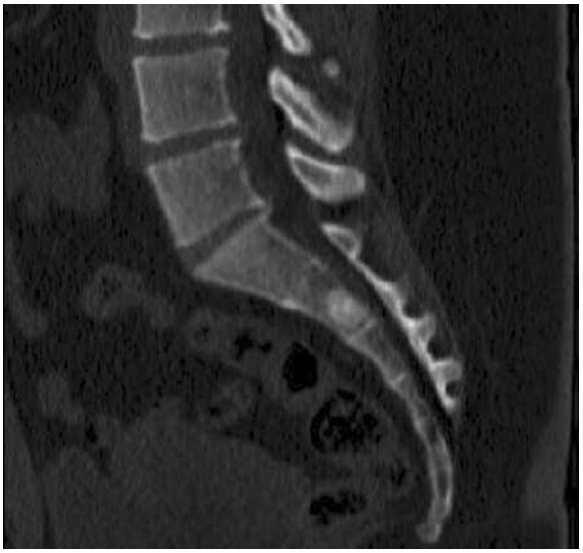

a

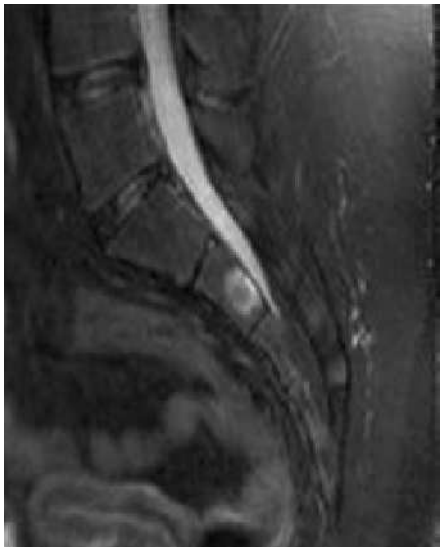

b

Fig. 33.9a–e. Benign notochordal cell tumors. Sagittal CT image (**a**) demonstrates a well-defined area of sclerosis within S2 which does not extend into the soft tissue. Sagittal T2 weighted (**b**) and coronal T1 weighted (**c–e**) *see next page*

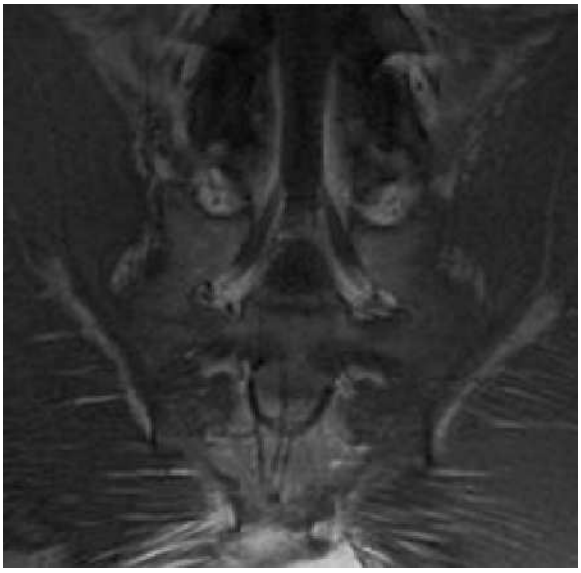

c

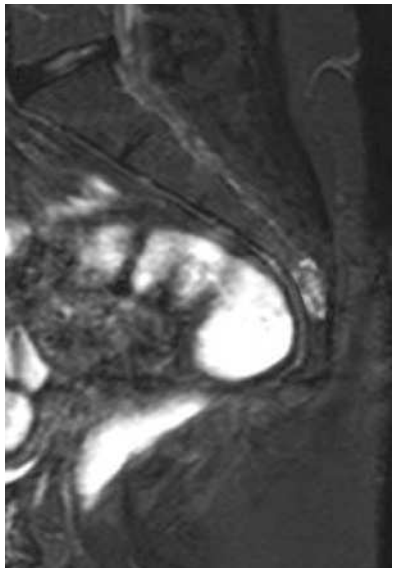

d

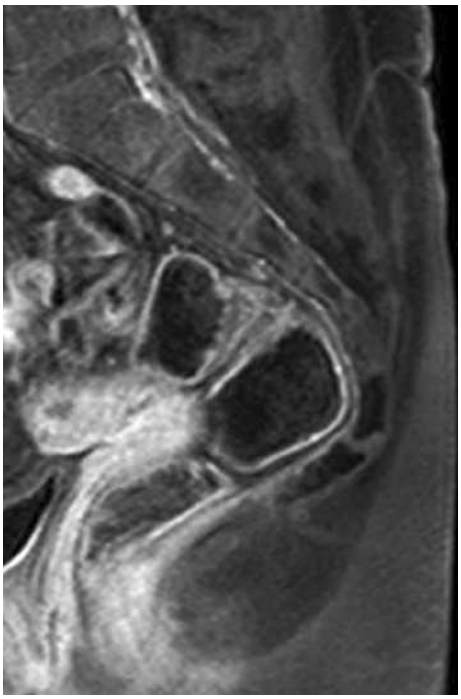

e

Fig. 33.9a–e. (*continued*) (**c**) images demonstrate corresponding areas of high T2 signal and low T1 signal, respectively. Note that the lesion is midline and entirely intracompartmental, unlike chordoma which almost always demonstrate extraosseous disease. Sagittal STIR image (**d**) in another patient demonstrates a well circumscribed lesion with heterogeneously increased signal within the coccyx. Corresponding post-contrast fat-suppressed T1 weighted image (**e**) demonstrates lack of enhancement

ymptomatic and found at autopsy. Larger lesions may be detected on CT or MR, and rarely by radiography. If detected radiographically, lesions appear as a vague area of sclerosis within the vertebral body. On CT lesions are sclerotic and notable for the absence of cortical destruction or soft tissue mass (Fig. 33.9a). MR demonstrates well-defined high T2-weighted signal and low T1-weighted signal intraosseous lesions which do not enhance with administration of intravenous gadolinium contrast (Fig. 33.9–e). Lesions do not show abnormal increased uptake on scintigraphy (Yamaguchi et al. 2008). The imaging features are also static, unlike that of chordoma. Histologically, benign notochordal cell tumors do not demonstrate lobularity, and lack nuclear atypia and syncytial cell cords (Kyriakos et al. 2003). This distinguishes giant notochordal rest as a separate entity from chordoma. Currently, imaging plays a significant role in sequential follow up of these lesions as an alternative to resection which is carries significant morbidity.

33.7.2 Plasmacytoma and Multiple Myeloma

Solitary plasmacytoma is almost always a precursor to multiple myeloma with a median progression of 2–3 years. The disease is most commonly seen in the fifth to seventh decades of life. Approximately 75% of patients with multiple myeloma will have radiographic findings. Four forms of skeletal involvement have been described: (1) plasmacytoma, (2) myelomatosis, (3) sclerosing myeloma, and (4) diffuse skeletal osteopenia (Angtuaco et al. 2004). Plasmacytomas typically involve the vertebral body. Lesions are not seen early in the course of disease, and are demonstrated radiographically when there has been 50% bone destruction. The tumor is usually lytic, sometimes expanded with a "soap bubble appearance" and should be distinguished from a lytic metastasis from slower growing primary such as kidney or thyroid cancer. Unlike metastases, the pedicles are usually spared early in the disease. Vertebral compression fractures are often present at diagnosis or develop during the course of multiple myeloma.

33.7.3 Lymphoma

Primary lymphoma of the bone is a rare manifestation of Hodgkin and non-Hodgkin lymphoma. Spinal involvement in lymphomas is more commonly a manifestation of late metastatic disease from hematogeneous spread. Primary bone lymphomas are usually non-Hodgkin lymphoma of the large B cell type. This malignancy peaks in the fifth to seventh decades with a strong male predilection (up to 8:1 male to female ratio) (Motamedi et al. 2004). Lesions can have a variable appearance. Most vertebral lymphomas are lytic. On radiographs and CT, the characteristic appearance is a thin walled expansive lesion within the vertebral body, with an occasional pathologic fracture. However, in Hodgkins disease there is a tendency to sclerosis, giving rise to the ivory vertebra. Vertebral, paraspinal, and epidural involvement are all manifestations of lymphoma in the axial spine. On MR imaging, fluid-fluid levels and blood degradation products may be seen (Kortman 1996). In Hodgkins disease, marginal erosion of contiguous vertebral bodies by enlarged nodes suggests the diagnosis. In patients older than 40, it may be impossible to distinguish radiographically lymphoma from metastasis and myeloma. Due to its strong male predilection, an aggressive malignant appearing lesion in the vertebrae in men between the ages of 20 and 40 should raise suspicion of lymphoma.

References

Ahlgren B, Morris G, Garfin S (1996) Cervical spine tumors. Spine State Art Rev 10:123–144

Akbarnia B, Merenda JR (1996) Benign tumors of the spine. Spine State Art Rev 10:71–88

Albrecht S, Crutchfield JS, Segall GK (1992) On spinal osteochondromas. J Neurosurg 77:247–252

Angtuaco EJC, Fassas ABT, Walker R, Sethi R, Barlogie B (2004) Multiple myeloma: clinical review and diagnostic imaging. Radiology 231:11–23

Bernstein M, Kovar H, Paulussen M, Randal RL, Schuck A, Teot LA, Juergens H (2006) Ewing's sarcoma family of tumors: current management. Oncologist 11:503–519

Boriani S, De Iure F, Campanacci L, Gasbarrini A, Bandiera S, Biagini R, Bertoni F, Picci P (2001) Aneurysmal bone cyst of the mobile spine: report on 41 cases. Spine 26:27–35

Diel J, Ortiz O, Losada RA, Price DB, Hayt MW, Katz DS (2001) The sacrum: pathologic spectrum, multimodality imaging, and subspecialty approach. RadioGraphics 21:83–104

Dormans J, Moroz L (2007) Infection and tumors of the spine in children. J Bone Joint Surg Am 89A:79–97

Hart RA, Boriani S, Biagini R, Currier B, Weinstein JN (1997) A system for surgical staging and management of spine tumors: a clinical outcome study of giant cell tumors of the spine. Spine 22(15):1773–1783

Ilaslan H, Sundaram M, Unni KK (2003) Vertebral chondroblastoma. Skel Radiol 32:66–71

Ilaslan H, Sundaram M, Unni KK, Dekutoski MB (2004a) Primary Ewing's sarcoma of the vertebral column. Skel Radiol 33(9):506–513

Ilaslan H, Sundaram M, Unni KK, Shives TC (2004b) Primary vertebral osteosarcoma: imaging findings. Radiology 230:697–702

Kortman K (1996) Diagnostic imaging of spinal canal and cord tumors. Spine State Art Rev 10:43–69

Kyriakos M, Totty WG, Lenke LG (2003) Giant vertebral notochordal rest: a lesion distinct from chordoma-discussion of an evolving concept. Am J Surg Pathol 27:396–406

Llauger J, Palmer J, Amores S, Bagué S, Camins A (2000) Primary tumors of the sacrum: diagnostic imaging. AJR Am J Roentgenol 174:417–424

Mirra JM, Brien E (2001) Giant notochordal hamartoma of intraosseous origin: a newly reported benign entity to be distinguished from chordoma. Report of two cases. Skel Radiol 30:698–709

Motamedi K, Ilaslan H, Seeger L (2004) Imaging of the lumbar spine neoplasms. Semin Ultrasound CT MRI 25:474–489

Moulopoulos L, Dimopoulos M (1997) Magnetic resonance imaging of the bone marrow in hematologic malignancies. Blood 90:2127–2147

Murphey MD, Andrews CL, Flemming DJ, Temple HT, Smith WS, Smirniotopoulos JG (1996) Primary tumors of the spine: radiologic-pathologic correlation. RadioGraphics 16:1131–1158

Murphey MD, Choi JJ, Kransdorf MJ, Flemming DJ, Gannon FH (2000) Imaging of osteochondroma: variants and complications with radiologicpathologic correlation. RadioGraphics 20(5):1407–1434

Murphey MD, Nomikos GC, Flemming DJ, Gannon FH, Temple HT, Kransdorf MJ (2001) Imaging of giant cell tumor and giant cell reparative granuloma of bone: radiologic-pathologic correlation. RadioGraphics 21(5):1283–1309

Rodallec M, Feydy A, Larousserie F, Anract P, Campagna R, Babinet A, Zins M, Drapé JL (2008) Diagnostic imaging of solitary tumors of the spine: what to do and say. RadioGraphics 28:1019–1041

Shaikh MI, Saifuddin A, Pringle J, Natali C, Sherazi Z (1999) Spinal osteoblastoma: CT and MR imaging with pathological correlation. Skel Radiol 28(1):33–40

Sundaram M (1996) Radiology of solitary tumors and tumor-like lesions of the vertebrae. Spine State Art Rev 10:25–41

Sundaram M (2006) Imaging of Paget's disease and fibrous dysplasia of bone. J Bone Miner Res 21:28–30

Yamaguchi T, Watanabe-Ishiiwa H, Suzuki S, Igarashi Y, Ueda Y (2005) Incipient chordoma: a report of two cases of early-stage chordoma. Mod Pathol 18:1005–1010

Yamaguchi T, Iwata J, Sugihara S, McCarthy EF, Karita M, Murakami H, Kawahara N, Tsuchiya H, Tomita K (2008) Distinguishing benign notochordal cell tumors from vertebral chordoma. Skel Radiol 37:291–299

Bony Pelvis

34

David Ritchie

CONTENTS

KEY POINTS

- Metastases and myeloma are common in the bony pelvis, whereas other bone tumours and tumour-like lesions are relatively uncommon.
- Primary malignant bone tumours of the pelvis are more common than benign tumours with chondrosarcoma, the most common primary malignant bone tumour in the mature pelvis (excluding myeloma), and Ewing's sarcoma, the most common in the immature pelvis.
- Osteochondroma is the most common benign tumour of the pelvis and eosinophilic granuloma the most common tumour-like lesion.
- The majority of tumours and tumour-like lesions arise in the ilium.
- Due to anatomical factors, delay in the diagnosis of pelvic bone tumours is not uncommon and lesions can grow to a relatively large size before detection.
- Although MR imaging is the cross-sectional imaging method of choice for assessing pelvic tumours, CT is often a useful complementary technique in identifying matrix and periosteal mineralisation and cortical destruction.

34.1 Introduction

Metastases and myeloma are common in the bony pelvis, whereas other bone tumours and tumour-like lesions are relatively uncommon. There are differences in the epidemiology of pelvic tumours compared with the same tumours at other locations as well as clinical considerations and variations in the imaging features. This chapter considers these differences, focuses on tumours

D. A. Ritchie, MD
Western Infirmary, Dumbarton Road, G11 6NT Glasgow, UK

with a predilection for the pelvis and discusses their imaging findings. There is an emphasis on discriminating features and differential diagnosis.

34.2 Imaging Bone Tumours and Tumour-like Lesions

34.2.1 Epidemiology

There are several series analysing tumours around the bony pelvis, but most are affected to an extent by tertiary referral patterns that skew the true incidence. Unless otherwise stated, the incidence data quoted have been calculated by combining authoritative texts on the subject (Unni 1996; Campanacci 1999). In this chapter, the bony pelvis includes the ilium, ischium and pubis.

By far the most common malignant bone tumours around the bony pelvis are metastases and myeloma, usually presenting in the elderly population; however, the true incidence is unknown, as many metastatic and myelomatous lesions do not present to specialised centres and may not be biopsied. Excluding metastatic disease and myeloma, and combining the remaining primary malignant bone tumours from Campanacci's and Unni's series (Table 34.1), 14.5% of all primary malignant bone tumours occurred in the pelvis, and of those, 78% occurred in the ilium, 17% in the pubis and 7% in the ischium (Unni 1996; Campanacci 1999). Chondrosarcoma is the most common primary malignant bone tumour, with a peak incidence in the fourth and fifth decades, whereas Ewing's sarcoma is the most common bone sarcoma in the immature pelvis. Only 4% of all benign bone tumours occurred in the pelvis, and of those, 73% were located in the ilium, 18% in the pubis and 9% in the ischium. Most benign lesions tend to present in the first two decades, and 44% of these are due to osteochondroma; however, the second most common benign lesion, giant cell tumour, has a peak incidence in the fourth decade and is rarely seen in the immature pelvis. In Campanacci's series of tumour-like lesions of bone around the pelvis, excluding brown tumours, 78% were located in the ilium, 12% in the ischium and 10% in the pubis. 50% of lesions were due to eosinophilic granuloma and 86% of those were located in the ilium. Multiplicity of lesions in an older adult usually indicates metastatic disease, multiple myeloma or lymphoma. In childhood, multiple lesions are more likely to be benign and the differential diagnosis includes polyostotic fibrous dysplasia, Langerhans' histiocytosis, multiple enchondromatosis (Ollier's disease) and hereditary multiple exostoses (diaphyseal aclasis).

Table 34.1. Incidence of primary bone tumours around the pelvis in descending order of incidence. Figures obtained by combining the results of Unni (1996) and Campanacci (1999)

Benign bone tumours (n=253)	Percentage	Primary malignant bone tumour (n=1,252)	Percentage
Osteochondroma	43	Chondrosarcoma	32
Giant cell tumour	18	Osteosarcoma	22
Osteoid osteoma	8	Ewing's sarcoma	22
Chondroblastoma	7	Lymphoma	14
Osteoblastoma	7	Fibrosarcoma	5
Chondromyxoid fibroma	6	Malignant fibrous histiocytoma	2
Chondroma	5	Malignant vascular tumour	2
Haemangioma	4		

In the benign group, the figures for osteochondroma are an underestimate as only the symptomatic lesions have been included. In the malignant group, metastases and myeloma have been excluded and the "lymphomas" contain patients with primary and generalised lymphoma

34.2.2 Clinical Aspects

Patients with musculoskeletal tumours often present with pain and/or swelling. Some tumours may present with a pathological fracture and other lesions, typically benign, may be detected as incidental findings; however, delay in the diagnosis of pelvic bone tumours is not uncommon and is often due to misdiagnosis. In one study of pelvic bone sarcomas, the diagnosis was initially missed in 44% of patients (Fig. 34.1; Wurtz et al. 1999). Some patients with pelvic tumours may present with non-specific pain that may be attributed to non-neoplastic conditions including osteoarthritis, bursitis, stress injury or referred pain from the lumbar spine (Thompson and Berg 1996). Furthermore, inadequate evaluation may result in inappropriate surgery. Some low-grade sarcomas may give a relatively long history suggesting benign disease. In patients with unexplained sciatica, further cross-sectional imaging of the pelvis may be required to exclude a pelvic tumour, which is often situated in the region of the sciatic notch.

34.2.3 Characterisation

34.2.3.1 Location

In the pelvis, the ilium is the most common site for malignant and benign bone tumours. Cartilaginous lesions are more frequently found in the region of the triradiate cartilage, but chondroblastoma and osteochondroma can also be found in the iliac crest at the site of the apophysis (Fig. 34.2). Giant cell tumours are typically subarticular or related to an old apophysis (Fig. 34.3). Marrow-related lesions, including myeloma, metastases, lymphoma, Ewing's sarcoma and Langerhans' histiocytosis, predominate in the ilium due to the abundance of red marrow.

34.2.3.2 Radiographic Features

Despite newer imaging techniques, the radiograph remains the initial imaging investigation of choice, although detection depends, to a certain extent, on radiographic technique, size and location, as well as aggressiveness, of the lesion. Lesions in the pubis or ischium are more easily detected since they contain less

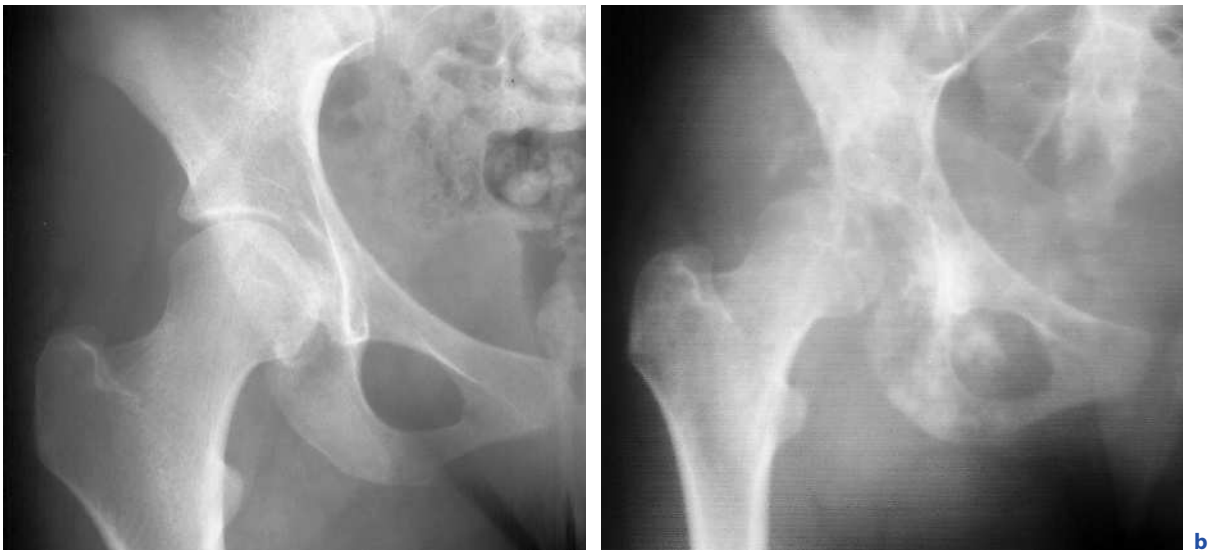

Fig. 34.1a,b. Osteosarcoma. **a** Anteroposterior (AP) radiograph. The subtle lysis of the medial acetabulum was initially overlooked. **b** AP radiograph. There is mixed lysis and sclerosis within the acetabulum and ischium with a large soft tissue mass containing amorphous mineralization. The tumour mass is causing subluxation of the hip

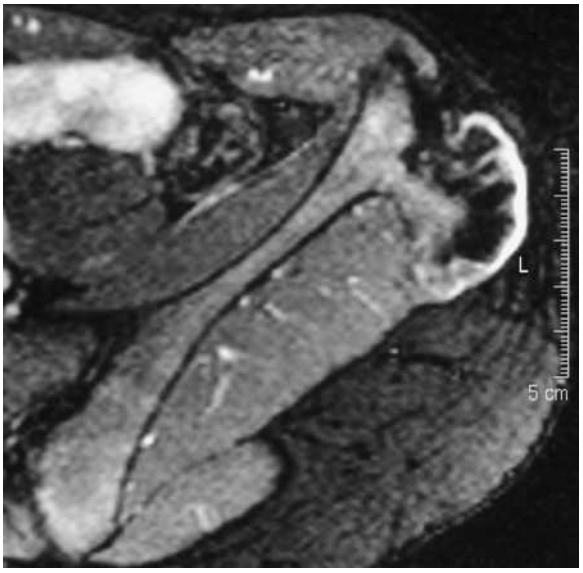

Fig. 34.2. Osteochondroma in adult male. Axial STIR MR image shows a polypoid lesion arising from the outer aspect of the ilium with continuity of cortex and marrow cavity and a thin unmineralised cartilage cap

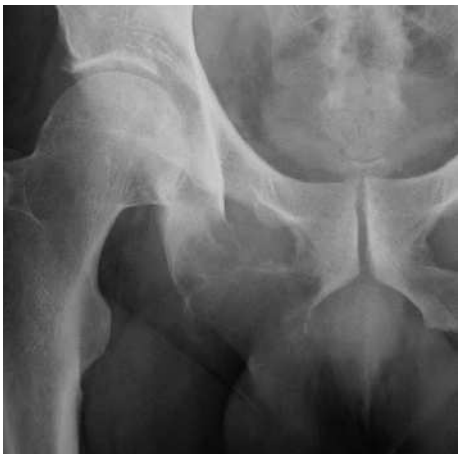

a

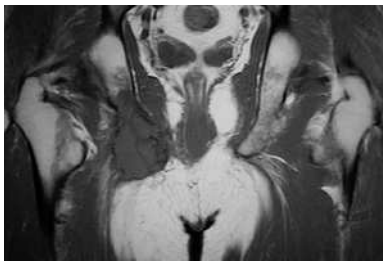

b

Fig. 34.3a,b. Giant cell tumour in a 49-year-old man. **a** AP radiograph shows a non-mineralising, expansile, lytic lesion arising in the right ischium with cortical destruction and apparent soft tissue infiltration inferiorly. **b** Coronal T1-weighted MR image confirms the expansile nature of the lesion. Giant cell tumours may occur at the site of an old apophysis

cancellous bone, whereas lesions arising in thick cancellous bone, such as the ilium, may be occult until there is enough destruction of the trabecular bone or evidence of cortical involvement. Some aggressive tumours, including round cell tumours, typically show a permeative pattern of bone destruction with little or no apparent cortical destruction; however, in such cases, close inspection of the radiograph may reveal subtle intracortical lucencies as well as a periosteal reaction. Unfortunately, the prominence of the overlying soft tissues and viscera around the pelvis means that some lesions, particularly those arising in the ilium, may be obscured until they reach a large size. Similarly, tumour mineralisation may be difficult to appreciate on a conventional radiograph, and CT may be required to confirm. Organised bone is characteristic of benign bone-forming lesions, such as an osteoblastoma, whereas malignant osteoid is described as fluffy, ill-defined, amorphous or cloud-like, and indicates an aggressive bone lesion such as osteosarcoma. Mineralised cartilage is variously described as flocculent, stippled, annular, comma shaped or popcorn calcification (Fig. 34.4). Identification of mineralised cartilage identifies the histological origin but does not distinguish between a benign or malignant tumour; however, a cartilaginous tumour in the pelvis is much more likely to be malignant than benign (Buirski et al. 1986; Unni 1996; Campanacci 1999). Periosteal reactions may occur with benign and malignant pelvic tumours and are more likely to be detected in the pubis or ischium rather than the ilium.

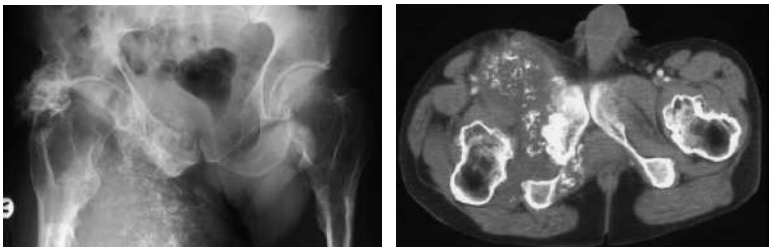

Fig. 34.4a,b. Diaphyseal aclasis with malignant transformation. **a** AP radiograph and **b** CT shows multiple osteochondromas with a large peripheral chondrosarcoma arising from the right pubis

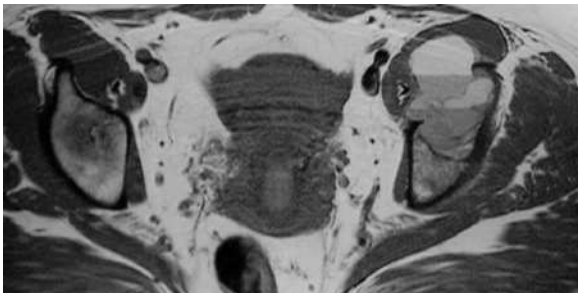

Fig. 34.5. Aneurysmal bone cyst in an 18-year-old man. Axial T2-weighted MR image confirms inhomogeneous lobulated lesion arising from the anterior aspect of the left iliac bone displacing the ilio-psoas muscle and containing fluid levels, in keeping with the sedimentation effect of static blood

34.2.3.3 Cross-sectional Imaging

The main role of bone scintigraphy (^{99m}Tc-methylene diphosphonate) is in the detection of metastatic disease, although it also plays an important role in the detection of osteoid osteomas. Ultrasound is useful for evaluating soft tissue components of bone lesions and guides biopsy. Computed tomography (CT) is superior to MR imaging at detecting cortical involvement, matrix and periosteal mineralisation and in certain cases both modalities may be complementary; however, for most bone tumours, MR imaging is required for optimal characterisation, pre-operative staging and suspected recurrence. MR imaging is also the most sensitive imaging technique for lesion detection, but care should be taken in interpretation as incidental findings may be discovered that are of no clinical relevance. As the anatomical site is large, adequate coverage will usually require a body coil.

On MR imaging, tissue characterisation based on signal intensities alone is not usually possible, as most lesions display non-specific low to intermediate signal intensity (similar to that of muscle) on T1-weighting and high signal intensity on T2-weighting. The appearances also vary with the type of tumour matrix and presence of mineralisation, necrosis and haemorrhage. Therefore, the same type of tumour may have different MR appearances; however, some lesions or parts of lesions may have more characteristic findings that may reduce the differential diagnosis. Cystic lesions, such as simple bone cysts, display homogeneous low signal intensity on T1-weighting, very high signal intensity on T2-weighting and show no or minimal rim enhancement. Fluid-fluid levels occur in various benign and malignant bony lesions and represent the sedimentation effect of blood. When seen in an expansile bone lesion in an adolescent, fluid-fluid levels are highly suggestive of an aneurysmal bone cyst (Fig. 34.5).

34.2.4 Staging

MR sequences in all three planes may be required for an adequate assessment. T1-weighted, fat-suppressed T2-weighted or STIR sequences all demonstrate contrast between osseous tumour and normal marrow, although peri-tumoral oedema may obscure the true tumour margin in both benign and malignant lesions. Indeed, benign lesions, such as eosinophilic granuloma, chondroblastoma and osteoid osteoma, all cause extensive surrounding inflammatory responses that can lead to confusion with a more aggressive process. Some authorities advocate a dynamic MR study to distinguish tumour from peri-tumoral oedema. The enhancement pattern is early with tumour and delayed with peri-tumoral oedema; however, this technique does not exclude isolated nests of tumour cells and it is prudent to include all abnormal marrow signal as suggestive of tumour for measurement purposes (Shapeero and Vanel 2000). Most of the oedema will resolve following chemotherapy and this can be verified on the re-staging MR scan prior to definitive surgery.

A lesion confined to a single bone within the pelvis is considered intra-compartmental, but more aggressive lesions may show extracompartmental spread at presentation (Anderson et al. 1999). Typically, most bone

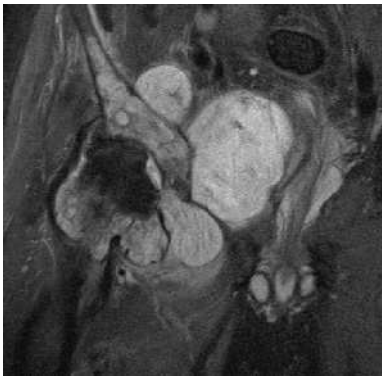

a

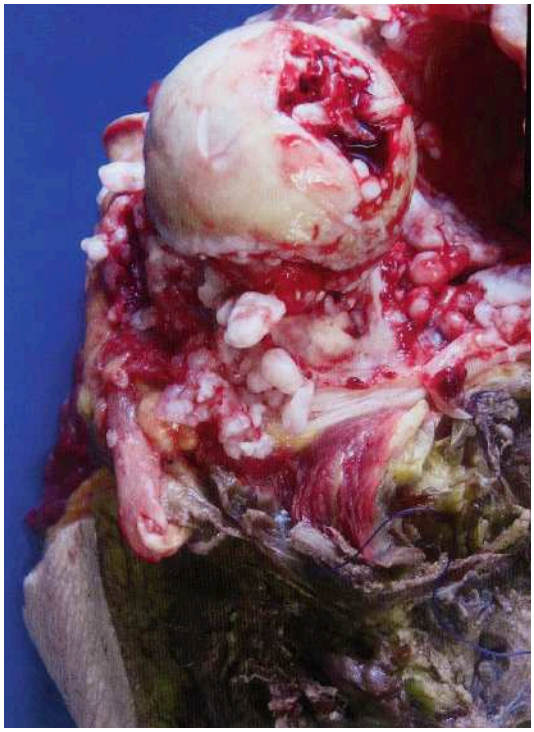

b

Fig. 34.6a,b. Chondrosarcoma in a 74-year-old man. **a** Coronal STIR MR image shows a large extracompartmental lesion arising from the right acetabulum with extensive infiltration of the right hip joint. **b** Specimen photograph following hind quarter amputation confirms multiple tumour nodules in the hip joint and femoral head

tumours are isointense with muscle on T1-weighted images, and optimal demonstration of soft tissue extent requires STIR or fat-suppressed T2-weighted sequences. For bone tumours that have spread into parosseous soft tissues, the normal low signal intensity cortex will typically display increased signal intensity due to tumour replacement. With some aggressive tumours, such as Ewing's sarcoma, the cortical destruction may be subtle, but close inspection of the cortex will often reveal diffuse infiltration.

Pathological fracture into the joint can be taken as unequivocal evidence of joint involvement, but the presence of a joint effusion by itself is an unreliable sign of joint involvement; however, the absence of an effusion has a high negative predictive value for joint invasion (Schima et al. 1994). In a series of 67 patients with primary bone sarcomas around the hip, involvement of the hip joint was suspected by pre-operative imaging in 29 cases and confirmed histologically in 15 cases (Ozaki et al. 2002). Intra-articular involvement was found in 39% of chondrosarcomas, 12.5% of osteosarcomas and in none of the Ewing's sarcomas (Fig. 34.6). The presence of cartilage disruption or mass inside the joint were more specific for intra-articular involvement than diffuse signal change or joint effusion. Most tumours infiltrated the joint through spread along the ligamentum teres. In another series by the same authors, analysing peri-articular primary bone sarcomas around the sacroiliac joint, infiltration of the joint was found in around half the patients with chondrosarcoma or osteosarcoma but in only 4% of patients with Ewing's sarcoma (Fig. 34.7; Ozaki et al. 2003a). Most of the tumours infiltrated through the posterior part of the joint. Transarticular spread across joints of limited mobility, such as the sacroiliac joints, is suggestive of a malignant lesion, although it can also occur with benign lesions (Chhaya et al. 2005; Whittingham-Jones et al. 2007).

Encasement of the neurovascular bundle usually contraindicates limb-salvaging surgery. Tumours that involve the femoral triangle and inner pelvis predispose to iliac/femoral neurovascular involvement, and lesions around the lateral sacrum, ischial tuberosity and posterior upper thigh predispose to involvement of the sciatic nerve. Fortunately, the prevalence of neurovascular involvement in musculoskeletal sarcomas is low (Panicek et al. 1997). MR imaging can demonstrate whether the tumour is in close contact or encasing the neurovascular bundle, but it cannot distinguish between mere contact from adherence or early invasion. Optimal contrast between neurovascular bundle and other tissues, including tumour, is best achieved on T1-weighted fat-saturated postintravenous gadolinium DTPA or proton-density (PD) fat-saturated sequences (Saifuddin et al. 2000).

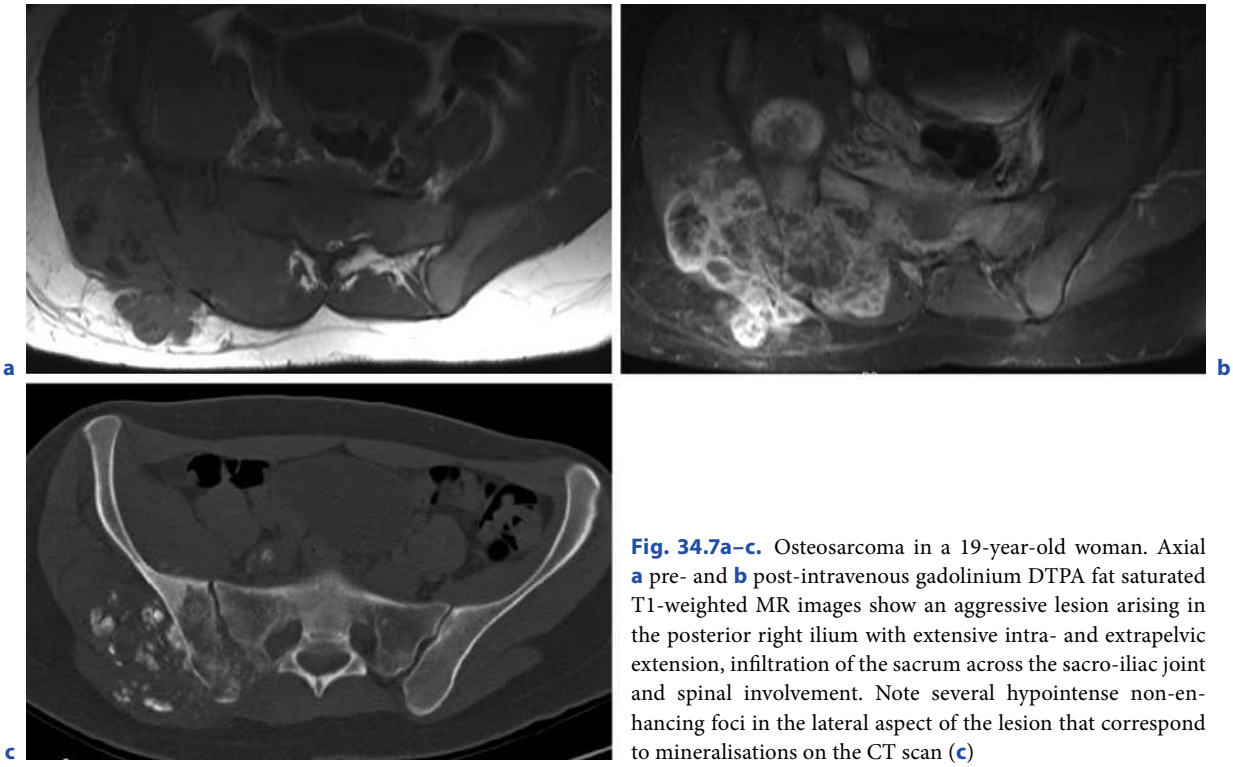

Fig. 34.7a–c. Osteosarcoma in a 19-year-old woman. Axial **a** pre- and **b** post-intravenous gadolinium DTPA fat saturated T1-weighted MR images show an aggressive lesion arising in the posterior right ilium with extensive intra- and extrapelvic extension, infiltration of the sacrum across the sacro-iliac joint and spinal involvement. Note several hypointense non-enhancing foci in the lateral aspect of the lesion that correspond to mineralisations on the CT scan (**c**)

34.3 Benign Bone Tumours and Tumour-like Lesions

34.3.1 Benign Mineralising Bone Lesions

Chondroblastoma is rare in the pelvis and only accounts for 7% of benign pelvic bone tumours. Most of them arise at the site of an old apophysis, usually around the triradiate cartilage of the acetabulum or the iliac crest (Matsuno et al. 1987). Pelvic lesions tend to occur in older patients compared with the more common location in the long bones, often in the third decade. Radiographs typically show a well-defined lytic lesion with or without sclerotic margins. Mineralisation is common but is often subtle and more easily detected on CT. Expansion should raise the possibility of a secondary aneurysmal bone cyst. On MR imaging, T2-weighted images typically show variable amounts of intermediate/low SI tissue that are due to haemosiderin, calcifications and chondroblast hypercellularity. A surrounding inflammatory response is common, and fluid-fluid levels may be present in cases with secondary aneurysmal bone cyst components. The presence of matrix mineralisation helps differentiate it from eosinophilic granuloma, Brodie's abscess and giant cell tumour. Uncommonly, chondroblastoma may follow a more aggressive course and metastatic disease has been described (Ramappa et al. 2000).

Chondromas (enchondromas) are rare in the pelvis, accounting for only 1.7% of all chondromas and 5% of all benign pelvic tumours. Radiologically, enchondromas are usually less than 5 cm in size and are characterised by a well-defined lytic lesion that may contain punctate or stippled calcifications. On MR imaging, T2-weighted images show multiple lobules of high signal intensity cartilage separated by thin, low-signal septae that enhance following intravenous contrast. Mineralised components show low signal intensity on all sequences. Differentiation from a low-grade chondrosarcoma may be difficult both radiologically and histologically (discussed further in the section on chondrosarcoma).

Osteoid osteoma (Fig. 34.8) occasionally involves the pelvis, accounting for only 1.7% of all osteoid osteomas and 8% of all benign bone tumours in the pelvis. Although radiographs may reveal a lucent or mineralised nidus with surrounding sclerosis, lesions in cancellous bone provoke little osteoblastic response and may be radiographically occult. With subarticular lesions, the reactive changes may provoke synovitis and effusion, and lesions may mimic a monoarthropathy (Mounach et al. 2008). Bone scintigraphy is useful, but CT is usually re-

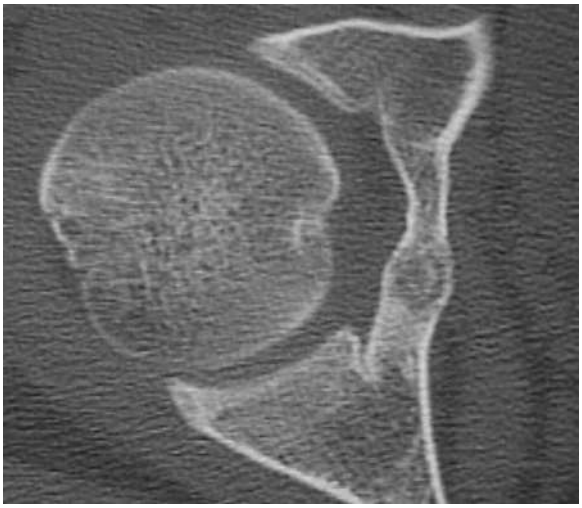

Fig. 34.8. Osteoid osteoma in an 18-year-old man. Axial CT image shows a small, partially mineralised slightly expansile nidus in the medial acetabulum

quired for precise localisation and helps in planning for CT-guided radiofrequency thermoablation (Papagelopoulos et al. 2006). On MR imaging, appearances can be confusing, as there is typically extensive marrow oedema and surrounding inflammatory changes that may obscure the nidus or suggest another process such as infection, trauma or tumour. The nidus may have variable signal intensity depending on the amount of fibrovascular tissue and mineralisation (Davies et al. 2002). Non-mineralised nidi typically show homogeneous enhancement, whereas enhancement in mineralised lesions results in the ring enhancement sign (Youseff et al. 1996). In the differential diagnosis, similar appearances can occur with a small bone abscess, but the presence of a sinus tract confirms infection.

Osteoblastoma is a rare tumour that is histologically similar to osteoid osteoma but is larger, more variable in appearance and, in the pelvis, similar in frequency to osteoid osteoma. The radiological appearances may also be similar, but osteoid osteoma tends to be less than 1 cm in size and osteoblastomas larger than 1.5 cm. Radiologically, subperiosteal lesions are often associated with a soft tissue mass and matrix mineralisation. In one series, seven of nine lesions were located in the acetabular region making treatment more difficult (Bettelli et al. 1989). Occasionally, some lesions display aggressive features with cortical destruction and infiltration of adjacent structures mimicking an osteosarcoma (Cheung et al. 1997).

34.3.2 Benign Lytic and Cystic Lesions

Giant cell tumour is an uncommon, locally aggressive tumour in the pelvis, but it is the second most common benign pelvic bone tumour accounting for 18% of all benign pelvic tumours. Most lesions occur in the fourth decade and occurrence in the immature skeleton is rare. Radiographically, lesions are typically osteolytic, expansile and subarticular in location, although they may also arise at the site of an old apophysis (see Fig 34.3). Lesions usually have a geographic pattern of bone destruction with a well-defined margin, although in up to 15% of cases, a more aggressive appearance may be seen with ill-defined margins and soft tissue infiltration. On MR imaging, lesions are inhomogeneous with variable signal intensity and often fluid-fluid levels due to secondary aneurysmal bone cyst formation. Foci of low or intermediate signal intensity on T2-weighted images are usually present and are due to collagen deposition, high cellularity and/or haemosiderin from previous haemorrhage. There is often inhomogeneous enhancement in the solid areas of the tumour that helps to differentiate it from primary aneurysmal bone cyst in the younger patient. CT is sensitive in demonstrating faint mineralisation in the periosteal shell and excludes intra-lesional mineralisation that might otherwise suggest an osteoblastic or cartilaginous tumour such as chondroblastoma or osteoblastoma. A solitary brown tumour can mimic a giant cell tumour, but other manifestations of hyperparathyroidism will usually be present. In the older patient, the differential diagnosis includes expansile metastasis, myeloma and primary bone sarcoma including chondrosarcoma. For giant cell tumour amenable to wide local resection, the prognosis is good, but for subarticular or large lesions, or lesions that also involve the sacrum, more radical treatment may be required and recurrence and complications are more common (Leggon et al. 2004).

Chondromyxoid fibroma is a rare benign cartilage tumour with mild predilection for the pelvis but only accounts for 6% of all benign bone tumours around the pelvis. Most lesions are found in the ilium usually around the triradiate cartilage or iliac crest. Radiographs typically show a well-defined, lobulated lytic lesion often with sclerotic margins. Expansion is common but may be difficult to appreciate in the ilium. Unlike most cartilaginous tumours, matrix calcification is uncommon and is seen in less than 10% of tumours. On MR imaging, lesion characteristics are non-specific with low signal intensity on T1-weighting and hyperintense signal intensity on T2-weighting. Chondromyxoid fibroma tends to present in the third decade and may be

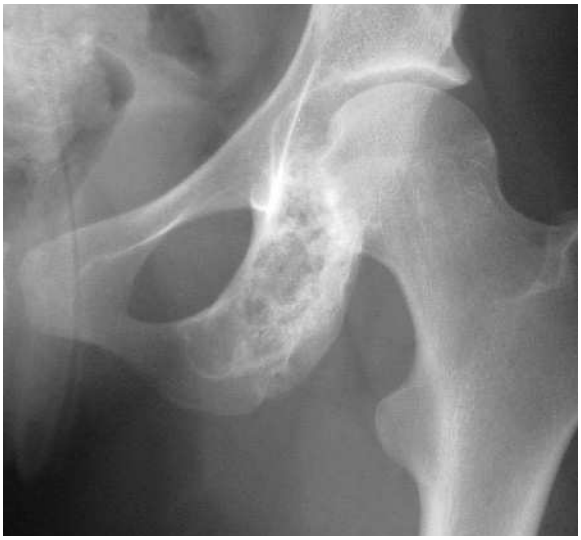

Fig. 34.9. Fibrous dysplasia in an 18-year-old woman. AP radiograph shows typical appearances with a slightly expansile lesion with prominent marginal sclerosis

radiologically indistinguishable from giant cell tumour, fibrous dysplasia, chondroblastoma or chondroma. Occasionally, chondromyxoid fibroma can have aggressive appearances mimicking a chondrosarcoma (Lersundi et al. 2005).

The simple (unicameral) bone cyst is rare in the pelvis. Lesions predominate in the iliac wing and, to a lesser extent, posterior ilium adjacent to the sacroiliac joint (Hammoud et al. 2005). Simple bone cysts are often incidental findings that probably originate during development but may not present until later in life. Radiographs reveal a well-defined lytic lesion often with a sclerotic rim. Expansion, if present, is usually only slight. On CT and MR imaging, lesions typically display fluid characteristics, although the density on CT and signal intensity on T1-weighted MR imaging may be greater than water due to high protein content. Fluid-fluid levels and solid areas representing reparative tissue may be seen in simple bone cysts complicated by fracture.

Aneurysmal bone cyst is a benign expansile lesion characterised by multiple blood-filled cystic cavities that are relatively uncommon in the pelvis. Approximately 6% of these cysts occur in the ilium, 2% in the pubis and 2% in the ischium. 80% of lesions occur between 5 and 15 years of age, typically arising around the triradiate cartilage. Most of the cysts are primary lesions, although aneurysmal bone cyst-like features can be found with other precursor lesions, including giant cell tumour, osteoblastoma, chondroblastoma and the rare telangiectatic osteosarcoma, and these are termed secondary lesions. For primary lesions, the imaging appearances mirror its evolution through various stages. In the early phase, radiographs show a markedly expansile lytic lesion that may have a "blown-out" appearance. The periosteal new bone may be barely perceptible due to the rapid rate of growth and may mimic an aggressive sarcoma (Campanacci 1999). In the stabilisation phase, the periosteal bone matures resulting in a surrounding mineralised shell, and in the healing phase, there is consolidation of the lesion with further thickening and maturation of the periosteal bone. Cross-sectional imaging is also useful (Mahnken et al. 2003). In the early phase, the thin rim of intact periosteal tissue gives a low signal intensity on all MR sequences and CT may reveal subtle periosteal mineralisation that is radiographically occult. MR imaging is more sensitive than CT at detecting fluid-fluid levels that result from the sedimentation effect of blood products within the cystic spaces (see Fig. 34. 5). In primary lesions, intravenous contrast confirms rim and septal enhancement, whereas in secondary lesions, the enhancement pattern depends on the extent and nature of the underlying lesion. It is worth stressing that telangiectatic osteosarcoma may resemble aneurysmal bone cyst both on imaging and histology, but the presence of thick nodular components, necrosis, soft tissue mass and matrix mineralisation should suggest osteosarcoma (Murphey et al. 2003).

Fibrous dysplasia is a relatively common developmental anomaly that commonly affects the bony pelvis in both monostotic and polyostotic forms. Polyostotic disease tends to present in the first decade with pain or pathological fracture or with endocrine problems (Albright's syndrome). Monostotic disease more commonly presents in the second decade as an incidental finding or after innocuous trauma. Radiographs show a well-defined, intramedullary, expansile lesion often with endosteal scalloping and sclerotic margin of variable thickness (Fig. 34.9). The matrix is variable ranging from lucent to sclerotic. MR imaging shows a hypointense or isointense signal intensity compared with muscle on T1-weighting and a variable signal intensity on T2-weighting depending on the cellularity and extent of the fibrous and mineralised components. Occasionally, fibrous dysplasia may be associated with muscular myxomas, known as Mazabraud syndrome.

Langerhans' cell histiocytosis is a relatively uncommon spectrum of diseases but does have a predilection for the pelvis. In one series, 20% of all lesions occurred in the ilium and it accounted for 50% of tumour-like lesions of the pelvis (Campanacci 1999). Its localised form, eosinophilic granuloma, accounts for 70% of cases and heals spontaneously. Patients present between the ages of 5 and 15 years with a slight male predominance. In

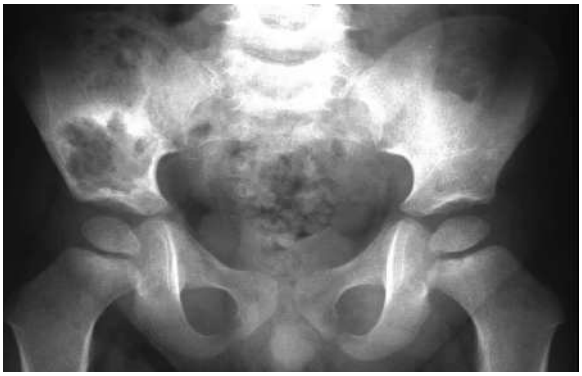

Fig. 34.10. Eosinophilic granuloma in a child. AP radiograph shows solitary lesion arising in the right ilium. Note the surrounding sclerosis and lamellar periosteal reaction laterally

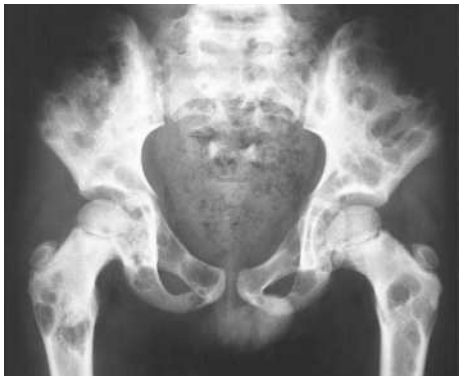

Fig. 34.11. Langerhans' cell histiocytosis in a child. AP radiograph shows multiple well-defined lytic lesions giving a "hole-within-a-hole" appearance. Some of the lesions have sclerotic margins

the early phase, radiographs and MR imaging typically demonstrate an aggressive pattern of bone destruction with ill-defined margins and lamellated periosteal reaction simulating Ewing's sarcoma, lymphoma or infection (Azouz et al. 2005; Ando et al. 2008); however, in the later healing phase, they have well-defined sclerotic margins simulating a benign bone tumour, including chondroblastoma, enchondroma, fibrous dysplasia or simple bone cyst (Fig. 34.10).

34.3.3 Benign Surface Lesions

Osteochondroma (exostosis) is the most common benign bone tumour of the pelvis accounting for 43% of benign bone tumours. It is a growth-plate aberration rather than a true tumour but is classified with benign chondrogenic tumours. Most pelvic lesions arise in the iliac bone (82%) and typically present with a mass or pressure effects on adjacent structures. Radiographically, lesions appear as a sessile or pedunculated exophytic outgrowth from the bone surface that shows continuity with the marrow cavity and cortex. The cartilage cap typically calcifies. A painful lesion or continued growth after maturity should raise the possibility of sarcomatous degeneration in the cartilage cap, although this is rare in solitary lesions (Murphey et al. 2000). A cap thickness of greater than 2 cm is suggestive of malignant transformation. The cartilage cap displays low signal intensity on T1-weighting and very high signal intensity on T2-weighting, due to its high water content, and is easily distinguished from adjacent muscle and ossific stalk (see Fig. 34.2). MR imaging is also helpful in excluding other complications including bursitis and pressure effects on adjacent structures. In the differential diagnosis, the lack of marrow continuity excludes periosteal chondroma and juxta cortical myositis ossificans. Medullary continuity may occur with parosteal osteosarcoma, but the cortex is destroyed and not remodelled as with osteochondroma.

34.3.4 Multiple Benign Bone Lesions

Several of the previously discussed benign solitary lesions, including Langerhans' cell histiocytosis, fibrous dysplasia, osteochondroma and enchondroma, may have multifocal involvement of the pelvis, and the imaging features are similar to those of solitary lesions. In Langerhans' cell histiocytosis, multifocal lesions may occur without extraskeletal involvement. In the pelvis, Langerhans' lesions may display a "hole-within-a-hole" appearance representing confluence of contiguous lytic lesions (Fig. 34.11; Stull et al. 1992); however, similar appearances may occur with metastatic disease, leukaemia/lymphoma, infection, fibrous dysplasia, Ollier's disease and cystic angiomatosis. In Ollier's disease (multiple enchondromatosis or enchondromatosis), the pelvis is commonly involved and the risk of sarcomatous transformation is 25%. In Maffucci's syndrome (enchondromatosis and soft tissue haemangiomas), the risk approaches 100%. In diaphyseal aclasis (hereditary multiple osteochondromatosis/exostoses), 9% of the lesions occur in the pelvis and most lesions are of the ses-

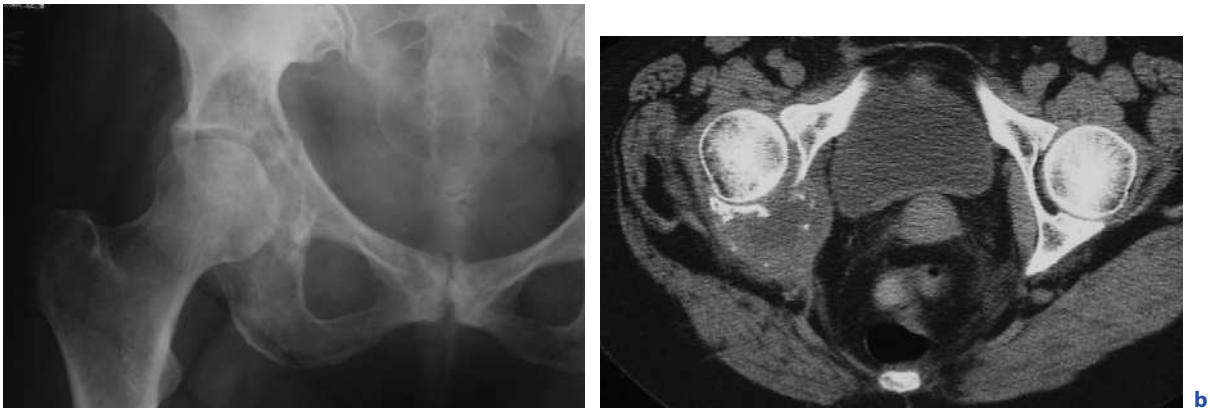

Fig. 34.12a,b. Post-irradiation osteosarcoma in a 62-year-old woman who had received radiotherapy for cervical carcinoma 20 years previously. **a** AP radiograph shows a pathological fracture of the right acetabulum due to an ill-defined lytic lesion that also involves the ischium. **b** CT shows extraosseous and intraarticular extension of the tumour and matrix mineralisations, in keeping with osteosarcoma

sile type. Small sessile lesions in the pelvis may create an undulating cortical contour on CT, termed the "wavy-pelvis sign" (Murphey et al. 2000). The reported incidence of sarcomatous degeneration has varied between 0.6 and 8% in different studies, but sarcomatous degeneration is probably more common in the pelvis than the appendicular skeleton (see Fig 34.4; Lee et al. 2002).

34.4 Malignant Bone Tumours

34.4.1 Malignant Mineralising Sarcomas

Chondrosarcoma is the most common primary bone sarcoma around the pelvis accounting for 32% of all primary bony malignancies excluding myeloma. Approximately 22% of all chondrosarcomas arise in the pelvis, and 71% of these arise in the ilium and around the acetabulum. Important prognostic factors include tumour grade and adequate surgical excision (Gelderblom et al. 2008). Low-grade lesions are more common than high-grade lesions and carry a much better prognosis. Low-grade lesions usually have a less aggressive geographic pattern of bone destruction that results in endosteal scalloping and cortical expansion; however, similar appearances can be found with enchondromas both radiologically and histologically, and differentiation may be difficult. On the other hand, the vast majority of cartilagenous tumours in the pelvis are malignant, and therefore all cartilagenous tumours of the pelvis should be viewed with suspicion. Cortical scalloping greater than two-thirds of the cortical thickness, lesion size greater than 5 cm, non-mechanical pain and patient age over 30 years are strongly supportive of chondrosarcoma (Murphey et al. 1998). On MR imaging, the non-mineralised chondroid matrix displays high signal intensity on T2-weighting and is separated into lobules by low-signal fibrovascular septae. In equivocal cases, dynamic contrast-enhanced MR imaging using Gd-DTPA has shown some success in differentiating chondroma from low-grade chondrosarcoma based on rate of enhancement, but an absolute distinction cannot be made (Geirnaerdt et al. 2000). CT is the most sensitive technique for detecting mineralisation and will detect mineralisation in over 90% of cases. In low-grade lesions, the mineralisation tends to have the classic "rings-and-arcs" pattern, whereas with higher-grade lesions, the mineralisation is more amorphous or stippled. High-grade lesions typically have a more aggressive appearance with permeative pattern of bone destruction, periosteal reaction and soft tissue extension. In dedifferentiated lesions, MR imaging will show features of both low- and high-grade components and recognition of the higher-grade components is important in planning the biopsy (Saifuddin et al. 2004). Soft tissue infiltration and transarticular spread are common and best assessed by MR imaging (see Fig. 34.6). In the differential diagnosis of higher-grade lesions, metastases and lymphoma can appear similar and are more likely if multifocal. Mineralisations are usually absent in myeloma and Ewing's sarcoma and only occasionally present in malignant fibrous histiocytoma and fibrosarcoma. Chondroblastic osteosarcoma should also be

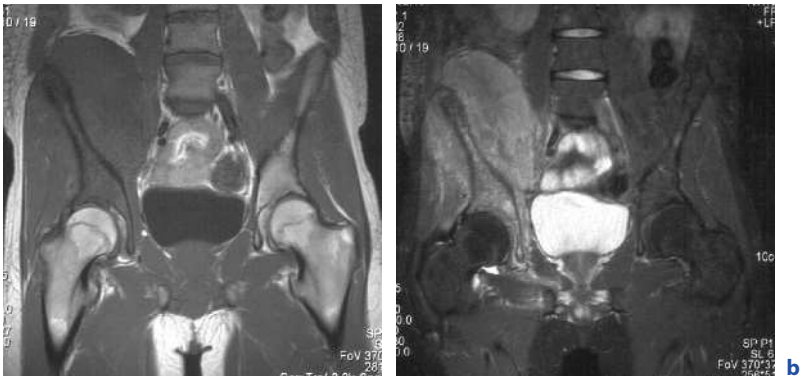

Fig. 34.13a,b. Ewing's sarcoma. Coronal **a** T1-weighted and **b** STIR MR images shows a large tumour involving most of the right ilium and acetabulum with soft tissue extension

considered but tends to occur in a much younger age group.

Osteosarcoma of the pelvis accounts for only 8% of all osteosarcomas but it is the second most common primary bony malignancy of the pelvis accounting for 22% of all primary malignancies excluding myeloma. The median age of pelvic osteosarcoma (20 years) is higher than that of extremity osteosarcoma (15 years), but the 3:2 male predominance is similar (Bielack et al. 2002; Ozaki et al. 2003b). Lesions occurring in older patients are often secondary to pre-existing conditions (López et al. 2003; Nakanishi et al. 2001). In one series, approximately 37% of all Paget's osteosarcomas and 29% of all radiation osteosarcomas occurred in the pelvis (Fig. 34.12; Unni 1996). Pelvic osteosarcomas have a much poorer prognosis than extremity osteosarcomas with 5-year survival rates of only 27–34% compared with 67% for extremity osteosarcomas (Bielack et al. 2002; Matsuo et al. 2005). Poor prognostic factors include secondary lesions, late detection, surgical limitations, involvement of sacrum, primary metastatic disease and poor response to chemotherapy. As elsewhere in the skeleton, over 90% are high-grade lesions but, unlike extremity lesions, the chondroblastic type appears to be more common than the osteoblastic type. Lesions predominate in the ilium and acetabular regions, but there is commonly spread into the other pelvic bones and sacrum (see Fig. 34.7; Matsuo et al. 2005). The radiological appearances are variable, but most lesions display a mixed lytic/sclerotic appearance with a moth-eaten or permeative pattern of bone destruction and soft tissue extension. Matrix chondroid or osteoid mineralisation is usually present and helps to differentiate from other sarcomas including Ewing's sarcoma. Periosteal reaction is common but more difficult to detect in the ilium. On MR imaging, lesions typically display low to intermediate signal intensity on T1-weighting and inhomogeneous high signal intensity on T2-weighting. Mineralised foci often display low signal intensity on all sequences. MR imaging is also useful in assessing suspicious lytic foci within pagetic bone. Preservation of fatty marrow signal intensity on T1-weighting excludes sarcomatous degeneration, whereas a reduction in signal intensity on T1-weighting should raise the possibility of sarcoma (López et al. 2003); however, a pathological fracture through non-sarcomatous pagetoid bone will also result in a reduction of signal intensity on T1-weighting.

34.4.2 Malignant Non-mineralising Sarcomas

Ewing's sarcoma is a high-grade round cell tumour with a predilection for the pelvis. Ewing's sarcoma of the pelvis accounts for 21% of all Ewing's sarcoma and 22% of all primary malignant bone tumours around the pelvis excluding myeloma. Ewing's sarcoma usually presents in a slightly younger age group than osteosarcoma with a peak incidence between 10 and 15 years. Prognostically, there is a significantly higher rate of metastatic disease with Ewing's sarcoma arising in the pelvis (38%) compared with the appendicular skeleton (16%). In addition, the long-term survival is only 15–20% for those with metastases at presentation compared with 50–70% for those without metastases (Bacci et al. 2007). Lesions are most commonly found in the ilium and may spread across the sacroiliac joint, but involvement of the hip joint is unusual. Radiographs show an aggressive lytic lesion with a moth-eaten or permeative pattern

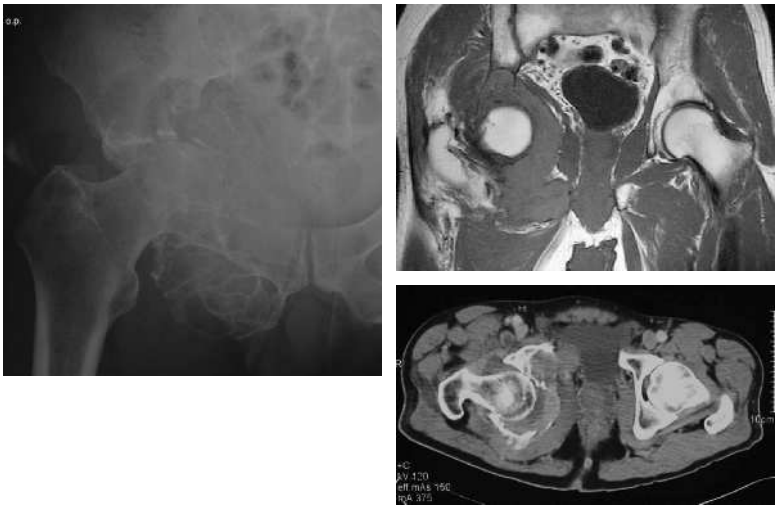

a,b c

Fig. 34.14a-c. Plasmacytoma in a 62-year-old man. **a** AP radiograph, **b** coronal T1-weighted MR image and **c** axial CT image show a pathological fracture/central right hip dislocation due to an expansile lytic lesion of the acetabulum. Histology confirmed plasmacytoma. The differential diagnosis includes expansile metastasis, giant cell tumour and chondrosarcoma

of bone destruction and lamellated periosteal reaction that may be difficult to detect in the pelvis (Mar et al. 2008). Although lesions do not produce a mineralised matrix, reactive sclerotic components may occur and are more common in the pelvis. On MR imaging, lesions are usually hypointense or isointense with muscle on T1-weighting but are of variable signal intensity on T2-weighting (Fig. 34.13). Components displaying low or intermediate signal intensity on T2-weighting are probably due to high cellularity. Haemorrhage and necrosis may also be present. In the differential diagnosis, the presence of matrix mineralisation should suggest an osteosarcoma, but this may be difficult to detect without CT. Acute osteomyelitis and eosinophilic granuloma may mimic Ewing's sarcoma as all three conditions may present with a fever and leukocytosis; however, eosinophilic granuloma tends to have a history of less than 2 weeks, osteomyelitis 2–4 weeks and Ewing's sarcoma 2–4 months. Both Ewing's sarcoma and lymphoma may present with an associated soft tissue mass, but lymphoma tends to present in an older age group.

Although malignant fibrous histiocytoma and fibrosarcoma are different pathological entities, they are discussed together as they have similar imaging appearances. Together, they account for 7% of malignant bone tumours around the pelvis. Approximately 9% of all malignant fibrous histiocytomas and 15% of all fibrosarcomas arise in the pelvis and most of these occur in the ilium. There is a wide age range but both peak in the fourth decade. In 20–30% of cases, both lesions may arise secondarily to pre-existing conditions, most commonly radiation treatment. Other associations include osteonecrosis, chronic osteomyelitis, Paget's disease, fibrous dysplasia, giant cell tumour, enchondroma and dedifferentiated chondrosarcoma. Radiographically, the spectrum of bone destruction is wide, but most show a lytic lesion with an aggressive pattern of bone destruction. Periosteal reaction and expansion are variable and dystrophic mineralisation is occasionally present (Papagelopoulos et al. 2000). On MR imaging, the signal characteristics are non-specific, but lesions may display an inhomogeneous, nodular signal pattern with peripheral enhancement (Link et al. 1998). If the collagen content is high, then a lower signal intensity on T2-weighting may be obtained. Foci of haemorrhage and necrosis may be present and extra-osseous tumour spread is frequent. The differential diagnosis in older patients includes metastases, myeloma and lymphoma, and if mineralisation is present, chondrosarcoma. In younger patients, osteosarcoma should also be considered, especially if mineralisation is present.

34.4.3 Non-sarcomatous Bone Malignancies

Multiple myeloma, a monoclonal proliferation of malignant plasma cells, is the most common primary malignant bone neoplasm around the pelvis with a peak incidence between the sixth and seventh decades and a 2:1 male predominance. The ilium is a common site for solitary plasmacytoma (Fig. 34.14), but conventional imaging may underestimate the disease extent, as 33% of patients with newly diagnosed solitary plasmacytoma by routine criteria in one study had additional lesions detected on MR imaging of the dorso-lumbar spine (Moulopoulos et al. 1995). Multiple myeloma typically shows multiple rounded, punched-out lytic lesions without sclerotic margins, although it may also present with diffuse demineralisation in 12–25% of patients and

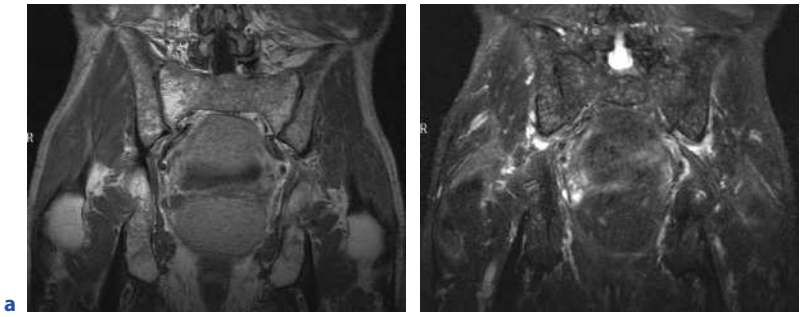

Fig. 34.15a,b. A 70-year-old man with anaemia and paraproteinaemia. Coronal **a** T1-weighted and **b** STIR sequences show diffuse infiltration of the pelvis with multiple small deposits in the sacrum, iliac and ischial bones. Histology confirmed diffuse myeloma

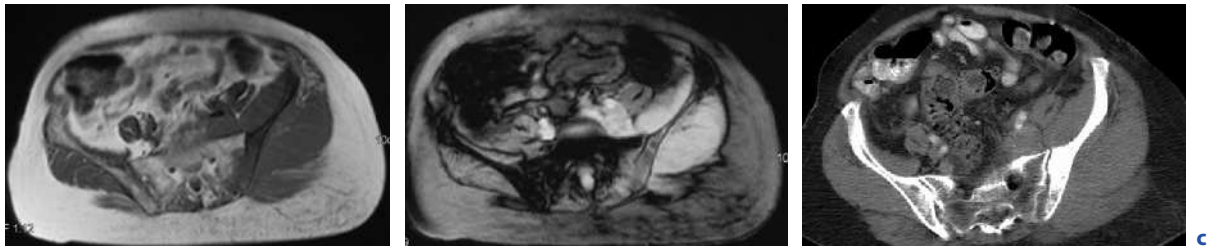

Fig. 34.16a–c. A 71-year-old woman with lymphoma. Axial **a** T1-weighted and **b** T2-weighted GE MR images and **c** axial CT image show a large left pelvic mass arising from the ilium with intra- and extrapelvic soft tissue extension and early infiltration of the left sacrum. Histology confirmed high-grade non-Hodgkin's lymphoma, B-cell type

sclerotic lesions in <1% of patients. On MR imaging, the features reflect the concentration and distribution of the tumour cells and five different patterns have been recorded: (1) normal bone marrow – histologically positive but insufficient infiltration to be detected on MR imaging; (2) focal infiltration; (3) diffuse homogeneous infiltration; (4) a combination of diffuse and focal involvement; and (5) "salt-and-pepper" pattern with low-grade diffuse disease interspersed by islands of high signal intensity fat (Fig. 34.15; Baur-Melnyk et al. 2005).

Metastatic lymphoma is common in the bony pelvis, whereas primary lymphoma of bone is rare. In one study, 18% of patients with osseous lymphoma had involvement of the pelvis, but only 2% had primary disease (Kirsch et al. 2006). In a large study of 237 patients with primary lymphoma of bone, 10.5% were located in the pelvis (Mulligan et al. 1999). Primary lymphoma carries a better prognosis than secondary lymphoma with 5-year survival rates of 88 and 51%, respectively (Kirsch et al. 2006; Beal et al. 2006). Secondary lymphoma can present with focal, multifocal or diffuse marrow involvement. Low-grade lymphoma is more likely to present with diffuse disease and detection by MR imaging will depend on the concentration of neoplastic cells within the marrow. Where the concentration of neoplastic cells is greater than 30%, then abnormal signal is usually detected on MR imaging, whereas concentrations of less than 20% are likely to show normal signal on MR imaging (Daldrup-link et al. 2007); however, most cases of secondary lymphoma show multifocal disease and this is readily detected on MR imaging. In focal disease, similar imaging appearances may be found with primary or secondary lymphoma. In primary lymphoma of bone, the majority of lesions display an aggressive, predominantly lytic appearance with a moth-eaten or permeative pattern of bone destruction, periosteal reaction and occasionally sequestra, but in the pelvis these features may be difficult to detect radiographically. Mixed lytic–blastic and blastic lesions are less common. On MR imaging, there is often a large parosseous soft tissue component (Krishnan et al. 2003). Infiltration of adjacent structures, including the sacroiliac joint, is not uncommon (Mulligan et al. 1999). Most lesions are isointense or hypointense to skeletal muscle on T1-weighting and display inhomogeneous and variable signal on T2-weighting (Fig. 34.16). The differential diagnosis is wide, as lymphoma has a wide age range. In the younger patient, the main differential diagnoses are Ewing's sarcoma, osteosarcoma, Langerhans' histiocytosis and osteomyelitis, and in the older patient, metastases and myeloma.

Metastases are, by far, the most common tumours around the bony pelvis. In a large series of bone metastases, 12% were located in the ilium (Campanacci 1999).

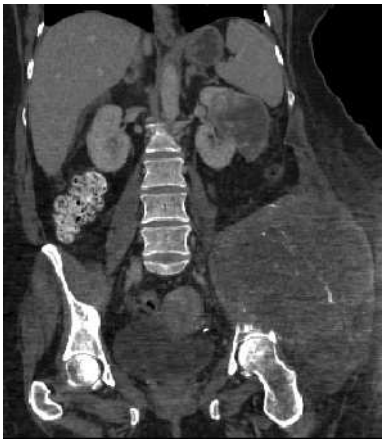

Fig. 34.17. A 75-year-old woman with left iliac metastasis from renal carcinoma. Coronal CT image shows huge expansile metastasis destroying most of the left iliac bone from a left renal carcinoma

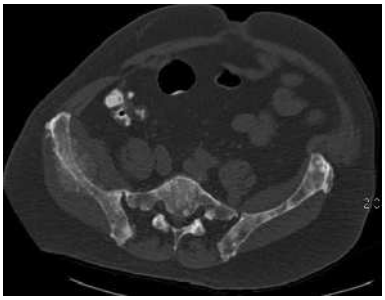

Fig. 34.18. A 62-year-old man with multifocal osteoblastic metastases. Axial CT image shows multiple osteoblastic metastases that were initially thought to be due to prostatic metastases, but histology confirmed metastatic osteosarcoma. Multiple pulmonary metastases were also present. There were no known risk factors for osteosarcoma

The majority of metastases are of lung, breast, prostate, colon, kidneys and bladder origin. In children, bone metastases may occur with neuroblastoma, rhabdomyosarcoma, osteosarcoma, Ewing's sarcoma, teratoma and Wilm's tumour. Radiographically, the majority of these lesions are lytic with a geographic or moth-eaten pattern of bone destruction and absent periosteal reaction. Occasionally, metastases have an expansile appearance indicating a slower rate of growth and often a renal or thyroid origin (Fig. 34.17). Prostatic metastases are usually sclerotic and breast, bladder and gastrointestinal primaries may be lytic, sclerotic or mixed. The MR imaging features are non-specific, but blastic metastases usually display low signal intensity on all sequences. A soft tissue component or the presence of a rim of high signal intensity around an osseous lesion (halo sign) usually indicates metastatic disease (Schweitzer et al. 1993). The differential diagnosis of osteolytic metastases includes myeloma and lymphoma, and if solitary, primary bone sarcoma including chondrosarcoma, malignant fibrous histiocystosis and fibrosarcoma. The differential diagnosis of sclerotic metastases includes bone islands, bone infarcts, Paget's disease, osteitis condensan ilii, and less commonly, lymphoma, Ollier's disease and sclerosing dysplasias (Fig. 34.18).

Acknowledgements

The author thanks J. Campbell of the Scottish Bone Tumour Registry for her assistance in collecting images, and A.M. Davies for several cases.

References

Anderson MW, Temple HT, Dussault RG, Kaplan PA (1999) Compartment anatomy: relevance to staging and biopsy of musculoskeletal tumours. Am J Roentgenol 173:1663–1671

Ando A, Hatori M, Hosaka M, Hagiwara Y, Kita A, Itoi E (2008) Eosinophilic granuloma arising from the pelvis in children: a report of three cases. Ups J Med Sci 113:209–211

Azouz EM, Saigal G, Rodriguez MM, Podda A (2005) Langerhans' cell histiocytosis: pathology, imaging and treatment of skeletal involvement. Pediatr Radiol 35:103–115

Bacci G, Balladelli A, Forni C, Longhi A, Serra M, Fabbri N, Alberghini M, Ferrari S, Benassi MS, Picci P (2007) Ewing's sarcoma family tumours. Differences in clinicopathological characteristics at presentation between localised and metastatic tumours. J Bone Joint Surg Br 89:1229–1233

Baur-Melnyk A, Buhmann S, Reiser M (2005) Role of MRI for the diagnosis and prognosis of multiple myeloma. Eur J Radiol 55:56–63

Beal K, Allen L, Yahalom J (2006) Primary lymphoma of bone: treatment results and prognostic factors with long-term follow-up of 82 patients. Cancer 106:2652–2656

Bettelli G, Capanna R, van Horn JR, Ruggieri P, Biagini R, Campanacci M (1989) Osteoid osteoma and osteoblastoma of the pelvis. Clin Orthop Relat Res 247:261–267

Bielack SS, Kempf-Bielack B, Delling G Exner GU, Flege S, Helmke K, Kotz R, Salzer-Kuntschik M, Werner M, Winkelmann W, Zoubek A, Jürgens H, Winkler K (2002) Prognostic factors in high-grade osteosarcoma of the extremities or trunk: an analysis of 1,702 patients treated on neoadjuvant cooperative osteosarcoma study group protocols. J Clin Oncol 20:776–790

Buirski G, Ratliff AH, Watt I (1986) Cartilage-cell-containing tumours of the pelvis: a radiological review of 40 patients. Br J Radiol 59:197–204

Campanacci M (1999) Bone and soft tissue tumours: clinical features, imaging, pathology and treatment, 2nd edn. Springer, Berlin Heidelberg New York

Cheung FM, Wu WC, Lam CK, Fu YK (1997) Diagnostic criteria for pseudomalignant osteoblastoma. Histopathology 31:196–200

Chhaya S, White LM, Kandel R, Wunder JS, Ferguson P, Agur A (2005) Transarticular invasion of bone tumours across the sacroiliac joint. Skeletal Radiol. 34:771–777

Daldrup-Link HE, Henning T, Link TM (2007) MR imaging of therapy-induced changes of bone marrow. Eur Radiol 17:743–761

Davies M, Cassar-Pullicino VN, Davies AM, McCall IW, Tyrrell PN (2002) The diagnostic accuracy of MR imaging in osteoid osteoma. Skeletal Radiol 31:559–569

Gelderblom H, Hogendoorn PC, Dijkstra SD, van Rijswijk CS, Krol AD, Taminiau AH, Bovée JV (2008) The clinical approach towards chondrosarcoma. The Oncologist 13:320–329

Geirnaerdt MJ, Hogendoorn PC, Bloem JL, Taminiau AH, van der Woude HJ (2000) Cartilaginous tumors: fast contrast-enhanced MR imaging. Radiology 214:539–546

Hammoud S, Weber K, McCarthy EF (2005) Unicameral bone cysts of the pelvis: a study of 16 cases. Iowa Orthop J 25:69–74

Kirsch J, Ilaslan H, Bauer TW, Sundaram M (2006) The incidence of imaging findings, and the distribution of skeletal lymphoma in a consecutive patient population seen over 5 years. Skeletal Radiol 35:590–594

Krishnan A, Shirkhoda A, Tehranzadeh J, Armin AR, Irwin R, Les K (2003) Primary bone lymphoma: radiographic-MR imaging correlation. Radiographics 23:1371–1383

Lee KC, Davies AM, Cassar-Pullicino VN (2002) Imaging the complications of osteochondromas. Clin Radiol 57:18–28

Leggon RE, Zlotecki R, Reith J, Scarborough MT (2004) Giant cell tumor of the pelvis and sacrum: 17 cases and analysis of the literature. Clin Orthop Relat Res 423:196–207

Lersundi A, Mankin HJ, Mourikis A, Hornicek FJ (2005) Chondromyxoid fibroma: a rarely encountered and puzzling tumor. Clin Orthop Relat Res 439:171–175

Link TM, Haeussler MD, Poppek S, Woertler K, Blasias S, Lindner N, Rummeny EJ (1998) Malignant fibrous histiocytoma of bone: conventional X-ray and MR imaging features. Skeletal Radiol 27:552–558

López C, Thomas DV, Davies AM (2003) Neoplastic transformation and tumour-like lesions in Paget's disease of bone: a pictorial review. Eur Radiol 13 (Suppl 4):L151–L163

Mahnken AH, Nolte-Ernsting CC, Wildberger JE, Heussen N, Adam G, Wirtz DC, Piroth W, Bücker A, Biesterfeld S, Haage P, Günther RW (2003) Aneurysmal bone cyst: value of MR imaging and conventional radiography. Eur Radiol 13:1118–11124

Mar WA, Taljanovic MS, Bagatell R, Graham AR, Speer DP, Hunter TB, Rogers LF (2008) Update on imaging and treatment of Ewing sarcoma family tumors: what the radiologist needs to know. J Comput Assist Tomogr 32:108–118

Matsuno T, Hasegawa I, Masuda T (1987) Chondroblastoma arising in the triradial cartilage. Report of two cases with review of the literature. Skeletal Radiol 16:216–222

Matsuo T, Sugita T, Sato K, Hotta T, Tsuchiya H, Shimose S, Kubo T, Ochi M (2005) Clinical outcomes of 54 pelvic osteosarcomas registered by Japanese musculoskeletal oncology group. Oncology 68:375–381

Moulopoulos LA, Dimopoulos MA, Smith TL, Weber DM, Delasalle KB, Libshitz HI, Alexanian R (1995) Prognostic significance of magnetic resonance imaging in patients with asymptomatic myeloma. J Clin Oncol 13:251–256

Mounach A, Nouijai A, Ghozlani I, Ghazi M, Achemlal L, Bezza A, El Maghraoui A (2008) Osteoid osteoma of the acetabulum: a case report. Rheumatol Int 28:601–603

Mulligan ME, McRae GA, Murphey MD (1999) Imaging features of primary lymphoma of bone. Am J Roentgenol 173:1691–1697

Murphey MD, Fleming DJ, Boyea SR, Bojescul JA, Sweet DE, Temple HT (1998) From the archives of the AFIP. Enchondroma versus chondrosarcoma in the appendicular skeleton: differentiating features. Radiographics 18:1213–1237

Murphey MD, Choi JJ, Kransdorf MJ, Flemming DJ, Gannon FH (2000) Imaging of osteochondroma: variants and complications with radiologic–pathologic correlation. Radiographics 20:1407–1434

Murphey MD, wan Jaovisidha S, Temple HT, Gannon FH, Jelinek JS, Malawer MM (2003) Telangiectatic osteosarcoma: radiologic–pathologic comparison. Radiology 229:545–553

Nakanishi K, Yoshikawa H, Ueda T, Araki N, Tanaka H, Aozasa K, Nakamura H (2001) Postradiation sarcomas of the pelvis after treatment for uterine cervical cancer: review of the CT and MR findings of five cases. Skeletal Radiol 30:132–137

Ozaki T, Putzke M, Burger H, Gosheger G, Winkelmann W, Lindner N (2002) Infiltration of sarcomas into the hip joint. Acta Orthop Scand 73:220–226

Ozaki T, Rodl R, Gosheger G, Hoffman C, Poremba C, Winkelmann W, Lindner N (2003a) Sacral infiltration in pelvic sarcomas: joint infiltration analysis II. Clin Orthop 407:152–158

Ozaki T, Flege S, Kevric M, Lindner N, Maas R, Delling G, Schwarz R, Hochstetter AR von, Salzer-Kuntschik M, Berdel WE, Jürgens H, Exner GU, Reichardt P, Mayer-Steinacker R, Ewerbeck V, Kotz R, Winkelmann W, Bielack SS (2003b) Osteosarcoma of the pelvis: experience of the Cooperative Osteosarcoma Study Group. J Clin Oncol 21:334–341

Panicek DM, Hilton S, Schwartz LH (1997) Assessment of neurovascular involvement by malignant musculoskeletal tumors. Sarcoma 1:281–283

Papagelopoulos PJ, Galanis E, Frassica FJ, Sim FH, Larson DR, Wold LE (2000) Primary fibrosarcoma of bone. Outcome after primary surgical treatment. Clin Orthop Relat Res 373:88–103

Papagelopoulos PJ, Mavrogenis AF, Kyriakopoulos CK, Benetos IS, Kelekis NL, Andreou J, Soucacos PN (2006). Radiofrequency ablation of intra-articular osteoid osteoma of the hip. J Int Med Res 34:537–544

Ramappa AJ, Lee FY, Tang P, Carlson JR, Gebhardt MC, Mankin HJ (2000) Chondroblastoma of bone. J Bone Joint Surg Am 82-A:1140–1145

Saifuddin A, Twin P, Emanuel R, Cannon SR (2000) An audit of MRI for bone and soft tissue tumours performed at referral centres. Clin Radiol 55:537–541

Saifuddin A, Mann BS, Mahroof S, Pringle JA, Briggs TW, Cannon SR (2004) Dedifferentiated chondrosarcoma: use of MRI to guide needle biopsy. Clin Radiol 59:268–272

Schima W, Amann G, Stiglbauer R, Windhager R, Kramer J, Nicolakis M, Farres MT, Imhof H (1994) Preoperative staging of osteosarcoma: efficacy on MR imaging in detecting joint involvement. Am J Roentgenol 63:1171–1175

Schweitzer ME, Levine C, Mitchell DG, Gannon FH, Gomella LG (1993) Bull's-eyes and halos: useful MR discriminators of osseous metastases. Radiology 188:249–252

Shapeero LG, Vanel D (2000) Imaging evaluation of the response of high-grade osteosarcoma and Ewing sarcoma to chemotherapy with emphasis on dynamic contrast-enhanced MR imaging. Semin Musculoskeletal Radiol 4:137–146

Stull MA, Kransdorf MJ, Devaney KO (1992) Langerhans cell histiocytosis of bone. Radiographics 12:801–823

Thompson RC Jr, Berg TL (1996) Primary bone tumors of the pelvis presenting as spinal disease. Orthopedics 19:1011–1016

Unni KK (1996) Dahlin's bone tumors: general aspects and data on 11,087 cases, 5th edn. Lippincott-Raven, Philadelphia, New York

Whittingam-Jones P, Hughes R, Fajinmi M, Lehovsky J, Saifuddin A (2007) Osteoblastoma crossing the sacro-iliac joint. Skeletal Radiol 36:249–252

Wurtz LD, Peabody TD, Simon MA (1999) Delay in the diagnosis and treatment of primary bone sarcoma of the pelvis. J Bone Joint Surg Am 81:317–325

Youssef BA, Haddad MC, Zahrani A, Sharif HS, Morgan JL, al-Shahed M, al-Sabty A, Choudary R (1996) Osteoid osteoma and osteoblastoma: MRI appearances and the significance of ring enhancement. Eur Radiol 6:291–296

Hand and Wrist

35

Nikhil A. Kotnis, A. Mark Davies and Steven L. J. James

CONTENTS

KEY POINTS

- Bone tumours of the hand and wrist are uncommon.
- The majority of these tumours are benign.
- Enchondroma is the commonest benign tumour.
- Chondrosarcoma is the commonest malignant primary tumour.
- Malignant tumours of the hand frequently have a better prognosis than tumours at other skeletal sites.

35.1 Introduction

Bone tumours affecting the hand and wrist are rare. Only 2% of a series of 4277 bone tumours were located in the hand or wrist (Dahlin 1995). Furthermore, primary bone tumours are uncommon when compared with tumours arising in the soft tissues of the hand. Haber described 2321 tumours of the hand with only 38 cases involving bone (cited by Garcia et al. 2001).

The majority of bone tumours that affect the hand are benign. Of a series of 469 cases reported by Campanacci and Laus (cited by Garcia et al. 2001), only ten were malignant tumours, six of which were metastases. The most frequent benign lesion is enchondroma and the most common malignant lesion is chondrosarcoma (Wilner 1982).

Radiographs are sufficient to allow accurate diagnosis in the majority of bone tumours of the hand and wrist. Computed tomography allows characterisation of tumour matrix and presence of bone destruction. MRI provides information regarding the extent of marrow involvement and soft tissue invasion.

N. A. Kotnis, MD
Department of Radiology, Royal Orthopaedic Hospital, NHS Foundation Trust, Bristol Road South, Northfield, Birmingham B31 2AP, UK

A. M. Davies, MBChB, FRCR
Department of Radiology, Royal Orthopaedic Hospital, NHS Foundation Trust, Bristol Road South, Northfield, Birmingham B31 2AP, UK

S. L. J. James, MD
Department of Radiology, Royal Orthopaedic Hospital, NHS Foundation Trust, Bristol Road South, Northfield, Birmingham B31 2AP, UK

This chapter reviews the most common benign and malignant bone neoplasms of the hand and wrist. The incidence, distribution and imaging characteristics of these tumours specific to this location are discussed.

35.2 Benign Tumours

35.2.1 Enchondroma

Enchondromas are located more frequently in the hand than any other part of the body, accounting for 45–65% of cases (Masada et al. 1989). 40% of all enchondromas of the body are located in the phalanges (Fig. 35.1) and 10% in the metacarpals. Carpal enchondromas are rare and account for approximately 2% of hand enchondromas (Takigawa 1971).

Typically, patients present with a pathological fracture following minor trauma. Alternatively, the tumour presents as a slowly enlarging mass or is discovered incidentally on radiographs obtained for other reasons.

Multiple hand enchondromas may be encountered in association with either Ollier's disease or Maffucci's syndrome. Ollier's disease is characterised by multiple enchondromas (Fig. 35.2) whereas the presence of multiple enchondromas in association with soft tissue haemangiomas is termed Maffucci's syndrome (Fig. 35.3). The distribution of lesions tends to be in either a monomelic or hemimelic pattern. Several authors have published an association with enchondromatosis and chondrosarcoma of the hand (Fig. 35.4). Higher rates of malignancy and frequent metastases in Ollier's disease and Maffuci's syndrome have been reported (Liu et al. 1987). There are, to date, only 7 reports in the literature of chondrosarcoma of the hand arising from a pre-existent benign solitary enchondroma, confirmed on histology and radiology. This may relate more to the difficulty of establishing the presence of a pre-existing unequivocally benign lesion when a relatively small calibre bone is involved.

Regarding imaging findings, radiographs show the tumour to be typically located in the meta-diaphyseal region of the tubular bones of the hand. It is classically a well-defined cystic, radiolucent intramedullary lesion containing thin internal trabeculations (Fig. 35.1). Cortical thinning and expansion of the bone are commonly seen. Associated chondroid calcifications are noted less often in enchondromas of the hand that at other skeletal locations. Enchondroma has a distinctive appearance on MR imaging, with multiple lobules of high signal intensity on T2W and STIR sequences. The high signal characteristic is due to the hyaline cartilage content in these lesions. Low signal septae are often seen separating the lobules. Low signal foci corresponding to chondroid matrix may also be apparent. MR imaging is also useful in evaluating the extent of soft tissue tumour in cases where malignant transformation is suspected.

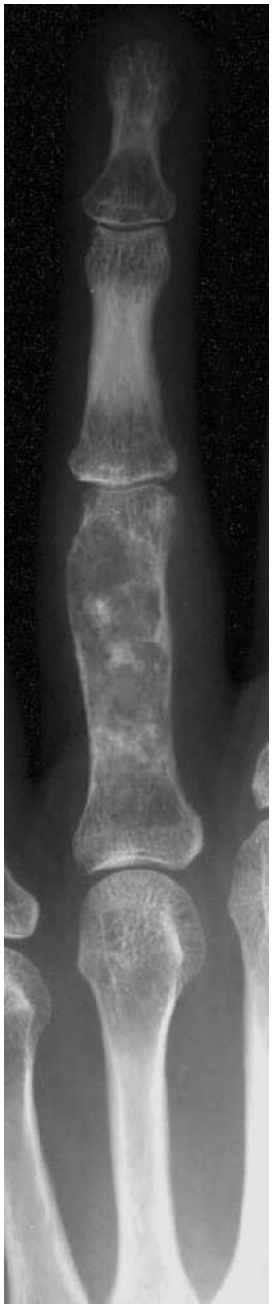

Fig. 35.1. Posteroanterior radiograph demonstrates an enchondroma in the proximal phalanx. Typical well-defined lesion with cystic areas, chondroid calcification, endosteal scalloping and thin internal trabeculation

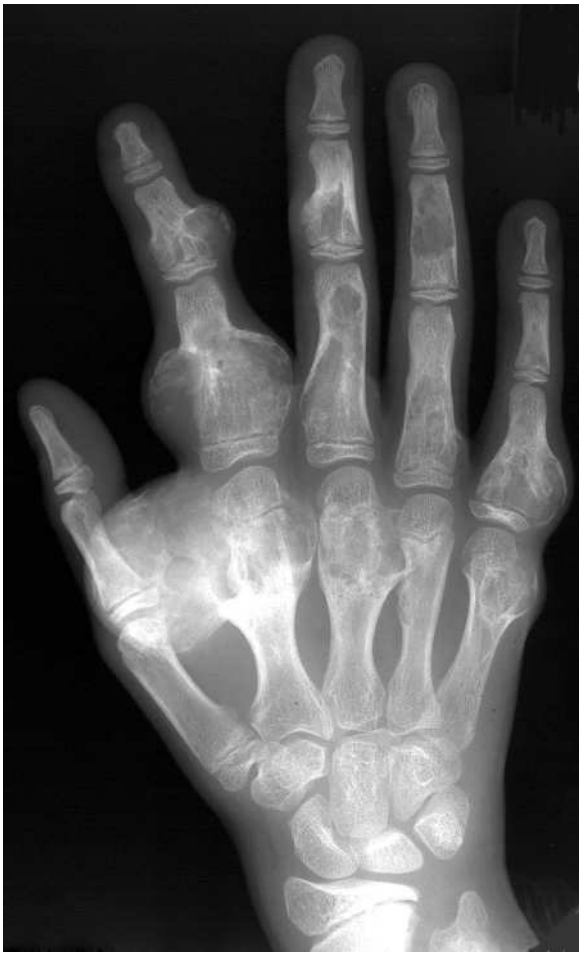

Fig. 35.2. Posteroanterior radiograph of the hand in a patient with Ollier disease. Multiple enchondromas are identified involving the metacarpals and phalanges

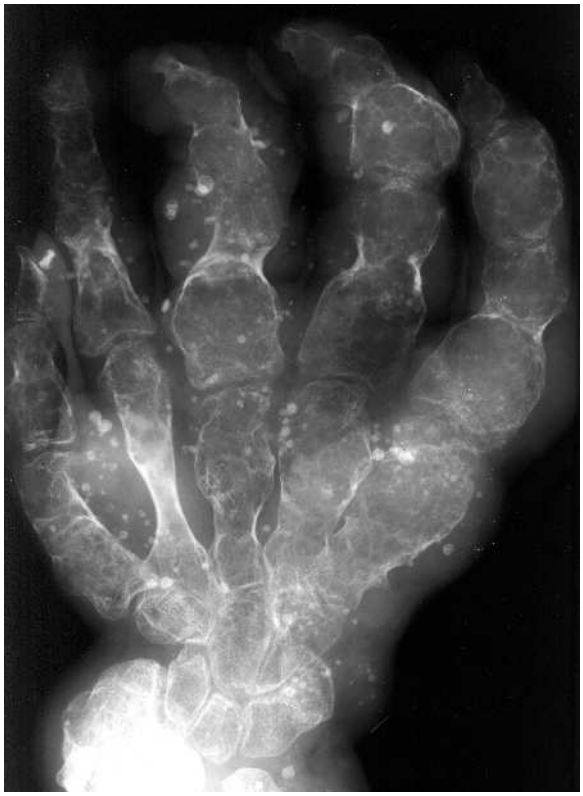

Fig. 35.3. Posteroanterior radiograph of the hand in a patient with Maffucci disease. There are multiple enchondromata with phleboliths in the soft tissue haemangiomas

35.2.2 Giant Cell Tumours of Bone

The distal radius is the third most common site of origin of giant cell tumour of bone (GCTOB), accounting for approximately 10% of cases. Only 2–3% of tumours arise in the bones of the hand (Minguella 1982; Athanasian 2004). A review of 1,228 cases of GCTOB, found almost 1% occurred in the metacarpals and 1% in the phalanges (Averill et al. 1980). Involvement of the carpal bones is very rare, though cases in the scaphoid, capitate, lunate, hamate and trapezium have all been described.

There is a slight female preponderance but the age range for GCTOB of the hand is similar to that at other locations (Sanjay et al. 1996; Athanasian et al. 1997). Earlier and higher rates of recurrence in GCTOB of the hand, compared to the tumour at other sites, have been reported (Patel et al. 1987). Of a series of 21 cases, 5% developed pulmonary metastases (Averill et al. 1980). Tumours of the distal radius have been implicated in the literature as the most common primary site in patients with pulmonary metastases (Athanasian et al. 1997).

Giant-cell reparative granuloma (GCRG) is a reactive process that may involve the small bones of the hand and it has been suggested that this lesion may be morphologically related or may constitute the same clinical entity as GCTOB (Gouin 2003). Others have however expressed a differing opinion (Murphey et al. 2001). These tumours may have an expansile, lytic ra-

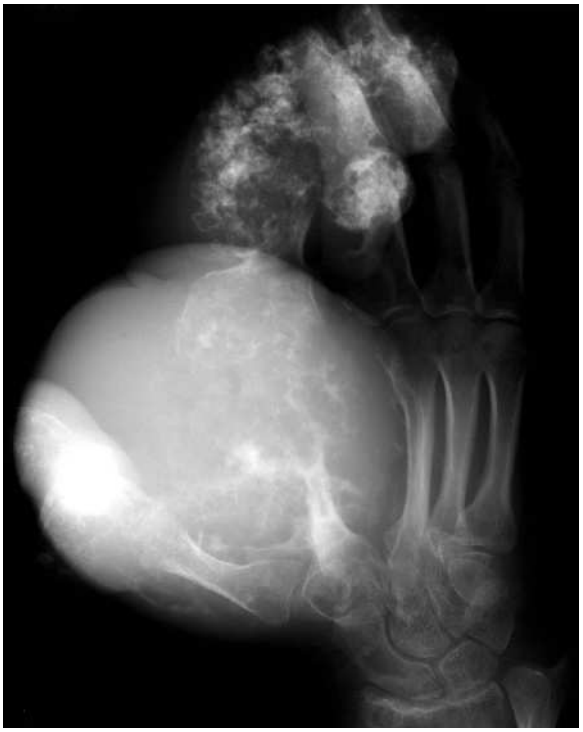

Fig. 35.4. Posteroanterior oblique radiograph of the hand demonstrates a chondrosarcoma in a patient with Ollier disease. There is destruction of the index finger metacarpal with an associated soft tissue mass

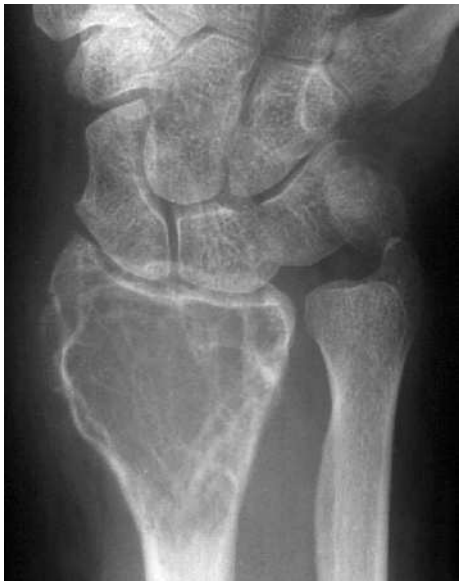

a

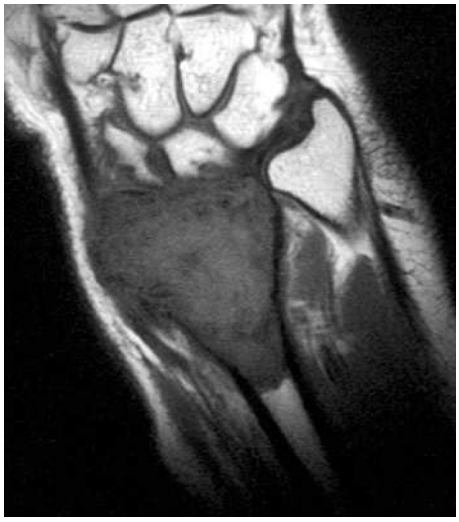

b

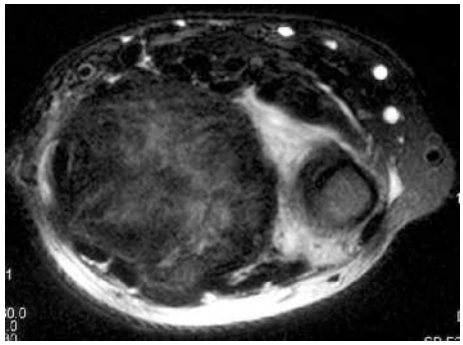

c

Fig. 35.5. **a** Posteroanterior radiograph demonstrates a typical giant cell tumour of the distal radius. A subarticular lucent lesion with internal trabeculation is identified. **b** Coronal T1-weighted MR image shows the intraosseous extent of the lesion with some internal low signal consistent with chronic haemosiderin deposition. **c** Axial fat-suppressed T2-weighted MR image shows the degree of expansion of the radius

diographic appearance and may demonstrate cortical destruction. GCRG most commonly affects the metaphysis of the phalanges, followed by the metacarpals and carpal bones. Pathological fracture and periosteal reaction are rarely seen.

Regarding imaging findings, lesions in the distal radius demonstrate an eccentric, expansile, lytic lesion located in a subarticular position involving the epiphysis and metaphysis as is typically seen elsewhere in the skeleton (Fig. 35.5a). The metacarpals and phalanges effectively represent the equivalent of a long bone in the hand. The tumour occurs in a more central location in the bones of the hand probably due to the limited volume of bone (Fig. 35.6). A narrow zone of transition is seen at the metaphyseal margin of the lesion and there is typically no matrix mineralization. Internal trabeculation is common but the pattern may vary from fine striations to coarse trabeculation. Periosteal reaction is unusual unless there is a complicating fracture (James and Davies 2005).

Technetium 99m bone scintigraphy may demonstrate a classic "doughnut" configuration with avid uptake at the periphery of the tumour and a relatively photopenic centre. The routine use of bone scintigraphy has been advocated by some authors where hand lesions are identified. The risk of multicentric involvement in hand lesions is estimated between 7–18% compared with <1% for tumours elsewhere (James and Davies 2005).

Lesions in the hand and wrist show similar MR imaging characteristics to GCTOB elsewhere in the body. MRI defines the intra- and extra-osseous extent of the tumour. Low signal intensity on all sequences can be seen which is indicative of chronic haemosiderin deposition in GCTOB (Fig. 35.5b, 35.5c; Aoki et al. 1996). Fluid-fluid levels may be demonstrated within the tumour mass indicating the presence of secondary aneurysmal bone cyst (ABC) formation.

35.2.3 Aneurysmal Bone Cysts

Aneurysmal bone cysts (ABC) of the hand are rare. In a series of 516 ABCs, only 17 lesions occurred in the hand (Fuhr and Hendron 1979). Involvement is most commonly seen in the metacarpals (52%) followed by the phalanges (36%) and carpal bones (4%; Platt and Klugman 1995). Trauma has been implicated in association with almost half of the published cases of hand ABC however many authors suggest this is coincidental and has simply drawn attention to a pre-existing lesion. Though locally aggressive and destructive, ABCs are not known to have metastatic potential.

Regarding imaging findings, radiographs of the hand demonstrate a central, expansile, lytic lesion which causes cortical thinning (Fig. 35.7). Subperiosteal ABCs

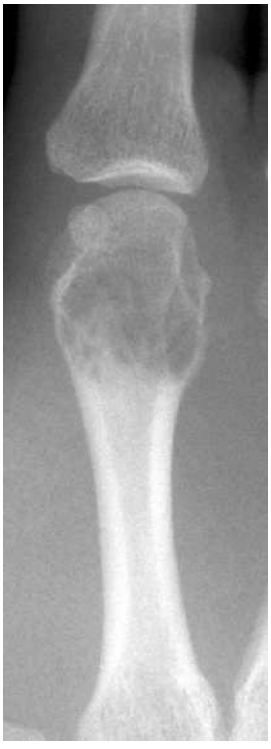

Fig. 35.6. Posteroanterior radiograph demonstrates a giant cell tumour in the distal metacarpal. A centrally located lytic lesion with internal trabeculation is identified

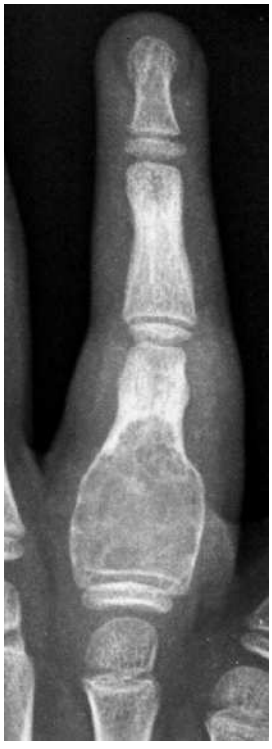

Fig. 35.7. Posteroanterior radiograph shows an aneurysmal bone cyst in the proximal phalanx. There is a lytic lesion with marked expansion and cortical thinning

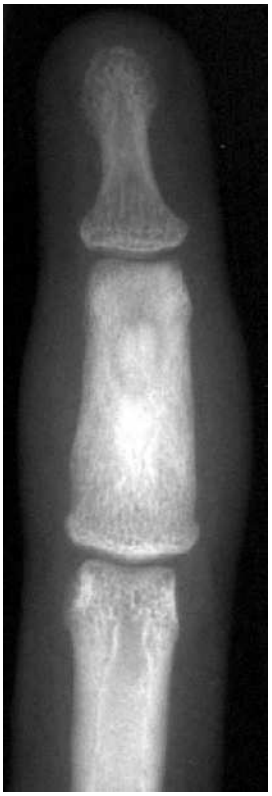

Fig. 35.8. Posteroanterior radiograph of the finger shows an area of sclerosis in the middle phalanx with a central nidus indicative of an osteoid osteoma

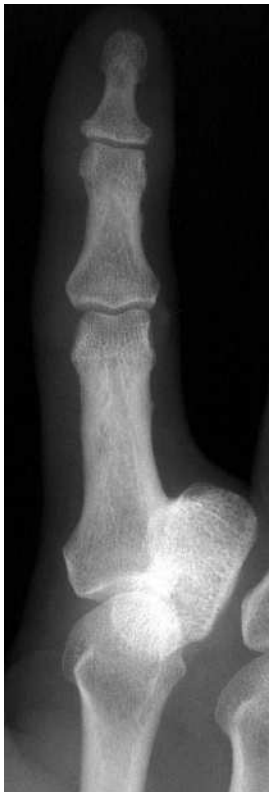

Fig. 35.9. Posteroanterior radiograph demonstrates a solitary osteochondroma arising from the base of the proximal phalanx

are eccentrically located but have rarely been reported in the hand. ABCs are normally epiphyseal or metaphyseal in location. A sclerotic margin may be present. Matrix trabeculations are sometimes observed and may be mixed or lytic. Pathological cortical fractures are associated with a periosteal reaction. When the lesion presents in the distal phalanx, significant bone destruction may occur. MR and CT imaging, as in other skeletal locations, may demonstrate fluid-fluid levels which are suggestive but not diagnostic of ABC.

35.2.4 Osteoid Osteoma

Approximately 10% of cases of osteoid osteoma involve the hand and wrist: 6% the phalanges, 2% the metacarpals and 2% the carpal bones (Jackson et al. 1977). Based on reports in the literature, painless osteoid osteoma appears to occur in the digits more frequently than in any other skeletal location (Basu et al. 1999; Lawrie et al. 1970; Rex et al. 1997; Wiss et al. 1983).

Osteoid osteomas may arise centrally in the medulla, in the cortex or in a subperiosteal location. As with other skeletal sites, the cortex is the most common location for osteoid osteomas of the hand and wrist. Subperiosteal lesions are extremely rare in the hand, with only a few reported cases (Crosby and Murphy 1988; Kayser et al. 1998; Shankman et al. 1997).

Regarding imaging findings, the typical radiographic appearance is that of a small, radiolucent lesion or nidus surrounded by an area of bone sclerosis (Fig. 35.8). Lesions noted in the subperiosteum have atypical radiographic findings. In a series of 18 patients with osteoid osteoma of the hand and wrist, only two had characteristic appearances on plain film (Marcuzzi et al. 2002). Initial radiographs in almost all of the patients were normal, with bony abnormality becoming visible from 6 to up to 25 months.

As with other skeletal locations, bone scintigraphy of osteoid osteoma of the hand and wrist shows a well-defined focal area of increased activity during all three phases of a technetium-99 MDP scan. Findings can be non-specific with diffuse uptake of radionuclide in the area of the lesion.

In cases where radiographs and bone scintigraphy are equivocal, CT should be obtained. This characteristically shows a lytic lesion with a central granular opacity surrounded by a sclerotic margin.

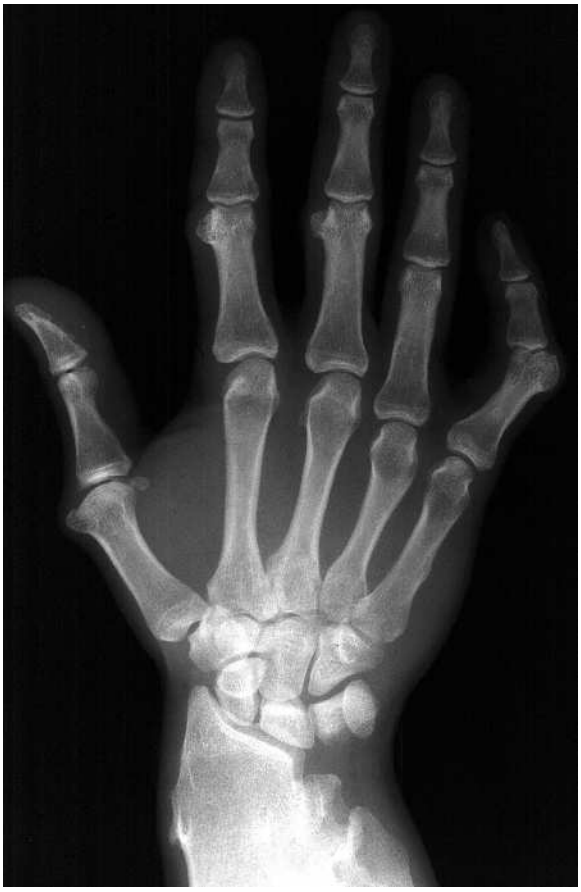

Fig. 35.10. Posteroanterior radiograph demonstrates multiple osteochondromas arising in the phalanges in a patient with hereditary multiple exostoses (HME) The lesion in the little finger proximal phalanx has caused an alignment abnormality at the level of the proximal interphalangeal joint. There is an associated Madelung deformity of the wrist

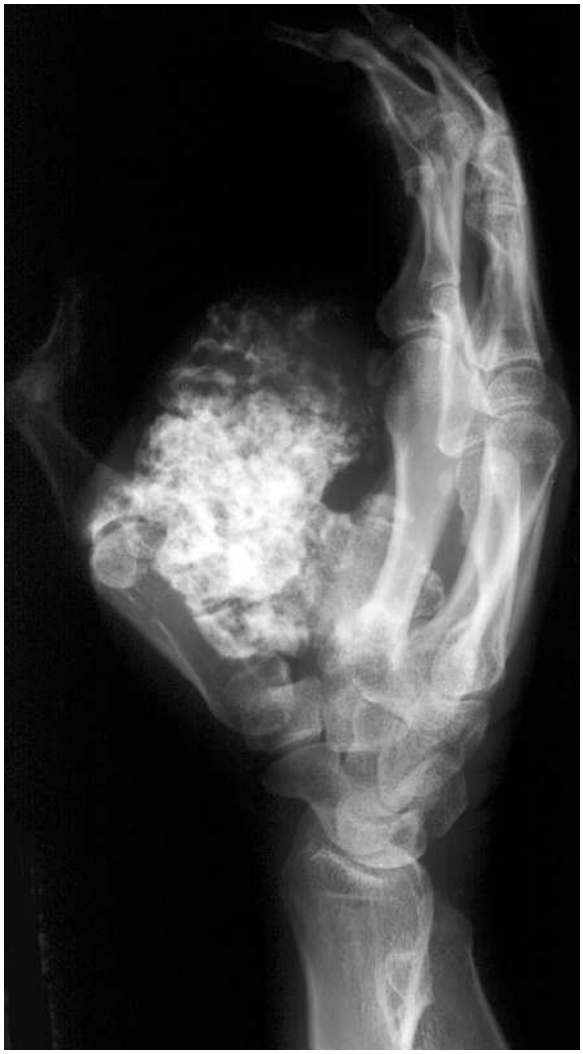

Fig. 35.11. a Lateral radiograph demonstrates malignant transformation in a patient with hereditary multiple exostoses. A large peripheral chondrosarcoma is identified in the web space between the thumb and index fingers. **b** *see next page*

35.2.5 Osteochondroma

Osteochondromas are the most common benign bone tumour; 90% are solitary and 10% are found in patients with hereditary multiple exostoses (HME). Only 4% of solitary osteochondromas involve the hands (Unni 1996). They are usually asymptomatic in the hand unless they lie in a position that interferes with function. Trigger finger and a mimic of mallet finger have been described (Al-Harthy and Rayan 2003; Murase et al. 2002). Carpal osteochondromas are rare. To our knowledge, only one chondrosarcoma of the hand developing from a solitary osteochondroma, has been reported in the literature (Cash and Habermann 1988).

The overall incidence of hand lesions is 79% in patients with HME (Solomon 1963). In this condition, the ulnar metacarpals and proximal phalanges are most commonly affected, with the thumb and distal phalanges less commonly involved. Multiple lesions are typical in these patients with an average of 11.6 exostoses per hand (Cates and Burgess 1991). They affect the forearm (40–60%) more commonly than the upper arm. It has been concluded that an increasing distal radius involvement in HME is associated with a greater severity of the disease process overall (Taniguchi 1995).

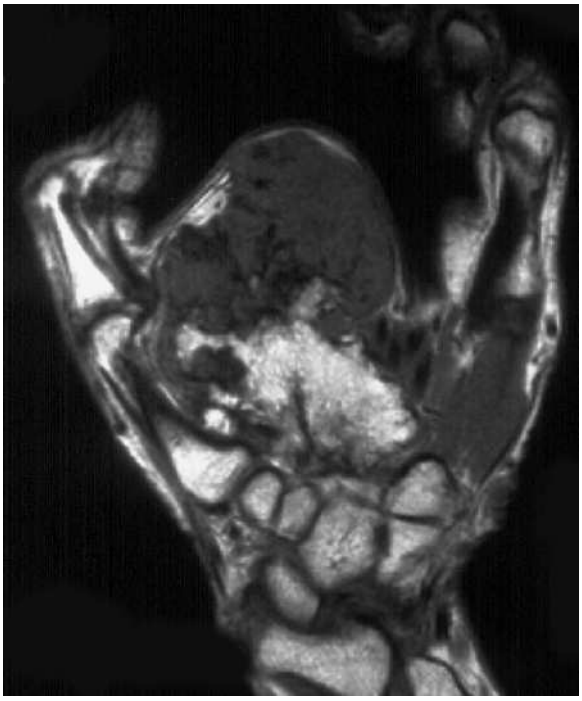

Fig. 35.11. (*continued*) **b** Coronal T1-weighted MR image shows the thickened cartilage cap

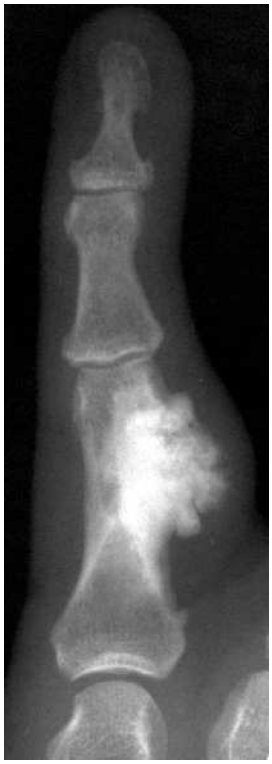

Fig. 35.12. Posteroanterior radiograph demonstrates a well-defined area of bony protuberance arising from the cortex of the proximal phalanx consistent with bizarre parosteal osteochondromatous proliferation

As with solitary osteochondromas, more peripherally located tumours are less likely to undergo malignant transformation in patients with HME. A chondrosarcoma of the hand arising in a patient with HME has twice been reported in the literature (Ostlere et al. 1991; Saunders et al. 1997).

Regarding imaging findings, radiographically osteochondromas of the hand are typically sessile lesions which show continuity with the underlying medullary cavity of the bone of origin (Fig. 35.9). Most osteochondromas related to HME are juxta-epiphyseal in location, with the non-epiphyseal end of bone being the next most common and the diaphysis the least common location (Fig. 35.10). Radiographs aid in demonstrating complications of osteochondromas such as fracture, growth disturbances, osseous deformity or malignant change (Fig. 35.11a). In children, osteochondroma may be extremely small and difficult to identify as a cause of finger deformity (Moore et al. 1983).

MR imaging provides precise information about thickness of the cartilage cap which has high signal intensity on T2 spin echo sequences and is important when assessing potential malignant transformation (Figure 35.11b). It also provides information regarding complications such as reactive bursa formation, neural impingement and vascular compromise.

35.3 Bone-Forming Surface Lesions

This group of conditions has been united under the collective term 'Proliferative periosteal processes of the phalanges' (Yuen et al. 1992). They are thought to result from subperiosteal haemorrhage. If this remains contained within periosteum, it can lead to Florid Reactive Periostitis. The condition is characterised radiographically by a lamellated, mature periosteal reaction with slight periosteal elevation and juxtacortical calcification in the adjacent soft tissues. It is most commonly seen in the proximal phalanx and typically affects patients in the second and third decades (James and Davies 2006). Once this matures, the periostitis becomes incorporated into the cortex and remodelling may lead to a broad-based cancellous protruberance known as bizzare parosteal osteochondromatous proliferation (BPOP).

A well marginated, calcified or osseous mass is seen to arise from cortex on radiographs (Fig. 35.12). Its lack of continuity with the medulla, which can be clearly demonstrated on CT, differentiates this lesion from an osteochondroma. It most commonly arises in the proximal and middle phalanges and typically presents in the third and fourth decades (Nora et al. 1983).

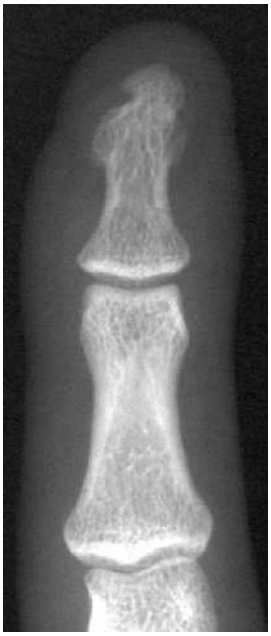

Fig. 35.13. Posteroanterior radiograph of the finger demonstrates a typical subungual exostosis of the distal phalanx

Other conditions in this group of disorders include Periostitis Ossificans, a juxta-cortical form of myositis ossificans; Turret Exostosis, thought to represent ossifcation of a subperiosteal haematoma and subungual exostosis (Fig. 35.13; James and Davies 2006).

35.4 Miscellanous Lesions

Chondroblastoma of the hand is extremely rare. Imaging features are similar to that of enchondroma except for their epiphyseal location. It may present as a large area of bone marrow and soft tissue oedema which is well depicted on MRI (Garcia et al. 2001). Osteoblastoma of the hand is also very rare but has been described in carpal, metacarpal and phalangeal bones (Wilner 1982).

Fibrous dysplasia of the hand and wrist is very uncommon. In a series of 225 cases of monostotic fibrous dysplasia, only 3 hand cases were reported (Schajowicz 1981). Of the cases described in the English speaking literature, the majority have been located in the metacarpal bone and have been of the monostotic form (Amillo et al. 1996; Gropper et al. 1985; Hayter and Becton 1984). An expansile, lytic lesion involving the shaft with a sclerotic border, trabeculations and a partially calcified matrix is described on plain radiography in one of these cases (Fig. 35.14; Gropper et al. 1985). Periosteal reaction on plain radiograph and soft tissue extension as delineated on MRI has been reported (Amillo et al. 1996). Pathological fracture through an

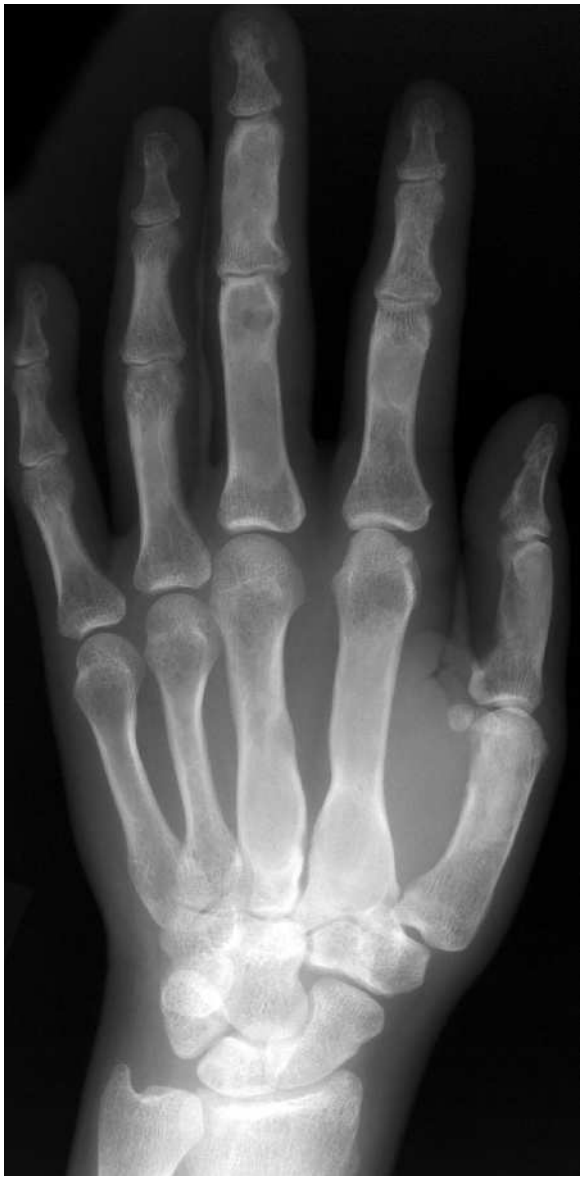

Fig. 35.14. Posteroanterior radiograph of the hand in a patient with polyostotic fibrous dysplasia. There are multiple well-defined ground-glass opacities involving the metacarpals and phalanges

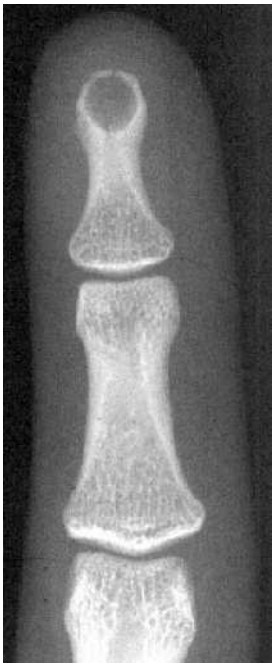

Fig. 35.15. Posteroanterior radiograph of the finger shows a well-defined lucency in the distal phalanx with a sclerotic margin consistent with an epidermoid inclusion cyst

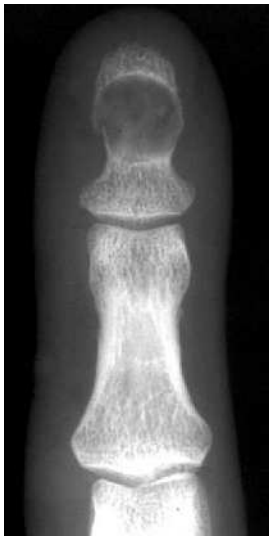

Fig. 35.16. Posteroanterior radiograph of the finger shows a well-defined lucency in the distal phalanx with a subtle sclerotic margin. There has been a pathological fracture with a cortical breach in this glomus tumour

involved metacarpal was the presenting feature in another case (Hayter et al. 1984).

Intraosseous epidermal cysts, or epidermal inclusion cysts, are squamous epithelial-lined benign cysts within bone. Peak incidence is within the 25–50 age group with a male to female ratio of 3:1 (Fisher et al. 1958). The most common site is the terminal phalanx of the left middle finger (Fig. 35.15; Fisher et al. 1958). On radiographs, they usually appear as a well-defined, unilocular, osteolytic lesion with a sclerotic margin and may exhibit spotty calcifications (Musharrafieh et al. 2002; Patel et al. 2006). Enchondroma is the major differential diagnosis but, unlike intraosseous epidermal cysts, it is rarely symptomatic in the absence of a fracture.

Glomus tumours are benign hamartomas. They arise from the normal glomus apparatus within subcutaneous tissue. The tumours mainly occur in women and are most commonly located in the distal phalanx (Fig. 35.16), usually in a subungual location (Dahlin et al. 2005). Intraosseous glomus tumours of the hand are extremely rare. Only ten had been reported in the literature by 1981 (Chan 1981). To our knowledge, only one further case has subsequently been described (Johnson et al. 1993). MRI has proved to be a valuable method of imaging glomus tumours (Theumann et al. 2002; Opdenakker et al. 1999). Most glomus tumours demonstrate high signal on spin echo T2-weighted sequences and avid enhancement post-gadolinium injection (Theumann et al. 2002). Cases have been reported where a tumour was present despite a negative MRI. On this basis it has been suggested that, in the correct clinical context, surgical exploration should be considered even if MRI findings do not support the diagnosis (Dahlin et al. 2005).

35.5 Malignant Tumours

35.5.1 Chondrosarcoma

Chondrosarcoma is the most common primary malignant tumour of the hand, yet when compared to it's occurrence at other skeletal locations, it is extremely rare. Of 635 chondrosarcomas reviewed, only 1.5% were recorded as arising in the hand and wrist (Unni 1996).

Chondrosarcoma of the hand tends to affect an older age group than at other sites with an average age of 61 (Saunders et al. 1997). They are more common in the proximal phalanx than the metacarpals (Fig. 35.17a, 35.17b). Three cases of chondrosarcoma arising in the carpal bones have been described. Chondrosarcomas

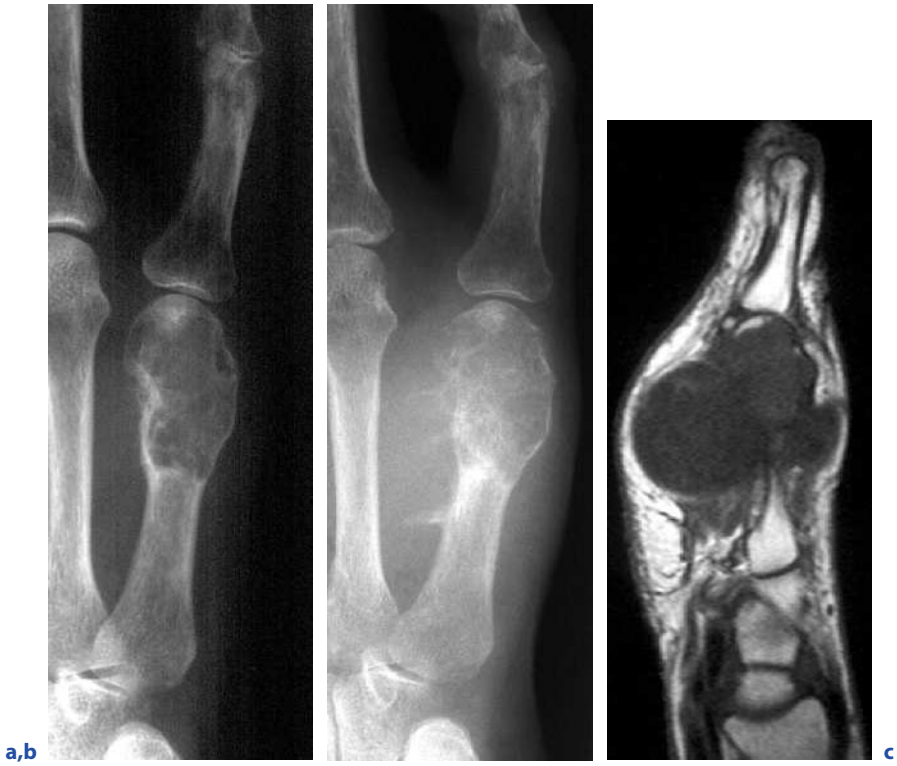

Fig. 35.17. **a** Posteroanterior radiograph of the finger shows a mildly expansile lesion in the distal aspect of the metacarpal. **b** Posteroanterior radiograph of the finger obtained 18 months later shows progression of the lesion. There is a spiculated periosteal reaction with an associated soft tissue mass in keeping with a chondrosarcoma. **c** Sagittal T1-weighted MR image and **d** axial fat-saturated T2-weighted MR image demonstrates the extent of the intraosseous and extraosseous components

arising from pre-existing solitary enchondromas or osteochondromas or in conditions of enchondromatosis (see Fig. 35.4) or multiple hereditary exostoses (see Fig. 35.11) are well documented in the literature. These "secondary" chondrosarcomas account for 27% of chondrosarcomas reported in the hand (Saunders et al. 1997). In all locations, 15–28% are secondary (Huvos and Marcove 1987; Salib 1967). Metastases occurred in only 1.8% of cases in a meta-analysis of 112 phalangeal chondrosarcomas (Bovee et al. 1999). The metastatic potential of chondrosarcoma in the hand is low unless dedifferentiated.

Regarding imaging findings, the tumours tend to originate near the site of the epiphyseal growth plate of the bone: proximally in the phalanx and distally in the metacarpals (Palimeri 1984; Roberts and Price 1977). They tend to arise from the medulla but rarely originate from periosteum.

Typical features on radiographs include cortical destruction, a wide zone of transition, matrix calcification, thickening and irregularity of any cartilaginous cap, pathological fracture and soft tissue extension (Fig. 35.17b). Extension of tumour across the joint in the hand has also been described (Patil et al. 2003). The appearance of surface chondrosarcomas is more variable and it is sometimes difficult to differentiate between a periosteal chondroma (Fig. 35.18) and juxtacortical chondrosarcoma (James and Davies 2005).

Soft tissue involvement was present in 77% of a series of 18 chondrosarcomas of the hand (Palimeri 1984). MRI is the best modality at detecting and estimating the extent of soft tissue component.

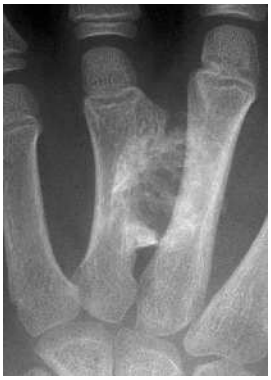

Fig. 35.18. Posteroanterior radiograph of the hand demonstrates a lesion arising from the metacarpal in keeping with a periosteal chondroma

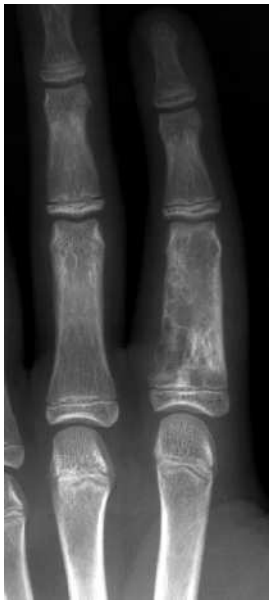

Fig. 35.19. Posteroanterior radiograph of the finger in a Ewing sarcoma shows an ill-defined area of lysis with mild expansion of the proximal phalanx

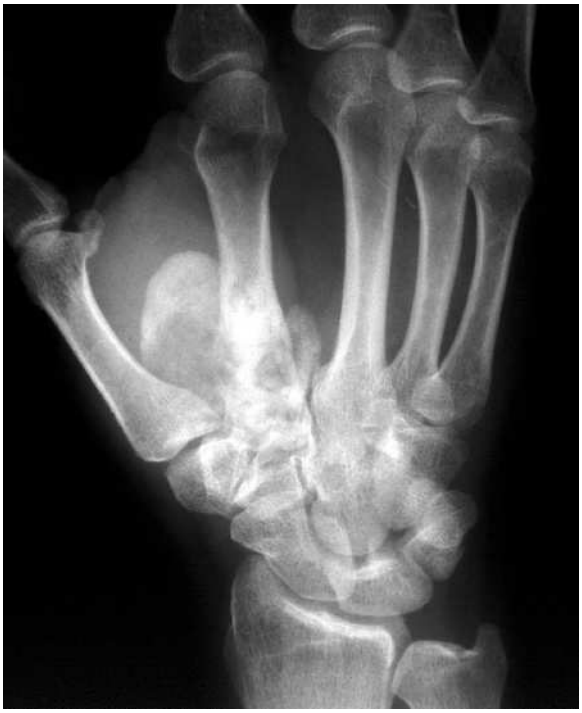

Fig. 35.20. Posteroanterior view of the hand demonstrates a densely ossified mass arising from the base of the index finger with an associate soft tissue mass in an osteosarcoma

35.5.2 Ewing's Sarcoma

Ewing's sarcoma (ES) arising in the hand accounts for 1% of all ES of bone (Dahlin and Unni 1986). The metacarpals are more commonly affected (Fig. 35.19) with occurrence in the phalanges relatively rare (Lacey et al. 1987). In a literature review of ES arising in the phalanges, the proximal phalanx was the most commonly affected bone (Yamaguchi et al. 1997). To our knowledge, the tumour has never been described arising within a carpal bone. Involvement in the radius and ulna is more common, respectively 2% and 1% (Wilner 1982).

Ewing's sarcoma of the hand occurs most commonly in boys and young men. The prognosis is better than for ES arising at other sites. This is thought to be due to less soft tissue in the extremities allowing for comparatively early presentation, diagnosis and excision with a wide margin (Yamaguchi et al. 1997).

Regarding imaging findings, as with ES at other locations, the characteristic permeative, lytic lesion with aggressive periosteal reaction and cortical destruction is seen in the majority of cases. The tumour tends to occur in the metadiaphyseal region of the short tubular bones (Baraga et al. 2001). A review of 43 cases of ES in the small bones of the hands and feet revealed that ES at these sites is less likely to be purely lytic and more

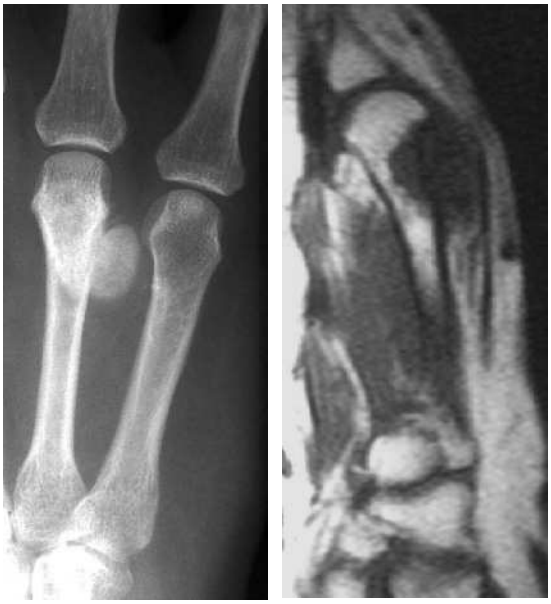

Fig. 35.21. **a** Posteroanterior radiograph of the finger demonstrates a well-defined densely calcified mass adjacent to the metacarpal in this parosteal osteosarcoma. **b** Coronal T1-weighted MR image demonstrates intraosseous extension into the metacarpal

commonly blastic or mixed than at other skeletal locations (Baraga et al. 2001). The presence of bony reaction and associated soft tissue mass often makes differentiation from osteomyelitis difficult. A juxtacortical soft tissue mass is present in 89% of cases and can be detected by MR imaging (Coombs 1993).

35.5.3 Osteosarcoma

Involvement of the small bones of the hand is extremely rare accounting for only 0.1 to 0.2% of osteosarcomas (Honoki et al. 2001). Many cases in the short tubular bones are secondary to underlying risk factors including previous radiation therapy, Paget's disease, trauma or multi-centric metastatic disease.

Osteosarcoma of the hand typically occurs in an older population than other skeletal sites with an average age of 45 years and the prognosis is generally better (Okada et al. 1993). The long duration of symptoms, long interval before local recurrence and excellent response to treatment suggest that lesions in this location are less aggressive (Okada et al. 1993).

The tumour arises in the metacarpals (Fig. 35.20) and phalanges but has not been reported in the carpal bones. There appears to be a greater propensity to arise from the surface of the bone occurring in 30% of hand lesions compared with 6.8% elsewhere in the skeleton (Dahlin and Unni 1986). The majority of these surface tumours are parosteal with only two reported periosteal osteosarcomas of the hand (Okada et al. 1993; Muir et al. 2008).

Regarding imaging findings, the radiographic findings are similar to the appearance of the tumour at other sites with matrix mineralisation, bone destruction and florid periosteal reaction. The tumour is generally intramedullary with extension into the soft tissues. Surface osteosarcomas however often appear as a densely calcified mass adjacent to a metacarpal or phalanx (Fig. 35.21a). They may be connected to bone by a stalk which can be demonstrated on CT. MRI better assesses the soft tissue involvement and degree of intramedullary extension (Fig. 35.21b). The lesion may be isointense on T1-weighted imaging and of high-signal intensity on T2-weighted imaging (Honoki et al. 2001).

35.5.4 Metastasis

Metastasis to hand is rare and accounts for approximately 0.1% of all metastatic lesions (Ghert et al. 2001). In a series of approximately 75,000 patients diagnosed with a primary malignancy, 5 patients with metastasis to the bones of the hand and wrist were identified (Amadio

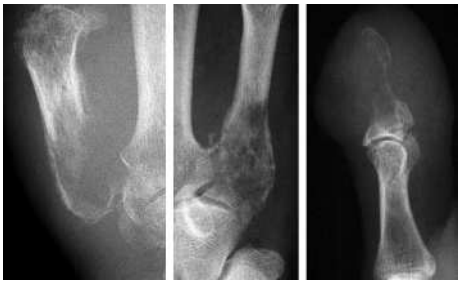

Fig. 35.22. Lateral radiographs in three different patients with metastases from bronchial carcinoma shows aggressive lytic lesions with cortical destruction and soft tissue extension

and Lombadri 1987). Although rare, it is important to be aware of the possibility of an acrometastasis as it can mimic other skeletal lesions such as infection or inflammatory arthritis both clinically and radiologically. Any bone in the hand and wrist can be involved, though the most commonly reported site is the terminal phalanx (Healy et al. 1986; Libson et al. 1987; Kerin 1983). No one phalanx is preferentially involved (Wu and Guise 1978). The carpus is less commonly affected, being involved in only 10% of cases in two large trials (Healy et al. 1986; Libson et al. 1987; Kerin 1983). The majority of patients are in their fifth decade or older.

Of skeletal wrist and hand metastases, 40–50% are from primary bronchial carcinoma (Fig. 35.22; Kerin 1983). This is thought to be due to the fact that primary tumours in the lung can shed cells directly into the systemic arterial circulation, whereas potential secondaries from other sites pass through the capillary bed of the lung or liver first. WOLFF and co-workers (1966) reported metastases from the breast accounting for 25% of bone secondaries in the hand (cited by Amadio and Lombadri 1987). Renal cell carcinoma accounts for 10% of lesions (Ghert et al. 2001). Metastases from the prostate, bladder, uterus and malignant melanoma have all been reported (Bouvier et al. 1971; Cerando 1951; Merek and Vortel 1949; Gelberman 1978). The prognosis for these patients is extremely poor with, in one series, 50% of patients dead within 6 months (Amadio and Lombadri 1987).

Regarding imaging findings, radiographically metastases of the hand appear most frequently as non-specific lytic, aggressive lesions which may be misdiagnosed as infection or an inflammatory arthritis particularly if there is no history of a primary tumour. Sclerotic forms have been described and are typical of metastatic osteosarcoma, but have also been seen with prostate and breast metastases (Abrahams 1995). Periosteal reaction is uncommon (Healy et al. 1986; Libson et al. 1987; Wu et al. 1978; Chung 1983; Kerin et al. 1958; Mulvey 1964). A soft tissue component is frequent but actual joint involvement is rare (Healey et al. 1986; Libson et al. 1987; Kerin et al. 1958; Mulvey 1964).

35.6 Conclusion

Bone tumours of the hand and wrist are infrequently encountered in general clinical practice. Clinical examination and radiography are often sufficient to allow an accurate diagnosis in the majority of cases at this site. Knowledge of their imaging characteristics is important in diagnosis.

The superficial location leads to earlier presentation, allowing expeditious diagnosis and treatment of malignant neoplasms. This often results in a better clinical outcome when compared to the same tumours at different skeletal sites. Though rare, it is important to keep the possibility of a malignant neoplasm in mind when encountered with an aggressive bone lesion in the hand or wrist.

References

Abrahams (1995) Occult malignancy presenting as metastatic disease to the hand and wrist. Skeletal Radiol 24:135–137

Al-Harthy A, Rayan GM (2003) Phalangeal Osteochondroma: a cause of childhood trigger finger. Br J Plast Surg, 56(2):161–163

Amadio P, Lombadri R (1987) Metastatic tumours of the hand. J Hand Surg 12A:311–316

Amillo S, Schweitzer D, San Julian M (1996) Monostotic fibrous dysplasia in the hand: a case report. J hand Surg Am, 21(2):290–292

Aoki J, Tanikawa H, Ishii K et al. (1996) MR findings indicative of haemosiderin in giant-cell tumor of bone: frequency, cause, and diagnostic significance. Am J Roentgenol 166:145–148

Athanasian EA (2004) Aneurysmal bone cyst and giant cell tumor of bone of the hand and distal radius. Hand Clin 20:269–281

Athanasian EA, Wold LE, Amadio PC et al. (1997) Giant cell tumors of the bones of the hands. J Hand Surg 22A:91–98

Averill RM, Smith RJ, Campbell CJ (1980) Giant cell tumors of the bones of the hand. J Hand Surg, 5A:39–49

Baraga JJ, Amrami KK, Swee RG et al. (2001) Radiographic features of Ewing's sarcoma of the bones of the hands and feet. Skeletal Radiol 30:121–126

Basu S, Basu P, Dowell JK (1999) Painless osteoid osteoma in a metacarpal. J Hand Surg Br 24(1):133–134
Bouvier M, Lejeune E, Queneau T et al. (1971) Les localisations du cancer secondaire des os. Rheumatologie 23:353
Bovee JVMG, Van der Heul RO, Taminiau AHM et al. (1999) Chondrosarcoma of the phalanx: a locally aggressive lesion with minimum metastatic potential. A report of 35 cases and a review of the literature. Cancer 86:1724–1732
Cash S, Habermann E (1988) Chondrosarcoma of the small bones of the hand: case report and review of the literature. Orthop Rev 17:365–369
Cates HE, Burgess RC (1991) Incidence of brachydactyly and hand exostosis in hereditary multiple exostosis. J Hand Surg Am 16(1):127–132
Cerando M (1951) Su una rara metasi falangea di carcinoma dell descica. Urologia 18:256
Chan CW (1981) Intraosseous glomus tumour: case report. J Hand Surg Am 6:368–369
Chung TS (1983) Metastatic malignancy to the bones of the hand. J Surg Oncol 24:99
Coombs RJ, Zeiss J, Paley KJ et al. (1993) Case report 802. Ewing's tumour of the proximal phalanx of the third finger with radiographic progression documented over a 6-year period. Skeletal Radiol 22:460–463
Crosby LA, Murphy RP (1988) Subperiosteal osteoid osteoma of the distal phalanx of the thumb. J Hand Surg Am 13(6):923–925
Dahlin DC (1995) Bone tumours, 3rd edn. General aspects and data on 6221 cases. Thomas, Springfield, Illinois
Dahlin DC, Unni KK (1986) Bone tumours, 3rd edn. Thomas, Springfield, Illinois
Dahlin LB, Besjakov J, Veress B (2005) A glomus tumor: classic signs without magnetic resonance imaging finding. Scand J Plast Reconstr Surg Hand Surg 39:123–125
Fisher R, Ruhn J, Skerrett P (1958) Epidermal cyst in bone. Cancer 11(3):643–648
Fuhr SE, Hendron JH (1979) Aneurysmal bone cyst involving the hand. A review and report of two cases. J Hand Surg 4:152–159
Garcia J, Bianchi S (2001) Diagnostic imaging of tumors of the hand and wrist. Eur Radiol 11:1470–1482
Ghert MA, Harrelson JM, Scully SP (2001) Solitary renal cell carcinoma metastasis to the hand: the need for wide excision or amputation. J Hand Surg 26A:156–150
Gouin F, Grimaud E, Redini F et al. (2003) Metatarsal giant cell tumor and giant cell reparative granuloma are similar entities. Clin Orthop 416:278–284
Gropper PT, Mah JY, Gelfant BM et al. (1985) Monostotic fibrous dysplasia of the hand. J Hand Surg Br 10(3):404–406
Hayter RG, Becton JL (1984) Fibrous dysplasia of a metacarpal. J Hand Surg Am 9(4):587–589
Healey JH, Turnbull ADM, Miedema B et al. (1986) Acrometastases. J Bone Joint Surg Am 68:743
Honoki K, Miyauchi Y, Yajima H et al. (2001) Primary osteogenic sarcoma of a finger proximal phalanx: a case report and literature review. J Hand Surg 26 A:1151–1156
Huvos A, Marcove R (1987) Chondrosarcoma in the young: a clinicopathologic analysis of 79 patients younger than 21 years of age. Am J Surg Pathol 11:930–942
Jackson RP, Reckling FW, Mantz FA (1977) Osteoid osteoma and osteoblastoma. Similar histologic lesions with different natural histories. Clin Orthop Relat Res 128:303–311
James SLJ, Davies AM (2005) Giant-cell tumours of the hand and wrist: a review of imaging findings and differential diagnoses. Eur Radiol 15:1855–1866
James SLJ, Davies AM (2006) Surface lesions of the bones of the hands: a pictorial review. Eur Radiol 16(1):108–123
Johnson DL, Kuschner, SH Lane CS (1993) Intraosseous glomus tumour of the phalanx. A Case report. J Hand Surg 18A:1026–1028
Kayser F, Resnick D, Haghighi P et al. (1998) Evidence of the subperiosteal origin of osteoid osteomas in the tubular bones: analysis by CT and MR imaging. Am J Roentgenol 170(3):609–614
Kerin R (1958) Metastatic tumours of the hand. J Bone joint Surg Am 40:263–277
Kerin R (1983) Metastatic tumors of the hand. J Bone Joint Surg Am 65:1331
Lacey SH, Danish EH, Thompson GH et al. (1987) Ewing sarcoma of the proximal phalanx of a finger. J. Bone Joint Surg Am 69:931–934
Lawrie TR, Alterman K, Sinclair AM (1970) Painless osteoid osteoma. A report of two cases. J Bone Joint Surg Am 52 (7):1357–1363
Libson E, Bloom R, Husband JE et al. (1987) Metastatic tumors of the bones of the hands and foot. Skeletal Radiol 16:387
Liu J, Hudkins P, Swee R et al. (1987) Bone sarcoma associated with Ollier's disease. Cancer 59:1376–1385
Marcuzzi A, Acciaro AL, Landi A (2002) Osteoid osteoma of the hand and wrist. J Hand Surg Br 27(5):440–443
Masada K, Fugiwara K, Yoshikawa H et al. (1989) Chondroma of the scaphoid. J Bone Joint Surg 71B:705
Merek S, Vortel V (1949) Metastases to thumbs 13 years after hysterectomy for cancer of the corpus uteri. Rohzl Chir 28:272
Minguella J (1982) Giant cell tumor of the metacarpal in a child of unusual age and site. The Hand 14:93–93
Moore JR, Cutis RM, Wiglis EPS (1983) Osteocartilaginous lesions of the digits in children: an experience with 10 cases. J Hand Surg 8:309–315
Muir TM, Lehman TP, Meyer WH (2008) Periosteal osteosarcoma in the hand of a paediatric patient: a case report. J Hand Surg 33A:266–268
Mulvey RB (1964) Peripheral bone metastases. Am J Roentgenol 91:155
Murase T, Moritomo H, Tada K et al. (2002) Pseudomallet finger associated with exostoses of the phalanx: a report of two cases. J Hand Surg 27A:817–820
Murphey MD, Nomikos GC, Flemming DJ et al. (2001) Imaging of giant cell tumor and giant cell reparative granuloma of bone: radiologic–pathologic correlation. Radiographics 21:1283–1309

Musharrafieh RS et al. (2002) Epidermoid cyst of the thumb. Orthopedics 25(8):862–863
Okada K, Wold LE, Baebout JW, Shives TC (1993) Osteosarcoma of the hand. Cancer 72:719–725
Opdenakker G, Gelin G, Palmers Y (1999) MR imaging of a subungual glomus tumor. Am J Roentgenol 172:250–251
Ostlere SJ, Gold RH, Mirra JM et al. (1991) Chondrosarcoma of the proximal phalanx of the right fourth finger secondary to multiple hereditary exostoses (MHE). Skeletal Radiol 20(2):145–148
Nora FE, Dahlin DC, Beabout JW (1983) Bizarre parosteal osteochondromatous proliferations of the hands and feet. Am J Surg Pathol 7(3):245–250
Palimeri T (1984) Chondrosarcoma of the hand. J Hand Surg 9A:332–338
Patel MR, Dessai SS, Gordon SL et al. (1987) Management of skeletal giant cell tumors of the phalanges of the hand. J Hand Surg 12 A:70–77
Patel K, Bhuiya T, Chen S (2006) Epidermal inclusion cyst of the phalanx: a case report and literature review. Skeletal Radiol 35:861–863
Patil S, Silva MV de, Crossan J et al. (2003) Chondrosarcoma of small bones of the hand. J Hand Surg Br 26(6):602–628
Platt AJ, Klugman DJ (1995) Aneurysmal bone cyst of the capitate. J Hand Surg Br 20B (1):8–11
Rex C, Jacobs L, Nur Z (1997) Painless osteoid osteoma of the middle phalanx. J Hand Surg Br 22(6):798–800
Roberts P, Price C (1977) Chondrosarcoma of the bones of the hand. J Bone Joint Surg 59B:213–221
Salib P (1967) Chondrosarcoma: a study of the cases treated at the Massachusetts General Hospital in 27 years (1937–1963) Am J Orthop:240–242
Sanjay BKS, Raj GA, Younge DA (1996) Giant cell tumours of the hand. J Hand Surg Br 21(5):683–687
Saunders C, Szabo RM, Mora S (1997) Chondrosarcoma of the hand arising in a young patient with multiple hereditary exostoses. J Hand Surg Br 22(2):237–242
Schajowicz F (1981) Fibrous dysplasia. In: Schajowicz F (ed) Tumours and tumorlike lesions of bone and joints. Springer, Berlin Heidelberg New York, pp 478–490
Shankman S, Desai P, Beltran J (1997) Subperiosteal osteoid osteoma: radiographic and pathological manifestations. Skeletal Radiol 267:457–462
Solomon L (1963) Hereditary multiple exostoses. J Bone Joint Surg 45B:292–304
Takigawa K (1971) Chondroma of the bones of the hand: a review of 110 cases. J Bone Joint Surg 53A:1591–1599
Taniguchi K (1995) A practical classification system for multiple cartilaginous exostosis in children. J Pediatr Orthop:15(5):585–591
Theumann NH, Goettmann S, Leviet D et al. (2002) Recurrent glomus tumors of the fingertips: MR imaging evaluation. Radiology 223:143–151
Unni KK (1996) Dahlin's bone tumours: general aspects and data on 11087 cases, 5th edn. Lippincott-Raven, Philadelphia, pp 71–108
Wilner D (1982) Radiology of bone tumors and allied disorders. Saunders, Philadelphia
Wiss DA, Reid BS (1983) Painless osteoid osteoma of the fingers: report of three cases. J Hand Surg Am 8(6):914–917
Wu KK, Guise ER (1978) Metastatic tumors of the hand. A report of six cases. J Hand Surg 3:271
Yamaguchi T, Tamai K, Saotome K et al. (1997) Ewing's sarcoma of the thumb. Skeletal Radiol 26:725–728
Yuen M, Friedman L, Orr W et al. (1992) Prolifertive periosteal processes of phalanges: a unitary hypothesis. Skeletal Radiol 21(5):301–303

Tumours and Tumour-Like Lesions of the Patella

36

Etienne Pluot, A. Mark Davies and Steven L. J. James

CONTENTS

KEY POINTS

- Benign neoplasms and tumour-like conditions represent 85% of lesions in the patella.
- Chondroblastoma, giant cell tumours, and aneurysmal bone cyst are the three commonest lesions.
- In patients older than 40 years of age, primary and secondary malignancies, intra-osseous ganglion, and gouty tophi should also be included in the differential diagnosis.
- The possibility of haematogenous osteomyelitis should be considered in children and teenagers between 5 and 15 years of age.
- The age, medical history and clinical context are of great help as the imaging features frequently are non-specific.

36.1 Introduction

Tumours and tumour-like lesions arising primarily from the patella are extremely rare, accounting for approximately 0.12% of all primary bone tumours. They may be incidentally diagnosed or present clinically with anterior knee pain, palpable mass lesion or joint stiffness. The most frequent conditions encountered are benign tumours and tumour-like conditions, representing up to 85% of lesions. Malignant lesions arising in the patella are uncommon, but should be considered in older patients (Ehara et al. 1989; Ferguson et al. 1997; Kransdorf et al. 1989; Linscheid and Dahlin 1966; Mercuri and Casadei 2001; O'Mara et al. 2000; Singh et al. 2008). Because of the sesamoid origin and size of the patella, typical features of bone tumours, as might be seen in the long bones, such as periosteal new bone formation, may be missing. This limits the

E. Pluot, MD
Musculoskeletal Fellow, Service de Radiologie B, Hôpital Cochin, 27 rue du Faubourg Saint Jacques, 75679 Paris Cedex 14, France

A. M. Davies, MD
Consultant Radiologist, Department of Radiology, Royal Orthopaedic Hospital, Birmingham B31 2AP, UK

S. L. J. James, MD
Consultant Radiologist, Department of Radiology, Royal Orthopaedic Hospital, Birmingham B31 2AP, UK

specificity of imaging in distinguishing between benign neoplastic, malignant and non-neoplastic lesions. Computed tomography (CT) and magnetic resonance (MR) imaging are used for surgical staging and operative planning. The purpose of this chapter is to review those conditions that may present as a "tumour" arising in the patella and indicate, where possible, the most likely diagnosis based on the imaging findings.

36.2 Benign Tumours

Benign neoplastic lesions are by far the commonest lesions arising in the patella, accounting for 39 to 69% of cases depending on the series. This particularly applies to patients presenting below 40 years of age. Giant cell tumour and chondroblastoma account equally for more than 50% of benign lesions and should, therefore, figure at the top of any list of differential diagnoses of patellar lesions in the younger age group.

36.2.1 Chondroblastoma

Chondroblastoma is a benign cartilage tumour that typically arises in the epiphysis of a long bone, most commonly occurring in the 2nd decade of life. The male: female ratio is 2:1. Chondroblastoma accounts for 1-3% of all benign primary bone tumours, involvement of the patella representing 4–6% of all cases of chondroblastoma (Moser et al. 1988; Schajowicz and Gallardo 1970; Springfield et al. 1985; Wolfe et al. 1995). Imaging appearances of chondroblastoma

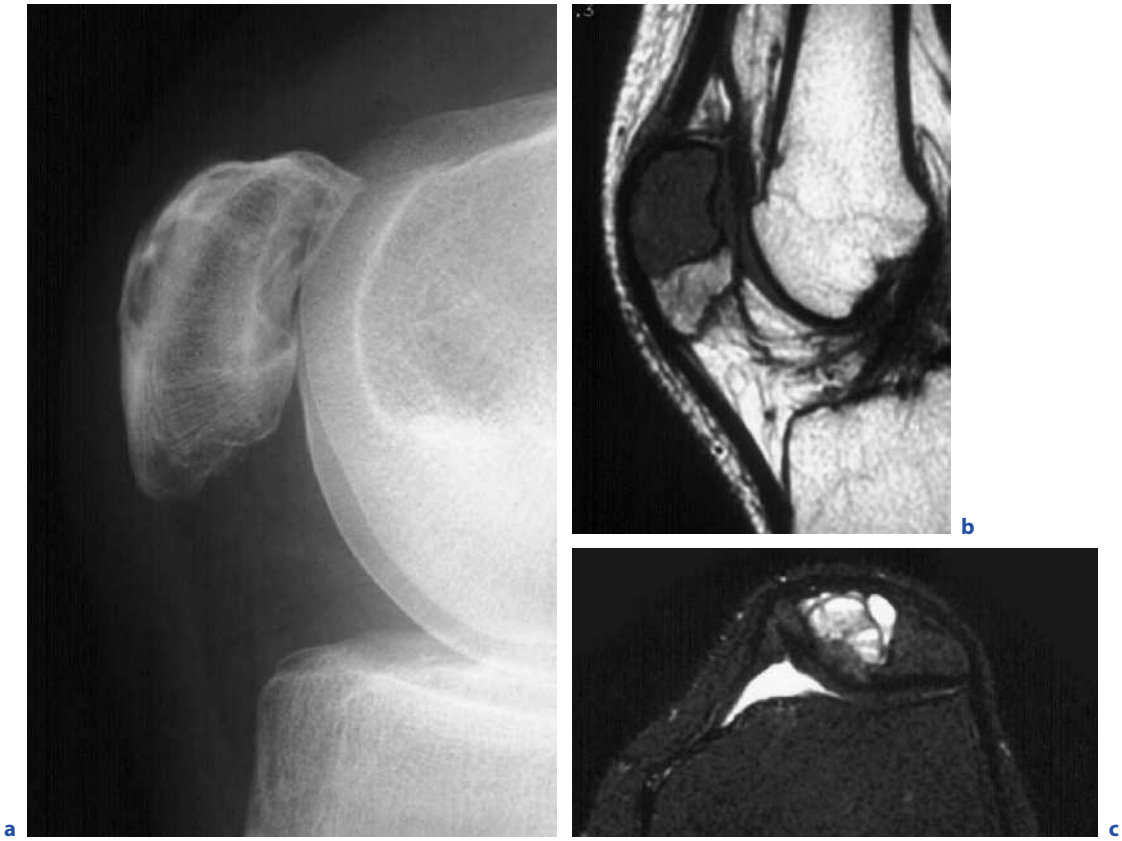

Fig. 36.1a–c. Chondroblastoma. **a** Lateral radiograph showing geographic bone destruction. **b** Sagittal T1-weighted image showing the lesion to be intermediate in signal intensity. **c** Axial T2-weighted image with fat suppression revealing fluid-fluid levels indicating secondary aneurysmal bone cyst formation

in the patella do not differ significantly from those in long bones. It appears radiographically as a round or lobulated focus of bone destruction, surrounded by a well-defined sclerotic rim (Fig. 36.1a). The size of the lesion ranges from 10 to 35 mm. The contour of the patella is usually preserved, unless the chondroblastoma is associated with a secondary aneurysmal bone cyst (ABC) formation. Matrix mineralization is frequently absent. CT can depict matrix mineralization, potential cortical expansion and soft-tissue involvement. Magnetic resonance imaging findings do not differ from other locations. MR imaging demonstrates low signal intensity on T1-weighted images (Fig. 36.1b) and variable signal intensity on T2-weighted images with foci of hypointense signal corresponding to the mineralization. Fluid-fluids levels can be observed, but are not specific, but do suggest an associated secondary ABC (Fig. 36.1c) (Trebse et al. 2001).

36.2.2 Giant Cell Tumour

Giant cell tumour (GCT) is a benign, locally aggressive neoplasm, typically affecting the subarticular portion of long bones during the 3rd decade of life. They arise in the metaphysis of long bones and reach the subarticular bone. Giant cell tumours represent 4–5% of all primary bone tumours, of which less than 1% involve the patella (Campanacci et al. 1987; Sung et al. 1982). Common clinical manifestations at the time of diagnosis are anterior knee pain, limited flexion and swelling. Pathological fractures occur in approximately 10–20% of cases. Pulmonary metastases are encountered in 2–3% of all patients with GCT. Two patients with pulmonary metastases were reported in a series of 11 patients with giant cell tumours of the patella (Agarwal et al. 2002). No major risk factor for metastatic disease in patients

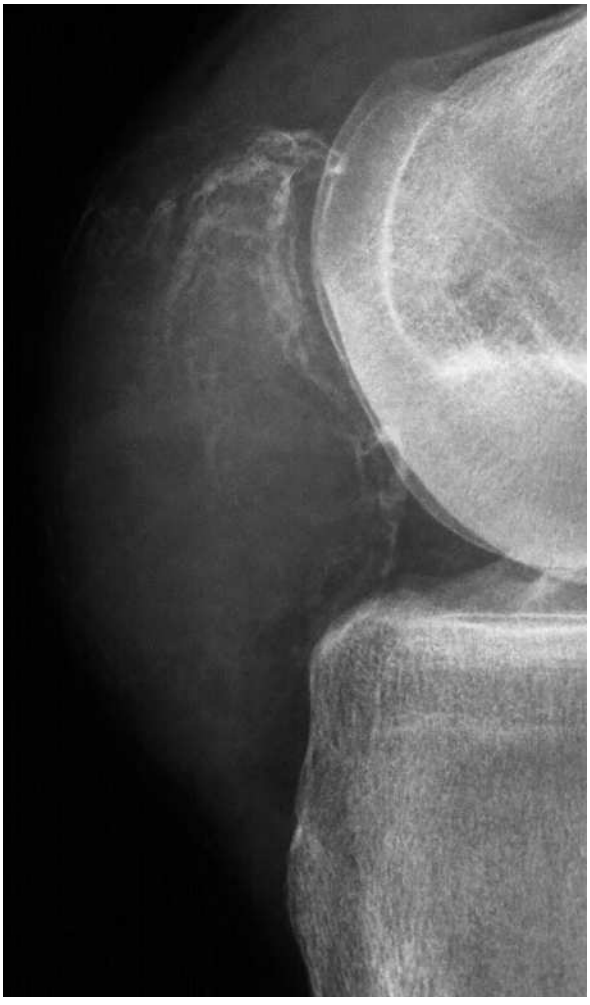

a

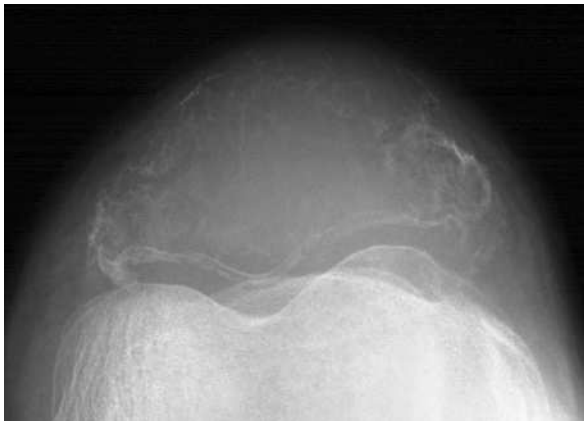

b

Fig. 36.2a–d. Giant cell tumour. **a** Lateral and **b** skyline radiographs showing destruction and expansion of the patella. (**c,d**) *see next page*

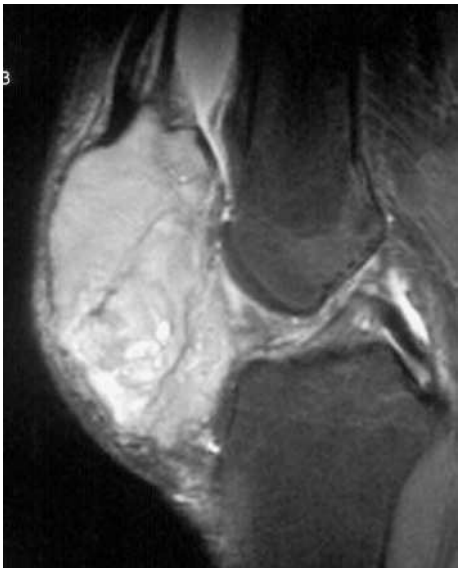

c

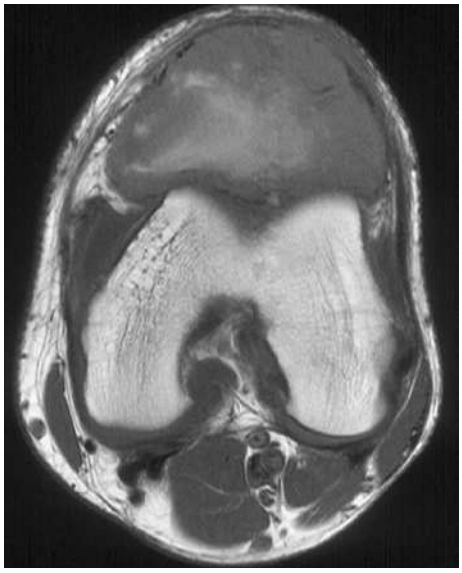

d

Fig. 36.2a–d. (*continued*) **c** Sagittal STIR and **d** axial T1-weighted images showing the lesion to be principally solid with some small cystic areas. The hyperintensity on the T1-weighted image suggests subacute haemorrhage possibly secondary to a fracture

with a GCT is clearly recognised (Rock 1990; Tubbs et al. 1992), but as suggested in Agarwal's series, surgical manipulation or pathological fracture of GCT of the patella could increase that risk. Imaging features in the patella are similar to that of GCT occurring in long bones. Radiographs and CT show a geographical pattern of bone destruction, with well- to ill-defined margins, involving more than 75% of the patella (Fig. 36.2a,b). Compared to chondroblastomas, GCT tends to be larger in size and therefore involves a greater proportion of the patella. Cortex thinning, bone expansion and "bubbly" appearance of the patella related to septa are typical (Fig. 36.3a,b). MR imaging demonstrates low to intermediate signal-intensity on T1-weighted images and intermediate to high signal intensity on T2-weighted images (Fig.36.2c,d). Low signal foci related to haemosiderin deposition within the tumour may be observed, and fluid-fluid levels would again suggest secondary ABC formation.

36.2.3 Other Benign Tumours

Various other benign tumours have been reported arising in the patella. The frequency of these lesions is far lower than the incidence of either chondroblastoma or GCT. These include simple bone cyst (Chaudhary et al. 2000; Wientroub et al. 1979), osteoma (Durig et al. 1975), osteoid osteoma (Bulas et al. 1992; Koos and Than 2005), osteoblastoma (De Coster et al. 1989), chondromyxoid fibroma, haemangioma (Bansal et al. 1974) and lipoma. Again, the imaging features in the patella do not significantly differ from similar lesions arising at other skeletal locations.

36.3 Malignant Tumours

Primary and secondary malignancies involving the patella are very rare, accounting for approximately 15% of patellar tumours. The most frequent aetiologies reported are metastasis, osteosarcoma, haemangioendothelioma and lymphoma (Fig. 36.3). Radiographically, most of them cannot be reliably distinguished from benign neoplasms. Clinical context, medical history and age of patient may raise the question of possible malignancy.

36.3.1 Metastases

Metastases very rarely arise in the patella, accounting for only 5% of all patellar tumours. Relatively poor

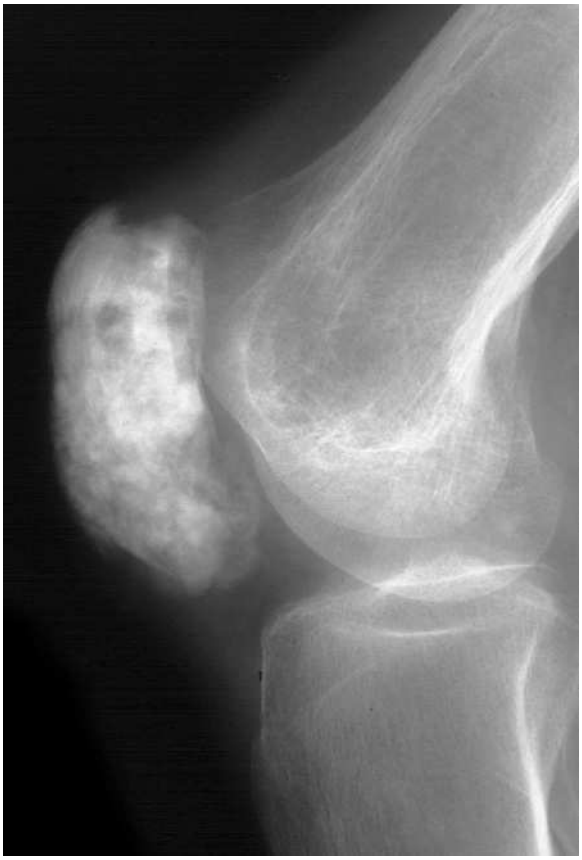

Fig. 36.3. Paget's osteosarcoma. The lateral radiograph shows Paget's disease of both the patella and distal femur. The lysis in the lower pole of the patella indicates malignant transformation to a sarcoma. Similar appearances might be seen with a metastasis in pagetic bone

vascularisation through an anastomotic peripheral arterial ring may explain the low frequency of metastases in the patella (Scapinelli 1967). Metastases from lung cancer appear to be the most frequently reported, possibly due to the high prevalence of lung cancer itself (Cooper and Mess 2000; Patel and Desai 1988; Pauzner et al. 1996). Other primary locations include carcinoma of the breast (Keeley 1973; Taylor 1964), kidney (Lim et al. 2007), colon, oesophagus and uterine cervix (Griener and Muller-Farber 2001; Urvoy et al. 1993), squamous cell carcinoma of the mouth (Singh et al. 1995) as well as melanoma (Jaeger et al. 1992).

36.3.2 Primary Malignant Tumours

Lymphoma (Cha et al. 1996), haemangioendothelioma and osteosarcoma (Mcgrath et al. 2006; Nagai et al. 1993; Okada et al. 1994) are the most frequent primary malignant tumours in the patella, each accounting respectively for approximately 4% of all patellar tumours. Demographics and radiological features are identical to other sites. Interestingly, no periosteal reaction should be expected as the patella, being a sesamoid bone, does not have a conventional periosteal layer. Malignant fibrous histiocytoma (Lopez-Barea et al. 1991), leiomyosarcoma (Inoue et al. 2001), plasmacytoma (Mcleod and Macnicol 1990) and angiosarcoma are rarely reported malignancies.

36.4 Tumour-Like Lesions

Tumour-like conditions account for approximately 40% of all patellar lesions. Aneurysmal bone cyst and osteomyelitis are the commonest non-neoplastic conditions in children and young adults, whereas the diagnosis of intraosseous gout and brown tumour of hyperparathyroidism should be favoured in adults older than 40 years of age.

36.4.1 Aneurysmal Bone Cyst

Aneurysmal bone cyst (ABC) is a benign bone lesion of unknown histiogenesis, but usually is not considered a true neoplasm. It typically occurs in children, with 80% of cases presenting under the age of 20 years. It is the third commonest lesion arising in the patella, after chondroblastoma and GCT, accounting for 10% of all patellar lesions and approximately 20% of tumour-like lesions in the patella. Again, the imaging features in the patella do not differ from other locations (Castro and Irwin 1996; Faris et al. 1978; Pevny and Rooney 1994). Fluid-fluids levels on CT or MR imaging (Fig. 36.4) strongly suggest the diagnosis of ABC, but should be considered with caution and should not exclude a primary bone lesion with secondary ABC or even malignancy. Indeed, due to the absence of a true periosteal layer around the patella, the typical signs suggesting malignancy, such as periosteal reaction with Codman's triangle, are missing.

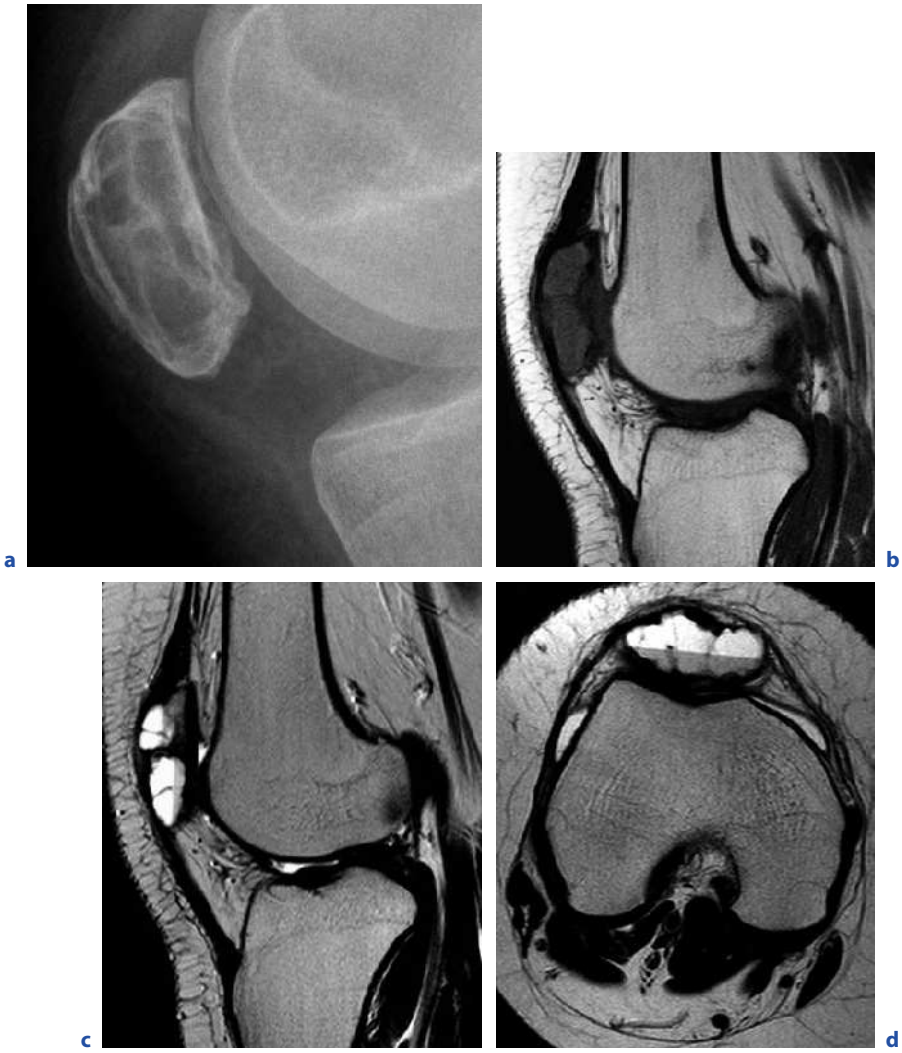

Fig. 36.4a–d. Aneurysmal bone. **a** AP radiograph showing a well-defined lytic lesion. **b** Intermediate signal intensity on the sagittal T1-weighted image and fluid-fluid levels on the **c** sagittal and **d** axial T2-weighted images

36.4.2 Osteomyelitis

Acute haematogenous osteomyelitis of the patella typically occurs between 5 and 15 years of age. It is rare in children younger than 5 years of age. This could be explained by the particular course of vascularisation of the patella, which is maximal during the ossification phase, while cartilaginous and fully ossified adult patella has a poor blood supply. A few cases in adults have been reported (Kankate and Selvan 2000), most of them involving immunocompromised patients (Vail and Urbaniak 1991). Staphylococcus aureus is the most common micro-organism causing the infection, which is usually limited to the patella and uncommonly spreads to the joint cavity. Tuberculosis should be mentioned as a possible cause, especially in immunocompromised patients, but tends to be multifocal rather than isolated in the patella. As previously mentioned for others aetiologies, no periosteal reaction should be expected. Again, imaging features of osteomyelitis of the patella lack specificity to discriminate it from other diagnoses and appear as a non-specific small radiolucency (Fig. 36.5). This is best demonstrated on CT (Fig. 36.5c) or MR imaging. Age group, clinical features and elevated haematogenous inflammatory markers are a help to suggest the diagnosis of infection.

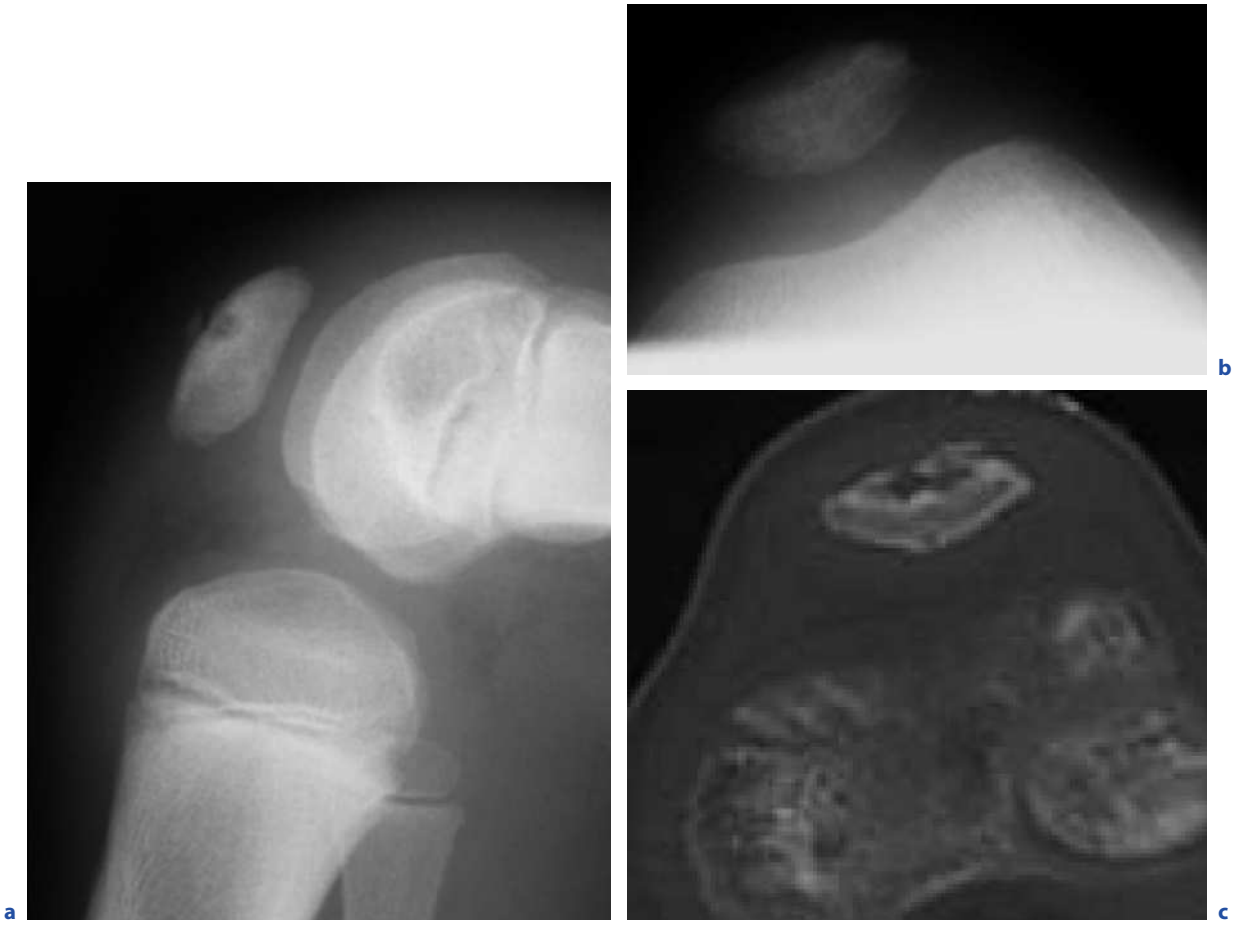

Fig. 36.5a–c. Osteomyelitis in a 7-year-old child. **a** Lateral and **b** skyline radiographs showing a small lytic lesion in the anterior patella. **c** Axial CT shows the lesion with a breach in the anterior cortex

36.4.3 Intraosseous Gout

Gout is a crystal-induced arthritis caused by a common disorder of uric acid that can lead to recurrent episodes of joint inflammation, tissue deposition of uric acid crystals and joint destruction. Patients with gout typically present with a history of acute monoarticular attacks affecting small joints in lower extremities. The first metatarsophalangeal joint is the initial joint manifestation in 50% of cases. Tophi are collections of uric acid crystals that can be found in the soft tissues of patients with chronic gout. Intraosseous tophi are rare findings, appearing as well-delineated lucent lesions. The foot and ankle are the most commonly involved joints, with the knee in third position. The patella is rarely affected, accounting for about 8% of patellar lesions (Fig. 36.6). Some authors reported a topographical predominance of intraosseous tophi in the superolateral aspect of the patella (Recht et al. 1994). The main characteristic of intraosseous tophi of the patella is the associated soft tissue mass, which presents usually with calcifications. Involvement of adjacent soft tissue is best demonstrated on CT or MR imaging (Fig. 36.6c). Gouty tophi have also been reported in bi-partite patella (Kobayashi et al. 2005) and as an underlying cause of pathological fracture (Aboulafia et al. 1999).

36.4.4 Other Tumour-Like Lesions

A number of very rare non-neoplastic disorders mimicking tumours have been reported arising in the patella. Each of these conditions represents less than 5% of all patellar lesions. Brown tumour in hyperparathyroidism, intraosseous ganglion (Tam et al. 1996), solitary bone cyst (Chaudhary et al. 2000), pigmented

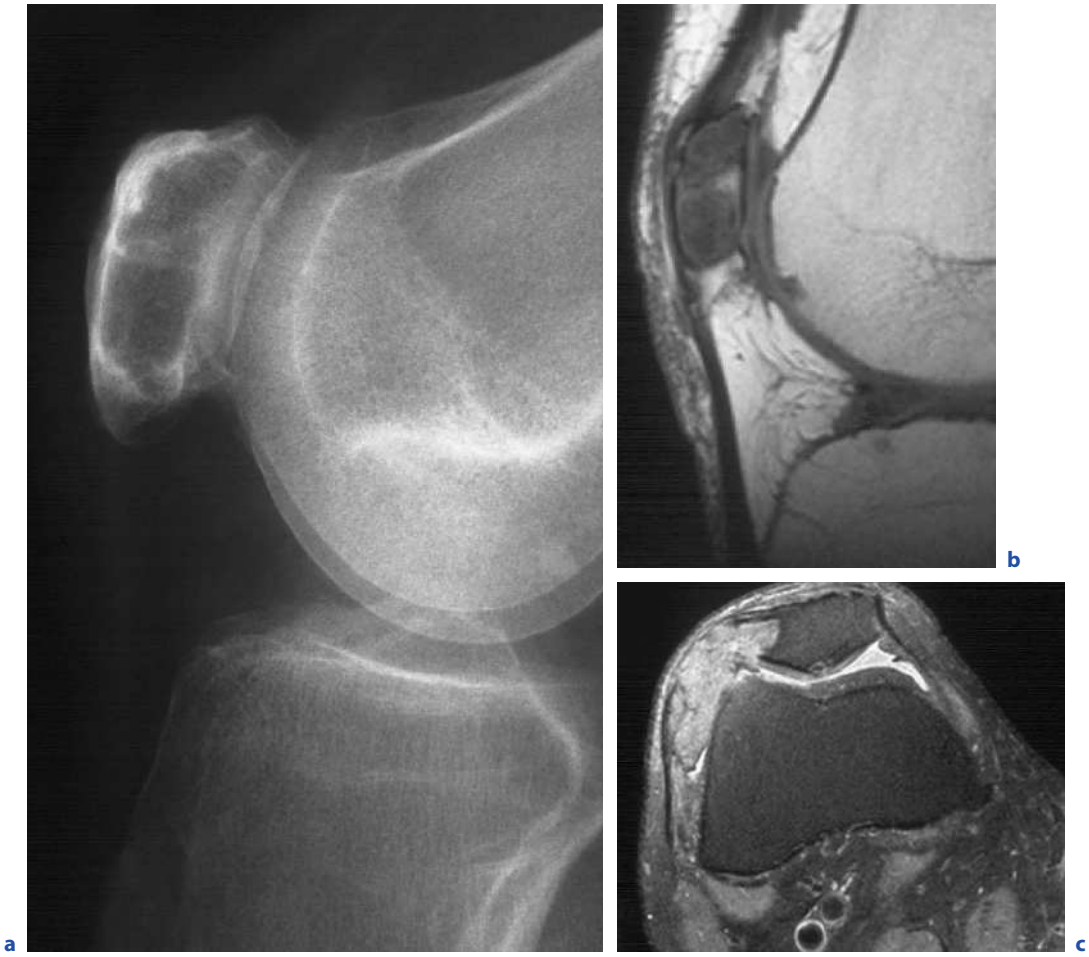

Fig. 36.6a–c. Gout. **a** Lateral radiograph showing geographic bone destruction. **b** Intermediate signal intensity lesion on T1-weighted image. **c** Extraosseous extension laterally on the T2-weighted image with fat suppression

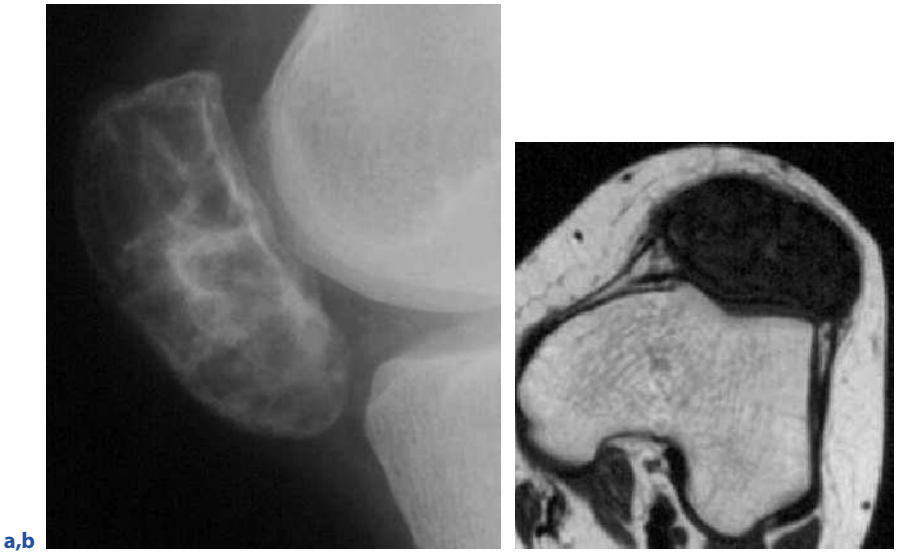

Fig. 36.7a–c. Brown tumour of hyperparathyroidism. **a** Lateral radiograph showing a septated lesion involving the whole patella. **b** Axial T1-weighted and **c** *see next page*

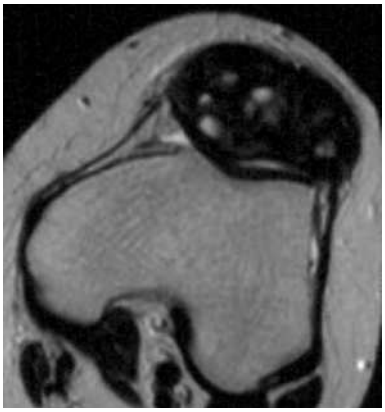

Fig. 36.7a–c. (*continued*) Brown tumour of hyperparathyroidism. **c** T2-weighted images showing a predominantly low signal intensity lesion due to old haemorrhage

villonodular synovitis, osteoma and the exceptional bizarre paraosteal osteochondromatous proliferation have all been reported. Brown tumours occur in primary or secondary hyperparathyroidism and consist of vascular, proliferating fibrous tissue, haemorrhage and reparative granulation tissue resulting from osteoclastic hyperactivity. They appear as well-defined, largely lytic lesions (Fig. 36.7a). MR imaging demonstrates low signal intensity of the lesion on both T1- and T2-weighted images, with possible hyperintense foci on T2-weighted images. The low signal intensity is likely due to repeated intralesional haemorrhage (Fig. 36.7b, c). Known clinical context, abnormal serum phosphate and calcium levels as well as other skeletal radiological findings are helpful in suggesting the correct diagnosis.

Acknowledgements. The authors wish to thank Dr. K. Woertler, Dr. S. Anderson and Dr. H. Kroon for some of the material used in this chapter.

References

Aboulafia AJ, Prickett B, Giltman L (1999) Displaced pathological patella fracture due to gout. Orthopedics 22:543–545

Agarwal S, Jain UK, Chandra T, Bansal GJ, Mishra US (2002) Giant-cell tumors of the patella. Orthopedics 25:749–751

Bansal VP, Singh R, Grewal DS, Bannerjee AK (1974) Haemangioma of the patella. A report of two cases. J Bone Joint Surg Br 56:139–141

Bulas RV, Hayes CW, Conway WF, Loughran T (1992) Case report 738: Osteoid osteoma of the patella. Skeletal Radiol 21:326–329

Campanacci M, Baldini N, Boriani S, Sudanese A (1987) Giant-cell tumor of bone. J Bone Joint Surg Am 69:106–114

Castro MD, Irwin RB (1996) Aneurysmal bone cyst of the patella. Am J Orthop 25:717–719

Cha S, Schultz E, McHeffey-Atkinson B, Sherr D (1996) Malignant lymphoma involving the patella. Skeletal Radiol 25:783–785

Chaudhary D, Bhatia N, Ahmed A et al. (2000) Unicameral bone cyst of the patella. Orthopedics 23:1285–1286

Cooper ME, Mess D (2000) Isolated skeletal metastasis to the patella. Am J Orthop 29:210–212

De Coster E, Van Tiggelen R, Shahabpour M et al. (1989) Osteoblastoma of the patella. Case report and review of the literature. Clin Orthop Relat Res:216–219

Durig M, Remagen W, Morscher E (1975) Primary osteoma of the patella: a case report (author's transl). Arch Orthop Unfallchir 83:289–293

Ehara S, Khurana JS, Kattapuram SV et al. (1989) Osteolytic lesions of the patella. AJR Am J Roentgenol 153:103–106

Faris WF, Rubin BD, Fielding JW (1978) Aneurysmal bone cyst of the patella. A case report. J Bone Joint Surg Am 60:711

Ferguson PC, Griffin AM, Bell RS (1997) Primary patellar tumors. Clin Orthop Relat Res:199–204

Griener B, Muller-Farber J (2001) Patellar metastasis of colon carcinoma. A rarity in differential diagnosis of acute knee pain. Case report. Unfallchirurg 104:778–781

Inoue S, Tanaka K, Sakamoto A et al. (2001) Primary leiomyosarcoma of the patella. Skeletal Radiol 30:530–533

Jaeger HJ, Kruegener GH, Donovan AG (1992) Patellar metastasis from a malignant melanoma. Int Orthop 16:282–284

Kankate RK, Selvan TP (2000) Primary haematogenous osteomyelitis of the patella: a rare cause for anterior knee pain in an adult. Postgrad Med J 76:707–709

Keeley CD (1973) Bilateral patellar metastases from carcinoma of the male breast. Can J Surg 16:328–329

Kobayashi K, Deie M, Okuhara A et al. (2005) Tophaceous gout in the bipartite patella with intra-osseous and intra-articular lesions: a case report. J Orthop Surg (Hong Kong) 13:199–202

Koos Z, Than P (2005) Rare localization of osteoid osteoma in the patella. Pediatr Radiol 35:929–930

Kransdorf MJ, Moser RP Jr, Vinh TN, Aoki J, Callaghan JJ (1989) Primary tumors of the patella. A review of 42 cases. Skeletal Radiol 18:365–371

Lim CT, Wong AS, Chuah BY et al. (2007) The patella as an unusual site of renal cell carcinoma metastasis. Singapore Med J 48:e314–319

Linscheid RL, Dahlin DC (1966) Unusual lesions of the patella. J Bone Joint Surg Am 48:1359–1366

Lopez-Barea F, Rodriguez-Peralto JL, Burgos-Lizalde E, Gonzalez-Lopez J, Sanchez-Herrera S (1991) Case report 639: Malignant fibrous histiocytoma (MFH) of the patella. Skeletal Radiol 20:125–128

McGrath BE, Schlatterer D, Mindell ER (2006) Case reports: Osteogenic sarcoma of the patella spread to lateral meniscus after arthroscopy. Clin Orthop Relat Res 444:250–255

McLeod GG, Macnicol MF (1990) Plasmacytoma of the patella. J R Coll Surg Edinb 35:195–196

Mercuri M, Casadei R (2001) Patellar tumors. Clin Orthop Relat Res:35–46

Moser RP Jr, Brockmole DM, Vinh TN, Kransdorf MJ, Aoki J (1988) Chondroblastoma of the patella. Skeletal Radiol 17:413–419

Nagai S, Okuda N, Azuma H, Suzuki M, Takahama M (1993) Osteosarcoma of the patella. A case report. Clin Orthop Relat Res:243–246

O'Mara JW Jr, Keeling J, Montgomery EA, Aaron AD (2000) Primary lesions of the patella. Orthopedics 23:328, 348, 370, 376–327

Okada K, Sato K, Abe E et al. (1994) Case report 858: Post-radiation osteosarcoma of the patella. Skeletal Radiol 23:471–474

Patel MR, Desai SS (1988) Patellar metastases. A case report and review of the literature. Orthop Rev 17:687–690

Pauzner R, Istomin V, Segal-Lieberman G, Matetzky S, Farfel Z (1996) Bilateral patellar metastases as the clinical presentation of bronchogenic adenocarcinoma. J Rheumatol 23:939–941

Pevny T, Rooney RJ (1994) Case report 876: Aneurysmal bone cyst of the patella. Skeletal Radiol 23:664–667

Recht MP, Seragini F, Kramer J et al. (1994) Isolated or dominant lesions of the patella in gout: a report of seven patients. Skeletal Radiol 23:113–116

Rock M (1990) Curettage of giant cell tumor of bone. Factors influencing local recurrences and metastasis. Chir Organi Mov 75:204–205

Scapinelli R (1967) Blood supply of the human patella. Its relation to ischaemic necrosis after fracture. J Bone Joint Surg Br 49:563–570

Schajowicz F, Gallardo H (1970) Epiphysial chondroblastoma of bone. A clinico-pathological study of 69 cases. J Bone Joint Surg Br 52:205–226

Singh HK, Silverman JF, Ballance WA Jr, Park HK (1995) Unusual small bone metastases from epithelial malignancies: diagnosis by fine-needle aspiration cytology with histologic confirmation. Diagn Cytopathol 13:192–195

Singh J, James SL, Kroon HM, Woertler K, Anderson SE, Davies AM (2008) Tumour and tumour-like lesions of the patella: a multicentre experience. Eur Radiol (in press)

Springfield DS, Capanna R, Gherlinzoni F, Picci P, Campanacci M (1985) Chondroblastoma. A review of 70 cases. J Bone Joint Surg Am 67:748–755

Sung HW, Kuo DP, Shu WP et al. (1982) Giant-cell tumor of bone: analysis of 208 cases in Chinese patients. J Bone Joint Surg Am 64:755–761

Tam W, Resnick D, Haghighi P, Vaughan L (1996) Intraosseous ganglion of the patella. Skeletal Radiol 25:588–591

Taylor GH (1964) Pathologic fracture of patella caused by metastatic carcinoma. N Y State J Med 64:430–431

Trebse R, Rotter A, Pisot V (2001) Chondroblastoma of the patella associated with an aneurysmal bone cyst. Acta Orthop Belg 67:290–296

Tubbs WS, Brown LR, Beabout JW, Rock MG, Unni KK (1992) Benign giant-cell tumor of bone with pulmonary metastases: clinical findings and radiologic appearance of metastases in 13 cases. AJR Am J Roentgenol 158:331–334

Urvoy P, Mestdagh H, Butin E, Lecomte-Houcke M, Maynou C (1993) Patellar metastasis from a large bowel adenocarcinoma. Acta Orthop Belg 59:409–411

Vail TP, Urbaniak JR (1991) Hematogenous patellar osteomyelitis associated with human immunodeficiency virus. Orthop Rev 20:788–790

Wientroub S, Salama R, Baratz M, Papo I, Weissman SL (1979) Unicameral bone cyst of the patella. Clin Orthop Relat Res:159–161

Wolfe MW, Halvorson TL, Bennett JT, Martin PC (1995) Chondroblastoma of the patella presenting as knee pain in an adolescent. Am J Orthop 24:61–64

Tumours of the Foot

37

David A. Ritchie

CONTENTS

KEY POINTS

- In contrast to the axial skeleton, metastases, myeloma and lymphoma are rare in the foot
- Ewing's sarcoma and chondrosarcoma are the most common primary malignant bone tumours in the immature and mature foot respectively with the majority in the calcaneus and metatarsal bones
- Osteoid osteoma is the most common benign bone tumour, often presents with atypical symptoms, frequently arises in the talar neck and may be radiographically occult
- Subungual exostosis is by far the most common tumor-like lesion and is distinct from a true osteochondroma
- In the calcaneus, giant cell tumours and chondroblastoma frequently occur in the apophysis posteriorly and adjacent to the posterior calcaneal facet (epiphyseal equivalent sites) whereas simple cysts and intraosseous lipoma typically arise in the anterior calcaneus in the region of the critical angle
- Lesions in the foot do not have to achieve a large size to become symptomatic and the small size of many bones means that involvement of an entire bone is not uncommon

37.1 Introduction

True osseous neoplasms of the foot are relatively uncommon and are greatly outnumbered by tumour-like conditions. There are significant differences in the epidemiology, clinical and imaging findings of foot tumours compared with the same tumours at more proximal locations. This chapter focuses on the more

D. A. Ritchie, MD
Consultant Radiologist, Western Infirmary, Dumbarton Road, Glasgow G11 6NT, UK

common types of tumour and tumour-like lesions that are found in the foot, emphasizes the imaging features and discusses their differential diagnosis.

37.2 Imaging Tumours and Tumour-like Lesions

37.2.1 Epidemiology

Bone tumours of the foot are uncommon, accounting for only 3.3% of all primary bone tumours (Unni 1996; Campanacci 1999). This is reflected in a large series of 307,601 soft-tissue and bony lesions of the foot where the true incidences of benign and malignant bone tumours were only 0.04% and 0.002%, respectively (Berlin 1995). However, some bone tumours have a predilection for the foot and this has been well documented in several series (Campanacci 1999; Unni 1996; Ozdemir et al. 1997; Murari et al. 1989; Casadei et al. 1991). Although the results of these series are skewed to a certain extent by tertiary referral patterns, the combined figures of two of these series have been collated and are presented in Table 37.1 and are also referred to in relevant sections of the text. Note that tumour-like lesions are not included in the table as they are not included in some of these series.

In contrast to the axial skeleton, primary bone sarcomas appear to be more common than metastases, myeloma or lymphoma in the foot. In Campanacci's series of 117 biopsied malignant bone tumours of the foot, the incidences of metastatic disease and myeloma were only 11% and 4% respectively, whereas the incidence of Ewing's sarcoma was 24% (Campanacci 1999). However, it is likely that the true incidences of metastatic disease and myeloma are higher as many lesions probably go unrecognized or are not biopsied in disseminated disease. Of the primary bone sarcomas, Ewing's sarcoma and chondrosarcoma are more common than osteosarcoma in the foot, with the majority arising in the calcaneus and metatarsal bones.

Of the benign tumours, osteoid osteoma is the most common lesion accounting for approximately 31% of all benign bone tumours. Osteoblastoma is less common than osteoid osteoma but histologically similar and both have a predilection for the talar neck. Giant cell tumour is the second most common benign bone tumour with an affinity for the talus and calcaneus (Biscaglia et al. 2000). Of the chondroid lesions, chondroma (enchondroma) is less common in the foot than in the hand but it accounts for 13% of benign bone tumours of the foot and is the most common benign bone tumour of the forefoot. Chondromyxoid fibroma is a rare benign cartilage tumour but 14% occur in the foot and it accounts for 10% of benign bone tumours at this site.

Table 37.1. Relative incidence of primary bone tumours in the foot. Figures obtained by combining the results of Unni, Campanacci, Murari and Casadei (Campanacci 1999; Unni 1996; Ozdemir et al. 1997; Murari et al. 1989; Casadei et al. 1991)

Benign lesion of bone (n=660)	Percentage of benign tumours	Primary malignant bone tumour (n=268)	Percentage of malignant tumours
Osteoid osteoma	31	Ewing's sarcoma	28
Giant-cell tumour	14	Chondrosarcoma	27
Enchondroma	13	Osteosarcoma	19
Osteoblastoma	11	Vasoformative tumours[a]	8
Chondromyxoid fibroma	10	Fibrosarcoma	6
Chondroblastoma	9	Malignant fibrous histiocytoma	4
Osteochondroma	9	Lymphoma	3
Others	3	Myeloma	3
		Others	2

[a]Vasoformative tumours include haemangioendothelioma and angiosarcoma

Of the tumor-like lesions, subungual exostosis is by far the most common bone lesion of all, accounting for over 96% of 3,850 bone tumor and tumor-like lesions of the foot (Berlin 1995). This reactive lesion usually arises on the dorsal aspect of the distal phalanx of the big toe should be differentiated from the much less common true osteochondroma. Although only 3% of simple bone cysts occur in the foot, bone cysts have a predilection for the calcaneus in adults accounting for 13% of benign tumors and tumor-like lesions in one series (Casadei et al. 1991). Aneurysmal bone cysts account for approximately 5% of benign tumour and tumour-like lesions of the foot and are most common in the calcaneus. Intraosseous ganglia are not uncommon in the foot. In a large study reviewing 213 cases, 8% were found in the foot (Murff and Ashry 1994).

37.2.2 Clinical Aspects

The compact small bone structure and paucity of soft tissues around the foot often results in early presentation and easily palpable lesions. In general, lesions tend to be smaller than their more proximal counterparts. It is important to be aware of any pre-existing lesions including enchondromatosis, Diaphyseal Aclasis or fibrous dysplasia and in the older age group, malignancy elsewhere. Some lesions including calcaneal cysts and intraosseous lipomas are usually incidental findings whereas other lesions, including chondroma may present with a pathological fracture. Several lesions may present with atypical clinical findings compared to the same lesion in other parts of the skeleton. For example, osteoid osteoma in the hindfoot is typically intraarticular or periarticular in location and may present as an inflammatory arthropathy. Furthermore, the typical night pain and response to non-steroidal anti-inflammatory drugs may be absent. Other patients with osteoid osteoma have presented with impingement, chronic sprains or trauma and a 3 year delay in diagnosis is not uncommon (Hussain et al. 2005). Although many lesions in the foot present at a similar age to their more proximal counterparts, some lesions may show significant variation. For example, in the foot, osteosarcoma most commonly presents in the fourth decade, two decades later than more proximal lesions. In older patients, multiplicity should suggest, metastases, myeloma or lymphoma, whereas the most common primary malignancy is chondrosarcoma. In one study of bone sarcomas of the foot, most patients presented with pain and/or a mass that was increasing in size and a median duration of 7 months (Shaylor et al. 2000).

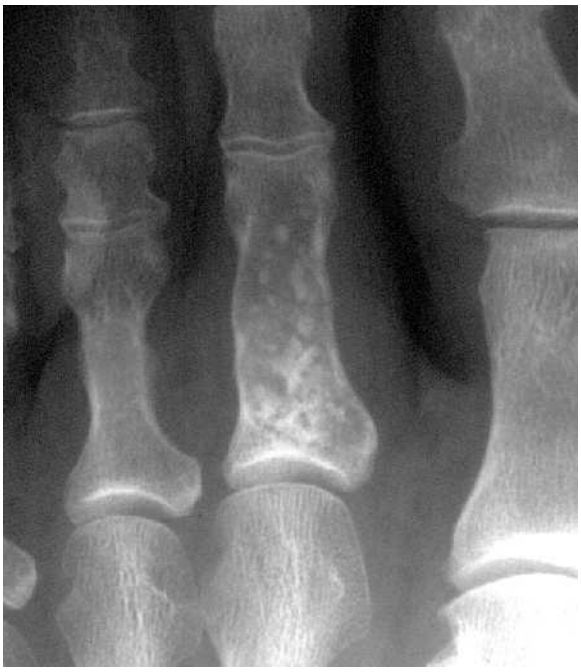

Fig. 37.1. Pathological fracture of the proximal phalanx of the second toe due to an enchondroma in a 30-year-old man. The radiograph shows characteristic punctuate mineralisations

37.2.3 Characterisation

37.2.3.1 Location

In general, most bone tumours, whether malignant or benign, tend to occur in the hind-/midfoot rather than the forefoot. When malignant tumours do occur in the forefoot, involvement of the metatarsals is much more common than the phalanges. On the other hand, benign tumours of the phalanges are not uncommon with the majority due to chondroma (Fig. 37.1). Some bone tumours have a predilection for a particular bone. Osteoid osteoma and osteoblastoma commonly arise at the talar neck, and simple bone cysts and intraosseous lipomas in the anterior third of the calcaneus (Figs. 37.2 and 37.3). The location of a tumour within a bone can also be described in transverse or longitudinal planes but differentiation of eccentric and central lesions in the forefoot in the transverse plane may be difficult due to the small cross-section of the bones. Similarly, in the longitudinal plane, since the physis of small foot bones is relatively

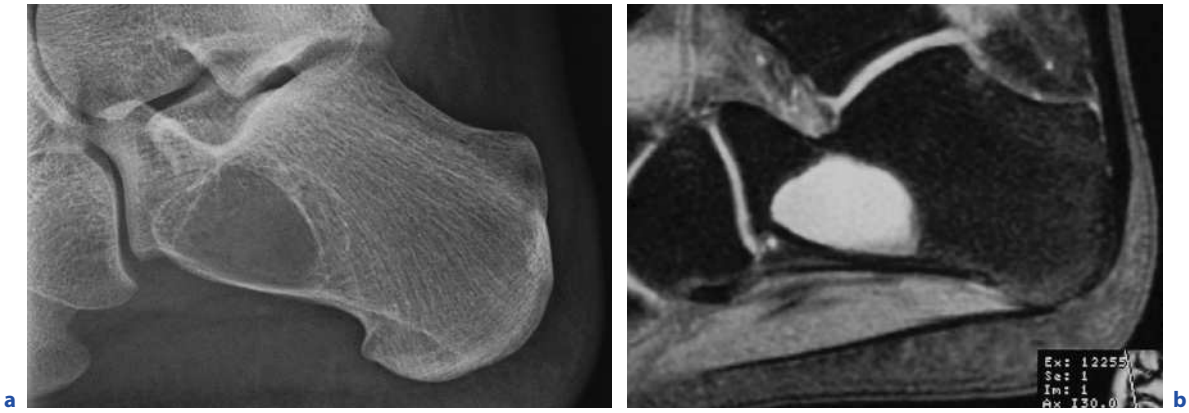

Fig. 37.2a,b. Incidental simple bone cyst in a 17-year-old male. **a** The radiograph shows a well defined intramedullary lytic lesion with sclerotic rim in the critical angle of the anterior calcaneus. **b** Sagittal STIR MR image showing a well defined homogeneous high signal intensity lesion in keeping with fluid

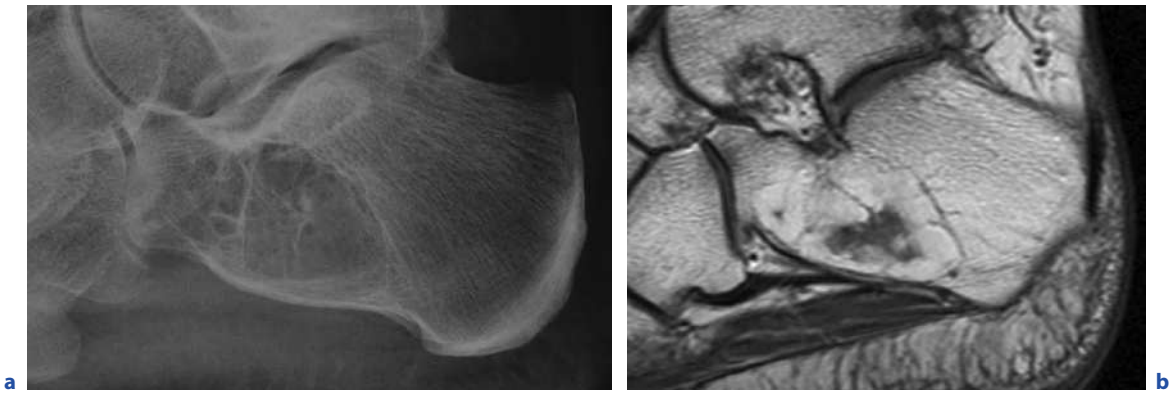

Fig. 37.3a,b. Intraosseous lipoma in a 29-year-old male. **a** Radiograph shows a slightly irregular, slightly expansile lesion with sclerotic margin in the critical angle of the anterior calcaneus. Centrally, there is dystrophic calcification that distinguishes it from a simple bone cyst. **b** Sagittal T1-weighted MR image shows high signal intensity mature fat in the peripheral portion of the lesion and low signal intensity centrally due to fluid, necrosis and mineralisation

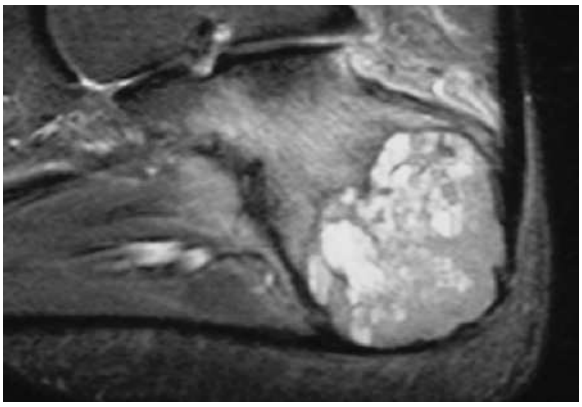

Fig. 37.4. Chondroblastoma in a 19-year-old male. Sagittal STIR MR image shows an irregular inhomogeneous lesion in the posterior calcaneus including the calcaneal apophysis. The high signal intensity foci are due to unmineralised cartilage and the intermediate foci are due to more cellular components. Note also the typical surrounding marrow oedema

small, differentiation of lesions into the various zones may not be possible. However, the calcaneus has identifiable sites that correspond to the physeal zones. The calcaneal apophysis and the subarticular portions of the upper and anterior calcaneus correspond to the epiphysis equivalent zone, the adjacent bone corresponds to the metaphyseal zone, and the central calcaneus to the diaphyseal zone. Chondroblastoma and giant cell tumours frequently occur in the apophysis posteriorly and adjacent to the posterior calcaneal facet, both epiphyseal equivalent sites (Fig. 37.4). Of the malignant bony lesions, metastases and Ewing's sarcoma tend to occur centrally in the body and tuberosity of the calcaneus, but osteosarcoma has no predilection for site.

37.2.3.2 Radiographic Features

It is usually possible to characterise the aggressiveness of the tumour from the radiograph, but when analysing the radiographic features in the foot, some modifications have to be borne in mind. Lesions in the foot do not have to achieve a large size to become symptomatic. The small size of many bones means that involvement of an entire bone is not uncommon. Early bone destruction and periosteal reaction are more easily detected in the small, thin tubular bones of the forefoot than in the larger bones of the midfoot and hindfoot. Intralesional mineralisation is readily detected and should suggest a lesion of osseous or cartilaginous origin (Fig. 37.1).

37.2.3.3 Cross-sectional Imaging

The main role of bone scintigraphy is in the distant staging of malignant tumours and it is of limited value in the assessment of benign bone tumours. However, it may play a significant role in the detection of osteoid osteoma (Fig. 37.5). The main role of CT and MR imaging is in staging but both may also be helpful in characterization. Both are accurate at depicting intralesional fat and fluid but CT is more accurate at detecting mineralization. In many cases, tissue characterisation based on density and signal intensities is not possible but some

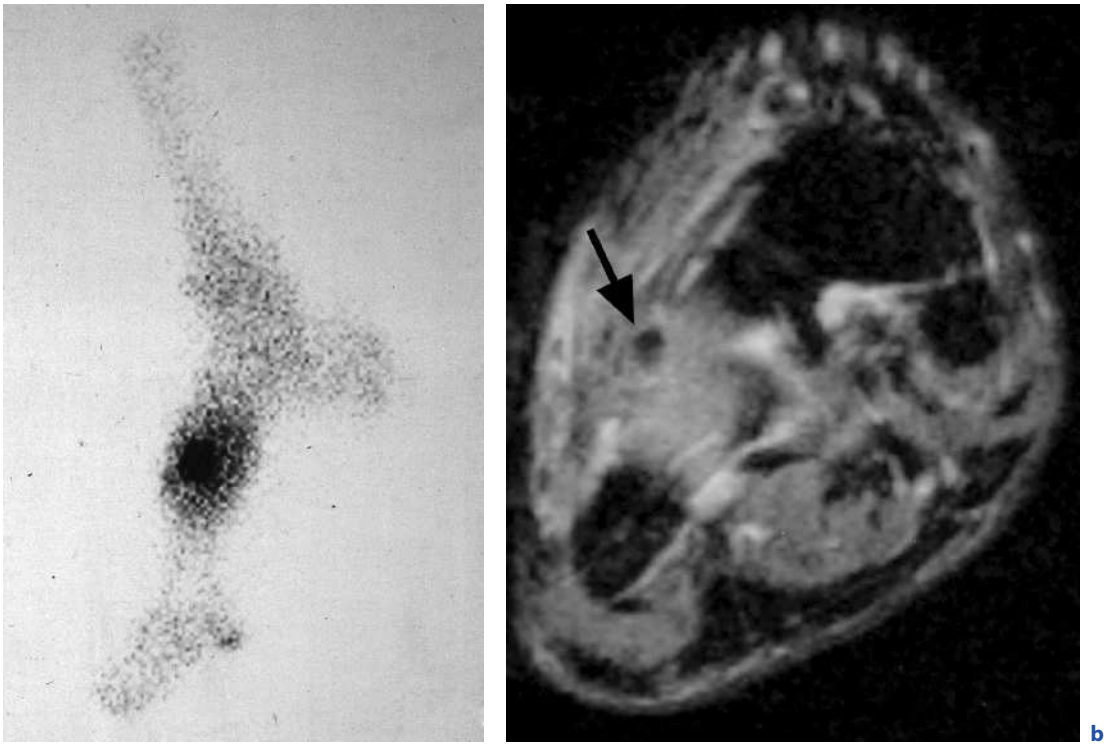

a b

Fig. 37.5a–e. Subperiosteal osteoid osteoma of the cuboid bone in a 53-year-old male with a 3 year history of foot pain. Radiographs were normal. Lateral bone scintigram (**a**) showing the "double density" sign in the midfoot region. Coronal STIR (**b**) (**c–e**) *see next page*

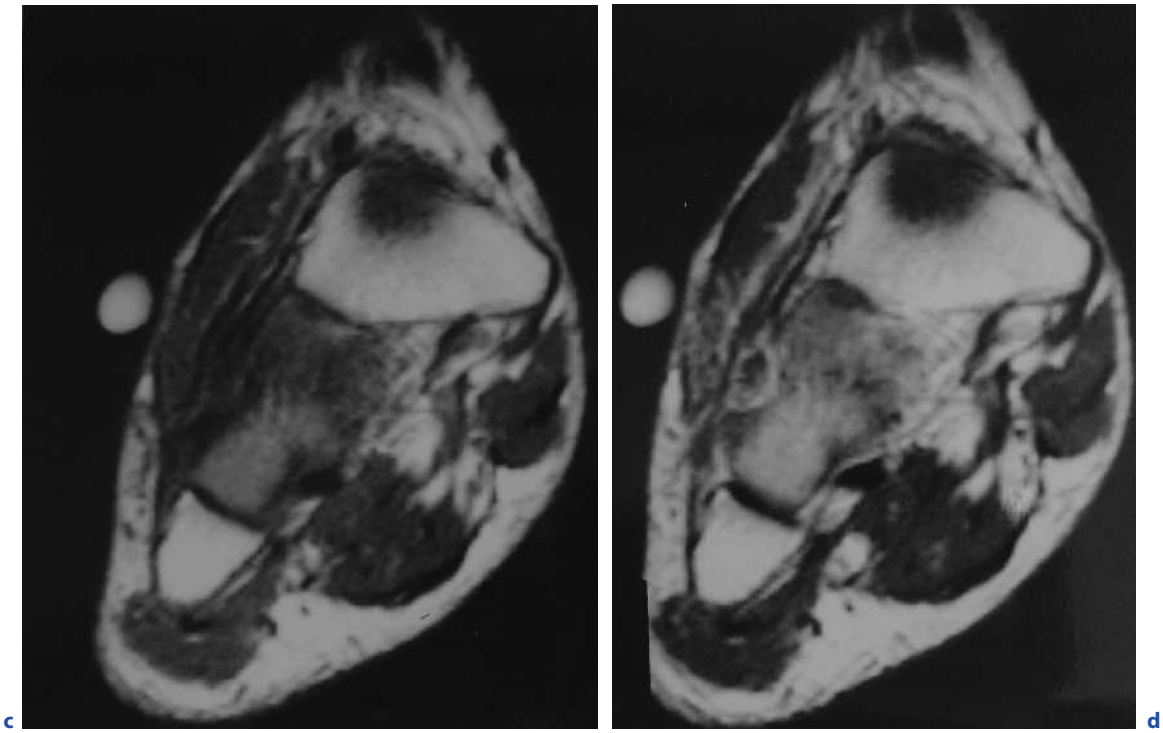

c d

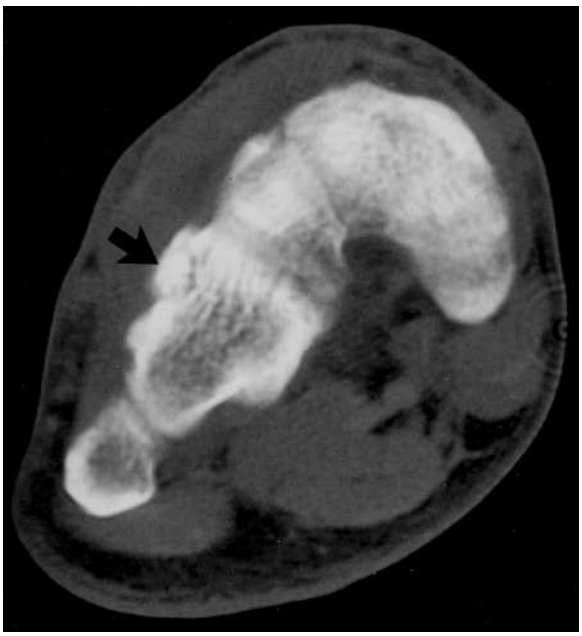

e

Fig. 37.5a–e. (*continued*) pre- (**c**) and post-intravenous (**d**) Gad DTPA T1-weighted MR images. Small hypointense, subperiosteal lesion arising from the dorsal aspect of the cuboid bone with marked oedema in the surrounding marrow and overlying soft tissues (*black arrow*). Note the marked rim enhancement around the central non-enhancing part of the nidus and more diffuse enhancement in the adjacent tissues. On the corresponding CT image at bone settings (**e**), prominent mineralization is confirmed within the non-enhancing part of the nidus (*black arrow*)

lesions may have characteristic findings. These include intraosseous ganglia, simple bone cysts and lipomas. The detection of fluid-fluid levels (sedimentation effect) in an expansile bone lesion in an adolescent is highly suggestive of an aneurysmal bone cyst, although fluid-fluid levels may also be seen in other lesions including giant-cell tumour and chondroblastoma (Fig. 37.6). Perilesional marrow oedema might suggest a sarcoma but this is not uncommon with several benign lesions including osteoid osteoma, osteoblastoma, stress fracture and infection. However, if there is also a fluid filled cavity with the "penumbra" sign on MR imaging then a bone abscess can be confidently diagnosed (Grey et al. 1998). Mature bone infarcts have a typical radio-

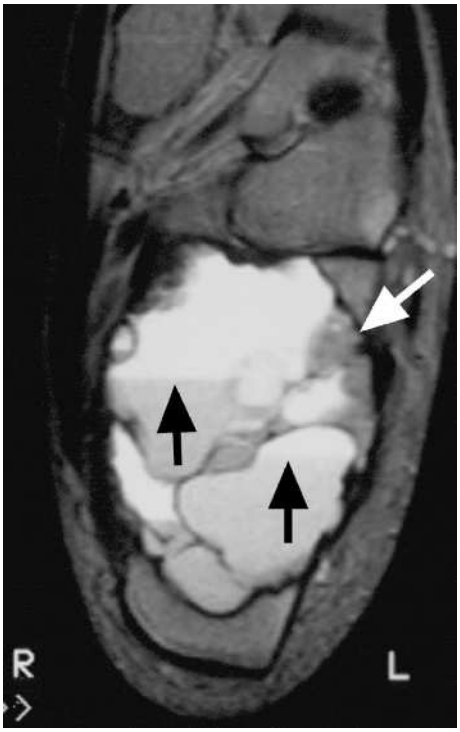

Fig. 37.6. Giant cell tumour with secondary aneurysmal bone cyst formation in a 22-year-old man. Transverse T2-weighted MR image shows a large, expansile lesion occupying most of the marrow cavity of the calcaneus. There are multiple fluid-fluid levels due to the sedimentation effect of blood products within the loculi of the lesion (*black arrows*). On the lateral aspect of the lesion, a small focus of intermediate signal intensity tissue represents solid tissue of the underlying giant cell tumour (*white arrow*)

graphic appearance but in early infarcts, radiographs may show non-specific mottled bone rarefaction, sometimes with mild reactive sclerosis, mimicking infection or malignancy. In this situation, MR imaging is helpful as it demonstrates the "double line" sign on T2-weighted images, diagnostic of osteonecrosis (Abrahim-Zadeh et al. 1998).

37.2.4 Management

Further management will depend on an analysis of the imaging features in conjunction with the patient's age and clinical presentation. Some benign lesions such as a bone island and intra-osseous lipoma are discovered incidentally and can be regarded as 'leave me alone' lesions that do not require further imaging, biopsy or follow-up. However, when a primary malignant, symptomatic benign or indeterminate lesion is suspected, local staging will be required to assess the tumour extent prior to biopsy and further management.

Accurate staging of foot tumours requires high quality cross-sectional imaging and optimal MR imaging involves high resolution coils and appropriate protocols. Focal lesions in the forefoot or hindfoot may only require MR imaging of those specific areas whereas more extensive lesions may need a scan of the whole foot. As the bones of the foot are in close proximity, scanning in all three planes is usually required. For lesions in the hindfeet, orthogonal planes are usually obtained but for lesions of the mid- and forefeet, the transverse images are usually performed in an oblique plane, parallel to the plane of the midfoot bones.

Most protocols include a combination of T1-weighted, T2-weighted and fat suppressed T2-weighted or STIR sequences.

The majority of bone sarcomas of the foot, whether low or high grade, are extracompartmental and infiltration of adjacent structures is common (Ogose et al. 1997; Shaylor et al. 2000). Extraosseous spread may result in a more radical resection but in general, a primary bone malignancy distal to the metatarsophlangeal joint should be considered for toe amputation or ray resection, whereas lesions of the hindfoot usually require below knee amputation. In one study of 23 bone sarcomas of the foot at a tertiary referral centre, inappropriate surgery had been performed initially in nine cases (Shaylor et al. 2000). Five of these patients required subsequent amputation, two of which were below-knee.

37.3 Benign Tumours and Tumour-like Lesions

37.3.1 Benign Mineralizing Lesions

Osteoid osteoma is the most common benign tumour of the foot with the majority found in the superior aspect of the talar neck and subarticular portions of the calcaneus. As with more proximal lesions, osteoid osteoma has a peak incidence in the second decade. The nidus usually measures less than 1 cm in size and is often mineralised, especially in cancellous lesions. Although cortical lesions in the forefoot are usually detectable on radiographs, the majority of lesions in the hind- and midfoot are intra-medullary or sub-periosteal, provoke little osteoblastic response and may be radiographically

occult (Fig. 37.5). Similarly, the characteristic 'double density sign' on bone scintigraphy, commonly seen in cortical lesions is often absent in intra-articular lesions due the generalized uptake of the associated synovitis. Cross-sectional imaging is usually required for confirmation and precise localization and CT is preferred over MR imaging. On MR imaging, the nidus of intra-articular lesions is often obscured by marrow oedema in 21% and is poorly identified in a further 29% (Davies et al. 2002). On the other hand, CT readily detects the nidus and helps plan arthroscopic or percutaneous resection or CT-guided thermoablation. However, patients often undergo MR imaging for unexplained foot pain and it is important to recognize the typical MR features of osteoid osteoma.

Osteoblastoma is histologically similar to osteoid osteoma and also has a predilection for a sub-periosteal location on the dorsal aspect of the talar neck. The nidi of most osteoblastomas are greater than 1.5 cm although up to 10% of osteoblastomas in the foot may also be less that 1 cm in size (Temple et al. 1998). Furthermore, other classical features of osteoblastoma including lack of surrounding sclerosis, expanded periosteal shell and soft tissue mass may also be present with subperiosteal osteoid osteoma. Matrix mineralization is present in over 50% of osteoblastomas. Occasionally, osteoblastoma can be locally aggressive with infiltration of adjacent structures (Miyayama et al. 1993). Rarely, true osteosarcomatous transformation with metastases has been recorded (Temple et al. 1998).

Chondroblastoma favours an epiphyseal or subarticular location, which accounts for the high incidence in the subarticular regions of the talus and calcaneus and calcaneal apophysis (Fink et al. 1997). In the foot, there is a higher male predominance (80%) and presentation tends to be in the third decade rather than the second decade with more proximal lesions. Radiographically, lesions are typically translucent, with well-defined, often sclerotic margins and mineralisation can be present in up to 54% (Davila et al. 2004). Endosteal scalloping or expansion is present in almost 70% and cystic features in 50%. Subchondral fractures are frequent but often radiographically occult. On MR imaging, lesions are typically inhomogeneous and surrounding marrow oedema is common (Fig. 37.4). On T2-weighted MR images, the solid components often contain variable amounts of intermediate/low signal intensity tissue due to haemosiderin, calcifications and chondroblastic hypercellularity. The cystic components often display fluid-fluid levels due to the sedimentation of altered blood products (Davila et al. 2004). Cystic components are also features of aneurysmal bone cyst, giant cell tumour, simple bone and ganglion cysts but the presence of mineralization should suggest a cartilaginous or osteoblastic neoplasm. Occasionally, a more aggressive appearance may be seen, termed 'aggressive' or 'malignant' chondroblastoma (Kyriakos et al. 1985).

Chondroma (enchondroma) is the most common benign bone tumour of the forefoot. Approximately 90% of foot chondromas occur in the forefoot and 75% of these are in the phalanges. Chondromas most commonly present with a painless swelling or pathological fracture in the third and fourth decades. Radiographs typically display a well-defined, expansile, lytic lesion that may contain punctate or stippled calcifications and a mean size of 2.7 cm (Fig. 37.1) (Gajewski et al. 2006). Periosteal chondroma is uncommon and usually displays a rim of reactive bone (Ricca et al. 2000). Cartilage tumours often have characteristic MR appearances. On T2-weighting, thin, low signal intensity, septae are noted between the lobules of high signal intensity cartilage. Following intravenous contrast, there is typically septal and peripheral enhancement. Mineralised components show low signal intensity on all sequences. It may be difficult to distinguish enchondroma from secondary chondrosarcoma due to malignant transformation in an enchondroma but, although rare, malignancy should be suspected where the lesion measures >5 cm^2 in size or arises in the mid- or hindfoot (Gajewski et al. 2006).

37.3.2 Benign Lytic and Cystic Lesions

Giant cell tumour of the foot is a locally aggressive tumour that predominates in the hindfoot, typically in the head/neck of the talus and tuberosity and subarticular portions of the calcaneus. It has a similar female predominance (2:1) to more proximal giant cell tumours but appears to present in slightly younger patients in the third decade. Lesions tend to display more aggressive features than lesions in large bones (Biscaglia et al. 2000). The majority of lesions have an ill-defined geographic pattern of bone destruction but up to a third have a more aggressive moth-eaten pattern with cortical destruction and soft tissue infiltration. Involvement of more than one bone is not uncommon. Lesions in the metatarsal bones are often expansile and involve most of the bone. Aneurysmal cyst components and haemorrhage are noted in up to 24% of giant cell tumours (Biscaglia et al. 2000). MR images typically show an inhomogeneous appearance, with foci of variable signal intensity and often fluid-fluid levels (Fig. 37.6). In the differential diagnosis, aneurysmal bone cyst can have similar appearances but tends to occur in younger pa-

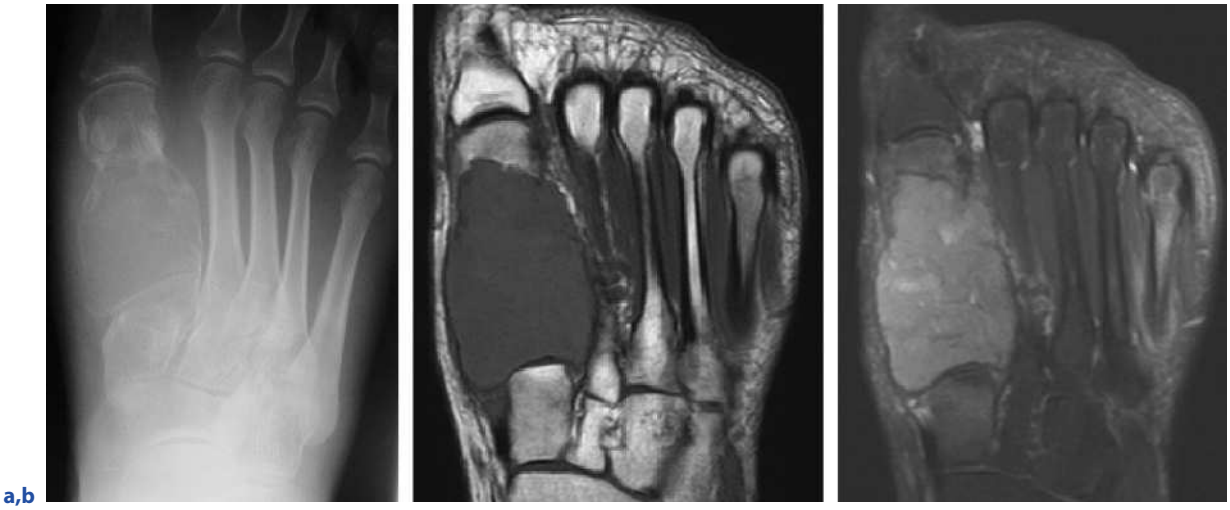

a,b c

Fig. 37.7a–c. Giant cell reparative granuloma of the first metatarsal bone in 22 year old man. AP radiograph (**a**) shows an unmineralised grossly expansile, lytic lesion involving the proximal portion and shaft of the 1st metatarsal bone with ill-defined cortical shell medially. Transverse T1-weighted (**b**) and intermediate-weighted (**c**) fat saturated MR images show a fairly homogeneous lesion with non-specific signal characteristics and intermediate signal intensity on T1-weighting and moderately hyperintense signal intensity on T2-weighting. Note also the stress fracture of the fifth metatarsal shaft with faint periosteal reaction and marrow oedema

tients, has a less aggressive pattern, lacks solid enhancing components and no soft tissue extension. Giant cell reparative granuloma may be indistinguishable from giant cell tumour but should be suggested if the patient is in the second decade and the lesion involves the forefoot (Fig. 37.7) (Murphey et al. 2001). More aggressive giant cell tumours in the second decade could mimic a Ewing's sarcoma although expansion would favour a giant cell tumour. Aggressive lesions in an older patient could mimic osteosarcoma but the presence of matrix mineralization excludes giant cell tumour. Giant cell tumour in the foot may recur more frequently than in long bone lesions and has the potential to undergo malignant transformation. Spontaneous malignant transformation is very rare (Agarwal et al. 2003). The rare multicentric giant cell tumour has a tendency to involve the feet but does not seem to carry an increased risk of pulmonary metastases (Cummins et al. 1996).

Chondromyxoid fibroma is a rare benign cartilage tumour that has a predilection for the foot, most commonly the metatarsals, calcaneus and phalanges. Radiographs typically show a slow-growing, well-defined, expansile, osteolytic lesion often with sclerotic margins (O'Connor et al. 1996). Matrix calcification is rare. In the small tubular bones of the foot, lesions often extend from the metaphysis into the diaphysis or epiphysis (Fig. 37.8). Occasionally, chondromyxoid fibroma can appear aggressive, mimicking a sarcoma. On MR imaging, lesions display inhomogeneous, intermediate to high signal intensity on T2-weighting due to chondroid, myxoid and fibrous components as well as intralesional haemorrhage. The margin of the lesion usually displays low signal intensity on all sequences, reflecting reactive bone.

Aneurysmal bone cyst can be defined as a benign, reactive, hyperaemic, expansile lesion characterized by thin walled blood filled cystic cavities. Lesions predominate in the tarsus and in particular, the posterior aspect of the calcaneus. In the thin tubular bones of the foot, lesions often expand the whole bone. Lesions are most common in the second decade and later presentation should raise the possibility of an underlying lesion, most commonly, a giant cell tumour (Fig. 37.6). In the initial phase, if growth is rapid, the periosteal reaction may be radiographically occult and the lesion may mimic an aggressive sarcoma. However, most foot lesions have a less aggressive appearance with a sharp zone of transition, cortical expansion and bony shelf/buttressing. Fluid levels, representing the sedimentation effect of blood, are frequently observed in aneurysmal bone cysts and are best demonstrated on MR imaging (Casadei et al. 1996). In primary lesions, intravenous

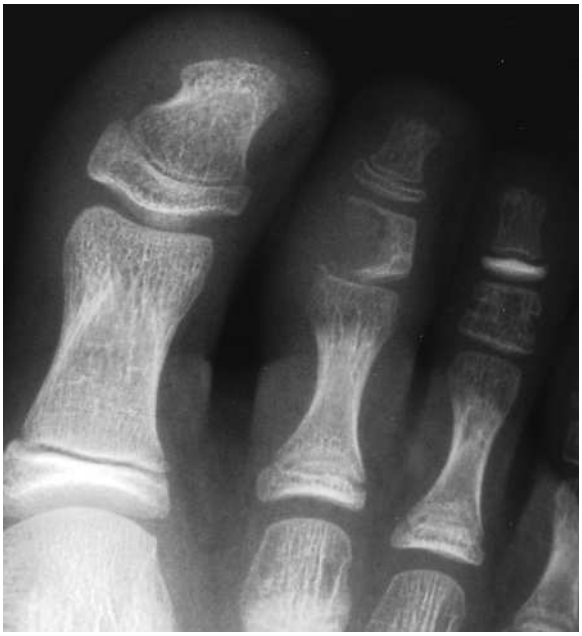

Fig. 37.8. Chondromyxoid fibroma in 12-year-old girl. AP radiograph shows a slightly irregular expansile lytic lesion of the medial aspect of the middle phalanx of the second toe. Some marginal sclerosis laterally, apparent cortical deficiency medially and breech of the articular margin proximally. Appearances are indistinguishable from an unmineralised enchondroma

contrast confirms rim and septal enhancement, whereas in secondary lesions the enhancement pattern depends on the extent and nature of the underlying lesion.

Simple bone cyst is uncommon in the foot but it does have a predilection for the calcaneus in adults. Some lesions present incidentally following minor trauma, whereas others present with chronic pain probably due to microfractures. Radiographs reveal a well-defined lytic lesion often with a sclerotic rim in the critical angle of the anterior third of the calcaneus. Pseudocysts can appear similar but are less well-defined, and internal trabeculations are often present (Stukenborg-Colsman et al. 1999). On CT and MR imaging, lesions often display fluid characteristics, although the density and signal intensity may be greater than water due to high protein content.

Intra-osseous lipoma is a rare benign tumour composed of mature adipose cells that also has a predisposition for the critical angle of the anterior calcaneus (Campbell et al. 2003). It is characterised by a well-defined, radiolucent lesion, less that 4 cm in size with a thin sclerotic rim (61%). There may be a central calcific density representing dystrophic calcification (62%) and expansion is present in up to 13% of cases (Fig. 37.3). On MRI, appearances will vary with the extent of necrosis and cyst formation but all contain at least some MR detectable fat. Calcific foci and cyst formation are common.

Intraosseous ganglia are juxta-articular cystic lesions that are much less common than their soft tissue counterparts. Most patients present in mid-adult life with intermittent pain. Radiographs show a well-defined, non-expansile, radiolucent, juxta-articular lesion with a well-defined sclerotic margin (Murff and Ashry 1994). On MR imaging, lesions are usually cystic and multiloculated and surrounding marrow oedema, soft tissue extension and an enhancing rim are common. A defect in the overlying cortex and fluid levels may also be present (Williams et al. 2004). Multilocular cystic lesions are commonly seen within the midcalcaneal body and are usually incidental findings. They are thought to arise from the anterior margin of the posterior facet of the subtalar joint (Elias et al. 2007).

37.3.3 Benign Surface Lesions

Osteochondroma (exostosis) should be differentiated from the much more common subungual exostosis that arises on the dorsal aspect of the distal phalanx of the big toe and lacks cartilage cap and marrow continuity with the underlying bone (Fig. 37.9a,b) (Lee et al. 2007). Radiographically, the lesions may be sessile or pedunculated, and the cartilage cap may show variable stippled or ring-shaped calcifications. Continued growth after maturity or pain should raise the possibility of sarcomatous degeneration, although this is rare in solitary lesions.

Bizarre parosteal osteochondromatous proliferation (BPOP) is an uncommon tumour-like lesion that is typically found on the surfaces of the proximal phalanges and metatarsal and metacarpal bones. It is most common in the third and fourth decades, has an equal sex incidence, and usually presents with a painless swelling (Walsh et al. 2006). Initially, the lesion is an immature mass of mineralisation within the soft tissues with no clear osseous attachment, but as it matures, radiographs show attachment to bone with a pedunculated or sessile base (Fig. 37.9c,d). It has been postulated that these lesions are part of a range of reactive lesions that includes florid reactive periostitis and turret exostosis (Dhondt et al. 2006). In the differential diagnosis, the lack of cortical flaring and medullary continuity excludes osteochondroma and the lack of marrow infiltration and soft

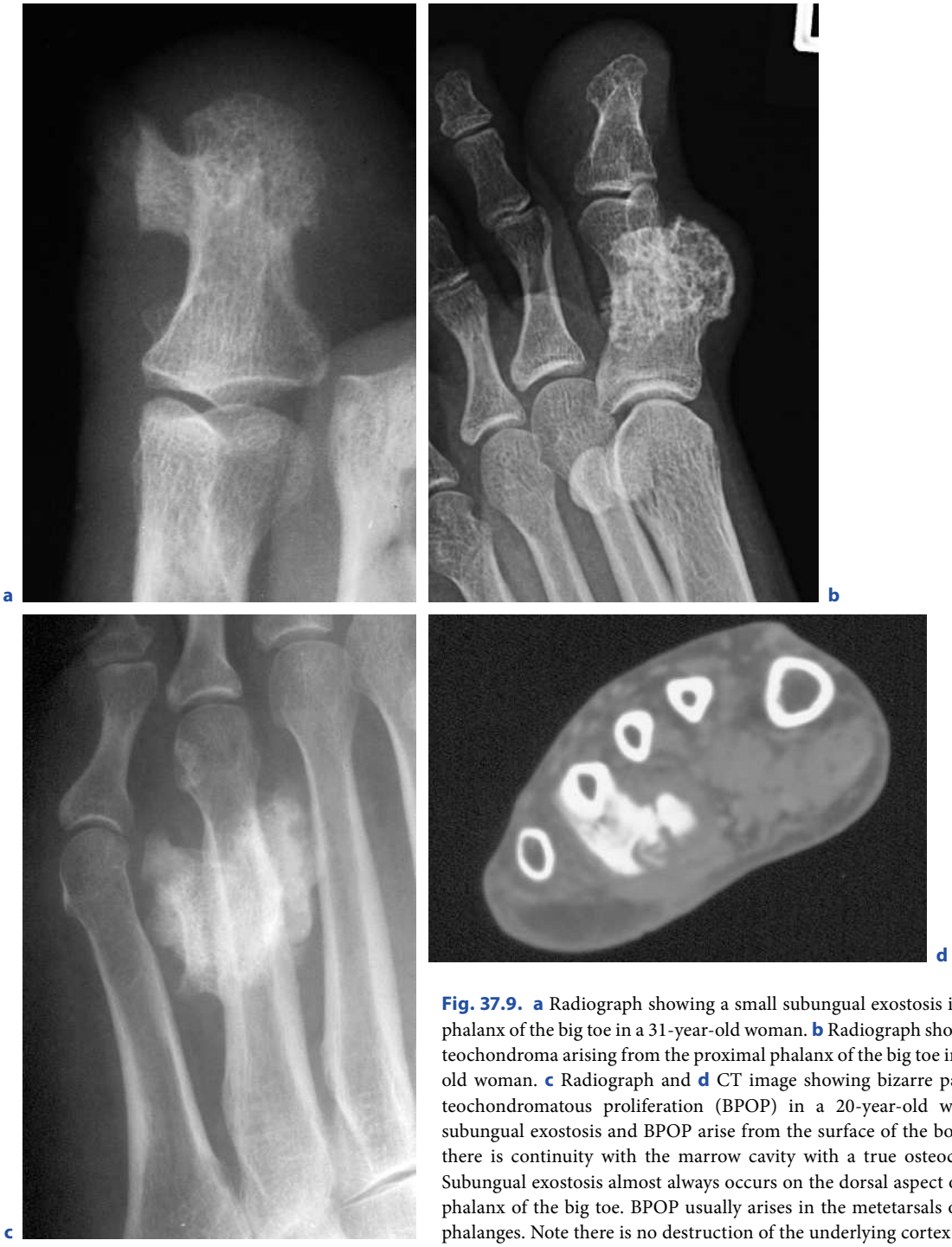

Fig. 37.9. **a** Radiograph showing a small subungual exostosis in the distal phalanx of the big toe in a 31-year-old woman. **b** Radiograph showing an osteochondroma arising from the proximal phalanx of the big toe in a 25-year-old woman. **c** Radiograph and **d** CT image showing bizarre parosteal osteochondromatous proliferation (BPOP) in a 20-year-old woman. The subungual exostosis and BPOP arise from the surface of the bone whereas there is continuity with the marrow cavity with a true osteochondroma. Subungual exostosis almost always occurs on the dorsal aspect of the distal phalanx of the big toe. BPOP usually arises in the metetarsals or proximal phalanges. Note there is no destruction of the underlying cortex

tissue mass makes bone sarcoma unlikely. Medullary involvement may be absent in the rare parosteal osteosarcoma but only one case has been described in the foot and marrow infiltration was present (Johnston et al. 1999).

37.3.4 Benign Multiple Lesions

Fibrous dysplasia is a relatively common developmental tumour-like lesion that rarely involves the foot in its

monostotic form. However, in its less common polyostotic form, 73% of patients show involvement of the foot. Polyostotic disease tends to present in the first decade with pain or pathological fracture or with endocrine problems (Albright's syndrome). Lesions are well defined and expansile usually with a sclerotic margin. The matrix is variable ranging from lucent to sclerotic. MR imaging shows a hypointense or isointense signal intensity compared with muscle on T1-weighting and variable signal intensity on T2-weighting depending on the amount of cellularity and fibrous and mineralised components (Isefuku et al. 1999). *Ollier's disease (multiple enchondromatosis)* is rare but the small tubular bones of the foot are the second most common site of involvement after the hand. In *Diaphyseal Aclasis (hereditary multiple exostoses),* 7% of the lesions occur in the foot. Malignant transformation may occur in up to 30% of patients with Ollier's disease and up to 8% of patients with Diaphyseal Aclasis although transformation in both conditions is rare in the foot.

37.4 Malignant Bone Tumours

37.4.1 Malignant Mineralising Sarcomas

Chondrosarcoma of the foot accounts for only 2.2% of all chondrosarcomas but is the second most common primary bony malignancy of the foot, accounting for 27% of lesions. The majority arise in the calcaneus and metatarsals and presentation is most commonly in the sixth and seventh decades. Chondrosarcoma of the hindfoot is more likely to metastasise than phalangeal chondrosarcoma, which only rarely metastasises and behaves as a locally aggressive lesion (Hatori et al. 2007; Bovee et al. 1999). The majority of lesions are low grade and centrally located with a geographic pattern of bone destruction. However, a more aggressive permeative pattern may also be found with higher grade lesions. In the feet, lesions are smaller than elsewhere in the skeleton, ranging between 2 cm and 5 cm in maximal size. In a large study of 75 lesions of the foot, endosteal erosion, cortical destruction and expansion were present in over 90%, ill-defined margins and a soft-tissue mass in 80%, and mineralisation in 74% (Ogose et al. 1997). The typical punctate calcifications are best shown on CT. On MR imaging, the signal characteristics may be similar to enchondroma, but chondrosarcoma should be strongly suspected where there is cortical destruction, periosteal reaction and soft-tissue infiltration (Hottya et al. 1999). Peripheral lesions are much less common than central lesions and usually arise from a pre-existing osteochondroma rather than periosteum (Fig. 37.10). The variants periosteal and clear cell chondrosarcoma of the foot and ankle have been reported but are extremely rare.

Osteosarcoma of the foot only accounts for 1% of all osteosarcomas but is the third most common primary bony malignancy of the foot accounting for 19% of ma-

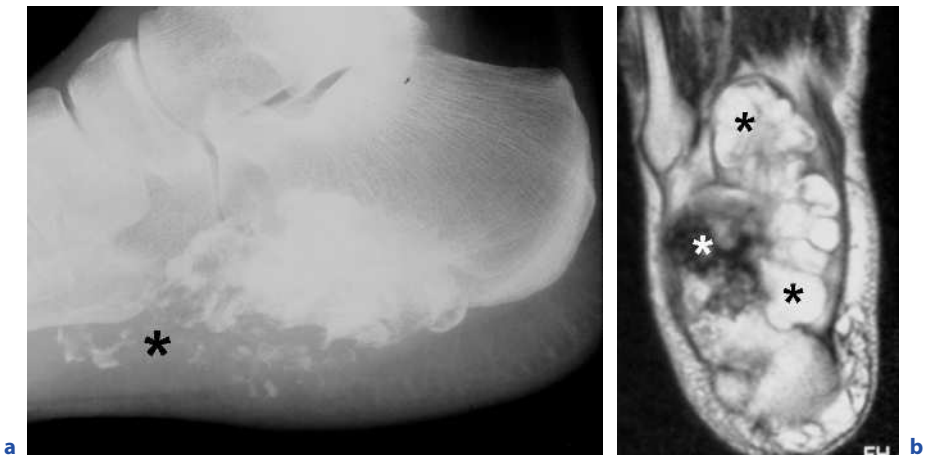

Fig. 37.10a,b. Peripheral chondrosarcoma of the calcaneus in a 43-year-old man. **a** The radiograph displays dense mineralisation over the anterior aspect of the calcaneus with punctate or stippled calcifications (*black asterisk*) in keeping with a cartilage-forming tumour. **b** Transverse T2-weighted MR image showing foci of low signal intensity mineralisation laterally (*white asterisk*) and lobules of high signal intensity unmineralised cartilage medially (*black asterisks*)

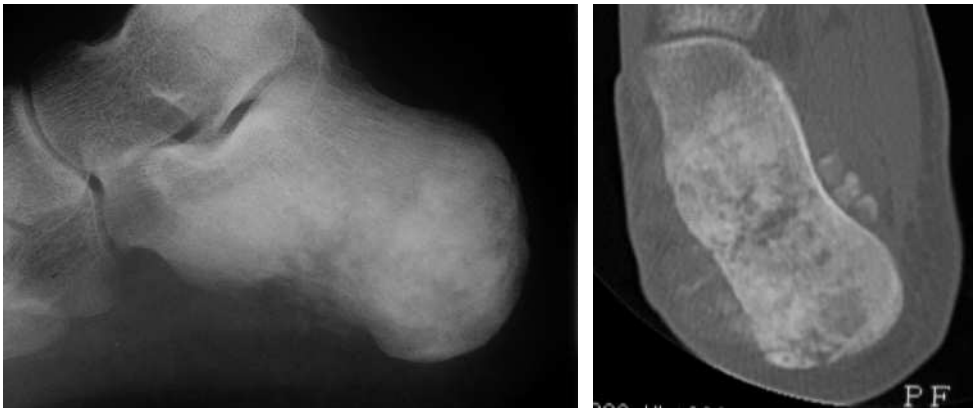

Fig. 37.11a,b. Osteosarcoma of the calcaneus in a 21-year-old female. **a** Lateral radiograph shows an ill-defined osteoblastic lesion in the mid- and posterior calcaneus with soft tissue mineralization inferiorly. **b** Transverse CT scan at bone settings confirms an osteoblastic lesion with mineralized osteoid matrix in the soft tissues

lignant primary bone tumours. Most lesions in the foot are intraosseous, osteoblastic and high grade (Choong et al. 1999). As many as 75% are located in the tarsus and 75% of those arise in the calcaneus. In contrast to osteosarcoma of the long bones, patients present most commonly in the fourth decade and the duration of symptoms can be up to 2 years. Radiographically, the majority of lesions show typical appearances with an aggressive moth-eaten or permeative pattern of bone destruction and usually soft-tissue extension. Occasionally, slow-growing lesions may be expansile with well-defined margins (Lee et al. 2000). Amorphous or cloud-like mineralisation is common and a lamellated or spiculated periosteal reaction is often present (Fig. 37.11). On MR imaging, lesions typically display low to intermediate signal intensity on T1-weighting and inhomogeneous high signal intensity on T2-weighting although mineralised foci typically display low signal intensity on all sequences. Paget's sarcoma and parosteal osteosarcoma of the foot are very rare (Johnson et al. 1999; de Waele et al. 2001).

37.4.2 Malignant Non-mineralising Sarcomas

Although only 4% of *Ewing's sarcoma* occur in the foot, Ewing's sarcoma is the most common primary bone sarcoma of the foot accounting for 28% of malignant bone tumours of the foot. Lesions are most commonly found in the calcaneus and metatarsal bones and usually present with a painful swelling in the second decade. There is a male predominance (2.3:1) and forefoot lesions usually have a shorter duration of symptoms than hindfoot lesions (Baraga et al. 2001; Adkins et al. 1997). Survival is much better in patients who present with localized disease and forefoot lesions. The prognosis is poor for the 11%–43% who have metastases at presentation (Adkins et al. 1997; Casadei et al. 2004). Most lesions in the tubular bones show "classic" appearances with an aggressive permeative pattern of bone destruction in a metadiaphyseal location and a soft-tissue mass (Fig. 37.12). In contrast, tumors in the tarsal bones are more likely to show more indolent features that may result in a delay in diagnosis (Baraga et al. 2001). The lack of mineralised matrix helps differentiate Ewing's sarcoma from osteosarcoma. On MR imaging, lesions are usually hypointense or isointense compared with muscle on T1-weighting and hyperintense and inhomogeneous on T2-weighting. Ewing's sarcoma often mimics osteomyelitis, both radiographically and clinically.

Malignant fibrous histiocytoma and *fibrosarcoma* are histologically different but are discussed together as they have similar imaging appearances. Fibrosarcoma is more common than malignant fibrous histiocytoma, but together they account for 10% of malignant bone tumours of the foot and ankle, and most present in the fourth decade (Unni 1996; Campanacci 1999). They most commonly occur in the hindfoot, and involvement of the forefoot is very rare. Radiographically, both lesions have a variable growth rate ranging from a geographic pattern of bone destruction to a more aggressive moth-eaten or permeative pattern with extensive bone destruction and soft-tissue infiltration (Link et al. 1998). The lack of mineralisation helps distinguish them from osteosarcoma or chondrosarcoma, although occa-

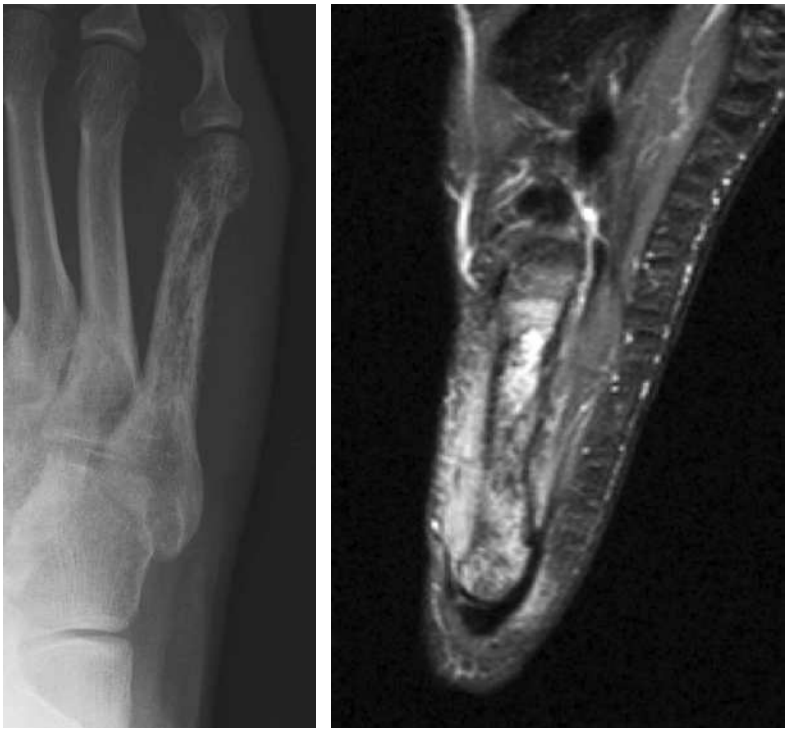

a b

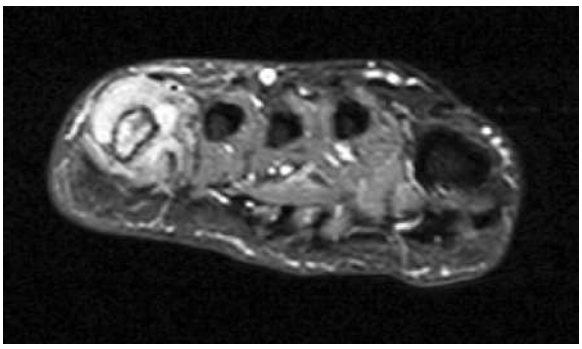

c

Fig. 37.12a–c. Ewing's sarcoma of the 5th metatarsal in a 22-year-old female. AP radiograph (**a**) displays a permeative pattern of bone destruction along the shaft of the 5th metatarsal with associated faint periosteal reaction. Sagittal (**b**) and coronal (**c**) fat suppressed intermediate weighted MR images confirm marrow replacement, cortical destruction and a parosseous soft tissue mass mainly on the dorsal aspect

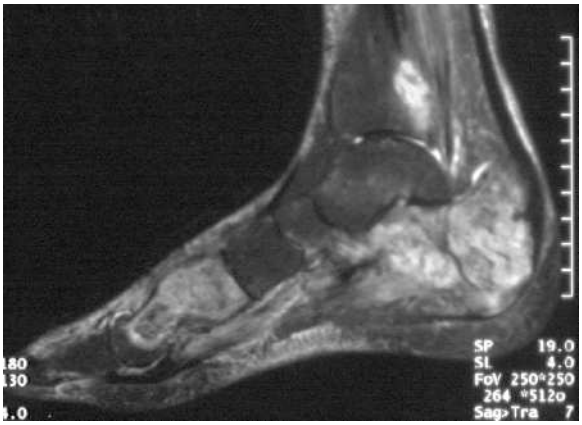

Fig. 37.13. Multifocal haemangioendothelioma in a 71-year-old woman. Sagittal STIR MR image showing several non-specific expansile lesions arising from the 1st metatarsal, calcaneus and distal tibia

sionally some mineralisation may be present. Lesions usually display non-specific intermediate signal intensity on T1-weighting and inhomogeneous high signal intensity on T2-weighting, although if the collagen content is high, then a predominantly lower signal intensity on T2-weighting may be noted. Foci of haemorrhage and necrosis may be present.

Haemangioendothelioma and *angiosarcoma* are more common in the soft tissues than bone but account for 8% of primary malignant bone tumours of the foot. Haemangioendothelioma is usually of intermediate aggressiveness and may be benign, whereas angiosarcoma is an aggressive malignant tumour with a poor prognosis (Bakotic et al. 1999). On radiographs, intermediate or low-grade lesions may present with lytic areas and a honeycombing appearance, whereas aggressive lesions demonstrate a permeative pattern of bone destruction and soft tissue infiltration. In haemangioendothelioma, multicentricity is common, and the small bones of the foot may be extensively involved (Fig. 37.13) (Boutin et al. 1996). MR imaging may show prominent vessels of variable signal intensity (depending on the blood flow) and fluid-fluid levels, but unlike haemangiomas, there is no fatty overgrowth.

37.4.3 Non-sarcomatous Bone Malignancies

Primary *lymphoma* of the foot is very rare, accounting for 3% of all primary bony malignancies of the foot and ankle. Secondary involvement to the foot is also rare and usually indicates widespread disease. Primary lymphoma has a wide age range but usually peaks in the fifth decade and is more common in males (2:1). Of the foot bones, the calcaneus is most commonly involved (Skorman and Martin 1999). Radiographically, lesions typically show an aggressive moth-eaten or permeative pattern of destruction and are predominantly lytic, although up to a third may have a mixture of lysis and sclerosis. Periosteal reaction, cortical destruction and soft-tissue extension are common. Sequestra may also be present. On MR imaging, most lesions are isointense or hypointense to skeletal muscle on T1-weighting and inhomogeneous and predominantly hyperintense on T2-weighting (White et al. 1996).

Multiple myeloma of the foot is rare, accounting for 0.3% of all myelomas and 3% of all malignant bone tumours of the foot. Solitary plasmacytoma is extremely rare in the foot and myeloma of the foot usually indi-

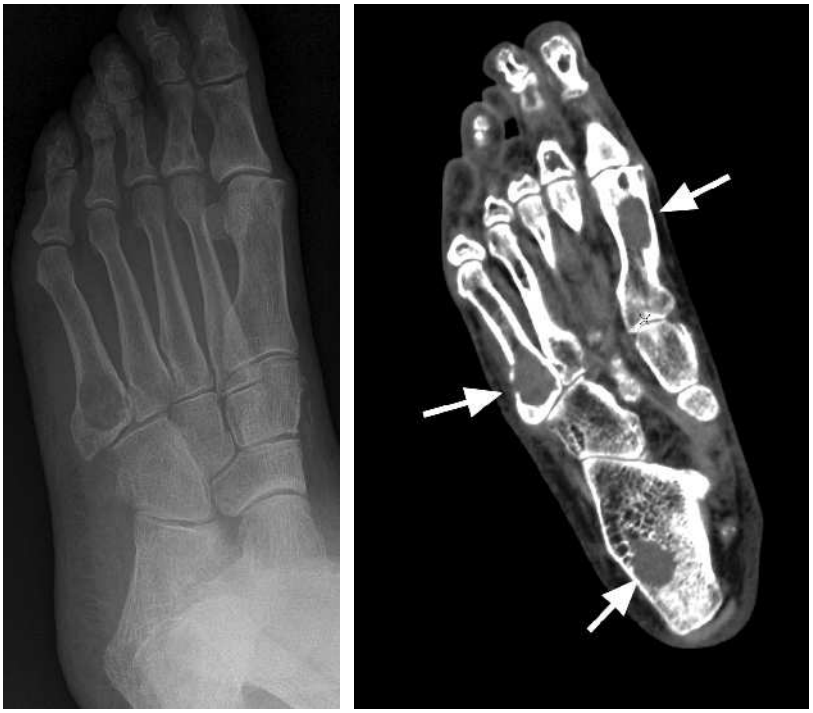

a, b

Fig. 37.14a,b. Myeloma of the 5th metatarsal bone in 73-year-old man. **a** Oblique radiograph shows a small lytic lesion in the base of the 5th metatarsal bone. **b** CT reformatted image at soft tissue settings shows further lesions in the 1st metatarsal shaft and the calcaneus (*arrows*). Biopsy confirmed myeloma. There was extensive involvement of the remainder of the skeleton

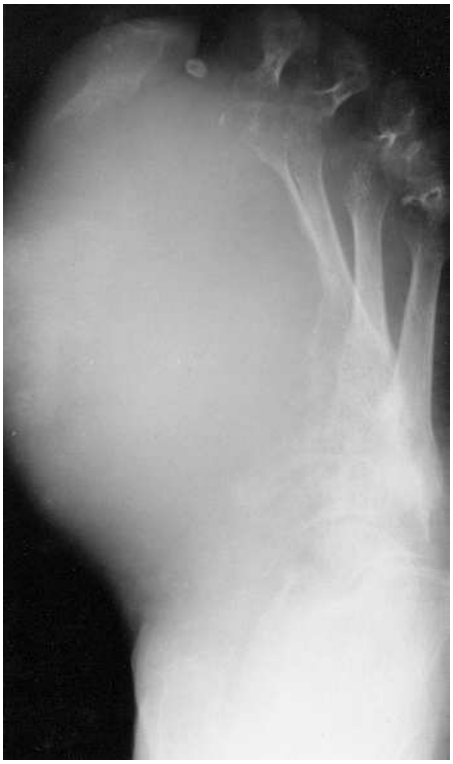

Fig. 37.15. Metastasis from colonic carcinoma. Marked destruction of the bones of the medial forefoot with a large soft-tissue mass

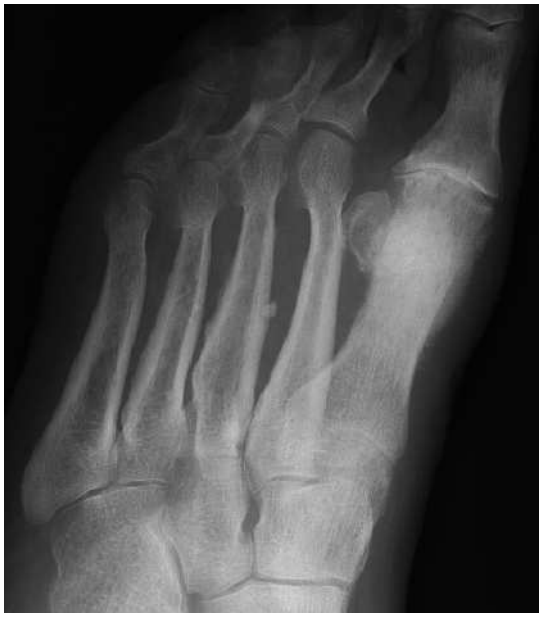

a

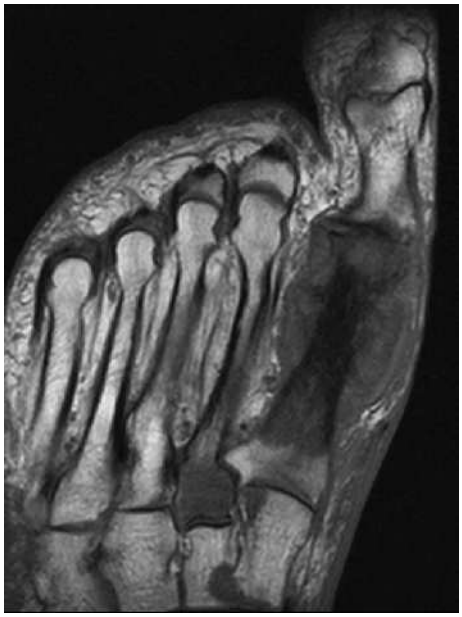

b

Fig. 37.16a,b. Prostatic metastases. **a** The oblique radiograph shows severe degenerative changes in the 1st metatarsophalangeal joint. In addition, there is also diffuse sclerosis and a periosteal reaction in the distal shaft of the 1st metatarsal bone that raised the possibility of primary mineralizing sarcoma or stress injury at an unusual site. **b** Transverse T1-weighted image of the forefoot showing an aggressive lesion arising from the first metatarsal bone with an associated parosseous soft tissue mass. Further intramedullary lesions are noted in the base of the second metatarsal and intermediate cuneiform bones. Biopsy of the 1st metatarsal bone confirmed prostatic metastasis and scintigraphy (not shown) confirmed widespread bone metastases

cates widespread involvement with marrow reconversion. Most of these involve the calcaneus (Daibata et al. 2005). Radiographically, lesions are osteolytic with a geographic pattern of bone destruction and variable margins (Fig. 37.14). The MR appearances are non-specific.

Metastases to the foot are rare, with a reported incidence of <0.3% (Libson et al. 1987). However, it is likely that the true incidence is higher in disseminated disease (Maheshwari et.al. 2008). Primary tumours are mostly due to adenocarcinoma from the colon (17%), kidneys (17%), lung (15%), bladder (10%), and breast (10%). Occasionally a foot metastasis may present without a known primary. In the foot, the tarsal bones are more commonly involved than the forefoot, and the majority of these occur in the calcaneus. Involvement of several foot bones is common and may result in massive bone loss (Fig. 37.15). Radiographically, 80% of metastases are purely osteolytic, but prostatic metastases are usually sclerotic, and breast, bladder and gastrointestinal primaries may be lytic, sclerotic or mixed (Fig. 37.16). The MR imaging features are variable.

Acknowledgements

The author would like to thank Jean Campbell of the Scottish Bone Tumour Registry for her assistance in collecting images and Dr A M Davies for several cases.

References

Abrahim-Zadeh R, Klein RM, Leslie D, Norman A (1998) Characteristics of calcaneal bone infarction: an MR imaging investigation. Skel Radiol 27:321—324

Adkins CD, Kitaoka HB, Seidl RK, Pritchard DJ (1997) Ewing's sarcoma of the foot. Clin Orthop 343:173–182

Agarwal K, Bajaj P, Aiyer HM, Sood LK (2003) Giant cell tumour of talus with osteosarcomatous transformation in a young male: a case report. Indian J Pathol Microbiol 46:215–217

Bakotic BW, Robinson M, Williams M, Van Woy T, Nutter J, Borkowski P (1999) Aggressive epithelioid hemangioendothelioma of the lower extremity: a case report and review of the literature. J Foot Ankle Surg 38:352–358

Baraga JJ, Amrami KK, Swee RG et al. (2001) Radiographic features of Ewing's sarcoma of the bones of the hands and feet. Skel Radiol 30:121–126

Berlin SJ (1995) Statistical analysis of 307,601 tumors and other lesions of the foot. J Am Podiatr Med Assoc 85:699–703

Biscaglia R, Bacchini P, Bertoni F (2000) Giant cell tumor of the bones of the hand and foot. Cancer 88:2022–2032

Boutin RD, Spaeth HJ, Mangalik A, Sell JJ (1996) Epithelioid haemangioendothelioma of bone. Skel Radiol 25:391–395

Bovee JV, Van der Heul RO, Taminiau AH et al. (1999) Chondrosarcoma of the phalanx: a locally aggressive lesion with minimal metastatic potential: a report of 35 cases and a review of the literature. Cancer 86:1724–1732

Campanacci F (1999) Bone and soft tissue tumours. Springer, Berlin Heidelberg New York

Campbell RS, Grainger AJ, Mangham DC, Beggs I, Teh J, Davies AM (2003) Intraosseous lipoma: report of 35 new cases and a review of the literature. Skel Radiol 32:209–222

Casadei R, Ferraro A, Ferruzzi A, Biagini R, Ruggieri P (1991) Bone tumors of the foot: epidemiology and diagnosis. Chir Organi Mov 76:47–62

Casadei R, Ruggieri P, Moscato M, Ferraro A, Picci P (1996) Aneurysmal bone cyst and giant cell tumor of the foot. Foot Ankle Int 17:487–495

Casadei R, Magnani M, Biagini R, Mercuri M (2004) Prognostic factors in Ewing's sarcoma of the foot. Clin Orthop Relat Res 420:230–238

Choong PF, Qureshi AA, Sim FH, Unni K (1999) Osteosarcoma of the foot: a review of 52 patients at the Mayo Clinic. Acta Orthop Scand 70:361–364

Cummins CA, Scarborough MT, Enneking WF (1996) Multicentric giant cell tumor of bone. Clin Orthop 322:245–252

Daibata M, Bandobashi K, Taguchi H (2005) Calcaneus involvement by multiple myeloma. Am J Hematol 80:311–312

Davies M, Cassar-Pullicino VN, Davies AM, McCall IW, Tyrrell PN (2002) The diagnostic accuracy of MR imaging in osteoid osteoma. Skel Radiol 31:559–569

Davila JA, Amrami KK, Sundaram M, Adkins MC, Unni KK (2004) Chondroblastoma of the hands and feet. Skel Radiol 33:582–587

de Waele S, Lonneux M, Vande Berg B, Nzeusseu A, Brasseur JP, Lecouvet FE (2001). Paget disease and osteosarcoma of the calcaneus. Clin Nucl Med 26:244–246

Dhondt E, Oudenhoven L, Khan S, Kroon HM, Hogendoorn PC, Nieborg A, Bloem JL, De Schepper A (2006) Nora's lesion, a distinct radiological entity? Skel Radiol 35:497–502

Elias I, Zoga AC, Raikin SM, Schweitzer ME, Morrison WB (2007) Incidence and morphologic characteristics of benign calcaneal cystic lesions on MRI. Foot Ankle Int 28:707–714

Fink BR, Temple HT, Chiricosta FM, Mizel MS, Murphey MD (1997) Chondroblastoma of the foot. Foot Ankle Int 18:236–242

Gajewski DA, Burnette JB, Murphey MD, Temple HT (2006) Differentiating clinical and radiographic features of enchondroma and secondary chondrosarcoma in the foot. Foot Ankle Int 27:240–244

Grey AC, Davies AM, Mangham DC, Grimer RJ, Ritchie DA (1998) The 'penumbra sign' on T1-weighted MR imaging in subacute osteomyelitis: frequency, cause and significance. Clin Radiol 53:587–592

Hatori M, Watanabe M, Kokubun S (2007) Chondrosarcoma of the distal phalanx of the great toe. J Am Podiatr Med Assoc 97:156–159

Hottya GA, Steinbach LS, Johnston JO, van Kuijk C, Genant HK (1999) Chondrosarcoma of the foot: imaging, surgical and pathological correlation of three new cases. Skel Radiol 28:153–158

Hussain A, Basu D, Irwin A (2005) Osteoid osteoma of the lateral cuneiform bone: presentation following trauma. Foot 15:133–136

Isefuku S, Hatori M, Ehara S, Hosaka M, Ito K, Kokubun S (1999) Fibrous dysplasia arising from the calcaneus. Tohoku J Exp Med 189:227–232

Johnson K, Davies AM, Mangham DC, Grimer RJ (1999) Parosteal osteosarcoma of a metatarsal with intramedullary invasion. Skel Radiol 28:111–115

Kyriakos M, Land VJ, Penning HL, Parker SG (1985) Metastatic chondroblastoma. Report of a fatal case with a review of the literature on atypical, aggressive, and malignant chondroblastoma. Cancer 55:1770–1789

Lee EY, Seeger LL, Nelson SD, Eckardt JJ (2000) Primary osteosarcoma of a metatarsal bone. Skel Radiol 29:474–476

Lee SK, Jung MS, Lee YH, Gong HS, Kim JK, Baek GH (2007) Two distinctive subungual pathologies: subungual exostosis and subungual osteochondroma. Foot Ankle Int 28:595–601

Libson E, Bloom RA, Husband JE, Stoker DJ (1987) Metastatic tumours of bones of the hand and foot. A comparative review and report of 43 additional cases. Skel Radiol 16:387–392

Link TM, Haeussler MD, Poppek S, Wortler K, Heindel W (1998) Malignant fibrous histiocytoma of bone: conventional X-ray and MR imaging features. Skel Radiol 27:552–558

Maheshwari AV, Chiapetta G, Kugler CD, Pitcher JD Jr, Temple HT (2008) Metastatic skeletal disease of the foot: case reports and literature review. Foot Ankle Int 29:699–710

Miyayama H, Sakamoto K, Ide M, Ise K, Hirota K, Yasunaga T, Ishihara A (1993) Aggressive osteoblastoma of the calcaneus. Cancer 71:346–353

Murari TM, Callaghan JJ, Berrey B, Sweet DE (1989) Primary benign and malignant osseous neoplasms of the foot. Foot Ankle 10:68–80

Murff R, Ashry HR (1994) Intraosseous ganglia of the foot. J Foot Ankle Surg 33:396–401

Murphey MD, Nomikos GC, Flemming DJ, Gannon FH, Temple HT, Kransdorf MJ (2001) From the archives of AFIP. Imaging of giant cell tumor and giant cell reparative granuloma of bone: radiologic-pathologic correlation. Radiographics 21:1283–1309

O'Connor PJ, Gibbon WW, Hardy G, Butt WP (1996) Chondromyxoid fibroma of the foot. Skel Radiol 25:143–148

Ogose A, Unni KK, Swee RG, May GK, Rowland CM, Sim FH (1997) Chondrosarcoma of small bones of the hands and feet. Cancer 80:50–59

Ozdemir HM, Yildiz Y, Yilmaz C Saglik Y (1997) Tumors of the foot and ankle: analysis of 196 cases. J Foot Ankle Surg 36:403–408

Ricca RL Jr, Kuklo TR, Shawen SB, Vick DJ, Schaefer RA (2000) Periosteal chondroma of the cuboid presenting in a 7-year-old-boy. Foot Ankle Int 21:145–149

Shaylor PJ, Abudu A, Grimer RJ, Carter SR, Tillman RM (2000) Management and outcome of surgical treatment of primary malignant tumours of the foot. Foot 10:157–163

Skorman SE, Martin R (1999) Primary lymphoma of the calcaneus with recurrence in the distal tibia: a case report. J Foot Ankle Surg 38:278–282

Stukenborg-Colsman C, Wulker N, Wirth CJ (1999) Cystic bone lesions of the calcaneus: a report of five cases. Foot Ankle Surg 5:33–38

Temple HT, Mizel MS, Murphey MD, Sweet DE (1998) Osteoblastoma of the foot and ankle. Foot Ankle Int 19:698–704

Unni K (1996) Dahlin's bone tumors: general aspects and data on 11,087 cases, 5th edn. Lippincott-Raven, Philadelphia

Walsh JC, Murphy D, Freihaut RB, O'Keane JC, Stephens MM (2006) Bizarre parosteal osteochondromatous proliferation of the fifth metatarsal (Nora's lesion) – Case report. Foot Ankle Surg 12:211–214

White LM, Siegel S, Shin SS, Weisman MH, Sartoris DJ (1996) Primary lymphoma of the calcaneus. Skel Radiol 25:775–778

Williams HJ, Davies AM, Allen G, Evans N, Mangham DC (2004) Imaging features of intraosseous ganglia: a report of 45 cases. Eur Radiol 14:1761–1769

Compartmental Anatomy

38

Kavita M. Patel and Nancy M. Major

CONTENTS

KEY POINTS

- Radiographic determination of tumor site (T) for the purpose of tumor staging requires an understanding of the compartmental boundaries of the upper and lower extremity.
- Knowledge of radiographic cross-sectional anatomy in the transverse plane is essential not only for determination of the intra or extra-compartmental nature of a bone tumor but also to prevent upstaging of surgical treatment due to contamination during image-guided percutaneous biopsy.
- A poorly planned biopsy can convert an intra-compartmental tumor into an extra-compartmental tumor by passing the biopsy needle through a previously unaffected compartment, potentially obviating the possibility for limb-sparing surgery.

38.1 Relevance of Compartmental Anatomy to Grading of Bone Tumors

In 1980, the Musculoskeletal Tumor Society, under the chairmanship of Dr. W. F. Enneking, proposed a staging system for bone and soft tissue tumors of the skeletal system (Enneking 1985; Enneking et al. 1980). Its purpose was not only to outline prognosis but also to guide surgical management. The three components of the staging system are grade (G), site (T), and presence of metastasis (M). Lesions are stratified as benign (G_0), low grade (G_1) or high grade (G_3) by incorporating histologic grade, radiologic appearance and clinical behavior, and require the triad of expertise of the pathologist, radiologist and orthopedic surgeon. Lesions are also stratified by site (T) as intra-capsular and in-

K. M. Patel, MD
Musculoskeletal Radiology Fellow (2007–2008), Duke University Medical Center, Durham, NC 27710, USA
N. M. Major, MD
Associate Professor of Radiology and Surgery, Biological Anthropology and Anatomy, Duke University Medical Center, Durham, NC 27710, USA

tra-compartmental (T_0), extra-capsular and intra-compartmental (T_1), and extra-compartmental (T_2). The presence (M_0) or absence (M_1) of metastases to either regional lymph nodes or distant organs, determines the third component of the Musculoskeletal Tumor Society (MTS) staging system (Enneking 1985). A combination of grade (G), site (T), and presence or absence of metastasis (M) ultimately stratifies the tumor as Stage I – low grade, Stage II – high grade or Stage III – metastatic. All metastatic lesions are classified as Stage III. Stage I and Stage II lesions are differentiated based on a combination of radiologic appearance and histologic grade (G) (Enneking 1985; Enneking et al. 1980).

The role of the musculoskeletal radiologist is to (1) determine tumor location, size and involvement of surrounding neurovascular structures (2) determine the radiographic component of tumor grade (G) and (3) determine tumor site (T). Radiographic criteria for determination of grade (G) include, in order of priority, characterization of the pattern of bony destruction (geographic, moth eaten or permeative), presence or absence of cortical penetration, presence or absence of a sclerotic rim, and presence or absence of an expanded cortical shell (Lodwick et al. 1980).

Radiographic determination of site (T) requires an understanding of the compartmental boundaries of the upper and lower extremity. Each bone is considered an individual compartment and tumors arising from bone are defined as intra or extra-compartmental based on breach of the adjacent bony cortex, periosteum or overlying articular cartilage, with extension into the adjacent soft tissues. The para-osseous space is a separate compartment and tumors arising in a para-osseous location are defined as intra or extra-compartmental based on extension into the adjacent bone or deep fascial planes. Tumors arising from the joint are defined as intra or extra-compartmental based on breach of the synovial and capsular tissues with extension out of the joint and into the adjacent soft tissues.

The three stages of malignant bone tumors are coupled with the designation of either A or B depending on whether the lesion is intra-compartmental (A) or extra-compartmental (B). Surgical treatment of bone tumors can be broadly categorized as either limb salvage (intra-capsular excision, marginal excision, wide "en bloc" excision or radical resection) or amputation, with or without disarticulation. Malignant intra-compartmental lesions require at least wide excision. Malignant extra-compartmental (B) lesions require radical resection of all involved compartments which may necessitate amputation (Toomayan et al. 2005). Knowledge of radiographic cross-sectional anatomy in the transverse plane is essential not only for determination of the intra or extra-compartmental nature of a bone tumor but also to prevent upstaging of surgical treatment due to contamination during image-guided percutaneous biopsy. Upstaging of a bone tumor by contamination of a previously tumor-free compartment could require a more extensive surgical procedure for treatment.

38.2 Compartmental Anatomy of the Upper and Lower Extremity

38.2.1 Compartments of the Thigh and Pelvic Girdle

Above the knee joint, the soft tissues of the lower extremity are divided into three compartments: anterior, posterior and medial (Figs. 38.1 and 38.2). The anterior compartment is the most proximal of the three compartments, and most proximally contains the tensor fascia lata and sartorius muscles at the level of the anterior superior iliac spine. More distally, the anterior compartment expands to include the rectus femoris muscle with its origin on the anterior inferior iliac spine, and the vastus medialis, vastus lateralis and vastus intermedius, from their origins on the proximal anterior femur. The distal aspect of the iliopsoas muscle, prior to its insertion on the lesser tuberosity, can be functionally classified in the anterior compartment, although its innervation differs from the other muscles of the anterior compartment, which are innervated by the femoral nerve. The anterior compartment is largest at the level of the mid-distal femoral diaphysis, where it occupies the anterior half of the thigh musculature. The sartorius muscles deserves special mention – it is classified as a structure in the anterior compartment with its proximal origin on the anterior superior iliac spine; however, the muscle crosses over the thigh, inferomedially towards the knee joint and joins with the insertions of the gracilis (medial compartment) and semi-tendinosis (posterior compartment) tendons at the pes anserine on the anteromedial tibia. The MTS staging system specifically delineates certain anatomical regions as extra-compartmental, because the loose fascial tissues of these spaces cannot restrict longitudinal spread of tumor (Enneking 1985; Enneking et al. 1980). Extra-compartmental spaces in the thigh include the groin and femoral triangle, which contains a main neurovascular bundle of the lower extremity. Tumor can spread between compartments along the neurovascular bundles.

The posterior compartment of the thigh is innervated by and contains the sciatic nerve as well as the

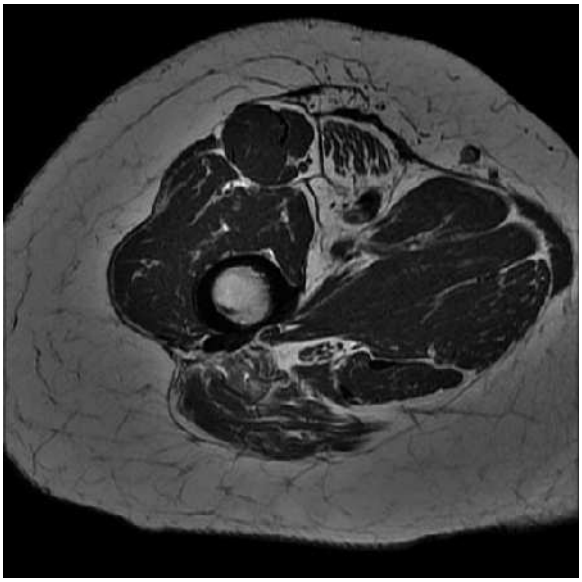

a

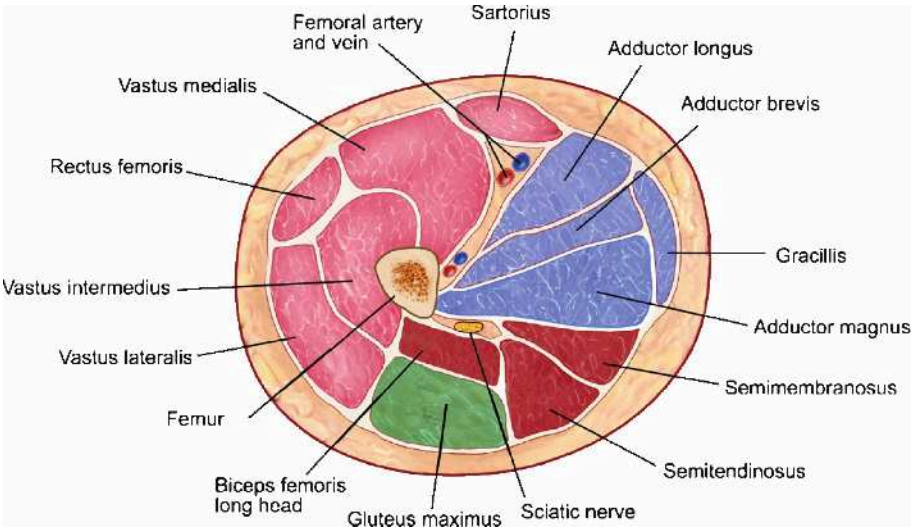

b

Fig. 38.1. **a** Transverse T1-weighted MR image of the proximal thigh. **b** Diagram in the transverse plane illustrating the contents of the anterior (*pink shading*), posterior (*red shading*) and medial (*blue shading*) compartments of the proximal thigh. The gluteus maximus (*green shading*) is extra-compartmental in the upper thigh and occupies its own compartment in the pelvic girdle

hamstring muscles. The posterior compartment includes the semitendinosis, semimembranosus and biceps femoris muscles from their insertion on the ischial tuberosity. The posterior compartment is largest at the level of the distal femur, where it occupies the posterior half of the musculature of the thigh.

Finally, the medial or adductor compartment of the thigh begins at the level of the pubic symphysis at the origin of the gracilis and the adductor muscles, namely the adductor magnus, adductor longus and adductor brevis. The adductor muscles insert distally on the linea aspera, located on the posterior shaft of the distal femoral diaphysis. The gracilis muscle inserts more distally at the pes anserine on the anteromedial tibia, with the sartorius (anterior compartment) and semi-tendinosis muscle (posterior compartment). The medial compartment is largest proximally, where it occupies nearly half of the musculature of the thigh and is innervated by the obturator nerve.

The pelvic girdle is a complex arrangement of bony structures and tendinous origins and mesenchymal tumors are considered intra-compartmental only if limited to the bone or the muscle of origin (Anderson et al. 1999) However, tumors of the bony pelvic girdle are generally quite advanced and already extra-compartmental at initial presentation. Superior to the hip joint, the pelvic soft tissues can be essentially divided into three compartments: the iliopsoas compartment, the gluteus medius/minimus compartment, and the gluteus maximus compartment (Bosch and Tscherne

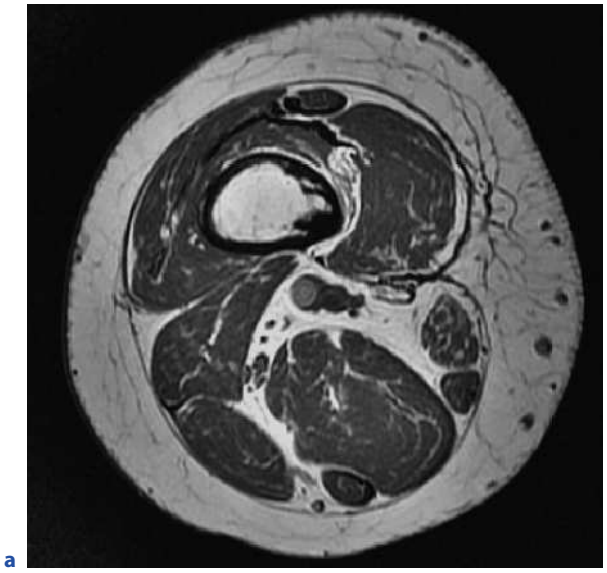

a

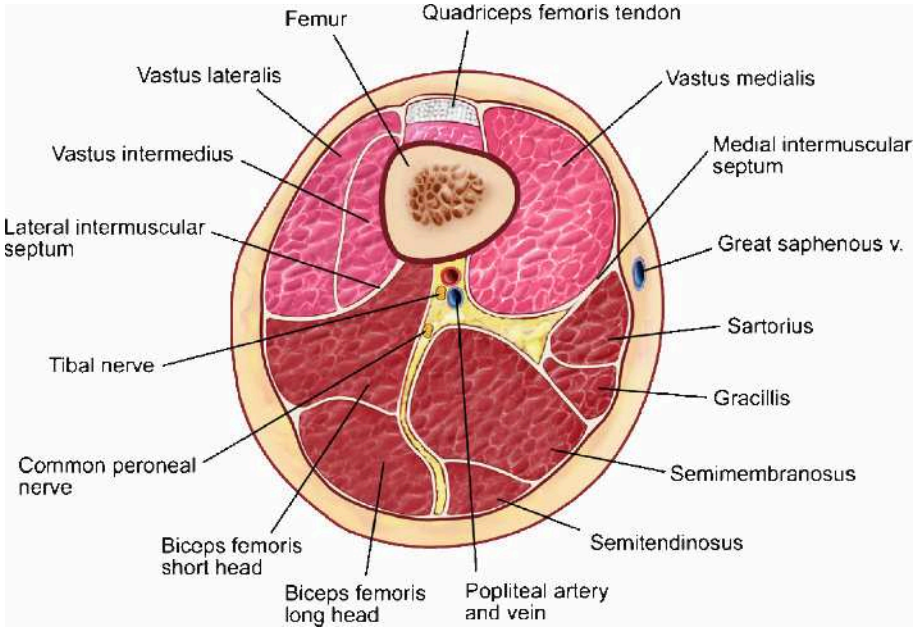

b

Fig. 38.2. **a** Transverse T1-weighted MR image of the distal thigh. **b** Diagram in the transverse plane illustrating the contents of the anterior (*pink shading*) and posterior (*red shading*) compartments of the distal thigh

1992). Both the gluteus medius/minimus compartment and the iliopsoas compartment lie within thick osteofibrous sheaths, divided from each other by the iliac bone and individually surrounded by the gluteal and iliac fascia, respectively (Bosch and Tscherne 1992). The gluteus maximus compartment is the most posterior and superficial compartment and is thinly invested within the gluteal fascia. The intra-pelvic region and neurovascular bundles of the lower extremity are classified as extra-compartmental spaces, meaning that spread to these regions would require a more radical surgical approach (Enneking 1985; Enneking et al. 1980). Some surgeons have reported good functional results with limb-sparing surgery despite tumor involvement of the sciatic nerve (Malawer and Sugarbaker 2001).

38.2.2 Compartments of the Lower Leg

Below the knee joint, the soft tissues of the lower extremity are divided into four compartments: anterior, lateral,

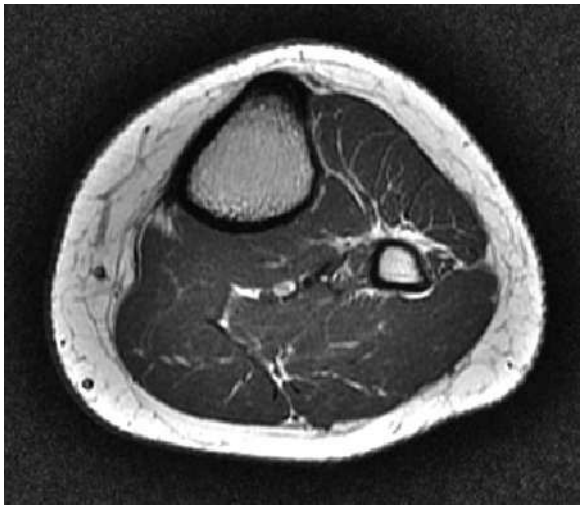

a

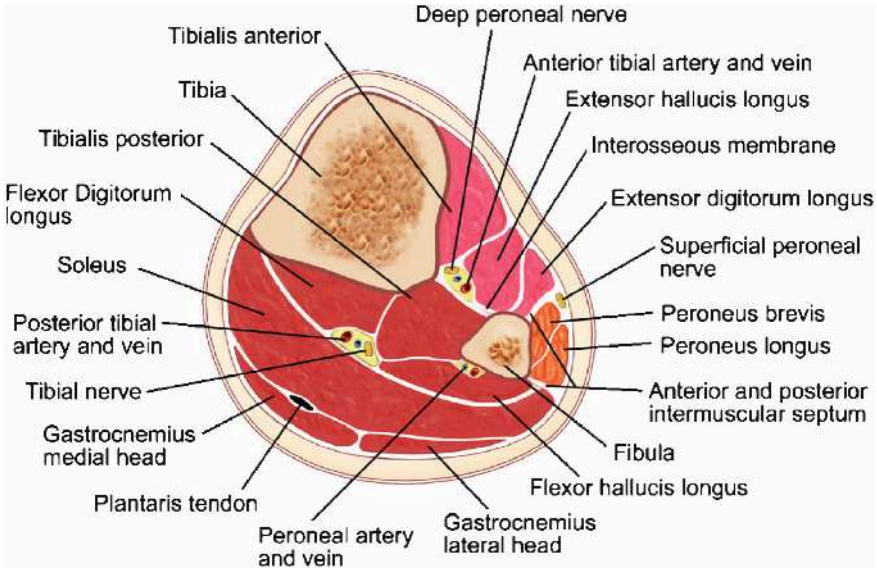

b

Fig. 38.3. **a** Transverse T1-weighted MR image of the proximal lower leg. **b** Diagram in the transverse plane illustrating the contents of the anterior (*red shading*), lateral (*orange shading*), and posterior (*pink shading*) compartments of the proximal lower leg

superficial posterior, and deep posterior (Figs. 38.3 and 38.4). Each of these compartments contains at least one neurovascular bundle, which also serves as its innervation. The muscles of the anterior or extensor compartment serve to dorsiflex the foot and include the tibialis anterior, extensor digitorum longus, extensor hallucis longus and peroneus tertius muscles. The anterior compartment contains and is innervated by the deep peroneal nerve and the muscles are supplied by the anterior tibial artery. The interosseous membrane traverses between the tibia and fibula, and separates the anterior compartment from the deep posterior compartment. The deep posterior compartment is innervated by the tibial nerve and contains the muscles which plantarflex the foot, including the tibialis posterior, flexor hallucis longus, flexor digitorum longus and the popliteus muscle proximally. The transverse intermuscular septum separates the deep posterior compartment from the superficial posterior compartment. The superficial posterior compartment is innervated by the tibial nerve and contains the muscles of the superficial calf. These muscles include the soleus and plantaris tendon, which

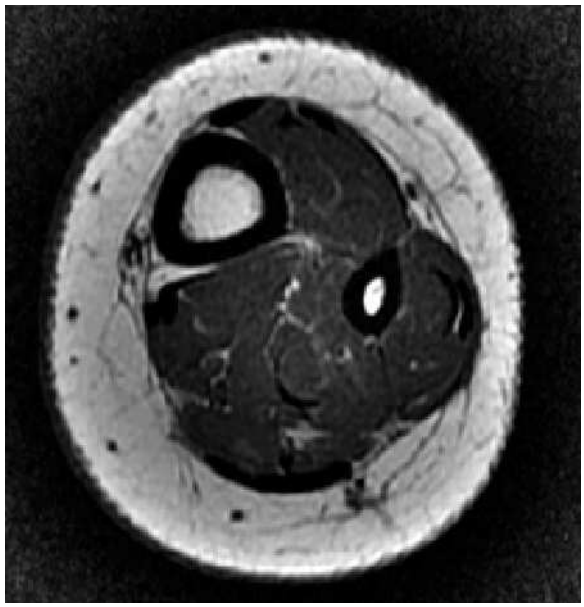

a

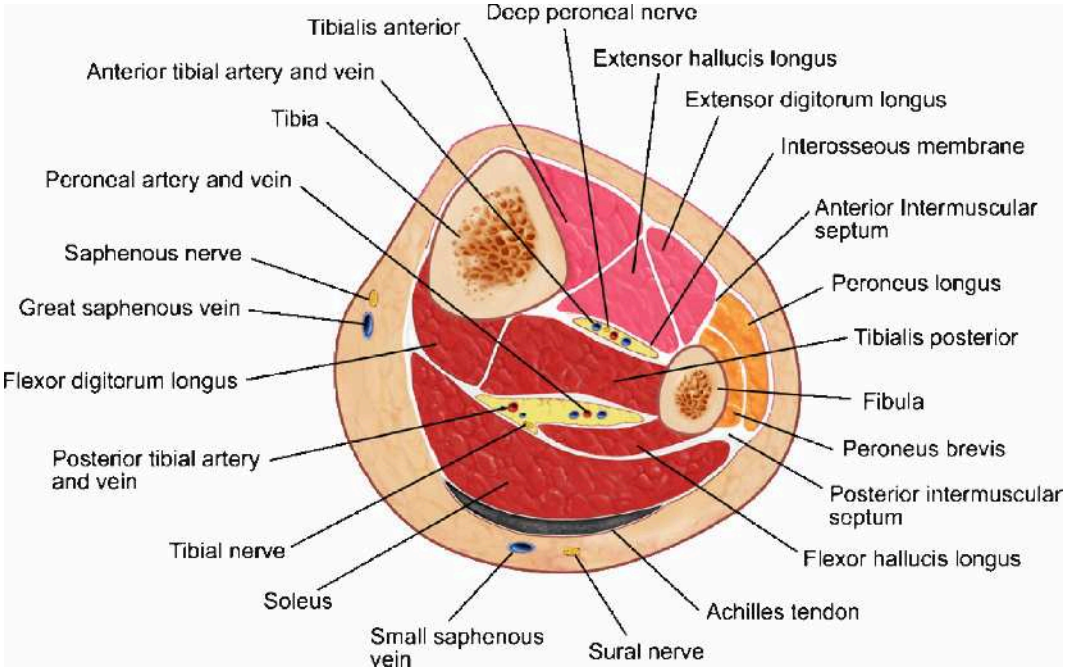

b

Fig. 38.4. **a** Transverse T1-weighted MR image of the distal lower leg. **b** Diagram in the transverse plane illustrating the contents of the anterior (*red shading*), lateral (*orange shading*) and posterior (*pink shading*) compartments of the distal lower leg

are deep to the medial and lateral heads of the gastrocnemius muscle. The anterior intermuscular septum separates the lateral compartment from the anterior compartment and the posterior intermuscular septum separates the lateral compartment from the posterior compartment. The lateral compartment is innervated by and contains the superficial peroneal nerve. The muscles of the lateral compartment of the leg serve to evert the foot, and include the peroneus brevis and peroneus longus. The MTS grading system delineates the popliteal fossa and neurovascular bundles of the lower extremity as extra-compartmental spaces because of the potential for longitudinal spread of tumor (Enneking 1985; Enneking et al. 1980).

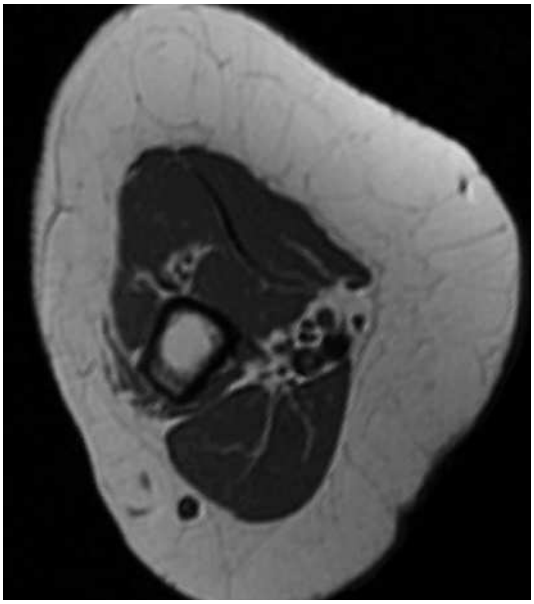

a

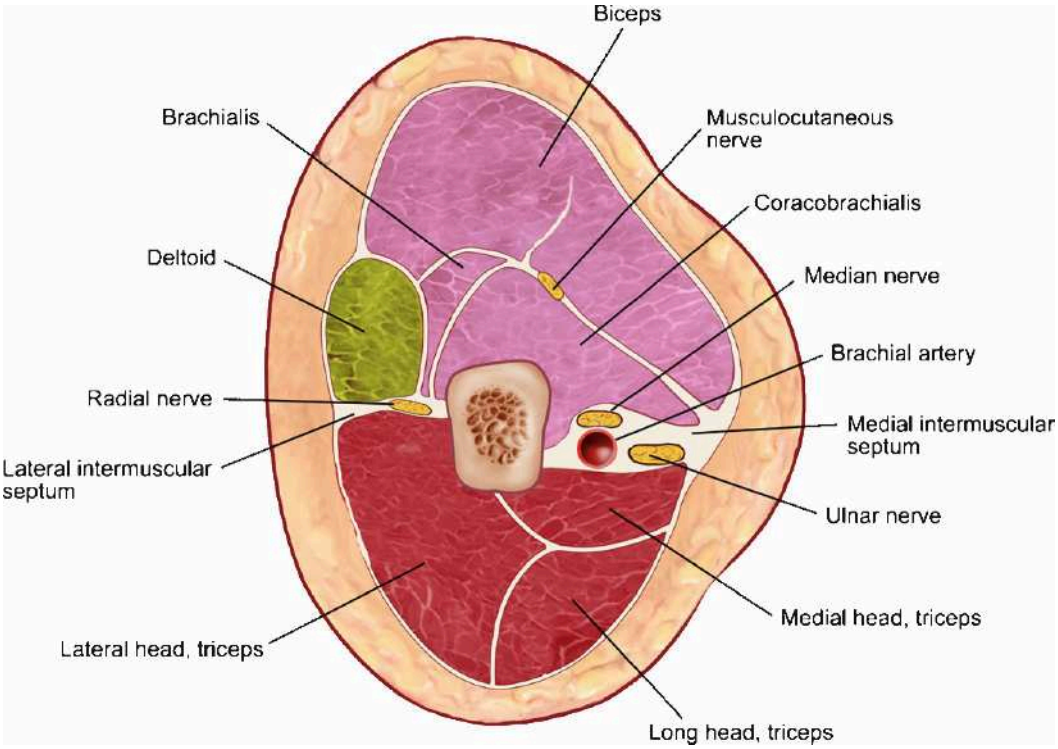

b

Fig. 38.5. **a** Transverse T1-weighted MR image of the proximal arm. **b** Diagram in the transverse plane illustrating the contents of the anterior (*pink shading*) and posterior (*red shading*) compartments of the upper arm. The deltoid muscle (*green shading*) is extra-compartmental in the arm and occupies the abductor compartment of the shoulder girdle. (Adapted with permission from Toomayan G, Robertson F, Major N, Brigman B (2006) Upper extremity compartmental anatomy: clinical relevance to radiologists. Skeletal Radiol 35:195–201)

38.2.3 Compartments of the Foot

The compartmental anatomy of the foot as it pertains to anatomical dissection is complex – some functional anatomy has been clinically elucidated through the analysis of various compartment syndromes (Goodwin et al. 1995). Because the MTS grading system is intended to stratify tumors based on prognosis and surgical treatment, the foot is divided into five compartments constituting the five individual rays. The mid-foot, hind-foot and dorsum of the foot are categorized as extra-compartmental spaces; the implication being that wide-excision of a tumor of the mid-foot or hind-

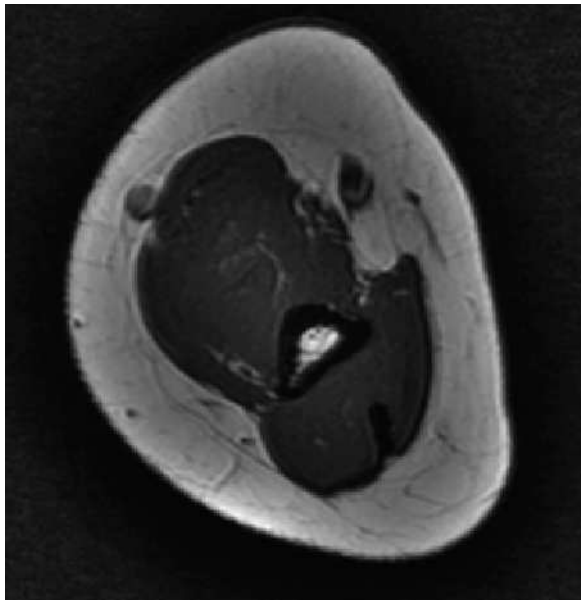

a

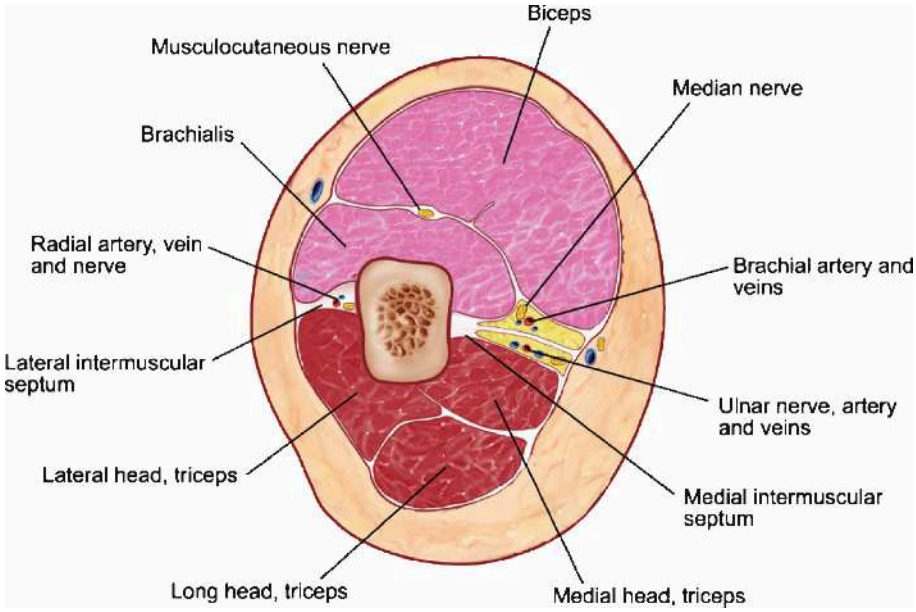

b

Fig. 38.6. **a** Transverse T1-weighted MR image of the distal arm. **b** Diagram in the transverse plane illustrating the contents of the anterior (*pink shading*) and posterior (*red shading*) compartments of the lower arm

foot is not possible because of ease of tumor spread in a compact space with thin fascial boundaries (Enneking 1985; Enneking et al. 1980). Wide-excision would render the remaining limb functionless, making amputation a more practical approach. The individual rays of the foot, however, have a more distinct fascial investment and if a tumor is confined to three or fewer rays, limb-sparing surgery/ray resection can be performed with a good functional outcome.

38.2.4 Compartmental Anatomy of the Upper Arm and Shoulder Girdle

The musculature of the upper arm is divided into an anterior compartment and a posterior compartment (Figs. 38.5 and 38.6). The bony humerus occupies a separate compartment and extra-compartmental spread of tumor occurs with cortical breakthrough of tumor into

a muscular compartment. Surgical treatment of extra-compartmental spread of a bone tumor of the humerus would require removal of the both the bone and soft tissue compartment containing tumor. The anterior and posterior compartments are divided by the medial and lateral intermuscular fascial septae (Toomayan et al. 2006). The anterior compartment is largest at the level of the distal humeral diaphysis, where is occupies nearly two/thirds of the musculature of the arm. The long and short heads of the biceps brachii fuse in the proximal arm from their respective origins on the supraglenoid tubercle and the coracoid process, and occupy the most superficial location in the anterior compartment. The brachialis muscle is located deep to the biceps muscle in the mid-distal arm and the coracobrachialis muscle is located deep to the biceps in a medial location in the proximal arm. The posterior compartment is entirely composed of the triceps brachii muscle. The long head and the lateral head of the triceps muscle originate from the infraglenoid tubercle and the posterior humeral shaft, and are located superficial to the medial head of the triceps muscles, which also originates from the posterior humeral shaft.

The periscapular space is designated as an individual compartment by the MTS Grading System. Anderson et al. (1999) described the soft tissues covering the dorsal scapula to occupy one compartment and include the infraspinatus, teres minor and rhomboid muscles; in this system, the supraspinatus muscle occupies a separate compartment. Malawer and Wittig (2001) described a classification system which incorporates functional compartmental anatomy for the purposes of reconstructive limb-sparing surgery of the shoulder girdle. A description of the six types of humeral and scapular resection is beyond the scope of this discussion; however, each type of resection is designated as Type A or Type B according to the status of the "abductor mechanism" – the main motor group of the shoulder joint, which includes the rotator cuff muscles and the deltoid muscle. A Type A resection is intra-compartmental with an intact abductor mechanism and a Type B resection is extra-compartmental with a partially or completely resected abductor mechanism. Resection of the abductor mechanism is generally required with extra-cortical spread of tumor from the proximal humerus or scapula (Malawer and Wittig 2001).

Tumor extension from the proximal humerus grows in a centripetal fashion elevating and displacing surrounding structures. Hence, tumor can be covered anteriorly by the intra-compartmental boundary of the subscapularis muscle. The subscapularis muscle tends to protect the neurovascular bundle of the brachial plexus and axillary vessels from tumor involvement (Malawer and Wittig 2001). The axillary space, periclavicular space and neurovascular bundles of the upper extremity are designated as extra-compartmental by the MTS Grading System because of the potential of unrestricted longitudinal spread of tumor, which may preclude limb-sparing surgery (Enneking 1985; Enneking et al. 1980).

38.2.5 Compartments of the Forearm

The compartmental anatomy of the forearm includes a dorsal and volar compartment (Figs. 38.7 and 38.8). Other staging systems include a third compartment of the "mobile wad" or radial compartment of the forearm, which is comprised of the brachioradialis muscle, extensor carpi radialis longus muscle and extensor carpi radialis brevis muscle (Boles et al. 2000). Yet, another system includes a fourth compartment by subdividing the dorsal compartment into deep and superficial components. However, for the purposes of tumor staging, the musculature of the forearm can be divided into volar and dorsal compartments, which are separated by the interosseous membrane (Toomayan et al. 2006). Superficially, the muscles of dorsal compartment serve to extend the wrist, and third, fourth and fifth digits; the muscle group includes, from radial to ulnar, the extensor carpi radialis brevis and longus, extensor digitorum, extensor digiti minimi, and extensor carpi ulnaris. In the two compartment system, the brachioradialis is classified in the dorsal compartment. The deep dorsal compartment contains the muscles that abduct and extend the first and second digit: the abductor pollicis longus, extensor pollicis brevis, extensor pollicis longus, and extensor indices. The supinator muscle is the deepest muscle of the dorsal compartment, and it functions to supinate the forearm.

The superficial muscles of the volar compartment serve to flex the wrist and fingers and pronate the forearm. The superficial group of muscles, from radial to ulnar, includes the pronator teres, flexor carpi radialis, palmaris longus, flexor digitorum superficialis, and flexor carpi ulnaris. The deep volar muscles are separated from the superficial muscles by a transverse septum, and include the flexor digitorum profundus, flexor pollicis longus, and the pronator quadratus, distally.

a

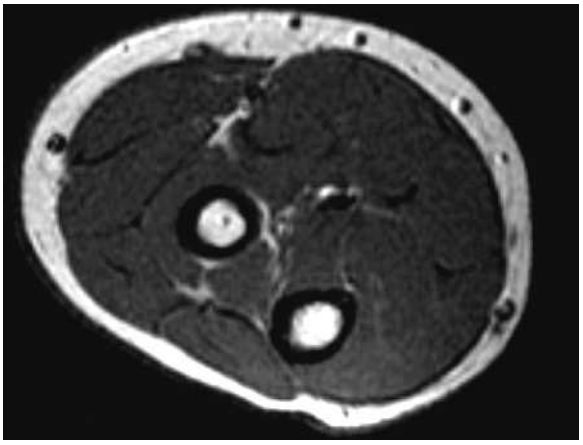

b

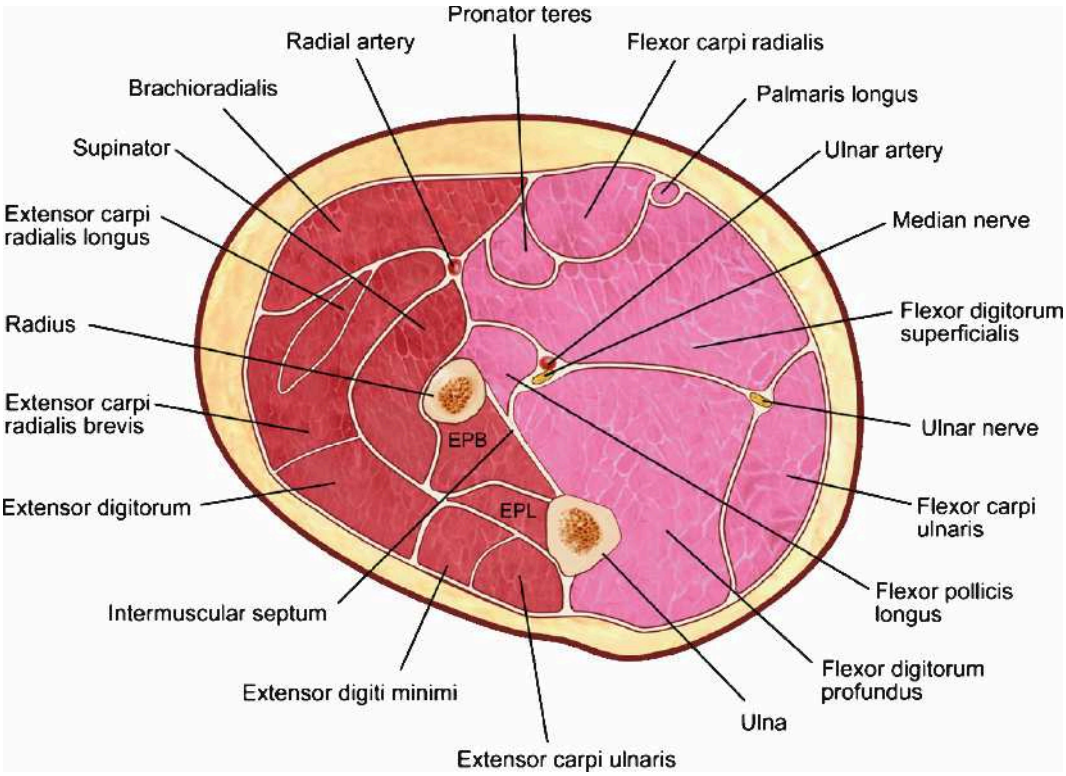

Fig. 38.7. **a** Transverse T1-weighted MR image of the proximal forearm. **b** Diagram in the transverse plane illustrating the contents of the dorsal (*pink shading*) and volar (*red shading*) compartments of the forearm. (Adapted with permission from Toomayan G, Robertson F, Major N, Brigman B (2006) Upper extremity compartmental anatomy: clinical relevance to radiologists. Skeletal Radiol 35:195–201)

38.2.6 Compartments of the Hand

The individual rays of the hand, including the five metacarpals, can be thought of as individual compartments, which can be individually resected with an acceptable functional result (Rock et al. 1993). Some authors have designated the palmar soft tissues as a separate compartment for the purposes of tumor resection (Anderson et al. 1999) and superficial palmar lesions can be treated with ray amputation (Rock et al. 1993). Deep lesions that extend into the carpal tunnel are best treated with partial or complete amputation (Athanasian 2004). Just as the mid-foot and hind-foot are considered separate compartments because of their compact nature, loose fascial planes and poor restriction to spread of tumor, Enneking (1985) designated the mid-hand as extra-compartmental. The extra-compartmental spaces of the forearm and hand also include the antecubital fossa and dorsum of the hand (Enneking 1985; Enneking et al. 1980), since tumor spread in these locations may require amputation.

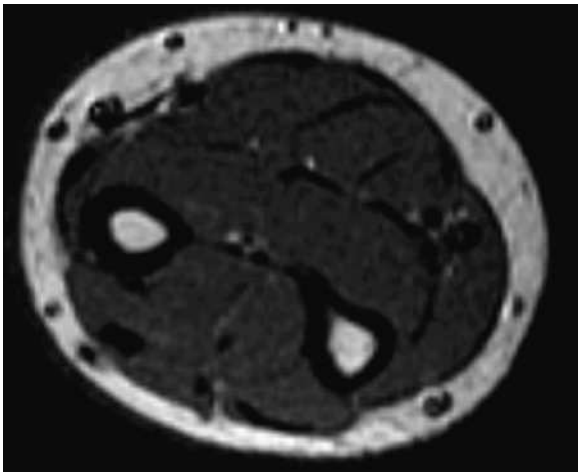

a

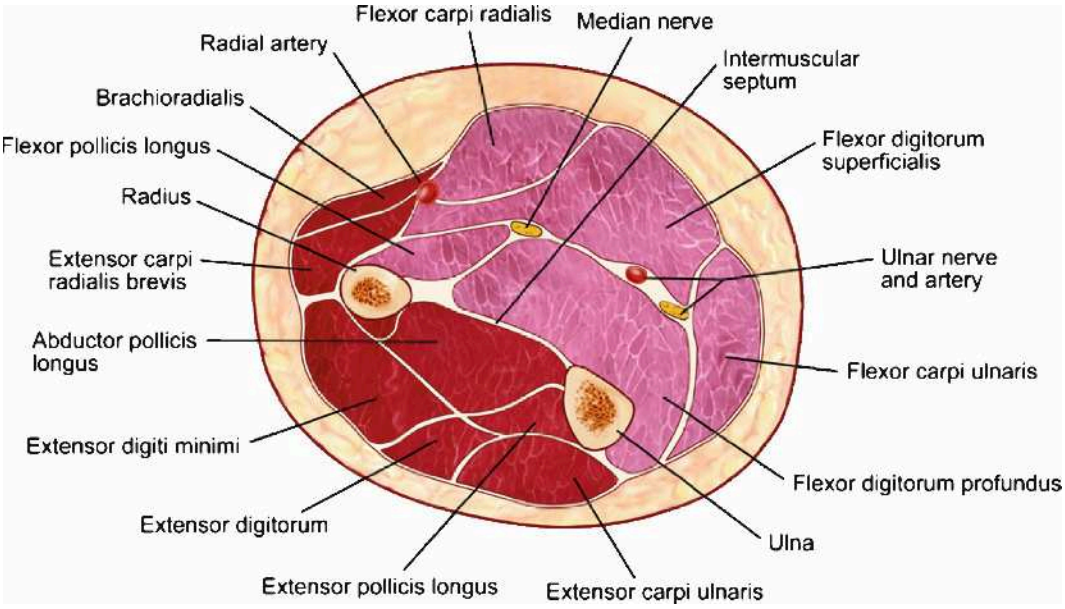

b

Fig. 38.8. **a** Transverse T1-weighted MR image of the distal forearm. **b** Diagram in the transverse plane illustrating the contents of the dorsal (*pink shading*) and volar (*red shading*) compartments of the forearm. (Adapted with permission from Toomayan G, Robertson F, Major N, Brigman B (2006) Upper extremity compartmental anatomy: clinical relevance to radiologists. Skeletal Radiol 35:195–201)

38.3 Relevance of Compartmental Anatomy to Biopsy Approach

The surgical plan for the resection of a bone tumor must guide the approach of the image guided percutaneous biopsy. Because malignant cells can seed the biopsy tract as the needle is inserted and removed, the biopsy tract must be excised along with the primary tumor. A poorly planned biopsy can convert an intra-compartmental tumor into an extra-compartmental tumor by passing the biopsy needle through a previously unaffected compartment, potentially obviating the possibility for limb-sparing surgery (Springfield et al. 1996; Mankin et al. 1996). The radiologist who is called upon to perform a percutaneous biopsy of a bone tumor is mandated to consult with the orthopedic surgeon, in order to prevent potential upstaging of the therapeutic procedure. The needle tract must avoid adjacent neurovascular bundles, be the shortest path between the skin and tumor, pass through the least number of compart-

ments, and be contained within the surgically excised tissue bloc.

Percutaneous biopsy of a malignant bone tumor of the proximal humerus should be performed through an anterolateral approach through the anterior third of the deltoid muscle, rather than through the posterior deltoid. The traditional approach through the deltopectoral interval can cause seeding of tumor into the pectoralis muscle compromising its use for reconstructive surgery (Bickels et al. 2001). Moreover, the deltoid is innervated from posterior to anterior and a biopsy through the posterior deltoid would necessitate removal of the more proximal nerve and result in denervation of the anterior deltoid (Anderson et al. 1999). Percutaneous biopsy of pelvic lesions should attempt to avoid the gluteal muscles, as preservation of this muscle group is necessary for functional status after limb-sparing surgery (Espinosa et al. 2008). Percutaneous biopsy of a distal femoral lesion should be performed from either an anteromedial or anterolateral approach, in order to avoid the rectus femoris and quadriceps extensor mechanism. Removal of this muscle group results in suboptimal function of the remaining limb (Anderson et al. 1999; Espinosa et al. 2008). A medial approach is preferred if the tumor is in close proximity to the femoral vessels, as this area will likely require exploration during surgery (Espinosa et al. 2008). The suprapatellar recess may extend a variable distance proximally, and should be avoided in order to prevent contamination of the knee joint (Espinosa et al. 2008). Percutaneous biopsy of a bone tumor of the tibia should be performed from a direct anterior approach, which not only affords the shortest distance between the tibial cortex and the skin surface but also avoids potential contamination of the posterior and lateral compartments of the lower leg (Anderson et al. 1999; Bickels et al. 2001).

References

Anderson MW, Temple HT, Dussault RG, Kaplan PA (1999) Compartmental anatomy: relevance to staging and biopsy of musculoskeletal tumors. AJR Am J Roentgenol 173:1663–1671

Athanasian EA (2004) Malignant bone and soft tissue sarcoma of the hand. J Am Soc Surg Hand 4(2):60–72

Bickels J, Jelinek J, Schmookler BM, Malawer M (2001) Biopsy of musculoskeletal tumors. In: Malawer M, Sugarbaker P (eds) Musculoskeletal cancer surgery: treatment of sarcoma and allied diseases. Kluwer Academic Publishers, Norwell, pp 37–45

Boles CA, Kannam S, Cardwell AB (2000) The forearm: anatomy of muscle compartments and nerves. AJR Am J Roentgenol 174:151–160

Bosch U, Tscherne H (1992) The pelvic compartment syndrome. Arch Orthop Trauma Surg 111:314–317

Enneking WF (1985) Staging of musculoskeletal neoplasms. Skeletal Radiol 13:183-194

Enneking WF, Spanier SS, Goodman MA (1980) A system for the surgical staging of musculoskeletal sarcoma. Clin Orthop 153:106–120

Espinosa LA, Jamadar DA, Jacobson JA, DeMaeseneer MO, Ebrahim FS, Sabb BJ, Kretschmer MT, Biermann JS, Kim S (2008) CT-guided biopsy of bone: a radiologist's perspective. AJR Am J Roentgenol 190:W283–W289

Goodwin DG, Salonen DC, Yu JS, Brossmann J, Trudell DJ, Resnick DL (1995) Plantar compartments of the foot: MR appearance in cadavers and diabetic patients. Radiology 196:623–630

Lodwick GS, Wilson AJ, Farrell C, Virtama P, Dittrich F (1980) Determining growth rates of focal lesion of bone from radiographs. Radiology 134:577–583

Malawer M, Sugarbaker P (2001) Resection of the posterior compartment of the thigh. In: Malawer M, Sugarbaker P (eds) Musculoskeletal cancer surgery: treatment of sarcoma and allied diseases. Kluwer Academic Publishers, Norwell, pp 265–277

Malawer M, Wittig JC (2001) Overview of resection around the shoulder girdle: anatomy, surgical considerations and classification. In: Malawer M, Sugarbaker P (eds) Musculoskeletal cancer surgery: treatment of sarcoma and allied diseases. Kluwer Academic Publishers, Norwell, pp 179–202

Mankin HJ, Mankin CJ, Simon MA (1996) The hazards of biopsy, revisited. J Bone Joint Surg Am 78:656–663

Rock MG, Wood MB, Fleegler EJ (1993) Reconstruction for tumors of the upper limb. In: Bogumill GP, Fleegler CJ (eds) Tumors of the hand and upper extremity. Churchill and Livingstone, Edinburgh, pp 413–434

Springfield DS, Dempsey S, Rosenberg A (1996) Biopsy: complicated and risky. J Bone Joint Surg Am 78:639–643

Toomayan GA, Robertson F, Major NM (2005) Lower extremity compartmental anatomy: clinical relevance to radiologists. Skeletal Radiol 34:307–313

Toomayan GA, Robertson F, Major NM, Brigman BE (2006) Upper extremity compartmental anatomy: clinical relevance to radiologists. Skeletal Radiol 35:195–201

Who Was Who in Bone Tumours

39

Etienne Pluot, A. Mark Davies and Steven L. J. James

CONTENTS

KEY POINT

- Our current knowledge of bone tumours is based on the research undertaken over the past 150 years by physicians and scientists from many different disciplines.

39.1 Introduction

Over the past three hundred years the medical fraternity has enthusiastically named diseases, symptoms and tests after their supposed discoverers. While some suggest that these eponyms often provide a less than truthful account of how diseases were discovered and advocate abandoning them, others argue that they should be preserved if only as a practical form of medical shorthand or aide-memoire to recall a particular disease or an association of different conditions. The purpose of this chapter is to provide the reader a brief diversion from the wearying task of absorbing the mass of information given in the preceding chapters. Listed in alphabetical order are potted biographies of some of the physicians and scientists whose names have become eponymous or synonymous with bone tumours. If nothing else it provides a fascinating insight into medical history and reveals that physicians from many different areas of expertise have contributed to our understanding of tumours and tumour-like lesions of bone. Apologies in advance to those, alive or dead, who feel that they have been unfairly omitted from the list.

Etienne Pluot, MD
Musculoskeletal Fellow, Service de Radiologie B, Hôpital Cochin, 27 rue du Faubourg Saint Jacques, 75679 Paris Cedex 14, France

A. Mark Davies, MBChB, FRCR
Consultant Radiologist, Department of Radiology, Royal Orthopaedic Hospital, NHS Foundation Trust, Bristol Road South, Northfield, Birmingham B31 2AP, UK

Steven L. J. James, MD, ChB, FRCR
Consultant Radiologist, Department of Radiology, Royal Orthopaedic Hospital, NHS Foundation Trust, Bristol Road South, Northfield, Birmingham B31 2AP, UK

39.2 Biographies

Albright, Fuller and McCune, Donovan James

Fuller Albright, an endocrinologist (born in Buffalo, 1900, died in Boston, USA, 1969), graduated from Harvard Medical School in 1924 and completed his residency at the Massachusetts General Hospital in Boston and John Hopkins Hospital in Baltimore, where he focused his attention on the parathyroid glands and calcium metabolism. He then spent two years in Vienna, working under the supervision of Jakob Erdheim, whom he considered a mentor thereafter. Albright returned to the United States in 1930 and was appointed to the medical faculty at Harvard, and spent the rest of his career at the Massachusetts General Hospital where he founded a biological laboratory and a clinic for clinical endocrinology. He showed a phenomenal capacity to describe new syndromes and explain their physiological basis, as well as to imagine and conceive methods to measure hormones levels in blood and urine. He thus described with Klinefelter and Reifenstein the eponymous syndrome, and explained how Turner's syndrome was correlated with elevated follicle-stimulating hormone. Among his massive scientific contributions, in 1937, Fuller Albright described in the *New England Journal of Medicine* "Syndrome characterized by osteitis fibrosa disseminata, areas of pigmentation and endocrine dysfunction, with precocious puberty in females. Report of five cases" that is the association of polyostotic fibrous dysplasia and precocious puberty. Albright's career was severely impaired by early Parkinson disease, for which he decided to undergo a new surgical treatment in 1956. Tragically, this intervention resulted in massive intracranial haemorrhage and left him comatose until his death in 1969. The American paediatrician Donovan James McCune (born 1902, died 1976), working at Columbia University, New York, published two articles on the same syndrome in 1936 and 1937, which is now known as the McCune-Albright syndrome.

Bloom, David

An American dermatologist, born in Warsaw, Poland, 1892. Bloom graduated from Berne University in 1919 after successive periods in Gdansk, Poland, and Freiburg, Germany. He then went to the USA and specialized in dermatology working at the Skin and Cancer Clinic in New York. In 1954, he published "Congenital telangiectatic erythema resembling lupus erythematosus in dwarfs; probably a syndrome entity" in the *American Journal of Diseases of Children*, based on the observation of three children presenting with growth retardation, dolichocephaly, facial sun-sensitive telangiectatic erythema, patchy areas of hyper- and hypopigmentation, and recurrent respiratory tract and gastrointestinal infections. This syndrome, known as Bloom's syndrome, was later further investigated, especially by James German, a geneticist of Cornell University, New York. German and Bloom, associated with Archibald, published in *Science* in 1965 "Chromosomal breakage in a rare and probably genetically determined syndrome of man", suggesting a chromosomal disorder causing the disease as well as establishing Bloom's syndrome as a state predisposing to cancers, such as osteosarcoma.

Brodie, Benjamin Collins, Sir

Born in Winterslow, 1783, died in Betchwork, England, 1862 (Fig. 39.1). He was a surgeon, physician, philosopher, writer and statesman. He received his early education from his father, the Rector of Winterslow until he came to London to study medicine in 1801. He was appointed house surgeon at St. George's Hospital and a member of the Royal College of Surgeons in 1805. He

Fig. 39.1. Brodie, Benjamin Collins, Sir (1783–1862). Provided by Bibliothèque de l'Académie Nationale de Médecine, Paris

became surgeon to King George IV in 1828 and subsequently to King William IV and to Queen Victoria in 1832. He was made a baronet in 1834 and elected President of the Royal College of Surgeons in 1844, president of the Royal Society and the first president of the General Medical Council in 1858. Although he carried out extensive research in various medical fields, most of his professional life was dedicated to bone and joint diseases. *Pathological and Surgical Observations on the Diseases of the Joints* was published in 1818 and passed through five editions until 1850. He described a type of subacute osteomyelitis in 1845, which to this day is known as Brodie's abscess.

Burkitt, Denis Parsons

Born in Enniskillen, Ireland, 1911, died in Gloucester, England, 1993 (Fig. 39.2). An English surgeon, he graduated from Edinburgh University in 1935 and became a fellow of Edinburgh's Royal College of Surgeons in 1938. He served with the Royal Army Medical Corps and was posted in Kenya, Somaliland and Uganda, where he settled after the end of World War II and remained until 1966. He published "A sarcoma involving the jaws of African children" in the *British Journal of Surgery* in 1958, describing fast growing swellings around the head and neck in children. He published "Malignant lymphoma in African children. A clinical syndrome" in *Cancer* in 1961 and suggested a possible link between the disease and an infectious agent, possibly transmitted by an insect, based on the geographical clustering of the cases. Michael Anthony Epstein and Yvonne Barr isolated a virus in a sample supplied by Burkitt in 1964, now known as Epstein-Barr virus. It is now recognized that Epstein-Barr's virus is associated with the development of B cell lymphoma, also known as Burkitt's lymphoma.

Fig. 39.2. Burkitt, Dennis Parson (1911–1993). Reproduced with kind permission of Dr. W. Reville, University College, Cork, Ireland

Fig. 39.3. Campanacci, Mario (1932–1999). Reproduced with kind permission of Dr L. Campanacci, Istituto Ortopedico Rizzoli, Bologna, Italy

Campanacci, Mario

Born in Parma, Italy, 1932, died 1999 (Fig. 39.3). An Italian orthopaedic surgeon, he graduated from Medical School at the University of Bologna in 1956. He joined the Istituto Ortopedico Rizzoli in 1958 where he directed the tumour pathology research laboratory from 1963, and became professor in 1975. He published seven books and more than 370 articles. He described in 1981 a lesion known as osteofibrous dysplasia involving the tibia and fibula, frequently referred to as a Campanacci lesion. He described in 1983 an association of multiple non-ossifying fibromas and various extra-skeletal abnormalities such as café-au-lait spots, mental retardation, hypogonadism or cryptorchidism, and ocular and cardiovascular malformations: the Jaffe-Campanacci syndrome. Campanacci founded the European Society of Muscular and Skeletal Oncology (EMSOS) in 1987.

Codman, Ernest Armory

An American orthopaedic surgeon and medical reformer, born in Boston, 1869, died in Ponkapong, USA, 1940 (Fig. 39.4). He graduated from Harvard Medical School in 1895 and completed his internship at the Massachusetts General Hospital. He carried out intensive investigations into the use of X-rays at Massachusetts General Hospital. In 1909, he described Codman's triangle—a diagnostic sign of osteosarcoma. Codman published "The use of X-rays in the diagnosis of bone diseases" in *Keen's Surgery*. In 1920, Codman established

Fig. 39.4. Codman, Ernest Amory (1869–1940). Reproduced with kind permission of Joint Commission, Illinois, USA

the first bone tumour registry in the United States in order to establish standards for tumour nomenclature and classification. Codman tumour was the original name, now no longer used, for chondroblastoma. He developed a special expertise in orthopaedic disorders of the shoulder, publishing a series of articles on the subject between 1906 and 1908, and in 1909 he devised an influential operative repair of the torn rotator cuff. Codman conceived the End Result Idea, a visionary concept at that time "which was merely the commonsense notion that every hospital should follow every patient it treats long enough to determine whether or not the treatment was successful, and to enquire 'if not, why not', with a view to preventing similar failures in the future". This idea was first considered as a lack of respect for tradition and the medical profession but brought to light the value of efficiency analysis, soon accepted by most institutions. The End Result Idea became the first tool used by the American College of Surgeons to standardize hospitals in the United States. It now provides the means for accurate evaluation of methods and practice in medical and surgical practice and clinical research. Today, the Joint Commission on Accreditation of Healthcare Organizations continues to reflect the fundamental purposes set forth by Codman in the early twentieth century in the United States.

Erdheim, Jakob and Chester, William

As Chief of the Pathology Institute of the Vienna city hospital, Jakob Erdheim (born 1874, died 1937) welcomed the American cardiologist William Chester (born 1903, died 1974) on a fellowship programme. Erdheim established in 1906 the relationship between the parathyroid glands and calcium metabolism and was the first to describe compensatory hyperplasia of the parathyroids following osteomalacia. William Chester published "Über lipoidgranulomatose" in *Virchows Archiv für pathologische Anatomie*, describing in two patients a rare lipidosis labelled Erdheim-Chester disease by Jaffe in 1972, who characterized it as non-Langerhans cell histiocytosis involving both skeleton and extra-skeletal organs.

Ewing, James

Born in Pittsburgh, USA, 25th December 1866, died 1943. An American pathologist, he suffered from osteomyelitis of the femur, for which he was confined to bed for two years when he was 14 years old. During this period, he entered various competitions and won a microscope, the tool on which his later career was based. He graduated from the New York College of Physicians and Surgeons in 1891, and completed his internship in Pittsburgh and New York. He travelled to Germany showing special interest in clinical and microscopic pathology. Ewing was appointed the first professor of pathology at Cornell University in 1899. Ewing published his book *Neoplastic Disease* in 1919, based on the experience accumulated at the Bellevue Hospital and the Memorial Hospital for the Study of Cancer and Allied Diseases. In 1920, he described a bone tumour he called *diffuse endothelioma* and established that the disease was distinct from lymphoma and neuroblastoma. This tumour was later labelled as "Ewing's tumor" by Codman in his bone tumour registry of the American College of Surgeons. Ewing was a strong supporter of radiation therapy rather than surgery, stating in 1922: "from the most unexpected source, experimental physics, a new and powerful weapon has been brought into play".

Gardner, Eldon John

An American geneticist, born in Logan, Utah, USA, 1909, died 1989. Gardner graduated in 1935 in zoology and chemistry from Utah State University and then completed a PhD in zoology at the University of California, Berkeley in 1939. After successive spells at Salinas Junior College, California and at the University of Utah, Salt Lake City, Gardner moved back to Utah State University, Logan, where he was appointed professor in 1948 and remained until his retirement in 1974. After several years spent exploring genetics in *Drosophila melanogaster*, he was invited by Fayette Stephens, one of the early human geneticists in the United States, to study various characteristics in Utah families, based on the Mormon genealogical records available in Salt Lake City. This cooperation proved to be successful as two

Fig. 39.5. Gaucher, Philippe Charles Ernest (1854–1918). Reproduced with kind permission of Dr. D. Wallach, Société Française d'Histoire de la Dermatologie, Paris, France

different papers were published in 1950 in the *American Journal of Human Genetics*, the first describing "Breast cancer in one family group" and the second depicting "Cancer of the lower digestive tract in one family group". In 1952, Gardner published a paper entitled "Hereditary pattern for multiple osteomas in a family group", followed in 1953 by one entitled "Multiple cutaneous and subcutaneous lesions occurring simultaneously with hereditary polyposis and osteomatosis". This association of familial polyposis and osteomas was termed Gardner's syndrome by Smith in 1958, and is now known to be a predisposing state for osteosarcoma, chondrosarcoma and liposarcoma.

Gaucher, Philippe Charles Ernest

Born in Champigny, France, 1854, died 1918 (Fig. 39.5). A French dermatologist, he described a case of splenomegaly in a 32-year-old woman, which he assumed was a form of spleen cancer. He published this case with postmortem histological findings in his doctorate thesis "De l'epithelioma primitif de la rate, hypertrophie idiopathique de la rate sans leucemie" in 1882. Gaucher was not aware at that time of the possible involvement of bones in what is now known as Gaucher's disease. The biochemical basis for the disease would be elaborated in 1965 by Brady.

Hand Alfred, Schüller Arthur and Christian, Henry

Alfred Hand (born in Scranton, USA, 1868, died 1949) graduated from the University of Pennsylvania in 1892 and completed his residency as a paediatrician. He then worked at various children's hospitals in Philadelphia as a physician and was appointed demonstrator of pathological histology at the University of Pennsylvania. He described in 1893 a disseminated form of Langerhans cell histiocytosis that he thought was due to tuberculosis. Arthur Schüller (born in Brno, Czechoslovakia, 1874, died in Melbourne, Australia, 1957) graduated from Vienna University in 1899 and soon began his career in neuropsychiatry. He immediately showed great interest in radiology and published in 1905 a comprehensive description of normal and pathological radiographic anatomy of the skull base in *Die Schädelbasis in Roentgenbilde*. Schüller was appointed a University Professor in 1914, just 6 months before the outbreak of World War I. Despite the war, Schüller maintained his position as the head of the neurology department and pursued his activities and research in radiology. He published in 1915 *Über eigenartige Schädeldefekte im Jugendalter («Landkartenschädel»)* depicting a "map-like skull" caused by bone defects in the membranous bones of the skull. Thus, his name was later linked to this particular form of Langerhans cell histiocytosis. After the war, he performed extensive research on what he called "neuroradiology" and was one of the first to perform pneumencephalography and ventriculography. In 1938, as Austria was annexed by Germany, Schüller and his wife had to flee to Oxford, England, where he was offered the opportunity to continue his research. Deeply shocked by the Nazi occupation in Europe and the fact that his two sons could not escape Austria, and were later reported murdered by the Nazis, Schüller and his wife emigrated to Australia in 1939. He worked as a radiologist in St Vincent's Hospital in Melbourne and had a room at his disposal in the anatomy department at Melbourne University, where he became an honorary research officer. Henry Christian (born in Lynchburg, 1876, died in Whitefield, USA, 1951) graduated as a Doctor of Medicine in 1900 from Johns Hopkins University in Boston. He was then appointed pathologist in Boston City Hospital and Boston Children's hospital, and finally Physician in Chief to the Peter Bent Brigham Hospital, where he remained until 1939. Besides his clinical duties, Henry Christian was deeply involved in teaching and held several positions at Harvard Medical School, including Dean of the Harvard Medical School at the age of 31. Inspired by Osler, he is renowned for having placed the students on the wards as clinical clerks, where they had the opportunity to do physical examinations and follow the course of patients in the hospital. He published in 1919 "Defects in membranous bones, exophthalmos, and diabetes insipidus: an unusual syndrome of dyspituitarism" in *Medical Clinics of North America*, completing the clinical triad of this particular form of Langerhans cell histiocytosis now known as Hand-Schüller-Christian disease.

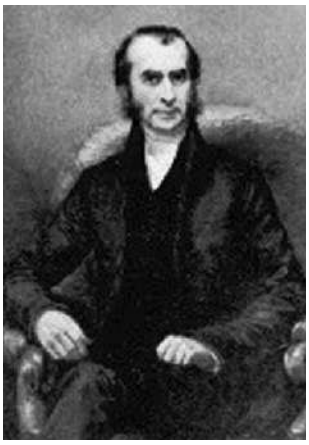

Fig. 39.6. Hodgkin, Thomas (1798–1866)

Fig. 39.7. Langerhans, Paul (1847–1888)

Hodgkin, Thomas

Born in Pentonville, England, 1798, died in Jaffa, Palestine, 1866 (Fig. 39.6). An English physician and pathologist, he commenced medical school at the United Hospitals of St. Thomas's and Guy's and graduated from Edinburgh University in 1823. He went to Italy and France in 1821, where he worked with Laënnec and became one of the early users of the stethoscope. First appointed physician at the London Dispensary, he was appointed lecturer in morbid anatomy and curator of the Pathology Museum at Guy's Hospital Medical School in 1925, where his career as a pathologist began. In 1832, he published "On some morbid appearances of the absorbent glands and spleen", giving an account of a disease described 33 years later by Samuel Wilks, now known as Hodgkin's lymphoma. Due to his ideas about preventive medicine and humanitarian and anti-slavery concerns, he progressively withdrew from medicine to devote his time to philosophical, geographical and ethnographical studies.

Jaffe, Henry Lewis

Born in New York, 1896, died in New York, USA, 1979. An American pathologist, he graduated from New York University School of Medicine in 1920 and served two internships in general medicine and surgery. He was appointed assistant pathologist and bacteriologist at Montefiore Hospital in 1922, then pathologist and director of laboratories at the Hospital for Joint Disease in 1925 at the tender age of 28! He continued as the head of this department until his retirement in 1964 and taught bone pathology at the Columbia College of Physicians and Surgeons, New York Medical College and Albert Einstein College of Medicine. Jaffe carried out extensive research on metabolic bone diseases, development, structure and pathological reaction of skeletal tissues, as well as describing specific skeletal abnormalities. He published more than 130 articles and two major books: *Tumours and Tumorous Conditions of Bones and Joints* in 1958 and *Metabolic, Degenerative, and Inflammatory Diseases of Bones and Joints* in 1972. Jaffe thoroughly described a number of bone conditions including osteoblastoma, osteoid osteoma, giant cell tumour, eosinophilic granuloma, pigmented villonodular synovitis, chondroblastoma, non-ossifying fibroma, chondromyxoid fibroma and aneurysmal bone cyst.

Langerhans, Paul

Born in Berlin, Germany, 1847, died in Funchal, Madeira, 1888 (Fig. 39.7). A German pathologist, he undertook his medical studies in Jena and then Berlin, where he became a close friend of Virchow's. He described the dendritic cells of the skin in 1868. The proliferation of histiocyte-like cells named Langerhans cells in bones and organs of reticuloendothelial system characterizes Langerhans cell histiocytosis or eosinophilic granuloma. Thanks to new histological staining techniques, he discovered in 1869 the pancreatic cells responsible for insulin production, known as Langerhans islets. His career was interrupted in 1874 by tuberculosis, while he was Professor at the University of Freiburg. He travelled to Italy, Switzerland and Madeira, where he began studying marine fauna with an unaffected energy.

Li, Frederick Pei and Fraumeni, Joseph F.

Frederick Pei Li, an American epidemiologist, born in Canton, China, 1940, graduated in physics from New York University and in demography from the University of Rochester and Georgetown University. He joined the National Cancer Institute in 1967 as an epidemiologist, mostly serving at the Dana-Farber Cancer Institute in Boston, where he was appointed head of the Division of Cancer Epidemiology and Control in 1991. He is now Professor of Clinical Cancer Epidemiology at the Harvard School of Public Health, Professor of Medicine at the Harvard Medical School and the Harry and Elsa Jiler American Cancer Society Clinical Research Professor. Joseph F. Fraumeni was born on 1 April, 1933, in Boston, Massachusetts. He received his undergraduate degree from Harvard College, an MD from Duke University and an MSc degree from the Harvard School of Public Health. In 1969, Dr. Frederick P. Li and Dr. Fraumeni reported a series of families featuring a genetic predisposition to sarcomas of bone and soft tissue, breast cancer and a variety of other neoplasms in "Soft-tissue sarcomas, breast cancer and other neoplasms: a familial syndrome?" in the *Annals of Internal Medicine*. The striking constellation of multiple cancers dispelled a prevailing dogma that familial predisposition is tumour-specific, and it suggested that genetic susceptibility pathways could be shared by a variety of cancers. In 1990, Drs. Li and Fraumeni collaborated with Drs. Stephen Friend and David Malkin to find germline mutations in the *p53* tumour suppressor gene as the pathogenic mechanism for the Li-Fraumeni syndrome. The findings stimulated new avenues of molecular research, especially since somatic mutations of the *p53* gene represent the critical genetic event in the development and progression of a large proportion of cancers in the general population.

Lodwick, Gwilym

Born in Mystic, USA, 1917. An American radiologist, he graduated from Iowa University Medical School in 1943. His medical education was interrupted due to his military service during World War II. He completed his residency in radiology in 1950 at the University of Iowa. Lodwick then completed a fellowship at the famous Armed Force Institute of Pathology in 1951. He was appointed radiologist and later chairman of the department of radiology at the University of Missouri-Columbia School of Medicine, where he spent almost three decades. His publications in the 1960s laid the foundation for much of the modern radiological approach to bone tumours. Of importance is his contribution to understanding the aggressivity of bone tumours on conventional radiographs. He first described the different patterns of tumour-related bone destruction in 1965 in "A systematic approach to the Roentgen diagnosis of bone tumors" published in *Tumors of Bone and Soft Tissue*. More than 40 years later, his systematic approach and the terminology he introduced continue to be taught to successive generations of radiology residents. Lodwick was also a pioneer in the field of radiology and informatics developing even in the early 1960s different programs in imaging modelling and computer-assisted diagnosis. He was thus nominated for a Nobel Prize of Medicine in 1975.

Maffucci, Angelo Maria

Born in Calitri, 1845, died in Pisa, Italy, 1903 (Fig. 39.8). An Italian pathologist, he graduated from Naples Medical School in 1872, starting his career as surgeon and pathologist in Naples Institute of Pathology in 1875. He was appointed Professor of general pathology in Messina in 1882, then Professor of Pathology at the University of Catania in 1883. From 1884 he became the first chairman of pathology at the University of Pisa. In 1881, he described "Di un caso encondroma ed angioma multiplo" published in *Contribuzione alla genesi embrionale dei tumori Movimento medico-chirurgico*, the association of an enchondroma with multiple angiomas, now known as Maffucci's syndrome. Maffucci also isolated the agent causing avian tuberculosis from his extensive experimental research on fowls and confirmed that avian tuberculosis had a different origin from the bovine and human forms. In the last years of his life his pioneering research provided the basis for future studies on tubercular vaccines from living bacilli.

Fig. 39.8. Maffucci, Angelo Maria (1845–1903). Reproduced with kind permission of Dr. R. Ciranni, Section History of Medicine, Pisa University, Pisa, Italy

Mazabraud, André

Born in Savigny, 1921, died in Clamart, France, 2006 (Fig. 39.9). A French rheumatologist and pathologist, he graduated from the faculty of Medicine of Paris during World War II. He then completed his residency in both pathology and rheumatology. He chose rheumatology as his speciality after he worked under Professor de Sèze at Lariboisière Hospital where he could correlate clinical presentations with radiological and histological features. After a year spent at the Institute of Pathology in Geneva, he was appointed pathologist in the laboratory attached to the rheumatology department at Lariboisière, where he remained until 1958. Mazabraud then went to the Mayo Clinic where he was offered the opportunity to review the collection of histological slides under the authority of David Dahlin, as well as preview Dahlin's famous textbook on bone tumours. This book convinced him to keep a record of all his radiological and histological findings for teaching purposes. Back from the USA, Mazabraud was appointed Chief of the Laboratory of Pathology at Cochin Hospital in Paris. During that period, Mazabraud also worked at Avicenne Hospital in Bobigny and Foch Hospital in Suresnes, where he studied the radiological and histological natural history of bone sarcomas. From 1969 to 1986, Mazabraud was appointed Chief of the Department of Pathology at the Curie Institute in Paris. In 1969, he reviewed the literature and proposed a syndrome associating single or multiple muscular myxomas with monostotic or polyostotic form of fibrous dysplasia of bone. This association had been previously described in 1926 by Henschen but now bears the name of Mazabraud's syndrome. Among his particularly rich scientific contributions, Mazabraud along with Aurias and assisted by Rimbaud, Buffe and Dubousset discovered the recurrent t(11;22) chromosomal translocation which characterizes the genetic abnormalities of Ewing's sarcomas.

Nora, Frederick

Born in Chicago, USA, 1952. In 1983, while undergoing his pathology residency at the Mayo Clinic, Rochester, USA, Nora co-authored a paper with the eminent skeletal pathologists Dr. David Dahlin and Dr. Krishnan Unni, first describing bizarre parosteal osteochondromatous proliferation. The name of this new entity proved too much of a mouthful for many. As a result, largely in the US, it has become known as Nora's lesion after the first author of the original paper. In Europe it tends to be known by the acronym BPOP.

Ollier, Léopold

Born in Les Vans, 1830, died in Lyon, France, 1900 (Fig. 39.10). A French orthopaedic surgeon, he underwent his medical education in Montpellier and speciality training in Lyon. He was appointed Chief Surgeon and Professor of Clinical Surgery at Lyon's Hotel-Dieu Hospital in 1860. Ollier carried out extensive research on periosteum and the subperiosteal osteogenetic layer and their role in bone formation, bone and joint resection, and bone and skin grafting. He described the condition first known as dyschondroplasia, now known as multiple enchondromatosis or Ollier's disease, characterized by abnormal development of enchondromas in the metaphysis and adjacent regions of the shafts and flat bones.

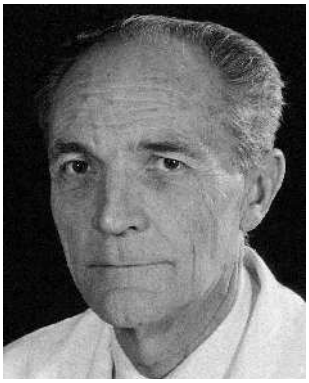

Fig. 39.9. Mazabraud, André (1921–2006). Reproduced with kind permission of F. Valenty and Dr. J. Dumont, Institut Curie, Paris, France

Fig. 39.10. Ollier, Léopold (1830–1900). Reproduced with kind permission of Maîtrise Orthopédique, Paris, France

Paget, James, Sir

Born in Yarmouth, 1814, died in London, England, 1899 (Fig. 39.11). An English surgeon and pathologist, he entered St. Bartholomew's Hospital in London aged 20, and graduated from the Royal College of Surgeons in 1836. Between 1836 and 1843, Paget spent time acquiring medical and scientific knowledge as he was appointed curator of the museum at St Bartholomew's Hospital and was responsible for the *Annual Reports on the Progress of Anatomy and Physiology*. He published in 1853 the two volumes of *Lectures on Surgical Pathology*, based on the work he had done in the museum, describing the minute changes of tissues revealed under the microscope. James Paget served as surgeon from 1847 to 1877 at St Bartholomew's Hospital and became professor of anatomy and surgery at the Royal College of Surgeons of England from 1847. He was elected fellow of the Royal Society in 1851, of which he was elected president in 1875. He was appointed Surgeon Extraordinary to Queen Victoria in 1858. Despite his phenomenal success in private practice—he had the largest surgical practice in London—Sir James Paget actively contributed to medical knowledge by making notable scientific contributions as well as writing important books on surgical pathology, tumours and surgery. In 1874, he published a paper "On disease of the mammary areola preceding cancer of the mammary gland", now known as Paget's disease of the nipple. In 1876, he published a complete and exhaustive case of a man with progressive bone deformity involving skull, spine, pelvic, lower limbs, compromised vision and deafness over twenty years, terminated by sarcoma of the radius. Clinical details as well as detailed postmortem findings with results of histological descriptions of the diseased bones were given. "On a form of chronic inflammation of bones (osteitis deformans)" was thus one of the first descriptions of Paget's disease, for which Sir James himself wrote: "a better name may be given when more is known of it". Sir James Paget was the first to describe several pathological conditions such as osteochondritis dissecans, as well as what is known today as Osgood-Schlatter disease, and was the first to recognize that the median nerve could be compressed at the wrist. The climax of his career was reached in 1881 when he was President of the International Congress of Medicine held in London, where prestigious orators such as Pasteur, Charcot, Virchow, Koch, Volkmann and Ollier all gave lectures.

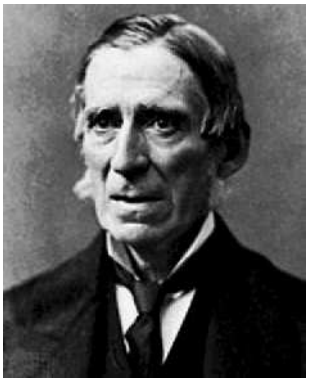

Fig. 39.11. Paget, James, Sir (1814–1899). © BIUM Paris

Fig. 39.12. Von Recklinghausen, Friedrich Daniel (1833–1906). © BIUM Paris

Von Recklinghausen, Friedrich Daniel

Born in Gütersloh, Germany, 1833, died in Strasbourg, Germany (now France), 1906 (Fig. 39.12). A German pathologist, he studied medicine in Bonn, then Würzburg, and graduated from Berlin University in 1855. He focused on pathology and worked during three semesters under Rudolph Virchow's authority. He travelled to Vienna, Rome and Paris before being appointed assistant pathologist at the Pathologischen Institut in Berlin between 1858 and 1864. He was appointed professor of pathology successively in Königsberg, 1865, Würzburg, 1866–1872, and finally Strasbourg 1872–1906, where he was elected Rector of the University in 1883. Von Recklinghausen explored a wide range of topics, from anatomy of connective tissue and inflammation to bone remodelling. He coined the term haemochromatosis and was the first to provide the link between haemo-

chromatosis and iron accumulation in different organs. In 1882, as a tribute to Rudolf Virchow, he described *Über die multiplen Fibrome der Haut und ihre Beziehung zu den multiplen Neuromen* and thus characterized the tumours of neurofibromatosis type 1. Among his famous colleagues were Julius Friedrich Cohnheim, Wilhelm von Waldeyer-Hartz, Karl Albert Ludwig Aschoff and Adolf Kussmaul, whose names all grace medical history!

Von Rothmund, August and Thomson, Matthew Sydney

August von Rothmund (born in Volkach, Germany, 1830, died 1906) graduated from the University of Munich in 1853. He completed his training in ophthalmology in Berlin, under the tutelage of Albrecht von Graefe, and subsequently worked in Prague and Vienna. He then returned to Munich where he ran a surgical policlinics and was in charge of teaching ophthalmology. He was appointed professor in 1859 and set up a university eye clinic in 1879. He published in 1868 "Über Cataracten in Verbindung mit einer eigenthümlichen Hautdegeneration" in *Archiv für Ophthalmologie*, depicting a rare condition characterized by skin abnormalities, juvenile cataract and nose deformity in an inbred community in the Alps. This condition was further described by Matthew Sydney Thompson, an English dermatologist (born in Earlsfield, England, 1894, died 1969). Thompson graduated from Cambridge University and was appointed senior dermatologist at King's College Hospital, London. He published "A hitherto undescribed familial disease" in 1923 and "Poikiloderma congenitale" in 1936 in the *British Journal of Dermatology*. This rare hereditary condition characterized by photosensitivity, skin abnormalities, juvenile cataract, skeletal dysplasia and predisposition to osteosarcoma and skin cancer is now referred to as Rothmund-Thomson syndrome.

Werner, C. W. Otto

A German physician, born in Flensburg, Germany, 1879, died 1936. He graduated from the Christian-Albrechts-Universität in Kiel in 1904. As a medical student he observed and described in 1903 a rare hereditary condition in four siblings presenting with markedly premature aging of the skin and cataracts. From 1906, Werner spent the rest of his life as a physician in a rural practice near the Danish border, only interrupted by his service in the German navy during World War I. The genetic disorder first described by Werner, affecting connective tissue throughout the body and predisposing to osteosarcoma among several other neoplasms, is also known as progeria adultorum, progeria of the adult and pangeria.

Subject Index

D

E

F

G

H

I

J

K

L

M

N

O

P

R

S

T

U

V

W

X

List of Contributors

Suzanne Anderson-Sembach, MD
Chair, Medical Imaging School of Medicine Sydney
The University of Notre Dame Australia
160 Oxford Street
Darlinghurst, Sydney NSM 2010
Australia

Email: andersonsembach@yahoo.com.au

Laura W. Bancroft, MD
Professor of Radiology, Adjunct Faculty
University of Central Florida
Orlando, FL 32816
USA
and
Radiologist, Florida Hospital
601 E. Rollins
Orlando, FL 32803
USA
and
Adjunct Faculty, Mayo Clinic
College of Medicine
Rochester, MN 55901
USA

Email: ljawb@hotmail.com

Johan L. Bloem, MD
Professor and Chairman of Radiology
Department of Radiology, C2S
Leiden University Medical Center
Albinusdreef 2
P O Box 9600
2300 R C Leiden
The Netherlands

Email: j.l.bloem@lumc.nl

Miriam A. Bredella, MD
Massachusetts General Hospital
Department of Radiology, Musculoskeletal Division
55 Fruit Street, Yawkey 6E
Boston, MA 02114
USA

Email: mbredella@partners.org

Peter Brys, MD
University Hospital Leuven
Department of Radiology
Herestraat 49
3000 Leuven
Belgium

Robert S. D. Campbell, FRCR
Department of Radiology
Royal Liverpool University Hospital
Prescot Street
Liverpool, L7 8XP
UK

Email: rob.campbell@rlbuht.nhs.uk

Victor N. Cassar-Pullicino, MD
Consultant Radiologist
Department of Radiology
The Robert Jones & Agnes Hunt Orthopaedic
and District Hospital NHS Trust
Oswestry, Shropshire SY10 7AG
UK

Email: pullicinov@hotmail.com

Peter Choong, MD
Department of Orthopaedics, University of Melbourne
Department of Surgery St. Vincent's Hospital
41 Victoria Parade, Fitzroy 3065, Victoria
Australia
Bone and Soft Tissue Tumour Service
Peter MacCallum Cancer Centre, St. Andrew's Place
East Melbourne 3002, Victoria
Australia

Email: sarcoma@bigpond.net.au

Alun Davies, MD
Department of Radiology
Royal National Orthopaedic Hospital Trust
Brockley Hill
Stanmore, Middlesex
London HA7 4LP
UK

Email: alungoronwy@hotmail.com

A. Mark Davies, MBChB, FRCR
Consultant Radiologist
Department of Radiology
Royal Orthopaedic Hospital
NHS Foundation Trust
Bristol Road South
Northfield
Birmingham B31 2AP
UK

Email: wendy.turner@roh.nhs.uk

A. M. de Schepper, MD
University Hospital Antwerp
Departmentt of Radiology
Wilrijkstraat 10
2650 Edegem
Belgium

Rainer Erlemann, MD
Professor
Department of Radiology
St. Johannes Hospital
Katholisches Klinikum Duisburg
An der Abtei 7–11
47166 Duisberg
Germany

Email: rainererlemann@t-online.de

Apoorva Gogna, MBBS, FRCR
Registrar, Department of Diagnostic Radiology
Singapore General Hospital
Outran Road
Singapore 169608
Republic of Singapore

Email: apoorvagogna@yahoo.com

Ruth A. R. Green, MBBS, MRCP, FRCR
Consultant Radiologist
Royal National Orthopaedic Hospital
Radiology Department
Brockley Hill, Stanmore
Middlesex HA7 4LP
UK

Email: ruth.green@rnoh.nhs.uk

D. Hobin, MB Bch, MRCPCH
Birmingham Children's Hospital
Steelhouse Lane
Birmingham, B4 6NH
UK

Ambrose J. Huang, MD
Massachusetts General Hospital
Department of Radiology, Musculoskeletal Division
55 Fruit Street, Yawkey 6E
Boston, MA 02114
USA

Email:ajhuang@partners.org

Sinchun Hwang, MD
Assistant Professor of Radiology
Weill Medical College of Cornell University
Department of Radiology
Memorial Sloan-Kettering Cancer Center
1275 York Ave
New York, NY 10065
USA

Email: hwangs1@mskcc.org

Hakan Ilaslan, MD
Section of Musculoskeletal Radiology,
Imaging Institute, Cleveland Clinic
Assistant Professor of Radiology
Cleveland Clinic Lerner School of Medicine of Case
Western Reserve University
Diagnostic Radiology/A21
Cleveland Clinic Foundation
9500 Euclid Avenue
Cleveland OH 44195
USA

Email: ilaslanh@ccf.org

Steven L. J. James, MD, ChB, FRCR
Consultant Radiologist
Department of Radiology
Royal Orthopaedic Hospital
NHS Foundation Trust
Bristol Road South
Northfield
Birmingham B31 2AP
UK

Email: steven.james@roh.nhs.uk

Karl J. Johnson, MB Bch, MRCP, FRCR
Consultant Paediatric Radiologist
Birmingham Children's Hospital
Steelhouse Lane
Birmingham B4 6NH
UK

Email: karl.johnson@bch.nhs.uk

Gernot Jundt, MD
Professor, Bone Tumor Reference Center
at the University Institute of Pathology
University Hospital Basel
Schoenbeinstrasse 40
4031 Basel
Switzerland

Email: gernot.jundt@unibas.ch

Amy W. Kao, MD
Diagnostic Radiology/Hb6
Cleveland Clinic Foundation
9500 Euclid Avenue
Cleveland OH 44195
USA

Email: kaoa@ccf.org

Susan V. Kattapuram, MD
Massachusetts General Hospital
Department of Radiology, Musculoskeletal Division
55 Fruit Street, Yawkey 6E
Boston, MA 02114
USA

Email: skattapuram@partners.org

Lars Gunnar Kindblom, MD, PhD
Department of Musculoskeletal Pathology at the Royal
Orthopaedic Hospital
NHS Foundation Trust
Robert Aitken Institute of Clinical Research
The Medical School
University of Birmingham
Birmingham B15 2TT
UK

Email: lars.kindblom@roh.nhs.uk

Monica Koplas, MD
Department of Radiology/Hb6
The Cleveland Clinic Foundation
9500 Euclid Ave.
Cleveland, OH 44195
USA

Email: koplasm@ccf.org

Nikhil A. Kotnis, MD
Department of Radiology
Royal Orthopaedic Hospital
NHS Foundation Trust
Bristol Road South
Northfield
Birmingham B31 2AP
UK

Email: nkotnis@hotmail.com

Mark J. Kransdorf, MD
Professor of Diagnostic Radiology
Department of Radiology
Mayo Clinic Jacksonville
4500 San Pablo Road
Jacksonville, FL 32224-3899
USA

Email: kransdorf.mark@mayo.edu

and
Department of Radiologic Pathology
Armed Forces Institute of Pathology
Washington, DC 20306-6000
USA

Radhesh K. Lalam, MD
Department of Radiology
The Robert Jones & Agnes Hunt Orthopaedic
and District Hospital NHS Trust
Oswestry, Shropshire SY10 7AG
UK

Karl Ludwig, MD
Associate Professor of Radiology
Department of Diagnostic Radiology
Orthopedic University Hospital
University of Heidelberg
Schlierbacher Landstraße 200a
69118 Heidelberg
Germany

Email: karl.ludwig@ok.uni-heidelberg.de

Nancy M. Major, MD
Associate Professor of Radiology and Surgery
Biological Anthropology and Anatomy
Duke University Medical Center
Durham, NC 27710
USA

Email: nancy.major@duke.edu

David Malfair, MD
Department of Radiology,
Vancouver General Hospital,
University of British Columbia
899 West 12th Avenue
Vancouver, Canada

Email:dmalfair@gmail.com

D. C. Mangham
Department of Musculoskeletal Pathology
The Robert Jones & Agnes Hunt Orthopaedic
and District Hospital NHS Trust
Gobowen, Oswestry
Shropshire SY10 7AG
UK

Sriram Mannava, MD
Diagnostic Radiology/Hb6
The Cleveland Clinic Foundation
9500 Euclid Avenue
Cleveland OH 44195
USA

Email: mannavs@ccf.org

Peter L. Munk, MD, CM, FRCPC
Professor of Radiology and Orthopaedic Surgery
Director, Musculoskeletal Division
Department of Radiology
Vancouver General Hospital & Health Sciences Centre
University of British Columbia
855 West 12th Ave
Vancouver, BC V5Z 1M9
Canada

Email: peter.munk@vch.ca

Mark D. Murphey, MD
Department of Radiologic Pathology
Armed Forces Institute of Pathology
Washington, DC 20306-6000
USA
and
Department of Radiology and Nuclear Medicine
Uniformed Services University of Health Sciences
Bethesda, MD 20814-4799
USA

Paul G. O'Donnell, FRCR
Royal National Orthopaedic Hospital
Radiology Department
Brockley Hill, Stanmore
Middlesex HA7 4LP
UK

Email: paul.o'donnell@rnoh.nhs.uk

David M. Panicek, MD
Professor of Radiology
Weill Medical College of Cornell University
Department of Radiology
Memorial Sloan-Kettering Cancer Center
1275 York Ave
New York, NY 10065
USA

Email: panicekd@mskcc.org

Kavita M. Patel, MD
Musculoskeletal Radiology Fellow (2007-2008)
Duke University Medical Center
Durham, NC 27710
USA

Email: kavita.mukund.patel@gmail.com

B. Peersman, MD
University Hospital Antwerp
Department of Radiology
Wilrijkstraat, 10
2650 Edegem
Belgium

Wilfred C. G. Peh, MBBS, MHSM, MD, FRCPE,
FRCPG, FRCR
Senior Consultant, Department of Diagnostic Radiology,
Alexandra Hospital
Clinical Professor, National University of Singapore
Programme Office, Singapore Health Services
5 Lower Kent Ridge Road
Singapore 119074
Republic of Singapore

Email: wilfred.peh@gmail.com

Etienne Pluot, MD
Musculoskeletal Fellow
Service de Radiologie B
Hôpital Cochin
27 rue du Faubourg Saint Jacques
75679 Paris Cedex
France

Email: e.pluot@voila.fr

David Ritchie, MD
Consultant Radiologist
Western Infirmary
Dumbarton Road
Glasgow, G11 6NT
UK

Email: d.a.r@o2.co.uk

Asif Saifuddin, MD
Department of Radiology
Royal National Orthopaedic Hospital Trust
Brockley Hill
Stanmore, Middlesex
London HA7 4LP
UK

Email: asaifuddin@aol.com

Darshana Sanghvi, MD, DNB
Department of Radiology
KEM Hospital and Seth GS Medical College, Parel
Mumbai 400 012
Maharashtra
India

Email: sanghvidarshana@gmail.com,
darshanasanghvi1@hotmail.com

Claus Simpfendorfer, MD
Cleveland Clinic
Diagnostic Radiology/A21
9500 Euclid Avenue
Cleveland, OH 44195
USA

Email:csimpfendorfer@yahoo.com

John A. Skinner, MD
Department of Bone and Soft Tissue Sarcoma Surgery
Royal National Orthopaedic Hospital Trust
Brockley Hill, Stanmore
Middlesex, London
HA7 4LP, UK

Email: john.skinner@ucl.ac.uk

Agustinus S. Suhardja, MD, MSc
Department of Radiology, C2S
Leiden University Medical Center
Albinusdreef 2
P.O. Box 9600
2300 RC Leiden
The Netherlands

Email: a_suhardja@ yahoo.com

Murali Sundaram, MD, FRCR
Section of Musculoskeletal Radiology, Imaging Institute,
Cleveland Clinic
Professor of Radiology,
Cleveland Clinic Lerner School of Medicine
of Case Western Reserve University
Diagnostic Radiology/A21
The Cleveland Clinic Foundation
9500 Euclid Avenue
Cleveland, OH 44195
USA

Email: sundarm@ccf.org

Bernhard J. Tins, MD
Department of Radiology
The Robert Jones & Agnes Hunt Orthopaedic
and District Hospital NHS Trust
Oswestry, Shropshire SY10 7AG
UK

Email: bernhard.tins@rjah.nhs.uk

Prudencia N. M. Tyrrell, MD
Department of Radiology
The Robert Jones & Agnes Hunt Orthopaedic
and District Hospital NHS Trust
Oswestry, Shropshire SY10 7AG
UK

Filip M. Vanhoenacker, MD, PhD
Department of Radiology
University Hospital Antwerp
Wilrijkstraat 10
2650 Edegem
Belgium

Email: filip.vanhoenacker@pandora.be

Filip van Kerkhove, MD
University Hospital Leuven
Department of Radiology
Herestraat 49
3000 Leuven
Belgium

Sophie Verbeke, MD
Department of Pathology, C2S
Leiden University Medical Center
Albinusdreef 2
P.O. Box 9600
2300 RC Leiden
The Netherlands

Koenraad Verstraete, MD, PhD
Full Professor of Radiology
Ghent University
Chief Department of Radiology
Ghent University Hospital – UZG/MR/1K12
De Pintelaan 185
9000 Ghent
Belgium

Email: koenraad.verstraete@rug.ac.be

Richard W. Whitehouse, MD
Department of Clinical Radiology
Manchester Royal Infirmary
Oxford Road
Manchester, M13 9WL
UK

Email: richard.whitehouse@cmmc.nhs.uk

Marc H. Willis, DO
Massachusetts General Hospital
Department of Radiology, Musculoskeletal Division
55 Fruit Street, Yawkey 6E
Boston, MA 02114
USA

Email: willismh@earthlink.net

Medical Radiology

Diagnostic Imaging and Radiation Oncology

Titles in the series already published

Diagnostic Imaging

Innovations in Diagnostic Imaging
Edited by J.H. Anderson

Radiology of the Upper Urinary Tract
Edited by E.K. Lang

The Thymus - Diagnostic Imaging, Functions, and Pathologic Anatomy
Edited by E. Walter, E. Willich, and W.R. Webb

Interventional Neuroradiology
Edited by A. Valavanis

Radiology of the Pancreas
Edited by A.L. Baert, co-edited by G. Delorme

Radiology of the Lower Urinary Tract
Edited by E.K. Lang

Magnetic Resonance Angiography
Edited by I.P. Arlart, G.M. Bongartz, and G. Marchal

Contrast-Enhanced MRI of the Breast
S. Heywang-Köbrunner and R. Beck

Spiral CT of the Chest
Edited by M. Rémy-Jardin and J. Rémy

Radiological Diagnosis of Breast Diseases
Edited by M. Friedrich and E.A. Sickles

Radiology of the Trauma
Edited by M. Heller and A. Fink

Biliary Tract Radiology
Edited by P. Rossi

Radiological Imaging of Sports Injuries
Edited by C. Masciocchi

Modern Imaging of the Alimentary Tube
Edited by A.R. Margulis

Diagnosis and Therapy of Spinal Tumors
Edited by P.R. Algra, J. Valk, and J.J. Heimans

Interventional Magnetic Resonance Imaging
Edited by J.F. Debatin and G. Adam

Abdominal and Pelvic MRI
Edited by A. Heuck and M. Reiser

Orthopedic Imaging. Techniques and Applications
Edited by A.M. Davies and H. Pettersson

Radiology of the Female Pelvic Organs
Edited by E.K. Lang

Clinical Applications of Magnetic Resonance in Cardiovascular Disease
Edited by J. Bogaert, A.J. Duerinckx, and F.E. Rademakers

Modern Head and Neck Imaging
Edited by S. Mukherji and J.A. Castelijns

Radiological Imaging of Endocrine Diseases
Edited by J.N. Bruneton - in collaboration with B. Padovani and M.-Y. Mourou

Trends in Contrast Media
Edited by H.S. Thomsen, R.N. Muller, and R.F. Mattrey

Functional MRI
Edited by C.T.W. Moonen and P.A. Bandettini

Radiology of the Pancreas 2nd revised edition
Edited by A.L. Baert, Co-edited by G. Delorme and L. Van Hoe

Emergency Pediatric Radiology
Edited by H. Carty

Spiral CT of the Abdomen
Edited by F. Terrier, M. Grossholz, and C. Becker

Radiology of Peripheral Vascular Diseases
Edited by E. Zeitler

Liver Malignancies
Diagnostic and Interventional Radiology
Edited by C. Bartolozzi and R. Lencioni

Medical Imaging of the Spleen
Edited by A.M. De Schepper and F. Vanhoenacker

Diagnostic Nuclear Medicine
Edited by C. Schiepers

Radiology of Blunt Trauma of the Chest
(Authors) P. Schnyder and M. Wintermark

Portal Hypertension
Edited by P. Rossi, P. Ricci, and L. Broglia

Recent Advances in Diagnostic Neuroradiology
Edited by Ph. Demaerel

Virtual Endoscopy and Related 3D Techniques
Edited by P. Rogalla, J. Terwisscha van Scheltinga, and B. Hamm

Transfontanellar Doppler Imaging in Neonates
(Authors) A. Couture and C. Veyrac

Multislice CT
Edited by M.F. Reiser, M. Takahashi, M. Modic, and R. Bruening

Diagnostic and Interventional Radiology in Liver Transplantation
Edited by E. Bücheler, V. Nicolas, C.E. Broelsch, and X. Rogiers

Pediatric Uroradiology
Edited by R. Fotter

Radiology of AIDS.
A Practical Approach
Edited by J.W.A.J. Reeders and P.C. Goodman

Pediatric Chest Imaging
Chest Imaging in Infants and Children
Edited by J. Lucaya and J.L. Strife

Radiological Imaging of the Small Intestine
Edited by N. Gourtsoyiannis

Magnetic Resonance Angiography. 2nd Revised Edition
Edited by I.P. Arlart, G.M. Bongartz, and G. Marchal

CT of the Peritoneum
(Authors) A. Rossi and G. Rossi

Pediatric ENT Radiology
Edited by S.J. King and A.E. Boothroyd

Applications of Sonography in Head and Neck Pathology
Edited by J.N. Bruneton. In Collaboration with C. Raffaelli and O. Dassonville

Radiological Imaging of the Ureter
Edited by F. Joffre and Ph. Otal

Imaging of the Knee.
Techniques and Applications
Edited by A.M. Davies and V.N. Cassar-Pullicino

Radiology of Osteoporosis
Edited by S. Grampp

Gastrointestinal Tract Sonography in Fetuses and Children
Edited by A. Couture

Imaging of Orbital and Visual Pathway Pathology
Edited by W.S. Müller-Forell

Imaging of the Larynx
Edited by R. Hermans

3D Image Processing.
Techniques and Clinical Applications
Edited by D. Caramella and C. Bartolozzi

Imaging and Intervention in Abdominal Trauma
Edited by R.F. Dondelinger

Perinatal Imaging. From Ultrasound to MR Imaging
Edited by F. Avni

Interventional Radiology in Cancer
Edited by A. Adam, R.F. Dondelinger, and P.R. Mueller

Radiological Imaging of the Neonatal Chest
Edited by V. Donoghue

Imaging of the Foot & Ankle.
Techniques and Applications
Edited by A.M. Davies, R.W. Whitehouse, and J.P.R. Jenkins

Pelvic Floor Disorders
Edited by C.I Bartram and J.O.L. DeLancey
Associate Editors: S. Halligan, F.M. Kelvin, J. Stoker

Imaging of the Pancreas.
Cystic and Rare Tumors
Edited by C. Procacci and A. J. Megibow

High-Resolution Sonography of the Peripheral Nervous System
Edited by S. Peer and G. Bodner

Radiology of the Petrous Bone
Edited by M. Lemmerling, K. Marsot-Dupuch, and S.S. Kollias

Imaging of the Shoulder.
Techniques and Applications
Edited by A.M. Davis and J. Hodler

Duplex and Color Doppler Imaging of the Venous System
Edited by G.H. Mostbeck

Multidetector-Row CT of the Thorax
Edited by U.J. Schoepf

Functional Imaging of the Chest
Edited by H.-U. Kauczor

Radiological Imaging in Hematological Malignancies
Edited by A. Guermazi

Radiology of the Pharynx and the Esophagus
Edited by O. Ekberg

Ultrasound of the Musculoskeletal System
S. Bianchi and C. Martinoli

Coronary Radiology
Edited by M. Oudkerk

Radiology and Imaging of the Colon
Edited by A.H. Chapman

Multislice CT
2nd Revised Edition
Edited by M.F. Reiser, M. Takahashi, M. Modic, and C.R. Becker

Dynamic Contrast-Enhanced Magnetic Resonance Imaging in Oncology
Edited by A. Jackson, D. Buckley, and G.J.M. Parker

Imaging in Treatment Planning for Sinonasal Diseases
Edited by R. Maroldi and P. Nicolai

MR Imaging in White Matter Diseases of the Brain and Spinal Cord
Edited by M. Filippi, N. De Stefano, V. Dousset, and J.C. McGowan

Diagnostic Nuclear Medicine
2nd Revised Edition
Edited by C. Schiepers

Handbook of Clinical Cardiac MRI
With Interactive CD-ROM
Edited by J. Bogaert, S. Dymarkowski, and A.M. Taylor

Focal Liver Lesions
Detection, Characterization, Ablation
Edited by R. Lencioni, D. Cioni, and C. Bartolozii

Multidetector-Row CT Angiography
Edited by C. Catalano

Radiology of the Stomach and Duodenum
Edited by A.H. Freeman and E. Sala

Paediatric Musculoskeletal Disease
Edited by D.J. Wilson

Magnetic Resonance Imaging in Ischemic Stroke
Edited by R. von Kummer and T. Back

Contrast Media in Ultrasonography
Basic Principles and Clinical Applications
Edited by E. Quaia

Imaging of the Hip & Bony Pelvis
Techniques and Applications
Edited by A.M. Davies, K.J. Johnson, and R.W. Whitehouse

Vascular Embolotherapy
Volume 1: A Comprehensive Approach
Edited by J. Golzarian, S. Sun, and M. Sharafuddin

Vascular Embolotherapy
Volume 2: A Comprehensive Approach
Edited by J. Golzarian, S. Sun, and M. Sharafuddin

Imaging of Kidney Cancer
Edited by A. Guermazi

Imaging of Occupational and Environmental Disorders of the Chest
Edited by P.A. Gevenois and P. De Vuyst

Contrast Media
Safety Issues and ESUR Guidelines
Edited by H.S. Thomsen

Virtual Colonoscopy
A Practical Guide
Edited by P. Lefere and S. Gryspeerdt

Spinal Imaging
Diagnostic Imaging of the Spine and Spinal Cord
Edited by J.W.M. Van Goethem, L. Van den Hauwe, and P.M. Parizel

Head and Neck Cancer Imaging
Edited by R. Hermans

Vascular Interventional Radiology
Angioplasty, Stenting, Thrombolysis and Thrombectomy
Edited by M. Cowling

Radiology of Osteoporosis
2nd Revised Edition
Edited by S. Grampp

Radiological Imaging of the Digestive Tract in Infants and Children
Edited by A.S. Devos and J.G. Blickman

MRI and CT of the Female Pelvis
Edited by B. Hamm and R. Forstner

Percutaneous Tumor Ablation in Medical Radiology
Edited by T.J. Vogl, T. Helmberger, M.G. Mack, and M.F. Reiser

Ultrasound of the Gastrointestinal Tract
Edited by G. Maconi and G. Bianchi Porro

Radiation Dose from Pediatric and Adult Multidetector Computed Tomography
Edited by D. Tack and P.A. Gevenois

Parallel Imaging in Clinical MR Applications
Edited by S.O. Schoenberg, O. Dietrich, and M.F. Reiser

Imaging of Orthopedic Sports Injuries
Edited by F.M. Vanhoenacker, M. Maas, J.L.M.A. Gielen

Clinical Functional MRI
Presurgical Functional Neuroimaging
Edited by C. Stippich

Screening and Preventive Diagnosis with Radiological Imaging
Edited by M.F.Reiser, G. van Kaick, C. Fink, and S.O. Schoenberg

Computed Tomography of the Lung
A Pattern Approach
J.A. Verschakelen and W. De Wever

Imaging in Transplantation
Edited by A. Bankier

Imaging in Percutaneous Musculoskeletal Interventions
Edited by A. Gangi, S.Guth, and A.Guermazi

Imaging of the Pancreas Acute and Chronic Pancreatitis
Edited by E.J. Balthazar, A..J. Megibow, and R. Pozzi Mucelli

Image Processing in Radiology
Current Applications
Edited by E. Neri, D. Caramella, and C. Bartolzzi

Measurements in Musculoskeletal Radiology
Edited by V.N. Cassar-Pullicino and A.M. Davies

Pediatric Chest Imaging
2nd Revised Edition
Chest Imaging in Infants and Children
Edited by J. Lucaya and J.L. Strife

Radiological Imaging of the Neonatal Chest
2nd Revised Edition
Edited by V. Donoghue

Imaging in Pediatric Skeletal Trauma
Techniques and Applications
Edited by K.J. Johnson and E. Bache

Pediatric Uroradiology
2nd Revised Edition
Edited by R. Fotter

Color Doppler US of the Penis
Edited by M. Bertolotto

Liver Radioembolization with Y90 Microspheres
Edited by J.I. Bilbao and M.F. Reiser

High Resolution Sonography of the Peripheral Nervous System
2nd Revised Edition
Edited by S. Peer and G. Bodner

Imaging Pelvic Floor Disorders
2nd Revised Edition
Edited by J. Stoker, S. Taylor, J. O. L. DeLancey

Intracranial Vascular Malformations and Aneurysms
From Diagnostic Work-Up to Endovascular Therapy
2nd Revised Edition
Edited by M. Forsting and I. Wanke

Coronary Radiology
2nd Revised Edition
Edited by Matthijs Oudkerk and Maximilian F. Reiser

Cardiothoracic Imaging with MDCT
Edited by M. Rémy-Jardin and J. Rémy

Multislice CT
3rd Revised Edition
Edited by M.F. Reiser, C.R. Becker, K. Nikolaou, and G. Glazer

MRI of the Lung
Edited by H.-U. Kauczor

Springer

Medical Radiology

Diagnostic Imaging and Radiation Oncology

Titles in the series already published

RADIATION ONCOLOGY

Lung Cancer
Edited by C.W. Scarantino

Innovations in Radiation Oncology
Edited by H.R. Withers and L.J. Peters

Radiation Therapy of Head and Neck Cancer
Edited by G.E. Laramore

Gastrointestinal Cancer - Radiation Therapy
Edited by R.R. Dobelbower, Jr.

Radiation Exposure and Occupational Risks
Edited by E. Scherer, C. Streffer, and K.-R. Trott

Radiation Therapy of Benign Diseases - A Clinical Guide
S.E. Order and S.S. Donaldson

Interventional Radiation Therapy Techniques - Brachytherapy
Edited by R. Sauer

Radiopathology of Organs and Tissues
Edited by E. Scherer, C. Streffer, and K.-R. Trott

Concomitant Continuous Infusion Chemotherapy and Radiation
Edited by M. Rotman and C.J. Rosenthal

Intraoperative Radiotherapy - Clinical Experiences and Results
Edited by F.A. Calvo, M. Santos, and L.W. Brady

Radiotherapy of Intraocular and Orbital Tumors
Edited by W.E. Alberti and R.H. Sagerman

Interstitial and Intracavitary Thermoradiotherapy
Edited by M.H. Seegenschmiedt and R. Sauer

Non-Disseminated Breast Cancer
Controversial Issues in Management
Edited by G.H. Fletcher and S.H. Levitt

Current Topics in Clinical Radiobiology of Tumors
Edited by H.-P. Beck-Bornholdt

Practical Approaches to Cancer Invasion and Metastases
A Compendium of Radiation Oncologists' Responses to 40 Histories
Edited by A.R. Kagan with the Assistance of R.J. Steckel

Radiation Therapy in Pediatric Oncology
Edited by J.R. Cassady

Radiation Therapy Physics
Edited by A.R. Smith

Late Sequelae in Oncology
Edited by J. Dunst and R. Sauer

Mediastinal Tumors. Update 1995
Edited by D.E. Wood and C.R. Thomas, Jr.

Thermoradiotherapy and Thermochemotherapy
Volume 1: Biology, Physiology, and Physics
Volume 2: Clinical Applications
Edited by M.H. Seegenschmiedt, P. Fessenden, and C.C. Vernon

Carcinoma of the Prostate
Innovations in Management
Edited by Z. Petrovich, L. Baert, and L.W. Brady

Radiation Oncology of Gynecological Cancers
Edited by H.W. Vahrson

Carcinoma of the Bladder
Innovations in Management
Edited by Z. Petrovich, L. Baert, and L.W. Brady

Blood Perfusion and Microenvironment of Human Tumors
Implications for Clinical Radiooncology
Edited by M. Molls and P. Vaupel

Radiation Therapy of Benign Diseases.
A Clinical Guide
2nd revised edition
(Authors) S.E. Order and S.S. Donaldson

Progress and Perspectives in the Treatment of Lung Cancer
Edited by P. Van Houtte, J. Klastersky, and P. Rocmans

Combined Modality Therapy of Central Nervous System Tumors
Edited by Z. Petrovich, L.W. Brady, M.L. Apuzzo, and M. Bamberg

Age-Related Macular Degeneration.
Current Treatment Concepts
Edited by W.E. Alberti, G. Richard, and R.H. Sagerman

Radiotherapy of Intraocular and Orbital Tumors
2nd revised edition
Edited by W.E. Alberti and R.H. Sagerman

Clinical Target Volumes in Conformal and Intensity Modulated Radiation Therapy
A Clinical Guide to Cancer Treatment
Edited by V. Grégoire, P. Scalliet, and K.K. Ang

Palliative Radiation Oncology
(Authors) R.G. Parker, N.A. Janjan, and M.T. Selch

Modification of Radiation Response
Edited by C. Nieder, L. Milas, and K.K. Ang

Advances in Radiation Oncology in Lung Cancer
Edited by B. Jeremic

Technical Basis of Radiation Therapy
Practical Clinical Applications
4th Revised Edition
Edited by S.H. Levitt, J.A. Purdy, C.A. Perez, and S. Vijayakumar

New Technologies in Radiation Oncology
Edited by W. Schlegel, T. Bortfeld, and A.-L. Grosu

Medical Radiology volume on Multimodal Concepts for Integration of Cytotoxic Drugs and Radiation Therapy
Edited by J.M. Brown, M.P. Mehta, and C. Nieder

Clinical Practice of Radiation Therapy for Benign Diseases
Contemporary Concepts and Clinical Results
Edited by M. H. Seegenschmiedt, H.-B. Makoski, K.-R. Trott, and L.W. Brady

CURED I – LENT - Late Effects of Cancer Treatment on Normal Tissues
Edited by P. Rubin, L.S. Constine, L.B. Marks, and P. Okunieff

CURED II LENT - Cancer Survivorship Research and Education
Late Effects of Cancer Treatment on Normal Tissues
Edited by P. Rubin, L.S. Constine, L.B. Marks, and P. Okunieff

Radiation Oncology
An Evidence-Based Approach
Edited by J.J. Lu and L.W. Brady

Primary Optic Nerve Sheath Meningioma
Edited by B. Jeremić and S. Pitz

Springer